1127-21
1521

JOURNAL OF
COLLOID SCIENCE

Editor-in-Chief
Victor K. La Mer, Columbia University, New York

Advisory Board

C. O. Beckmann
K. F. Bonhoeffer
J. A. Christiansen
P. J. W. Debye
John T. Edsall
I. Fankuchen
John D. Ferry
Wilfried Heller
John G. Kirkwood
E. C. Lingafelter
L. G. Longsworth
S. G. Mason
J. Th. G. Overbeek

R. Ruyssen
William Seifriz
Leo Shedlovsky
Theodore Shedlovsky
Robert Simha
R. H. Smellie
Jacinto Steinhardt
The Svedberg
Hugh S. Taylor
Arne Tiselius
Robert D. Vold
Bernard Vonnegut
Ralph W. G. Wyckoff

Bruno H. Zimm

VOLUME 11

1956

ACADEMIC PRESS INC.—PUBLISHERS
NEW YORK, N. Y.

JOURNAL OF COLLOID SCIENCE **11,** 1–14 (1956)

PSEUDOPLASTIC FLOW: VISCOMETRY, CORRELATIONS OF SHEAR STRESS VS. SHEAR RATE, AND PREDICTION OF LAMINAR FLOW IN TUBES

Edward W. Merrill

Department of Chemical Engineering, Massachusetts Institute of Technology, Cambridge, Massachusetts

Received October 14, 1955

ABSTRACT

The relations of shear stress τ to shear rate D for low molecular weight polyisobutylenes dissolved in cyclohexane were studied in a coaxial cylinder viscometer. Flow curves of τ vs. D were found invariably to be typical of pseudoplastic fluids, without dependency on time of shear, and were well correlated by empirical equations of the form: $\tau = bD^s$, wherein b and s are experimental constants depending on concentration C and temperature T. It is shown that ln b is linear in $\sqrt{C}$ and in $1/T$. The correspondence of b as a measure of anomalous flow with viscosity η (defined as $\tau = \eta D$) for Newtonian flow is suggested. For a pseudoplastic fluid whose shear stress-shear rate relation can be described mathematically as $\tau = bD^s$, an equation is derived to relate volumetric flow rate through a straight tube to pressure gradient, for conditions of laminar flow. This equation is similar in form to the Hagen-Poiseuille formula for flow of Newtonian fluids. Tube-flow experiments with pseudoplastic fluids in tubes are described which confirm the validity of the equation.

INTRODUCTION

In numerous studies reported in the literature on the relation of viscosity to the temperature, concentration, and molecular weight of polymer solutions, the polyisobutylenes have been examined in particular because of their stability and relative ease of characterization. Usually these studies have been conducted under conditions of low concentration or low rate of shear, or both at once, in order to assure Newtonian flow. Under such conditions of measurement, whereby the solution viscosity and also the relative and intrinsic viscosity are not functions of rate of shear, the evaluation of high polymer configuration has met with substantial success.

In the studies described in this article, solutions of low molecular weight dissolved in cyclohexane, having substantial concentration, were tested in a coaxial cylinder viscometer for the shear stress-shear rate relation over a range of shear rates up to 6000 reciprocal seconds or more. This relation was found to be characteristic of that type of non-Newtonian flow called pseudoplasticity. These pseudoplastic curves have been fitted with good precision by a simple empirical equation of the form $\tau = bD^s$, wherein τ is shear stress, D is shear rate, and b and s are experimentally determined constants. Although equations of this form have been criticized for not contributing to the understanding of the basic molecular mechanics of the fluid and for not yielding any term that has the dimensions of viscosity, they may serve a useful purpose in providing an accurate mathematical description of the shear stress-shear rate relation of a fluid, by which at least elementary cases of flow may be calculated.

This paper is accordingly divided into two parts. In the first part the basic shear stress-shear rate relations were determined for low molecular weight polyisobutylene in cyclohexane, as functions of temperature and concentration. The resulting experimental curves were then fitted by empirical equations of the form $\tau = bD^s$, and the variations of b and s with temperature and concentration were correlated.

In the second part, a general equation is derived for predicting the flow rate-pressure gradient relation in straight tubes of circular cross section, for a fluid in laminar flow that obeys the empirical relation: $\tau = bD^s$. The equation was verified by experiments on two different pseudoplastic fluids that follow the relation $\tau = bD^s$, one of them being polyisobutylene in cyclohexane, the other ammonium alginate in water.

Part I: Viscometry and Correlation of Polyisobutylene Solutions

Experimental

Solutions were prepared for viscometry by weighing out in aluminum foil dishes samples of the commercial polyisobutylene investigated, viz., grade LMH of the Enjay Corp., which has a viscosity-average molecular weight of 80,000 as reported by the manufacturer. The polymer in its dish was placed in a screw cap jar, and the desired amount of cyclohexane was weighed in. The jar was then sealed with the screw cap, provided with a Vinylite-coated paper gasket. Additionally, to insure against solvent loss, the neck and cap of the jar were painted with collodion solution. The jar and its contents were shaken in a bottle shaker until an apparently homogeneous solution was obtained, and the solution was then stored in the sealed jar until the viscometric test was made. The aluminum weighing dish was allowed to remain in the jar. Periodic checks confirmed constancy of weight and thus of original concentration.

The coaxial cylinder viscometer used for these tests (*1*) is an improved model of an earlier type (*2*). The distinguishing features of the earlier viscometer, viz., small annular clearance (0.006 in.) between mechanically aligned cylinders, the measurement of shear stress and shear rate as essentially point values, and pressure injection of test fluid, have been retained in the model used in these experiments. In the present viscometer, temperature control has been substantially improved by providing both the inner cylinder (the rotor) and the outer cylinder (the stator) with closed water channels just beneath the shearing surfaces, through which a continuous supply of water is pumped under pressure from a thermostatic bath controlled to ±0.2°C. The fluid under test in the annular space is thereby maintained at a substantially uniform temperature.

Viscometric Results and Correlation of Shear Stress versus Shear Rate

The solutions of the LMH polyisobutylene in cyclohexane examined in this study were in concentrations of 10.0%, 15.0%, 20.0%, and 25.0% by

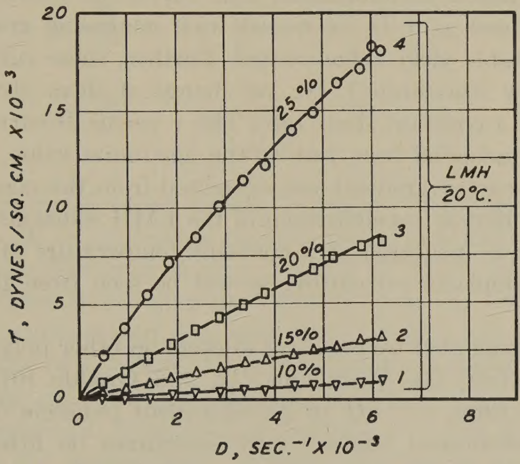

FIG. 1. Linear scale plots of shear stress τ vs. shear rate D for various weight % concentrations of LMH polyisobutylene in cyclohexane.

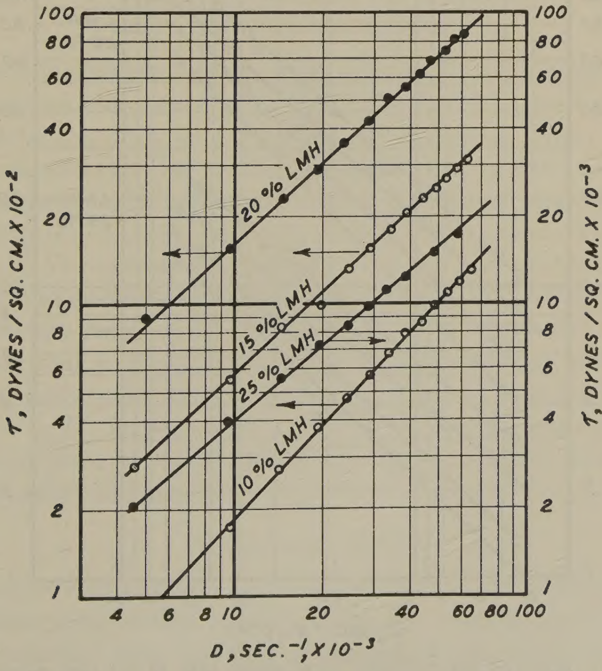

FIG. 2. Log-log plots of shear stress τ vs. shear rate D for different wt. % concentrations of LMH polyisobutylene in cyclohexane at 20°C.

weight, all of which were tested at 20°C. In addition, the 20% and 25% solutions were tested at 10°, 30°, and 40°C.

Except for the 10% solution, which was nearly Newtonian, all other solutions showed the anomalous curves of stress versus shear rate (τ vs. D) commonly called pseudoplastic, i.e., curves in which the apparent viscosity η, defined as τ/D, decreased with increasing gradient, but for which no detectable yield value existed. Further, these curves showed no time-dependency (thixotropy), i.e., no change of shear stress with duration of shear at a constant shear rate. The τ versus D curves obtained as shear rate was increased from zero to the maximum value, were identical with those obtained as gradient was decreased from the maximum to zero.

It was found that as concentration of the LMH solutions increased, the τ versus D curves measured at a constant temperature of 20°C. showed increasing pseudoplastic curvature, as will be seen from the linear scale plots in Fig. 1.

As has been suggested by previous workers on other polymeric systems, for example, Alfrey (3), Weltmann (4), and Grodde (5), an empirical equation of the form $\tau = bD^s$ or its equivalent (wherein b and s are experimentally determined values), may sometimes be fitted to the flow curves of high polymer solutions. In the present study this type of corre-

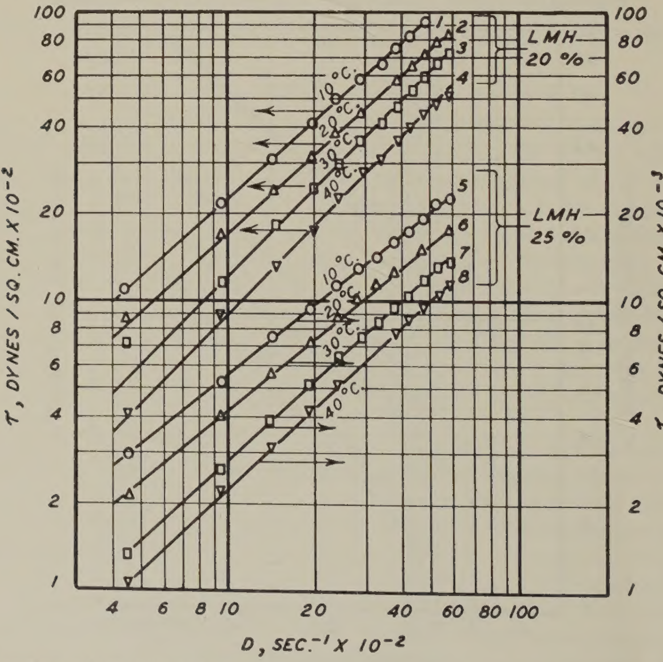

FIG. 3. Log-log plots of shear stress τ vs. shear rate D for two concentrations of LMH polyisobutylene in cyclohexane for different temperatures.

TABLE I

Values of the Experimental Constants in the Equation: $\tau = bD^s$

Polymer	Conc., g/100 g.	Temp., °C.	b	s
LMH	10	20	0.185	1.0
	15		0.848	0.94
	20		3.4	0.90
	25		11.6	0.85
LMH	20	10	6.75	0.85
		20	3.40	0.90
		30	1.87	0.95
		40	1.00	0.985

lation has been found to be notably successful. The experimental values of τ vs. D for all concentration studies and all temperature studies have been plotted *logarithmically* in Figs. 2 and 3. It will be noted that straight lines result, whose slopes give the values of s in the empirical equation cited. Once s is determined, the coefficient b is then calculable as any experimental value of τ divided by corresponding D raised to the s power. Table I presents values of b and s, determined from Fig. 2, for all the solutions herein examined. Equations of the form $\tau = bD^s$ will be seen to fit the data both for temperature variation at constant concentration and for variation in concentration at constant temperature.

Concentration Effects

Previous investigators, among them Alfrey (3), have suggested a linear relation between the logarithm of viscosity and the square root of polymer concentration on a weight basis, for Newtonian fluids. When, however, the concentration of polymer is higher, and in particular, the rates of shear imposed on the solution are of the order of magnitude of thousands of reciprocal seconds, as in the present study, non-Newtonian $\tau - D$ curves result. Viscosity then is a function of the rate of shear, so that the value of $\eta(D)$ to be used in a correlation of $\ln \eta$ vs. $\sqrt{C}$ becomes a problem.

In the present study of LMH polyisobutylene solutions in cyclohexane, it was found that a general correlation of isothermal flow properties with respect to concentration of solution was achieved by plotting $\ln b$ vs. $\sqrt{C}$, wherein $b = \tau/D^s$, instead of $\ln \eta$ vs. $\sqrt{C}$. The coefficient b in this equation is independent of shear rate D, though it no longer has the dimensions of viscosity. This is shown as curve 1 of Fig. 4.

Temperature Effects

In the same way that the linear correlation of $\ln b$ with $\sqrt{C}$ in the realm of pseudoplastic flow appears to be the counterpart of $\ln \eta$ versus $\sqrt{C}$ in Newtonian flow, the flow properties of the LMH solutions at a constant concentration were found to be influenced by temperature in

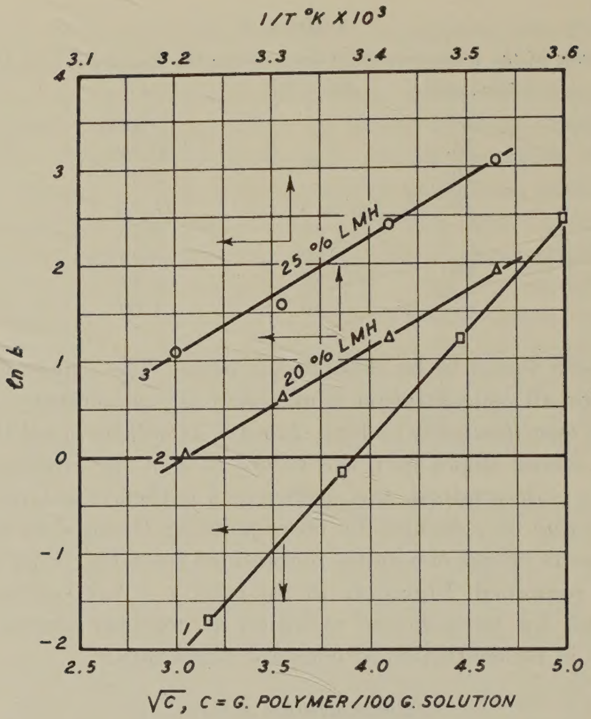

FIG. 4. Correlation of ln b with $\sqrt{C}$ and with $1/T$. Curve 1: ln b vs. $\sqrt{C}$, LMH solutions at 20°C. Curve 2: ln b vs. $1/T$, 20% LMH. Curve 3: ln b vs. $1/T$, 25%LMH

such a way that a plot of ln b vs. $1/T$ yields a straight line, whereas in the domain of Newtonian flow, ln η is linear in $1/T$. This relation is shown as curves 2 and 3 of Fig. 4 for 20% and 25% (by weight) solutions of LMH in cyclohexane.

PART II: EQUATION FOR LAMINAR FLOW IN STRAIGHT TUBES OF CIRCULAR CROSS SECTION, AND EXPERIMENTAL VERIFICATION

Derivation of the General Equation

Consider a straight tube of circular cross section, in which a liquid is flowing isothermally, in steady state, and in laminar flow. Let the section for analysis be sufficiently removed from the inlet so that the boundary layers have met at the axis and have produced a stable velocity profile.

Consider as the system for analysis a cylindrical control volume coaxial with the tube, having a length ΔL and a radius r. The radius r may be varied from zero at the axis to the inside tube radius r_w. Steady-state flow requires a balance of forces in the flow direction on the cylindrical control volume such that

$$-\Delta P \cdot \pi r^2 = \tau \cdot 2\pi r \Delta L, \qquad [1]$$

where ΔP = pressure drop across the length ΔL,
r = radius of element,
ΔL = length of element, and
τ = shear stress.

In the conventional Hagen-Poiseuille development for a Newtonian fluid, the Newtonian equation $\tau = \eta(dV/dr)$, where η = viscosity and dV/dr = velocity gradient or shear rate (elsewhere called D), is substituted in Eq. [1], and integration proceeds to give expressions for point velocity V as a function of r, and for total volumetric flow rate Q, as:

$$V = \frac{-\Delta P/\Delta L}{2\eta} \cdot [r_w^2 - r^2], \qquad [2]$$

$$Q = \frac{\pi(-\Delta P/\Delta L)}{8\eta} \cdot r_w^4. \qquad [3]$$

In the case of a pseudoplastic fluid that follows the empirical relation $\tau = b(dV/dr)^s$, substitution of this relation into Eq. [1] followed by integration will yield

$$V = \left(\frac{-\Delta P/\Delta L}{2b}\right)^{1/s} \cdot \frac{r_w^{1/s+1} - r^{1/s+1}}{1/s+1}, \qquad [4]$$

$$Q = \frac{\pi}{1/s+3} \cdot \left(\frac{-\Delta P/\Delta L}{2b}\right)^{1/s} \cdot r_w^{1/s+3}. \qquad [5]$$

Equations [4] and [2] become identical, and Eqs. [5] and [3] become identical, as $s \rightarrow 1$ and $b \rightarrow \eta$, i.e., as the pseudoplastic fluid approaches Newtonian behavior.

The experiments described below relate to the verification of Eq. [5] by the measurement of $-\Delta P/\Delta L$ as a function of Q for three different values of r_w and for two different pseudoplastic fluids, for which the values of b and s were previously determined in the coaxial cylinder viscometer.

EXPERIMENTAL

As the polyisobutylene solutions in cyclohexane referred to in Part I show a relatively limited variation in b and s, it was decided that for the verification of Eq. [5] a more conclusive proof would be had if a pseudoplastic fluid having markedly different values of b and s from those of the polyisobutylene solutions was also tried. Consequently, two different polymer solutions were prepared: *(1)* a nominal 23 wt. % solution of LMH polyisobutylene in cyclohexane, for which b and s were found to be on the average 3.5 and 0.9, respectively; *(2)* a nominal 3 wt. % aqueous solution of ammonium alginate, for which b and s averaged 125 and 0.47, respectively. Each of these solutions was made up in a single 4-gal. batch, the solvent and polymer being paddled for at least 24 hours, until homogeneity was achieved.

The experimental arrangement for testing is illustrated schematically in Fig. 5. A Hycar-lined Moyno 3L2 pump driven by a U. S. Varidrive No. 4500 ¾ h.p. unit was used to control flow rate. This combination was chosen because the Moyno pump is slip-free in the pressure range of interest, and the flow rate is thus linear in

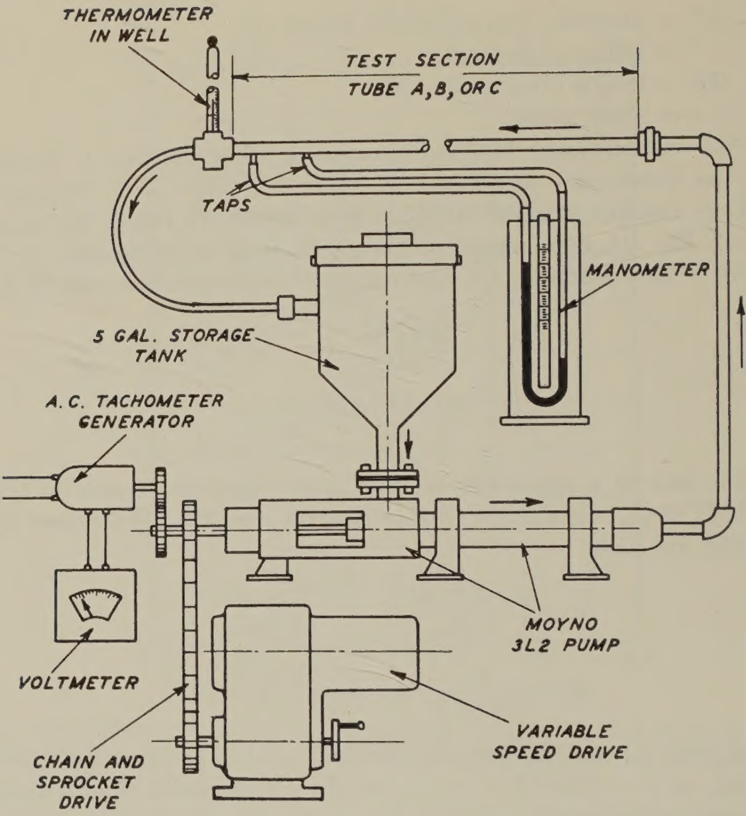

FIG. 5. Schematic diagram showing arrangement of apparatus for tube-flow experiments.

pump r.p.m. The Moyno pump is also essentially pulse-free—a necessity with respect to accurate manometer reading. The Varidrive unit was so overpowered for the average load of these experiments that once set at a given speed, the speed was unaffected by changes in pumping pressure and the like.

The test section consisted of a 6-ft. length of straight tube, through which the fluid was pumped at a preselected constant rate. Three tube diameters were used: A, 0.463 cm.; B, 0.709 cm.; C, 1.395 cm. Pressure taps were installed with a spacing convenient for reading by a mercury U-tube manometer. The first pressure tap was located at least 70 diameters downstream from the inlet end of the tube, to minimize the end effect. In every run the fluid under test in the straight pipe was allowed to fill both arms of the manometer as a supernatant fluid above the mercury, with no air space.

Prior to runs with the pseudoplastic fluids, the pump throughput was calibrated as a function of r.p.m. with a Newtonian fluid, viz., aqueous solution of glucose having a viscosity of 2.43 poises at 25°C., the temperature of calibration. The rotor speed of the pump was measured with an accuracy of $\pm\frac{1}{2}\%$ by an a.-c. tachometer generator, geared directly to the input shaft, and a suitable voltmeter. The pump was found to deliver 9.37 cm.[3] per revolution, and thus a plot of flow in cubic centimeters per second versus tachometer voltage was obtained. The Newtonian glucose solution was pumped through the system at various flow rates, with each of tubes *A*, *B*, and *C*, and the pressure drop was measured. Concordance with the Hagen-Poiseuille law (Eq. [3]) was found, and thus the pump calibration, tube measurements, and the like were verified. The temperature of the test section tube was not controlled. Instead, the runs were all made at ambient room temperature with actual temperature of the effluent from the test section noted for each run. Owing to the large volume of holdup in the storage tank, the relatively low amount of energy dissipation in the fluids, and the essentially uniform temperature of all the apparatus, the fluid, and the ambient air before a run, the maximum variation in temperature for any series of runs with a given tube diameter was ±1°C. around a mean value, which was in the vicinity of 25°C. For each run, the manometer and the thermometer were read simultaneously. Owing to the proximity of the two, it is believed that the reported temperatures correspond closely to the temperature of the fluid as it passed the manometer.

Results

The basic viscometric data, obtained with the use of the coaxial-cylinder viscometer referred to above, are presented in Fig. 6, plotted logarithmically. Figure 6 shows the shear stress-shear rate relations for the LMH polyisobutylene solution at 23.3°C. and 27.7°C., and for the am-

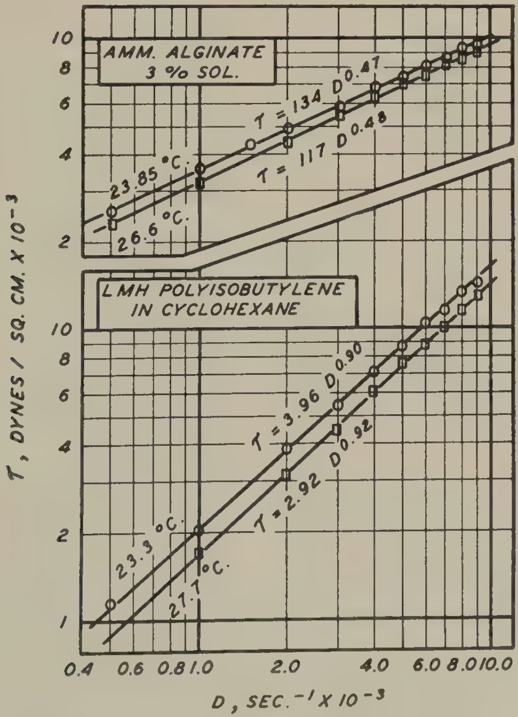

FIG. 6. Log-log plots of shear stress τ vs. shear rate D for fluids used in tube-flow runs, obtained by coaxial cylinder viscometer.

monium alginate solution at 23.85°C. and 26.6°C. The two different temperatures were selected so as to bracket closely the range of operation in the tube-flow experiments. The flow equation for each temperature level and each fluid is noted against the curve, expressed in the form $\tau = bD^s$, the constants b and s being determined as indicated above.

The results of the tube-flow experiments are summarized in Table II. The value of measured flow rate, noted as Q_m, was fixed by the pump r.p.m. The pressure gradient $\Delta P/\Delta L$ was computed from the mercury

TABLE II

Measured and Calculated Flow Rates Q_m and Q_c as Function of Pressure Gradient $\Delta P/\Delta L$

Fluid and tube	Run no.	$\Delta P/\Delta L$, dynes $\times 10^{-3}$/cm.^{2}	Temp., °C.	b	s	Q_m, cm.^{3}/sec.	Q_c, cm.^{3}/sec.
LMH polyisobutylene in cyclohexane *A* tube Radius 0.2315 cm.	1	31.8	25.5	3.37	0.910	20.2	21.0
	2	36.6	25.5	3.37	0.910	23.7	24.0
	3	39.2	26.0	3.24	0.912	25.3	26.6
	4	43.9	26.2	3.19	0.913	29.2	30.7
	5	51.2	26.3	3.17	0.913	35.4	36.7
	6	56.8	26.3	3.17	0.913	37.8	40.7
	7	60.7	27.0	3.02	0.917	47.0	45.0
LMH polyisobutylene in cyclohexane *B* tube Radius 0.355 cm.	1	16.4	23.8	3.88	0.902	52.3	54.2
	2	19.2	24.0	3.82	0.903	64.0	64.8
	3	22.7	24.5	3.65	0.906	79.6	78.8
	4	26.2	24.8	3.58	0.907	89.6	93.0
	5	12.2	24.9	3.53	0.907	40.2	41.3
	6	7.35	24.5	3.65	0.906	21.5	22.9
	7	8.16	24.5	3.65	0.906	27.5	25.0
	8	10.0	25.0	3.52	0.908	33.7	32.8
Ammonium alginate 3% aqueous sol. *B* tube Radius 0.355 cm.	1	22.6	26.0	120	0.477	41.5	44.4
	2	24.2	26.2	119	0.478	48.7	48.9
	3	25.6	26.3	119	0.478	56.2	56.2
	4	26.6	26.6	117	0.480	61.7	60.9
	5	27.9	27.0	115	0.481	69.3	69.0
	6	29.5	27.1	114	0.481	78.7	79.2
	7	16.1	26.7	117	0.480	21.3	21.3
	8	18.3	27.0	115	0.481	28.3	28.6
	9	20.5	27.0	115	0.481	34.5	36.7
Ammonium alginate 3% aqueous sol. *C* tube Radius 0.698 cm.	1	4.33	22.4	141	0.465	40.8	35.0
	2	5.01	22.4	140	0.466	51.8	49.5
	3	5.83	23.5	135	0.469	67.8	69.6
	4	6.14	23.9	134	0.470	78.0	76.7
	5	6.55	24.4	130	0.472	92.0	91.7
	6	6.75	24.8	127	0.473	100.3	100.0

manometer reading in conjunction with the spacing of the taps on the particular tube being used. In predicting the value of flow rate that should occur by Eq. [5] and indicated as Q_c in Table II, the following method was used. The value of s for a particular tube-flow run was determined by linear interpolation between the s values obtained from the viscometric runs shown in Fig. 6, based on the temperature reported for the run. In the light of the correlations found in Part I, the value of b was determined by interpolation on a plot of ln b vs. $1/T$, between the b values obtained from the viscometric runs. With b and s thus computed and r_w known, the observed pressure gradient $\Delta P/\Delta L$ was substituted into Eq. [5], which gave the value of Q_c shown in the last column of Table II.

In most of the runs summarized in Table II, Q_m is slightly lower than Q_c, but random reversals occur. The general trend of positive error in Q_c is believed to lie in one of the following causes. (*1*) The tachometer-generator geared to the Moyno pump is excited by a constant voltage a.-c. source, obtained through a Variac. Slight change in line voltage, and thus excitation of the tachometer, will give output voltage readings that are in error by a constant factor with respect to the voltage readings on which the pump calibration was made. (*2*) The shear stress in the coaxial cylinder viscometer is measured as the output of a resistance wire transducer that is excited by a d.-c. voltage source. Variation of this d.-c. voltage source from that existing at the time of calibration will cause the observed values of shear stress to be in error by

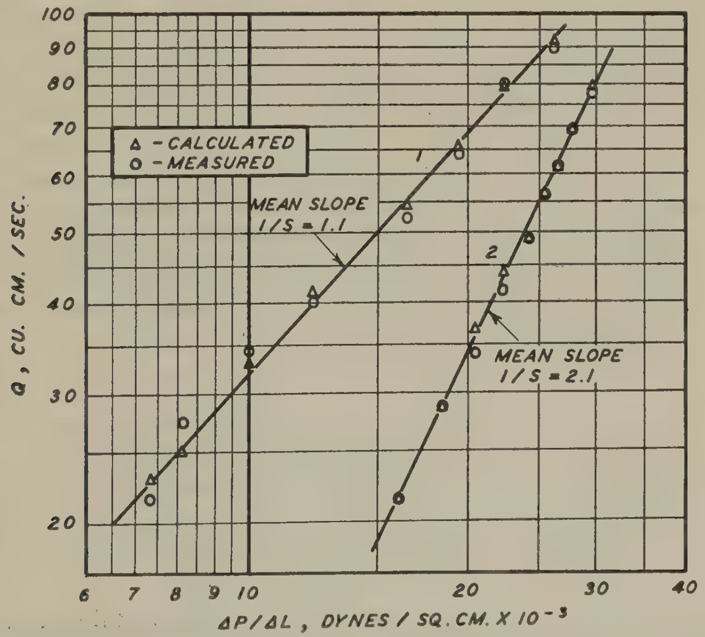

FIG. 7. Log-log plots of flow rate Q versus pressure gradient $\Delta P/\Delta L$. Curve 1: LMH polyisobutylene in cyclohexane; tube B. Curve 2: 3% aqueous ammonium alginate; tube B.

a constant factor. Although every effort was made to check these factors, both in the viscometer and in the tube-flow circuit, before the runs, it is evident that an error of one or both of these types appeared. Fortunately the value of s as determined from Fig. 6 is independent of the error in shear stress, so long as the error is constant, and constancy is likely as the viscometric determinations are made in a very short time, e.g., a few minutes. Thus it would be possible from viscometric data and one *accurate* tube-flow experiment to correct the value of b to match the values of Q_m and Q_c. By using the same percentage correction of b in other runs, all the data would be essentially concordant.

According to Eq. [5], in the isothermal laminar flow of a pseudoplastic fluid through straight tubes, the flow rate should be proportional to the pressure gradient raised to the $1/s$ power. The most nearly isothermal series of runs, viz., ammonium alginate in tube B and polyisobutylene solution in tube B, have been thus plotted logarithmically in Fig. 7. In the alginate series, the mean value of s was 0.479; hence its reciprocal was 2.09. The slope of the mean line drawn through the Q_c points is found to be about 2.1. In the polyisobutylene series the mean value of s was 0.905, of which the reciprocal was 1.105. The slope of the mean line drawn through the experimental points is 1.11.

Discussion

Oldroyd (6) and Toms (7) have suggested that immediately next to a boundary surface, fluids such as polymer solutions, which in bulk are isotropic, may become anisotropic owing to the hindrance of rotation of the polymer molecules by the wall. If this were the case, shear rate would no longer be a unique function of shear stress immediately next to the wall, and for this case Oldroyd and Toms suggest the use of an effective slip coefficient in the calculation of the flow rate-pressure gradient relation. A method of test for anisotropic wall effect is to plot curves of ϕ vs. $1/\tau_w$ for the same fluid flowing in tubes of different diameters. Herein ϕ is the apparent fluidity as calculated by the Hagen-Poiseuille relation, and τ_w is the shear stress at the wall. As ϕ is the reciprocal of viscosity η, Eq. [3] shows that:

$$\phi = \frac{8Q}{\pi r_w^4(-\Delta P/\Delta L)}, \tag{6}$$

and from Eq. [1], the shear stress at the wall will be

$$\tau_w = \frac{(-\Delta P/\Delta L)r_w}{2}. \tag{7}$$

If isothermal plots of ϕ vs. $1/\tau_w$ for the same fluid in tubes of different diameters do not lie on the same curve, then the presence of an anisotropic wall layer of fluid is indicated, the shear stress-shear rate relation of which is not the same as in the bulk of the fluid.

In the present study of the laminar flow of polyisobutylene solution and an ammonium alginate solution, each through two different tubes, plots of ϕ vs. $1/w$ were made by using both measured values of flow rate Q_m and smoothed values as obtained from Fig. 7. Although the temperatures at which the individual measurements were made differed slightly, it is found that a single curve can be drawn through the points representing polyisobutylene flow through tubes A and B, and ammonium alginate flow through tubes B and C, both for measured flow rate values (Q_c) and smoothed values. It is, therefore, concluded that for these pseudoplastic solutions, the anisotropic wall effect discussed by Oldroyd and Toms must be so small as to be undetectable within experimental error. Obviously the wall effect must depend on the molecular configuration of the polymer molecules in the particular solvent. Further research will be directed toward the study of higher molecular weight polymers and higher concentrations.

ACKNOWLEDGMENTS

The Dewey & Almy Chemical Co., Division of W. R. Grace & Co., of Cambridge, Mass., supported this research by a substantial grant under which the coaxial-cylinder viscometer was developed, and by provision of the apparatus used in the tube-flow experiments. The author is especially indebted to Mr. Dunbar L. Shanklin, Mr. Theodore C. Browne, Mr. S. R. Ballou, and Mr. A. J. Leydon of the Dewey & Almy Chemical Co. for their continual aid and cooperation. The author also wishes to acknowledge the experimental work carried out in the Chemical Engineering Department of M.I.T. by Mr. A. J. Mackenzie on the temperature effects in polyisobutylene solutions, by Mr. G. Aitken and Mr. R. J. Miller on the concentration effects in polyisobutylene solutions, and by Mr. Z. A. Dakekian and Mr. R. C. Engelken, who constructed the tube-flow apparatus and performed the studies therewith.

The considerable assistance of Prof. H. S. Mickley in reviewing the manuscript, and of Prof. H. C. Weber, Mr. Henry Chasen, and Mr. H. H. Carter, all of the Chemical Engineering Department of M.I.T. in advice on construction and instrumentation is gratefully acknowledged. Mr. Carter also prepared the drawings.

SUMMARY

It is concluded from the first part of this study that the pseudoplastic flow relation of low molecular weight polyisobutylenes in cyclohexane may be well fitted with empirical equations of the form $\tau = bD^s$, and further that b is analogous to viscosity η of a Newtonian fluid in that ln b is linear in $1/T$ and $\sqrt{C}$. These relations provide a reasonable basis for interpolation of flow properties of such fluids with respect to temperature and concentration.

In the second part of the paper, the empirical equation $\tau = bD^s$ is used to derive an equation for laminar isothermal flow in straight tubes similar to the Hagen-Poiseuille relation for Newtonian fluids. The accuracy of this equation is shown by experiments on the laminar flow in straight tubes of two pseudoplastic fluids that follow a shear stress-shear rate relation expressible as $\tau = bD^s$, one of these fluids being of the type studied in the first part of this paper.

References

1. Merrill, E. W., "A coaxial cylinder viscometer for non-Newtonian fluids," to be published in the *Journal of the Instrument Society of America*.
2. Merrill, E. W., *J. Colloid Sci.* **9,** 7 (1954).
3. Alfrey, T., "Mechanical Behavior of High Polymers," p. 33. Interscience, New York, 1948.
4. Weltmann, R., N.A.C.A. Technical Note 3397, Washington, D. C., February, 1955.
5. Grodde, K. H., *Erdöl u. Kohle* **6,** 380 (1953).
6. Oldroyd, J. G., *J. Colloid Sci.* **4,** 333 (1948).
7. Toms, B. A., *J. Colloid Sci.* **4,** 511 (1948).

JOURNAL OF COLLOID SCIENCE **11**, 15–20 (1956)

GELS OF METHYL SILICONIC ACID

I. METHOD OF FORMATION AND ENERGY OF ACTIVATION

Charles B. Hurd and Alan R. Winterberger

Butterfield Chemical Laboratory, Union College, Schenectady, New York

Received August 29, 1955

Abstract

Sodium methyl siliconate, $CH_3Si(OH)_2ONa$, forms gels, when mixed with solutions of acetic, hydrochloric, or tartaric acid. Compared to sodium silicate and acid sols, which set to form silicic acid gels over a wide range of pH, from about 0 to 11, the siliconate and acid mixtures gel only in the range of pH 10.5 to 11.2, and only in solutions of fairly high concentrations.

The energy of activation of setting of siliconate gels varies between 19,000 and 20,000 cal., compared to 24,000 cal. for alkaline gels of silicate and phosphoric acid.

Viscosity versus time curves resemble those with silicate. The electrical conductivity of the siliconate gels increases more as the gel sets than is the case with silicate gels, representing a structure of lower resistance. The siliconate condensation polymers are the type intermediate between the polysilicic acids and the polysiloxanes. The siliconate gels are softer and more cloudy than silicic acid gels.

Introduction

A new organo silicon compound, sodium methyl siliconate, $CH_3Si(OH)_2ONa$, has provided a different material from sodium silicate, for the production of gels. It is available in aqueous solution as SC-50 from the maker, the General Electric Silicone Plant, Waterford, New York (1).

In a continuation of our series of studies on silicic acid gels, we have investigated the effect of temperature and pH upon gels made from sodium methyl siliconate and acids.

Materials

The siliconate is called sodium "T" for short because of its trifunctional nature, being the monosidium salt of a tribasic acid. It can be converted to a di- or tri-sodium salt by sodium hydroxide. It is water-soluble. When dried without prolonged contact with air, it forms a product believed to be a condensation polymer, $(CH_3SiO_2Na)_n$. It differs from sodium silicate, ordinarily used for preparing silicic acid gels, in the ratio $SiO_2:Na$. In the siliconate the ratio is no higher than 1:1 for a water-soluble compound. With silicate, compounds with ratios as high as 2:1 are still water-soluble.

Further information on this new compound may be obtained, if desired, from the maker (1).

The acids used were reagent grade. Distilled water used for the solutions had been recently boiled. Solutions were standardized by regular analytical methods.

EXPERIMENTAL METHODS

Our method for preparing gels was similar to that used with solutions of sodium silicate for many years (2), namely, to mix aqueous solutions of the sodium methyl siliconate with dilute solutions of acetic acid or other acids. The acid presumably forms methyl siliconic acid, a weak acid, which then condenses, splitting out water, to form the gel.

Solutions of the sodium methyl siliconate and of the acid were placed in 100-ml. Pyrex beakers in a water thermostat, covered by watch glasses. They were mixed by pouring the siliconate solution into the acid solution, then pouring back and forth quickly. The gel mixture, in one beaker, covered by a watch glass, was kept in the thermostat until it had set, as judged by the "tilted rod" test (2, 3). We used 25 ml. of the siliconate solution and 55 ml. of the acid solution and water to give a total of 80 ml., although the 0°C. runs, using 160 ml. of mixture, were made in 250-ml. Erlenmeyer flasks with paraffined stoppers, the same technique as we have used with silicic acid gels (2).

All pH measurements of gel mixtures were made with a Beckman glass electrode pH meter. These measurements gave us some difficulty, owing to drift in the pH reading. Measurements of the electrical conductivity were made with an RC-1B conductance bridge, made by Industrial Instruments, Inc. The cell was especially constructed so that the electrodes could be withdrawn from the gel when set. Viscosity measurements were made in an ordinary Ostwald type viscometer pipette.

RESULTS

Our attempts to prepare gels by mixing solutions of the siliconate, diluted to one-third the concentration received, with acid solutions of various kinds and concentrations or with solutions of acidic salts such as ammonium chloride, failed. The results were either clear solutions, which refused to set in several weeks time, regardless of temperature, or solutions containing a white precipitate.

A potentiometric titration of this sodium methyl siliconate, 1.23 N in Na content, with 1.91 N HAc, gave a simple titration curve. The steepest part of the curve, shown in Figure 1, came at pH = 7.8. Up to 10 ml. acid, the solution was clear; it was cloudy from 10 through 13 ml. and had a precipitate above 13 ml. The mixture did not gel. This titration with the

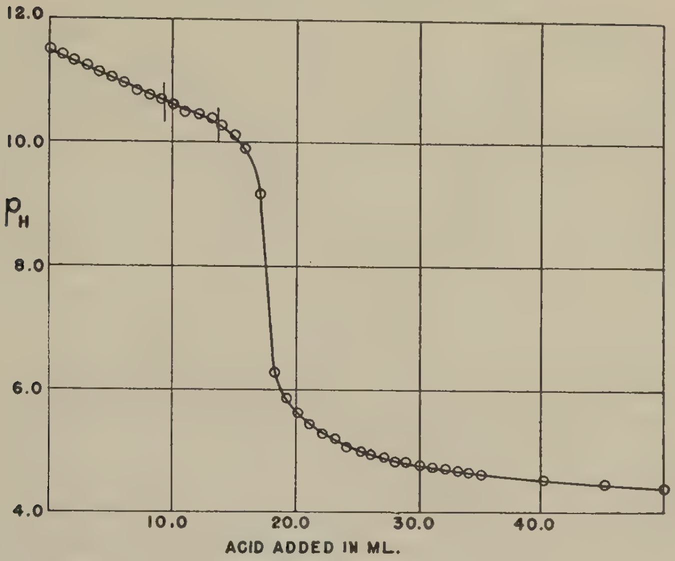

FIG. 1. Titration of 1.23 *N* Na methyl siliconate with 1.91 *N* HAc.

cloudy solution and the precipitate forming, is completely different from the situation when sodium silicate solution is used, as is the failure of the final result to set to a gel.

Although our attempts to produce gels using the sodium methyl siliconate diluted with water and mixed with acid failed, we were able to produce gels by using the siliconate in its original concentration. The NaOH equivalent of this material is 3.78 *N*. Gels were formed using acetic, hydrochloric, or tartaric acids. Four mixtures were used for each acid. Runs were made at 35°, 25°, and 0°C. The methods for making these tests have been described many times (2, 4).

Gels could be produced only in the alkaline range within pH limits of approximately 11.15 to 10.60. A decrease in pH caused by higher acid concentration resulted in more rapid setting. With a pH less than 10.50, white precipitates resulted, while for pH values above 11.20, the mixtures did not set in several weeks. In this narrow pH range, the mixture of the siliconate solution and acid solution was clear at first. It became opalescent before setting. The tilted rod test worked as it does with silicic acid gels. These siliconate gels are opalescent and somewhat more cloudy than alkaline silicic acid gels. They are softer than silicic acid gels of the same silica content.

Table I shows a set of typical results using acetic acid, 1.91 *N*, and the siliconate as received, NaOH $\Bumpeq$ = 3.78 *N*. Each mixture contained Na equivalent to 1.18 *N* NaOH and siliconate equivalent to 1.18 g. mols. $CH_3SiO_{1.5}$ per liter.

TABLE I

Time of Set of Gels of Sodium Methyl Siliconate and Acetic Acid at 25° C.

Mixture	Normality of HAc	pH	Time of set (sec.)
A	0.358	11.10	10,080
B	0.476	10.75	350
C	0.596	10.70	95
D	0.715	10.58	45

TABLE II

Energy of Activation of Setting of Gels Prepared from Sodium Methyl Siliconate and Acetic, Tartaric, or Hydrochloric Acid

Mixture	Acetic acid		Tartaric acid		Hydrochloric acid	
	Q	pH	Q	pH	Q	pH
A	23,000	11.10	20,000	11.15	—[a]	11.15
B	21,500	10.75	19,100	11.05	19,100	11.00
C	21,300	10.70	18,600	10.90	16,100	10.90
D	12,300[b]	10.58	17,200	10.70	13,800	10.75
Average	19,500		18,700		16,300	

[a] Did not set.
[b] May be in error.

Results using other temperatures for the acetic acid mixtures, as well as those containing tartaric or hydrochloric acid, were similar.

As we have done with gels from sodium silicate and various acids, we have plotted the logarithm of time of set against reciprocal absolute temperature and determined the energy of activation from the slope of these curves (2). These siliconate gels being in the basic range can best be compared with those of sodium silicate and phosphoric acid, reported by Hurd and Marotta (4), who found the energy of activation to be 24,870 cal. at pH = 10.5. Results for the siliconate gels are given in Table II.

The acid solutions were not of exactly the same normality: acetic 1.91 N, tartaric 1.89 N, and hydrochloric 1.84 N.

The D runs for acetic acid seem out of line. Lower results were found for Q for the HCl mixtures here, which is in agreement with the behavior of sodium silicate–hydrochloric acid gels (5), though it should be noted that those results were reported for acid gels. We have no data on Q for alkaline gels from sodium silicate and hydrochloric acid.

The values of Q reported here for gels from sodium methyl siliconate and acetic acid do not agree as well with those for tartaric acid as do the results reported (6) for similar acids used with silicate. Siliconate gels are much more difficult to produce.

Measurements of electrical conductance here show more change, namely, from 0.27 ohm^{-1} up to about 0.32 ohm^{-1} when just set, than was found with silicic acid gels some years ago (7, 8). As the siliconate gels stand after setting, the conductivity decreases to about 0.30.

We are not reporting the results for viscosity of the mixtures of siliconate and acid solutions, as a function of time elapsed since mixing, since the curves are like those for mixtures of solutions of sodium silicate and acid. Results for the latter have been reported. The viscosity of the mixture remains essentially that of water until just before the mixture sets, when the viscosity time curve swings up smoothly to high values and breaks off as the mixture sets.

Discussion

To interpret these data, one should first note the formula for sodium methyl siliconate, $CH_3Si(OH)_2ONa$, and its acid, methyl siliconic acid, $CH_3Si(OH)_3$. The latter is trifunctional compared to orthosilicic acid, $Si(OH)_4$, which is tetrafunctional. The 3 OH groups in methyl siliconic acid permit linear condensation and cross linkage just as orthosilicic acid does, but more difficulty should be shown by the trifunctional acid than by the tetrafunctional. Our data bear this out. We have only been able to form gels in the narrow pH range from 10.5 to 11.2 here. We were unable to form any gels in the acid range, the material always forming a white precipitate.

Compare this narrow range of pH to the case of gels of silicic acid which form from solutions with pH values of -0.5 (9) to approximately 11 (4), and one senses the difficulty of gel formation here. In addition, silicic acid gels form in quite dilute solutions.

Our curves for log time of set against reciprocal T were linear, which adds confidence in our Q values. Nonlinear curves for alkaline silicic acid gels have been reported (10) by others. Our Q values vary more here, as shown in Table II, within the permitted pH range than do corresponding values for silicic acid gels, but our difficulty with pH variation has been mentioned. Our value here of about 20,000 cal. compares roughly with about 24,000 for alkaline silicic acid gels with phosphoric acid (4). We were not able here to work out a relation between time of set and pH.

We suggest the same mechanism of setting of these siliconic acid gels as has been proposed for silicic acid gels (11, 12), namely, condensations between adjacent molecules producing long chains and eventually cross linkages to form the gel. When the ionization constant of methyl siliconic acid is available to compare with that of orthosilicic acid (13), where $K_1 = 2 \times 10^{-10}$, it will undoubtedly show that siliconic acid is weaker.

Our data on viscosity and conductivity here serve to strengthen our assumption concerning the mechanism.

If one more OH group, in the methyl siliconic acid, is replaced by a CH_3, we have dimethyl silan diol, the monomer for condensation into linear polymers known as siloxanes. Gels are not formed, since cross linkage is impossible with a difunctional monomer.

The siliconate thus supplies the missing link between dimethyl silan diol and orthosilicic acid. It forms gels as it should, being capable of cross linkage, but it forms them much less readily than tetrafunctional orthosilicic acid.

References

1. Silicones Product Data—SC-50, Sodium Methyl Siliconate, also AD 19-A. General Electric Co., Waterford, N. Y.
2. Hurd, C. B., and Miller, P. S., *J. Phys. Chem.* **36,** 2194 (1932), and other papers of the series.
3. Hurd, C. B., and Letteron, H. A., *J. Phys. Chem.* **36,** 604 (1932).
4. Hurd, C. B., and Marotta, A., *J. Am. Chem. Soc.* **62,** 2767 (1940).
5. Hurd, C. B., Frederick, K. J., and Haynes, C. R., *J. Phys. Chem.* **42,** 85 (1938).
6. Hurd, C. B., *J. Phys. Chem.* **40,** 21 (1936).
7. Mylius, F., and Groschuff, E., *Ber.* **39,** 116 (1906).
8. Hurd, C. B., and Swanker, H. J., *J. Am. Chem. Soc.* **55,** 2607 (1933).
9. Hurd, C. B., and Barclay, R. W., *J. Phys. Chem.* **44,** 847 (1940).
10. Munro, L. A., and Pearce, J. A., *J. Phys. Chem.* **44,** 1024 (1940), and other articles by Munro and associates.
11. Hurd, C. B., Raymond, C. L., and Miller, P. S., *J. Phys. Chem.* **38,** 663 (1934), and other papers in the series, particularly (4).
12. Hurd, C. B., Smith, M. D., Witzel, F., and Glamm, A. C., Jr., *J. Phys. Chem.* **57,** 678 (1953).
13. Treadwell, W. D., and Wieland, W., *Helv. Chim. Acta* **13,** 842 (1930)

JOURNAL OF COLLOID SCIENCE **11**, 21–33 (1956)

DETERMINATION OF SURFACE AREAS OF CARBON BLACKS BY SOAP ADSORPTION

Samuel H. Maron, Edward G. Bobalek and Shiu-Ming Fok

Department of Chemistry and Chemical Engineering, Case Institute of Technology, Cleveland, Ohio

Received August 15, 1955

Abstract

A method is presented for the determination of the surface area of carbon blacks by adsorption of laurate or myristate soaps from aqueous solution. It involves conductometric titration of the blacks in aqueous dispersion with the respective soaps. Comparison of results obtained by this method on eleven samples of various blacks with nitrogen adsorption data indicates that up to a nitrogen area of 50 m.^{2}/g. the two methods yield identical results if areas of 23.2 and 35.2 Å^2 are employed for the laurate and myristate molecules, respectively. However, for the finer blacks the two methods yield divergent surface areas, with those by nitrogen being the larger. These differences are ascribed to surface irregularities present in the higher area blacks, which can be expressed as a surface roughness factor, f, defined as the ratio of the area of a black as determined by nitrogen adsorption to that given by the soap titration. These roughness factors have a value of unity for the smaller area blacks, and increase for the finer blacks to values above two.

Since a nitrogen molecule is small and can be accommodated in spaces inaccessible to larger molecules, nitrogen areas appear to be too large for correlation with rubber reinforcement. On the other hand, the areas given by larger molecules, such as soap, should be much nearer to those involved in the interaction of carbon black and rubber.

Introduction

Among the various properties of carbon blacks which affect their reinforcing action in rubber, a very significant one is the surface area of the blacks (2, 4, 9). These areas can be determined by iodine adsorption (15), nitrogen adsorption (3), and electron microscopy (5). Whereas each method can yield consistent results, it is frequently difficult to reconcile the results of different methods for the same materials. This lack of agreement among the methods makes it difficult to establish the significance of the term "surface area," particularly as it applies to the problems of rubber compounding.

Furthermore, the electron microscope and nitrogen adsorption methods are rather involved, and require special apparatus. Although the iodine adsorption method is simple, serious error can result in its use owing to chemical interaction of the iodine with unsaturated substances present in the blacks.

There obviously exists a need for a simple and reliable procedure for measuring the area of carbon blacks. A review of the literature, and some unpublished results of Maron and Elder, suggested that soap titration may provide a solution to this problem. Horovitz (11) demonstrated the usefulness of this method with charcoal by using surface tension to determine the concentration of soap in presence of the adsorbent. A simple conductometric soap titration method was developed by Maron *et al.* (12) for the determination of surface area and particle size of the polymer in synthetic rubber latices. Harkins (10) mentioned that the above method can be applied successfully to carbon blacks, but he did not publish any details of technique or results. Again, Weatherburn and co-workers (14, 16) studied the adsorption of soap by carbon blacks, but they made no attempt to use the data for surface area calculations.

Preliminary studies made in this laboratory showed that the conductometric soap titration method, found practical for surface area determinations in latices, could readily be adapted to carbon blacks. Consequently, a study was undertaken (*a*) to establish the conditions required for simple and precise conductometric titration of carbon blacks with soap solutions, and (*b*) to correlate the areas obtained by soap titration with those given by low-temperature nitrogen adsorption.

Applicability of the Soap Titration Method to Carbon Black

The soap titration method for the determination of the surface area and particle size of synthetic latices has been described by Maron and co-work-

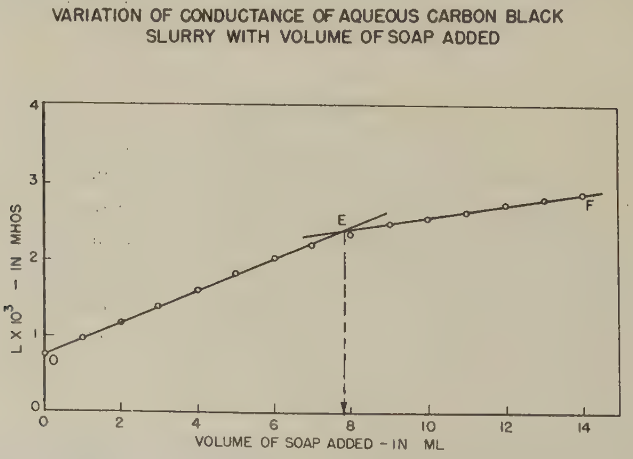

FIG. 1. Variation of conductance of aqueous carbon black slurry with volume of soap added.

ers (12). When a given weight of carbon black in aqueous dispersion is titrated with soap solution in a manner analogous to that employed for latex, and the conductances plotted against the volume of added soap solution, curves such as the one shown in Fig. 1 are obtained. These are very similar to the ones obtained with latex, and hence we shall suppose, as was done with latex, that point E corresponds to the appearance of micelles in solution, and that *at this point the carbon black is covered with only a monolayer of soap*. Evidence for the validity of these suppositions will be given below.

Maron *et al.* (12) have shown that at point E

$$C = S_a m + C_f, \tag{1}$$

where in this instance C would be the total concentration of soap in the carbon black slurry, expressed in moles per liter, S_a the number of moles of soap adsorbed per gram of black at the critical micelle concentration (cmc), m the total concentration of carbon black in the slurry in grams per liter, and C_f the concentration in moles per liter of unadsorbed soap in the solution (cmc). Further, since S_a and C_f should be constants (12), a plot of C vs. m should be linear with slope S_a and intercept C_f. Figure 2 shows a typical plot of C vs. m obtained in the present work. The linearity of the plot indicates that the anticipated consequences of the hypothesis are fulfilled.

Added confirmation of the validity of the above argument is provided by the fact that the value of S_a can be obtained also by a back titration method (12), in which soap-deficient latex is used to adsorb excess soap added to carbon black. Any amount of soap present beyond C in a sample should be adsorbed by the latex, until an end point is reached at which we have an equilibrium distribution of the soap among the carbon black sur-

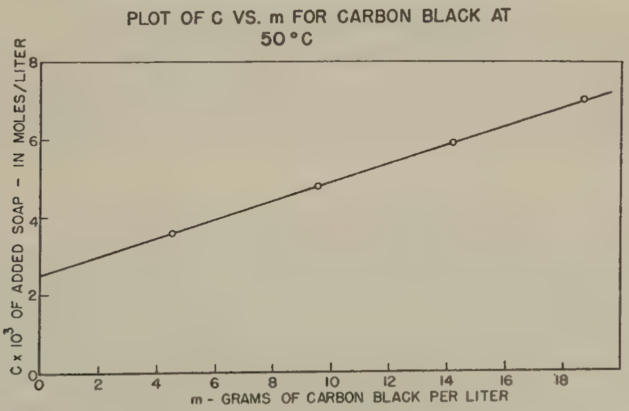

FIG. 2. Plot of C vs. m for carbon black at 50°C.

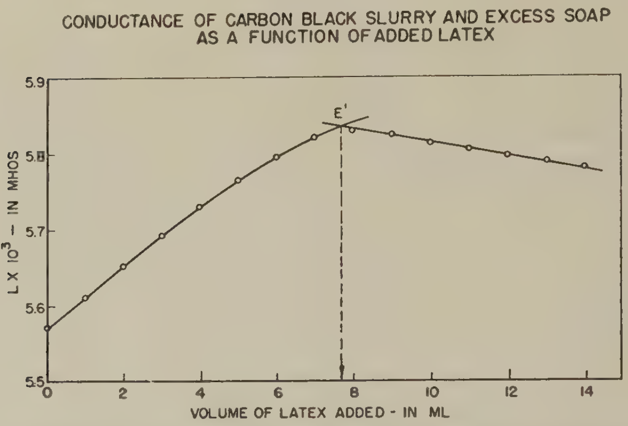

Fig. 3. Conductance of carbon black slurry and excess soap as a function of added latex.

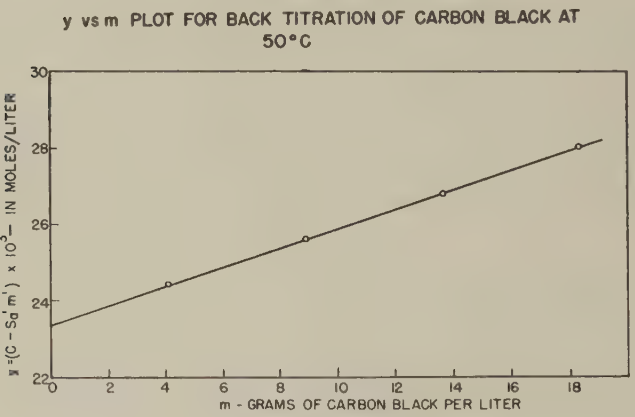

Fig. 4. Plot of y vs. m for back titration of carbon black at 50°C.

face, the rubber surface, and the soluble soap in the solution at the cmc. A typical back titration curve is shown in Fig. 3. Point E' is analogous to point E in Fig. 1, but now both the carbon black surface and the rubber surface are covered with a monolayer of soap. It can be shown that for this situation Eq. [1] becomes

$$y = C - S_a'm' = S_a m + C_f' \qquad [2]$$

where S_a' is the moles of added soap adsorbed per gram of rubber as determined by direct titration of the latex alone with soap, m' is the concentration of rubber at point E' in grams per liter, and C_f' is the cmc of the soap in the carbon black-latex slurry. Consequently, a plot of y vs. m should yield a straight line with slope also equal to S_a. Such a plot is shown in Fig. 4. A comparison of the S_a values given by the two methods will be presented later.

From S_a the average surface area per gram of carbon black, A, follows as

$$A = S_a A_s N \times 10^{-20} \qquad [3]$$

where A_s is the effective area in Å^2 occupied by a soap molecule on the black surface at the cmc, and N is Avogadro's number. The area given by Eq. [3] is in square meters per gram, m.^{2}/g., of the black.

EXPERIMENTAL PROCEDURES

1. Preparation of Standard Soap Solutions

The oleic and lauric acids used were obtained from the Amend Drug and Chemical Company, New York, New York; the myristic acid was obtained from the Eastman Kodak Company, Rochester, New York. All samples were designated as C.P. grades. Weighed amounts of these fatty acids were dissolved in equivalent quantities of carbonate-free NaOH and KOH, the solution diluted with distilled water, and then held at nearly reflux temperature for several hours until they clarified. To make sure that the soap solutions contained no free fatty acid, a determination of the latter was run by the direct conductometric titration method of Maron, Ulevitch, and Elder (13), and any acid found was neutralized by the addition of the requisite quantity of alkali.

The soap solutions thus prepared were diluted with distilled water to the desired strength, and then analyzed for soap content by conductometric titration with HCl (13). Since the soaps were to be used at 50°C., they were kept at this temperature and sampled with pipettes also calibrated at 50°C.

2. Carbon Black Samples

Eleven carbon black samples, ranging in nitrogen area from 22 to 132 m.^{2}/g., were used in this study. These, along with the nitrogen areas, were supplied us through the courtesy of the Columbian Carbon Company of New York City. They embraced Furnex, Statex 93, Statex M, Statex B, Statex K, Micronex W-6, and Standard Micronex. The only treatment given the received samples was drying for 3 hours at 90°C. in a vacuum oven.

3. Determination of C and m by Direct Soap Titration

Half- to two-gram samples of carbon black and 100 ml. of freshly boiled, distilled water were placed in the glass conductivity cell illustrated in Fig. 5. The cell was assembled, immersed in a 50°C. thermostat, and sufficiently strong stirring started to prevent settling of black. This stirring was maintained throughout an experiment. When thermal equilibrium was established, a resistance reading was taken. Soap was then added in 1- or 2-ml.

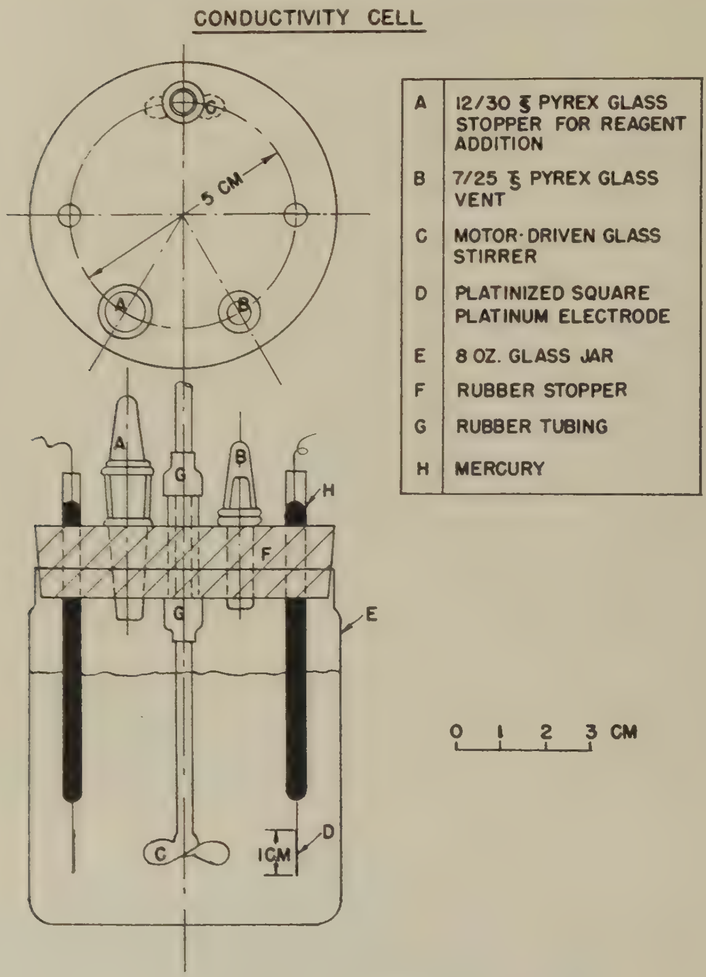
CONDUCTIVITY CELL
5 CM
A
B
C
D
E
F
G
H
1CM
A 12/30 $\mathfrak{F}$ PYREX GLASS STOPPER FOR REAGENT ADDITION
B 7/25 $\mathfrak{F}$ PYREX GLASS VENT
C MOTOR-DRIVEN GLASS STIRRER
D PLATINIZED SQUARE PLATINUM ELECTRODE
E 8 OZ. GLASS JAR
F RUBBER STOPPER
G RUBBER TUBING
H MERCURY
0 1 2 3 CM

Fig. 5. Conductivity cell.

volumes through A, and after a few minutes the resistance reading was again taken.

It was found that several minutes were sufficient to attain equilibrium after each addition, and to obtain resistance readings which did not change thereafter. This procedure of adding soap and taking resistance readings was continued until enough points were obtained to yield a plot such as shown in Fig. 1.

Resistance measurements were made with a 1000-cycle Leeds and Northrup Campbell-Shackleton bridge. Throughout the temperature used was 50.0° ± 0.1°C.

For each black sample the above procedure was repeated with several concentrations of carbon so as to yield at least three and usually four values of C and m to be plotted as in Fig. 2. The constants S_a and C_f of the straight lines obtained in every case were evaluated by least squares.

4. Determination of y and m in Back Titration with Latex

Interpretation of the back titration data requires a determination of the rubber content of the latex used and also its capacity for soap adsorption. These quantities were determined in a manner already described (12). In order to avoid the complications involved in the use of latices containing mixed soaps, a latex was selected which contained the same type of soap (sodium laurate) as was used in the direct titration of the blacks.

The latex titrations of black were conducted as follows. A weighed sample of carbon black was placed in the conductivity cell, 100 ml. of boiled, distilled water were added, and then the desired quantity of soap solution. The assembled cell was placed in the thermostat, and stirring started. Latex was now added in 1-ml. volumes, and the resistance readings taken a few minutes after each addition. The titration was continued until enough points were obtained to construct a curve such as given in Fig. 3, from which the end point E' was determined. The values of y and m were calculated from the data for the end point of the titration. This titration of excess soap was repeated for several initial concentrations of carbon black in order to get at least three values of y and m, which were plotted as in Fig. 4 to yield S_a and C_f'.

RESULTS AND DISCUSSION

Before detailed investigation of the various blacks was undertaken, it was decided to ascertain first what may be the effects on adsorption of (*a*) the pH of the blacks, (*b*) the extraction of the blacks, (*c*) pelletization of the black, and (*d*) the nature of the soap cation. To investigate the effect of pH of the blacks, the S_a and C_f values were determined by titration with potassium oleate for Statex K (pH = 9) and Micronex W-6 (pH = 5). Next to fresh samples of these carbons in aqueous dispersion was added enough KOH to raise the pH to 9.5, and the dispersions were retitrated with oleate to determine again S_a and C_f. It was thus found that wereas this adjustment of pH modified the C_f slightly, S_a remained the same as before pH adjustment.

Similar comparative experiments made with straight Philblack-0 and with toluene-extracted Philblack-0 also showed no effect on the S_a values of the black. As to the effect of pelletization of the black, pelletized and nonpelletized Spheron 9 gave again the same value of S_a in both cases. Finally, the effect of the nature of the soap cation on adsorption was studied by using potassium and sodium soaps with the same anion group. Both soaps yielded identical results for a given type of black, so that only the

TABLE I

Adsorption of Fatty Acid Soaps by Carbon Blacks at 50°C.

Carbon black sample	Laurate		Myristate		Oleate	
	No. of detns.	$S_a \times 10^4$ *(moles/gram)*	No. of detns.	$S_a \times 10^4$ *(moles/gram)*	No. of detns.	$S_a \times 10^4$ *(moles/gram)*
Furnes (a)	1	1.73	1	1.13	1	1.02
Statex 93 (a)	2	2.39 ± 0.02	2	1.54 ± 0.01	2	1.53 ± 0.03
Statex 93 (b)	2	2.30 ± 0.01	2	1.52 ± 0.01	3	1.46 ± 0.03
Statex M	2	3.08 ± 0.02	2	2.04 ± 0.01	2	1.90 ± 0.03
Statex B (a)	2	3.47 ± 0.03	—	—	2	2.17 ± 0.04
Statex B (b)	2	3.21 ± 0.07	3	2.21 ± 0.09	2	2.07 ± 0.03
Statex K (a)	1	3.84	—	—	2	3.18 ± 0.04
Statex K (b)	2	3.94 ± 0.00	2	2.57 ± 0.00	2	3.09 ± 0.02
Micronex W-6 (a)	2	4.38 ± 0.00	1	2.83	1	3.40
Micronex W-6 (b)	2	4.17 ± 0.07	2	2.67 ± 0.01	2	3.86 ± 0.05
Std. Micronex	3	4.35 ± 0.02	3	2.95 ± 0.10	2	3.87 ± 0.01
C_f *(moles/liter)*	21	0.0218 ± 0.0005	18	0.0070 ± 0.0004	21	0.0025 ± 0.0003

TABLE II

Comparison of the Back and Direct Titration Procedures

Carbon black sample	$C_f \times 10^3$ *(moles/liter)*		$S_a \times 10^4$ *(moles/gram)*	
	Direct titration	Back titration	Direct titration	Back titration
Statex B (b)	21.7	23.9	3.21	3.05
Std. Micronex	21.9	23.4	4.35	4.82

soap anion is important in adsorption. In view of this fact only potassium soaps were used in all subsequent experiments.

Table I summarizes the adsorption data obtained on the eleven samples of seven types of carbon black by titration with laurate, myristate, and oleate soaps. At the bottom of the table are listed also the average values of C_f found for the entire series of blacks with a particular soap. It may be seen that for a particular soap C_f is a constant, as it should be, if C_f represents the cmc of the soap. Further, the C_f's obtained here are in good agreement with the generally accepted values for the critical micelle concentrations of these soaps (6, 7, 8, 12).

As a check on some of the S_a values given in Table I, Table II shows a comparison of results obtained with two blacks on direct titration with soap and on back titration with latex. The good agreement obtained by the two methods is evidence for the fact that no changes occur in the surface areas of the blacks owing to different possible extents of dispersion in presence of excess soap. If variable conditions of dispersion existed, it would be unlikely that the original S_a direct titration values could be recovered so well by back titration. The concordance of results indicates that the effective surface area of the carbon black is a constant independent of the amount of soap present, and hence it must be presumed that it represents the actual surface area of the carbon black.

Another check on the consistency of the observed S_a values follows from the following considerations. If a given carbon black be titrated with several soaps, then by Eq. [3] its area should be given by

$$A = S_{a_1}A_{s_1}N \times 10^{-20} = S_{a_2}A_{s_2}N \times 10^{-20} = S_{a_3}A_{s_3}N \times 10^{-20}$$

and hence

$$\frac{S_{a_1}}{S_{a_3}} = \frac{A_{s_3}}{A_{s_1}} \text{ and } \frac{S_{a_2}}{S_{a_3}} = \frac{A_{s_3}}{A_{s_2}}.$$

Consequently, if the soap area ratios are constant, the ratios of the S_a's should also be constant and independent of the nature of the substrate. The most logical condition for the constancy of the area ratios would be the constancy of the individual soap areas, since it is not very probable that both areas would change equally so as to preserve the value of the ratio. In Table III, columns 2 and 3, are listed the slope ratios thus calculated for myristate and oleate to laurate soaps. It will be observed that in line with expectations the myristate-laurate ratio is a constant within experimental error, whereas this is not the case for the oleate-laurate ratio. These results indicate that, whereas the carbons behave nonspecifically with respect to adsorption of laurate and myristate, the adsorption of oleate is more specific and is not independent of the nature of the surface. This specificity of oleate adsorption may well be associated with the presence of unsaturation

TABLE III

Ratio of S_a Values for Adsorption of Soaps by Carbon Blacks

Carbon black sample	Slope ratios	
	$\frac{\text{Myristate}}{\text{Laurate}}$	$\frac{\text{Oleate}}{\text{Laurate}}$
Furnex (a)	0.653	0.590
Statex 93 (a)	0.644	0.640
Statex 93 (b)	0.661	0.635
Statex M	0.662	0.617
Statex B (a)	—	0.625
Statex B (b)	0.688	0.645
Statex K (a)	—	0.828
Statex K (b)	0.652	0.784
Micronex W-6 (a)	0.646	0.776
Micronex W-6 (b)	0.640	0.926
Std. Micronex	0.678	0.890

TABLE IV

Surface Areas and Roughness Factors of Carbon Blacks

Carbon black sample	A_{N_2} ($m^2/g.$)	Apparent soap areas A_s (Å²)		A_c ($m.^2/g.$)		Surface factor $f = A_{N_2}/A_c$	
		Laurate	Myristate	Laurate $A_s = 23.2$ Å²	Myristate $A_s = 35.2$ Å²	Laurate	Myristate
Furnex (a)	22.3	21.4	32.8	24.1	23.9	0.93	0.93
Statex 93 (a)	31.2	21.7	33.7	33.3	32.6	0.94	0.96
Statex 93 (b)	33.9	24.5	37.0	32.0	32.2	1.06	1.05
Statex M	42.8	23.1	34.9	43.0	43.2	1.00	0.99
Statex B (a)	48.0	23.0	—	48.4	—	0.99	—
Statex B (b)	50.0	25.9	37.6	44.9	46.8	1.11	1.07
		23.3 ± 1.2	35.2 ± 1.7				
Statex K (a)	68.4	29.6	—	53.6	—	1.27	—
Statex K (b)	94.6	39.9	61.1	55.0	54.5	1.72	1.74
Micronex W-6(a)	103.9	39.4	61.0	61.1	59.9	1.72	1.73
Micronex W-6(b)	106.2	42.3	66.1	58.2	56.5	1.83	1.88
Std. Micronex	132.0	50.4	74.3	60.6	62.4	2.18	2.12

in the soap molecule, and it may thus be of interest as a means of studying the nature of the carbon black surface. However, of the soaps tried here, only laurate and myristate appear to be suitable as adsorbates for surface area determination.

Since the B-E-T nitrogen areas A_{N_2} have been determined for all the blacks used here, they may be employed, along with observed S_a's, to find by means of Eq. [3] the effective cross-sectional areas of the laurate and myristate molecules on the various carbon black surfaces. The areas thus found are given in columns 3 and 4 of Table IV. Inspection of these two columns reveals that the values of A_s for a given soap are constant up to a nitrogen area of about 50 m.²/g. Thereafter the A_s values increase progressively with increase in the observed nitrogen areas.

This indicated increase in apparent surface area occupied by a soap molecule on the blacks of surface area above 50 m.²/g. is inconsistent with the results shown in Table III for the ratio of laurate to myristate areas. The latter data indicate quite conclusively that the areas per soap molecule are constant within experimental error. The only way to resolve this inconsistency is by supposing that the soap areas are not changed, but that on carbons of surface area greater than 50 m.²/g. the two methods, nitrogen adsorption, on the one hand, and soap adsorption, on the other, yield different results for the surface area. Since the two methods yield concordant results for carbons of area below 50 m.²/g., the molecular soap areas derived from these can be taken as the invariant molecular areas applicable also to all the other carbons above this limit. On this basis the areas occupied by molecules of laurate and myristate become, respectively, 23.2 ± 1.2 and 35.2 ± 1.7 Å^2.

These values of the areas show conclusively that at the titration end point we are dealing with monolayers of soap on the black surfaces. The cross-sectional area of a straight-chain fatty acid soap in a condensed monolayer is about 21 Å^2. If the soap were adsorbed in multilayers, the area per soap molecule would be less than 21 Å^2, whereas if it were adsorbed in expanded monolayers the molecular area would be greater than this figure. The results obtained for the soap areas indicate that the laurate exists on the carbon black surface at the cmc in a slightly expanded monolayer, and the myristate in one considerably more expanded. Incidentally, the areas found for these two soaps on polymer substrates (12) were, respectively, 41.4 and 34.1 Å^2. This difference in magnitude as well as order emphasizes the importance of the effect of nature of the substrate in the adsorption of soap at the cmc.

Using the soap areas obtained above, the surface areas of the various blacks have been calculated by means of Eq. [3], and they are given in columns 5 and 6 of Table IV. Up through Statex B these values of A_c show good concordance between themselves as well as with A_{N_2}. Past this black, however, the agreement is good only between the results for the two soap titrations.

It is our belief that the latter discrepancy arises from a combination of two factors, namely, the structure of the carbon black surface and the size of soap molecules compared to those of nitrogen. Were the surface perfectly regular, then it is to be anticipated that both soaps and nitrogen would have equal access to the entire surface, and the two methods should yield then the same results. On the other hand, were the surface of the black irregular as a result of presence of porosity or surface elevations, then it can be readily visualized that a small molecule like nitrogen could well get into spaces unavailable to larger molecules like soaps. Under such conditions we would obtain a larger surface area by nitrogen than by soap adsorption. The results in Table IV show that such is actually the case.

Without getting into a deeper discussion of the nature of the carbon black surface, it is possible to treat the above effect of surface structure in terms of a *surface roughness factor*, f. Anderson and Emmett (1) have observed that surface areas determined by the B-E-T method using nitrogen frequently were greater than the areas determined by electron microscopy. They ascribed this difference, as above, to surface structure, and defined a surface roughness factor as the ratio of the nitrogen to electron microscopically determined areas. A similar approach can be used here. We shall define as the surface factor the ratio of nitrogen to soap areas; i.e.,

$$f = A_{N_2}/A_c. \qquad [4]$$

This quantity, f, which can be determined from a combination of nitrogen and soap adsorption data, should be a measure of extent of surface irregularity of the blacks, and should be the larger the greater the extent of this irregularity.

Values of f calculated from A_{N_2} and A_c are shown in the last two columns of Table IV. It will be observed, first, that the surface factors deduced from the results of laurate and myristate titrations are in excellent agreement for all the blacks listed. Second, for the blacks of area up to 50 m.²/g., the surface factor is essentially unity, as should be the case when nitrogen and soap adsorption data yield the same surface area. Finally, above 50 m.²/g. the surface factor is greater than unity, and increases as the nitrogen surface area of the blacks becomes larger. A similar relation between roughness factors and nitrogen areas is observable in Anderson and Emmett's (1) data on comparison of nitrogen and electron microscope areas of blacks.

Conclusions

The results presented above for the determination of the surface areas of carbon blacks in the range of 20 to 130 m.²/g. indicate that the soap titration procedure given here offers a very convenient and reliable means of estimating the surface areas of such blacks. The fact that above 50 m.²/g. the soap titration method yields a lower surface area than nitrogen adsorption is an indication that correlations between reinforcing powers of blacks and nitrogen areas can not possibly be valid. The nitrogen molecule is much smaller than a rubber molecule, and hence it can occupy positions on an irregular surface which would be totally inaccessible to a bulky polymer molecule. For this reason adsorption of a soap molecule, which is closer in size and shape characteristics to a polymer molecule, should yield a much better approximation of the black surface area accessible to rubber, and hence a better correlation may be anticipated between soap areas of blacks and rubber reinforcement than between the latter and nitrogen areas.

Finally, a comparison of soap and nitrogen adsorption areas offers a means for evaluation of the extent of carbon black surface irregularity through the surface factor. It may well be that this factor as well plays a significant role in rubber reinforcement.

Acknowledgments

This work was performed as a part of a research project sponsored by the Office of Synthetic Rubber, Federal Facilities Corporation, in connection with the Government Synthetic Rubber Program.

The authors also wish to thank Dr. C. W. Sweitzer of the Columbian Carbon Company for making available to us the calibrated carbon black samples used in this study.

References

1. Anderson, R. B., and Emmett, P. H., *J. Appl. Phys.* **19**, 367 (1948).
2. Blake, J. T., *Ind. Eng. Chem.* **20**, 1084 (1928).

3. Brunauer, S., Emmett, P. H., and Teller, E., *J. Am. Chem. Soc.* **60,** 309 (1938)
4. Godfrey L. Cabot, Inc., "The Evaluation of Carbon Blacks in Natural and Synthetic Rubbers," December 14, 1948.
5. Godfrey L. Cabot, Inc., "The Particle Size and Surface Area of Several Types of Commercial Carbon Blacks," January 21, 1949.
6. Corrin, M. L., and Harkins, W. D., *J. Am. Chem. Soc.* **69,** 679 (1947).
7. Corrin, M. L., Klevens, H. B., and Harkins, W. D., *J. Chem. Phys.* **14,** 480 (1946).
8. Ekwall, V. P., and Lindblad, L. G., *Kolloid-Z.* **94,** 42 (1941).
9. Goodwin, N., and Park, C. R., *Ind. Eng. Chem.* **20,** 620, 706, 1088 (1928).
10. Harkins, W. D., *J. Am. Chem. Soc.* **69,** 1428 (1947).
11. Horovitz, K., *Phys. Rev.* **29,** 617 (1927).
12. Maron, S. H., Elder, M. E., Ulevitch, I. N., and Moore, C., *J. Colloid Sci.* **9,** 89, 104, 263, 347, 353, 382 (1954).
13. Maron, S. H., Ulevitch, I. N., and Elder, M. E., *Anal. Chem.* **21,** 691 (1949).
14. Reade, M. A., Weatherburn, A. S., and Bayley, C. H., *Can. J. Research* **27F,** 426 (1949).
15. Smith, W. R., Thornhill, F. S., and Bray, R. I., *Ind. Eng. Chem.* **33,** 1303 (1941).
16. Weatherburn, A. S., Rose, G. R. F., and Bayley, C. H., *Can. J. Research* **27F,** 179 (1949).

JOURNAL OF COLLOID SCIENCE **11**, 34–38 (1956)

A SPECTROPHOTOMETRIC METHOD FOR THE DETERMINATION OF CATIONIC DETERGENTS

A. V. Few[1] and R. H. Ottewill

Department of Colloid Science, The University, Cambridge, England

Received August 25, 1955

ABSTRACT

A method has been developed for the determination of cationic detergents in aqueous solution at concentrations of ca. 10^{-5} M. The analysis depends upon the formation of a complex between the detergent and an anionic dye, and the quantitative extraction of the complex into an organic phase in which the dye itself is insoluble. The intensity of color in the organic phase is then directly proportional to the concentration of detergent. Satisfactory analyses have been achieved using octyltrimethylammonium bromide (±5%), dodecyltrimethylammonium bromide, cetyltrimethylammonium bromide, and dodecylpyridinium bromide (±2%). The method is insensitive to wide variations in pH and salt concentration of the detergent solution.

INTRODUCTION

During the course of a recent study of the binding of dodecyltrimethylammonium bromide by bovine plasma albumin (1), it became necessary to analyze solutions of the detergent in the concentration range 10^{-4} to 10^{-5} M. Whilst the titrimetric method of Epton (2) for anionic detergents can be adapted for the determination of cationic detergents, its limitation to the range 3×10^{-3} to 8×10^{-3} M rendered it too insensitive for the present purpose. However, Karush and Sonenberg (3) have developed a colorimetric method for the estimation of long-chain alkyl sulfates at concentrations of 5×10^{-6} M. The principle of the method depends upon the formation of a stoichiometric complex between the anionic detergent and a dye of opposite polarity, and the extraction of the colored complex into an immiscible organic phase. The applicability of this method to the analysis of cationic detergents in very dilute solution seemed possible provided that certain conditions were fulfilled. These are that the dye should have only anionic groupings (e.g., $-SO_3^-$), be sufficiently soluble in the aqueous phase, and completely insoluble in the organic phase, whilst the complex (detergent + dye) should transfer quantitatively to the latter. A dye satisfying these conditions is Orange II [p-(β-naphthol-azo) benzene sulfonic acid] and this has been successfully employed for the estimation of several cationic detergents, using chloroform as the organic phase.

---

[1] Member of Scientific Staff of the Medical Research Council.

EXPERIMENTAL METHODS

Orange II

This was prepared by diazotization of sulfanilic acid followed by coupling with β-naphthol under the normal conditions. The product was purified by recrystallizing three times from aqueous ethanol and dried *in vacuo*. A stock solution was prepared by dissolving the dye in $0.1M$ sodium chloride solution, and stored in the dark. Continual shaking of an aliquot of the dye solution with chloroform failed to produce any coloration of the organic phase, as measured by a spectrophotometer. Karush and Sonenberg (3) found difficulty when using pararosaniline and rosaniline by the fact that considerable color transfer to the organic phase occurred, before the addition of anionic detergent.

Detergents

The *n*-alkyl quaternary ammonium bromides (C_8, C_{12} and C_{16}) and *n*-alkyl pyridinium bromide (C_{12}) were prepared in the laboratory by the reaction of pure samples (Eastman Kodak Co.) of the alkyl bromides with the appropriate bases. For the quaternary ammonium detergents the reaction was carried out at 18°C. for 16 hours in dry acetone solution using a slight excess (1.1 mole) of the base. The dodecyl pyridinium bromide was prepared by refluxing the reactants at 115°C. for 3 hours. The detergents were recrystallized from moist acetone, dried, and Soxhlet extracted for 8 hours with 60°–80°C. (b.p.) petroleum ether. The products were finally recrystallized twice from moist acetone and dried *in vacuo*.

Colorimetric Determination

Estimations of the color intensity of the organic phase were made using a Unicam photoelectric quartz spectrophotometer type SP 500. Cells of path length 1 cm. were employed. The dye in aqueous solution and the complex in chloroform solution both had absorption maxima at 485 mμ, hence optical density measurements were taken at this wavelength. Beer's Law was obeyed over the concentration range studied in the investigation.

Analytical Procedure

Four milliliters of detergent solution, 1 ml. of dye solution and 5 ml. of A.R. chloroform were pipetted into clean C 19 glass-stoppered test tubes. The tubes were then shaken 50 times, centrifuged for 5 min., and ca. 4 ml. of the organic phase transferred to the spectrophotometer cells. At this stage a period of 5 min. was allowed for small water droplets, occasionally formed during the transference of the liquid to the cells, to disperse before readings of optical density were taken. It was found that after ca. 15 shakes, transference of the complex to the organic phase was almost complete, and that after this continued shaking produced a constant optical density of the organic phase. An arbitrary number of 50 shakes was employed to standardize procedure.

The concentration of dye (0.4×10^{-4} *M*) was chosen so that the maximum optical density, i.e., when complete transfer of the dye had occurred, was ca. 0.7 using an optical path length of 1 cm. This ensured that the most sensitive portion of the spectrophotometer scale was used for the measurements.

RESULTS AND DISCUSSION

Figure 1 illustrates the curves of optical density vs. molar concentration obtained using the detergents octyl-, dodecyl-, and cetyl-trimethylammonium bromide (OTAB, DTAB, CTAB) and dodecylpyridinium bromide (DPyB) in 0.1 *M* NaCl. In all cases a good linear relationship was found between optical density and concentration of detergent. With the exception of OTAB, this linear relationship holds until an optical density of ca. 0.72 is reached, when transfer of the dye to the organic phase is complete and further detergent causes no increase in the optical density. It is significant that this plateau occurs at a detergent concentration of 0.4×10^{-4} *M*, the molar concentration of dye employed, indicating a 1:1 complex between the dye and detergent. This is only to be expected since

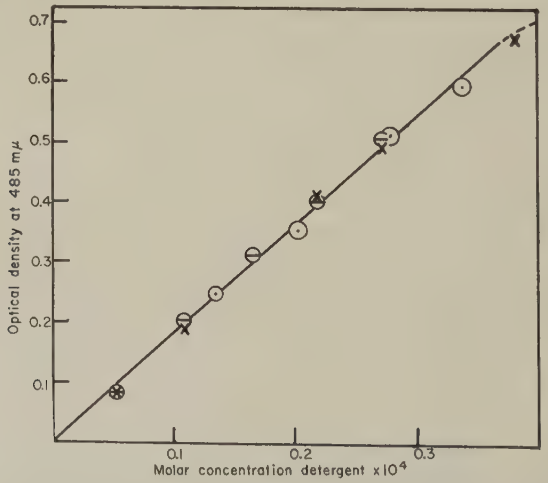

FIG. 1. Plot of optical density (485 mμ) versus the molar concentration of detergent, —⊖— *n*-octyltrimethylammonium bromide; —⊙— *n*-dodecyltrimethylammonium bromide; —⊘— *n*-cetyltrimethylammonium bromide; and —×— *n*-dodecylpyridinium bromide. Aqueous solvent: 0.1 *M* sodium chloride; organic solvent: chloroform.

the dye Orange II contains only one sulfonate group per molecule. The optical densities obtained for CTAB and DPyB, at the same molar concentrations, fall slightly below those for DTAB. It is considered that this is not due to differences in the molar absorption coefficient for the various detergent/dye complexes but to a trace of impurity $\ngtr 2\%$ present in the CTAB and DPyB. With the short-hydrocarbon chain detergent OTAB a reproducible linear relationship was also obtained, but in this case incomplete transference of the complex occurred and the slope of the curve was only ca. ¼ that found for the former detergents.

Figure 2 compares the experimental curve for the estimation of DTAB in 0.1 *M* NaCl with those obtained with DTAB in 0.01 *M* HCl (pH 2.2), in 0.1 *M* $NaHCO_3$ (pH 8.3), and in water. With these conditions reasonable agreement is obtained with the results in 0.1 *M* NaCl, indicating that the complex was stable over a wide range of pH and salt concentration.

Although the formation of the detergent/dye complex is unaffected by the above changes in the composition of the aqueous phase, the transference of the complex is critically dependent upon the nature of the organic phase. A variety of organic solvents were investigated as possible alternatives to chloroform, using DTAB as test detergent. Of these, only the partially chlorinated hydrocarbons, e.g., tetrachloroethane and trimethylene chlo-

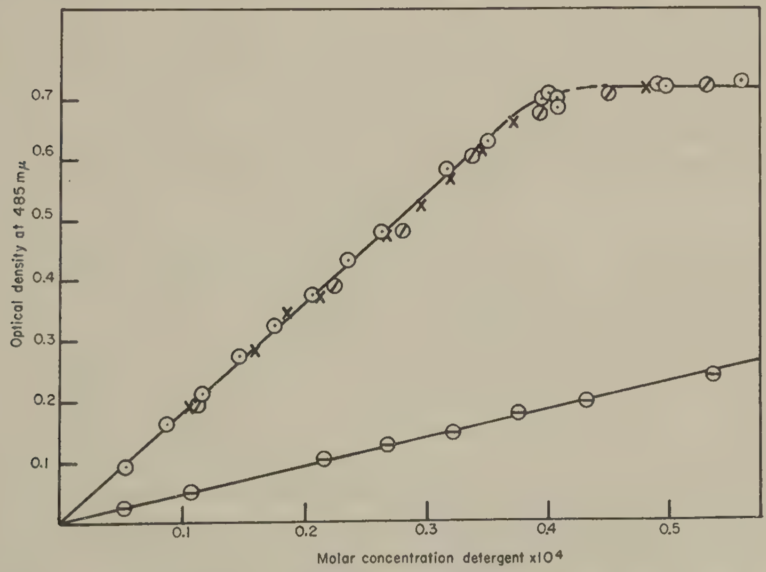

FIG. 2. Plot of optical density (485 mμ) versus molar concentration of *n*-dodecyltrimethylammonium bromide. Detergent in water —⊙—, in 0.01 *M* hydrochloric acid (pH 2.2) —×—, and in 0.1 *M* sodium bicarbonate (pH 8.3) —⊖—. Full drawn curve represents data for the detergent in 0.1 *M* sodium chloride. Organic solvent: chloroform.

ride, allowed complete transference of the complex. With chlorobenzene, ethylene dibromide, and ethyl acetate only a partial transference occurred; with carbon tetrachloride, hexane, and benzene no transference occurred; whilst the free dye was soluble in *iso*-amyl alcohol and cyclohexanone.

It was observed that in all cases where the complex was not transferred to the organic solvent, an intense band of color developed in the aqueous phase adjacent to the liquid/liquid interface. This indicates that with these organic solvents the complex is able to adsorb only on the unstable emulsion interface formed by shaking, and on subsequent breakdown and separation into two phases the complex desorbs into the aqueous phase. The solubility of the complex in partially chlorinated hydrocarbons is clearly connected with their capacity for dissolving the long-chain cationic detergents. Qualitative solubility tests of DTAB in the various solvents mentioned above (with the exception of *iso*-amyl alcohol and cyclohexanone, which were rejected by virtue of the solubility of the free dye itself) showed a similar behavior to that of the detergent/dye complex. Thus a good solvent for the detergent also favored transfer of the complex.

The spectrophotometric method described here has been found satisfactory for the estimation of cationic detergents in dilute solution: at concentrations of 10^{-5} M the reproducibility for C_{12} and C_8 n-alkyl detergents is ±2% and ±5%, respectively. Analysis of detergent solutions at concentrations below 10^{-5} M, without loss in sensitivity, is clearly possible by the use of spectrophotometer cells of longer path length.

ACKNOWLEDGMENTS

We wish to thank Dr. J. H. Schulman, O.B.E., and Dr. P. Johnson for helpful discussions, and the Nuffield Foundation for financial assistance (R.H.O.).

REFERENCES

1. FEW, A. V., OTTEWILL, R. H., AND PARREIRA, H. C., *Biochim. et Biophys. Acta* **18,** 136 (1955).
2. EPTON, S. R., *Trans. Faraday Soc.* **44,** 226 (1948).
3. KARUSH, F., AND SONENBERG, M., *Anal. Chem.* **22,** 175 (1950).

JOURNAL OF COLLOID SCIENCE **11**, 39–47 (1956)

CHEMICAL RELAXATION OF STRESS IN POLYURETHANE ELASTOMERS

J. A. Offenbach* and A. V. Tobolsky

The Frick Chemical Laboratory, Princeton University, Princeton, New Jersey

Received November 17, 1955

ABSTRACT

Chemical stress relaxation behavior of polyester urethane elastomers and a polyether elastomer have been determined over a temperature range of 90° to 130° C. Since both polyether and polyester samples have approximately the same rate of stress decay, it has been necessary to exclude ester-ester interchange as a reaction mechanism, and regard the known thermal lability of the urea and urethane groups as indicative of possible sites of network scission. A likely possibility for the weak link is the tri-substituted urea (biuret) cross-linkage.

INTRODUCTION

In a recent series of communications from the Bayer Laboratories (1–8), the preparation and properties of a new series of polyurethane elastomers obtained from polyesters and diisocyanates have been described. These elastomers, under the generic term of Vulcollan, are analogous with the product known as Adiprene B, which has very recently been announced by the Du Pont Laboratories (9). This latter material differs chemically from the Vulcollan in that the main network chain is composed of polyether segments rather than polyester segments. All of these synthetic elastomers have been found to display excellent properties with respect to tear strength, tensile strength, abrasion resistance, rebound resilience, resistance to swelling in common organic solvents, and resistance to aging, deterioration from exposure to air or ozone. However, noticeable deleterious effects of temperature on elastic modulus and tensile strength were noted (3), indicating that chemical changes were occurring.

The applicability of measurement of relaxation of stress at constant strain has been found useful in following chemical network degradation for many polymeric substances, examples being natural rubber, in which oxidative scission of chains was the prime factor (10), and disulfide rubbers (11, 12), and silicone elastomers (13, 14), in which mutual exchange of network bonds was thought to be responsible for decay of stress.

---

* This article is based upon a dissertation snbmitted by Jack A. Offenbach in partial fulfillment of the requirements for the degree of Doctor of Philosophy at Princeton University.

The basic link between the mechanical behavior of a crosslinked polymer and its chemical constitution is given by the fundamental equation of rubber elasticity (5):

$$f = NkT\left(\alpha - \frac{1}{\alpha^2}\right), \qquad [1]$$

where f is the stress based on original cross section, N is the number of network chains per unit volume of rubber, and α is the strain, or relative elongation. At constant strain and temperature, the stress at any time should be proportional to the number of network chains maintaining stress per unit volume. Even if there were departure from this theory, it would be expected that a decay of stress would still be related to a decrease in the number of network chains maintaining stress. Since a dynamic equilibrium between breaking of bonds and reformation of new bonds is possible, "intermittent" measurements are made in which the sample is stretched only for a period of time necessary to determine the stress, and then released to its initial position. The latter measurement is believed to represent the difference between the rate of scission of bonds and the rate of formation of new bonds, whereas a continuous measurement of decay of stress is thought to measure only the decay of bonds, since any new bonds formed would be in equilibrium with the strained condition and not contribute to the stress.

Experimental

Materials

Samples of Vulcollans, prepared essentially as in patents and publications of the Bayer Company, were obtained from the U. S. Rubber Company, and used without any further treatment. Three basic types of compounds were investigated. Common to all three was the starting material, a polyester of molecular weight approximately 2000, prepared from adipic acid and a mixture of ethylene and propylene glycols. The constituents of the three samples were as follows:

A. Polyester, diphenylmethane diisocyanate, and water as "crosslinking agent."

B. Polyester, naphthalene 1,5-diisocyanate, and butanediol 1,4 as "crosslinking agent."

C. Polyester, toluene 2,4-diisocyanate, and an aromatic diamine as "crosslinking agent."

A sample of Adiprene B was kindly furnished us by the DuPont Laboratories.

Equipment and Procedure

All measurements were made on an instrument previously described (10), except that the relaxometer was modified for use of strip samples. This proved very advantageous and convenient for these studies. A full description of this modification is given elsewhere (16).

RESULTS AND DISCUSSION

Stress relaxation behavior of the three Vulcollans and DuPont Adiprene B have been studied over a temperature range of 90° to 130°C. and an extension of 20%. Extension was not included as a variable, since it was shown to have little or no effect in other polymeric systems exhibiting stress decay due to cleavage of chemical bonds.

Our data have been presented in terms of percentage of residual stress, $100f/f_0$, as a function of logarithmic time. The original stress present in the

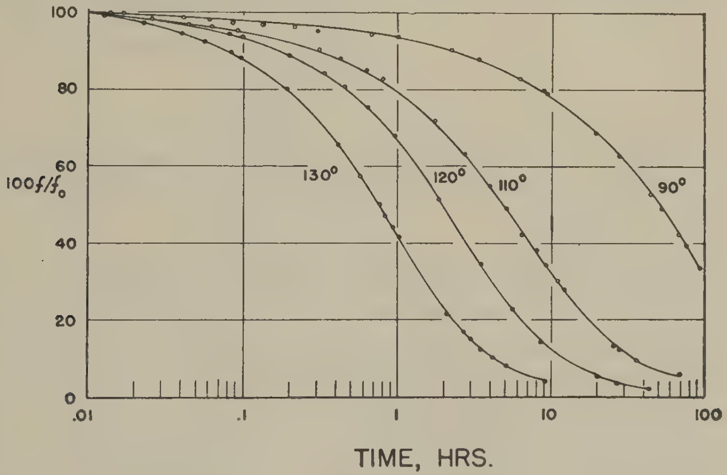

FIG. 1. Continuous stress relaxation of Vulcollan A.

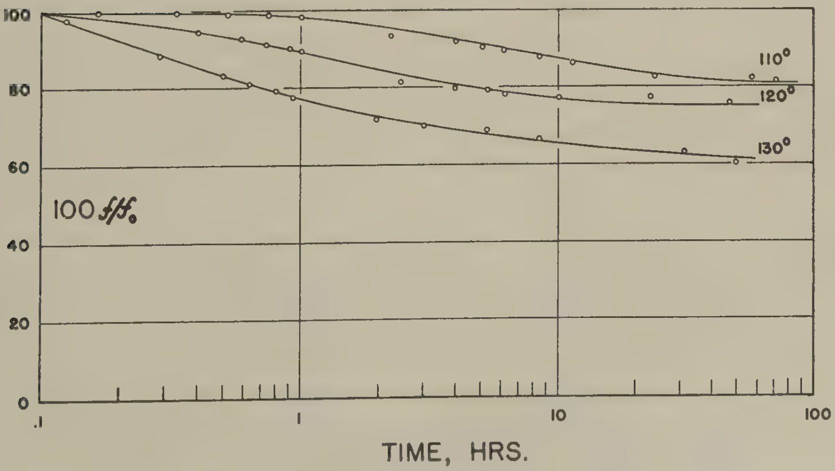

FIG. 2. Continuous stress relaxation of polyurethanes at 120°C.

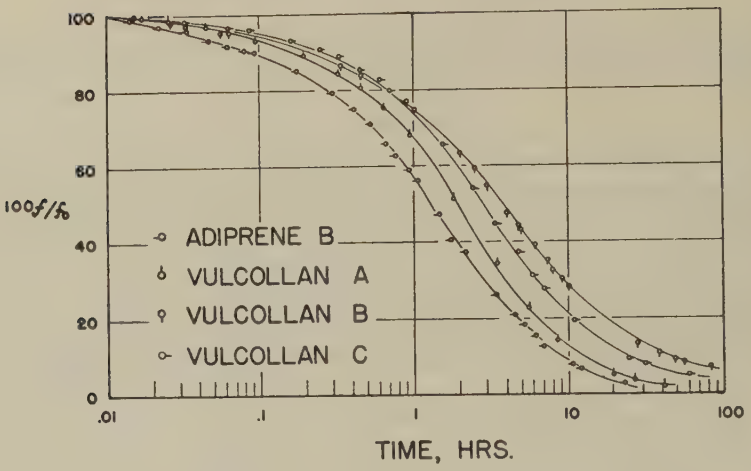

Fig. 3. Temperature dependence of relaxation times.

sample was determined by graphical extrapolation to an arbitrary time, 0.01 hour in the case of continuous measurement, and 0.1 hour for intermittent measurements.

Absolute magnitudes of the initial modulus were reproducible within 5% or better and duplicate determinations plotted on a relative basis were completely superposable. The data for the continuous runs for Vulcollan A are presented in Fig. 1, and the intermittent data for Adiprene B in Fig. 2. Comparison of stress decay curves for all samples at 120°C. is made in Fig. 3. Common to all four samples is the fact that all appear to approach zero stress asymptotically and that the greater portion of the decay takes place within two cycles of logarithmic time. Such behavior is similar to that shown by polysulfide rubber (11, 12), natural rubber (10), and silicone rubber (13). In these materials chemical scission of bonds was deduced to be the underlying factor. None of the linear polymers which stress relax owing to internal flow processes have ever shown a two-cycle decay, but extend over many cycles of logarithmic time. Of course, predominantly chemical relaxation effects would be expected in an extended three-dimensional structure such as polyurethane rubber, in which flow would be ruled out as a rate-controlling step.

For natural rubber and polysulfides at high temperatures, a good fit was found to the equation $f/f_0 = e^{-t/\tau}$, in which τ is a characteristic relaxation time, and this also approximately fits the chemical stress decay of polyurethane rubbers. The magnitude of τ may be calculated as the reciprocal of the time required for the force to reach $1/e$ of its initial value. By identification of $1/\tau$ with a chemical rate constant k, it is then possible to determine an activation energy for the process. A composite plot of $-\log \tau$ or $\log k$ vs. $1/T$ is given in Fig. 4. Activation energies were computed from the

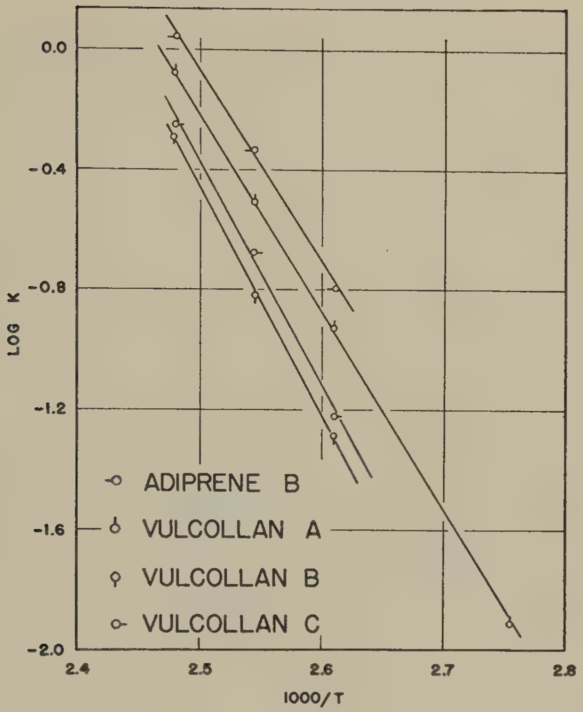

FIG. 4. Intermittent relaxation of Adiprene B.

TABLE I

Sample	Activation energy
Vulcollan A	29.9 ± 2
Vulcollan B	35 ± 1
Vulcollan C	34 ± 3
Adiprene B	30.5 ± 0.5

slopes in the usual way and are summarized in Table I. It is seen that all have the same order of magnitude, and the sample which shows the most rapid stress decay (Adiprene B) relaxes only about 2.5 times as fast as the Vulcollan B, which is the slowest.

Referring to Fig. 2, the results of the intermittent runs are in marked contrast to the continuous stress relaxation. The intermittent curves for Vulcollan C are similar to this. Since the decay of stress here is due to the difference between the rate of bond formation and the rate of bond cleavage, it is apparent that considerable reformation of bonds is taking place.

Effects of Added Substances

Preliminary experiments were begun to determine the effects of extraneous chemical substances introduced into the rubber. Vulcollan A was immersed in water at 90°C. for 1 hour, with weight increase of 2%, and then its stress decay characteristics determined at 90°C. in an atmosphere containing water vapor. No difference between treated and untreated polymer was discernible in either the continuous or intermittent relaxation curves. To determine the effect of incorporated hydroxyl groups, a compound was sought in which a high degree of weight retention was available at elevated temperatures. A specimen of Vulcollan B was immersed in polyethylene glycol "300" at 80°C. for 1 hour. There resulted an initial weight increase of 16%, and at the end of 40 hours in a circulating oven at 110°C., about half of this quantity was still present in the rubber. A marked physical change had also appeared, in that the rubber became very soft and possessed very low tear strength. More quantitative information is provided by the comparison of the continuous stress relaxation curves for both the untreated sample and the one in which polyethylene glycol was present. For the untreated sample at 110°C., the time to attain $1/e$ of the initial retractive force is 19 hours, contrasted with 6.8 hours for the treated sample. The mechanism for this reaction is not yet known; the glycol groups could presumably exchange with the main-chain polyester linkages or possibly with the urethane linkages.

Structure of Polymers

A brief review of the general methods of preparation of these polymers will reveal the labile points at which network scission might be expected. The basic process may be divided into chain formation, chain lengthening, and network formation. Common to all three Vulcollans was the starting material of polyester of molecular weight 2000, prepared from adipic acid and a mixture of ethylene and propylene glycols. By addition of a 30% excess of a diisocyanate, generally aromatic, it was possible to link two or three of these chains together by formation of urethane bonds. Further lengthening of the chains is possible through the following processes, outlined by the Bayer papers:

A). Addition of water will cause the elimination of carbon dioxide between two isocyanate groups through formation of a substituted urea bridge, viz.,

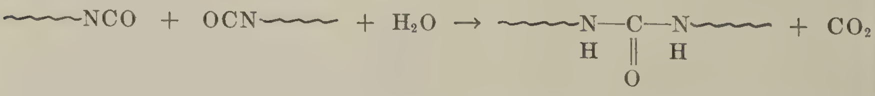

$$\sim\sim NCO + OCN\sim\sim + H_2O \rightarrow \sim\sim\underset{H}{N}-\underset{\underset{O}{\|}}{C}-\underset{H}{N}\sim\sim + CO_2$$

B). Addition of a glycol proceeds by linking two polyester chains through formation of adjacent urethane groups, viz.,

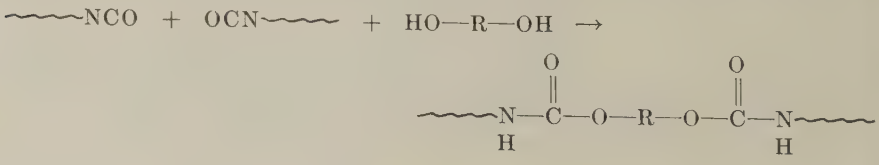

$$\sim\sim NCO + OCN\sim\sim + HO-R-OH \rightarrow \sim\sim\underset{H}{N}-\overset{\overset{O}{\|}}{C}-O-R-O-\overset{\overset{O}{\|}}{C}-\underset{H}{N}\sim\sim$$

C). Addition of a diamine leads again to the coupling of two polyester chains through adjacent urea groups, viz.,

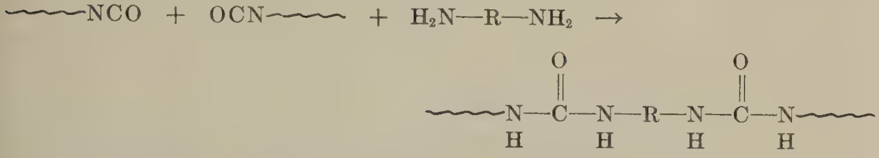

$$\sim\sim\sim NCO + OCN\sim\sim\sim + H_2N{-}R{-}NH_2 \rightarrow \sim\sim\sim\underset{H}{N}{-}\overset{O}{\overset{\|}{C}}{-}\underset{H}{N}{-}R{-}\underset{H}{N}{-}\overset{O}{\overset{\|}{C}}{-}\underset{H}{N}\sim\sim\sim$$

Cross-linking in the case of (*A*) and (*C*) is thought to proceed via reaction of the hydrogen atoms in the newly formed urea groups with isocyanate polyester chains still present. Analogous reactions of low molecular weight disubstituted ureas have been found to proceed in this manner, through formation of new urea linkages, giving a substituted biuret structure. In like manner it is reasonable to assume that the hydrogen atoms in the newly formed urethane groups of (*B*) furnish the sites for cross-linking. Lower molecular weight analogues of this reaction are likewise known. In the elastomer formation, however, it is at present not known whether one or both of the urethane hydrogens are capable of further reaction.

Complete information regarding the formation and structure of Adiprene B is not at present available, although it is known that the main network chains are formed from polyethers, rather than polyesters, and the chain lengthening process also proceeds via formation of urethane bonds.

Possibilities for Bond Scission

1. Ester cleavage. Referring again to the experimental stress relaxation data, it seems reasonable to rule out the possibility of stress decay by virtue of ester-ester interchange, since parallel behavior is shown by the polyether urethane as well. In addition, previous experiments in this laboratory (17) show that a much slower chemical decay of stress is present in elastomeric polyester vulcanizates of both the Paraplex type and the similar polyester rubbers of the succinic acid-propylene glycol type (vulcanized by benzoyl peroxide) which were originated in the Bell Telephone Laboratories. For example, in a continuous stress relaxation experiment at 130°C., the time required to reach $1/e$ of the initial value of the modulus was 75 hours for the Bell Telephone rubber. These times varied from 34 hours to 240 hours for the Paraplex series. On the other hand, for the Vulcollan type rubbers the relaxation times were approximately 1 hour at 130°C.

2. Urethane cleavage. Simple low molecular weight urethanes are known to be thermally unstable. The presence of the corresponding isocyanates has been noted by Hofmann (18) upon distillation of phenyl, tolyl, and naphthyl urethanes. An extensive investigation has been made by Petersen and others (4) on decomposition products of urethanes formed from low molecular weight diisocyanates. By use of their "Cellit" (acetylcellulose) test, it was possible to define a characteristic decomposition temperature for each urethane. For many of these compounds characteristic temperatures of 180°C. were found, although a few extended as low as 120°–130°C. It is therefore not impossible that urethane cleavages in the elastomer are responsible for the observed stress decay.

3. Disubstituted ureas. Simple low molecular weight disubstituted ureas are also known to be thermally unstable. Utilization of the thermal decomposition of substituted ureas has led to the synthesis of isocyanates by vaporization of ureas in the presence of hydrogen chloride (19), although a temperature of 370°C. was required for 99% dissociation. Qualitatively the presence of isocyanates has been observed in liquid phase decomposition of ureas (20), in solution (21), and by distillation of molten disubstituted ureas (22), and treatment of molten ureas with phosphoric anhydride (18) or dry hydrogen chloride (23). The difficulty of applying this decomposition as a synthetic method lies in the recombination of products. This recombination appears relevant to the interpretation of our intermittent stress curves, which measure the net change between bonds cleaved and bonds reformed.

In many cases the cross links are very probably trisubstituted urea linkages. These would also be a possible site for bond scission, and we feel instinctively that this is a very likely possibility.

4. Urethane vs. substituted urea linkages as the labile sites. It has not been possible, with the data at hand, to ascertain more definitely the actual site of network scission.

If scission were to occur at cross links only, the relaxation time at a given temperature would be independent of the modulus of the specimen, i.e., independent of the concentration of cross linkages. If the scission occurs at urethane linkages between cross links, then the relaxation time would be inversely proportional to the number of urethane linkages between cross links, i.e., it would be shorter for specimens of low modulus. For certain rubbers the substituted urea linkages might occur only at the cross links.

A possible clue as to which bonds are being attacked might be obtained by studying rubbers prepared from polyesters of different degrees of polymerization.

REFERENCES

1. MÜLLER, E., *et al.*, *Angew. Chem.* **64**, 523 (1952). Translated in *Rubber Chem. and Technol.* **26**, 493 (1953).
2. HÖCHTLEN, A., *Kunststoffe* **40**, 221 (1950).
3. BAYER, O., *et al.*, *Angew. Chem.* **62**, 57 (1950). Translated in *Rubber Chem. and Technol.* **23**, 812 (1950).
4. PETERSEN, S., *Ann.* **562**, 205 (1949).
5. SIEFKEN, W., *Ann.* **562**, 75 (1949).
6. HEBERMEHL, R., *Farben, Lacke, Anstrichstoffe* **8**, 123 (1948).
7. BAYER, O., *Angew. Chem.* **59**, 257 (1947).

8. Bayer, O., *Ann.* **549,** 286 (1941).
9. Hill, F. B., Young, C. A., Nelson, J. A., and Arnold, R. G., presented at the Detroit meeting of the Division of Rubber Chemistry, May 4–6, 1955. Reported in *Chem. Eng. News* **33,** 2079 (1955).
10. Tobolsky, A. V., Prettyman, I. B., and Dillon, J. H., *J. Appl. Phys.* **15,** 380 (1944).
11. Stern, M. D., and Tobolsky, A. V., *J. Chem. Phys.* **14,** 93 (1946).
12. Mochulsky, M., and Tobolsky, A. V., *Ind. Eng. Chem.* **40,** 2155 (1948).
13. Johnson, D. H., McLoughlin, J. R., and Tobolsky, A. V., *J. Phys. Chem.* **58,** 1073 (1954).
14. Osthoff, R. C., Bueche, A. M., and Grubb, W. T., *J. Am. Chem. Soc.* **76,** 4659 (1954).
15. Mark, H., and Tobolsky, A. V., "Physical Chemistry of High Polymeric Systems," p. 330. Interscience, New York, 1950.
16. Offenbach, J. A., Ph.D. Thesis, Princeton University, 1955.
17. Andrews, R. D., Ph. D. Thesis, Princeton University, 1948.
18. Hofmann, A. W., *Ber.* **3,** 653 (1870).
19. Bennett, W. B., Saunders, J. H., and Hardy, E. E., *J. Am. Chem. Soc.* **75,** 2101 (1953).
20. Eckenroth, H., and Wolf, M., *Ber.* **26,** 1463 (1893).
21. Iwakura, Y., and Nakakubo, K., *Bull. Tokyo Inst. Technol.* **13,** 25 (1948).
22. Hofmann, A. W., *Ber.* **14,** 2725 (1881).
23. Habich, A., and Limpricht, H., *Ann.* **109,** 101 (1859).

JOURNAL OF COLLOID SCIENCE **11**, 48–50 (1956)

VISCOELASTIC PROPERTIES OF CRYSTALLINE POLYMERS: POLYETHYLENE

E. Catsiff, J. Offenbach, and A. V. Tobolsky

The Frick Chemical Laboratory, Princeton University, Princeton, New Jersey

Received November 17, 1955

The viscoelastic behavior with respect to time and temperature of linear polymers in which crystalline regions are present are in marked contrast to that shown by a typical linear amorphous polymer such as polyisobutylene. Recently published data obtained in this laboratory for the stress relaxation of polytrifluorochloroethylene are illustrative of the differences which may be expected (1). In addition to a much slower decay of stress throughout the transition region of polytrifluorochloroethylene, an extension of the transition region through a wider temperature range is also manifested. The presence of specific structural features such as the amount of crystallinity and orientation of crystallites vitiates the general equivalence of time and temperature through a horizontal translation in logarithmic time (2), and also introduces a vertical translation along the log modulus axis. It was of interest to characterize the viscoelastic properties of another crystalline polymer, polyethylene, and to correlate it with measurements of crystallinity and birefringence.

The accompanying diagram illustrates the variation of the logarithm of the relaxation modulus as a function of log time for varying temperatures between −65°C. and 105°C., a few degrees below its melting temperature. Measurements were made on samples of polyethylene, Monsanto E-73, up to 80°C. on the glassy state relaxometer described in a recent article (3) and continued beyond that temperature by means of the Firestone Relaxometer (4), especially adapted for strip samples (5). Agreement between the two methods is shown by the coincidence of data obtained at 80°C. Extensions corresponding to the curves at 90°C. and 105°C. were 10%; those at other temperatures were 5% or less. An extension of 10% at 80°C. resulted in a modulus which was 20% lower than at 5% extension.

A notable similarity exists between polyethylene and polytrifluorochloroethylene. For both polymers, the transition region between rubbery and glassy modulus is spread over a wider temperature range than for an amorphous polymer and in this region relaxation is not rapid. The rela-

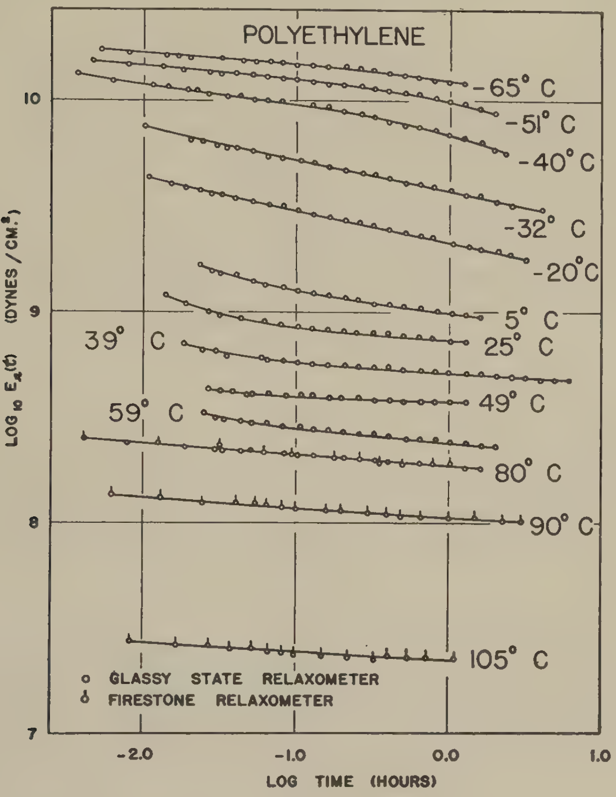

Fig. 1

tively larger decrease of 0.01 hour modulus values with increasing temperature especially near the melting point has its origin in the relatively large decrease of crystallinity as the melting temperature is approached. Determinations of percentage of crystallinity and shear modulus as a function of temperature bear out this correlation (6).

Little or no relaxation of the birefringence between 40°C. and 100°C. has been previously noted, although its initial value progressively decreases with increasing temperature (7). The stress relaxation curves obtained by these workers (7) between 40°C. and 100°C. are also in general agreement with those of this writing. X-ray determinations of scattering intensity of a stretched sample of polyethylene are also indicative of the approximate constancy with time of the percentage of crystallinity and orientation at a particular temperature (8). Both birefringence and X-ray results indicate a marked decrease in per cent crystallinity and in orientation of the stretched samples as the temperature is raised, particularly near the melting point, but time effects seem to be small. This agrees with the stress relaxation data.

References

1. Tobolsky, A. V., and Andrews, R. D., *J. Phys. Chem.* **59**, 989 (1955).
2. Tobolsky, A. V., and Andrews, R. D., *J. Chem. Phys.* **13**, 3 (1945).
3. Catsiff, E., and Tobolsky, A. V., *J. Colloid Sci.* **10**, 375 (1955).
4. Tobolsky, A. V., Prettyman, I. B., and Dillon, J. H., *J. Appl. Phys.* **15**, 380 (1944).
5. Offenbach, J. A., Ph.D. thesis, Princeton University, 1955.
6. Nielsen, L. E., *J. Appl. Phys.* **25**, 1209 (1955).
7. Stein, R. S., Krimm, S., and Tobolsky, A. V., *Textile Research J.* **19**, 8 (1949).
8. Krimm, S., and Tobolsky, A. V., *J. Polymer Sci.* **7**, 57 (1951).

JOURNAL OF COLLOID SCIENCE **11**, 51–59 (1956)

THE SIZES OF MOLECULES ADSORBED AT THE BENZENE-WATER INTERFACE

N. Pilpel

Research Organisation B. I. Callender's Cables Ltd.,
38 Wood Lane, London W. 12, England

Received September 22, 1955

Abstract

The force area characteristics of adsorbed films of some ketones and alcohols at the benzene-water interface have been investigated. It has been found possible to relate the film characteristics to the sizes of the molecules concerned. The technique may thus be of assistance in identifying other surface-active compounds.

Introduction

The structures of surface-active compounds can often be determined by studying the characteristics of their monolayer. The structures of acids, esters, sterols, hormones, and other complex organic molecules have all been investigated by this technique. In the past, most of the work has been carried out on monolayers at the air-water interface. Relatively little has been done at the oil-water interface.

The reason for this is the experimental difficulty involved. There are few compounds which are insoluble in both oil and water and whose monolayers at this interface can therefore be studied directly with a Langmuir Trough. Again, the operation of this instrument at the oil-water interface is a matter of considerable difficulty (1). In the case of surface-active compounds which are soluble in one or other of the two phases it is necessary to calculate force-area characteristics of the adsorbed film. This involves employment of the Gibbs' adsorption equation and may, in certain cases, result in considerable errors.

The oil-water interface, however, is of considerable interest in both biological and nonbiological systems. It frequently happens that it is the more convenient one to use. Thus in trying to categorize the hydrophilic compounds which occur in mineral oils, it is convenient to float the oil on water and study the film which is adsorbed at the interface between the two liquids. Very little work of this nature has so far been published. The aim of the present work has been to extend the experimental data, and to see whether a convenient relationship between monolayer characteristics and molecular structure can be discovered. Such a relationship at the oil-water interface might assist considerably in identifying the hydrophilic compounds which develop in mineral oils.

EXPERIMENTAL

The experiments now reported were carried out at the benzene-water interface. Ketones and alcohols were used to produce the adsorbed films, and the characteristics of these determined by application of the Gibbs' equations.

Preparation of Materials. High-grade commerical materials were purified by standard methods. B.D.H. "molecular weight" benzene was used without further purification. The water for interfacial tension measurements was distilled twice through all-glass apparatus. Melting points, boiling points, and refractive indices of the materials finally employed agreed well with reliable literature values.

Measurements. Solutions of known concentration were prepared in benzene. Interfacial tensions were measured at 20°C. with the Du Noüy tensiometer using the platinum ring. The scale reading at rupture of the interfacial film was converted into interfacial tension by substituting into the following equation (2):

$$\gamma = P\{0.725 + (0.0145\, P/C^2(D - d))^{\frac{1}{2}}\}. \tag{1}$$

Here γ = interfacial tension in dynes/cm.
P = scale reading at rupture in dynes/cm.
C = circumference of platinum ring (here 4 cm.)
D = density of water at 20°C.
d = density of sample at 20°C.

Freezing points of the solutions were measured in the standard form of Beckman apparatus.

RESULTS

The experimental results are set out in Table I. In these tables N_S is the molar concentration of the solute; γ the interfacial tension; and θ the freezing point depression. Γ denotes the surface excess of the adsorbed molecules, the superscripts 1, N, and U referring to the three conventions used for defining the position of the oil-water interface. These conventions have been fully explained elsewhere (3, 4).

The relevant equations now used for calculating the surface excesses are

$$\Gamma_S^{(1)} = -\frac{N_S}{N_0}\frac{T_0^2}{LT}\frac{\partial\gamma}{\partial\theta}; \tag{2}$$

$$\Gamma_S^{(N)} = \Gamma_S^{(1)}/(1 + N_S/N_0); \tag{3}$$

$$\Gamma_S^{(U)} = (\Gamma_S^{(N)}A_0 + N_S)/(N_0A_0 + N_SA_S). \tag{4}$$

TABLE I

Interfacial Tensions and Freezing Point Depressions of Solutions in Benzene

N_S	γ, dynes/cm.	θ, °C.	$-\frac{\partial\gamma}{\partial\theta}$	$\Gamma_S^{(1)}$	$\Gamma_S^{(N)}$	$\Gamma_S^{(U)}$	A, A²	F, dynes/cm.
					gram moles/cm.² × 10¹⁰			
				Acetophenone				
0.000	34.2	0	—	—	—	—	—	—
0.0106	30.8	0.781	2.85	0.812	0.805	0.529	316	3.4
0.0191	29.5	1.418	1.93	0.995	0.975	0.663	250	4.7
0.0288	28.0	2.210	1.55	1.21	1.18	0.828	200	6.2
0.0514	26·2	3.723	1.05	1.52	1.43	1.07	156	8.0
0.0855	24.3	6.196	0.612	1.52	1.39	1.19	140	9.9
0.1048	23.4	7.496	0.491	1.53	1.37	1.26	132	10.8
0.1311	22.5	9.250	0.394	1.58	1.37	1.38	121	11.7
				Benzil				
0.0000	34.0	0	—	—	—	—	—	—
0.0036	32.9	0.238	5.09	0.485	0.485	0.513	324	1.1
0.0106	30.8	0.686	4.25	1.20	1.19	1.27	131	3.2
0.0258	26.9	1.702	3.12	2.19	2.12	2.31	72.1	7.1
0.0360	25.2	2.375	2.04	2.01	1.94	2.20	76.0	8.8
0.0530	23.6	3.470	1.32	1.96	1.86	2.24	74.6	10.4
0.0855	21.9	4.713	1.02	2.53	2.31	2.94	56.9	12.1
				Benzophenone				
0.0000	33.8	0	—	—	—	—	—	—
0.0040	32.6	0.273	2.76	0.293	0.291	0.319	521	1.2
0.0085	31.9	0.580	2.28	0.518	0.514	0.572	290	1.9
0.0211	30.4	1.442	1.38	0.790	0.776	0.925	180	3.4
0.0427	28.6	2.934	1.02	1.21	1.16	1.45	115	5.2
0.0655	27.4	4.473	0.661	1.23	1.14	1.60	104	6.4
0.0810	26.9	5.441	0.475	1.11	1.00	1.56	107	6.9
0.1109	26.1	7.336	0.345	1.14	0.916	1.69	98.6	7.7
				Benzoyl acetone				
0.0000	34.0	0	—	—	—	—	—	—
0.0018	33.8	0.114	2.19	0.105	0.105	0.118	1410	0.2
0.0039	33.6	0.246	2.08	0.217	0.215	0.244	682	0.4
0.0086	32.9	0.544	1.87	0.431	0.427	0.489	341	1.1
0.0196	31.6	1.278	1.74	0.925	0.905	1.04	160	2.4
0.0471	29.1	2.859	1.69	2.22	2.12	2.45	67.7	4.9
0.0630	27.8	3.621	1.45	2.59	2.43	2.86	58.1	6.2
0.0800	26.9	4.225	1.21	2.78	2.50	3.05	54.5	7.1
				Cyclohexanone				
0.0000	33.9	0	—	—	—	—	—	—
0.0050	31.9	0.365	4.28	0.571	0.571	0.609	274	2.0
0.0181	28.9	1.287	2.66	1.31	1.29	1.42	118	5.0
0.0333	26.6	2.312	1.99	1.82	1.75	1.97	84.4	7.3
0.0602	23.6	4.118	1.53	2.58	2.42	2.85	58.5	10.3
0.0798	21.9	5.310	1.28	2.95	2.71	3.28	50.8	12.0

TABLE I—*Continued*

N_S	γ, dynes/cm.	θ, °C.	$-\frac{\partial\gamma}{\partial\theta}$	$\Gamma_S^{(1)}$	$\Gamma_S^{(N)}$	$\Gamma_S^{(U)}$	A, A.^{2}	F, dynes/cm
				gram. moles/cm.^{2} $\times 10^{10}$				
				Phorone				
0.0000	34.0	0	—	—	—	—	—	—
0.0046	33.0	0.294	2.32	0.283	0.283	0.314	541	1.0
0.0110	32.2	0.696	1.77	0.522	0.520	0.596	279	1.8
0.0351	30.0	2.180	1.34	1.28	1.24	1.48	113	4.0
0.0664	27.8	4.125	0.965	1.82	1.70	2.16	76.9	6.2
0.0910	26.5	5.847	0.652	1.73	1.52	2.18	76.3	7.5
0.1100	25.7	7.166	0.548	1.79	1.45	2.23	74.6	8.3
				Decanol				
0.0000	34.2	0	—	—	—	—	—	—
0.0050	30.5	0.339	15.0	2.00	1.99	2.02	82.5	3.7
0.0098	27.0	0.592	13.5	3.54	3.50	3.58	46.7	7.2
0.0194	24.0	0.961	7.71	3.94	3.84	4.07	40.9	10.2
0.0380	20.6	1.400	5.00	5.21	4.81	5.30	31.5	13.6
0.0655	18.8	1.978	3.54	6.60	6.18	6.65	25.1	15.4
0.1079	16.3	2.636	2.20	7.08	6.38	7.21	23.1	17.9
				Octanol				
0.0000	34.0	0	—	—	—	—	—	—
0.0040	30.0	0.278	18.8	2.00	2.00	2.03	82.4	4.0
0.0106	24.5	0.638	10.0	2.85	2.81	2.89	57.7	9.5
0.0212	21.4	1.021	5.85	3.36	3.31	3.46	48.2	12.6
0.0355	19.7	1.401	3.90	3.78	3.65	3.90	42.8	14.3
0.0592	18.1	1.925	3.16	5.28	5.07	5.51	30.2	15.9
0.0991	16.0	2.745	2.21	6.45	5.88	6.59	25.4	18.0

T_0 is the freezing point of the solvent benzene.
L its latent heat of fusion.
T the absolute temperature.
A_S is the area per molecule of the polar solute which may be taken as 22 A.^{2} without significant error.
A_0 that of the benzene molecule which is taken as 24 A.^{2}.
N_0 is the mole fraction of the solvent.

The area, A, per polar molecule in the adsorbed film is given by:

$$A = \frac{1}{\Gamma_S^{(U)}}, \qquad [5]$$

the force, π, in the surface being obtained from

$$\pi = \gamma_0 - \gamma, \qquad [6]$$

where γ_0 is the interfacial tension of the pure solvent.

As the force π is increased the area per polar molecule decreases. The

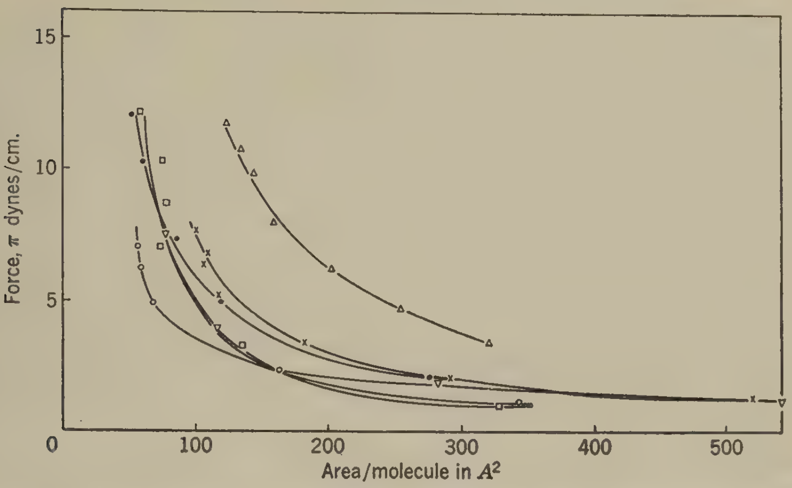

FIG. 1. Force-area curves for ketones adsorbed at the benzene-water interface. △ Acetophenone; □ Benzil; × Benzophenone; ○ Benzoyl acetone; • Cyclohexanone; ▽ Phorone.

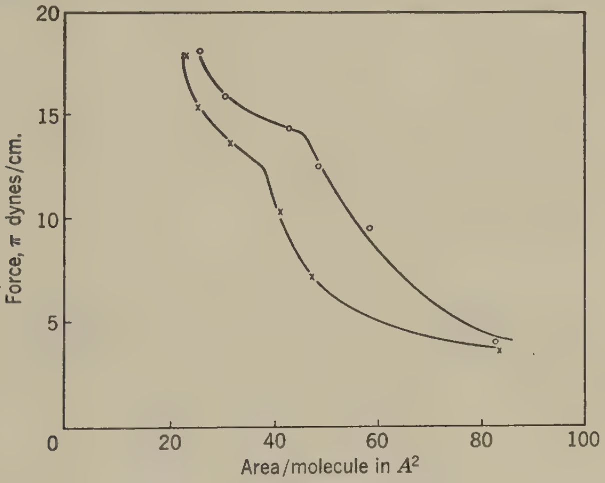

FIG. 2. Force-area curves for alcohols adsorbed at the benzene-water interface. ⊙ Octanol; × Decanol.

resulting πA curves have been plotted in Figs. 1 and 2 for the compounds now studied.

The curves are subject to two main sources of error.

Firstly there are the errors of measurement. Freezing points are probably correct to within ±0.005°C., interfacial tensions to within ±0.2 dynes/cm. But the error involved in deriving $\partial\gamma/\partial\theta$ from the slope of the γ versus θ curve is probably of the order of ±5% and may be greater when the slope is steep.

Secondly the equations used for calculating the surface excesses are strictly valid only under ideal conditions. These are not realized in practice. One important condition is that only very dilute solutions ($<0.01\ M$) are used. At concentrations $>0.05\ M$ the assumption that the solute molecules are unassociated is no longer true. This is shown by departure from linearity of the plots of freezing point against concentration, particularly for the alcohols. Some allowance however, is made for this by the θ term in Eq. [2].

The fact, however, that the πA curves for the simple straight-chain alcohols become asymptotic at about 21 $A.^2$ supports the validity of the treatment, since direct measurement with the Langmuir Trough at the air-water interface has shown this to be the area at close packing of these molecules (5).

DISCUSSION

The πA curves obtained by the present method are incomplete. For the ketones the greatest force that can be applied to the adsorbed film is about 12 dynes/cm., while for the alcohols it is about 18 dynes/cm. Nevertheless some useful deductions can be made.

The ketones give smooth πA curves and there is no indication of a change of state in the adsorbed film. The alcohols, however, exhibit points of inflexion between 12 and 14 dynes/cm. and this is ascribed to a change of state from liquid expanded to liquid condensed.

Langmuir has shown (6) that expanded films at the air-water interface obey an equation of the type

$$(\pi - \pi_0)(A - A_0) = C. \qquad [7]$$

In this π_0 is a measure of the van der Waals' forces between nonpolar groups, while A_0 is the co-area of the polar heads. This equation has been shown to apply also to insoluble films of proteins at the oil-water interface (7).

TABLE II

Cross-Sectional Areas of Molecules

Substance	π_0, *dynes/cm.*	C	A_0, A^2	Calculated area, A^2
Acetophenone	−0.8	1188	30.3	35.4
Benzil	+0.5	194	47.1	56.2
Benzophenone	+0.5	350	47.3	47.8
Benzoyl acetone	+0.7	94	42.1	49.0
Cyclohexanone	+0.4	421	18.2	26.5
Phorone	+0.5	245	42.2	44.2
Decanol	+1.9	92	29.7	—
Octanol	−2.3	405	21.5	—

It is now found that over the liquid expanded region the present πA curves obey the Langmuir equation quite satisfactorily. Numerical values of π and A taken from the curves have been substituted into Eq. [7]. The resulting values of π_0, A_0, and C are set out in Table II. It is seen that in all cases, π_0 numerically is small. This is to be expected since the hydrophobic tails of the adsorbed molecules are dissolved in the oil phase. The negative value of π_0 in the case of acetophenone must be attributed to a combination of experimental error, weakness in the method of calculation, and departure from the ideal behavior predicted by the Langmuir equation.

If it is assumed that condensation of the films takes place when the spheres of influence of the molecules begin to overlap, it follows that A_0 should be a measure of the area occupied by each molecule when these begin to "touch." The ketones now used have relatively rigid molecules and for them "touching" is more or less synonymous with close packing. This explains why their curves exhibit no condensed region. In the case of the alcohols however, the molecules have a long chain of C and H atoms, which can be tilted from the vertical at the benzene-water interface. Interaction between the molecules can commence before close packing and this accounts for the region in which the adsorbed film is condensed.

It is now possible to see whether the values of A_0 obtained from the Langmuir equation do in fact agree with the cross-sectional areas of the molecules concerned. For illustration the case of acetophenone is considered.

At the benzene-water interface the adsorbed molecules will be orientated as shown in Fig. 3. The molecules are planar. If one assumes an angle of 110° between the benzene ring and the methyl group, and uses published values of bond lengths (8, 9), it is found that the distance xx in Fig. 3 is

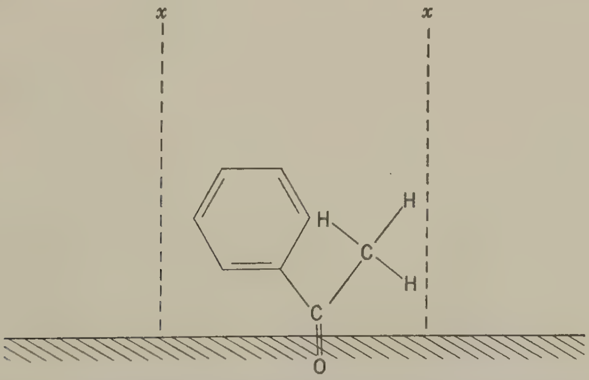

FIG. 3. Acetophenone molecule at the benzene-water interface.

about 6.6 A. Multiplying this by 5.4 A. (the assumed thickness of the benzene ring[1]) gives a cross-sectional area of 35.6 A.^{2} This compares with an A_0 value of 30.3 A.^{2}.

The molecules of the remaining ketones have been assumed to have the same orientation at the interface as acetophenone. The thickness of the phorone molecule has been taken as 4.6 A. (the distance between the centers of neighboring $—CH_2—$ chains), while the $C{=}C—CH_3$ angle is assumed to be 124°. The cross-sectional areas thereby calculated are compared in Table II with A_0 values derived from the πA curves.

It is seen that for the six ketones the calculated areas differ from the values of A_0 by less than 10 A.^{2}. This agreement is considered very reasonable in view of the several assumptions that have been made in deriving πA curves, in calculating values of A_0, and in calculating the cross-sectional areas of the molecules concerned. (For example, the C—C—C angle in cyclohexanone has been taken as 109° (9). At the interface it is likely to be greater than this as a result of deformation of the molecules (10). This would account for the low value of A_0 obtained).

We now consider the πA curves of the two long-chain alcohols. Both exhibit regions in which the adsorbed film is presumably condensed (11). The condensed portions of the curves tend to a minimum area of about 20 A.^{2}, which is near to the figure of 21 A.^{2} for close-packed straight-chain alcohols.

The expanded regions of the curves obey the Langmuir equation fairly well, though not as well as the ketones. For octanol A_0 is 21.5, while for decanol it is 29.7. These admittedly rather approximate values are both greater than 21 A.^{2}, which indicate that at the interface the molecules are tilted from the vertical, so that interaction between the nonpolar tails occurs before close packing of the OH heads.

On this assumption one would expect the values of A_0 to coincide with the points of inflexion in the πA curves. That they do not must be attributed to departure from ideal behavior of the expanded films.

It appears then, for the compounds now studied, that A_0 gives some indication of the area occupied by each molecule when interaction between them commences. In the case of the rigid ketones interaction coincides with "touching" and A_0 can be taken as the cross-sectional areas of the molecules. In the case of long-chain alcohols tilting occurs and A_0 is thus greater than the cross-sectional area. For such compounds the required area is given by the value of A when the πA curve becomes asymptotic.

This correlation between πA characteristics and the sizes of the molecules may be of assistance in identifying unknown compounds adsorbed at the oil-water interface.

---

[1] This assumption leads to values of the cross-sectional areas of benzene, cholestanol, etc., in reasonable agreement with the accepted values.

ACKNOWLEDGMENTS

The author wishes to thank the directors of British Insulated Callender's Cables for permission to publish this work. He is indebted to Mr. T. Platts Mills for carrying out the measurements.

SUMMARY

The force-area characteristics of adsorbed films of some ketones and alcohols at the benzene-water interface have been investigated on the assumption that the adsorbed film is monomolecular and that Gibbs' equations hold. For small, relatively rigid molecules it has been possible to relate the film characteristics to the sizes of the molecules concerned, and the method may therefore be of assistance in identifying other surface-active molecules adsorbed at the interface.

REFERENCES

1. ASKEW, F. A., AND DANIELLI, J. F., *Proc. Roy. Soc (London)* **A155**, 695 (1936).
2. A.S.T.M. Standards, p. 1116 (1949).
3. GUGGENHEIM, E. A., AND ADAM, N. K., *Proc. Roy. Soc. (London)* **A139**, 218 (1933).
4. HUTCHINSON, E., *J. Colloid Sci.* **3**, 219 (1948).
5. ADAM, N. K., "Physics and Chemistry of Surfaces." Oxford University Press, Oxford, 1952.
6. LANGMUIR, I., *J. Chem. Phys.* **1**, 756 (1933).
7. ALEXANDER, A. E., AND TEORELL, T., *Trans. Faraday Soc.* **35**, 727 (1939).
8. SYRKIN, Y. K., AND DYATKINA, M. E., "Structure of Molecules," Ch. 9. Butterworths, London, 1950.
9. PINSKER, Z. G., "Electron Diffraction," Ch. 11. Butterworths, London, 1953.
10. ADAM, N. K., "Physics and Chemistry of Surfaces," p. 78. Oxford University Press, Oxford, 1952.
11. HUTCHINSON, E., AND RANDALL, D., *J. Colloid Sci.* **7**, 151 (1952).

JOURNAL OF COLLOID SCIENCE **11,** 60–68 (1956)

VARIATION OF CONTACT ANGLE AND STRUCTURE WITH MOLECULAR LENGTH AND SURFACE DENSITY IN ADSORBED FILMS OF FATTY ACIDS

W. C. Bigelow and L. O. Brockway

Department of Chemistry, University of Michigan, Ann Arbor, Michigan

Received November 23, 1955

ABSTRACT

Films of fatty acids from 12 to 22 carbons were prepared by adsorption on glass microscope slides from cetane solutions. Variations in density were achieved (*1*) by using a range of concentrations with a fixed short time of immersion and (*2*) by subsequent immersion in cetane of the most dense films.

Electron diffraction patterns showed an increasing average tilt of the molecules relative to the surface normal with decreasing length of the molecules but no apparent change in tilt with variations in surface density. The contact angles exhibited by drops of cetane on the films decreased markedly from a maximum of 43–44° when the density of the adsorbed molecules on the surface was decreased, but were independent of the variations in tilt and length of the molecules.

INTRODUCTION

Previous investigations (1, 2) have shown that polar organic compounds, such as the fatty acids and the corresponding alcohols, amines, and amides, adsorb from solution in nonpolar organic solvents onto clean solid surfaces to form films which have the interesting property of being very poorly wetted by the solutions and the pure nonpolar solvents. As the film-covered surfaces are withdrawn from the solutions, the liquid recedes, leaving the film-covered surfaces dry. Drops of the solutions or of the pure nonpolar solvents which are subsequently placed on the surfaces show contact angles of as much as 40° and move about freely as the surfaces are tilted. To describe these properties briefly the films are commonly referred to as being "oleophobic."

Although these oleophobic films have been studied rather extensively, their detailed structure has not yet been determined nor related to their oleophobic properties. In the early studies of the formation and properties of the films (1), it was concluded that they consisted of monolayers of closely packed polar molecules in which the molecules were attached to the surfaces by their polar groups and were oriented with their hydrocarbon chains perpendicular to the substrate surfaces. The outer surfaces of the ilms were thus considered to consist of a nearly continuous array of methyl groups, and the difference in the character of this methyl-rich surface and the predominantly methylenic organic liquids was proposed as the basic reason for the incomplete wetting of the hydrocarbon films by the nonpolar hydrocarbon liquids. Subsequent electron diffraction studies (3, 4) confirmed these basic structural concepts, but showed that the molecules were, on the average, tilted several degrees in random directions from the surface normal, and evidence was obtained indicating that the average tilt varied depending on the roughness of the substrate surfaces. More recently (5) electron microscope studies of the films have led to the proposal of a structural model in which the molecules associate in cluster or micelles about 100 A. in diameter. Owing to the difference in the diameters of the hydrocarbon chains and the polar groups, this model proposes that the molecules tilt toward the centers of the micelles somewhat like the corn stalks in a corn shock. This general arrangement for the molecules is consistent with observations on the rate of evaporation of the adsorbed molecules from the surfaces at elevated temperatures (6). A further interesting feature of this model is the proposal that the average tilt of the adsorbed molecules should decrease as the length of the hydrocarbon chains of the molecules increases.

The present investigation was undertaken to obtain more information on the factors affecting the structures and the oleophobic properties of the ilms. The principal factors which have been considered here are: (*1*) variations in the length of the polar molecules and (*2*) variations in the average density of the polar molecules on the surfaces. Studies have been made of films of each of the fatty acids from 12 to 22 carbon atoms in ength. In addition the films have been prepared and treated in ways designed to introduce systematic variations in the average density of molecules on the surfaces. The structures of the films were examined by electron diffraction, and their oleophobic properties evaluated by measuring the advancing contact angles of drops of cetane placed on the films.

Experimental Methods

The films studied here were prepared on glass microscope slides by adsorption from cetane solutions. The fatty acids used include: lauric, myristic, palmitic, stearic, arachidic, and behenic acids. These acids were urnished by the Chemical Division of the Procter and Gamble Company and were all reported to be at least 95% pure. Their respective melting points were: 44.1°, 57.5°, 63.7°, 69.4°, 76.0°, and 80.5°C. The cetane was a commercial grade material having a melting range of 17.3°–17.8°C. To nsure its freedom from adsorbable impurities, the cetane was passed repeatedly through columns of activated silica gel and alumina until drops placed on both strongly alkaline and strongly acid water showed no tendency to spread. This has been shown to be a satisfactory test for the absence of polar impurities for solvents used in preparing films by adsorption from solution (1).

Glass microscope slides were chosen as substrates for the films because electron microscopic studies (7) have shown their surfaces to be highly polished to a uniformly smooth condition, and it was hoped to avoid variations in the roughness of the substrate and to eliminate the tedious polishing procedures which would be necessary to produce comparable surfaces on metals or minerals.

Some difficulty was encountered in cleaning the slides so that they would adsorb films having reproducible properties. After considerable experimentation, a procedure was adopted consisting of the following sequence of operations: (*1*) thorough washing in a hot detergent (Tide) solution, (*2*) thorough rinsing with hot water, (*3*) immersion for 10 to 15 minutes in cold chromic-sulfuric acid cleaning solution, (*4*) thorough rinsing with steaming distilled water running directly from a still equipped with a block-tin condenser, (*5*) immersion for 30 minutes in hot distilled water followed by a final rinse with the steaming distilled water. The slides were then hung at one corner with stainless steel wire clips in a clean drying oven with a stainless steel interior and were dried at 150°C. for 4 hours. Upon removal from the oven they were stored until use in glass-stoppered bottles. In all these operations the slides were handled with acid-cleaned, glass-tipped tweezers, and extreme care was exercised to avoid scratching or marring their surfaces. Even with most careful adherence to this procedure variations were occasionally observed in the behavior of slides cleaned in different batches. Therefore, slides for a given series of experiments were cleaned at the same time, and comparisons have been made only for slides cleaned in the same batch. All the glass-stoppered bottles and other glassware used in these experiments were cleaned by a process similar to that used with the slides.

The electron diffraction examinations were made by the reflection method using a General Electric electron diffraction instrument operating at an electron-accelerating potential of 35 kv. Some difficulties were encountered owing to the accumulation of electrostatic charges on the nonconducting glass slides. The usual procedure of bombarding the surfaces with low-energy electrons was found to destroy the monolayers in many instances and therefore could not be used. It was found that good patterns could be obtained by using a low-intensity electron beam and an angle of incidence of the beam relative to the slides which was somewhat larger than is generally used in reflection studies. Consequently, the first-order reflections from the adsorbed molecules were usually masked by the shadow of the slides, and the patterns showed a rather high background which caused some difficulty in the analysis of the patterns. The interpretation of the electron diffraction patterns in terms of the structure of the monolayers has been described by Karle and Brockway (4).

The contact angles of the cetane drops were determined by the sessile drop, or drop-on-plate, method. To insure that the drops exhibited advancing angles, they were formed on the surfaces with a hypodermic syringe which was operated through micrometer screw controls permitting the tip of the syringe to be slowly withdrawn from the drops while the cetane was being ejected and the drops were growing in size. The contact angles (θ) of the drops were calculated from their maximum heights (h) and maximum widths (w) using the formula $\tan \theta/2 = 2h/w$. This relationship is valid for drops having the shape of spherical segments but has been shown by Mack (8) to be applicable in general only to drops which are less than 0.5 mm. in diameter. To insure compliance with these conditions, all of the drops measured here were smaller than this. The drop dimensions were measured with a horizontal telescope equipped with a 5× objective and a 12.5× filar micrometer eyepiece. With this instrument measurements could be reproduced to ±.002 mm., which corresponds to an uncertainty of no more than 0.5° in the determination of the contact angles.

RESULTS

Two series of experiments were used to study the effects of the average density of the adsorbed molecules on the structure and oleophobic properties of the films. The first of these, which also included studies of the effects of variations of the length of the adsorbed polar molecules, was carried out with films of each of the fatty acids prepared from solutions ranging in concentrations from 1×10^{-4} to 5×10^{-2} molal, using a constant period of immersion of 5 seconds for depositing the films from each solution. The period of immersion was chosen relatively short so that it would be unlikely that the adsorption process would be completed in the more dilute solutions. The density of adsorbed molecules would then increase with increasing concentration of the solutions.

TABLE I

Average Advancing Contact Angles for Drops of Cetane on Fatty Acid Films Deposited on Glass Surfaces by 5-Second Immersion in Solutions of Different Concentration[a]

Acid	Molal concentrations of solutions					
	1×10^{-4}	5×10^{-4}	1×10^{-3}	5×10^{-3}	1×10^{-2}	5×10^{-2}
Behenic	—	—	44°	N.S.	N.S.	N.S.
Arachidic	43°	43°	44°	N.S.	N.S.	N.S.
Stearic	42°	44°	44°	44°	N.S.	N.S.
Palmitic	N.O.	N.O.	41°	44°	44°	N.S.
Myristic	N.O.	N.O.	36°	43°	44°	N.S.
Lauric	N.O.	N.O.	25°–36°	39°	42°	43°

[a] Each value is the average for not less than 5 different drops on each of 5 different slides; the individual measurements lay within ±1° of the average (except for lauric acid at 10^{-3} molal).

N.O.—not oleophobic.

N.S.—indicated concentration exceeds solubility.

The results of the contact angle measurements on the films formed under these conditions are summarized in Table I. Films prepared from sufficiently concentrated solutions of each acid showed maximum contact angles of 43–44°. The concentrations required for this were near the solubility limits for the various acids at room temperature and ranged from about 1×10^{-3} molal for arachidic acid to about 5×10^{-2} molal for lauric acid. With decreasing solution concentrations, the contact angles decreased, the effect being somewhat greater for the shorter acids than for the longer ones. Below concentrations ranging from about 1×10^{-3} molal for lauric and myristic acids to about 1×10^{-4} molal for stearic and arachidic acids, periods of immersion greater than 5 seconds were required to produce oleophobic films.

Electron diffraction studies were made on each of the slides after completion of the contact angle measurements and on several additional slides prepared immediately before insertion into the diffraction camera. Diffraction patterns consisting of well-defined, arced layer lines were obtained from all films except those of lauric acid. These patterns are similar to those reported by Brockway and Karle (3) in previous studies of acid films deposited by adsorption from solution, and by Germer and Storks (9) in studies of monolayers deposited by the Langmuir-Blodgett technique. For reasons as yet unknown, the photographs from the slides bearing the lauric acid films contained no features characteristic of long-chain organic molecules. The diffraction patterns from the other acids were analyzed, using the general principles outlined by Karle and Brockway (4), for indications of variations in the arrangement of the adsorbed molecules. Comparison of patterns from monolayers of the different fatty acids showed a slight increase in the curvature of the layer lines as the length of the fatty acids decreased. This is indicative of an increase in the average tilt of the molecules from the surface normal as the length of the hydrocarbon chains decreases. The average tilts estimated for the different acids are as follows: behenic and arachidic, 2°; stearic, 4°; palmitic, 6°; myristic, 8°. These values were arrived at by estimating the maximum slope of the layer lines in a number of patterns for each acid, averaging, and considering this angle to be approximately equal to the average molecular tilt of the molecules. The general trend indicating an increase in the average tilt with a decrease in chain length of the molecules is considered to be reliable, although the separate values for the angles are probably not better than ±3°. It is probable that the maximum molecular tilt in each case is as much as twice these average values. There were no detectable differences in the arcing of the layer lines in the patterns from solutions of different concentrations of the same acid, though the layer lines in patterns from the films prepared from the more dilute solutions were generally less intense relative to the background scattering than those from films prepared from the more concentrated solutions.

Slides which were immersed in the very dilute acid solutions for periods too short to produce oleophobic films were also examined by electron diffraction for evidence of oriented adsorbed molecules. A 1×10^{-5} molal arachidic acid solution failed to produce oleophobic surfaces on slides immersed for a period of 15 minutes. After the liquid remaining on these slides was removed by centrifugation, very weak layer line diffraction patterns were obtained. Slides immersed in this solution for periods of 30 minutes and 3 hours were oleophobic over parts of their surfaces and gave somewhat stronger layer line patterns. Slides immersed for 20 hours were oleophobic over their entire surfaces and produced layer line diffraction patterns of intensities comparable to those from films prepared from the more concentrated solutions. All these patterns were carefully compared with those obtained from films prepared from the more concentrated solutions, and there was no noticeable difference in the arcing of the layer lines.

The second series of experiments to determine the effects of variations in the molecular densities of the films on their structure and properties was made with films of arachidic and stearic acids. These films were prepared from the 1×10^{-3} molal solutions, using a 5-second period of immersion, and were subsequently immersed for short periods in pure cetane to redissolve some of the adsorbed molecules. It was found that the films would generally retain their oleophobic properties after immersion in the cetane for periods of as much as 7 to 10 minutes, but that the contact angles decreased from the initial values of 43–44° to values just above 30° as the period of immersion was increased within these limits. Contact angle values observed in typical experiments with each acid are given in Table II. Each of these values is the average for measurements made on five or more drops. Electron diffraction patterns obtained from the depleted films were care-

TABLE II

Advancing Contact Angles (θ) of Drops of Cetane on Fatty Acid Films Before and After Immersion in Cetane

Slide	θ before immersion	Time of immersion	θ after immersion
		Stearic Acid Films	
A	44° ± 1°	1 min.	40° ± 1°
B	44	2	37
C	44	3	37
D	44	5	33
E	44	6	31
F	44	8	Not oleoph.
		Arachidic Acid Films	
A	44° ± 1°	1 min.	40° ± 1°
B	43	3	39
C	44	3	38
D	44	5	35
E	45	7	32
F	44	8	Not oleoph.

fully compared with patterns from undepleted films. A decrease in the intensity of the layer lines, relative to the background, accompanied the decrease in the contact angles, but there were no detectable changes in the shapes of the layer lines such as would indicate changes in the orientation of the adsorbed molecules.

A few experiments were also carried out with films of monopalmitin and monostearin formed by immersing microscope slides for 5 seconds in 1×10^{-3} molal solutions of these compounds in the purified cetane. Drops of cetane showed advancing contact angles which averaged 41 ± 1° on these films, and electron diffraction patterns of the arced layer line type were obtained from them. The patterns were generally less well defined than the patterns from the acid films and were correspondingly more difficult to interpret. The arcing of the layer lines was found to be somewhat greater than in the patterns of any of the acids, although there was no detectable difference between patterns from the two monoglycerides. The best estimate of the average molecular tilt was 12–15°.

DISCUSSION

From the contact angle measurements it is concluded that the most important factor in determining the oleophobic properties of films of fatty acids, and similar polar organic compounds, adsorbed on solid surfaces is the density of the adsorbed molecules on the surfaces. Although a quantitative relationship has not been established, it has been shown that the dependence is a direct one such that decreases in the densities of the films are accompanied by decreases in their oleophobic properties. This is particularly evident from the data of the depletion experiments recorded in Table II. In these experiments, the contact angles exhibited by drops of cetane on films of stearic and arachidic acids decreased from 44° to nearly 30° when the films were immersed in pure cetane to dissolve some of the adsorbed molecules from the surfaces. The contact angle variations shown in Table I for films formed from acid solutions of different concentrations are also consistent with this conclusion, for with a constant short period of immersion the number of molecules adsorbed on the surfaces would be expected to increase with the concentrations of the solutions.

It is also concluded that the length of the adsorbed polar molecules is not a major factor in determining the oleophobic properties of the films. The same maximum contact angle of 43–44° was observed for drops of cetane on films of all the acids which were prepared from their nearly saturated solutions (Table I). Wide variations in the contact angles of drops on films from the same acid were observed in the cases of myristic and lauric acids (Table I) and of arachidic and behenic acids (Table II).

These conclusions are reasonable when it is considered that the oleophobic phenomena must arise from the replacement of the high-energy surface of the substrate with a low-energy hydrocarbon surface upon which the hydrocarbon liquids do not spread. Since the van der Waals forces attracting the molecules of liquid to the surface are operative over distances of only a few Ångstrom units, it is clearly the characteristics of the outer surfaces of the films and not their thickness which determine their oleophobic properties. For the ideal case of dense, insoluble films on completely smooth substrates, the oleophobic properties should be the same for films of acids only a few carbon atoms in length as for acids of many carbon atoms such as those studied here.

In practice, however, the roughness of the substrate surface may be large compared with the dimensions of the polar molecules, and increasing the length of the molecules may well improve their ability to form films having the required surface characteristics. It is suggested that this accounts for the difference between the present results and those reported previously (1) for films adsorbed on rolled platinum foil which showed an increase in contact angles with increasing chain length of amine films. The glass microscope slides used here were probably smoother than the rolled foil.

The electron diffraction studies show variations in the average tilt of the axes of the polar molecules from the normal to the substrate which are related to the lengths of the molecules. In films of the 14-carbon myristic acid the average tilt is estimated to be 6° more than in films of the 20-carbon arachidic acid. The molecular tilt also appears to depend on the size of the polar group as indicated by the fact that the tilt of the molecules in films of monostearin and monopalmitin is considerably greater than in films of acids of the same length. The other notable feature observed in the diffraction patterns is that the intensity of the layer lines relative to the background scattering decreases in films treated to give decreasing contact angles.

Consideration of both the diffraction and contact angle observations shows no correlation between the contact angles and the tilt or length of the molecules. Films from the most concentrated solutions of the different acids show the same contact angles but different tilts. Soaking the films in pure cetane reduces the contact angle but does not change the tilt appreciably. The assumption that soaking reduces the surface density of adsorbed molecules is supported by the observed decrease in intensity of the diffraction patterns.

It is of interest to consider the diffraction results in connection with the structural models which have been proposed for the films. The most interesting of these is the micelle model which was proposed by Epstein. This model is generally consistent with the electron diffraction observations and takes into account such general structural features as the randomness in direction of the tilt of the molecules and the occurrence of a range of values of tilt. In addition it provides for the increase of the average molecular tilt with a decrease in chain length and with an increase in the size of the polar groups, as was observed here.

The early concept that the outer surfaces of the films must consist of closely packed methyl groups in order for the films to be oleophobic must be modified somewhat. Since the molecules show considerable tilt from the normal to the average surfaces, it is apparent that even in the most dense films considerable numbers of methylene groups of the hydrocarbon chains of the adsorbed molecules must be exposed in the surfaces of the films. Furthermore, the oleophobic properties persist even after considerable depletion of the films when even greater numbers of the methylene groups, and even some areas of the substrate surfaces, are undoubtedly exposed.

It must be emphasized that both of the above models were developed for ideally smooth substrates. Surfaces in practice are nearly always rough on a molecular scale, and this could have a pronounced effect on the proportion of methyl and methylene groups exposed in the surfaces of the films as well as on the energetics of the formation of micelles. The correlation of molecular tilt with chain length should include the influence of surface roughness. The molecular tilt observed in diffraction patterns is measured relative to the average surface and should be used only cautiously in deducing the tilt at the actual point of attachment in deriving structural models. A direct effect of surface roughness on tilt has already been noted (3) for cerotic acid films on platinum in which the observed maximum tilt of 30° on rough rolled platinum decreased to nearly 0° when the platinum was given a careful metallographic polish. This effect should be even greater for acids of shorter chain length. Further studies of adsorbed films certainly should include the effect of surface roughness on their structures and oleophobic properties.

ACKNOWLEDGMENT

The authors wish to express their appreciation to the Procter and Gamble Company for the pure fatty acids used in this research.

REFERENCES

1. Bigelow, W. C., Pickett, D. L., and Zisman, W. A., *J. Colloid Sci.* **1**, 513 (1946).
2. Bigelow, W. C., Glass, E., and Zisman, W. A., *J. Colloid Sci.* **2**, 563 (1947).
3. Brockway, L. O., and Karle, J., *J. Colloid Sci.* **2**, 277 (1947).
4. Karle, J., and Brockway, L. O., *J. Chem. Phys.* **15**, 213 (1947).
5. Epstein, H. T., *J. Phys. & Colloid Chem.* **54**, 1053 (1950).
6. Karle, J., *J. Chem. Phys.* **17**, 500 (1949).
7. Williams, R. C., and Epstein, H. T., private communication.
8. Mack, G. L., *J. Phys. Chem.* **40**, 159, 169 (1936).
9. Germer, L. H., and Storks, K. H., *J. Chem. Phys.* **6**, 280 (1938).

JOURNAL OF COLLOID SCIENCE **11**, 69–76 (1956)

MEASUREMENTS RELATED TO THE FUNDAMENTAL PROCESSES OF AEROSOL ELECTRIFICATION

R. H. Woessner and Ross Gunn

Physical Research Division, U. S. Weather Bureau, Washington, D. C.

Received August 24, 1955

Abstract

With the object of illuminating the fundamental processes responsible for the electrification of aerosols, a number of measurements have been made to compare the initial distribution of charges carried by various aerosols with their final equilibrium state. Measurements have been made on freshly condensed water droplets and sulfur particles, on both freshly dispersed and aged silica dust particles, and on sprayed water droplets; all lying within the 1- to 2-μ radius range.

The measurements show that when numerous ions are formed within the aerosol space the particle charges are not completely discharged but rather the ions greatly hasten the attainment of an equilibrium distribution. Moreover, it is found that irrespective of the initial measured distribution of charges, the final equilibrium distribution approaches a Gaussian curve whose width is dependent upon the mean particle radius and is usually symmetrical about the axis of zero charge.

Because the infrequent collision of water droplets can hardly produce appreciable electrification by friction, and because the equilibrium charge on water droplets and that on silica particles of the same size are indistinguishable, it is concluded that the maintained charges on aerosols are a direct consequence of the diffusion of the ambient atmospheric ions onto the particles. The equilibrium distributions approach the theoretical form recently worked out by Ross Gunn.

I. Introduction

A basic understanding of the physics of cloud stability and the processes responsible for their coagulation and precipitation requires a detailed knowledge of the distribution of electrical charge on cloud particles. Moreover, it is important to understand the basic processes whereby cloud droplets acquire charge and redistribute this charge as equilibrium is approached. Preliminary measurements of the electrical charge carried by fog droplets have been made by Wigand (1) and by Reeder and Paquette (2). Many data are available on the distribution of charge carried by silica and other dusts, but there is little information on the character of the aging process and the final equilibrium distribution. Measurements by Gillespie and Langstroth (3) and Kunkel (4) have shown that aging or systematic changes in the observed distributions normally continue for a number of hours after the dusts are dispersed. The equilibrium distribution of charges on condensed oil droplets have also been reported by Lissowski (5).

In order to illuminate the fundamental processes responsible for the equilibrium we have examined the initial and final electrical states of a number of aerosols generated in quite different ways. All of the collected data were obtained on droplets having radii lying in the 1- to 2-μ range. These measurements permit one to determine the fractional number of the particles carrying any selected number of positive or negative ions. Such distributions have been determined, first, for silica dust that has been dispersed by a sudden burst of air. This dust is highly electrified initially by frictional processes, and the character of the charge distribution is observed to change systematically with age until an equilibrium state is established. A second type of aerosol was produced by the condensation of water upon electrically neutral sodium chloride nuclei. The charges were determined immediately after the generation of the droplets and found to be negligible. After the droplets had been aged the charge distribution was again determined. For comparison with water droplets so formed, a similar aerosol was made by atomizing a weak salt solution. In this case the droplets were initially found to be highly charged. Finally another solid aerosol was formed by the condensation of sulfur vapor. This produced large numbers of sulfur particles which were initially observed to be all neutral but which acquired through aging an equilibrium distribution of charge much like that observed on the aerosols mentioned above.

The classical hypothesis that the random electrification of aerosols arises from the frictional interaction of the particles is not questioned when conditions are favorable. However, it is a well-established fact of atmospheric electricity that any highly insulated and charged body will discharge to $1/\epsilon$ (37 %) of its initial value in a time τ given by (6)

$$\tau = \frac{1}{4\pi\lambda}, \qquad [1]$$

where λ is the total conductivity of the environment. The substitution of observed values suggests that in ordinary air most of the initial charge on any selected particle would vanish in an hour. Therefore, unless further frictional collisions between the particles take place to restore the electrification carried by the aerosol, it will discharge. Usually the particles are small and a brief calculation will show that they seldom collide in the air after the aerosol is once dispersed. Thus it seems evident that some other mechanism must be invoked to account for the *maintenance* of the observed equilibrium charge distribution.

Our laboratory measurements show that the aging may be greatly hastened by the introduction into the environment of the aerosol of large numbers of ions. Although we have not experimentally examined the matter in detail, it appears that the time to approach equilibrium is roughly equal to the discharge time given by Eq. [1], when the actual conductivity *within the dust cloud* is employed (Eq. 25 of Ref. 7). For example, the aging time for a typical silica dust cloud in ordinary air is something like 2 hours or more. But if the cloud is exposed to a large number of ions, produced, for example, by X-rays, then it is found that the aerosol comes to an equilibrium in approximately a minute. In view of the observed profound reduction in the time to reach equilibrium which results from the introduction of ions into the environmental air, it appeared that a study of the conversion of the initial to the final distribution of charges might provide valuable information on the fundamental processes responsible for the observed electrification.

A detailed analysis of droplet charging by the diffusion of atmospheric ions onto their surface has recently been worked out by one of us (7, 8), and measurements have been made to determine if the behavior of aerosols is consistent with this analysis. The analysis showed that the fractional number of particles in an aerosol carrying a given number of elementary charges x is expressed by

$$\frac{F_x}{F_t} = \frac{e}{(2\pi akT)^{1/2}} \exp\left[\frac{-\left(x - \dfrac{akT}{e^2}\ln\dfrac{\lambda_+}{\lambda_-}\right)^2}{2\left(\dfrac{akT}{e^2}\right)}\right], \qquad [2]$$

where F_x is the number of particles carrying x elementary charges, F_t is the total number of particles, e the electronic charge, a the droplet radius, k the Boltzmann constant, T the absolute temperature, and λ_+ and λ_- are the positive and negative conductivities, respectively. Equation [2] is a typical Gaussian distribution that is symmetrical about the axis of zero charge when the positive and negative electrical conductivities are equal. As the ratio of these conductivities change, the axis of symmetry, which measures the mean charge on the particles, is displaced towards the sign of the predominant conductivity. However, inside a cloud the positive and negative conductivities are not very different and the distribution then centers about zero charge. In some of the preliminary investigations the positive and negative conductivities within the aerosol were measured and were found to be approximately equal. In the remaining investigations the observed symmetry of the experimental curves was interpreted to mean that the conductivities are nearly equal. We have found special cases in which the axis of symmetry is displaced. These cases will be reported elsewhere. In all cases the expression of Eq. [2] is found to describe very well the equilibrium distribution on cloud and other aerosol particles. Our measurements show that whereas there is much scatter when analyses are made on less than 1000 droplets, more data invariably smooth out these irregularities.

II. APPARATUS

The apparatus employed in this investigation is basically an adaptation of an arrangement first used by Wells and Gerke (9) in investigations of charged smoke particles. The radius and the electric charge of the aerosol particles were determined directly from the observed displacements of the particles that result from the impressed electrical and gravitational forces. A horizontal electric field was cyclically applied to the droplets in an unsymmetrical time sequence in order that the sign of the charge on each particle as well as its magnitude could be determined. The rate of fall was used to determine the radius of each individual particle. The displacements were photographed and analyzed by projection and measurement on a translucent screen.

III. THE MEASUREMENTS

Using the above apparatus, the sign and number of elementary charges carried by each particle and its radius were determined. The distribution of the fractional numbers carrying any assigned number of ions was then plotted as shown in the accompanying figures. Between 250 to 600 individual measurements were made to determine each curve.

Curve *C* of Fig. 1 gives the observed distribution for silica dust particles immediately after they are dispersed by a blast of clean air. It may be noticed that large numbers of the particles carry large positive and negative charges. However, when this same aerosol is exposed to large numbers of positive and negative ions produced within the cloud volume by X-rays, then within a minute the distribution is converted to that shown in Fig. 1,*B*.

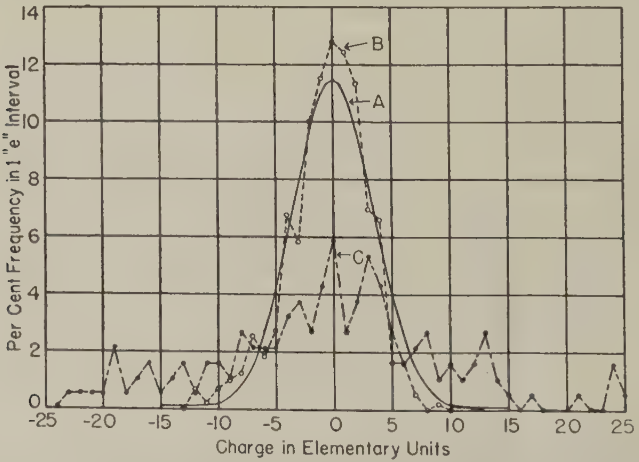

FIG. 1. Silica dust disbursed by air blast. *A*. Calculated according to Eq. [2] ($a = 0.7\,\mu$). *B*. Aged by exposure to copious ionization. *C*. Initial distribution.

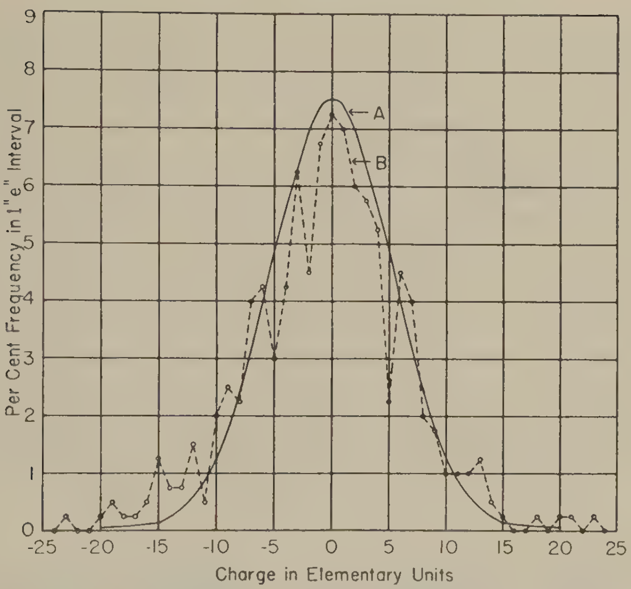

FIG. 2. Water cloud condensed on neutral NaCl nuclei. The condensed cloud was initially uncharged. *A*. Calculated according to Eq. [2] ($a = 1.63\ \mu$). *B*. Aged by exposure to copious ionization.

For comparison with these observed distributions one may draw Fig. 1,*A*, which, according to Eq. [2], represents the equilibrium distribution for particles having the mean observed radius of 0.7 μ. The experimental curves naturally show some statistical scatter since only 545 individual particle measurements are represented. These measurements seem representative of aerosols initially electrified by frictional contacts that result from their energetic dispersal.

An aerosol was next formed by the *condensation* of water vapor onto vaporized sodium chloride nuclei. After its formation, but before it was aged with ions, this type of aerosol is found to be essentially uncharged. Less than 2% of the particles are charged, and these generally possessed only one elementary unit. When this aerosol is aged by the introduction of numerous ions the equilibrium charge distribution is observed to be that shown in Fig. 2,*B*. The average observed radius of the droplets was 1.63 μ. This experimentally observed curve was obtained by measurements on some 2500 individual cloud droplets. Again for comparison the distribution shown in Fig. 2,*A*, was calculated from Eq. [2] for droplets of the observed mean radius.

As a further check, a water cloud was produced by an atomizer that disbursed a water solution containing traces of sodium chloride. When these drops reached equilibrium the concentration of salt corresponded closely to that employed in the foregoing experiment. It was observed that these drops were very highly charged initially owing presumably to the energetic disruption of the water surfaces. However, upon the introduction of numerous ions into the cloud, the initial electrification largely vanished and the equilibrium charge distribution shown by the dashed curve in Fig. 3,*B* was established. Approximately equal numbers of positive and negative droplets were then observed with about 8.5% of them remaining

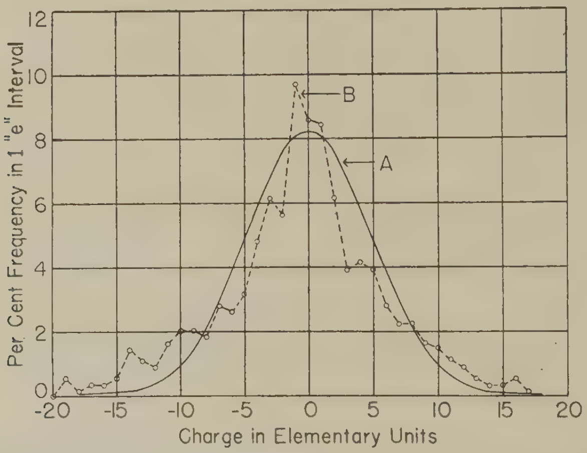

FIG. 3. Water cloud formed by spraying. Droplets highly charged initially and widely scattered. *A*. Calculated according to Eq. [2] ($a = 1.35\,\mu$). *B*. Aged by exposure to copious ionization.

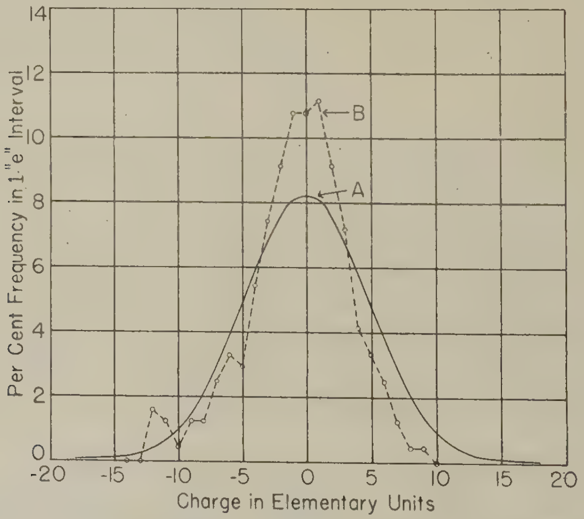

FIG. 4. Sulfur cloud condensed from vapor. Initially uncharged. *A*. Calculated according to Eq. [2] ($a = 1.35\,\mu$). *B*. Aged by exposure to copious ionization.

neutral. The solid line of Fig. 3,*A*, represents the theoretical curve of Eq. [2] for droplets having the observed mean radius of 1.35 μ.

The measurements all show that an aerosol that has just been formed by condensation from its own vapor is initially uncharged. For example, a sulfur-particle aerosol of this type was formed from the vapor and its initial neutral state verified by measurement. When this sulfur-particle aerosol was exposed to copious ionization for 2 minutes, the equilibrium electrification shown by the broken line in Fig. 4,*B*, was immediately established. This distribution approximates that calculated from Eq. [2] and shown as a solid line in Fig. 4,*A*.

In addition to the above results it was frequently observed that the equilibrium distributions, once established, continued for more than an hour after they were first produced, quite irrespective of the intensity of ionization to which they were subsequently subjected. It is presumed that this state would continue until the aerosol was precipitated.

IV. Conclusion

The foregoing experiments show rather clearly that the aging of aerosols depends critically upon the intensity of the gaseous ionization. An aerosol in the laboratory subject to the ordinary ions in the air ages in from 2 to 6 hours. By increasing the ionization and conductivity of the environmental air by the use of X-rays or any other ionizer, an equilibrium distribution may be established in a minute or so. The ions in the region therefore are ultimately responsible for the equilibrium.

The initial electrification of an aerosol by mechanical means that separate charge by frictional contact, is not questioned. But the continued maintenance of this electrification does not seem to be consistent with the above-demonstrated properties. It may be noticed that the copious ionization employed in the above experiments would normally discharge in a relatively short time, any charge placed on the particles by the occasional frictional exchange of charge due to collision. Therefore, the observed electrification must somehow be maintained by other processes.

The above-summarized measurements show that the charge distributions for aerosols of fundamentally different initial electrifications come to essentially the same final equilibrium distribution whenever they are aged by exposure to large numbers of atmospheric ions. Aerosols of initially neutral particles or very highly charged particles establish substantially the same type of equilibrium distribution in times that are roughly inversely proportional to the intensity of the ionization or the electrical conductivity of the air. This establishes that the fundamental charging process is ionic in nature. The data, moreover, suggest that surface-active forces of oriented molecules play a minor role in the establishment of the equilibrium.

A careful theoretical analysis of aerosol charging given in an earlier paper by one of us appears to describe the final equilibrium distribution very well indeed (7, 8). Accordingly, it is concluded that both theoretical and experimental analyses show that the observed charge distribution appearing on typical stable aerosols is fundamentally due to ionic diffusion.

REFERENCES

1. WIGAND, A., *Physik. Z.* **27,** 803 (1926).
2. REEDER, S. D., AND PAQUETTE, R. G., Univ. of Wash. Oceanographic Labs. Ref. No. 51-2 (1951).
3. GILLESPIE, T., AND LANGSTROTH, G. O., *Can. J. Chem.* **30,** 1056–1068 (1953).
4. KUNKEL, W. B., *J. Appl. Phys.* **21,** 833–837 (1950).
5. LISSOWSKI, P., *Acta Physicochim. U.R.S.S.* **13,** 157–192 (1940).
6. GUNN, R., *Terrestrial Magnetism and Atm. Elec.* **40,** 79–106 (1935).
7. GUNN, R., *J. Meteorol.* **11,** 339–347 (1954).
8. GUNN, R., *J. Colloid Sci.* **10,** 107–119 (1955).
9. WELLS, P., AND GERKE, R., *J. Am. Chem. Soc.* **41,** 312 (1919).

JOURNAL OF COLLOID SCIENCE 11, 77–79 (1956)

THE SWELLING OF ORGANOPHILIC MONTMORILLONITES IN LIQUIDS

R. Greene-Kelly

Rothamsted Experimental Station, Harpenden, Herts, England

Received November 28, 1955

Abstract

The crystalline swelling of amine montmorillonites is shown to take place in certain liquids. The relation between the steric requirements of the intercalated molecules is discussed.

Introduction

Jordon has shown (1) the macroscopic swelling of amine montmorillonites in nitrobenzene and toluene-methanol mixtures to be negligible until the intercalated amine possessed a chain length of 10 carbon atoms. The possibility of crystalline swelling of amine montmorillonites was not studied. The work reported here shows that certain amine montmorillonites which show no crystalline swelling in water will expand when immersed in suitable solvents.

Experimental

The amine montmorillonites were prepared as in earlier work (2) and the X-ray diffraction technique was similar. The oriented flakes were mounted in thin Pyrex glass capillaries which were filled with the selected liquid and sealed off. These capillaries were mounted in the X-ray camera and oriented so that the plane of the flake was parallel to the plane of the slit collimated beam.

Results and Discussion

Table I shows the effect of immersion of a number of amine montmorillonites in selected solvents. A comparison of the results shows that the amines differ widely in their ability to modify the swelling behavior of montmorillonite. For example, benzene, which does not enter sodium montmorillonite, will expand pyridyl and piperidyl montmorillonite and yet has no effect on triethylammonium montmorillonite. Clearly the sorption of molecules by these modified montmorillonites may be dependent not only on the pore space available but also on interaction with the cation so as to produce pore space of more suitable dimensions.

TABLE I

Showing the Influence on the 001 Spacing (Calculated from the Spacings of Higher Orders) of Immersion of Various Amine Montmorillonites in Selected Liquids. The Results Obtained with Sodium Montmorillonite Are Included for Comparison

	KX
Sodium montmorillonite	
Degassed 100° d_{001}	9.6
In water	>100
In glycerol[b]	17.8
In pyridine	
Dry	14.8
Wet	23
In benzene	9.6
In methanol[a]	16.8
In piperidine	14.7
In α-picoline	15.7
In quinoline	16.9
Triethylammonium montmorillonite	
Air dry d_{001}	13.3
In water	13.3
In glycerol	13.3
In pyridine	15.0
In benzene	13.2
Piperidyl montmorillonite	
Air dry d_{001}	13.3
In water	13.3
In glycerol	14.5
In piperidine	14.7
In pyridine	14.7
In benzene	14.7
Pyridyl montmorillonite	
Air dry d_{001}	12.5
In water	12.5
In glycerol	14.0
In pyridine	14.8
In α-picoline	15.6
In quinoline	16.7
In benzene	15.0
In methanol	12.5
4-Ethyl pyridyl montmorillonite	
Air dry d_{001}	12.8
In water	12.8
In glycerol	14.1

[a] From reference 3.

[b] Brown (4) has found 14 KX spacings with K^+ and Tl^+ montmorillonite and glycerol.

The spacings obtained when swelling occurs fall into two groups: Firstly those which are identical to that obtained with sodium montmorillonite and which are determined by the shape and size of the entering molecule, and secondly those where the spacing is governed by the cation in a new orientation. Triethylammonium montmorillonite in pyridine is an example of the first type, and piperidyl montmorillonite in glycerol of the second type. In several cases both the entering molecule and the cation may simultaneously satisfy their demands for close vertical packing, for example, pyridyl montmorillonite in benzene. It is interesting to note that similar molecular dimensions are not always a sufficient reason for simultaneous close packing; for example, α-picoline could adopt a configuration whereby its space-limiting dimensions are identical to pyridine yet it chooses a pore space 0.8 KX greater, presumably to satisfy the imposed charge distribution in the interlamellar space. Within the experimental accuracy it can be concluded that the orientation of molecules in these two-component complexes is substantially the same as in the corresponding one-component complexes; there is no evidence, for example, of solution leading to new arrangements as have been found with water and pyridine in sodium montmorillonite (5). An apparent exception to this generalization occurs with the pyridyl montmorillonite-glycerol system, but here glycerol molecules in fact determine the spacing, for it is known that montmorillonite saturated with large ions can form 14 KX complexes in addition to the 17.8 KX complexes with sodium or calcium montmorillonite (4).

REFERENCES

1. JORDAN, J. W., *Mineralog. Mag.* **28,** 598 (1949).
2. GREENE-KELLY, R., *Trans. Faraday Soc.* **51,** 412 (1955).
3. MACEWAN, D. M. C., *Trans. Faraday Soc.* **44,** 349 (1948).
4. BRINDLEY, G. W., "X-ray Identification and Structure of Clay Minerals," p. 116. Mineralog. Soc., 1951.
5. GREENE-KELLY, R., *Clay Min. Bull.*, to be published.

JOURNAL OF COLLOID SCIENCE 11, 80–95 (1956)

APPLICATION OF REE-EYRING GENERALIZED FLOW THEORY TO SUSPENSIONS OF SPHERICAL PARTICLES

Samuel H. Maron and Percy E. Pierce

Physical Chemistry Laboratory, Department of Chemistry and Chemical Engineering, Case Institute of Technology, Cleveland, Ohio

Received September 30, 1955

Introduction

Ree and Eyring have presented recently a generalized theory of flow by means of which they were able to represent satisfactorily the viscosity of solid plastic systems and polymer solutions (1, 2). However, in view of the complexity of the systems considered and the lack of extensive systematic data, they could not explore in greater detail all the implications of the theory, nor could they rely exclusively on the theory for evaluation of all the quantities involved.

At about the same time Maron and Fok (3) completed an extended investigation of the flow behavior of X-667 synthetic latex, which is an aqueous suspension of spherical particles of butadiene-styrene copolymer, stabilized by adsorbed potassium oleate. In this study the average particle size of the disperse phase was measured, and the effects of the following variables were determined: Shear stress from 50 to 800 dynes/cm.^{2}; concentration from 0 to 0.60 volume fraction, v; and temperature from 20° to 50°C. Further, the latex flow was found to be Newtonian below *ca.* $v = 0.25$, and non-Newtonian above this concentration.

These extensive data on the X-667 latex lend themselves particularly well to a detailed test of the generalized flow theory of Ree and Eyring, as well as to an examination of the concentration and temperature dependence of the parameters involved. The results of this investigation are presented in the present paper.

Theoretical Considerations

The Ree-Eyring theory considers a non-Newtonian system to be composed of a number of flow units of different relaxation times, and gives for the viscosity η, defined as F/G, where F is the shear stress and G the rate of shear, the expression

$$\eta = \sum_{n=1}^{n} \frac{x_n \beta_n}{\alpha_n} \frac{\sinh^{-1} \beta_n G}{\beta_n G}. \qquad [1]$$

In this equation x_n is the fractional area occupied by the nth flow unit on the shear surface, and

$$\alpha_n = \frac{(\lambda\lambda_2\lambda_3)_n}{2kT} \tag{2}$$

$$\beta_n = \frac{1}{[(\lambda/\lambda_1)2k']_n}, \tag{3}$$

where k is the Boltzmann constant, T the temperature, the subscript n refers to the particular flow unit involved, and the summation has to be extended to all the flow units present. Here $\lambda_2\lambda_3$ is the cross-sectional area of a given flow unit, λ the distance a unit moves between equilibrium positions, λ_1 the distance between planes of flow units of a given kind, and k' the rate constant for passage of a given flow unit over the potential energy barrier. On substitution into Eq. [3] of the absolute rate theory expression for k', namely,

$$k' = \frac{kT}{h} e^{-\Delta F_n^*/RT}, \tag{4}$$

where ΔF_n^* is the free energy of activation for flow of the nth unit, β_n becomes

$$\beta_n = \frac{h\lambda_{1n}\, e^{\Delta F_n^*/RT}}{2kT\lambda_n} \tag{5}$$

$$= \frac{h\lambda_{1n}\, e^{-\Delta S_n^*/R}\, e^{\Delta H_n^*/RT}}{2kT\lambda_n}. \tag{6}$$

Equation (6) follows on insertion of $\Delta F_n^* = \Delta H_n^* - T\Delta S_n^*$, where ΔH_n^* and ΔS_n^* are, respectively, the heat and entropy of activation for flow.

For the latex system under consideration we may assume the presence of only two types of flow units, namely, water, whose behavior may be taken as Newtonian, and the latex particles, whose flow may be non-Newtonian. For this condition Eq. [1] takes the form

$$\eta = \frac{x_1\beta_1}{\alpha_1} + \frac{x_2\beta_2}{\alpha_2}\left(\frac{\sinh^{-1}\beta_2 G}{\beta_2 G}\right) \tag{7a}$$

$$= a + b\,\frac{\sinh^{-1}\beta_2 G}{\beta_2 G} \tag{7b}$$

where

$$a = \frac{x_1\beta_1}{\alpha_1} \tag{8}$$

and

$$b = \frac{x_2\beta_2}{\alpha_2}. \tag{9}$$

The subscript 1 refers to the medium and 2 to the latex particles. From Eq. [6] β_2 becomes

$$\beta_2 = \left[\frac{h\lambda_{12}\, e^{-\Delta S_2^*/R}}{2k\lambda_2}\right]\frac{e^{\Delta H_2^*/RT}}{T}. \tag{10}$$

Again, on substitution of Eqs. [2] and [10] into Eqs. [8] and [9] we get

$$a = \left[\frac{hx_1\lambda_{11}\, e^{-\Delta S_1^*/R}}{(\lambda\lambda_2\lambda_3)_1\lambda_1}\right] e^{\Delta H_1^*/RT} \tag{11}$$

and

$$b = \left[\frac{h\lambda_{12}\, x_2\, e^{-\Delta S_2^*/R}}{(\lambda\lambda_2\lambda_3)_2\lambda_2}\right] e^{\Delta H_2^*/RT}. \tag{12}$$

Equation [7] should represent the variation of η with G at any given temperature and concentration with a set of three parameters a, b, and β_2. In turn, these parameters should be functions of volume fraction and temperature in line with Eqs. [10]–[12].

DEPENDENCE OF VISCOSITY ON SHEAR STRESS

To obtain a, b, and β_2 at any given v and T, values of β_2 were selected, the quantities $\theta = (\sinh^{-1}\beta_2 G)/\beta_2 G$ calculated for the various rates of shear at which viscosities were observed in the non-Newtonian region, and the η's plotted vs. the corresponding θ's. Adjustments were then made in β_2 until the plots became linear, in which case the slope of the line yields b, and the intercept gives a. By this procedure it was found possible to obtain satisfactory straight lines for all the available data at the various concentrations and temperatures, and to arrive at the coefficients given in Table I.

With these parameters, Eq. [7] reproduces well the $\eta - G$ curves, as

TABLE I

Parameters of Viscosity Equation for X-667 Latex

v	20.13°C.			29.94°C.			39.74°C.			50.00°C.		
	$a \times 10^2$	$b \times 10^2$	$\beta_2 \times 10^3$	$a \times 10^2$	$b \times 10^2$	$\beta_2 \times 10^3$	$a \times 10^2$	$b \times 10^2$	$\beta_2 \times 10^3$	$a \times 10^2$	$b \times 10^2$	$\beta_2 \times 10^3$
0.2990	3.04	0.507	3.87	2.46	0.390	2.94	2.03	0.327	2.26	1.70	0.261	1.73
0.3970	5.41	1.88	5.46	4.31	1.57	4.08	3.58	1.30	3.13	2.98	1.08	2.43
0.4398	7.29	4.33	6.67	5.85	3.52	5.05	4.88	2.84	3.91	4.10	2.34	2.98
0.4876	10.7	9.97	8.93	8.67	7.67	6.67	7.30	6.23	5.13	6.01	5.51	3.92
0.5390	19.3	37.0	13.5	15.7	31.6	10.2	13.0	24.1	7.81	10.8	19.7	5.95
0.5603	25.7	59.7	17.9	21.0	49.1	13.2	17.4	44.4	10.1	14.4	37.7	7.75
0.5866	43.0	148.0	27.0	37.0	113.0	20.0	31.1	91.1	15.4	26.6	75.7	11.8
0.6017	62.0	277.0	40.0	50.6	230.0	29.4	41.8	192.0	22.2	34.7	160.0	16.9

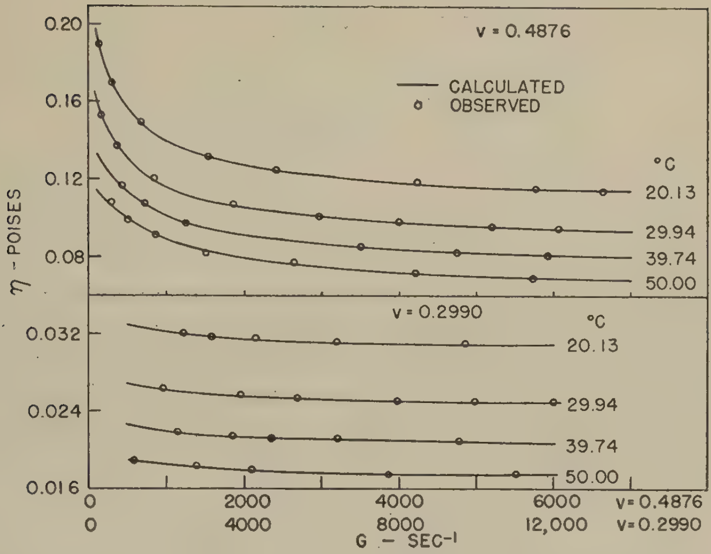

FIG. 1. Comparison of observed and calculated viscosities.

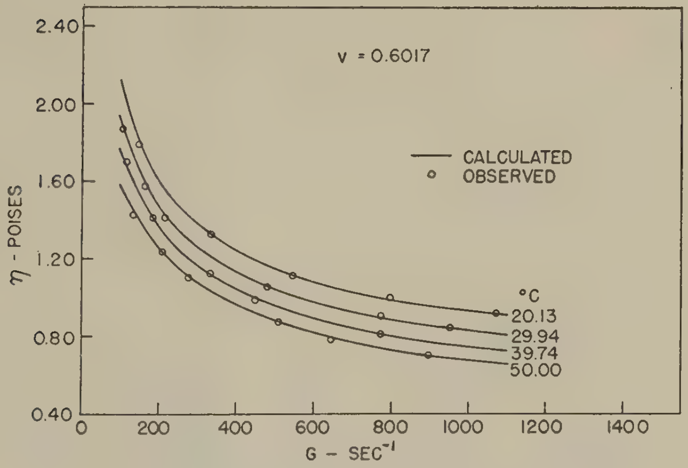

FIG. 2. Comparison of observed and calculated viscosities.

may be seen from the typical plots shown in Figs. 1 and 2. In these plots the solid curves are those given by the use of the appropriate parameters in Eq. [7], while the points are experimentally observed.

DEPENDENCE OF PARAMETERS ON CONCENTRATION

For any constant temperature it has been found possible to express the variations of the three parameters with volume fraction v by means of the relations

$$a = \frac{x_1\beta_1}{\alpha_1} = \frac{K_a}{(1 - \epsilon_a v)^2} \qquad [13]$$

$$b = \frac{x_2\beta_2}{\alpha_2} = K_b\left[\frac{(\epsilon_b v)^2}{(1 - \epsilon_b v)^3}\right] \qquad [14]$$

and

$$\beta_2 = \frac{K_\beta}{(1 - \epsilon_\beta v)}. \qquad [15]$$

In these equations the K's are constants dependent on temperature, and the ϵ's are temperature-independent constants. The values of the K's and ϵ's found are given in Table II. How well these equations reproduce the parameters as a function of v may be judged from Figs. 3–5, where the solid curves are those calculated by means of Eqs. [13]–[15], and the points correspond to the values given in Table I.

TABLE II

Values of Constants for Eqs. [13]–[15]

Temp., °C.	$K_a \times 10^8$	$K_b \times 10^3$	$K_\beta \times 10^8$	ϵ_a	ϵ_b	ϵ_β
20.13	9.42	3.98	2.08	1.453	1.490	1.572
29.94	7.66	3.30	1.53	1.453	1.490	1.572
39.74	6.24	2.88	1.20	1.453	1.490	1.572
50.00	5.19	2.41	0.920	1.453	1.490	1.572

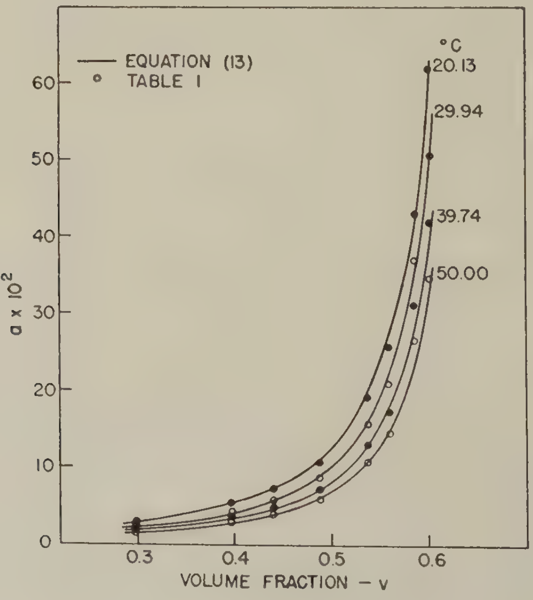

FIG. 3. Comparison of calculated and fitted a values.

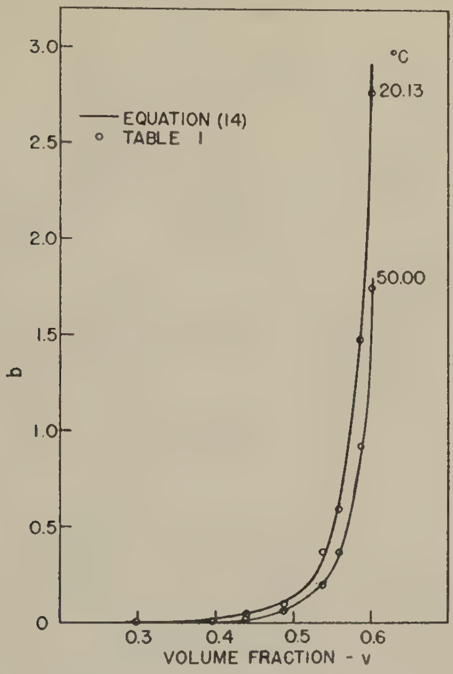

FIG. 4. Comparison of calculated and fitted b values.

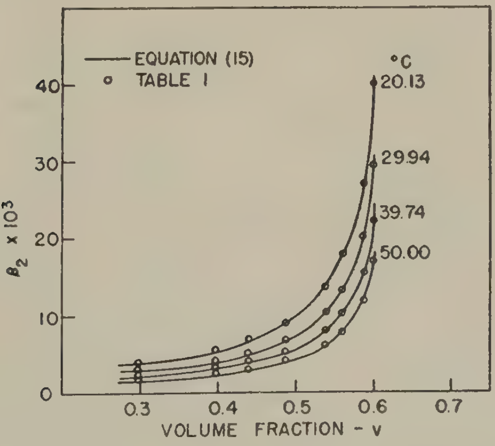

FIG. 5. Comparison of calculated and fitted β_2 values.

DEPENDENCE OF FLOW CONSTANTS ON TEMPERATURE

Comparison of Eqs. [10]–[12] with Eqs. [13]–[15] suggests that, if the quantities in the brackets of the former equations are temperature-independent, the variations of K_a, K_b, and K_β with temperature should be given by

$$K_a = K_a^0 e^{\Delta H_1^*/RT} \qquad [16]$$

or

$$\log K_a = \log K_a^0 + \frac{\Delta H_1^*}{2.303RT} \qquad [17]$$

$$K_\beta = \frac{K_\beta^0 e^{\Delta H_2^*/RT}}{T} \qquad [18]$$

or

$$\log K_\beta T = \log K_\beta^0 + \frac{\Delta H_2^*}{2.303RT} \qquad [19]$$

and

$$K_b = K_b^0 e^{\Delta H_b^*/RT} \qquad [20]$$

or

$$\log K_b = \log K_b^0 + \frac{\Delta H_b^*}{2.303RT}. \qquad [21]$$

If the ΔH^*'s are independent of temperature, it is to be expected from these equations that plots of log K_a, log K_b, and log $K_\beta T$ vs. $1/T$ should

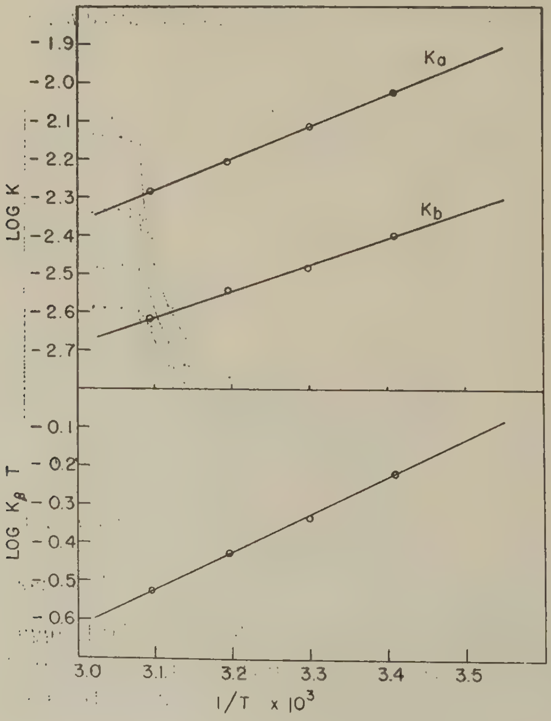

FIG. 6. Temperature dependence of K's.

TABLE III

Constants for Eqs. [16]–[21]

$\Delta H_1^* = 3780$ cal./mole	$K_a{}^0 = 0.144 \times 10^{-4}$
$\Delta H_b^* = 3110$ cal./mole	$K_b{}^0 = 0.191 \times 10^{-4}$
$\Delta H_2^* = 4530$ cal./mole	$K_\beta{}^0 = 2.55 \times 10^{-4}$

be linear, with ΔH^*'s following from the slopes and the K^0's from the intercepts. These plots, shown in Fig. 6, are in fact linear, and yield the constants listed in Table III.

It should be emphasized that this linearity indicates also that the ΔH^*'s are independent as well of concentration, i.e., that the energies of activation for flow of both the water and the latex particles remain constant over the entire range of composition of the dispersions. This fact can be confirmed through the following considerations. The parameter a gives the contribution made by the water to the observed viscosity. Consequently, on setting $v = 0$ in Eq. [13], we should get $a = K_a = \eta_0$, where η_0 is the viscosity of water at the temperature in question. Comparison of the K_a's in Table II with the viscosities of water at the various temperatures shows that these agree within 5–6%. In view of the large extrapolation, the agreement must be considered satisfactory. An even more illuminating comparison is obtained by plotting log η_0 vs. $1/T$ between 20° and 50°C. The straight line thus obtained yields $\Delta H_1^* = 3780$ cal./mole and $K_a{}^\circ = 0.150 \times 10^{-4}$. This ΔH_1^* is identical with that given in Table III, while the $K_a{}^\circ$ value is very close to the observed 0.144×10^{-4}.

However, from Eqs. [10] and [12] it is to be expected that ΔH_2^* should be identical with ΔH_b^*, whereas Table III indicates that such is not the case. This discrepancy suggests that the assumption made above, namely, that the quantities in the brackets of Eqs. [10] and [12] are temperature-independent, is not correct for at least one of these. If in Eq. [10] it is taken that ΔS_2^* is constant, then it may be expected that any temperature dependence of λ_{12}, if present, will be essentially identical to that of λ_2, and hence the entire quantity in the brackets should not depend on T. Consequently, the energy of activation derived from K_β should be that of the latex particles, or ΔH_2^* in Table III. On the other hand, whereas the quantity $(\lambda_{12}e^{-\Delta S_2^*/R}/\lambda_2)$ in Eq. [12] may be independent of T by the above argument, this may not be the case for $(\lambda\lambda_2\lambda_3)_2$, and hence ΔH_2^* will not be identical with ΔH_b^*. The difference between ΔH_2^* and ΔH_b^* observed may be reconciled by assuming that $(\lambda\lambda_2\lambda_3)_2$ varies with T according to the relation

$$(\lambda\lambda_2\lambda_3)_2 = (\lambda\lambda_2\lambda_3)_2{}^0 e^{\Delta H_3/RT} \qquad [22]$$

where ΔH_3 is a constant. On this basis Eq. [12] becomes

$$b = \left[\frac{h\lambda_{12}x_2 e^{-\Delta S_2^*/R}}{(\lambda\lambda_2\lambda_3)_2{}^0\lambda_2}\right] e^{(\Delta H_2^* - \Delta H_3)/RT} \qquad [23]$$

and hence ΔH_b^* in Eq. [20] is

$$\Delta H_b^* = \Delta H_2^* - \Delta H_3 . \qquad [24]$$

On substitution of the values of ΔH_b^* and ΔH_2^* from Table III, we obtain $\Delta H_3 = 1420$ cal./mole.

The dependence of $(\lambda\lambda_2\lambda_3)_2$ on temperature observed here is different from that found by Ree and Eyring (1) for solid plastics. In the latter instance the volume of the flow unit varied linearly with T, making thus α_n independent of temperature. Here, however, the volume of the latex flow unit appears to vary according to Eq. [22], and hence α_2 will not be independent of the temperature.

COMPLETE EQUATIONS FOR FLOW PARAMETERS

On assembly of the various equations and constants, we can finally represent the parameters a, b, and β_2 as functions of v and T by the following relations:

$$a = \left[\frac{K_a^0}{(1 - \epsilon_a v)^2}\right] e^{\Delta H_1^*/RT} \qquad [25]$$

$$b = \left[\frac{K_b^0(\epsilon_b v)^2}{(1 - \epsilon_b v)^3}\right] e^{\Delta H_b^*/RT} \qquad [26]$$

and

$$\beta_2 = \left[\frac{K_\beta^0}{(1 - \epsilon_\beta v)}\right] \frac{e^{\Delta H_2^*/RT}}{T} . \qquad [27]$$

From these equations it follows that when $v = 0$, $a = \eta_0 = K_a^0 e^{\Delta H_1^*/RT}$, $b = 0$, and $\beta_2 = \frac{K_\beta^0 e^{\Delta H_2^*/RT}}{T}$. Again, when $\epsilon v = 1$, all these quantities go to infinity. Consequently between $v = 0$ and $\epsilon v = 1$ the range of variation of these quantities is a from $\eta_0 \rightarrow \infty$; b from $0 \rightarrow \infty$; and β_2 from $\frac{K_\beta^0 e^{\Delta H_2^*/RT}}{T} \rightarrow \infty$.

FLOW OF LATEX IN NEWTONIAN REGION

Maron and Fok (3) have found that the latex under discussion showed Newtonian flow up to a concentration of ca. $v = 0.25$. From the above equations giving the parameters as functions of v, it should be possible to calculate the viscosities in the Newtonian region even though the parameters were evaluated from the non-Newtonian flow data above $v = 0.25$.

For the case where both the water and the latex particles are Newtonian, $\sinh^{-1}\beta_2 G/\beta_2 G = 1$, and Eq. [7] becomes

TABLE IV

Comparison of Calculated and Observed Relative Viscosities in Newtonian Region

Volume fraction v	Relative Viscosity, η_r							
	20.13°C.		29.94°C.		39.74°C.		50.00°C.	
	Calc.	Obs.	Calc.	Obs.	Calc.	Obs.	Calc.	Obs.
0.0000	1.00	1.00	1.00	1.00	1.00	1.00	1.00	1.00
0.0306	1.10	1.09	1.10	1.09	1.10	1.09	1.10	1.10
0.0515	1.17	1.16	1.17	1.16	1.17	1.17	1.17	1.18
0.1010	1.39	1.36	1.39	1.36	1.39	1.37	1.39	1.38
0.1795	1.91	1.82	1.91	1.85	1.91	1.84	1.92	1.85
0.2481	2.67	2.48	2.68	2.49	2.69	2.53	2.70	2.53

$$\eta = a + b. \qquad [28]$$

Hence on substitution of Eqs. [25] and [26] for a and b we get

$$\eta = \left[\frac{K_a^0}{(1 - \epsilon_a v)^2}\right] e^{\Delta H_1{}^*/RT} + \left[\frac{K_b^0(\epsilon_b v)^2}{(1 - \epsilon_b v)^3}\right] e^{\Delta H_b{}^*/RT}. \qquad [29]$$

Again, $\eta_0 = K_a^0 e^{\Delta H1^*/RT}$. Consequently, the relative viscosity, η_r, is given by

$$\eta_r = \frac{\eta}{\eta_0} = \frac{\left[\dfrac{K_a^0}{(1 - \epsilon_a v)^2}\right] e^{\Delta H_1{}^*/RT} + \left[\dfrac{K_b^0(\epsilon_b v)^2}{(1 - \epsilon_b v)^3}\right] e^{\Delta H_b{}^*/RT}}{K_a^0 e^{\Delta H_1{}^*/RT}}$$

$$= \frac{1}{(1 - \epsilon_a v)^2} + \frac{B(\epsilon_b v)^2}{(1 - \epsilon_b v)^3}, \qquad [30]$$

where

$$B = \frac{K_b^0}{K_a^0} e^{(\Delta H_b{}^* - \Delta H_1{}^*)/RT}. \qquad [31]$$

Table IV gives a comparison of the relative viscosities measured by Maron and Fok (3) with those calculated by Eq. [30]. The agreement is in general satisfactory.

LIMITING CONDITIONS FOR FLOW

(*a*) $\beta_2 G \rightarrow 0$: When $\beta_2 G \rightarrow 0$, $\theta = \sinh^{-1}\beta_2 G/\beta_2 G \rightarrow 1$, and Eq. [7*b*] reduces to $\eta = a + b$, i.e., the flow becomes Newtonian. This condition can be attained when either β_2 or G becomes very small. Since β_2 decreases rapidly with lowering of concentration, Newtonian flow will set in when v is decreased sufficiently to meet the above condition. With synthetic latices of various types it has been observed that the flow is Newtonian at volume fractions below *ca.* 0.25, and hence at $v = 0.25$ and below β_2 is sufficiently small to make θ essentially equal to unity over the entire range of G values used in the various studies.

However, even though β_2 may not be small, it is possible to keep β_2G small by keeping G low. Under such conditions the flow at volume fractions above 0.25 will become Newtonian as G approaches zero. This transition from non-Newtonian to Newtonian flow on decrease of G at the higher concentrations has been observed by Maron and Belner (4).

(*b*) $\beta_2G \rightarrow \infty$: When $\beta_2G \rightarrow \infty$, $\theta \rightarrow 0$, and by Eq. [7*b*] $\eta = a$, i.e., the flow becomes Newtonian, and the viscosity is due entirely to solvent. This is true only when $G \rightarrow \infty$ and not when $\beta_2 \rightarrow \infty$, as will be seen below. Such behavior at high shear rates has been observed in many colloidal systems, including latex (5), and has been predicted by Ostwald and Auerbach (6).

(*c*) $v \rightarrow 0$: If the divisions indicated in Eq. [30] are performed, then we obtain on collection of terms

$$\eta_{sp} = \eta_r - 1 = 2\epsilon_a v + (3\epsilon_a^2 + B\epsilon_b^2)v^2 + (4\epsilon_a^3 + 3B\epsilon_b^3)v^3 + \cdots \quad [32]$$

In Eq. [32] v is the volume fraction of the latex particles only, and not of these plus the adsorbed soap which they carry, namely, v_t. The relation between v_t and v is, as shown by Maron, Madow, and Krieger (7), $v_t = \gamma v$, where γ depends on the length of the adsorbed soap molecule and the volume-to-surface average diameter of the latex particles. For the X-667 latex in question $\gamma = 1.119$. On substitution of $v = v_t/\gamma$ into Eq. [32], we get

$$\frac{\eta_{sp}}{v_t} = \frac{2\epsilon_a}{\gamma} + \left(\frac{3\epsilon_a^2 + B\epsilon_b^2}{\gamma^2}\right)v_t + \left(\frac{4\epsilon_a^3 + 3B\epsilon_b^3}{\gamma^3}\right)v_t^2 + \cdots \quad [33]$$

When $v_t \rightarrow 0$,

$$\left(\frac{\eta_{sp}}{v_t}\right)_{v\rightarrow 0} = \frac{2\epsilon_a}{\gamma} \quad [34]$$

or $2\epsilon_a/\gamma = 2(1.453)/1.119 = 2.60$. This result agrees well with the predicted Einstein value of 2.50 for the limiting value of (η_{sp}/v) for suspensions of spheres.

Equation [33] also predicts that the values of the higher coefficients will depend on the ϵ's and B. Since ϵ_a and ϵ_b both are functions of the type of packing of the spheres and the particle size distribution, the values of the coefficients of v should also depend on these factors. Further, since B, Eq. [33], involves T, they should also depend somewhat on the temperature. The values of the second coefficient calculated between 20° and 50°C. range from 5.76 to 5.84, and those of the third coefficient range from 11.6 to 11.9.

(*d*) $\epsilon v \rightarrow 1$: When $\epsilon v \rightarrow 1$, then according to Eqs. [25] and [26] a and b both become infinite, and so does the viscosity. At the same time β_2 also goes to infinity. The volume fraction of polymer at which this occurs is $v = 1/\epsilon$, and the total volume fraction of polymer plus adsorbed soap is $v_t = \gamma/\epsilon = 1.119/\epsilon$. Substituting the values of ϵ_a, ϵ_b, and ϵ_β, we obtain for v_t 0.77, 0.75, and 0.71. For rhombohedral close packing of uniform spheres v_t at which $\eta = \infty$ should be 0.74, and slightly higher than this for nonuniform spheres. The results obtained are in good agreement with these expectations.

EVALUATION OF "MOLECULAR" PARAMETERS

On comparison of Eqs. [8], [11], and [25] it is seen that

$$\left(\frac{x_1\beta_1}{\alpha_1}\right)_{\text{red.}} = \frac{K_a^{\;0}}{(1-\epsilon_a v)^2} = \frac{x_1 h\lambda_{11} e^{-\Delta S_1{}^*/R}}{(\lambda_2\lambda_3)_1\lambda_1{}^2}, \tag{35}$$

where red. represents the quantity reduced for temperature dependence. Similarly we get from Eqs. [9], [12], [23], and [26]

$$\left(\frac{x_2\beta_2}{\alpha_2}\right)_{\text{red.}} = \frac{K_b^{\;0}(\epsilon_b v)^2}{(1-\epsilon_b v)^3} = \frac{x_2 h\lambda_{12} e^{-\Delta S_2{}^*/R}}{(\lambda\lambda_2\lambda_3)_2{}^0\lambda_2} \tag{36}$$

and from Eqs. [10] and [27]

$$(\beta_2)_{\text{red.}} = \frac{K_\beta^{\;0}}{(1-\epsilon_\beta v)} = \frac{h\lambda_{12} e^{-\Delta S_2{}^*/R}}{2k\lambda_2}. \tag{37}$$

Before anything further can be done with these equations, it is necessary to obtain x_1 and x_2.

(*a*) *Evaluation of* x_1 *and* x_2.[1] Consider a volume V of the dispersion, containing n spherical particles of average radius R. Let this volume be rectangular in cross section with total area A_t and height L. If we pass through this volume an arbitrary plane parallel to the base, then the probability that the plane will pass through a particle of the disperse phase at a distance between r and $r + dr$ from the center of the particle is $2dr/L$. Again, the area cut through the sphere by the plane is $\pi(R^2 - r^2)$. Hence the average area per particle cut by the drawn plane is

$$A_{\text{av.}} = \int_0^R \frac{2\pi(R^2 - r^2)\,dr}{L} = \frac{4\pi R^3}{3L} = \frac{4\pi R^3 A_t}{3V}$$

since $V = A_t L$. $A_{\text{av.}}$ is the area occupied by a single particle of disperse phase in the plane. The total area occupied by the particles in the plane s then $nA_{\text{av.}}$, and this divided by the total area of the plane, A_t, gives then x_2, namely,

$$x_2 = \frac{nA_{\text{av.}}}{A_t} = \frac{n}{A_t}\left[\frac{4\pi R^3 A_t}{3V}\right] = \frac{4/3\pi R^3 n}{V}.$$

[1] The authors are indebted to Prof. I. M. Krieger for suggesting the derivation which follows.

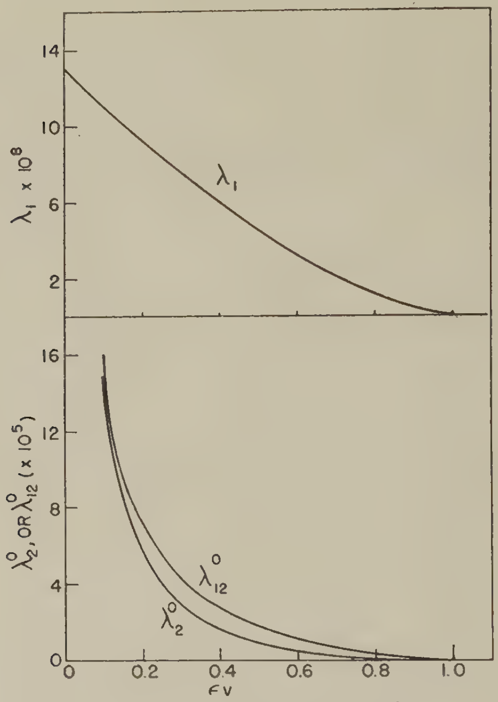

FIG. 7. Dependence of λ_1, $\overset{0}{\lambda_2}$, and $\overset{0}{\lambda_{12}}$ on ϵv.

The right-hand side of this equation is also the expression for the volume fraction, v. Consequently, $x_2 = v$, and $x_1 = (1 - v)$.

However, x_2 cannot take on all values of v from zero to unity, since when $\epsilon v \rightarrow 1$ the particles touch, and the entire shear stress is carried by the disperse phase. This fact suggests that $x_2 = \epsilon v$ rather than v, and that $x_1 = (1 - \epsilon v)$. Since the values of the various ϵ's are fairly close to each other, no distinction will be made among them below.

(*b*) *Water*. On substituting $x_1 = (1 - \epsilon v)$ into Eq. [35] and solving for λ_1, we get

$$\lambda_1 = \left[\frac{h\lambda_{11}e^{-\Delta S_1^*/R}}{(\lambda_2\lambda_3)_1 K_a{}^\circ}\right]^{1/2} (1 - \epsilon v)^{3/2}. \qquad [38]$$

Since Glasstone, Laidler, and Eyring (8) have shown that for water $\Delta H_v = 2.45\ \Delta F_1^*$, where ΔH_v is the heat of vaporization of water and ΔF_1^* the free energy of activation for its flow, use of this relation along with ΔH_1^* yields $\Delta S_1^* = -0.71$ e.u./mole between 20° and 50°C. Again, λ_{11} may be taken as the diameter of a water molecule, 3.92×10^{-8} cm., while $(\lambda_2\lambda_3)_1$, the diameter squared. On this basis

$$\lambda_1 = 13.0 \times 10^{-8}(1 - \epsilon v)^{3/2} \text{ cm.} \qquad [39]$$

At the top of Fig. 7 is shown a plot of λ_1 vs. ϵv. This quantity varies from 13.0 A., i.e., approximately three molecular diameters, for pure water to zero at $\epsilon v = 1$, where flow ceases.

(*c*) *Polymer Particles.* Division of Eq. [36] by [37] yields

$$\left(\frac{x_2}{\alpha_2}\right)_{\text{red.}} = \frac{2kx_2}{(\lambda\lambda_2\lambda_3)_2^0} = \frac{K_b^0}{K_\beta^0}\frac{(\epsilon v)^2}{(1-\epsilon v)^2} \qquad [40]$$

from which, on substitution of $x_2 = \epsilon v$, we obtain

$$(\lambda\lambda_2\lambda_3)_2^0 = \frac{2kK_\beta^0}{K_b^0}\frac{(1-\epsilon v)^2}{\epsilon v} \qquad [40a]$$

$$= 3.68 \times 10^{-15}\frac{(1-\epsilon v)^2}{\epsilon v}. \qquad [40b]$$

$(\lambda_2\lambda_3)_2$, the cross-sectional area of the latex particle flow unit, may be taken to be D^2, where $D = D_s + 2(27.5) = 1440$ A. Here D_s is the volume-to-surface average particle diameter, and 27.5 A. is the length of the adsorbed potassium oleate molecule. Thus λ_2^0 becomes

$$\lambda_2^0 = \frac{2kK_\beta^0}{D^2K_b^0}\frac{(1-\epsilon v)^2}{\epsilon v} \qquad [41a]$$

$$= 1.78 \times 10^{-5}\frac{(1-\epsilon v)^2}{\epsilon v}, \qquad [41b]$$

from which, by Eq. [22], λ_2 follows as

$$\lambda_2 = \lambda_2^0 e^{\Delta H_3/RT} = 1.78 \times 10^{-5}\frac{(1-\epsilon v)^2}{\epsilon v} e^{\Delta H_3/RT}. \qquad [42]$$

The exponential term in the last relation is equal to 11.47 at 20.13°C., 10.59 at 29.94°C., 9.84 at 39.74°C.; and 9.15 at 50.0°C. The plot of Eq. [41], given in Fig. 7, shows that λ_2^0 decreases from infinity at $v = 0$ to zero at $\epsilon v = 1$. These limits also apply to λ_2.

As will be shown below, $\lambda_{12} = \infty$ when $v = 0$, and this is also true of λ_2. Consequently $(\beta_2)_{\text{red.}}$, which is equal to K_β^0 at $v = 0$, must become by Eq. [37]

$$K_\beta^0 = \frac{h}{2k} e^{-\Delta S_2^*/R}, \qquad [43]$$

from which we get $\Delta S_2^* = -32.1$ e.u./mole. Substituting this value of ΔS_2^* and Eq. [42] for λ_2 into Eq. [37], we obtain

$$\lambda_{12} = 1.78 \times 10^{-5}\left(\frac{1-\epsilon v}{\epsilon v}\right) e^{\Delta H_3/RT}, \qquad (44)$$

or

$$\lambda_{12}^0 = \frac{\lambda_{12}}{e^{\Delta H_3/RT}} = 1.78 \times 10^{-5}\left(\frac{1-\epsilon v}{\epsilon v}\right). \qquad [45]$$

The plot of λ_{12}^0 vs. ϵv, given in Fig. 7, shows that λ_{12}^0 like λ_2^0 varies from infinity at $v = 0$ to zero at $\epsilon v = 1$, but its rate of decrease is not as rapid as that of λ_2^0; i.e., at intermediate concentrations the distance between shear planes of latex particles is larger than the distance between equilibrium positions occupied by the latex particles. When $\epsilon v = 1$ the particles touch, and hence the distance between them is reduced to zero, as is, also, the distance between equilibrium positions.

ACKNOWLEDGMENT

The work described herein was performed as part of the synthetic rubber research project sponsored by the National Science Foundation.

SUMMARY

The generalized flow theory of Ree and Eyring has been applied successfully to the extensive data of Maron and Fok (3) on the flow behavior of X-667 latex in both the Newtonian and non-Newtonian regions. By postulation of the presence of two flow units, a Newtonian water unit and a latex particle flow unit which may be non-Newtonian, an equation involving three parameters was obtained which reproduced very well dependence of the viscosity on rate of shear at all temperatures and concentrations. Further, the theory predicted the correct dependence of the parameters on temperature, from which could be obtained the heats of activation for flow of both the water and latex particles. Both heats of activation were found to be independent of concentration, with that of the water being the same as for the pure liquid.

The theory does not predict the concentration dependence of the parameters. However, empirical equations for such dependence were deduced, from which it was possible to ascertain the values of the parameters in the Newtonian range below a volume fraction $v = 0.25$, and to calculate therefrom Newtonian relative viscosities in good agreement with the observed ones at all temperatures and concentrations. Further, on extrapolation to $v = 0$, η_{sp}/v_t was found to be 2.60 as against the expected Einstein value of 2.50 for suspensions of spheres, while extrapolation to infinite viscosity gave a volume fraction in very good agreement with that expected for the rhombohedral close packing of nonuniform spheres.

From the combination of the theoretical and empirical equations were obtained also expressions for the values of the "molecular" parameters of the theory as functions of temperature and concentration, and the entropy of activation for the flow of the latex particles. The distance between equilibrium positions of the water molecules was found to vary from 13 A. to zero between $v = 0$ and the volume fraction at which the viscosity becomes infinite. On the other hand, the distances between equilibrium posi-

tions and planes of latex particles varied from infinity to zero between the same concentration limits.

REFERENCES

1. REE, T., AND EYRING, H., *J. Appl. Phys.* **26,** 793 (1955).
2. REE, T., AND EYRING, H., *J. Appl. Phys.* **26,** 800 (1955).
3. MARON, S. H., AND FOK, S. M., *J. Colloid Sci.* **10,** 482 (1955).
4. MARON, S. H., AND BELNER, R. J., *J. Colloid Sci.*, in press.
5. MARON, S. H., AND SISKO, A. W., Unpublished results.
6. OSTWALD, W., AND AUERBACH, R., *Kolloid-Z.* **38,** 261 (1926).
7. MARON, S. H., MADOW, B. P., AND KRIEGER, I. M., *J. Colloid Sci.* **6,** 584 (1951).
8. GLASSTONE, S., LAIDLER, K. J., AND EYRING, H., "The Theory of Rate Processes," p. 492. McGraw-Hill, New York, 1941.

JOURNAL OF COLLOID SCIENCE 11, 96–106 (1956)

THE LIESEGANG PHENOMENON

II. ADDITION OF PROTECTING AGENTS

A. Packter*

Clay Development Laboratory, F. W, Berk & Co., London Colney, Herts, England.

Received March 2, 1955; revised July 7, 1955

ABSTRACT

The present work demonstrates that the formation of clearly defined rhythmicity is intimately related to the stability of the sol prior to precipitation. The various factors affecting this stability have been analyzed for their effect on the periodicity. It is shown that excess silver ion causes rapid flocculation and blurred precipitation zones. On the other hand, the spacing coefficient is shown to increase in the presence of peptizers for the precipitated substance.

The periodicity observed in gels may be used as a method for investigating the stability of colloidal sols.

INTRODUCTION

When rhythmic precipitation occurs in a gel medium, the position of the rings of precipitate follow a geometric progression law, $x_n = ak^n$, where x_n is the position of the nth ring, from the origin of diffusion; a and k are constants, k being known as the spacing coefficient. Previous work (2) has shown that sol protection (by adsorption) and diffusion are important factors in the rhythmic precipitation, and the spacing is related to the initial concentration (C_0) of the diffusion cation, according to the relation,

$$(k - 1) = A + B/C_0,$$

where the constant A is a measure of this former effect. When any of the reacting ions is removed from the system by adsorption or complex formation, an increase in A should follow.

This effect has been studied with silver, copper, and lead salts peptized by ammonia, and simple organic acids. Rhythmic precipitation has been followed, using two methods: (a) by diffusion of the reacting *anion* into the gel containing the complex metal ammonia ion; (b) by diffusion of the reacting *cation* into the gel containing the anion, together with the protecting agent. We have found with both methods that for a given cation-anion ratio, B remains constant, whereas A increases with the protecting agent-sol ratio, according to a Freundlich relation. A parallelism is observed in the increase in A, on the one hand, and the stability of the corresponding sols in aqueous suspension, on the other.

---

* Present address: Glaxo Laboratories Ltd., Greenford, Middlesex, England.

Many salts, hitherto leading to unclear stratification, now give a well-defined periodic behavior, and the rhythmicity can be investigated with a higher degree of accuracy. The quantitative study of rhythmic precipitation may be used to define and measure the stability of the sols of such insoluble precipitates as have been studied in this work.

Experimental

1. *Sols in Aqueous Solution*

a. Addition of Ammonia. The peptization of silver and copper salts by ammonia, and the stability of the peptized sols in presence of excess of the reacting ions, have been investigated.

An aqueous solution of the reacting cation is added to an equal volume of solution of the reacting anion, with increasing proportions of ammonia. The stability of the sol obtained in aqueous solution and in 5% gelatine suspension is observed.

The onset of turbidity in these systems generally occurs within a very narrow time limit (e.g., 1 sec. in 1000 sec.) and coagulation, concurrent with optimum turbidity, has been determined visually. The sol stability is defined as t, the time of coagulation, between the mixing of the two solutions and the appearance of the optimum turbidity (1). The effect of added protecting agents on the stability has been investigated by following the *peptization ratio* $C_p{}^*/C_s$, where $C_p{}^*$ is the concentration of protecting agent that causes complete peptization of the equivalent sol, and C_s is the sol concentration. (All C values are expressed in gram equivalents per liter.) Complete peptization occurs when a system is obtained which is stable for over 24 hours and which shows no visible light scattering or turbidity and no variation in color during this period.

(1) The peptization ratios of equivalent sols. The peptization ratio generally remains constant for the salts examined for the sol concentration range, 0.0005 M–0.01 M, and varies markedly with the nature of the precipitated salt.

It is seen from Table IA that the peptization ratio is greatest for the silver salt of least solubility, and increases in the order oxalate, chromate, phosphate, arsenate, chloride, bromide. The values observed, however, are not in agreement with those derived from application of the mass action law to the equilibrium,

$$Ag^+ + 2NH_3 \leftrightarrow [Ag\cdot 2NH_3]^+$$

with the instability constant, $K = 6.8 \times 10^{-8}$.

The peptization ratio in 5% gelatine suspensions is increased for silver

TABLE IA

Peptization Ratios of Precipitates for Sol Concentration Range 0.0005 M–0.01 M

	Aqueous solution	5% gelatine suspension
Silver oxalate	2.0	2.5
Silver chromate	2.5	3.0
Silver phosphate	5.0	6.0
Silver arsenate	6.0	8.0
Silver chloride	25.0	25.0
Silver bromide	>100	>100
Copper phosphate	2.0	—
Copper arsenate	2.0	—
Copper chromate	2.0	—

TABLE IB

Peptization Ratios

(Complex copper salts)

	0.00125 *M*	0.0025 *M*	0.005 *M*	0.01 *M*
Copper pyridine thiocyanate	0.4	0.7	1.0	2.0
Copper chromate basic	6.0	8.0	8.0	8.0
Copper oxinate	100	500	>1000	>1000

salts owing to the uptake of ammonia by the gelatine. Copper salts, on the other hand, are *completely peptized* by 5% suspensions of alkaline gelatine at pH 11 without any further addition of ammonia.

In the case of complex or chelate copper compounds, the peptization ratio increases with the sol concentration, as shown in Table I*B*.

(*2*) *The stability of equivalent sols to excess of reacting ions.* Although the stability of the equivalent sols as measured by coagulation time is marked at the peptization ratio (time for turbidity, $t = 24$ hr.), rapid flocculation is observed when the ammonia present in the system is 0.8–0.9 of this value. The poor stability of such systems is due to the presence of free cation.

In the same way, fully peptized silver salt sols may be flocculated when an excess of silver is present, of about 1.1–1.3, depending on the nature of the salt. It therefore appears that although a good stability of silver salt sols may be obtained in the presence of ammonia, these sols are readily flocculated by an excess of silver ion. (This result accounts for the lack of rhythmicity and the flocculation observed whenever silver nitrate is diffusing into a gel containing the reacting anion in the presence of ammonia.)

The fully peptized sols at equivalent anion-cation ratio are, however, much less sensitive to excess anion. It is found that flocculation is observed only when the anion concentration is over 100 times the equivalent ratio. On the other hand, when the degree of peptization, and hence the stability of the sol, is decreased by reducing the ammonia concentration by

5%–25%, it is found that the flocculating effect of the anion may be readily observed. (Refer to Fig. 1 for 0.005 M silver chromate systems.) At any ammonia-sol concentration ratio (C_{NH_3}/C_s), the stability decreases with excess anion concentration, according to the Tuller-Fulmer relation (5),

$$\log_{10} t = \log_{10} t_0 - b\bar{C}_A/C_c \qquad [1]$$

where $\bar{C}_A/C_c$ is the excess anion-cation concentration ratio; and t_0 is the stability of the equivalent sol (for which $\bar{C}_A/C_c$ is zero). The symbol b is a constant that represents the fall in stability at unit excess anion concentration, varies inversely as the ease of destabilization of the ammonia peptized sol, and increases rapidly with fall in C_{NH_3}/C_s below the peptization ratio, according to the relation, $b = \beta(C_{NH_3}/C_s)^{-m}$. Rapid coagulation (at $t = 1$ sec.) occurs at some particular $\bar{C}_A/C_c$ value that mainly depends on the value of $(1/b)$. The results shown in Table II exemplify the type of behavior observed with 0.01 N silver salt sols.

It follows that the sols obtained by this method are less readily flocculated by excess anion than by excess cation. In other words, their sta-

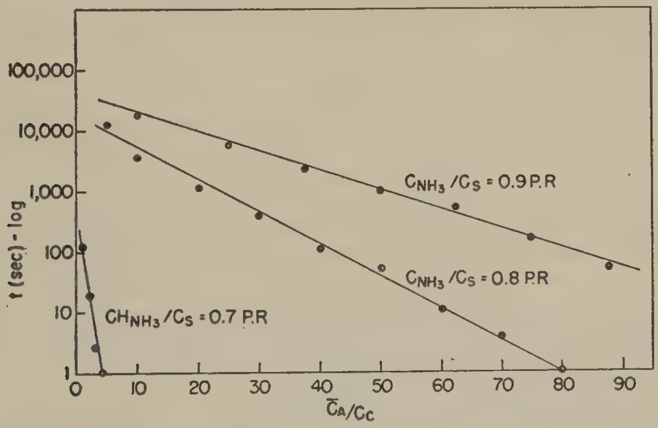

FIG. 1. Flocculation of ammonia peptized 0.005 M silver chromate sols by excess anion. Variation in stability with excess anion-cation concentration ratio.

TABLE II

Excess Anion-Cation Concentration Ratio for Rapid Coagulation (turbidity in 1 sec.)

Ammonia/silver ion concentration ratio	Chromate	Oxalate	Chloride
0.95 P.R.	>100	35	15
0.90	>100	2	1.5
0.85	>100	<0.1	<0.1
0.80	80	<0.1	<0.1
0.75	4	<0.1	<0.1

bility is greater, and the study of rhythmic precipitation according to method (*a*) should lead to a quantitative investigation of the periodicity and the effects of the diffusing flocculating ion.

b. Addition of Organic Acids. Silver, copper, and lead salts are peptized by a large number of simple organic acids and anions (1).

The order of protecting power for a series of acids may vary from salt to salt for a particular metal cation, but generally the following results have been observed.

Silver salts. Dicarboxy acids > chelating acids > nonchelating acids.

Copper salts. Amino acids > hydroxy and dicarboxy acids > nonchelating acids.

Lead salts. Dicarboxy acids > hydroxy acids > amino acids.

Excess cation flocculates the organic acid peptized sols; and the stability falls according to the Tuller-Fulmer relation (Eq. [1]).

1. *Rhythmic Precipitation in Gel Systems*

a. Peptization by Ammonia. The rhythmic precipitation of the above silver and copper salts protected by ammonia has been followed in test tubes by diffusing solutions of the *anion* into 5% gelatine gel containing 0.01 M silver nitrate or 0.005 M copper sulfate, with increasing concentrations of ammonia.

In all instances the spacing coefficient (k) varies with the initial concentration (C_0) of the diffusing anion, according to the relation (*cf.* ref. 2)

$$(k - 1) = A + B/C_0 . \qquad [2]$$

In this relation, B/C_0 represents the diffusion effects that vary inversely as C_0 ; and A measures the contribution of the sol protection by the gel medium.

Increasing the concentration (C_p) of the protecting agent maintains B constant, while A increases rapidly, up to a limiting value (Figs. 2*A*, 2*B*) when complete peptization is attained.

The increase observed follows the relation

$$\Delta A = (A_c - A_0) = \alpha[C_p/C_s]^n \qquad [3]$$

where A_0 is the A value in the absence of ammonia, and A_c is the A value at concentration C_p of ammonia. The symbols α and n are constants: α is the increase in A for $C_p/C_s = 1$. C_s is the sol concentration.

Using silver salts (Fig. 1), the increase in A for a given C_p/C_s ratio as measured by α is greatest for the oxalate and decreases in the same order as has been found in aqueous systems for the protection of the corresponding salt by ammonia. The values of n may vary over a wide range from 0.3 to 2.0.

b. Peptization by Organic Acids. The rhythmic precipitation has been

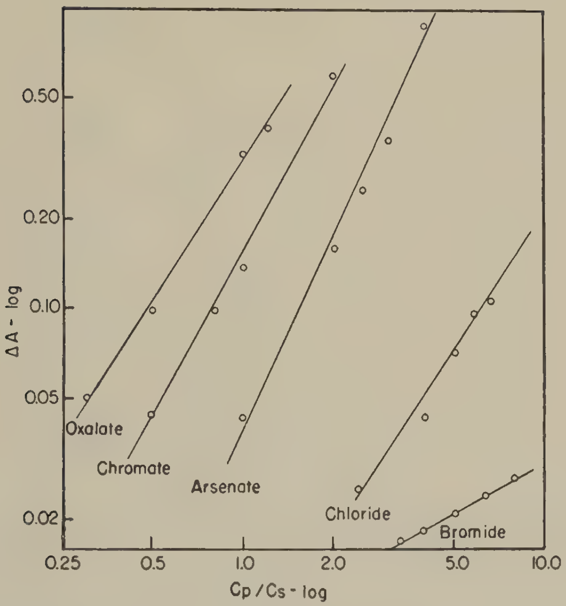

FIG. 2A. Precipitation of 0.01 *N* silver salts by excess anion (*N* solution), in 5% gelatine gels. Variation in spacing with ammonia-silver ion concentration ratio.

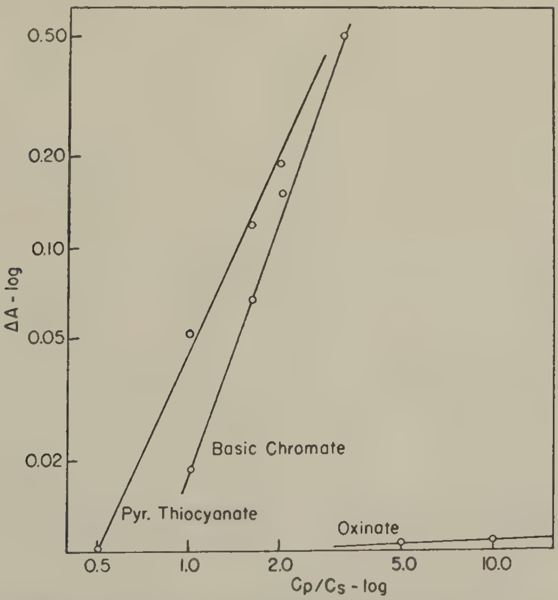

FIG. 2B. Precipitation of 0.01 *N* cupric salts, by excess anion (*N* solution), in 5% gelatine gels. Variation in spacing with ammonia-cupric ion concentration ratio.

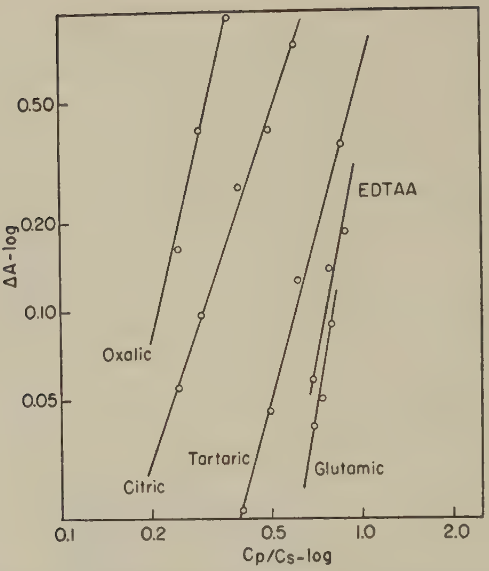

FIG. 3. Precipitation of 0.05 M silver chromate in 5% gelatine gels (0.003 M Cl′). Variation in spacing with acid-silver ion concentration ratio.

followed by causing solutions of the cation to diffuse into gelatine and agar gels, containing the anion together with increasing concentration of the protecting agent.

The spacing coefficient varies with the initial concentration (C_0) of the diffusing cation according to the relation (ref. 2)

$$(k - 1) = A + B/C_0 .$$

Increasing the concentration (C_p) of protecting agent maintains B constant, while A increases as in Eq. [1].

We have shown in a previous work (1) that the increase in stability, as measured by coagulation time of the corresponding aqueous sol on addition of protecting agent, is also a function of C_p/C_s . Hence the values of ΔA for a particular system are directly related to the stability of this sol.

The onset of complete peptization in gel systems, however, is not related to some specific sol stability (of, e.g., 24 hr.). Other factors which affect the rate of crystal growth may lead to nonappearance of precipitate, at relatively low A values.

(1) Silver salts in gelatine. The protecting effect of a series of organic acids has been followed on the 0.005 M Ag_2CrO_4 system, precipitated in 5% Coignet gelatine gels (0.003 M to Cl′). The increase in spacing is partly due to the fall in pH of the gelatine (2). The values of ΔA, corrected for this factor, are presented in Fig. 3.

(2) Silver salts in agar. The addition of citric or glutamic acid to 1%

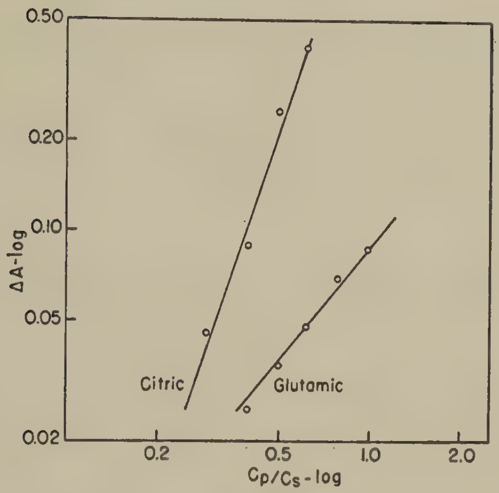

FIG. 4. Precipitation of 0.005 M silver chromate in 1% agar gels (0.001 M Cl′). Variation in spacing with acid-silver ion concentration ratio.

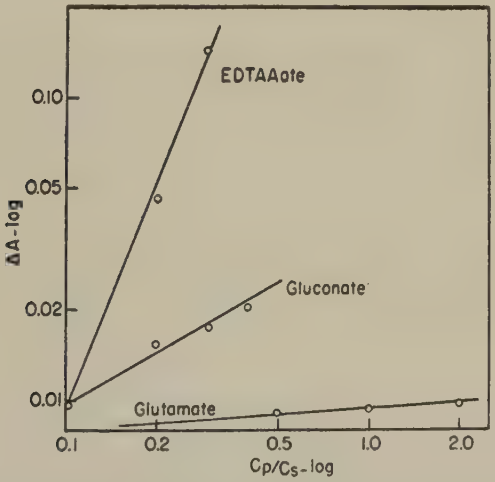

FIG. 5. Precipitation of 0.005 M lead iodide (basic) in 5% gelatine gels. Variation in spacing with anion-lead ion concentration ratio.

agar gels (0.001 M to Cl′) leads to rhythmic precipitation of 0.005 M silver chromate, in rings of small black crystals. Values of ΔA are presented in Fig. 4.

(3) *Lead salts in gelatine.* Lead iodide is precipitated in gelatine gels as a series of rings separated by opaque yellow sol and the rhythmicity can be followed only by complicated photoelectric techniques (3). Addition of organic anions (at pH > 8) leads to the well-defined rhythmic precipita-

tion of basic lead iodide, as a series of thick yellow rings, separated by clear colorless sol.

The ΔA values are presented in Fig. 5 for the 0.005 M system.

In all cases, the increase in A for any value of C_p/C_s follows the order of peptization of the corresponding aqueous sol.

DISCUSSION

We have shown in a previous work (1) that peptization of insoluble metal salts by organic acids and anions is due to adsorption of these protecting agents onto the micelle of the *metal salt sol* rather than to withdrawal of free *cation* to form a metal ion-organic acid complex; the concentration of protecting agent required for complete peptization is not found to vary stoichiometrically with the concentration of the reacting anion. The negatively charged gelatine and organic acid protected sols are in turn coagulated by excess cation; the excess cation preferentially removes part of the peptizer and the fall in stability of the aqueous suspensions varies with excess cation concentration according to the relation proposed by Tuller and Fulmer (5) for the coagulation of sols of silver salts, ferric oxide, etc.

The peptization ratios for insoluble metal salt systems "protected" by ammonia (presented in Tables I*A* and I*B*), although following the order of the saturation solubilities in distilled water, are also not related in any simple way to the values derived by application of the mass action law to the equilibrium,

$$Ag^+ + 2NH_3 \leftrightarrow [Ag \cdot 2NH_3]^+$$

The experimental data indicate that peptization by ammonia is caused by complex formation with the insoluble copper or silver *salt* (MX) according to the equilibrium,

$$MX + aNH_3 \leftrightarrow [M \cdot aNH_3]X,$$

followed by protection of the complex metal salt sol by adsorption of further ammonia, as proposed by Dey (6). The decrease in stability of the positively charged ammonia peptized sols also varies with excess anion concentration according to the Tuller-Fulmer relation; and this result demonstrates that coagulation occurs by preferential discharge of the adsorbed ammonia by the excess anion. The increase in b values with fall in the ammonia-salt concentration ratio shows that discharge by anion occurs more readily as the amount of adsorbed ammonia is reduced.

Two factors determine the spacing in rhythmic precipitation: diffusion, on the one hand, and adsorption and subsequent stabilization of a sol on the other; and the rhythmicity is mainly defined by the constant A in the spacing relation discussed in an earlier work (2),

$$(k - 1) = A + B/C_0 .$$

As we have previously shown (1), the increase in stability of an insoluble metal salt sol from t_1 to t_2, caused by addition of protecting agent at concentration C_p, is given by the relation,

$$\log_{10} t_2/t_1 = F(C_p/C_s), \tag{4}$$

where F is a constant for the particular metal salt-protecting agent system in aqueous solution.

Destabilization by excess of reacting ion (at concentration $\bar{c}$) follows the general relation,

$$\log_{10} t = \log_{10} t_0 - b(\bar{c}/C_s), \tag{1a}$$

where in turn $b = \beta(C_p/C_s)^{-m}$. The addition of protecting agent thus necessitates an increase in the excess ion concentration ($\Delta\bar{c}$) to reach rapid coagulation (at $t = 1$ sec.) and precipitation. Comparison of [4] and [1a] gives:

$$\begin{aligned}\Delta\bar{c} &= F/b(C_p/C_s)\\ &= F/\beta(C_p/C_s)^{1+m}.\end{aligned} \tag{5}$$

This in turn leads to an increase in the constant A of the spacing relation [2]; and ΔA will be a function of $\Delta\bar{c}$, i.e., of F and (C_p/C_s).

Such a relation, $\Delta A = \alpha(C_p/C_s)^n$, is indeed observed experimentally over a wide range of C_p/C_s values.

The increase in spacing observed in gel media runs parallel to the increase in stability of the corresponding aqueous sol; and the constant α is related to F, and also varies inversely as the peptization ratios for a series of salts with common cation.

The techniques used by Liesegang and subsequent workers (3, 4) have generally led to systems of thick diffuse rings separated by partially coagulated turbid sol that do not lend themselves to quantitative recording, except by special photoelectric instruments; whereas, although more sharply defined rings are obtained in systems rhythmically precipitated in two dimensions (4, 7), the low spacing coefficients ($k < 0.005$) can be determined only by high-power optical magnification. Values for the spacing are thus rarely given in the literature, and workers in this field have generally estimated the rhythmicity by counting the number of visible rings.

This work has shown that the lack of clarity is due to the high flocculating power of the diffusing cation on the peptized sol first formed (between successive rings). However, whenever a greater sol stability is obtained by the presence of protecting agents, the periodic precipitation is well defined, and the general laws governing the phenomenon may be determined with accuracy. Such substances as silver oxalate, chloride, and bromide (8–10), and lead iodide (3) that have failed to show rhythmicity in gelatine, exhibit good rhythmic behavior and higher spacing coefficients on addition of suitable protecting agents.

ACKNOWLEDGMENT

This work has been carried out at Kings College, London. I wish to thank Professor Sir E. K. Rideal and Dr. R. Matalon for helpful discussion and advice.

REFERENCES

1. PACKTER, A., AND MATALON, R. *Discussions Faraday Soc.* **18,** 161 (1954).
2. MATALON, R., AND PACKTER, A., *J. Colloid Sci.* **10**(1), 46 (1955).
3. SCHEMJORKIN, J., *Kolloid. Z.* **58,** 325 (1932).
4. VEIL, S., "Les Periodicités de Structure," Hermann & Cie., Paris, 1935.
5. TULLER, E. F., AND FULMER, E. J., *J. Phys. Chem.* **52,** 787 (1948).
6. DEY, A. K., *J. Colloid Sci.* **3**(5), 473 (1948).
7. SERB-SERBINA, N. N., *Kolloid-Z.* **62,** 79 (1933).
8. FISCHER, L., *Acta Univ. Latviensis, Kim. Facultat,* p. 261 (1930).
9. SCHRAUM, K., *Kolloid-Z.* **66,** 108 (1944).
10. GHOSH, S., *J. Indian Chem. Soc.* **7,** 509 (1930).

JOURNAL OF COLLOID SCIENCE 11, 107–109 (1956)

LETTERS TO THE EDITOR

DIFFUSION BATTERY

The method given for end effect corrections in the subject paper (1) by use of two batteries of the same cross-section but different lengths, is incorrect. As applied to the batteries described, the method depends on the aerosol concentration distribution 4.92 cm. from the long battery channel entrance being completely random, which will not be the case. Although the method as given avoids gross errors owing to the high turbulence in the channel entrances, calculations have shown that its use can introduce errors of up to 20% in the diffusion coefficient when no end effects exist and results are not extrapolated to zero flow.

However, this does not invalidate the data or conclusions of the paper. An extrapolation of the diffusion constants obtained by the large battery alone to zero flow gave diffusion constants identical with those obtained by the method described in the paper. It was apparent that the extrapolation to zero flow is the only essential part of the correction procedure; use of a shorter battery to correct the data obtained by a longer one is unnecessary and undesirable.

REFERENCE

1. THOMAS, JESS W., *J. Colloid Sci.* **10**, 246 (1955).

Whirlpool-Seeger Corp.
St. Joseph, Michigan

JESS W. THOMAS

Received December 7, 1955

THE CHARGING OF AEROSOLS BY IONIC DIFFUSION

In connection with the paper by R. Gunn (1) dealing with this subject we would like to mention a similar theoretical and experimental study of this problem made by us before the World War II (2, 3). From the differential equation for the diffusion of gaseous ions towards a charged absorbing sphere (the effects of the mirror forces and of the concentration jump at the surface of the sphere being neglected) the following expression was derived for the stationary charge distribution on the droplets of a fog in a bipolar ionic atmosphere

$$n_{+i} = n_0(D_+\nu_+)^i(D_-\nu_-)^{-i}\exp(-i^2e^2/2akT) \qquad [1]$$

and a similar expression for n_{-i}. In these expressions n_{+i} and n_{-i} are the numbers of the droplets per unit volume, with i positive and negative elementary charges, respectively, n_0 are the number of those with a zero charge, a is the droplet radius, ν, the number of ions per unit volume and D their diffusion coefficient. The expressions are fairly accurate when $ie^2/akT < 1$. If the usually small difference between $D_+\nu_+$ and $D_-\nu_-$ is neglected, the Boltzmann equation [2] is valid.

$$n_{+i} = n_{-i} = n_0 \exp(-i^2e^2/2akT). \tag{2}$$

To the same form can be reduced Eq. [12] in Gunn's paper if $D_+\nu_+ = D_-\nu_-$.

In the experimental part of our work the size and the charge of about 2500 individual thermally produced oil droplets with radii ranging from 0.14 to 0.22 μ and from 1.0 to 2.0 μ were determined ultramicroscopically. The air in the fog chamber was highly ionized by radium, as in Gunn's experiments, and the stationary state of charging was reached in a very short time. All measured droplets were divided according to their radii in the following groups: 0.14–0.16 μ; 0.17–0.19 μ; 0.20–0.22 μ; 1.0–1.3 μ; 1.3–1.6 μ; and 1.6–2.0 μ, and in each group the distribution calculated by means of Eq. [2] was compared with the experimentally determined distribution. The agreement was reasonably good in almost all cases. In accordance with the fact that $D_- > D_+$ the number of negatively charged droplets was slightly ($\sim$10%) larger than that of positive droplets. In Gunn's experiments with water droplets an opposite relationship was found, apparently owing to some secondary effects (photoemission, double-layer field, etc.).

REFERENCES

1. GUNN, R., *J. Colloid Sci.* **10,** 107 (1955).
2. LISSOWSKI, P., *Acta physicochim. U.R.S.S.* **13,** 157 (1940).
3. FUCHS, N., *Bull. acad. sci. U.R.S.S., Sér. géograph. et geophys.*, **11,** 341 (1947).

Institute for Scientific Information,
Academy of Sciences of the U. S. S. R.,
Moscow, U. S. S. R.

N. FUCHS
P. LISSOWSKI

Received August 25, 1955

REPLY TO LETTER TO THE EDITOR BY N. FUCHS AND P. LISSOWSKI

I am glad to acknowledge the oversight of the Russian papers mentioned in the above Letter to the Editor, but must point out that the papers are not at all similar. A careful reading of their papers will show that their Reference 3 above has little or no bearing on the subject matter of my work. The experimental measurements on oil droplets of Reference 2 are of interest, generally confirm our expressed conclusions, and are creditable. On the other hand, I cannot agree with much of the analysis of Reference 2, and, certainly the papers and derived equations are not at all similar. For example, Gunn's basic aerosol equation (Eq. 12 of Reference B below) cannot be transformed to their basic Eq. 1 above by any means. It should be noticed that only the normalized forms of the basic derived equations degenerate to the same Boltzmann relation under the highly specialized restriction imposed in the above letter. This degenerate agreement, therefore, is not particularly significant and implies, principally, that classical statistics were employed.

The fact that ions diffuse onto droplets and electrify them has been known a long time. For example, J. S. Townsend (1914) worked out expressions for the electrification of droplets by diffusion and applied his results to the measurement of the elementary charge. An important part of my 1954 and 1955 papers (Reference A and B below) was based on my old 1935 work which emphasized that each cloud droplet in a bipolar ionized atmosphere acted as if it were one pole of a gaseous concentration cell. Expressions were adopted for the systematic droplet charge that closely approximates the values used in Reference B below, and these principles were applied to a useful quantitative theory of rain electrification. My recent papers consider a number of important physical factors not mentioned in the Russian work and obtained expressions that cannot be transformed to their basic relations. I, therefore, fail to find recognizable similarity in the referenced works. Doubtful readers should consult the originals.

REFERENCES

A. GUNN, R., "Diffusion charging of atmospheric droplets by ions, and the resulting combination coefficients," *J. Meteorol.* **11,** 339–347 (1954).
B. GUNN, R., "The statistical electrification of aerosols by ionic diffusion," *J. Colloid Sci.* **10,** 107–119 (1955).
C. TOWNSEND, J. S., "Electricity in Gases." Oxford Press, 1914.
D. GUNN, R., "Electricity of rain and thunderstorms," *Terrestrial Magnetism and Atm. Elec.* **40,** 79–106 (1935).

Physical Research Division,
U. S. Weather Bureau,
Washington, D. C.
ROSS GUNN

Received October 20, 1955

JOURNAL OF COLLOID SCIENCE 11, 110–111 (1956)

BOOK REVIEWS

Glass-reinforced Plastics. Edited by PHILLIP MORGAN, The New York Philosophical Library, New York, 1954. 248 pp. Price $10.00.

Since the wartime success in the utilization of glass-reinforced plastics in aircraft, the usefulness of these materials has been widened considerably. In view of this increase in use there has been a constant demand for information on these materials in a single source. This book provides such a source and presents the essential facts covering the materials and their use in various processes and applications. It will go far toward bringing some semblance of understanding to a field which has to a certain extent been shrouded in secrecy. The authors bring to the specialist the elementary principles of fields in which he may not be directly involved, but a knowledge of which will enable him to have a better understanding of the field as a whole. A copy of this book should be on the desk of everyone engaged in a phase of reinforced plastics work.

The types and treatments of glass fibers used in this work are given, together with the properties of laminates of each. Polyesters are discussed in detail, both as to preparation and use. Phenolics, epoxides, and silicones are treated at some length while miscellaneous resins which have been used in this field are referred to. The various molding techniques are described, and there is a very excellent chapter on the mass production of pipe and rod. Other chapters cover the application of reinforced plastics in the aircraft, automotive, electrical, and boat-building industries.

That the book was assembled hastily is self-evident. Considerable overlapping occurs in Chapters II, III, and IV on the discussion of polyesters, and the subject of glass treatment is covered in detail in two places. There are also errors which can be attributed to proof-reading such as "the difunctional monomers methyl acrylate, methyl methacrylate, vinyl acetate. . . ." Some of the tables are quite adequate while others leave much to be desired. However, these criticisms do not detract from the overall value of the book. The authors are to be commended for their efforts to bring together in one place information on this growing field.

R. E. DAVIES, Summit, New Jersey

Microscopy of Ceramics and Cements. By HERBERT INSLEY AND VAN DERCK FRÉCHETTE. Adademic Press Inc., New York 10, New York, 1955. 286 pp. Price $7.50.

This book deals with clay minerals and products, cements, glass and vitreous enamels, refractories, slags and foundry sands, and abrasives. It should be in every laboratory where any of these are investigated. For advanced students in ceramics, or in inorganic chemistry or mineralogy, who are likely to work with these materials, it is filled with examples and suggestions for further studies.

It very properly presupposes knowledge of optical crystallography, although it covers the adaptation of the usual techniques to the study of fine-grained aggregates, and other special methods. Excellent selected bibliographies for each section deal with topics that the authors cannot present at length but that are essential reading for further work. Numerous photomicrographs are included, all of high quality considering the difficulty of the specimens. A well-reproduced color chart of retardation vs. thickness is a valuable feature.

The discussions are particularly stimulating because they consider what happens in the specimen and not merely its static components. Perhaps phase diagrams here and there would be convenient for reference, but even without them physical and inorganic chemists should find the book interesting reading, and could hardly resist looking into some of the references.

The value of an encyclopedic work such as this is comes not only from what it includes for the seeker of special information, but in what it suggests to him from outside this specialty. By writing it, the authors have committed themselves to an ever-increasing coverage in later editions. It is hoped that this may include more on abnormalities and service failures, and an improved chapter on abrasives.

C. W. Mason, Ithaca, New York

The Nucleic Acids: Chemistry and **Biology** (*in 2 vols*). Edited by Erwin Chargaff and J. N. Davidson. Academic Press, New York, 1955. Vol. I, 692 pp. Price $16.80. Vol. II, 576 pp. Price $14.50.

The efforts of the editors and a total of thirty-three contributors have gathered together in these two large volumes an enormous amount of detailed information about the nucleic acids, their constituents, and what is known of the part they play in various aspects of cellular biology. The plan of the work is exhaustive. Nearly 2400 references to the original literature are given in Volume I alone. By far the largest number of these references are of comparatively recent date, and a very substantial part are the product of the last ten years. This compendium will, therefore, be of great value to all those working with nucleic acids and their constituents, or to those concerned with their role in biology.

The contributions in the first volume are devoted to the organic and physical chemistry and the physical properties of the nucleic acids: their isolation, resolution into, and characterization of, their components, characteristic reactions, and determination of their chemical structure. The second volume deals extensively with biological aspects: the extent to which nucleic acids are found in cells and tissues; cytochemical techniques for their detection and estimation; their occurrence and distribution in cell nuclei, and particularly in chromosomes; their occurrence in cytoplasm; biosynthesis of their constituents and of the nucleic acids themselves; metabolic aspects; and their role in growth and in infection, and as genetic determinants.

It is not easy for a single specialist to evaluate every contribution. The work as a whole suffers slightly, as is inevitable in one of this structure, from only partly successful integration, and a certain amount of duplication occurs in the work of various contributors. This appears to be deliberate rather than by editorial oversight, since the work is not of such a character that every reader might be expected to read it as a whole. For the biochemist or biologist whose own speciality lies elsewhere this is a disadvantage. For the latter an additional chapter (even though necessarily a long one) which would outline and summarize and thus provide a convenient orientation in this complex and rapidly expanding field, would have been welcome.

Jacinto Steinhardt, Cambridge, Massachusetts

JOURNAL OF COLLOID SCIENCE **11,** 113–123 (1956)

OSCILLOMETRIC INVESTIGATION OF PRECIPITATION AND DISSOLUTION RATES OF SPARINGLY SOLUBLE SULFATES

Peter J. Lucchesi

Department of Chemistry, Illinois Institute of Technology, Chicago, Illinois

Received January 3, 1956

Abstract

The rate of formation of $BaSO_4$, $PbSO_4$, and $SrSO_4$ from their supersaturated aqueous solutions have been followed oscillometrically by continuously recording the rate of decrease of conductance of the solution during precipitation. The sample is capacitance-coupled to the tank circuit of a commercially available oscillometer which resonates at 5 megacycles. Rates are reported as a function of temperature, agitation, and initial concentration of reagents. Initial rates of formation of the precipitates are measured continuously during the first few seconds of the precipitation by impressing the off-balance signal on a recorder. In order to follow precipitation and dissolution rates with the apparatus, it is necessary to choose systems which can be studied in the concentration region where the instrument is sensitive to changes in ionic concentration. In general, the results are in qualitative agreement with the diffusion theory, but the rates depend upon the order of addition of reagents in a manner which indicates that such factors as the electrokinetic potential at the solid surface are of considerable importance.

Introduction

The kinetics of precipitation of sparingly soluble salts have been studied by a variety of experimental techniques since the early work of von Weimarn (1, 2). These techniques have included interferometric (3, 4, 5), light-scattering (6, 7), potentiometric (8), and polarographic (9) methods. Recently, Diehl (10, 11) has reported work on the $BaSO_4$ system using a high-frequency conductometric titration apparatus.

The oscillometric technique (12) employs a tuned circuit resonating at its natural frequency, as determined by the values of the inductance and capacitance of its tank circuit. The sample under investigation is coupled to the oscillator through its inductance or capacitance. In the instrument used in this work, the sample forms the principal dielectric component of the condenser of the circuit. Therefore, changes in sample conductivity or dielectric constant, or both, produce changes in the capacitance of the resonant circuit and, hence, alter the natural frequency. This change is measured by restoring the frequency of the circuit to its prior value by means of calibrated parallel capacitors. Alternatively, the off balance signal can be impressed on a recording instrument for continuous recording.

The oscillometric technique is rapid and convenient, and it offers the advantage of eliminating the need for immersing electrodes in the sample solution.

Since it has been reported (13, 14) that in dilute aqueous salt solutions the changes in dielectric constant are negligible compared with conductance changes, the changes in conductance during precipitation or dissolution of ionic salts can be followed oscillometrically. The present work reports the results of experiments on the formation of $SrSO_4$, $BaSO_4$, and $PbSO_4$ from their supersaturated aqueous solutions. Attempts to apply the method to the determination of dissolution rates are also reported.

EXPERIMENTAL

1. Apparatus

The oscillometer was the E. H. Sargent Model V. This circuit resonates at 5 megacycles, and the sample solution is capacitance-coupled to the tank circuit. The standard sample cell was provided with a glass coil through which was passed thermostated water from a water bath. The water bath was equipped with a heater and a freon compressor, so that the temperature of the circulating water could be varied at will in the range 0–40°C. In the low temperature range, the temperature of the sample in the cell could be regulated to ±0.1°. In the range 15–40°C., the temperature could be regulated to ±0.05°. Fluctuations in temperature of such magnitude are well within tolerance. In general, the rate of precipitation decreases with increasing temperature, and the conductance of the solution increases. The net effect on the measured rate is such that a temperature control of ±0.1° was found to be entirely within the reproducibility of the measurements. Since part of this research was concerned with a study of the effect of agitation, stirring was provided when needed by means of an electronically controlled stirring motor. The output of the oscillometer was fed to a voltage divider and then to a fast response Leeds and Northrup Speedomax recorder. Thus, precipitation in the sample decreased the conductance and drove the circuit off resonance, the signal giving on the recorder a continuous representation of the decrease in conductance of the solution with time. It is, of course, necessary to use a recorder of rapid response so that the rate of recording is faster than the rate of change of conductance. For the Speedomax employed, the response of the recorder was faster than the measured rates by about a factor of 10.

2. Limitations

One important limitation of the apparatus narrows the range of salts whose dissolution or precipitation rates can be studied. At 25.0°C., the change in instrument response with increasing concentration of ionic salts in water is given in Fig. 1 for $SrCl_2$, $BaCl_2$, Na_2SO_4, and K_2SO_4.

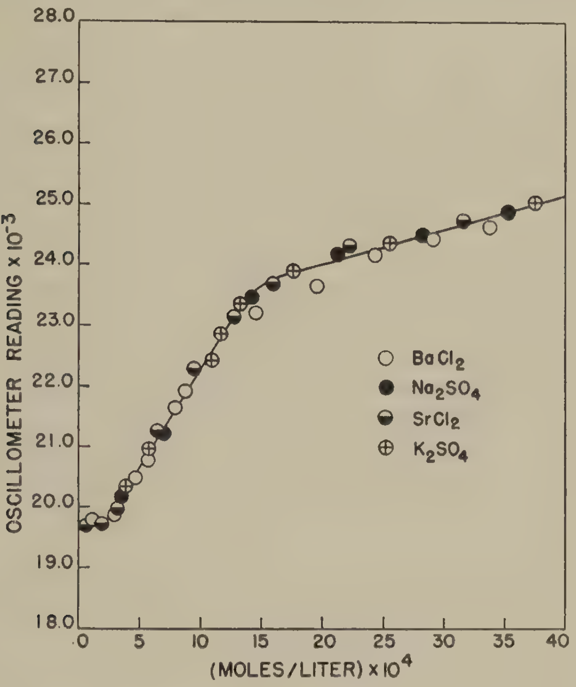

FIG. 1. Oscillometer response versus concentration of electrolyte at 25.0°C.

Within the reproducibility of the data, all points fall on the same curve. However, it is apparent that in very dilute solutions and in solutions more concentrated than approximately 0.002 M, the sensitivity of the instrument with changing concentration is very poor. In the intermediate range, the sensitivity is good and the response varies linearly with electrolyte concentration. In order to measure precipitation rates, it is necessary to work at concentrations such that the rates are followed entirely in the range of maximum sensitivity. If the original ionic concentration is on the plateau of the curve, and if during the precipitation the concentration falls to the sensitive region, the recorded rate will merely reflect the changing sensitivity of the instrument. On the other hand, when dissolution rates are measured in pure water, we are working at the other extreme where the instrument is again insensitive to small concentration changes. The curve recorded is flat until the solute concentration becomes large enough so that the system is in the sensitive range of the instrument. A straight line is then obtained corresponding to the dissolution rate of the salt in an aqueous solution of its ions at the concentration at which the instrument becomes sensitive. Hence, initial rates in pure water cannot be measured, and no rates can be obtained for salts whose solubility is below the sensitive region.

3. Procedure

In one series of experiments, the thermostated cell was filled with 100 ml. of an aqueous solution 0.001 M in $PbCl_2$, $BaCl_2$, or $SrCl_2$. With the solution held at constant temperature, K_2SO_4 was added by spraying into the solution 1.0 ml. of an aqueous solution 0.1 M in K_2SO_4. Both solutions were at the same temperature. The addition was accomplished by means of a plunger device which drove the solution through a capillary sealed to the end of a calibrated pipet. Hence, the initial concentrations on mixing were approximately 0.001 in $SO_4^=$ and in cation. In another series of experiments, a 10-ml. cell was used which was fitted with an outer jacket through which thermostated water was pumped. The reagents were sprayed into the cell in such a manner that they met in a stream and were mixed before entering the cell. In these experiments, 5 ml. of 0.001 M K_2SO_4 solution were mixed with the same volume of 0.001 M solution of the cation. The results obtained with these mixing techniques agreed with each other within the reproducibility of duplicate measurements using the same mixing procedure.

Immediately upon mixing, the recorder registered a sharp increase in reading due to the increase in electrical conductivity of the solution. In some cases this was followed by an induction period after which the conductivity began to decrease. The nature of the curves recorded is demon-

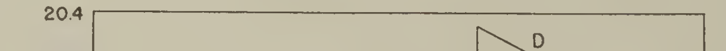

FIG. 2. Change in conductance of solution during formation of $BaSO_4$ at 25.0°C. (A) mixture of 50 ml. 0.0001 M $BaCl_2$ and 50 ml. 0.0001 M $Na_2SO_4 \cdot 10H_2O$. (B), (C), and (D) change in response of instrument on successive additions of 1 ml. aqueous solution containing 1 mg. Na_2SO_4.

strated in Fig. 2. This curve was redrawn from the recorder plot of the $BaSO_4$ system. The initial portion is linear for approximately 10–20 sec. and then begins to taper off. The rates reported in this paper are in number of recorder divisions traversed by the pen during the first 60-sec. time interval, and as such they represent the initial rate of formation of the precipitate from its supersaturated solution. For the relatively insoluble $BaSO_4$, these rates could be measured in less than 1 min., depending upon the length of the induction period. Figure 2 shows the results obtained when successive portions of Na_2SO_4 were sprayed into a $BaCl_2$ solution. The sharp increases in response are due to the increased conductivity on addition of sulfate, and the subsequent decreases give the rate of formation of $BaSO_4$. The slopes of these lines decrease in magnitude, indicating that the rate decreases as the Ba^{++} concentration in the solution decreases. After each addition, the net conductivity is increased, since the net process involves replacement of a Ba^{++} ion by 2 Na^+ ions.

4. Materials and Solutions

All salts used for preparation of standard solutions were Mallinckrodt A R grade. Solutions were made by weighing to 0.1 mg. on an analytical

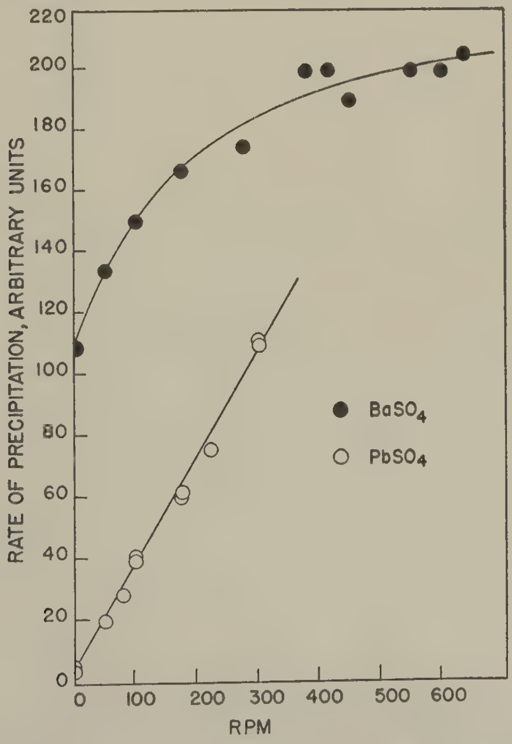

FIG. 3. Effect of stirring on rate of formation of $BaSO_4$ and $PbSO_4$ at 25.0°C.

balance and all volumetric apparatus was calibrated. Water was singly distilled and had a pH of approximately 6.6.

Results

1. *Dissolution Rates*

For the reasons outlined above, attempts to measure initial dissolution rates in pure water were not successful. It was not difficult, however, to measure these rates in solutions which originally contained dissolved ionic solutes in concentrations approximately 0.0001 *M*; i.e., in the sensitive range of the instrument. For example, by embedding $SrSO_4$ crystals on the surface of plastic stirrers previously softened by treating with acetone, the initial rate of dissolution in 0.0003 *M* HCl was easily obtained directly from the recorder plots, which were linear. Since these measurements cannot be directly compared with the precipitation experiments in pure water, the data are not given in this paper.

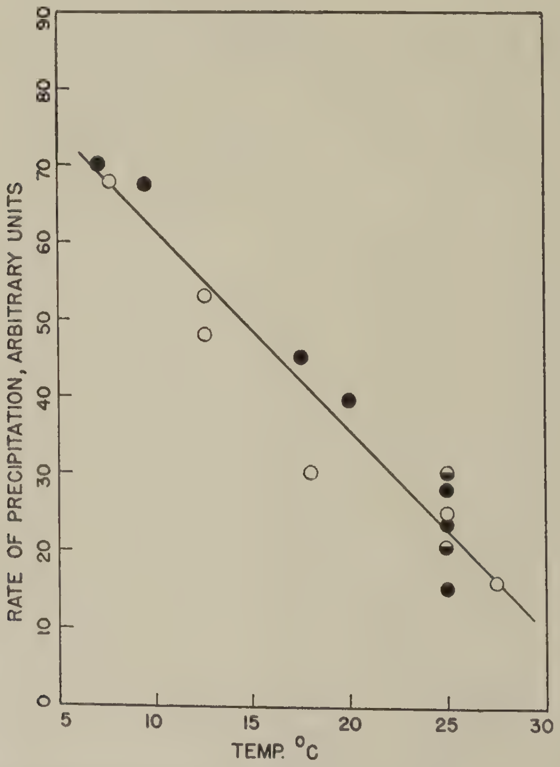

Fig. 4. Effect of temperature on rate of formation of $BaSO_4$ at initial Ba^{++} and $SO_4^{=}$ concentration of 0.001 *M*. Three different experiments are given by unshaded, half-shaded and shaded points.

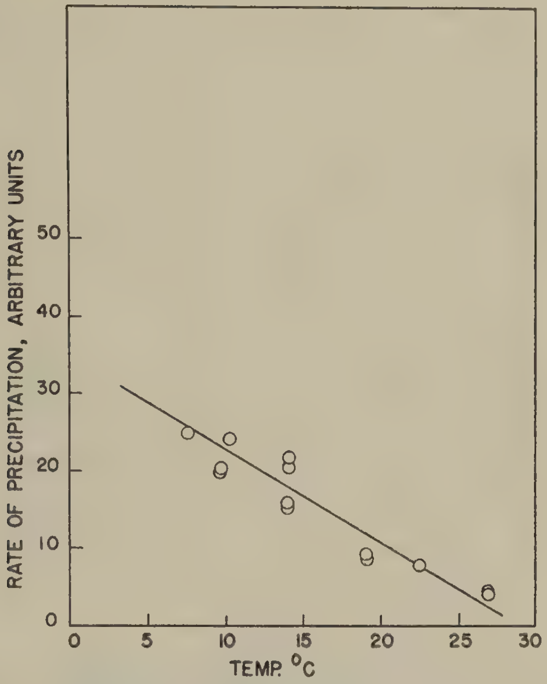

FIG. 5. Effect of temperature on rate of formation of $SrSO_4$ at initial Sr^{++} and $SO_4^{=}$ concentrations of 0.001 M.

2. Precipitation Rates

The rate of formation of $BaSO_4$ from water at 25.0°C. and at initial Ba^{++} and $SO_4^{=}$ concentrations of 0.001 M is plotted in Fig. 3 as a function of stirring rate. This graph also includes similar data for the $PbSO_4$ system. The rate obtained on mixing, with no external agitation, is plotted as a function of the temperature for $BaSO_4$ and $SrSO_4$ in Fig. 4 and Fig. 5, respectively. It was of interest to study these rates at constant concentration (0.001 M) of anion and varying concentration of cation and vice versa. These data are given for the $BaSO_4$ system in Fig. 6. At 25.0°C., it was found that the rate of formation of $SrSO_4$ was the same, within the reproducibility of the measurements, as that of $PbSO_4$, despite the greater solubility of the former. For the $PbSO_4$ system, the rate obtained on adding 1.0 ml. solution 0.1 M in Pb^{++} to 100 ml. solution 0.001 M in $SO_4^{=}$, at 25.0°C., was approximately double the rate observed when the order of addition was reversed.

3. Experimental Error

For the $BaSO_4$ system, the average deviation from the mean of a set of identical experiments was found to be 12% in the least favorable case.

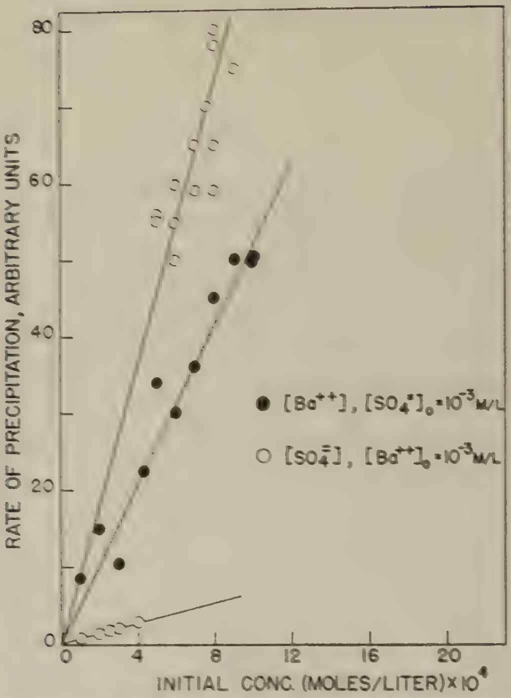

FIG. 6. Rate of formation of $BaSO_4$ at 25.0°C. as a function of Ba^{++} concentration at constant $SO_4^=$ concentration (0.001 M), and as a function of $SO_4^=$ concentration at constant Ba^{++} concentration (0.001 M).

For the more soluble $SrSO_4$ and $PbSO_4$, the reproducibility was poorer and was of the order of 17%. The principal difficulty was found to be a result of spurious pulses registered by the oscillometer during low-temperature experiments. These were a result of condensation of water on the terminals around the outer surface of the sample cell. More reproducible results were obtained when the thermostated water was circulated through a glass coil immersed in the solution than in the jacket type cell which was thermostated by circulating water through its outer jacket. The reproducibility of the results appeared to decrease with increased stirring in the $SrSO_4$ solutions, and the same effect was observed for low-temperature experiments in the $PbSO_4$ solutions. However, the trend observed was an increased rate of formation of $PbSO_4$ at lower temperatures and a rate that increased slightly with stirring in the $SrSO_4$ solutions. These trends are considered reliable, but the uncertainty in the quantitative data is too large to warrant presentation in the graphs.

4. Induction Period

In many cases, an induction period was observed before precipitation began. In $SrSO_4$ solutions, this period was observed to be as long as 3–5 min. Induction periods were also observed in the $BaSO_4$ studies, and they ranged from 5–45 sec. However, the length of the induction period depended on the concentration and the order of addition of the reagents. For example, in the $PbSO_4$ and $BaSO_4$ experiments, the induction period was nvariably longer when the cation was added to the sulfate solution than t was when the order of addition was reversed. Also, when 1.0 ml. of the Ba^{++} solution was added to 100 ml. of the solution 0.001 M in $SO_4^=$, the nduction period increased with increasing concentration of Ba^{++}; i.e., with increasing degree of supersaturation.

Discussion

In a general way, the data obtained reveal a qualitative agreement with the diffusion theory as proposed by Noyes and Whitney (15), and later modified by Nernst (16), Berthoud (17), and others (18, 19). This theory considers the process of crystal growth as diffusion controlled, or as a combination of the transport process and the reaction at the surface of the growing crystal. In general, the treatment predicts a rate proportional to the surface area, the difference between the instantaneous concentration of the reagents and the equilibrium solubility of the salt, and to the diffusion coefficient of the depositing species across the crystal-solution interace. The rate should also increase with increasing stirring of the solution. Qualitatively, the experimental facts support these predictions. For example, the rates increase markedly with stirring, they decrease with increasing temperature or decreasing solubility of the salt, and, at constant concentration of anion (or cation), increase with increasing concentration of cation (or anion).

However, a more quantitative examination of the data reveals that the mechanism involved in the formation of the precipitate is more complex han the mechanism pictured in the diffusion theories. For example, the ffect of temperature on the rate of formation of $BaSO_4$ and $SrSO_4$ is much greater than the known temperature coefficient of their solubility n water. In the range 0°–26°C., the solubility of $BaSO_4$ increases by approximately 50% and that of $SrSO_4$ by 33% (20, 21).

An interesting variation is observed when the rates are measured at constant Ba^{++} or Pb^{++} concentration and varying $SO_4^=$ concentration, and vice versa. The rate of formation of $PbSO_4$ is faster, at room temperaure, when Pb^{++} ions are added to $SO_4^=$ than in the reverse case.

Similarly, as evident from Fig. 6, addition of $SO_4^=$ to Ba^{++} gives a slower ate of formation than the reverse case, but at $SO_4^=$ concentrations greater han 0.004 M the effect appears to be reversed, and addition of $SO_4^=$ to Ba^{++} gives faster rates than obtained when the order is reversed. Hence, n dilute solutions, the addition of $SO_4^=$ to a forming $BaSO_4$ or $PbSO_4$ precipitate is more difficult than the addition of the cation. At higher conentrations, in the case of $BaSO_4$, the reverse is observed.

It seems reasonable to assume that the rate of formation of these precipitates is influenced to a large extent by factors such as the electrokinetic potential at the surface of the precipitate and by the sign of the charge on the surface. Unfortunately, the available data on the electrokinetic potential of $PbSO_4$, $SrSO_4$, and $BaSO_4$ are in some cases conflicting. Thus Buchanan (22–24) reports these potentials are positive in aqueous alcoholic solutions and reports the $BaSO_4$ potential in its saturated aqueous solution as positive. However, this appears to vary markedly with surface structure and temperature, and it may even change sign in the presence of impurities. On the other hand, Ruyssen (25, 26) reports that in a saturated solution crystals of $BaSO_4$ are negatively charged, and that the electrokinetic potential changes sign in $BaCl_2$ solutions. Since the potential and its sign depend upon the composition of the solution, the temperature, and the surface regularities, it is not surprising that the observed rates of formation of the precipitates vary with the order of addition of reagents and with the temperature in a manner only qualitatively explained by the diffusion mechanism.

Such surface factors appear to be important in exchange studies. For example, very recent work indicates the rate of exchange between $SO_4^{=}$ ions in saturated aqueous solutions and solid $PbSO_4$ differs from the rate of exchange of Pb^{++} ions (27).

ACKNOWLEDGMENT

The author gratefully acknowledges the financial support provided by Research Corporation in support of this research.

REFERENCES

1. VON WEIMARN, P. P., "Zur Lehre von den Zuständen der Materie", Bd I, Test; Bd II, 1913.
2. VON WEIMARN, P. P., "Die Allgemeinheit des kolloiden Zustandes." Th. Steinkopff, Dresden, 1925.
3. KRUEGER, G. C., AND MILLER, C. W., *Phys. Rev.* **86**, 623 (1951).
4. BERG, W. F., *Proc. Roy. Soc.* (*London*), **164A**, 79 (1938).
5. THOMSON, G. P., *Proc. Phys. Soc.* (*London*) **61**, 403 (1948).
6. TEZAK, B., *Arch. Kem.* **23**, 30 (1951).
7. LAMER, V. K., AND DINEGAR, R. H., *J. Am. Chem. Soc.* **73**, 380 (1951).
8. QUINTIN, M., *Compt. rend.* **226**, 494 (1948).
9. KRYUKOVA, T. A., *J. Phys. Chem.* (*U.S.S.R.*) **13**, 693 (1939).
10. DUKE, F. R., BEVER, R. J., AND DIEHL, H., *Iowa State Coll. J. Sci.* **23**, 297 (1949).
11. BEVER, R. J., CROUTHAMEL, C. E., AND DIEHL, H., *Iowa State Coll. J. Sci.* **23**, 289 (1949).
12. SHERRICK, P. H., DAWE, G. A., KARR, R., AND EWEN, E. F., "Manual of Chemical Oscillometry." Sargent, Chicago, 1954.
13. WALDEN, P., *Z. physik. Chem.* **115**, 177 (1925).
14. DEBYE, P., "Polar Molecules." Dover Publications, New York, 1945.
15. NOYES, A. A., AND WHITNEY, W. R., *Z. physik. Chem.* **23**, 689 (1897).
16. NERNST, W., *Z. physik. Chem.* **47**, 52 (1904).

7. Berthoud, A., *J. Chem. Phys.* **10,** 624 (1912).
8. Valeton, J. J. P., *Z. Krist.* **59,** 135 (1924).
9. Friedel, G., *Bull. soc. franç. minéral.* **48,** 12 (1925).
0. Kolthoff, I. M., and Sandell, E. B., "Textbook of Quantitative Inorganic Analysis," p. 60. Macmillan, New York, 1953.
1. Lucchesi, P. J., Ph.D. thesis, New York University, June, 1954.
2. Buchanan, A. S., and Heyman, E., *Proc. Roy. Soc. (London)* **195A,** 150 (1948).
3. Buchanan, A. S., and Heyman, E., *Nature* **164,** 29 (1949).
4. Buchanan, A. S., and Heyman, E., *J. Colloid Sci.* **4,** 137 (1949).
5. Ruyssen, R., and Loas, R., *Nature* **162,** 741 (1948).
6. Ruyssen, R., *J. Phys. Chem.* **44,** 265 (1940).
7. Nelson, L. B., Ph.D. thesis, New York University, June, 1955.

JOURNAL OF COLLOID SCIENCE **11,** 124–134 (1956)

VERIFICATION OF A NEW EQUATION IN THE STUDY OF THE SLOW COAGULATION OF LYOPHOBIC SOLS BY DIFFERENT TECHNIQUES

Amal K. Bhattacharya and Abani K. Bhattacharya

Department of Chemistry, Agra College, Agra, India

Received June 14, 1955

Abstract

The relation between the concentration of the electrolyte and the time of coagulation expressed by a new equation was checked employing the data, available in the literature, on the dependence of the time of coagulation on the concentration of the electrolyte. These data consist of results obtained from studies on (*1*) viscosity, (*2*) light absorption, (*3*) extinction coefficient, and (*4*) counting of particles.

The time of coagulation, t, obtained by each of the above methods was plotted against $1/(C - a)$. Straight lines were obtained for each set of values according to the relation expressed by $\frac{1}{C - a} = \frac{n}{m} t + \frac{1}{m}$, which can be readily deduced from the equation, $C = a + \frac{m. 1/t}{n + 1/t}$. Here C is concentration and a, m, and n are constants.

Thus it is shown that the relation between the concentration of electrolyte and time for the same stage of coagulation is well expressed by the above equation, irrespective of the method used.

I. Introduction

The relation between the concentration of the electrolyte and the time of coagulation of As_2S_3, $Cr(OH)_3$ and $Fe(OH)_3$ sols has been communicated in a series of publications by Bhattacharya and Kumar (1, 2). The time of coagulation, t, and the concentration, C, of the electrolyte could be represented by the equation, $C = a + \frac{m.1/t}{n + 1/t}$, where m and n are constants and a is another constant obtained graphically from the intercept on the concentration axis of C versus $1/t$ curves. This equation reduces to the form, $\frac{1}{C - a} = \frac{n}{m} t + \frac{1}{m}$. By plotting $1/(C - a)$ against t, it was shown that straight lines were obtained in the study of slow coagulation, confirming the linearity of the foregoing equation. Extensive studies of coagulation have been carried out by many workers in this field, such as Smoluchowski (15), Freundlich (4), Zsigmondy (18), Weiser (16), Westgren (17), Kruyt and Van Arkel (9, 10), Dhar and Ghosh (3), Mukherjee (14) and Joshi (6, 7). In spite of their extensive work the fact remains that no suitable expression is found in the literature which correlates the concentration of the electrolyte with the time of slow coagulation. In order to confirm our new equation, the times corresponding to the same stage of coagulation with different concentrations of electrolytes were determined from the available data as follows.

1. *Study of Slow Coagulation*

a. By Viscosity, Light Extinction, and Light Transmission Methods. Gann (5) studied the slow aggregation of colloidal particles of Al_2O_3 by measuring the changes in the time of efflux at different time intervals through the capillary of a viscometer.

Kruyt and Troelstra (12) measured the percentage of extinction of light during the coagulation of AgI sol at different time intervals.

Mukherjee (14) studied the coagulation of an As_2S_3 sol by the change in intensity of the transmitted light at different intervals of time.

They determined the variations of the above properties with time using several concentrations of different electrolytes. Characteristic curves were obtained by plotting the magnitude of variations in the physical property studied against the intervals of time.

The stage of coagulation was defined by drawing a line parallel to the time axis. This line cut the family of curves (one curve for each different concentration of the electrolyte). It was assumed that the same value of viscosity or light extinction or transmission connotes the same state of aggregation and hence of coagulation. The time intervals at the same stage of coagulation for different concentrations of the electrolyte could now be easily read from the curves. Having thus obtained the values of the time of coagulation t at the same stage for known concentration C, the C versus $1/t$ curve was plotted. This curve cuts the C-axis when $1/t$ is equal to zero, i.e., when t tends to infinity. This intercept on the C-axis gives the value of the constant a.

Since the concentration of the electrolyte is already known, $1/(C - a)$ could be plotted against t and straight lines were obtained in all cases according to the equation, $\frac{1}{C - a} = \frac{n}{m} t + \frac{1}{m}$. The value of $1/m$ was now determined from the intercept on the $1/(C - a)$ axis, when $t = 0$. The tangent of the angle with the t axis is equal to n/m. Thus $1/m$ or m being known, n was calculated. In this way the constants, a, m, and n were determined.

b. By Counting the Number of Particles. Kruyt and Van Arkel (9–11) observed the slow and rapid coagulations of a selenium sol by counting the number of particles at different intervals of time at different concentrations of electrolytes. In this paper the times of coagulation for different concentrations of the electrolyte at the same stage were given in tables. Hence C versus $1/t$ and also $1/(C - a)$ versus t curves were drawn, and the values of the constants were determined as already stated.

It may be noted that the curves of C versus $1/t$ as well as $1/(C - a)$ versus t will refer to a particular stage of slow coagulation as obtained by drawing a line parallel to the t axis and cutting the curves for different concentrations of the electrolyte added to the sol. If we take different stages of coagulation, the straight lines obtained by plotting $1/(C - a)$ versus t will not be identically the same.

TABLE I

(See Figs. 1 and 2)

Coagulation stage expressed in ϕ (time of efflux)	Conc. of electrolyte, C (*mM/l.*)	Time of coagulation, t (*mins.*)	$1/t \times 10^3$	a (*mM/l.*)	$\frac{1}{C - a} \times 10^3$	m (*mM/l.*)	n (*min.*$^{-1}$)
75	100	29.54	33.85	50	20	62.5	6.875
	90	50.00	20.00		25		
	80	68.18	14.66		33		
	70	150.00	6.667		50		
70	100	11.36	88.04	50	20	62.5	13.125
	90	25.00	40.00		25		
	80	38.64	25.88		33		
	70	81.82	12.22		50		
	60	195.45	5.116		100		
65	100	6.82	146.6	50	20	62.5	21.25
	90	13.64	73.31		25		
	80	25.00	40.00		33		
	70	52.27	19.13		50		
	60	127.27	7.857		100		

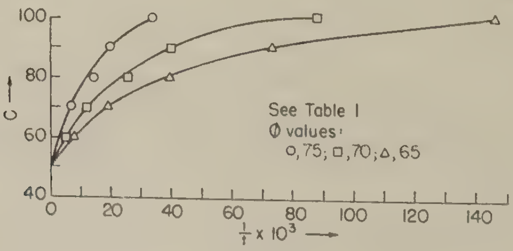

FIG. 1

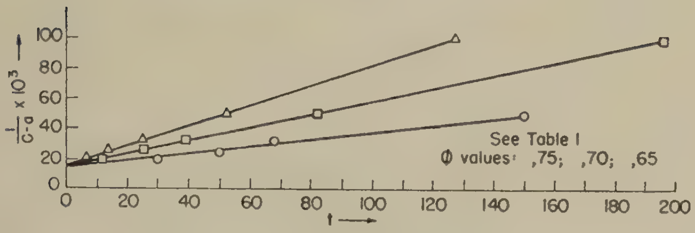

FIG. 2

II. OBSERVATIONS

1. Gann's Experiments on Viscosity Changes during Coagulation

a. Electrolyte: KCl.

TABLE II

(See Figs. 3 and 4)

Coagulation stage expressed in extinction, E	Conc. of electrolyte, C ($mM/l.$)	Time of Coagulation, t ($mins.$)	$1/t \times 10^3$	a ($mM/l.$)	$\frac{1}{C-a} \times 10^4$	m ($mM/l.$)	n ($min.^{-1}$)
0.5	126.92	8	0.125	70	175.7	113.6	34.08
	135.58	5	0.200		152.5		
	149.04	3	0.333		126.5		
	167.30	2	0.500		102.8		
0.4	111.54	8	125	70	240.8	113.6	56.8
	123.08	5	200		188.4		
	134.61	3	333		154.8		
	144.23	2	500		134.7		
	173.08	1	1000		97.01		
0.3	92.31	8	125	70	448.2	113.6	127.8
	103.84	5	200		295.5		
	115.38	3	333		220.4		
	124.04	2	500		185.1		
	142.31	1	1000		138.3		

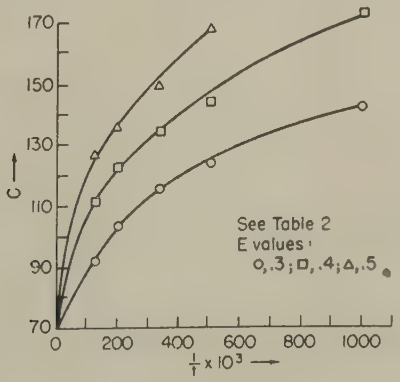

FIG. 3

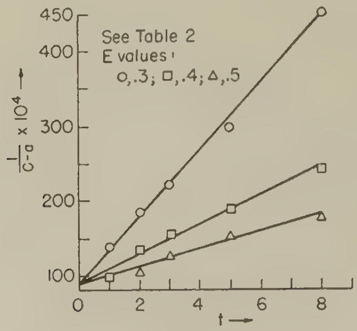

FIG. 4

2. Kruyt's and Troelstra's Experiments on Extinction of Light during Coagulation

b. Electrolyte: KNO_3.

3. Mukherjee's Experiments on Transmission of Light during Coagulation

a. Electrolyte: NaCl.

TABLE III

(See Figs. 5 and 6)

Coagulation stage expressed in transmission, (Deflection θ) (*mm.*)	Conc. of electrolyte, C (N)	Time of coagulation t (*mins.*)	$1/t \times 10^2$	a (N)	$\frac{1}{C-a}$	m (N)	n (*min.*$^{-1}$)
70	0.091	2.222	45.01	0.076	66.67	0.05	0.035
	0.083	5.000	20.00		142.90		
	0.077	32.220	3.10		1000.00		
80	0.091	1.111	90.01	0.076	66.67	0.05	0.060
	0.083	2.500	40.00		142.90		
	0.077	20.000	5.00		1000.00		
90	0.091	0.833	120.00	0.076	66.67	0.05	0.0925
	0.083	1.805	55.41		142.90		
	0.077	13.330	7.50		1000.00		

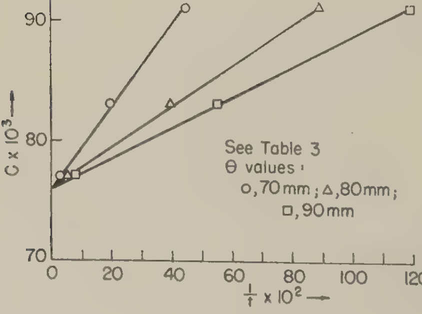

FIG. 5

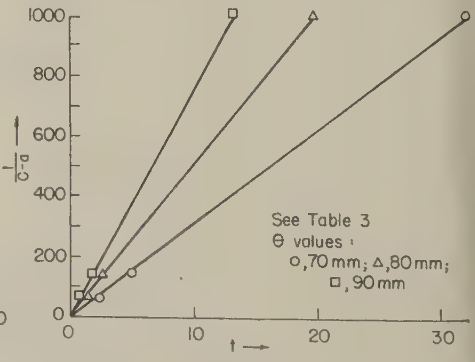

FIG. 6

b. Electrolyte: $BaCl_2$.

TABLE IV

(See Figs. 7 and 8)

Coagulation stage expressed in transmission (deflection θ) (*mm.*)	Concn. of electrolyte, C (N)	Time of coagulation t (*mins.*)	$\frac{1}{t} \times 10^3$	a (N)	$\frac{1}{C - a}$	m (N)	n (*min.*$^{-1}$)
20	0.00200	4.0	250.0	0.0014	1667	0.00125	0.001375
	0.00182	7.5	133.3		2381		
	0.00167	13.0	76.9		3704		
	0.00154	30.0	33.3		7143		
25	0.00200	2.0	500.0	0.0014	1667	0.00125	0.002750
	0.00182	4.0	250.00		2381		
	0.00167	6.5	153.80		3704		
	0.00154	14.5	68.97		7143		
30	0.00200	1.0	1000.0	0.0014	1667	0.00125	0.006125
	0.00182	2.0	500.0		2381		
	0.00167	3.0	333.3		3704		
	0.00154	6.0	166.7		7143		

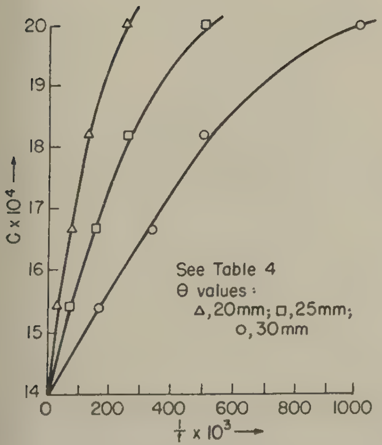

FIG. 7

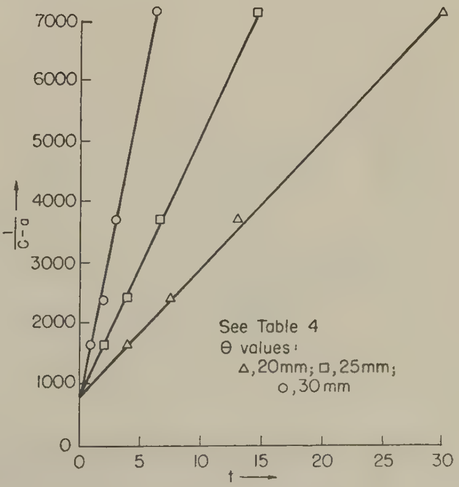

FIG. 8

c. Electrolyte: $Al_2(SO_4)_3$.

TABLE V

(See Figs. 9 and 10)

Coagulation stage expressed in transmission (deflection θ) (*mm.*)	Concn. of electrolyte C (N)	Time of coagulation, t (*mins.*)	$\frac{1}{t} \times 10^3$	a (N)	$\frac{1}{C - a}$	m (N)	n (*min.*$^{-1}$)
25	0.000400	5.238	190.9	0.00034	16670	0.0002	0.00042
	0.000385	8.095	123.5		22420		
	0.000370	13.000	76.9		32890		
27.5	0.000400	2.70	370.4	0.00034	16670	0.0002	0.00084
	0.000385	4.10	243.9		22420		
	0.000370	6.37	157.0		32890		
30	0.000400	1.36	735.3	0.00034	16670	0.0002	0.00164
	0.000385	2.27	440.5		22420		
	0.000370	3.18	314.5		32890		

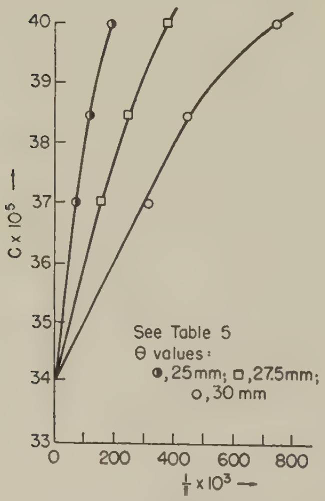

FIG. 9

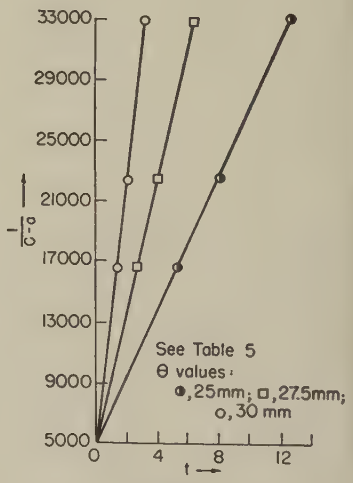

FIG. 10

*4. Kruyt's and van Arkel's Experiments on Counting of Particles during Coagulation**

a. Electrolyte: KCl.

TABLE VI

(See Figs. 11 and 12)

Concn. of electrolyte (*mM/l.*)	No. of particles at $t = 0$	Time of coagulation, t (*hours*)	$\frac{1}{t} \times 10^5$	a (*mM/l.*)	$\frac{1}{C - a} \times 10^4$	m (*mM/l.*)	n ($hr.^{-1}$)
20	33.5×10^9	2777	36.01	10	1000	43.48	23.91
40	33.5×10^9	417	60.02		333		
50	33.5×10^9	55.5	239.8		250		

* Data falling in the region of slow coagulation only, as stated by Kruyt and Van Arkel, have been recorded.

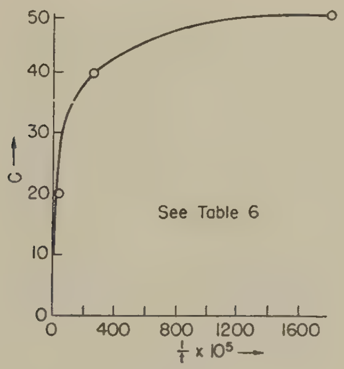

FIG. 11

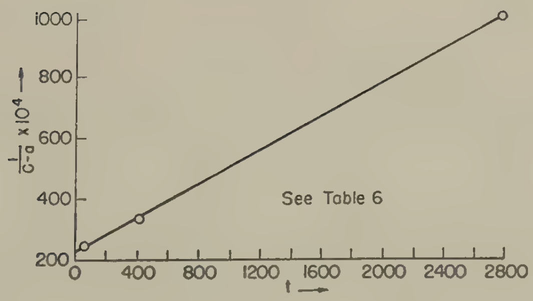

FIG. 12

b. Electrolyte: $BaCl_2$.

TABLE VII

(See Figs. 13 and 14)

Concn. of electrolyte ($mM/l.$)	No. of particles at $t = 0$	Time of coagulation, t (hrs)	$\frac{1}{t} \times 10^3$	a ($mM/l.$)	$\frac{1}{C - a} \times 10^2$	m ($mM/l.$)	n ($hour^{-1}$)
2	33.0×10^7	55.55	18.00	1.3	500.00	4.167	4.445
3	33.0×10^7	7.222	138.5		83.33		
4	33.0×10^7	1.944	514.4		45.45		

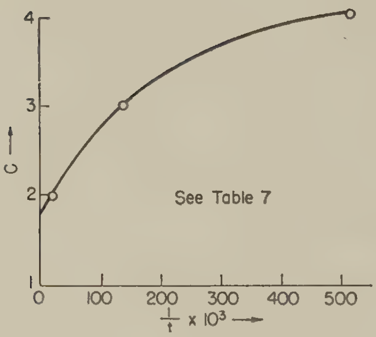

FIG. 13

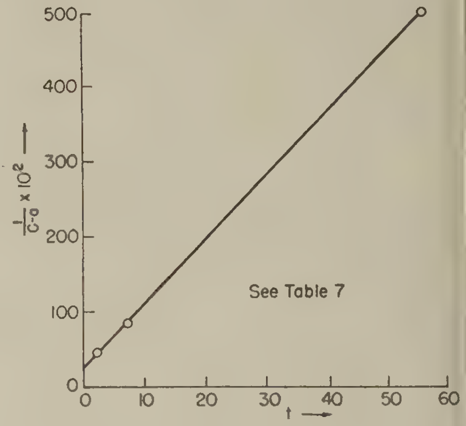

FIG. 14

III. DISCUSSION

Interpretation of the Constants

When C is plotted versus $1/t$, the curve cuts the C-axis and the intercept at $1/t = 0$ is given by a, i.e., a is the value for $t \to \infty$. This means that the stability of the sol remains unaffected up to a concentration given by a, and a has been designated as the "critical stability concentration" of the electrolyte for the sol. When $1/t$ is very large compared to n, i.e., when t is very small, as happens in the region of rapid coagulation, n in the new equation can be neglected so that $C = a + m$ or $C - a = m$, or more strictly $C - a \to m$ in the rapid coagulation zone. Therefore m represents the concentration of the electrolyte above the critical value, a, which will produce instantaneous coagulation. On the other hand, if n happens to be very large as compared to $1/t$, $1/t$ can be neglected in the denominator and the equation reduces to $C = a + \frac{m}{n}(1/t)$. This is a linear equation which was in agreement with the straight curve obtained for a few cases only.

In order to interpret n let us consider an alternative form of the equation, $C - a = m/(nt + 1)$. Working out the dimensions of the equation we find that $nt + 1$ should be dimensionless, and this can be possible only when n has the dimension, time^{-1}. Hence n can be put $1/t$ or k/t. Substituting $n = 1/t$ in the equation we get $C - a = m/2$. If $n = k/t$ is substituted, $C - a = m/(k + 1)$. This means that n is a characteristic constant for the sol and shows that the sol will be coagulated in a time interval t given by $(1/k + 1)$ times the m (the quantity for instantaneous coagulation). Hence we connect n with the sensitiveness or susceptibility of the sol to the electrolyte and n becomes equal to k when $t = 1$. But the susceptibility of the sol particles may depend on a large number of factors, such as size and shape of the particles, charge and zeta potential, thickness and interaction of the double layers, adsorption, ion exchange, and changes in the dielectric constant.

It is interesting to observe in the tables that the order of decrease in the values of n, at different stages of coagulation, directly indicates the greater and greater degree of aggregation of the coagulating particles. In viscosity determinations, n decreases with an increase in the time of efflux, ϕ. Similarly n decreases as the extinction percentage increases and with a decrease in the intensity of light transmission, measured by the deflection, θ, in the galvanometer. From the variations in the values of n at different stages of coagulation it becomes evident that n depends upon all the factors which determine the stability of the sol, and hence it can assume a definite value with different concentrations of the electrolyte at a particular stage of coagulation or degree of aggregation of the colloidal particles. When the same stage of coagulation is reached, where the net effect of the physical factors determining the stability of the sol may be visualized to remain the same, on adding different concentrations of the electrolyte, n will have a constant value corresponding to the same degree of aggregation. This has been actually observed (see curves, $1/(C - a)$ against t).

Acknowledgments

The authors express their deep gratitude to the late Prof. J. W. McBain, F.R.S., Director of the National Chemical Laboratory of India, Poona, and to Prof. W. E. Garner, F.R.S., for their keen interest in the progress of this work.

References

1. Bhattacharya, A. K., and Kumer, R., *J. Indian Chem. Soc.* **28,** 179 (1951; *ibid.* **28,** 638 (1951).
2. Bhattacharya, A. K., and Kumar, R., *J. Indian Chem. Soc.* **29,** 687 (1952); *ibid.* **29,** 759 (1952).
3. Dhar, N. R., and Ghosh, S., *J. Phys. Chem.* **30,** 294 (1926).
4. Freundlich, H., *Kolloid-Z.* **23,** 163 (1918).
5. Gann, J. A., *Kolloidchem. Beih.* **8,** 64 (1916).
6. Joshi, S. S., *J. Indian Chem. Soc.* **10,** 329 (1933).
7. Joshi, S. S., *J. Indian Chem. Soc.* **11,** 133 (1934).
8. Kruyt, H. R., and Van Arkel, A. E., *Chemisch Weekblad* **16,** 220 (1919).

9. Kruyt, H. R., and Van Arkel, A. E., *Rec. trav. chim.* **39,** 656 (1920).
10. Kruyt, H. R. and Van Arkel, A. E., *Rec. trav. chim.* **40,** 169 (1921).
11. Kruyt, H. R., and Van Arkel, A. E., *Kolloid-Z.* **32,** 29 (1923).
12. Kruyt, H. R., and Troelstra, S. A., *Kolloid-Beih.* **54,** 225 (1945).
13. Mukherjee, J. N., and Sen, K. C., *J. Chem. Soc.* **115,** 461 (1919).
14. Mukherjee, J. N., *J. Chem. Soc.* **125,** 785 (1924).
15. Smoluchowski, von, M., *Z. physik. Chem.* **92,** 129 (1917).
16. Weiser, H. B., *J. Phys. Chem.* **25,** 399 (1921).
17. Westgren, A., *Arkiv Kemi, Mineral. Geol.* **7,** (No. 6) 1918.
18. Zsigmondy, R., *Z. physik. Chem.* **92,** 600 (1918).

OURNAL OF COLLOID SCIENCE **11**, 135–149 (1956)

THE USE OF MONODISPERSE LATEXES IN AN ELECTRON MICROSCOPE INVESTIGATION OF THE MECHANISM OF EMULSION POLYMERIZATION[1]

E. B. Bradford, J. W. Vanderhoff, and T. Alfrey, Jr.

hysical Research Laboratory, The Dow Chemical Company, Midland, Michigan

Received December 9, 1955

ABSTRACT

Monodisperse polystyrene latexes are useful in electron microscope investigations f the mechanism of emulsion polymerization: (*1*) as calibration standards in particle iameter determinations, (*2*) in determining the relative rates of growth of different ize particles, and (*3*) in illustrating the effect of varied emulsifier concentrations n seeded emulsion polymerizations.

Previously measured monodisperse latexes, dispersed on a substrate along with he particles to be measured, were used as calibration standards. The accuracy, reroducibility, and limitations of this method of measurement are discussed.

The relative rates of growth of different size particles in a seeded emulsion polyierization were determined by polymerizing monomer in a seed latex comprised of mixture of two monodisperse latexes. The total particle volume increase was in toichiometric agreement with the volume of added monomer. A mathematically erived relationship of relative particle growth is presented. The effect of varied mulsifier concentrations is shown; too high concentrations yield "new" particles, oo low concentrations result in excessive coagulum.

INTRODUCTION

Monodisperse polystyrene latexes have enjoyed wide acceptance in the eld of electron microscopy (1). Samples of the original 580G Lot 3584 tex were distributed to many laboratories, and a compilation of particle iameter determinations showed agreement among several methods of easurement (2). Later a series of monodisperse polystyrene latexes were repared for wide distribution to other laboratories (3). The particle diamters of this series, ranging from 880 to 11,720 A., were determined by a O diffraction grating replica technique.

These monodisperse polystyrene latexes are of great value in investigaons elucidating the mechanism of emulsion polymerization. If the parcle diameter of a monodisperse latex is known with accuracy, the colloidal stem it comprises may be characterized as to the number of particles, surface area of particles, etc. In addition, if these accurately measure particles can be used as a calibration standard in the measurement o particles of other sizes, the time-consuming SiO diffraction grating replic technique can be circumvented. The purpose of this investigation was t determine the utility of these uniform particles as calibration standard and to illustrate how they may be used to elucidate the mechanism o emulsion polymerization.

---

[1] Presented, in part, at the thirteenth annual meeting of the Electron Microscope ciety of America, Pennsylvania State University, October 27–29, 1955.

MONODISPERSE POLYSTYRENE LATEXES AS CALIBRATION STANDARDS

The use of polystyrene particles from the latex, 580G Lot 3584, as calibration standards has been investigated by many electron microscopists. The compilation of particle diameter determinations by Gerould (2) indicated most investigators found a value of about 2590 A.; a few found higher values, however. Scott (4) encountered discrepancies reminiscent of instrumental fluctuations and irradiation effects. Kern and Kern (5) found that the particle diameter increased when the particles were shadowed obliquely. Ellis (6) found, as did Scott, that the second drop of diluted latex on a specimen increased the diameter of the original particles. He attributed this to the deposition of soluble materials on the latex particles. Watson and Grube (7) found anomalies at high electron intensities and recommended using a specimen composed of uniform particles deposited on a grating replica as a calibration standard.

Recently it was shown that accurate, reproducible particle diameter determinations may be carried out using a SiO diffraction grating replica-stainless steel grid technique (3). The polystyrene latex particles are dispersed directly on a SiO replica of a 30,000 line/inch diffraction grating. The replica is supported by a stainless steel grid; grids of metals such as copper and phosphor-bronze result in particle growth under electron irradiation. Only one photographic exposure is made in a grid opening to decrease the possibility of particle growth due to irradiation. Thus each exposure is calibrated internally as regards magnification; this compensates for any fluctuation in magnification from exposure to exposure. This technique in general yields accurate, reproducible particle diameter measurements; however, the preparation of a separate diffraction grating replica for each latex sample is tedious, time-consuming, and expensive where large numbers of samples are to be measured. If carefully measured polystyrene particles could be used as calibration standards the saving would be considerable.

In order to determine the utility of these latexes as calibration standards, the following experiments were carried out. Two monodisperse polystyrene latexes from our standard series, Runs No. LS-057-A (hereafter designated as 57) and LS-063-A (hereafter designated as 63), were used.

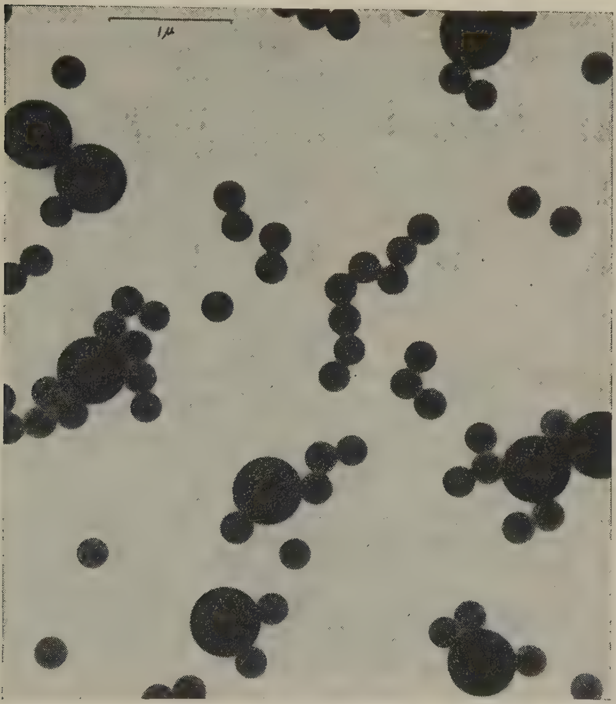

Fig. 1. Typical electron micrograph of a dispersion of two monodisperse latexes.

The particle diameters of these latexes had been determined as 2640 A. and 5570 A., respectively, using the SiO diffraction grating replica-stainess steel grid technique (3). In the first experiment the two latexes were mixed. A drop of the diluted latex mixture was dried on a collodion membrane supported by a 200 count copper lektromesh grid. Since it had been previously shown (3) that no particle growth trend was observed using copper grids *if* the intensity of the electron beam was kept low and each exposure was made in a different grid opening, copper grids were used in hese experiments to eliminate the possibility of magnetic effects. A series of exposures was made in the EMB electron microscope. A different grid opening was used for each exposure. A typical electron micrograph is hown in Fig. 1. The disparity in particle diameters enables one easily to distinguish between the two distributions. The larger particles (63) were measured using a 6.5 power measuring magnifier and the magnification of ach exposure was calculated from these measurements. This magnification was then used to calculate the particle diameter of 57. The data are hown in Table I.

The average particle diameters of 57 agree very well with the 2640 A. value determined previously.

TABLE I

Particle Diameter of Latex 57 Determined Using Latex 63 as a Calibration Standard (Latexes Mixed before Drying)

Exposure number	No. of particles measured (63)	Average magnification	No. of particles measured (57)	Avg. particle diameter (57), *A.*
10067 A	5	7640 ×	20	2660
C	5	7660 ×	21	2660
D	6	7590 ×	21	2650
10077 A	9	7650 ×	25	2690
C	8	7600 ×	25	2660

TABLE II

Particle Diameter of Latex 57 Determined Using Latex 63 as a Calibration Standard (Latex 63 Deposited First, Then Latex 57)

Exposure number	No. of particles measured (63)	Average magnification	No. of particles measured (57)	Avg. particle diameter (57), *A.*
10068 A	7	7610 ×	22	2660
B	9	7630 ×	16	2660
C	4	7630 ×	11	2680
D	8	7590 ×	17	2660
E	8	7600 ×	22	2680

In order to determine the effect of successively drying the particles on a membrane, a drop of diluted 63 latex was dried first, then a drop of diluted 57 was dried on the same specimen grid. Again the larger particles were measured and the magnification calculated. This magnification was used to calculate the diameter of the smaller particles. The data are shown in Table II.

Again the average particle diameters of 57 agree very well with the 2640 A. value determined previously.

In order to determine the effect of the reverse order of particle addition the following experiment was carried out. A drop of diluted 57 latex was dried on a collodion membrane. Then a drop of diluted 63 latex was dried onto the same membrane. Again the larger particles were measured and the the magnification of the exposure calculated. This magnification was used to calculate the diameter of the smaller particles. The data are shown in Table III.

Again these average particle diameters agree very well with the value obtained previously.

The over-all average diameter of 57 determined using 63 as a calibration standard (three different methods of sample preparation) was 2664 A. and the standard deviation, σ, was 42 A. This differs by 24 A. from the "true" value ($\bar{D}$ = 2640 A., σ = 60 A.)—i.e., that obtained using the SiO diffraction grating replica-stainless steel grid technique. The statistical *t*-test shows that this difference may or may not be indicative of analytical bias and invites further experimentation (now in progress). On the other hand when the *t*-test is applied to the individual averages (mixtures of latexes: $\bar{D}$ = 2661 A., σ = 45 A.; 63 dried first, then 57: $\bar{D}$ = 2666 A., σ = 40 A.; 57 dried first, then 63: $\bar{D}$ = 2667 A., σ = 40 A.), the calculated *t*-values fall far below the critical *t*-value at the 1 per cent probability level. Thus the three different procedures of sample preparation yield essentially the same result although this result may be expected to be 18–33 A. (95 per cent confidence limits) higher than the "true" value. However, since the differences expected are only about 1 per cent of the "true" particle diameter, the errors incurred are probably not serious. It is interesting to note that this difference is of the same order of magnitude as the limit of accuracy of the particle measurements (the particle diameter measurements were estimated to the nearest 0.02 mm. using a 6.5 power measuring magnifier; this value, 0.02 mm., is equivalent to 26 A. at 7600× magnification). From these data it appears that, if care is used, these particles can be employed as calibration standards with an accuracy of about 1 per cent.

Since the effect of electron irradiation on latex spheres has been discussed extensively in the literature (2, 3, 6, 7), polystyrene particles of different sizes were studied under identical conditions of irradiation. Samples of the same two latexes were diluted and mixed before a drop was

TABLE III

Particle Diameter of Latex 57 Determined Using Latex 63 as a Calibration Standard (Latex 57 Deposited First, Then Latex 63)

Exposure number	No. of particles measured (63)	Average magnification	No. of particles measured (57)	Avg. particle diameter (57), *A*.
10069 B	5	7670 ×	12	2710
C	6	7680 ×	18	2690
D	6	7640 ×	14	2670
10458 A	7	7540 ×	11	2650
B	4	7560 ×	12	2650
C	5	7560 ×	7	2650
D	6	7540 ×	9	2650

TABLE IV

Effect of Five Minutes Irradiation on Polystyrene Latex Particles of Two Different Sizes in the Same Field

Exposure number	No. of particles	Average particle diameter (63), *mm*.	Per cent increase	No. of particles	Average particle diameter (57), *mm*.	Per cent increase
10077						
A (before)	9	4.26	4.5	25	2.06	12.6
B (after)	9	4.45		25	2.32	
C (before)	8	4.23	4.4	25	2.02	13.6
D (after)	8	4.42		25	2.29	

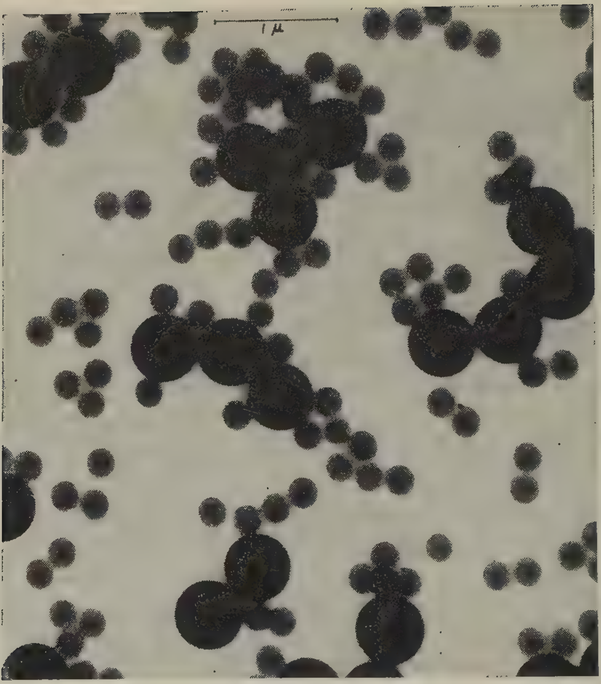

FIG. *a*

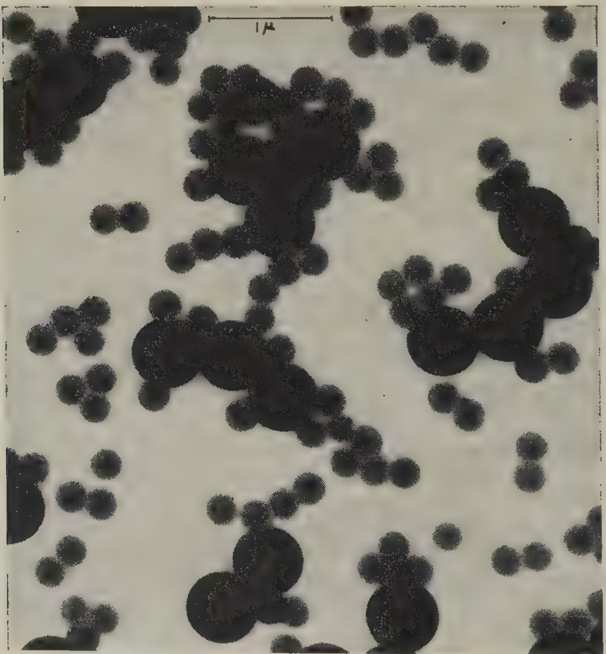

FIG. *b*

FIG. 2. Monodisperse polystrene latexes of different sizes (*a*) before and (*b*) after 5 min. irradiation in the electron microscope.

ried onto a collodion membrane supported by a copper grid. The speci-
en was inserted into the electron microscope and an exposure was made
a typical area containing particles of both distributions. After 5 min.
intense irradiation under the electron beam a second exposure of the
me particles was made. The data are summarized in Table IV.

The original diameter of the larger particles was approximately twice
at of the smaller particles. However, it is interesting to note that the
er cent increase of the smaller particles is about three times that of the
rger ones. In order to determine the actual amount of growth, the mag-
fication of each pair of exposures (before and after) was calculated using
e larger particles before irradiation as a calibration standard. The average
article diameter of 63 increased 250 A. and 240 A., whereas the average
article diameter of 57 increased 340 A. and 360 A., respectively. Therefore
can be concluded that the diameter of the smaller particles increases
a considerably greater rate than the diameter of the larger ones. This
enomenon will be the subject of a future investigation. A typical electron
icrograph of the particles before and after irradiation is shown in Fig. 2.

Kinetics of Competitive Growth

Various aspects of the preparation of monodisperse colloids hav beeen
scussed in the literature (8) and have been utilized by LaMer (9) in the
reparation of monodisperse sulfur sols. Whether the process involved is a
recipitation, a crystallization, or a polymerization, the essential condition
ems to be the supplying of a fixed number of nuclei which subsequently
row to much larger size with no nucleation occurring during this growth
eriod.

Let us consider a swollen latex particle in a typical seeded emulsion
olymerization. Let V represent the volume of polymer in the given par-
cle, and D the diameter of the sphere this amount of polymer would form.
hus V and D are the volume and diameter of the *unswollen* latex particle.
et us assume that the rate of polymerization of a given particle will de-
end upon the diameter, D, in the form of a power law:

$$\frac{dV}{dt} = kD^n. \qquad [1]$$

ere k may vary with the nature of the environment—i.e., with catalyst
ncentration, retarder concentration, temperature, etc. During the
urse of a reaction, k may even vary with time. However, at any one
stant in a particular emulsion polymerization it is assumed to be the
me for particles of all sizes. Since $V = \frac{\pi}{6}D^3$, we obtain:

$$\frac{1}{D} \cdot \frac{dD}{dt} = \frac{2k}{\pi} \cdot D^{n-3}. \qquad [2]$$

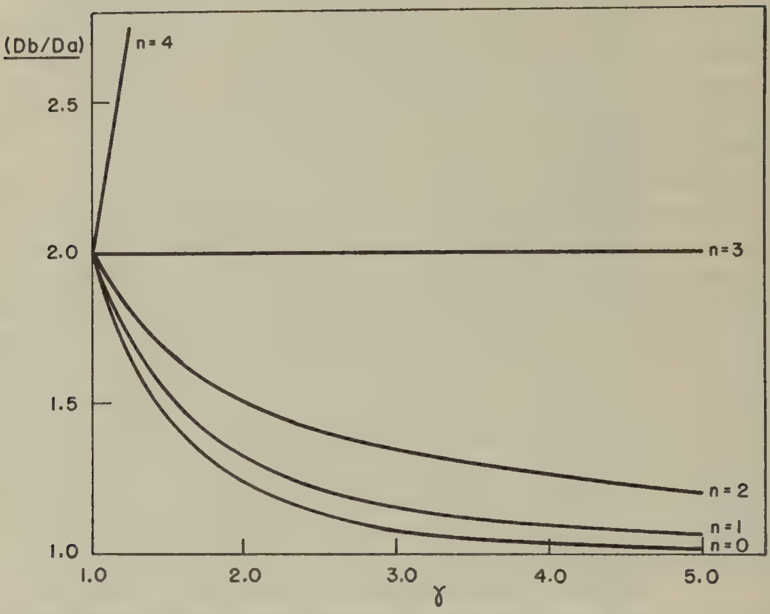

FIG. 3. Theoretical variation of D_b/D_a with γ at integral values of n when $\alpha = 2.00$.

Inspection of Eq. [2] indicates that if $n = 3$, the *relative* rate of diameter growth is independent of size. If $n < 3$, the smaller particles will grow faster than the larger ones and tend to catch up with them. In this case the particle size distribution will be self-sharpening. If $n > 3$, the distribution will broaden, relatively, during the growth reaction.

The integration of Eq. [2] produces:

$$D^{3-n} - D_0^{3-n} = \frac{2(3-n)}{\pi} \int_0^t k(t)\, dt. \qquad [3]$$

Consider now two different groups of latex particles growing from seeds having the initial sizes, D_{a_0} and D_{b_0}, and growing to the final sizes, D_a and D_b.

$$D_b^{3-n} - D_{b_0}^{3-n} = D_a^{3-n} - D_{a_0}^{3-n} = \frac{2(3-n)}{\pi} \int_0^t k(t)\, dt. \qquad [4]$$

Let us now define two ratios, α and γ:

$$\alpha = \frac{D_{b0}}{D_{a_0}} \qquad \text{and} \qquad \gamma = \frac{D_a}{D_{a_0}}$$

and solve Eq. [4] for the ratio of final diameters, D_b/D_a:

$$\frac{D_b}{D_a} = \frac{1}{\gamma} \cdot [\gamma^{3-n} + \alpha^{3-n} - 1]^{1/(3-n)}. \qquad [5]$$

This equation shows how the relative diameters of two different groups of latex particles vary with increasing conversion. This function is plotted against γ in Fig. 3 for the case where $\alpha = 2$ (i.e., some of the seed particles are twice the diameter of the others). Smith (10), in his treatment of emulsion polymerization theory, has indicated that the rate of polymerization per particle is approximately the same for all growing latex particles. This would lead to a very rapid convergence of (D_b/D_a) toward unity, as shown by the curve $n = 0$ in Fig. 3. However, the most direct way to determine n is to seed an emulsion polymerization with particles of two different initial

TABLE V

Stoichiometry of Competitive Particle Growth in Emulsion Polymerization

Sample number	$\frac{\text{Monomer}}{\text{Polymer}}$	%$K_2S_2O_8$	Measured vol. inc., A.^{3}, $\times 10^{-24}$			Theoret. volume inc., A.^{3} $\times$ 10^{-24}
			57	63	Total	
A-1	$\frac{1}{1}$	0.020	0.245	1.61	1.86	1.91
A-2	$\frac{1}{1}$	0.20	0.251	1.66	1.91	1.91
A-3	$\frac{1}{1}$	1.00	0.246	1.46	1.71	1.91
B-1	$\frac{2}{1}$	0.020	0.548	3.17	3.72	3.81
B-2	$\frac{2}{1}$	0.20	0.551	3.35	3.90	3.81
B-3	$\frac{2}{1}$	1.00	0.577	3.69	4.27	3.81
C-1	$\frac{5}{1}$	0.020	1.58	7.96	9.54	9.52
C-2	$\frac{5}{1}$	0.20	1.60	8.06	9.66	9.52
C-3	$\frac{5}{1}$	1.00	2.90	10.7	13.6	9.52
D-1	$\frac{10}{1}$	0.020	3.93	17.2	21.1	19.1
D-2	$\frac{10}{1}$	0.20	3.88	15.9	19.8	19.1
D-3	$\frac{10}{1}$	1.00	8.06	19.4	27.5	19.1

sizes, allow them to compete with each other for monomer in the same system, and measure their sizes after the polymerization reaction.

Experimental Results on Competitive Growth of Latex Particles

The same two monodisperse polystyrene latexes, 57 (2640 A.) and 63 (5570 A.), were mixed together in approximately equal particle concentrations. Styrene monomer was added to the seed charges and the samples were polymerized to completion at 70°C. Various potassium persulfate catalyst concentrations (0.02, 0.20, and 1.00%—based on the aqueous phase) were used. The particle diameters after polymerization were determined using 57 as a calibration standard. No "new" particles were formed. The total measured volume increase of the particles agreed stoichiometrically with the volume increase expected if all the added monomer polymerized completely. This is shown in Table V. The stoichiometric agreement is best at the lower catalyst concentrations.

The experimentally determined values of (D_b/D_a) are plotted against γ in Fig. 4. In this case n seems to be about 2.5. This is much greater than the value $n = 0$ predicted by Smith (10). However, the latexes used by Smith were considerably smaller in diameter and probably were not as uniform as those employed here. Some deviation from $n = \sim 2.5$ is indicated for high monomer/polymer ratios at a catalyst concentration of

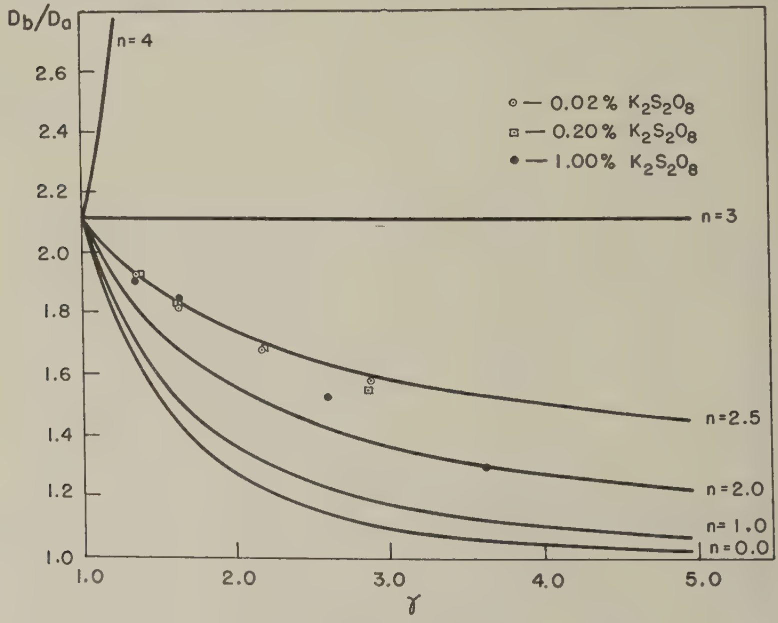

Fig. 4. Experimental variation of D_b/D_a with γ when $\alpha = 2.11$.

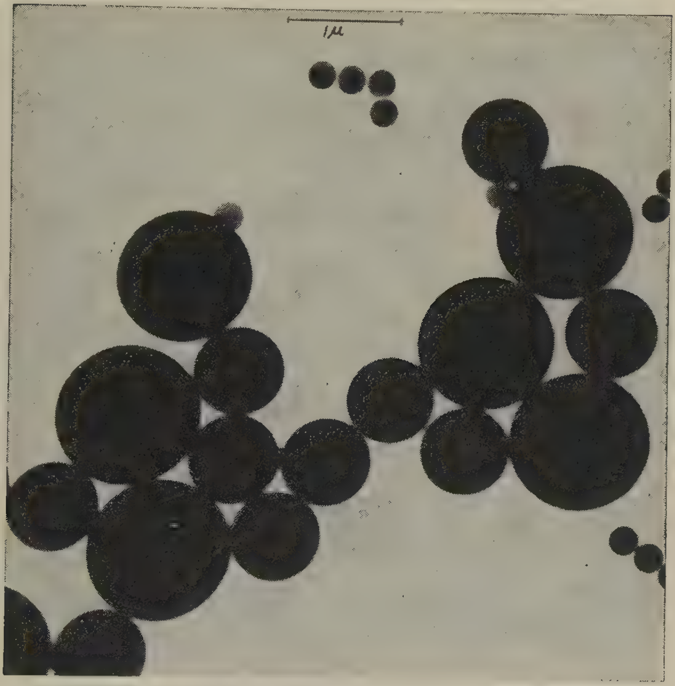

FIG. 5. Typical electron micrograph from which competitive growth measurements were made.

.00 %. More extensive experiments, now in progress, will elucidate com-
etitive particle growth for particles of various sizes under widely varying
xperimental conditions. A typical electron micrograph from which these
easurements were made is shown in Fig. 5. The two final particle size
stributions are easily distinguishable from one another and from the
libration particles.

EFFECT OF SOAP CONCENTRATION ON SEEDED EMULSION POLYMERIZATION

In order to utilize the self-sharpening tendency of growing latex par-
le distributions, and to achieve a more uniform final product, two fur-
er conditions must be met: (*1*) no "new" seed particles can be permitted
form during the reaction, and (*2*) the agglomeration of latex particles
ust be prevented. This can be accomplished by controlling the soap
ncentration. If the soap concentration is too low, the latex will be un-
ble and aggregation will occur; if the soap concentration is too high,
ew" particles will form.

A series of polymerizations using 57 as a seed latex illustrates these prin-
les. In each polymerization the amount of soap (based on added mono-

TABLE VI

Effect of Soap Concentration in Seeded Emulsion Polymerization

Sample number	% Additional soap (based on monomer)	% Coagulum (based on monomer)	"New" particle initiation
1	0.00	7.5	None
2	0.20	3.7	None
3	0.95	0.07	None
4	1.70	None	None
5	2.45	None	None
6	3.57	None	~0.2 × 10^{13}/cc.
7	4.70	None	13 × 10^{13}/cc.
8	5.57	None	41 × 10^{13}/cc.

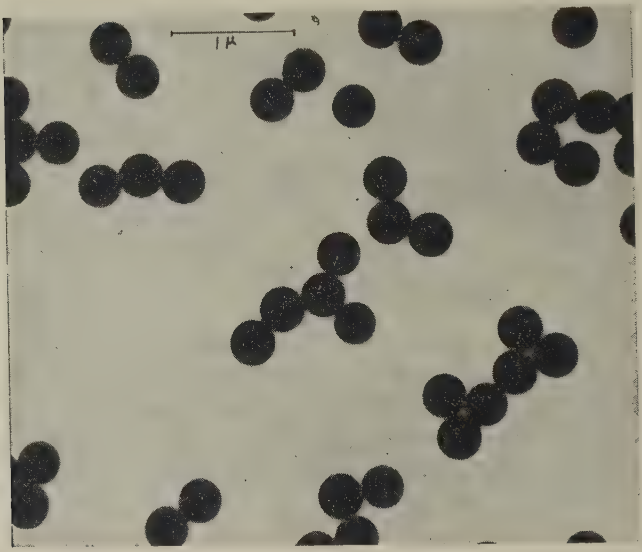

FIG. 6. Typical electron micrograph illustrating the effect of 0.00–2.45% soap added in a seeded emulsion polymerization.

mer) was increased. This experiment is similar to one previously carried out with a polyvinyltoluene latex by Vitkuske *et al.* (11). Table VI shows the results of these experiments.

At the lower soap concentrations coagulum was formed, whereas at higher concentrations a new crop of small particles was initiated. However, there is a broad range of soap concentrations between the disappearance of coagulum and the initiation of "new" particles. Figures 6, 7, 8, and 9 are electron micrographs of the final latexes. Figure 6 is typical of Samples

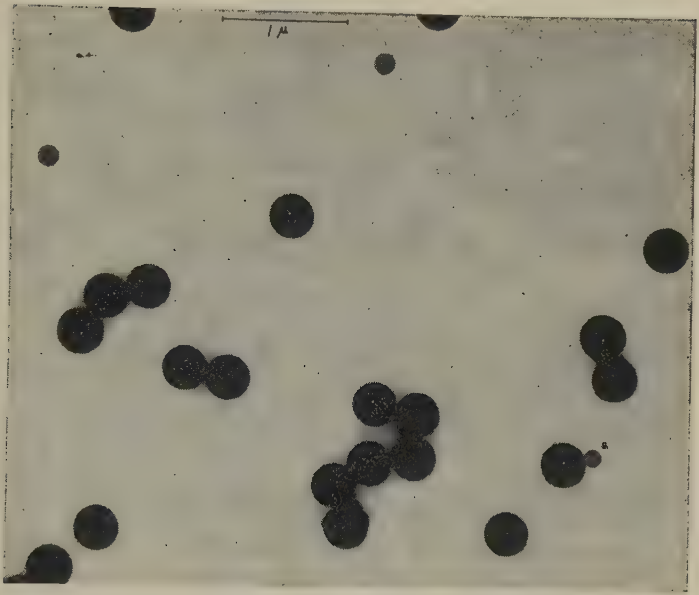

FIG. 7. Electron micrograph illustrating the effect of 3.57% soap added in a seeded emulsion polymerization.

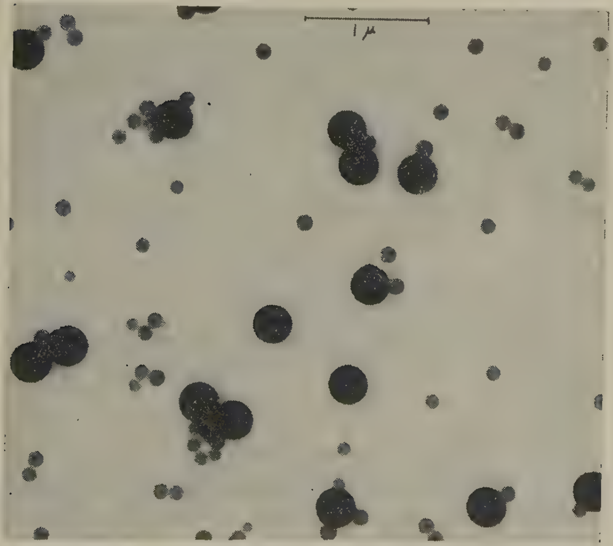

FIG. 8. Electron micrograph illustrating the effect of 4.70% soap added in a seeded emulsion polymerization.

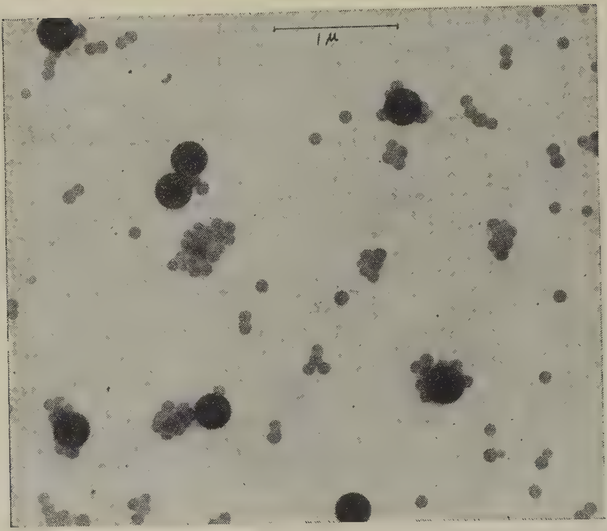

Fig. 9. Electron micrograph illustrating the effect of 5.57% soap added in a seeded emulsion polymerization.

1–5, where there were no "new" particles initiated. In Fig. 7 (Sample 6) a few "new" particles are evident. Figure 8 (Sample 7) shows more "new" particles, and a still greater number is seen in Fig. 9 (Sample 8). As the soap concentration increases, the "new" particles become smaller and more numerous while the final particle diameter of the original seed particles decreases. The numbers of "new" particles in Samples 6–8 were calculated from the difference between the experimentally determined total volume increase and the volume increase expected if all the monomer polymerized completely. These values are shown in Table VI. The concentration of particles in the original seed latex (57) was 2.2×10^{13}/cc. These experiments illustrate the importance of soap concentration in seeded emulsion polymerizations.

ACKNOWLEDGMENTS

The authors wish to acknowledge the assistance and cooperation of W. D. Keiser, H. E. Campbell, L. E. Morford, and W. D. Holzhausen, of the Physical Research Laboratory.

REFERENCES

1. Backus, R. C., and Williams, R. C., *J. Appl. Phys.* **20,** 224 (1949); *ibid.* **21,** 11 (1950); Gerould, C. H., *ibid.* **21,** 183 (1950); Ming Feng, I., *ibid.* **22,** 820 (1951).
2. Gerould, C. H., *J. Appl. Phys.* **21,** 183 (1950).
3. Bradford, E. B., and Vanderhoff, J. W., *J. Appl. Phys.* **26,** 864 (1955).
4. Scott, G. D., *J. Appl. Phys.* **20,** 417 (1949).
5. Kern, S. F., and Kern, R. A., *J. Appl. Phys.* **21,** 705 (1950).

6. Ellis, S. G., *J. Appl. Phys.* **23,** 728 (1952).
7. Watson, J. H. L., and Grube, W., *J. Appl. Phys.* **23,** 793 (1952).
8. Reiss, Howard, *J. Chem. Phys.* **19,** 482 (1951); LaMer, V. K., and Dinegar, R., *J. Am. Chem. Soc.* **72,** 4847 (1950).
9. LaMer, V. K., and Barnes, M. D., *J. Colloid Sci.* **1,** 71 (1946); LaMer, V. K., and Dinegar, R., *J. Am. Chem. Soc.* **72,** 4847 (1950).
0. Smith, W. V., *J. Am. Chem. Soc.* **70,** 3695 (1948).
1. Vitkuske, J. F., Vanderhoff, J. W., Bradford, E. B., and Alfrey, T., Jr. Presented at the 128th meeting of the American Chemical Society, Minneapolis, Minnesota, September, 1955.

JOURNAL OF COLLOID SCIENCE **11**, 150–157 (1956)

THE LIESEGANG PHENOMENON
III. THE STRUCTURE OF THE GEL MEDIUM

A. Packter*

Clay Development Laboratory, F. W. Berk & Co., London Colney, Herts, England.

Received March 2, 1955; revised July 7, 1955

ABSTRACT

The effects of (*1*) hydrogen ion, and formaldehyde, (*2*) chloride ion, and detergents, have been investigated on the rhythmicity of silver chromate precipitated in gelatine gels and compared with their action on the corresponding aqueous suspensions.

The results throw light on the structure of the set gel, and its influence on the precipitation of the above salt.

INTRODUCTION

In a previous work (1), we have demonstrated the parallelism between the adsorption factor, *A*, in the rhythmic precipitation of metal salts in gelatine gels, and the stability of the corresponding sol in the aqueous suspension. Further experiments have indicated that adsorption and sol peptization in the set gel may also be affected by the actual structure of the gel.

Whereas the stability of sols in the aqueous suspension increases continuously with the gelatine concentration, the rhythmicity of silver chromate precipitated in the corresponding set gel remains constant after a limiting value of 2%–3%. Low concentrations of hydrogen ion and aldehydes, on the other hand, show far greater effects on the spacing in the set gels than corresponds to the increase in stability of the aqueous sol; whereas traces of electrolytes and detergents, which have a marked flocculating effect on this system, show no such effect on the corresponding aqueous suspension.

The results indicate that at gelatine concentrations above 3%, the structure of the set gel becomes more and more interlinked, and no further free carboxyl or amino groups are available for protection of the silver chromate sol. Chloride ion and anionic detergents discharge NH_3^+ groups along the polypeptide chain, and this leads to marked reduction in protecting power; while addition of hydrogen ions and formaldehyde leads to increasing availability of free carboxyl groups and increases the spacing coefficient.

---

* Present address: Glaxo Laboratories Ltd., Greenford, Middlesex, England.

In the aqueous suspensions, this interlinking of polypeptide chains occurs to far less a degree, and the effect of the above reagents is correspondingly less marked.

The flocculent-silver ion ratio at which maximum flocculation occurs is a measure of the amount of free carboxyl or amino group adsorbed onto the sol surface. The stability of silver chromate sols in gelatine is shown to fall very rapidly with increase in concentration of the reacting ions, while the adsorbed protecting agent is more readily discharged from the concentrated sols.

EXPERIMENTAL

1. Aqueous Suspensions

The flocculation and peptization of silver chromate sols by formaldehyde, chloride ion, and long-chain anionic detergents has been investigated.

Experimental Technique. As in previous paper (1).

Materials.

Gelatine. As supplied by the British Gelatine Works; all electrolyte and free amino acids removed by treatment with ion-exchange resins.

Alcohols, Amines, etc. Twice redistilled under vacuum.

Sodium Dodecyl Sulfate (S.D.D.S) Prepared synthetically by interaction of pure lauryl alcohol with chlorosulfonic acid in chloroform. The crude sulfate is dried, washed with acetone, and recrystallized from aqueous alcohol.

TABLE I

Peptization Ratios of Amino Acids for Silver Chromate Sols

Addition of formaldehyde

A. Glycine (pH 4)

	Glycine	1 Glycine/1 HCHO	1 Glycine/10 HCHO
0.0005 *M* sol	40	12	10
0.001 *M* sol	200	25	12.5
0.0025 *M* sol	>500	50	16

B. Glutamic Acid (pH 4)

	G.A.	1 G.A./1 HCHO	1 G.A./10 HCHO
0.0005 *M* sol	0.7	0.6	0.6
0.001 *M* sol	1.5	1.5	1.5
0.0025 *M* sol	2.0	2.0	2.0
0.005 *M* sol	>10.0	5.5	4.0

(5% suspension)

C. Gelatine (pH 5)

	No addition	0.1 *M* HCHO	*M* HCHO
0.001 *M* sol	1.13	1.09	0.63

Cetyl Trimethyl Ammonium Acetate (*C.E.T.A.A.*) B.D.H. "CETAB" is treated with its equivalent of alcoholic caustic potash. The crude hydroxide solution is filtered, neutralized with 5 *N* acetic acid; and after removal of the bulk of the alcohol by distillation, the acetate is recrystallized twice from acetone.

a. Flocculation by Traces of Anion. Whereas traces of Cl′ ion discharge the Ag^+ stabilized silver chromate sols (1) and increase the rate of coagulation, the *gelatine protected* sols have been found to be completed unaffected up to $C_{Cl'} = 0.05\ N$.

b. The Effect of Aldehydes on the Peptizing Power of Amino Acids. We have shown in a previous work (1) that the peptizing power of amino acids and gelatine for silver salts is very much dependent on the hydrogen ion concentration. Fall in pH < 5 leads to increasing availability of free carboxyl groups, with decrease in the *peptization ratio.*

Similar results have been obtained by addition of aldehydes to these protecting agents. Some typical results are presented in Table I.

It is seen that formaldehyde interacts with the amino acids at their isoelectric point, to liberate free carboxyl groups, with a corresponding rise in protecting power. (No appreciable change in pH occurs.)

High concentrations (0.2 *M–M*) of formaldehyde, however, are generally required to cause an appreciable effect.

2. Gel Systems

Experimental Technique. As in previous work (2).

a. Variation in Concentration of the Gel Medium. The effect of variation in concentration (C_G) of the gel medium on the rhythmicity has been followed for silver chromate precipitated in gelatine gels. (Refer to Table II.)

Increase in $C_G > 3\%$ leads to no corresponding increase in the spacing. (The rate of *crystal growth,* however, may further decrease with rise in C_G. At $C_G > 5\%$, silver chromate is precipitated in indistinct planes of barely visible crystals.)

b. The Addition of Electrolytes (and Detergents). The effects of these

TABLE II

Rhythmic Precipitation of Silver Chromate in Coignet Gelatine Gels

	A values	
C_G	0.005 *M*	0.01 *M*
2%[a]	0.005	0.005
3[a]	0.014	0.010
4	0.021	0.014
5	0.021	0.014
6	0.021	0.014

[a] The rigidity of these gels is enhanced by addition of 0.5% agar.

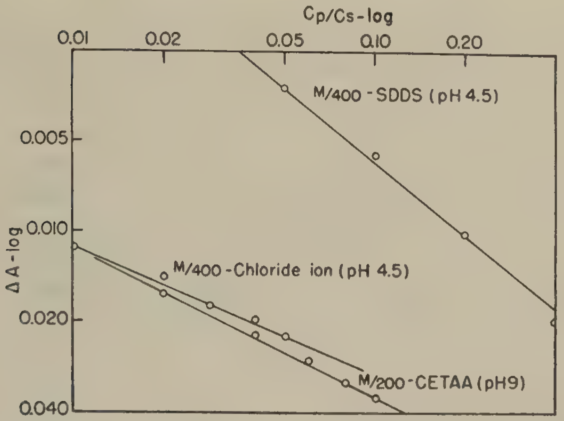

FIG. 1. Flocculation of silver chromate, precipitated (by excess anion), in 5% gelatine gel. Variation in spacing with flocculant-silver ion concentration ratio.

TABLE III

Flocculation of Silver Chromate in 5% Gelatine Gels (pH 4.5) by Chloride Ion

	A_0	$[C_{\mathrm{Cl}'}/C_s]_{\max}$	α
0.00125 *M* sol	>0.500	>1.000	<0.01
0.0025 *M* sol	0.160	0.100	0.05
0.005 *M* sol	0.048	0.030	0.16
0.01 *M* sol	0.005	0.002	>0.30

reagents are best studied by diffusing excess CrO_4'' ion (normal solution) into the gel containing silver nitrate, together with varying amounts of the reagent under investigation. (If the cation is diffused into the gel, excess Ag^+ ion would interact with certain of these materials (*cf.* ref. 2).)

(*1*) *Chloride ion* ($pH < 5$). Whereas chloride ion has no effect on the aqueous gelatine peptized suspension of silver chromate, a marked flocculation is observed in the set gel, at very low Cl'/Ag^+ concentration ratios.

At high initial CrO_4'' concentration ($>0.5\ N$), the variation in B—in the relation $(k - 1) = A + B/C_0$,—may be neglected, and $\Delta A = \Delta k$.

The decrease in A is connected to $C_{\mathrm{Cl}'}/C_s$ according to a Freundlich type of relation

$$-\Delta A = \alpha \left[\frac{C_{\mathrm{Cl}'}}{C_s}\right]^n \qquad [1]$$

where α and n are constants, and C_s is the sol concentration. α is the value of ΔA at $C_{\mathrm{Cl}'}/C_s = 1$. This relationship is demonstrated in Fig. 1.

Beyond some *minimum* spacing, a repeptization is observed.

The values of $C_{\mathrm{Cl}'}/C_s$ corresponding to the minimum value of A are shown in Table III, together with the values of α and A_0 (the A value obtained in the absence of flocculating agent).

The stability of the sols—as measured by the $C_{\text{Cl}'}/C_s$ value for maximum flocculation—decreases rapidly with rise in sol concentration. The value of α increases at the same time, demonstrating that the adsorbed gelatine is more readily discharged from the more concentrated sol.

Previous work (2) on the variation of A_0 with hydrogen ion concentration has indicated that this constant is determined by the adsorption of carboxyl groups onto the sol. There is, indeed, a direct correlation between A_0 and $[C_{\text{Cl}'}/C_s]$ which is also a measure of the adsorbed carboxyl groups.

(2) Long-chain anions. $pH < 5$. In acid gelatine, detergents such as S.D.D.S. and sodium oleate behave in a similar manner to the chloride ion. (Refer to Table IV.)

The flocculation effect is less marked owing to the uptake of detergent by the gelatine (3).

$pH > 7$. In alkaline gelatine, S.D.D.S. peptizes silver chromate systems.

(3) Long-chain cations. $pH > 7$. In *alkaline* gelatine traces of cationic detergents also flocculate the silver chromate system. The fall in A is again given by Eq. [1]. (Fig. 1.)

Repeptization occurs at higher C_F/C_s ratios.

The C_F/C_s ratios for maximum flocculation are presented in Table V, together with the values of α and A_0.

As with chloride and long-chain anion, the flocculation effect increases with rise in C_s.

A_0 is seen to depend on the adsorption of free amino groups.

$pH < 5$. In *acid* gelatine, C.E.T.A.A. peptizes silver chromate.

c. *The Addition of Aldehydes.* The effect of addition of aldehydes has been investigated on the 0.005 M silver chromate system precipitated in 5% Coignet gelatine gels.

TABLE IV

Flocculation of Silver Chromate in 5% Gelatine Gels (pH 4.5) by Sodium Dodecyl Sulfate

	$^a[C_F/C_s]_{\max}$	α
0.0025 M sol	0.02	0.040
0.005 M sol	0.30	0.030
0.01 M sol	1.20	0.025

$^a C_F$ = concentration of flocculant.

TABLE V

Flocculation of Silver Chromate in 5% Gelatine Gels (pH 9.0) by Cetyl Trimethyl Ammonium Acetate

	A_0	$[C_F/C_s]_{\max}$	α
0.0025 M sol	>0.300	>0.250	<0.01
0.005 M sol	0.150	0.080	0.14
0.01 M sol	0.020	0.005	>0.50

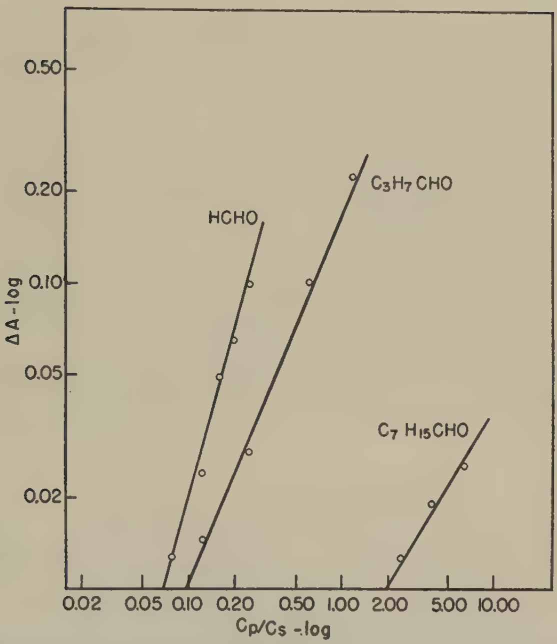

FIG. 2. Peptization of 0.0025 *M* silver chromate, precipitated in 5% gelatine gel. Variation in spacing with aldehyde-silver ion concentration ratio.

Formaldehyde gives a marked increase in spacing at low HCHO/Ag^+ ratios, whereas the higher aldehydes are less effective. (Refer to Fig. 2.)

It is seen that complete peptization is reached at very much lower HCHO concentrations than has been found with the aqueous 5% gelatine suspensions.

DISCUSSION

In the previous work (2) we have noted the parallelism between the adsorption factor *A*, in the spacing relation for rhythmic precipitation (of insoluble metal salts in gelatine gels), and the stability of the corresponding sol in aqueous suspension. The experimental data of this work demonstrate that the adsorption and sol protection in the set gel may also be appreciably affected by the actual structure of the gel.

Marked flocculation effects have been observed on addition of very low concentrations of certain electrolytes to silver chromate systems in gelatine gels. These cannot be due to an interaction with the reacting ions, since withdrawal of about 1%–2% of silver or chromate ion by adsorption or complexing would lead at most to a slightly enhanced stability of the "supersaturated" system, and an *increase* in the spacing coefficients (2).

On the other hand, dilute electrolyte solutions may cause appreciable modifications of the physicochemical properties of protein suspensions and gels (4, 5); while reagents such as formaldehyde which react with the ϵ-amino groupings of the lysine residues in gelatine also cause marked changes in structure (6). The internal structure of a gelatine gel—which is mainly determined by the interlinking of adjacent carboxyl and amino groups—will be especially sensitive to slight variations in electrical properties in the region of the isoelectric point (4, 7) and at gelatine concentrations above 3 %, where very few such free amino or carboxyl groups may be available for protection of metal salt sols. (Refer to Table II.)

It thus appears that the flocculation and peptization effects observed are caused by such modifications in the physicochemical make up of the gel medium; and the following mechanism is proposed. (The flocculating action of traces of chloride ion has indeed been discussed in an earlier work (2).)

1. Flocculation by Electrolytes, etc.

The flocculating action of traces of chloride ion has been discussed in a previous work (2). In *acid* gelatine, the negative ions discharge NH_3^+ groups along the polypeptide chain; the uncharged amino groups will consequently associate with adjacent uncharged carboxyl groups, thereby reducing the number available for adsorption onto the silver chromate sol. Anionic detergents behave similarly, owing to the interaction between the NH_3^+ group and the RSO_4' or $RCOO'$ anion (3). Traces of cationic detergents, on the other hand, flocculate the silver chromate system in *alkaline* gelatine, by discharging COO' groups, and consequent reduction in the number of free amino groups for adsorption onto the sol.

The flocculant-sol concentration ratio at which the maximum flocculation is observed enables a rough estimate to be made of this adsorption. Although a 5 % suspension may in the fluid state contain about 0.0625 N free glutamic acid, and 0.05 N free lysine residues (5), the limiting spacing reached in the set gels suggests that the greater part of such groups are no longer available, as the gel structure is formed by interlinking of adjacent polypeptide chains. It is seen in fact, that even with the 0.0025 M sol in acid gelatine where peptization is quite marked ($A > 0.150$), only about 0.001 N free carboxyl groups are adsorbed onto the sol; whereas in alkaline gelatine, only about N/2500 free amino groups are adsorbed onto the 0.005 M sol. With increase in particle size of the sol, the protection falls to a marked extent, since the ordered structure of the set gel will limit the adsorption onto the larger sol particles, formed at higher concentrations of the reacting ions.

2. Peptization by Hydrogen Ion: Formaldehyde

Increase in spacing is observed when additional free carboxyl groups are made available for adsorption onto the silver chromate sol, as by the addition of low concentrations of acetic acid (1) or of formaldehyde (4) to the gelatine suspensions.

In the set 5% gels at the isoelectric point of gelatine (pH 5), marked peptization ($A > 0.200$) of 0.0025 M silver chromate sols is obtained on addition of 0.002 N formaldehyde, or about 0.002 N acetic acid, and liberation of similar amounts of free carboxyl groups. In view of the various assumptions made, these results are in good agreement with those estimated from flocculation experiments.

In the fluid suspensions (at pH < 5), the polypeptide chains are far more mobile, and the effect of traces of all the above reagents will be correspondingly far less marked. Very much higher concentrations of hydrogen ion and formaldehyde are required for complete peptization of the silver chromate sols; while chloride ion shows no corresponding flocculating effect.

ACKNOWLEDGMENTS

This work has been carried out at Kings College, London. I wish to thank Professor Sir E. K. Rideal for his helpful interest.

REFERENCES

1. PACKTER, A., AND MATALON, R. *Discussions Faraday Soc.* **18,** 161 (1954).
2. MATALON, R., AND PACKTER, A., *J. Colloid Sci.* **10**(1), 46 (1955).
3. MATALON, R., AND SCHULMAN, J. H., *Discussions Faraday Soc.* **6,** 27 (1949).
4. LOEB, J., "Proteins and the Theory of Colloidal Behaviour," Ch. 5. McGraw Hill, London, 1924.
5. KRUYT, H. R., "Colloid Science," Vol. 2, Ch. 7. Elsevier Publishing Co., Amsterdam, 1949.
6. FRENCH, D., AND EDSALL, J. T., *Advances in Protein Chem.* **2,** 277 (1945).
7. FERRY, J. D., *Advances in Protein Chem.* **4,** 1 (1945).
8. CHIBNALL, A. C., *Proc. Roy. Soc.* (*London*) **B131,** 136 (1942).

JOURNAL OF COLLOID SCIENCE **11,** 158–166 (1956)

HYDROPHOBIC MONOLAYERS ON PLATINUM, MICA, AND SILIC

D. J. O'Connor[1] and J. V. Sanders

Division of Tribophysics, C.S.I.R.O., University of Melbourne, Australia

Received January 3, 1956

ABSTRACT

The wetting behavior of plates of platinum, mica, and silica has been determin
after their immersion in aqueous solutions of two anionic and two cationic detergen
(sodium cetyl sulfate, potassium laurate, and cetyl trimethylammonium bromid
dodecyl trimethylammonium bromide) over the range of concentrations M to 10^{-9}
In general, a surface becomes hydrophobic to the solution at a low concentration b
is completely wetted by a more concentrated solution (ca. 10^{-3} M) of the same co
pound. The anionic detergents, however, wet silica over the whole range of conce
trations. The concentrations which define the limits of the hydrophobic range
solutions have been determined. These are interpreted in terms of adsorption of o
or two monolayers of the long-chain ions at the liquid-solid interface.

INTRODUCTION

When a solid is immersed in a solution of a long-chain compound unde
certain circumstances an oriented monolayer is adsorbed on its surfac
Zisman has shown that this adsorbed monolayer lowers the surface energ
of the solid and makes the surface hydrophobic or oleophobic. The effec
has been observed with dilute solutions of many long-chain amphoteri
compounds in aqueous and nonaqueous liquids (1–3). However, the gen
eral experience of washing procedures, and flotation studies (4), and th
experiments of Kahan (5) show that more concentrated aqueous solution
of detergents will usually wet solids. It appears, therefore, that there is a
intermediate concentration at which the wetting properties of the solutio
change. In the experiments to be described, the wetting behavior of som
aqueous detergent solutions has been determined over a wide range of con
centrations by observations of whether a clean specimen of platinum, mica
or silica retains a liquid film or exhibits a hydrophobic surface when re
moved from the solutions. It is confirmed that if a surface becomes hydro
phobic in dilute solutions, it will, in general, be completely wetted by mor
concentrated solutions. With increasing concentration there is thus
critical concentration where the surface first becomes hydrophobic, an
another critical concentration of a larger value at which the surface is re

---

[1] Now at United Kingdom Atomic Energy Authority, Atomic Energy Researc
Establishment, Harwell, Berks., England.

etted by the solution. The two critical concentrations have been determined for the three solids in solutions of both anionic and cationic compunds of two different chain lengths.

EXPERIMENTAL

The wetting behavior of aqueous solutions of sodium cetyl sulfate (Na-S), cetyl trimethylammonium bromide (CTAB), dodecyltrimethylammo-um bromide (DTAB), and potassium laurate (KL) was examined on ean platinum, mica, and silica over the concentration range M to 10^{-9}. The solid specimens were made into the form of flat plates about 1 cm. 0.5 cm. × 0.1 mm., with a hole near one edge through which a loop of tinum wire was threaded. The surface of the platinum specimen was rolled, the mica was cleaved, and the silica had a smooth, fired surface. e platinum and the silica were chemically cleaned and flamed to red at, and the mica cleaved on both sides immediately before being used. e specimens were hung on a hook at the end of a glass rod and suspended the dipping cell, above the liquid, to cool. The dipping cell, illustrated Fig. 1, contained about 20 ml. of the solution to be tested. When the an plate was cool it was lowered into the solution; it was withdrawn r 1 min. and examined for 15 sec. to determine its wetting behavior.

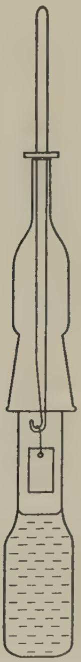

FIG. 1. The dipping cell showing a specimen suspended above the solution.

It was then replaced in the solution and examined again after 2, 3, 5, 10, 20 30, and 60 min. All the tests were carried out at room temperature (21° ± 4°C.). All solutions were made from high-purity, doubly distilled, wate of specific conductivity $< 10^{-6}\ \Omega^{-1}\ \text{cm.}^{-1}$, and stored in stoppered Pyre glass flasks. They were aged for at least 1 day before being used. Excep for the KL solutions which were brought to pH 10 with KOH, all solution were tested at their natural pH. The glass dipping cell was cleaned wit hot chromic acid, washed in tap water, then distilled water, and finall rinsed with conductivity water. The platinum and silica plates were cleane before every experiment. The surface-active chemicals were high-purit laboratory-prepared samples.

RESULTS

The surfaces of the three solids are completely wet by all the solution at very low concentrations (10^{-9} *M*) so that when the specimen plate i removed from the solution it retains a visible, continuous, liquid film. I general, as the concentration is increased, a part of the surface, usuall near the lower edge, becomes hydrophobic to the solution. This area increases with longer times of immersion. Solutions of greater concentration produce a larger hydrophobic area until at a particular concentration th whole specimen becomes hydrophobic. In this state when the plate i removed from the solution it sheds any liquid and can be withdrawn com

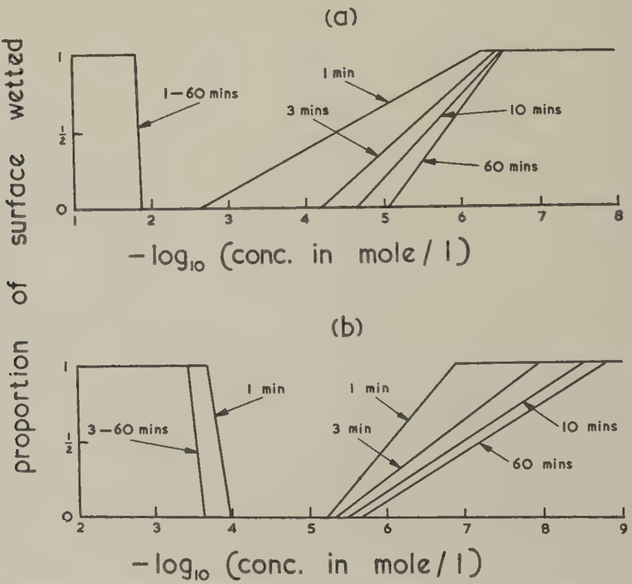

FIG. 2. The average wetting behavior as a function of concentration for variou times of immersion of specimens of (a) platinum in DTAB, and (b) mica in CTAB.

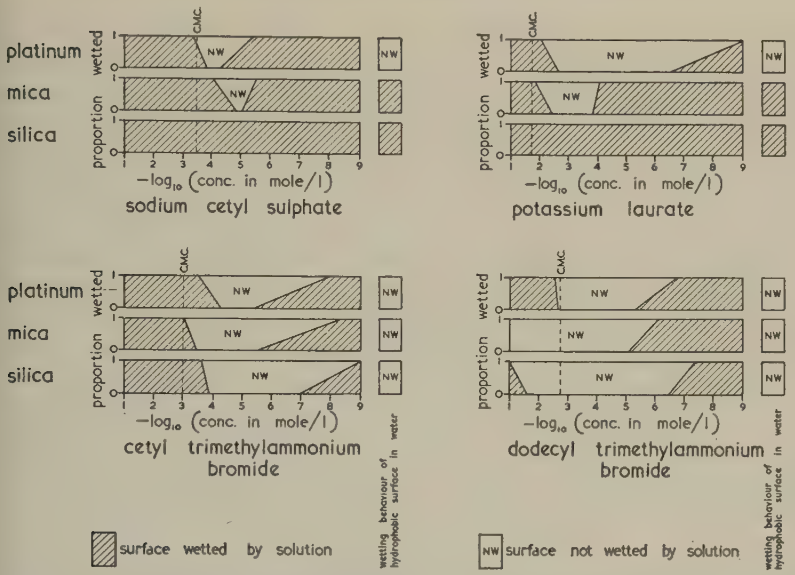

FIG. 3. The wetting behavior of platinum, mica, and silica when removed from
etergent solutions after one hour's immersion. The slanting boundaries have the
me significance as in Figure 2.

letely dry. This concentration, at which the change to nonwetting of the
hole specimen occurs, we shall call the first critical concentration (C_1).
s the concentration is increased still further a second critical concentra-
on (C_2) is reached at which the surface is again completely wetted by the
olution, so that when the specimen is withdrawn from the solution it
tains a continuous liquid film on the surface.

In these experiments no attempt has been made to correct the concen-
ations of the dilute solutions for adsorption on the walls of the con-
iners, so that the values less than 10^{-6} M are not quantitatively signifi-
ant, especially for the cationic compounds. When the concentration is
eater than about 10^{-6} M, there are more adsorbate molecules present
the solution than is necessary to provide a close-packed monolayer on
l the surface exposed to the solution in the dipping cell and the values
ecome authentic.

At concentrations near the critical values the proportion of surface
etted depends upon the time of immersion of the plate. Two examples are
ven in Fig. 2, where the proportion of area wetted is plotted against con-
ntration for immersion times up to 1 hour, for (*a*) platinum in DTAB,
d (*b*) mica in CTAB. Immersion times of more than 1 hour produce no
rther change. The time effect is always more pronounced for the first
an for the second critical concentration, the increase in hydrophobic
a taking place mainly in the first 10 min. Equilibrium at the second

critical concentration is attained, however, within about 5 min. The overall effect of increasing the time of immersion is to broaden the range of concentrations within which a completely hydrophobic surface is obtained.

The results for an immersion time of 1 hour in the two cationic and two anionic detergents are presented in Fig. 3. This shows that there is a restricted range of concentrations over which the specimens may be removed with a hydrophobic surface for all the specimen-detergent pairs except the silica-anionic combinations. The slanting lines indicate, as in Fig. 2, that at concentrations less than the first critical concentration, and slightly less than the second, only a part of the area retains a liquid film.

The surfaces which were hydrophobic to the solutions were tested in another cell containing pure water, and the wetting behavior determined. As can be seen in Fig. 3, specimens which were hydrophobic to solutions were also hydrophobic to water except for surfaces produced on mica and silica by the two anionic detergents. The other hydrophobic surfaces were not wetted even after prolonged washing in water.

Discussion

The First Critical Concentration (C_1)

The first critical concentration is the minimum concentration at which the adsorption is sufficient to lower the surface energy of the whole of the solid area to such a value that a finite contact angle is observed.

The presence of an oriented monolayer on some selected hydrophobic surfaces was confirmed by an examination of the specimens by electron diffraction. The diffraction patterns exhibited the diffuse bands typical of monolayers of compounds of this type (6), but indicated that the molecules were not quite so well oriented as, for example, in monolayers of the fatty acids adsorbed from paraffin solutions (7).

The very low values of C_1 (e.g., 10^{-7} M for silica in CTAB), whilst being only qualitative, indicate strong adsorption. The larger values such as ca. 10^{-5} M for platinum and mica in NaCS signify that the surfaces are incapable of removing all the long-chain material from solution as a hydrophobic monolayer. This corresponds to the results of Zisman (1), who found that platinum would not remove all the octadecyl alcohol molecules from a solution in a nonpolar solvent.

The time dependence of the wetting behavior at concentrations near C_1 may be only partly a real effect. It is possible that extra molecules may be collected from the liquid-air surface when the plate passes through the interface. However, usually the lower portion of the specimen becomes hydrophobic first, whereas the upper part is the first to pass through the interface in all withdrawals made for examination subsequent to the first dip.

The differences in behavior of the three solids can be reasonably explained y a consideration of the different processes by which the monolayer is dsorbed. For the particular solids chosen, the adsorption mechanisms ust be different. Platinum will physically adsorb surface-active ions by irtue of the free mobility of the electrons in the surface. Adsorption will ot depend upon the charge of the ion, and consequently a hydrophobic ayer will be formed in cationic and anionic detergent solutions. However, referential adsorption occurs on silica, where hydrolysis of the surface nd subsequent dissociation of surface hydroxyl groups leaves the surface egatively charged. The anionic reagents are not adsorbed to any extent, nd the surface is completely wet throughout the concentration range of aCS and KL. CTAB and DTAB are strongly bound to this surface, probbly by an ion-exchange process (8). The cleavage face of mica contains in ddition to SiO_2 groups some K and Al ions which provide sites for the ossible adsorption of anions. Mica can thus become hydrophobic in NaCS nd KL, as well as in the cationic solutions, but a higher concentration of dsorbate is necessary in the case of the anionic reagents. The weak atachment of the anionic monolayer to mica allows it to be desorbed by ashing to give a hydrophilic surface. This is the only example in this set f experiments of a surface which is hydrophobic to a solution but which ecomes hydrophilic to water when it is rinsed.

The combinations of long-chain compounds and solids used in these exeriments thus provide a range of adsorption forces. The value of C_1 indiates the strength of this bond. It is to be expected that the value of C_1 ould depend upon the pH of the solution, but as yet no measurements ave been made at other pH values.

The Second Critical Concentration (C_2)

With the single exception of mica in DTAB, surfaces which are hydrohobic at intermediate concentrations can be wetted again at higher conntrations to give a sharp value for C_2. For a given surface-active comound the value of C_2 differs only slightly for the three solids.

Since C_2 is the concentration at which the liquid will just be retained as film on the surface, we have

$$\gamma''_{LV} = \gamma''_{SV} - \gamma''_{SL},$$

here γ_{LV} is the surface tension of the liquid,
γ_{SV} is the surface tension of the solid + monolayer,
d γ_{SL} is the interfacial tension between solid + monolayer and the liquid,

′ indicating that the values are at concentration C_2. The equality is, of urse, justified only at the critical point of change from wetting to nontting. Figure 4 shows how the two critical states of change of wetting havior can occur. The full curve represents the change in γ_{LV} with con-

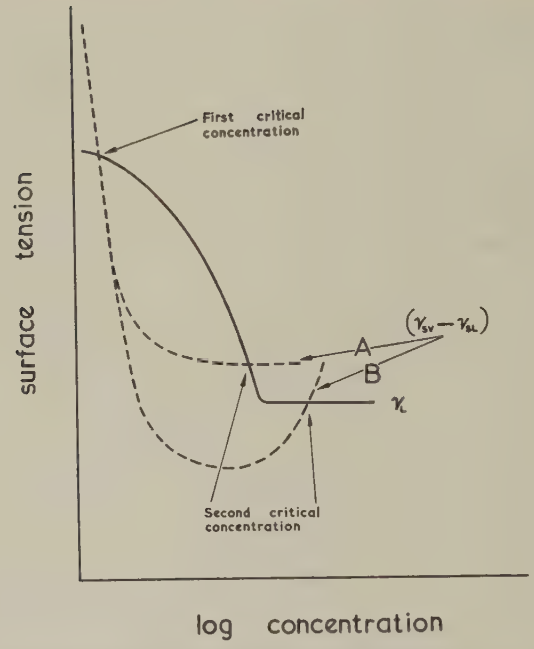
First critical concentration
surface tension
$(\gamma_{sv}-\gamma_{sL})$
A
B
γ_L
Second critical concentration
log concentration

FIG. 4. The variations of surface tensions with concentration (schematic only).

centration, and the dotted curves two possible ways in which $\gamma_{SV} - \gamma_{SL}$ can change. At very low concentrations γ_{LV} is about 70 dyne cm.$^{-1}$, and γ_{SV}, being that of the clean solid surface, is much greater; wetting occurs and therefore $\gamma_{LV} < \gamma_{SV} - \gamma_{SL}$. Adsorption increases with concentration, γ_{SV} is reduced to such a value that the surface becomes hydrophobic, and so $\gamma_{LV} > \gamma_{SV} - \gamma_{SL}$. The contact angle becomes greater than zero when the curve of γ_{LV} against concentration crosses that of $\gamma_{SV} - \gamma_{SL}$ (Fig. 4). With increasing concentration γ_{LV} drops to about 30 dyne cm.$^{-1}$ at the critical concentration for micelle formation (C.M.C.) and then remains constant. Wetting may occur in two ways, viz.,

A. If $\gamma_{SV} - \gamma_{SL}$ reaches a constant value before γ_{LV}, the curves will cross again at a concentration less than the C.M.C. (curve *A*) to give rewetting.

B. If, on the other hand, rewetting occurs at a concentration greater than the C.M.C., $\gamma_{SV} - \gamma_{SL}$ must have increased, since γ_{LV} is constant. It is unlikely that γ_{SV}, being the surface tension of the solid covered with a fairly close-packed monolayer, can increase; the change must therefore occur in the interfacial tension γ_{SL}. Wetting by this mechanism is shown schematically by curve *B*, which must have a turning point.

Further consideration shows that rewetting by the first method will be restricted. If Young's equation is applied to a drop of solution making a contact angle θ with the hydrophobic surface, then

$$\gamma_{LV} \cos \theta = \gamma_{SV} - \gamma_{SL}.$$

Wetting by the first process implies that there is no turning point in curve A, or that $\gamma_{SV} - \gamma_{SL}$ is always greater than the minimum value of γ_{LV}. If the hydrophobic surface exhibits a large contact angle, then $\gamma_{SV} - \gamma_{SL}$ must be quite small; if, for instance, θ reaches 90°, $\gamma_{SV} - \gamma_{SL} = 0$ at that concentration. Under such conditions the curve of $\gamma_{SV} - \gamma_{SL}$ against concentration must have a turning point to allow rewetting. If this curve is to have no turning point (mechanism *A*), $\gamma_{SV} - \gamma_{SL}$ must always be greater than the minimum value of γ_{LV}, viz., about 30 dyne cm.$^{-1}$. Since the maximum value of γ_{LV} is 72 dyne cm.$^{-1}$, the maximum contact angle allowable for rewetting by mechanism *A* is given by $72 \cos \theta = 30$ or $\theta = 65°$. This s only an upper limit to the maximum contact angle, since it will occur at some concentration where γ_{LV} is less than 72 dyne cm.$^{-1}$. If the hydrophobic surface exhibits a maximum contact angle greater than 65°, then rewetting by mechanism *A* is not possible. In general, paraffinic carbon compounds which have more than about ten carbon atoms in the chain, f adsorbed strongly, form close-packed monolayers which cause contact angles to be greater than 65°. It seems unlikely, therefore, that mechanism *A* will operate under the conditions of these experiments.

As mentioned above, when mechanism *A* is inoperative, rewetting is aused by lowering of the interfacial tension. It seems reasonable to assume hat this occurs as a result of additional adsorption of the long-chain material within the aqueous phase at the liquid-solid interface. One would xpect a reduction in interfacial energy for such a system if the adsorbed molecules were packed with the terminal CH_3 groups pointing out of the olution towards the corresponding groups of the monolayer on the solid. uch a system is equivalent to a lamellar micelle in solution. At the C.M.C. lamellar micelle could easily form, and in fact rewetting occurs frequently t concentrations close to the C.M.C. (Fig. 3). Double-layer adsorption f this type has been postulated previously (9, 10) and has been observed y adsorption measurements of sodium dodecyl sulfate on barium sulfate 11). The present experiments indicate that the effect is quite general. he failure of solutions of DTAB up to a concentration of *M* to wet mica a peculiar exception. There are several possible explanations but the hoice of the correct one requires further experiments.

The results are directly applicable to washing and rinsing procedures. f the appropriate solution is used, an article may be removed from a rinsg bath in a hydrophobic state and any excess solution on the surface will main as small relatively thick drops. If the drops are removed by some eans other than evaporation, an apparently clean surface will be left.

If, however, the drops evaporate, they will leave stain marks. Thus if articles are to be dried by a draining-evaporation process, it is preferable to remove the article from the rinse with a thin continuous film on the surface. This will evaporate quickly and leave a relatively clean, dry surface. The experiments show that these conditions may be obtained by using appropriate concentrations of the detergent in the rinsing bath.

REFERENCES

1. Bigelow, W. C., Pickett, D. L., and Zisman, W. A., *J. Colloid Sci.* **1,** 573 (1946).
2. Bigelow, W. C., Glass, E., and Zisman, W. A., *J. Colloid Sci.* **2,** 563 (1947).
3. Shafrin, E. G., and Zisman, W. A., "Monomolecular Layers", ed. by H. Sobotka. American Association for the Advancement of Science, 1954.
4. Sutherland, K. L., and Wark, I. W., "Principles of Flotation." Australian Inst. Mining and Metallurgy, Melbourne, 1955.
5. Kahan, G. J., *J. Colloid Sci.* **6,** 571 (1951).
6. Karle, I., and Brockway, L. O., *J. Chem. Phys.* **15,** 213 (1947).
7. Menter, J. W., and Tabor, D., *Proc. Roy. Soc.* (*London*) **204A,** 514 (1951).
8. O'Connor, D. J., and Buchanan, A. S., *Australian J. Chem.* **6,** 278 (1953).
9. Held, N. A., and Khainsky, I. A., *Kolloid-Z.* **76,** 26 (1936).
   Held, N. A., and Samochwalov, K. N., *Kolloid-Z.* **72,** 13 (1935).
10. Schulman, J. H., and Smith, T. D., *Kolloid-Z.* **126,** 20 (1952).
11. Cuming, B. D., and Schulman, J. H., "Recent Developments in Mineral Dressing." Institution of Mining and Metallurgy, London, 1953.

OURNAL OF COLLOID SCIENCE 11, 167–170 (1956)

A POSSIBILITY FOR THE DETERMINATION OF MOLECULAR WEIGHTS OF COLLOIDAL PARTICLES BY ULTRACENTRIFUGATION IN AN ELECTRIC FIELD

A. Scheludko

Institute for Physical Chemistry, University of Sofia

Received January 17, 1956

This paper examines theoretically the behavior of solutions of colloidal articles or macromolecular matter under the simultaneous application of entrifugal and stopping electrical fields.

1. We shall examine the behavior of a colloidal solution placed in the ltracentrifuge in a rectangular cell, the two sides of the latter, perpendiclar to the radius of rotation, representing two electrodes. An electrical ield is applied to these electrodes, either using contacts through the axis f the rotor, or in some other way. In accordance with the electric charge f the colloidal particles the electrodes are connected in such a way that he force of the electric field acts in a direction opposite to the centrifugal orce. This stopping electric field has an intensity ϕ. We suppose that no lectrolysis occurs in the cell; this is the case with nonaqueous (nonconucting) solutions. The cell is rotated with an angular velocity ω.

We assume that the colloidal solution contains identical noninteracting articles, each with an electrophoretic mobility, u, in the solvent used. xcluding the very first moment of application of the fields, for the exernal force acting on a particle located at a distance x from the axis of otation, we have

$$vB = uB\varphi - m\omega^2 x \qquad [1a]$$

hen the relative mass of the particle is $m > 0$ ($v = dx/dt$ is the rate of irectional movement of the particle, and B is the constant of friction), nd

$$vB = m\omega^2 x - uB\varphi \qquad [1b]$$

hen the relative mass is $m < 0$.

At a distance

$$x_0 = \frac{uB}{m} \cdot \frac{\varphi}{\omega^2} \qquad [2]$$

e force acting on the particles is zero and the movement of the particles both sides of x_0 will be in opposite directions: when $m > 0$ the particles will move away from $x = x_0$ and when $m < 0$ they will move towards $x = x_0$. In the latter case after a sufficiently long time there will be a maximum in the concentration of the particles at $x = x_0$.

If there are several components in the solution, each with a different uB/m, and $m < 0$, the components will be separated along the radius of rotation with respective maxima of their concentration at x_{0_1}, x_{0_2}, etc. From the positions of these maxima for each component the values of $(uB/m)_1$, $(uB/m)_2$, etc., can be determined. These values differ from the sedimentation constants by the factor u.

2. For dilute solutions, after a state near the equilibrium is established, the concentration of each component around x_0, sufficiently apart from the electrodes, will be

$$C_x = C_{\max} e^{-(m\omega^2/2kT)(x-x_0)^2}. \qquad [3]$$

Here C_x is the particle concentration at a distance x from the axis of rotation, $C_{\max}$ is the concentration at x_0, k and T being the Boltzmann constant and the absolute temperature, respectively. For these components for which the values of x_0 can be sufficiently well resolved, the molecular weights can be determined using the conventional methods.

3. The resolving power, i.e., the smallest difference in x_0 for which we still can determine separately the masses of two types of colloidal particles, behaving very similarly by ultracentrifugation in an electric field, depends on the following condition. The distance between x_{0_1} and x_{0_2} must at least equal the sum of $\delta_1 + \delta_2$, δ being the distance from x_0, for which the decrease in concentration is large enough to allow, according to Eq. [3], the determination of the masses of the particles. For this purpose it is convenient to use this value of δ for which Eq. [3] has an inflection point. Here dc/dx has maximal value and hence, the precision for the determination of m is greatest. For this case we have

$$\delta = \frac{1}{\omega}\sqrt{\frac{kT}{m}}. \qquad [4]$$

Therefore the condition determining the resolving power is given by

$$x_{0_1} - x_{0_2} = \delta_1 + \delta_2 \approx 2\delta.$$

4. Since the particles move in opposite directions with respect to x_0, it could be supposed that soon after the application of the external fields and long before the sedimentation equilibrium is reached, there should be established a certain extreme value of the concentration at x_0. This supposition, however, does not prove to be correct.

At the beginning of sedimentation, the diffusion, being much smaller than the migration, can be neglected, and we have the simplified equation

$$\frac{\partial c}{\partial t} = -v\frac{\partial c}{\partial x} - C\frac{dv}{dx}.$$

Bearing in mind Eq. [1*b*], the solution of this equation is of the type $= C_0e^{Bt}$, and it should be true that $dc/dx = 0$ for all values of x. Thereore extreme values of the concentration at $x = x_0$ could be expected after significantly longer time of sedimentation.

5. The stopping electrical field will prolong the time necessary for esablishing the equilibrium distribution. This time for a distance δ from x_0 an be roughly approximated according to the methods used in common ltracentrifugation. We accept that the time for establishing the equilibium at a given place is proportional to the time necessary for the migraion of a particle from the sides of the cell up to this particular place. By omparing the time for migration with and without the stopping field, and t_0, respectively, we have

$$\frac{t}{t_0} = \frac{\ln \dfrac{x_1 - x_2}{x_2 - x_0}}{\ln \dfrac{x}{x_2}}.$$

Iere x_1 is the distance from the axis of rotation to the outer side of the ell, x_0 is in the middle of the cell, and $x_2 = x_0 + \delta$. The length of the cell or the calculation of t is taken to be $2(x_1 - x_0)$, and for the calculation of is $x_1 - x_2$.

6. For a better illustration of the preceding elementary discussions oncerning the behavior of colloidal particles under ultracentrifugation in an lectric field we shall examine a numerical example. Let us have dispersed articles with a molecular weight, $M = 100{,}000$, specific gravity $\Delta_1 = 1$, nd electrophoretic mobility $u = 10^{-5}$ cm.sec^{-1} volt^{-1}, the solvent being hloroform of viscosity $\eta = 0.58 \times 10^{-2}$ and specific gravity $\Delta_2 = 1.48$. hloroform is selected as solvent for several reasons—it has a relatively igh specific gravity, does not conduct electricity, excluding in this way ne complications which could be caused by electrode processes, and stly, the electrophoretic mobility in chloroform (1), as in other nonqueous polar solvents, retains a measurable value. In the above-cited aper, the electrophoretic mobility of glass in chloroform is given a value bout 20 times lower than in water. For this reason we accept $u = 10^{-5}$, ., about 30 times lower than the ordinary values of electrophoretic obility in water. The data for electrophoretic mobilities in nonaqueous lvents are very scarce, stating only that these are lower than for water. or this reason we shall examine in some details the influence of u for ultrantrifugation in electric field.

According to the values accepted above for the relative mass of the parcles we find that $m = 8 \times 10^{-20}$, where $m = M/N_L(1 - \Delta_2/\Delta_1)$, and asming a spherical form, $B = 3.8 \times 10^{-8}$, where $B = 6\pi\eta\sqrt[3]{\dfrac{3M}{4\pi N_L\Delta_1}}$.

For common ultracentrifuges with $w = 10^3$ rev. sec.$^{-1}$, radius of the rotor 5 cm., and length of the cell 3 cm., we can accept $x_0 = 3$ cm., which means that the maximum in the concentration will be located somewhere in the middle of the cell. For the realization of this case, according to Eq. [2] we must apply an electrical field $\phi = 0.63$ volt, or 1.9 volts between the electrodes of the cell. This shows that even if u was 100 times smaller, i.e., 3,000 times smaller than ordinary electrophoretic mobilities in water, the potential difference between the electrodes of the cell should be only about several hundred volts, which can be achieved without any special difficulties. These considerations make us believe that the lowering of the electrophoretic mobility by nonaqueous solvents, which alone can be used under our conditions, would not represent any difficulty for ultracentrifugation in an electrical field.

In the case of the example discussed above, we obtain the reasonable value of 0.7 cm. for δ. For the time of settling, according to the dimensions of the cell, x_0 and δ, we find that $t \approx 3.5\ t_0$. Compared with common ultracentrifugation we have an increase in the time of settling of about 3 to 4 times.

REFERENCE

1. FAIBROTHER, F., AND BALKIN, M., *J. Chem. Soc.* **1931**, 389.

OURNAL OF COLLOID SCIENCE 11, 171–176 (1956)

A TYNDALLOMETRIC STUDY CONNECTING ELECTROLYTE CONCENTRATION AND TIME OF COAGULATION

Amal K. Bhattacharya

Physical Chemistry Section, Chemical Laboratories, Agra College, Agra

Received October 20, 1955

ABSTRACT

The equation, $C = a + \frac{m \cdot 1/t}{n + 1/t}$, where C and t are the concentration of the elecrolyte and time of coagulation, respectively, and a, m, and n are constants, has een tested from the tyndallometric data obtained from the time-tyndallograms nd time-disperseodograms. At the same stage of coagulation the time of coagulaion t was plotted against $1/(C - a)$. Straight lines were obtained for each set of alues according to the relation $1/C - a = \frac{n}{m}t + \frac{1}{m}$, which can be readily derived rom the equation.

It was shown by Bhattacharya and Kumar (1) that the concentration of he electrolyte C and time of coagulation t of arsenious sulfide, chromium ydroxide, and ferric hydroxide sols can be represented by the equation, $= a + \frac{m \cdot 1/t}{n + 1/t}$, where m and n are constants and a is another constant btained graphically from the intercept on the C-axis of $C - 1/t$ curves. he above equation can be reduced to the form $\frac{1}{C - a} = \frac{n}{m}t + \frac{1}{m}$. It was hown that straight lines were obtained by plotting $1/(C - a)$ against t, onfirming the linearity of the foregoing equation.

In order to confirm the merit of this equation by following a more preise experimental technique, the times corresponding to the same stage of oagulation with different concentrations of the electrolytes were deterined from the time-tyndallograms and time-disperseodograms obained by Težak and co-workers (3), who studied the coagulation of silver alide sols in *statu nascendi*. Characteristic curves were obtained by them the time-tyndallograms, where the tyndallometric value was plotted gainst time, as well as in the time-disperseodograms, where the radius the colloidal particle in millimicrons was plotted against time using veral concentrations of the coagulating electrolyte.

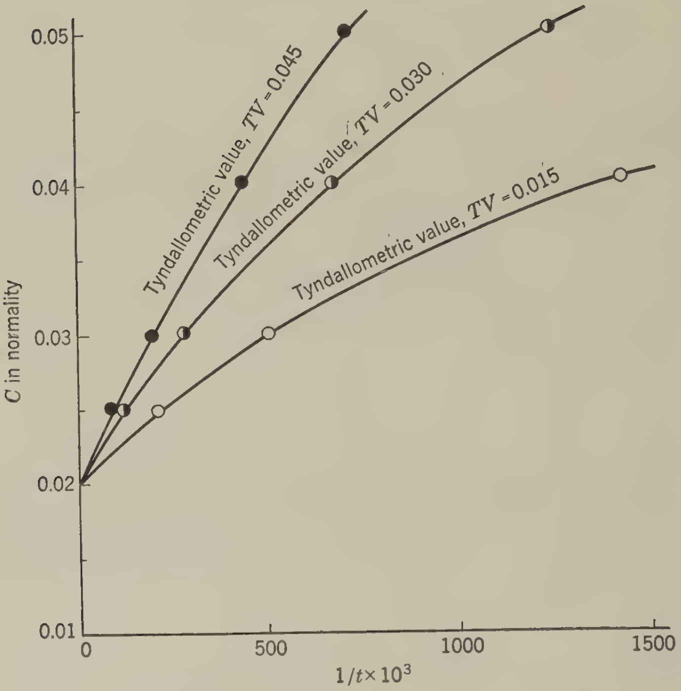

Fig. 1. Concentration against reciprocal of time of coagulation as determined from the time-tyndallograms at different stages of coagulation, denoted by different tyndallometric values.

Experimental Arrangement[1]

A nephelometric method was used for the observation of the formation of the precipitate. The setup consisted of a tyndallometer (Trübungsmesser, C. Zeiss) in combination with a Pulfrich photometer (C. Zeiss). The temperature of the measuring chamber was kept constant by using a thermostat (Hoppler's ultrathermostat). In order to determine the particle size the so-called tyndallometric, dispersion quotients, DQ_T, have been used. This DQ_T method was developed by Težak (4) following the results which Teorell (2) obtained in an investigation of the relation between the coefficient of light extinction and the particle size in colloidal systems.

Verification of the Equation

The same stage of coagulation was determined by drawing a line parallel to the time axis which cut the other axis and the tyndallometric curves for the different concentrations of the electrolyte assuming that the same tyndallometric value or the same radius of the particle connotes the same state of aggregation and hence of coagulation. The time intervals at the

[1] A detailed account of the experimental arrangements has been mentioned by Težak and co-workers (3).

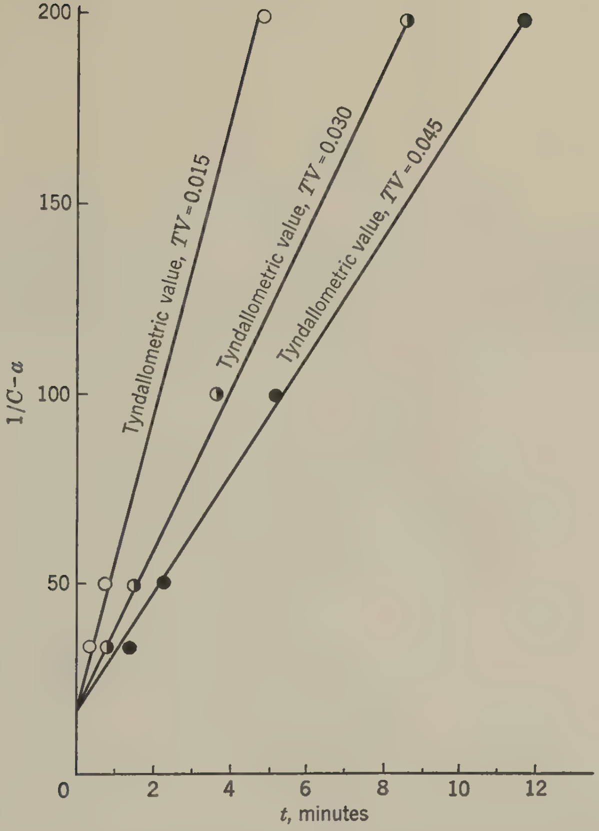

FIG. 2. The value $1/(C\text{-}a)$ against time of coagulation as determined from the ime-tyndallograms at different stages of coagulation, denoted by different tyndallo-etric values.

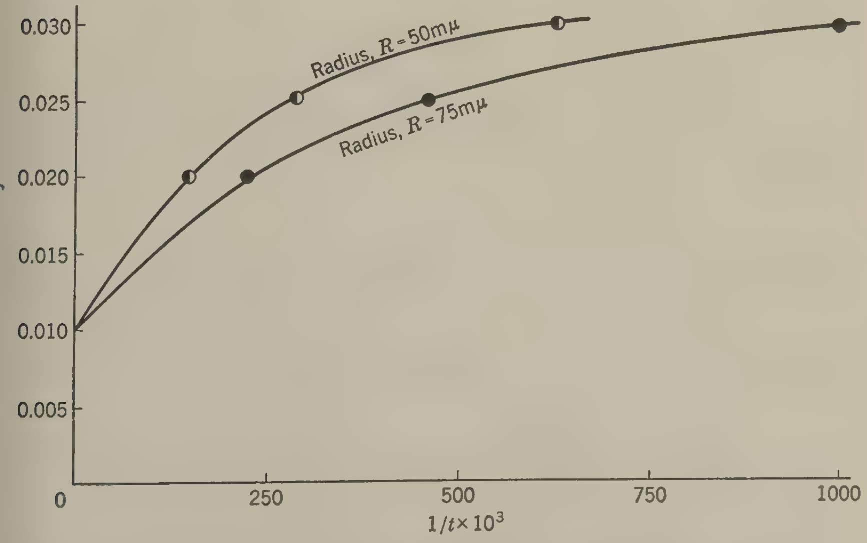

FIG. 3. Concentration against reciprocal of time of coagulation as determined m the time-disperseodograms at different stages of coagulation, denoted by dif-rent radii of particles.

same stage of coagulation for different concentrations of the electroly were read from the curves. Having thus obtained the values of the tim of coagulation t at the same stage for known concentrations C, the C-1 curve was plotted (Figs. 1 and 3). The curve cuts the C-axis when 1 is equal to zero, i.e., when t tends to infinity. This intercept on the C-ax gave the value of the constant a. Since the concentration of the electrolyt is already known, $1/(C - a)$ was plotted against t (Figs. 2 and 4), whe straight lines were obtained in all cases according to the equation $\frac{1}{C - a}$ = $\frac{n}{m}t + \frac{1}{m}$. $1/m$ was now determined from the intercept on the $1/(C - a$ axis when $t = 0$. The tangent of the angle with the t axis is equal to n/m Thus $1/m$ or m being known, n was calculated. In this way the constant a, m, and n were determined (Table I).

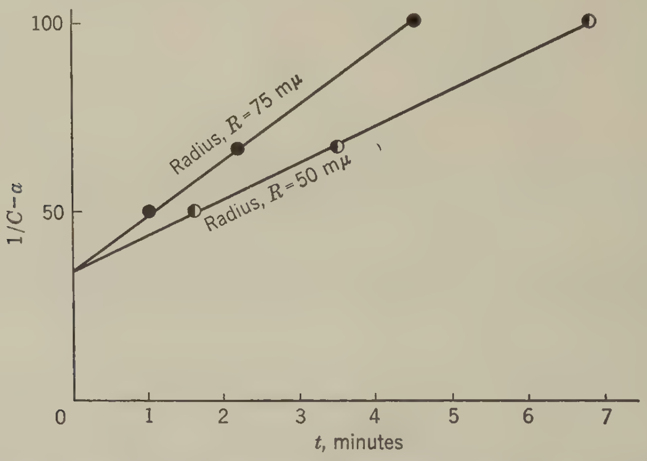

FIG. 4. The value $1/(C\text{-}a)$ against time of coagulation as determined from the time-disperseodograms at different stages of coagulation, denoted by different radi of particles.

TABLE I

Calculation of the Constants a, m, and n from the Time-Tyndallograms and Time-Disperseodograms at Different Stages of Coagulation

Time tyndallograms				Time disperseodograms			
Stage	a	m	n (T^{-1})	Stage	a	m	n (T^{-1})
	M	M		mμ	M	M	
T.V. = 0.015	0.02	0.0588	0.229	$R = 50$	0.01	0.0294	0.0137
T.V. = 0.030	0.02	0.0588	0.123	$R = 75$	0.01	0.0294	0.0215
T.V. = 0.045	0.02	0.0588	0.091	$R = 100$[a]	0.01	0.0294	0.0343

[a] Not shown in the figure.

DISCUSSION

Interpretation of the Constants a, m, and n

When C and $1/t$ are plotted the curve cuts the C-axis and the intercept ; $1/t = 0$ is given by 'a', i.e., a is the value for $t \rightarrow \infty$. This means that ie stability of the sol remains unaffected up to a concentration given y a, which has been designated as the "critical stability concentration" ' the electrolyte for the sol. When $1/t$ is very large as compared to n, e., when t is very small as happens in the rapid coagulation region, n in be neglected so that $C = a + m$ or $C - a = m$ or more strictly $C - a \rightarrow$ in the zone of rapid coagulation. Therefore m represents the concen- ation of the electrolyte above the critical value a which will produce in- antaneous coagulation.

In order to interpret n consider an alternative form where $C - a =$ $/(nt + 1)$. Working out the dimensions of the equation we find that ; $+ 1$ should have no dimension and this can be possible only when n as the dimension T^{-1}. Hence n can be put equal to $1/t$ or k/t. Substituting $= 1/t$ in the new equation we get $C - a = m/2$ or if $n = k/t$ is sub- ituted, $C - a$ becomes equal to $m/(k + 1)$. This means that n is a charac- ristic constant for the sol, which shows that the sol will be coagulated in me interval t by $1/(k + 1)$th fraction of m (quantity for instantaneous agulation). Hence we connect n with sensitiveness or susceptibility of e sol to the electrolyte which becomes equal to k when $t = 1$. But the sceptibility of the sol particles may be dependent on a large number of ctors such as size and shape of the particles, charge and zeta potential, ickness and interaction of the double layers, and last but not the least e adsorption, ion exchange, and changes in the dielectric constant, etc.

It is interesting to observe from the above table that n decreases with creasing tyndallometric value as also with the decrease in the radius of e colloidal particle, or in other words, the order of decrease in the values n directly indicates the greater and greater degree of aggregation of the agulating particles. Further from the variations in the values of n at fferent stages of coagulation it becomes evident that n depends upon the ctors which determine the stability of the sol and hence can assume a finite value with different concentrations of the electrolyte at a particu- r stage of coagulation or degree of aggregation of the colloidal particles. hen the same stage of coagulation is reached where the net effect of the ysical factors determining the stability of the sol may be visualized to main the same by adding different concentrations of the electrolyte, n ll have a constant value corresponding to the same degree of aggregation. is has been actually observed (vide $1/(C - a)$ and t curves).

ACKNOWLEDGMENT

Grateful thanks are due to Professor Santi R. Palt., D.Sc., F.R.I.C., F.N.I., Professor of Physical Chemistry, Indian Association for the Cultivation of Science, Calcutta, and Professor A. K. Bhattacharya, D.Sc., F.R.I.C., Head of the Chemistry Department, Agra College, Agra for their kind interest and helpful suggestions in this piece of work.

REFERENCES

1. BHATTACHARYA, A. K., AND KUMAR, R., *J. Indian Chem. Soc.*, **28**, 179, 638 (1951); *ibid.* **29**, 687, 759 (1952).
2. TEORELL, T., *Kolloid-Z.*, **53**, 322 (1930); *ibid.* **54**, 58, 150 (1931).
3. TEŽAK, B., MATIJEVIC, E., AND SCHULZ, K., *J. Phys. & Colloid Chem.* **55**, 1557 (1951).
4. TEŽAK, B., *Z. physik. Chem.* **A175**, 219 (1935); *Kolloid-Z.* **74**, 16 (1936).

OURNAL OF COLLOID SCIENCE 11, 177–183 (1956)

ALIBRATION OF LIQUID AEROSOL COLLECTORS BY DROPLETS CONTAINING UNIFORM SIZE PARTICLES

N. H. Farlow and F. A. French

U. S. Naval Radiological Defense Laboratory, San Francisco 24, California

Received November 10, 1955

Abstract

A simple and rapid method has been developed for determining micro-drop vol-nes by the inclusion of uniform size solid particles in water drops. Corn smut spores 7.8 μ average size and latex spheres of 0.514 μ mean size have been used to calibrate sensitive surface which can collect and measure water aerosol droplets having ameters ranging from 1 to 100 μ. The method is especially valuable in the drop size nge 1 to 10 μ where other calibration techniques fail. No elaborate equipment is cessary. Precision is greatly improved by utilizing arithmetic mean calculations minimize statistical error. A calibration curve is presented relating droplet size to llecting surface spot size. The method enables the use of the polyvinyl alcohol-ver nitrate-hydrogen peroxide film for water aerosol sampling with satisfactory ecision.

The difficulty of accurately calibrating water aerosol collecting surfaces demonstrated by the efforts to calibrate soot and magnesium oxide slides , 2), dye films (1), chemically processed surfaces (3), and special ion indi-ting surfaces for droplet collection (3, 4). The basic difficulty in such cali-ation is relating the droplet volume to the impression the volatile droplet akes on the sensitive collecting surface. The individual volumes involved e on the order of 10^{-13} to 10^{-7} ml. for 1- to 100-μ diameter droplets. Sta-tical considerations become laborious if large collections of polydisperse rosols are analyzed for tracer solutes and these analyses are used to relate op volume with resulting spot size on the collecting surface. Thus, the stem of calibration most often employed is a comparison of droplets col-cted in a grease matrix with the impressions made by the same droplet stribution on the collecting surface. This method of calibration requires at very large numbers of both grease-enclosed droplets and collecting rface impressions be measured to deduce even the roughest correlation. aborate equipment is often necessary to reduce droplet evaporation en-untered in the dual collection system.

The method presented here is independent of droplet size-frequency dis-butions, does not require a separate droplet size measurement, and neces-ıtes only a relatively small number of drop impression measurements.

The precision of the spot diameter measurement, likewise, need not be high to produce a reliable calibration.

Principle of the Method

The theory of chemical aliquots may be applied to a suspension of solid particles of uniform size, provided they are small and the suspension is vigorously stirred. Under these conditions, any small droplet will contain the same proportion of solid particles as the original suspension. Utilizing this hypothesis, a water-sensitive chloride ion indicating collecting surface (3) has been calibrated. Droplets landing on this transparent film diffuse along the surface and into the film, forming microscopic craters. The diameters of these impressions are about twice those of the droplets forming them. The calibration of droplet size with spot size is effected by first aspirating droplets from a master suspension onto the film. The number of solid particles per unit volume of the master suspension is determined by pycnometer or haemacytometer methods. The diameter of the impression formed is measured and a count made of the solid particles in the spot area. There is a statistical variation in the number of solid particles a given size drop will contain. To minimize this statistical error a number of spots of a given size must be measured and the solid particles within them counted and averaged. This average number of solid particles per given spot size is used to compute the volume of the droplet forming the spot. This computation is easily made by simple proportion since the number of particles per unit volume has already been determined on the master suspension. This calculated volume is the sum of the volumes of the water and the solid particles. Since only the liquid portion of each droplet diffuses into the film and forms the spot, the solid particle volume must be subtracted from the calculated volume of the droplet. This difference is the effective volume of the water drop and the diameter of the spot it produces. A calibration point is thus obtained.

Experimental Details

In order to calibrate the sampling surfaces throughout the 1- to 100-μ drop size range, it was necessary to employ two sizes of solid particles. For the droplet size range 30 to 100 μ, plant spores of the common corn smut[1] were used. These spores, having a density about 1.3 g./cc. are amazingly uniform in size at 7.8 ± 0.3 μ and almost spherical. For the droplet size range 1 μ to 30 μ it was necessary to use smaller particles. Uniform polystyrene latex spheres[2] suspended in water were found to be ideal for this procedure. These spheres are sized by the manufacturer and in this case were 0.514 μ in diameter with a standard deviation of ± 0.011 μ.

[1] Corn husks containing this fungus were obtained from the University of California Herbarium, Berkeley, California, through the courtesy of Dr. Lee Bonar.

[2] Dow Chemical Co., Physical Research Lab, 2-280 Bldg., Midland, Michigan.

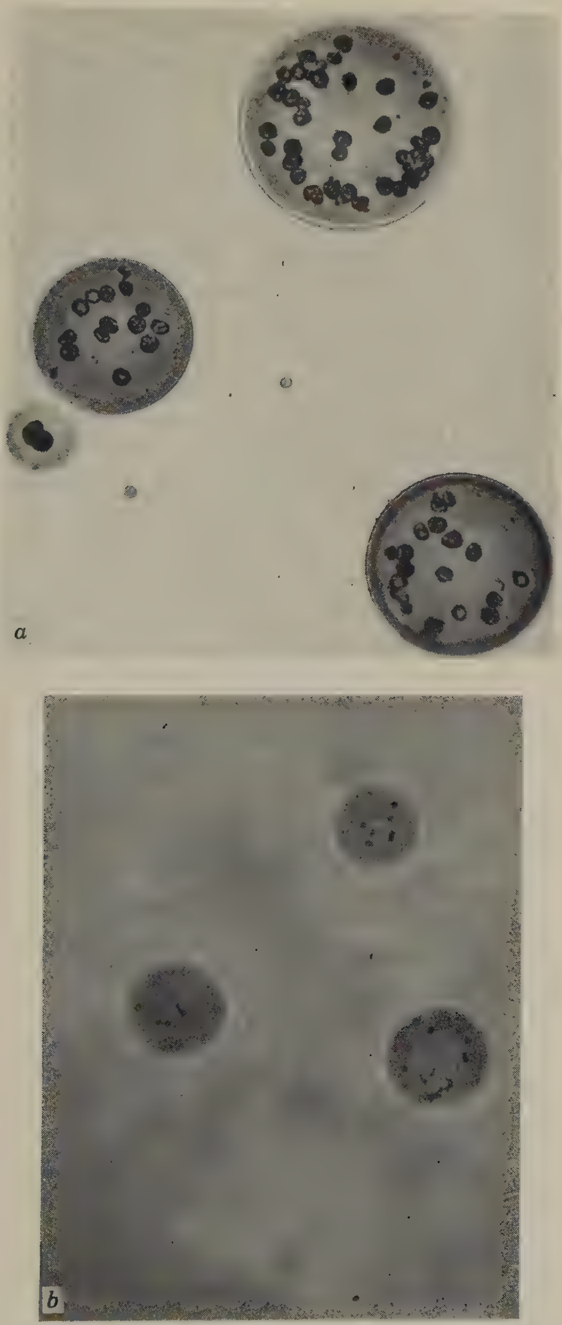

FIG. 1. Photomicrograph of droplet impressions on the sensitive collecting sur- ce. (*a*) (*upper*) Impressions containing corn smut spores (magnification 232 ×).) (*lower*) Impressions containing latex spheres (magnification 1200 ×).

Corn Smut Spore Calibration

Two water suspensions were made with the corn smut spores. Eight samplings were taken from each suspension and the number of spores per cubic millimeter determined by conventional haemacytometer methods. These measurements were averaged and the mean spore concentrations were found to be 198,000 ± 4500 spores/mm.^{3} and 206,000 ± 4000 spores/mm.^{3} with probable errors of 2.3% and 2%, respectively. From these vigorously agitated suspensions water aerosols were aspirated and impacted on sensitive collecting surfaces (3). The droplets, impacting on the film, diffused into the material, leaving the spores on the surface. Standard development methods associated with the film technique (3) defined the drop spread area (Fig. 1*a*). Microscopic measurements with a micrometer eyepiece were then made of each spot diameter and tabulated with the number of spores in that spot. All spots of a given diameter were then listed together. The number of spores associated with each were totaled and averaged. This arithmetic mean number of spores per given spot size was then used in a simple proportion calculation to determine the total volume of the drop plus spores. The spore volume was subtracted yielding the volume of water which caused the given spot. Table I lists the various spot sizes measured and the diameters of the drops which produced each spot. Probable error measurements are tabulated and will be discussed later.

TABLE I

Calibration with Latex Spheres and Corn Smut Spores

Film spot diameter (μ)	Arithmetic mean droplet diameter (μ)	Probable error of the mean (μ)	Probable error (%)
	Latex Sphere Suspensions		
2	3.08	±0.11	±5
3	2.73		
4	3.05		
5	3.68	±0.02	±0.6
6.3	4.38		
7.5	4.88	±0.11	±2
8.3	5.66		
10	6.53	±0.06	±1
13.3	8.09	±0.07	±1
16.7	9.95	±1.35	±1.5
26.7	15.2		
33.4	18.4		
	Corn Smut Spores		
31	18.9		
52	29.5	±0.54	±2
84	47.6		
90	52.0	±0.20	±0.4
135	75.5	±1.1	±1
180	98.1	±1.7	±2

Latex Sphere Calibration

The solid content of the latex suspension was determined by gravimetric methods. Information on the mean particle size and density was supplied by the manufacturer. From this data the concentration of latex spheres was found to be 1.240 × 10^{12} ± 0.007 × 10^{12} particles per milliliter, a probable error of 0.6%. In order that a countable number of spheres would result in each droplet aspirated in the size ranges 1 μ to 30 μ, it was necessary to dilute the latex preparation. The dilution ratios of latex to water were 1:10, 1:25, 1:50, 1:75, 1:100, and 1:200. The various dilutions were aspirated and the droplets collected on the sensitive films. The spots were developed (Fig. 1*b*), the impression diameters measured, and the number of spheres per spot counted. The same averaging method used for the spore technique was utilized here to reduce statistical variations in number of spheres per given size droplet. By methods similar to those used for the spore techniques, the drop diameter-spot diameter relationships were determined (Table I).

A total of 3000 droplet impressions containing over 20,000 spores or latex spheres were measured and counted in this calibration. Either an eyepiece graticule containing circles of varying diameters or a micrometer eyepiece was used to measure each spot size. The spores or latex spheres were rapidly ounted using a hand tabulator.

Velocities of impaction up to 170 m.p.h. were investigated. The relationhip of spot size with drop size remained unchanged throughout the range. Variations of humidity during the collection of droplets on the film had ttle effect on the calibration.

The calibration points of spot diameter with drop diameter (Table I) are lotted (Fig. 2) and a straight line drawn connecting the points.

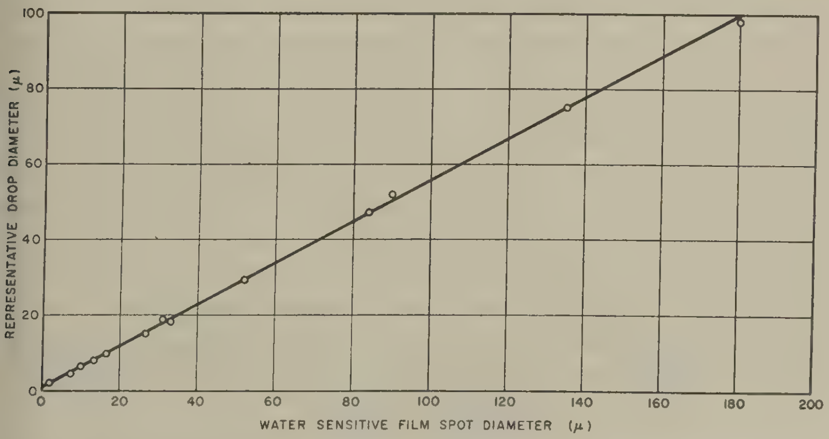

FIG. 2. Calibration curve relating film spot diameter with droplet diameter.

ERROR DISCUSSION

A basic assumption of the method is that the theory of aliquots can be applied to suspensions of uniform small particles. That this assumption is reasonably valid can be seen from the concentration measurements of spores per unit volume by the haemacytometer technique. The probable error of 2 % is sufficiently small to preclude the propagation of large errors due to inadequate stirring of the master suspension. The small particle size of the latex suspension is even more favorable for sustaining the assumption in the small droplet range. The propagation of errors in other phases of the experiment probably overshadows this error.

Besides the usual microscope and operator biases, there are two inherent errors of the method which cannot be eliminated. The first is introduced by the mere physical presence of comparatively large spores in the droplets. It is to be expected that a small amount of water will adhere to the spore surface and evaporate rather than contribute to the spreading of the droplet along and into the film. Thus, the spot formed tends to be smaller than it would have been without the spores. The second inherent error is due to the presence of an unknown quantity of surface-active agent in the latex preparation. Dilutions of latex in water from 1/10 to 1/200 show a slight, but reproducible, trend towards greater droplet spreading on the film with higher surface-active agent concentration. Averaging similar values obtained with different dilutions helps reduce the error due to this effect.

Errors must also be expected when using solid particles only 0.5 μ in diameter. Even though they need only be counted, their size is approaching the practical limit of the microscope. Magnifications up to 600 × were used on the smaller drop ranges in order that reasonably accurate sphere counts could be made. Because of the system of averaging fairly large counts, fractional particles result in the calculations and are carried through. They are not to be construed as indicating great experimental accuracy.

Three independent experiments were conducted to determine certain of the calibration points. For these various points the probable errors (6) have been computed (Table I). These error values represent the cumulated errors due to operator bias, instrument deficiencies, and inherent statistical errors of the method. Some points appear to be more biased than others. This is indicative of operator fatigue from long hours at the microscope. Such biases are difficult to appraise mathematically, but probably contribute a major share of the error in aerosol measurement technique. In general the probable error is largest in the small particle range, being about 5 %; in the larger size range it is about 2 %. Errors due to micrometer eyepiece measurements of spot diameters are not formally appraised. They contribute to the error calculated in the mean droplet diameter.

APPLICATIONS

Use of the uniform size spores and latices both alone and as a droplet ontaminant shows promise as a means of checking sampling instrument ias, isokinetic characteristics, and efficiency. Uniform particles as a drop-et volume indicator may have use in micro-analytical chemistry as a cali-rating mechanism. Aerosol droplet agglomeration and evaporation, and hemical reactions between aerosol droplets offer studies wherein the ethod may be useful.

ACKNOWLEDGMENT

Appreciation is expressed for the suggestions and assistance given by Mr. J. W. endricks. The editorial assistance of Mr. J. Todd is sincerely appreciated.

REFERENCES

. Schaefer, V. J., "The preparation and use of water sensitive coatings for sampling cloud particles," General Electric Co., AAF Technical Report 5539; AAF Air Materiel Command, Wright Field, Dayton, Ohio, January 24, 1947, pp. 103–130.
. May, K. R., *J. Sci. Instr.* **27**, 128 (1950).
. Farlow, N. H., "A Physico-Chemical System for Water Aerosol Measurements," *J. Colloid Science* **11**, 184–191 (1956).
. Crozier, W. D., "Airborne particle study," Research and Development Division, New Mexico School of Mines, Contract N7ONR-405, Task 1, Project #NR 082-013, March 1949.
Farlow, N. H., "An improved halide ion sampling surface for water aerosols," *Rev. Sci. Instr.* **25**, 1109–1111 (1954).
Scarborough, J. B., *Numerical Mathematical Analysis*, 511 pp. Johns Hopkins Press, Baltimore, 1950.

JOURNAL OF COLLOID SCIENCE 11, 184–191 (1956)

A PHYSICOCHEMICAL SYSTEM FOR WATER AEROSOL MEASUREMENT

N. H. Farlow

U. S. Naval Radiological Defense Laboratory, San Francisco, California

Received November 10, 1955

Abstract

The need for a durable, precision collecting surface for water aerosols has led to the development of a new transparent 35-mm. film sensitive to distilled water and sea water fog droplets in the size range 1 to 100 μ. The droplet indicating film is polyvinyl alcohol containing silver nitrate and hydrogen peroxide coated on a substrate of 35-mm. cellulose acetate film leader stock. A unique development process employing gaseous phenylhydrazine, ammonia, water vapor, and ultraviolet light from a sun lamp defines the impressions left by the droplets. The salt water impressions are sharply distinguished from distilled water spots by intense color differences. The chloride detection mechanism allows the identification of droplets containing as little as 0.02% sodium chloride. Special techniques are developed which allow collections of radioactive water droplets to be identified by radioautographic methods.

Historical

Early in the quest for positive indicating surfaces upon which fog or rain droplets might leave measurable impressions, such materials as sooted glass slides became very popular (1, 9–11). Their major deficiencies were lack of definition for droplets smaller than 10 μ and fragility of the soft carbon coating. Much work was done to correlate the size of the impression with that of the original droplet, but conflicting spot types tended to confuse the issue (9). Magnesium oxide coatings were substituted (7) because they had finer particle sizes and were easier to distribute over the slide. Rough calibrations were made using this material (1), but resolution difficulties still prevented the register of less than 10-μ diameter droplets.

During the same year carbon black slides were introduced, the petrolatum-mineral oil slide was developed (5). This method with several important improvements (7, 8) has become one of the most reliable laboratory means of collecting droplets. The technique involves inverting a warm vaseline-mineral oil coated cover glass over a solidified grease-coated collecting slide containing impinged droplets. It is not adaptable for general field use. To get away from the fragile soot and oxide coatings and the difficult grease methods, thin dye films bound with gelatin, polyvinyl alcohol, ethylhydroxycellulose, and others were tried (9). Deleterious huidity effects and poor small droplet response hindered the usefulness of ese methods. Specialized surfaces to indicate contaminating ions such as lides (2, 4), carbonates, nickel, cobalt, and copper (3) were developed.

All the above materials have been useful for certain applications. How-er, there is an evident need for a sampling surface which combines a nsitivity to distilled water droplets with specialized ion identification, ggedness in the field, and reliability in the small particle range. The com-nation of these properties into one collecting surface together with meth-ls for detecting radioactive droplets is the purpose of this investigation.

Description of the Method

From this investigation has evolved a new type of transparent film mpling strip. Its base is a 35-mm. film of cellulose acetate on which a clear ater solution of polyvinyl alcohol-silver nitrate-hydrogen peroxide is dip ated and dried. The sensitive mechanisms of this sampling strip are best scribed in four phases: (*1*) the physical impression made by water drop-s on the film, (*2*) the chemical reaction of sea water droplets and their otochemical development, (*3*) the vapor phase chemical development of stilled water impressions, and (*4*) the radioautographic methods adapted r radioactive droplet detection. Because of the interacting complexity of ese combined film properties, a brief discussion of each phase follows.

Phase 1. Water droplets in the size range 1 to 100 μ produce permanent ater-like impressions on dried gelatin or polyvinyl alcohol films by dis-rting the water-soluble film (Fig. 1*a*). The raised peripheral lips of these aters create optical "lens effects" under the microscope, thereby making e craters visible. Their diameters are accurately measurable down to the -μ size; below this, the resolution is difficult. Both sea water and distilled ater droplets make identical spots. Experiments show that polyvinyl ohol (PVA) is superior to gelatin in crater formation and humidity sistance; hence, PVA was chosen as the water-sensitive material.

Phase 2. Hydrogen peroxide buffered silver nitrate is introduced into e plastic mix to promote a precipitation reaction between the sea water loride ions and the silver. The resultant silver chloride precipitates only thin the bounds of the saline droplet spread on the film. By photochemi-lly reducing the silver chloride to colloidal silver, strong color differences e produced between the distilled water and sea water spots. The sea water ots are deep red-brown; the others are transparent (Fig. 1*b*). The rapid ver chloride reduction is accomplished by high-intensity sun lamp posure.

Phase 3. The accidental use of phenylhydrazine vapors on a droplet pinged film led to the discovery of the "developable" properties of tilled water spots. Distilled water droplet impressions become well de-d and colored (Fig. 1*c*) even in the difficult 1- to 10-μ range when exposed

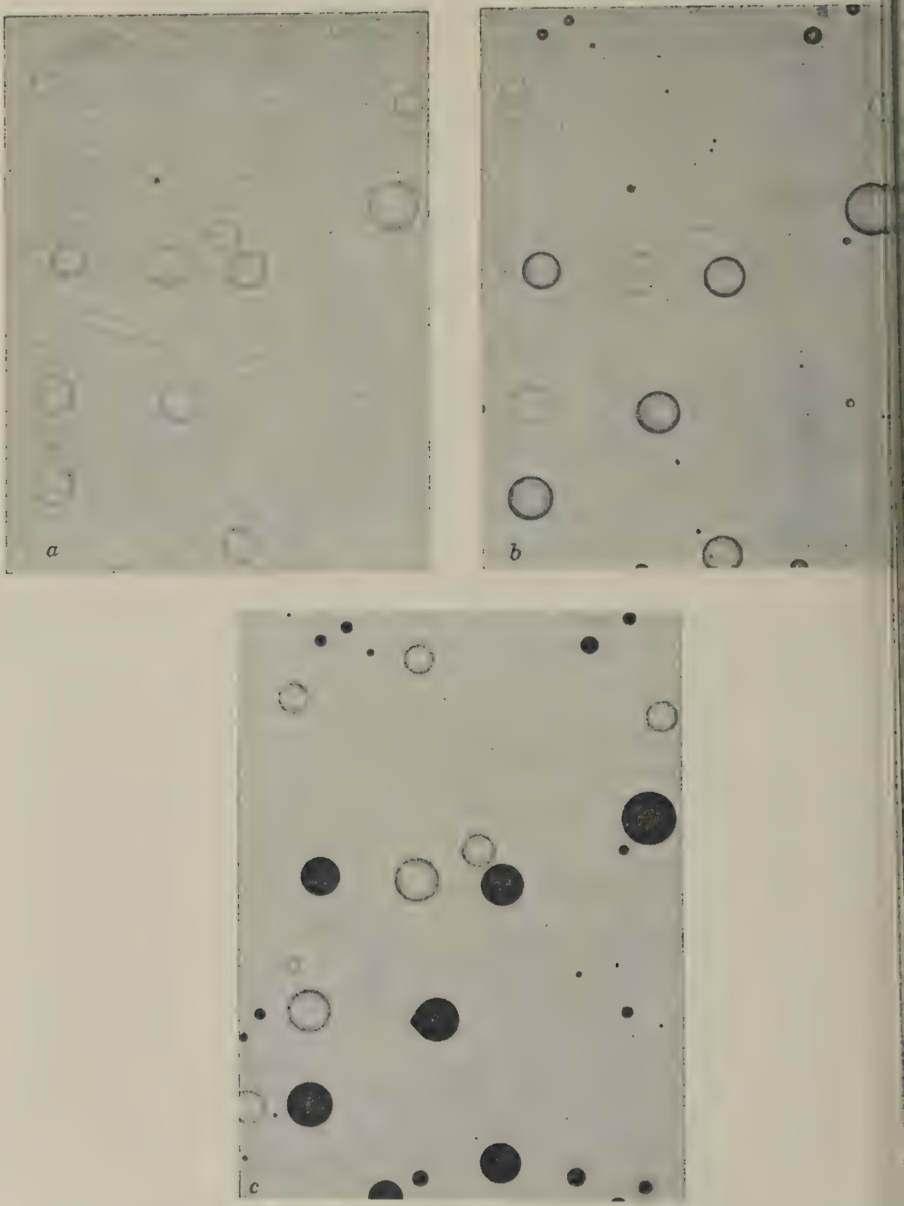

FIG. 1. Various stages of development of droplet impressions on the sensitive film (magnification 360 ×). (*a*) Undeveloped salt and distilled water droplet impressions. (*b*) The same impressions after sun lamp development. (*c*) The same impressions after sun lamp and phenylhydrazine development.

vapors of water, phenylhydrazine, and ammonia. The mechanism of this eaction is conjectural but differences of silver nitrate concentration within ie drop spread area are thought to be contributing factors.

Phase 4. The water droplet collecting film is found to be insensitive to igh-activity radiation. In order that radioactive droplets might be deected, the radioautographic techniques of LaRiviere and Ichiki (6) were dapted for film usage. By coating the chemically developed droplet iminged film with a transparent water repellent varnish,[1] photographic uclear emulsions could be applied directly to the film surface for autoraphing. Subsequent emulsion development, fixing, and washing does not arm the protected droplet impressions.

LABORATORY PROCEDURES

Film Preparation. Laboratory amounts of the film are most easily made y the following techniques.

A distilled water solution containing 30% by weight of PVA[2] is made by irring the dry powder into cool water with strong agitation. The solution heated to 80°C. and stirred continuously until the powder is completely issolved. The clear solution is allowed to stand for several hours, to cool nd debubble. To this cool, bubble-free mixture is gently added dilute itric acid until a pH of 5 is reached. A solution of hydrogen peroxide and lver nitrate is stirred in so that the final mixture has by weight 20% PVA, % silver nitrate, 0.3% hydrogen peroxide, and the remainder distilled ater.

Cellulose acetate base films[3] are first etched in saturated potassium hyroxide solution so that the coating will properly wet and adhere to the urface. The film is thoroughly washed in distilled water, then dip coated the coating solution. The coated films or slides are dried at 40°C. or less hile hanging in a vertical position. Using this mixture at room temperaure will produce a water-sensitive coating about 1 mil thick on each side f the dipped base.

Spot Development. Small-scale spot development can be accomplished ith simple apparatus. The sea water impressions are first photochemically educed by several minutes exposure 2 in. from the sun lamp. Then the istilled water spots are chemically developed by exposure to phenylhydrane vapor. Practice is required to achieve the proper degree of development nd care must be exercised to control certain film variables discussed later this paper. For the small film vapor development, place about 30 ml. of phenylhydrazine in a liter beaker and heat until white fumes appear. Remove the beaker from the hot plate and add 5 to 10 ml. of 30% ammoni water. Droplet impinged film strips are thrust into the vapor above th liquid and held until the surface is silvered. Condensation of vapors ont the film can be avoided by preheating the film to near 80°C. Moistening th heated film over hot water improves the development, but care must b taken that no condensation occurs. Because of the toxic nature of phenylhydrazine, all work should be done in a hood; handling should be with gloves and tongs. After sun lamp and phenylhydrazine development, sea water spots will appear deep red-brown, whereas pure water spots are gray or brownish. All spots are well defined in the range 1 μ and larger; they ar perfectly circular and accurately measurable.

---

[1] "Krylon," acrylic spray, Krylon, Inc., Philadelphia, Pennsylvania.

[2] Elvanol 51-05, E. I. Du Pont de Nemours, Inc., Electrochemicals Dept., Wilington, Delaware.

[3] Eastman Kodak Co., #3 clear safety 35-mm. film with positive perforations, chester 4, New York.

EXPERIMENTAL INVESTIGATIONS

Chloride Sensitivity. Because of salt content variation in sea fogs, it is important to know the limits of film chloride detectability. Solutions of varying salinity were aspirated with a small volume aerosol generator system (4). Fourteen 2-in. strips of 35-mm. sensitive film were cut from a master film batch. Each strip was impinged with two aerosols of differing salinity (Table I). The droplet size range of these aerosols was 1 μ and greater. Each film strip was then divided into three sections. Each section was developed periodically over the time indicated. Before development each section was halved. One half of the section was developed with phenylhydrazine vapors; the other half was first exposed for 2 min. at 2 in. from a sun lamp, then chemically developed.

With this test arrangement, it is seen that a brief sensitization of the silver chloride areas with ultraviolet light greatly enhances the spot color contrast with subsequent phenylhydrazine development. A 2-min. sun lamp exposure alone is not enough clearly to develop the lower concentration chloride droplets, but by combining the sensitizing system with vapor reduction, considerable development time can be saved and water spot contrast increased.

Table I indicates that the lower limit of saline sensitivity occurs with droplets containing 0.02% sodium chloride by weight. With proper standards, a pure sea water droplet can easily be distinguished from droplets containing lesser amounts of sodium chloride.

Vapor Phase Components. The essential components of the vapor phase reduction system are water vapor, phenylhydrazine vapor, and ammonia.

The chemical reduction operates essentially as follows. Consider first a film containing only impressions of distilled water droplets. These droplets have by some mechanism changed the local silver nitrate concentration on the film in their spread area. The water vapor in the reducing system opens up the plastic structure and carries the phenylhydrazine vapors into the

TABLE I
Chloride Sensitivity

Film ample	Aerosol 1	Aerosol 2	Development of color contrast between aerosols[a]					
			1 wk		3 wk		5 wk	
			$\phi NHNH_2$	Sun + $\phi NHNH_2$	$\phi NHNH_2$	Sun + $\phi NHNH_2$	$\phi NHNH_2$	Sun + $\phi NHNH_2$
1	Dist. H_2O	3% NaCl	S	VS	S	VS	W	S
2	Dist. H_2O	2% NaCl	S	VS	M	VS	M	S
3	Dist. H_2O	1% NaCl	S	S	M	VS	W	W
4	Dist. H_2O	0.2% NaCl	M	S	W	S	N	W
5	Dist. H_2O	0.02% NaCl	W	W	W	W	N	N
6	Dist. H_2O	0.002% NaCl	N	N	N	N	N	N
7	0.02% NaCl	0.002% NaCl	N	N	N	N	N	N
8	0.2% NaCl	0.02% NaCl	N	W	W	M	N	N
9	1% NaCl	0.02% NaCl	S	S	M	S	M	S
10	1% NaCl	0.2% NaCl	M	M	M	VS	M	S
11	2% NaCl	0.2% NaCl	W	M	W	S	W	S
12	2% NaCl	1% NaCl	W	M	W	S	W	W
13	3% NaCl	1% NaCl	W	M	M	VS	W	S
14	3% NaCl	2% NaCl	W	W	N	W	W	W

[a] VS—Very strong color contrast. S—Strong color contrast. M—Moderate color ontrast W—Weak color contrast. N—No color contrast.

lm where the silver reduction begins. At the same time, ammonia, acting a fashion similar to its role in classical chemical silvering, retards the ilver crystal size growth while also aiding the penetration of the reducing gent. The rate of reaction is identical throughout the system. However, wing to the infinitesimal difference in silver nitrate concentration in the rop area, the degree of silvering in the spot is different. This variance from he background silver gives the color contrast necessary to define the pure ater impression. The inhibiting effect on silver crystal growth by ammonia is valuable in preventing the formation of a surface haze of silver hich can mask the color differences between spot area and adjacent film. f such a haze does occur, it is removable with a soft cloth. The temperature t which the redox reaction takes place is important, for it determines not nly the concentration of water vapor and phenylhydrazine but also the ltimate size to which the silver crystals can grow under the vapor conditions. In general, the higher the temperature, the larger the ultimate silver rain size.

Consider now the more clear-cut action of the system on salt water drop- t impressions. In this droplet area is a colloidal dispersion of silver loride from the saline-silver nitrate reaction. A brief sensitization by the sun lamp has partially photo-reduced the chloride crystals. Under the vapo chemical action, the reduction to silver proceeds much more rapidly and t a greater extent than does the distilled water droplet area. Thus sharpl contrasting spots of two aerosol types are produced.

Temperature Effects. The effect of elevated temperatures on the dry film is not harmful. Rigorous temperature tests show conclusively that continuous exposure to 70°C. temperatures for 34 days does not seriously deteriorate the film properties either before or after impingement with aerosol Although film darkening at the upper temperature range is considerable it does not interfere with the droplet indicating properties.

Humidity Effects. Because of its great affinity for water droplets, the film is necessarily sensitive to changes in humidity. Mild humidity variation does not affect the formation of the crater-like impression. However, the chemical reduction of the silver nitrate is affected. Extensive experiments were carried out to determine the effect of humidity on the film. Sensitive film strips were exposed for periods of 24 hr. to 9 months in relative humidities of 0 to 72%. These same strips were then impinged with water and salt water aerosols and again exposed to the various humidities for 24 hr. to 19 days. At the end of the test periods the strips were photochemically and chemically developed and the spots rated according to qualities of resolution, color, and contrast. From extensive experiments employing a large variety of time-humidity combinations, the following general conclusions were reached. Films stored for extended periods of time before use as aerosol collectors retain their sensitive properties when kept in environment of 50% relative humidity or less. Film strips which have been impacted with droplets can be stored prior to chemical development for several weeks without impairment of sensitivity so long as the relative humidity remains below 70%. Once the droplet spots have been developed by photochemical and chemical processing, the impressions are permanently fixed in size and color characteristics.

Fluctuations of moisture content during the actual development of the film in the chemical vapor bath have produced complex and as yet unexplained variations of spot development. Such moisture variations produce great differences in colloidal silver grain size which lead to color combinations of spectral brilliance. To avoid the oftentimes disastrous fluctuations, elaborate control systems were devised to reproducibly control the chemical vapor concentrations in the development process (12).

Special Requirements. The film is moderately photosensitive and must be stored in total darkness. To permit long-term storage of film samples under field conditions where wide humidity fluctuations might be expected, sealed polyethylene bags are used and the wrapped films stored in sealed film cans. Films, under proper conditions, can be stored as long as nine months without impairment of sensitivity.

CALIBRATION OF THE FILM

The sampling surface calibration of spot size with original drop size has en completed in the 1- to 100-μ droplet diameter range. The procedure, ta, and curves are presented in a separate report.

APPLICATION

One of the most interesting potential applications of the technique is in e study of the effect of various nucleii on the size distribution of a liquid rosol. The true effects of such "cloud-seeding" materials are still largely eculative. A continuous sampling of size distribution both before and ter "seeding" should give quantitative data about possible particle size owth. The use of radioisotopes in liquid aerosols for studies on droplet glomeration, investigations of air stream flows, and smog applications ers a wide variety of problems in which the material may be useful.

ACKNOWLEDGMENTS

Credit is given to the invaluable assistance of Mr. F. A. French on organic chemi- aspects of this work. The editorial assistance of Mr. Jarvis Todd is greatly ap- eciated.

REFERENCES

BLANCHARD, D. C., "The use of sooted screens for determining raindrop size and distribution," G. E. Research Lab. Occasional Report #16, Project Cirrus, U. S. Army Contract #W-36-039-SC-38141, Schenectady, New York, November, 1949.

BOYCE, S. C., "Source of atmospheric salts," *Science* **113,** 620 (1951).

CROZIER, W. D., "Airborne particle study," Research and Development Division, New Mexico School of Mines, Contract N70NR-405, Task 1, Project #NRO82-013, March 1949.

FARLOW, N. H., "An improved halide ion sensitive sampling surface for water aerosols," *Rev. Sci. Instr.* **25,** 1109 (1954).

FUCHS AND PETRJANOFF, *Nature* **139,** 111 (1937).

LARIVIERE AND ICHIKI, *Nucleonics*, **110,** #9, 22–24, 1952.

MAY, K. R., *J. Sci. Instr.* **22,** 187 (1945).

MAY, K. R., *J. Sci. Instr.* **27,** 128 (1950).

SCHAEFER, V. J., "The preparation and use of water sensitive coatings for sampling cloud particles," General Electric Co. A.A.F. Technical Report 5539. A.A.F. Air Material Command, Wright Field, Dayton, Ohio, January 24, 1947.

STOKER, R. L., *J. Appl. Phys.*, **17,** 243–245 (1946).

STRAZHEVSKY, L., *Tech. Phys. U.S.S.R.* **4,** 978 (1937).

FARLOW, N. H., U. S. Naval Radiological Defense Laboratory Technical Report #49, May 1955.

OURNAL OF COLLOID SCIENCE 11, 193–194 (1956)

BOOK REVIEWS

Gas kinetics: An Introduction to the Kinetics of Homogeneous Gas Reactions. y A. F. Trotman-Dickenson, Lecturer in Physical Chemistry in the University Edinburgh. Academic Press Inc., 125 East 23rd St., New York 10, New York, 1955. + 322 pp. Price $8.00.

This book fills an important gap in the literature of chemical kinetics. Other ecent books have a much wider field and hence discuss gas reactions in a much less etailed way, and in most cases have also a much more theoretical bias. There has ng been a need for a book such as the present one which covers basic theory, but at the same time definitely written from an experimental point of view. Nothing hich covers the same general field has appeared since Schumacher's *Chemische asreaktionen*, which is now nearly twenty years out of date. The author has himself ade contributions to almost all branches of the subject, and is eminently qualified write such a book.

The initial chapter discusses the relation of chemical kinetics to thermodynamics, ond dissociation energies, etc. The second chapter gives an excellent and concise ccount of the theories of chemical kinetics. This is followed by chapters on uni- olecular decompositions and bimolecular combinations, transfer reactions, and dical decompositions and additions. For a book of only slightly over three hundred ages the references are unusually numerous and complete, although not many of em are later than 1953.

This is an excellent book, and is both clear and critical. It can be strongly recom- ended to all workers in the field, and as an authoritative introduction to the subject r students of chemical kinetics. The book is well produced, and the price is reason- ble.

E. W. R. Steacie, Ottawa, Canada

A Course in Modern Techniques of Organic Chemistry. By R. P. Linstead, J. A. Lvidge, and Margaret Whalley, Academic Press Inc., New York, 1955. 190 pp. rice $5.00.

This little volume contains material which is part of a course at the Imperial ollege of Science and Technology in London.

The range of material covered is quite large and has been conveniently divided to three parts: Techniques of Purification and Separation (including adsorption, artition, paper and ion-exchange chromatography, multiple fractional extraction, nophoresis on filter paper, isolation and purification of protein, fractional distilla- on, vacuum sublimation, final purification of solids and of liquids for analysis), pecial Reaction Techniques (vacuum line technique, catalytic hydrogenation at low d high pressure, reaction in a Carius tube, vapor phase reactions, reactions in quid ammonia, use of lithium aluminum hydride, preparative electrolysis and onolysis) and Techniques of Quantitative Analysis and Allied Physical Measure- ents (semi micro carbon and hydrogen, micro Kjeldahl, active hydrogen, molecular eight, potentiometric titration, polarographic analysis, colorimetric analysis, sorption spectrometry by use of visual and photoelectric instruments).

The chapters are written extremely concisely with a minimum of theoretical discussion, the emphasis being on the description of actual experiments involving the particular method or technique under consideration. References are given for further elaboration of the subjects covered. There can be little quarrel with the choice of topics, although some tabulation of data might have been included in connection with some chapters such as on ultraviolet absorption. The omission of infrared data is unfortunate.

Some slight drawback of the book is that it is designed for use with specific British equipment (chapters on potentiometric titration, colorimetric analysis, polarographic analysis, absorption spectroscopy). This affects only a small part of the volume, however, and should not detract from its general usefulness not only in connection with a course, but as a handy bird's-eye view of a variety of topics encountered in research work. From that point of view it is highly recommended.

GILBERT STORK, New York, New York

The Elements of Chromatography. By TREVOR I. WILLIAMS (Oxford). 90 pages, 36 figures including 7 colored plates and a photograph of David T. Day. Published by the Philosophical Library, New York, and printed by Blackie and Son, Ltd., Glasgow. Price $3.75.

This delightfully written little book and beautiful example of the printers' art is highly recommended to all who wish to read a short and concise book on chromatography.

A great deal of fundamental information is provided in this skillful presentation.

ARTHUR W. THOMAS, New York, N. Y.

JOURNAL OF COLLOID SCIENCE 11, 195–213 (1956)

EXPERIMENTAL INVESTIGATIONS ON THE LIGHT SCATTERING OF COLLOIDAL SPHERES[1]

I. The Specific Turbidity

Richard M. Tabibian, Wilfried Heller, and Joseph N. Epel

Chemistry Department, Wayne University, Detroit, Michigan

Received March 23, 1956

INTRODUCTION

The use of light scattering for determining the size and shape of particles of colloidal or subcolloidal size dates back more than half a century. The first extensive discussion of experimental light-scattering phenomena was carried out by Tyndall in 1868. The first significant work on the theory of the problem was done by Rayleigh in 1871 (1).

In spite of the fact that the basic theoretical development had been completed and useful experimental techniques had been developed at a rather early date, the systematic experimental investigation and practical application of light scattering had been lagging until about fifteen years ago. The reasons for this were twofold. First of all, prior to the modern development of protein chemistry and of synthetic materials, it was rather difficult to obtain colloidal and macromolecular systems of well-defined and fairly uniform particle size. Secondly, and this may have been the main reason, the need for information on the dimensions or molecular weights of colloidal or macromolecular units was at no time as compelling as it has become, for various reasons, during the last fifteen years.

The modern era of extensive theoretical refinements and intensive experimental application of light scattering began in the early 40's almost simultaneously in three closely related fields. (*a*) The need to know more about the mechanism of growth and the rate of growth of polymer particles in synthetic latices and about the role of soap micelles in emulsion polymerization led to the application of light scattering to these systems on a large scale (2, 3). This application was greatly aided by the conversion of classical equations into more attractive practical forms (3, 9). (*b*) At about the same time, large-scale experiments were carried out by LaMer (4) and collaborators with the aim of getting more information on the size of particles in

---

[1] The exploratory first part of this work (J. N. Epel) was supported by a grant from the Research Corporation; the later large scale investigations (R. M. Tabibian) were supported by the U. S. Office of Naval Research.

aerosols in an expansion of earlier work on aerosols by Engelhard and Friess (5), Paranjpe *et al.* (6), and Ruedy (7). (*c*) The successful application of light scattering to the determination of molecular weights of proteins (8) together with the new impetus given to the refinement of the theory primarily by Debye (9) and Zimm (10), led to extensive application of light scattering to solutions of macromolecular systems.

1. Brief Survey of Theories

In the classical theory of light scattering in disperse systems, based upon the electromagnetic theory of light, the scattering particles are considered as dipoles (11). This theory is limited to small α-values,[2] i.e., to particles which are small compared to the wavelength of the incident light. If α is not small enough ($\alpha > 0.4$), the particle (or macromolecule) may be considered, instead, as an assembly of dipoles whose oscillations are out of phase. The treatment of this case is also relatively simple if it is assumed that the field exciting the dipoles is identical with the primary electromagnetic field which is equivalent to neglecting the contribution of the scattered field. This means, in practical terms, that a relative refractive index, m,[3] approaching 1.0 must be assumed. Rayleigh (12) and, independently, Gans (13) worked out the respective theory. The resulting equation is, therefore, generally referred to as the Rayleigh-Gans equation. The latter is, as will be shown in a later paper, quite satisfactory over an extended range of intermediate α-values which shrinks rapidly with increasing m. Equivalent to the Rayleigh-Gans theory and leading, for spheres, to the same numerical results is the very recent application by Debye of his earlier theory of X-ray scattering (14) to the case of light scattering (15).

A more general treatment for spheres, also on the basis of the electromagnetic theory, is that given by Mie in 1908 (16). It has the considerable advantage over the others in that it is applicable to any α and m. Here, each particle, considered as a dipole if small compared to the wavelength,[4] may be represented at larger α-values as an assembly of interdependent dipoles. This means that the excitation of each dipole is assumed to depend not only on the primary field but rather on the total field as affected by the excitation of other dipoles in the same assembly. As α increases, the increase in the number of dipoles leads successively to quadrupolar, octupolar, and multipolar contributions to the total scattering. The consideration of the contributions of all these "partial waves," both electric and magnetic—together with the preceding element of rigorousness—makes the evaluation of the Mie equations quite laborious for any set of α and m parameters, more so the larger α and m. There have, therefore, been several attempts either to simplify the Mie treatment by means of approximations or to develop a simpler related treatment such that the limitations imposed upon m or α as implied in the Rayleigh, Rayleigh-Gans, or Debye treatment are less severe. Theoretical data are then obtained more easily for a far more extensive α or m range but at the cost of a reduction in accuracy within the ranges of approximate validity. Nevertheless, they are of major interest in a specific number of cases. Particularly noteworthy are the results of Van de Hulst (17). One case which will be considered in detail elsewhere leads to acceptable approximate results which are applicable to small and moderately small m values and to both intermediate and larger α-values but not for smaller or very large α-values. Hart and Montroll (18) obtained equations the results of which agree with those of the Mie theory to 5% or even better for a fairly wide range of rather large intermediate α-values but not for smaller or very large α-values. Considering the use of visible light, the upper limit of this intermediate α-range pertains to large microscopic particles. Far more serious is the fact that the α-values below which a useful application is excluded, correspond, according to our survey, to particle diameters of 495, 260, and 195 mμ for m equal to 1.20, 1.33, and 1.50, respectively, if the wavelength in vacuo $\lambda_0 = 5461$ A.

---

[2] $\alpha = \pi D/\lambda$, where D is the diameter of the spheres and λ the wavelength of the incident light in the medium.

[3] $m = \mu_2/\mu_1$, where μ_2 is the refractive index of the particle and μ_1 that of the medium.

[4] The results in this limiting case are identical with those of the first Rayleigh theory.

While all preceding treatments of light scattering are based upon assuming discrete particles, molecules, or segments thereof as a source of light scattering, an alternate approach also proved possible. It was proposed by Smoluchowski (19) and Einstein (20). Here, light scattering is treated as a phenomenon of fluctuations in density in the case of pure liquids and fluctuations of concentration in the case of liquid mixtures. Einstein's brief approach to the latter case was carried out in detail by Raman (21) and by Gans (22) and, again, independently by Debye (9). The equations arrived at on the basis of the fluctuation theory opened to light scattering the wide field of pure liquids and simplified the treatment of solutions containing nonspherical solutes. On the other hand, it must be borne in mind that the respective equations apply only to instances where the relative refractive index of the solute does not differ appreciably from 1.0 and where the dimensions of the solute particles are small compared to the wavelength used.

2. Objectives of Present Investigation

The primary objective of this investigation was to establish methods and procedures for the precise and accurate determination of particle sizes from light scattering considering, to begin with, spheres only. Since it was desired not to limit the method to particles of any particular size range or to particles of small relative refractive indices, the Mie equations had to be used. Light-scattering functions on the basis of this theory had been calculated for isolated values of the various parameters by Blumer and others (23, 24). Systematic computations were carried out only recently by A. N. Lowan and associates (25) and also by Houghton and Chalker (26) for relative refractive indices 1.33–2.0 and 1.33, respectively. These data are applicable to aerosols. Therefore, extensive computations had to be carried out in this laboratory for the range $\alpha = 0.2$ to 15.0 and $m = 1.05$ to 1.30, which covers virtually all possible cases of nonabsorbing spheres dispersed in a liquid exclusive of the upper microscopic range only (diameters greater than 2 microns if visible light is used) (27). Values up to $\alpha = 6.0$ were determined by Pangonis (28) using a desk calculator. Electronic calculations for the larger α-values were carried out by L. R. Langdon and H. J. McCarty of the Computation Laboratory of Wayne University.[5] While this work was proceeding additional extensive computations by Gumprecht and Sliepcevich (29), again primarily concerned with aerosols, became available.

Implicit additional objectives of the present investigation were: (*a*) a rigorous experimental verification of the Mie theory, using for that purpose the electron microscope as an independent criterion of particle size,[6] and (*b*) a critical evaluation of the various possible sources of error in light-scattering measurements. The investigation covered measurements of (*1*) the total turbidity, (*2*) the total scattering at an angle of 90°, (*3*) the state of polarization of the laterally scattered radiation as expressed by depolarization and "scattering ratio," (*4*) the turbidity spectra, and (*5*) the Tyndall spectra. The present paper will deal with the total turbidity.

3. Definition of Turbidity

The intensity of a beam of light passing through a solution or suspension is attenuated as a result of scattering. The fractional decrease in the intensity of the primary beam is, in analogy to the Lambert-Beer law:

$$-dI/I = RN\,dx, \tag{1}$$

where R is the total radiation scattered by a single particle per unit intensity of incident light,[7] N is the number of particles per cubic centimeter in a system sufficiently dilute to exclude significant multiple scattering, and x is the length of the light path in the scattering solution. Integration yields

---

[5] We are indebted to Professor A. Jacobson, Director of the Computation Laboratory, for making its facilities generously available to us. We also wish to acknowledge the valuable theoretical assistance of Prof. A. F. Stevenson in problems of programming.

[6] This is not the first attempt to verify the Mie equations. However, it had never been possible before to work with systems that approach monodispersity as closely as desirable for such a check. In addition, in the case of gold or sulfur sols and other similar systems, uncertainties with respect to the complex refractive index exclude any rigorous comparison between experiment and theory.

[7] The quantity R which has the dimensions of *cm*^{2} is also referred to as the scattering cross-section and $R/\pi r^2$, where r is the radius of the sphere, as the scattering coefficient.

$$I/I_0 = e^{-RNx}. \tag{2}$$

The product RN is equivalent to the "apparent" or "conservative" (30) absorption coefficient per centimeter of light path and is generally called the turbidity τ. Therefore

$$\tau = \ln (I_0/I)/x. \tag{3}$$

The specific turbidity is obtained by dividing τ by the total volume of all the spheres in 1 c.c., i.e., by their volume fraction ϕ. For practical purposes, it is more useful to express the concentration on a weight basis, i.e.,

$$\tau/c' = (\tau/\phi)(\rho_{12}/\rho_2), \tag{4}$$

where c' is the weight, in grams, of the scattering particles per gram of disperse system and ρ_2 and ρ_{12} are the density of the particles and entire system, respectively. Considering for reasons of experimental convenience, rather $1/100$ of τ/c'

$$\tau/c = 1/100\, (\tau/c') \equiv 1/100\, (\tau/\phi)(\rho_{12}/\rho_2), \tag{5}$$

where c is now the concentration in grams per 100 grams of disperse system.

To eliminate interference of multiple scattering the experimental specific turbidity, measured at finite concentrations, must be extrapolated to zero concentration. The quantity of primary interest is therefore the limiting specific turbidity.

$$(\tau/c)_0 = \lim_{c \to 0} (\tau/c). \tag{6}$$

This is the quantity to be compared with the theoretical specific turbidity derived from the Mie equations for the particular wavelength used and the pertinent m-values.

4. APPARATUS

The measurements were carried out with a precision apparatus designed in this laboratory (31). Since it is to be described in detail in a forthcoming publication, it will be sufficient to point out a few of those features which are particularly pertinent to a discussion of the results given here. A schematic diagram is shown in Fig. 1, in which features pertinent to measurements of angular light scattering have been omitted. The apparatus consists of three main sections: the illuminating unit I, the monochromator II, and the scattering unit III.

The illuminating unit contains interchangeably a mercury vapor lamp, type AH-4, or a tungsten ribbon filament lamp. The work reported here was carried out exclusively with the former. After passing through the monochromator and prior to entering the scattering unit, the light beam traverses the compensator C which compensates for the partial polarization produced by the constant deviation prism in the monochromator and by the reflecting glass plate R. Two 10-cm. cylindrical absorption cells with corex windows are used for the scattering system and reference liquid (here water), respectively. These are mounted on a special carriage which is designed to bring the two cells alternately into the light path. In order to prevent secondary scattering from reaching the phototube, the scattering cell (i.e., the cell containing the scattering system) is painted black and a diaphragm D_6 placed at the exit window.

The primary beam entering the scattering cell assembly SC at A_3 is characterized by a solid angle of 1×10^{-4} steradian. Translating this into a quantity which can be more easily visualized, the vertex of the planar projection of the light cone has a half-angle of 0.33 degree. Hereafter when

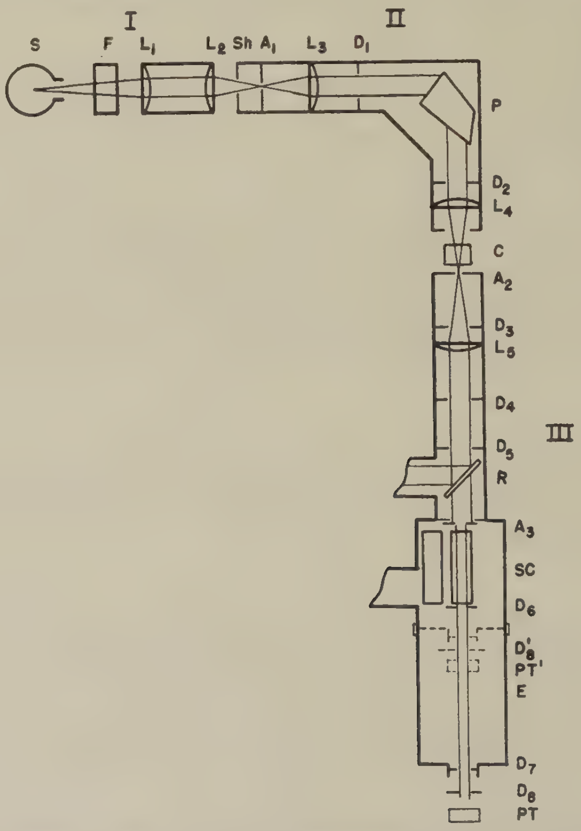

FIG. 1. Schematic diagram of the light scattering apparatus. S light source, F infrared filter, L lenses, Sh shutter, A variable apertures, D fixed diaphragms, P constant deviation prism, C compensator, R reflector plate, SC scattering cell assembly, PT phototube positions, E detachable extension.

referring to the solid angle, this vertex angle will be used for the sake of convenience. Thus, the primary beam entering the scattering cell is nearly parallel. This is of paramount importance in the case of large particles where forward scattering is appreciable.

The primary beam on leaving the scattering cell is superimposed by a scattered beam. The reduction and definition of the solid angle of the latter beam are of considerable importance, as will be seen in the following paper. This is accomplished by inserting a diaphragm D_8 in front of the photomultiplier tube. For particularly rigorous work this diaphragm is preceded by a narrower diaphragm D_7 yielding the smallest solid angle used. By shifting the photomultiplier tube and D_8 to PT', additional variations of the solid angle become possible. Its smallest and largest values, expressing them in terms of one-half the vertex angle, are 0.4 to 8.2 degrees. The value pertinent to the results reported below is 1.0 degree.[8] This is obtained by placing the phototube in the PT position and omitting D_7. The distance between the phototube and scattering cell is 29 cm.

The photomultiplier tube can be protected from high light intensities by placing a neutral gray filter either directly in front of the phototube or in a holder at the exit end of the water-filled reference cell.

A multiplier photometer model 520M manufactured by the Photovolt Corporation, New York City, is used for the measurements. This is a line operated instrument utilizing an IP21 photomultiplier tube.

5. Experimental Procedure

In order to verify the Mie theory it was necessary to have particles which were both spherical and as uniform in size as possible. Fairly monodisperse polystyrene and polyvinyltoluene latices provided by the Plastics Basic Research and Physics Division of the Dow Chemical Company[9] came closest to fulfilling these conditions and, hence, were used as model systems. An additional advantage of these substances was that they exhibited no absorption in the visible portion of the spectrum.

Verification of data obtained from the Mie theory presupposed the use of an independent, alternate method of comparative size determination. Electron microscopy was the alternate method chosen. Independent electon microscopic size determinations were carried out by Dr. J. H. L. Watson of the Edsel B. Ford Institute for Medical Research and Dr. E. B. Bradford of the Dow Chemical Company. The results of their studies are shown in Table I. The Bradford values reported under I as well as those reported by Watson were obtained by standard electron microscopic techniques. The

---

[8] It will be seen later that this angle is small enough so as not to affect the $(\tau/c)_0$ values.

[9] In this respect we are indebted to Drs. R. S. Spencer, F. E. Towsley, and particularly J. W. Vanderhoff of the Dow Chemical Company.

TABLE I

Particle Sizes of Latices from Electron Microscopy

Sample No.	E. B. Bradford			J. H. L. Watson	
	Average Diameter, $m\mu$		Standard Deviation, $m\mu$	Average Diameter, $m\mu$	Standard Deviation, $m\mu$
	I	II			
S-153*	45	—	—	65	8
41	119	120	4	—	—
39	132	134	2	—	—
S-138*	135	—	—	155	16
40	144	144	4	—	—
S-139*	150	—	—	180	20
42	177	163	4	—	—
S-151*	219	—	—	258	10
7065*	252	238	35	263	36
2023*	230	249	9	218	8
S-137*	223	—	—	260	17
2022*	254	—	10	258	9
580G*	259	—	—	289	7
7194*	275	271	47	299	57
6	304	—	7	—	—
2012	—	381	—	373	11
43B	439	445	6		
44A	470	492	5		
063-A*	—	557	—		
43C	535	558	9		
44B	595	620	7		
066-A*	—	814	—		
44C	770	824	11		

* Starred samples are polystyrene; all others are polyvinyltoluene.

Bradford values II are very recent determinations or redeterminations by means of a precision technique involving the deposition of particles on a silica replica grating, thereby resulting in an internally calibrated micrograph. All the Watson values and eight of the Bradford values I were obtained by numerical analysis of the electron micrographs in this laboratory. All other counts were carried out at the Dow Laboratories. The differences between the three sets of electron microscopic values are in some instances appreciable. Possible reasons for such variations have been discussed by Watson (32). Among the various causes, that due to calibration uncertainties is eliminated by the technique of internal calibration (Bradford II). It may be noted that the data in the 2nd and 5th columns are those used in a preceding note (33).

The latex samples as received contained 30–50% solids. The preparation of diluted latex for the light-scattering measurements was carried out in the following manner. A small amount of latex was diluted with freshly prepared double distilled water in a centrifuge bottle of 250-ml. capacity to reduce the concentration to about 0.5–1.0%. The diluted latex was then centrifuged at about 350 *g* for 20 minutes to remove any agglomerates that might have been present. One hundred milliliters of the supernatant suspension were pipetted into a flask. The polymer concentration was determined by accurately weighing out (to 0.1 mg.) about 25 g. of this suspension and evaporating it to dryness in a partial vacuum at 80° and then weighing the dried solids.[10] A series of dilutions was made volumetrically from the remainder of the centrifuged latex by adding double distilled water to portions measured with a 10-ml. burette into volumetric flasks. The volume additivity, verified in these systems, allowed the concentration to be expressed in grams per 100 g. for any of the diluted samples obtained.

These samples were kept in pyrex glassware which had been carefully cleansed and subsequently steamed out for several minutes. To safeguard against any changes taking place in the samples upon prolonged standing at room temperature, all measurements were made within 3 days of the time when they were first prepared.

Experimentally, the turbidity is determined by filling one cell with the latex suspension and the other with doubly distilled water. Consecutive measurements of the intensity of light passing through the cell containing distilled water, I_0, and that passing through the latex, I, permit a direct calculation of τ and τ/c at a given concentration. The measurements are carried out for systematically varied values of the concentration in order to arrive, by extrapolation, at the significant quantity $(\tau/c)_0$.

All measurements of the turbidity reported here were made at room temperature (25°C. ± 3°) using the mercury green line ($\lambda_0 = 5461$ A.). Measurements at other wavelengths will be reported later in connection with turbidity spectra.

The transmittance of the two matched "Beckman" cells was found to be not strictly identical and to vary in a nonsystematic fashion with time.[11] The resulting potential error, although very small, was eliminated by frequent calibrations of the cells.

6. Experimental Results

Figures 2 and 3 show the variation of the turbidity with concentration for polyvinyltoluene and polystyrene, respectively. In all instances the data fall fairly well onto the straight lines drawn, i.e., τ is very nearly proportional to c within the concentration range investigated. On the assumption

---

[10] The nonpolymeric percentage of the dried solids was negligible as verified by centrifuging out the polymer from a latex and evaporating the supernatant liquid to dryness.

[11] This was found to be due to a very thin polymer deposit on the faces of the cell. This was removed periodically.

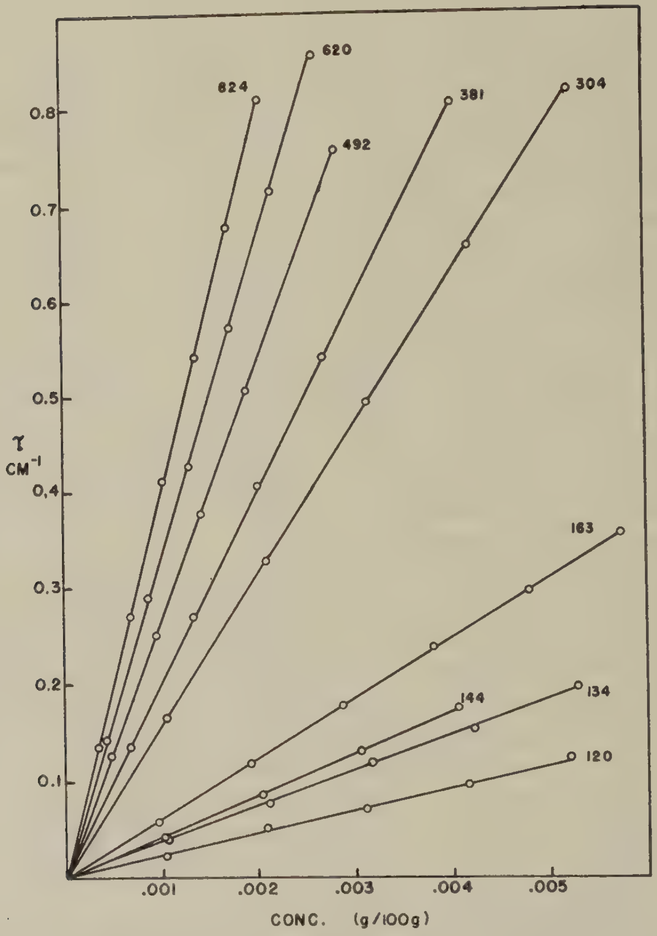

FIG. 2. Concentration dependence of turbidity (polyvinyltoluene). Parameter: particle diameter in millimicrons (Bradford II).

of a strict linearity of the τ vs. c plots[12] the slopes of these lines would be identical to the limiting specific turbidity, $(\tau/c)_0$.[13] A related but more rigorous procedure for obtaining $(\tau/c)_0$ is the plotting of τ/c vs. c and extra-

---

[12] At higher concentrations, pronounced deviations from the straight lines are to be expected but this range was not explored as not being of interest to the immediate purpose.

[13] The data for $D = 238$ and 249 millimicrons depart from the general pattern of an increase in slope with D which is theoretically necessary within the range of α-values investigated. This must be attributed to an accidental interchange of electron microscopic specimens or of data obtained therefrom. A conclusive check was impossible owing to lack of material. This explanation is supported by the fact that two sets of earlier electron microscopic data (Bradford I and Watson) in Table I give the expected opposite sequence for the D-values.

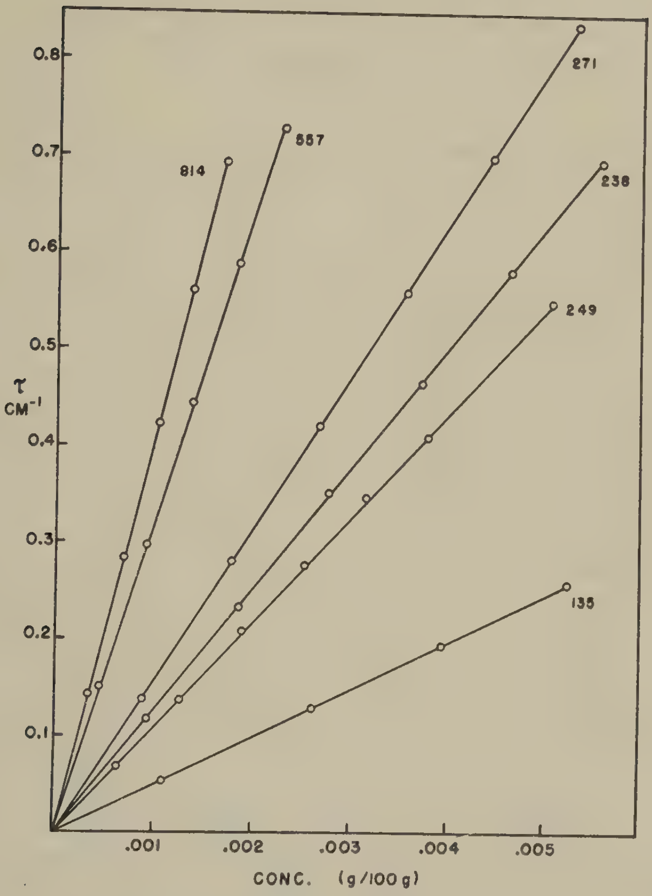

FIG. 3. Concentration dependence of turbidity (polystyrene). Parameter: particle diameter in millimicrons (Bradford II).

polation of the straight lines thus obtained to zero concentration. A few examples are given in Fig. 4 for intermediate particle sizes. The three uppermost curves have a slightly negative slope which is also found with still larger particles. This indicates that the range of concentrations within which τ/c is strictly proportional to c is more limited the larger the particle size. This is in agreement with expectation since deviations from linearity expected at larger concentrations are due to multiple scattering which, at a given concentration, is stronger the larger the particle size.

Typical numerical data for a latex with rather small particle size and for another with large particle size are given in Table II.

The scattering of the τ/c values, small as it is, is due to uncertainties in τ as well as in c. Plots of the type of Fig. 4 allow a fairly good evaluation of the overall precision obtainable in such measurements. The deviation of

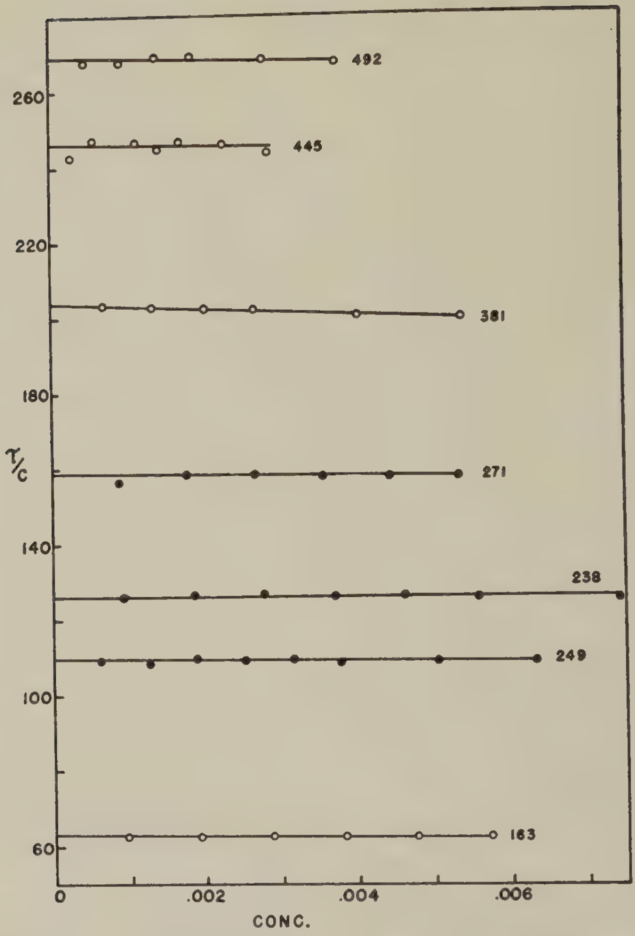

FIG. 4. Concentration dependence of the specific turbidity ○: Polyvinyltoluene; ●: Polystyrene; Parameter: particle diameter in millimicrons. (Bradford II).

the individual points from the lines is, at the worst, 2 % and in most cases less than 1 %. The precision of the $(\tau/c)_0$ values is therefore better than 1 % throughout. Consequently, the precision of the particle diameters, calculated from $(\tau/c)_0$, is better than 0.33 % throughout. This defines the normal precision for properly conducted turbidimetric particle size determinations with properly constructed equipment. In four instances a check was carried out on the reproducibility of data by repeating after widely spaced periods of time all operations, i.e., samples were taken from the same stock latices,[14] in one case as much as two years later, and in each instance the concentration and optical properties were determined independently. The maximum

---

[14] These were kept in a refrigerator at all times.

TABLE II

Data Illustrating the Dependence of τ/c on Concentration

(Polyvinyltoluene latices)

Sample No.	$c^a \times 10^3$	τ(cm.$^{-1}$)	τ/c
42 (diameter: 163 mμ)	0.000	0.000	(62.7)[b]
	0.9536	0.05944	62.33
	1.907	0.1192	62.51
	2.861	0.1792	62.64
	3.814	0.2398	62.87
	4.768	0.2977	62.44
	5.722	0.3569	62.37
	7.629	0.4737	62.09
	9.536	0.5934	62.23
44C (diameter: 824 mμ)	0.000	0.000	(397)[b]
	0.3420	0.1355	396.2
	0.6840	0.2716	397.1
	1.026	0.4118	401.4
	1.368	0.5424	396.5
	1.710	0.6775	396.2
	2.052	0.8129	396.2

[a] Grams of solids per 100 g. of latex.

[b] $(\tau/c)_0$.

deviation from the mean $(\tau/c)_0$ did not exceed 1.5%. Included in this are deviations due to conceivable minute changes in these latices which were, on the whole, remarkably stable at ~5°C.

7. Comparison of Results with Theory

In order to make an accurate comparison of experimental results and theory, m and ρ_2 have to be known. A separate study carried out in this laboratory by Thomas L. Pugh (34) furnished those data. The density ρ_2 for polystyrene and polyvinyltoluene is 1.057 and 1.026 g./c.c., respectively, at 25.0°C. The relative refractive index, m, against water for $\lambda_0 = 5461$ A. is 1.199 and 1.188, respectively (35). With these and the electron microscopic data at hand, a conclusive comparison became possible.[15]

The solid lines in Figs. 5 and 6 represent the theoretical $(\tau/c)_0$ vs. diameter (D) curves obtained for the case of polystyrene and polyvinyltoluene at $\lambda_0 = 5461$ A. on the basis of the theoretical $(\tau/c)_0$ vs. α relationship de-

---

[15] The polymer particles contain a surface film of stabilizer. This has two conceivable effects. First, it would make the optically effective particles slightly larger than the polymer spheres. This difference, being larger the smaller the particle size, does not enter here since the electron microscopic diameter includes the surface film. Secondly, the refractive index of the surface layer is slightly lower than that of the latex particle, thus reducing the m value. Since the experimentally determined m value was also pertinent to the surface-coated polymer particles, this effect also is eliminated.

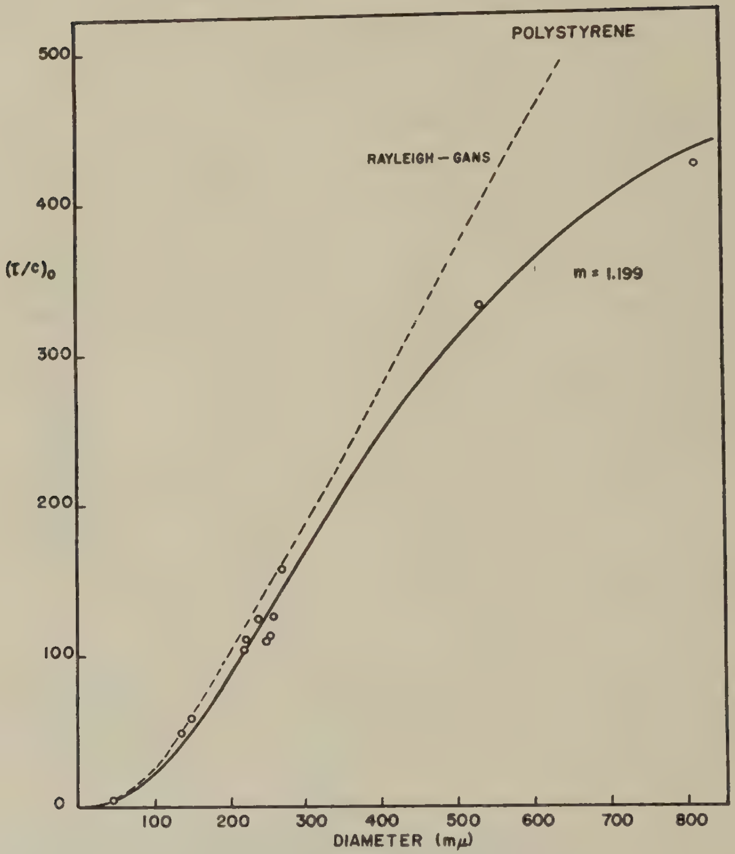

FIG. 5. Variation of the limiting specific turbidity with particle diameter (polystyrene) (Bradford II diameters).

rived from the Mie theory (36) taking into account the respective values of m and ρ_2 given above. The experimental data indicated by circles, using the Bradford II values for D, fit the theoretical curve very well in the case of polystyrene, the deviations being more in the nature of scattering rather than systematic. In the case of polyvinyltoluene the experimental points are throughout somewhat below the theoretical curve, more so the larger the diameter. The dotted theoretical curve, however, fits the data very well. This curve was calculated assuming an m value of 1.185. It is, therefore, inviting to assume that the small discrepancy between the experimental data and the fully drawn theoretical curve ($m = 1.188$) is due here to an error to the extent of 0.25 % in the determination of the refractive index of the polymer (34). This is within the limit of uncertainty in those experiments.[16]

[16] The effect of a change in m of as little as 0.003 shows the extreme importance of

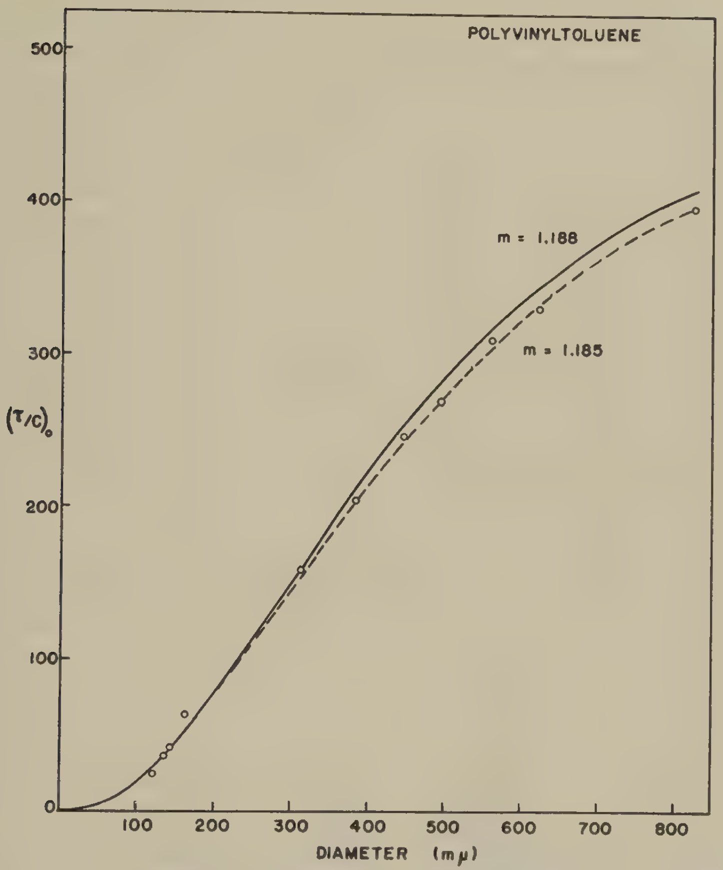

FIG. 6. Variation of the limiting specific turbidity with particle diameter (polyvinyltoluene) (Bradford II diameters).

A more exacting numerical comparison of the particle diameters obtained from light scattering by means of the Mie theory and those obtained by electron microscopy is given in Tables III and IV. The former were obtained by converting the experimental $(\tau/c)_0$ values to particle diameters by means of the pertinent theoretical $(\tau/c)_0$ vs. D curves. The per cent deviations given in the 5th and 7th and in the 5th columns, respectively, of these tables are rather small considering that they are affected by both the un-

---

accurate refractive index measurements if full advantage is to be taken of the precision inherent in turbidity measurements as defined above. While the accuracy of m-determinations as approximately defined above is the best obtainable with interferometric data in view of the necessity of a double extrapolation to both zero concentration and zero scattering, the latter requirement can henceforth be eliminated by a theoretical aid promising an appreciable increase in accuracy of m-values. This will be discussed fully in a later paper.

TABLE III

Comparison of Particle Diameters from Turbidity, D_0, and Electron Microscopy, D_e (Polyvinyltoluene)

Sample No.	$(\tau/c)_0$ (cm.$^{-1}$)	D_e(mμ) Bradford II	D_0(mμ) $m = 1.188$	% Deviation	D_0(mμ) $m = 1.185$	% Deviation
41	22.9	120	112	−6.7	112	−6.7
39	37.0	134	137	2.2	138	3.0
40	42.7	144	146	1.4	149	3.5
42	62.7	163	176	8.0	182	11.6
6	159[a]	304[b]	—	—	—	—
2012	204	381	372	−2.4	382	0.3
43B	246	445	432	−2.9	447	0.4
44A	269	492	469	−4.7	485	−1.4
43C	310	558	540	−3.2	558	0.0
44B	331	620	583	−6.0	610	−1.6
44C	397	824	772	−6.3	—	—

[a] Data obtained by T. L. Pugh.

[b] Bradford value I.

TABLE IV

Comparison of Particle Diameters from Turbidity, D_0, and Electron Microscopy, D_e (Polystyrene)

Sample No.	$(\tau/c)_0$ (cm.$^{-1}$)	D_e(mμ)	D_0(mμ) $m = 1.199$	% Deviation
S-153	5.1	45[a]	63	40.0
S-138	49.4	135[a]	149	10.4
S-139	59.0	150[a]	163	8.7
S-151	104.2	219[a]	224	2.3
S-137	110.9	223[a]	233	4.5
2023	109.4	249	231	−7.2
7065	126.0	238	252	5.9
2022	113.0	254[a]	236	−7.1
580G	126.0	259[a]	252	−2.7
7194	158	271	290	7.0
063A	331[b]	557	538	−3.4
066A	422[b]	814	765	−6.0

[a] Bradford values I; all others are Bradford values II.

[b] Data obtained by T. L. Pugh.

certainties in the specific turbidities from light scattering defined in the preceding section and the far larger uncertainties involved in electron microscopy.

It is quite apparent that the experiments described here can be considered as a conclusive proof of the validity of the Mie theory. Strictly speaking this statement applies thus far only to the α-range covered here experimentally, i.e., to diameters up to approximately 1 micron on using the green Hg-line. There is no doubt, however, that the statement can be generalized to cover any larger α-values. Not settled yet, however, is the question as to whether or not turbidity data obtained experimentally at still larger α-values are reliable, primarily because of additional experimental difficulties. In a few preliminary exploratory experiments with latices containing large microscopic spheres greater than 1 micron, $(\tau/c)_0$ values lower than those expected were obtained.

Because of the widespread use of the Rayleigh-Gans theory for particle size determinations, it is of interest to compare the experimental data also with the theoretical data derived from this theory. The respective turbidity function, evaluated for $\lambda_0 = 5461$ A.,

$$(\tau/c)_0 = [(1.4389 \times 10^2)/(\alpha)](m^2 - 1)^2 f(m') \qquad [7]$$

contains the α-dependent quantity $f(m')$ which thus far had been evaluated numerically only by Rayleigh (12). Additional $f(m')$ values were calculated primarily in order to extend the α-range which had terminated at the value of 4.32. They are given together with the Rayleigh values (the latter are identified by asterisks) in Table V. The theoretical turbidity curve thus obtained is dotted in Fig. 5. It is clear that the experimental data in Fig. 5 deviate appreciably from this alternate theoretical turbidity curve. The minimum deviation of the turbidity is, with the exception of a very narrow

TABLE V

Values of $f(m')$ (Eq. [7])

α	$f(m')$
$\pi/8$	0.0530*
0.4	0.0569
0.6	0.2666
$\pi/4$	0.7097*
0.8	0.7570
1.0	1.6180
$3\pi/8$	2.718*
$\pi/2$	6.1077*
1.6	6.4027
$5\pi/8$	10.534*
2.0	10.999
$3\pi/4$	16.156*
2.6	20.470
$7\pi/8$	23.448*
π	32.336*
$9\pi/8$	42.382*
3.6	44.159
$5\pi/4$	53.477*
4.0	55.683
$11\pi/8$	65.958*
5.0	90.915
8.0	244.92
10.0	388.00

* Calculated by Rayleigh.

α-range of ±0.2 centered at $\alpha = 2.6$, in excess of 5 % and increases beyond 20 % at α-values of less than 0.8 and more than 4.5. The use of the Rayleigh-Gans equation and of the equivalent Debye equation (37) must therefore be confined to the proper m-range and, in addition, to the proper α-range if useful data are to be obtained. A quantitative definition of these ranges will be given in a forthcoming paper.

SUMMARY

Specific turbidities were measured on 23 nearly monodisperse polystyrene and polyvinyltoluene latices containing rigid spherical particles. The uniform diameters varied systematically from 45 to 824 millimicrons. The particle diameters calculated from the turbidity data by means of the Mie theory agreed so well with electron microscopic diameters that the results can be regarded as a conclusive proof of the Mie theory. A precision apparatus and the general experimental technique are described which allow one to determine particle diameters with a precision of better than 0.33 %, which far exceeds the precision obtainable with the electron microscope. It is shown that the refractive index of the scattering spheres must be determined very exactly in order to obtain, in addition, highly accurate particle diameters. Evaluation of the turbidity data by means of the Rayleigh-Gans theory shows that it can give quantitatively significant particle diameters only for a very limited size range if the relative refractive index is near 1.2.

REFERENCES

1. A fairly representative review on the theoretical and experimental work done during this early period is given by R. Gans in "Handbuch der Experimentalphysik," Vol. 19, p. 346. Akademische Verlagsgesellschaft, Leipzig, 1928. Part of the more recent work in this field has been reviewed by G. Oster (*Chem. Revs.* **43,** 319 (1948)) as well as by P. Doty and J. T. Edsall (*Advances in Protein Chem.* **6,** 35 (1951)).
2. Various reports to the Office of Rubber Reserve from 1943 to 1946 by W. Heller and co-workers, University of Chicago. While the material in these reports remained unpublished, the results were instrumental for the formulation of the theory of the mechanism of emulsion polymerization as summarized by W. D. Harkins (*J. Am. Chem. Soc.* **69,** 1428 (1947)).
3. Various, partially unpublished reports to the Office of Rubber Reserve since 1943 by P. Debye and co-workers, Cornell University; *cf.* reference (9).
4. LAMER, V. K., AND SINCLAIR, D., Office of Scientific Research and Development, Reports No. 1668 and 1857 (1943); *cf. Chem. Revs.* **44,** 245 (1949).
5. ENGELHARD, H., AND FRIESS, H., *Kolloid-Z.* **81,** 129 (1937).
6. PARANJPE, G. R., NAIK, G. Y., AND VAIDYA, P. B., *Proc. Indian Acad. Sci.* **A9,** 333, 352 (1939).
7. RUEDY, R., *Can. J. Research* **A21,** 79, 99 (1943); *ibid.* **A22,** 53 (1944).
8. PUTZEYS, P., AND BROSTEAUX, J., *Trans. Faraday Soc.* **31,** 1314 (1935).
9. DEBYE, P., *J. Appl. Phys.* **15,** 338 (1944).

10. Doty, P., Zimm, B., and Mark, H., *J. Chem. Phys.* **12,** 144 (1944); *ibid.* **13,** 159 (1945); and later papers by Zimm and associates.
11. Lord Rayleigh, *Phil. Mag.* **12,** 81 (1881). Rayleigh had arrived at essentially the same results in an earlier treatment (*Phil. Mag.* **41,** 447 (1871)) not based on the electromagnetic theory.
12. Lord Rayleigh, *Proc. Roy. Soc.* (*London*) **84A,** 25 (1911); *ibid.* **90A,** 219 (1914).
13. Gans, R., *Ann. Physik* **76,** 29 (1925).
14. Debye, P., *Ann. Physik* **46,** 809 (1915).
15. Regarding the latter, widely used, but not published theory, see the reviews mentioned in reference (1).
16. Mie, G., *Ann. Physik* **25,** 377 (1908).
17. Van de Hulst, H. C., "The Optics of Spherical Particles." Duwaer & Sons, Amsterdam, Netherlands, 1946.
18. Hart, R. W., and Montroll, E. W., *J. Appl. Phys.* **22,** 376 (1951).
19. Smoluchowski, M., *Ann. Physik* **25,** 208 (1908).
20. Einstein, A., *Ann. Physik* **33,** 1275 (1910).
21. Raman, C. V., and Ramanathan, K. R., *Phil. Mag.* **45,** 213 (1923).
22. Gans, R., *Z. Physik* **17,** 371 (1923).
23. Blumer, H., *Z. Physik* **32,** 119 (1925); *ibid.* **38,** 304 (1926).
24. Shoulejkin, W., *Phil. Mag.* **48,** 307 (1924); *cf.* reference (5).
25. Tables of Scattering Functions for Spherical Particles, National Bureau of Standards, Washington, D. C., Government Printing Office, 1948.
26. Houghton, H., and Chalker, W., *J. Opt. Soc. Amer.* **39,** 955 (1945).
27. These Tables of scattering functions will be published in the near future by the Wayne University Press, Detroit, Michigan.
28. Pangonis, W. J., Dissertation, Wayne University, Detroit, 1952.
29. Gumprecht, R., and Sliepcevich, C., "Tables of Scattering Functions for Spherical Particles." Engineering Research Institute, University of Michigan, Ann Arbor, 1951.
30. Heller, W., and Quimfe, G., *J. Phys. Chem.* **46,** 765 (1942).
31. Herrington, K., Dissertation, Wayne University, Detroit, 1950.
32. Watson, J. H. L., and Grube, W. L., *J. Appl. Phys.* **23,** 793 (1952).
33. Heller, W., Epel, J. N., and Tabibian, R., *J. Chem. Phys.* **22,** 1777 (1954).
34. Heller, W., and Pugh, T. L., 128th Meeting of the American Chemical Society, Minneapolis, Minnesota, September, 1955.
35. The refractive index data given here differ slightly from preliminary ones used in an earlier publication (reference (33)). Details of the work by T. L. Pugh will be published in the near future.
36. Heller, W., and Pangonis, W., *J. Chem. Phys.* **22,** 948 (1954).
37. Doty, P., and Steiner, R. (*J. Chem. Phys.* **18,** 1211 (1950)) derived from the Debye theory a turbidity function which, because of the equivalence of this and the Rayleigh-Gans theory, is not needed. If evaluated, this function would furnish a curve identical with the dotted curve in Fig. 5.

JOURNAL OF COLLOID SCIENCE **11**, 214–225 (1956)

FREQUENCY AND TEMPERATURE DISPERSIONS OF HIGH POLYMERS

Shigeharu Onogi and Kyuzaburo Ui

Department of Textile Chemistry, Faculty of Engineering, Kyoto University, Kyoto, Japan

Received March 20, 1956

INTRODUCTION

The frequency and temperature dependences of viscoelasticity of high polymers are of practical as well as theoretical interest.

The relaxation spectra of amorphous and plasticized high polymers differ more or less from those of highly oriented crystalline polymers, such as cellulosic materials, particularly on the long-time side (1). The spectra of oriented crystalline polymers are very great, and little subject to the time scale, whereas those of typical amorphous polymers are small at long times and become greater with the shortening of the relaxation time from about 1 second, until they approach almost the same order of magnitude as those of oriented crystalline polymers at around 10^{-7} to 10^{-8} second. In this region, therefore, the elastic dispersion with respect to frequency can be observed on amorphous polymers (2).

Low temperatures produce the same state of affairs as high frequencies, changing amorphous polymers from the rubbery to the glassy state. Thus the dispersion with respect to temperature occurs in the vicinity of the glass temperature (3, 4).

Other high polymers show intermediate behaviors between these two extremes, and the relaxation time at which the maximum of the spectrum appears shifts to the long-time side to some extent in accordance with the nature of the polymer.

These two dispersions, "frequency dispersion" and "temperature dispersion," are quite similar to each other, suggesting that there exists some intimate relationship between them. The quantitative discussion of such relationships must be made on the basis of the experimental data obtained for a given material by varying extensively both the frequency and temperature, but the available data on this are very scanty at present.

This paper is concerned with the application of the recently proposed general law relating to the time scale and temperature for the viscoelastic behavior in amorphous polymeric systems. From the experimental curves of the dynamic response as a function of temperature at a given frequency, the response as a function of frequency at a specified temperature can be computed. This is done by making an assumption concerning the relaxation spectrum and thereby obtaining the "characteristic temperature" for the material.

This procedure has been tested by means of the data of the dynamic experiments on two types of polyvinylidene-vinyl chloride copolymer; it has also been tested with the published data on polyvinyl chloride-dimethyl thianthrene. Between the computed and the measured value good agreement is obtained in the former case, and excellent agreement in the second.

REDUCTION OF VARIABLE-TEMPERATURE DATA TO VARIABLE-FREQUENCY DATA

As mentioned by Ferry and Fitzgerald (5), the assumption that all relaxation times depend identically on temperature is supported by numerous data on various linear polymers. According to these authors, the customary exponential expression between the relaxation time and the absolute temperature with a constant activation energy is not valid, but the following algebraic one is fit to describe quite well the temperature dependence in various substances, such as a wide variety of polymers, polymer solutions, organic glass-forming liquids, and inorganic glasses (6, 7):

$$\log a_T = -c_1(T - T_s)/(c_2 + T - T_s), \qquad [1]$$

where a_T represents the ratio of any relaxation time at temperature T to its value at a reference temperature T_s, which is suitably chosen for each system and lies about 50°C. above the glass transition temperature; c_1 and c_2 are the universal constants and found to be 8.86 and 102.

Employing this, the relaxation time τ at temperature T can be given by

$$\log \tau = \log \tau_s - c_1(T - T_s)/(c_2 + T - T_s), \qquad [2]$$

where τ_s is the value of τ at T_s. When one uses any other reference temperature T_0 than the characteristic temperature T_s, τ must be given by the following equation in terms of T_0 and the corresponding relaxation time τ_0:

$$\log \tau = \log \tau_0 - c_1c_2(T - T_0)/(c_2 + T - T_s)(c_2 + T_0 - T_s). \qquad [3]$$

Accordingly, the real and imaginary parts of the complex dynamic modulus and some other dynamic properties measured in variable-temperature experiments at a given frequency ν_0 can be reduced to the variable-frequency data at a specified temperature T_0 by plotting them against the following "reduced frequency" ν:

$$\log \nu = \log \nu_0 - c_1c_2(T - T_0)/(c_2 + T - T_s)(c_2 + T_0 - T_s). \qquad [4]$$

In reverse, of course, the variable-frequency data can also be reduced to the variable-temperature data.

Moreover, in performing this reduction, it is possible to determine the distribution of relaxation times from the variable-temperature dynamic data as well as from the variable-frequency data.

Thus, for instance, the frequency dispersion can be predicted from the temperature dispersion, and so far as the above algebraic expression for the temperature dependence of τ is valid, the predicted dispersion should be the same as the actual one obtainable from variable-frequency experiments.

For practical performance of these reduction processes it is required that the characteristic temperature T_s be known. It can suitably be chosen from the shift factor a_T as a function of temperature, which can be determined from the experimental results of the frequency dependences of the complex dynamic modulus and some other viscoelastic properties at various temperatures. As will be shown later, T_s can also be determined from the experimental curves of the real and imaginary parts of the complex dynamic modulus as a function of temperature at a given frequency, though only approximate.

EXPERIMENTAL METHODS

The real and imaginary parts of the complex dynamic modulus, E' and E'', of two kinds of commercial polyvinylidene-vinyl chloride fiber of 250 deniers, one of which (*1*) contains only plasticizer while the other (*2*) contains plasticizer and pigment, were measured by means of the vibrating reed method at constant frequency (100 ± 2 cycles per second) and over a temperature range from $-20°$ to 80°C. In addition to this, the frequency dependence of E' of the fiber 1 was measured with the same method at various temperatures from -12 to 42°C. and over a frequency range from about 20 to 120 cycles per second. The details of the apparatus and measuring techniques have been described elsewhere (8–10), and the vibrator, in the present case, was set in the thermostat to perform the experiments at constant temperature.

The variable-frequency experiments at constant temperature were carried out quite independent of the experiments on variable-temperature described above, by employing four experimental methods according to the frequency range.[1] In the frequency range from about 0.2 to 10 cycles per second, the free damping oscillation method was employed; from 50 to 220 cycles per second, the stretch-vibrometer similar to that of Lyons (11); from 1 to 5 kc., the longitudinal-wave resonance, and in higher range, the longitudinal-wave transmission method originating from Nolle (12, 13) were

[1] These experiments were performed by courtesy of Assistant Professor H. Kawai of the Department.

used, respectively. The details of the apparatus and measuring techniques have also been described elsewhere (1).

RESULTS

The real and imaginary parts of the complex dynamic modulus, E' and E'', of the polyvinylidene-vinyl chloride fiber 1 and 2 obtained by the variable-temperature experiments are plotted against the reciprocal absolute temperature x $(=1/T)$ in Figs. 1 and 2, respectively. These results show typical temperature dispersions over the temperature range about −20 to 60°C., and the maximum values of E'' for these samples are found at 14.4 and 7.9°C., respectively.

Figure 3 shows the frequency dependence of E' of the fiber 1 at various temperatures. Shifting each curve in the figure along the abscissa by a suitable distance, which corresponds to log a_T, a composite curve referred

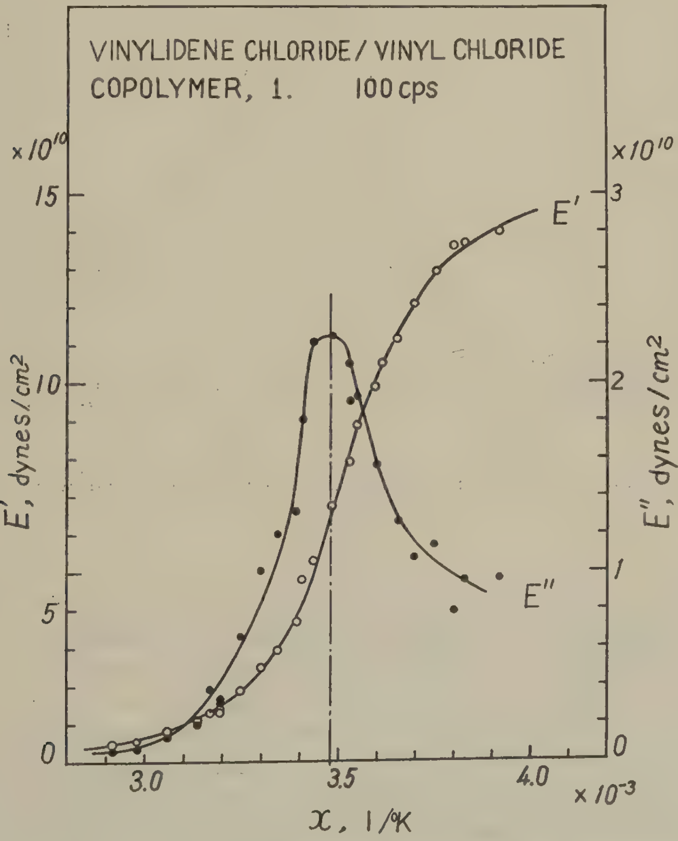

Fig. 1. E' and E'' vs. reciprocal absolute temperature for polyvinylidene-vinyl chloride fiber 1.

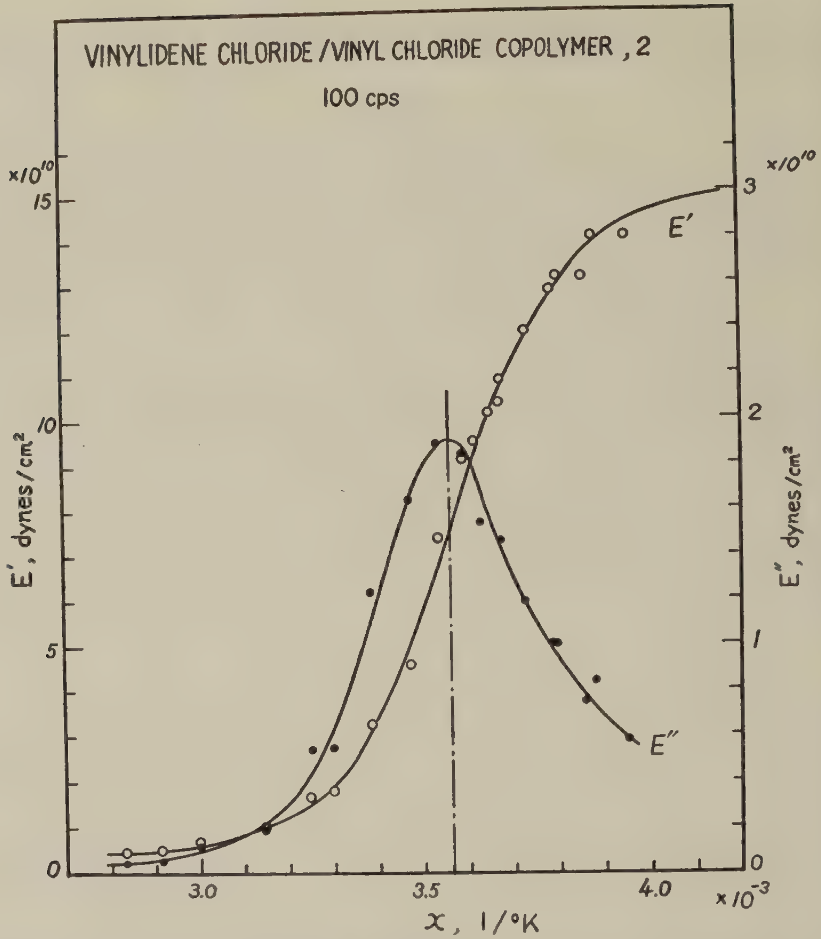

FIG. 2. E' and E'' vs. reciprocal absolute temperature for polyvinylidene-vinyl chloride fiber 2.

to a specified temperature can be obtained. Figure 4 shows such a composite curve referred to 23°C., and in Fig. 5 the evaluated values[2] of log a_T are plotted (with open circles) against temperature in contrast with those calculated from Eq. [1] with assuming $T_s = 312$ (solid circles and curve). Good agreement can be seen between them. The results of the variable-frequency experiments for the fiber 1 at 23.5°C. are dotted in Fig. 6. The values of E' and E'' disperse over the whole frequency range covered, and the maximum value of the latter appears at around 3 kc.

---

[2] The value for 3°C. is not certain but rather arbitrary.

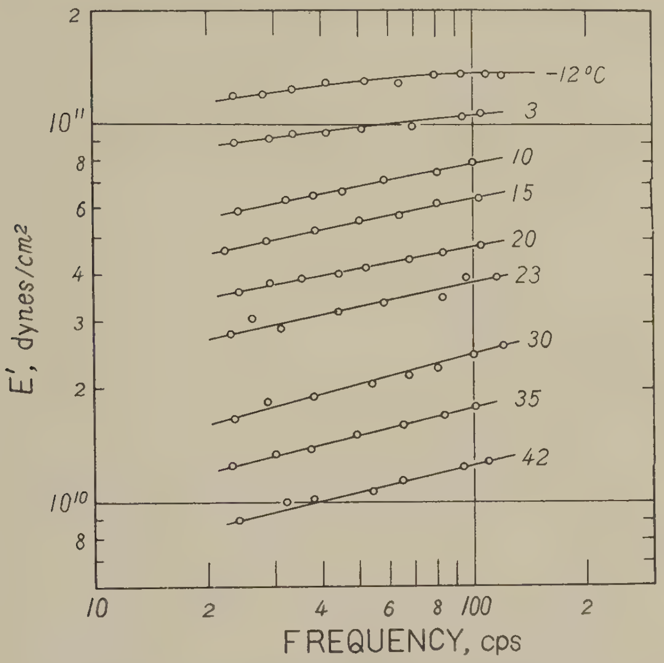

FIG. 3. Frequency dependence of E' for polyvinylidene-vinyl chloride fiber 1 at nine temperatures as indicated.

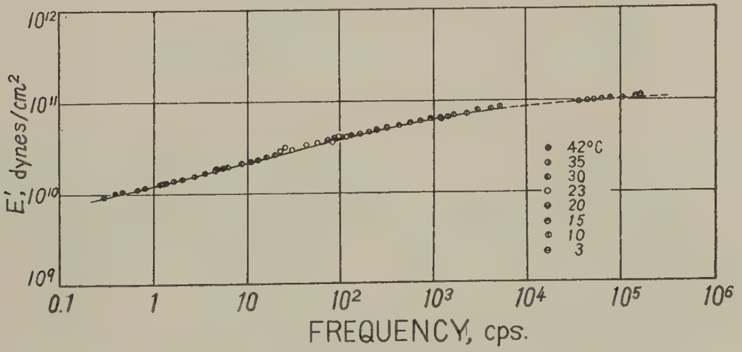

FIG. 4. Real part of the complex dynamic modulus reduced to 23°C., plotted against reduced frequency.

DISCUSSION

It is found at once from Figs. 1 and 6 that the maximum values of E'' of the polyvinylidene-vinyl chloride fiber 1 measured by the variable-frequency and variable-temperature experiments are quite equal. Moreover, it seems that the limiting values of E' at both sufficiently high frequency and low temperature are also equal. Such a special feature can also be found

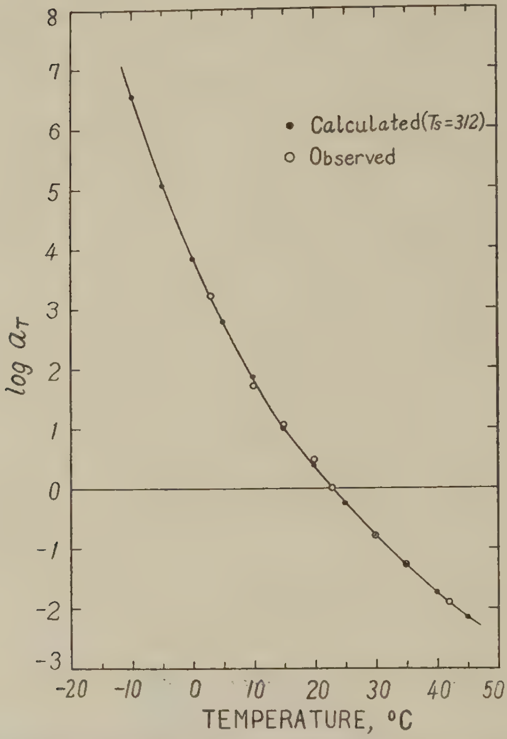

FIG. 5. Logarithm of reduction factor a_T plotted against temperature (open circles, observed; solid circles, calculated with T_s = 312).

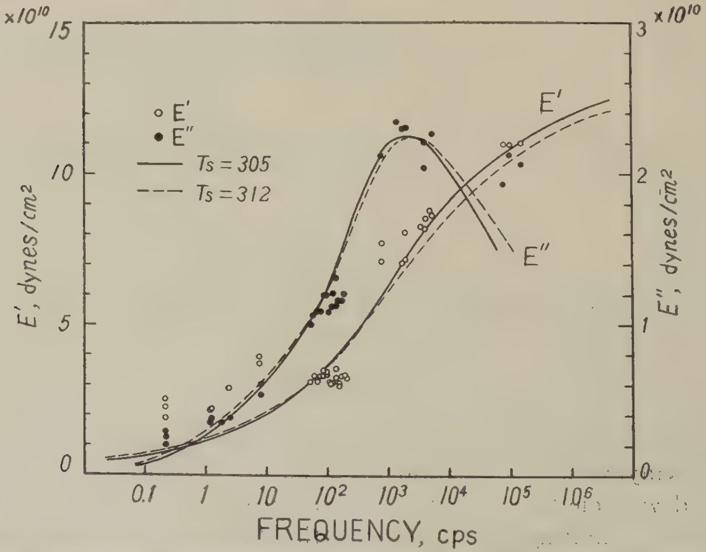

FIG. 6. Frequency dependences of E' and E'' for the polyvinylidene-vinyl chloride fiber 1 (dots: obtained from variable-frequency experiments; lines: reduced from the variable-temperature data in Fig. 1).

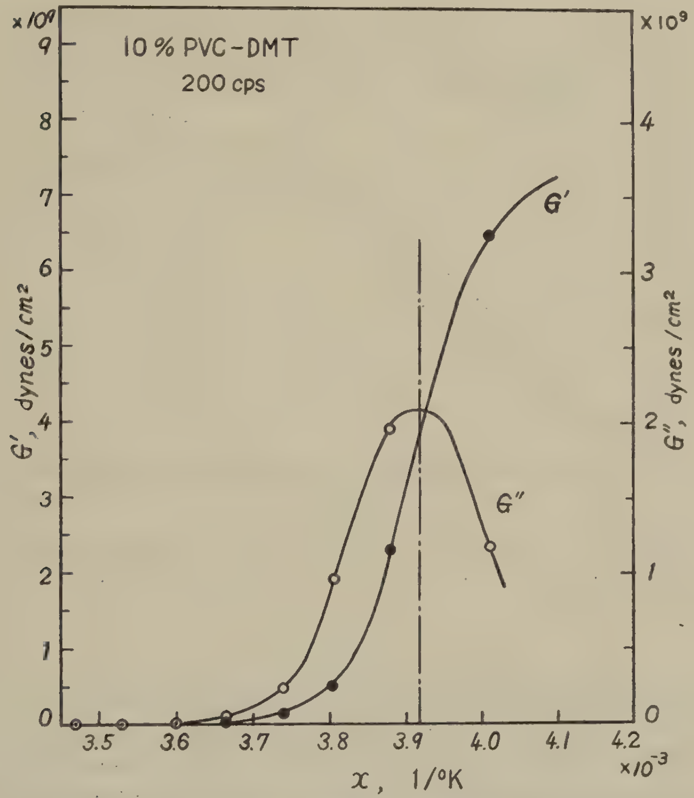

FIG. 7. G' and G'' vs. reciprocal absolute temperature for 10% PVC-DMT gel. (After E. R. Fitzgerald and J. D. Ferry).

in the dynamic data on the polyvinyl chloride-dimethyl thianthrene gel (10% PVC by volume) obtained by Fitzgerald and Ferry (14), who carried out dynamic measurements with the electromagnetic transducer method in the frequency range of about 30 to 5000 cycles per second and at −23.55 to 25.00°C. In Fig. 7, the real and imaginary parts of the complex dynamic shear modulus, G' and G'', at 200 cycles per second are plotted against x, and in Fig. 8, those measured by varying the frequency at −0.2°C. are dotted. The maximum values of G'' in these data are quite equal to each other.

So far as these substances are concerned, therefore, it seems proper to consider that the height of the relaxation spectrum in the frequency-dispersion region is independent of temperature. The only remarkable difference between both the dispersions is that the temperature dispersion takes place rather sharply over a comparatively narrow temperature range, whereas the frequency dispersion takes place gradually over an extensively wide range of frequency. And it is very significant to ascertain whether the two dispersions are reducible to each other according to Eq. [4] or not.

The two pairs of solid and dashed curves in Fig. 6 show the results of

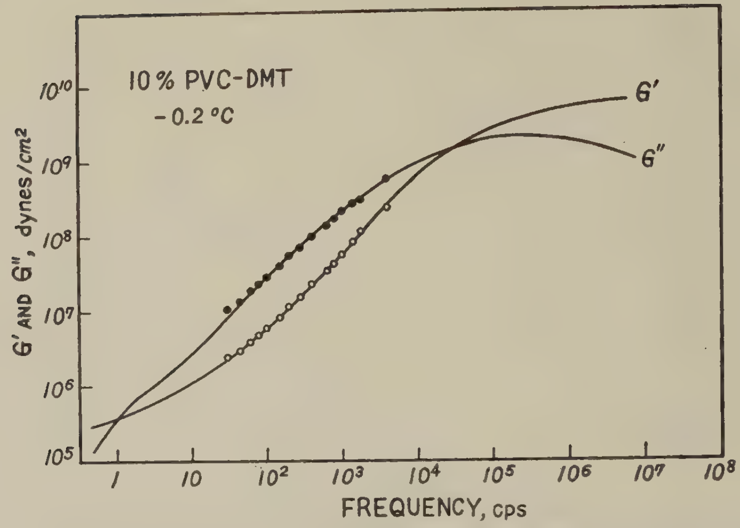

FIG. 8. Frequency dependences of G' and G'' for the 10% PVC-DMT gel (dots: obtained from variable-frequency experiments; lines: reduced from the variable-temperature data in Fig. 7).

reduction of the temperature dependences of E' and E'' for the polyvinylidene-vinyl chloride fiber 1 shown in Fig. 1 according to Eq. [4]. The reference frequency ν_0 in this case is 100 cycles per second, and the reference temperature T_0 is 296.5°K. The solid curves in the figure show the results of reduction with $T_s = 305$, which is calculated from Eq. [5] mentioned below with the assumption of a *wide* box distribution, while the dashed curves represent the results reduced with $T_s = 312$, which has been determined from a_T shown in Fig. 5. As mentioned above, the dots in the figure show the results of the variable-frequency experiments at 23.5°C. ($= T_0$).

The above value of T_s of 305 was calculated from the variable-temperature data according to the following equation:

$$T_s = c_2 - \frac{\sqrt{\dfrac{2.303 c_1 c_2 E_0}{m}} - 1}{x_m}. \qquad [5]$$

This can be derived by assuming for the complex dynamic modulus the box distribution of relaxation times and the above-mentioned temperature dependence of τ, namely, Eq [1]. Then, E' and E'' can be given as a function of temperature as follows:

$$E' = E_s + \frac{E_0}{2} \ln \frac{1 + \omega^2 \tau_{ms}^2 e^{2f(x)}}{1 + \omega^2 \tau_{ls}^2 e^{2f(x)}}, \qquad [6a]$$

$$E'' = E_0(\tan^{-1} \omega\tau_{ms} e^{f(x)} - \tan^{-1} \omega\tau_{ls} e^{f(x)}), \qquad [6b]$$

where E_s is the static modulus, E_0 is the height of the box distribution assumed, τ_{ls} and τ_{ms} are, respectively, the lower and the upper limits of the distribution at T_s, and $f(x)$ is given from Eq. [1] as follows:

$$\begin{aligned} f(x) &= -2.303c_1(T - T_s)/(c_2 + T - T_s) \\ &= -2.303c_1(1 - T_s x)/[1 + (c_2 - T_s)x]. \end{aligned} \tag{7}$$

E'' has a maximum value,

$$E''_{\max} = \frac{\pi}{2} E_0 \qquad (\tau_{ms} \gg \tau_{ls}), \tag{8}$$

at reciprocal temperature x_m which satisfies

$$e^{f(x_m)} = \omega^{-1}(\tau_{ms}\tau_{ls})^{-1/2}. \tag{9}$$

On the other hand, the slope of the tangent of the $E' - x$ curve at x_m, m, is given as

$$\begin{aligned} m &= E_0 f'(x) \qquad\qquad (\tau_{ms} \gg \tau_{ls}) \\ &= E_0 \Delta H_a(x_m)/R \\ &= 2.303\, c_1 c_2 E_0/[1 + (c_2 - T_s)x_m]^2, \end{aligned} \tag{10}$$

where R is the gas constant and $\Delta H_a(x)$ is the apparent activation energy for the relaxation processes. This results immediately into Eq. [5]. The above value of T_s of 305 is obtained by using

$$E_0 \left(= \frac{2}{\pi} E''_{\max} \right) = 1.43 \times 10^{10},$$

$$m = 3.47 \times 10^{14}, \qquad \text{and} \qquad x_m = 3.48 \times 10^{-3}.$$

Leaving the subject of the derivation of Eq. [5] and turning back to Fig. 6, it is to be noticed that both the solid and dashed curves agree fairly well with the variable-frequency data in the whole frequency range covered, with the exception of small difference in E' and E'' at the low and high frequency ends, respectively. The lower T_s, in general, the sharper the reduced curve becomes, and therefore the solid curve is sharper than the dashed one. But the difference is rather small and the former agrees with the measured values as well as the latter.

With the assumption of a single relaxation time instead of the above box distribution, one obtains Eq. [5] with m replaced by $2m$. In this case E_0 is given as $2E''_{\max}$, and T_s is found to be 284°K. This value is too small to yield good agreement. It appears that the sharper the relaxation spectrum, the smaller the calculated value of T_s is, and that the value of T_s calculated from Eq. [5] is always somewhat smaller than the true one, since the actual spectrum is always broader than the box distribution assumed. But it is much better to assume a box distribution than to assume a single relaxation time. Thus, we cannot expect the correct value of T_s from Eq. [5], but when we have the variable-temperature data alone and no available data concerning the shift factor a_T, Eq. [5] is very useful to calculate T_s and hence to reduce the data to the variable-frequency data.

The same state of affairs as mentioned above can be found in the case of PVC-DMT gel mentioned above. The value of T_s calculated from Eq. [5] is 288, whereas that reported in Ref. 6 is 293. Here again the calculated value is smaller by 5°, but the results of reduction do not differ so much.

The two curves in Fig. 8 show the results of reduction of the temperature dependences of G' and G'' shown in Fig. 7. The values T_0, T_s, and ν_0 in this case are, respectively, 272.8°K. (−0.2°C.), 293°K, and 200 cycles per second. Here again the dots in the figure show the values of G' and G'' measured actually at −0.2°C. by varying the frequency. They lie almost on the corresponding curves, showing that the frequency dispersion predicted from the temperature dispersion coincides quite well with the actual one, and that the above algebraic expressions for the temperature dependence of τ and for the reduced frequency are valid.

SUMMARY

The real and imaginary parts of the complex dynamic modulus of two kinds of commercial polyvinylidene-vinyl chloride fiber have been measured by means of several measuring methods at −20° to 80°C. over the frequency range 0.2 to 10^5 cycles per second. Both the variable-temperature and variable-frequency data show typical dispersions in the experimental ranges covered, being similar to each other.

By employing the algebraic expression for the temperature dependence of the relaxation time given by Ferry and his schools, the variable-temperature data can be reduced to the variable-frequency data, and vice versa. For polyvinylidene-vinyl chloride fiber and PVC-DMT gel, the frequency dispersion predicted from the temperature dispersion exhibits its agreement with the actual case.

ACKNOWLEDGMENTS

The authors wish to express their sincere gratitude to Professor M. Horio for his kind guidance and encouragement for their studies. They also wish to acknowledge their indebtedness to Assistant Professor H. Kawai of the Department for his experimental support, and to Professor J. D. Ferry of the Department of Chemistry, University of Wisconsin, for his helpful discussion. They are also indebted to the Research Institute for Synthetic Fibers, Japan, for financial support.

REFERENCES

1. FUJINO, K., KAWAI, H., AND HORINO, T., *Textile Research J.* **25**, 722 (1955).
2. See, for example, IVEY, D. G., MROWCA, B. A., AND GUTH, E., *J. Appl. Phys.* **20**, 486 (1949).

3. Nolle, A. W., *J. Polymer Sci.* **6,** 1 (1950).
4. Schmieder, K., and Wolf, K., *Kolloid-Z.* **127,** 65 (1952); *ibid.* **134,** 149 (1953).
5. Ferry, J. D., and Fitzgerald, E. R., *Proc. 2nd Intern. Congr. Rheology*, p. 144 (1954).
6. Williams, M. L., *J. Phys. Chem.* **59,** 95 (1955).
7. Williams, M. L., Landel, R. F., and Ferry, J. D., *J. Am. Chem. Soc.* **77,** 3701 (1955).
8. Horio, M., Onogi, S., Nakayama, C., and Yamamoto, K., *J. Appl. Phys.* **22,** 966 (1951).
9. Horio, M., and Onogi, S., *J. Appl. Phys.* **22,** 971 (1951).
10. Horio, M., and Onogi, S., *J. Appl. Phys.* **22,** 977 (1951).
11. Lyons, W. J., *Textile Research J.* **19,** 123 (1949).
12. Nolle, A. W., *J. Acoust. Soc. Amer.* **19,** 194 (1947).
13. Nolle, A. W., *J. Appl. Phys.* **19,** 753 (1948).
14. Fitzgerald, E. R., and Ferry, J. D., *J. Colloid Sci.* **8,** 1 (1953).

JOURNAL OF COLLOID SCIENCE 11, 226–236 (1956)

ON CONCENTRATED SOLUTIONS OF POLYELECTROLYTES. I. SPINNABILITY AND NON-NEWTONIAN VISCOSITY

Hiroshi Inagaki

Institute for Chemical Research, Kyoto University, Kyoto, Japan

Received September 14, 1955; revised January 17, 1956

INTRODUCTION

It is the purpose of the present study to correlate the characteristic structure of concentrated solutions of a linear polyelectrolyte with measurements of spinnability and non-Newtonian viscosity. Although a number of investigations have recently been made of polymers carrying electric charges, they have mainly been confined to dilute solutions and gels, with particular interest in clarifying the effects of charges on the shape and size of coiled molecules by means of the statistical treatment. Concentrated solutions of polyelectrolytes have attracted little attention, because it has been presumed that the electrolyte characteristics of polyelectrolytes would disappear in solutions of high concentration. In fact, the viscosity-concentration relations for such systems are similar to those for neutral polymers, and the anomalies characteristic of dilute polyelectrolyte solutions cannot be observed at high concentrations.

This does not imply, however, that concentrated solutions of polyelectrolytes are identical with those of neutral polymers. As a matter of fact, it has been found that the polyelectrolytic characteristics are still prominent even in highly concentrated solutions when such irreversible processes as viscoelastic behavior are investigated. For example, it is shown in this paper that an addition of caustic alkali to a concentrated solution of a polyelectrolyte results in a remarkable enhancement of the spinnability and a diminution of the dependence of viscosity upon shear-rate, while these effects are not observed in solutions of neutral polymers.

The "spinnability" of the solutions was measured by drawing up a rod from the surface of the solution at a given rate. The length of "liquid-thread" which could be drawn up in this way is called the "spinnability." This length may depend upon the degree of orientation of dissolved chain molecules in the direction of drawing and the interaction between the molecules.

The essential factors which characterize the behavior of polyelectrolytes in solution are the forces resulting from coulombic interactions. In concentrated solutions the interaction may be confined to intermolecular ones among polyions and would be such that the polyions be thereby arranged so as to make the overall interaction energy a minimum. This state we shall hereafter call the "structure" of the solution. The addition of an alkali to such a solution will make the electric double layer around the polyions denser and the interaction force diminish, thus "loosening" the structure of the solution. This will enhance the spinnability and reduce the shear-rate dependence of the viscosity. Demonstration of this behavior was attempted in this work using 2–7% aqueous solutions of sodium carboxymethyl cellulose containing various amounts of caustic soda.

Experimental

Material

Commercial sodium carboxymethyl cellulose of high viscosity was used in these experiments. Its molecular weight was estimated to be about 90,000 from measurements of the intrinsic viscosities in solutions containing various amounts of sodium chloride. Reference was made to data of Pals and Hermans (1) who had obtained relations between the intrinsic viscosity and the added NaCl concentration for several samples of sodium carboxymethyl cellulose of known molecular weights. The degree of substitution of the sample was determined to be 0.960 by means of conductometric titration; this was also checked by determination of the ash content.

In order to remove the inorganic salts contaminating the sample, the material was shaken with a mixture of one part of water and nine parts of methanol, allowed to stand for 10 hours at about 50°C., and then filtered through a fine filter. This procedure was repeated until the filtrate had become entirely free of the chloride ion, which was confirmed by the silver nitrate test. The purified material was dissolved in pure water or in caustic soda solutions of various concentrations. To effect the complete dissolution each solution was heated at a temperature somewhat lower than 60°C. for several days.

Measurement of Spinnability

An apparatus similar to that of Scherer (2) was constructed with several modifications. A glass rod immersed in a test solution is driven up at a constant rate by a mechanical device. As the rod is pulled up from the solution, it draws a liquid thread, which is attenuated towards the solution surface and eventually broken off when the rod reaches a certain height. The length of the liquid thread drawn up before the break occurs is here referred to as the "spinnability" of the given solution under given experimental conditions. An electric circuit comprising a triode vacuum tube and relays was devised so that the movement of the rod could be stopped automatically as soon as the circuit was opened by the break of an electrically

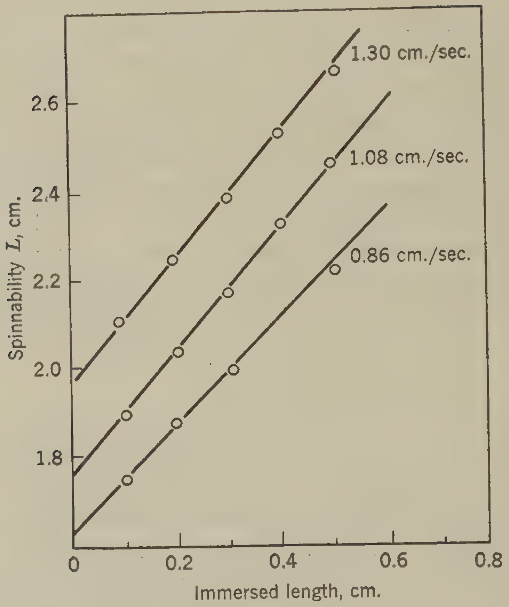

FIG. 1. Relations between spinnability and immersed length of rod at different rates of drawing.

conductive liquid thread. If the solution is not sufficiently viscous, the measured length of the liquid thread does not yield the correct measure of the spinnability (in the sense we are using in this paper), because in that case the effluence of the liquid over the rod also contributes to the length of liquid thread. In the present experiments, however, solutions of sufficiently high viscosity were used and the drawing was effected at comparatively high speeds in order to eliminate this source of error. Scherer used a gear system for driving the rod, while we substituted for it a vertically mounted piston-cylinder system (3). A piston falls down by its own weight in a vertical cylinder at a constant rate, expelling the air through a vent. The rate of falling of the piston can be controlled by varying the opening of this vent. The piston is connected by a flexible wire to the top of the rod. Thus the rod is pulled up smoothly as the piston falls down in the cylinder. This device proved to be very satisfactory since the liquid thread is so susceptible to the slightest vibration caused by the driving of gears.

The spinnability of a solution will depend upon the rate of drawing, and the radius and immersed length of the rod. Measurements showed that the spinnability at a given rate of drawing and a given rod radius varies linearly with the immersed length of the rod,[1] as illustrated in Fig. 1. The intrinsic spinnability, denoted by L_0, is then defined as the value of spinnability corresponding to zero immersed length of the rod. The relation between the rate of drawing and spinnability was found not to be linear, in contrast with Erbring's results (4). In the discussion which follows, spinnability values cited refer to those at zero immersed rod length, 1.1 cm./sec. drawing rate and 0.4 cm. rod radius. All the spinnability measurements were carried out at 25°C.

---

[1] As the immersion of the rod is deeper, a thicker thread of solution is drawn up. This results in the enhancement of spinnability.

Measurement of Structural Viscosity

A horizontal capillary viscometer similar to the Bingham viscometer (5) was used. Two large air reservoirs were connected to the viscometer and compressed air was applied to the solution at one end of the capillary. The viscometer and one of the air reservoirs were immersed in a thermostat to avoid fluctuations of the temperature and pressure. The capillary tube was made interchangeable so that desired shear rates may be obtained for solutions having different viscosities. Because in the case of highly viscous solutions a certain amount of the solution remains on the wall of the bulb of the viscometer, the actual efflux volume differs from the theoretical value. A special microburette was designed and used for determining actual efflux volumes.

Corrections for the kinetic energy of flow, surface tension, and Bingham's effect were omitted in this study, because numerical examination had proved that they were insignificant under conditions of the present experiments.

The viscosity, η^*, of a solution may be calculated as a function of shear rate S from data obtained with capillary viscometers, according to the equation (6):

$$\eta^* = Pa/2lS,$$

$$S = (1/\pi a^3)\,[3Q + P(dQ/dP)],$$

where a and l are the radius and length of the capillary, respectively, P is the applied pressure, and Q is the rate of flow. The shear rate, S, can be obtained graphically from the plot of Q *vs.* P according to the second equation. Viscosity measurements were also carried out at 25°C.

Figure 2 shows representative plots of η^* against S. Approximate linear relations are obtained when these are plotted on a log-log graph, as shown in Fig. 3. The slopes of these straight lines, that is, $-(d \log \eta^* / d \log S)$, were utilized as measures for the "strengths of structure" of respective solutions. It is of interest to note that this slope has a close relation with the spinnability, as demonstrated later.

In order to investigate the effect of temperature upon the viscosity and its dependence on shear rate, measurements were carried out at 20, 30, 40, and 50°C. for solutions of different alkalinities, that is, nil, 0.4, 2.00, and

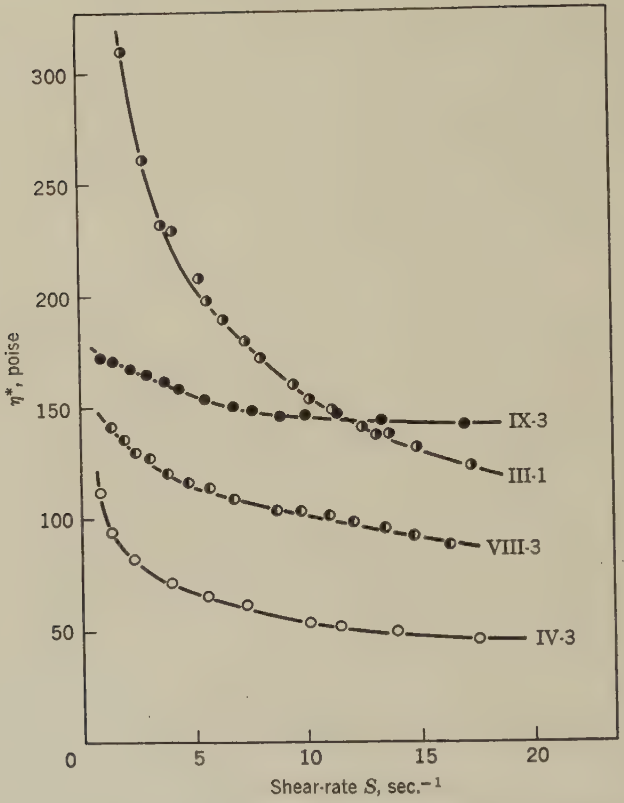

FIG. 2. Plots of viscosity *vs*. shear rate. Numbers attached to the curves correspond to the experiment numbers in Table I.

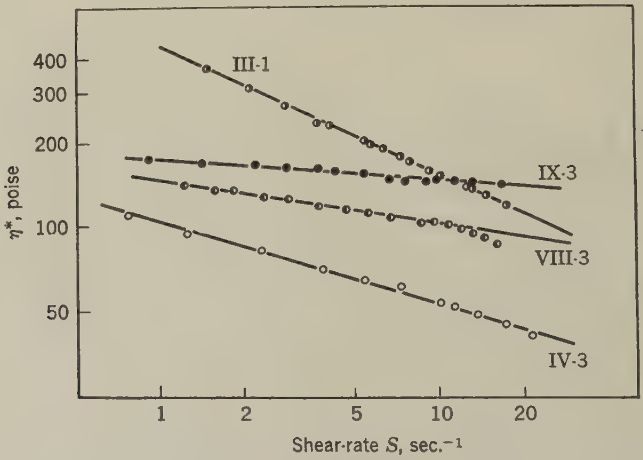

FIG. 3. Log-log plots of the viscosity curves shown in Fig. 2.

TABLE I

Concentration of caustic soda (*moles/liter*)	Experimental no.	Concentration of polymer C(*g/100 g.*)	Viscosity η_0 (*poise*)	$-(d \log \eta^*/d \log S)$	Spinnability L_0 (*cm.*)
Pure water	I-1	2.86	650	0.56	0.60
	I-2	1.70	422	0.53	0.57
0.0032	II-1	3.35	327	0.43	1.15
	II-2	3.06	265	0.42	1.10
	II-3	2.72	215	0.42	1.08
	II-4	2.58	180	0.39	1.11
0.0114	III-1	3.68	615	0.45	—
	III-2	2.01	(33)	0.40	—
0.096	IV-1	4.35	459	0.36	1.75
	IV-2	4.24	384	0.31	1.70
	IV-3	4.08	270	0.31	1.59
	IV-4	3.91	—	0.30	—
0.101	V-1	3.35	75	0.28	—
0.315	VI-1	5.57	240	0.21	2.52
	VI-2	4.79	120	0.21	2.47
	VI-3	4.58	111	0.23	—
0.768	VII-1	5.32	131	0.14	—
0.970	VIII-1	8.00	560	0.14	3.32
	VIII-2	6.27	248	0.17	3.25
	VIII-3	5.91	192	0.15	3.30
	VIII-4	5.74	141	0.13	3.10
1.650	IX-1	7.43	439	0.06	4.14
	IX-2	7.24	281	0.08	4.11
	IX-3	7.03	195	0.09	4.00
	IX-4	6.69	128	—	3.65

4.00%. In these measurements, a different sample of sodium carboxymethyl cellulose was used, which had a molecular weight almost equal to that of the former sample but had a degree of substitution of 0.540.

RESULTS

Effects of Alkali Added

Table I summarizes data obtained for spinnability and $-(d \log \eta^*/d \log S)$. In the fourth column of the table, viscosity values, η_0, obtained by the falling ball method are included. It is interesting to note from the table that the values of $-(d \log \eta^*/d \log S)$ are little affected by the polymer concentration and changed markedly with the amount of alkali added; the absolute value of $-(d \log \eta^*/d \log S)$ decreases rapidly with increasing alkalinity. Because the value of $-(d \log \eta^*/d \log S)$ is almost constant at a given alkalinity, independent of the polymer concentration, the average value was computed at each alkalinity. This is plotted against the amount of alkali added in Fig. 4. The numerical results are given in Table II. From Table I the value of intrinsic spinnability, L_0, corresponding to a

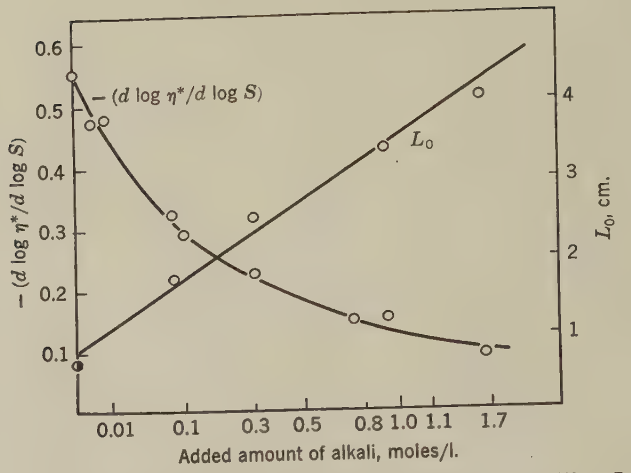

FIG. 4. Plots of $-(d \log \eta^*/d \log S)$ and of intrinsic spinnability L_0 *vs*. concentration of alkali added. The abscissa scale is the square root of alkali concentration.

TABLE II

Series no.	Alkalinity (*moles/liter*)	$-(d \log \eta^*/d \log S)$	L_0 at $\eta_0 = 300$
I	Pure water	0.55	0.6
II	0.0032	0.42	1.1
III	0.0114	0.43	—
IV	0.096	0.32	1.7
V	0.101	(0.28)	—
VI	0.315	0.22	2.5
VII	0.768	(0.14)	—
VIII	0.970	0.15	3.3
IX	1.650	0.08	4.0

TABLE III

Temp., °C.	$-(d \log \eta^*/d \log S)$			
	Exp. No.			
	1	2	3	4
20.0	0.36	0.32	0.16	0.08
30.0	0.35	0.32	0.16	0.08
40.0	0.36	0.32	0.15	0.08
50.0	0.32	0.32	0.16	0.08
Polymer conc., (*g./100g.*)	3.00	3.54	5.00	6.01
Alkalinity (*moles/liter*)	Nil	0.10	0.50	1.00

falling ball viscosity value (η_0) of 300 poises, was determined at each alkalinity. The results are recorded in Table II and plotted graphically in Fig. 4. It is seen from this figure that the intrinsic spinnability so defined increases almost linearly with the square root of the alkali concentration.

Temperature Dependence of $-(d \log \eta^*/d \log S)$

It was found that viscosities for the solutions investigated decreased with increasing temperature, describing curves almost parallel with each other, while the values of $-(d \log \eta^*/d \log S)$ remained constant independent of temperature at a given alkalinity. The numerical results appear in Table III. It can be seen from the table that the only factor which influences the slope of the log η^* *vs.* log S plot is the concentration of caustic soda added.

DISCUSSION

Solutions of polyelectrolytes even as dilute as 1–2% concentrations exist in a state which may be defined as a gel rather than a fluid, while solutions of neutral polymers at corresponding concentrations behave like a fluid in the sense of high polymer chemistry. When an alkali is added, the gel-like mass of a polyelectrolyte solution tends to behave like an ordinary viscous fluid. This fact indicates that the structure of aqueous solutions of polyelectrolytes is greatly modified by the presence of simple electrolytes. Busse (7) has suggested that such a gel-like state of aqueous polyelectrolyte solutions should be attributed to the electrostatic interaction between the double layers covering the colloidal particles. In the concentrated poly-

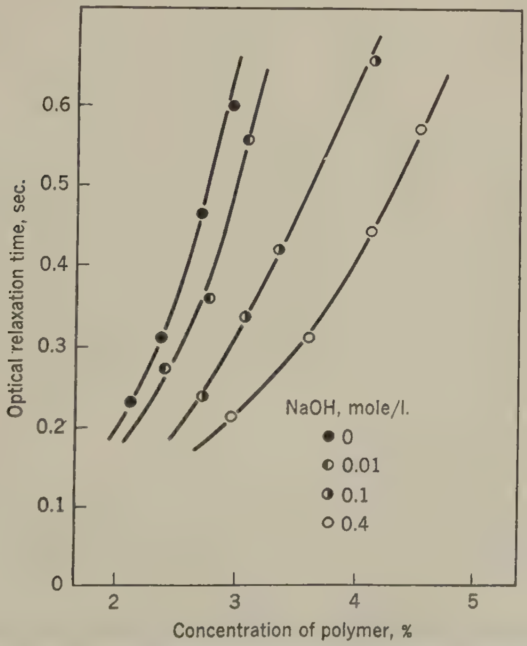

FIG. 5. Plots of relaxation time of streaming birefringence *vs.* polymer concentration at a certain shear rate (30.0 sec.$^{-1}$).

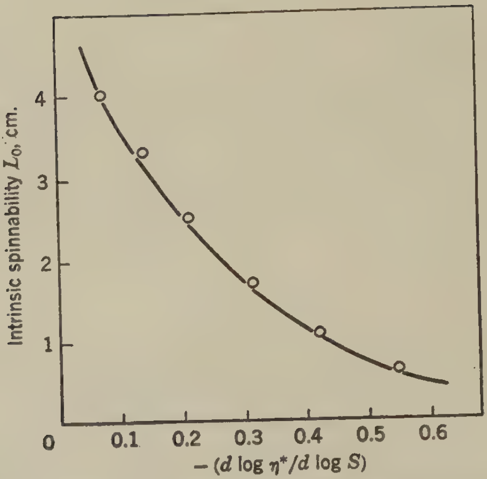

FIG. 6. **Relation between intrinsic spinnability and** $-(d \log \eta^*/d \log S)$.

electrolyte solutions studied in the present work, the interaction between the polyions is dominant, and the intramolecular interaction may be disregarded, because of the close packing of the polyions in solution.

The structure of the solution considered here is such that the overall electrostatic energy resulting from the intermolecular interaction between polyions is at its minimum. Such a structure of polyelectrolyte solutions is, therefore, distinguished from the network structure as produced by entanglement of neutral polymer chains in solution. Its "strength" will be controlled by the thickness of the double layer around the polyions. The double layer in concentrated polyelectrolyte solutions, although quite dense even in pure water solutions, can be condensed further by the addition of simple electrolytes. This causes the structure of the solution to "loosen" and makes it easy for polyions to translate or orient in response to an external force applied to the system. The spinnability should then be increased, because it is associated with the ease with which polymer chains are oriented in the direction of drawing, as discussed by Nitschmann and Schrade (8). The results given in Fig. 4 and those of Nakagawa (9) confirm this interpretation.

A support for the idea presented above for the structure of concentrated polyelectrolyte solutions may be obtained from measurements on streaming birefringence. The relaxation time of streaming birefringence is a measure of the rotary diffusivity of macromolecules, which, in the case of concentrated solution, depends mainly on the intermolecular interactions involved. According to the work made by Joly (10), the relaxation time is expected to decrease with decrease in the intermolecular interaction, which provides, in the present case, a measure for the strength of the structure of the solution. Experiment on streaming birefringence is now being in progress in this institute for almost the same system as investigated in this work; the relaxation time is measured using an apparatus similar to that of Conner and Donnelly (11). (The details of this experiment will be described in a forthcoming publication.) Some of the results so far obtained are given in Fig. 5. It can be seen from the figure that the relaxation time at a certain shear rate (30.0 sec.^{-1}) and concentration increases with decreasing added alkali concentration and shows magnitudes of order of 10^{-1} sec., which are larger than those obtainable in dilute polyelectrolyte solutions. This may support the idea proposed in the above and, furthermore, suggests that the intramolecular interaction in a polyion has almost disappeared in comparison with the intermolecular one at as high concentrations as studied here.

The temperature dependence of $-(d \log \eta^*/d \log S)$ as found here with solutions of carboxymethyl cellulose seems to be of a peculiar nature, in contrast with the case of neutral polymer solutions. It is expected that increasing the temperature would promote the thermal motion of polymer molecules and, therefore, make the structure of solution less firm. If so, the absolute value of $-(d \log \eta^*/d \log S)$ would decrease with increasing temperature. The fact that carboxymethyl cellulose solutions do not follow this prediction suggests that the structure produced by the electrostatic interaction is of a different nature than brought about by molecular entanglement of polymer chains.

The relation between the spinnability and the quantity $-(d \log \eta^*/d \log S)$ is shown graphically in Fig. 6. This type of relation may be of general interest from the rheological point of view, because it is supposed that spinnability of a solution may closely be correlated with non-Newtonian behavior of its viscosity, irrespective of what sort of intermolecular interactions produce the structure of the solution. If so, study of this relation will afford information about the state of entanglement between neutral polymer chains in concentrated solutions. In future, such data may play an important role in investigating qualities of spinning dopes used in textile industries.

ACKNOWLEDGMENTS

The author wishes to thank Professor M. Horio and Dr. H. Fujita for reading the manuscript, and members of the "Research Group on High Polymers, Kyoto University" for interesting discussions. He also wishes to record his thanks for the valuable assistance of Messrs. K. Kiyohara and S. Sakurai, and for the financial support from the Research Institute for Synthetic Fibers, Japan.

SUMMARY

The spinnability and non-Newtonian viscosity of concentrated solutions of sodium carboxymethyl cellulose (concentration 2–7%) were measured

over a range of concentration of caustic soda added. The plots of log η^* (η^* is viscosity) *vs.* log S (S is shear rate) were linear for all cases investigated. Their slopes, that is, $-(d \log \eta^*/d \log S)$, were used for characterizing the strength of structure of the solution under shear. It was found that the spinnability is increased, while the slope, $-(d \log \eta^*/d \log S)$, is decreased, with increasing alkalinity of the solution. In order to interpret these results, it was assumed that there is a certain order of polyions in solution in which the overall interaction energy is at its minimum. In other words, the existence of a certain type of structure was presumed in concentrated polyelectrolyte solutions. The decrease in $-(d \log \eta^*/d \log S)$ was then shown to be attributed to the "loosening" of the "structure." It was also shown, based on this assumption, that the less tight the structure of solution the greater the spinnability is. This is in line with the prediction that the orientation of chain molecules in the direction of drawing is made easy as the structure of solution is loosened. The addition of an alkali results in making the double layer around the polyion denser, and thus the structure of solution less tight owing to the decrease in electrostatic interaction between polyions. This consequence, when combined with the above-mentioned, explains qualitatively the behavior found experimentally. It is important to note through these considerations that the electrolyte behavior of polyelectrolyte solutions is still conspicuous even at high concentrations. The quantity, $-(d \log \eta^*/d \log S)$, for a given solution was almost independent of the temperature over the range studied.

REFERENCES

1. PALS, D. T. F., AND HERMANS, J. J., *Rec. trav. chim.* **71,** 433 (1952).
2. SCHERER, P. C., *Rayon Textile Monthly* **26,** 67 (1945).
3. NAKAGAWA, T., *Bull. Chem. Soc. Japan* **25,** 88 (1952); INAGAKI, H., *Bull. Research Inst. Synthetic Fibers, Japan* **11,** 144 (1954).
4. ERBRING, H., *Kolloid-Beih.* **44,** 171 (1936).
5. BARR, G., "A Monograph of Viscometry," p. 53. Oxford University Press, 1936.
6. CLARK, O., AND DEUTSCH, M., *J. Appl. Phys.* **21,** 713 (1950).
7. BUSSE, W. F., *J. Phys. Chem.* **36,** 2862 (1932).
8. NITSCHMANN, NS., AND SCHRADE, J., *Helv. Chim. Acta* **31,** 312 (1948).
9. NAKAGAWA, T., *Bull. Chem. Soc. Japan* **25,** 93 (1952).
10. JOLY, M., *Kolloid-Z.* **126,** 77 (1952).
11. CONNER, W. P., AND DONNELLY, P. I., *Ind. Eng. Chem.* **43,** 1136 (1951).

JOURNAL OF COLLOID SCIENCE **11**, 237–239 (1956)

THE REINFORCEMENT OF RUBBER BY CARBON BLACK. A STUDY OF THE COHESION BETWEEN THE PARTICLES OF FILLER

R. S. Bradley

Department of Inorganic and Structural Chemistry, University of Leeds, England

Received September 1, 1955

ABSTRACT

The force of cohesion between carbon particles in filled rubber has been calculated on the basis of London forces, and has been shown to be inadequate to explain the high tensile strength of filled rubber.

In spite of the immense amount of labor devoted to the problem, the action of carbon black in reinforcing rubber remains obscure. Rival theories may be divided into the so-called physical and chemical. In the latter some kind of cross-linking between rubber molecular via carbon particles is imagined to occur. Even if this is true, however, there will always be present, in addition, the physical interaction due to London forces. So far as the writer is aware, no calculation has been published of the magnitude of this physical interaction. It is the purpose of this paper to make a reasonable numerical estimate of the cohesion in rubber due to carbon black, and by comparing with experimental values to decide whether in fact the reinforcement is mainly physical in origin.

For simplicity the tensile strength has been chosen as a criterion of reinforcement, since it is comparatively easy to calculate the force required to separate the carbon particles and since the abrasive action on rubber tires during wear does involve the pulling apart of the material. It is realized, however, that no one physical property can give an unequivocal estimate of the reinforcement.

The writer's interest in the subject began with a theoretical and experimental study of cohesion between spheres (1) in which it was shown that the force of attraction between two spheres of radii r_1, r_2 containing q attracting molecules per cm.^{3} is given by

$$\text{Force} = \frac{\pi^2 q^2 \lambda}{36} \frac{r_1 r_2}{r_1 + r_2} \frac{1}{d^2}, \qquad [1]$$

where d is the shortest distance between the surfaces of the spheres and the law of force between molecules whose centers are distant r cm. apart is given by: force of attraction $= \lambda/r^7$ i.e., the London type of force. Equation [1] holds only if $d \ll r_1$ and r_2. Later work by Hamaker (2) gave for the *energy* between two equal spheres of radius r for any value of d and for London forces

$$\text{Energy} = \frac{\pi^2 q^2 \lambda}{72} \left(\frac{1}{x^2 + 2x} + \frac{1}{x^2 + 2x + 1} + 2 \ln \frac{x^2 + 2x}{x^2 + 2x + 1} \right) \qquad [2]$$

where $x = d/(2r)$. (This result has been rewritten to be consistent with Eq. [1], since Hamaker takes the force to be $6\ \lambda'/r^7$ and the energy λ'/r^6.) The force between a sphere and a bulk solid with a plane surface distant d from the spherical surface, at right angles to the surface along a line through the center of the sphere, is $\pi^2 q^2 \lambda r/(36d^2)$.

It is clear from these results that the force of attraction between spheres decays rapidly with the distance between them, and little error will be introduced if the calculation is confined, as a first approximation, to nearest neighbors. The particles of carbon in filled rubber appear approximately spherical, and it will be assumed that they are all of equal radius, and in the same spatial relation as close packed spheres. We may then calculate the distance between the spherical surfaces, along the line of centers, if the density of the filled rubber is known. For the latter additivity of volumes is assumed, taking a value 2 g.cm.$^{-3}$ for the density of carbon black particles.

For the estimation of λ the Slater-Kirkwood (3) method is most convenient. The structure of carbon black appears to be distorted graphitic, and it may be assumed to be sufficiently accurate that the average polarizibility per carbon atom is the same as in graphite. This gives an estimate of $\lambda = 1.1 \times 10^{-58}$ dyne cm.^{7}, based on bond refractivities, for carbon atom interactions.

From the number of particles per cm.^{2} on either side of a section made in filled rubber the contribution of the carbon to the force per cm.^{2} required to pull the section apart can be calculated from Eq. [1], with the results recorded in Table I. In this calculation no allowance has been made for the fact that carbon black spheres (*a*) displace rubber, causing a reduction in the rubber-rubber interaction, and (*b*) interact with the rubber on the opposite side of the section which is pulled apart. The natural tensile strength of rubber, especially artificial rubber, may be assumed to be small

TABLE I

Contribution to Tensile Strength of Force between C Particles

% by wt. of filler	Radius of C particle, *cm.*	Contribution to tensile strength, *dynes cm.*$^{-2}$
50	1.8×10^{-6}	2.3×10^4
80	1.8×10^{-6}	2.1×10^6
50	10^{-6}	1.3×10^5
80	10^{-6}	1.2×10^7

compared with that of graphite, and these contributions will not affect the order of magnitude of the results above. It is clear from Table I that even at the high loading of 80 wt. % the increase in tensile strength is far below that found experimentally, e.g., G.R.S. loaded with 50% carbon has a tensile strength of the order of 10^8 dynes cm.^{-2} (4).

The conclusion is that physical forces are not responsible for the great increase in tensile strength of GRS and other artificial rubbers when filled with carbon black. It should be noted, however, that the same cannot be said without further examination for the effect on the modulus, which is unfortunately a much more difficult problem.

My thanks are due to Mr. Merton Studebaker, of the Phillips Chemical Co., for his interest in this work and for many stimulating discussions.

References

1. Bradley, R. S., *Phil. Mag.* **13,** 853 (1932).
2. Hamaker, H. C., *Physica* **4,** 1058 (1937).
3. Slater, J. C., and Kirkwood, J. G., *Phys. Rev.* **37,** 683 (1931); de Boer, J., *Trans. Faraday Soc.* **32,** 10 (1936).
4. Parkinson, D., *Brit. J. Appl. Phys.* **2,** 273 (1951).

JOURNAL OF COLLOID SCIENCE **11**, 240–243 (1956)

STUDIES ON THE RHEOLOGICAL PROPERTIES OF HUMIC ACID FROM COAL

P. N. Mukherjee and A. Lahiri

Fuel Research Institute, Jealgora, India

Received January 23, 1956

ABSTRACT

The viscosity of the alkali salts of humic acids has been measured at different dilutions, both in aqueous and salt solutions. From the abnormal viscosity (η_{sp}/C)-concentration relationship obtained for these systems, it is concluded that they can be considered as polyelectrolytes.

INTRODUCTION

The constitution of humic acids is intimately linked with the constitution of coal, since these acids represent a very important intermediate stage in the process of coalification from vegetable matter (1). The constitution of humic acids has been a subject of investigation for a long time. Although the chemical properties of these complex acids are fairly well known (2) and the functional groups present in the acids, e.g., —COOH, phenolic —OH, C═O, and —O·CH_3 have been identified, the number of rings present in the acids and the points of attachment of these reactive groups in the molecules have not yet been established. In the present investigation, the character and behavior of the alkali salts of humic acids have been studied by measurement of viscosity in aqueous and salt solutions.

EXPERIMENTAL

Humic acids were prepared by aerial oxidation of a sample of low rank coal (Jambad-Bowla Seam, Raniganj Coalfield) at 200°C. for 200 hours in an air oven. The humic acids, thus formed, were extracted by digestion of the oxidized coal with (N) NaOH solutions, followed by precipitation of the acids by addition of hydrochloric acid. The acids thus isolated were dialyzed to remove the last traces of mineral impurities. For the preparation of the alkali salts, the pure humic acids were treated with a stoichiometric proportion of NaOH and the sodium salt was precipitated from solution by addition of an excess of absolute alcohol. The salts were washed free of alkalis by 90% alcohol and finally dried *in vacuo* at 50°C.

The viscosity measurements of the sodium salts of humic acids were

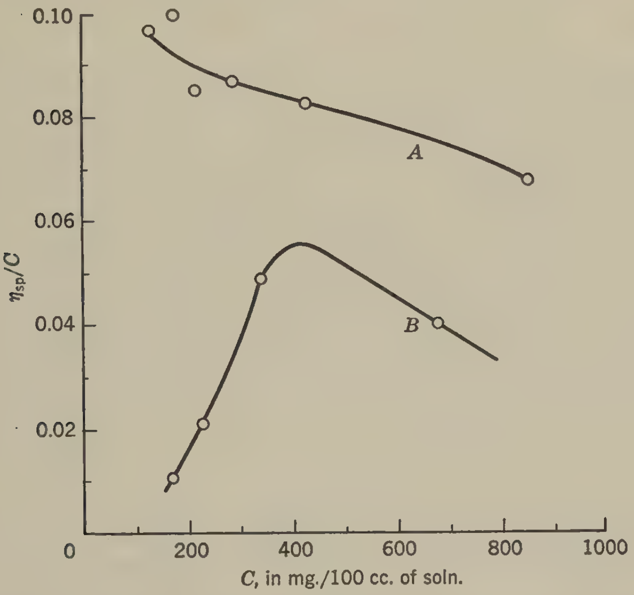

FIG. 1. Change of reduced viscosity of sodium humate. Curve *A*: Water solution. Curve *B*: Sodium chloride solution.

carried out with an Ostwald viscometer having a flow time of 170 sec. with distilled water at 35.13°C. ± 0.02°C.

RESULTS

The viscometric measurements of the solution of sodium humates in water were made at different dilutions at 35.13°C. ± 0.02°C. and the calculated values of reduced viscosity (η_{sp}/C, where $\eta_{sp} = \eta/\eta_0 - 1$; η and η_0 being the viscosity of the solution and solvent, respectively) are presented in curve *A*, Fig. 1. The measurement of the viscosity of solutions at different concentrations of sodium humate was done at a constant sodium chloride concentration (20.78×10^{-3} g.eq./l.) and the results are represented in curve *B*, Fig. 1.

DISCUSSION

It is evident from curve *A* that the reduced viscosity rises rapidly with diminishing concentration of sodium humate—a property characteristic of polyelectrolytes. For a neutral polymer, the reduced viscosity varies linearly with dilution in the dilute region and the curve gives a positive slope with the *C* axis. For a polyelectrolyte (3) (i.e., a high molecular weight substance which behaves simultaneously as an electrolyte containing a number of ionizable groups along the polymer chain), however, the reduced viscosity rises rapidly with dilution. The latter type of behavior has been observed in case of a number of substances by different workers (3–7).

According to Fuoss (3) the difference in behavior between the two classes of polymers may be explained in the following way. For a neutral polymer, the chain is coiled up in solution and the extent of coiling is not appreciably affected by dilution, in the very dilute region. For a polyelectrolyte, on the other hand, at high dilution almost all the ionizable groups will be dissociated and the chain will be left fully charged electrically. Under these conditions, the repulsion between similarly charged groups in the chain will be a maximum and the chain will assume a fully extended condition with maximum separation between similarly charged centers. At lower dilutions, the degree of dissociation of the ionizable groups will be smaller and as a consequence the chain will be only partially extended. Hence, it follows that with progressive dilution the chain will be gradually extended. The rise in reduced viscosity with dilution in the case of a polyelectrolyte can thus be explained. In the case of simple electrolytes, the positive and negative charges are capable of independent movement in solution and hence the possibility of an abnormal viscosity relationship does not arise.

The interesting viscosity relationships observed in the case of sodium humate may therefore be attributed to the increased intramolecular coulombic repulsion with increased electrolytic dissociation brought about by dilution.

The relationship between the reduced viscosity and different dilutions of sodium-humate solution, at constant sodium chloride concentration, as shown in curve *B*, is significant. The curve shows a well-defined maximum at a concentration of sodium humate where the ionic concentration of sodium from sodium-humate is nearly equal to that from sodium chloride. At lower sodium-humate concentration, the curve shows the behavior of a neutral polymer whereas at higher sodium-humate concentration, it shows the typical behavior of a polyelectrolyte.

According to Fuoss (3, 4) this marked effect of the simple electrolyte on the reduced viscosity of polyelectrolytes may be explained in terms of the mass-action effect. Increase in concentration of positive ions in solution will decrease the degree of dissociation of the ions from Na-humate. This will therefore cause a reduction in the intramolecular coulombic repulsion in the polymer chain and thus favor the coiling up of the chain. This will happen when the sodium ion concentration from sodium chloride is greater than that from sodium-humate. Under these conditions, almost all the ionizable groups in sodium-humate will remain undissociated and the molecules will remain in the coiled-up state. This explains the behavior of sodium humate solutions at higher dilutions. At concentrations where the sodium ion concentration from sodium-humate is higher than that from NaCl, there will be a partial dissociation of Na-humate, with the result that the molecules will be stretched to a certain extent. At this stage it will simulate the behavior of typical polyelectrolytes.

Whether the above explanations are applicable to the system of sodium humate solution is a matter for further consideration. The difficulty arises from the fact that humic acids and their salts cannot be regarded as high polymers as their molecular weights lie in the range from 300 to 1200. One explanation is that although the molecular weights of humic acids as measured by different methods (8) indicate a comparatively lower value, in solution a large number of units may be linked together by hydrogen bonding or some similar mechanism, thereby forming a polymer chain-like structure. Another possibility is that the molecular weights of humic acids, as reported in the literature, may not represent the true values. In some cases, molecular weights of a much higher order (2350–26000) have also been reported (9).

REFERENCES

1. WAKSMAN, S. A., "Humus," pp. 261–288. Williams & Wilkins, Baltimore, 1938.
2. WAKSMAN, S. A., "Humus," pp. 22–64. Williams & Wilkins, Baltimore, 1938.
3. FUOSS, R. M., AND STRAUSS, U. P., *J. Polymer Sci.* **3,** 246, 602 (1948).
4. FUOSS, R. M., AND CATHERS, G. I., *J. Polymer Sci.* **4,** 97, 121 (1949).
5. PALS, D. T. F., AND HERMAN, J. J., *J. Polymer Sci.* **3,** 879 (1948).
6. BALAZS, E. A., AND LAURENT, T. C., *J. Polymer Sci.* **6,** 665 (1951).
7. BASU, S., AND DAS GUPTA, P. C., *J. Colloid Sci.* **7,** 53 (1952).
8. LOWRY, H. H., "Chemistry of Coal Utilization," Vol. 1, pp. 352–353. Wiley, New York, 1945.
9. KING, J. G., "Fuels, Solid, Liquid & Gaseous," p. 73. Edward Arnold, London, 1953.

JOURNAL OF COLLOID SCIENCE **11**, 244–249 (1956)

KINETICS OF POLYMERIZATION OF METHYLMETHACRYLATE INITIATED BY THE SYSTEM BENZOYL PEROXIDE-DIMETHYLANILINE

K. F. O'Driscoll and A. V. Tobolsky

The Frick Chemical Laboratory, Princeton University, Princeton, New Jersey

Received January 17, 1956

ABSTRACT

The rates of polymerization and the degrees of polymerization produced in methylmethacrylate by the initiator-activator system benzoyl peroxide-dimethylaniline were studied at low temperatures. The initiation of polymer chains appears to result from a bimolecular reaction between amine and peroxide, since the temperatures used were below those at which benzoyl peroxide alone would appreciably initiate polymerization. The activation energy for initiation is calculated to be 12.8 kcal.

INTRODUCTION

For the polymerization of styrene initiated by the system benzoyl peroxide-dimethylaniline, the following relation obtains at low temperatures (1)

$$R_p = C([Bz_2O_2][DMA])^{0.5} \qquad [1]$$

where R_p is the *initial* rate of polymerization in moles per liter per second, [M], $[Bz_2O_2]$, and [DMA] are the concentrations of monomer, benzoyl peroxide, and dimethylaniline in moles per liter, and C is a function of temperature alone.

Recently, Imoto *et al.* (2) have shown that, for methylmethacrylate polymerization initiated by the system benzoyl peroxide-dimethylaniline at 30° C., the observed rate of polymerization may be expressed as the sum of two rates

$$R_p = C_1[Bz_2O_2]^{0.5} + C_2([Bz_2O_2][DMA])^{0.5}. \qquad [2]$$

This is, however, an approximation which is valid only for polymerizations carried out at sufficiently low temperatures so that the contribution of the benzoyl peroxide alone is small compared to that of the benzoyl peroxide-dimethylaniline system. In actuality, the rates of *initiation* are additive, and, since the rate of initiation is proportional to the square of the rate of polymerization, a more exact expression would be

$$R_p^2 = C_1^2[Bz_2O_2] + C_2^2[Bz_2O_2][DMA]. \qquad [3]$$

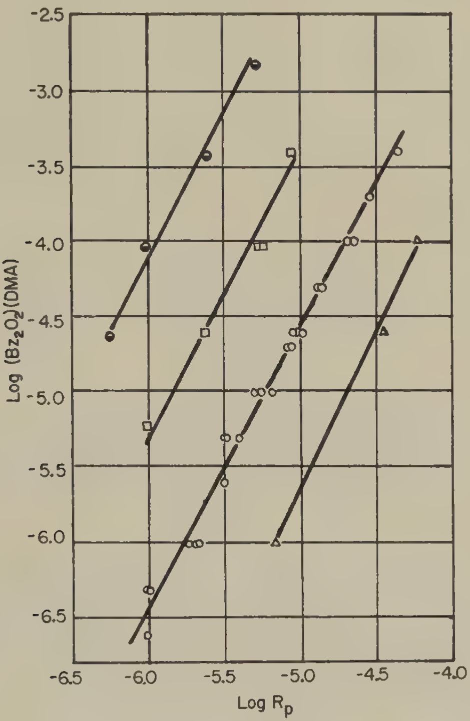
-2.5
-3.0
-3.5
-4.0
-4.5
-5.0
-5.5
-6.0
-6.5
Log (Bz₂O₂)(DMA)
-6.5
-6.0
-5.5
-5.0
-4.5
-4.0
Log Rₚ

FIG. 1

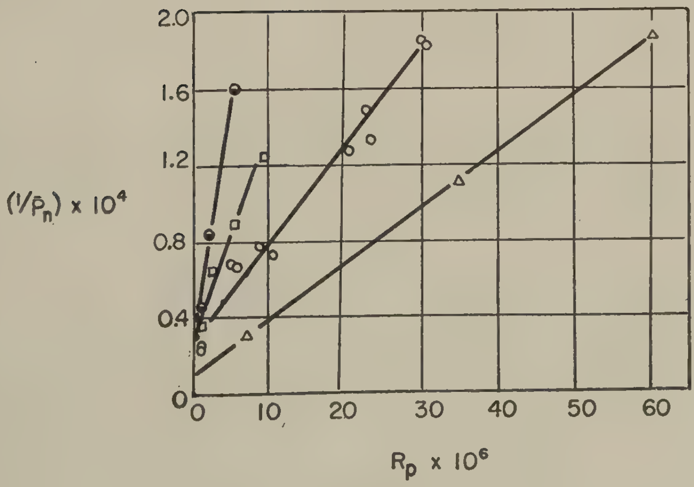
2.0
1.6
1.2
0.8
0.4
0
(1/P̄ₙ) x 10⁴
0
10
20
30
40
50
60
Rₚ x 10⁶

FIG. 2

In this paper we show that the initial rate of polymerization of pure methylmethacrylate initiated by the system benzoyl peroxide-dimethylaniline is dependent only on the square root of the product $[Bz_2O_2][DMA]$, when the temperature is below that at which benzoyl peroxide alone will significantly initiate polymerization. The experiments were carried out in pure methylmethacrylate at 20°, 0°, −16°, and −40° C. The relation between $1/\bar{P}_n$ (reciprocal number average degree of polymerization) and R_p was obtained at all four temperatures. From this data the activation energy of the initiation reaction is calculated.

EXPERIMENTAL

The experimental procedure for measuring R_p has been described previously (3). All polymerizations were carried out to less than 5% conversion. The value of $\bar{P}_n$ was calculated by means of the relationship (4)

$$\bar{P}_n = 1772\,[\eta]^{1.25}. \qquad [4]$$

The dimethylaniline was purified as in reference 1. Recrystallized benzoyl peroxide was used. The methylmethacrylate was purified by washing with 5% sodium hydroxide to remove inhibitor, drying over anhydrous potassium carbonate, and distilling under nitrogen at 100 mm. taking a good middle cut.

The temperature of polymerization was controlled to within ±0.1° at 20° and 0° C., ±1° at −16° C., and ±2° at −40° C.

Catalyst concentrations were varied from 0.0005 to 0.040 mole per liter of benzoyl peroxide and dimethylaniline. The ratio of benzoyl peroxide to dimethylaniline was varied from 40:1 to 1:40.

RESULTS

The results of the experimental work are presented in Figs. 1 and 2. Figure 1 shows a plot of log R_p *versus* log Bz_2O_2 DMA; these lines correspond to the general expression

$$R_p = C([Bz_2O_2][DMA])^{0.5}. \qquad [5]$$

TABLE I

T (°C.)	$A'/[M]^2$	A'	$R_p/([Bz_2O_2][DMA])0.5$	$R_i'/[Bz_2O_2]\,[DMA]$
20	2.96	272	6.00×10^{-3}	214×10^{-6}
0	5.24	490	2.16×10^{-3}	49.0×10^{-6}
−16	12.5	1210	0.454×10^{-3}	5.14×10^{-6}
−40	28.0	2840	0.118×10^{-3}	0.784×10^{-6}

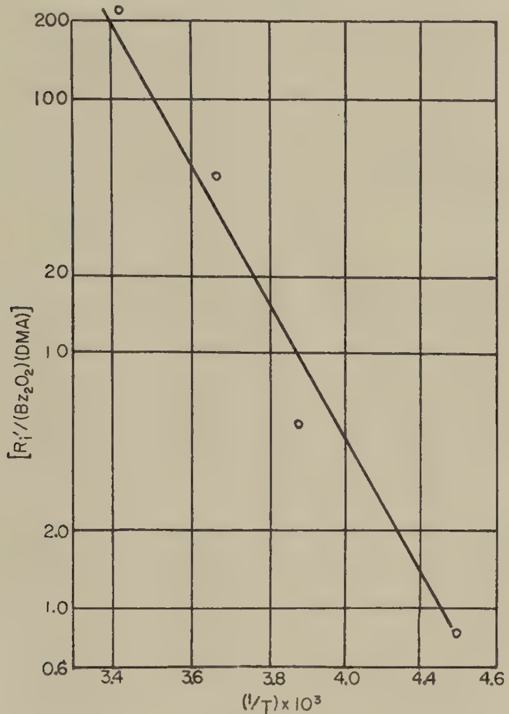

FIG. 3

Figure 2 shows a plot of $1/\bar{P}_n$ *versus* R_p. These lines correspond to

$$1/\bar{P}_n = C_{tr,m} + \frac{A'}{[M]^2} R_p . \qquad [6]$$

Using Eqs. [5] and [6], the rate of initiation, R'_i, may be calculated for the various temperatures by means of the expression

$$R'_i = \frac{2A'}{[M]^2} R_p^2 \qquad [7]$$

Values for the variables as obtained experimentally from Eqs. [5] and [6] are tabulated in Table I. A plot of log R'_i/Bz_2O_2 DMA *versus* $1/T$ (reciprocal absolute temperature) was made as shown in Fig. 3, which is represented by the equation

$$R'_i/[Bz_2O_2][DMA] = 5.4 \times 10^{11} e^{-12,800/RT}. \qquad [8]$$

The values of A' tabulated in Table I are plotted in Fig. 4 *versus* $1/T$. Also included in this plot are the values of A' previously collected (5).

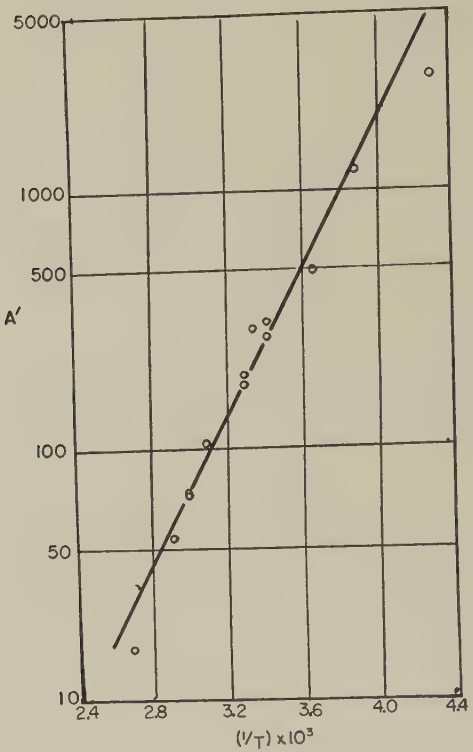

FIG. 4

Owing to the extension of the temperature range the equation presented in reference 5:

$$A' = 3.00 \times 10^{-4} e^{8,180/RT} \qquad [9]$$

is now modified to be

$$A' = 4.65 \times 10^{-3} e^{6,390/RT} \qquad [10]$$

DISCUSSION

In reference 1 it was suggested that at 0° C. radicals are produced from dimethylaniline and benzoyl peroxide by a bimolecular mechanism. In the present work Eqs. [5], [6], and [8] affirm this over a range of temperature and show moreover that the activation energy for the initiation reaction is 12.8 kcal. It should be noted that the reaction between benzoyl peroxide and dimethylaniline is extremely wasteful from the viewpont of radical production. Imoto (6) has shown the reaction to yield only about 25% of the theoretical amount of radicals at 50° C. in styrene.

The value for $R'_i/[Bz_2O_2][DMA]$ at 0° C. may be compared with the same value obtained for styrene in reference 1: for methylmethacrylate the value is 49.0×10^{-6}, whereas for styrene the value is 30.7×10^{-6}.

This work was sponsored by the Office of Ordnance Research, Department of the Army.

REFERENCES

1. TOBOLSKY, A. V., AND MELTZER, T. H., *J. Am. Chem. Soc.* **76,** 5178 (1954).
2. IMOTO, M., CHOE, S., AND TAKATSUGI, H., *J. Chem. Soc., Japan, Ind. Chem. Sect.* **58,** 451 (1955).
3. TOBOLSKY, A. V., AND JOHNSON, D. H., *J. Am. Chem. Soc.* **74,** 938 (1952).
4. TOBOLSKY, A. V., AND BAYSAL, B., *J. Polymer Sci.* **8,** 529 (1952).
5. TOBOLSKY, A. V., AND FERINGTON, T. E., *J. Colloid Sci.* **10,** 536 (1955).
6. IMOTO, M., OTSU, T., AND OTA, T., *Makromol. Chem.* **16,** 10 (1955).

JOURNAL OF COLLOID SCIENCE **11**, 250–253 (1956)

EFFECT OF OLEIC ACID AND SODIUM HYDROXIDE ON THE SOLUBILIZATION OF BUTANOL-1 AND 3-METHYL BUTANOL-1 IN AQUEOUS SOLUTION OF SODIUM OLEATE

A. N. Bose and K. N. Mehrotra

Department of Chemistry, Lucknow University, India

Received February 20, 1956

Introduction

McBain and Lissant (1) and Spring and Howard (2) observed that lauric acid increases the solubility of hydrocarbons in aqueous solution of sodium and potassium laurate. In the present work the extent of solubilization of butanol-1 and 3-methyl butanol-1 in aqueous solution of sodium oleate containing free oleic acid and free sodium hydroxide has been determined with a view to finding out if the free acid and sodium hydroxide have any influence on the solubility of these alcohols.

The viscosity of the solutions has also been determined with a view to finding out the nature of the micelles formed.

Materials Used

Oleic acid was Kahlbaum (Analar). Sodium hydroxide was prepared from sodium B.D.H. (Analar) in conductivity water. Merck (Reagent grade) butanol-1 and 3-methyl butanol-1 after further purification had the following boiling points: Butanol-1, 117°–118°C. 3-Methyl butanol-1, 129°–130°C.

Experimental Method

Exact solubilities of alcohols were not determined but attempts were made to prepare 5 %, 10 %, 20 %, 30 %, 40 %, 50 %, 60 %, 70 %, 80 %, and 90 % solutions of alcohols in 25 %, 50 %, 75 %, and 100 % neutralized acid and in excess of sodium hydroxide by the method used by Smith (3).

Viscosities were determined at 35° ± 0.05°C. in a thermostat by means of Ostwald's viscometer. Densities were determined by means of a pycnometer. The results obtained are given in Tables I and II.

Results and Discussion

In 25 % neutralized oleic acid, solutions of 75 %, 80 %, and 90 % butanol-1 and 90 % 3-methyl butanol-1 could be prepared. The solubility of water in butanol-1 at 34°C. is 20.5 % and that in 3-methyl butanol-1 is 10.18 %; this

TABLE I

Viscosity of the System: Water-Sodium Oleate and Butanol-1 in Presence of Free Acid and Alkali

Viscosity in millipoise; Temperature 35° ± 0.05°C.

Butanol-1, %	Percentage of oleic acid neutralized				Concentration of NaOH		
	25	50	75	100	0.2*N*	0.4*N*	0.6*N*
5	—	—	19.08	16.17	22.36	79.14	121.00
10	—	28.99	22.35	18.62	21.80	27.52	30.52
20	—	—	26.20	25.20	25.85	—	—
30	—	—	29.47	28.32	—	—	—
40	—	—	32.81	30.98	—	—	—
50	—	—	33.74	32.42	—	—	—
60	—	—	34.89	33.13	—	—	—
70	—	—	29.51	29.94	—	—	—
80	25.01	26.03	26.93	28.07	—	—	—
90	23.12	24.26	25.03	25.99	—	—	—

TABLE II

Viscosity of the System: Water-Sodium Oleate and 3-Methyl Butanol-1 in Presence of Free Acid and Alkali

3-Methyl butanol-1, %	Percentage of oleic acid neutralized				Concentration of NaOH	
	25	50	75	100	0.2*N*	0.4*N*
5	—	—	—	18.62	152.3	—
10	—	—	—	39.09	105.2	45.45
20	—	—	—	57.23	—	—
70	—	—	—	52.12	—	—
80	—	—	—	39.50	—	—
90	30.48	32.21	34.40	34.59	—	—

shows that only a very small amount of water was solubilized in butanol-1 and no water was solubilized in 3-methyl butanol-1.

In 50% neutralized oleic acid, solutions of 10%, 75%, 80%, and 90% butanol-1 and 90% 3-methyl butanol-1 could be prepared. This shows that for butanol-1 both hydrophilic oleomicelles and lipophilic hydromicelles (see Schulman and Riley (4)) were formed. But for 3-methyl butanol-1 water was not solubilized.

Solutions of all concentrations of butanol-1 were prepared in 75% and 100% neutralized acid. For 3-methyl butanol-1 solutions of 85% and 90% alcohols were prepared in 75% neutralized acid but in completely neutralized acid solutions of 5%, 10%, 20%, 70%, 80%, and 90% alcohol concentrations could be prepared; therefore, for this alcohol it can be concluded that neutral sodium oleate acts as a better solubilizer than the acid soap. Spring and Howard (2), on the other hand, found the acid soap to be a better solubilizer than the neutral soap for the solubilization of benzene. This difference in behavior is due to the fact that the loci of solubilization of alcohols, which are polar compounds, are different from those for benzene.

The solubility of butanol-1 and 3-methyl butanol-1 decreased as the alkali concentration was increased.

Viscosity of Butanol-1 System

From the results given in Table I it is observed that for 25 % and 50 % neutralized acid, the viscosity of 80 % solution is more than that of 90 % alcohol solution. This is due to the fact that the micelle in the former solution is bigger than in the latter.

In the case of 75 % and completely neutralized acid solutions, the viscosity at first increases up to 60 % alcohol concentration and then decreases with the increase in alcohol concentration. This is probably due to the fact that below 60 % alcohol concentration hydrophilic oleomicelles are present and above 60 % alcohol concentration lipophilic hydromicelles are formed. Above 60 % alcohol concentration the decrease in viscosity is due to the decreasing size of the micelles.

In the alkaline region, viscosity increases considerably as the alkali concentration increases. This is due to the increasing tendency to form gel with the increase in the concentration of alkali. Formation of gel in presence of salts has also been observed by Pilpel (5).

In the presence of excess of alkali, viscosity decreases as the alcohol concentration increases. This is due to the fact that the gel formation tendency decreases with the increase in concentration of butanol-1. The explanation given by Pilpel (5) is that in the presence of short-chain alcohols, the radii of both spherical and cylindrical micelles decrease and hence the tendency to form gel also decreases.

Viscosity of 3-Methyl Butanol-1 Systems

The behavior of the 3-methyl butanol-1 system is similar to that of the butanol-1 system.

Summary

The solubilizing capacity of aqueous solutions of acid soap and neutral soap for butanol-1 and 3-methyl butanol-1 has been determined. It has been observed that the amount of butanol-1 solubilized is the same in aqueous solutions of 75 % neutralized and completely neutralized oleic acid. But for 3-methyl butanol-1 neutral soap acts as a better solubilizer than the acid soap. This is due to the fact that the loci of solubilization of both free acid and the alcohol are the same.

It has been concluded from the viscosity determinations for these sys-

tems that two types of micelles are formed. The first type of micelles exists below 60 % butanol-1 concentration and the second type above 60 %.

REFERENCES

1. McBAIN, J. W., AND LISSANT, K. J., *J. Phys. & Colloid Chem.* **55,** 655 (1951).
2. SPRING, S., AND HOWARD, JR., *J. Colloid Sci.* **9,** 380 (1954).
3. SMITH, E. L., *J. Phys. Chem.* **36,** 1401 (1932).
4. SCHULMAN, J. H., AND RILEY, D. P., *J. Colloid Sci.* **3,** 383 (1948).
5. PILPEL, N., *J. Colloid Sci.* **9,** 285 (1954).

JOURNAL OF COLLOID SCIENCE **11**, 254-259 (1956)

MEASUREMENTS OF THE SYSTEMATIC ELECTRIFICATION OF AEROSOLS

Ross Gunn and R. H. Woessner

Office of Physical Research, U. S. Weather Bureau, Washington, D. C.

Received March 5, 1956

ABSTRACT

The distribution of the fractional numbers of aerosol particles carrying assigned charges was measured for the case where the positive and negative light ion conductivities of the environment were *unequal*. The maximum of the distribution is displaced toward the sign of the charge that corresponds to the ion having the predominant conductivity. With a measured ratio of $\lambda_+/\lambda_- = 0.8$; about 95% of the particles carried negative charges and had an average value of $-12\ e$. The magnitude of both the observed mean charge and the distribution corresponds closely to the *aerosol electrification equation* recently worked out by the senior author. The investigations show that ionic diffusion is responsible for the equilibrium electrification of perhaps most aerosols.

I. INTRODUCTION

The free electrical charge carried by aerosol particles frequently plays an important part in determining the physical characteristics of the aerosol. In a number of earlier papers (1–3) the fundamental character of the electrification transferred to typical aerosol particles was considered, and it was shown that the mean charge, averaged with respect to sign, depended critically upon the ratio of the positive and negative light ion conductivities of the aerosol environment. In this paper one considers the experimentally determined systematic electrification of water droplets condensed from saturated clean air in which the positive and negative light ion conductivities are quite different. It is found that under these circumstances the sign of the mean systematic charge is the same as the sign of the predominant light ion conductivity.

Earlier analyses and measurements of the electrical charge communicated to insulated spheres, supported in a small wind tunnel and operating with ionized air having a known conductivity ratio, showed clearly (4) that ionic diffusion is responsible for the electrification and its magnitude is dependent on the conductivity ratio of the positive and negative light ion conductivities. It has been shown (1) that the average charge Q transferred to a particle whose radius is *larger* than the mean free path of the ions in the environment, is given by

$$Q = \left[1 + F\left(\frac{aVe}{2\pi kTu}\right)^{1/2}\right]\frac{akT}{e}\ln\frac{\lambda_+}{\lambda_-} \tag{1}$$

where F is a numerical constant approximating unity that depends on the detailed air flow about the particle, a is the particle radius, k is the Boltzmann constant, T is the absolute temperature, e is the elementary charge, λ_+ and λ_- are the respective light ion conductivities of the environmental air, V is the systematic particle velocity relative to its environment, and u is the mean ionic mobility in the transition layer just outside the particle. Since the falling velocity V of most aerosol particles is small, Eq. [1] may usually be reduced to

$$Q = \frac{akT}{e}\ln\frac{\lambda_+}{\lambda_-} = ye \tag{2}$$

where y, obviously, is the number of elementary charges corresponding to Q and defines the maximum of the distribution curve given by Eq. [3] and Figs. 1 and 2.

Because large numbers of particles supported in an ionized atmosphere normally capture the more mobile negative ions faster than the positive ions and thus tend to establish equality of conductivity between the posi-

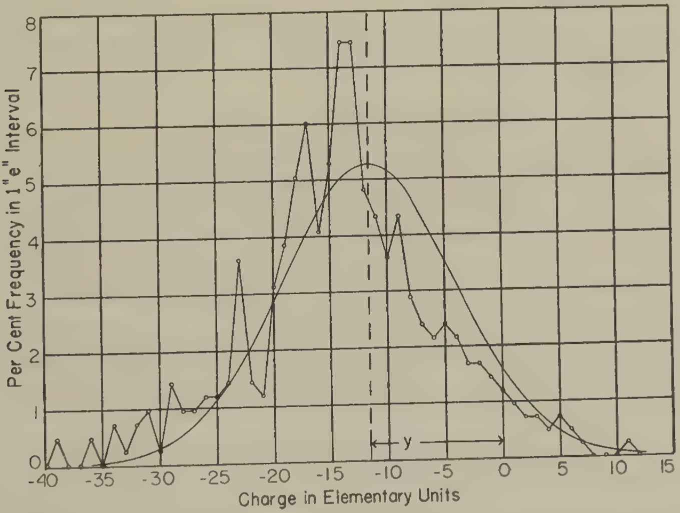

FIG. 1. Measured fractional number of pure water droplets carrying assigned numbers of elementary charges. Average radius = 3.32 μ with a mean deviation of 0.65 μ. Measured conductivity ratio $\lambda_-/\lambda_+ = 1.22$ so that $y = -11.7$, as calculated from Eq. [2]. Number of droplets measured = 416. Smooth curve is Eq. [3].

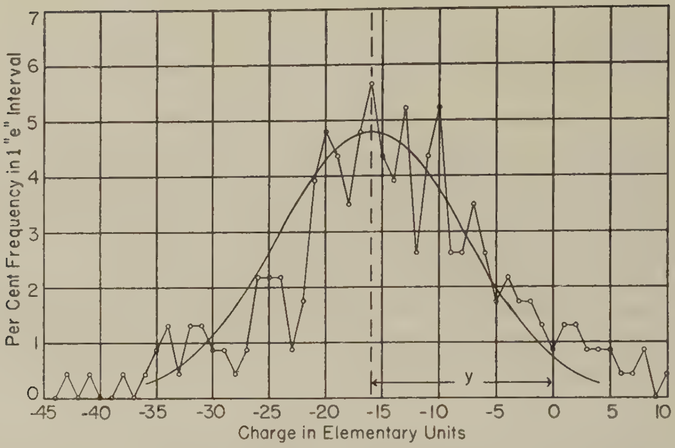

FIG. 2. Measured fractional number of pure water droplets carrying assigned numbers of elementary charges. Average radius = 4.0 μ with a mean deviation of 0.8 μ. Measured conductivity ratio $\lambda_-/\lambda_+ = 1.26$ so that $y = -16$, as calculated from Eq. [2]. Number of droplets measured = 230. Smooth curve is Eq. [3].

tive and negative ions; there was a possibility that the phenomena fully established for a single sphere (4) would not be evident in a cloud of suspended particles. Accordingly, it seemed worth while to measure the distribution of electrification among the particles of an aerosol under carefully controlled conditions, wherein the environmental conductivity ratio of the positive and negative light ions was known. Such measurements are summarized herewith.

II. EXPERIMENTAL PROCEDURE

The apparatus employed in this investigation is an adaptation of the method first used by Wells and Gerke (5) in their investigation of charged smoke particles. Their method employed a chamber wherein the particles were subject to periodic horizontal electrical forces as well as the steady forces of gravity. By the use of Stokes' law, the radius and electrical charge of each aerosol particle was then determined directly from the observed displacements of the particles that result from gravitational and cyclically impressed electrical forces. The rate of fall of each droplet was used to determine its radius.

As reported in an earlier communication (3) it is found that newly formed cloud droplets are essentially neutral but they quickly acquire an equilibrium charge upon exposure to copious ionization. This accumulation of charge normally is accomplished in ordinary clear air in some hours, but may be greatly expedited by the use of X-rays or other ionizing sources. Care was taken in our experiments to clean the air introduced into the cloud chamber so that ions could not rapidly attach themselves to the large numbers of condensation nuclei normally suspended in ordinary air. These nuclei reduce the conductivity of the air and tend to promote equality of conductivity for the positive and negative ions (6). The air was carefully cleaned by passing it first through a layer of copper wool and then through 2 inches of loose cotton before it was introduced into a chamber saturated with water. This clean air was then slightly cooled to form a cloud at a temperature about ½°C. above ambient. The cloud chamber was exposed to X-rays of such an intensity that many ions normally existed in the space between the cloud droplets. In the presence of such ionization it was found that the ratio of the negative conductivity to the positive conductivity (λ_-/λ_+) approximated 1.2 to 1.3, in spite of the relatively large number of cloud droplets in the environmental air. The newly formed cloud was aged in the chamber for some minutes and then drawn through a standard Gerdien conductivity apparatus. The positive and negative ionic conductivities were independently determined by measuring the current to the central electrode by the use of a standard high resistance and a vibrating reed electrometer. This conductivity ratio was measured both before and after every reported run and if appreciable fluctuation occurred, the measurements were discarded.

Considerable effort was made to obtain a cloud of droplets having a uniform size. The cloud was formed by condensation in clean air and subsequently aged. The mean deviation of droplet size is indicated in the captions of each figure.

III. The Measurements

Using the above apparatus in the manner outlined, the sign and number of elementary charges carried by each particle and its radius were determined. The distribution of the fractional numbers carrying any assigned number of ions was then plotted as shown in the accompanying figures. Between 200 and 500 individual measurements were made to determine each curve. Figures 1 and 2 are representative samples of a number of measurements and these show very clearly that the fractional number of *uncharged* droplets in an environment where the conductivity ratios differ appreciably from unity is small. All measurements show that when the negative conductivity exceeds the positive conductivity a large majority of cloud droplets bear a negative charge. The number of negative charges, y, corresponding to the maximum of the distribution curve Eq. [3] is immediately calculable from Eq. [2], assuming that the relative fall velocity V of the particles is small.

IV. Discussion

Employing straightforward kinetic theory methods it was shown in earlier papers (1, 2) that the magnitude and distribution of the charges on aerosol particles were determined primarily by the probability of capture of the light ions in the atmosphere. These bombard the droplet as a result of their thermal motions and the relative probability of capture is measured by the ratio of the conductivities of the light ions. Thus, a Gaussian-like distribution symmetrical about the zero charge axis is produced whenever the conductivity ratio λ_+/λ_- is unity. However, if the positive and negative conductivities are appreciably different the distribution curve is systematically displaced towards the sign of the predominant ion. Carrying out an analysis of this concept Ross Gunn has shown (2) that the fractional number of particles F_x/F_t carrying a given number of elementary charges x is given by the *basic aerosol electrification equation*

$$\frac{F_x}{F_t} = \frac{e}{(2\pi akT)^{1/2}} \exp\left[\frac{-\left(x - \dfrac{akT}{e^2}\ln\dfrac{\lambda_+}{\lambda_-}\right)^2}{2\left(\dfrac{akT}{e^2}\right)}\right], \qquad [3]$$

where F_x is the number of particles per unit volume, carrying x elementary charges, and F_t is the total number of particles per unit volume. This basic equation describes not only the random charge carried by aerosol particles but also the systematic charge that is made evident in the foregoing measurements. For the purpose of comparing this diffusion theory with our measurements, we have plotted as smooth curves in Figs. 1 and 2 the distribution predicted by Eq. [3] using measured values for the conductivity ratio and the mean particle radius. It may be seen that the theoretical expression of Eq. [3] well describes the observations and predicts the systematic displacement of the distribution curves towards the negative charge just as the measured values of the conductivity ratio indicated on each curve imply. Our earlier measurements showed that if as many as 2500 droplets were measured the statistics were greatly improved and irregularities of the experimental curve as shown by Figs. 1 and 2 largely disappeared.

V. CONCLUSION

This series of analytical and experimental studies (1–4) shows very clearly the importance of ionic diffusion processes in establishing the observed free charges on aerosol particles. The basic charge distribution equation given above represents the observed phenomena as well as the measured data. The equation predicts not only the statistical charging and distributions observed when the conductivities of the positive and negative ions are equal, but also when the conductivity ratios differ from unity. This experimental investigation supports, in every detail, the view that the electrification of *aged* aerosols is due to the thermal diffusion of light ions that are normally present throughout the atmosphere.

REFERENCES

1. GUNN, ROSS, "Diffusion charging of atmospheric droplets by ions, and the resulting combination coefficients." *J. Meteorol.* **11,** 339–347 (1954).
2. GUNN, ROSS, "The statistical electrification of aerosols by ionic diffusion." *J. Colloid Sci.* **10,** 107–119 (1955).
3. WOESSNER, R. H., AND GUNN, ROSS, "Measurements related to the fundamental processes of aerosol electrification." *J. Colloid Sci.* **11,** 69–76 (1956).
4. PHILLIPS, B. B., AND GUNN, ROSS, "Measurements of the electrification of spheres by moving ionized air." *J. Meteorol.* **11,** 348–351 (1954).
5. WELLS, P., AND GERKE, R., *J. Am. Chem. Soc.* **41,** 312 (1919).
6. PHILLIPS, B. B., ALLEE, P. A., PALES, J. C., AND WOESSNER, R. H., An experimental analysis of the effect of air pollution on the conductivity and ion balance of the atmosphere. *J. Geophys. Research* **60,** 289–296 (1955).

JOURNAL OF COLLOID SCIENCE 11, 260–271 (1956)

THE EFFECT OF METHYLCELLULOSE ON THE ELECTROLYTE STABILITY OF DILUTE SYNTHETIC LATEXES[1]

F. L. Saunders and J. W. Sanders

Plastics Basic Research Laboratory, The Dow Chemical Co., Midland, Michigan

Received March 20, 1956

ABSTRACT

The effect of Methocel (Dow methylcellulose) on the electrolyte stability of dilute synthetic latexes has been studied using a centrifuging technique in conjunction with turbidity measurements as a means of determining stability.

Stability studies on dilute styrene latexes appear to conform to the general concepts associated with hydrophobic colloids.

The effect of the addition of Methocel on the electrolyte stability of the dilute latex is similar to the sensitizing and protecting action exhibited by certain hydrophilic colloids on hydrophobic colloids. The protecting effect occurs at approximately theoretical surface coverage of the latex particles by a monolayer of Methocel. The electrolyte stability under these conditions is much less sensitive to small changes in electrolyte concentration. The molecular weight of the Methocel does not appreciably affect the amount necessary for the protecting action.

With addition of emulsifier to the diluted latex, the amount of Methocel required for the protecting effect is decreased and precluded from adsorption when the particles are covered by emulsifier.

INTRODUCTION

In many commercial applications of synthetic latex, it is often desirable to add a protective colloid or a thickening agent to the latex to improve its process behavior. The question is often raised, how do such compounds function in terms of an interfacial or adsorption phenomenon and their effect on the colloidal stability of the latex. Since hydrophilic colloids are generally used in these applications and latexes are characteristic of hydrophobic colloids, it suggests a study similar to the well-known investigations of the effect of hydrophilic colloids on the electrolyte stability of hydrophobic colloids.

The electrolyte stability of a dilute synthetic latex may be considered in terms of the general concepts associated with hydrophobic colloids. The stability is primarily controlled by the interaction of the electrical double layer of the latex particles formed by adsorption of emulsifier ions. Such a system is usually sensitive to electrolyte addition and its stability may be represented by a coagulation value. The coagulation value as defined here corresponds to the electrolyte concentration in millimoles per liter necessary to produce complete coagulation under a given set of conditions. A factor which is also of interest in a stability study of this nature is the sensitivity of the colloid to electrolyte additions, which is a relative indication of the hydrophobic or hydrophilic nature of the colloid. In general, the sensitivity of the system to coagulation by electrolyte addition decreases as the colloid becomes more hydrophilic.

---

[1] Presented before the Division of Colloid Chemistry at the 126th Meeting of the American Chemical Society New York, New York, September, 1954.

When a hydrophilic colloid is added to a hydrophobic one, a sensitizing and protecting effect is often observed. The hydrophilic colloid is adsorbed on the surface of the hydrophobic particle which alters its interfacial properties and, therefore, its stability. The sensitizing effect is usually found at low concentrations of the hydrophilic colloid and results in a region where the coagulation value is lower than that of the original colloid. At higher concentrations, the protective action is produced where the colloid is less susceptible to coagulation by electrolytes. The exact nature of these effects is not known; however, in a qualitative manner the sensitization has been attributed to formation of agglomerates of the hydrophobic particles held together by the hydrophilic ones. The protecting action is due to complete coverage of the hydrophobic particles by the hydrophilic colloid (1). The protected particles acquire the stability properties of the hydrophilic colloid.

To study this phenomenon in detail as it applies to a latex system, the effect of methylcellulose on the electrolyte stability of a dilute monodisperse latex has been investigated. The methylcellulose served as a protective hydrophilic colloid in this system. The thickening effect was eliminated by using dilute latexes of less than 2% polymer solids.

During the course of this investigation, a paper by Diehle, Kraemer, and Klaus (2) appeared which reports a similar study by a somewhat different technique. While the present investigation confirms part of their results, considerable effort has been given to important related aspects of the problem, which to our knowledge have not been previously considered.

Experimental

The latexes used for the stability studies were laboratory preparations which were essentially monodisperse as indicated by electron micrographs. Table I lists the average particle diameters and polymer compositions of the various latexes which were studied. The coagulating electrolytes were prepared from reagent grade salts dissolved in distilled water. The methylcellulose solutions were prepared from Dow Methocel, made up as 1% solutions.

The coagulation values were determined by adding 1 ml. of the electrolyte to a 10-ml. sample of the dilute latex and centrifuging the sample in a

TABLE I

Reference Number and Particle Diameter of Latexes Studied

Latex No.	Composition	Particle diam. microns
1	Styrene	0.330
2	Styrene	0.184
3	Saran	0.125

clinical type centrifuge. After 5 minutes of mild centrifuging (3300 r.p.m.), the coagulated material separated from the system leaving a serum containing the uncoagulated latex. A sample of the serum was quickly withdrawn and diluted with a known amount of nonionic soap solution (Nonisol-100). This was done to prevent further coagulation and to dilute the sample for subsequent turbidity measurement on the diluted serum with reference to a calibration curve. The calibration curve was obtained from turbidity measurements on diluted samples of the original latex of known concentration. The turbidity measurements were made utilizing a 10-mm. path-length cell in conjunction with a B-S light-scattering photometer manufactured by the Phoenix Precision Instrument Co. The initial concentration of the latex used in each series of coagulation experiments was determined by centrifuging a 10-ml. sample of the latex with 1 ml. of distilled water in place of the electrolyte and the concentration of the latex was obtained from the turbidity-concentration curve. For the polystyrene latex under these conditions, an insignificant amount of the latex was centrifuged down in the absence of added electrolyte. By selecting a suitable range of electrolyte concentrations, the degree of coagulation was controlled to produce values between 0 and 100% coagulation. When these values were plotted as per cent coagulated vs. log *c*, where *c* is the concentration of electrolyte in millimoles per liter based on total volume, the upper range of the coagulation curve was extrapolated to the 100% coagulation value. The electrolyte concentration at this intercept represents the coagulation value for these conditions.

RESULTS AND DISCUSSION

Coagulation Values: Effect of Valency of Coagulating Ion

To illustrate this method of measuring latex stability and to verify the applicability of the Schulze-Hardy rule to latex systems (3), coagulation of Latex #1 consisting of 0.82% polymer solids was produced by NaCl, $CaCl_2$, and $AlCl_3$. The Schulze-Hardy rule states that the flocculating power of an electrolyte depends upon the valence of the ion which has a charge opposite to that of the colloid particle. From consideration of a theory of the interaction of the double layers on hydrophobic sol particles, Verwey (4) concludes that for monovalent, divalent, and trivalent ions, the coagulation values should be in the ratio $1:(\frac{1}{2})^6: (\frac{1}{3})^6$ or 100:1.6:0.13.

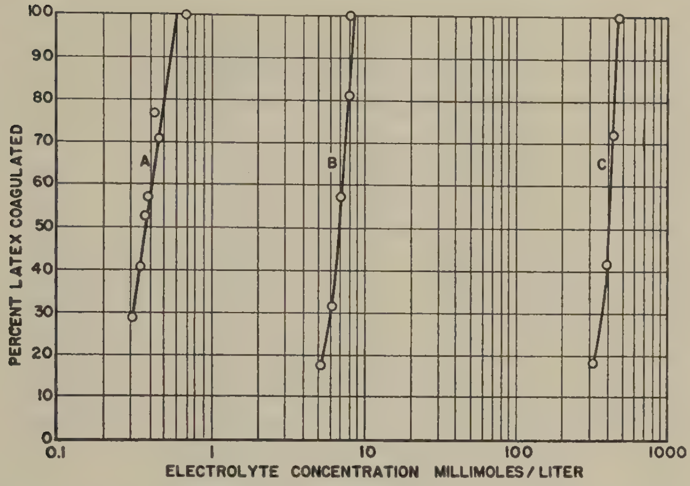

FIG. 1. Dependence of coagulation value on valence of coagulating electrolyte. *A*—$AlCl_3$; *B*—$CaCl_2$; *C*—NaCl.

Since the latex particles are negatively charged, the coagulation values of the mono-, di-, and trivalent salts should conform to this relationship.

In Fig. 1 is shown the dependence of coagulation on electrolyte concentration for the three electrolytes considered. The coagulation values obtained from these data by extrapolation to the 100% coagulation are 470, 8.8, and 0.6 millimoles per liter for the Na, Ca, and Al salts. These values represent a ratio of approximately 100:1.8:0.13. This is in good agreement with the ratio 100:1.6:0.13 as derived by Verwey for the Schulze-Hardy relationship.

Effect of Methocel on Latex Stability

The effect of Methocel on the electrolyte stability of the latex was determined by adding small amounts of the Methocel solution to the dilute latex, maintaining a constant polymer composition. The per cent of the latex coagulated for each electrolyte addition was determined as previously described.

The effect of 15 cps. grade Methocel on the electrolyte stability of Latex #1 containing 0.82% polymer solids is shown in Fig. 2. The coagulating electrolyte was $CaCl_2$. The data as presented are intended to indicate a coagulation value, the electrolyte concentration at 100% coagulation, as well as the sensitivity of the latex to electrolyte additions. Curve *A* represents the coagulation of the original diluted latex with no addition of Methocel. It is to be noted that the stability is very sensitive to small changes in electrolyte concentration, as indicated by the slope of the line. The effect of Methocel on stability is shown by curves *B–F* for an in-

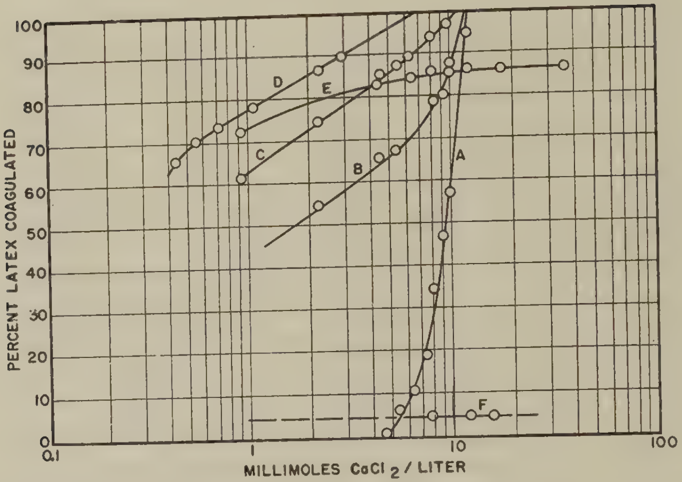

FIG. 2. Dependence of latex coagulation on Methocel and electrolyte concentration. Per cent Methocel on solids. *A*—0.00; *B*—0.31; *C*—0.61; *D*—1.22; *E*—1.83.

crease in Methocel concentration from 0.31% to 1.83% based on polymer solids. It is evident that the stability is decreased up to a Methocel concentration of 1.53%, Curve *E*, where it appears to remain constant at all electrolyte concentrations considered. Subsequent additions of Methocel produce an increase in the stability and apparently the stability is insensitive to the electrolyte addition. Curve *F* represents this latter case where essentially no coagulation is produced. Since the data are not suitable for extrapolation to obtain a coagulation value for each Methocel concentration, the relative stability has been considered as the per cent of the latex remaining in suspension at a given electrolyte concentration. In Fig. 3 is shown the dependence of stability on Methocel concentration for several electrolyte concentrations. The three curves represent three electrolyte concentrations which indicate that the general shape of the stability curve is the same for different concentrations of the coagulating electrolyte. The stability increase after the initial sensitizing action appears to occur at a relatively constant Methocel concentration.

To study this effect under different surface area conditions, several of the latex parameters were varied as well as the composition of the latex. In Fig. 4 is presented a composite plot of the stability of the various latex systems as a function of the weight of Methocel per square Angstrom of latex surface area. The Methocel concentration was plotted in this manner to permit a comparison of the stability with the surface coverage of the particles by the Methocel. Curves *A* and *B* represent the stability of Latex #1 consisting of 0.82% and 1.74% polymer solids coagulated by 5 millimoles per liter $CaCl_2$. The stability shown in Curve *C* is for Latex #2,

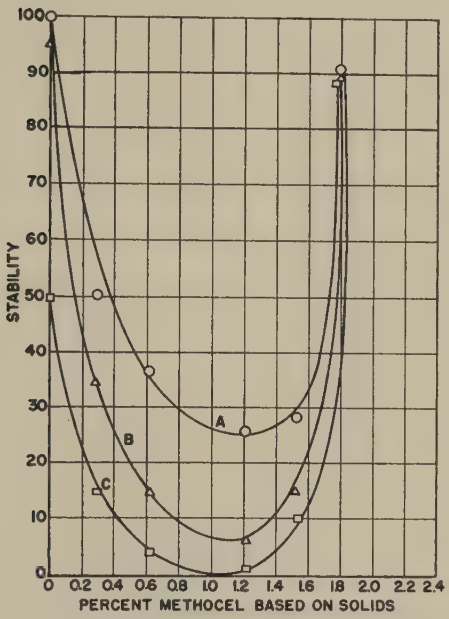

FIG. 3. Dependence of latex stability on Methocel and electrolyte concentration. Coagulating electrolyte $CaCl_2$. *A*—1 mM./l.; *B*—5 mM./l.; *C*—10 mM./l.

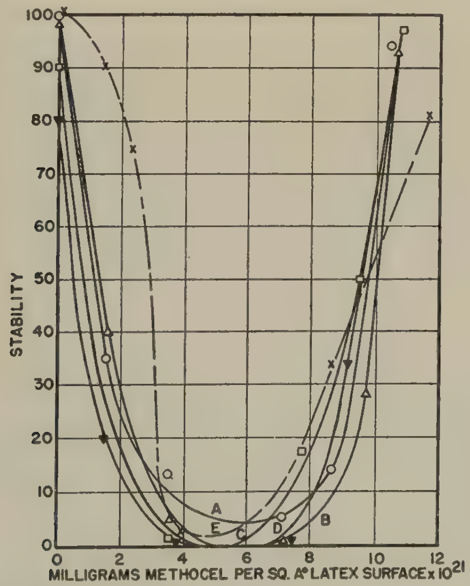

FIG. 4. Dependence of latex stability on surface coverage by Methocel. *A*—latex #1,0.82% solids, 5 mM./l. $CaCl_2$; *B*—latex #1, 1.74% solids, 5 mM./l. $CaCl_2$; *C*—atex #2, 0.88% solids, 5 mM./l. $CaCl_2$; *D*—latex #2, 0.88% solids, 350 mM./l. aCl; *E*—latex #3, 1.47% solids, 5 mM./l. $CaCl_2$.

0.88% polymer solids coagulated by 5 millimoles per liter $CaCl_2$. The same latex coagulated by 350 millimoles per liter NaCl is given in Curve *D*. The two electrolytes were used to determine whether the stability curves were affected by the valence of the coagulating ion. It appears that there is no appreciable difference in the amount of Methocel necessary to produce the protecting action against coagulation by the mono- and divalent coagulating ions. Latex #3 of 1.47% solids coagulated with 5 millimoles per liter $CaCl_2$ is shown in Curve *E*.

The increase in stability which is shown in Figure 4 appears to occur in a narrow range of Methocel concentrations for all the systems considered, suggesting that this effect may be due to a surface coverage phenomenon whereby the particles are covered by a monolayer of Methocel. If this is the case, the amount of Methocel necessary to produce the protecting action can be predicted from consideration of the total surface area of the latex particles and the amount of surface area covered by a Methocel molecule. The dimensions of the cellobiose unit have been determined by X-ray measurements which give approximately 40 A^2 as the area covered by a glucose unit (5). This should be a good approximation for the Methocel monomer molecule of molecular weight 190. Diehle *et al.* (2) make use of a value equivalent to 40 A^2 as the area covered by a methylcellulose monomer unit.

Based on the assumption that each Methocel monomer unit covers 40 A^2 as a monolayer, 7.9×10^{-21} mg. of Methocel would cover 1 A^2 of surface area. Consideration of Fig. 4 indicates that this value would correspond to the Methocel concentration where the latex stability increases after the minimum. Therefore, the increase in stability or protective effect after the sensitization appears to coincide fairly well with the Methocel concentration necessary to produce surface coverage. This is only a first approximation, since the amount of Methocel in the aqueous phase has not been considered as well as the initial coverage of the latex by the emulsifier; however, they tend to cancel each other.

The decrease in stability or sensitizing action is accompanied by a decrease in mobility of the suspended particles (2) which indicates that the zeta-potential is decreased and is a prime factor in determining the stability of the latex system. It has also been observed that in this region where the latex is sensitized by the Methocel there is limited aggregation before the addition of the coagulating electrolyte (6). At complete surface coverage of the particles by the Methocel, the aggregates appear to disperse and the particles are stabilized by the hydrophilic nature of the protective Methocel layer.

The preceding considerations have been limited to a relatively low molecular weight Methocel. Since molecular weight might be a factor influencing the surface coverage or protecting action due to steric effects (7),

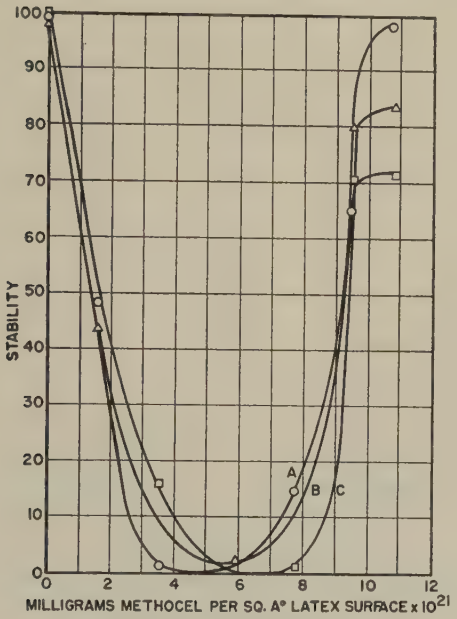

FIG. 5. Dependence of latex stability on Methocel molecular weight. *A*—15 cps. *B*—400 cps.; *C*—4000 cps.

several higher molecular weights were considered. Three different grades of Methocel were considered; the viscosities of their 2% solutions were 15, 400, and 4000 cps. The effect of the molecular weight of Methocel on the electrolyte stability of the dilute latex is shown in Fig. 5. The latex, #1 of 0.82% polymer solids, was coagulated with 5.0 millimoles per liter $CaCl_2$. There appears to be only a small dependence on the molecular weight for producing the increase in stability or protective effect. The small difference in protective action is probably due to experimental variations in preparation and coagulation of the various latex systems.

The Effect of Added Emulsifier on the Protective Action of Methocel

In many cases, it has been observed that the addition of emulsifier to a concentrated latex influences the effect of Methocel as a thickener, as well as the final stability of the latex system. Since the systems considered previously contained relatively little free emulsifier and very little surface coverage by the emulsifier, indicated by surface tensions in the vicinity of 70 dynes per centimeter, the effect of further emulsifier addition on the electrolyte stability has been studied.

The latex system used for this phase of the investigation was Latex #1 of 0.82% solids. The added emulsifier was an alkyl-aryl sulfonate added as a powder to the dilute latex. The concentration of the added emulsifier

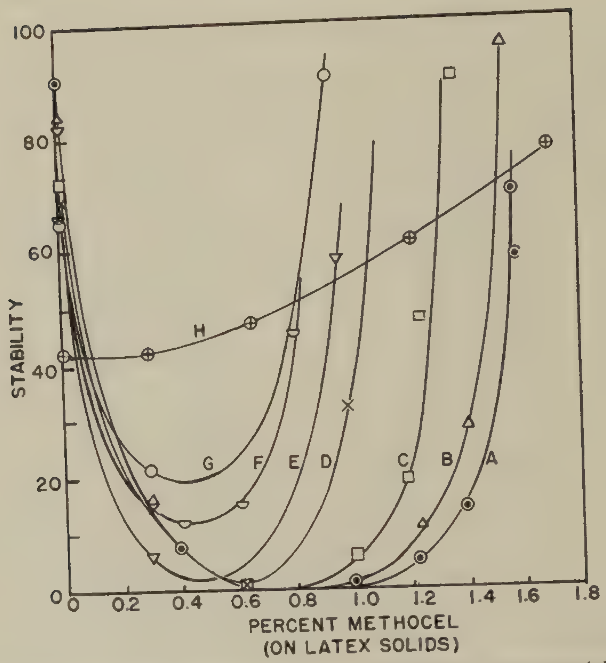

FIG. 6. Dependence of latex stability on Methocel concentration with added emulsifier. Emulsifier concentration g./g. latex solids. *A*—0.00; *B*—0.008; *C*—0.015; *D*—0.026; *E*—0.037; *F*—0.060; *G*—0.10; *H*—0.80.

was recorded in grams of active emulsifier per gram of latex solids. The surface tension of the resulting latex was also determined to indicate the relative amount of emulsifier in the water phase. A duNoüy Tensiometer was used for these measurements.

The effect of added emulsifier on the electrolyte stability curves when Methocel was added to the latex is presented in Fig. 6. Curves *A–H* represent increasing amounts of emulsifier added to the dilute latex. The stability curves shown in Fig. 6 were obtained from per cent coagulation vs. electrolyte concentration curves as previously described. The coagulating electrolyte concentration was 5 millimoles per liter $CaCl_2$. The various emulsifier additions and the surface tension of the latex before the addition of the Methocel are given in Table II.

From Fig. 6, it is evident that the presence of the emulsifier affects the behavior of the Methocel as a protective colloid. With an increase in emulsifier concentration, the protective effect is observed at a lower Methocel concentration. The calculated surface coverage of the latex particles by Methocel for this latex occurs at approximately 1.4% based on polymer solids. The lower initial stability of the latex with increasing emulsifier content is due to the presence of electrolyte in the added emulsifier. As a

TABLE II

Emulsifier Concentration and Surface Tension of Latexes Presented in Figure 6

Added emulsifier g./g. latex solids	Surface tension of latex, *dynes/cm.*	Curve in Fig. 6
0.000	73	A
0.008	68	B
0.015	65	C
0.026	58	D
0.037	52	E
0.060	45	F
0.10	36	G
0.80	33	H

result, the stability is less to a given concentration of added electrolyte. The stability of a latex is generally increased by an increase in adsorbed emulsifier ions and decreased by an increase in ionic strength. For these dilute latexes at high emulsifier concentration, the latter effect appears to be the dominating factor. Nevertheless, Fig. 6 serves to illustrate the effect of added emulsifier on the sensitizing and protecting effect of Methocel.

The interpretation of the data presented in Fig. 6 appears to depend in part upon the distribution of the added emulsifier between the aqueous phase and the particle. Maron *et al.* (8) have shown by surface tension titration of a latex with emulsifier, that the minimum in surface tension corresponds to micelle formation and surface coverage of the particle. Therefore, if one assumes that the minimum in surface tension of the latex indicates surface coverage of the particles by the emulsifier, the addition of emulsifier up to this point would result in decreasing the free-surface area of the particles. From consideration of Fig. 6, it appears that with ncreasing soap concentration and consequently increasing coverage by the emulsifier, it takes less Methocel to produce the stabilizing effect. This uggests a competition between Methocel and the emulsifier for the paricle surface with the emulsifier having the greater affinity. In the dilute atex with no addition of emulsifier, there is only a small amount of emulifier on the particle surface and the added Methocel effectively covers the ntire surface. With increased coverage of the particle by the emulsifier, a maller amount of Methocel is necessary to produce complete coverage of he particle. Finally, when the surface is covered by the emulsifier, the Methocel is precluded from adsorption and has little effect on the stability f the latex.

One aspect of the electrolyte stability which is not shown by Fig. 6 is he sensitivity of the latex system to electrolyte addition. For curves *A–E*, ll the stability vs. electrolyte concentration curves were similar to those Fig. 3, in which the sensitivity of the latex to electrolyte addition beme less with an increase in Methocel concentration. However, this was t the case for the latexes with sufficient emulsifier to bring the surface

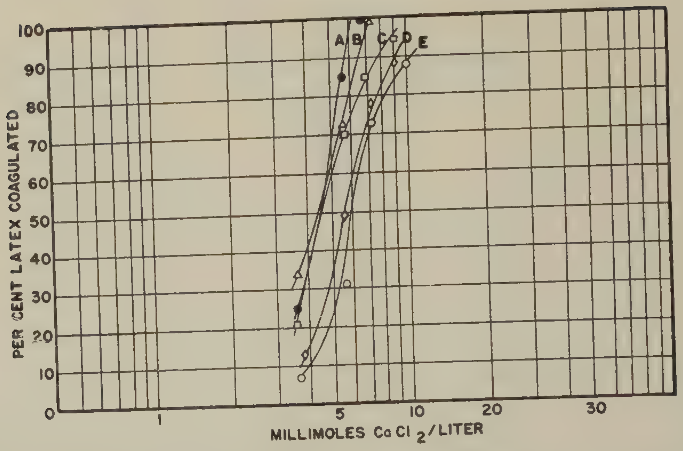

FIG. 7. Dependence of latex coagulation on Methocel and electrolyte concentration in presence of excess emulsifier. Per cent 15 cps. Methocel based on solids. *A*—0.00; *B*—0.31; *C*—0.61; *D*—1.22; *E*—1.59.

tension near the minimum of 33 dynes per centimeter, such as those represented by curves *G* and *H*. In these systems, subsequent addition of Methocel did not produce a decrease in the sensitivity of the latex to electrolyte, but merely shifted the curve retaining a rather steep slope. This situation is shown in Fig. 7 for the latex considered in Curve *H* of Fig. 6. Comparison of Figs. 2 and 7 indicate a definite change in the effect of Methocel on the stability of the latex to electrolyte concentration. The sensitivity of the latex appears to remain the same at all concentrations of added Methocel. This indicates that the stability is controlled by the adsorbed emulsifier ions, and the hydrophilic Methocel has no significant effect on the stability.

SUMMARY

The effect of Methocel on the electrolyte stability of dilute latexes appeared to be similar to the sensitizing and protecting action observed when certain hydrophilic colloids are added to hydrophobic colloids. When a small amount of Methocel was added to a dilute latex, the Methocel was adsorbed at the polymer-water interface. As a result, the zeta-potential was reduced, aggregates formed, and the electrolyte stability decreased. When sufficient Methocel was present to cover the surface of the particles, a protective action was produced which stabilized the particles by the hydrophilic nature of the Methocel layer. In latex systems where there was little emulsifier, the protecting action appeared to occur when the surface of the particles was covered by a monolayer of Methocel. The molecular weight of the Methocel did not appreciably affect the amount necessary to produce the protective action.

When additional emulsifier was added to the latex, the protecting action f the Methocel took place at a lower Methocel concentration. The proecting action appeared to depend upon the complete surface coverage of he particles by adsorption of emulsifier and Methocel in an additive maner. The greater the amount of Methocel necessary to produce surface overage, the greater was the hydrophilic nature of the protected particles. Vith increased amounts of emulsifier, less Methocel was necessary to roduce surface coverage and consequently the colloid was less hydrohilic. With complete coverage by emulsifier, the Methocel did not appear o be adsorbed and the latex stability was controlled primarily by the ouble layer associated with the adsorbed emulsifier.

Acknowledgments

The authors wish to acknowledge the assistance of Drs. Turner Alfrey and J. W. 'anderhoff in providing the monodisperse latexes and that of J. H. Oswald in obtainng the experimental data. We also thank Dr. W. Heller of Wayne University for his aluable suggestions and discussions concerning this work.

References

. Kruyt, H. R., "Colloid Science," Vol. 1. Wiley, New York, 1950.
. Diehle, O., Kraemer, H., and Klaus, W., *Kolloid-Z.* **130**, 105 (1953).
. Heller, W., and Oppenheimer, H., Paper presented at the 110th meeting of the American Chemical Society, Chicago, Illinois, September, 1946.
. Verwey, E. I., and Overbeek, J. Th. G., "Theory of the Stability of Hydrophobic Colloids." Elsevier, Amsterdam, 1948.
. Ott, E., "Cellulose and Cellulose Derivatives." Interscience, New York, 1943.
. Frantz, G. C., Sanders, J. W., and Saunders, F. L., to be published.
. Heller, W., and Pugh, T. L., *J. Chem. Phys.* **22**, 1778 (1954).
. Maron, S. H., Elder, M. E., and Ulevitch, I. N., *J. Colliod Sci.* **9**, 89 (1954).

JOURNAL OF COLLOID SCIENCE **11**, 272–285 (1956)

FACTORS AFFECTING THE SOLUBILITY OF NONIONIC EMULSIFIERS

William N. Maclay

The B. F. Goodrich Company, Research Center, Brecksville, Ohio

Received January 28, 1956

ABSTRACT

The effect of detergents, electrolytes, and organic liquids on the cloud point of Triton X-100, a nonionic emulsifier of the alkylphenol/polyethylene oxide type, is described. The lowering of the cloud point in dilute aqueous solution by electrolyte is a linear function of the ionic strength. The observed salting-out effect for the alkali metal and multivalent cations is roughly in the order of decreasing ion hydration. Crystalline nonelectrolytes cause only slight cloud point changes.

Nonpolar liquids and anionic detergents significantly raise the cloud point of the nonionic emulsifier. As the polarity of the organic solubilizate is increased by introduction of double bonds and more polar constituent groups, the increase in cloud point is less marked. Aromatics and polar aliphatics even cause the cloud point to be sharply decreased.

The cloud points of mixtures of nonionic emulsifiers lie intermediate between the cloud points of solutions of the pure components.

INTRODUCTION

Most nonionic surface-active agents are prepared by reacting a water-insoluble material, such as an alkyl phenol, with ethylene oxide so that the product is an oil-soluble group attached to a water-soluble polyethylene oxide chain. The overall degree of water or oil solubility of the material may be varied by changing the ratio of the hydrophilic and the hydrophobic portions of the molecule.

The high water solubility of the polyethylene oxide chain is due to hydrogen bonding between the solvent and the ether oxygen atoms in the chain. Since hydrogen bonding is a temperature-sensitive phenomenon, for each nonionic emulsifier molecule there exists a temperature at which the degree of hydration of the hydrophilic portion is just insufficient to solubilize the remaining hydrocarbon fragment. Consequently, the emulsifier separates from the solution. In spite of the broad molecular weight distribution which characterizes most commercial preparations (1), this is generally a well-defined temperature and is called the "cloud point." Usually, for a given hydrophobic unit, a molecule with a large polyethylene oxide tail can exist in solution at a higher temperature owing to a greater amount of hydrogen bonding than can a molecule with a shorter polyethylene oxide tail, so that the magnitude of the cloud point is roughly proportional to the water solubility of the material.

The following will convey some idea of the extent of hydration of a typical nonionic emulsifier. Triton X-100 is the adduct of *t*-octylphenol and 8 to 10 moles of ethylene oxide. The average molecular weight is about 680. Kushner and Hubbard (2) calculate from their viscosity data that 43 molecules of water are kinetically bound to each micellar Triton molecule at room temperature. Since the Triton molecule contains 10 ethylene oxide units, there are 10 ether oxygens which are capable of hydration. Each of these would accommodate about 2 water molecules so that approximately half of the bound water is actually hydrogen-bonded while half is trapped by these solvated tentacles extending into the solvent.

Weiden and Norton (3) have pointed out that as a third component such as benzene or phenol is added to nonionic detergent solutions, the cloud point is significantly lowered. This phenomenon was attributed to the decreased hydrophilic character of the detergent micelle resulting from the incorporation of the third component (or solubilizate). Livingston (4) suggested that pH may have an important effect on the cloud point lowering by phenols.

This paper presents experimental results on the effect of various additives on the cloud point of dilute aqueous solutions of Triton X-100.

EXPERIMENTAL

Triton X-100 was used as received from the Rohm and Haas Company, who offer this material as an essentially 100% active agent. Anionic and other nonionic surface-active agents were also the unmodified commercial preparations. Solubilizates were either distilled commercial grade materials or Eastman white label stock. The salts were Baker and Adamson reagent grade.

Cloud points were measured in 4-dram screw cap vials. Approximately 12.5 g. of 2% detergent solution was weighed in, followed by varying small amounts of the third component. Free space in the vial was about 2 ml. For the electrolyte systems, stock salt solutions were prepared to which were added the required amount of Triton. In the case of Triton/water/ lodecane/ethylene dichloride systems, stock Triton/water/dodecane nixtures were prepared and agitated for 2 days on a shaker. Portions of this homogenized stock were weighed into the vials as above and weighed ımounts of ethylene dichloride were added as indicated.

The vial was attached horizontally to the shaft of a Müller Vibro Mixer Fisher Scientific Co.) by means of a special fixture devised from a hose lamp. The cloud point was determined while the vial was agitated in a emperature-controlled bath of dioctyl phthalate. The Vibro Mixer proided a 120 c.p.s. mechanical oscillation of variable (low) amplitude so

TABLE I

Cloud Point-Concentration Relationship for Triton X-100

Wt. % Triton	Cloud point, °C.
0.25	64
0.50	64
2.0	64
4.0	64
7.0	65
10.0	66
13.0	67
16.0	68.5
20.0	70
33.0	76

that efficient mixing could be achieved during continuous observation of the tube contents. Temperature was regulated by a Cenco-deKhotinsky thermoregulator. The regulator was adjusted manually until a temperature just below the cloud point was reached. A slow and careful increase in temperature then permitted accurate observation of the point of clouding. Check determinations were run on each cloud point. In general, a system was observed to cloud about one degree higher on heating than it cleared on cooling. It is the higher temperature that was recorded as the cloud point.

The pH measurements were made on a Beckman Model G laboratory pH meter.

Results and Discussion

The cloud points of aqueous solutions of Triton X-100 are substantially constant over a wide concentration range as shown in Table I. The present study was made using 2% solutions unless otherwise indicated.

The precipitation of Triton molecules out of solution above the cloud point was demonstrated by holding a quantity of 2% Triton solution at 76°C. for 24 hours, whereupon it was found that a detergent-rich phase had separated. The top layer, 0.12 weight per cent in Triton, weighed about 17 times as much as the bottom layer, which was 32.6 weight per cent in Triton. The upper layer, displaying no cloud point under 100°C., was probably made up largely of the higher polyethylene oxide fractions of this normally polydisperse product. The concentrated layer had a sharp cloud point at 76°C. Prolonged heating at a higher temperature might effect a more complete separation of Triton from solution. Fineman and co-workers (5) have shown that foaming of this type of agent decreases sharply above the cloud point owing to separation of the solute.

When a solubilizate such as benzene is added to the Triton solution, as shown in Fig. 1, the cloud point is depressed. Other aromatics such as phenol and aniline likewise cause the cloud point to be lowered. This

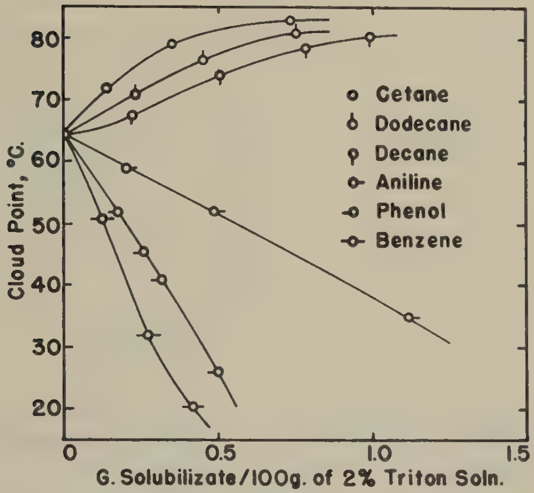

FIG. 1. The effect of solubilizates on the cloud point of 2% Triton X-100 solutions.

property of cloud point lowering is useful in a practical way in determining the apparent cloud points of very hydrophilic nonionic emulsifiers. Since the cloud points of such materials may exceed the boiling point of the solution, the direct measurement is experimentally inconvenient. By adding in increments a material such as benzene, a cloud point exceeding 100°C. may be determined from measurements at lower temperatures by extrapolation of the cloud point depression curve to zero solubilizate concentration.

A system which was 2% in Triton and contained 0.483 weight per cent phenol exhibited a cloud point of 24.5°C. Upon standing at room temperature for 1 day, a phase separation occurred. The volume of the upper layer was estimated to be 12 times that of the lower layer. The cloud points of the layers were 34° and 62°C., respectively. Analytical data on the composition of each phase are required before further interpretation of this phenomenon can be made since, as pointed out by Weiden and Norton (3) and as shown in Fig. 2 for ethylene dichloride, a given amount of solubilizate produces a greater lowering in cloud point for a dilute Triton solution than for a more concentrated one.

The presence of phenol in both layers of the Triton/phenol system was demonstrated by adding ferric chloride which reacts with phenol in aqueous solution to produce a blue coloration. Since the coloration in the top layer was extremely slight, it was concluded that both the phenol and the Triton were concentrated in the bottom layer. In a similar experiment with Triton and sodium sulfate, the volume ratio of the layers was reversed. In this case the bottom layer was the larger. The presence of salt

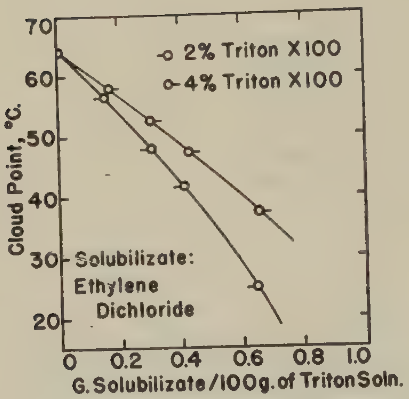

FIG. 2

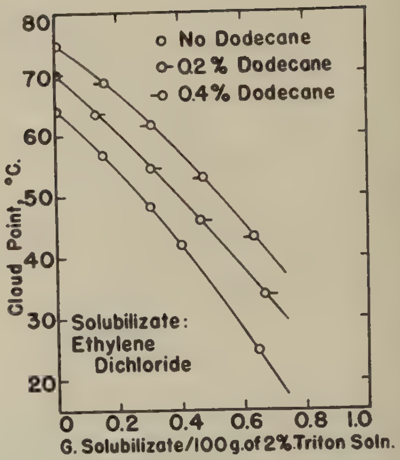

FIG. 3

FIG. 2. The effect of emulsifier concentration on the cloud point lowering by a solubilizate.

FIG. 3. The additivity of cloud point effects.

in both layers was indicated by the addition of barium chloride solution. The partition of Triton was not determined.

The ability to change the cloud point is not confined to aromatics, although from the limited amount of data reported here it would appear that they are particularly active. It is seen in Fig. 1 that not only do added solubilizates effect a decrease but also some solubilizates can bring about an increase in the cloud point of Triton X-100 solutions. No adequate explanation of this phenomenon can be offered at this time. It is interesting to note, as in Fig. 3, that the effects are additive. That is, the addition of dodecane to the Triton/ethylene dichloride system serves to displace upwards the normal cloud point depression curve.

The ability of the longer chain hydrocarbons to elevate the cloud point of Triton solutions increases as a function of hydrocarbon chain length. This is seen in Fig. 1 and even more clearly in Fig. 4, where the cloud point function for 19 solubilizates is plotted against concentration. For the higher molecular weight hydrocarbons, the cloud point curves level off at solubilizate concentrations of 1% or less. Increased polarity arising from the introduction of a double bond serves to decrease the ability of the solubilizate to elevate the cloud point. This is seen in a comparison of tetradecene-1 with the other hydrocarbons in Fig. 4. The unsaturated C_{14} chain is less active in elevating the cloud point than is the saturated C_{10} material. The curve for C_{14} mercaptan lies below the curve for tetradecene-1. This provides a direct comparison between two types of polar groupings. The introduction of sufficient polarity in the solubilizate may even serve

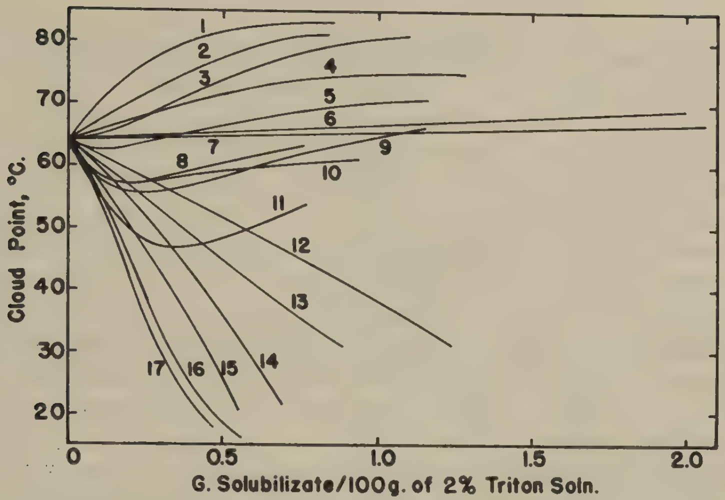

FIG. 4. The effect of solubilizates on the cloud point of 2% Triton X-100 solutions. Solubilizates: 1. Cetane; 2. Dodecane; 3. Decane; 4. Tetradecene-1; 5. *n*-Tetradecyl mercaptan; 6. Acetone; 7. Citric acid; 8. *n*-Octene; 9. Hexane; 10. 2-Ethyl hexene; 11. Cyclohexane; 12. Aniline; 13. Butyl acetate; 14. Ethylene dichloride; 14. Phenol and oleic acid; 16. Lauryl alcohol and nitrobenzene; 17. Benzene.

to reverse the effect of the solubilizate on the cloud point. For example, oleic acid, which contains both double bond and carboxyl grouping, lowers the cloud point significantly at all measured concentrations. Similarly, the polar alcohol group shifts the curve downward as may be observed by comparing lauryl alcohol with dodecane. Esters likewise depress the cloud point as seen in the case of butyl acetate. The effect of a ketone group is intermediate. Acetone causes a gradual increase in cloud point as does methyl ethyl ketone, the curve for which, although not shown, is almost flat and lies just below the one shown for acetone. Thus the polarity argument appears to be a reasonably consistent one in the case of the aliphatics. The fact that fewer data are available on aromatics does not permit one to carry this point of view forward for that class of compounds. It is to be noted, however, that benzene sharply depresses the cloud point.

The influence of solubilizate polarity on the magnitude of the cloud point lowering might be partly rationalized as follows. Nonpolar solubilizates are held tightly in the interior of the micelles where the immediate environment is likewise nonpolar. More polar solubilizates are also held in the oil soluble micelle center but are held there less tightly and would tend to migrate toward the outside owing to the polar attraction of the polyethylene oxide chains. This decreases the hydrophilic nature of the nearest ethylene oxide units which results in a loss of some hydration. The net effect might then be to make the system resemble an emulsifier with a shorter ethylene oxide chain, i.e., the cloud point is lowered. As more and more solubilizate is introduced, more and more hydrogen-bonded water molecules are released to the environment until the point is reached where the entire emulsifier molecule finds itself in an atmosphere sufficiently rich in solubilizate that the system remains turbid at all temperatures. This extreme state is real and places a limitation on the amount of solubilizate which can be added to the Triton system to produce sharp cloud points. Even before this point is reached, the cloud points tend to be more and more diffuse at higher solubilizate concentrations. The turbidity at high solubilizate concentrations may also be due in part to droplets of excess solubilizate, particularly at the lower temperatures. This explanation does not, of course, account for an increase in cloud point as a function of added solubilizate nor does it render the appearance of a minimum in the curve more understandable.

The effect of cyclization is shown in a comparison of hexane with cyclohexane in Fig. 4. The initial slope of the cyclohexane curve is greater than that for hexane, although both exhibit the same general characteristics. The cyclohexane curve is intermediate between the hexane and the benzene curves. Little effect can be attributed to chain branching as is seen in a comparison of *n*-octene with 2-ethyl hexene. The branched chain has the slightly lower cloud point curve.

The suggestion by Livingston (4) that the cloud point function may be pH-sensitive has been examined. Measurements of pH were made on samples of the phenol/Triton system where, as expected, the pH decreases as phenol concentration increases. This is shown in Table II. The influence of pH on the cloud point was then determined by measuring the cloud point of 2% Triton in disodium phosphate/citric acid buffer mixtures with no added solubilizate. Figure 5 reveals the linear relationship obtained over a pH range of 2 to 9 units. The cloud point is seen to change 22°C. over

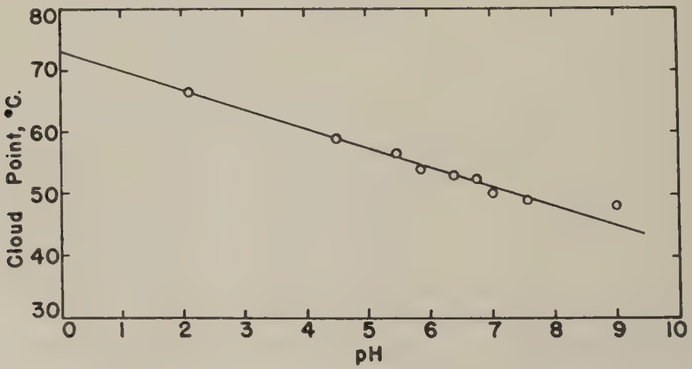

FIG. 5. The apparent variation of cloud point with pH of buffered 2% Triton X-100 solutions.

TABLE II

Cloud Point and pH of the Phenol/Triton System

g. phenol/100 g. 2% Triton soln.	pH	C.P., °C.
0	6.73	64
0.1778	6.83	52
0.2606	6.60	45.5
0.3198	6.55	41
0.4963	6.40	26
0.5984	6.32	18

TABLE III

Contributions of Buffer Components to the Cloud Point of Triton X-100

g. Na_2HPO_4/100 g. 2% Triton soln.	pH	C.P., °C.
0	6.73	64
0.4924	8.87	61
0.9711	8.98	58
1.450	8.92	55.5
1.943	9.00	52.5
2.65	9.00	48

g. citric acid/100 g. 2% Triton soln.	pH	C.P., °C.
0	6.73	64
0.5220	2.33	65
0.9844	2.20	65.5
1.459	2.10	66
1.90	2.10	66.5

the indicated pH range. Now the cloud point of an unbuffered 2% Triton solution is 64°C. and its pH is 6.7. At this pH, Fig. 5 indicates a cloud point of 52°C. This clearly implies the existence of a salt effect on the cloud point.

Consequently, the effects of disodium phosphate and citric acid on the cloud point of Triton X-100 solutions were measured separately. As seen in Table III, the solutions containing phosphate cover a wide range in cloud point variation while the pH of these solutions varies less than two tenths of a pH unit. Citric acid causes a very slight increase in cloud point and the pH values are, of course, very low. In both cases, the cloud point is a linear function of the concentration of the added third component. From these two curves it may be shown that the cloud point functions for citric acid and disodium phosphate are additive. That is, the cloud points for the buffer mixture can be calculated from the known individual contributions of the two components using a linear equation.

These facts strongly suggest that pH, of itself, does not directly affect the cloud point and solubility of nonionic emulsifiers of the polyethylene oxide type. According to Livingston (4), pH does affect the solubility of

TABLE IV

HCl/Triton Solutions

pH	C.P., °C.
1.4	64
3.0	64
5.2	64
7.2	64

phenols (or phenolates) which may therefore influence the magnitude of the effect of these materials on the cloud point.

It should be possible to separate pH effects, if they exist, from electrolyte effects on the cloud point if there were available a method to vary one without introducing effects from the other. This has been done by adding small amounts of hydrochloric acid to large volumes of 2% Triton solution so that the pH could be varied at extremely low electrolyte concentrations. The data in Table IV indicate that the total electrolyte concentration is the important variable. The pH has been varied over a six-unit range, yet the electrolyte level is, in all cases, too low to influence the cloud point.[1]

From the foregoing, it would appear then that a solubilizate may affect the water solubility of a nonionic emulsifier in either of two ways: (*a*) by changing the structure of the micelle by penetration or (*b*) by dissolving in the water phase and thus changing the environment of the micelles. For materials insoluble in water such as benzene and other hydrocarbons, mechanism (*a*) must apply. In the case of strong electrolytes (vide infra) and other water-soluble addends, mechanism (*b*) pertains. The work of Livingston (4) suggests that, for phenols, pH has an indirect effect on cloud point since, by changing pH, the water solubility of the phenol is influenced and hence an environmental change in the medium around the micelle is effected.

At the higher levels, salts exert a profound influence as may be seen in Fig. 6, where the cloud points of Triton solutions are plotted as a function of added electrolyte. Certain solution properties of nonelectrolytes, notably the activity coefficient, vary directly with the ionic strength of the medium rather than with the square root of the ionic strength as is the rule for electrolytes. It is interesting to note in this case that the cloud point curves for a nonionic emulsifier are linear in the ionic strength of the added electrolyte.

Comparing the monovalent cations, the effectiveness in cloud point lowering increases in the order lithium, sodium, and potassium for the case of the chlorides. This is the order of increasing ionic radii and there-

---

[1] This conclusion is, however, confused by the fact that the behavior of the nonionics in mineral acid solutions differs from their behavior in salt solutions. The ether linkages are weakly cationic and will form oxonium salts with mineral acids. These salts should be more water-soluble than the free nonionic emulsifier.

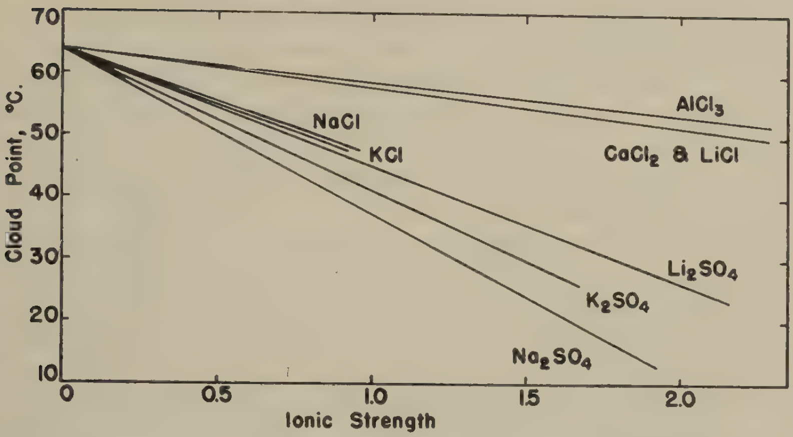

FIG. 6. The effect of electrolytes on the cloud point of 2% Triton X-100 solutions.

fore decreasing ion hydration. For the sulfates, the order of sodium and potassium is reversed. For the multivalent ions, calcium, with a larger crystallographic radius than aluminum, depresses the cloud point more at a given ionic strength, although the difference is not great. In view of the nature of this phenomenon, it would appear likely that the concepts of ion size and hydration should enter into the picture. However, the expected order is reversed.

Harned and Owen have summarized the results of several determinations of the activity coefficients of neutral molecules in aqueous salt solutions (6). Their data for the salt effects on the activity coefficients of nitrous oxide, ethylene, diacetone alcohol, and ethyl acetate bear marked similarity to the results reported here in several respects:

a. The logarithm of the activity coefficient is linear in the ionic strength of the medium.

b. The effects are in the same direction as the cloud point data. That is, increased salt concentration leads to decreased solubility of the nonionic solute.

c. The order of influence of the individual electrolytes is the same:

Order of Decreasing Log γ	Order of Decreasing Influence on Cloud Point
Na_2SO_4	Na_2SO_4
	K_2SO_4
	Li_2SO_4
NaCl	KCl, NaCl
KCl	
LiCl	LiCl, $CaCl_2$
$CaCl_2$	
$AlCl_3$	$AlCl_3$

Note, too, that the electrolyte series are oriented in the same direction, i.e., the same salts produce the most profound effects in each case. The great similarity in these effects on such dissimilar molecules should especially be noted. Harned and Owen proceed to point out that the electrostatic influence is an important part of the salting-out effect. The role of the ionic radius is confused, since the theoretical prediction of the order of effects does not agree with the observed results.

It is known that electrolytes tend to dehydrate lyophilic colloids. This salting-out effect of an ion is generally larger, the smaller its size and the greater the charge it carries. As pointed out above, this does not seem to be true for the Triton systems. The salting-out effect of an electrolyte has been attributed to the congregation of dipolar molecules of the polarizable solvent around the ions of the added electrolyte. Owing to this attraction between the ions and the solvent, there is a tendency for the solvent to displace a less polar solute from the vicinity of any particular ion. The observed decrease in solubility may thus be due to the preferential orientation of solvent molecules around the ions.

It is interesting to compare these results with those of Doscher, Myers, and Atkins (7), who measured the turbidities and viscosities of Triton solutions in the presence of added electrolyte. These workers report the order for cations of increasing effectiveness in raising turbidities to be lithium, potassium, and sodium. Aluminum was somewhat lower than calcium. If it may be assumed that the order of increasing turbidity should correspond in our case with the order of increasing effectiveness as a cloud point depressant, then our results are in agreement with those of Doscher *et al.*, with the exception of the sodium and potassium chlorides. These two curves on Fig. 6 are almost coincident, however, so that any disagreement is mild. The observed order of salting out for the alkali metal ions Na > K > Li does not agree with the lyotropic series in which lithium precedes sodium. The order for the anions is correct. It might be expected that the multivalent cations, aluminum and calcium, would be more effective than the monovalent alkali metal ions in salting out the Triton but this is contrary to experience. Doscher attributes this behavior to interaction of the multivalent metal ions with the polyethylene oxide chains of the nonionic detergent which produces a salting-in rather than a salting-out effect.

As was the case with the organic liquids, polarity is important among crystalline materials. Crystalline nonelectrolytes exert only mild effects on the cloud point. A solution that is 2% in Triton and 18% in sucrose clouds 1½ degrees lower than it would if there were no sucrose present. Moreover, for a less polar crystalline nonelectrolyte such as urea, the effect is reversed. A solution which is 2% in Triton and 20% in urea has a cloud point which lies 14°C. above the normal Triton cloud point.

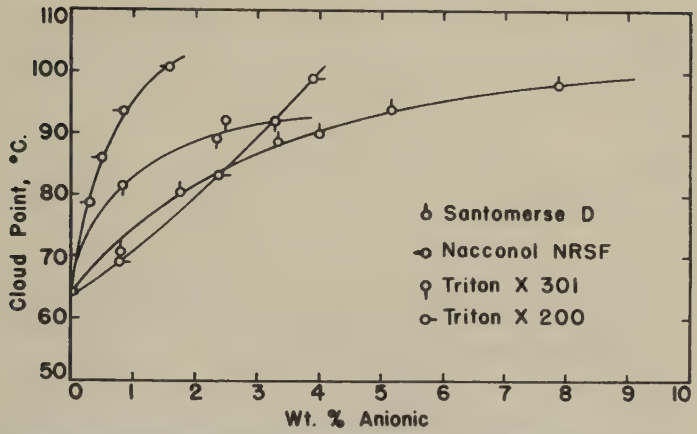

FIG. 7. The effect of anionic emulsifiers on the cloud points of dilute solutions of Triton X-100. (For an explanation of the abscissas, see text.)

Mixtures of nonionic and anionic surface-active agents are important in certain industrial applications. Thus, it is of interest to determine the extent to which the presence of an anionic material modifies the solubility behavior of the nonionic agent. Cloud point measurements were made on systems composed of mixtures of 2% solutions of Triton X-100 and several anionic materials. It was found that, in the absence of a solubilizate, small amounts of anionic agent raise the cloud point of the nonionic. The mixtures generally do not display the sharp cloud points characteristic of the Triton X-100 alone, but rather cloud over a 10°–20°C. temperature range so that it is often impossible to find the cloud point in the usual sense. It does prove to be possible in some cases to determine within 1°C. the temperature at which the mixtures start to cloud, i.e., a blue haze first appears. This has been done for the Triton X-100/Triton X-200 and the Triton X-100/Nacconol NRSF systems where, in Fig. 7, this apparent cloud point is plotted against the weight per cent anionic component in the anionic/nonionic mixture. It should be borne in mind that in all cases the total detergent concentration is 2%. It is to be understood that the point of complete turbidity lies some 10°–20°C. higher. For the Triton X-100/Santomerse D and Triton X-100/Triton X-301 systems, some turbidity existed over an extremely wide temperature range. In these instances, the temperature at which the system became opaque was recorded as the apparent cloud point. No attempt was made to complicate these systems further by adding a solubilizate. It is to be expected that this would render the cloud point even more diffuse and any significant measurement would be impossible.

It is suggested that the above phenomenon finds its basis in the formation of mixed micelles. That is, if anionic agents which, of course, have no

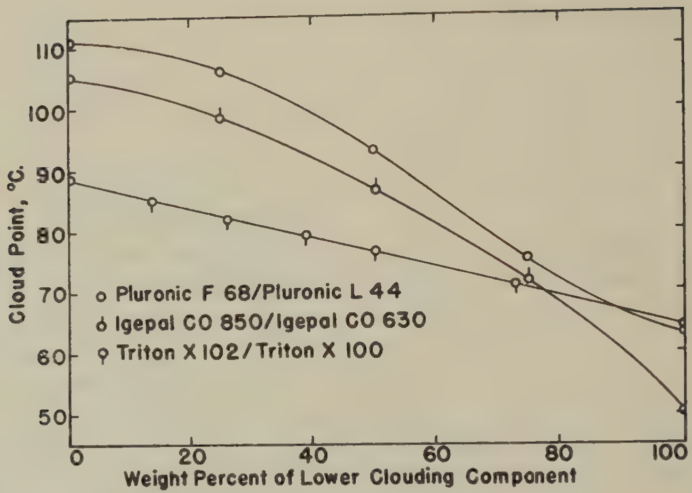

FIG. 8. The cloud points of mixed nonionic emulsifier solutions. Cloud points of 2% solutions of the pure components: Pluronic F68, 111°C.; Igepal CO850, 105°; Triton X-102, 88.5°; Pluronic L44, 63°.; Igepal CO630, 50°; Triton X-100, 64°.

cloud points, enter into the formation of micelles with the nonionic, rather than each molecular species forming its own type of micelle, then at temperatures exceeding the nonionic cloud point, the anionic serves as a solubilizer for the now insoluble nonionic. If each formed its own micelle, there is little reason to expect the cloud point to be greatly changed by the presence of the anionic material. On the other hand, it is unlikely that the two species enter micelles in any prescribed stoichiometric proportions so that some micelles contain higher proportions of the anionic than others, with the result that the solubility behavior of different mixed micelles in the same solution is different. This could explain the diffuse nature of the cloud point in these mixed systems. Lack of data on micelle formation in nonionic and mixed anionic/nonionic systems prevents a quantitative treatment of this phenomenon.

The dilute solution cloud point of a mixture of nonionic emulsifiers lies somewhere intermediate between the cloud points of the two components. The exact temperature at which the mixture clouds is dependent upon the relative amounts of each component present. The variation is linear for the case of mixtures of 2% solutions of Triton X-100 and Triton X-102. These two materials are identical except that Triton X-102 contains on the average, 2–4 more ethylene oxide units per chain than does Triton X-100. Two cases of positive deviation from additivity are also to be seen in Fig. 8 for the Pluronic and Igepal mixtures. Components in each of these pairs differ only in polyethylene oxide content. This behavior gives some indication of the manner in which the cloud point of a polydisperse nonionic emulsifier could be influenced by the type of molecular weight distribution which characterized it. It is quite apparent that long polyethylene oxide chains successfully solubilize the shorter homologues.

ACKNOWLEDGMENT

The helpful assistance of T. W. Hughes, who performed many of the measurements, is gratefully acknowledged.

REFERENCES

1. MAYHEW, R. L., AND HYATT, R. C., *J. Am. Oil Chemist's Soc.* **29**, 357 (1952).
2. KUSHNER, L. M., AND HUBBARD, W. D., *J. Phys. Chem.* **58**, 1163 (1954).
3. WEIDEN, M. H. J., AND NORTON, L. B., *J. Colloid Sci.* **8**, 606 (1953).
4. LIVINGSTON, H. K., *J. Colloid Sci.* **9**, 365 (1954).
5. FINEMAN, M. N., BROWN, G. L., AND MYERS, R. J., *J. Phys. Chem.* **56**, 963 (1953).
6. HARNED, H. S., AND OWEN, B. B., "The Physical Chemistry of Electrolytic Solutions," p. 398. Reinhold, New York, 1950.
7. DOSCHER, T. M., MYERS, G. E., AND ATKINS, JR., D. C., *J. Colloid Sci.* **6**, 223 (1951).

JOURNAL OF COLLOID SCIENCE 11, 286–287 (1956)

LETTER TO THE EDITORS

ON A HIDDEN ASSUMPTION IN THE STATISTICAL THEORY OF ION EXCHANGE OF DAVIS AND RIBLE

In 1950 Davis (1) and Davis and Rible (2) published a statistical treatment of ion exchange equilibria in systems involving polyvalent ions analogous to Guggenheim's treatment of mixtures with zero energies of mixing (3). Attention should be drawn to the fact that in the calculation of the value for q both Davis and Rible and Guggenheim tacitly assume that no site has two neighbors that are nearest neighbors one of another at the same time. In paragraph 9 of his article Guggenheim hints at this inaccuracy, which he considers to be small in three-dimensional arrays. Of the two-dimensional arrays the triangular array ($z = 6$), which possesses the above characteristics, corresponds with atomic configurations in silicate minerals, for example, and is mentioned by Davis among the three most probable cases (1).

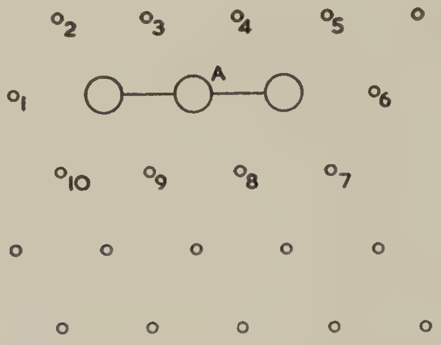

Placing a triatomic linear molecule or a trivalent ion A on a triangular array one can count 10 sites adjacent to A, whereas Guggenheim's formula (2.1) gives $qz = 14$. If one chooses to include one of the sites 3, 4, 8, or 9, one mode only remains in two of the three lines through the chosen site for placing a second trivalent ion; on the third line parallel to A all three modes remain. So for these four sites $m_J = (2 + 3)/9 = 5/9$ and $q_J = 5/3$, whereas formula (7) of Davis and Rible gives $q_J = 7/3$.

Although there may be some doubt as to the validity of the theoretical considerations, the formulas obtained give a good description of the experimental results, as was shown by Krishnamoorty and Overstreet (5). Their experiments also fit the "statistical formulas" better than the description by means of "equivalent percentages", proposed by Kressman and Kitchener (4).

REFERENCES

1. DAVIS, L. E., *J. Colloid Sci.* **5**, 71 (1950).
2. DAVIS, L. E., AND RIBLE, J. M., *J. Colloid Sci.* **5**, 81 (1950).
3. GUGGENHEIM, E. A., *Proc. Roy. Soc. (London)* **A 183**, 203 (1944).
4. KRESSMAN, T. R. E., AND KITCHENER, J. A., *J. Chem. Soc.* **1949**, 1201.
5. KRISHNAMOORTY, C., AND OVERSTREET, R., *Soil Sci.* **69**, 41 (1949).

Laboratory of Agricultural Chemistry,
Agricultural University,
Wageningen, Netherlands

Received February 20, 1956

A. H. BLOKSMA

JOURNAL OF COLLOID SCIENCE **11,** 288–293 (1956)

BOOK REVIEWS

Handbook of Hydrocarbons. By S. W. Ferris, Sun Oil Company, Marcus Hook, Pennsylvania. Academic Press Inc., New York, 1955. 324 pp. Price $8.50.

Table A (19 pages) lists 675 hydrocarbons in order of their boiling points. In Table B they are arranged in groups of the same empirical formula and same type (alkane, alkene, etc.) with 752 references to the original literature.

Table C gives the alternate names for these hydrocarbons with a key to Table B. Table D gives formulas for the cyclic hydrocarbons.

This compilation should be very useful to anyone working in the oil industry.

Victor K. La Mer, New York, New York

Physicochemical Calculations. By E. A. Guggenheim and J. E. Prue. Interscience Publishers, Inc., New York, 1955. xii, 491 pp. Price $7.

This book is the result of the authors' recognition of the need for "an up-to-date and representative collection of material with which to illustrate instruction in . . . many important fields of experimental work . . . unsuited to the teaching laboratory." The book contains 171 problems which have been based upon publications in physical chemistry and chemical physics, much of which is recent. The selection is diversified and is grouped as follows:

Atomic and Molecular Weights
Avogadro's Number
Molecular Velocities
Interatomic Distances
Moments of Inertia
Characteristic Frequencies
Electric Moments and Polarizabilities
Energies and Enthalpies
Entropies
Heat Capacities
Equation of State
Mixtures of Non-Electrolytes
Electrolyte Solutions
Conductance and Diffusion of Electrolytes
Gaseous Equilibria
Chemical Equilibria Involving Solids
Solution Equilibria
Acid-Base Equilibria
General Electrolyte Equilibria
Solid Surfaces
Liquid Surfaces
Gas Kinetics
Solution Kinetics
Radioactivity.

The object of each problem is first concisely stated and each is further divided into four sections as follows:

1. Data, including detailed reference to the sources.
2. Introduction, in which a brief outline of theory and method of calculation are given.
3. Calculation—in which a complete numerical calculation is presented with units clearly indicated.
4. Discussion—in which brief but enlightening remarks assess the results and relate them to other work when possible.

The problems are on an advanced level and are suited for review or instruction in graduate work, but many of them are also suitable for use in the more comprehensive undergraduate courses in physical chemistry being given in many colleges and universities. The complete numerical solutions are especially valuable for those using the book for self-instruction.

Since the value of such a book as a teaching aid is greatly enhanced if the student (or teacher) first reviews theory in a suitable text in cases where it is not familiar, the addition of text book references (where possible), for persons of limited background, would have been an extra convenience.

R. H. Smellie, Jr., Hartford, Connecticut

Electrolyte Solutions. The Measurement and Interpretation of Conductance, Chemical Potential and Diffusion. By R. A. Robinson, D.Sc., Ph.D., F.R.I.C., Professor of Chemistry, University of Malaya, Singapore, and R. H. Stokes, Ph.D., D.Sc., F.R.A.C.I., A.R.I.C., Reader in Physical Chemistry, University of Western Australia. Academic Press Inc., 125 East 23rd Street, New York 10, N. Y., 1955. xiii + 512 pp., 15 × 22.5 cm. Price $9.50.

The subtitle indicates a vertical division into three fields and a horizontal division into two stages. The level of the target reader seems to be the student who has had a first course in physical chemistry which omitted the study of electrolytes, but any more advanced reader will also find much to interest him.

Measurement can also be divided into two stages, obtaining numbers in the laboratory, and converting them into usable numbers. The first of these is the best handled part of the book, and a laudable effort is made to play up those workers who have specialized in the development and use of extremely precise apparatus but who have not contributed to interpretation. For most measurements the reader can understand the principles from the text and can find the details of the best techniques from the references. Many of the more useful results are given in the appendices.

There are a few surprising lapses, of which I give two examples. Almost a page (198) is given to a discussion of the measurements of the electromotive force of the cell H_2 | HCl | AgCl | Ag in the thesis of N. J. Anderson with T. F. Young, which is not available to most readers, but the discussion is limited to the fact that AgCl reacts at the platinum electrode. This is due to the unorthodox cell, in which all components were present at each electrode, which is probably completely unusable with any other system. No mention is made of the extreme precision of the results, which may also depend on the unorthodox cell, or of the fact that Anderson agrees with Carmody in obtaining a potential 0.2 mv. lower than the accepted value of less careful workers.

More important is the erroneous statement (p. 24) that deviation from the perfect gas law is unimportant if "the vapour pressures of solution and solvent are always of similar magnitude." The fact is that if ln a_A is replaced by ln p_A/p_A^0 the resulting osmotic coefficient does not approach unity at zero concentration unless the vapor is a perfect gas. It follows naturally that they do not discuss corrections to the vapor pressure measurements for deviations from the perfect gas laws, and do not mention the important fact that in their comparative measurements, the activity of the water, as well as its pressure, is the same as in the standard solution. This is one reason why we prefer the older term, "isotonic," which Bousefield rejected in favor of "isopiestic" because to him "isotonic" connoted ideal solutions.

It is surprising to read a discussion of diffusion which does not mention Einstein, but his contributions are given. It is surprising to me to read a discussion of electrolytes which names Kirkwood only in connection with the theory of dielectrics. Kirkwood's more direct contributions are not mentioned.

The phenomena of electrolyte solutions must be interpreted by a combination of the physical and the chemical approaches. Many of the phenomena may be explained either way. An example is "salting out" which may be attributed to decrease in dielectric constant by the material salted out, or to removal of the solvent by chemical reaction with the material which salts out. If expression of the phenomena in chemical terms is included in chemical interpretation, this book represents the extreme in that direction. The existence of equivalent physical approaches is often not even suggested.

The statistical entropy in terms of volume fractions (Flory-Huggins, or free-volume) is discussed, but only the statistical entropy in terms of mole fractions (ideal) is used. The Debye theory is used in the form applicable to solutions of rigid, spherical ions, all of the same size, which do not alter the dielectric constant or the volume of the solution. All the rest of the free energy of mixing is attributed to solvation, with equilibrium constant so large that the solvation is independent of the concentration, or to association, although Bjerrum's physical interpretation of association is discussed at length.

There is no mention of the treatment of ions of different sizes or those with nonspherical symmetry. This omission and the discussion of the higher approximations of the Boltzmann exponential run the danger of leading the unwary reader to two dangerous pitfalls. The first is failure to see that ignoring an effect is as definite an assumption about it as determining it by even a crude approximation, and is often a much worse one. The second is an obsession about nonintegrability, or lack of linear superposition. The application of the Debye method to the higher terms in the Boltzmann exponential does involve nonintegrability, and the same difficulty may affect other extensions, but it does not influence the terms proportional to the concentration and is probably always less serious than other approximations. The method of Mayer is discussed, but no mention is made of the fact that this method avoids the difficulties of nonintegrability.

The choice of Bjerrum's method of treating the higher approximations as association may be justified because it is easily extended to other kinds of association. The reader is worried unnecessarily as to whether Bjerrum chose the equilibrium constant well. This constant must agree with the second osmotic virial coefficient, which has been calculated by Gronwall, LaMer, and Sandved, by Kirkwood, and by Mayer with three quite different approaches. All give the same answer, but Kirkwood's expression is more convenient.

A chemical interpretation of hydration must attribute to each ion a hydration number which is an integer and independent of the ions with which it is associated. The numbers obtained by the authors obey neither of these criteria. Glueckauf (*Trans. Faraday Soc.* **51**, 1235 (1955)) has recently applied volume-fraction statistics to this problem and in the electrostatic treatment has assumed that the anhydrous component, not the hydrated ions, does not change the volume of the solution, but uses otherwise the same simplified form used here. He obtains hydration numbers about half those found by Robinson and Stokes. For the alkali and alkaline earth halides he gets integers to about ¼ mole per mole, which is closely that of random numbers, and additivity to about ¼ mole per mole. Of course the anhydrous component also has volume, and electrolytes do affect the dielectric constant. Consideration of these factors will lead to different values of the hydration numbers. A reader who does not like any of these numbers may turn to the salting out of nonelectrolytes and to transport properties, where he will find a large variety.

Space is lacking to discuss properly the treatments of conductance and of diffusion. If read with a proper disrespect for the hydration numbers, the whole book should be interesting and instructive to either a newcomer or the more advanced reader.

George Scatchard, Cambridge, Mass.

Ultrasonic Engineering with Particular Reference to High Power Applications. By Alan E. Crawford. Academic Press Inc., New York; Butterworths Scientific Publications, London, 1955. Volume 7, 344 pp. Price $8.

"In the past the subject of ultrasonics has been considered to be in the physicists' field of action; but with the advent of such established ultrasonic processes as metal coating and cleaning it must leave the laboratory and enter the province of the process engineer." . . . "The object of this book is to collect together and correlate the mass of data on applications and effects of ultrasonic waves, and to cover the basic methods of generation."

After defining his purposes in this manner, the author, who has considerable practical experience in ultrasonic engineering, presents a brief outline of the theory of ultrasonic waves and cavitation. A hundred-page discussion of sound generators follows; piezoelectric transducers, magnetostriction transducers and generators, jet generators, and electromagnetic transducers are treated clearly and competently.

The second half of the book deals with: precipitation and agglomeration; emulsification and dispersion; chemical applications; metallurgical applications; coating of metals; biological and medical applications; and ultrasonic instruments and control gear.

Of particular interest to the reader of this journal will be the sections on smoke, dust, and mist precipitation; agglomeration and precipitation in liquids; rheopexy and dilatancy; emulsification in liquid-in-liquid systems; dispersion of solids-in-liquids; ore separation; ultrasonic action on sediments, precipitates, and gels; liquid-in-gas systems; ultrasonic cleaning; surface treatment of metals, ultrasonic soldering, and tinning; polymerization, depolymerization; also, the chapter on ultrasonics in biology and medicine, which, however, gives barely an outline of these vast, very complex, and potentially very useful fields of work.

Ultrasonic Engineering would be more useful to the reader (and fairer to many investigators in these fields) if the references to the literature were considerably more numerous and, in some instances, more accurate. Likewise, many a reader undoubtedly would be grateful for information on the range of the proven usefulness of the numerous and widely varied processes which have been described in the literature, and for an evaluation of their economics.

In spite of these minor shortcomings, this competent, unpretentious, easily readable, well-printed, and pleasantly made book is a most useful addition to the literature. It will be welcome to all those who want to acquaint themselves in a convenient manner with the rapidly expanding field of ultrasonic engineering.

Karl Sollner, Bethesda, Md.

Ionography. Electrophoresis in Stabilized Media. By Hugh J. McDonald, D.Sc., Professor of Biochemistry, Stritch School of Medicine of Loyola University, Chicago, Ill. In collaboration with Robert J. Lappe, M.S., Research Assistant, Department of

Biochemistry, Loyola University; Edward P. Marbach, Ph.D., Associate Chemist, American Meat Institute Foundation and Research Associate (Instructor), Department of Biochemistry, University of Chicago; Robert H. Spitzer, M.S., Research Assistant, Department of Biochemistry, Loyola University; and Matthew C. Urbin, Ph.D., Associate Chemist, Chemical Division, Corn Products Refining Company, Argo, Ill. The Year Book Publishers, Inc., 200 East Illinois Street, Chicago 11, Ill., 1955. x + 268 pp. 14.5 × 22 cm. Price $6.50.

In the past five or six years, electrophoresis in stabilized media has become a research tool widely used by those interested in separation and identification of natural products. In addition to a discussion of the method, this book contains the first complete literature survey in this new field (865 references).

Included in this book are: a description of the types of apparatus used, discussions on nomenclature, experimental methods, and mobility determinations and their relation to mobilities determined by the moving boundary method. As pointed out in the preface, the principles shown are based mainly upon the authors' own experimental work using their apparatus (horizontal paper strip in a gas atmosphere); however, other techniques are discussed in some detail. The survey of the literature covers applications of the method to proteins, peptides, and amino acids; carbohydrates; lipoproteins; enzymes, hormones, and vitamins; inorganic substances and miscellaneous others. In this regard, the book is excellent.

There are, however, several points of discussion which do not contribute greatly to the value of this book. The experiments on the relationship of molecular weight to mobility described in the early part of the book go unexplained, and one must assume that some of the results are fortuitous. The lengthy criticism of the "tortuous path" theory of Kunkel and Tiselius and the development of their own "barrier" theory are not convincing. The term "thermodynamic activity" is used in an unfortunate way, leaving the reader quite dubious as to the validity of the equations developed and of the theory itself. Although it appears unlikely that any one term to describe electrophoresis in stabilized media will be universally accepted, the authors encourage the use of the term "ionography" in preference to the quite commonly used "paper electrophoresis," "zone electrophoresis," "electrochromatography," and other similar terms.

There has certainly been need in this field for a thorough discussion of the various techniques and their applications, as well as a complete literature survey. *Ionography* satisfies this need well.

ROBERT R. BECKER, New York, New York

The Principles of Chemical Equilibrium. BY K. G. DENBIGH. New York: Cambridge University Press, 32 E. 57th St., 1955. xxi + 491 pp. Price $7.50.

This is essentially a textbook of chemical thermodynamics for students of chemistry and chemical engineering; a certain amount of molecular and kinetic theory is introduced, and Part III, 147 pages, is almost entirely devoted to statistical mechanics. The level is about that of first-year graduate students in American universities. There is only minor emphasis on specific problems of chemical engineering.

Part I, 108 pages, is devoted to the first and second laws, thermodynamic functions and formulas, development of partial molar quantities and chemical potential, etc. Part II, 223 pages, contains chapters on applications to gases and gas reaction equilibria, phase rule and phase equilibria, ideal and nonideal solutions, and reaction equilibria in solutions. The treatment is very largely in terms of the Gibbs chemical potential. Fugacity and activity are treated logically and well illustrated; electrical cells and electrolyte solutions in general receive only brief treatment.

In Part III, statistical mechanics is used as an introduction to theory of heat capacity of crystals, to presentation of the third law, and for brief treatment of "regular solutions" and of adsorption. The last chapter discusses kinetics. Many readers will deplore the very late introduction of the third law, which thus loses its perspective among the methods of calculating equilibrium constants. There is no mention of the enthalpy and free energy functions such as $(G^0 - H_0^0)/T$, although these are widely tabulated and are compiled from thermal as well as from statistical and spectroscopic data.

The book contains much well-written, provocative exposition and discussion. It is quite adequate in its applications of thermodynamics to the systems chosen. In comparison with the other leading books in its field it merits high rating. This is not to say that it does not also deserve severe criticism. For example, the treatment of heat theory and the second law is classical and sometimes lacking in logic; the usual confusion between "heat" and "thermal energy" is well maintained. There is pressure today, especially among the followers of Brønsted, to revise and extend the interpretation of the second law to cover all forms of energy. Work cannot be obtained from systems all of whose energy is equipotential; work can be expressed as the integral of a potential-quantity product, and entropy is the quantity term in thermal energy. The unique position of "heat" is not that it can be only in part converted to work, but that entropy can be created in irreversible processes.

In such respects Denbigh's book is quite disappointing. It is difficult to criticize individual statements when they are made from an outmoded point of view. As an example, it is pointed out (p. 21) that we do not expect a vessel of water to cool spontaneously while lifting a weight from the floor. It would seem equally important to point out that we do not expect to obtain electrical energy from two identical electrodes immersed in the same solution, or motion from a piston with the same gas pressure on both sides. We do not expect the vanes of a radiometer to turn if equally blackened and equally illuminated on all sides.

In discussing the oxidation of carbon (pp. 71–72) the author points out that ΔG and ΔH have nearly the same value, and that on combustion ". . . almost as much energy is obtained as heat as would have been obtained as work, if the process had been carried out reversibly. The wastefulness of the process is in the subsequent conversion of the thermal into mechanical energy." This reviewer disagrees; the wastefulness is in the irreversible combustion; heat and thermal energy are not the same thing. The viewpoint needs to be changed. In the combustion entropy has been created at a higher temperature and may now be degraded in potential. The thermal energy available depends on the temperature gradient available.

We must also object to certain statements about electrical cells (pp. 161–162). "The essential aspect of the cell is the fact that the equilibrium composition of the reaction system is not the same as it would be in the absence of a potential difference between the two electrodes; if the potential difference is E the reactants and products come to a certain state of equilibrium, whereas if the cell is short-circuited they come to a quite different state of equilibrium." Actually, of course, the contents of an electrical cell are never in a state of equilibrium; the materials are so chosen that reaction is negligible, a matter of kinetics, until the circuit is completed. In the example cited by Denbigh, hydrogen and mercurous chloride are quite capable of direct reaction, from a thermodynamic standpoint.

We repeat that this book compares very favorably with others in its field. The development and application of thermodynamic functions and formulas have much to recommend them. The book will be of best use under the guidance of an alert and experienced teacher.

Cecil V. King, New York, New York

ANNOUNCEMENT

The *Journal of Colloid Science* is preparing a special issue consisting of Numbers 4 and 5 of this Volume, dedicated to Sir Eric Rideal. This special issue will appear in September and will contain papers written by his friends and pupils as a tribute to his scientific achievement in the field of colloid science.

ERRATUM

Volume 11, Number 1, February, 1956. In the article entitled "A Spectrophotometric Method for the Determination of Cationic Detergents" by A. V. Few and R. H. Ottewill, the legend for Figure 1 on page 36 refers to Figure 3 on page 37. The legend for Figure 2 on page 37 refers to Figure 1 on page 36.

Eric K. Rideal

JOURNAL OF COLLOID SCIENCE **11**, 295 (1956)

Dedication

In 1924, Cambridge University established the first chair of Colloid Science and appointed Eric Rideal the Professor. He envisaged this new discipline as cutting across old barriers, and comprising those parts of science, ranging from meteorology through physics and chemistry to biology, which deal with systems in which surface energy arising from fine division becomes dominant. As the subject grew, it embraced the study of large kinetic units and their morphology.

It is fitting on the occasion of Sir Eric's retirement from active academic posts that the journal bearing the name of the science he has fostered should dedicate a special number contributed by the students he has stimulated and trained.

As Sir Eric's first postdoctoral student, I recall vividly the popular lecture he gave in Cambridge in 1922, entitled, "Measuring Molecules with a Meter Stick." He demonstrated on the lecture platform to the delight of his listeners, by using only the simplest equipment, how much could be learned first-hand about the sizes and shapes of molecules when spread as monolayers. My own present interest in surfaces stems in no small part from this enthusiastic and prophetic approach.

As Associate Editor, Sir Eric has given this journal valuable support and encouragement from the date of founding in 1946. The Editorial Staff and Publishers offer this issue as a token of appreciation for his untiring efforts in contributing to the success of the journal. It is our wish that Sir Eric continues to have happy years in which he can enjoy life and have the satisfaction of seeing his scientific offspring develop.

VICTOR K. LA MER
Editor-in-Chief

JOURNAL OF COLLOID SCIENCE **11**, 296–298 (1956)

Sir Eric Rideal—An Appreciation

Heredity, Sanderson's preparatory school at Oundle, and Cambridge in the late-classical period of J. J. Thomson served to mold and determine the future scientific career of Sir Eric Rideal. The processes of learning were complete by the time World War I broke out in the summer of 1914. The first academic year after the war Rideal spent in the University of Illinois. It was perhaps fortunate for England that a large state university contrasted so radically with Cambridge. Smoking, also, was, at that time, prohibited on the Illinois campus. Rideal found himself much more at home on the Princeton campus, which he visited several times during the year. He did not find in Princeton what proved later to be Princeton's principal asset to him. It was on the boat in 1920 returning to England that he first met the gracious Princeton lady who was subsequently to become his charming wife.

The threat of submarine warfare compelled England to take steps in 1916–17 to learn how the nitrogen of the air could be fixed and the ammonia converted to nitric acid. Rideal and Partington were withdrawn from the Somme barges where, as lieutenants in the Royal Engineers, they had supervised water supplies for the troops. Together they elucidated the catalytic ammonia oxidation process on platinum gauze and formulated pilot plant and production procedures. Greenwood had a small group of men working on synthesis proper, he being the only man with previous experience in high-pressure synthesis. The writer was assigned the task of learning how to produce the nitrogen-hydrogen mixture. Since this was a major fraction of the total cost from an economic standpoint, it was decided that Rideal should join in the effort. There ensued a happy, fruitful eighteen months of collaboration. A number of problems for the Army as well as in the production of synthesis gas were solved. We were dubbed the Siamese twins, and it would be difficult to decide who was responsible for this or that advance. And, together, during the same period, we wrote a book *Catalysis in Theory and Practice* to try to define a scientific content of the subject. A good friend who reviewed the book guessed which of us had written the individual chapters. His guess was wrong because he used the wrong measuring stick.

We parted company early in 1919, each resolved to find some more science to put into a second edition of the book if it should ever reach such a state. Rideal elected to pursue kinetics, the writer to concentrate on adsorption by catalysts. That was the way we started, but over the years we each crossed over from one domain to the other.

From these early years a few researches may be cited. With Hurst, Rideal examined the ratio CO:H_2 burnt in presence of copper catalysts promoted with palladium. With Norrish he studied the catalytic influence of oxygen in reaction at a liquid sulfur-hydrogen interface. Together, also, they studied the influence of surfaces on the reaction between ethylene and bromine vapor which indicated a nonhomogeneous process, catalyzed by glass, cetyl alcohol, or paraffin wax to varying degrees. With a joint study on the sensitization by chlorine of hydrogen-oxygen mixtures to visible light, Norrish was launched, as were so many of Rideal's subsequent students, on the pathway to academic honors and chairs of chemistry.

A new phase in Rideal's career was developing simultaneously which culminated in the newly established school and chair of Colloid Science at Cambridge. In 1924 he was examining the destruction of rennin at an air-liquid interface and with Schofield was examining mono-layers on water as two-dimensional gases. They showed that as the length of the hydrocarbon chains in the fatty acids increases, the lateral adhesion between the gaseous films in the surface increases. The measurements of surface pressure using the Langmuir trough led also to measurements of "surface potential," the contact potential between the liquid and air. Early measurements by Guyot and Frumkin gave place to the detailed studies of Schulman and Rideal (1931). They compared surface potentials with surface pressures and refined the techniques of the potential measurement.

Side by side with the work on surface films the work on solid surfaces was prosecuted vigorously. Undoubtedly the most important work in the Cambridge School in this period was the work initiated and carried through by Roberts on the adsorptive properties of clean tungsten filaments. This work ushered in an entirely new era in the investigation of metal surfaces. The incredibly accurate measurements of Roberts on flashed tungsten filaments indicating the rapidity of many processes of chemisorption on clean surface, the use of Pirani gauges for measuring adsorption at low pressures of the order of 10^{-5} mm., the use of the accommodation coefficient of helium and neon to follow the adsorption process, all these techniques opened up a new era in adsorption by metals which Beeck, Tompkins, and many others have developed from their original beginnings in Cambridge. In the early thirties the advent of deuterium opened up a new phase of kinetic studies both homogeneous and heterogeneous. Farkas and Melville as postdoctoral students in Rideal's laboratory made basic advances in this area. The existence of isotopic exchange side by side with hydrogenation of ethylene was a major result from these studies.

Toward the end of the 1930's the study of reactions in surface films was in full swing including physical processes of adsorption and penetration as well as chemical reactions proper. Differences of penetration by sodium cetyl sulfate with films of cholesterol and cholesterol acetate had significance in the interpretation of biological processes as, for example, blood lyses. Interaction between amine films and a soluble acid substance, e.g., phenol, gave no change in surface pressure but change in the dipole moment vector. Dihydroxy phenols could give rise to cross-linking. Hydrolysis of esters was followed by change in surface potential as well as surface area. The oxidation of the double bond in oleic acid films with dissolved permanganate was shown to be a function of surface pressure; at low pressures the double bond was in the surface layer and oxidizable, at high pressures it was squeezed out of the surface and lined up in the hydrocarbon chain, inaccessible to the oxidant.

During World War II Rideal was engaged once more in scientific service to his country, this time at a high level of responsibility. Physical chemists have reason for gratitude to him also for his Presidency of the Faraday Society continuously during all the long war years. This unique record is paralleled by his Presidency both of the Chemical Society and of the Society of Chemical Industry, surely a trio of honors not achieved by any other. The Professorship in Colloid Science lasted from 1930 to 1946, when Rideal succeeded Sir William Bragg and followed in the footsteps of Davy and Faraday as Fullerian Professor of Chemistry in the Royal Institution and Director of the Davy-Faraday Laboratory. This phase lasted three years, from 1946 to 1949. One suspects that the erstwhile Cambridge don missed the youth and vitality of the undergraduate. He returned to university work as Professor of Physical Chemistry at King's College, London, from 1950 until his retirement in 1955. It is impossible to think of Rideal away from a laboratory and so, even in his retirement, he will be found in a small group of laboratories, with an assistant or two, at Imperial College, London.

In his Sabatier lecture to the Society of Chemical Industry in 1943 Rideal suggested a mechanism of interaction between a van der Waals layer and a chemisorbed layer on surfaces. As the Rideal-Eley mechanism this theory has been competitive with that originally put forward by Langmuir, in which both reactants occupy competitively the chemisorbed layer. Later work of Rideal with Trapnell on evaporated tungsten films appears to favor the Langmuir concept but the two views are still much debated. The last five years of research have been as bewilderingly diversified as any of the periods in his active life which preceded it. Two or more generations of physical chemists now working in all the five continents testify to the breadth and range of his mind and the vitality which even physical disabilities or administrative difficulties could not quench. His life of service to physical chemical and colloid science has earned the gratitude that is written into these tributes from his friends. *Ad multos annos.*

Hugh Taylor

April 7, 1956

JOURNAL OF COLLOID SCIENCE **11**, 299–307 (1956)

DRAINAGE OF LIQUID FROM SURFACES OF DIFFERENT RUGOSITIES

J. J. Bikerman

Department of Civil and Sanitary Engineering, Massachusetts Institute of Technology, Cambridge, Massachusetts

Received March 26, 1956

I. INTRODUCTION

In 1950 the effect of surface roughness on sliding of drops along a solid surface was studied (1); in this paper, rugosity is correlated with the rate of drainage of liquid present as a continuous sheet.

Stainless steel plates of six standard finishes were coated with oil and suspended vertically. The amount of oil remaining on a plate was measured after suitable time intervals by weighing the plate on an analytical balance. The relation between this amount and the average height (h_{rms}) of surface hills, as determined by two commercial stylus instruments, was ascertained; at a first approximation, the liquid drained at such a rate as if a layer, h_{rms} thick and adjacent to the solid, did not participate in the flow.

II. THEORY OF THE METHOD

As long as the liquid has a Newtonian viscosity, the theory is simple and to a considerable extent known (2, 3).

The shaded portion of Fig. 1 represents the plate. Here δ is the variable thickness of the oil film. The coordinate h is vertical and directed downward, and the coordinate x is normal to the plate and directed from the plate into the liquid.

If u is the velocity of liquid at a given point at a given moment, η is viscosity, g acceleration due to gravity, ρ the density of liquid minus the density of air, and $n = g\rho/\eta$, then, in analogy to the formula for the flow between two parallel walls,

$$u = n\delta x - \frac{n}{2} x^2, \qquad [1]$$

and the volume draining down in unit time for unit width of the plate is

$$\int_0^\delta u \, dx = \frac{n}{3} \delta^3. \qquad [2]$$

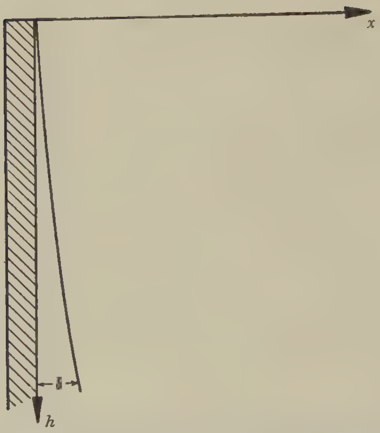

FIG. 1. Diagram of a plate (shaded) with oil draining from it; x is distance from the solid-liquid interface, δ thickness of the liquid film, h distance from the top of the film.

At a given h, the change of thickness in time, i.e., $\partial\delta/\partial\tau$, is equal to the volume of liquid (per unit width) entering, minus the volume leaving the space between the levels h and $h + dh$ in unit time. Thus,

$$\frac{\partial\delta}{\partial\tau} = -n\delta^2\frac{\partial\delta}{\partial h}. \qquad [3]$$

From the theory of partial derivatives

$$\left(\frac{\partial h}{\partial\tau}\right)_\delta = -\frac{(\partial\delta/\partial\tau)_h}{(\partial\delta/\partial h)_\tau} = n\delta^2. \qquad [4]$$

Hence, for a constant δ,

$$\int dh = n\delta^2\int d\tau.$$

The constant of integration is zero, if at zero time the liquid is gathered near $h = 0$; hence,

$$h = n\delta^2\tau, \text{ i. e., } \qquad \delta = \left(\frac{h}{n\tau}\right)^{1/2} \qquad [5]$$

Thus, an equation is arrived at which has been derived previously (2) by means of a guess and dimensional analysis.

Substitution of [5] into [2] and introduction of the letter w for the width of the plate gives Eq. [6] for the volume of liquid which passes downward through any level in unit time:

$$-\frac{dV}{d\tau} = \frac{nw}{3}\delta^3 = \frac{wh^{3/2}}{3n^{1/2}\tau^{3/2}}; \qquad [6]$$

V is the volume of liquid present on the plate. If the height of the wetted part of the plate is H, the volume of liquid reaching the bottom of the plate in unit time is $wH^{3/2}/3n^{1/2}\tau^{3/2}$ and the volume retained after time τ is

$$V = V_0 - \frac{wH^{3/2}}{3n^{1/2}} \int_{\tau_0}^{\tau} \tau^{-3/2}\, d\tau = V_0 - \frac{2wH^{3/2}}{3n^{1/2}} (\tau_0^{-1/2} - \tau^{-1/2}). \qquad [7]$$

At the first glance it would seem natural to set zero time as the lower limit of integration. However, Eq. [1] neglects the inertia terms and thus cannot be true at the start of the experiment; also some time must pass before the liquid profile (initially determined by the mode of application of the film) acquires the shape defined by Eq. [5]. Thus, in theory, τ_0 is the time needed for Eq. [5] to become correct. In practice, τ_0 was taken to be 30 min. for the more viscous, and 10 min. for the less viscous, oil. Volume V_0 is that present on the plate at time τ_0. As, theoretically, no oil remains on the plate after an infinite time,

$$V_0 = \frac{2wH^{3/2}}{3n^{1/2}\tau_0^{1/2}} \qquad [8]$$

and

$$V = \frac{2wH^{3/2}}{3n^{1/2}\tau^{1/2}}. \qquad [9]$$

III. Experimental Procedure

Nine plates of stainless steel (austenitic 18-8, Type 302) were used. Their finish numbers and the height h_{rms} of surface hills (for the definition of h_{rms} see, e.g., ref. 5) are shown in Table I. Before each experiment they were twice degreased in freshly distilled trichloroethylene.

Two oil samples were employed. The vacuum oil had density 0.893 g./cm.^{3}; its viscosity was 7.40 g./cm.sec. at 25°C. and 9.35 g./cm.sec. at 21°C. The medicinal liquid paraffin had density 0.856 and its viscosity at 21°C. was 1.95 g./cm.sec.

As only one side of each plate had a definite finish, this side only was used. The plates were laid horizontally on the unfinished face, and oil was

TABLE I

Height h_{rms} of Surface Hills, in microns

	Plates, 5 cm. wide						Plates, 7.5 cm. wide		
Finish No.	1	2D	2B	4	6	7	2D	2B	4
Previous determination	3.15	0.91	0.33	0.038	0.094	0.025			
New determination	3.83	0.94	0.17	0.043	0.102	0.030	0.28	0.12	0.05

poured on them first so as to wet the whole (or almost the whole) working surface (5.0 x 4.7 cm. for the smaller and 7.5 x 8.1 cm. for the larger plates), while the rest of the oil was put next to the upper edge of the wetted area to satisfy the conditions of integration leading to Eq. [5]. About 0.15 g. oil was put on the small, and about 0.60 g. on the large, plates; in agreement with Eq. [7], no effect of the initial volume could be discerned. Then the plates were suspended vertically in a desiccator (to protect them from dust) in such a manner that the lower portion of the wetted side was in contact with a porous clay wafer covered with filter paper; in this way the oil, instead of accumulating as a cylindrical drop at the bottom edge of each plate, was taken up by the bibulous material as soon as it reached the level of the filter paper. The plates, with the oil on them, were then weighed on an analytical balance at suitable intervals.

IV. EXPERIMENTAL RESULTS

Only the results of the last four series, each performed twice, are reported here. In the expression for V (see Eq. [9]) w and H were varied by using plates of two different sizes, and n was varied by using two different liquids and, for one of the liquids, two different temperatures. The small plates having finishes 4 and 6 were not used in these series, as previous experiments showed that they behaved very similarly (but a little more erratically) to finish 7.

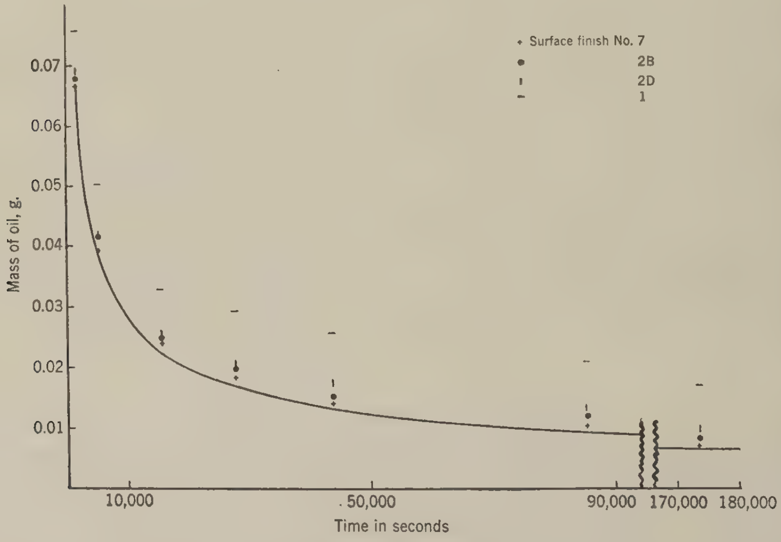

FIG. 2. Rate of drainage; small plates. Ordinate is mass of vacuum oil retained on the plate after time plotted along the abscissa at about 25°C. Continuous curve is calculated for a smooth interface and the experimental points are for surfaces whose rugosity increases from No. 7 (crosses) to No. 1 (horizontal bars).

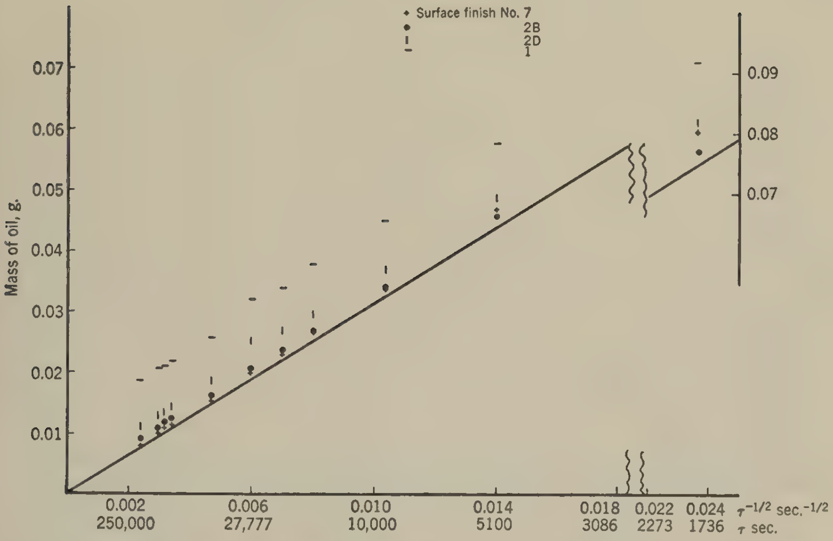

FIG. 3. Rate of drainage; small plates. Ordinate is mass of vacuum oil retained on the plate at 21°C. Abscissa is $1/\sqrt{\tau}$, τ being time in seconds. Straight line is calculated. The experimental points refer to surfaces of a rugosity increasing from No. 7 (crosses) to No. 1 (horizontal bars).

Figure 2 presents the results for small plates, vacuum oil, and room temperature which oscillated between 24.8° and 25.6°C. In Eq. [9], n was 118 cm.$^{-1}$ sec.$^{-1}$, w was 5.0 cm., H 4.7 cm., and, consequently, $V = 3.12\ \tau^{-1/2}$ cm.^{3}, if τ is expressed in seconds. The abscissa of Fig. 2 is time (in seconds), and the weight of oil on the plate (that is, 0.893 V g., as the density of the oil is 0.893) is plotted along the ordinate. The solid line is the calculated weight, i.e., $3.12 \times 0.893\ \tau^{-1/2}$ g. The horizontal dashes, the vertical dashes, the circles, and the crosses are the experimental points for the finishes No. 1, No. 2D, No. 2B, and No. 7, respectively.

In Figures 3, 4, and 5 the ordinate is still the weight of the oil remaining on the plate but the abscissa represents $\tau^{-1/2}$ (τ being time in seconds) rather than τ itself; according to Eq. [9], the weight should be a linear function of $\tau^{-1/2}$, and the theoretical straight line calculated from that equation is drawn on each of the figures.

Figure 3 summarizes the experiments on small plates and vacuum oil at 21°C. The n was 92.2 cm.$^{-1}$ sec.$^{-1}$; hence $V = 3.54\ \tau^{-1/2}$ cm.^{3} and the weight of oil: $3.16\ \tau^{-1/2}$ g., if τ is in seconds. For Fig. 4, small plates and medicinal paraffin were used at 21°C. The n was 430.5 cm.$^{-1}$ sec.$^{-1}$, V was $1.64\ \tau^{-1/2}$ cm.^{3}, and the weight of oil was $1.404\ \tau^{-1/2}$ g. Figure 5 shows the data on large plates and medicinal paraffin oil at 21°C. The n was, of course, again 430.5 cm.$^{-1}$ sec.$^{-1}$, but w was 7.5 cm. and H was 8.1 cm., whence $V = 5.55\ \tau^{-1/2}$ cm.^{3}, and the theoretical weight of oil: $4.76\ \tau^{-1/2}$.

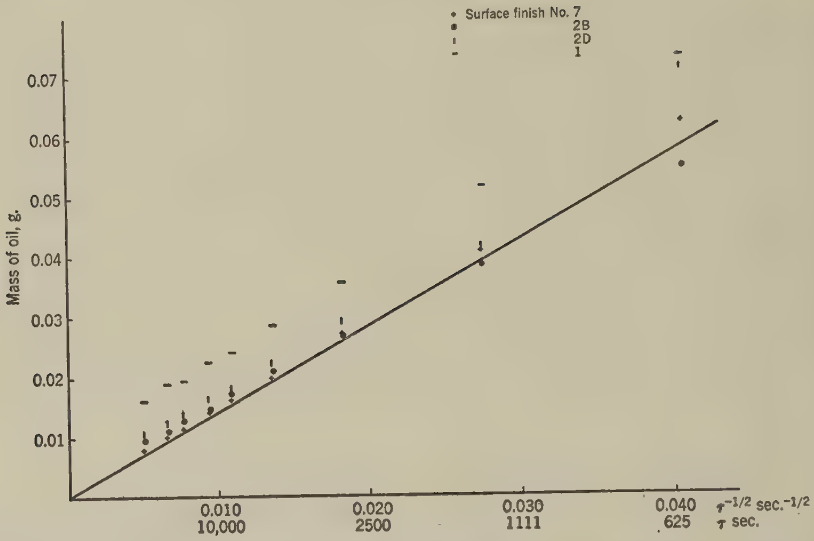

FIG. 4. Rate of drainage; small plates. Ordinate is mass of medicinal paraffin oil retained on the plate at 21°C. Abscissa is $1/\sqrt{\tau}$, τ being time in seconds. Straight line is calculated. The experimental points refer to surfaces of a rugosity increasing from No. 7 (crosses) to No. 1 (horizontal bars).

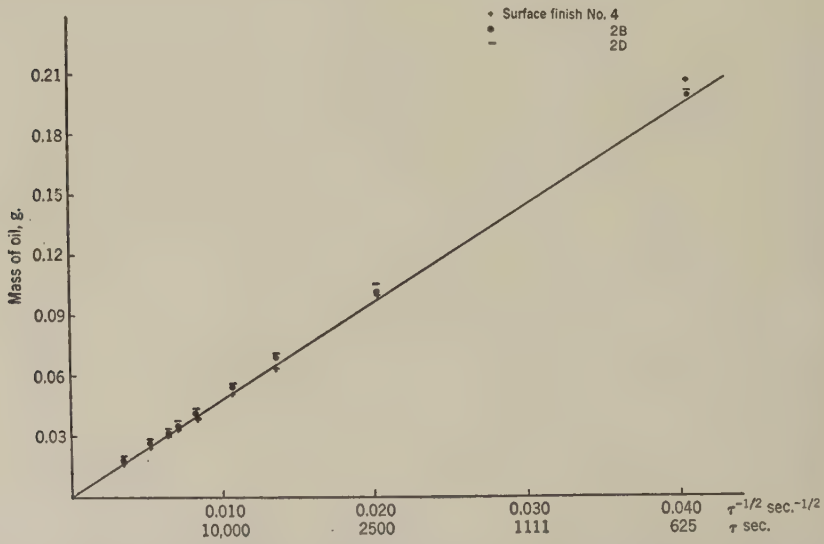

FIG. 5. Rate of drainage; large plates. Ordinate is mass of medicinal paraffin oil retained on the plate at 21°C. Abscissa is $1/\sqrt{\tau}$, τ being time in seconds. Straight line is calculated. The experimental points refer to surfaces whose rugosity increased from No. 4 (crosses) to No. 2D (horizontal bars).

V. The Meaning of the Results

1. The above graphs demonstrate that, in every instance, the amount of oil remaining on the smoothest plate (No. 7 or No. 4) was in almost quantitative agreement with the theoretical prediction. There are three known causes for the deviations still observed:

a. The steady flow for which Eq. [9] is valid takes time to materialize. As the exact moment at which Eq. [9] started to be valid is not known, the time scale may be a little incorrect; however, the uncertainty of the time scale affects the readings at the extreme right of Fig. 3, Fig. 4, and Fig. 5 but cannot significantly change the results of later readings; e.g., to bring the first value for finish No. 7 in Fig. 4 onto the theoretical line, it would be sufficient to assume that the time of the first reading was 529 sec. rather than 600 sec. (as shown by the watch), and this difference of 71 sec. would be negligible for the rest of the curve.

b. The value of H may be in error by, perhaps 1%, or, for large plates, as much as 2% because the boundaries of the initially wetted area were not straight.

c. Equation [9] neglects capillarity. Capillary effects were observed on all plates; visual inspection showed that some oil rose and wetted the plates above the initial level, and the visibly wet area after the drainage was larger than before it; e.g., in the series of graph 3 the wet area initially was 23.5 cm.^{2} for all plates but expanded during the drainage to 35.5 cm.^{2}, 32 cm.^{2}, 27 cm.^{2}, and 26 cm.^{2} for plates No. 1, 2D, 2B, and 7, respectively.

2. Whereas the deviation of the smoothest plates from the theory is small, rough plates retain much more oil than either the theory predicts or the smooth plates do. If the first few per cents of the drainage time are disregarded (see *1a* above), it is found that the difference between the oil amounts on two plates of different rugosities changes but little with time. For instance, in the series of graph 4, the mass of oil on plate No. 1 was greater than that on plate No. 7 by 0.0084, 0.0079, 0.0080, 0.0082, 0.0078, 0.0089, and 0.0083 g. in the last 7 readings. When plate No. 7 was compared with less rough plates, the difference in the amounts retained was about as constant, absolutely, but the relative error naturally was greater; thus (oil on 2B) minus (oil on 7) in the same series was −0.0001, 0.0006, 0.0010, 0.0006, 0.0011, 0.0009, and 0.0013 g.

Table II lists the mean differences between the oil amounts on a coarse and the smoothest plate, disregarding the earlier readings.

3. If the excess *amount* retained by a rough surface, as compared with a smooth one, is divided by the density of the oil to obtain the excess *volume* and then by the final wetted area (see *1c* above), the thickness of the oil film, which apparently does not take part in the drainage, is obtained.

TABLE II

Excess Oil Retained by Rough Surfaces and the Thickness of the "Immobile Layer"

Plate pairs	Graph 2		Graph 3		Graph 4		Graph 5	
	Amount *(grams)*	Thickness *(microns)*	Amount *(grams)*	Thickness *(microns)*	Amount *(grams)*	Thickness *(microns)*	Amount *(grams)*	Thickness *(microns)*
No. 1-No. 7	0.0102	3.2	0.0115	3.6	0.0082	2.9		
No. 2D-No. 7	0.0027	0.94	0.0030	1.1	0.0023	0.84		
No. 2B-No. 7	0.0013	0.54	0.0005	0.22	0.0008	0.35		
No. 2D-No. 4							0.0033	0.52
No. 2B-No. 4							0.0016	0.26

This "thickness of an immobile layer" also is shown in Table II. If its values are compared with the profilometer readings of Table I:

Finish No. 1: thickness of immobile layer	2.9–3.6;	h_{rms} 3.15–3.83
Small No. 2D:	0.84–1.1;	h_{rms} 0.91–0.94
Small No. 2B:	0.22–0.54;	h_{rms} 0.17–0.33
Large No. 2D:	0.52;	h_{rms} 0.28
Large No. 2B:	0.26;	h_{rms} 0.12

the main conclusion of the present study emerges, namely, that the thickness of the "immobile layer" is approximately equal to the average height of hills on the solid surface along which the liquid flows.

VI. Implications

1. The existence of an apparently stagnant liquid layer adjacent to a solid or, from another point of view, of an apparently enhanced viscosity of this layer was often considered to be a proof of long-range forces emanating from a solid surface; see, e.g., ref. 4 and a review in ref. 5. As a rule, the rugosity of the surface was overlooked in those experiments. The observation formulated in the preceding section demonstrates that the effects previously attributed to long-range forces are more likely to be due to surface roughness, as stated in ref. 5.

It was postulated (6) that surface asperities, by preventing a rectilinear flow of liquid next to the solid, reduce the magnitude of electrokinetic effects (which, it is known, originate in the interfacial film). The present work supplies a partial confirmation for this view.

2. The effect of rugosity on the slow movement of a liquid at a solid surface should be taken into account in many laboratory and industrial operations. Lubrication comes to mind first. Here, however, adhesive joints only are considered.

When such a joint is made by placing an excess of liquid adhesive on a solid and pressing another solid against the first, the adhesive, in being squeezed out, flows along two solid surfaces in a manner fully analogous to that studied in the present paper. Therefore, the amount of liquid remaining between the solids, after the joint was allowed to set under a given pressure for a given time, depends on rugosity. As the strength of a joint depends on the thickness of the "glue line," it must vary also with surface roughness. Maintaining the external conditions of glue setting (such as pressure and time) constant does not guarantee formation of comparable joints, as long as rugosity is not constant or not known.

3. It was hoped to use the rate of drainage as a measure of surface roughness. In its present form the method seems to be about as exact as that using a stylus, but takes an incomparably longer time. Should it be possible to accelerate the test, it might still prove useful because of its extreme simplicity and low cost.

ACKNOWLEDGMENT

It is gratefully acknowledged that the work reported above was financed by Lord Manufacturing Company, Erie, Pennsylvania, represented by Mr. D. M. Alstadt, Supervisor of Basic Research.

SUMMARY

Two hydrocarbon oils were allowed to drain from stainless steel plates of 9 different roughnesses. The theory of the drainage was derived; its predictions were approximately fulfilled by the smoothest plates. On the rough plates an apparently stagnant liquid layer existed whose thickness was nearly equal to the average height of hills on the solid surface, as determined with two stylus instruments.

This result (*a*) refutes one of the proofs for the existence of long-range molecular forces, (*b*) confirms the hypothesis that the magnitude of electrokinetic phenomena is reduced by rugosity, (*c*) shows the necessity of considering roughness in adhesion measurements, and (*d*) renders possible a new method of measuring surface roughness.

REFERENCES

1. BIKERMAN, J. J., *J. Colloid Sci.* **5**, 349 (1950).
2. JEFFREYS, H., *Proc. Cambridge Phil. Soc.* **26**, 204 (1930).
3. DERYAGIN (DERJAGUIN), B. V., *Compt. rend. Acad. Sci. U.R.S.S.* **39**, 13 (1943).
4. KARASEV, V. V., AND DERYAGIN, B. V., *Kolloid. Zhur.* **15**, 365 (1953).
5. BIKERMAN, J. J., "Surface Chemistry for Industrial Research," p. 249. Academic Press, New York, 1948.
6. BIKERMAN, J. J., *J. Phys. Chem.* **46**, 724 (1942).

JOURNAL OF COLLOID SCIENCE **11,** 308–313 (1956)

THE ABSOLUTE RATE OF CERTAIN FIRST-ORDER REACTIONS ON METAL SURFACES

A. J. B. Robertson

Department of Chemistry, King's College, Strand, London, England

Received March 26, 1956

ABSTRACT

The probability of reaction per collision of a reactant molecule with a catalytic surface (P) is considered. If E is the experimental activation energy, it is found that P for a number of reactions on metals is in the range of $\exp(-E/RT)$ to $10^4 \exp(-E/RT)$. This is not in agreement with the theory of an immobile transition state. A mobile transition state is proposed, and the transfer of energy from the solid to the adsorbed gas is briefly considered.

INTRODUCTION

Consider a gaseous reactant in contact with a metallic surface on which a catalyzed reaction is occurring. We shall consider only first-order reactions (usually decompositions) for which the rate of chemical transformation in molecules per second is proportional to the reactant pressure. The number of reactant molecules colliding per second with the catalyst is also proportional to the reactant pressure, and therefore the probability of reaction per collision with the catalyst, which we denote P, is independent of gas pressure. In discussing these reactions it is convenient to consider P rather than a first-order constant or a rate in molecules reacting per square centimeter of catalyst. The value of P should be independent of the size of the reaction vessel and the surface area of the catalyst. When P is constant, the probability of reaction of any particular molecule which strikes the catalytic surface is independent of the presence of other molecules on the surface and in the gas phase. Some new determinations of P for several reactions in this Laboratory, and calculations from published data, permit a simple generalization to be proposed.

TRANSITION STATE THEORY EQUATIONS FOR P

To formulate explicit expressions for P by the transition state theory, some model of the transition state is necessary. Temkin (1) assumed an immobile transition state, and deduced equations for the absolute reaction rate using methods somewhat similar to those whereby Fowler (2) obtained the Langmuir isotherm for an ideal localized monolayer. Glasstone, Laidler, and Eyring (3), however, showed that explicit expressions for the rate of various surface processes are more simply obtained when the adsorption sites are treated as reactants and assigned a partition function. A general account has been given by Laidler (4), whose symbols we shall employ. For a first-order process the rate of reaction in molecules per square centimeter of catalyst per second is

$$v = c_g c_s \frac{kT}{h} \frac{f_\ddagger}{F_g f_s} \exp\left(\frac{-\epsilon_0}{kT}\right) \qquad [1]$$

and for a diatomic molecule, for example, this becomes

$$v = c_g \tfrac{1}{2} sL \frac{kT}{h} \frac{\sigma}{\sigma_\ddagger} \frac{h^3}{(2\pi mkT)^{3/2}} \frac{h^2}{8\pi^2 IkT} \exp\left(\frac{-\epsilon_0}{kT}\right) \qquad [2]$$

if a cancellation of the vibrational partition functions in $f_\ddagger$ and F_g is assumed. But the number of molecules striking the catalyst per square centimeter per second is

$$n = \frac{c_g kT}{(2\pi mkT)^{\frac{1}{2}}}. \qquad [3]$$

From Eqs. [2] and [3]

$$P = \tfrac{1}{2} sL \frac{\sigma}{\sigma_\ddagger} \frac{h^2}{2\pi mkT} \frac{h^2}{8\pi^2 IkT} \exp\left(\frac{-\epsilon_0}{kT}\right). \qquad [4]$$

In Eq. [4], $\frac{1}{2}s$ is of the order of unity; L is about 10^{15} sites per square centimeter, and a consideration of the magnitude of the other terms for small molecules shows that the theory of an immobile transition state must give a value for P some powers of ten less than $\exp(-\epsilon_0/kT)$. Also, for more complex molecules, the partition function F_g becomes larger, and P becomes still less compared with $\exp(-\epsilon_0/kT)$. If E is the experimental Arrhenius activation energy, $\exp(-\epsilon_0/kT)$ is only slightly different from $\exp(-E/RT)$, and thus the predictions from the immobile transition state theory can be compared with experiment. Generally, a grave discrepancy is found.

Some Experimental Measurements of P

In our experiments, P varied for different reactions from a value nearly equal to $\exp(-E/RT)$ to a value exceeding $\exp(-E/RT)$ by a factor approaching 10^4. Two series of investigations have been carried out. In the first, with D. J. Fabian, the decomposition of ethane and propane on a platinum filament was examined by a mass spectrometric method, by which a direct determination of reaction rate was made at pressures of 10^{-4} to 10^{-7} mm. On a new and active filament, properly treated, both ethane and propane lost one hydrogen atom, to give ethyl and propyl radicals, respectively, which evaporated from the filament. With use, the filament activity changed, probably as a result of carbonization, and the reaction changed to molecular dehydrogenation to ethylene and propylene, respectively. The value of P was determined by assuming equality between the geometrical area of the filament and its true area. For ethane forming ethyl radicals the result was $P = 10^{3.5} \exp(-E/RT)$, and for the molecular dehydrogenation it was $P = 10^{1.3} \exp(-E/RT)$. The partition function F_g (for unit volume) for ethane is known, and on inserting this in Eq. [1] an equation analogous to [2] can be obtained, which gives a value for the preexponential term. This theoretical value is too small by a factor of 10^{11} for the ethyl radical formation, and by a factor of 10^9 for the ethylene formation. For propane, the experimental results were very similar, and the disagreement with the immobile transition state theory is worse. In the second series of investigations, with A. J. Crocker, formic acid was decomposed to carbon dioxide and hydrogen at pressures of about 10^{-3} mm. on polycrystalline copper and on three separate faces (100, 110, and 111) of single copper crystals. In all cases the surfaces were rendered smooth by electrolytic polishing, and P was again computed by assuming equality of the true and geometrical area. The value of P was always of the order of $\exp(-E/RT)$. Similar results have been found in other laboratories. Osberghaus and Taubert (5) determined P for the surface decomposition of methyl chloride at very low pressure by a mass spectrometric method, and found $P = 10^{3.3} \exp(-26 \text{ kg.-cal. mole}^{-1}/RT)$.

The theory of the immobile transition state advanced by Temkin was applied by him to interpret data of Van't Hoff, and an equation analogous to [2], but for a polyatomic molecule, accounted for the absolute rate of the decomposition of phosphine on glass. We agree with these calculations. Glasstone, Laidler, and Eyring (3) adduced two further examples to which, they state, the immobile transition state theory can be applied, namely, the decomposition of nitrous oxide on gold, investigated by Hinshelwood and Prichard (6), and the decomposition of hydrogen iodide on platinum, investigated by Hinshelwood and Burk (7). For nitrous oxide on gold, however, Hinshelwood and Prichard show that P is nearly equal to $\exp(-E/RT)$. We agree with these calculations. For hydrogen iodide on platinum, Hinshelwood and Burk do not consider P; but we can assume that the dimensions of the apparatus and the catalytic filament were the same as those with nitrous oxide, and then show by comparison of the two sets of data that P for hydrogen iodide is less than that for nitrous oxide by a factor of only 5.5. Thus we have the very interesting result, observed in three laboratories, that P for decomposition reactions on metals is in the range of $\exp(-E/RT)$ to $10^4 \exp(-E/RT)$, where E is the apparent Arrhenius activation energy for the reaction in question.

The Immobile Transition State Theory Applied to Nitrous Oxide

From our previous deductions we see that the absolute rate of the nitrous oxide decomposition on gold is not accounted for by the immobile transition state theory. Since nitrous oxide is a linear molecule, Eq. [2] can be applied. Let us put $\frac{1}{2}s = 2$, $L = 10^{15}$ sites per square centimeter, $\sigma/\sigma_{\ddagger} = 1$, and $I = 66 \times 10^{-40}$ g. cm.². For $\exp(-\epsilon_0/kT)$ we put $\exp(-E/RT)$, where the experimental activation energy is 29 kcal. per mole. Then the absolute rate in molecules per square centimeter of catalyst at 1211°K. is

$$v = c_g \times 6.85 \times 10^{-8}.$$

But the volume of the bulb was about 50 cm.³ and the area of the catalyst was 0.316 sq. cm. The total number of molecules is $50c_g$ and the first-order rate constant is 4.3×10^{-10} sec.$^{-1}$. This is about a million times less than the experimental value. The theory fails, in agreement with our previous deductions; the discrepancy is so great that it is not worth while allowing for the small difference between $\exp(-\epsilon_0/kT)$ and $\exp(-E/RT)$, or for the fact that the mean temperature of the gas is not the same as that of the catalytic wire.

THE INTERPRETATION OF THE LARGE VALUES OF P

The fact that P is of the order of magnitude of $\exp(-E/RT)$ does not necessarily imply that only those molecules react which strike the surface with sufficient kinetic energy. Let us suppose that all the molecules striking the surface are first adsorbed as molecules, and they can then either evaporate or react. For all normal reaction rates, the probability of evaporation will be much greater than that of reaction, for any molecule. An adsorption isotherm for the molecularly adsorbed layer in equilibrium with gas at pressure p can then be formulated, neglecting reaction. For a first-order evaporation of the adsorbed molecules it is

$$kp = CB_e \exp\left(\frac{-L}{RT}\right) \qquad [5]$$

where kp is the number of molecules striking 1 sq. cm. per second, C is the number of adsorbed molecules per square centimeter, and B_e is the frequency factor for evaporation of molecules adsorbed with a heat L per mole. Recently, Dewing and Robertson (8) described a direct method for investigating the condensation and subsequent evaporation of molecules by projecting a molecular beam on to a spinning rotor, and collecting the gas evaporating from the rotor at different points. For the only system investigated in this way so far (hydrogen on superficially oxidized nickel) Eq. [5] was followed closely. For the rate of reaction in molecules per square centimeter per second we have the analogous equation

$$R = CB_r \exp\left(\frac{-E_t}{RT}\right), \qquad [6]$$

where E_t is the true or surface activation energy and B_r is the frequency factor for reaction. Combining Eqs. [5] and [6], and noting that kp is the number of molecules striking 1 sq. cm. per second, gives

$$P = \left(\frac{B_r}{B_e}\right) \exp\left(\frac{-E}{RT}\right), \qquad [7]$$

where E, the apparent activation energy, is $E_t - L$. Thus for P to exceed $\exp(-E/RT)$, the transfer of vibrational energy from the surface to the adsorbed molecule must be more efficient than the transfer of translational energy perpendicular to the surface to the molecule as a whole. Usually, thermal accommodation coefficient measurements are interpreted in the opposite way, but the experimental evidence seems inconclusive. Some decisive experiments on this problem seem desirable. A large value for B_r also implies no loss of entropy when an adsorbed molecule is converted to a transition state, and perhaps even a gain of entropy. Since, at the high temperatures involved in the experiments, the molecularly adsorbed layer probably has considerable mobility, the transition state must also be mobile. Let us suppose that the transition state is so mobile that its partition function is that of a two-dimensional gas. The equilibrium between gaseous molecules and mobile transition states is one between a three-dimensional and a two-dimensional gas, in which surface sites do not participate. The equation to be used instead of [1] is

$$v = c_g \frac{kT}{h} \frac{F_\ddagger}{F_g} \exp\left(\frac{-\epsilon_0}{kT}\right). \qquad [8]$$

We assume a cancellation of the rotational and vibrational terms in $F_\ddagger$ and F_g, and insert into $F_\ddagger$ an expression for the translational partition function per unit area of a two-dimensional gas. Combining with Eq. (3] then gives

$$P = \exp\left(\frac{-\epsilon_0}{kT}\right). \qquad [9]$$

We note that a transition state with supermobility is needed to explain some of the experimental results, or, in terms of Eq. [7], the transition state gains entropy. Some evidence has been found, notably by Gwathmey, for a surface mobility of metal atoms induced by the occurrence of a reaction on the metal, and it seems possible that a mobile transition state may be associated with a mobile metal atom or atoms, when P exceeds the value given by Eq. [9].

I thank Sir Eric Rideal for his interest, and both the Research Fund of the University of London and the Institute of Petroleum, for grants in support of this work.

References

1. Temkin, M., *Acta Physicochim. U.R.S.S.* **8,** 141 (1938).
2. Fowler, R. H., *Proc. Cambridge Phil. Soc.* **31,** 260 (1935).
3. Glasstone, S., Laidler, K. J., and Eyring, H., "The Theory of Rate Processes." McGraw-Hill, New York, 1941.
4. Laidler, K. J., *in* P. H. Emmett, ed., "Catalysis," Vol. 1. Reinhold, New York, 1954.
5. Osberghaus, O., and Taubert, R., *Z. physik. Chem. (Frankfurt)* **4,** 264 (1955).
6. Hinshelwood, C. N., and Prichard, C. R., *Proc. Roy. Soc. (London)* **A108,** 211 (1925).
7. Hinshelwood, C. N., and Burk, R. E., *J. Chem. Soc.* **127,** 2896 (1925).
8. Dewing, J., and Robertson, A. J. B., *Discussions Faraday Soc.* **17,** 102 (1954).

JOURNAL OF COLLOID SCIENCE **11,** 314–316 (1956)

COLORS EXHIBITED BY THIN FILMS ON METAL

U. R. Evans

Emeritus Reader in the Science of Metallic Corrosion, Cambridge University,
Cambridge, England

Received January 9, 1956

The beautiful colors produced when a bright metal surface is gently heated in air or exposed to an atmosphere containing hydrogen sulfide, are today almost universally acknowledged as due to interference between light reflected, respectively, from the outer and inner surfaces of a film, which may be oxide, sulfide, or, as indicated by Vernon (1), an oxide film containing sulfur. It may seem strange to recall that 30 years ago scientists of eminence considered that the cause was not interference between light reflected from the two surfaces, but diffraction caused by some repeated structure within the film, or some other feature independent of thickness as such. The main difficulty to accepting the interference theory was that, if the sequence of colors appearing when, say iron, was gently heated (straw yellow, red-mauve, violet, dark blue, light blue . . .) was due to gradual increase in thickness, the colors should appear in reverse order if the thickness of the film was gradually reduced. This had been tried. Iron heated to the blue range was abraded in an attempt to make the film thinner; but instead of the blue's becoming violet, then red-mauve, and finally straw yellow, the color merely became weaker and finally disappeared. Possibly the size of the abrasive particles used exceeded the film thickness, or the abrasive action was such as to drag away the film in tiny flakes, or (what is now known to happen very easily) the film was broken up and pushed into the relatively malleable metal. Clearly a better method was required for reducing the film thickness.

In 1925, the author (2) used what is now known as "reductive dissolution" for producing this gradual and uniform thinning. When iron covered with ferric oxide films is cathodically treated in weakly acid solution, the iron from the oxide passes into solution as ferrous ions, and the film is uniformly thinned; the rate of thinning depends solely on the current density and can therefore be controlled. He took a strip of iron, heated it at one end so as to produce the usual sequence of colors, and subjected the lower part (only) to reductive dissolution, keeping the upper half dry to serve as a comparison. It was soon found that the colors moved backwards relatively to those on the dry half, thus realizing the reverse change. This removed the main difficulty to the interference theory.

The manner in which the interference bands pass across the spectrum as the thickness increases was afterwards studied by Constable (3). Further papers by the author (4, 5) showed why the colors are weak or absent when very transparent films are present on very smooth and highly reflective surfaces, and why the wavelengths missing from the specular reflection are present in scattered light—another fact once considered to be inconsistent with the interference theory.

It may be remarked that reductive dissolution—first utilized for testing the interference theory of colors—was afterwards found to be important in other ways, as shown by various investigators working in the author's laboratory. Miley (6) used the principle to obtain rough measurements of the color-film thickness, by observing the coulombage needed for the complete destruction of the oxide, and more precise electrometric measurements, also based on reductive dissolution, were later carried out by D. Eurof Davies (7). Pryor (8) studied the reductive dissolution of ferric oxide, not only as a film, but also as pure ferric oxide powder, which, although only slightly and slowly attacked by direct exposure to dilute acid, is readily attacked when floated on mercury and exposed to the same acid under cathodic conditions. Reductive dissolution explains why stainless steel containing chromium will resist dilute acid under conditions where unalloyed iron is rapidly attacked. The oxide present on unalloyed iron readily suffers reductive dissolution, since, at pores or film defects which appear spontaneously, the cell

Metal (anode) | acid | ferric oxide (cathode)

destroys the film by cathodic reduction; this can be avoided if the iron specimen is made an anode, or if chromic acid is present, which is reduced in preference to ferric oxide; under such circumstances the author (9) found it possible to expose tinted iron specimens in acid without the rapid destruction of the colors which normally occurs. In films containing chromium, the instability of the divalent condition in chromium makes reductive dissolution difficult, and dissolved oxygen can now play the part of the chromic acid. Berwick (10) found that stainless steel (unheated and thus carrying only an invisible film) could remain in dilute acid without attack, provided that oxygen was present; when the oxygen was entirely removed, vigorous attack took place.

In calculating film thicknesses from color, it was at one time assumed that the phase change on reflection was always 0 or π. Tammann (11), who (even in 1920) believed that the colors were due to interference, made this assumption when he used the development of colors to follow the thickening of iodide and other films. For this and other reasons, the simple method which he used for calculating the thickness (division of the thickness of the air film giving the same color as the film on the metal by the refractive index of the film substance) gives erroneous results, as was shown in the author's laboratory by Bannister (12), who compared the thicknesses of the same films by four different methods (microgravimetric, coulometric, nephelometric, and Tammann's simple color method); the first three methods agreed, but the fourth gave divergent results. Bannister, however, calibrated the color scale against microgravimetric measurements and was then able to use the color comparisons to study the thickening-law for silver iodide films produced when silver was immersed in a chloroform solution of iodine.

The specific phase change has been studied in detail by Winterbottom (13) and more recently by Charlesby and Polling (14), whose work on the colors produced on tantalum by anodic polarization in ammonium borate solution deserves special attention. The color sequence runs through numerous "orders," red appearing several times. The phase change at the metal-oxide interface was measured with some accuracy; it varies with wavelength, being 0.2 π at 2700 A. and 0.8 π at 8000 A.

REFERENCES

1. VERNON, W. H. J., *Trans. Faraday Soc.* **23,** 113 (1927); especially p. 122.
2. EVANS, U. R., *Proc. Roy. Soc.* (*London*) **A107,** 228 (1925).
3. CONSTABLE, F. H., *Proc. Roy. Soc.* (*London*) **A115,** 570 (1927).
4. EVANS, U. R., *Chemistry & Industry* **1926,** 211; on p. 212, 4 lines from bottom "$\lambda/2$, $3\ \lambda/2$, $5\ \lambda/2$" should read "$\lambda/4$, $3\ \lambda/4$, $5\ \lambda/4$."
5. EVANS, U. R., *Kolloid-Z.* **69,** 129 (1934).
6. EVANS, U. R., AND MILEY, H. A., *Nature* **139,** 283 (1937).
7. DAVIES, D. E., EVANS, U. R., AND AGAR, J. N., *Proc. Roy. Soc.* (*London*) **A225,** 443 (1954).
8. PRYOR, M. J., AND EVANS, U. R., *J. Chem. Soc.* **1949,** 3330; *ibid.* **1950,** 1259–1276 (4 papers in all).
9. EVANS, U. R., *J. Chem. Soc.* **1930,** 478.
10. BERWICK, I. D. G., AND EVANS, U. R., *J. Appl. Chem.* **2,** 576 (1952).
11. TAMMANN, G., *Z. anorg. u. allgem. Chem.* **111,** 78 (1920).
12. EVANS, U. R., AND BANNISTER, L. C., *Proc. Roy. Soc.* (*London*) **A125,** 370 (1929).
13. WINTERBOTTOM, A. B., *Trans. Faraday Soc.* **42,** 487 (1946); also Appendix (p. 802) to U. R. Evans' "Metallic Corrosion, Passivity and Protection," Arnold, London, 1946 ed.
14. CHARLESBY, A., AND POLLING, J. J., *Proc. Roy. Soc.* (*London*) **A227,** 434 (1955).

JOURNAL OF COLLOID SCIENCE 11, 317–323 (1956)

THE "MACROMOLECULAR LESION" INVOLVING DEOXYRIBONUCLEIC ACID IN RADIOBIOLOGY AND RADIOTHERAPY

J. S. Mitchell

Professor of Radiotherapeutics, University of Cambridge, England

Received January 27, 1956

Introduction

Far too little is known about the molecular mechanism of the therapeutic action of ionizing radiations. An important problem at the present time is to ascertain whether or not inhibition of synthesis of deoxyribonucleic acid (DNA) after therapeutic doses of radiation is a primary biological process.

The problem is more difficult than it was at first thought to be. The inhibition of additional formation of DNA after irradiation appears to be the most radiosensitive metabolic process observed so far in the cells of malignant tumors. It is found that in tumor cells for some hours after irradiation *in vivo* with single doses of X-radiation of 1000 r or more, e.g., in the Ehrlich ascites tumor after 1250 r (1, 2) and the Yoshida sarcoma after 1000 r (3), the formation of new DNA is stopped and the content of DNA per cell remains substantially unchanged. At the same time there is a more or less normal progressive and roughly proportional increase in the mean cell volume and content of ribonucleic acid (RNA), nitrogen, and water.

The relations between the inhibition of synthesis of DNA and the processes of mitotic inhibition and chromosome breakage, and the ultimate death of the tumor cells after therapeutic irradiation, are incompletely understood. The work of Howard and Pelc (4) suggests that in *Vicia faba* seedlings the immediate delay in entering division which results from irradiation cannot be attributed to delay in DNA synthesis and that delay in entering division and chromosome breakage behave differently in relation to irradiation. Holmes and Mee (5) showed similarly that the process of DNA synthesis in regenerative hyperplasia in the rat liver is easily inhibited by irradiation before the actual synthesis begins and that delay of mitosis and chromosome breakage do not necessarily depend on inhibition of DNA synthesis. Studies of the regenerating liver and normal tissues of the mouse led Kelly and Payne (6) to the working hypothesis that

DNA turnover per se is not radiosensitive and that its depression after irradiation might be a consequence of mitotic inhibition. Pelc and Howard (7) suggest that different mechanisms of action are responsible for the inhibition of DNA synthesis and the reduction of growth rate in bean roots.

Only limited information is available about the relative biological efficiencies of fast neutrons and X- or γ-radiation for the various processes involved. For depression of P^{32} uptake in lymphomatous tissue in the mouse by fast neutrons and X-rays, Scott (8) found a value of the X/n ratio of roughly 6, which corresponds to a value of the relative biological efficiency of about 2.4 (9). In these experiments the neutrons possibly caused greater regression of the tumor than did the X-rays, but the doses used were not sufficient to produce permanent retrogression. However, this value of the relative biological efficiency is about the same as that obtained for inhibition of "takes" of the tumor (10) and production of chromosome abnormalities (11). In the bean roots in the meristematic resting cells, Howard and Pelc (4) found that doses of neutrons smaller than a dose of X-rays by a factor of at least 2.5 produced the same reduction of the number of cells synthesizing DNA during 12 hours following irradiation. There is often considerable experimental error in the measurement of relative biological efficiency. However, these values of the relative biological efficiency for inhibition of uptake of P^{32} appear to be roughly the same as those for lethal effects and production of chromosome abnormalities in the same material but almost certainly higher than those for mitotic inhibition (see, for example, references 12–14).

A further problem is that even large doses of X-radiation, e.g., 9000 r, reduce the uptake into DNA of P^{32} as phosphate and C^{14} as acetate, glycine, and adenine only to about 50%, when there is no destruction of cells and when effects of shock are avoided (compare references 15 and 5). This reduction does not seem to be accounted for by action of the radiation on cells in a sensitive stage only. One must raise the possibility of two alternative metabolic pathways of synthesis of DNA, one radiosensitive and one radioresistant, or even two types of DNA, with turnover of different radiosensitivity.

On general grounds it seems reasonable to assume that complete and permanent inhibition of synthesis of new DNA would stop the growth of a malignant tumor. This by itself would not necessarily lead to death of the cells, but it is likely that such damage to the duplicating mechanism of DNA would render the DNA incapable of carrying out its normal functions in relation to cell metabolism. However, there appears to be no direct experimental evidence about this.

In considering the effect of a therapeutic dose of radiation which leads to permanent retrogression and healing, it is suggested that as a first approximation the radiation stops the duplication of the DNA present, i.e., it stops the formation of new DNA in an amount equal to that present at the time of irradiation. It is recognized that after the irradiation some cells may succeed in passing through several divisions before dying but other cells degenerate with or without attempted division. The importance of the stroma reaction in removing the tumor cells injured by the radiation and perhaps in preventing their recovery (16, 17) must be emphasized, but it is unlikely that this process has any direct effect on the primary radiobiological process. It is suggested that the stroma reaction may be chemotactic and due to diffusible metabolites liberated from the tumor cells injured by the radiation.

It would appear to be particularly important to find out the details of the mechanism by which X- and γ-rays interfere with the synthesis of DNA and nucleoproteins in proliferating cells in order to try to provide a more rational starting point for the chemotherapy of cancer.

Ultraviolet Photomicrographic Studies

Although the methods of classical histology show no obvious changes shortly after irradiation, experimental studies which I have carried out over a number of years with the use of ultraviolet photomicrography have shown disturbances of cellular nucleic acid metabolism in several types of cells within relatively short times, even some minutes after irradiation. In my early work on the accumulation of pentose nucleotides in cytoplasm after irradiation and inhibition of synthesis of deoxyribonucleic acid by irradiation (reference 18(*a*), 18(*b*)—pts. 1, 2, and 3), a substantial increase in cytoplasmic absorption at 2537 A. was found in a number of human malignant tumors at 80 minutes after irradaition. The magnitude of the change was consistent with the presence in the irradiated cytoplasm of ribonucleotides in local concentration often of the order of 3%. In further work (19, 20) experiments using ribonuclease in conjunction with quantitative ultraviolet photomicrography showed that the cytoplasmic nucleotides accumulating after irradiation were mainly ribopolynucleotides closely resembling and probably identical with ribonucleic acid. Extraction methods showed characteristic nucleotide absorption with maximum at the wavelength 2620 A. It is important to note that the increase in ribonucleotide absorption occurs almost entirely after irradiation with doses less than 750–1000 r; at higher doses usually there is no increase in concentration of ribonucleotide absorption and often a definite decrease, presumably owing to interference with less radiosensitive processes in the disturbance of cellular nucleic acid metabolism (see reference 21). Subsequent experiments have detected increased cytoplasmic absorption in a biopsy of a human basal-celled carcinoma of the skin taken immediately after delivery of 40 r of γ-radiation in 43 minutes.

It is of interest that Euler and Hevesy (22) observed an increase in the specific activity of the nucleic acid phosphorus at 2 hours after irradiation of the Jensen rat sarcoma with small doses of 77–310 r, though the main result in this classical paper is the reduction of P^{32} turnover in DNA after irradiation with doses of 460–7000 r.

Histochemical studies by Petrakis, Ashler, and Ferkel (23) of the effects of total body irradiation on the liver cells of the rat showed an initial increase in cytoplasmic RNA during the first 24 hours after 600 r and a decrease later; after 1500 r there was a decrease during the first 3 hours, then an increase during the next 3 hours to 40% above the controls, and a decrease at 24 hours.

In studies of the effect of X-rays on the Ehrlich ascites tumor, Forssberg and Klein (2) found that the amount of ATP and ADP per cell showed a considerable but transient increase soon after irradiation; the surplus amount disappeared at a high rate and in an approximately linear fashion between 35 and 100 minutes after irradiation.

Since 1940 I have been carrying out experiments on the irradiation of tissue cultures mainly of chick fibroblasts *in situ* on the stage of the ultraviolet microscope. Very little of this work has yet been published because of the difficulties of precise quantitative interpretation. The result of an experiment in which chick fibroblasts in culture (provided by Mrs. I. Simon-Reuss) received a dose of 435 r of X-radiation delivered in 6 min. has been published (24). There appeared to be an increase in cytoplasmic absorption at 2537 A and also an increase in diffusible absorbing material in the photograph taken at between 2 to 6 min. after the end of the X-ray exposure. At about 87 min. after the irradiation the characteristic absorption was lost, the cells were breaking down, and there appeared to be gross damage to the chromosomes.

A great many control experiments were carried out which showed that the ultraviolet radiation used for these exposures did not produce effects comparable with those observed after exposure to X-rays. There was evidence of a hyperchromatic effect after the first photographic exposure, but there was no obvious change in ultraviolet absorption for about 20 subsequent photographic exposures. Visible light only was used for focusing. It is now reasonably certain that under the conditions of most experiments of this type, the ultraviolet radiation used for the photographic exposures produces effects in the living cells which are not negligible, including blockage of the course of mitosis. Accordingly attempts are being made to develop methods with much lower intensity of ultraviolet light.

More recently, Dr. G. H. Hjort, who worked with me in Cambridge, has used the methods of ultraviolet photomicrography to study the effects of total body irradiation with doses between 75 and 1200 r on the lymphocytes of lymphoid tissue in adult rats. The sections were prepared from frozen dehydrated tissue. It has been found that an increase in nucleotide type of absorption mainly in the cytoplasm can be detected as early as 15 minutes after irradiation, and this biochemical change appears before any morphological changes can be detected. There is, however, wide variability in the behavior of different cells in respect to these changes, and much further quantitative examination of the experimental material is necessary.

Ionic Efficiency

It is useful to express the effects of irradiation on inhibition of synthesis of deoxyribonucleotides by means of a crude estimate of the ionic efficiency (*cf.* reference 19). In a typical small human tumor, e.g., an early squamous carcinoma of the skin, it is possible to effect a permanent cure by administration of a single dose of 2250 r of γ-radiation such as that of Ir^{192} of mean energy 0.38 m.e.v. It will be assumed as a first approximation that this dose of radiation ultimately stops the formation of an amount of new DNA equal to that already present in the proliferating part of the tumor. In a typical example, the mean diameter of the nuclei of the tumor cells was 6.86 μ and the mean DNA content per nucleus was found by ultraviolet photomicrographic absorption measurements to be 7.8×10^{-12} g. (compare, e.g., reference 25). Hence there are approximately 1.44×10^{10} monomeric deoxyribonucleotides of average molecular weight 327 per nucleus. A dose of 2250 r of γ-radiation corresponds to the formation within each nucleus, of average volume 169 μ^3, of $2250 \times 169 \times 1.79 = 6.81 \times 10^5$ ion pairs. Hence the ionic efficiency, which is the number of monomeric deoxyribonucleotides whose formation (or duplication) is inhibited per ion pair, is 2.11×10^4. Such a value would correspond to inhibition of formation of one polymeric molecule of DNA of molecular weight 6.9×10^6. This value is essentially identical with the value of about 6×10^6 obtained in a number of recent measurements of the weight of DNA molecules extracted from calf thymus (26), herring sperm heads (27, 28), *E. coli* (29), and pneumococcus transforming principle (30). Such good agreement is almost certainly fortuitous, since the method of calculation is crude.

However, the calculations suggest that one ion pair stops the formation of one molecule of DNA. The possibility of a direct action mechanism involving DNA or possibly a DNA-protein must be raised. The mediation of the now well-recognized radiochemical mechanism involving the formation of H atoms and OH radicals and H_2 and H_2O_2 is likely. However, the distinction between direct and indirect mechanisms of action is less clearly defined than previously thought since the demonstration of protection and oxygen effects in the irradiation of solid polymers (31).

It may be suggested that damage anywhere in the DNA molecule stops self-duplication. It is tempting to speculate that there is a mechanism of separation involved in the duplication of DNA which may be likened to the opening of a "zipper," and that this can be blocked by the changes produced by one ion pair occurring anywhere in the sensitive region in the whole length of the duplicating system.

However, quite apart from the details of the mechanism, these considerations suggest that therapeutic doses of γ-radiation produce what may be termed a "macromolecular lesion" involving effectively the whole of the DNA or DNA-protein in the tumor. Thus this lesion appears to be an important type of damage concerned in the mechanism of the therapeutic action of ionizing radiations. The details of its relation to mitotic inhibition and chromosome breakage are not clear. In considering the role of inhibition of synthesis of new DNA it is not unlikely that there are different biochemical effects at different levels of radiation dose.

A consequence of these considerations which should be capable of experimental test is that it is possible that the molecular weight of the DNA is lower in radioresistant tumors than in radiosensitive tumors and that there may be an approximate proportionality between the molecular weight of the DNA and the radiosensitivity of cells in general. It is, of course, almost certain that other factors are involved especially when comparing cells from different species and different types of organism. One problem is the difficulty of measurement of the molecular weight of the DNA and the DNA-proteins *in vivo.* The radiosensitivity may be expressed quantitatively in terms of the reciprocal of the dose required to produce some measurable effect such as permanent retrogression of 50% of tumors in the assessment of radiocurability.

The concept of a "macromolecular" lesion renders possible a common mechanism of lethal action of ionizing radiations on proliferating cells and by the process of acute cytolysis observed in the small lymphocyte and some highly radiosensitive tumor cells.

SUMMARY

Evidence is presented which suggests that an important type of damage produced by therapeutic doses of ionizing radiation is a "macromolecular lesion" involving deoxyribonucleic acid (DNA) or DNA-protein.

Experimental studies by means of ultraviolet photomicrography have shown disturbances of cellular nucleic acid metabolism within relatively short times, even some minutes, after irradiation.

In a typical example of a small human tumor curable by radiotherapy, a crude estimate of the ionic efficiency shows that one ion pair is associated with inhibition of formation of one polymeric molecule of DNA of molecular weight about 7×10^6.

Further experimental studies are suggested.

REFERENCES

1. KLEIN, G., AND FORSSBERG, A., *Exptl. Cell Research* **6,** 211 (1954).
2. FORSSBERG, A., AND KLEIN, G., *Exptl. Cell Research* **7,** 480 (1954).

3. Gardella, J. A., and Lichtler, E. J., *Cancer Research* **15**, 529 (1955).
4. Howard, A., and Pelc, S. R., *Heredity, Suppl.* **6**, 261 (1953).
5. Holmes, B. E., and Mee, L. K., *in* "Radiobiology Symposium" (Z. M. Bacq and P. Alexander, eds.), p. 220. Butterworth, London.
6. Kelly, L. S., and Payne, A. H., *Acta Radiol. Suppl.* **116**, 693 (1954).
7. Pelc, S. R., and Howard, A., *in* "Progress in Radiobiology" (Mitchell, J. S., Holmes, B. E. and Smith, C. L., eds.), p. 8. Oliver and Boyd, Edinburgh, 1956.
8. Scott, K. G., *Radiology* **46**, 173 (1946).
9. Aebersold, P. C., and Anslow, G. A., *Phys. Rev.* **69**, 1 (1946).
10. Axelrod, D., Aebersold, P. C., and Lawrence, J. H., *Proc. Soc. Exptl. Biol. Med.* **48**, 251 (1941).
11. Marshak, A., *Radiology* **39**, 621 (1942).
12. Gray, L. H., Mottram, J. C., Read, J., and Spear, F. G., *Brit. J. Radiol.* **13**, 371 (1940).
13. Gray, L. H., and Scholes, M. E., *Brit. J. Radiol.* **24**, 285 (1951).
14. Zirkle, R. E., *in* "Radiation Biology" (A. Hollaender, ed.), Vol. 1, Part 1, Ch. 6, p. 315. McGraw-Hill, New York, 1954.
15. Hevesy, G., *Acta Radiol. Suppl.* **116**, 423 (1954).
16. Cramer, W., *10th Sci. Rept. Impl. Cancer Research Fund, London*, p. 95 (1932).
17. Lasnitzki, I., *Brit. J. Radiol.* **20**, 240 (1947).
18(*a*) Mitchell, J. S., *Nature* **145**, 105 (1940); (*b*) *Brit. J. Exptl. Pathol.* **23**, 285, 296, 309 (1942).
19. Mitchell, J. S., *Brit. J. Radiol.* **16**, 339 (1943).
20. Mitchell, J. S., 21st Ann. Rept. Brit. Empire Cancer Campaign, p. 62 (1944).
21. Hamilton, L. D., Ph.D. thesis, Cambridge, 1952; also unpublished work.
22. Euler, H. v., and Hevesy, G. v., *Kgl. Danske Videnskab. Selskab, Biol. Medd.* **17** (No. 8) (1942).
23. Petrakis, N. L., Ashler, F. M., and Ferkel, R. L., Naval Radiol. Def. Lab. Rept. AD-126B.
24. Mitchell, J. S., *in* "Radiobiology Symposium" (Z. M. Bacq and P. Alexander, eds.), p. 314. Butterworth, London, 1955.
25. Vendrely, R., *in* "The Nucleic Acids" (E. Chargaff and J. N. Davidson, eds.), Vol. 2, Chapter 19, p. 155. Academic Press, New York, 1955.
26. Reichmann, M. E., Rice, S. A., Thomas, C. A., and Doty, P., *J. Am. Chem. Soc.* **76**, 3047, 1954.
27. Alexander, P., and Stacey, K. A., *Trans. Faraday Soc.* **50**, 303 (1954).
28. Alexander, P., and Stacey, K. A., *Biochem. J. (London)* **60**, 194 (1955).
29. Rowen, J. W., and Norman, A., *Arch. Biochem. and Biophys.* **51**, 524 (1954).
30. Fluke, D., Drew, R., and Pollard, E., *Proc. Natl. Acad. Sci. U. S.* **38**, 180 (1952).
31. Alexander, P., and Charlesby, A., *in* "Radiobiology Symposium" (Z. M. Bacq and P. Alexander, eds.), p. 49. Butterworth, London, 1955.

JOURNAL OF COLLOID SCIENCE 11, 324–326 (1956)

CHEMICAL PHYSICS AT THE NATIONAL GALLERY, LONDON

F. I. G. Rawlins

National Gallery, London, England

Received February 16, 1956

The care of art treasures has progressed notably during the present century. For this, two basic concepts are mainly responsible, at least so far as paintings are concerned. The first is that pictures (especially those of "classical" art) are layer structures—almost a rough large-scale version of the *Schichten-gitter* of the crystallographer—and the second recognizes that, in the last resort, the well-being of such a stratified system is a problem in energetics. Thus, we are confronted by many of the elemental questions of chemical physics, combined at certain points with a touch of engineering, such as would have delighted the heart of Willard Gibbs. In our own day, an approach of this kind is facilitated by the contemplation of certain aspects of colloid science and surface chemistry, thus indicating a debt to Sir Eric Rideal, and the atmosphere pervading his laboratory at Cambridge when the present author was a research student there some 30 years ago.

From the point of view of conservation, it is well to recollect that the stratified object in mind, namely, a painting, is of necessity immersed in an environment of a certain relative humidity. It is this which occasions an exchange of energy between the layers and the surrounding air. The aim of the scientist is to reduce this exchange to a minimum, or, graphically expressed, to narrow the area of the hysteresis loop representing input and output of moisture. Wood, upon which many ancient pictures are painted, may be considered as a complex pseudo-colloid, possessing an approximately hexagonal symmetry. Its reactions to temperature and changes in moisture content (compared with dry weight) may therefore be expected to show anisotropic characters with respect to the direction of grain. Largely owing to this feature, strains are set up in the ground, paint, and surface layers above, and most cases of deterioration can be traced to the corresponding stresses. Theoretically, the water-vapor differential of canvas is opposite to that of wood, i.e., it shrinks when wet and expands when dry, but artists' canvas does not behave so; on account of the priming, its hygroscopic nature overpowers the normal molecular reorientation of the cellulose chains. Experiments carried out in the years before the World War II demonstrated clearly that equilibrium between support (wood or canvas) and its environment would be obtained at a relative humidity of around 58% at a temperature of approximately 63°F. Upon thermodynamic principles of this nature, the National Gallery's wartime deep-shelter repository was designed, and the experience so gained was in fact carried into permanent practice with the establishment of air-conditioning in part of the London building as soon as practicable after the cessation of hostilities. This matter of a satisfactory *modus vivendi* for great paintings has been discussed first because, manifestly, it is futile to apply chemical or physical methods to them individually, if year in year out they are being subjected to distortions akin to those found in reciprocating machinery, and which lead, first to "fatigue," and then possibly to ultimate collapse. Given, therefore, a reasonable "climate," we can hope to initiate means whereby pictures themselves can be scientifically treated.

Two major enquiries present themselves at once. One is the constitution of the natural resins (so widely used in the arts for surface coatings), and the other is the diffusion effect of organic solvents upon old linoxyn films, a factor of fundamental importance for a deeper understanding of the complicated process of cleaning.

I. Chromatography of Natural Resins

Paint media and varnishes have always been an intractable subject from the point of view of analysis; their constitution is most involved. For dammar and mastic (and no doubt for others, too), the distinction between the alcohol-soluble α-resene, and the alcohol-insoluble β-resene has a sound basis. The former has been found to be a complex mixture of triterpene alcohols, ketones, ketols, and so on, whereas the β-resene is a mixture of polymeric materials covering a wide range of molecular weights and of low oxygen content. The techniques of chromatography have proved of great value in this field.

II. Diffusion in Films

This general problem covers several associated matters: the process of diffusion of solvents into varnish, the solvent power of mixed liquids, and the mechanical properties of swollen varnishes. A beginning has been made upon all these. Optical methods (interference especially) have been used to tackle diffusion, the advance of the penetrant liquid causing a change in refractive index and thus a change of the Fizeau fringes from which the concentration gradient can be found. As regards solvent power, critical mixtures of organic liquids have been demonstrated with marked effect upon the degree of swelling. Mechanically, linoxyn bears some resemblance to rubber, and useful analogies may be expected from tests in rubber technology.

The study of new materials for use in the arts has not been neglected.

Examples are cold-setting adhesives, and the possibilities of Polythene and Saran as moisture barriers. In fact, one of the outstanding difficulties is, and has been, to evolve a completely satisfactory method of measuring the moisture permeability of surface films, in spite of several attempts by various workers on an industrial scale.

In general, the preoccupation of the laboratory with urgent *ad hoc* activities has not prevented, as the foregoing will have shown, due attention being devoted to long-term considerations, particularly of a kind stemming from the pioneer work of Sir Eric Rideal and his School.

ACKNOWLEDGMENTS

A substantial part of the studies described in this article has been carried out by the author's colleagues, Dr. A. E. Werner (now at the British Museum) and Miss R. J. Plesters. In addition, the development of chromatographic techniques and of the work upon linoxyn films are the contributions of the two Scholars on the Nuffield Foundation, Mr. J. S. Mills, and Mr. Ian Graham, who have undertaken research in this laboratory during the past few years.

JOURNAL OF COLLOID SCIENCE 11, 327–339 (1956)

A KINETIC STUDY OF THE REACTION BETWEEN FERRIMYOGLOBIN AND HYDROGEN PEROXIDE

Philip George and D. H. Irvine*

Department of Colloid Science, The University, Cambridge, England

Received March 1, 1956

ABSTRACT

The reaction between ferrimyoglobin, $Fe^{+}_{Mb}(H_2O)$, and hydrogen peroxide results in a one-equivalent oxidation of the hemoprotein giving a higher oxidation state of the molecule whose structure is best represented as a complex ferryl ion, $Fe_{Mb}O$. A kinetic study of the formation of this compound, ferrylmyoglobin, shows that there are two reaction paths, the acidic form of ferrimyoglobin, $Fe^{+}_{Mb}(H_2O)$, reacting with H_2O_2, and either the alkaline form, $Fe_{Mb}OH$, reacting with H_2O_2, or the acidic form reacting with O_2H^-.

Two possible reaction mechanisms for the formation of ferrylmyoglobin are examined in the light of the quantitative kinetic data obtained. The first involves the production of an OH radical in a reaction similar to that usually written for the ferrous ion reaction, except that the oxidation states are all higher by 1 in the ferrimyoglobin reaction. The second involves the initial formation of a +5 oxidation state in the rate-determining step, which then undergoes extremely rapid reduction to ferrylmyoglobin by reducing groups present in the system (i.e., in the protein part of the molecule). In the latter mechanism, ferrimyoglobin would conform to the same pattern of oxidation-reduction behavior shown by the hemoprotein enzymes, peroxidase and catalase.

INTRODUCTION

Ferrimyoglobin is a hemoprotein in which the prosthetic group, ferric protoporphyrin, is joined to a protein of molecular weight 17,000. When H_2O_2 is added to it a red compound is formed having well-defined spectroscopic characteristics (1). This compound was originally thought to be a complex of the enzyme-substrate type, and the view was strengthened by the work of Chance (2), who showed that the kinetics of the reactions of H_2O_2 and alkyl hydroperoxides with peroxidase and catalase, hemoproteins similar in structure to ferrimyoglobin, could be satisfactorily explained using a modification of the Michaelis-Menten mechanism of enzyme action.

In previous papers (3–6) we showed conclusively that the red compound is not an enzyme-substrate complex but a higher oxidation state of ferrimyoglobin, one oxidation equivalent above ferrimyoglobin, capable of being formed by other oxidizing agents besides peroxides. In other words, it reacts as if the iron is in the oxidation state +4. Other experimental studies showed the site of oxidation to be the iron atom itself, and not some other point in the very complicated molecule. Since it represents the first well-authenticated case of a stable derivative of quadrivalent iron, it is of interest in inorganic chemistry; and the reaction by which it is formed with hydrogen peroxide is of significance from the physicochemical standpoint for the following reason.

---

*Present addresses: P.G. Department of Chemistry, The University of Pennsylvania, Philadelphia. D.H.I. Department of Chemistry, University College, Ibadan, Nigeria.

Our earlier investigations showed that in the reaction of ferrimyoglobin with H_2O_2 a transient oxidizing entity was produced along with the stable red compound (3). This entity has many of the properties of the OH radical, and the chemistry of the ferrimyoglobin-H_2O_2 reaction can be satisfactorily accounted for on the assumption that it is formed:

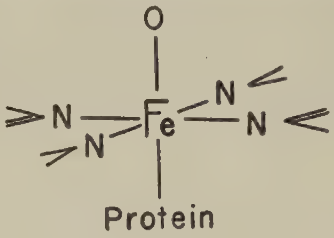

FIG. 1.

$$Fe^{3+}_{Mb}\,(H_2O) + H_2O_2 \rightarrow Fe^{IV}_{Mb} + OH + \text{etc.} \qquad [1]$$

where Fe^{3+}_{Mb} (H_2O) denotes ferrimyoglobin and Fe^{IV}_{Mb} the higher oxidation state. On this basis, therefore, there is a formal similarity to the first step in the reaction between the ferrous ion and hydrogen peroxide when it is written in the form

$$Fe^{2+}_{aq} + H_2O_2 \rightarrow Fe^{3+}_{aq} + OH + OH^-, \qquad [2]$$

the chief difference being that in the hemoprotein case the oxidation numbers are higher by 1 throughout.

Measurements of the change in pH which accompanies the formation of the higher oxidation state by potassium chloriridate, and also of the pH variation of the equilibrium constant for this reaction, show 2 moles of H^+ to be liberated per mole of ferrimyoglobin oxidized (6), i.e.,

$$Fe^{3+}_{Mb}\,(H_2O) + IrCl_6^{2-} \rightleftharpoons Fe^{IV}_{Mb} + 2H + IrCl_6^{3-} + \text{etc.} \qquad [3]$$

The structure which best fits these data, in relation to other reactions of the higher oxidation state, is that of a coordination compound of the hypothetical ferryl ion, FeO^{2+}, with four of the six bonds about the iron atom within the octahedral complex to pyrrolic nitrogen atoms of the porphyrin ring, the fifth linking the iron to a group in the protein, and the sixth binding the oxygen atom which characterizes the ferryl ion type of structure (Fig. 1). The higher oxidation state is thus conveniently referred to as "ferrylmyoglobin."

The present paper deals with the kinetics of its formation by H_2O_2 under various conditions of pH, temperature, and ionic strength. The significance of the results, and in particular the energetics, are discussed in the light of previous knowledge of the chemistry of the reaction and similar reactions of peroxidase and catalase.

EXPERIMENTAL

Materials. Ferrimyoglobin was prepared according to the method described previously (3). The H_2O_2 was pure 97% (w/w) free from inhibitors, kindly supplied by Laporte Chemicals Ltd.

Measurement of Rates. The rate of formation of ferrylmyoglobin was determined by measuring the change of optical density with time at a suitable wavelength (409 mμ), using a Unicam Quartz spectrophotometer adapted for work at constant temperature.

RESULTS

1. *The Effect of pH on the Rate of Formation*

Experiments were restricted to the pH region between 8.0 and 9.5, where it was known from previous investigations that only slight destruction of the hemoprotein molecule occurred during the oxidation (3). Within this region good second-order plots were obtained up to 80% reaction, but beyond this deviations from linearity were noticed. This was to be expected since, through side reactions, a little more than 1 mole of H_2O_2 is required to give 1 mole of ferrylmyoglobin. Figure 2 shows some of the second-order plots obtained at 22.0°C. and $I = 0.02$, and in Table I the values of the second-order constant, $k_{obs.}$, are listed for different pH values at four temperatures.

Inspection of the data shows that $k_{obs.}$ decreases slightly as the pH increases from about 8.0 to 8.5, but more markedly in the range 8.5 to 9.5. This effect could arise through the ionization of the peroxide molecule or a group in ferrimyoglobin itself, which is known to have a pK of about 9.0 (7). This group is believed to be a water molecule coordinated to the iron atom in the acidic form, for the ionization is accompanied by a profound alteration in the spectra of the ferrimyoglobin comparable to that resulting from the formation of its cyanide and azide complexes. In these reactions the change in magnetic susceptibility, from that appropriate to a "predominantly ionic" structure to that of a "predominantly covalent" struc-

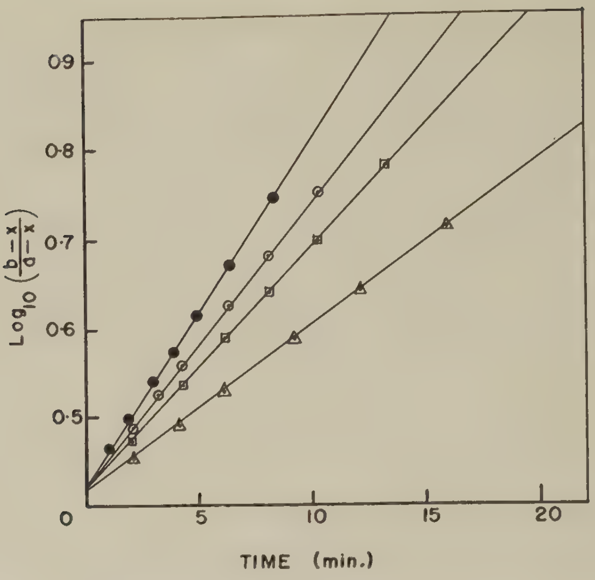

Fig. 2. Second-order plots for the ferrimyoglobin-H_2O_2 reaction at 22°C. and I = 0.02 at pH 8.02: ●; 8.43: ⊙; 8.81: ⊡; and 9.26: △.
Ferrimyoglobin concentration, $a = 4.34 \times 10^{-6}M$;
H_2O_2 concentration, $b = 11.49 \times 10^{-6}M$;
Ferrylmyoglobin concentration, x at time t.

TABLE I

Variation with pH of the Observed Second-Order Velocity Constants ($k_{obs.}$, l. mole^{-1} sec.$^{-1}$) for the Reaction of H_2O_2 with Ferrimyoglobin at I = 0.02

(a) T = 15.0 ± 0.1

pH	$k_{obs.}$
8.07	121 ± 2
8.27	106 ± 2
8.48	100 ± 3
8.66	92 ± 2
8.86	76 ± 2
9.08	68 ± 2

(b) T = 22.0 ± 0.2

pH	$k_{obs.}$
8.02	203 ± 5
8.22	183 ± 6
8.43	170 ± 3
8.61	165 ± 3
8.81	143 ± 2
9.03	118 ± 4
9.26	98 ± 2
9.46	85 ± 3

(c) T = 29.7 ± 0.3

pH	$k_{obs.}$
8.38	282 ± 11
8.56	251 ± 6
8.76	224 ± 7
8.98	211 ± 7
9.21	181 ± 11

(d) T = 36.0 ± 0.4

pH	$k_{obs.}$
8.34	473 ± 11
8.52	413 ± 11
8.72	335 ± 9
8.94	311 ± 12
9.17	277 ± 9

ture, leaves little doubt that the cyanide and azide are bonded to the iron. The ionization in question can thus be represented by the equation

$$\mathrm{Fe}_{\mathrm{Mb}}^{+}(\mathrm{H_2O}) \underset{}{\overset{K_{\mathrm{Fe}}}{\rightleftharpoons}} \mathrm{Fe_{Mb}OH} + \mathrm{H}^+ \qquad [4]$$

with the acidic form carrying a net charge of + 1, since two of the three positive charges of the ferric iron are cancelled by negative charges on two of the pyrrolic nitrogen atoms of the porphyrin ring. The corresponding formula for ferrylmyoglobin is $\mathrm{Fe_{Mb}O}$.

If the peroxide reacted exclusively through its anion, O_2H^-, then in the pH range 8.0 to 8.5, $k_{\mathrm{obs.}}$ would be approximately proportional to $1/\mathrm{H}^+$. The data in Table 1 are clearly inconsistent with this mechanism. But the two following mechanisms give identical kinetic expressions which account very well for the observed variation. First, if acidic and alkaline ferrimyoglobin react with peroxide with velocity constants k_a and k_b

$$\mathrm{Fe}_{\mathrm{Mb}}^{+}(\mathrm{H_2O}) + \mathrm{H_2O_2} \xrightarrow{k_a} \mathrm{Fe_{Mb}O} + \text{etc.}$$

$$\mathrm{Fe_{Mb}OH} + \mathrm{H_2O_2} \xrightarrow{k_b} \mathrm{Fe_{Mb}O} + \text{etc.},$$

$k_{\mathrm{obs.}}$ would vary with hydrogen ion concentration according to the equation

$$k_{\mathrm{obs.}} = \frac{k_a\mathrm{H}^+}{K_{\mathrm{Fe}} + \mathrm{H}^+} + \frac{k_b K_{\mathrm{Fe}}}{K_{\mathrm{Fe}} + \mathrm{H}^+}, \qquad [5]$$

where K_{Fe} is the ionization constant. This may be rearranged to give

$$k_{\mathrm{obs.}}(K_{\mathrm{Fe}} + \mathrm{H}^+) = k_a\mathrm{H}^+ + k_b K_{\mathrm{Fe}}. \qquad [5a]$$

On the other hand, if acidic ferrimyoglobin exclusively reacts with H_2O_2 and O_2H^-, with the velocity constants k_a and k'_b,

$$\mathrm{Fe}_{\mathrm{Mb}}^{+}(\mathrm{H_2O}) + \mathrm{H_2O_2} \xrightarrow{k_a} \mathrm{Fe_{Mb}O} + \text{etc.}$$

$$\mathrm{Fe}_{\mathrm{Mb}}^{+}(\mathrm{H_2O}) + \mathrm{O_2H^-} \xrightarrow{k'_b} \mathrm{Fe_{Mb}O} + \text{etc.}$$

then the rate equation is given by

$$k_{\mathrm{obs.}} = \frac{\mathrm{H}^+}{(K_{\mathrm{Fe}} + \mathrm{H}^+)}\left[\frac{k_a\mathrm{H}^+}{K_p + \mathrm{H}^+} + \frac{k'_b K_p}{K_p + \mathrm{H}^+}\right] \qquad [6]$$

where K_p is the ionization constant of hydrogen peroxide. Since $K_p \approx 2 \times 10^{-12}$, for the range of hydrogen ion concentration employed, $\mathrm{H}^+ \gg K_p$, so this equation can be simplified and rearranged to give

$$k_{\mathrm{obs.}}(K_{\mathrm{Fe}} + \mathrm{H}^+) = k_a\mathrm{H}^+ + k'_b K_p, \qquad [6a]$$

which is identical in form with Eq. [5a]. With the use of the values of K_{Fe} obtained from the work of George and Hanania (7), the resulting plot of

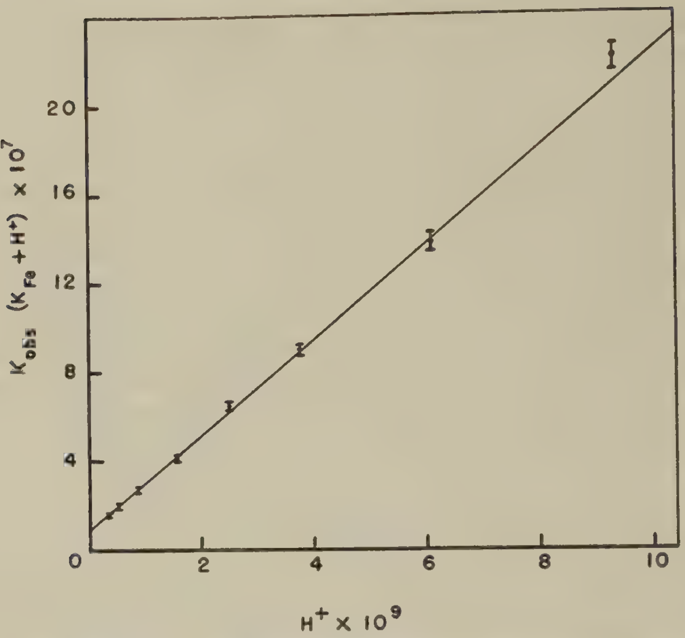

FIG. 3. Plot of $k_{obs.}(K_{Fe} + H^+)$ against H^+ for data obtained at 22°C. and I = 0.02. K_{Fe} is the ionization constant, $Fe^+_{Mb}\,(H_2O) \rightleftharpoons Fe^+_{Mb}OH + H^+$.

TABLE II

Variation with Temperature of the Velocity Constants k_a and k_b(l. mole^{-1} sec.$^{-1}$) for the Reaction of H_2O_2 with the Acidic and Alkaline Forms of Ferrimyoglobin

T, °C	k_a	k_b
15.0 ± 0.1	122 ± 2	22.0 ± 1.5
22.0 ± 0.2	220 ± 6	49.0 ± 3.0
29.7 ± 0.3	320 ± 16	140 ± 15
36.0 ± 0.4	607 ± 33	197 ± 22

$k_{obs.}\,(K_{Fe} + H^+)$ against H^+ is linear, as shown for the data at 22.0°C. and I = 0.02 in Fig. 3. Hence on this analysis alone both mechanisms are equally valid. Values of k_a have been obtained from the slopes of the lines at the four temperatures used, but values of k_b were arrived at by plotting $k_{obs.}\,(K_{Fe} + H^+)/H^+$ against $1/H^+$. This method was used in preference to that of utilizing the intercepts on the previous plots because, although subject to large errors, it was much more sensitive. The values of k_a and k_b are recorded in Table II, and from the latter k'_b can be evaluated from the relationship $k_bK_{Fe} = k'_bK_p$ which follows from the comparison of Eqs. [5*a*] and [6*a*].

It may be noted that in the plot of $k_{obs.}\,(K_{Fe} + H^+)$ against H^+ in Fig. 3, the point corresponding to the most acidic solution pH 8.02, does not lie on the straight line, and that the discrepancy is outside the limit of experimental error. Now it is known that there is another ionizable group in ferrimyoglobin, possibly on the amino acid residue to which the ferric protoporphyrin is attached, whose ionization affects the velocity constants, and hence the equilibrium constants for the formation of ferrimyoglobin fluoride, and cyanide (8–10). It has a pK of about 6.1 at 20°C. This ionization, therefore, is very likely the cause of the discrepancy. Dalziel and O'Brien (11) have observed a similar effect in the reaction of H_2O_2 with ferrihemoglobin, a hemoprotein of molecular weight 68,000 with four ferric protoporphyrin groups attached to it, which also possesses similar "heme-linked" ionizable groups (12). Unfortunately, in solutions acid to pH 8.0, since side reactions occur involving irreversible oxidation and destruction of the protoporphyrin (3), a reliable quantitative investigation of the participation of these ionizing groups cannot be made.

2. *The Effect of Temperature*

From plots of $\log_{10} k_a$ and $\log_{10} k_b$ against $1/T$ the activation energies were evaluated, and together with data for the variation of K_{F_0} and K_p with temperature (7, 13), the activation energy for the reaction with velocity constant k'_b was calculated, giving

$$\begin{aligned} k_a &= 10^{11.7\pm0.7} \text{ exp. } - (12{,}600 \pm 1000)/RT \\ k_b &= 10^{16.5\pm2.2} \text{ exp. } - (20{,}000 \pm 3000)/RT \\ k'_b &= 10^{17.4\pm2.2} \text{ exp. } - (17{,}600 \pm 2500)/RT \end{aligned}$$

3. *The Effect of Ionic Strength*

A direct experimental determination of the effect of ionic strength on the rate constant $k_{obs.}$ was impracticable because changing the ionic strength changed the pH of the buffer solution. It was therefore decided to estimate the effect by measuring the rate constant at a known ionic strength, determining the pH of the solution, and making a comparison with the constant calculated from Eqs. [5*a*] and [6*a*] according to various ionic strength variations of k_a and k_b, of k_a and k'_b. With the spectrophotometric technique employed it was not possible to carry out experiments in the absence of air, and absorption of carbon dioxide by very dilute buffer solutions in the pH range about 9.0 prevented an investigation of the ionic strength effect in this particular range, where the term containing k_b or k'_b makes a significant contribution to $k_{obs.}$. Data obtained at a pH of about 8.2 are given in Table III. On the assumption that k_a, and k_b or k'_b, are independent of ionic strength, calculated values of $k_{obs.}$ agree quite well with the experimental values, as shown by the comparison of columns 3 and 4. Since at this pH the term containing k_b or k'_b contributes only about 8% of $k_{obs.}$, the variations of $k_{obs.}$ with ionic strength would in any case be very little affected by any variation of k_b or k'_b, and it may be concluded that k_a, which contributes the remaining 92%, is therefore inde-

TABLE III

The Effect of Ionic Strength on the Rate Constant at $T = 25.0°C$.

I	pH	$k_{obs.}$	$k_{calc.}$
0.16	8.10	240 ± 6	235 ± 8
0.04	8.18	230 ± 5	227 ± 8
0.02	8.21	225 ± 5	224 ± 8
0.01	8.24	230 ± 10	222 ± 8
0.005	8.25	250 ± 5	222 ± 8
0.0025	8.23	245 ± 5	226 ± 8

pendent of ionic strength within experimental error. This is good evidence that k_a does not correspond to a reaction between ionic species, and it therefore supports the conclusion drawn from the kinetic analysis that the reaction involves the undissociated H_2O_2 molecule.

4. The Effect of Added Reducing Agents on the Rate of the Reaction

Previous experiments had shown that if a reducing agent was added to ferrimyoglobin before the addition of H_2O_2, then, provided the concentration of reducing agent did not exceed that of the ferrimyoglobin, ferrylmyoglobin was formed to almost the same extent as in the absence of the reducing agent (3). Measurement of the rate of formation under these conditions showed that this was also unaffected by the presence of the following reducing agents, ferrocyanide and iodide ions, tartaric acid, and mannitol. In these reactions deviations from second-order kinetics were observed after about 60% reaction. This can be attributed to partial reduction of the higher oxidation state by the reducing agent. When excess reducing agent was used, however, the couple ferrylmyoglobin/ferrimyoglobin acted as a catalyst for the oxidation of the reducing agent by peroxides. An account of this will be published elsewhere.

Discussion

The difficulty in making a choice between two reaction mechanisms that lead to the same dependence of velocity constant on hydrogen ion concentration is not unfamiliar in reaction kinetics. In the ionic-iron-hydrogen peroxide system, the electron transfer $Fe^{3+} + O_2^- \rightarrow Fe^{2+} + O_2$ is preferred to the hydrogen atom transfer $FeOH^{2+} + HO_2 \rightarrow Fe^{2+} + H_2O + O_2$ from a comparison with corresponding reactions of the cupric ion (14). In the oxidation of hydroquinones by ferric ions the electron transfer step $Fe^{3+} + Q^- \rightarrow Fe^{2+} + Q$ is preferred to hydrogen atom transfer in $FeOH^{2+} + QH \rightarrow Fe^{2+} + H_2O + Q$ in view of the magnitudes of the entropy of activation and the overall entropy change (15). In the present case no choice can yet be made between $Fe_{Mb}OH$ reacting with H_2O_2, and Fe^{+}_{Mb} (H_2O) reacting with O_2H^-; moreover in the case of such hemoprotein reactions a special difficulty can arise as the following considerations show.

The values of the temperature-independent factors for these two reactions are $10^{16.5\pm2.2}$ and $10^{17.4\pm2.2}$, respectively. High values are more appropriate to reactions between oppositely charged ions (16), so this criterion appears to favor the latter reaction, viz., $\mathrm{Fe}^{+}_{\mathrm{Mb}}\,(\mathrm{H_2O}) + \mathrm{O_2H^-}$. However, in the pH range 8 to 9.5 where the measurements were made, which is alkaline with respect to the isoelectric point of myoglobin, studies of the variation of the ionization constant, K_{Fe}, as a function of ionic strength, indicate that the ionization is accompanied by a change in charge on the iron atom of -2 to -3, provided the simple Debye-Hückel theory is applicable to these systems (7). In other words, the net negative charge on the protein as a whole, which titration studies show is of the order -10 in this pH range (6), results in the iron atom "carrying" an effective negative charge of -2 in its acidic form and -3 in its alkaline form. This being so, the reaction of $\mathrm{Fe}^{+}_{\mathrm{Mb}}\,(\mathrm{H_2O})$ with $\mathrm{O_2H^-}$ would involve species with charges of -2 and -1 and so the magnitude of the temperature-independent factor really favors the other alternative, $\mathrm{Fe_{Mb}OH}$ reacting with $\mathrm{H_2O_2}$.

There is little doubt, however, that the chief reaction path in the pH range 8 to 9 entails $\mathrm{Fe}^{+}_{\mathrm{Mb}}\,(\mathrm{H_2O})$ reacting with $\mathrm{H_2O_2}$, and the heat of the reaction can be calculated using thermochemical and bond energy data from the literature to compare with the observed activation energy of 12.6 ± 1 kcal./mole. If it is assumed, as the evidence would appear to indicate, that an OH radical is formed together with ferrylmyoglobin in the oxidation by $\mathrm{H_2O_2}$, and that one $\mathrm{H^+}$ is liberated, the first step in the reaction of $\mathrm{H_2O_2}$ with acidic ferrimyoglobin would be given by the equation:

$$\mathrm{Fe}^{+}_{\mathrm{Mb}}\,(\mathrm{H_2O}) + \mathrm{H_2O_2} \rightarrow \mathrm{Fe_{Mb}O} + \mathrm{H_3O^+} + \mathrm{OH}\bullet \qquad [7]$$

The heat of this reaction can be calculated from the heat of the following steps (6):

$$\mathrm{Fe}^{+}_{\mathrm{Mb}}\,(\mathrm{H_2O}) + \mathrm{IrCl_6^{2-}} \rightarrow \mathrm{Fe_{Mb}O} + 2\mathrm{H^+} + \mathrm{IrCl_6^{3-}} - 9.0 \pm 1.0\ \text{kcal./mole} \qquad [8]$$

$$\mathrm{IrCl_6^{3-}} + \mathrm{H^+} \rightarrow \mathrm{IrCl_6^{2-}} + \tfrac{1}{2}\mathrm{H_2} - 30.5 \pm 0.5\ \text{kcal./mole} \qquad [9]$$

$$\mathrm{H_2O_2} + \tfrac{1}{2}\,\mathrm{H_2} \rightarrow \mathrm{OH}\cdot + \mathrm{H_2O} + 21.6 \pm 2.0\ \text{kcal./mole} \qquad [10]$$

to give the value -17.9 ± 3.5 kcal./mole. The heat of reaction [10] is 22.3 kcal./mole according to the standard heats of formation quoted by Latimer (17) for $(\mathrm{H_2O})_{\mathrm{l}}$, $(\mathrm{H_2O_2})_{\mathrm{aq.}}$ and $(\mathrm{OH}\cdot)_{\mathrm{g}}$ together with the values of 10.5 and 1.4 kcal./mole for the heats of solution of OH and $\mathrm{H_2}$, respectively, adopted by Evans, Hush, and Uri (18). From the bond energy data compiled by these authors, the heat of reaction [10] is found to be 20.8 kcal./mole. A mean value of 21.6 has been taken as the best approximation and the uncertainty put at ±2.0 kcal./mole.

The endothermicity of reaction [7] is thus 17.9 ± 3.5 kcal./mole, and the observed activation energy 12.6 ± 1.0 kcal./mole. Although the discrepancy is quite small, amounting to only 0.8 kcal./mole if the highest activation energy and lowest endothermicity are chosen, these calculations suggest that reaction [7] may not be the actual rate-determining step. Consideration should therefore be given to a second reaction mechanism which could satisfy the energetics and still be consistent with the other experimental observations. This entails a rate-determining step in which peroxide effects a two-equivalent oxidation, giving a compound in which the iron is in the oxidation state +5, followed by the very rapid reduction of this compound to ferrylmyoglobin by reducing matter present in the system.

$$\mathrm{Fe}^{+}_{\mathrm{Mb}}\,(\mathrm{H_2O}) + \mathrm{H_2O_2} \xrightarrow[\text{step}]{\text{rate-determining}} \mathrm{Fe}^{\mathrm{V}}_{\mathrm{Mb}} + \text{etc.}$$

$$\mathrm{Fe}^{\mathrm{V}}_{\mathrm{Mb}} \xrightarrow{\text{single-equiv. reduction}} \mathrm{Fe}_{\mathrm{Mb}}\mathrm{O} + \text{etc.}$$

The assumption of a rapid reduction step is essential to account for the fact that the rate of formation of ferrylmyoglobin is unaffected by the addition of reducing agents, and for the observation that during the course of the reaction only the two species, ferrimyoglobin and ferrylmyoglobin, have been detected spectrophotometrically. On this hypothesis, the reactions previously attributed to the OH radical would be assigned to the single-equivalent oxidation products formed by the attack of the +5 oxidation state on the reducing matter present, e.g., groups on the protein. Transient radical species could easily result from an attack of this kind. The reaction which was taken to indicate the presence of the OH radical, namely, the luminol test, would also occur with these other species, provided they were strong enough oxidizing agents. The complex ion, Ru (dipy)$_3^{3+}$, with $E_0 = 1.35$ v., and the permanganate ion, $E_0 = 0.56$ v., were found to oxidize luminol with an intense luminescence, showing this test not to be a characteristic of the OH radical as such, but merely an indication of its great oxidizing power and the rapidity with which it reacts.

In this connection it is interesting to note that Cahill and Taube (19) have recently presented evidence which suggests that in the ferrous ion-hydrogen peroxide system, two-equivalent oxidation to give a quadrivalent iron compound is the important initiating reaction

$$\mathrm{Fe}^{2+}_{\mathrm{aq.}} + \mathrm{H_2O_2} \rightarrow \mathrm{Fe}^{\mathrm{IV}}_{\mathrm{aq.}} + \text{etc.}$$

However, the detailed kinetics have been explained so far only by a free radical mechanism in which the OH· radical is formed initially as in reaction [2]: the need to postulate the formation of a quadrivalent iron compound, possibly the ferryl ion, arose only when high ferric ion concentrations were present (14, 20).

An interesting feature of the ferrimyoglobin-hydrogen peroxide reaction is the contrast between the rate data for the two reaction paths. In the reaction of H_2O_2 with the acidic form, the activation energy 12.6 ± 1.0 kcal./mole is relatively low, favoring the reaction, whereas the entropy

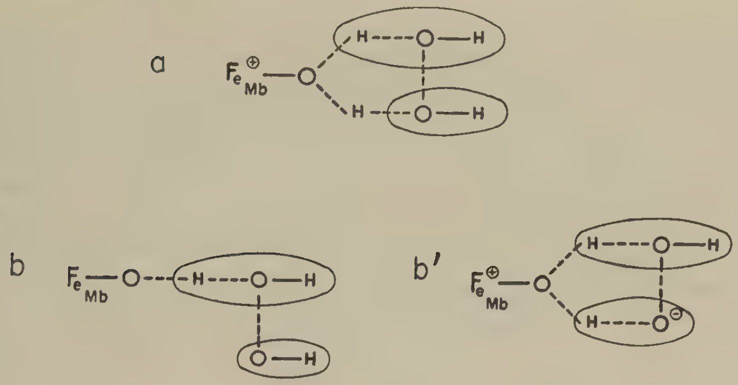

Fig. 4.

of activation, calculated to be −6.6 ± 1.5 e.u., is unfavorable. In the case of the alkaline form reacting with H_2O_2, or alternatively the acidic form reacting with O_2H^-, the activation energies, 20.0 ± 3.0 and 17.6 ± 2.5 kcal./mole are much higher, but the entropies of activation are favorable, +15 ± 10 and + 19.5 ± 10 e.u., respectively. Since the formation of ferrylmyoglobin requires the removal of both hydrogen atoms bonded to the oxygen in the coordinated water molecule of acidic ferrimyoglobin, or the single hydrogen atom attached in the OH group of the alkaline form, the various transition states can be pictured as shown in Fig. 4, for the mechanism involving OH radical production. According to the second mechanism involving the initial formation of a +5 oxidation state, provided this also had a bonded oxygen atom structure, the required alignment of the reactants would be substantially the same. The negative entropy of activation of reaction *a* could be attributed to the special orientation required for the H_2O_2 molecule, with the peroxidic oxygen atoms bridging the hydrogen atoms of the coordinated water molecule. In view of the favorable entropy of activation for the second path, the need for no special orientation in reaction *b*, in contrast to reaction *b′* which resembles reaction *a* in this respect, could be regarded as evidence that this is the more likely of the two alternatives. The differences in activation energy agree with this interpretation. It is likely that in ferrylmyoglobin a strong Fe—O bond is formed, and this could also be the case in the +5 state. But there is already quite a strong Fe—O bond in the alkaline form of ferrimyoglobin, since kinetic studies show this form to be unreactive in cyanide and fluoride complex formation (9), whereas, when the acidic form reacts, the formation of the Fe—O bond in the higher oxidation state would provide a greater balance of energy to offset the loss from bond-fission.

Finally a comparison may be drawn between the reaction of peroxides with ferrimyoglobin and with the enzymes peroxidase and catalase, two similar hemoproteins in so far as they have the same prosthetic group. In both of the enzyme systems the participation of two intermediate compounds is well established. One of these resembles ferrylmyoglobin, in that it is a single-equivalent oxidation product; the other is either a two-equivalent oxidation product, or a peroxide complex, i.e., containing H_2O_2 or O_2H^- as the ligand (21). Recent studies (22) favor the +5 oxidation state, and the interrelationship of the various compounds can be expressed by the following scheme, where Fe_p^{3+} denotes the ferriprotoporphyrin prosthetic group of peroxidase or catalase, and AH_2 denotes a reducing agent,

$$Fe_p^{3+} + H_2O_2 \xrightarrow[\text{oxidation}]{\text{2-equiv.}} Fe_p^{V} + \text{etc.}$$

$$\begin{tikzcd}
Fe_p^{V} + AH_2 \arrow[r, "\text{one-equiv.}", "\text{reduction}"'] & {[Fe_p^{IV}\cdot AH]} \arrow[r, "\text{separation}"] \arrow[d] & Fe_p^{IV} + AH + \text{etc.} \arrow[d, "+AH_2"] \\
& Fe_p^{3+} + A + \text{etc.} & Fe_p^{3+} + \text{etc.} \\
& \text{Catalase Action} & \text{Peroxidase Action}
\end{tikzcd}$$

The catalytic action of peroxidase involves, in turn, the two single-equivalent reduction steps, $Fe_p^{V} \rightarrow Fe_p^{IV}$ and $Fe_p^{IV} \rightarrow Fe_p^{3+}$ (23). Although the action of catalase appears to involve a distinct two-equivalent reduction, $Fe_p^{V} \rightarrow Fe_p^{3+}$, it is more likely, for two reasons, that a single-equivalent reduction of Fe_p^{V} occurs initially and then a further reduction of Fe_p^{IV} within the reaction "cage," a small fraction escaping during each cycle. Firstly, the Fe_p^{IV} compound of catalase is actually formed progressively during the course of the oxidation of those reducing agents which appear to undergo the two-equivalent oxidation (24), and secondly, in the presence of the appropriate reducing agent (aromatic amines or phenols), catalase action, just like that of peroxidase (25), proceeds by the two distinct single-equivalent reduction steps. If the ferrimyoglobin reaction gives a +5 oxidation state, the reaction of all three hemoproteins would fit into the same pattern of oxidation-reduction behavior, the differences being of degree rather than kind. The greater catalytic activity of peroxidase and catalase would then be attributable primarily to the higher speed of the initial two-equivalent oxidation of the prosthetic group. The indiscriminate reduction of the +5 state of myoglobin to ferrylmyoglobin would also distinguish the two systems, through the waste of oxidizing capacity. On the other hand, if the ferrimyoglobin reaction proceeds with OH radical formation, then the smaller catalytic activity would be attributable essentially to the lower speed of the single-equivalent oxidation of the ferrimyoglobin.

REFERENCES

1. KEILIN, D., AND HARTREE, E. F., *Proc. Roy. Soc. (London)* **B117,** 1 (1935).
2. CHANCE, B., "The Enzymes," Vol. 2, Part 1, p. 428. Academic Press, New York, 1951.

3. George, P., and Irvine, D. H., *Biochem. J.* **52,** 511 (1952).
4. George, P., and Irvine, D. H., *Biochem. J.* **55,** 230 (1953).
5. George, P., and Irvine, D. H., *Biochem. J.* **58,** 188 (1954).
6. George, P., and Irvine, D. H., *Biochem. J.* **60,** 596 (1955).
7. George, P., and Hanania, G. I. H., *Biochem. J.* **52,** 517 (1952).
8. George, P., and Hanania, G. I. H., *Biochem. J.* **56,** xxxvii (1954).
9. George, P., and Hanania, G. I. H., *Biochem. J.* **56,** xxxviii (1954).
10. George, P., and Hanania, G. I. H., *Discussions Faraday Soc.* No. **20,** 216 (1955).
11. Dalziel, K., and O'Brien, J. R. P., *Biochem. J.* **56,** 648 (1954).
12. Wyman, J., Jr., *Advances in Protein Chem.* **4,** 410 (1948).
13. Evans, M. G., and Uri, N., *Trans. Faraday Soc.* **45,** 224 (1949).
14. Barb, W., Baxendale, J. H., George, P., and Hargrave, K. R., *Trans. Faraday Soc.* **47,** 462 (1951).
15. Baxendale, J. H., Hardy, H. R., and Sutcliffe, L. H., *Trans. Faraday Soc.* **47,** 963 (1951).
16. Glasstone, S., Laidler, K. J., and Eyring, H., "The Theory of Rate Processes." McGraw-Hill, New York, 1941.
17. Latimer, W. M., "Oxidation Potentials." Prentice-Hall, New York, 1952.
18. Evans, M. G., Hush, N. S., and Uri, N., *Quart. Revs.* (*London*) **6,** 186 (1952).
19. Cahill, A. E., and Taube, H., *J. Am. Chem. Soc.* **74,** 2312 (1952).
20. Barb, W., Baxendale, J. H., George, P., and Hargrave, K. R., *Trans. Faraday Soc.* **47,** 591 (1951).
21. George, P., and Irvine, D. H., *Brit. J. Radiol.* **27,** 131 (1954).
22. George, P., *Science* **117,** 220 (1953).
23. George, P., *Biochem. J.* **54,** 267 (1953).
24. Chance, B., *J. Biol. Chem.* **179,** 1341 (1949).
25. George, P., *Biochem. J.* **52,** xix (1952).

JOURNAL OF COLLOID SCIENCE **11,** 340–351 (1956)

EXPERIMENTAL STUDIES ON THE LIGHT-SCATTERING METHOD AND ITS CALIBRATION

W. J. Hughes, P. Johnson, and R. H. Ottewill

Department of Colloid Science, The University, Cambridge, England

Received March 20, 1956

INTRODUCTION

In a previous paper from this laboratory (1), a simple, inexpensive, and yet accurate light-scattering photometer was described and its performance was demonstrated. The light-scattering envelope showed freedom from extraneous scattering and molecular weight determinations for bovine serum albumin gave values which, though slightly higher than that accepted generally on the basis of all physical data, were in line with those of other light-scattering workers. Such values utilized a calibration based upon the turbidity of a suitable aqueous fluid and there is no reason to doubt its inherent soundness. However, for some experimental work the use of nonaqueous calibrating solutions is desirable, but such a calibration (using a solution of polystyrene in toluene) resulted in molecular weights for bovine serum albumin which were some 20% low. On the other hand, the turbidity at $\lambda = 5461$ A. of "Cornell" polystyrene in 0.5% solution in toluene (2), based upon the nonaqueous calibration, was in good agreement with the generally accepted value determined by Brice, Halwer, and Speiser (3).

Whereas aqueous and nonaqueous systems *within themselves* behaved consistently, it seemed likely that the discrepancy arose as a result of refraction effects occurring between the aqueous bath fluid and the contents of the rectangular light-scattering cell. It should be mentioned that the apparatus, in achieving high sensitivity, used a converging beam of light, and it seemed probable that the application of the usual cone angle correction for the scattered beam was not sufficient for solutions which differed in refractive index from the bath fluid. To retain the optical blackening on various parts of the apparatus, only aqueous bath fluids were permissible, so that refraction was unavoidable whenever nonaqueous light-scattering solutions were used. On this view the reasonable value of the turbidity for the "Cornell" polystyrene solution probably arose from the cancellation of refraction effects in the calibration and measuring procedures. Such cancellation would not, of course, occur when a nonaqueous calibration was applied to an aqueous scattering system.

Another possible (though improbable) cause was that the "receiving" system of the apparatus was almost seeing past the edge of the light beam through the cell. Thus any added refraction effects might worsen the situation, and difficulties of the type described by Hermans and Levinson (4) could be expected. Whatever the nature of the calibrating fluid, its turbidity, upon which the calibrations depend, was determined by a Unicam spectrophotometer. Any errors arising in this procedure should therefore affect both aqueous and nonaqueous fluids.

In the work described here, a systematic attempt to explain the calibration discrepancy was made, culminating in the design of a new "universal" apparatus (5) which, it is found, can be safely used for light-scattering liquids of any refractive index and which still largely retains the simplicity of the earlier model.

Experimental

The light-scattering apparatus used initially has already been fully described (1, 2), and only salient points will be mentioned here. The entrance slit, of length 2.0 cm., was illuminated by an 80-watt Hg arc fed by a stabilized 200-volt a.-c. supply. An image of the slit, at unit magnification, was projected within the rectangular light-scattering cell (internal dimensions 5 × 5 × 1 cm.), which was situated centrally in the lower part of a conical flask (diameter of base 12.5 cm.) containing an aqueous bath liquid. The cell was surrounded by a suitable system of blackened baffles and, except for the windows, the outside of the conical flask was painted dull black. Scattered light was focused by means of a lens upon an R.C.A. 931A electron multiplier tube, masked by a slit of length 1.5 cm., which actuated a sensitive galvanometer (Tinsley type 4500 A.). The whole receiving system could be rotated about a vertical axis through the center of the light-scattering cell.

In using the apparatus a secondary standard block, usually of Transpex[1] (polymethyl methacrylate), was used and all galvanometer deflections were taken relative to the standard block scattering in the 90° position to the incident beam. Thus experimental readings were independent of slow variations in the intensity of the lamp or in the sensitivity of the electron multiplier system. The 5461 A line of the Hg arc, isolated by a Wratten 77 (or 77A) filter, was used unless otherwise stated. When required, the 4358 A line was obtained by using a combination of Ilford 809 and 601 filters.

Materials

The following calibrating substances were used:

Turnip Yellow virus (T.Y.V.), kindly supplied by Dr. R. Markham (6) as a crystalline solid under saturated ammonium sulfate, which could be stored for several months at 4°C. It was used in phosphate buffer (pH = 6.4; I = 0.05) at a concentration of up to 0.5%.

---

[1] Supplied by I.C.I. Ltd.

Ludox[2], a silica suspension in water, was diluted to 1%–2% with distilled water.

Polystyrene[3] (DC/PJ 3—with a turbidity at $\lambda = 5461$ A in ½% toluene solution of 7.88×10^{-4} cm.$^{-1}$ (2)) was used, as in previous work, in toluene/ethanol solution which was prepared as follows: 2 g. polystyrene were dissolved in toluene and the volume made up to 100 ml., to which 36 ml. of absolute ethanol were added to give slight opacity. The dissymmetry of such solutions was 1.10 ± 0.015 and appropriate correction was made to the 90° deflections in calibration experiments. Such corrections were not used for the aqueous calibrating solutions.

Several reference substances were also used. Armour crystalline bovine serum albumin and lysozyme, as well as a series of transfusion dextrans in 0.9% NaCl provided by the Medical Research Council, were used in aqueous solution. Polystyrene samples, distributed by the International Union of Chemistry, were also used in methyl ethyl ketone solution.

Aqueous solvents were made up from distilled water and A.R. chemicals. Sulfur-free toluene was stood over sodium wire and distilled. Carbon disulfide was repeatedly shaken with clean mercury until no discoloration was produced, dried over $CaCl_2$, and twice distilled; only the middle third was collected. Methyl ethyl ketone was washed with saturated aqueous K_2CO_3, dried over anhydrous K_2CO_3 and Na_2SO_4, and fractionally distilled. Absolute ethyl alcohol was used.

Aqueous solutions were filtered before use through "gradacol" membranes (7), organic solvents and solutions through No. 4 or 5 sintered glass filters. Dissymmetries of ca. 1.02 and 1.01 were routinely obtained for aqueous and organic solvents, respectively.

In determining absolute turbidities, the clarified solution, in the 5-cm. light-scattering cell was examined against solvent in a matched cell in the Unicam spectrophotometer (Model SP500) immediately before and after measurement in the light-scattering apparatus. Slit widths up to 0.02 mm. only were employed in the spectrophotometer, in which the photocell normally receives light from a cone of semiangle 2°. In experiments quoted later, the effect of reducing the cone angle is considered.

The Cone Angle Correction

When the scattered light leaves the cell through a plane face, refraction occurs and if scattering liquids of varying refractive index are to be compared, this must be done on the basis of identical angles for the cones of

[2] Kindly supplied by E. I. Dupont de Nemours and Co., Inc.

[3] Kindly supplied by Distillers Co. Ltd.

scattered light. For the apparatus described the corrections, worked out in detail elsewhere (8, 9), assume a particularly simple form. Thus let I'_{90} (obs.) be the galvanometer deflection caused by the scattering of a solution of refractive index n_c, placed in the cell which is surrounded by a cylindrical bath of liquid of refractive index n_b. It is assumed that the dimensions of the bath are large compared with the linear dimensions of the scattering volume; thus scattered light leaves the bath radially. Then if I'_{90} (corr.) is the actual galvanometer deflection in absence of refraction effects (i.e., $n_b = n_c$),

$$I'_{90}(\text{corr.}) = I'_{90}(\text{obs.}) \left(\frac{n_c}{n_b}\right)^2. \qquad [1]$$

In practice, the ratio of the actual galvanometer deflection for the scattering solution to that of the standard block is utilized, and since n_b may vary between experiments, refraction effects may modify the standard block deflection. It is thus necessary to correct the latter to some standard condition. For this purpose, it is customary to choose water as the bath liquid. Let S_{st} be the galvanometer deflection if Transpex of refractive index n_{st} filled the bath and S_0 with water of refractive index n_0. Then by analogy with [1]

$$S_0 = S_{st} \left(\frac{n_0}{n_{st}}\right)^2. \qquad [2]$$

Similarly with a liquid of refractive index n_b in the outer bath, the observed deflection ($S_{\text{obs.}}$) becomes

$$S_{\text{obs.}} = S_{st} \left(\frac{n_b}{n_{st}}\right)^2. \qquad [3]$$

Thus we have

$$\begin{aligned} S_0 &= S_{st} \left(\frac{n_b}{n_{st}}\right)^2 \cdot \left(\frac{n_0}{n_b}\right)^2 \\ &= S_{\text{obs.}} \left(\frac{n_0}{n_b}\right)^2. \end{aligned} \qquad [4]$$

Thus the ratio of the actual corrected galvanometer deflection for the scattering solution to that for the standard block is

$$I_{90}(\text{corr.}) = \frac{I'_{90}(\text{corr.})}{S_0} = \frac{I'_{90}(\text{obs.}) \left(\frac{n_c}{n_b}\right)^2}{S(\text{obs.}) \left(\frac{n_0}{n_b}\right)^2} = \frac{I'_{90}(\text{obs.})}{S(\text{obs.})} \left(\frac{n_c}{n_0}\right)^2, \qquad [5]$$

in which it is to be noted that n_b no longer occurs.

Assuming a system of ideal Rayleigh scatterers and corresponding proportionality between turbidity τ (or Rayleigh ratio) and the scattered intensity at 90° to the incident beam, we have

$$\tau = C\mathrm{I}_{90}(\mathrm{corr.}) \tag{6}$$

$$= C\left(\frac{n_c}{n_0}\right)^2 \frac{\mathrm{I}'_{90}(\mathrm{obs.})}{S(\mathrm{obs.})} \tag{7}$$

$$= C(\mathrm{obs.})\,\frac{\mathrm{I}'_{90}(\mathrm{obs.})}{S(\mathrm{obs.})} \tag{8}$$

where

$$C = C(\mathrm{obs.})\left(\frac{n_0}{n_c}\right)^2 \tag{9}$$

Thus if the cone angle correction were the only refraction correction involved in the apparatus, the constant C of a given apparatus, connecting the turbidity (or Rayleigh ratio) with the corrected galvanometer deflection for the 90° direction, could be obtained from measurements of τ and I_{90} (obs.) on a solution of any known refractive index. Again it is to be noted that the refractive index of the bath n_b is not involved in Eq. [9].

Table I contains data obtained in a test of these conclusions. It is clear that the C values of Table I, (after correction for exit cone angle effect) are not constant for scattering solutions of differing refractive index, so that Eq. [9] cannot be regarded as a complete correction procedure for the convergent-beam light-scattering apparatus described. It is also to be noted, however, in line with Eq. [9] that, for a given scattering solution, changes in the refractive index of the bath fluid do not affect C_{obs}. Further, even

TABLE I

Effect of Variation of Liquid in Cell and Outer Bath on Calibration Constant

Scattering Solution	Bath Liquid	n_b	n_c	$C_{\mathrm{obs}} \times 10^3$	$C \times 10^3$ (from Eq. [9])
T.Y.V. in phosphate buffer	Water	1.333	1.333	4.36	4.36
Ludox in water	Water	1.333	1.333	4.30	4.30
Ludox in water	Aqueous $CaCl_2$	1.384	1.333	4.30	4.30
Polystyrene in toluene/EtOH	Water	1.333	1.466	4.13	3.42
Polystyrene in toluene/EtOH	Aqueous $CaCl_2$	1.426	1.466	4.33	3.58
Polystyrene in EtCOMe/EtOH	Water	1.333	1.384	3.82	3.54
Polystyrene in EtCOMe/EtOH	Aqueous $CaCl_2$	1.384	1.384	3.84	3.56

when a given scattering solution is surrounded by a bath liquid of identical refractive index, the C value varies with n_c. This result probably appears surprising at first sight, but it should be recalled that refraction effects would not be absent in such cases with the Transpex block.

A similar series of experiments was performed with a carbon disulfide solution, in a rectangular cell, as secondary standard in place of the usual Transpex block, which allowed the use of organic solvents in the surrounding bath. Substantially similar results were obtained.

Optical Tests

It was thought possible that whereas the receiver of the apparatus could not "see" outside the edge of the light beam with aqueous scattering solutions (which have been mainly studied), this might not be true for organic solvents. Thus experiments were carried out, with aqueous and nonaqueous scattering solutions, in which the depth of the beam was increased by enlarging the source slit by small though significant amounts; the final slit masking the electron multiplier tube was shortened. These modifications were made both separately and concurrently and the constant C was evaluated for each arrangement (Table II). It seems clear from Table II that the receiving system is "seeing" well within the light beam as it was designed to do (1, 2).

Parallel Beam Experiments

Since possible refraction effects at the exit beam are largely eliminated by the application of the cone angle correction, the outstanding possibility of similar effects occurring at the entry of the light beam remained. As the light beam enters the conical liquid bath, not only is it deviated but also its convergence is affected, whilst further refraction may occur at the plane face of the scattering solution. To assess theoretically the whole effect

TABLE II

Optical Tests of Apparatus

Normal length of illuminating slit = 2.0 cm.
Normal length of receiving slit = 1.5 cm.

Solution	Length of receiving slit (cm.)	Illuminating Slit 2.5 cm.		Illuminating Slit 2.0 cm.	
		I_{90}	$C \times 10^3$	I_{90}	$C \times 10^3$
Polystyrene in toluene/ethanol	1.0	0.157	3.66	0.157	3.66
	1.5	0.157	3.66	0.159	3.58
T.Y.V. in phosphate buffer	1.0	2.03	4.31	2.01	4.33
	1.5	Normal calibration		—	4.35
Ludox suspension	1.0	8.30	4.42	8.36	4.37
	1.5	8.42	4.34	8.53	4.28

TABLE III

Experiments with a Parallel Beam of Light

Solution	n_c	C_{obs}	$C \times 10^3$ (Eq. [9]).	M Wt. of Bovine Serum Albumin
T.Y.V. in phosphate buffer	1.333	4.87	4.87	77,000
		4.82	4.82	76,300
Polystyrene in toluene/ethanol	1.466	5.67	4.70	74,600
		5.75	4.77	75,400
Polystyrene in EtCOMe/EtOH	1.384	4.92	4.57	72,300
		4.56	4.52	71,500
Mean			4.69	74,500 ± 2500

of changing n_b and n_c on the incident intensity at the scattering volume would thus have been very difficult. Accordingly the optics were considerably simplified by removing the liquid bath and by using a parallel beam of incident light. Since the latter strikes the plane face of the scattering solution at normal incidence, the volume of liquid illuminated does not vary as its refractive index is changed. Table III contains the summarized results and includes a calculation of the molecular weight of bovine serum albumin based upon the different C values.

Within the experimental error of this set of experiments, C is a constant independent of the refractive index of the scattering solution. The molecular weight value for bovine serum albumin, 74,500 ± 2500, agrees well in absolute magnitude and in its scatter with that reported by other light-scattering workers (e.g., Edsall *et al.* (9)). In view of the modified optics, it is of interest that the C value of Table III agrees so closely with those of previous tables; in explanation it is to be remembered that I_{90} readings are taken relative to the same Transpex standard block.

PARALLEL BEAM APPARATUS

Table III thus indicates strongly the disappearance of the calibration discrepancy with the use of an incident parallel beam of light rather than a convergent one. However, a more conclusive proof was obtained by constructing an entirely new apparatus provided with an accurately parallel incident beam. To reduce refraction effects and spurious reflections, a cylindrical brass liquid bath with plane glass entrance and exit windows and a cylindrical strip of glass for the passage of scattered light was constructed around the rectangular light-scattering cells already described (Fig. 1). A system of baffles was designed to prevent light from the cell corners reaching the receiving system, and apart from the glass surfaces, the whole assembly was blackened by the Relonol[4] process. It was thus

---

[4] Details kindly made available by British Scientific Instruments Research Association.

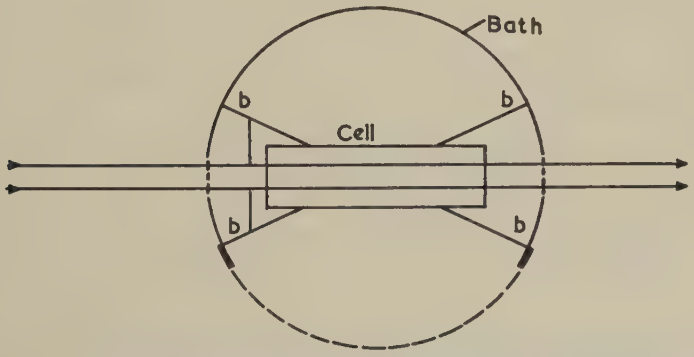

FIG. 1. Light-scattering cell and surrounding liquid bath (*b*—blackened baffles; - - - - —windows).

possible to use aqueous or nonaqueous fluids in the bath. The loss in sensitivity which resulted from the use of parallel rather than convergent incident light was more than regained by the use of a cathode-follower amplifier by which current amplification of up to 1000 could be obtained without instability. An IP 21 electron multiplier was used in a receiving system which was very similar to that of the original apparatus. As the secondary standard for this apparatus, a polished glass block[5] of suitable turbidity replaced the Transpex block; it could be immersed in organic as well as aqueous liquids. Light-scattering envelopes for the range $\theta = 40°$ to 140° (θ being the angle made by the direction of scattering with the incident direction) were determined for aqueous and nonaqueous solutions and solvents. Within this range, no irregular reflections occurred. Further by examination of the fluorescence from a dilute fluorescene solution, the lack of any geometrical dissymmetry was demonstrated (5).

The validity of the cone angle correction was shown for an aqueous Ludox suspension and a toluene solution of polystyrene by measuring the change in scattering with varying refractive index of the bath fluid. Since nonaqueous fluids were used for this purpose and the glass standard block was not then available, the actual galvanometer deflections I'_{90} were multiplied by $(n_c)^2/(n_b)$ and plotted against $(n_b)^2$ (see Eq. [1]). Figure 2 gives such plots which approximate closely to horizontal lines: the scatter of points occurring is probably largely due to lamp fluctuations. Thus the cone angle correction appears to be valid.

For a test of the calibration of the instrument (Table IV), solutions similar to those of Table I were used.

Within experimental error the constant C is thus independent of the nature of the scattering solution, in confirmation of the indications of

---

[5] We are grateful to Mr. R. D. Maurer of Corning Glass Works for the gift of the glass from which the block was made.

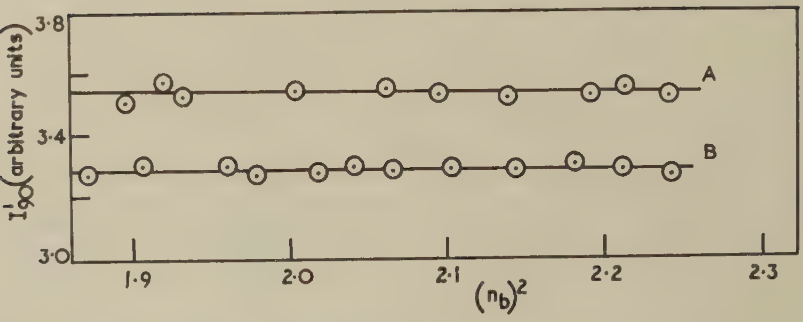

FIG. 2. The validity of the cone angle correction. A plot of corrected galvanometer deflection against the square of the refractive index of the bath liquid $(n_b)^2$ for Ludox in water (*A*) and polystyrene in toluene/ethanol (*B*).

TABLE IV

Calibration of "Universal" Light-Scattering Instrument
(Bath liquid—water (n_b = 1.333)

Scattering Solution	n_c	Dissymmetry I_{60}/I_{120}	Depolarization	$C \times 10^3$	
Ludox in water	1.333	1.01$_0$	0.004	5.36	5.32
	1.333	1.01	0.007	5.31	
	1.333	1.01$_8$	0.008	5.29	
	1.333	1.01$_3$	0.004	5.33	
T.Y.V. in phosphate buffer:	1.333	1.01$_9$	0.006	5.34	5.29
pH = 6.4	1.333	1.04$_1$	0.009	5.26	
I = 0.05	1.333	1.02$_2$	0.010	5.28	
Polystyrene in toluene/ethanol	1.466	1.09$_6$	0.009	5.42	5.44
	1.466	1.10$_1$	0.007	5.52	
	1.466	1.11$_0$	0.008	5.49	
	1.466	1.09$_6$	0.007	5.36	
	1.466	1.10$_2$	0.009	5.40	

Table III. The somewhat higher value for toluene/ethanol solutions could well arise from a slight loss of alcohol by evaporation between the spectrophotometer and light-scattering measurements. Accordingly the accepted C value for the apparatus is 5.30×10^{-3} cm.$^{-1}$.

Whilst calibrating liquids of differing refractive index thus gave the same apparatus constant, it was possible that the absolute turbidity values provided by the spectrophotometer were in error. The chief uncertainty would appear to arise from the possibility that appreciable scattered light (in addition to that transmitted) is reaching the spectrophotometer photocell. Accordingly additional stops consisting of 5-mm. holes in blackened metal plates were fitted at each end of the light-scattering cells, by which the semi-cone angle for light reaching the photocell was reduced from the normal value of 2° to *ca.*1°. The calibration constant C, determined on an

TABLE V

Light-Scattering Data for Reference Substances

Solute	Solvent	Dissymmetry I_{60}/I_{120}	Present authors		Other workers		Ref.
			Mol. Wt. (± 2%)	$2B \times 10^4$[a]	Mol. Wt.	$2B \times 10^4$[a]	
Lysozyme	0.1 M NaCl	1.06	15,500	0	14,800	−6	(11)
Bovine serum albumin	0.1 M NaCl and phosphate buffers	1.02	72,200	—	72,000 ± 5000	—	(9) (12) (13)
Dextran fractions							
No. 1	0.9% NaCl	1.02	72,500	11.6	74,600	9.1	(14)
No. 2	0.9% NaCl	1.01	77,500	10.2	80,000	9.3	(14)
No. 3	0.9% NaCl	1.04	244,000	5.5	230,000	6.2	(14)
Polystyrene[b]							
No. 3	Methyl ethyl ketone	1.06[c]	124,000	1.6	110,000	3.2	(15)
No. 1	Methyl ethyl ketone	1.07[c]	366,000	2.3	334,000	2.4	(15)

[a] From the equation $\frac{Hc}{\tau} = \frac{1}{M} + 2Bc$.

[b] Distributed by International Union of Chemistry. In the report by Frank and Mark (15), these fractions, 1 and 3, were termed II and IV, respectively.

[c] I_{45}/I_{135}.

aqueous Ludox suspension, now had the values 5.32, 5.30, 5.33, 5.36 to be compared with 5.33, 5.31, 5.37, 5.38 ($\times 10^{-3}$ cm.$^{-1}$) obtained in absence of the additional stops. It can thus be accepted that the scattered light normally accepted by the photocell is a negligible fraction of the total. The use of narrow slits and the following of accepted practice for spectrophotometry (10) make further systematic spectrophotometer errors unlikely.

Further checks on the accuracy of the absolute calibration have been obtained by examination of standard reference materials and comparison with results published by other workers and obtained mainly on Brice-Speiser instruments. Some such data have already been published from this laboratory (1), and further more general comparisons are included in Table V. Of the results in aqueous solution, those for dextran deserve special mention. Each group of measurements was made independently and was complete before the interchange of results was made. The differences are somewhat larger than is desirable, but they are probably partly due to the varying optical rotation of the samples which were used for determining concentration. With the excellent agreement for lysozyme and bovine serum albumin, and for higher molecular weight proteins already reported (1), it seems clear that for aqueous systems and molecular weights of 15,000 to 350,000, the techniques described here and in previous papers are in substantial agreement with those based upon the Brice-Speiser photometer (3, 12, 13). For the International Union of Chemistry polystyrenes (Nos. 1 and 3) a refractive index increment of 0.219 was used; molecular weights, though somewhat higher than the mean values reported by Frank and Mark (15), are within or close to the range of values given. Values of the slope term in the plot of light-scattering data against concentration, and of the dissymmetry are well within the ranges of values reported.

Finally, the turbidity of polystyrene DC/PJ3 in ½% toluene solution at $\lambda = 5461$ A. was redetermined on the new light-scattering instrument as 7.86×10^{-4} cm.$^{-1}$ to be compared with 7.88×10^{-4} cm.$^{-1}$ previously reported (2). On the same relative scale the "Cornell" polystyrene under the same conditions had the value 12.5×10^{-4}, in substantial agreement with values supported by Zimm (17).

Discussion

From the comparison of Tables III and IV with Table I, it seems clear that the calibration anomaly, reported by Goring and Johnson (1) and confirmed in the present work, arises from the convergence of the incident light beam and the consequent complexities of the geometrical optics. When the convergent light beam is replaced by a well-defined parallel beam of light, it is quite valid to calibrate an apparatus with a liquid which may have a substantially different refractive index from the systems being studied. However, in such cases, calibration liquids should satisfy other criteria (1). In particular they should show no selective absorption and give stable, symmetrical, and reproducible scattering with low depolarization and accurately measurable transmission readings.

In view of the widespread availability of spectrophotometers of high performance, calibrations based upon their use for determining the absolute turbidities of suitable calibrating solutions have many advantages. Provided well-matched cells are available (preferably the *actual* light-scattering cells), the turbidity can be accurately and quickly determined for a variety of calibrating fluids, and frequent rechecking is feasible. In view of the comparatively large transmission of suitable calibrating fluids, the absolute accuracy attainable is not all that could be desired, but it is probably no worse than for alternative methods. Ultimately such determinations are based upon the photometric scale of the spectrophotometer, but over a wide range of transmission values considerable reliability in this matter has been shown (10). On the other hand, the use of a purified organic solvent (e.g., benzene), for which a certain turbidity (usually determined elsewhere) is assumed, requires the assumption of the same state of purification as was previously attained in the case of the standard solvent, its scattering is small and of doubtful constancy, and its depolarization is usually high. Nor is the standard turbidity, determined by specialized experiments, entirely free from suspicion (16, 17). Similar criticisms apply equally to the use of standard transmission or reflection diffusers as means of providing absolute calibrations, though they are of great convenience as secondary standards.

Acknowledgments

We gratefully acknowledge grants from the British Rayon Research Association (to W.J.H.) and from the Nuffield Foundation (to R.H.O.), and we are indebted to the Medical Research Council for permission to quote results on dextrans and to the British Scientific Instruments Research Association for information on the Relonol process.

Summary

In calibrating a light-scattering apparatus, the existence of a discrepancy between results obtained from aqueous and nonaqueous calibrating fluids has been confirmed and its origin investigated. It arises from the convergence of the incident light beam and consequent complications of the geometrical optics. It no longer occurs when parallel incident light is used. A new light-scattering instrument employing parallel incident light has been constructed, tested, and utilized for the investigation of several reference substances. Satisfactory agreement with the results of several other investigations is reported.

References

1. Goring, D. A. I., and Johnson, P., *Trans. Faraday Soc.* **48,** 367 (1952).
2. Goring, D. A. I., Thesis, Cambridge, 1953.
3. Brice, B. A., Halwer, M., and Speiser, R., *J. Opt. Soc. Amer.* **40,** 768 (1950).
4. Hermans, J. J., and Levinson, S., *J. Opt. Soc. Amer.* **41,** 460 (1951).
5. Hughes, W. J., and Johnson, P., Paper in preparation.
6. Markham, R., *Discussions Faraday Soc.* **11,** 221 (1951).
7. Goring, D. A. I., and Johnson, P., *J. Chem. Soc.* **1952,** 33.
8. Carr, C. I., and Zimm, B. H., *J. Chem. Phys.* **18,** 1616 (1950).
9. Edsall, J. T., Edelhoch, H., Lontie, R., and Morrison, P. R., *J. Am. Chem. Soc.* **72,** 4641 (1950).
10. Gibson, K. S., and Balcom, M. M., *J. Opt. Soc. Amer.* **37,** 593 (1947).
11. Halwer, M., Nutting, G. C., and Brice, B. A., *J. Am. Chem. Soc.* **72,** 2786 (1951).
12. Dandliker, W. B., *J. Am. Chem. Soc.* **76,** 6036 (1954).
13. Tietze, F., and Neurath, H., *J. Biol. Chem.* **194,** 1 (1952).
14. Weissberg, S. G., Private communication.
15. Frank, H. P., and Mark, H., *J. Polymer Sci.* **10,** 129 (1953).
16. Rousset, A., and Lochet, R., *J. Polymer Sci.* **10,** 319 (1953).
17. Zimm, B. H., *J. Polymer Sci.* **10,** 351 (1953).

JOURNAL OF COLLOID SCIENCE **11**, 352–355 (1956)

PARTIAL MOLAL VOLUMES IN ALKYL SULFATE SOLUTIONS

Eric Hutchinson and Carol S. Mosher

Department of Chemistry, Stanford University, Palo Alto, California

Received March 26, 1956

ABSTRACT

Measurement of the partial molal volumes of *n*-hexyl and *n*-octyl alcohol in sodium decyl and dodecyl sulfate solutions shows that for these materials dissolution occurs with almost no change in apparent volume. From the partial molal volumes of sodium decyl and dodecyl sulfate it appears that the "hydrocarbon center" of the micelle is a slightly looser structure than in liquid hydrocarbons. Added salts and higher alcohols have very little effect on the partial molal volumes of these alkyl sulfates.

In a recent paper (1) the three-component system composed of sodium alkyl sulfate–water–additive has been treated as a two-phase system consisting of an aqueous phase containing single electrolyte ions and additive molecules, on the one hand, and a micellar phase composed of alkyl sulfate ions (and gegenions) and additive in a binary mixture on the other. Some reservations must be made about calling an object as small as a micelle a true phase, but it was demonstrated that a general interpretation of these systems, in agreement with the usual laws of solutions, was possible on this basis. Attention was focused on the ideality or otherwise of the binary micellar solutions. This paper deals with the partial molal volumes of the components of the micellar solutions.

Partial molal volumes at 25°C. were evaluated from density data from the following equations.

$$V_1 = \frac{M_1}{\rho} - \frac{(n_0M_0 + n_1M_1 + n_2M_2)}{\rho^2}\left(\frac{\partial \rho}{\partial n_1}\right)_{P,T,n_0,n_2} \qquad [1]$$

$$V_2 = \frac{M_2}{\rho} - \frac{(n_0M_0 + n_1M_1 + n_2M_2)}{\rho^2}\left(\frac{\partial \rho}{\partial n_2}\right)_{P,T,n_0,n_1} \qquad [2]$$

In these equations

n_0, n_1, n_2 = mole number of water, alkyl sulfate, and additive.

M_0, M_1, M_2 = corresponding mole weights.

ρ = density of solution.

V_1, V_2 = partial molal volume of alkyl sulfate and additive.

P, T = pressure and temperature.

The additive (component 2) consisted in some cases of sodium chloride or sodium sulfate; in others it consisted of *n*-hexyl or *n*-octyl alcohol.

The densities of the solutions were measured in pycnometers having the shape given in Fig. 1, holding approximately 20 ml. of solution.[1] The solutions were equilibrated in a thermostat at 25°C. ± 0.005°C. Sodium chloride and sodium sulfate of analytical grade were used. *n*-Hexyl and *n*-octyl alcohols were obtained by the catalytic reduction of carefully purified methyl esters of hexanoic and octanoic acids. The alkyl sulfates were prepared by a standard procedure (2).

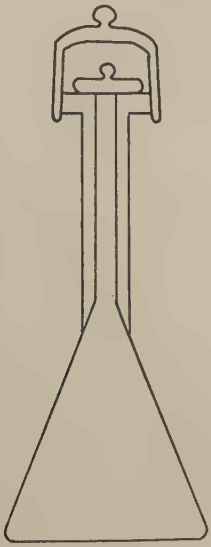

FIG. 1

RESULTS

Over the range of solutions studied the densities of the solutions above the C.M.C. were linear functions of the mole numbers. These densities are summarized in the equations below, which were obtained from the straight-line plots computed by the method of least squares. All data refer to 25°C.

$$\rho = a + b\, n_1 \text{ (or } a + b\, n_2\text{) g./ml.}$$

Sodium decyl sulfate in water.

$a = 0.9973_7$, $b = 0.04148_4$, $\bar{V}_1 = 216.5$ ml. ± 2.5

Sodium decyl sulfate in 0.0927_7 molal sodium chloride.

$a = 1.0013_4$, $b = 0.04030_2$, $\bar{V}_1 = 216.9$ ml. ± 2.5

---

[1] Details of the use of these pycnometers as well as the extended density data are available in Technical Report 5. ONR Contract N6 ONR 25130, Stanford University.

Sodium decyl sulfate in 0.1006_9 molal sodium sulfate.
$a = 1.0098_6$, $b = 0.03833_4$, $V_1 = 216.9$ ml. ± 2.6

Sodium decyl sulfate in 0.05245_6 molal *n*-octyl alcohol.
$a = 0.9962_2$, $b = 0.03969_2$, $V_1 = 216.9$ ml. ± 2.4

n-Hexyl alcohol in 0.2000 molal sodium decyl sulfate.
$a = 1.0063_0$, $b = -0.02121_5$, $V_2 = 123$ ml. ± 0.7

n-Octyl alcohol in 0.2035_8 molal sodium decyl sulfate.
$a = 1.0058_7$, $b = -0.2715_0$, $V_2 = 158.2$ ml. ± 0.5

Benzene in 0.2000 molal sodium decyl sulfate.
$a = 1.0061_9$, $b = -0.00973_0$, $V_2 = 87.4$ ml. ± 0.1

Sodium dodecyl sulfate in 0.0488_8 molal *n*-octyl alcohol.
$a = 0.9964_5$, $b = 0.03456_9$, $V_1 = 250.3$ ml. ± 2.6

n-Octyl alcohol in 0.1994_2 molal sodium dodecyl sulfate.
$a = 1.0040_5$, $b = -0.02358_4$, $V_2 = 154.8$ ml. ± .3

The partial molal volumes of the various components showed some variation with concentration, as indicated in the data above and as shown in Fig. 2. The average partial molal volumes of *n*-hexyl and *n*-octyl alcohol—123.3 ml. and 158.2 ml., respectively—in sodium decyl sulfate may be compared with the molal volumes of these compounds at 25°C., viz., 125.9 ml. and 157.8 ml. The difference between the partial molal volume of *n*-octyl alcohol in sodium decyl and sodium dodecyl sulfate solutions is

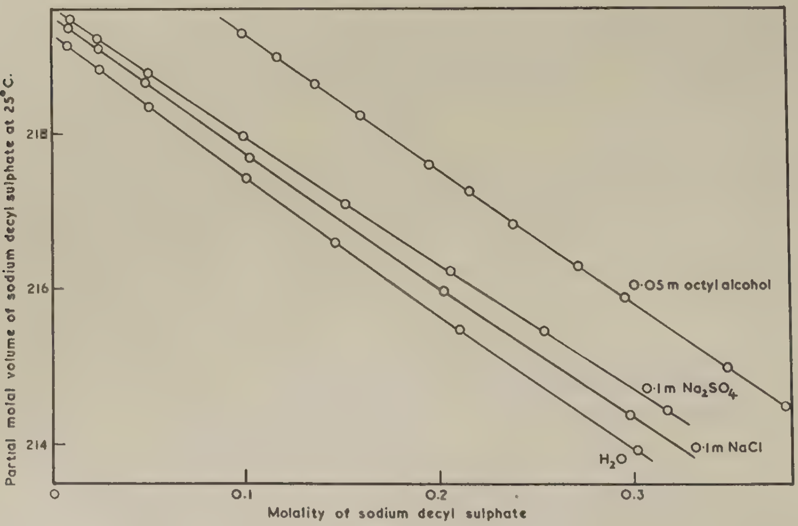

FIG. 2

outside the error of measurement but is quite small. Thus the solutions of these alcohols in micelles exhibit no marked nonideality as far as volume change on mixing is concerned. Similarly with benzene the partial molal volume in sodium decyl sulfate micelles, 87.4 ml., compares favorably with the molal volume of pure benzene, 89.4 ml.

The effect of additives on the partial molal volume of sodium decyl sulfate is almost negligible. Since the effect of electrolyte additives is thought to be twofold, viz., to increase the size of the micelles and to decrease their net charge (3), this result is a little surprising. It demonstrates that, if these postulated effects are real, they exert virtually no change on the closeness of packing or organization in the micelle. Although we have not obtained the partial molal volume of sodium dodecyl sulfate in pure water, it seems reasonable to assume that the effects of additives—either electrolytes or nonelectrolytes—is similarly small. Therefore, taking the partial molal volume of sodium dodecyl sulfate in *n*-octyl alcohol solutions as being the same as in pure water, the change in partial molal volume in going from decyl sulfate to dodecyl sulfate is 33.4 ml., as compared with 32.5 ml. between liquid *n*-hexyl alcohol and *n*-octyl alcohol. This difference is small but, we believe, real. It is to be compared to the corresponding difference of 27.4 ml. in going from decanoic to dodecanoic acid (4) in the solid state. Thus the alkyl sulfate micelle appears to have a slightly looser structure than paraffinic hydrocarbons.

ACKNOWLEDGMENT

This work was carried out as part of a program supported by the Office of Naval Research under Contract N6 ONR 25130 with Stanford University.

REFERENCES

1. HUTCHINSON, E., INABA, A., AND BAILEY, L. G., *Z. physik. Chem.* (N.F.) **5**, 344 (1955).
2. DREGER, E. E., *et al.*, *Ind. Eng. Chem.* **36**, 610 (1944).
3. PHILLIPS, J. N., AND MYSELS, K. J., *J. Phys. Chem.* **59**, 325 (1955); KLEVENS, H. B., *Chem. Revs.* **47**, 1 (1950).
4. GARNER, W. E., AND RYDER, E. A., *J. Chem. Soc.* **127**, 720 (1925).

JOURNAL OF COLLOID SCIENCE **11**, 356–376 (1956)

THE ADSORPTION OF ALCOHOLS AND PHENOLS FROM NONPOLAR SOLVENTS ON TO ALUMINA

D. J. Crisp

Department of Colloid Science, Cambridge, and Marine Biology Station, University College of North Wales, Bangor, Wales

Received April 5, 1956

Introduction

The early literature on adsorption from solution of substances on to solid-liquid interfaces is for the most part devoted to the measurement of the quantities of various substances adsorbed at a high concentration. There are also many measurements of the heats and free energies of wetting. Adsorption isotherms, especially at low surface coverage, are seldom given. The changes in energy, orientation, and mobility of molecules when they displace molecules of solvent from the solid-liquid interface can best be understood from the heats, free energies, and entropies of the adsorption process in dilute solution. The fundamental thermodynamic quantities will presumably be independent of the specific area or quality of the particular sample of powder used, provided the molecular structure of the adsorbing surface is the same.

The work described in this paper serves to illustrate several experimental approaches by which heats and energies of adsorption can be measured on good adsorbates such as alumina, by employing the surface film balance as an analytical method (1, 2).

Experimental Methods

Samples of alumina were kept over phosphorus pentoxide in a desiccator, and transferred to a dry stoppered adsorption tube 10 cm. long and 1.5 cm. in diameter for each experiment. Benzene used as solvent was dried over sodium wire and redistilled just prior to making up solutions. The liquid adsorbates (propyl and ethyl alcohols) were dried over quicklime, and the solid adsorbates (long-chain alcohols and phenols) were recrystallized and kept over phosphorus pentoxide.

In the first experiments surface-active agents were used as adsorbates. Ten milliliters of solution in dry benzene were delivered into an adsorption tube containing a weighed quantity, approximately 1 g., of dry alumina powder, and shaken up. After the alumina had settled, the concentration of the supernatant solution was determined on a Langmuir trough after any necessary dilution to bring the concentration to the order of 1 mg./ml. Comparison with the original concentration gave the amount of solute adsorbed on the powder. Since very small quantities of the order of 0.1 ml. are sufficient for analysis, it is possible to take repeated samples without seriously altering the system or depleting the liquid phase. If the adsorption tube and its contents are maintained in a thermostat at a series of temperatures, the effect of temperature on the adsorption equilibrium can be measured and from this a heat of adsorption can be deduced. Similarly by successive additions of small quantities of solution or of pure solvent, the process of adsorption and desorption can be followed progressively.

In another type of experiment a short-chain member of an homologous series was added by means of a microsyringe to a system containing a long-chain homolog adsorbed on alumina, in order to study competitive adsorption. The energy of adsorption of the short-chain member can then be determined, on certain assumptions, from the consequent rise in concentration of long-chain substance in solution as a result of desorption. In analyzing the concentration of the long-chain member on the surface balance the short-chain homolog does not interfere, since it dissolves immediately into the water underlying the surface film.

Phenol solutions were analyzed colorimetrically by means of a modified diazotization and coupling reaction carried out simultaneously on the unknown solution and on known standards. One milliliter of the benzene solution containing phenol was removed from the adsorption tube and made miscible with water by adding 12 ml. of ethyl alcohol and making up to 20 ml. with distilled water. Coupling was carried out by adding 1 ml. of 50% sodium acetate solution, 0.5 ml. of diazotized paranitraniline, and after an interval of 1 minute, 1 ml. of 20% sodium carbonate.

Direct calorimetric methods for measuring the heat changes on mixing and adsorption were made by means of a simple vacuum calorimeter in which the mixing was carried out by breaking a bulb of thin glass containing alumina powder or solution as described by Hutchinson (3). The temperature change was measured by a thermistor, employing a Wheatstone bridge circuit and sensitive galvanometer to reduce the thermistor current to the minimum possible. It was found necessary to cease stirring when measuring the temperature, in order to keep a uniform temperature difference between the thermistor and the surrounding fluid; otherwise drifts of resistance are observed because of changes in the flow of heat from thermistor to solution when the convection pattern is altered after breaking the bulb. The bulbs were prepared from 5 mm. diameter glass tubing blown to a capacity of 3–5 ml., and carefully annealed to avoid heat changes caused by breaking a highly strained bulb. The bulb reached initial thermal equilibrium with the fluid in the calorimeter after an hour.

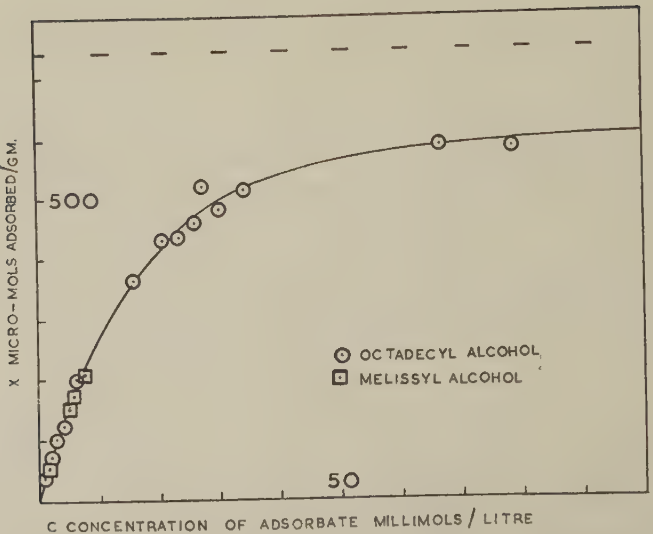

Fig. 1. Adsorption isotherms on alumina for octadecyl and melissyl alcohol from benzene solution. The dotted line represents the maximum capacity of the powder.

Discussion and Results

Adsorption Isotherms by Direct Method

Adsorption isotherms for two long-chain aliphatic alcohols, octadecyl and melissyl, on a sample of alumina powder A, are shown in Fig. 1. It will be seen that when expressed in moles per gram of powder (x) adsorbed at a molar concentration c in benzene, the isotherms are practically identical, though the isotherm for melissyl alcohol is restricted because of its limited solubility. A second sample of alumina B was then used to determine isotherms for cetyl, octadecyl, and melissyl alcohols.

The isotherms of both samples of alumina were of Langmuirian form, a graph either of x/c against x or of c/x against c approximately closely to straight lines (Fig. 2). From such an isotherm the maximum capacity of the powder x_0 may be deduced from the limiting condition $x \rightarrow x_0$ as $c \rightarrow \infty$. The isotherms may then be expressed independently of the specific area of the sample of powder by plotting the fraction of surface covered by adsorbent, θ $(= x/x_0)$, against its molar concentration in solution c. As can be seen from Fig. 3, a fundamental relation applies to all three alcohols and both samples of alumina.

Adsorption isotherms of cholesterol and phenol were determined on alumina A. The adsorption of these compounds did not fit the Langmuirian isotherm as closely as did the results with aliphatic alcohols, but could be fitted sufficiently closely to permit estimates of x_0 and θ to be obtained.

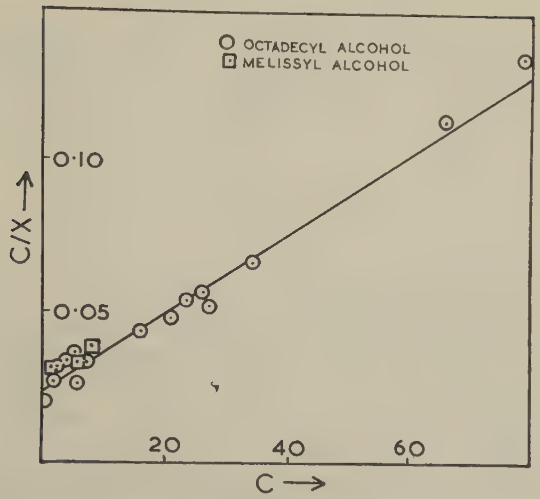

FIG. 2. Graph of c/x against c for two long-chain alcohols adsorbed on alumina; c = concentration in millimoles/l., x = micromoles adsorbed per gram of powder.

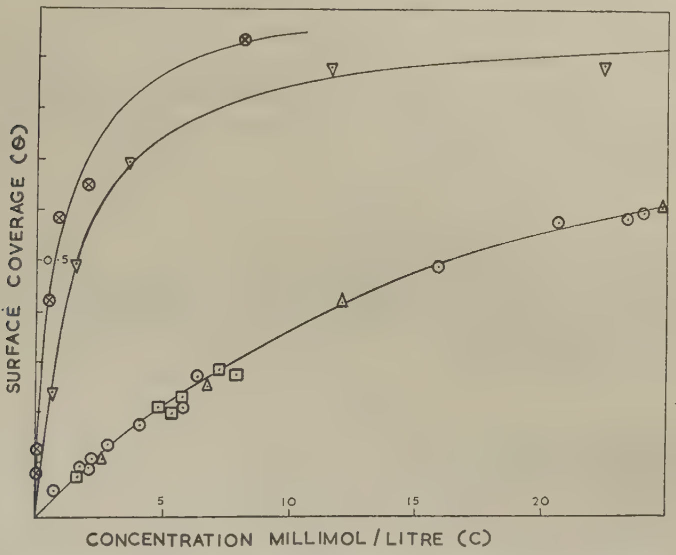

FIG. 3. Adsorption isotherms expressed as fraction of surface covered, θ, against concentration, c, in millimoles/l.

⊙ Octadecyl alcohol
⊡ Melissyl alcohol
△ Cetyl alcohol
▽ Cholesterol
⊗ Phenol

TABLE I

Substance	Maximum adsorption x_0 *(micromoles per g. of powder)*	Area of condensed film at air-water interface A_0 (Å²)	Estimate of available area of powder $x_0 A_0$ (*m.²/g.*)
Octadecyl alcohol	740	20.5	91
Cholesterol	420	38.0	96
Phenol	640	23.0	88

These isotherms are also shown in Fig. 3. They rise more steeply from the concentration axis than do those of the alcohols. Phenol was almost quantitatively adsorbed except at very low concentration. Attempts to extend this investigation to the carboxylic acids were not successful, however, since after initial adsorption the fatty acid disappeared slowly and completely from solution, indicating a possible interaction beyond that of unimolecular adsorption.

The adsorption isotherms for alcohols, cholesterol, and phenol offer three independent estimates of the available area of powder A. If the assumption is made that the cross-sectional area of these molecules at maximum adsorption ($x = x_0$) is equal to their specific area when spread as a condensed film at an air-water interface, the estimates given in Table I are obtained. They are reasonably consistent and suggest that the adsorption of surface-active compounds may be used to obtain a convenient estimate of the available surface area. Since these substances are of a similar type and cross-sectional area, a larger surface might nevertheless be available to much smaller molecules.

The Free Energy of Adsorption

Fowler (1935) has shown that if the Gibbs free energy of adsorption ΔG of a substance is independent of the quantity adsorbed on fixed sites of the adsorbent, then whatever the actual mechanism of adsorption, the Langmuirian isotherm must follow

$$\theta = Kc(1 - \theta). \qquad [1]$$

With the use of the concentration scale the free energy is

$$\Delta G = -RT \log_e \frac{c_s f_s}{cf} \qquad [2]$$

where c, c_s, are the concentrations in solution and in the surface phase, respectively, and f and f_s are their respective activity coefficients.

To relate surface and bulk concentrations an arbitrary surface thickness τ and limiting area A_0 of the adsorbed molecule must be assumed. If the surface activity $c_s f_s$ is assumed to approximate to the molecular concentration in the free surface space

$$c_s f_s = \frac{1}{(A - A_0)\tau}, \qquad [3]$$

where A is the surface area occupied by the adsorbed molecule in the plane of the solid surface, A_0 is the limiting area, and τ the free space available in the direction perpendicular to the solid surface. Putting $f = 1$, $\theta = A_0/A$, then clearly if $\theta = \frac{1}{2}$, $c = K^{-1}$ (Eq. [1]) and $A = 2A_0$, so that

$$\Delta G = -RT \log_e \frac{K}{A_0 \tau} . \qquad [4]$$

At 20°C.

$$\Delta G = -1340 \left[\log_{10} \frac{K}{A_0} + 5.52 \right],$$

where A_0 is in Ångström units and c in Eq. [1] is measured as micromoles/ml. (millimoles/l.).

It will be noted that if the surface phase were regarded as a homogeneous region, τ would represent that part of its thickness across which the adsorbed molecules are free to undergo thermal movement. It is not equal to the thickness of the layer of adsorbed molecules, nor will it necessarily vary with the size of the adsorbed molecule. Langmuir took a value of 5.4 A. for molecules at the air-water interface in calculating energies of adsorption, and similar dimensions (6.0 A.) were assumed by Kemball and Rideal (4) for the mercury-air interface. On the basis of a similar assumption, the values of free energy change on adsorption from benzene solution to alumina for a number of substances are given in Table II. The value of K was obtained from the adsorption isotherms and A_0 from the area of the condensed film (Table I), except in those instances where K was deduced from experiments involving competitive adsorption (see below).

Competitive Adsorption

When only one of a pair of adsorbents, A, can be readily analyzed, then, with certain assumptions, the adsorption constant K_B of a competing ad-

TABLE II

Substance	Method	Adsorption coefficient K (*millimolar*$^{-1}$) at temperature indicated	Assumed area occupied per molecule (Å²)	Free energy of adsorption ΔG (*cal/gram/mole*) assuming $\tau = 5$ Å.
Melissyl alcohol $C_{31}H_{63}OH$	Direct adsorption	0.062 (19°C.)	20	3960
Octadecyl alcohol $C_{18}H_{37}OH$	Direct adsorption	0.060 (20°C.)	20	3900
Cetyl alcohol $C_{16}H_{33}OH$	Direct adsorption	0.060 (18°C.)	20	3930
Propyl alcohol C_3H_7OH	Displacement of octadecyl alcohol	0.084 (19°C.)	20	4170
Cholesterol $C_{27}H_{45}OH$	Direct adsorption	0.55 (19°C.)	38	4890
Phenol	Direct adsorption	4.0 (21°C.)	23	6330
	Displacement of ethyl alcohol	3.10 (20°C.)	23	6200

sorbent B can be measured from its effect in displacing the substance A, provided of course that the isotherm constant K_A is known.

Certain sites on the adsorbate will be common to A and to B. Let the fraction of these covered by A be θ_A' and by B, θ_B'.

Then the Langmuir isotherm becomes (5)

$$\theta'_A = \frac{K_A c_A}{1 + K_A c_A + K_B c_B};$$

$$\theta'_B = \frac{K_B c_B}{1 + K_A c_A + K_B c_B}.$$

It is possible that some sites may for stereochemical or other reasons be suitable for adsorbing only A or only B. For such exclusive sites

$$\theta''_A = \frac{K_A c_A}{1 + K_A c_A}$$

$$\theta''_B = \frac{K_B c_B}{1 + K_B c_B}$$

The total fraction of surface covered is then given by

$$\theta_A = \theta_A''\epsilon_A + \theta_A'(1 - \epsilon_A),$$

$$\theta_B = \theta_B''\epsilon_B + \theta_B'(1 - \epsilon_B),$$

where ϵ_A and ϵ_B are fractions of the total sites available to A and B, respectively, that are occupied exclusively.

Combining the above expressions

$$\frac{\theta_A}{\theta_B} = \frac{K_A c_A}{K_B c_B} \cdot \frac{(1 + K_A c_A + K_B c_B \epsilon_A)(1 + K_B c_B)}{(1 + K_B c_B + K_A c_A \epsilon_B)(1 + K_A c_A)}. \qquad [5]$$

If now we assume that A or B is able to occupy all the available sites and that no sites are available to one or the other exclusively,

$$\epsilon_A = \epsilon_B = 0$$

and Eq. [5] simplifies to

$$\frac{K_A}{K_B} = \frac{\theta_A c_B}{\theta_B c_A}. \qquad [6]$$

a). Octadecyl and Propyl Alcohols. In the first example of competitive adsorption, the coefficient K_B of propyl alcohol was determined by the ability of propyl alcohol to displace octadecyl alcohol from alumina. The adsorption coefficient K_A for octadecyl alcohol was known, and the capacity of the powder for propyl alcohol was assumed to be the same as its capacity

x_0 for octadecyl alcohol (i.e., $\epsilon_A = \epsilon_B = 0$). An initial adsorption of octadecyl alcohol from solution was carried out, followed by a further addition of octadecyl alcohol solution to obtain a second point on the isotherm. Provided these points fitted reasonably to the previously determined curve, the experiment was continued by adding small quantities of dry propyl alcohol by a graduated microsyringe, shaking, and leaving to stand. The amount of octadecyl alcohol in solution was then determined by surface film analysis. This process was repeated several times to obtain sets of values for θ_A, θ_B, c_A, and c_B as follows:

The total quantity of both constituents q_A and q_B in the system and the volume of solution v is known at any time, allowance being made for withdrawals of solution for test. The concentration of A, c_A, is determined by analysis. Then

$$\theta_A = \frac{q_A - vc_A}{mx_0} \qquad [7]$$

where x_0 = total capacity of 1 g. of powder and m = mass of powder. Competitive adsorption may be expressed in the form explicit for θ_B

$$\theta_B = 1 - \theta_A - \frac{\theta_A}{K_A c_A}.$$

From θ_B we may derive c_B, from the equivalence of mass given by

$$c_B = \frac{q_B - mx_0 \theta_B}{v}.$$

Table III gives the results of four sets of experiments. In Fig. 4 the values of θ_B/θ_A are plotted against c_B/c_A on a logarithmic scale. This gives a straight line at 45° to the axis, indicating proportionality between the two quantities as demanded by Eq. [6]. This line, substituted into Eq. [6] with c_A and c_B expressed in molar concentrations, gives $K_B = 1.4\ K_A$, indicating closely similar energies of adsorption despite the great difference in chain length (Table II).

b). *Alcohol and Phenol.* The second example of the use of a competitive system to determine the energy of adsorption can be illustrated by the adsorption of phenol on alumina. Direct measurement of the isotherm gave $K = 4.05$ when c was expressed as moles/ml. $\times 10^{-6}$, but the method was not very accurate because of the very low concentrations at which the phenol was adsorbed. As an alternative method a known amount of phenol (A) was adsorbed from a dilute solution in benzene. This initial adsorption took up virtually all the phenol. Ethyl alcohol (B) was then added in increasing amounts to displace the phenol, which was measured colorimetrically. The concentration of phenol in solution was thus obtained,

TABLE III

Competitive Adsorption between Octadecyl Alcohol (A) and Propyl Alcohol (B)

Powder capacity (mx_0) as mg. octadecyl alcohol	Total propyl alcohol (q_B) (*mg.*)	Conc. of octadecyl alcohol (C_A) (*mg./ml.*)	θ_A	θ_B (calc.)	C_B (Calc.) (*mg./ml.*)
115	0	1.72	0.284	0	0
115	0	1.17	0.200	0	0
115	7.0	1.57	0.165	0.36	negative
115	46.0	2.76	0.087	0.77	3.50
130	0	4.96	0.525	0	0
130	9.75	5.85	0.447	0.205	0.348
130	58.03	8.30	0.277	0.573	3.33
130	131.4	10.55	0.138	0.805	14.1
130	897	11.8	0.023	0.968	122
146	0	1.20	0.205	0	0
146	0	0.63	0.135	0	0
146	8.0	0.74	0.119	0.18	0.107
146	15.9	0.834	0.106	0.32	0.275
146	23.5	0.918	0.095	0.44	0.485
146	30.9	0.99	0.085	0.53	0.75
146	46.25	1.11	0.067	0.66	1.41
146	74.5	1.35	0.043	0.814	3.14
146	151.5	1.545	0.024	0.906	8.40
146	948	1.635	0.0045	0.983	62.0
160	0	10.0	0.705	0	0
160	8.0	11.6	0.632	0.125	0.47

and from it the amount remaining adsorbed on the powder by Eq. [7] above.

$$\theta_A = \frac{q_A - vc_A}{mx_0}.$$

The distribution of the competing substance B is then given by the equation:

$$c_B = \frac{q_B - mx_0\theta_B}{v} = \frac{\theta_B}{K_B(1 - \theta_A - \theta_B)},$$

in which q_B is the total amount of B added, v the volume of solution, and K_B is taken as 0.062 (in micromoles) as for the other alcohols. Hence this equation can be solved as a quadratic in θ_B.

Table IV gives the results of this experiment. Figure 5 shows $\log_{10}(c_B/c_A)$ plotted against $\log_{10}(\theta_B/\theta_A)$ as before, and the slope is again seen to be unity, indicating that Eq. [6] applies in this case, although the values of K_A and K_B are very different. From Fig. 5 the value of $K_A/K_B = 38.5$, giving a free energy difference of 2180 cal. between alcohol and phenol.

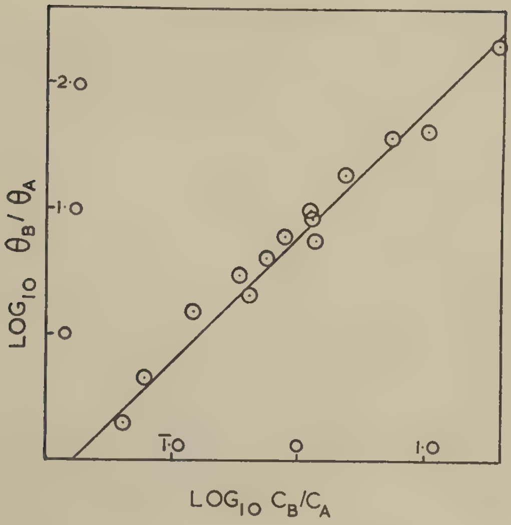

FIG. 4. Competitive adsorption between octadecyl alcohol (A) and propyl alcohol (B).

Log$_{10}$ C_B/C_A = logarithm of ratio of concentrations of A and B in benzene solution.

Log$_{10}$ θ_B/θ_A = logarithm of ratio of surface of alumina covered by A and B.

TABLE IV

Competitive Adsorption between Phenol (A) and Ethyl Alcohol (B)

mx_0 (*micromoles*)	v (*ml.*)	q_B (*micromoles*)	C_A (*micromoles/ml.*)	θ_A	C_B (*micromoles/ml.*)	θ_B
1140	16.0	0	0 (?)	0.107	0	0
1140	17.7	5,220	1.02	0.0875	240	0.85
1140	15.4	22,070	3.08	0.052	1360	0.92
1140	18.7	105,600	3.97	0.016	5660	0.97
609	14.6	0	0 (?)	0.171	0	0
609	14.7	1,920	0.55	0.158	100	0.72
609	11.6	3,350	1.88	0.133	247	0.81
609	10.4	6,510	2.92	0.116	580	0.86
609	8.35	11,955	4.70	0.091	1360	0.895
609	12.05	96,500	6.23	0.0235	8000	0.97

This gives a value for the adsorption energy of phenol of about 6200 cal., in fair agreement with that obtained by the direct method. It will be noted that this example differs from the previous in that the adsorption coefficient K_B of the competing substance was known, and that of the initially adsorbed material K_A was deduced from the experiment.

An attempt was made to measure the competitive adsorption of water by displacement of a long-chain alcohol. This experiment was unsuccessful

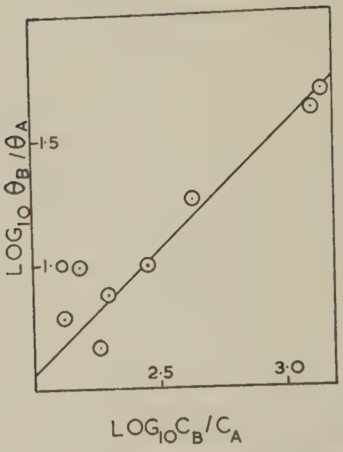

FIG. 5. Competitive adsorption between phenol (A) and ethyl alcohol (B). Axes as in Fig. 4.

because the displacement by low concentrations of water was less than expected, while the desorption of water, which should have taken place when dry benzene was added to the system, did not in fact occur. The system therefore did not behave as predicted by Eq. [6], but rather as would have been expected if water were at first adsorbed slowly and perhaps irreversibly on sites not all accessible to the long-chain alcohol.

Few experiments have been carried out on competitive adsorption. Using the results obtained by Butler and Ockrent (6), Kemball, Rideal, and Guggenheim (7) showed that a similar system of independent competition, based on the Volmer isotherm for mobile monolayers, may be postulated to account for the adsorption of propyl and ethyl alcohol on water.

Heats of Adsorption

Recently a number of investigators have drawn attention to the different meanings which may be given to the term "heat of adsorption," especially in regard to its use for the vapor-solid interface (8). Hill (9) suggested defining the heat change at constant surface pressure; Everett (10) lists four possible definitions, including Hill's, and points out that those which assume a constant surface area are the more useful since they correspond with the calorimetric heat. For condensed systems the differential heat at constant area and external pressure ($\Delta\bar{H}$) is the obviously appropriate definition.

The differential heat of adsorption $\Delta\bar{H}$ may be measured most conveniently by the temperature coefficient of the free energy change, using the Gibbs-Helmholtz equation:

$$\Delta\bar{H} = \Delta G - T\left(\frac{\partial \Delta G}{\partial T}\right)_p,$$

in which Δ refers to the transfer of material from unit activity in solution to unit activity on the surface of the adsorbate, employing the concentration scale in the definition of activity, and T is the absolute temperature.

Substitution of Eqs. [1] and [4] into the Gibbs-Helmholtz equation gives

$$\Delta\bar{H} = R\left[\frac{\partial \log_e \theta/c(1-\theta)}{\partial(1/T)}\right]. \qquad [8]$$

The results of experiments on adsorption over a range of temperatures are therefore plotted in the form of $\log_{10}(\theta/c(1-\theta))$ against $1/T$. They give straight lines, the slope of the line giving $\Delta\bar{H}$ directly. In some experiments, particularly those with cholesterol, the position of the line varied slightly with θ, the fraction of surface covered, either because of experimental error or because of the fact that the system did not follow the Langmuir isotherm exactly. However, the slope of the lines from which the heats of adsorption are calculated were in reasonably good agreement with each other, as can be seen from Fig. 6.

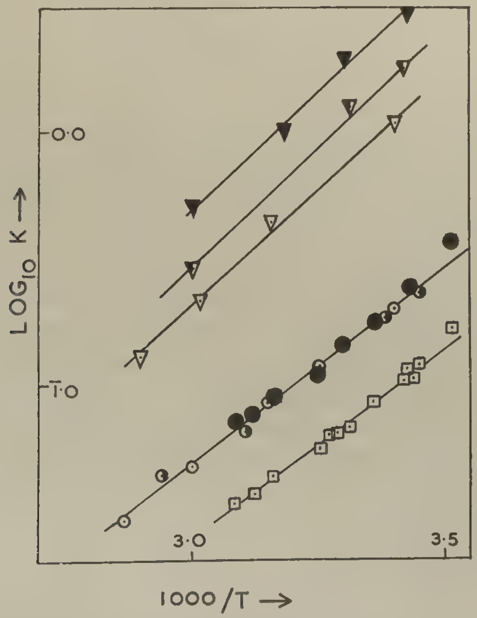

FIG. 6. Graph of logarithm of Langmuir adsorption constant, $K = \theta/(1-\theta)c$, where c is in mg./ml., plotted against reciprocal of absolute temperature $1/T$.

⊙ Octadecyl alcohol $\theta = 0.1$–0.25
◐ Octadecyl alcohol $\theta = 0.25$–0.4
● Octadecyl alcohol $\theta = 0.25$–0.45
⊡ Melissyl alcohol $\theta = 0.1$–0.3
▽ Cholesterol $\theta = 0.1$–0.2
▼ Cholesterol $\theta = 0.4$–0.5
⧨ Cholesterol $\theta = 0.7$–0.9

The heat change associated with adsorption was also measured by direct calorimetry, but as the method involved the measurement of small temperature differences, it was less precise than the method based on the temperature variation in the coefficient of adsorption. In these experiments a sample of alumina is mixed with a solution of adsorbate in a calorimeter. Since only that part of the heat change which is produced by the process of adsorption is required, any other heat changes, such as those involved in wetting the powder by the solvent, and also any heats of mixing between solvent and adsorbate must be eliminated.

In the first series of experiments alumina was placed dry in the bulb and was wetted by the fluid in the calorimeter when the bulb was broken. The heat of wetting of alumina by the solvent alone was first measured (H_1); in this case the calorimeter was filled with dry benzene. Next the heat of wetting of alumina by a solution of octadecyl alcohol in benzene (H_2) was determined, and the amount of alcohol adsorbed was measured simultaneously by the surface balance. Allowance was then made for the heat change due to wetting by benzene, the heat of adsorption being

$$\Delta H = \frac{(H_2 - H_1)}{n}$$

n being the number of gram moles adsorbed per gram of powder. By using a large volume of solution of adsorbate little change in concentration was produced during adsorption, so that the differential heat of mixing of the adsorbate with the solvent (heat of solution) remained sensibly constant. When the solutions were dilute, this heat of mixing approximated to that at zero concentration.

In the second method the bulb was filled with powder together with sufficient benzene to wet it thoroughly, no heat measurement being made during this operation. The bulb was then broken into a fairly dilute solution of adsorbate, the resulting heat change and amount adsorbed being measured as before. Preliminary experiments indicated that mixing a solution of octadecyl alcohol and benzene at the dilutions used involved no appreciable heat change. Since the heat of wetting by solvent is automatically eliminated by this procedure, the heat produced by adsorption should be measured directly.

The second method was applied also to measure the heat of adsorption of octyl alcohol from benzene, the amount adsorbed being deduced from a knowledge of the capacity of the powder and the isotherms of other alcohols, in the assumption that octyl alcohol behaved similarly. For the stronger solutions of octyl alcohol allowance had to be made for the heat of mixing with benzene on the basis of the experimentally determined curve for heats of mixing (Fig. 7). Table V summarizes the results. It will first be noticed that the values obtained by calorimetry showed considerable variation

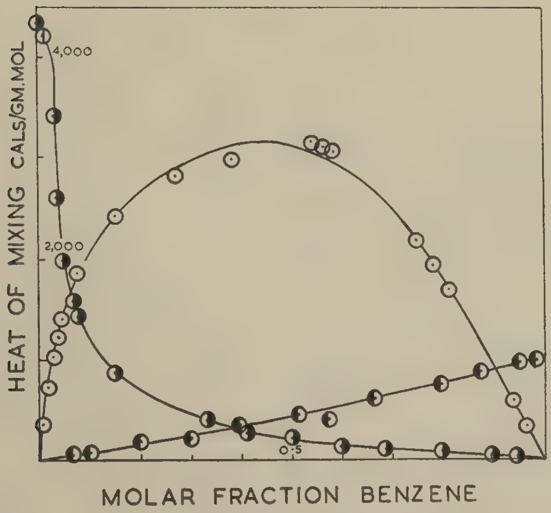

FIG. 7. Heats of mixing for octyl alcohol and benzene.
⊙ Integral heat
◑ Partial molar heat of mixing of octyl alcohol $\Delta\bar{H}_A$
◐ Partial molar heat of mixing of benzene $\Delta\bar{H}_B$

and that those obtained at comparable surface coverage by the more direct method, in which the powder wetted by benzene was added to a solution of adsorbate, are higher than those obtained by subtraction of the heat of wetting by benzene from the heat of wetting by the solution. There appears to be no theoretical reason why the two methods should give significantly different results. It is possible that wetting of the dry powder, as distinct from powder already thoroughly wetted, was somewhat slower, so that part of the heat was evolved slowly and failed to be included in the heat measured by the experimental method. This might have made both heats of wetting and their difference too low. The rates of change of temperature in the calorimeter gave no indication that this was so, however. A second possibility is that an unsuspected source of heat might have accompanied each experiment, and this bias would have been eliminated only in the method involving the difference of two heats of wetting. The fact that the variability in the results was greater than the probable error in the measurement of temperature change, points to the latter as the more probable cause of the observed differences and suggests that the true calorimetric value lies in the region of 8000 cal./gram mole for the alcohols. Nevertheless even this lower value for the heats of adsorption is slightly higher than the values obtained from the temperature dependence of the coefficient of adsorption. Such a difference would not be surprising, since the former gives an integral heat, whereas the latter method gives the differential heat of adsorption. If the surface contains sites of different energy or if, as is

TABLE V

Heats of Adsorption

Method and Corrections Applied	Substance	Powder capacity (*millimoles/g.*)	Conc. of solution millimoles after adsorption	Coverage	ΔH
A. Direct calorimetry Mixed wetted powder and octyl alcohol solution. Corrected for heat of mixing.	Octyl alcohol	1100	35	0.67	10,500
			38	0.69	9,420
			65	0.79	10,550
			770	0.98	5,950
			780	0.98	6,700
Mixed dry powder and octadecyl alcohol solution. Corrected for heat of wetting by benzene.	Octadecyl alcohol	740	44	0.73	8,200
			37	0.70	8,750
			34	0.69	9,100
Mixed wetted powder and octadecyl alcohol solution.		740	37	0.70	10,500
			37	0.70	11,000
B. Temperature dependence of adsorption coefficient	Melissyl alcohol	780		0.1–0.3	7,540
	Octadecyl alcohol	780		0.1–0.45	7,350
	Cholesterol	420		0.1–0.2	8,520
				0.4–0.5	8,850
				0.7–0.9	8,650

clearly shown to be the case in Fig. 7, the differential heat of mixing (solution) of the adsorbate falls as its concentration c rises, the differential heat of adsorption will not remain constant but will fall as c and θ increase. Thus at a concentration of about 0.8 M the heat of solution of octyl alcohol is some 3000 cal./gram mole less than its value extrapolated to zero concentration, so that its heat of adsorption is correspondingly low (see Table V). Below a concentration of 0.15 M, at which the surface is still almost fully covered, the heat of solution of this alcohol is not much less than its value extrapolated to zero (Fig. 7), so that if a high initial heat of adsorption were postulated in this range it could only be due to sites of higher energy which were occupied first. The proportion of high-energy sites cannot be large however, because this situation would not be consistent with the Langmuir isotherm (5, 11, 12). Moreover the values of the differential heat of adsorption do not change appreciably with surface coverage.

There is a further difference between the calorimetric and differential heats, which arises from the derivation of the adsorption coefficient K which enters into Eq. [8]. In defining K, the assumption was made that the adsorbed phase occupied a free space perpendicular to the surface of thickness τ. The thickness of the interphase is assumed to remain constant independently of changes in temperature.

In fact, however, there will probably be an increase in τ with rise of temperature, implying an entropy term corresponding to the vibration of the molecule perpendicular to the surface. The energy associated with this will not be included in the differential heat of adsorption $\Delta\bar{H}$ as defined above, but if it exists it will be included in the heat measured calorimetrically. The influence of changes in τ on $\log_e K$ is relatively small, so that the probable difference due to this cause would not be a large one in the case of a strongly adsorbed molecule. Thus Kemball (13), making the same assumption in the measurement of entropies of adsorption of vapors on mercury, found that the observed entropies agreed well with those calculated on theoretical grounds.

Several factors therefore may contribute to the difference between the adsorption heat measured by the (isosteric) differential method and the integral heat measured calorimetrically.

The actual values of ΔH for the different compounds show two important features. Firstly, there is no noticeable increase in the heat of adsorption in the alcohols with increase in length of the hydrocarbon chain. Secondly, there is a rise in the differential heat of adsorption as the hydroxyl group becomes more acidic. The values of ΔH are much lower than those given by Hutchinson (3) for adsorption of similar compounds on to ionic crystals.

State of Molecules Adsorbed on Alumina

In one-component adsorption the measurement of the entropy of adsorption, employing the Langmuir or any other convenient isotherm, may give definite information concerning the state of the adsorbed phase (see references (13–17). However, the analogous application of the Langmuir isotherm to a two-component system in the form used here ignores not only the association in the solvent of adsorbate molecules but also the competition for the surface of the adsorbent which must exist even in dilute solutions between molecules of solvent and adsorbate. This competition becomes more evident as the concentration of adsorbate increases (see references 18, 19). Thus although the isotherm may apply to dilute solutions where the chemical potential of the solvent is sensibly constant, the process of adsorption is more complex than that of a one-component system, in that molecules are not simply adsorbed or desorbed but exchange with adsorbed solvent molecules. The heats and free energies of adsorption therefore vary with the solvent used (2, 3). No attempt will therefore be made to interpret the absolute values of heat and entropy changes.

The fact that the Langmuir isotherm offers the most convenient reference system for adsorption on alumina from nonpolar solvents indicates nevertheless that the adsorbed molecules form a localized monolayer (5, 11). The isotherm is applicable over practically the whole range of θ, pointing, on the one hand, to the uniformity in energy of the adsorption sites and, on the other, to the high energy of adsorption compared with the energy associated with lateral bonds (12). This is clearly borne out by comparing the free energies and heats for members of an homologous series. There is practically no change in the molar free energy of adsorption from propyl alcohol (C_3) to melissyl (C_{31}), nor in the heat of adsorption between octyl (C_8) and melissyl (C_{31}). Evidently in dilute solution only the polar groups take part in adsorption. The hydrocarbon chains remain in exactly the same state whether the polar groups are in solution or are attached to the surface of the adsorbent. The condition of long-chain molecules adsorbed on to alumina from nonpolar solvents is thus analogous to their adsorption at an oil-water interface (20) except that at the solid interface they are localized to fixed sites. Since the hydrocarbon chains of the adsorbed molecules are freely dissolved in the solvent, there can be little or no lateral interaction, and the condition necessary for the Langmuir type of adsorption is maintained even for high surface coverage. These conclusions are in agreement with the observations of Manunta (21) and Cassidy (22), who found no difference in adsorption of fatty acids of differing chain length from petrol ether solution. Cassidy's curves do not fit the Langmuirian isotherm, but judging from the initial slopes and maximum capacity the free energy of adsorption of a fatty acid appears to be at least 6500 cal./gram mole.

The Traube Rule

The Traube rule (23) was first put forward to describe the increase in surface activity of a substance at an air-water interface which results from the addition of a hydrocarbon group to the molecule. Langmuir (24) showed that the Traube rule was an expression of the additivity of the molar free energy of adsorption which at this interface was about −625 cal./gram mole for each additional CH_2 group. The rule has been shown to apply to adsorption of vapors on to air-water surfaces (25; ref. 26, $\Delta G_{CH_2} = -500$ cal.); to the mercury surface (ref. 15, $\Delta G_{CH_2} = -930$ cal. for the gaseous film, −650 cal. for the condensed film at 25°C.); to penetration into neutral (27) and ionized monolayers (ref. 28, $\Delta G_{CH_2} = -800$ cal.). In all the above examples the hydrocarbon chain partakes in the adsorption process; it enters a different field of force and so undergoes an energy change.

When adsorption takes place on to a solid surface the role of the hydrocarbon chain is less clear. Several writers have reported a reversal of the Traube rule for molecules adsorbed under these conditions. However, Broda and Mark (29) have pointed out that both on theoretical grounds and as a result of experiment (30) any increase in chain length should increase the tendency of molecules to adsorb. Most if not all of the instances quoted in contradiction to this view result from confusion between the total amount adsorbed, which may decrease with chain length, and the energy of adsorption, which may either be independent of chain length or may increase with it. In theory the rule should be reversed only where the hydrocarbon chain is forced to enter a higher energy state; such a system is not easy to envisage. A paper by Holmes and McKelvey (31), which is frequently quoted as an example of the reversal of the Traube rule, gives isotherms for fatty acids adsorbed from toluene on to silica gel. They show that the higher acids adsorb in decreasing amounts, especially if the comparison is made at high concentration. However, if the isotherms for the series are scaled to the same maximum adsorption there is no definite trend in the initial slopes and therefore none in the energies of adsorption. Elder and Springer (32) suggest that whereas acetic and formic acids may adsorb more strongly on silica gel because of hydrogen bonding, the decrease in total adsorption of higher members of the series is due to their increased molecular size, not to the effect of the nonpolar chain. The results of Bartell and Fu (33) for adsorption of organic acids on silica gel from carbon tetrachloride point to the same conclusion, for although the adsorption maxima are higher for the smaller acid molecules, when the data are plotted as Langmuir isotherms there appears to be little change in energy from formic to butyric acid, the average value of the molar free energy ΔG for these members of the series being about -3600 cal./gram mole.

Illiin (34), reviewing results obtained with charcoal, points out that the apparent reversal of Traube's rule which is found in adsorbing fatty acids from water on to certain types of charcoal, is due to the ultrapore structure which limits the entry of the larger molecules. The highly active hydrofuge type with a lower proportion of ultrapores gave the usual increase in adsorption with chain length. Linner and Williams (35), though suggesting that if the amount of fatty acids adsorbed at a standard concentration decreased as the chain length increased it constituted a "reversal of Traube's rule," correctly interpreted the effect as being due to a difference in the available surface area. Differences brought about by activation treatment (36–38) affect the adsorption properties of charcoals considerably. In spite of these differences charcoals generally show an increased energy of adsorption with chain length for organic molecules adsorbed from aqueous solution (39). Amiot (40) obtained agreement with the Langmiur equation for adsorption of alcohol from aqueous solutions, and his values representing the "Intensity of Adsorption," presumably the Langmuir adsorption coefficient, show that isoamyl alcohol adsorbs 190 times as readily as methyl, corresponding to ΔG_{CH_2} of -770 cal. This appears a remarkably high value, since it is almost the same as the drop in energy of a CH_2 group in passing from a water to an oil phase (41). Linner and Gortner (42) also obtained a Langmuir isotherm for acids adsorbed on "Norit" charcoal, but the value for ΔG_{CH_2} calculated from their estimates of the Langmuir constant was only −320 cal. Fowkes and Harkins (43) measured adsorption of fatty acids and other substances on paraffin wax from the changes in contact angle and surface tension, and also obtained Langmuirian isotherms. In this case the value of ΔG_{CH_2} was about −650 cal./gram mole, which is of the same order as the energy change in passing from an aqueous to a nonpolar oil. Evidently when substances are adsorbed from aqueous solution on to charcoal the hydrocarbon chain interacts with the solid by dispersion forces, very much as it would interact with a solid or liquid hydrocarbon (*cf.* ref. 44). When the polar group is ionized, adsorption is negligible (38), the energy of adsorption being greatly reduced just as it is at the oil-water interface because of the electric potential set up (45).

SUMMARY

1. The isotherms for adsorption from benzene solution on to dry alumina were measured by means of the surface balance for a number of surface-active materials, chiefly alcohols. The isotherms were of Langmuirian form, described by $\theta/c(1 - \theta) = K$, where K is the Langmuir adsorption coefficient.

2. Competitive adsorption was followed between two alcohols, and between an alcohol and a phenol. The two adsorbates followed the Langmuirian equation independently, and the coefficient of adsorption of one could be deduced from the coefficient of the other.

3. When one of the competing substances was water, competitive adsorption did not appear to follow the Langmuir isotherm, since the water did not desorb normally.

4. The isosteric or differential heats of adsorption of several surface-active substances were measured from the temperature dependence of the Langmuir adsorption coefficient. The calorimetric or integral heats were also measured and were somewhat higher than the differential heats.

5. The heats and free energies of adsorption were in all cases independent of the length of the hydrocarbon chain. The free energy and probably also the heat of adsorption in the series alcohol, phenol, fatty acid increased as the hydroxyl group became more acidic.

6. The molecules are believed to be adsorbed on fixed sites of approximately uniform energy. At low concentration of adsorbate its nonpolar region remains dissolved in the solvent and is not affected by adsorption. The presence of solvent minimizes lateral forces and thus allows the Langmuirian relationship to hold good over a wide range of surface coverage.

7. The Traube rule, if applied to energies of adsorption, is probably generally valid for adsorption on solid surfaces. The so-called exceptions are thought to be due to the smaller surface area often available to larger molecules rather than to any decrease in their molar energy of adsorption.

8. The adsorption of polar substances from nonaqueous solutions appears to be little influenced by the hydrocarbon chain with silica as the adsorbent just as with alumina. On the other hand, the energy of adsorption of organic molecules from aqueous solution on to charcoal increases with increasing length of the hydrocarbon chain.

References

1. Crisp, D. J., *Proc. Intern. Congr. Pure and Appl. Chem., London, 1947* (1947).
2. Hutchinson, E., *Trans. Faraday Soc.* **43,** 439 (1947).
3. Hutchinson, E., *Trans. Faraday Soc.* **43,** 443 (1947).
4. Kemball, C., and Rideal, E. K., *Proc. Roy. Soc. (London)* **A187,** 53 (1946).
5. Fowler, R. H., *Proc. Cambridge Phil. Soc.* **31,** 262 (1935).
6. Butler, J. A. V., and Ockrent, C., *J. Phys. Chem.* **34,** 2842 (1930).
7. Kemball, C., Rideal, E. K., and Guggenheim, E. A., *Trans. Faraday Soc.* **44,** 948 (1948).
8. Drain, L. E., *Science Progr.* **42,** 608 (1954).
9. Hill, T. L., *J. Chem. Phys.* **17,** 520 (1949).
10. Everett, D. H., *Trans. Faraday Soc.* **46,** 453 (1950).
11. Everett, D. H., *Trans. Faraday Soc.* **46,** 942 (1950).
12. Graham, D., *J. Phys. Chem.* **57,** 665 (1953).
13. Kemball, C., *Proc. Roy. Soc. (London)* **A187,** 73 (1946).
14. Barrer, R. M., *Trans. Faraday Soc.* **40,** 374 (1944).
15. Kemball, C., *Proc. Roy. Soc. (London)* **A190,** 117 (1947).
16. de Boer, J. H., and Kruyer, S., *Koninkl. Ned. Akad. Wetenschap. Proc.* **B55,** 451 (1952).
17. de Boer, J. H., and Kruyer, S., *Koninkl. Ned. Akad. Wetenschap. Proc.* **B56,** 67, 236, 415 (1953).
18. Kipling, J. J., *Quart. Revs. (London)* **5,** 1, 60 (1951).
19. Kipling, J. J., and Tester, P. A., *J. Chem. Soc.* **1952,** 4123.
20. Alexander, A. E., and Teorell, T., *Trans. Faraday Soc.* **35,** 727 (1939).
21. Manunta, C., *Helv. Chim. Acta* **22,** 1156 (1939).
22. Cassidy, H. G., *J. Am. Chem. Soc.* **62,** 3073 (1940).
23. Traube, I., *Ann.* **265,** 27 (1891).
24. Langmuir, I., *J. Am. Chem. Soc.* **39,** 1848 (1917).
25. Michelli, L. I. A., *Phil. Mag.* **3,** 895 (1927).
26. Cassel, H., and Formstecher, M., *Kolloid-Z.* **61,** 18 (1932).
27. Pankhurst, K. G. A., *Proc. Roy. Soc. (London)* **A179,** 393 (1942).
28. Crisp, D. J., "Surface Chemistry," p. 65. Butterworth, London, 1947.
29. Broda, A., and Mark, H., *Z. physik. Chem.* **A180,** 392 (1937).
30. Baum, A., and Broda, E., *Trans. Faraday Soc.* **34,** 797 (1938).
31. Holmes, H. N., and McKelvey, J. B., *J. Phys. Chem.* **32,** 1522 (1928).
32. Elder, A. L., and Springer, R. A., *J. Phys. Chem.* **44,** 943 (1940).
33. Bartell, F. E., and Fu, Y., *J. Phys. Chem.* **33,** 678 (1929).
34. Illiin, B., *Z. physik. Chem.* **A155,** 403 (1931).
35. Linner, E. R., and Williams, A. P., *J. Phys. Chem.* **54,** 605 (1950).
36. King, A., *J. Chem. Soc.* **1937,** 1489.
37. Bartell, F. E., and Lloyd, L. E., *J. Am. Chem. Soc.* **60,** 2120 (1938).
38. Kipling, J. J., *J. Chem. Soc.* **1948,** 1483.

39. Freundlich, H., *Kapillarchemie* **I,** 257 (1930).
40. Amiot, R., *Compt. rend.* **202,** 1852 (1936).
41. Butler, J. A. V., *Trans. Faraday Soc.* **33,** 229 (1937).
42. Linner, E. R., and Gortner, R. A., *J. Phys. Chem.* **39,** 35 (1935).
43. Fowkes, F. M., and Harkins, W. D., *J. Am. Chem. Soc.* **62,** 3377 (1940).
44. Boyd, G. E., and Harkins, W. D., *J. Am. Chem. Soc.* **64,** 1195 (1942).
45. Cassie, A. B. D., and Palmer, R. C., *Trans. Faraday Soc.* **37,** 156 (1941).

JOURNAL OF COLLOID SCIENCE **11**, 377–390 (1956)

A SURFACE EQUATION OF STATE FOR CHARGED MONOLAYERS

J. T. Davies

Department of Chemical Engineering, University of Cambridge,
Tennis Court Road, Cambridge, England

Received April 5, 1956

Abstract

The force-area characteristics of charged films adsorbed at the *air-water* surface should not be compared with the previously published theoretical treatment of Davies—this treatment applies only to charged films at the *oil-water* surface. By taking cohesive energy as well as electrical repulsion into account, a new equation has been derived for air-water films. This equation is compared with recent experimental results.

Introduction

Over the last few years studies on detergents spread as insoluble monolayers (1–4) and in adsorbed films (2, 5–9) have shown conclusively that an electrical charge on a monolayer may profoundly alter its free energy and surface tension. The surface dipole moments (10) and the amounts and rates of adsorption (11) are likewise affected by the electrical charge.

Several different equations have been proposed to account for the electrical effects. Cassie and Palmer (12), for example, suggested:

$$\pi^{\pm}(A - A_0) = 1.5\,kT, \qquad [1]$$

where $\pi^{\pm}$ is the film pressure (surface tension lowering) of either a positively or a negatively charged film, A is the area available in the surface to each long-chain ion, and A_0 is the cross-sectional area of the latter. The Boltzmann constant and the absolute temperature are represented by k and T. Equation [1] gives values of the product $\pi^{\pm}(A - A_0)$ which are usually far too low, especially for charged films at the oil-water interface.

Recently Brady and Brown (7) have reported that a value $2kT$ for the product $\pi^{\pm}(A - A_0)$ is in quite good agreement with experiment for films of sodium lauryl sulfate adsorbed at the air-water interface, though their range of A is small (52–90 A.^{2}), whereas Pethica (9) finds that the product is less than $1kT$ for films of sodium lauryl sulfate when 0.145 M NaCl is present, also at the air-water surface.

These authors (7, 9) have compared these results for *air-water* films with an equation of state put forward by Davies (13) for films at the *oil-water* interface. This equation predicts that for the low salt concentrations the product $\pi^{\pm}(A - A_0)$ for charged films at the *oil-water* interface tends to $3kT$. Like other and earlier results for charged films at *air-water* surfaces (1, 13), however, those of Pethica and of Brady and Brown give products considerably less than $3kT$ (e.g., octadecyltrimethylammonium ions give about $1kT$ (13)). If, on the other hand, the equation of Davies (13) is applied to films at the *oil-water* interface, there is quite fair agreement with experiment for both cationics and anionics (8, 13). The values of the product then approach $3kT$.

This paper deals with the reason for the lower product measured for films at the air-water surface compared with that at the oil-water surface: the cohesion between the hydrocarbon chains at the air-water surface (11) causes such monolayers to be more condensed (and hence less ideal in behavior) than in the presence of oil (13, 14). This is illustrated in Fig. 1.

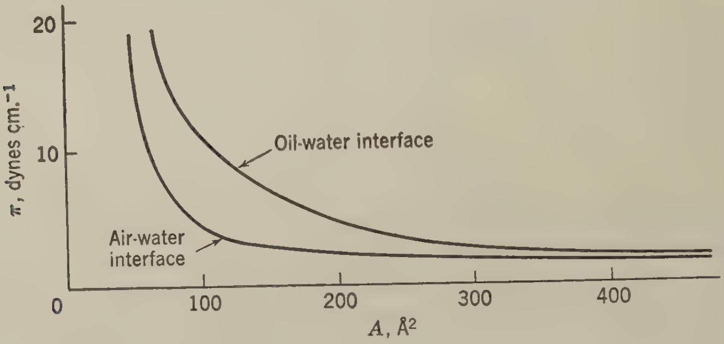

FIG. 1. Force-area curves for $C_{18}H_{37}N(CH_3)_3^+$ at oil-water and air-water interfaces. Substrate is 0.01 N HCl (11).

FILMS AT THE AIR-WATER SURFACE

Exact interpretation of the results of Brady and Brown (7) and of Pethica (9), as well as of the earlier air-water data (1, 2, 13), requires knowledge of both electrical and cohesive energies. It is the purpose of this paper to suggest values for these energies. At the air-water surface π^0 (the surface pressure of an uncharged film) will not, in general, be equal to π_c, the surface pressure due to kinetic energy. Both kinetic pressure (π_c) and cohesive pressure (π_s) contribute to the total surface pressure (π^0) of the uncharged film: $\pi^0 = \pi_c + \pi_s$. This subscript notation is that of Guastalla (15). Now $\pi_c = kT/(A - A_0)$ (11) and if π_s were also a known function of chain length and A, we could relate π^0 and A, obtaining an explicit equation of state for films at an air-water surface:

$$(\pi^0 - \pi_s)(A - A_0) = kT \qquad [2]$$

If now the film is charged (e.g., made up of long-chain quaternary ammonium ions), an electrical repulsive pressure $\Delta\pi$ must also be allowed for (13). If this is separable from the cohesion, the total pressure ($\pi^{\pm}$) of a charged film at the air-water surface will be made up of three independent components:

$$\pi^{\pm} = \pi_c + \pi_s + \Delta\pi.$$

For any given film $\Delta\pi$ can be evaluated (13) if the ionic concentration of the underlying solution and the charge density on the film are known.

Further since $\pi_c(A - A_0) = kT$, the equation of state now becomes:

$$(\pi^{\pm} - \pi_s - \Delta\pi)(A - A_0) = kT. \quad [3]$$

THE COHESIVE ENERGY

1. *High Areas*

At high areas the cohesive energy π_s will now be shown to vary in accord with the empirical equation:

$$\pi_s = -Kn/A^{3/2}. \quad [4]$$

Here n is the number of —CH_2— groups in each surface-active molecule or ion. This leads to the equation of state for cohering uncharged films (from Eq. [2]):

$$(\pi^0 + Kn/A^{3/2})(A - A_0) = kT. \quad [5]$$

Guastalla (16, 17) was the first to suggest a cohesive pressure correction varying as $A^{-3/2}$. He determined (as $\pi_0 - \pi_c$) the cohesion in films of unionized myristic acid at the air-water surface; accurate experimental data over a wide range of A showed that $\pi_s A^{3/2}$ was constant, having a value of -7600 when π_s is expressed in dynes cm.$^{-1}$ and A in A.^{2}. For lauric acid $\pi_s A^{3/2}$ is similarly found to be -5560 (18). Guastalla did not investigate the variation of the cohesive energy with n; he considered that the cohesion was caused by the dipoles of the polar groups (17). However, while confirming the dependence of cohesion on $A^{-3/2}$, Phillips (19) found that it varied markedly with n. Further, films at the *oil-water* interface show no cohesion, and we therefore consider that all cohesion originates at the air-water surface in van der Waals' forces of attraction between the —CH_2— groups of adjacent hydrocarbon chains.

While the dependence of cohesion on $A^{-3/2}$ (Eq. [4]) is thus confirmed for uncharged films, the variation of π_s with n must now be tested. This is done in Fig. 2*a*, where $-\pi_s A^{3/2}$ is plotted for various uncharged compounds with different chain lengths (16, 18, 19). Though there are clearly specific effects, the relation $-\pi_s A^{3/2} = Kn$ is approximately obeyed within the region of $n = 11$ to $n = 17$. Thus for uncharged films Eq. [4] is a fair approximation in this range: K has a value of 400 per —CH_2— group when π_s is in dynes cm.$^{-1}$ and A in A.^{2}.

If now a cohering film at the air-water surface is electrically charged, we have by substitution from Eq. [4] into Eq. [3]:

$$(\pi^{\pm} + Kn/A^{3/2} - \Delta\pi)(A - A_0) = kT, \qquad [6]$$

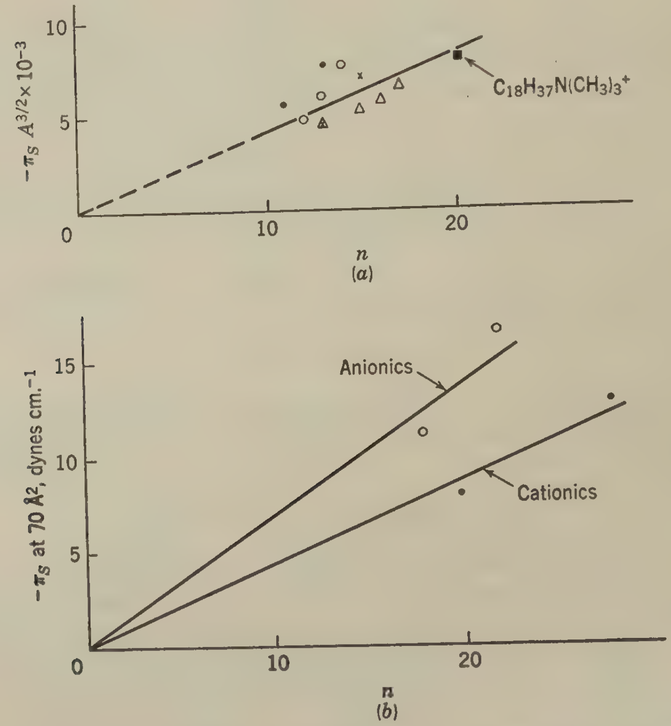

FIG. 2. (a) Plot of $-\pi_s A^{3/2}$ vs. n (number of —CH_2— groups) for uncharged films at the air-water interface (high-area region). The roughly linear relationship over the range $n = 11$ to $n = 17$ leads to Eq. [4]. Full circles, data for acids (16, 18). Open circles, data for acids (19). Crosses, data for nitriles (19). Triangles, data for esters (19). The full square is calculated for a cationic film from the data in Fig. 4 below.

(b) Plot of π_s at 70A.^{2} vs. n for long-chain sulfates and quaternary ammonium ions at the air-water interface (low-area region). Here n is the number of —CH_2— groups effective in producing cohesion; π_s has been derived from Eq. [7] using the results of this paper and of refs. 13 and 19. The lines are represented by Eq. [8].

which is the required equation of state for a charged film at the air-water surface. Further, $\Delta\pi$ can be explicitly calculated (13).

To test directly whether, as assumed in Eqs. [3] and [6], the cohesive energy may still be calculated from Eq. [4] if the film is charged (i.e., whether π_s and $\Delta\pi$ are independent at high areas) consider two films at the same areas and on the same aqueous substrates, but one at the oil-water interface (no cohesion, $\pi_s = 0$) and the other at the air-water surface. With subscripts *o* and *a* to denote this difference, we therefore have:

$$\pi_o^{\pm} - \pi_a^{\pm} = -\pi_s. \qquad [7]$$

Thus π_s is easily deduced at different areas from data such as those in Fig. 1. In Fig. 3, $-\pi_s$ is shown for films of octadecyltrimethylammonium ions. Values from Fig. 3 at areas from 225 A.^{2} to 100 A.^{2} are plotted logarithmically in Fig. 4, in which the slope of the plot of log $(-\pi_s)$ against

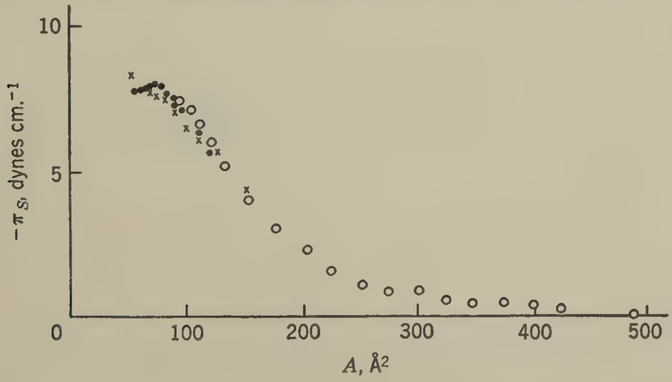

FIG. 3. Cohesive pressure $(-\pi_s)$ for $C_{18}H_{37}N(CH_3)_3^+$ ions, evaluated using Eq. [7] and data of ref. 11.

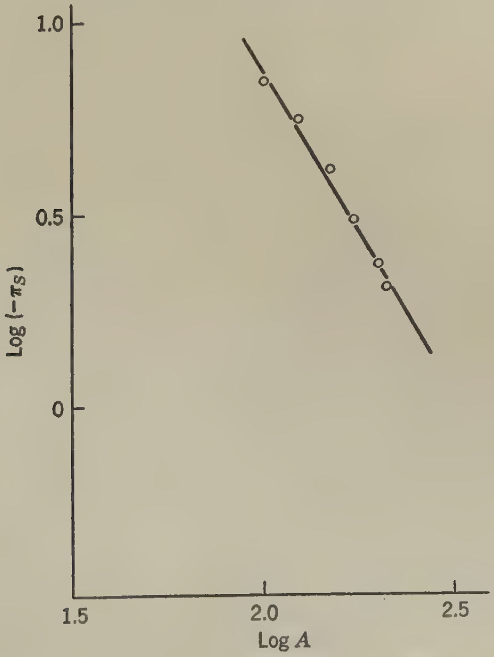

FIG. 4. Logarithmic plot of data of Fig. 3. Slope of line is −1.6; *cf*. Eq. [4].

log A is -1.6, in agreement with the value -1.5 in Eq. [4]. Further, from the data of Fig. 4, $-\pi_s A^{3/2}$ is found to be 8000, and since 20 —CH_2— groups are effective in films of octadecyltrimethylammonium ions (11), the cohesive constant K in these films is still 400, as in neutral films (see point in Fig. 2*a*). This confirms the assumption that π_s and $\Delta\pi$ are independent in the high-area region.

2. Low Areas

If, however, A is less than 100 A.^{2} for cationics or 71 A.^{2} for anionics, we shall show that:

$$\left.\begin{aligned}\pi_s &= -0.4\,n \text{ dyne cm.}^{-1} \text{ for cationics}\\ \pi_s &= -0.67\,n \text{ dyne cm.}^{-1} \text{ for anionics}\end{aligned}\right\}. \qquad [8]$$

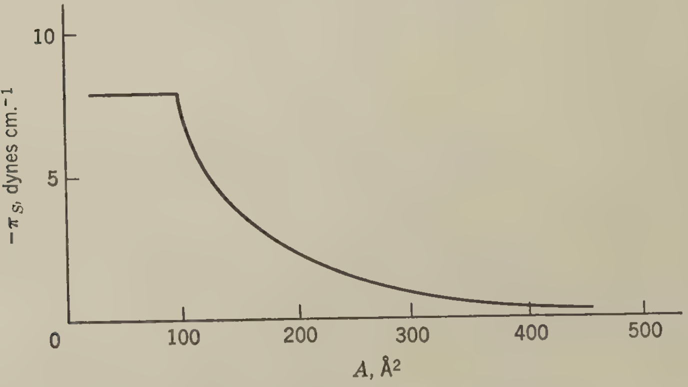

FIG. 5. Idealized curve for cohesion in films of $C_{18}H_{37}N(CH_3)_3^+$ at the air-water surface on 0.01 N HCl, from points of Fig. 3.

The charged films at low areas thus appear to behave similarly to Langmuir's duplex expanded films, in which π_s (or F_0) is constant at different areas (20). This constant cohesion at low areas is suggested by the data of Fig. 3 (points having been taken from Fig. 1 and from references 11, 13, and 19); it is seen that the cohesion in octadecyltrimethylammonium films remains nearly constant at 8 dynes cm.$^{-1}$ as A is reduced below about 90 A.^{2}. This is idealized in the line and curve of Fig. 5, which cut at 100 A.^{2} for cationics; in general, the area below which the cohesive pressure does not increase further is obtained by equating [4] and [8].

In this low-area region π_s is considerably less than in Langmuir's neutral films; the surface cohesion for a neutral molecule with 20 —CH_2— groups, for example, is about 21 dynes cm.$^{-1}$ compared with 8 dynes cm.$^{-1}$ for the corresponding charged film of octadecyltrimethylammonium ions. This difference may well arise from the strong electrical repulsion at low areas —the long-chain ions in the surface tend to be distributed evenly over the surface and local clustering (which leads to more effective cohesion) is thus prevented in charged films. Thus π_s is no longer completely independent of electrical effects, though allowance can be made for this (as in Eqs. [8]); in this way separability of electrical and cohesive effects is still possible.

The variation of π_s with n, the number of —CH_2— groups in each chain, is again very marked in the low-area region. Langmuir's data (20) for neutral films show that π_s is approximately proportional to n for expanded films in the range of n from 11 to 20. Though results for charged films are fragmentary (Fig. 2*b*), the lines drawn in the figure (and which lead to Eqs. [8]) are not inconsistent with experiment.

At first sight the different cohesive energies between the hydrocarbon chains of surface-active cationics and anionics may appear surprising. There are, however, other differences between the two types of surface-active ions; for example, much more oil can be solubilized in cationic than in anionic micelles (21, 22) owing to the tighter cohesion in the latter. The long-chain anions carry their charge on the exposed oxygen atoms of the head group; the counter ions may therefore polarize this and so lie close under the head group, permitting the hydrocarbon chains to pack fairly closely. With cationics, however, the charged nitrogen atom is both enlarged and protected from polarization by the attached hydrogen or methyl groups; the counter ions cannot fit snugly and so the surface film at low areas may be expected to be more disordered, as is also the micelle. The finding (Fig. 2*b*) that cohesion is more important in films of anionics than in films of cationics is thus not unexpected.

THE EQUATIONS OF STATE AT THE AIR-WATER SURFACE

If $A > 100$ A.^{2}, for cationics, or 71 A.^{2}, for anionics, we have, by substituting in [6] for K and $\Delta\pi$ (13):

$$\left(\pi^{\pm} + 400n/A^{3/2} - 6.1c^{1/2}\left\{\cosh \sinh^{-1} \frac{134}{Ac^{1/2}} - 1\right\}\right)(A - A_0) = kT. \qquad [9]$$

In the low-area region we have, using Eq. [8] for π_s:

$$\left(\pi^{\pm} + \beta n - 6.1c^{1/2}\left\{\cosh \sinh^{-1} \frac{134}{Ac^{1/2}} - 1\right\}\right)(A - A_0) = kT, \qquad [10]$$

where c is the concentration of uni-univalent electrolyte in the solution, and where β is 0.4 for cationics and 0.67 for anionics. If, however, $Ac^{1/2} < 38$, these equations may be simplified, respectively, with an error of not more than 2%, to:

$$\pi^{\pm}(A - A_0) = 3kT - 6.1(A - A_0)c^{1/2} - \frac{2kTA_0}{A} - \frac{400n(A - A_0)}{A^{3/2}} \qquad [11]$$

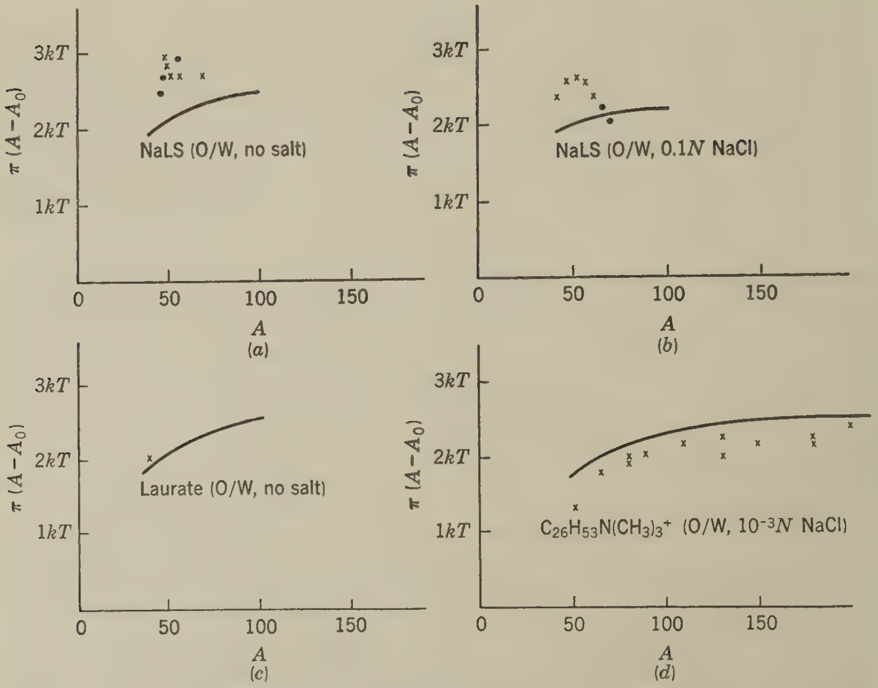

FIG. 6. Plots of product $\pi^{\pm}(A - A_0)$ vs. A (in A.²) for ionized films at the *oil-water* interface. Comparison is made with the appropriate theoretical equations (Eqs. [10] and [12] with $\pi_s = 0 = \beta$), represented by full lines throughout.

(*a*) Films of lauryl sulfate ions adsorbed from water. Experimental figures are those of Cockbain (8). Where the Gibbs equation was used to calculate adsorptions, the factor 2 was retained, and these results (full circles) agree well with direct measurement (crosses). Points at areas above 60 A.² could not accurately be determined from the Gibbs equation and such points are omitted. The value of A_0 used here is 20 A.² throughout.

(*b*) Films of lauryl sulfate ions adsorbed from 0.1 N NaCl. Here A_0 is 20A.² throughout. Cockbain (8) used the Gibbs equation with a factor of 1 in calculating all points. The full points are calculated from an extrapolation of Cockbain's experimental data.

(*c*) Films of laurate ions adsorbed from solutions of pH 11. Data taken from Cockbain and McMullen (6), who used the Gibbs equation with factor 2 since no salt was present; $A_0 = 20$ A.².

(*d*) Films of $C_{26}H_{53}N(CH_3)_3^+$ spread on 10^{-3} N NaCl (13). Here $A_0 = 30$ A.².

and

$$\pi^{\pm}(A - A_0) = 3kT - 6.1(A - A_0)c^{1/2} - \frac{2kTA_0}{A} - \beta n(A - A_0). \quad [12]$$

A further simplification is possible if both $A\sqrt{c}$ and $\sqrt{c}$ are small, as is true for sodium lauryl sulfate adsorbed in the absence of salt. Then:

$$\Delta\pi \approx \frac{2kT}{A}.$$

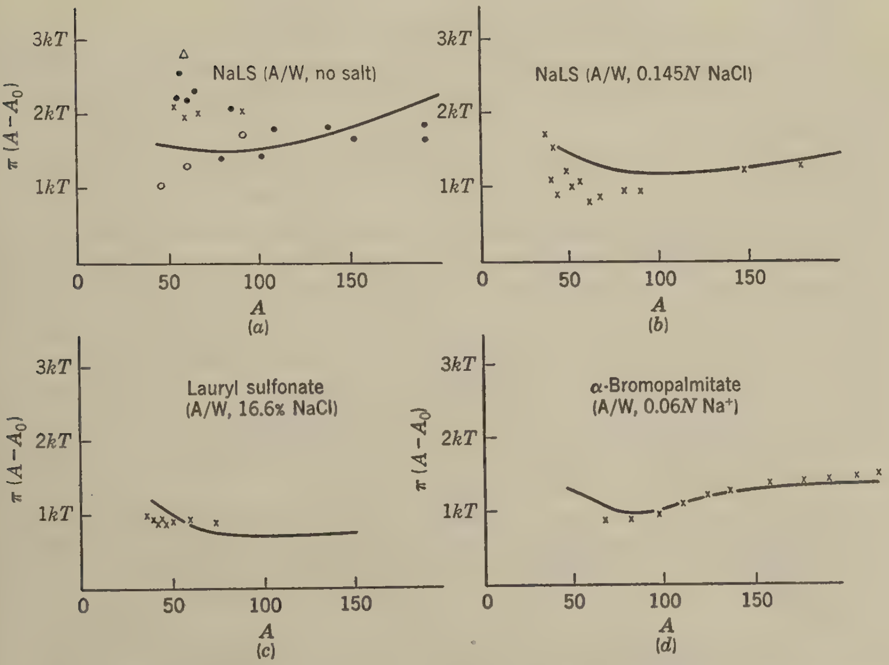

FIG. 7. Plots of product $\pi^-(A - A_0)$ vs. A (in A.^{2}) for ionized films at the *air-water* surface. Comparison is made with the appropriate theoretical equations (Eqs. [9], [10], [11], [12]), represented by full lines throughout.

(*a*) Films of lauryl sulfate ions adsorbed from water: closed circles, data of Pethica (9); open circles, data of Hutchinson (5); crosses, data of Brady and Brown (7); triangles, data of Miles and Shedlovsky. A_0 is 20A.^{2} throughout. All points are calculated from experimental figures using the Gibbs equation with a factor of 2.

(*b*) Films of lauryl sulfate ions adsorbed from 0.145 N NaCl; results are those of Pethica (9), using the Gibbs equation with a factor of 1 and with A_0 as 20A.^{2}.

(*c*) Films of lauryl sulfonate spread on 16.6% NaCl; results are those of Brady (2), with A_0 as 20A.^{2}. Points at 60A.^{2} and 75A.^{2} have been calculated from an extrapolation of Brady's force-area curve.

(*d*) Films of α-bromopalmitate spread on 6×10^{-2} N Na$^+$. Points are from the data of Crisp (1), and A_0 is taken as 25A.^{2}.

An approximate equation of state for low areas can now be obtained by substituting the appropriate terms into Eq. [3]. Thus

$$(\pi^{\pm} - \pi_s - \Delta\pi)(A - A_0) = kT \qquad [3]$$

becomes:

$$\left(\pi^{\pm} + \beta n - \frac{2kT}{A}\right)(A - A_0) = kT, \qquad [13]$$

which is valid for films at low areas (<71 A.^{2} for anionics) adsorbed on substrates of very low total electrolyte concentration.

COMPARISON WITH EXPERIMENT

For films at the *oil-water* interface, $\pi_s = 0$, and so Eqs. [10] and [12] with $\beta = 0$ should apply. Comparison with various experimental data is made in Fig. 6.

In Figs. 7 and 8 experimental data for adsorbed and insoluble films at the *air-water* interface are shown. They are compared with Eqs. [9] and [10], or with the simpler forms (Eqs. [11] and [12]) where possible. Three points may be noted from the figures. Firstly, the air-water values of the product $\pi^{\pm}(A - A_0)$ (using A_0 values obtained from insoluble films of the same type) are considerably lower than for the same films at the oil-water interface, often by as much as $1kT$ (*cf.* Figs. 6*a* and 7*a*; 6*b* and 7*b*, 6*d* and 8*a*). Secondly, the theoretical equations cover the experimental rise in the product at areas below 80 or 100 A.^{2}. Thirdly, the most soluble films (lauryl sulfate in the absence of added salt) show products rather higher than calculated, as seen in Figs. 6*a* and 7*a*.

A direct test of the form of the cohesive pressure corrections is also possible, using the data of Fig. 1 for octadecyltrimethylammonium films.

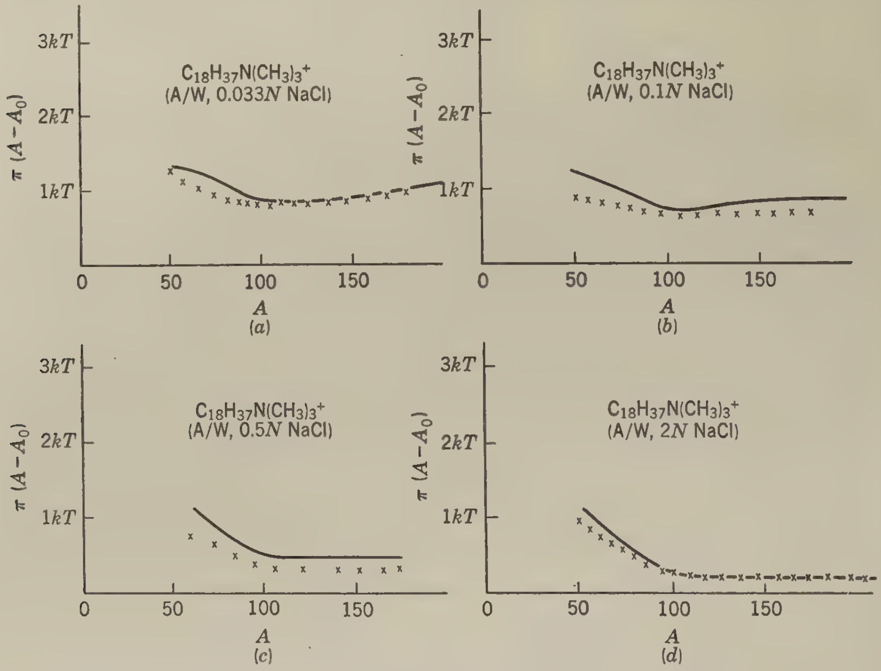

FIG. 8. Plots of product $\pi^+(A - A_0)$ vs. A (in A.^{2}) for charged films of octadecyltrimethylammonium ions spread at the *air-water* surface. Points are taken from the curves of Davies (13) with A_0 as 30A.^{2}. Comparison is made with the appropriate theoretical equations (Eqs. [9], [10], [11], [12]) represented by full lines throughout.

(*a*) Films on 0.033 N NaCl; (*b*) on 0.1 N NaCl; (*c*) on 0.5 N NaCl; (*d*) on 2 N NaCl.

TABLE I

Measured and Calculated Cohesive Pressures for Monolayers of Octadecyltrimethylammonium Ions at the Air-Water Interface, with $c = 0.01\ N$

Area per long-chain ion ($A.^2$)	$-\Pi_s$ (*dynes cm.*$^{-1}$) from experimental data of ref. (11) using Eq. [7]. *cf.* Fig. 3	$-\Pi_s$ (*dynes cm.*$^{-1}$) *calculated from Eqs.* [4] *and* [8]
	High-area region	
400	0.4	1.0
300	0.8	1.5
200	2.4	2.8
150	4.2	4.3
100	6.8	8.0
	Low-area region	
90	7.3	8.0
80	7.5	8.0
70	7.8	8.0
60	8.0	8.0
50	8.0	8.0

In Table I the cohesive pressure has been determined from the experimental data by applying Eq. [7]; the calculated values were obtained from Eqs. [4] and [8].

DISCUSSION

1. The Value of A_0

In the calculation of the points and curves of Figs. 6 and 7, it has been assumed that A_0 is 20 A.^{2}, as in insoluble, condensed films of $C_{22}H_{45}SO_4'$. This assumption was made to avoid introducing a further empirical factor into the surface equation of state. There is, however, a growing body of evidence to suggest that A_0 is higher in adsorbed "soluble" films than in spread films or even in the less soluble adsorbed films. Pethica (9), for example, takes A_0 for the lauryl sulfate ion to be 31 A.^{2}, while Cockbain (8) suggests that the 25 A. used in his calculations may be too low. Brady and Brown (7) consider 30.5 A.^{2} reasonable, though Cook and Talbot (23) suggest that A_0 is as high as 50 A.^{2}.

On this assumption that A_0 is indeed higher in "soluble" (weakly adsorbed) monolayers of long-chain ions, the data for films of lauryl sulfate adsorbed in the absence of salt have been recalculated with $A_0 = 33$ A.^{2}, this giving the best fit between the points and the calculated curves; *cf.* Figs. 6*a* and 7*a*, and 9*a* and 9*b*.

The approximate equation of state for low areas and low ionic strengths (Eq. [13]) has been compared with experiment in Figs. 9*c* and 9*d*, again with $A_0 = 33$ A.^{2}, and with $\beta = 0$ for films at the oil-water interface.

2. The Reason for the Larger A_0 *in the More Soluble Films*

Cockbain (8) suggests that A_0 is greater in the more soluble films because some of the hydrocarbon chain extends, in a coiled form, into the aqueous

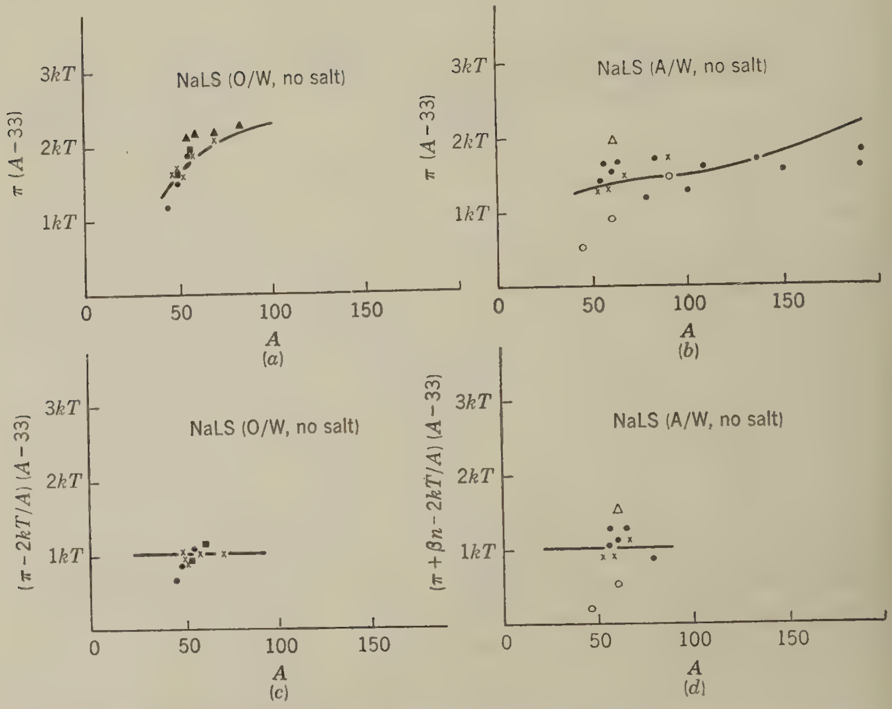

FIG. 9. Effect of taking A_0 as 33 A.^{2} for soluble films. Comparison of experimental points with theoretical equations represented by full curves.

(*a*) Plot of $\pi^{-}(A - 33)$ vs. A for sodium lauryl sulfate adsorbed at the oil-water interface in the absence of salt; crosses and circles as in Fig. 6*a*. Squares refer to results of Haydon and Phillips (24); triangles refer to results for dodecyltrimethylammonium ions (24). Curve is plot of Eqs. [11] and [12].

(*b*) As in (*a*) but at air-water surface: crosses, circles, and triangle as in Fig. 7*a*. Curve is plot of Eqs. [11] and [12] with no cohesion correction.

(*c*) Test of Eq. [13] for low areas and low electrolyte concentrations. Data are for sodium lauryl sulfate adsorbed at the oil-water interface ($\beta = 0$) in the absence of salt. Circles and crosses as in Fig. 6*a*. Squares from data of ref. (24) for lauryl sulfate. Line at $1kT$ represents Eq. [13].

(*d*) As in (*c*), but at air-water interface, with $\beta n = 8$. Crosses, circles, and triangle as in Fig. 7*a*. Line at $1kT$ represents Eq. [13].

phase. To the present author this seems reasonable; this tendency for A_0 to increase will be enhanced if n is small (less cohesive force to pull the chains out of the water or to orient them) and if the electrical potential on the film is high (i.e., A small or c low), which increases the tendency to pull the chains into the water.

The same conditions (n, A, c lower) make the film more soluble, i.e., the long-chain ions are less strongly adsorbed.

3. *The Empirical Equation of Brady and Brown*

To fit their data for sodium lauryl sulfate adsorbed at the air-water surface Brady and Brown (7) suggested the empirical equation:

$$\left(\pi^{\pm} - \frac{kT}{A}\right)(A - 30.5) = kT. \qquad [14]$$

This relation is numerically close to Eq. [13] over the range of areas 50 A.^{2} to 70 A.^{2}; here kT/A is about 7 and βn is 8. Clearly, however, this numerical agreement cannot hold over a wider area range, nor with longer chains (larger n), nor with cationics (β lower). A more detailed investigation of this would seem worth while.

CONCLUSION

That charged films at the air-water surface (7, 9, 13) do not obey the equations of Davies (13) for *oil-water* films is shown to be due to neglect of the cohesive pressure between the hydrocarbon chains. Whereas charged monolayers of long-chain quaternary ions at the *oil-water* interface are known to behave in accord with the equations of Davies (13), it is shown here that the same films at the *air-water* surface obey fairly closely Eqs. [9], [10], [11], [12], [13] in which the cohesive pressure has been introduced. The latter equations are also consistent with the rather chaotic published measurements on adsorbed films of sodium lauryl sulfate, both with and without added salt.

ACKNOWLEDGMENT

The author is grateful to Sir Eric Rideal, F.R.S., for stimulating discussions in the early stages of the preparation of this paper.

REFERENCES

1. CRISP, D. J. "Surface Chemistry." Butterworth, London 65, 1949.
2. BRADY, A. P., *J. Colloid Sci.* **4,** 417 (1949).
3. ASKEW, F. A., AND DANIELLI, J. F., *Trans. Faraday Soc.* **36,** 785 (1940).
4. ALEXANDER, A. E., AND TEORELL, T., *Trans. Faraday Soc.* **35,** 727, 733 (1939).
5. HUTCHINSON, E., *J. Colloid Sci.* **3,** 413 (1948).
6. COCKBAIN, E. G., AND MCMULLEN, A. I., *Trans. Faraday Soc.* **47,** 322 (1951).
7. BRADY, A. P., AND BROWN, A. G., "Monomolecular Layers," p. 33. American Association for the Advancement of Science, 1954.
8. COCKBAIN, E. G., *Trans. Faraday Soc.* **50,** 874 (1954).
9. PETHICA, B. A., *Trans. Faraday Soc.* **50,** 413 (1954).
10. DAVIES, J. T., *Nature* **167,** 193 (1951).
11. DAVIES, J. T., *Trans. Faraday Soc.* **48,** 1052 (1952).
12. CASSIE, A. B. D., AND PALMER, R. C., *Trans. Faraday Soc.* **37,** 156 (1941).
13. DAVIES, J. T., *Proc. Roy. Soc.* (*London*) **A208,** 224 (1951).
14. HUTCHINSON, E., "Monomolecular Layers," p. 161. American Association for the Advancement of Science, 1954.

15. GUASTALLA, J., *Compt. rend.* **228,** 820 (1949).
16. GUASTALLA, J., *Cahiers phys.* **10,** 30 (1942).
17. GUASTALLA, J., *J. chim. phys.* **43,** 184 (1946).
18. TER MINASSIAN-SARAGA, L., *J. chim. phys.* **52,** 80 (1955).
19. PHILLIPS, J. N., Thesis, Univ. of London, 1954.
20. LANGMUIR, I., *J. Chem. Phys.* **1,** 756 (1933).
21. KLEVENS, H. B., *Kolloid-Z.* **128,** 61 (1952).
22. MCBAIN, M. E. L. AND HUTCHINSON, E., "Solubilization," pp. 63, 64, 67, 79, 80, 85. Academic Press, New York, 1955.
23. COOK, M. A., AND TALBOT, E. L., *J. Phys. Chem.* **56,** 412 (1952).
24. HAYDON, D. A., AND PHILLIPS, J. N., *Nature*, in press (1956).

JOURNAL OF COLLOID SCIENCE **11**, 391–397 (1956)

THE COALESCENCE OF LIQUID DROPS

M. Linton and K. L. Sutherland

Division of Industrial Chemistry, C.S.I.R.O., Melbourne, Australia

Received April 13, 1956

Abstract

Liquid drops floating on a surface of the same liquid were studied using high-speed photography. The coalescence of a drop with the underlying surface or with another drop on collision is delayed by the air film trapped between the opposing surfaces which deform on approaching each other. A drop remains in contact with the underlying surface for a time proportional to its size. When two floating drops collide they bounce or coalesce after a time proportional to the cube of the size of the smaller drop. Drops of diameter smaller than 0.05 cm. coalesce readily with other drops, whereas those larger than 0.1 cm. in diameter are more likely to bounce. These results have a bearing on the coalescence of colliding jets, mist, and raindrops.

Introduction

The phenomenon of drops of a liquid floating on a surface of the same liquid was described in 1881 by Reynolds (1), who observed raindrops remaining on a dust-free water surface for some seconds before coalescing with the underlying water. Surface-active agents cause floating drops to last longer, and hence we suggested that they would hinder coalescence of droplets in a cloud. Telford (private communication) tested this suggestion in a wind tunnel, but found that small drops formed from solutions of surface-active agents coalesced just as rapidly as drops of pure water. We sought the reason for this apparent anomaly by a study of coalescence processes.

Experimental

The solution used to form floating drops was 0.1% w/v cationic detergent (I.C.I. "Cetavlon" containing 75% cetyl trimethyl ammonium bromide) in distilled water. Qualitatively this solution behaved like a wide variety of sprayable liquids. A fine jet which broke into drops was played at an angle of about 30° at a point off-center on a surface of the same solution contained in a glass vessel 3 cm. in diameter. The drops bounced off the surface and off the wall and then floated individually or in the form of a drop raft (Plate I, *A*). The drops were photographed from above at film speeds up to 2700 frames/sec., the speed being estimated from a timing trace.

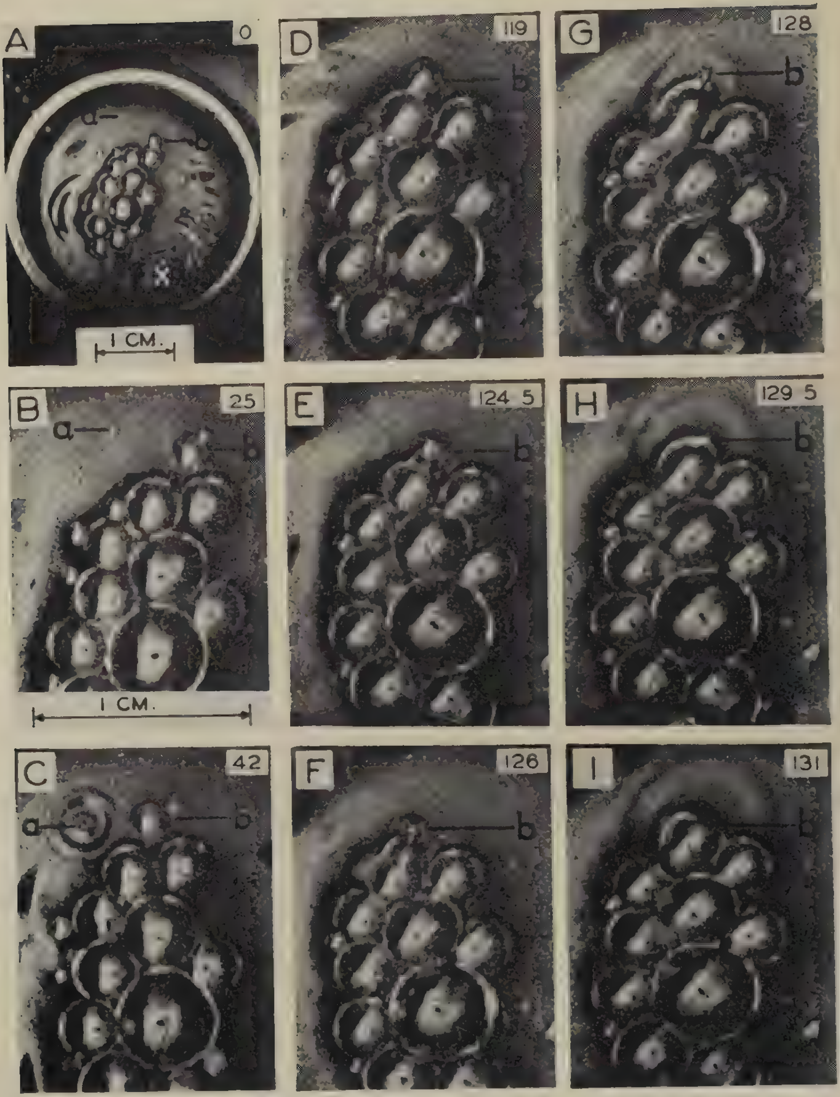

PLATE I. Selections from frames of film (at *ca.* 2000 frames/sec.) of drops of "Cetavlon" solution, floating on the same solution, individually, and in apparent contact in a drop raft.

Scales are as shown. The numbers marked on the frames are the times in milliseconds from frame *A*.

A: Overall view of vessel, jet entering from top left and hitting the surface near *X*.

A small drop "*a*" (*A–C*) coalesces with the surface, forming a wave pattern (*C*). A medium size drop "*b*" bounces from a larger drop (*A* and *B*), and then from a smaller drop (*A–C*). Drop "*b*" collides with a larger drop at the edge of the raft (*D*) and coalesces with it, showing rapid development of necks (*E* and *F*), a small protuberance (*G* and *H*), and oscillation (*I*).

The coalescence of a drop with the underlying surface was revealed by a wave pattern (Plate I, *C*). Occasionally the drop coalesced in stages (*cf.* (2)), a secondary drop being ejected a few millimeters into the air.

Drops colliding with each other remained in contact for a period, the time of apparent contact, and then separated or bounced ("*b*," Plate I, *A–C*) or coalesced ("*b*," Plate I, *D–I*). The onset of coalescence was shown by a "neck" which widened within a few milliseconds ("*b*," Plate I, *E–G*) causing oscillations ("*b*," Plate I, *I*) the amplitude and period of which increased with the size of the drops involved. During coalescence protuberances often formed (Plate I, *G* and *H*), and occasionally one would detach as a secondary drop.

The life of a drop is measured from its appearance on the surface to the appearance of the wave pattern produced by its disappearance and could usually be determined to ±5 msec. For bounce or coalescence on collision the error in the time of contact was about 1 msec. The drop diameters were measured to ±0.01 cm. by comparison with the known size of the vessel. Since drop sizes ranged from 0.02 to 0.24 cm. there was a considerable error in measuring the smaller drops.

RESULTS

Figure 1 shows the time of apparent contact (t in milliseconds) for coalescence between a floating drop and the free liquid surface in relation to the drop diameter (d in centimeters). The best linear fit on a double logarithmic plot is:

$$t = 2 \times 10^3\, d^{0.78}. \qquad [1]$$

However, a simpler relation:

$$t = 4 \times 10^3\, d \qquad [2]$$

is consistent with the results.

The times of apparent contact for mutual bounce and coalescence between two drops were found to depend on the diameter of the smaller drop as shown in Fig. 2. A relation which represents the results is:

$$t = 1.8 \times 10^4\, d^3. \qquad [3]$$

These results, as shown by the two curves in Fig. 2, strikingly bear out the visual observations that drops less than 0.1 cm. in diameter coalesce with one another much more rapidly than with a free liquid surface. In qualitative accord with relations [1]–[3] are the visual observations (1, 3, 4) that single drops a few millimeters in diameter float for about 2 sec. Some of the larger drops shown in Plate I were present throughout the 2.5 sec. duration of the film.

The scatter of the experimental results indicates that the errors of

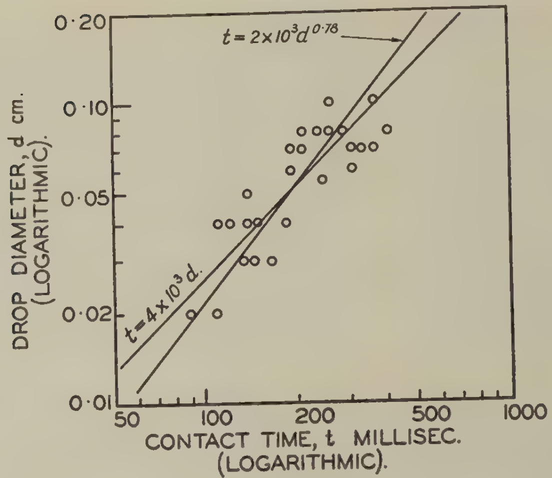

FIG. 1. Coalescence with the underlying surface. Variation of apparent contact time with drop size.

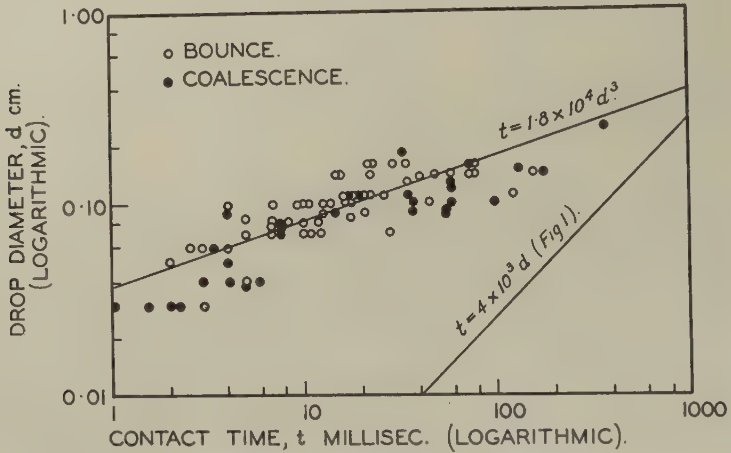

FIG. 2. Bounce and coalescence between colliding drops floating on the surface. Variation of apparent contact time with the size of the smaller drop involved.

measurement are outweighed by uncontrolled factors such as a variation in velocity of impact and oscillations of the surface or of the drops.

Figure 3 shows that in mutual collision drops smaller than 0.05 cm. in diameter are more likely to coalesce than are drops larger than 0.10 cm. The larger drops often bounce many times. The increased probability of coalescence with decrease in drop size seems to be related to the decrease in contact time as expressed by relation [3]. The above observations agree with the high percentage of coalescences observed by Telford *et al.* (5)

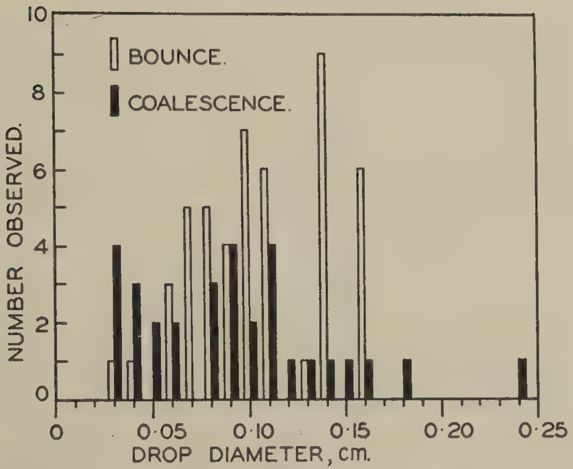

FIG. 3. The dependence of the frequency of bounce and coalescence on the size of the smaller of two colliding drops.

for a mist of 0.015 cm. water drops, and also for drops of "Cetavlon" solution (private communication).

DISCUSSION

The Mechanism of Floating Drops

Newton's rings can be seen between the floating drops and the underlying liquid surface (6). These indicate an air gap of 0.1–1.0 μ in thickness. That an air film can be formed is shown by the observation of Riedel (7) that drops of soap solution falling from a sufficient height can penetrate a plane liquid surface and remain completely surrounded by an air film of thickness 6 μ for a drop 0.3 cm. diameter. We observed this same phenomenon with "Cetavlon" solution. Small air bubbles are also trapped in the underlying liquid or the remaining drop after coalescence. By replacing air by other media, including viscous oils, Mahajan found that the life of floating drops increased more or less linearly with the viscosity of the surrounding medium (8). By means of interference rings, Deryaguin and Prokhorov (9) studied an air gap between two drops of a volatile liquid pressed against each other. A stream of unsaturated air passing around the drops caused the diffusion of air and vapor through the gap sufficient to prevent coalescence indefinitely. In some recent work they showed that the vapor saturation also played an appreciable although less important part in the coalescence of moving water drops and drop mists (9).

We considered the application, to this problem, of two simple models used by Elton (10) in his studies of the approach of a gas bubble in a liquid to a solid surface. In the first model a sphere approaches a plane in a viscous medium and this gives a calculated rate of approach much greater than the observed rate.

When floating drops are obtained the underlying liquid is depressed and the drops are flattened. Thus the approach of the two opposing surfaces might resemble that of two curved parallel discs. If we take two plane parallel discs as equivalent for our second model, the time t to approach from an initial separation h_1 cm. to a final separation h_2 is (10):

$$t = \frac{3\pi\eta D^4}{64mg}\left(\frac{1}{h_2^2} - \frac{1}{h_1^2}\right), \tag{4}$$

where D is the disc diameter (in our case the diameter of the equivalent deformed area), η the viscosity of the air between the discs (1.8×10^{-4} poise), mg is the force on the discs (in our case the weight of the drop). If $h_2 \ll h_1$, the $1/h_1^2$ term can be neglected. If D is proportional to d, relation [4] agrees in form with relation [2]. With the assumption of plausible values of D and h, the calculated times can be made to agree with the experimental. Hence the disc model is at least plausible.

There is experimental evidence that the flow of entrapped air between the two liquid surfaces does not alone control the stability of the floating drops. We have confirmed that dust and electric charges hinder or completely prevent the formation of floating drops.

The increased stability of floating drops with decrease in surface tension is ascribed to the increased deformation of the drops and underlying surface and consequently to the larger area of the air gap. A monolayer of insoluble surface-active material also increases drop stability, but an excess has the same effect as dust.

The Mechanism of Mutual Bounce and Coalescence of Floating Drops

Large drops floating in the form of a drop raft show flattening between drops (Plate I). Again the considerable times for which large drops rest against each other and the rapidity of coalescence after a neck forms suggest that it is an air film between the deformed surfaces which controls coalescence. Thus, qualitatively, the factors discussed above which influence the stability of floating drops will similarly influence mutual coalescence. However, the contact time depends on the forces between the drops and hence on the slope of the surface surrounding the drops. The slope probably depends on the experimental arrangement, the number and size of drops constituting the raft as well as the surface tension and density of the liquid.

Bounce and Coalescence of Colliding Jets

From the above results we would expect, as Lord Rayleigh found (11), that small drops from two jets which collide in the air would rapidly coalesce and that large drops would bounce. Some factors affecting floating drops influence colliding jets similarly. Thus soluble surface-active agents facilitate bounce but dust and electric charges prevent bounce (11).

CONCLUSIONS

The coalescence of a drop with a free surface or with another drop on collision is delayed by the air film trapped between the opposing surfaces which deform on approaching each other. The delay increases with the size of the drop because of the increased volume of air trapped. The delay is such that on mutual collision floating drops of 0.1 cm. diameter readily bounce but drops of 0.05 cm. are more likely to coalesce. Drops colliding in jets behave similarly. The results should have a bearing on the coalescence of rain drops and mists of the size range studied, i.e., > 0.01 cm.

ACKNOWLEDGMENT

We gratefully acknowledge the assistance of F. D. Lugton with the high-speed photography and preparation of Plate I.

REFERENCES

1. REYNOLDS, O., *Chem. News* **44**, 211 (1881).
2. WARK, I. W., AND COX, A. B., *Nature* **136**, 182 (1935).
3. MAHAJAN, L. D., *Kolloid-Z.* **69**, 16 (1934).
4. KATALINIC, M., *Z. Physik* **38**, 511 (1926); *Nature* **127**, 627 (1931); *ibid.* **136**, 916 (1935).
5. TELFORD, J. W., THORNDIKE, N. S., AND BOWEN, E. G., *Quart. J. Roy. Meterol. Soc.* **81**, 241 (1955).
6. MAHAJAN, L. D., *Z. Physik* **84**, 676 (1933).
7. RIEDEL, W., *Kolloid-Z.* **83**, 31 (1938).
8. MAHAJAN, L. D., *Phil. Mag.* [7], **10**, 383 (1930).
9. PROKHOROV, P., *Discussions Faraday Soc.* **18**, 41 (1954).
10. ELTON, G. A. H., *Proc. Roy. Soc. (London)* **A194**, 259 (1948).
11. LORD RAYLEIGH, *Proc. Roy. Soc. (London)* **27**, 406 (1879); *ibid.* **29**, 71 (1879); *ibid.* **34**, 130 (1882).

JOURNAL OF COLLOID SCIENCE **11**, 398–418 (1956)

RECENT WORK ON SPREAD MONOLAYERS, ADSORPTION AND DESORPTION

L. Ter Minassian-Saraga

Laboratoire de Chimie Physique, Faculté des Sciences, Paris

Received April 15, 1956

INTRODUCTION

The work carried out at our laboratory during the last ten years[1] on the properties of spread or adsorbed monolayers can be divided into three categories:

I. The behavior of protein films spread on aqueous substrates at various pH and salt concentrations.

II. The study of the surface potential of very dilute ("gaseous") spread or adsorbed films and of heterogeneous films, for substances showing a two-dimensional phase change.

III. The study of isotherms, of the laws and mechanism of desorption for a slightly soluble spread monolayer; the study of the validity of Gibbs equation.

This work is a continuation of the research on spread monolayers carried out by J. Guastalla with the two surface balances or "manometers" devised by this author.

Surface Manometer and Micromanometer

These apparatuses (Figs. 1 and 2) are of the Langmuir "differential" type and they are direct-reading. A float separates two parts of the surface of the substrate. The film is spread on one of them (left compartment on the figures). The pressure exerted by the film on the float gives rise to a restoring force which is measured by the displacement of a spot on a scale.

In the case of the *surface manometer* (3) (Fig. 1), the float is made of paraffin-coated mica and is attached to the frame by two vaseline-coated silk threads. The float displaced by the film causes the deviation of a "pendulum-like element" from its equilibrium position; the deviation of this element (magnified by an optical device) is proportional to the hori-

---

[1] The study of spread monolayers is an old tradition at the Laboratoire de Chimie Physique de la Faculté des Sciences, Paris; A. Marcelin had undertaken this research as early as 1913.

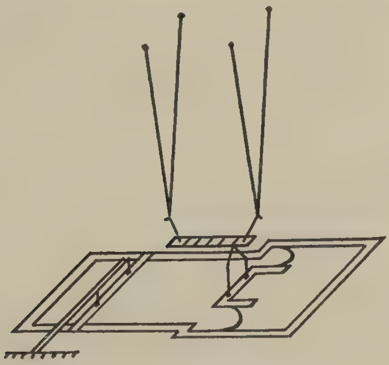

FIG. 1. Surface manometer.

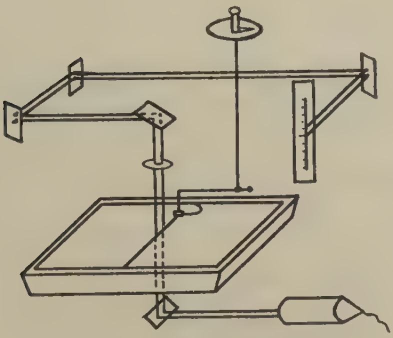

FIG. 2. Surface micromanometer.

zontal restoring force. The weight of the pendulum-like element determines the sensitivity of the apparatus, which can attain 0.02 dyne/cm.

In the case of the *surface micromanometer* (2) (Fig. 2) the float is substituted by a vaseline-coated silk thread floating at the surface of the substrate and kept under a known tension. The thread takes a curved shape owing to the film pressure, and the displacement of the mid-point of the thread is proportional to the pressure.

The tension of the silk thread determines the sensitivity of the apparatus, which can attain 0.001 dyne/cm.

J. Guastalla (2–7) has verified the following results (already predicted by N. K. Adam (1)) from a study of very dilute films of several fatty substances and proteins; at extreme film dilutions the equation of state for monolayers becomes analogous to the three-dimensional Boyle-Mariotte law:

$$p\sigma = kT, \tag{1}$$

where p = surface pressure in dynes/cm.; σ = surface area in A^2/molecule, k = Boltzmann constant; T = absolute temperature. This result embodies the fundamental principle of the method suggested by J. Guastalla for the determination of the molecular weights of spread proteins (4-6).

I. STUDY OF THE BEHAVIOR OF PROTEIN FILMS SPREAD ON THE SURFACE OF AQUEOUS SUBSTRATES AT VARIOUS PH'S OR SALT CONCENTRATIONS (8, 9)

Certain molecular properties, such as size and weight, of proteins spread on substrates at various pH's or salt concentrations, can be studied by means of surface manometers. N. Benhamou has investigated several proteins, for example, oxyhemoglobin. She has shown that the pH ranges of stability for the spread protein and for the protein in solution are about the same (note that in the first case the pH of the substrate has to be considered).

J. Guastalla's method (4) was used for molecular weight determinations. The method subsequently suggested by Bull (10, 12) is analogous.

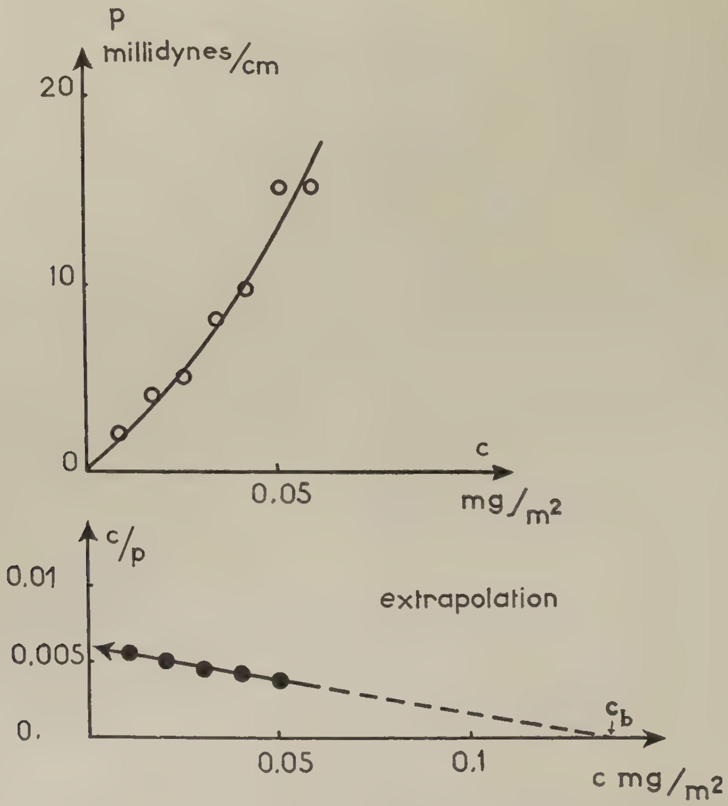

FIG. 3. Compression results for very dilute films of oxyhemoglobin. Substrate pH 3.1.

The compression curves of the very dilute spread film were studied. The corresponding isotherms can usually be represented by the equation:

$$p(S - b) = \frac{RT}{M},$$

where S = area/g. of protein, b = cosurface, M = molecular weight, and R = gas constant. This can be rearranged to give:

$$(1 - bC) = \left(\frac{RT}{M}\right)\frac{C}{p},$$

where C = concentration in g./unit area. If C/p is plotted as a function of C (Fig. 3), a straight line is obtained which, when extrapolated to $C = 0$, permits the calculation of the molecular weight and, when extrapolated to $C/p = 0$, leads to the "cosurface" concentration ($1/b$).

Figures 4 and 5 show, for example, the behavior of oxyhemoglobin molecules spread on the surface of substrates having a pH <8. The molecules of this protein dissociate at about pH 6. Between pH 4 and 5 stable units having a molecular weight of about 35,000 are found. When substrates of lower pH are used, a gradual splitting occurs which leads to smaller units (probably globin of molecular weight equal to 11,000 at pH = 2).

The very compressed protein films show a "collapse point" (11, 13); N. Benhamou has pointed out that the variation of the molecular area and of the average film thickness at the collapse point can lead to an interpretation of the mechanism of the splitting which she observed while making molecular weight determinations in very dilute films.

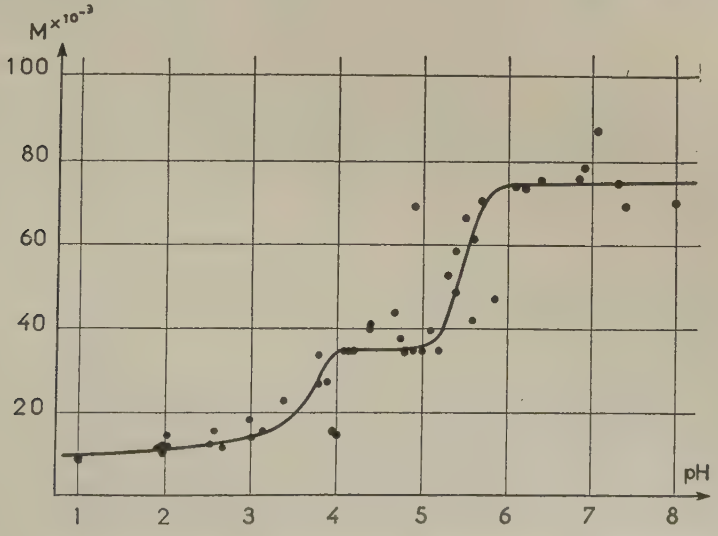

FIG. 4. Molecular weight of oxyhemoglobin as a function of substrate pH.

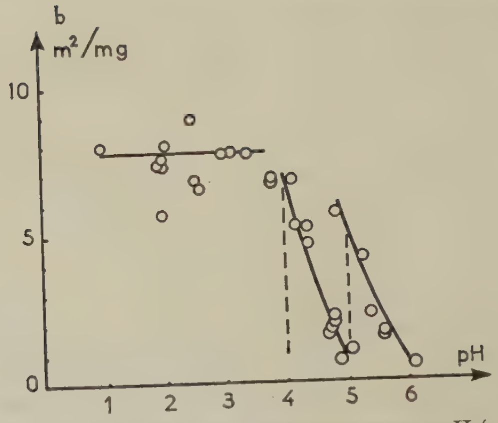

FIG. 5. Variation of "cosurface" as a function of substrate pH (oxyhemoglobin).

TABLE I

Results for Oxyhemoglobin

Substrate	pH	Mol. wt.	p_c collapse, pressure, (*dynes/cm.*)	C_c (*mg./m.*^{2})	e (*A.*)	c (*A.*)^2
$KH_2PO_4 + K_2HPO_4$) 0.04 molar	6.9	70,000	22	3.4	26	3,400
K Biphthalate 0.025 molar and KOH	4.5	35,000	22	1.8	14	3,200
HCl 0.01 molar	2	11,000	20–21	2	15	900

The molecular area σ_c is equal to $M/C_c N$, where C_c is the film concentration at the collapse point and N is Avogadro's constant.

If the density of the protein in the film is equal to the density d of the crystal, the film mean thickness e is given by the relation: $e = 10\ C_c/d$ in A. The e and σ_c values calculated by N. Benhamou (9) are shown in Table I.

At the first splitting the molecule breaks up horizontally so that each resultant molecule has half the height of the original molecule (σ_c of the resulting molecule is substantially equal to σ_c for oxyhemoglobin at the isoelectric point); when the final splitting occurs the molecules could be broken up vertically, the thickness of the film remaining unchanged (14–15 A.).

II. SURFACE POTENTIAL MEASUREMENTS (20–23)

The surface potentials are determined by the well-known method of the ionizing electrode (16). The device used (23) is very accurate and permits, in particular, the determination of very low surface potential values of monolayers, constituted by fatty acids (myristic acid and lauric acid), in the state called "gaseous." Simultaneously, the surface pressures of the same monolayers have been studied using surface manometers.

Figure 6 shows the plot of the surface potential ΔV against the mono-

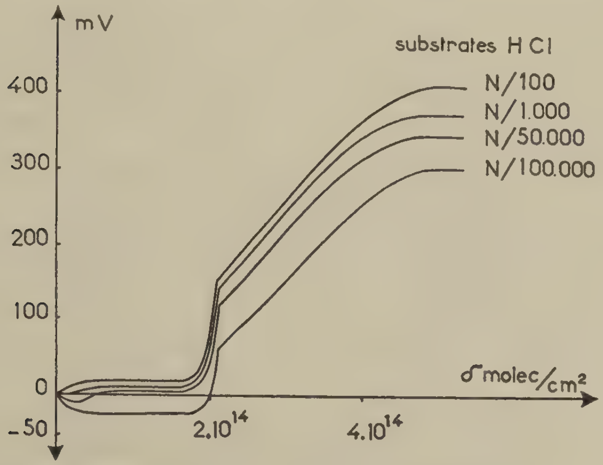

FIG. 6. Surface potential (millivolts) of myristic acid with substrates of HCl solution.

layer concentration δ for the whole range of concentrations of stable myristic acid films spread on substrates at different pH values.

The surface potential of fatty acid monolayers in the "gaseous state" adsorbed or spread on the surface either of distilled water (19–21) or of very dilute hydrochloric acid (concentration lower than 10^{-4} N) is negative; when the acidity increases, the concentration range of films showing a negative potential diminishes and when the pH of the substrate becomes lower than the value 4, the values of the negative potentials are of the same order of magnitude as the experimental error.

The analytical form of the curves of surface potential has been predicted by J. Guastalla (17). This relation can be written as follows:

$$V = 12\,\pi m\,(\delta - K\delta^{3/2})$$

where m is the apparent vertical dipole moment of the carboxyl group.

The value of m may be calculated from the slope of the tangent at the origin to the curves of Fig. 7. When the substrate contains very little acid (less than $2 \times 10^{-5}M$ HCl), the value $m = 1.7$–1.8 Debye is obtained at any pH of the substrate.

Several authors (14, 15, 18) have observed that measurements of ΔV are very difficult in the "transition" region when the mean concentration of the film is intermediate between the "evaporation" point and the "condensation" point.

J. Michel (23) has shown that the results may depend on the measuring technique adopted. Thus a small electrode placed near the surface registers values of ΔV which diminish as a function of time and tend to the value obtained for the monolayer in the so-called "saturated vapor" state, whatever the mean concentration of the film may be (Fig. 8, curve I).

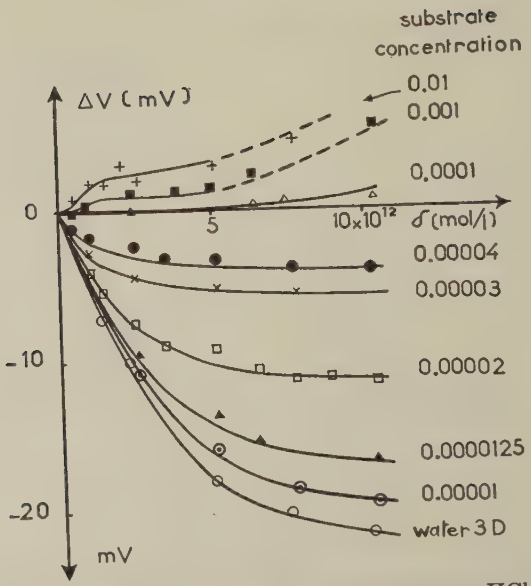

FIG. 7. Surface potential of myristic acid. Substrates: HCl solutions.

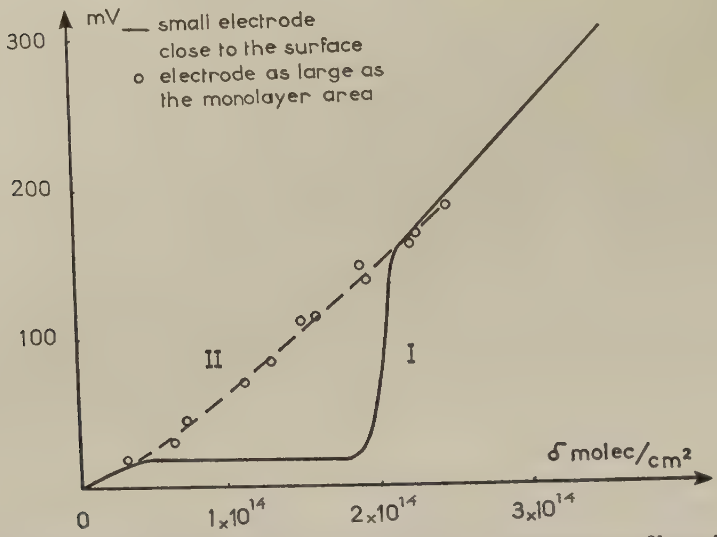

FIG. 8. Effect of electrode type on surface potential of heterogeneous films of myristic acid. Substrate: $10^{-2}N$ HCl.

However, if the measurements are carried out quickly with an electrode placed away from the surface and having a surface area as large as that of the film, the ΔV values obtained for heterogeneous monolayers vary as a continuous function of the mean monolayer concentration (Fig. 8, curve II).

After having shown that this phenomenon was independent of the presence of the Polonium source and was caused only by the electrode, J. Michel has assumed that the electrode itself (the grating) has driven away the molecular aggregates (portions of the condensed phase), and that the film in the state called "saturated vapor" is the only one able to maintain itself in the presence of the electrode.

Finally J. Michel has shown that the surface potential curves of adsorbed films have the same characteristics as the potential of spread films. J. Michel (21), like several other authors (24), has measured the variation of surface potential of a solution as a function of time, in order to study the kinetics of adsorption during the first few seconds after the formation of a fresh surface.

III. STUDY OF THE SPREAD MONOLAYER, OF ADSORPTION AND DESORPTION

All experiments were carried out on the same substance (lauric acid), the liquid substrate or solvent consisting of a 10^{-2} *M* hydrochloric acid solution.

1. *Spreading and Adsorption of Lauric Acid*

The study of the isotherm of the spread monolayer, initiated by N. K. Adam (25), was taken up again using the surface manometers of J. Guastalla (see Introduction).

Since the film is slightly soluble, its surface pressure *p* tends to diminish as a function of time. The experiment should be performed "point by point," i.e., for each film concentration the substance is spread, the film thus obtained is compressed immediately, the pressure is plotted as a function of time, and the resulting curve is extrapolated to zero time. The

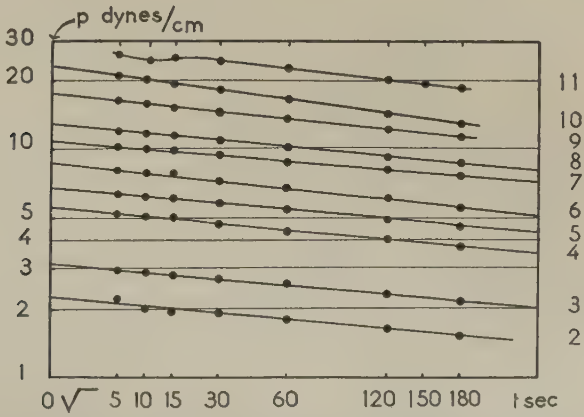

FIG. 9. Variation of surface pressure as a function of time. Lauric acid. Substrate: $10^{-2}N$ HCl; 20°C. The curves 2–11 correspond to original molecular areas equal to: 49.7, 40.2, 37.1, 35.5, 34, 32, 31.1, 28.6, 27.1, 22.6 A.^{2}.

desorption studies (see below) have led to a method of extrapolation according to which log p is plotted as a function of the square root of time ($\sqrt{t}$), (Fig. 9). The p_0 values thus obtained are then plotted as a function of the area (σ) of the molecules making up the original spread monolayer, and the isotherm is thus established (Figs. 10 and 11). The equation of

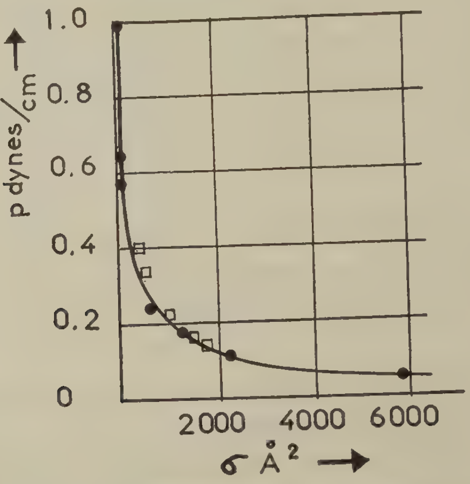

FIG. 10. Lauric acid in the gaseous state. Substrate: $10^{-2}N$ HCl. □ Adam (14–16°C.). ● present study (19°C.).

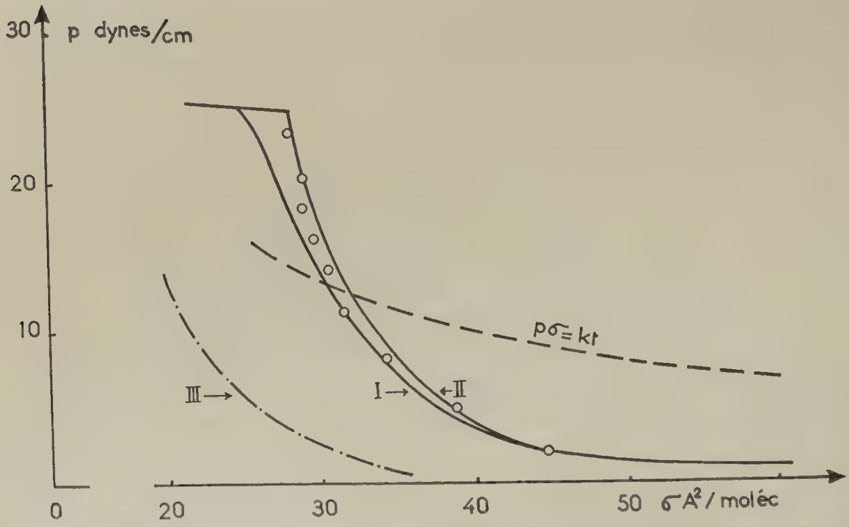

FIG. 11. Lauric acid at 20°C. Substrate: $10^{-2}N$ HCl. I: extrapolation of p-t plot; II extrapolation of log p − $\sqrt{t}$ plot; III Harkins (31); ○ Adam (25).

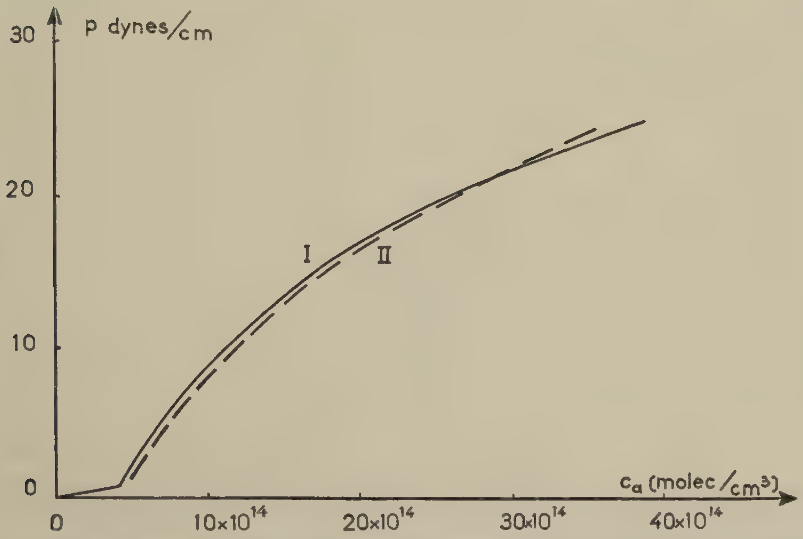

FIG. 12. Adsorption curves for lauric acid. Solvent: $10^{-2}N$ HCl; 21°C. ± 1 (46); I: experimental; II: calculated.

state for a film of lauric acid in the state called "expanded" has the analytical form suggested by J. Guastalla (7), as follows.

$$p = kT\delta + B\delta^{3/2} + A\delta^{5/2}, \quad [2]$$

where A and B are constants.

The experimental study of the adsorption, i.e., the measuring of the surface tension lowering $p = \Delta\gamma$ at equilibrium for different lauric acid solutions (28, 40), leads to the *adsorption curve* (p is plotted against the concentration of the solution c_a) (Fig. 12).[2]

Let us consider now the verification of the Gibbs equation which can be written:

$$dp = \delta kTd \ln c_a, \quad [3]$$

where $\delta = 1/\sigma$ is equal to the surface concentration of the monolayer in molecules/cm.².

The verification of the Gibbs equation was attempted by two different methods:

1. The value of δ is obtained by graphical differentiation (25, 40) of the adsorption curve. The variation of σ as a function of p is shown on Fig. 13, curve I, which is called the calculated isotherm of the adsorbed monolayers.

---

[2] A similar study was carried out for several cationic detergents, which belonged to a homologous series and were strong electrolytes. In particular, experiments were carried out in the presence of mineral salt at different concentrations (49, 50).

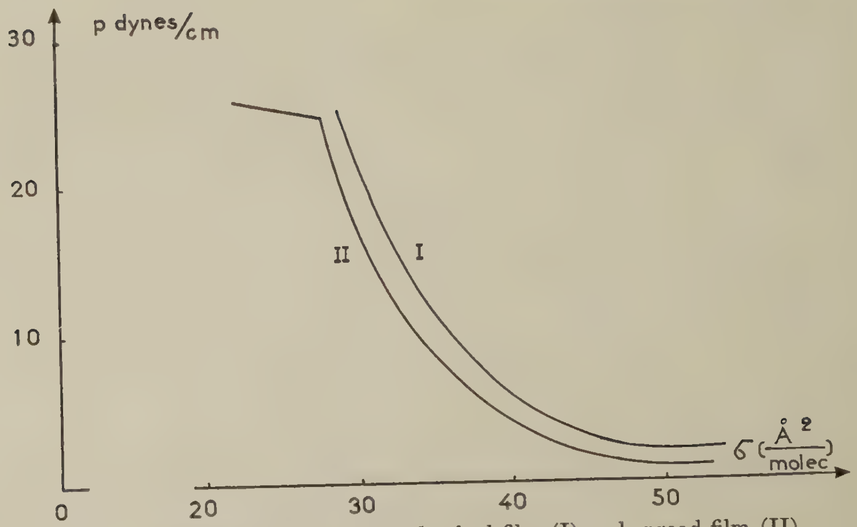

FIG. 13. Isotherms of lauric acid adsorbed film (I) and spread film (II).

Let us suppose with Langmuir (34) that the spread and the adsorbed monolayers are identical. In order to verify the Gibbs equation, the calculated isotherm of the adsorbed monolayer is compared with the isotherm of the spread monolayer.

The agreement between the two curves was found to be satisfactory, in comparison with the results of other authors (36).

2. After elimination of p between Eqs. [2] and [3] the relation [3] is integrated to give (40, 46):

$$\log c_a = 1.105 \times 10^{-21}\delta^{3/2} - 6.15 \times 10^{-7}\delta^{1/2} + \log \delta + \log A, \qquad [4]$$

where A is the integration constant.

Finally after elimination of δ between Eqs. [2] and [4] p is obtained as a function of c_a/A; this last function is the calculated adsorption curve, provided the integration constant is evaluated; this can be done with the help of one point taken from the experimental curve; it has thus become possible to compare the calculated adsorption curve with the experimental one. The agreement is satisfactory, as can be seen from Fig. 12.

The two series of measurements (adsorption curve and isotherm) allow the calculation of the ratio $K_d = c_a/\delta$ corresponding to a given surface pressure and concentration c_a; this ratio is called the desorption coefficient; its variation as a function of p (46) is shown in Fig. 14.

2. Desorption of Spread Monolayers of Lauric Acid (30, 42, 43, 47)

This phenomenon was studied in two different ways, either by keeping the pressure of the film constant, in which case the area of the monolayer decreases, or by keeping the area constant, in which case the pressure of the film decreases as a function of time.

These two kinds of experiments were carried out at constant temperature with the help of a temperature-controlling device which was originated in this laboratory (45).

(*A*) *Desorption of a Monolayer Kept under Constant Pressure.* The desorption experiments under constant pressure were carried out with the help of a surface barostat (30) (Fig. 15), a modified surface manometer with a pendulum-like element on which a platinum wire is fixed. The wire forms part of an electrical relay circuit which sets a motor going whenever the pendulum-like element is displaced because of a slight decrease of the surface pressure (0.05 dyne/cm.). The motor moves the piston which compresses the film until the initial pressure is obtained.

During a desorption experiment, the displacement of the piston permits the measurement of the area *S* of the film as a function of time. The results of a typical experiment are represented by plotting the logarithm of *S* as a function of *t* (Fig. 16). The plot thus obtained, called the desorption curve, has two parts: a curved part at the beginning and a linear portion for higher values of *t*.

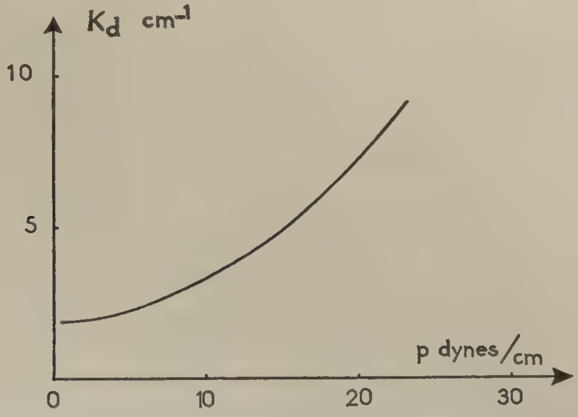

FIG. 14. Desorption ratio ($K_d = c_a/\delta$) for lauric acid dissolved in $10^{-2}N$ HCl at 20°C.

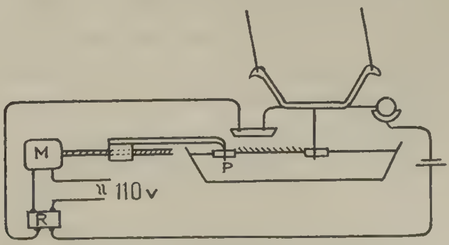

FIG. 15. Surface barostat.

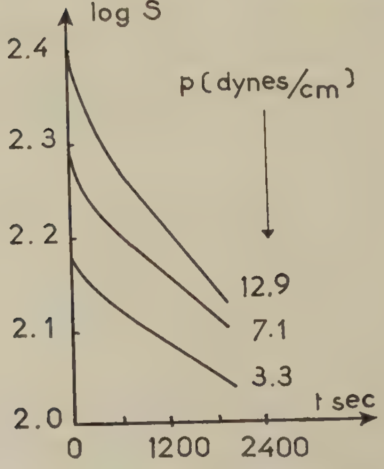

FIG. 16. Desorption curves for lauric acid at 19.5 ± 0.5°C. Substrate: $10^{-2}N$ HCl.

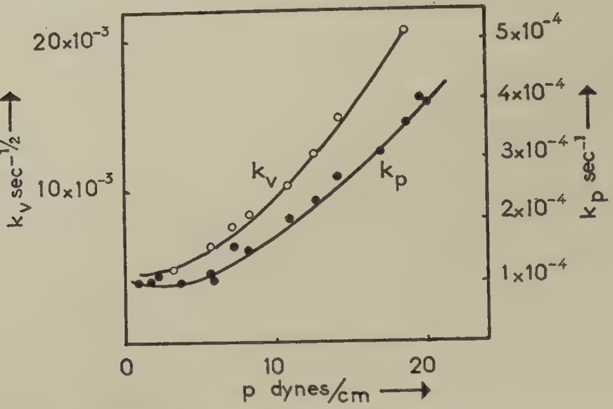

FIG. 17. Influence of pressure on desorption of lauric acid monolayers maintained at constant pressure with a substrate $10^{-2}N$ HCl; 19.5 ± 0.5°C.

The results obtained for a substrate at given pH and temperature are reproducible, provided that the depth of the liquid substrate is always the same. This condition is in agreement with the mechanism of desorption.

The steepness of the desorption curve increases with pressure, but the lapse of time corresponding to the first portion of the desorption curve seems to be independent of the pressure (15–20 minutes) (Fig. 16).

Physical meaning of the desorption curves.[3] Let N be the number of molecules of the monolayer. Its area is then equal to S:

$$S = \sigma N. \tag{5}$$

---

[3] The reference (47) contains a more detailed discussion of desorption.

The slope $K(t)$ of the tangent to the desorption curve at any point is called the rate of desorption. It can be defined by the following relationship:

$$K(t) = -\frac{dS}{S\,dt} = -\frac{\sigma\,dN}{S\,dt} = \sigma\Phi(t), \qquad [6]$$

where $\Phi(t) = -(1/S)(dN/dt)$; this last term is by definition the number of molecules lost per unit time and per unit surface, i.e., the rate of diffusion at the surface. The integral of $K(t)$ between zero and t gives:

$$\int_0^t K(t)\,dt = \ln\frac{S_0}{S} = \frac{1}{\delta}\int_0^t \Phi(t)\,dt, \qquad [7]$$

which represents the desorption curve. The quantity $\ln(S_0/S)$ stands for the number of molecules that have crossed a unit surface in time t.

Desorption experiments at constant pressure and constant molecular area permit the calculation of the diffusion rate by means of relation [6].

The particular form of the desorption curve indicates that the rate of diffusion varies as a function of time at the beginning of an experiment; therefore the desorption rate is also *variable.* After a certain lapse of time, the rate of desorption becomes *stationary,* independent of time, and is indicated by the linear form of the desorption curve.

Mechanism of desorption. At the beginning of a desorption experiment, just after spreading, the film is in contact with the pure substrate. The molecules of the film may acquire the activation energy corresponding to a possible potential barrier and thus may become able to penetrate the substrate and mix with the adjacent molecules of this phase. This process (*a*) is called dissolution.

By a consecutive process (*b*), the dissolved molecules may diffuse away from the surface into the liquid substrate. The rate of desorption is controlled by the slower rate of the two processes (*a*) and (*b*).

We have adopted the following working hypothesis: Because of the rapidity with which dissolution occurs, the desorption is diffusion-controlled; the dissolved molecules may then accumulate close to the surface, and from the beginning of an experiment an equilibrium could be established between the film and an infinitely thin region of solution immediately below the surface. This equilibrium is supposed to be identical to the adsorption equilibrium between a solution of concentration c_a and an *adsorption* film of the same p and δ as those of the spread desorbing film (the identity of the two kinds of films has been assumed previously (34)).

The diffusion occurring after dissolution would proceed into the substrate away from the region of concentration c_a.

Kinetics of desorption. Stationary state of desorption (*linear part of adsorption curve* (*Fig. 16*)). According to the above-mentioned working hypothesis, the rate of desorption can be constant only if the diffusion proceeds through a calm liquid layer, called "diffusion layer" of mean thickness ϵ, in which a constant concentration gradient exists.

We assume therefore that (Fig. 18) a convection current could exist beyond the depth ϵ; these currents are thought to carry away the desorbed molecules and to maintain in this part of the substrate an infinitely small solute concentration, since the substrate volume is very large.

This hypothesis has led (47) to a law for the variation of the film area as a function of time:

$$\ln S = cte - \frac{c_a D}{\delta \epsilon} t = cte - K_d \frac{D}{\epsilon} t, \qquad [8]$$

where D = diffusion constant of the molecules constituting the desorbing monolayer.

The hypothesis was verified in a simple direct way. The trough containing the experimental substrate was heated by a weak lamp. The convection current intensity was thus increased without producing any substantial change in the temperature of the substrate.

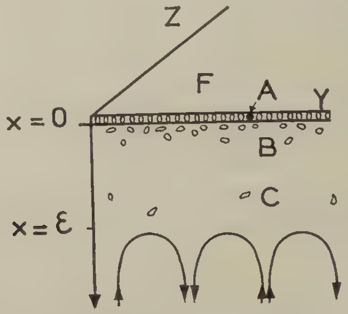

FIG. 18. Representation of diffusion layer and convection currents.

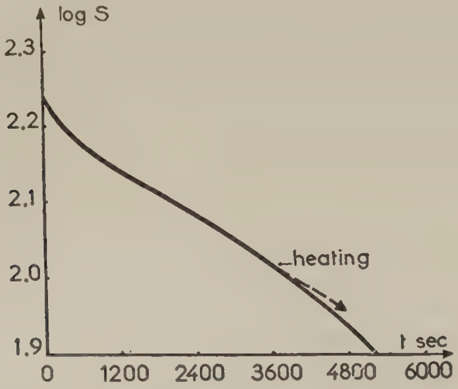

FIG. 19. Influence of liquid movement on desorption of lauric acid; p = 6 dynes/cm.; 19.5 ± 0.5°C.

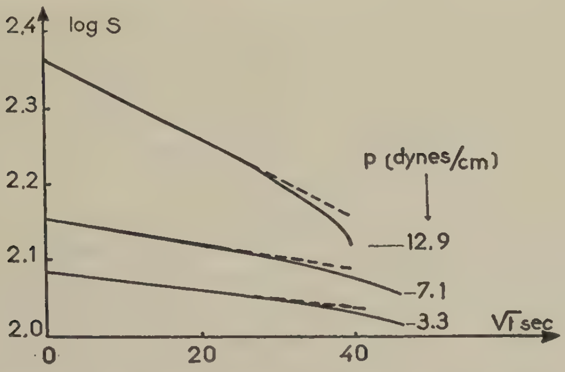

FIG. 20. Desorption at constant pressure for lauric acid. Variable desorption. Substrate: $10^{-2}N$ HCl; 19.5 ± 0.5°C.

Since ϵ decreases with the increase in the intensity of the convection currents, the desorption rate should increase according to relation [8]; this increase was in fact observed (Fig. 19).

Variable rate of desorption (parabolic portion of the desorption curve (Fig. 16)). During the time interval corresponding to the variable rate of desorption, the molecules which have desorbed immediately after spreading of the film will not yet have reached the depth ϵ; the concentration gradient at the surface will vary as a function of time during the same interval.

After these first desorbed molecules have traveled more than the distance ϵ the concentration gradient will become constant and the rate of desorption will also become constant.

The theoretical law (47) giving the variation of the film area as a function of time will, under these conditions, take the following form:

$$\ln S = \ln S_0 - 2\,\frac{c_a}{\delta}\sqrt{\frac{D}{\pi}}\sqrt{t} = \ln S_0 - 2K_d\sqrt{\frac{D}{\pi}}\sqrt{t}. \qquad [9]$$

According to this last relation $\ln S$ is a linear function of $\sqrt{t}$ (see Fig. 20).

Influence of the film pressure. The rate of desorption increases with the film pressure during the interval studied (2–20 dynes/cm.) (Fig. 17).

The desorption intensity is defined either by k_v (slope of the tangent at the origin of the curves represented in Fig. 20) for the variable rate of desorption or by k_p (slope of the linear portion, Fig. 16) for the constant rate of desorption. According to relations [8] and [9]:

$$\left\{\begin{aligned} k_v &= 2K_d\sqrt{\frac{D}{\pi}} \\ k_p &= K_d\,\frac{D}{\epsilon} \end{aligned}\right. , \qquad [10]$$

where K_d is a function of the film pressure only (D and ϵ being constant). The relations [10] could be experimentally verified, since the rates k_v and k_p are proportional to K_d (Figs. 21 and 22). The slope of the straight line shown on Fig. 21 is proportional to D. The value of $D = 7.4 \times 10^{-6}$ cm.^{2}/sec. was obtained at 19.5°C. This result is satisfactory in view of the results obtained by other methods (see Table II).

The value of ϵ can now be calculated from the slope of the line representing k_p as a function of K_d. It is found to be 1.2 mm.

Several authors have assumed the existence of a diffusion layer in the case of heterogeneous physical processes (27, 29, 35, 41).

The values calculated for ϵ by these authors are generally lower, since

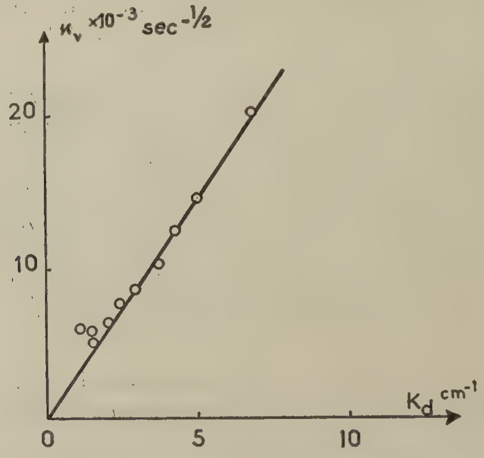

FIG. 21. Variation of the desorption rate as a function of desorption ratio for lauric acid at 19.5°C. Variable state of desorption.

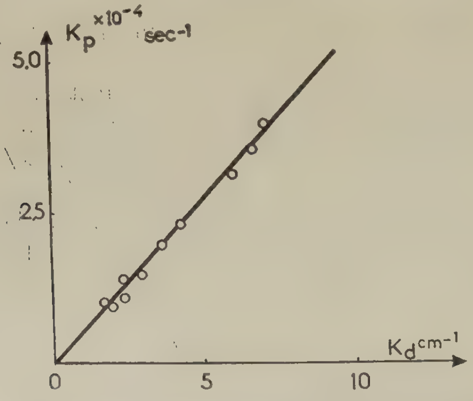

FIG. 22. Variation of the desorption rate as a function of the desorption ratio for lauric acid at 19.5°C. Stationary rate of desorption.

the experiments were carried out in such a manner that the liquid phase was strongly stirred. When the stirring of the liquid was caused by convection currents (29) only, the calculated ϵ value (0.5 mm.) is of the same order of magnitude as the one found by the present method.

Experimental evidence for the existence of a diffusion layer and of convection currents. According to Benard (26) the convection currents are made visible by the motion of aluminum particles in a water suspension.

A suspension of this type was placed in an optical cell, which was illuminated along a vertical direction and examined along a horizontal plane.

When a monolayer of myristic acid is spread at the surface of the aqueous suspension, the aluminum particles leave the surface region and migrate beyond a depth $\epsilon = 0.5$ mm. (Fig. 23).

According to Benard, the interpretation of this experiment is the following: the convection currents of the substrate stop at a depth of 0.5 mm., which corresponds approximately to the thickness of the diffusion layer determined by means of desorption measurements ($\epsilon = 1.2$ mm.).

Moroever, this experiment confirms the views of Landt and Volmer (33) and of Merigoux (38), who assumed that owing to the friction which may exist between a film and the liquid substrate, there will be no movement near the surface of the liquid.

The layer ϵ disappears when the suspension is stirred but reappears again after a few minutes and will then persist for several hours.

Desorption of myristic acid (47). It was found that myristic acid monolayers, which are considered to be stable, desorb very slowly; the desorption curves (Fig. 24) for these films are of the same form as those found for lauric acid.

It was therefore concluded that:

TABLE II

Values of Diffusion Constants by Various Methods

Authors	$D \times 10^6$ cm²/sec.	t(°C.)	Substances
McBain *et al.* (37)	8.1	25	K Laurate
Lamm *et al.* (32)	7.5	20	Na Laurate
This work	7.4	19	Lauric acid
Calc. (Einstein relation) (30)	5.8	19	Lauric acid

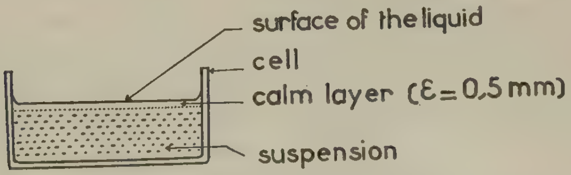

FIG. 23. Apparatus for examining diffusion layer.

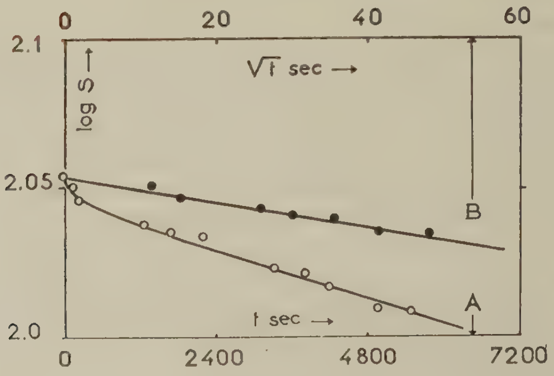

FIG. 24. Desorption at constant pressure for myristic acid. Substrate: $10^{-2}N$ HCl ~ 20°C.

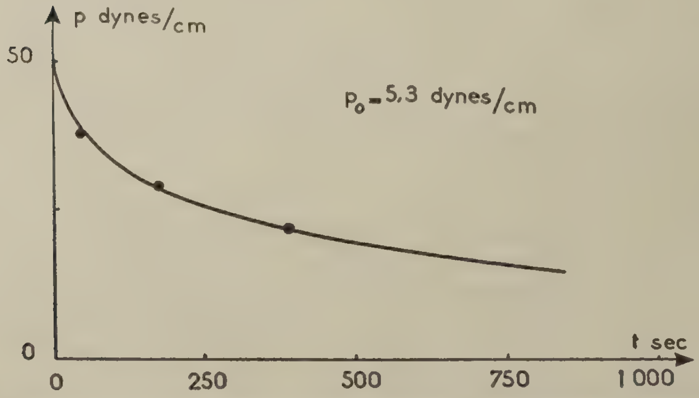

FIG. 25. Desorption at constant area for lauric acid; ● calculated; — experimental.

The desorption of myristic acid may also be diffusion-controlled, the diffusion proceeding inside a diffusion layer.

The concentration of the region of substrate immediately below the film may then have the equilibrium value c_a.

(B) Desorption at Constant Area (*44*, *47*). This study was carried out by means of the surface manometer, for lauric acid spread on $10^{-2}N$ HCl. The film is spread and then compressed to a given area. The decrease of pressure as a function of time (Fig. 25) is recorded. In this case c_a, the concentration in the liquid layer immediately below the film, is also variable. It was shown that, provided these variations are very small during an experiment, the rate of diffusion at the surface can be written:

$$-\frac{d\delta}{dt} = \frac{c_a(t)\sqrt{D}}{\sqrt{\pi t}} = -\frac{1}{K_d}\frac{dc_a}{dt}.$$

This equation, when integrated and transformed, leads to the relation

$$-\ln \frac{c_a}{c_0} = C\sqrt{t} \quad \text{or} \quad \ln \frac{p}{p_0} = -C'\sqrt{t}, \qquad [11]$$

which forms the basis of the extrapolation method shown in Fig. 9.

CONCLUSION

The study of the behavior of spread oxyhemoglobin has shown that in definite substrate conditions the molecular weight of this *spread* substance (as for other proteins) may be close to that of the native protein *in solution.*

The measuring of surface potential for spread heterogeneous films of myristic acid has shown that the electrode interferes with the film below. It was found that the surface potentials of very dilute films of fatty acids spread on distilled water are negative and tend to a negligible value when the substrate pH decreases.

The study of the desorption of films maintained under constant pressure has shown that the desorption of the fatty acid molecules (lauric and myristic acids) may be diffusion-controlled; the diffusion proceeds through a layer immediately below the film, this layer being of macroscopic thickness. During desorption, an extremely thin layer of substrate adjacent to the film has the concentration c_a, which is that of a solution in equilibrium with an *adsorbed* film which is identical with the *spread film.*

Theoretical laws were proposed in agreement with the above-mentioned mechanism. The experimental verifications of these laws were found to be satisfactory: the variation of the film area at constant pressure as a function of time could be predicted and the correct value of the diffusion constant was calculated. It appears therefore that in this case the possibly existing potential barrier to desorption would have to be very low.[4] It was therefore assumed that the stability of the spread monolayers of certain fatty acids may be due to a very low rate of desorption.

The author wishes to express her thanks to Dr. H. A. Zutrauen for his assistance in translating this paper.

REFERENCES

1. ADAM, N. K., AND JESSOP, G., *Proc. Roy. Soc.* (*London*) **A110,** 423 (1926).
2. GUASTALLA, J., *Compt. rend.* **206,** 993 (1938).
3. GUASTALLA, J., *Compt. rend.* **208,** 973 (1939).
4. GUASTALLA, J., *Compt. rend.* **208,** 1078 (1939).
5. GUASTALLA, J., *Cahiers phys.* **13,** 5 (1943).
6. GUASTALLA, J., *Cahiers phys.* **10,** 30 (1942).

---

[4] Ward and Brooks (48) were led to an analogous conclusion when studying the transfer of fatty acids of low molecular weight across an oil-water interface.

7. Guastalla, J., *J. chim. phys.* **44,** 306 (1946).
8. Benhamou, N., *J. chim. phys.* **48,** 5 (1951).
9. Benhamou, N., *J. chim. phys.* **53,** 32, 44 (1956).
10. Bull, H. B., *J. Am. Chem. Soc.* **67,** 4 (1945).
11. Bull, H. B., *Advances in Protein Chem.* **3,** 95 (1947).
12. Bull, H. B., *J. Biol. Chem.* **185,** 27 (1950).
13. Neurath, H., and Bull, H. B., *Chem. Revs.* **23,** 391 (1938).
14. Adam, N. K., and Harding, J. B., *Proc. Roy. Soc. (London)* **A138,** 411 (1932).
15. Dervichian, D., *Ann. phys.* [11] **8,** 361 (1937).
16. Guyot, J., *Ann. phys.* [10] **2,** 506 (1924).
17. Guastalla, J., *Compt. rend.* **224,** 1498 (1947).
18. Harkins, W. D., and Fischer, E. K., *J. Chem. Phys.* **1,** 852 (1933).
19. Isemura, T., and Hotta, H., *Bull. Chem. Soc. Japan* **23,** 193 (1950).
20. Michel, J. "Surface Chemistry," p. 127. Butterworths, London, 1949.
21. Michel, J., *Mem. serv. chim. etat (Paris)* **37,** 55 (1952).
22. Michel, J., *J. chim. phys.* **47,** 25 (1950).
23. Michel, J., Thesis.
24. Posner, A. M., and Alexander, A., *Trans. Faraday Soc.* **45,** 651 (1949).
25. Adam, N. K., *Chem. Revs.* **3,** 172 (1926).
26. Benard, H., *Ann. chim. et phys.* [7] **23,** 62 (1901).
27. Brunner, *Z. physik. Chem.* **47,** 56 (1904).
28. Frumkin, A., *Z. physik. Chem.* **116,** 466 (1925).
29. Glasstone, S., "Introduction to Electrochemistry," p. 448. Van Nostrand, 1942.
30. Guastalla, J., and Mibashan-Sharaga, L., "Surface Chemistry," p. 103. Butterworths, London, 1949.
31. Harkins, W. D., and Fischer, E. K., *J. Chem. Phys.* **1,** 852 (1933).
32. Lamm, V. O., and Högberg, H., *Kolloid-Z.* **91,** 10 (1940).
33. Landt, E., and Volmer, M., *Z. physik. Chem.* **122,** 398 (1926).
34. Langmuir, I., *J. Am. Chem. Soc.* **39,** 1848 (1917).
35. Langmuir, I., and Schaeffer, V. S., *J. Am. Chem. Soc.* **59,** 2400 (1937).
36. McBain, J. W., and Davies, G. P., *J. Am. Chem. Soc.* **49,** 2230 (1927);
    McBain, J. W., and Ford, T. F., *J. Am. Chem. Soc.* **58,** 378 (1938);
    McBain, J. W., and Humphreys, C. W., *J. Phys. Chem.* **36,** 300 (1932).
    McBain, J. W., and Swain, R. C., *Proc. Roy. Soc. (London)* **A154,** 608 (1936).
    McBain, J. W., and Wood, L. A., *Proc. Roy. Soc. (London)* **A174,** 286 (1940).
37. McBain, J. W., and Tsun Hsien Liu, *J. Am. Chem. Soc.* **53,** 57, (1931).
38. Merigoux, R., Thesis, *Rev. opt.* (Paris) (1938).
39. Mibashan-Sharaga, L., *Compt. rend.* **228,** 548 (1949).
40. Mibashan-Sharaga, L., *Compt. rend.* **228,** 822 (1949).
41. Nernst, W., *Z. physik. Chem.* **47,** 52 (1904).
42. Sharaga, L., *Compt. rend.* **231,** 46 (1950).
43. Sharaga, L., *Compt. rend.* **231,** 335 (1950).
44. Sharaga, L., *Compt. rend.* **233,** 135 (1951).
45. Ter Minassian-Saraga, L., *J. chim. phys.* **52,** 80 (1955).
46. Ter Minassian-Saraga, L., *J. chim. phys.* **52,** 99 (1955).
47. Ter Minassian-Saraga, L., *J. chim. phys.* **52,** 181 (1955).
48. Ward, A. F. H., and Brooks, L. H., *Trans. Faraday Soc.* **48,** 1124 (1952).
49. Zutrauen, H. A., and Ter Minassian-Saraga, L., *J. chim. phys.* **52,** 353 (1955).
50. Zutrauen, H. A., *J. chim. phys.* **53,** 54 (1956).

JOURNAL OF COLLOID SCIENCE 11, 419–427 (1956)

SOME SURFACE STUDIES OF ANTIFOAMS

J. G. Hawke and A. E. Alexander

School of Applied Chemistry, New South Wales University of Technology, Sydney, Australia

Received April 5, 1956

INTRODUCTION

In order to overcome the problem of foaming in steam boilers several types of chemical compounds have been developed in recent years, one large group of such compounds being broadly classed as polyamides (1, 2). Compared with materials previously used, such as castor oil, they are substantially superior in stability and effectiveness, the amounts required being only of the order of a few p.p.m.

A number of theories of their mode of action have been put forward, based largely on laboratory boiler tests (1, 2), although a few surface studies have been reported (3). An examination of these theories in the light of general surface phenomena made it appear that certain aspects at least were open to question. The present investigation of the film-forming properties of a number of these polyamides was therefore undertaken, and the results certainly substantiate these earlier doubts. Some new suggestions are advanced based on the present findings, but it is clear that much further work needs to be done before the basic physicochemical phenomena involved in the activity of these antifoams can be established on a firm basis.

EXPERIMENTAL

Two series of compounds have been investigated, namely, the diacylated piperazines 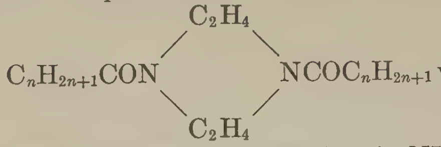 $C_nH_{2n+1}CON\begin{matrix}C_2H_4\\ \\ C_2H_4\end{matrix}NCOC_nH_{2n+1}$ with $n = 11, 13, 15, 17$, and the diethylene triamines $R\cdot CO\cdot NH(CH_2)_2\cdot NH(CH_2)_2\cdot NH\cdot CO\cdot R$ with $R = 15$ and 17 (both the stearyl and oleyl derivatives in the latter case). These compounds were kindly donated to us by the late Dr. A. L. Jacoby, and full analytical data have been given in his earlier publications (2, 3).

Monolayers were spread from solution in benzene containing about 2% ethyl acetate to assist spreading. In some cases addition of up to 10%

chloroform was necessary to effect solution. Surface pressure (Π) vs. area (A) curves were usually obtained on a simple type of film balance (4) with a hanging mica strip instead of the horizontal float. This apparatus gave an accuracy of *ca.* 0.1 dyne/cm. At the higher temperatures some measurements were made with a du Noüy surface tension apparatus. Surface potentials (ΔV) were measured in the usual manner with an ionizing air electrode (5), the surface viscosity and rigidity being assessed qualitatively by blowing talcum powder on the surface. Surface moments (μ) were calculated by means of the usual equation $\Delta V = 4\pi\mu/A$. Equilibrium spreading pressures (Π_S) were obtained by spreading a few crystals on the previously cleaned surface and measuring the change in surface tension either with the hanging plate or du Noüy apparatus.

RESULTS

The results for the spread monolayers of the various piperazines are given in Figs. 1–3. Figure 1 shows the variation in the Π-A, ΔV-A and μ-A relationship with chain length, Fig. 2 the variation with temperature for the dimyristyl compound. The results in Fig. 2 were obtained by the hanging plate method except for those at 72°C., which were obtained from the du Noüy apparatus. The effect of acidity was examined with several compounds with extremely similar results, those for the dimyristyl compound being given in Fig. 3.

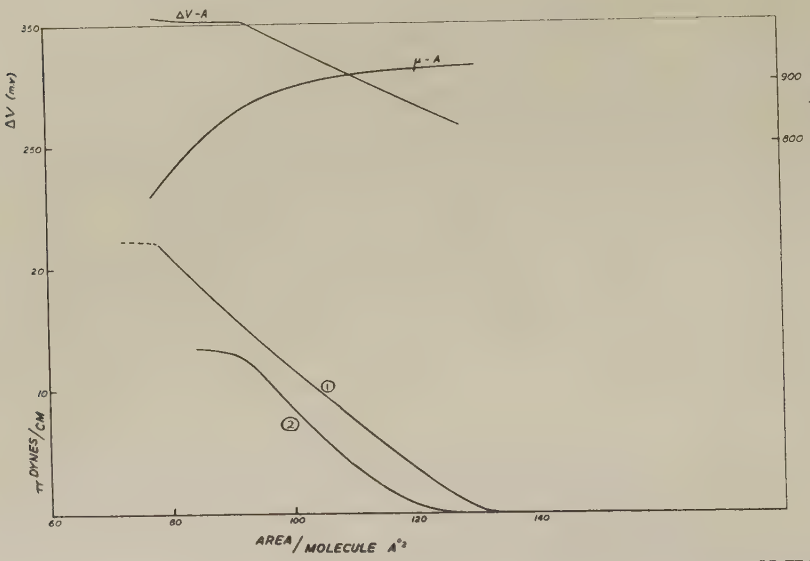

FIG. 1. Π-A, ΔV-A, and μ-A curves for the various piperazines on 0.01 N HCl. (*1*) Π-A for distearyl, dipalmityl, and dimyristyl compounds (mean value). (*2*) Π-A for dilauryl compound.

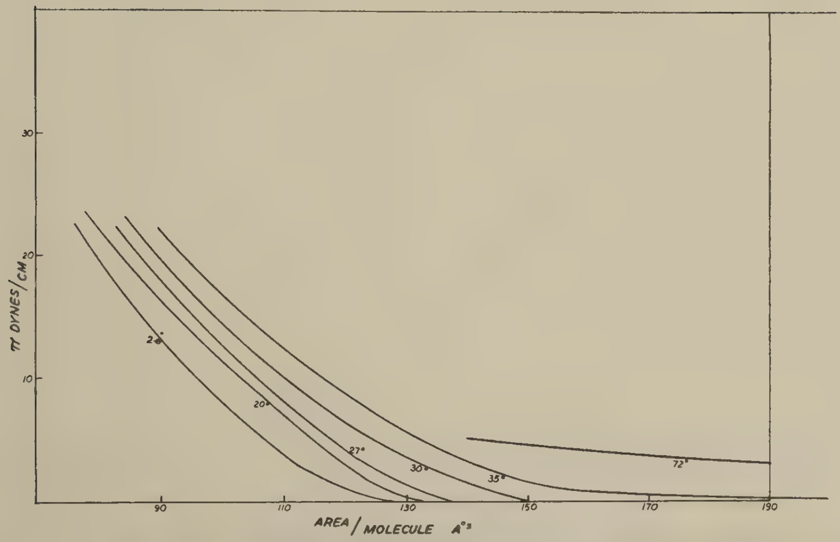

FIG. 2. Π-*A* curves for dimyristyl piperazine on 0.01 *N* HCl at various temperatures.

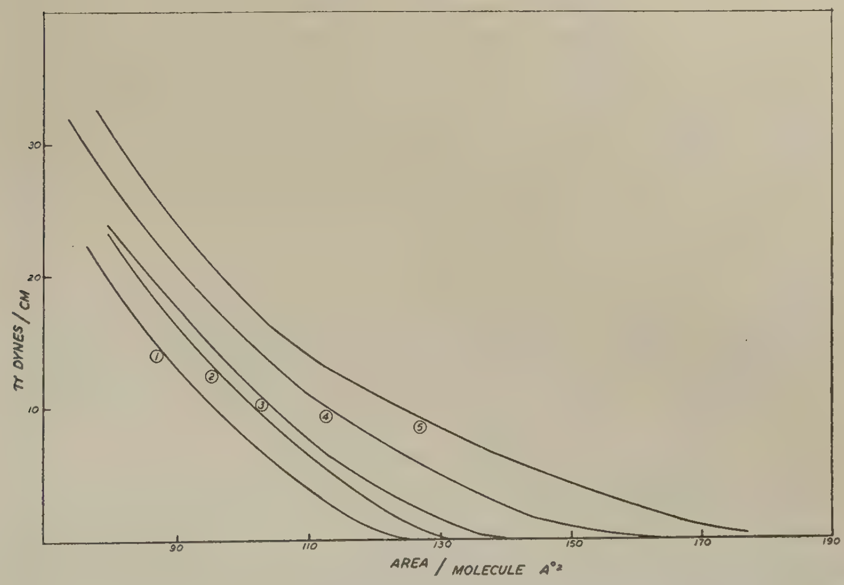

FIG. 3. Π-*A* curves for dimyristyl piperazine at various acidities at room temperatures.

(*1*) 0.01 *N* HCl.
(*2*) 0.1 *N* HCl.
(*3*) *N* HCl.
(*4*) 5.3 *N* HCl.
(*5*) 10.6 *N* HCl.

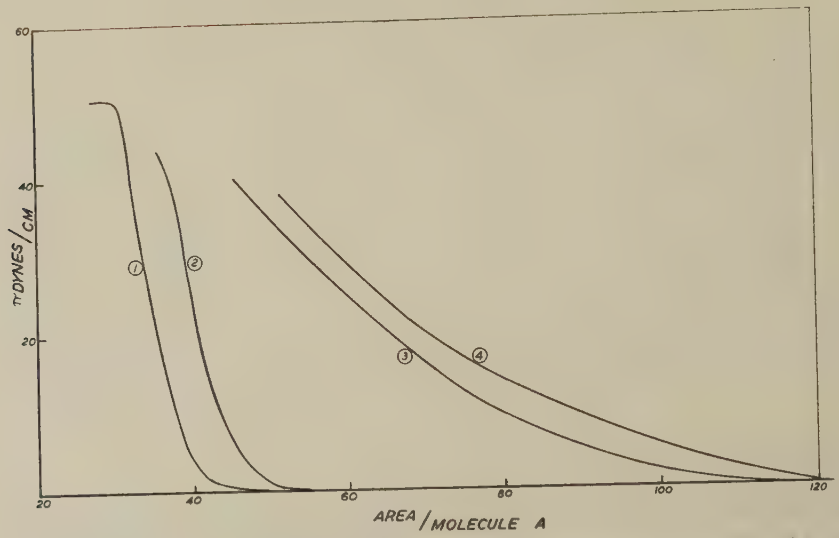

FIG. 4. Π-A curves for distearyl and dioleyl diethylene triamines on 0.01 N and 5.3 N HCl at room temperatures.

(*1*) Distearyl compound (0.01 N HCl).
(*2*) Distearyl compound (5.3 N HCl).
(*3*) Dioleyl compound (0.01 N HCl.)
(*4*) Dioleyl compound (5.3 N HCl).

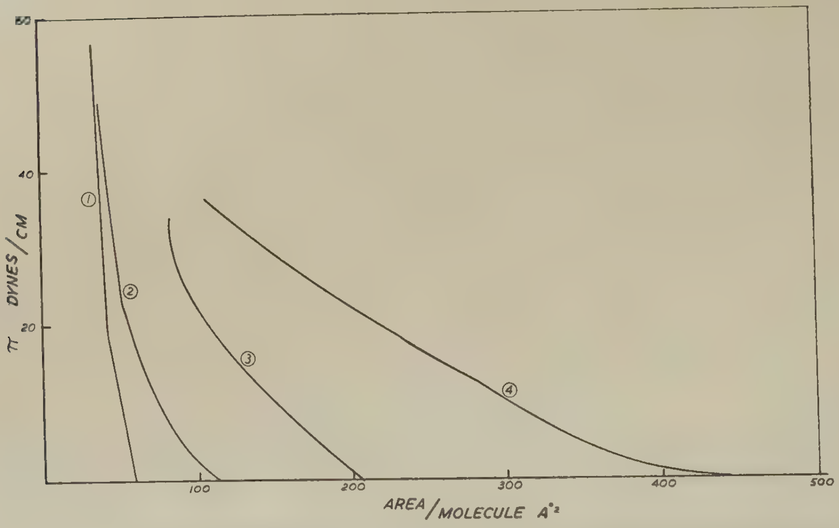

FIG. 5. Π-A curves for dipalmityl diethylene triamine on 0.01 N HCl at various temperatures.

(*1*) 13.3°C.
(*2*) 32.0°C.
(*3*) 45.0°C.
(*4*) 55.0°C.

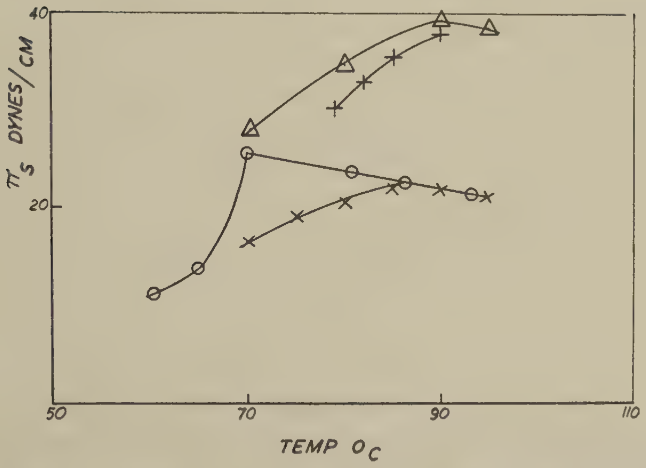

FIG. 6. Equilibrium spreading pressures (Π_S) as a function of temperature for two piperazines and two triamines.

△ Dioleyl diethylene triamine.
+ Distearyl diethylene triamine.
○ Dimyristyl piperazine.
× Distearyl piperazine.

Figures 4 and 5 show the results for the monolayers of the triamines. The results for the equilibrium spreading pressures (Π_S) at various temperatures are given in Fig. 6, two piperazines (dimyristyl and distearyl) and two triamines (dioleyl and distearyl) being chosen for this purpose.

DISCUSSION

Before considering the mechanism of antifoam action it is necessary to consider the results for the spread monolayers, in order to determine, as far as possible, the molecular configuration at the air/water interface.

1. The Structure of the Spread Monolayers

At room temperature (18.5–20.5°C.) all the piperazines gave monolayers of the liquid expanded type, quite fluid at all areas. This behavior shows at once that appreciable hydrogen bonding between the head groups is absent (6), which is not surprising in view of their chemical nature. The expansion on strong acids is again not unexpected, being shown by compounds such as ethers and acids (7).

At the cohering point of the monolayer the configuration of the head group is probably as shown below:

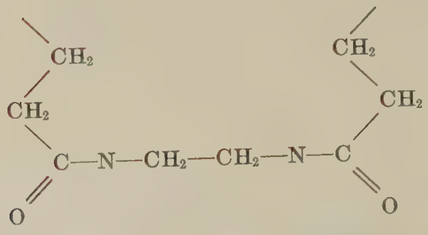

(*a*) Head group in elevation (i.e., viewed parallel to surface)

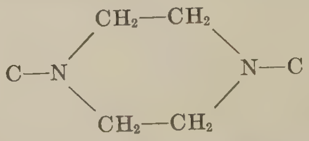

(*b*) Head group in plan (i.e., viewed perpendicular to surface)

Calculations from a scale drawing of the structure, on the assumption of planar nitrogen and with covalent and van der Waals' radii as given by Pauling (8), gave about 75 A.^{2} as the area of the head group including the first few CH_2 groups (the remaining part of the chain could, if necessary, fold back inside the area of the ring). This value is clearly very much less than the experimental limiting area of about 120 A.^{2}—a behavior which is typical of liquid expanded films in general.

The results for the surface moment (μ) show that at areas below about 100 A.^{2} some head-group reorientation is occurring, but it does not seem possible to relate this to any specific change such as a tilting of the head group by rotation around the N—C bonds.

At the higher temperatures the piperazines give gaseous films, in the case of the dimyristyl compound, for example, the results at 72°C. obeying the equation $\Pi(A\text{-}31) = 503$, this being the well-known equation of state for an imperfect gaseous film.

The monolayers given by the triamines are seen to differ considerably from those of the piperazines. At room temperature the dioleyl compound gives a typical liquid expanded film with cohering area of about 110 *A*.^{2}. The distearyl compound, on the other hand, gives a very rigid solid film, with an extrapolated area at zero compression of about 40 A.^{2}. Such a difference between a saturated and its cis mono-unsaturated relative has been noted in many other systems. The behavior of the distearyl compound strongly suggests marked hydrogen bonding between the head groups, probably through the 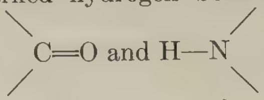 $>C{=}O$ and $H{-}N<$ groups. (The observed tendency for the dilute benzene solutions to form gels probably arises from the same cause.)

Calculation from a scale model (Catalin Molecular Models) showed that the head groups, if fully extended parallel to the surface, would occupy about 65 A.^{2}, so that with the distearyl compound the orientation of the head group must be substantially different. However, examination of the model showed that, by suitable rotation, the head group can be folded up in such a manner as to fit almost exactly into the area of the two paraffin chains (i.e., *ca* 40 A.^{2}).

The two important features of the high-temperature results are the physical nature of the films and the magnitude of the equilibrium spreading pressures. The fluid nature even of the distearyl triamine at temperatures near the boiling point of water shows that the tendency for head group hydrogen bonding is largely broken down by thermal agitation under such conditions. The magnitude of the equilibrium spreading pressures at the high temperatures should be noted and also their variation with the chemical nature of the head group and comparative independence of chain length and unsaturation (see Fig. 6).

2. The Mechanism of Antifoam Action

The bearing of the present results upon the mechanism of antifoam action can now be considered. The theory suggested by Jacoby and Thompson for compounds of the polyamide type is summarized by them as follows (9); "In the presence of an adsorbed layer of surface-active insoluble material, the collapse of a foam bubble may be accompanied by a syneresis (10) or formation in the adsorption layers of dehydrated aggregates of the surface-active material. It has been observed that certain monolayers, although they may actually stabilize the bubble film while they are in the liquid state, lose this ability at once when the solid (brittle) state is attained (10). This indicates that one of the conditions for stabilization is the great mobility of the molecules of the adsorption layers, and if this mobility is lost by attainment of the solid state, the adsorption layers may contribute to the rupture of the bubble film. It is likely that the syneresis described above results essentially in the formation of patches of monolayer in the brittle state which are incapable of redispersion at a rate equal to or greater than the velocity of destruction of the bubble film." "The theory of antifoam action referred to above suggests that hydrogen bonding promotes antifoam action by enhancing the syneretic effect and creating a greater tendency for the monolayer to reach the solid or brittle state, as shown by Alexander (11)."

The monolayer results obtained in the present investigations, in particular the fluidity and the expanded nature of *all* films at the higher temperatures, makes the above explanation improbable. The fact that the melting point of all the compounds lies well below the operating temperatures of normal commercial boilers provides additional support to this argument.

A tentative alternate theory is advanced below but much further work on surface behavior at high temperatures will be necessary before any finality is likely to be reached.

The important factors in promoting antifoam action are believed to be:

a). A high insolubility in water at the normal operating temperatures (i.e., >100°C. and usually much higher).

b). A moderate degree of surface activity at the steam/water interface.

c). The ability to form fluid films at the steam/water interface (i.e., at the high temperatures existing in boilers).

d). A low tendency for adsorption on the suspended particles in the boiler as well as on the heating surfaces.

e). High chemical stability in the boiler.

Of these factor (*e*) is obvious and will not be considered further.

The possession of high insolubility (as judged by monolayer standards which are of course quite different from bulk solubility standards) ensures that the antifoam is virtually entirely concentrated in the region where it is most essential, i.e., at the free steam/foam surface. This would arise from the steam bubbles' coming into contact with the colloidal particles of antifoam (the antifoam is usually added in dioxane solution to the feedwater), resulting in some surface spreading and subsequent transport to the uppermost foam surface.

The surface spreading due to the lowering of the steam/water interfacial tension could have a number of effects, although their relative importance is hard to assess at this stage. A moderate degree of surface activity (say, *ca.* 20 dynes/cm.) would probably suffice to displace most solid suspended particles from the interface (unless they were unusually hydrophobic), and it would appear that such interfacial particles are one of the major factors in promoting excessive foaming in boilers. Further, the lowering in surface tension would damp out violent movements at the surface when the bubble collapses, and would also assist draining by allowing easier deformation of two bubbles in close contact. A low tendency for adsorption on the suspended particles is essential to keep them as hydrophilic as possible. Reactive soluble molecules, such as fatty acids present in oily contamination, would tend to make such particles hydrophobic and thus to increase their tendency to concentrate at the foam surface.

SUMMARY

The surface behavior at the air/water interface of a number of paraffin-chain compounds used as antifoams in steam boilers has been studied. The compounds were chiefly diacylated piperazines (C_{11}, C_{13}, C_{15}, and C_{17}), together with dipalmityl, distearyl, and dioleyl diethylene triamines. The effects of acidity of the substrate and temperature were examined using spread monolayers, and in addition equilibrium spreading pres-

sures were measured at higher temperatures (up to 95°C.). The results show that certain aspects of current theories of antifoam action need correction and some alternative suggestions are advanced.

ACKNOWLEDGMENTS

Part of this work was carried out (by J.G.H.) at the University of New England and we wish to acknowledge the assistance given during that period by Mr. V. R. Stimson.

REFERENCES

1. JACOBY, A. L., AND THOMPSON, W. H., *Proc. 7th Ann. Water Conf. Engrs. West. Penn.* **1947**, 31.
2. JACOBY, A. L., *J. Phys. & Colloid Chem.* **52**, 689 (1948).
3. JACOBY, A. L., AND JOHNSON, C. E., *J. Phys. & Colloid Chem.* **53**, 9 (1949).
4. ALEXANDER, A. E., *Nature* **159**, 304 (1947).
5. ALEXANDER, A. E., AND JOHNSON, P., "Colloid Science." Oxford University Press, 1949.
6. ALEXANDER, A. E., *Proc. Roy. Soc. (London)* **A179**, 470 (1942).
7. SCHULMAN, J. H., AND HUGHES, A. H., *Proc. Roy. Soc. (London)* **A138**, 436 (1932).
8. PAULING, L., "The Nature of the Chemical Bond." Cornell University Press, Ithaca, 1948.
9. Reference 2, p. 692.
10. TRAPEZNIKOV, A. A., AND REBINDER, P. A., *Compt. rend. acad. sci. U.R.S.S.* **18,** 427 (1938).
11. ALEXANDER, A. E., *Proc. Roy. Soc. (London)* **A179,** 486 (1942).

JOURNAL OF COLLOID SCIENCE **11,** 428–434 (1956)

THE FRACTIONATION OF POTATO STARCH BY CENTRIFUGATION IN ALKALI

H. Baum[1] and G. A. Gilbert

Department of Chemistry, The University, Birmingham 15, England

Received April 5, 1956

Abstract

Potato starch can be fractionated into its branched and unbranched components by the centrifugation of dispersions of undamaged granules in dilute alkali. The branched component, amylopectin, appears to be completely insoluble in this medium, and the unbranched component, amylose, completely soluble. There is no evidence to suggest that covalent bonds exist in the granule between amylose and amylopectin. The separation of the components by centrifugation is shown to be very efficient because of the exclusion of amylose from the sediment of highly swollen amylopectin particles. If the volume occupied by the sediment is used in conjunction with Einstein's theory for spheres to calculate the intrinsic viscosity of the amylopectin, a value of 2.9 is obtained compared with a measured value of 2.2. Amylose is found to have an intrinsic viscosity of 5.5, and the sum of the weighted values of the intrinsic viscosities of the separated components is found to equal that of whole starch.

Introduction

Owing to their size and nature, the molecules of starch are very sensitive to oxidation and hydrolysis. But starch occurs in its native form as compact resistant granules which must be "dispersed" before chemical or physical examination is possible. There is always the possibility, therefore, that changes have occurred during this essential preliminary of dispersion, and that the observed properties of starch are not exactly those of native starch. The broad features of the chemical structure of starch can hardly be affected by these considerations, nor can the repeatedly confirmed observation that most varieties of starch consist of two distinct components, amylose and amylopectin, one of which is a linear and the other a branched polysaccharide.

The properties most likely to be affected during dispersion of the starch are the molecular size of the components, and their content of "anomalous" groups, the term used for groups which appear to be present in minute amount but which exert a disproportionate effect on the course of enzyme action on the components. Confirmation that treatment with oxygen can introduce anomalies which limit the extent of the phosphorolysis of amylose has recently been obtained (1).

---

[1] Present address: Department of Biochemistry, University College of South Wales, and Monmouthshire, Cardiff, Wales.

Evidence is also available of the influence of dispersion and fractionation on the molecular weight of amylopectin. Witnauer, Senti, and Stern (2) measured the degree of polymerization of potato amylopectin by the method of light scattering, and obtained the respective values of 220,000 and 86,000 for two samples which apparently differed only in the details of their preparation. The authors concluded that the difference in size could be due to inadvertent chemical degradation. One can deduce from the amount of degradation required to reduce the figure of 220,000 to 86,000, that if only half this amount of degradation had occurred during the preparation of the sample having the higher degree of polymerization, then the original size of the amylopectin could have been comparable to that of the starch granule itself. The upper limit of the molecular size of amylopectin is thus undetermined.

It is obviously desirable to compare different methods of dispersion and fractionation, and in the present paper a method is described which avoids conditions that are known to degrade starch. Use is made of the insolubility of amylopectin in cold dilute alkali—a fact which was appreciated in the early days of starch chemistry (3), but which has been lost sight of in the intervening years.

Experimental

The method of fractionation will be illustrated by an experiment with spring-harvested new potatoes. The potato tissue was blended for 1 min. in 1% NaCl solution in an "Atomix" blender, and the blend filtered through muslin into a large volume of 1% NaCl solution. The sediment of starch was washed by decantation first with 1% NaCl solution and then with distilled water. It was stored under distilled water at 2–3°C.

A slurry of this starch in a little distilled water was poured into NaOH solution through which nitrogen was being bubbled, to give 200 ml. of a 0.79% dispersion of starch in 0.5 N NaOH. The vessel used as a "disperser" has been described previously (4). After 30 min. at 15°C., a portion of the dispersion was poured into a stainless steel centrifuge tube and the tube capped. The tubes held about 43 ml. The rest of the dispersion was diluted (in the disperser, with 0.5 N NaOH) to a concentration of 0.53%, and 127.9 ml. removed into three centrifuge tubes. Further dilutions were made and then samples taken at concentrations of starch of 0.28% and 0.051%. The samples were then centrifuged in a Servall centrifuge (6-in. rotor) for 2 hr. at 15,500 r.p.m. (40,000 g). The dispersion separated into a water-clear supernatant solution and a sharply delimited opalescent gelatinous sediment (occupying half the tube in the case of the 0.53%

sample). With little disturbance, 1-ml. samples of the supernatant solutions were taken at a depth of about 6 ml., for staining with iodine by the method of Hassid and McCready (5). The optical density of the stain of each supernatant was then compared with that of the corresponding whole starch dispersion. Results are given in Table I.

Only the tubes containing the 0.53% dispersion were proceeded with further. From these the bulk of the supernatant solution (A) was withdrawn very carefully with a transparent syringe. A small intermediate cut (B) was next taken from the region which included the surface of the sediment, and made up to 42 ml. with 0.5 N NaOH after being transferred to another centrifuge tube. The main sediments (C) were mixed in their tubes with more 0.5 N NaOH, and then recentrifuged as before at the same time as the intermediate cut. After centrifugation, (B) was separated into a supernatant solution (D) and a sediment (E). The tubes containing (C) gave supernatant solutions (F) and sediments (G). The sediments (G) were mixed with more NaOH solution and recentrifuged once again to give a supernatant solution (H) and a sediment (I).

Sediment (I), which contained the major part of the amylopectin, was diluted with water to 100 ml. and brought with 3.5 N acetic acid to pH 5.2. When 1.4 vol. of ethanol were added, a sticky aggregate formed which was separated by decantation and centrifugation (2000 r.p.m.). No material which stained with iodine was left in the solution. The aggregate was washed with ethanol-water (1.4:1 by vol.) and then swollen in water. After reaggregation with 1.4 vol. of ethanol, the aggregate was washed with the same mixture and was by then free of salt. Finally, a homogeneous dispersion of the amylopectin, representing the final product, was formed by shaking the aggregate with warm water in a flask containing a small curved spatula to break up lumps of gel. The concentration of the dispersion was determined by evaporating a portion in the presence of alcohol (which prevents the formation of a moisture-retaining "glass"), followed by dry-

TABLE I

Enrichment Factor of the Supernatant Amylose Solution

Concentration of starch (%)	Optical density of iodine stain of		Ratio (b/a)	Enrichment factor
	(a)	(b)		
	Starch dispersion	Supernatant amylose solution		
0.791	3.28	4.10	1.25	2.32
0.530	2.20	2.31	1.05	1.95
0.277	1.15	0.90	0.78	1.44
0.051	0.211	0.123	0.58	1.08
0.000			0.54*	1.00

* By extrapolation.

ing at 70°C. under high vacuum. The "blue value" (6) of the dispersion was determined by heating portions for 3 min. with dilute NaOH, neutralizing, and staining with iodine (5). Sediment (E) was worked up similarly.

The supernatant solution (A), which contained most of the amylose, was neutralized with *N* HCl and shaken with *t*-amyl alcohol (7). Amylose precipitated immediately in the cold in a flocculent form. The mixture was warmed and cooled and then centrifuged. No iodine-staining material could be detected in the supernatant solution, showing that no fractionation was occurring at this stage, and that the amyl alcohol was acting merely as a convenient precipitant. The precipitate was washed on the centrifuge with cold *t*-amyl alcohol-saturated water until free from salt. This precipitate represented the final product of amylose. It was analyzed by dissolving it in hot water, from which the amyl alcohol was blown off, and staining samples with iodine for the determination of "blue value." Concentration and yield were determined as for the amylopectin above.

The supernatants (D), (F), and (H) were neutralized with acetic acid and precipitated with *t*-amyl alcohol. No iodine-staining material remained in solution, nor was a further precipitate formed on the addition of 1.4 vol. of ethanol. The precipitates were too small to be worked up separately and were therefore combined. Salt was removed by washing with *t*-amyl alcohol-saturated water, and "blue value" and yield were determined as before.

Results and Discussion

In the experiment above, in which 679 mg. of the starch from new potatoes was dispersed at a concentration of 0.53% in 0.5 *N* NaOH, 99 mg. of amylose, of "blue value" 1.23, was recovered from the supernatant solution (A). The combined precipitates from supernatant solutions (D), (F), and (H) gave 38 mg. of amylose of "blue value" 1.15. Allowing for 3 mg. of amylose removed from the supernatant solutions for staining with iodine, this yield corresponded to a total of 21% by weight of amylose of an average "blue value" of 1.21 in the whole starch. ("Blue values" were measured routinely (6) with a Hilger Spekker absorptiometer in conjunction with Kodak No. 8 filters. Calibration showed that a "blue value" of 1.21 was raised to 1.36 if the optical density of the iodine stain was measured at 6800 Å on a Unicam spectrophotometer.)

The main amylopectin sediment weighed 508 mg. and had a "blue value' of 0.176. Corresponding figures for the minor sediment were 26 mg. and 0.200. These amounts together corresponded to a content of 79% by weight of amylopectin of "blue value" 0.177 in the whole starch. Only 5 mg. of the original starch remained unaccounted for.

The volume occupied by the amylopectin and made unavailable to the amylose can be calculated from the dependence of the concentration of the amylose in the supernatant solution on the concentration of the dispersion. If all the volume was available to the amylose, the concentration of the supernatant solution would rise in direct proportion to that of the dispersion, but in point of fact it rises much more rapidly, as Table I shows. The ratio of the optical density of the iodine stain of the supernatant solution to that of the dispersion is tabulated there as a function of the concentration of the dispersion. Extrapolation of this ratio (which proves to be a linear function of the concentration) to zero concentration gives the value which the ratio would have if no exclusion of the amylose took place. The limiting value is 0.54. At a concentration of starch of 0.53% the value of the ratio has risen to 1.05, and the amylose has therefore been concentrated by a factor of 1.95. Therefore, of the 127.9 ml. of dispersion, only 127.9/1.95 ml., i.e., 65.6 ml. could have been available to the amylose. Hence, by difference, the volume occupied by the amylopectin was 62.3 ml. This calculated volume compares well with the observed volume of the sediment, which was 66.5 ml.

If 540 mg. (approx.) of amylopectin occupy 62.3 ml. when swollen in 0.5 *N* NaOH, the specific volume of the amylopectin is 115. According to the Einstein equation for the intrinsic viscosity of a suspension of spherical particles, $[\eta] = 0.025 \times$ specific volume, and, therefore, if the amylopectin particles behaved as spheres, the intrinsic viscosity of the amylopectin would be 2.9. In fact, the measured value is 2.2 (see below, and also ref. 8). Since factors such as free-draining, shape, and anomalous viscosity have not been taken into account, only the rough similarity of these figures can be pointed out.

Most of the development work on the method was carried out on starch from autumn-harvested King Edward potatoes. Even after the starch had been kept under distilled water for six months at 2°C. (without freezing, which damages the granules), good yields of amylose of "blue value" 1.1 and of amylopectin of "blue value" 0.16 were obtained, but it is preferable to use freshly prepared starch.

A preliminary study was made of the intrinsic viscosity of the components of this starch. All measurements of viscosity were made in 0.5 *N* NaOH at 20°C. as described previously (4, 8). The starch itself, of "blue value" 0.40, had an intrinsic viscosity of 2.85. After centrifugation of a 0.45% dispersion for 2 hr. at 15,000 r.p.m., the intrinsic viscosity of the dispersion, after the components had been remixed, was unchanged, but the specific viscosity at 0.225% concentration had fallen from 1.33 to 1.21. The amylose in the supernatant solution had an intrinsic viscosity of 5.5, and the amylopectin in the sediment, after a second centrifugation in fresh 0.5 *N* NaOH as before, a value of 2.2. On the assumption that the fractions represent respectively 21% and 79% of whole starch, the weighted sum of their viscosities amounts to 2.89, which corresponds closely to the measured value of 2.85 for whole starch. The components therefore contribute independently to the intrinsic viscosity of whole starch.

A portion of the supernatant amylose solution was brought to pH 7 with HCl, left overnight, and then made alkaline again for the measurement of intrinsic viscosity. This was found to have remained practically unchanged at 5.4. However, when the amylose was heated in the absence of salt in neutral solution at 100°C. in nitrogen, its intrinsic viscosity fell to approximately 4. Heating similarly in 1% NaCl solution brought about a further reduction to about 3, in agreement with previous results (8).

It is not essential to use forces as high as 40,000 *g* to carry out the fractionation in alkali. Successful results have been achieved even at 20,000 *g*. At 40,000 *g* there is a slight depletion of the amylose near the meniscus owing to some sedimentation of the amylose itself.

Summary

The present results give final support to the earlier view (3) that amylopectin is insoluble in dilute alkali. Whether this insolubility is conferred by covalent bonds, and the amylopectin molecule is comparable in size to the starch granule, or whether it is due to aggregation, is not apparent from these experiments, but at least it is clear that there are no bonds in the starch granule between amylose and amylopectin which resist the action of dilute NaOH solution (contrast ref. 9).

The separation of amylose from amylopectin by centrifugation in dilute alkali is surprisingly efficient because amylose is excluded from the sediment of swollen amylopectin particles. In a 0.5% dispersion of starch, about half the volume is occupied by amylopectin and unavailable to amylose, and this leads to an enrichment of the supernatant solution in amylose by a factor of two. Calculations based on the swollen volume of the amylopectin show that the intrinsic viscosity of amylopectin conforms very roughly to Einstein's law, but it would be premature to attempt a more exact comparison. The intrinsic viscosities of the two components appear to be additive in dispersions of whole starch. If "alkali-fractionated" amylose is heated in water or salt solution, its intrinsic viscosity falls from the high value of 5.5 to values obtained previously (8) for amylose prepared by fractionation in neutral solution.

Acknowledgment

We are grateful to Mr. N. D. Scott for carrying out some of the viscosity measurements.

REFERENCES

1. BAUM, H., GILBERT, G. A., AND SCOTT, N. D., *Nature* **177,** 889 (1956).
2. WITNAUER, L. P., SENTI, F. R., AND STERN, M.D., *J. Polymer Sci.* **16,** 1 (1955).
3. GATIN-GRUZEWSKA, Z., *Compt. rend.* **146,** 540 (1908).
4. BAUM, H., GILBERT, G. A., AND WOOD, H. L., *J. Chem. Soc.* **1955,** 4047.
5. HASSID, W. Z., AND MCCREADY, R. M., *J. Am. Chem. Soc.* **65,** 1154 (1943).
6. BOURNE, E. J., HAWORTH, W. N., MACEY, A., AND PEAT, S., *J. Chem. Soc.* **1948,** 924.
7. LANSKY, S., KOOI, M., AND SCHOCH, T. J., *J. Am. Chem. Soc.* **71,** 4066 (1949).
8. BAUM, H., AND GILBERT, G. A., *Chemistry & Industry* **1954,** 489, **490.**
9. BAUER, A. W., AND PACSU, E., *Textile Research J.* **23,** 870 (1953).

JOURNAL OF COLLOID SCIENCE **11**, 435–444 (1956)

PENETRABILITY OF MOLECULAR LAYERS

Harry Sobotka

Department of Chemistry, The Mount Sinai Hospital, New York, New York

Received March 26, 1956

Abstract

The deviation of the deposition ratio from unity in Blodgett and Langmuir's building-up process is discussed. The loosening up of the crystalline array in films, compared to the substance in bulk, is considered in the light of certain melting point phenomena. There is a difference in principle between the permeability of membranes and the penetrability of molecular layers. Several examples for the latter phenomenon are given. A hypothesis is proposed for the phenomena of penetration and skeletonization. Substances in molecular layers exist in an exceedingly dynamic state.

Introduction

The building-up technique, developed by Blodgett and Langmuir, leads to the deposition of mixed films, consisting of fatty acids and of their salts with bivalent metals. Any explanation of the reactivity and penetrability of built-up films presupposes a working hypothesis that answers the question of the arrangement of the two different molecular species in the film.

The deposition ratio of built-up films, i.e., the quotient "area of H-layers/area of AB-layers" approaches unity (1), but the most precise measurements yield a ratio of 0.96. The built-up film appears to be stretched out by *ca.* 4%. The forces which hold the molecules in place in an H-film are threefold: the van der Waals' forces between the aliphatic chains, the interaction of the polar groups with the "gegenions" accumulating in the hypophase near the boundary (2), and the external lateral pressure or "push." Upon building-up the third factor disappears and leaves the cohesion of the film to the van der Waals' forces and to the anchoring of the polar groups on the metal surface.

A likely explanation for the deviation of the value of the deposition ratio from unity would be a greater slanting angle of the stearic acid molecules upon deposition. The increase in area per molecule of about 4% would correspond to an increase by the same percentage of the cosine of the angle formed between the molecules and the horizon and to a corresponding decrease of the angle itself. Even in the original H-film this angle is less than 90% and seems to be a function of the length of the carbon chain and of the disposition of the cations at the base of the film.

Depending upon the pH of the hypophase, larger or smaller proportions of the fatty acid molecules are neutralized; in other words the higher the pH of the hypophase, the higher the content of bivalent metal in the film (3). We are working on the confirmation by radioactive techniques of the analytical data of Langmuir and Schaefer. The quantity and size of the metalion exert a perceptible influence on the overall height and the cross section of the individual molecules. The evaluation of this effect is not simple, especially in respect to the interferometric determination of the thickness, which requires exact data for the refractive index and density of these soaps.

For our present purpose, especially as we are not concerned with absolute values of film thickness, we accept the assumption that the influence of the metalions on refractive index and density may be neglected.

Since we are dealing with mixed layers, consisting of metal stearate and stearic acid, the next question arises as to the regularity of the arrangement. Blodgett found that the thickness of such mixed films decreases when they are exposed for a few seconds to an organic solvent such as benzene. The decrease is expressed in a "lowering" of the interference colors of the first order. Treatment of the film at this stage with a drop of hexadecane will restore the original colors. The explanation of this phenomenon is as follows: the benzene had removed free acid from the film, leaving behind a skeleton of the barium soap. This skeletonized film is then refilled with the hydrocarbon of practically identical refractive index. One important condition for this experiment is that at least two-thirds of the stearic acid molecules exist as barium soaps. If we contemplate the hexagonal array of a layer, it becomes obvious that a stable skeleton will be obtained only if the holes left by the free stearic acid molecules, upon removal, form a regular pattern with no two positions contiguous to one another. Thus, the skeleton will assume the pattern of an empty beehive. Figure 1 shows a possible plan for this arrangement.

The measured thickness of fatty acid monolayers is in good agreement with the assumption that they form a zigzag line within a plane and are more or less slanted against the surface normal. The van der Waals' forces

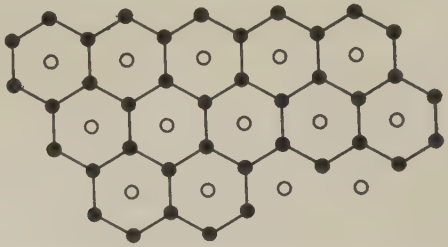

FIG. 1. Hexagonal array of stearic acid-barium stearate layer. Solid dots signify barium ions, open circles hydrogen ions.

increase with the length of the chain and, thus, the molecules become more "crowded" and their cross section attains lower values, about 10–15% smaller, for higher acids such as lignoceric acid with a chain of 24 carbon atoms.

At this point, we must mention an observation which at first sight seems puzzling but which offers what seems to be the true explanation for the deposition coefficient 0.96, discussed above. The interferometric measurement of multilayer films gives values for their thickness which, divided by the number of dippings, yields a thickness per double layer of 48.35 A. The same films, when studied by X-ray crystallographic methods, yield a periodicity of 50.1 A. between subsequent layers of barium ions—a discrepancy far out of the reach of experimental error (4). It appears that the built-up layers contain holes aggregating 4% of the total surface and that these defects accumulate so that the second layer may fill up the holes of the first layer, but in itself carry 8% holes and so forth. After the deposition of 25 layers, one layer will have disappeared by filling up the holes in the other 24 layers. Thus, a count of 25 layers by dipping yields only 24 actual layers. This hypothesis finds support in the observation that the smoothness of the building-up process shows periodic fluctuations; it runs smooth at the beginning, becomes rougher and requires slowing-up in the up-and-down movement by the time 10–15 layers are deposited, and resumes its smoothness around 25 layers.

As had been mentioned before, X-ray diffraction pictures of built-up monolayers of stearic acid show hexagonal configuration, whereas stearic acid in bulk crystallizes in the rhombic system, which is about 10% more densely packed. The acid in bulk has a transition point from the rhombic to the hexagonal system a few degrees below its melting point. This evidence indicates the lesser cohesion in the two-dimensional state and may incidentally explain its greater penetrability. As we have shown (5), films of fatty acids are ripped off under certain conditions by dilute solutions of serum albumin. In the course of these studies we have found that above a certain temperature, characteristic for each acid, the "ripping-off reaction" becomes nonspecific and proceeds in the absence of albumin with pure buffer solution. This loosening up of the two-dimensional array occurs with palmitic acid 30° C. below its melting point, with stearic acid 25° C. below its melting point, and with arachidic acid less than 20° C. below its melting point in the bulk phase. This observation points to the increasing share of the van der Waals' forces with lengthening of the chain.

By the same token, terminally branched fatty acids become opaque soon after deposition and display extreme volatility more than 40° C. below their melting point in bulk. Some of them, the neo-acids, form only opaque films right upon deposition, betraying their inability to fit the terminal tertiary butyl groups into a crystalline array (6).

The question of melting point of thin films has been studied by G. Karagounis (7) in Zurich from quite a different angle. Karagounis was interested in a method for the determination of the total surface of finely divided powders. Wilhelm Ostwald had observed that, when spread sufficiently thin, salol was taken up by quartz powder in such a manner that it did not elicit crystallization of melted and undercooled salol. He assumed that the salol layer on quartz was amorphous.

Karagounis tried to determine the minimum or critical coverage ("Belegungsdichte" = B_C) necessary to render the salol-covered powder effective as a seed for the undercooled melt. The critical coverage is determined by preparing samples of the powder, say, of a metal or of a metal oxide salt, with various quantities of the covering substance, applied under certain precautions from ether solution. The critical coverage seems to be reached when a coherent monomolecular layer is completed and when the formation of a second layer starts, in other words, when a three-dimensional array begins to form. The specific surface

$$F_S = \frac{B_C}{D_m \cdot d},$$

where d is the density and D_m the minimal thickness of the layer. At this critical point many of the properties of the powder change rather abruptly. Below this point the characteristics hardly differ from those of the pure powder; above, it has a fatty or, if crystalline, a sandy touch. Below the critical coverage the powder, say, aluminum oxide or a metal, is hydrophilic; when placed on water it is wetted and sinks. Above the critical coverage the powder is as hydrophobic as the covering substance, say, salol or p-chlorophenol, and floats. The electric resistance of the powder also sharply increases at this point. This reminds one of the electrophoretic properties of glass powders or plastics which, when completely covered by a layer of protein, behave exactly like the protein itself.

In the course of these experiments, Karagounis observed a phenomenon which he interprets as a lowering of the melting point in thin layers, and it is for this reason that his work is discussed here in a little more detail. Samples of the metal or oxide powder are covered with given amounts of a low-melting organic substance such as salol or naphthylamine or ethylanthracene. All of them show, when carefully purified, a great tendency to form undercooled melts at room temperature. The samples, when kept at room temperature or below, act as seeds in the undercooled bulk phase of the substance. Samples of the coated metal powder were then heated to various temperatures and tested for their seeding ability. Those heated above a certain temperature—which is reproducible within 1°–2°—seemed to have melted, because they did not function as seeds, when brought back to room temperature.

The value of this "melting point" of a thin layer depends on its thickness. The dependence of this melting point depression on both the nature of the compound and the nature of the powder is interpreted by Karagounis as an effect of the π-electrons in the molecules of the compound: the more π-electrons, the greater the melting point depression under comparable conditions. It is assumed that the π-electrons are absorbed by the metallic hypophase into its electropositive "holes" and that, thus, the cohesion of the layer decreases. This was tested with ethylanthracene on silver-tin alloys. The number of unoccupied spaces in the pure metals is substantially higher than in the various alloy phases. A minimum of electropositive holes is found in the γ-alloy (73 silver: 27 tin) which also shows a minimum of electrical conductivity. The melting point curve shows the effect of ethylanthracene on the melting point depression, which decreases from 30°C. on the pure metals to 18°C. on the alloy.

In the case of melting point depressions and lowering of cohesion in fatty acid films, observed by Beischer (8) and by ourselves (5), we can safely exclude the π-electron hypothesis. It must be mentioned that Karagounis himself emphasizes that his conclusions may not be applied to all systems. Cases in point are the melting point depression of naphthylamine on lead sulfide and of *p*-cresol on sodium chloride, in which cases smaller but definite effects of the same nature were observed. Unfortunately, those compounds which lend themselves to spreading and building-up of monomolecular layers, lack in general the tendency to form undercooled melts. Nevertheless, it will be of interest to study the effect of the chemical nature of the underlying plate upon the melting behavior of fatty acid films.

Whatever the ultimate causes of the loosening up of matter in the two-dimensional as compared to the three-dimensional state, it gives rise to two phenomena, which seem to be typical for this state of matter. The one is the turning around of molecules without disturbance of the general lineup in which they are found.

Under certain conditions, fatty acids and also sterols, when subject to the Blodgett building-up process, build up on the downtrip of the plate only and not on the uptrip; in other words, they form a so-called "X-film" consisting of AAAA···· instead of ABABAB···· layers. Porter (9) studied potentials across built-up stearic acid slides and found that in Y-films the potentials of the alternating A- and B-layers cancel one another. On the other hand, potentials up to 6 and 8 volts are built up in X-films with a sequence of 100–200 A-layers. These X-films seem to represent a metastable state, higher in energy than Y-films, and spontaneous drops of the potentials to practically zero were observed during these measurements.

The same turning around of alternate sheets or layers was observed in X-ray diffraction studies, when X-films, which were expected to yield a distance of 25 A. between the barium ions, invariably yielded twice this distance and proved identical with Y-films, into which they had been converted by the irradiation (3).

It has been shown by Langmuir on molecular models that they may turn around 180° along their longitudinal axis without requiring any additional elbow space at the turning point. In fact, two adjacent chains may turn around by a ring-around-the-rosy movement without any lateral disturbance. Although the "how" of this turning around reaction is perfectly within the realm of geometric possibility, its "why," the energetics of the reaction, still forms a major puzzle.

Penetrability

In the description of the properties of monomolecular films it has become apparent that the forces of cohesion in this state of matter are smaller than one would venture to predict by extrapolation from the three-dimensional state, where molecules, vicinal in the third dimension, contribute cohesional forces. We use purposely the term penetrability for monolayers, in order to distinguish the phenomenon from that of permeability, applicable to membranes. In the latter, whether of biological origin or of synthetic nature, permeability depends on the number, size, and electrical charges of their pores. We suggest that the penetrability of mono- and oligomolecular films be due not to pores or fortuitous defects in predetermined sites but to the continuous opening and closing of their molecular array in the course of their thermic motion.

Rothen had carried out, about 10 years ago, a series of experiments where systems of antigens and antibodies and of enzymes and substrates were operative across blankets up to 250 A. thick, consisting of stearic acid layers or also of equally thick Formvar layers. He attributed these effects to long-range forces, but it was subsequently demonstrated by Trurnit (10) and by Singer (11) that his experimental results could be explained by the bodily penetration of one partner of the system across the blanket.

We had previously noticed a phenomenon which could only be explained by bodily penetration (1). The oleophilic or oleophobic, the hydrophilic or hydrophobic, character of films, a characteristic of considerable interest in two-dimensional chemistry, may be determined by the measurement of the contact angles of droplets of the respective liquids placed on a Blodgett slide. We found that the surface of mono- or multilayers of steric acid shows a contact angle of about 80° with water, i.e., the surface is strongly hydrophobic. On the other hand, a drop of water placed on a monolayer of a protein film, e.g., a built-up film of serum albumin, will spread with a contact angle of zero. If a double layer of stearic acid is superimposed on a film of albumin, the contact angle with water will be around 40° and only upon additional superimposition of a few double layers of stearic acid will this value reach 80°–81°, the value for pure stearic acid films.

Another phenomenon of similar nature, which defies explanation by long-range forces, was observed with isostearic acid, an isomer of normal stearic acid, terminating in an isopropyl group (6). This acid may be built-up to form optically clear films, resembling stearic acid in appearance, but of slightly lower thickness. However, in contrast to the normal acid, which preserves its optical perfection and the depth of its interference colors for more than 15 years at New York room temperatures, the isoacid films become opaque over night and, if not kept at 0° C. but at room temperature, rapidly lose their thickness as seen by the interference colors. Clearly, the molecules of both acids are subject to thermic oscillations, both in the direction of the chain and in a circular manner. In the case of the normal chain the van der Waals' forces will pull the molecule back into its equilibrium position. Contrariwise, in the case of the isostearic acid, some molecules will first move upwards and subsequently perform a circular motion, which will make it impossible for the molecule to be drawn back into the film; hence, the molecule will eventually work itself upwards against a continuously decreasing cohesive force and will end up lying on the surface of the film. Since this surface is oleophobic and altogether poor in energy, the isostearic acid molecules will sublimate with astounding velocity. This phenomenon is confined to the free acids, whilst the barium soaps remain behind; thus, a skeletonized film will eventually result. If a Y-film of isostearic acid is immediately covered with a Y-film of 6 to 10 layers of normal stearic acid, sublimation of the isostearic acid proceeds at practically the same rate as from a free isostearic acid film. The isostearic acid has penetrated 10 layers of *n*-stearic acid at a speed exceeding its rate of sublimation.

All these phenomena, taken together, teach us that monomolecular and oligomolecular films exist in a most dynamic state, in which the molecules continuously exchange place. Whether they do this by squeezing through superimposed layers or by a turning-over mechanism in the manner of a turnstile, or by a combination of both, remains an interesting subject for investigation.

Skeletonization

The removal of fatty acids by organic solvents from mixtures with their metal salts in surface films has been mentioned previously. Similarly, albumin was found (5) to remove the free fatty acid only, leaving behind a skeleton of the barium salt. This situation does not affect the quantitative measurement of the decrease, since the optical measurement is based on the refractive index of the layer, which is an additive property. That the films are skeletonized may be proved by refilling with water. The interference colors of films, refilled with water, are of course slightly "lower" because of the lower refractive index of water.

Stearic acid molecules not only penetrate through superimposed layers of the stearic acid-barium stearate mixture, but they pass without any evident encumbrance through as many as 14 layers (250 A.) of cholesterol, when exposed to the albumin solution. Moreover, a film, thus skeletonized, may be refilled with water molecules penetrating again—this time in the opposite direction—through the cholesterol blanket.

DISCUSSION

Kinetics

We propose the following mechanism for skeletonization. The molecules of the organic solvent or of albumin undergo a number of collisions with the surface of the built-up film. These collisions are defined as effective if they result in the removal of a molecule of fatty acid from the top layer. The holes thus created in the top layer are instantaneously distributed throughout the film or, in other words, fatty acid molecules from the lower layers migrate upwards until the holes are evenly dispersed throughout the film. But this equilibrium is continuously disturbed by the removal of molecules from the top layer. Thus, the reaction rate decreases more slowly than it would in a monomolecular reaction, since the decrease of removable molecules is partly compensated by the migration from beneath. The free acid which is the only removable species in these reactions, comprises in our case about one-third to one-fourth of the film; hence the apparent removal of three layers is equivalent to the exhaustive skeletonization of 10 layers or to the one-third skeletonization of 30 layers or to the one-fifth skeletonization of 50 layers. Accordingly, in a thick film the top layer will be depleted more slowly of available fatty acid molecules and a higher reaction rate will be maintained. We have been able to verify this point (12); a 35-layer film lost 3.0 layers during the first 10 minutes of exposure to the albumin solution; under otherwise equal experimental conditions 4.6 layers were ripped off from a 51-layer film.

The specificity of the ripping-off reaction offers an excellent tool for the differentiation between two fatty acids, especially between palmitic or stearic acid on the one hand and the longer chain acids on the other hand. If we form mixed films of lignoceric and stearic acids on a hypophase of pH = 7.6, containing barium ion, and build them up in the customary manner, we obtain a film containing lignocerate ion, stearate ion, barium ion, and hydrogen ion; the anions in the relation 1:1 and the cations in the relation 1:1, i.e., two equivalents barium: one equivalent hydrogen. Thus, the film might be considered to consist of 1/3 barium lignocerate, 1/3 barium stearate, 1/6 lignoceric acid and 1/6 stearic acid. From among these four species only free stearic acid may be removed by albumin, so that the total of removable molecules would amount to 1/2 only of those that may be ripped off from a simple barium stearate-stearic acid film. In preliminary experiments (12) it has been observed that the rate of removal is substantially identical for the lignoceric-stearic and for the pure stearic film; experiments to ascertain the limit of skeletonization in these films are under way. The above result teaches an important fact, namely, that anions and cations in the film are not specifically correlated one with another. The position resembles a solution of four ionic species, two cations A and B, say, barium and calcium, and two anions, C and D, e.g., NO_3' and Cl', which will react as if it contained AC, AD, BC, and BD. If one of these molecular species, say, AC, is removed by a reaction, e.g., barium nitrate by crystallization, it will be virtually replenished from AD + BC; eventually species BD, in the example calcium chloride, will prevail in the mother liquor. Similarly, as the ripping-off reaction specifically removes hydrogen stearate, more of it will form and correspondingly increasing amounts of barium lignocerate will constitute the remaining skeleton.

Geometric Relationships

Pure fatty acids in bulk and in layers formed by adsorption crystallize in at least three allomorphic forms (13). The situation with built-up films of a mixture of free acid and barium soap is different. From X-ray crystallographic evidence (14) we are led to assume that the ions in each layer form a hexagonal network.

The distance between two cationic layers has been determined by X-ray crystallography for stearic acid-barium stearate films at 50.1 A. The length of the unit cell comprising two stearic acids and one atom of barium, computed from the atomic distances and valence angles, is approximately 51.05 A. Thus, the molecules are slanted with an angle of 10°–12°. Since no X-ray data are available for films containing lignoceric and other acids, nor for their deposition ratio, it cannot be stated at present whether their slanting angle differs substantially.

In this array the barium ions form a beehive network and the hydrogen ions are situated in the centers of the hexagons. Each barium ion neutralizes one carboxylic group from the layer above it and one from the layer below. The hydrogen ions are arranged in pairs, which neutralize two neighboring carboxyl groups by polar and hydrogen bonding, in other words, the fatty acid occurs in dimers. Neither the protons nor the metal ions appear to be definitely correlated to individual pairs of carboxyl groups, but must be imagined to be equidistant from six carboxylic groups, three above and three below.

The skeletonization of stearic films proceeds as follows. First, the free stearic acid molecules are dissolved from the top layer and each of them carries with it its counterpart from the second layer; clearly, the hydrogen bonds are strong enough to overcome the cohesional forces that are holding back the second molecule.

If we now could look down the resulting shaft, we should see the three terminal methyl groups of stearic acid molecules of the third layer pointing upwards at a lateral distance of *ca.* 3.0 A. from the center of the bottom of the shaft. One of the three will now be squeezed up the shaft to the surface, carrying with it the two nearest protons from the next ionic layer and the corresponding fatty acid from the fourth layer. What is the driving force in this transfer mechanism? It cannot be repulsion by electrostatic forces at the polar level of the layers, since we know that hydrocarbons are likewise subject to skeletonization reactions, nor would one wish to invoke an unprecedented solid-state analogue of surface tension. We believe that the force which overcomes the frictional resistance is the lateral mechanical pressure. Whereas the external pressure is relaxed in the building-up process, the cohesional van der Waals' forces continue operating. Aliphatic acids display a bulge at their carboxylic end, imparting to them clublike shape. Thus, any lateral pressure will be strongest at the level of the carboxylic groups and will tend to displace them in a direction perpendicular to the film. While they cannot escape downwards, they find an easy path through the holes left by the skeletonization of the layer immediately above. The absorption of hydrocarbons or water in the refilling reaction deals with molecules lacking a bulge.

This hypothesis is supported by the following observation: the thickness of stearic and of lignoceric films, as compared with the calculated length of the molecules, indicates a slant of *ca.* 11° (see above). Mixed films of stearic and lignoceric acid on the molecular ratio 1:1 are about 1.05 A. thicker than the calculated average, per layer, taking into account the difference in molecular weight (12). We interpret this difference by a more perpendicular position of the molecule in these mixed films with a slanting angle near zero. This position may be achieved by the squeezing of the free carboxylic groups of the stearic acid molecules into a plane of lower lateral pressure.

ACKNOWLEDGMENT

The experimental work was supported in part by U. S. Public Health Service Grant C-1791.

REFERENCES

1. LANGMUIR, I., SCHAEFER, V. J., AND SOBOTKA, H., *J. Am. Chem. Soc.* **59**, 1751 (1937).
2. DIXON, J. K., JUDSON, C. M., AND SALLEY, D. J., "Monomolecular Layers," H. Sobotka, ed., p. 63. American Association for the Advancement of Science, Washington, 1954.
3. LANGMUIR, I., AND SCHAEFER, V. J., *J. Am. Chem. Soc.* **58**, 284 (1936).
4. BERNSTEIN, S., *J. Am. Chem. Soc.* **62**, 374 (1940).
5. SHER, I. H., AND SOBOTKA, H., *J. Colloid Sci.* **10**, 125 (1955).
6. SOBOTKA, H., ROSENBERG, S., AND BIRNBAUM, A., *J. Colloid Sci.* **5**, 567 (1950).
7. KARAGOUNIS, G., *Helv. Chim. Acta* **36**, 282, 1681 (1953); *ibid.* **37**, 805 (1954).
8. BEISCHER, D. E., in H. Sobotka, ed., "Monomolecular Layers," p. 107. American Association for the Advancement of Science, Washington, D. C., 1954.
9. PORTER, E. F., AND WYMAN, J. JR., *J. Am. Chem. Soc.* **60**, 1083 (1938).
10. TRURNIT, H. J., *Science* **111**, 1 (1950).
11. SINGER, S. J., *J. Biol. Chem.* **182**, 189 (1950).
12. Unpublished results with Dr. M. Demeny.
13. VON SYDOW, E., *Arkiv Kemi* **9**, 231 (1956).
14. HAVINGA, E., AND DE WAEL, J., *Chem. Weekblad* **34**, No. 43 (1943).

JOURNAL OF COLLOID SCIENCE **11,** 445–450 (1956)

PROTEIN INTERACTIONS WITH LECITHIN AND CEPHALIN MONOLAYERS

D. D. Eley and D. G. Hedge

University of Nottingham, England

Received April 16, 1956

Abstract

A surface trough has been used to study protein/lipid interactions by a development of the Schulman-Rideal injection technique. From the adsorption isotherms obtained the structure of the complexes has been determined. The lipids used—distearin, dipalmitoyl cephalin, and distearoyl lecithin—were synthetic materials, and the proteins were bovine plasma albumin and sheep insulin. The results indicated that the first sublayer of adsorbed protein combined with distearin and cephalin through the peptide bonds, probably by means of hydrogen bonding or ion-dipole association. With lecithin, however, the interaction appeared to be ionic. In all cases the indications were that a second layer of native protein was adsorbed.

Introduction

The fundamental importance of surfaces in biological systems has been stressed earlier in reviews by Danielli and Davies (1) and by Cheesman and Davies (2); indeed, it is evident that most of the reactions occurring in living organisms occur at surfaces. The structure of an artificial lipoprotein layer has been determined in a recent paper (3), and this was compared to the picture of the plasma membrane as put forward by Danielli and Davson (4). By the use of a modification of the injection technique of Schulman and Rideal (5), complexes between stearic acid and cholesterol and various proteins were shown to be stabilized by interaction—probably hydrogen bonding—between the polar groups of the lipids and the peptide bonds of the proteins. The thermodynamics of the adsorption process indicated further stabilization by cohesion between nonpolar side chains of the reacting molecules (6).

In the present work the study of lipid-protein interactions at the air/water interface has been extended by the use of more complex lipids, in order to determine the effect of introducing different groups into the lipid monolayer.

Experimental

Apparatus and Materials

Surface pressures were measured by the single horizontal wire torsion balance, accurate to 0.02 dyne/cm., used in the earlier work (3).

Crystallized bovine plasma albumin (BPA) was obtained from Armour Laboratories, and sheep insulin from Burroughs Wellcome & Co. Buffer solutions were prepared from A. R. reagents and water which had been distilled from alkaline permanganate. BPA solutions were made up in conductivity water and insulin in 0.01 *N* HCl, and they were discarded after one month.

The lipids used were α,α'-distearin, α,α'-dipalmitoyl cephalin, and α,β-distearoyl lecithin. Samples of the purified substances, prepared by synthesis, were presented by Dr. T. Malkin and Dr. T. H. Bevan, of the University of Bristol. They were dried over P_2O_5 *in vacuo* for 24 hours before use.

Procedure

Monolayers of the lipids were spread from chloroform-benzene solution using an Agla micrometer syringe. The method of following the interactions was similar to that described previously for the simpler lipids (3). Injection of BPA under distearin and dipalmitoyl cephalin was carried out using a 0.05 *M* acetate buffer of pH 4.8 as substrate; a 0.04 *M* phosphate buffer of pH 7.4 was used for the injection of BPA and insulin under distearoyl lecithin films. In all cases the ionic strength was made up to 0.15 with sodium chloride. Doty and Schulman (7) were unable to obtain adsorption of injected proteins by lecithin films using an initial surface pressure of 14 dyne/cm., but, in the present work, reduction of this quantity to 2 dyne/cm. allowed a considerable rise in surface pressure to be obtained, and this lower value was used throughout. The experiments were carried out at a room temperature of about 17°C.

RESULTS

The effect of varying the amount of protein injected on the increase in surface pressure, $\Delta\pi$, was demonstrated by plotting the two variables against each other. In order to show the amount of protein in relation to the amount of lipid spread, a second graph was drawn of $\Delta\pi$ versus the ratio of the number of protein molecules, n_p, to the number of lipid molecules, n_L. The latter relationship, for distearin and lecithin adsorption of BPA, is shown in Fig. 1. Cephalin/protein interactions followed a similar pattern. It is seen that the adsorption curves show the same characteristics as those obtained for cholesterol and stearic acid (3). The discontinuities in the isotherms can then be taken to indicate the completion of separate layers of protein, and the nature of the lipoprotein complex can be determined using the same method as was applied to the simpler lipids, by making the basic assumption that all the injected protein is adsorbed at the lipid surface.

The weights of protein required to complete one and two layers, and

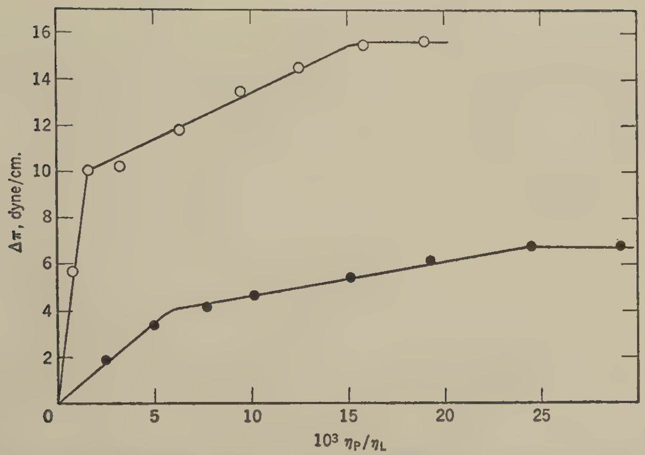

FIG. 1. The variation of surface pressure increase, $\Delta\pi$, with molecular ratio, n_p/n_L, of BPA to distearin (open circles) and lecithin (full circles).

TABLE I

Adsorption of BPA and Insulin by Lipid Monolayers

Lipid	Protein	No. of layers	n_L/n_p	Wt. of protein (*mg.*)	$\Delta\pi$ (dynes/cm.)
Distearin	BPA	1	625	0.01	10.0
	BPA	2	64	0.087	15.6
Cephalin	BPA	1	330	0.021	10.8
	BPA	2	84	0.063	14.0
Lecithin	BPA	1	160	0.023	4.1
	BPA	2	41	0.077	6.8
Lecithin	Insulin	1	28	0.024	16.3
	Insulin	2	7	0.073	18.4

TABLE II

Specific Areas of Adsorbed Proteins

Lipid	Protein	Specific area of protein ($m.^2/mg.$) 1st layer	2nd layer
Distearin	BPA	2.6	0.30
Cephalin	BPA	1.1	0.38
Lecithin	BPA	1.0	0.34
Lecithin	Insulin	1.0	0.36

the corresponding molecular ratios of lipid/protein, n_L/n_p, are shown in Table I. A knowledge of the weight of protein in each layer and the total surface area allows a calculation of the specific area of the protein to be carried out. The specific areas of the first and second sublayers are shown in Table II.

Discussion

An examination of the figures shown in Table I indicates marked differences between the behavior of distearin, cephalin, and lecithin. Whereas the ratios n_L/n_p for cholesterol and stearic acid (3) approximated to the number of amino acid residues in the protein—588 and 103 for BPA and insulin, respectively (8)—in the present work only the diglyceride shows this simple 1/1 ratio of peptide bond to lipid molecule for the first layer of protein. Complex formation by distearin may then be compared to that found with cholesterol, in which the hydroxyl group and the peptide bonds interact. Since in the first layer of protein only one group in the distearin takes part in the adsorption, the active center here is again the hydroxyl group. The absence of any ionic character in distearin points to a hydrogen bond mechanism, as with the simpler lipids.

A further point of similarity between distearin and cholesterol is apparent from the specific areas given in Table II, for the first layer of BPA under distearin has an area of 2.6 m.^{2}/mg., compared to 2.4 m.^{2}/mg. under cholesterol. This is due to the similar spacing of the hydroxyl groups, approximately at the corners of rectangles 10 A. by 4 A., in condensed films of both lipids. With the phospholipids, on the other hand, the specific areas of the first layers are constant at about 1 m.^{2}/mg., indicating an extent of surface denaturation similar to that found at the air/water interface. The second sublayer of protein has roughly the same area for all the lipids. Since the values are comparable with those obtained for stearic acid and cholesterol (3), this second layer would appear to consist of native protein.

Considering the first sublayer of BPA under dipalmitoyl cephalin, n_L/n_p is seen to be much smaller than for distearin. With allowance for the observation that, in all other cases, the ratio was somewhat larger than the number of amino acid residues in the molecule, the difference being attributed to an edge effect (3), the figure of 330 corresponds to half the number of residues in BPA. This indicates that each molecule of cephalin interacts with two peptide linkages in the protein.

In order to determine the particular groups in cephalin active in the adsorption process the results of the previous studies are considered. It is evident that the groups involved must be polar; furthermore, the distearin results show that the ester groupings take no part in the interaction. From this evidence combined with steric considerations it follows that the only two available groups are the phosphate and the amino groups. The protein is, then, arranged with one peptide bond under an amino group and the next under a phosphate group. This necessitates some reorientation of the ethanolamine residue, but the dimensional feasibility of this arrangement has been shown by molecular models. As to the type of bonding operative in this system, no definite conclusions can be drawn. Surface potential studies by Few and Schulman (9) have shown that, at pH 4.8, the amino group is fully charged and the phosphate group is partly charged. It would be possible, therefore, for strong hydrogen bonds to be formed between these two groups and two peptide adjacent bonds. On the other hand, ion-dipole association could occur between the two charged groups of cephalin and peptide bond dipoles, in a similar manner to that suggested by Pankhurst (10).

The difference in the behavior of the phospholipids from that of the simpler lipids is even more pronounced with lecithin, as the molecular ratio n_L/n_p for the first layer of BPA is only half that obtained for cephalin. With both insulin and BPA n_L/n_p is seen to be about one quarter of the total number of residues. Thus, if the interaction is of the same character as before, these results indicate that each lecithin molecule reacts with four peptide bonds. However, since lecithin differs from cephalin only in the substitution of three methyl groups for the hydrogen atoms of the amino group, there can be no more than two groups available for interaction with peptide bonds. The presence of these methyl groups rules out hydrogen bonding from the positive end of the molecule. A possible mechanism is ion-dipole association between the two charged groups of lecithin and two peptide bonds, there being two other peptide bonds not contributing to the interaction. However, the use of molecular models has indicated that the bulk of the choline residue renders this arrangement sterically unlikely.

In view of the evidence against the use of peptide bonds here the most likely mechanism seems to be ionic attraction. At pH 7.4 all the carboxyl groups in the protein will be fully charged, taking a pK of 3–4. According to Waugh (8) the maximum negative side-chain charge of BPA is 124, which is of the same order as the value of n_L/n_p for the first sublayer of BPA under lecithin. Similarly, the maximum negative charge of insulin (8) is 17, compared to 28 for the molecular ratio of the first layer of this protein. Although the discrepancies found here are rather large, the general indication is that the interaction here is between the positively charged groups of the lecithin film and the negatively charged groups of the protein. This agrees with the conclusions of Booij (11), who, in discussing the role of lecithin in the protoplasmic membrane, stated that only the negative groups of the protein are of importance for the complex relations with lecithin.

The biological implications of this work are evident when the complexes formed here are compared with the Danielli and Davson model of the plasma membrane (4). Previous work on lipoproteins led Dervichian (12) to conclude that the bonding is of an ionic character, nonionic lipids being included by means of van der Waals' lipid-lipid association. The present work on glyceride derivatives and the previous work on the simpler lipids seem to indicate that this is not the complete story, since complex formation between proteins and nonionic lipids is possible. Where bulky charged groups are present in the lipid, as in lecithin, however, ionic association predominates.

ACKNOWLEDGMENTS

The authors wish to express their thanks to the Department of Scientific and Industrial Research for a maintenance grant to D.G.H., and to Dr. T. Malkin and Dr. T. H. Bevan (University of Bristol) for the gift of the specimens used.

REFERENCES

1. DANIELLI, J. F., AND DAVIES, J. T., *Advances in Enzymol.* **11,** 35 (1951).
2. CHEESMAN, D. F., AND DAVIES, J. T., *Advances in Protein Chem.* **9,** 439 (1954).
3. ELEY, D. D., AND HEDGE, D. G., *Discussions Faraday Soc.* on Membrane Phenomena, April, 1956, to be published.
4. DANIELLI, J. F., AND DAVSON, H., "Permeability of Natural Membranes," p. 60. Cambridge Univ. Press, 1943.
5. SCHULMAN, J. H., AND RIDEAL, E. K., *Proc. Roy. Soc.* (*London*) **B122,** 29 (1937).
6. ELEY, D. D., AND HEDGE, D. G., to be published.
7. DOTY, P., AND SCHULMAN, J. H., *Discussions Faraday Soc.* **6,** 21 (1949).
8. WAUGH, D. F., *Advances in Protein Chem.* **9,** 325 (1954).
9. FEW, A. V., AND SCHULMAN, J. H., *Biochem. et Biophys. Acta* **10,** 302 (1953).
10. PANKHURST, K. G. A., "Surface Chemistry," p. 109. Butterworths, London, 1949.
11. BOOIJ, H. L., *Discussions Faraday Soc.* **6,** 150 (1949).
12. DERVICHIAN, D. G., *Discussions Faraday Soc.* **6,** 7 (1949).

JOURNAL OF COLLOID SCIENCE **11**, 451–470 (1956)

ACTIVITY OF TRYPSIN-LIPID COMPLEXES AT OIL/WATER INTERFACES

M. J. Fraser[1] **and J. H. Schulman**

Department of Colloid Science, University of Cambridge, England

Received May 14, 1956

ABSTRACT

Adsorption of trypsin at lipid-stabilized oil/water interfaces has been studied as a function of the nature of the interface. The adsorption of the enzyme, with corresponding changes in the activity expressed, is found to be related to the charge and nature of the lipid polar groups at the interface and to the charge and nature of the polar groups of the protein. Interactions between enzyme and lipid at the interface are paralleled in bulk with soluble lipid homologs. The loss in activity of the enzyme at the interfaces studied is thought to be due to a general structural unfolding of the molecule. Provided that the unfolding process has not gone too far, desorption of the surface enzyme can lead to partial recovery of activity.

Some of the problems involved in the study of the effect of changes in the general structure of the protein on the enzymatic activity by the present methods are discussed. It is concluded that a determination of whether or not these partially "denatured" enzymes can work at lower efficiency necessitates careful investigation of the kinetic and thermodynamic properties of the adsorbed, partially unfolded enzyme.

INTRODUCTION

The study undertaken here may be considered one approach to a much more general field of enquiry, namely, the expression of activity of enzymes *in vivo* (1–3). The turnover of substrate by an intracellular enzyme may be modified by many factors, for example, permeability barriers may limit the supply of substrate or the enzyme may be working at a suboptimal pH. On the other hand, its activity may be considerably altered by virtue of being combined, on a morphological level, with structured organelles such as the cell membrane, mitochondria, microsomes, or nuclear material, or, on a chemical level, by combination with lipids, polysaccharide, nucleic acid, specific inhibitors, or certain inorganic ions. Indeed, an activity of an intracellular enzyme may, even under certain conditions, be apparently completely masked (4). The cell physiologist, as opposed to the enzymologist, is interested, on both the chemical and morphological levels, in how these changing factors can be related to changes in the physiological state of the cell.

---

[1] 1851 Exhibition Scholar.

In the present investigation this approach to the problems of structure and function has been restricted to the chemical level in the study of the activity of enzymes adsorbed at various lipid interfaces. Two broad divisions of the problems, which may or may not be easily distinguishable in practice, immediately suggest themselves: combination of enzyme with lipid resulting in modification of the activity by direct changes in the active center or in modification of the activity by a general structural alteration of the molecule, indirectly affecting the active center. It is the latter physicochemical problem that is of most concern here. The questions arise: "What part does the overall structure of the protein play in the activity of an enzyme?" "Can partially 'denatured' enzymes work at lower efficiency?" "To what extent is the denaturation[2] reversible?" Information on both types of enzyme-lipid interactions from bulk studies can throw light on the interfacial problem. For example, the usual methods of following "denaturation," such as viscosity and solubility changes, increase in flow birefringence, and increase in available —SH groups and phenolic —OH groups (5), may be employed. Few studies have yet attempted to correlate these changes with losses in enzymatic activity, especially at interfaces, and it is difficult to know whether the effects are through direct blocking of the active center or general structural modification. To distinguish between these effects the choice of enzymes and lipids studied should be such that there is no interaction with the active center.

A previous study (6) of the heme-enzyme, catalase, showed that it could be adsorbed at various lipid-stabilized oil/water interfaces in states varying from fully active to inactive monolayers and multilayers, depending upon the lipid used and the conditions of adsorption employed. An emulsion technique (7) was used, choosing oil-soluble lipid stabilizers to minimize the interaction between the protein and lipid in the bulk aqueous phase. Adsorption of catalase (I.P. = 6.8) on to negatively charged oil/water interfaces, stabilized by anthracene-C_{21}-sulfonate, mixed lauryl phosphates, and cephalin, occurred readily at acid pH, whereas adsorption on to positively charged interfaces, stabilized by octadecatrimethyl ammonium bromide (C_{18}TAB) mixed with *n*-lauryl alcohol, cholesterol, and other straight-chain and cyclic alcohols, took place at alkaline pH. The negatively charged lipids were thought to interact chiefly with the $-NH_3^+$ groups on the protein, whereas the positively charged lipids interacted chiefly with the $—COO^-$ groups (6, 8, 9), there being probably little or no direct interaction with the active center, the heme iron. The interaction of long-chain sulfates and sulfonates with proteins at a pH acid to I.P. is very strong (9, 10). In bulk, 10^{-3} *M* sodium dodecyl sulfate at pH = 5.3

---

[2] Denaturation is taken in the sense of a nonproteolytic structural modification of the protein (5).

completely inactivates catalase, while well over 20 mg./m.^{2} of catalase adsorb on to the anthracene-C_{21}-sulfonate–stabilized oil/water interface, the inner 10 mg./m.^{2} being completely and irreversibly inactivated. The specific area of a fully unfolded protein monolayer at a clean air/water interface is $\sim$1.0 m.^{2}/mg., while at a clean oil/water interface it is $\sim$1.8 m.^{2}/mg. (11); thus on the sulfonate-stabilized interface we have something like 8–10 layers of fully unfolded protein very tightly bound with no recovery of catalase activity on desorption, on top of which are many layers of only partially unfolded protein. These exhibit more and more activity as one moves from the interface, and from these more and more activity may be recovered on desorption of the enzyme.

Adsorption of catalase on to oil/water interfaces stabilized with the long-chain phosphates, which have less effect on catalase activity in bulk, results in less uptake of the enzyme, diffuse monolayers only being formed. There is correspondingly less reduction in activity. The same holds for the phospholipid cephalin, where the charged groups responsible for adsorption are also phosphates. In both cases there is a partial recovery of activity on desorption of the enzyme from the interface.

The adsorption of catalase on to the positively charged C_{18}TAB interface may be compared with the action of the soluble dodecyl trimethyl ammonium bromide (DTAB) in bulk, which is weak (12). Here only small amounts of enzyme adsorb with little or no reduction in activity and nearly complete recovery of activity when the enzyme is desorbed. Here the monolayers are diffuse and comprised of "native" or only slightly unfolded protein.

Where unfolding of the surface enzyme molecules was thought to occur with loss of activity, it was found that the activation energy (μ) for the enzyme-substrate reaction became progressively higher, and the μ values for the surface enzyme were all higher than those in bulk. Desorption from the cephalin-stabilized interface led to a return of the μ to its bulk value (6).

To sum up then, the loss in activity of the enzyme when it was adsorbed at an interface was correlated with the degree of unfolding of the protein. The unfolding at lipid-stabilized interfaces was brought about chiefly by polar group interaction, whereas at the air/water and oil/water interfaces the unfolding was due to interaction of nonpolar groups. Provided that the unfolding process did not go to completion, as it did at the clean air/water and oil/water interfaces, desorption of the enzyme from the interface resulted in partial to complete restoration of activity.

It was considered of great interest to study the adsorption on to these oil/water interfaces of another enzyme without a prosthetic group and with a very different chemical function. The choice of trypsin for this study has many advantages. Trypsin may be prepared in a fairly pure form (13). It is considered to be a very stable enzyme under conditions where appreciable autolysis does not occur and is able to survive precipitation by trichloroacetic acid (14, 15). Also, Northrop (16) reports that it can undergo reversible heat denaturation. It is a protein of small molecular weight (14) (17,000) having a very high I.P. (17) (∼11.0) and contains large amounts of lysine and arginine which give rise to many end $—NH_2$ groups (17) in the protein. Its active center is thought to involve an uncharged imidazole group (15) (pK = 6.25 at 25°C.) and it is not thought that there are any $—NH_3^+$ groups nearby (18). Thus although this study is most likely to be restricted to studying the adsorption of trypsin on to negative surfaces, since it is positively charged over its entire range of activity (pH 5–10) (15, 19), one is not likely to obtain direct blocking of the active center by long-chain sulfonate, sulfate, phosphate, or fatty acid anions. These react with the many charged $—NH_3^+$ groups present. The discovery of Schwert *et al.* (20) that trypsin catalyzes the hydrolysis of arginine and lysine esters enables one to use a very simple substrate to follow its activity. Thus instead of following the protease activity of trypsin using casein or hemoglobin as substrate, one may measure its esterase activity using benzoyl arginine ethyl ester (BAEE) as substrate, greatly simplifying the interpretation of the results.

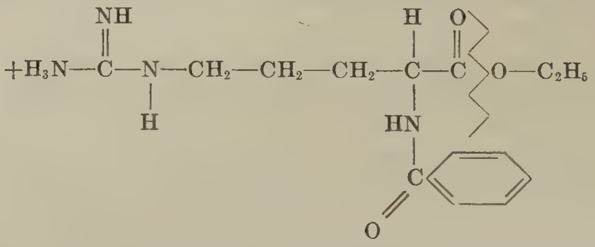

Benzoylarginineethylester (BAEE) showing where the hydrolysis by trypsin takes place

Experimental

Materials

1. The trypsin used throughout these experiments was taken from a stock solution of the redissolved trichloroacetic acid precipitate described by Northrop, Kunitz, and Herriott (13). This had been well dialyzed against 0.01 *M* HCl and stored in a refrigerator. The enzyme gave the same activity under standard conditions over a period of months. Two different preparations of the enzyme were used.

2. The benzoyl arginine ethyl ester (BAEE) was prepared by the method of Bergmann, Fruton, and Pollok (21).

3. All emulsions were made with pure Nujol as the oil phase. Most of the stabilizers have been described elsewhere (6). Very pure samples of synthetic and natural sodium taurocholate and sodium cholate prepared by E. Stenhagen (Uppsala) were used. A sample of egg phospholipid containing considerable lecithin was aslo used on which no further attempt at purification was made.

Methods

1. The preparation of emulsions stabilized by anthracene-C_{21}-sulfonate, lauryl phosphate, C_{18}TAB-*n*-lauryl alcohol, and C_{18}TAB-cholesterol has been described elsewhere (6). The preparation of oleic acid-glyceryl monooleate and oleic acid-glyceryl monooleate-bile salt emulsions is described by Frazer *et al.* (26). All emulsions, other than that stabilized with C_{18}TAB and mixtures, were examined in a medium of 0.1 *M* NaCl, which was 0.01 *M* in NaH_2PO_4. The pH was adjusted to the required value in each case with small amounts of strong NaOH or HCl. The C_{18}TAB-stabilized emulsions were made up in 0.1 *M* NaCl, which was 0.01 *M* in NH_4Cl, for phosphate interacts strongly with the trimethyl ammonium ion (22). When the suspension of emulsion was adjusted in pH the required amount of trypsin was added for adsorption. In most cases the extent of adsorption could be measured by centrifuging up the oil droplets and determining the activity remaining in the subnatant. Where 100% adsorption occurred the activity of the surface enzyme was easily determined on the suspension (6).

Fine suspensions of cholesterol (saturated solution) and of egg phospholipid were prepared by pipetting 2 ml. of petroleum ether (b.p. 30–60°C.) solution (0.14 g. phospholipid/ml.) into 40 ml. of warm (~45°C.) saline buffer and shaking vigorously for 5–10 minutes.

2. Assay of trypsin activity, measuring the rate of hydrolysis of BAEE, has been described previously (15). All measurements except where stated were made at room temperature (18–21°C.), and during any group of measurements the temperature did not vary more than 0.5°C. The substrate concentration used in every case was 3×10^{-3} *M* with respect to BAEE, well above the K_m value of 1.0×10^{-5} *M*. All activities were measured in 0.1 *M* NaCl, which is 0.01 *M* in phosphate or ammonium ion as above.

3. Microscopic electrophoretic mobility measurements on the emulsion particles in the presence and absence of trypsin were made over a wide range of pH in 0.1 *M* NaCl, which is 0.01 *M* in phosphate or ammonium ion using an Abramson cell (23–25). Measurements were made at room temperature and the potential applied to the tube was 110 v. Each point represented in the following curves is the average of 10–15 readings of the movement of different particles in the field. A mobility of 10 "units" in the curves presented corresponds to *ca.* 4×10^{-5} cm./sec./v./cm.

RESULTS

1. Interactions with Sulfates and Sulfonates

In Fig. 1 the effect of small concentrations of sodium dodecyl sulfate (S.D.S.) on trypsin esterase activity in bulk over the pH range 5.0–9.5 in 0.1 *M* NaCl plus 0.01 *M* phosphate is shown. Activities are not measured in the strong buffering range of phosphate (pH ~6.2–7.2), as the measurements by the method used become inaccurate. At pH = 5.0 it is seen that concentrations of S.D.S. as low as 1.7×10^{-3} *M* completely inactivate trypsin, whereas even at pH = 9.5, where the enzyme still bears a high net positive charge, the activity can be reduced to as low as 13% by 6.9×10^{-3} *M* S.D.S. The activation by low concentrations of S.D.S. is irreversible, and no activity is regained on raising the pH. Bulk concentrations of the polycyclic sulfonate, sodium taurocholate (bile salt), up to 1.2×10^{-2} *M* do not affect trypsin esterase activity at pH = 8.0. Three different samples of the compound were used, a crude natural preparation, a chromatographically purified natural preparation, and a pure synthetic preparation.

Saturated solutions of the aromatic sulfonates methyl orange and Congo red in 0.1 *M* NaCl + 0.01 *M* phosphate, pH = 8.0, also had no effect on trypsin esterase activity.

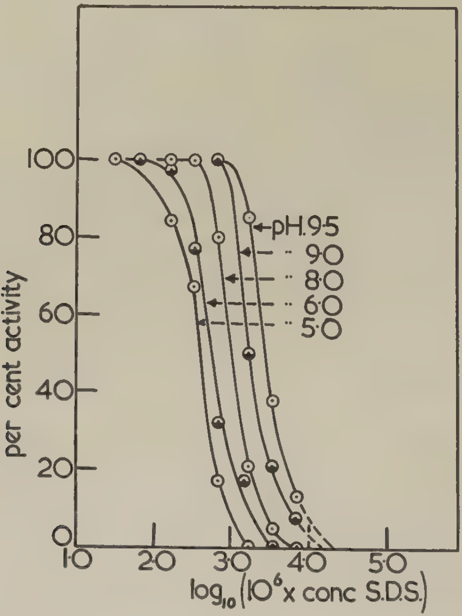

FIG. 1. Effect of S.D.S. on trypsin esterase activity in 0.1 *M* NaCl + 0.01 *M* phosphate over pH range 5.0–9.5.

Concentrations of trypsin giving 10–20 mg. protein per square meter (m.^{2}) of an anthracene-C_{21}-sulfonate–stabilized emulsion cause immediate flocculation of the emulsion at pH = 4.0 and below. Under these conditions all the enzyme was adsorbed on to the interface, as the clear subnatant brought to pH = 8.0 had no activity. The flocculation time is greatly lengthened if the emulsion is much diluted, and if diluted ~100-fold (from say 0.4 m.^{2}/ml.) there is no apparent flocculation within several hours but floccules may be seen microscopically, as was found in the process of making mobility measurements (see below). At concentrations of trypsin below approximately 8–10 mg./m.^{2} flocculation did not occur, and at pH values above 4.0 there was no flocculation in the presence of "excess" protein ($>$10 mg./m.^{2}).

In Table I is shown the effect of pH, time of adsorption, and ratio of protein to surface on the activity of trypsin esterase in the presence of the anthracene-C_{21}-sulfonate–stabilized emulsion. Where the adsorption is carried out beyond the range of measurable activity, i.e., below pH = 5.0, the samples are returned to the optimum pH = 8.0 and the activity recovered is recorded. All activities are reported as percentages of the bulk controls at any given pH. In general, the loss in activity increases with decreasing pH, with time allowed for adsorption before the activity measurement is begun, and with increasing available surface area. Throughout all activity measurements the rates of hydrolysis of BAEE were linear with time, some being measured over a period of as much as 10–20 minutes. The activities usually dealt with (in range 1.0–10.0 mg./m.^{2}) are thus more stable in time than the measurements made at pH = 8.0 at a ratio of protein to surface of 0.4 mg./m.^{2} would seem to indicate (see measurements made at 1.7 mg./m.^{2}). Thus, 2 minutes was chosen as the standard time of adsorption, and most figures presented in Table I are averages of duplicates agreeing to within ~7%. Attempts at recovering activity by shifting the pH of adsorption to a more alkaline value for measurement of activity show that once the activity has been lost completely (in practice <2–3%, the error of measurement), it cannot be recovered; if only partially lost, some recovery is possible.

The adsorption of trypsin on to oil droplets stabilized with anthracene-C_{21}-sulfonate was also followed by observing the change in electrophoretic mobility of the particles in the presence of protein by the microscopic technique of Abramson (23, 25). The change in mobility of the particles with increasing ratios of protein to surface at pH = 4.0 is shown in Fig. 2(*A*). The particles have initially a high negative charge which is reduced to zero when the surface concentration of trypsin is ~10 mg./m.^{2}. It is in this region where flocculation of the emulsion occurs. On addition of further protein more is adsorbed and the particles become positively charged reaching a constant value, probably approaching the mobility of the pro-

TABLE I

Trypsin Esterase Activity in the Presence of an Anthracene-C_{21}-Sulfonate–Stabilized Emulsion in 0.1M NaCl + 0.01M Phosphate. Effects of pH, Time of Adsorption, and Ratio of Protein/Surface Are Shown.

pH of adsorption	pH of activity measurement	Time of adsorption (*mins.*)	Ratio of protein/surface (*mg./m.^{2}*)	Activity (*% of control*)
9.5	9.5	2	1.0	35%
9.0	9.0	2	1.0	37%
8.5	8.5	2	1.0	43%
8.0	8.0	2	1.0	42%
7.5	7.5	2	1.0	39%
6.0	6.0	2	1.0	<3%
6.0	6.0	2	1.6	<3%
6.0	6.0	2	3.3	<3%
6.0	6.0	2	5.0	32%
6.0	6.0	2	10.0	66%
5.0	5.0	2	1.0	<3%
5.0	5.0	2	5.0	<3%
5.0	5.0	2	8.0	13%
5.0	5.0	2	10.0	32%
8.0	8.0[a]	2	1.0	47%
6.0	6.0[a]	2	1.0	58%
5.0	8.3	2	1.0	<3%
5.0	8.3	2	5.0	<3%
5.0	8.3	2	8.0	27%
5.0	8.3	2	10.0	60%
4.0	8.0	2	1.0	<3%
4.0	8.0	2	5.0	<3%
4.0	8.0	2	10.0	<3%
8.0	8.0	2	0.04	<3%
8.0	8.0	1	0.4	64%
8.0	8.0	5	0.4	11%
8.0	8.0	10	0.4	10%
8.0	8.0	60	0.4	<2%
8.0	8.0	1	1.7	55%
8.0	8.0	10	1.7	25%
8.0	8.0	20	1.7	13%
8.0	8.0	60	1.7	9%

[a] 1.6×10^{-3} *M* DTAB added.

tein itself in bulk at this pH. It is known that all the protein added is adsorbed on to the surface up to a concentration of at least 25 mg./m.^{2} The effect of pH on adsorption of trypsin on to this sulfonate-stabilized interface is readily shown in Fig. 3, where the mobilities of the emulsion particles in the presence (*B*) and absence (*A*) of 10 mg./m.^{2} of trypsin are shown. The mobility of the particles increases slowly with increasing pH. If the lowering of the mobility of the particle at any given pH is plotted against the electrophoretic mobility of trypsin in bulk taken from the data of Duke, Bier, and Nord (19) (see inset, Fig. 3), a straight-line

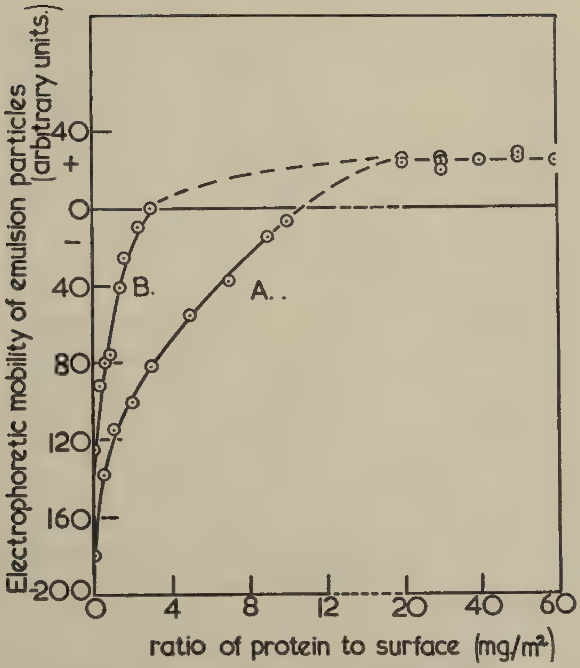

FIG. 2. Electrophoretic mobility of particles stabilized with anthracene-C_{21}-sulfonate (*A*) and lauryl phosphate (*B*) in the presence of increasing amounts of trypsin. Medium of 0.1 *M* NaCl + 0.01 *M* phosphate adjusted to pH = 4.0.

relationship is seen to hold. This shows that the adsorption of trypsin on to this interface is chiefly related to the net charge on the protein.

Two experiments were done to determine the activation energy for the surface enzyme-BAEE hydrolysis with the sulfonate system. The conditions used were adsorption (0.6 mg./m.²) at pH = 8.0 in 0.1 *M* NaCl + 0.01 *M* phosphate, where at the room temperature of 20°C. the activity of the adsorbed enzyme is 45% of the control. Measurements were made over the temperature range 18–40°C. The μ value for the control (*cf.* ref. 15) was 10,000 cal./mole, whereas the values for the surface enzyme were 8900 and 13,900 cal./mole. The difference between surface and bulk values is thus not significant. Linear Arrhenius plots for the surface enzyme were obtained up to 34°C., but above this temperature the activity fell off very rapidly, apparently because of drastic heat inactivation on the surface.

2. *Interactions with Phosphates*

With emulsions stabilized with mixed lauryl phosphates (chiefly primary and secondary phosphates) there is the possibility that some interaction with trypsin may occur in bulk, especially with disodium lauryl phos-

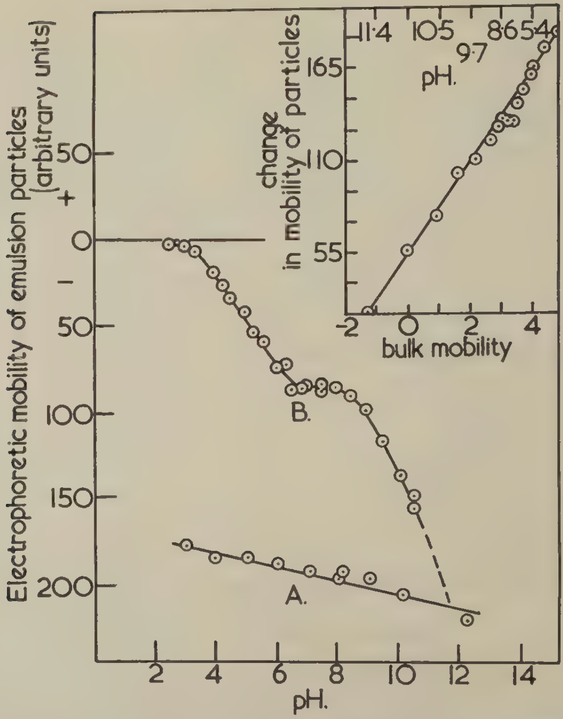

FIG. 3. Effect of pH on the electrophoretic mobility of anthracene-C_{21}-sulfonate-stabilized Nujol particles in 0.1 *M* NaCl + 0.01 *M* phosphate in the absence (*A*) and presence (*B*) of 10 mg./m.^{2} of trypsin. The inset shows a plot of the change in the mobility of emulsion particles due to adsorption of trypsin against the mobility of trypsin in bulk taken from the data of Duke, Bier, and Nord (19).

phate. Under the conditions employed for studying the activity of the adsorbed enzyme there is not likely to have been appreciable interaction in the bulk phase, for when the oil phase was removed by centrifugation the clear subnatant had no effect on the activity of trypsin brought from pH = 4.0 to pH = 8.0 for testing. There was also no effect when twice the amount of emulsion was tested for "free phosphate," but with ten times the usual amount the trypsin esterase activity was reduced to 60% of that of the control. The possibility that a considerable part of this reduction was due to emulsion particles still present in the subnatant cannot be excluded, as the separation of the two phases became more difficult with large amounts of emulsion. At pH = 4.0 flocculation of the emulsion occurred when the ratio of protein to surface reached ~4 mg./m.^{2}, and it was found that 99.5%, 90%, 80%, and 62% of the enzyme was adsorbed (the subnatants were tested at pH = 8.0) at ratios of 4, 5, 7.5, and 10

TABLE II

Trypsin Esterase Activity in the Presence of Lauryl Phosphate-Stabilized Emulsion in 0.1M NaCl + 0.01M Phosphate. Standard Time of Adsorption of 2 Mins. Allowed. Effects of pH and Ratio of Protein/Surface are Shown.

pH of adsorption	pH of activity measurement	Ratio of protein/ surface (*mg./m.*^{2})	Activity (*% of control*)
8.0	8.0	0.25	~0%
8.0	8.0	0.50	27%
8.0	8.0	0.75	41%
8.0	8.0	1.00	55%
8.0	8.0	2.00	66%
4.0	8.0	0.25	~0%
4.0	8.0	0.50	14%
4.0	8.0	0.75	20%
4.0	8.0	1.00	38%
4.0	8.0	2.00	—

mg./m.^{2}. Thus about 4 mg. of trypsin was adsorbed readily per square meter at pH = 4.0 in 0.1 *M* NaCl plus 0.01 *M* phosphate.

The data presented in Table II show the effects on trypsin esterase activity of adsorption at pH's = 4.0 and 8.0. As on the sulfonate-stabilized interface more activity is lost when larger areas are available for adsorption and unfolding. Unlike adsorption on the sulfonate interface a considerable amount of activity may be recovered at pH = 8.0 after adsorption at pH = 4.0. That the lauryl phosphate-stabilized oil/water interface will take up 3–4 mg./m.^{2} of trypsin at pH = 4.0 is confirmed by (*B*) presented in Fig. 2, showing the change in electrophoretic mobility of the emulsion particles in the presence of increasing amounts of protein. In the presence of a great excess of protein the mobility of the particles reaches the same value as that of the sulfonate-stabilized particles in the presence of excess protein, probably approaching that of the bulk trypsin at this pH.

Electrophoretic mobility measurements on emulsion particles stabilized with mixed lauryl phosphates presented in Fig. 4 show: (*1*) that the mobility of the emulsion particles alone increases slowly with increasing pH (*A*), as with the sulfonate; (*2*) the mobilities here are all lower in value at the same pH; and (*3*) the adsorption of trypsin at different pH's on to the surface takes roughly the same form (*B*) as that on the sulfonate-stabilized interface. Mobilities below pH = 4.0 are positive because more than 3 mg./m.^{2} are adsorbed, the measurement being carried out in the presence of "excess" protein (~10 mg./m.^{2}). The inset to Fig. 4 shows the plot of the change in the mobility of the emulsion particles due to the adsorption of trypsin against the bulk mobility of trypsin. A linear relationship is shown in pH region 4.0–9.0, but above this pH the lowering due to adsorption of protein is higher than expected on the basis of the net charge on the trypsin.

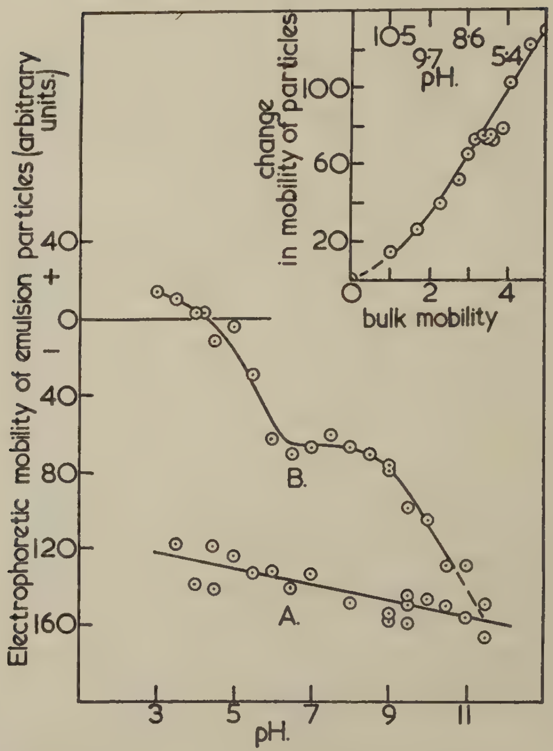

Fig. 4. Effect of pH on the electrophoretic mobility of lauryl phosphate-stabilized Nujol particles in 0.1 M NaCl + 0.01 M phosphate in the absence (A) and presence (B) of 10 mg./m.^{2} of trypsin. The inset shows a plot of the change in the mobility of emulsion particles due to adsorption of trypsin against the mobility of trypsin in bulk taken from the data of Duke, Bier, and Nord (19).

3. Interactions with Fatty Acid

Concentrations of sodium oleate of 1.6×10^{-3} M in 0.1 M NaCl + 0.01 M phosphate reduced the activity of trypsin to $<12\%$, 42%, 51%, 59%, and 53% of the controls at pH's 6.0, 7.5, 8.0, 8.5, and 9.0, respectively. The loss of activity at pH = 6.0 is only partially reversible, for if the pH of the sample is brought to 8.0 the residual activity is only 29% that of the control, instead of the expected 51%. All these samples showed a slight turbidity, the sodium oleate (partially oleic acid at pH = 6.0) probably being above its micelle point under these conditions. A thick emulsion stabilized by a mixture of oleic acid and glyceryl monooleate (26) is quite stable at alkaline pH where the fatty acid is fully ionized. At acid pH, however, inversion of the emulsion will occur if enough oil phase is present, or breaking, if there is a predominance of the aqueous phase. The breaking time may be considerably lengthened by using much-diluted emulsion.

Under the conditions used here to measure activities of trypsin in the presence of emulsion (above pH = 6.0) electrophoretic mobilities of the particles in 0.1 *M* NaCl + 0.01 *M* phosphate no breaking was observed to occur. Measurements on any sample were not made longer than 20 minutes.

Trypsin was not effective in flocculating the dilute fatty acid-stabilized emulsions at any pH even over long periods of time. The particles that did float up at acid pH showed as extensive breaking as in controls without trypsin. The data presented in Table III show the effect of pH, time of adsorption, and ratio of protein to surface on the activity of trypsin esterase in the presence of the oleic acid-glyceryl monooleate–stabilized emulsion. With respect to the effects of time of adsorption and surface available for adsorption (ratio of protein/surface large), the results are qualitatively the same as those found for adsorption on to the sulfonate- and phosphate-stabilized interfaces. As these quantities increase in value the losses in activity become greater. With respect to pH, however, the results are totally different. Loss in activity above pH = 8.0 is not appreciable; the loss seems to be greatest in the region of pH = 6.7 and is partially reversible on changing the pH to above 8.0. At pH = 6.0 the loss is not as great as at pH = 6.7, under the same conditions. The measurements made with this system are much more variable than with the

TABLE III

Trypsin Esterase Activity in the Presence of Oleic Acid-Glyceryl Monooleate–Stabilized Emulsion in 0.1M NaCl + 0.01M Phosphate. Effects of pH, Time of Adsorption, and Ratio of Protein/Surface are Shown.

pH of adsorption	pH of activity measurement	Time of adsorption (*mins.*)	Ratio of protein/ surface (*mg./m.*^{2})	Activity (*% of control*)
8.3	8.3	2	0.83	98%
6.7	8.3	2	0.83	83%
8.7	8.7	2	0.65	85%
7.5	7.5	2	0.65	110%
7.0	7.0	2	0.65	59%
6.7	6.7	2	0.65	<8%
6.2	6.2	2	0.65	66%
8.3	8.3	2	0.04	90%
7.5	7.5	2	0.04	62%
6.7	8.3	2	0.04	50%
6.7	8.3[a]	5	0.04	37%
6.7	8.3[a]	5	0.04	37%
6.0	8.3	5	0.04	64%
6.2	6.2	5	0.08	32%
6.2	6.2	5	0.16	36%
6.6	6.6	5	0.08	15%

[a] Experiments on 2 different days.

sulfonate and phosphate systems, and these activity values presented are probably reliable only to within ±10%.

More light is thrown on these results when the electrophoretic mobilities of the emulsion particles are examined over a wide pH range in the presence and absence of excess trypsin (~5 mg./m.^{2}). The results presented in Fig. 5 show that, as expected, the mobility of the emulsion particles alone (*A*) drops from a large negative value at alkaline pH to zero at very acid pH, showing an apparent surface pK $\simeq$ 5.5. Above pH = 8.0 no trypsin adsorbed on to this interface, but just below this in the region 6.2–7.2 there appeared to be a strong adsorption (*B*), falling off to approximately zero also at lower pH values where the surface loses

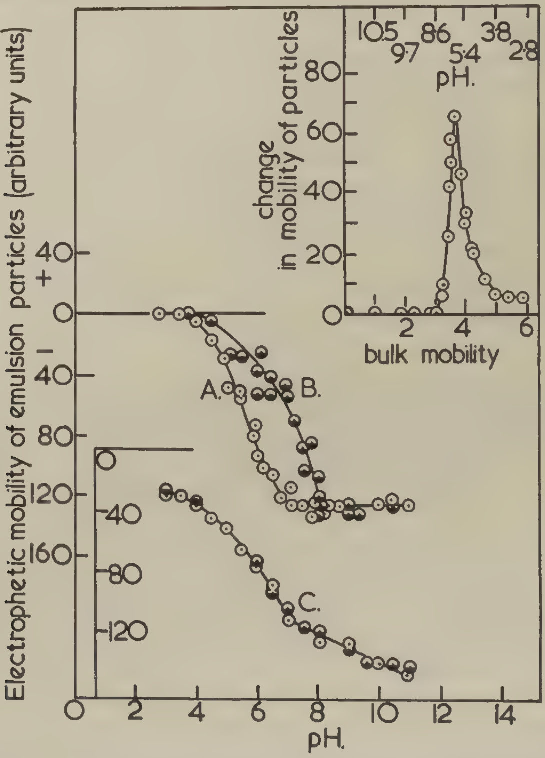

FIG. 5. Effect of pH on the electrophoretic mobility of oleic acid-glyceryl monooleate–stabilized Nujol particles in 0.1 *M* NaCl + 0.01 *M* phosphate in the absence (*A*) and presence (*B*) of 10 mg./m.^{2} of trypsin. The inset shows a plot of the change in mobility of emulsion particles due to adsorption of trypsin against the mobility of trypsin in bulk taken from the data of Duke, Bier, and Nord (19). Curve (*C*) shows the effect of pH on the electrophoretic mobility of oleic acid-glyceryl monooleate-sodium taurocholate–stabilized particles in the absence (open circles) and presence (half circles) of trypsin under the same conditions. Much taurocholate remains in the bulk phase.

its charge. A plot of the change of electrophoretic mobility of the particles that occurs when trypsin is added at any given pH (a measure of the amount of adsorption of the protein) against the electrophoretic mobility of trypsin in bulk (which is proportional to the net charge on the protein at a given pH) thus shows the very curious curve presented in the inset to Fig. 5.

Attempts were made also to study the adsorption on to an oil/water interface stabilized with oleic acid, glyceryl monooleate, and bile salt (sodium taurocholate) by following the changes in electrophoretic mobility of the emulsion particles at various pH's. As may be seen in Fig. 5 (*C*) there was no apparent adsorption of protein (over the whole pH range), probably because of the appreciable interaction of the relatively soluble bile salt with the trypsin in bulk. The curve is seen to show the properties of both fatty acid and sulfonate. Above pH = 8.0, where all the fatty acid is ionized, there is a slow increase in mobility with increasing pH, as with the sulfonate system, and below pH = 8.0 the fatty acid is titrated but not to zero mobility because of the taurocholate present.

4. Examination of Other Systems

Repeated attempts were made in order to determine whether or not trypsin adsorbed on to oil/water interfaces stabilized with C_{18}TAB + *n*-lauryl alcohol and C_{18}TAB + cholesterol at pH = 8.0 in 0.1 *M* NaCl + 0.01 *M* NH_4^+. With the former system the electrophoretic mobilities of the particles were measured on three samples and found to be +93, +90, and +93 units. When trypsin was added in ratios 8.3 and 6.6 mg./m.^{2} of surface the mobility was usually lowered slightly but erratically to about +70 units, with some samples even showing flocculation (zero mobility). Hocking (24, 25) has also found considerable variability in mobility measurements on similar systems. The same was found to be the case for the C_{18}TAB-cholesterol system, where the mobilities at pH = 8.0 (+85 and +83 units) were lowered to +60–63 units. It is thought that the lowerings were due to contamination by phosphate, with which trimethyl ammonium bromide compounds strongly interact, as no adsorption (within 2% error) occurred when the oil phase was separated off by centrifugation and the subnatant tested for activity. In these experiments excess surface was used. Also, there was no effect on trypsin esterase activity by these systems over the pH range 6.0–9.0.

There was found to be no adsorption of trypsin on to uncharged (zero mobility) particles of cholesterol or egg phospholipid particles as tested on fine suspensions of these substances at pH's 4.0 and 8.0 in 0.1 *M* NaCl + 0.01 *M* phosphate by electrophoretic mobility measurements and centrifugation experiments. Also there was no observed effect on trypsin esterase activity at pH = 8.0 by these suspensions.

5. *Adsorption of Trypsin at the Air/Water and Oil/Water Interfaces*

In confirmation of previous observations (see 27, 28) trypsin unfolded at the clean air/water and oil/water interfaces loses its activity completely and irreversibly. Monolayers of trypsin were spread at the air/water interface on 0.1 *M* NaCl + 0.01 *M* phosphate at pH = 8.0 for 20 minutes. The films were then collapsed and the protein was removed as fairly robust fibers, and added to saline phosphate at pH = 2.5, in which they appeared to redissolve. When 4 times the usual amount of protein was collected and tested for activity at pH = 8.0 no activity whatever could be detected.

Trypsin was inactivated at the oil/water interface by shaking 20 times the normal amount of trypsin usually used in an activity measurement in saline phosphate at pH = 8.0 with increasing amounts of a hydrocarbon fraction (b.p. 125–155°C., chiefly nonane) until droplets that were unstably emulsified suddenly coalesced. No activity whatever was found to remain, the method being capable of detecting 0.5% of the original activity present. A control sample, shaken without hydrocarbon, did not lose any detectable amount of activity on this treatment and very little froth formation occurred.

Discussion

In almost every case investigated it is seen that the adsorption of trypsin on to lipid-stabilized oil/water interfaces is a function of the charge on the interface. No detectable adsorption occurs when the protein and interface are of the same charge (C_{18}TAB-*n* lauryl alcohol or C_{18}TAB cholesterol interfaces) or of zero charge (cholesterol or egg phospholipid particles). Adsorption occurs best on the negatively charged sulfonate- and phosphate-stabilized interfaces, and the fatty acid ester–stabilized interface below pH = 8.0. With the negative interfaces the amount of adsorption not only is proportional to the charge on the interface but is a function of the nature of the polar groups with which the protein interacts. At pH = 4.0, for example, the sulfonate-stabilized particles (whose mobility is −180 unit as compared with −130 unit of the phosphate-stabilized particles) can take up over 25 mg. trypsin/m.^{2}, whereas the phosphate-stabilized particles take up only 4 mg. trypsin/m.^{2} at pH = 6.7 and the fatty acid-stabilized particles (mobility of −110 unit) take up less than 0.5 mg./m.^{2}. That the nature of the interface is important is also seen in the anomalous position of the fatty acid-stabilized interface above pH = 8.0. Here no trypsin is adsorbed, though there is bulk interaction with oleate anions. Appreciable adsorption occurs only in the region pH = 6.2–7.2 where the fatty acid is 72–95% ionized, i.e., about 20% of the groups are in the undissociated form. Whether the unionized—COOH groups act in the adsorption by H-bonding with polar groups in the protein or act to space the charged fatty acid groups on the interface is not known. A "spacer" molecule (6), however, already exists at this interface in the form of the neutral glyceryl monooleate. If any extensive adsorption of trypsin on to this interface occurred at $pH = 8.0$ or above it would be expected that the intestinal tryptic activity would be greatly inhibited, much the same as intestinal lipase activity is inhibited when sodium cetyl sulfate is fed to rats (29).

Where the charge and composition of the interface remain relatively constant over a wide pH range (on the sulfonate- and phosphate-stabilized particles) another important factor in the adsorption is seen to be the charge on the protein. The decrease in mobility of the particles, taken to be proportional to the amount of protein adsorbed, was found to be linearly proportional to the bulk mobility of the protein, which is a measure of its net charge. In the case of adsorption on the phosphate interface at alkaline pH there is apparently more protein adsorbed than expected, and this may be accounted for by the strong interaction between phosphate and amine groups (30, 31).

In all cases studied the losses in enzymatic activity are seen to parallel the strength of adsorption, and with the strongest adsorption (e.g., on to the sulfonate and phosphate interfaces at $pH < 5.0$) there is complete and irreversible loss in trypsin esterase activity. With weaker adsorption the losses in activity are less, and the recoveries on desorption or partial desorption are correspondingly greater. Most of these interactions with sulfonate, phosphate, and fatty acid are considered to be with the $—NH_3^+$ groups of trypsin, which are not thought to be involved in the active center (18), uncharged imidazole group (15). Further evidence of this fact may be stated in the reports that acetylation (32) of the $—NH_3^+$ groups or blocking with formaldehyde (33) does not affect trypsin esterase activity. Also the long-chain polycyclic sulfonate, sodium taurocholate (bile salt), which was found here to interact with trypsin in bulk to prevent its adsorption on to the interface stabilized with oleic acid, glyceryl monooleate, and sodium taurocholate, has no effect on trypsin esterase activity up to concentrations of $\sim 10^{-2}\ M$, nor do appreciable concentrations of the aromatic sulfonates, methyl orange and Congo red. These molecules may bind the exposed $—NH_3^+$ groups on the trypsin surface without opening up the molecule as the long-chain sulfonates do (10), but probably do not bind on the active center. As a result of these considerations, the loss in enzymatic activity that occurs when trypsin adsorbs on to the interfaces stabilized with sulfonate, phosphate, or fatty acid, is thought to be due to the same interactions that occur in the adsorption of the protein at these oil/water interfaces, and to be mediated through a general structural unfolding of the molecule. If the unfolding process does not proceed too far then activity may be restored under favorable circumstances.

The action of S.D.S. in bulk on trypsin esterase activity parallels the adsorption on to the anthracene-C_{21}-sulfonate–stabilized interface. Williams *et al.* (34) report that the critical micelle concentration of S.D.S. in 0.1 M NaCl is 1.6×10^{-3} M, above which micelles of molecular weight 32,400 (112 molecules of S.D.S.) form, and this is probably little affected by pH changes. Appreciable inactivation of the enzyme apparently occurs only above the micelle point (Fig. 1). The effect of increasing pH is to weaken the interaction of the enzyme with the micelles, just as with the sulfonate-stabilized particles (see below and Table I, Fig. 3). The concentration of protein present is small compared to the concentration of S.D.S., being of the order of 0.012 mg./ml. ($\sim 7 \times 10^{-7}$ M). Wills has previously suggested that the loss of many enzyme activities in the presence of S.D.S. is due to adsorption on to micelles. The inhibition of trypsin esterase activity does not follow a normal type of competitive or noncompetitive inhibition, as shown by plotting the curves in Fig. 1 in the form: reciprocal of activity vs. conc. inhibitor. A linear plot is usually obtained, whereas the data of Fig. 1 give a hyperbolic curve.

It also appears that the interaction of trypsin with oleate micelles leads to loss of esterase activity even above pH = 8.0, where no adsorption on to oleate-glyceryl monooleate–stabilized interface takes place. At low pH, where the fatty acid is in the undissociated form, there is apparently no adsorption on to this interface, contrary to what occurs at a hydrocarbon oil/water interface. Adsorption of proteins on oleic acid droplets, however, apparently does occur in 0.01–0.05% protein solutions (35).

On the basis of the present data it cannot be stated unequivocally that the partial activity of the surface trypsin is exhibited by partially unfolded protein. It is not known whether the loss in activity of a "native" trypsin molecule through unfolding parallels the general structural opening up of the protein, e.g., as measured in bulk by viscosity and solubility changes, birefringence of flow, exposure of —SH and phenolic —OH groups, etc. (6). It is quite possible that a certain amount of structural alteration (e.g., acetylation, formalation, heat and urea denaturation) of the molecule could take place without affecting the activity. A striking example of this has recently been reported by Hill and Smith (36) in which 120 amino acid residues of the original 180 in the proteolytic enzyme papain may be removed without loss in activity. Further alteration (possibly at or near the active center) could suddenly trigger a complete loss of activity. In some cases studied here this may be so, e. g., interaction of trypsin with sulfates (S.D.S. in bulk) and sulfonates (surface adsorption), at acid pH where the activity is irreversibly lost. However, where the activity on adsorption is not irreversibly lost there remains the possibility that unfolded protein is exhibiting partial activity. There are several other cases of reversible "denaturation" of this protein, that by heat and more recently that by urea, where the criterion for denaturation has been activity loss in the first case (16) and activity coupled with viscosity measurements in the second case (37). Where one has a sample of enzyme treated by "denaturing agents" or adsorbed at an interface, exhibiting partial activity, is the activity exhibited by a fraction of fully active molecules (not necessarily "native" with respect to structural changes) or is it exhibited by all of the molecules partially active? The question is very difficult to answer in practice; and the answer may well be different for different enzymes, e.g., those with and without prosthetic groups.

Where a competitive or noncompetitive type of inhibition of the enzyme resulting from a combination of inhibitor with the active center can be ruled out, the loss of enzymatic activity must result from an effect of the inhibitor on the general stereochemical configuration of a part or the whole of the protein molecule. If strained configurations of the molecule can work at lower efficiency, exhibiting partial activity, then it is possible that kinetic and thermodynamic studies will enable one to differentiate between losses in activity by a drastic (all-or-none effects) or a slight modification of the structure of the active center. For example, one might expect the combination of the substrate with the enzyme to be much more difficult and hence predict an increase in the K_m and activation energy for this reaction. The increase in activation energy for the overall catalase H_2O_2 reaction of the surface-adsorbed enzyme has been previously (6) related to a general structural unfolding of the molecule. With trypsin only one such study has been made, unfortunately in the unfavorable (irreversible loss of activity) case of adsorption at the sulfonate-stabilized interface. The same activation energies for the surface and bulk enzyme-substrate reactions would seem to indicate that the loss in activity at this interface is an all-or-none effect. Such a mechanism has been proposed for the structural unfolding of protein molecules in bulk by long-chain sulfates (9). At present, few data with which to elucidate the role of the general protein structure in enzymatic activity, either in the "simple" bulk cases or for the complex interfacial enzymes, are available.

Aside from the physicochemical problems involved in this work, a point of interest to the cell physiologist is that intracellular enzymes by virtue of being combined with lipids at some interface could be expressing only part, or possibly none, of their potential activity. Splitting, or change in physical state, of these complexes by some environmental change could lead to expression of full activity, thus partaking in, if not "causing," a change in the physiological state of the cell. This is a possible mechanism for the evocation of intracellular enzyme activities alternative to *de novo* synthesis of an enzyme.

ACKNOWLEDGMENTS

The authors wish to thank B. R. Hammond of this laboratory for a generous supply of benzoyl arginine ethyl ester and Dr. H. Gutfreund for one of the samples of trypsin

used in these experiments. We are indebted to Dr. H. Gutfreund especially, and to Dr. A. V. Few and Dr. B. A. Pethica, for many helpful discussions.

REFERENCES

1. Danielli, J. F., *Nature* **156,** 468 (1945).
2. Claude, A., *Advances in Protein Chem.* **5,** 423 (1949).
3. Schneider, W. B., *3rd Intern. Congr. Biochem. Brussels, Rapport,* p. 143, 1955.
4. Schneider, W. B., *J. Histo. Cytochem.* **1,** 212 (1953).
5. Neurath, H., Greenstein, J. C., Putnam, F. W., and Erickson, J. O., *Chem. Revs.* **34,** 157 (1944).
6. Fraser, M. J., Kaplan, J. G., and Schulman, J. H., *Discussions Faraday Soc.* **20,** 44 (1955).
7. Elkes, J. J., Frazer, A. C., Schulman, J. H., and Stewart, H. C., *Proc. Roy. Soc. (London)* **A184,** 102 (1945).
8. Pallansch, M. J., and Briggs, D. R., *J. Am. Chem. Soc.* **76,** 1396 (1954).
9. Putnam, F. W., *Advances in Protein Chem.* **4,** 79 (1948).
10. Wills, E. D., *Biochem. J.* **57,** 109 (1954).
11. Alexander, A. E., and Teorell, T., *Trans. Faraday Soc.* **35,** 727 (1939).
12. Few, A. V., Ottewill, R. H., and Parreira, H. C., *Biochim. et Biophys. Acta* **18,** 136 (1955).
13. Northrop, J. H., Kunitz, M., and Herriott, R. M. "Crystalline Enzymes," p. 226. Columbia University Press, New York, 1948.
14. Gutfreund, H., *Trans. Faraday Soc.* **50,** 624 (1954).
15. Gutfreund, H., *Trans. Faraday Soc.* **51,** 441 (1955).
16. Northrop, J. H., *J. Gen. Physiol.* **16,** 323 (1932).
17. Bier, M., and Nord, F. F., *Arch. Biochem. and Biophys.* **33,** 320 (1951).
18. Neurath, H., and Schwert, G. W., *Chem. Revs.* **46,** 69 (1950).
19. Duke, J. A., Bier, M., and Nord, F. F., *Arch. Biochem. and Biophys.* **40,** 425 (1952).
20. Schwert, G. W., Neurath, H., Kaufman, S., and Snoke, J. E., *J. Biol. Chem.* **172,** 221 (1948).
21. Bergmann, M., Fruton, J. S., and Pollok, H., *J. Biol. Chem.* **127,** 643 (1939).
22. Matalon, R., and Schulman, J. H., *Discussions Faraday Soc.* **6,** 21 (1949).
23. Abramson, H. A., *Trans. Faraday Soc.* **35,** 5 (1940).
24. Hocking, C. S., and Schulman, J. H., International Conference on Biochemical Problems of Lipids, p. 39. Brussels, 1953.
25. Hocking, C. S., Ph.D. dissertation, University of Cambridge, England, 1953.
26. Frazer, A. C., Schulman, J. H., and Stewart, H. C., *J. Physiol. (London)* **103,** 306 (1944).
27. Rothen, A., *Advances in Protein Chem.* **3,** 123 (1947).
28. Cheesman, D. F., and Davies, J. T., *Advances in Protein Chem.* **9,** 439 (1954).
29. Frazer, A. C., *J. Physiol. (London)* **102,** 329 (1943).
30. Schulman, J. H., and Cockbain, E. G., *Trans. Faraday Soc.* **36,** 661 (1940).
31. Alexander, A. E., and Schulman, J. H., *Trans. Faraday Soc.* **36,** 960 (1940).
32. Jansen, E. F., Nutting, M.-D. F., Jang, R., and Balls, A. K., *J. Biol. Chem.* **179,** 189 (1949).
33. Bernhard, S. A., *Biochem. J.* **59,** 506 (1955).
34. Williams, R. J., Philips, J. N., and Mysels, K. J., *Trans. Faraday Soc.* **51,** 728 (1955).
35. Cumper, C. W. N., and Alexander, A. E., *Australian J. Sci. Research* **A4,** 372 (1951).
36. Hill, R. L., and Smith, E. L., *Biochim. et Biophys. Acta* **19,** 376 (1956).
37. Harris, J. F., *Nature* **177,** 471 (1956).

JOURNAL OF COLLOID SCIENCE 11, 471–478 (1956)

ELECTROCHEMICAL STUDIES IN ANHYDROUS FORMIC ACID. III.

THE SUPPRESSION OF POLAROGRAPHIC OVERCURRENTS (MAXIMA)

F. Sebba and T. A. Pinfold

Department of Chemistry, University of Capetown, South Africa

Received April 5, 1956

ABSTRACT

The appearance of polarographic overcurrents (maxima) in anhydrous formic acid was found to depend on the relative concentrations of the electroreducible ion and the supporting electrolyte. The overcurrents were easily suppressed at relatively low concentrations of the supporting electrolyte, i.e., about 0.3 M. The unusual behavior was attributed to the monomeric molecules of formic acid which are capillary-active. The increase of supporting electrolyte caused a corresponding increase in the ionic strength which, it is postulated, weakened the hydrogen bonds in the dimeric formic acid molecule. This led to a greater concentration of monomeric molecules which was responsible for the suppression of the overcurrent.

INTRODUCTION

As it will be shown that the peaks on polarographic waves, hitherto known as "maxima," are variables passing through maximum values, in order to avoid the clumsy expression "maximal maxima" it has been decided to refer to them as "overcurrents"; this is a better description than the noncommittal term "maxima." The overcurrent is defined as the difference between the peak value of the current and the residual current from which the wave started in a polarogram.

No information on the electrocapillary curve of mercury in anhydrous formic acid has yet been published. In view of its relationship to the fact that the polarographic overcurrent occurs with some elements and does not occur with others, the measurement of this curve was undertaken.

The dependence of the overcurrent on supporting electrolyte concentration has been shown in the case of overcurrents existing on the waves for the electroreduction of oxygen by Varasova (3) and Rasch (4), of mercuric cyanide by Dillinger (5), and of uranyl salt solutions by Herasymenko (6). These authors showed that as the supporting electrolyte concentration was increased, the overcurrent at first increased and then decreased. At the maximum overcurrent the supporting electrolyte concentration was found to be directly proportional to the concentration of the electroreducible species. Complete suppression of the overcurrent was not mentioned except by Herasymenko in the case of uranyl salts and was ascribed to adsorption of reduction products which suppress the overcurrent. That large concentrations of supporting electrolyte are normally required before the overcurrents are suppressed was recognized by Heyrovsky and Simunek (7), who maintained that the overcurrents "are suppressed by surface-active matter, active anions or great concentrations of electrolytes." If this is so the graph of the overcurrent value against supporting electrolyte concentration in aqueous solution would be as shown by the complete curve in Fig. 5 (full and dotted lines).

Experimental

A description of the polarographic cell used, details of the quinhydrone-in-formic acid electrode (Q.F.A.E.) and the saturated calomel-in-formic acid electrode (S.C.F.A.E.), together with the polarographic characteristics of nine inorganic cations have been published elsewhere (1, 2).

To measure the values of the overcurrents and diffusion currents, a centimeter scale was firmly mounted in front of the polarograph and the position of the light spot recorded visually. This had the advantage over photographic recording of allowing larger deflections of the galvanometer and thus increased the accuracy of the measurements.

In the examination of the variation of the overcurrent with concentration of supporting electrolyte, the ratio of the overcurrent to the diffusion current, called β, was plotted. One advantage of plotting the ratio instead of overcurrent value, was that the former depended much less on changes in the drop time, being the ratio of two quantities both of which were dependent on this time of dropping.

The electrocapillary curves were plotted by noting the drop time of mercury from the capillary.

Results

The electrocapillary curves were measured at sodium formate concentrations of 0.05 M, 0.1 M, 0.25 M, 2.0 M, 4.0 M, and 5.5 M in anhydrous formic acid. The curve was flattened near the maximum, the flat portion extending over a potential of about 0.25 volt; otherwise the curve was of normal shape. The electrocapillary maximum in a 0.25 M sodium formate-formic acid solution was -0.55 volt vs. S.C.F.A.E. No shift to more negative potentials was observed on increasing the sodium formate concentration; this showed the formate ion to be capillary-inactive. This is in agreement with the observations of Rasch (4). Had the formate ion been adsorbed at the mercury-solution interface a change of the potential at the maximum to more negative values, due to the adsorption of a negative ion, would have been observed. The potential of the maximum after correcting for the liquid junction potential between anode and cathode compartments was actually found to shift in a positive direction. The corrected potential of the maximum at a sodium formate concentration of 0.05 *M* was -0.58 volt vs. S.C.F.A.E. and at 5.5 *M* was -0.40 volt vs. S.C.F.A.E. This suggests that, as the sodium formate concentration is increased, some positive ion is being adsorbed more and more at the mercury-solution interface.

Formic acid has been shown to be capillary-active. It was found that if added to aqueous solutions during a polarographic investigation it was capable of suppressing overcurrents. Furthermore, formic acid behaves in exactly the same way as methyl red in its effects on the somewhat curious curves obtained by Lingane (8) in the polarographic investigation of indium in 1 *M* aqueous potassium chloride. This suggests that formic acid is itself capillary-active. The species present in pure anhydrous formic acid are largely dimeric molecules in equilibrium with monomeric molecules and formate ions. That the formate ions are not capillary-active is shown by the failure of the electrocapillary maximum in formic acid to shift to more negative values. It is unlikely that the dimer will be capillary-active, the carbonyl and hydroxyl groups being hydrogen-bonded to those of another molecule. It is thus believed that the monomeric formic acid molecules are responsible for the capillary activity and the suppression of the overcurrent and that it is the positive hydroxyl group which is adsorbed at the mercury-solution interface. Increase of the concentration of the monomer should thus shift the electrocapillary curve to more positive values, which is what was shown to occur. It is thus postulated that increase of the sodium formate concentration increases the ionic strength of the medium; this tends to weaken the hydrogen bonding in the dimer with the production of monomeric molecules. As the ionic strength will increase linearly with concentration of a uni-univalent salt such as sodium formate, the increase of monomeric formic acid is believed to be a linear function of the sodium formate concentration.

It has been shown (2) that of the elements studied polarographically in formic acid, only bismuth, antimony, lead, and tin, the half-wave potentials of which are appreciably more positive than the electrocapillary maximum potential, give rise to overcurrents. The values of the ratio β at various concentrations of sodium formate, used as a supporting electrolyte, are plotted in Figs. 1–4. These curves show similar behavior to those in aqueous solution (Fig. 5) in that the overcurrent increases, passes through a maximum, and then decreases. With the exception of tin, the curves were found to be reproducible, and, as found in aqueous solution, the concentration of supporting electrolyte at the maximum value of ratio β was directly proportional to the concentration of the electroreducible ion. Unlike bismuth,

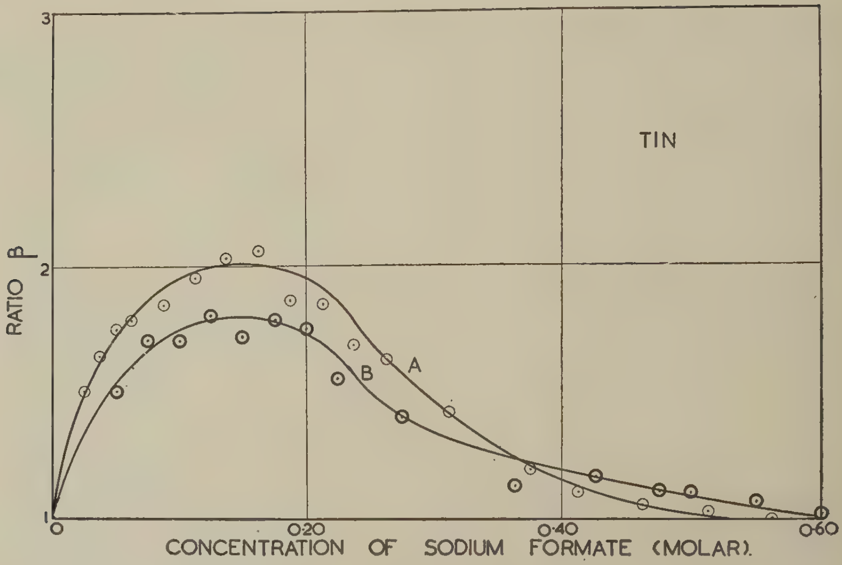

FIG. 1. Concentration of tin in gram ions per liter: Curve *A*—2.45 × 10^{-3}; Curve *B*—1.25 × 10^{-3}.

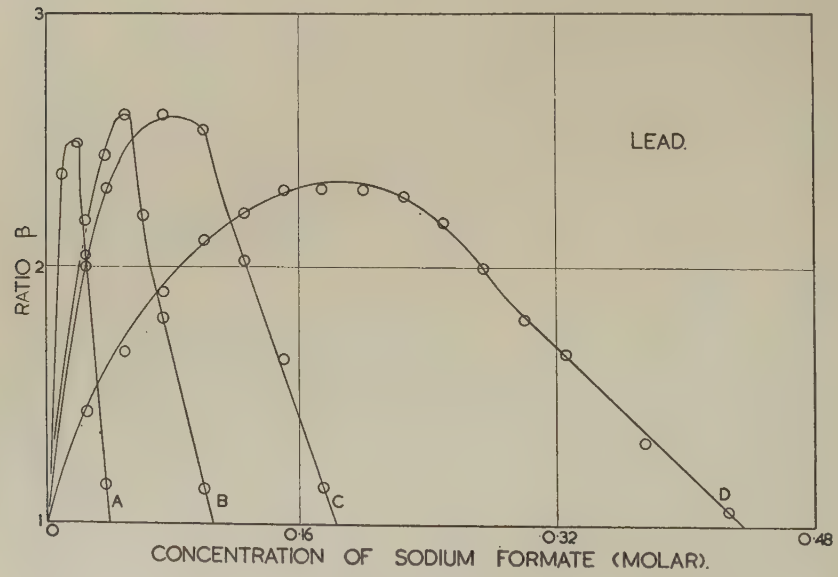

FIG. 2. Concentration of lead in gram ions per liter: Curve *A*—0.13 × 10^{-2}; Curve *B*—0.24 × 10^{-2}; Curve *C*—0.39 × 10^{-2}; Curve *D*—0.87 × 10^{-2}.

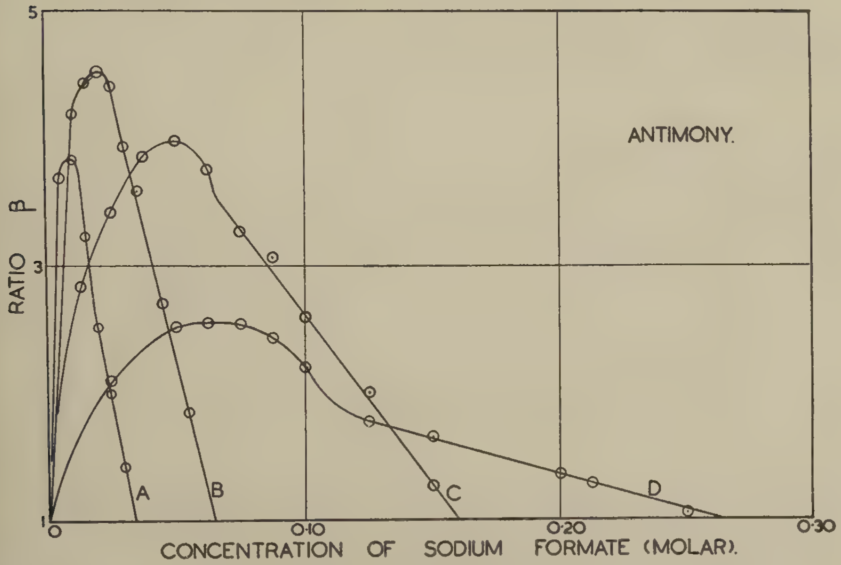

Fig. 3. Concentration of antimony in gram ions per liter: Curve *A*—0.25×10^{-3}; Curve *B*, 0.49×10^{-3}; Curve *C*—1.23×10^{-3}; Curve *D*, 1.96×10^{-3}.

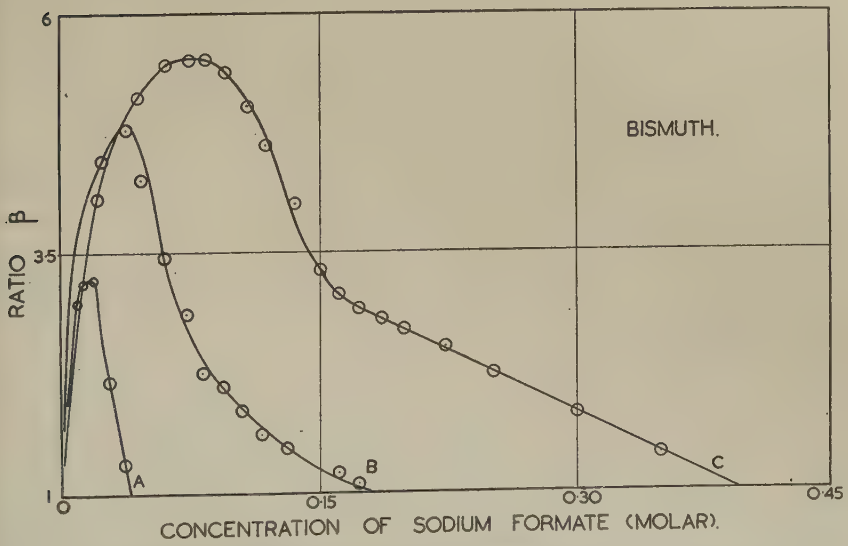

Fig. 4. Concentration of bismuth in gram ions per liter: Curve *A*—0.32×10^{-3}; Curve *B*—0.70×10^{-3}; Curve *C*—1.50×10^{-3}.

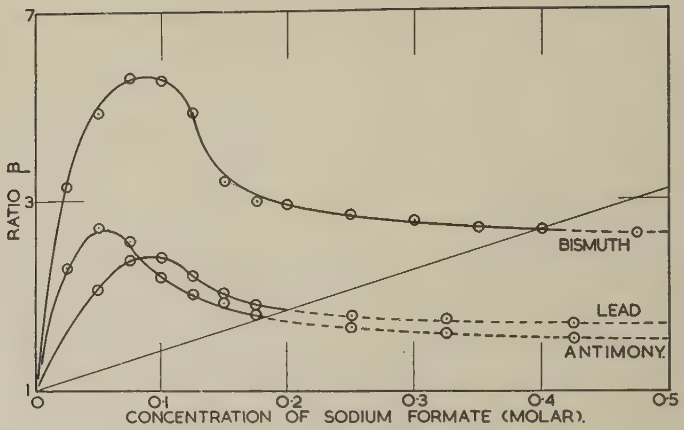

Fig. 5. Curves as in aqueous solution.

antimony, and lead, the overcurrents of tin were only gradually suppressed over a relatively large concentration range.

It was discovered that if an arbitrary choice of some linear function which would suppress the overcurrent, is made and plotted on the curves found for aqueous solution (Fig. 5) and the resultant of the two curves drawn, the curves obtained are identical in form to those plotted in Figs. 2–4. The linear function which suppresses the overcurrent is believed to be the increase of monomeric formic acid molecules with increasing sodium formate concentration.

According to the theory of Antweiler (9) and von Strackelberg (10), the overcurrents observed in this investigation would be due to streaming of the electrolyte caused by the presence of the mercury-solution interface of formate ions, these negative ions having been attracted there by the positively charged mercury drop. With increasing concentration of the formate ion the streaming increases, causing a correspondingly higher value of the overcurrent. The cations of the supporting electrolyte, in this case sodium ions, tend, however, to block out the electroreducible species at the mercury-solution interface. The effect on the overcurrent is such that after its initial increase, it passes through a maximum value and decreases. This explains the phenomenon noted by previous workers (3–6) and also in this investigation, that the supporting electrolyte concentration required to give the maximum overcurrent value is directly proportional to the electroreducible ion concentration. The higher this electroreducible ion concentration, the higher must be the supporting electrolyte concentration to cause a decrease in the overcurrent. A very much larger supporting electrolyte concentration would be required before the indifferent cations are present in such excess as to shut out the electroreducible species completely and so suppress the overcurrent. In formic acid, however, there is the added effect of monomeric formic acid molecules, which, being readily adsorbed at the mercury-solution interface, tend to shut out the electroreducible ions to a much greater extent, causing the suppression of the overcurrent at low supporting electrolyte concentrations.

If the behavior of antimony ions be cited as an example (Fig. 3), it can be seen that increase of the electroreducible ion concentration causes at first an increase in the maximum overcurrent and then a decrease, the latter being almost nonexistent at high electroreducible ion concentrations. This effect can be explained by consideration of Fig. 6. The concentration of indifferent electrolyte at the maximum overcurrent increases on increasing the concentration of the electroreducible ion. The maximum overcurrent consequently moves more towards the depreciating straight line which has correspondingly a higher value, giving rise to resultant curves with lesser values for the maximum overcurrent. To this must be added the fact that the rate of streaming must itself reach a maximum value owing to increase of the viscosity of the solution. (The viscosity of a 0.5 *M* sodium formate-formic acid solution is 22.1 millipoises (11), over twice the value for an aqueous solution of the same sodium formate concentration.) Thus in Figure 6 the maximal overcurrent value increases because of a greater rate of streaming, due to increase in the sodium formate concentration (curve *B* is higher than curve *A*). At curve *B*, however, the rate of streaming has reached its maximum value and on further increase of the supporting electrolyte concentration to curve *C* a slight decrease in the streaming rate, and consequently a decrease in the maximal overcurrent, is observed owing to the greater viscosity of the solution.

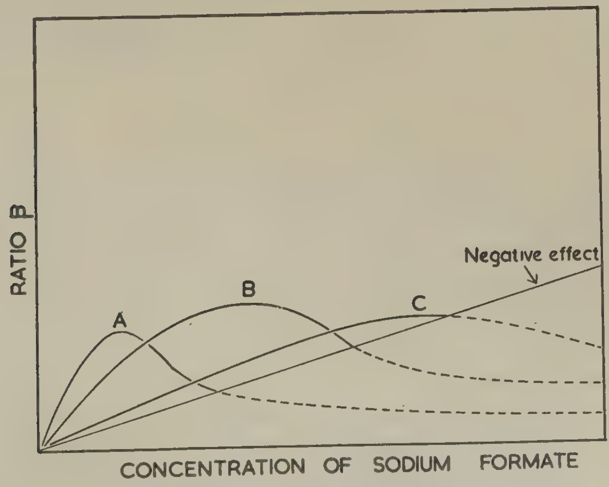

FIG. 6. Schematic representation of the decrease in ratio β on increase of the electroreducible ion concentration.

The poor reproducibility of the measurements of ratio β made for tin ions was due partly to a very pronounced decrease in the diffusion current as the sodium formate concentration was increased. This lowering of the diffusion current was due to the formation of a formato-stannous complex formed by tin, in the presence of formate ions (2). The anomalous behavior of the overcurrents of tin, in that they were not sharply suppressed on increasing the supporting electrolyte concentration has not been explained. In the formation of a formato complex, tin is unique amongst the four elements investigated, and it is possible that its unusual behavior may be due to this factor.

ACKNOWLEDGMENTS

The authors wish to express their sincere appreciation to the Council for Scientific and Industrial Research, Pretoria, for a bursary to one of us (T.A.P.).

REFERENCES

1. PINFOLD, T. A., AND SEBBA, F., *J. Am. Chem. Soc.* **78,** 2095 (1956).
2. PINFOLD, T. A., AND SEBBA, F., *J. Am. Chem. Soc.* **78** (1956).
3. VARASOVA, E., *Collection Czechoslov. Chem. Communs.* **2,** 8 (1930).
4. RASCH, J., *Collection Czechoslov. Chem. Communs.* **1,** 560 (1929).
5. DILLINGER, M., *Collection Czechoslov. Chem. Communs.* **1,** 638 (1929).
6. HERASYMENKO, P., *Trans. Faraday Soc.* **24,** 267 (1928).
7. HEYROVSKY, J., AND SIMUNEK, R., *Phil. Mag.* **7,** 951 (1929).
8. LINGANE, J. J., Ph.D. thesis, University of Minnesota, Minneapolis, 1938. See I. Kolthoff and J. Lingane, "Polarography," p. 519, Interscience, New York, 1952.
9. ANTWEILER, H., *Z. Elektrochem.* **44,** 831 (1938).
10. VON STRACKELBERG, M., *Z. Elektrochem.* **45,** 466 (1939).
11. SCHLESINGER, H. I., AND MARTIN, A., *J. Am. Chem. Soc.* **36,** 1586 (1914).

JOURNAL OF COLLOID SCIENCE **11**, 479–495 (1956)

CAPILLARY CONDENSATION IN SINGLE PORES

R. M. Barrer, N. McKenzie, and J. S. S. Reay

Chemistry Department, Imperial College of Science and Technology,
London, S. W. 7, England

Received March 8, 1956

ABSTRACT

The processes of filling and emptying single capillaries have been quantitatively considered for a wetting liquid for capillaries in the form of cones, wedges, double cones, hollow spherical caps, cylinders with hemispherical ends, and the pore space between solid cylinders and spheres. A quantitative examination has been made of hysteresis involving several kinds of rigid capillaries with reentrant angles. The isotherms have been calculated, irreversible work and entropies associated with the hysteresis have been evaluated, and the scanning behavior of groups of capillaries has been indicated for typical pore systems. In such pore systems the domains of Everett and Enderby are clearly connected with the pores with reentrant angles. The domains for such rigid pores should normally be noninteracting.

Condensation isotherms in cone- or wedge-shaped capillary systems, or between solid cylinders, may lead to isotherms having the contour of Types III, IV, or V in Brunauer's (1) classification. Thus capillary shape may be a factor in explaining the form of sorption isotherms.

1. Introduction

Analysis of pore distributions in microporous sorbents is often made in terms of Kelvin's equation

$$RT \ln \frac{p}{p_0} = -\frac{2\sigma V_L}{r}, \qquad [1]$$

where r denotes the radius of curvature of a hemispherical meniscus of a liquid having a surface tension σ and molecular volume V_L. A plane surface of the liquid exerts a vapor pressure p_0 and the hemispherical meniscus a vapor pressure p. However, many menisci cannot be spherically symmetrical, for example, those formed between parallel plates, in wedge-shaped cavities, or around points of contact between separate particles. Indeed, in many real menisci the two radii of curvature must be opposite in sign. Inspection of the literature shows a number of discussions of capillary condensation (2–6), but these are fragmentary and not always correct (*cf.* Section 2*g*), and no adequate exploration appears to have been made of the shapes of pure condensation isotherms in single capillaries of different forms. Because of this and because of the fictitious character of pore size distributions derived by assuming that menisci are always spherically symmetrical (Kelvin's equation), we have been led to consider condensation isotherm contours in individual pores of different shapes.

Microporous media sometimes possess a characteristic pore morphology. Graphite, vermiculite, and montmorillonite consist of flakes and must provide many wedge-shaped cavities, and spaces between nearly parallel lamellae. Halloysite crystallites are bent round to form hollow cylindrical rolls (7). Attapulgite and sepiolite, two minerals with very high gas-sorbing capacities, consist of fine laths in a tangled mass (8). Spherulitic crystals and particles (e.g., analcite) provide cavities of the type to be expected in various packings of spheres (9), for instance, tetrahedral and octahedral interstices for close-packed equal spheres. In many gels the cavities and pores are less distinctive, and in most systems whether gel or crystal there is usually a distribution of capillary sizes and shapes. Nevertheless there remains the possibility of substantial homogeneous groups of capillaries which may sometimes give the isotherms the form typical of that in a single capillary. These contours we shall show are very characteristic of the capillary shapes.

At any point on a meniscus in equilibrium there are two radii of curvature, r_1 and r_2. Surface tension then produces a hydrostatic pressure difference ΔP across the interface such that

$$\Delta P = \sigma\left(\frac{1}{r_1} + \frac{1}{r_2}\right). \qquad [2]$$

The meniscus must have such a form that $(1/r_1 + 1/r_2)$ is constant at every point on its surface. The uniform value of ΔP then produces a change in the vapor pressure of the meniscus-forming liquid from p_0 to p such that

$$RT \ln \frac{p}{p_0} = -\sigma V_L \left(\frac{1}{r_1} + \frac{1}{r_2}\right). \qquad [3]$$

Equation [3] leads to Eq. [1] for a hemispherical concave meniscus and to Cohan's (10) equation

$$RT \ln \frac{p}{p_0} = -\frac{\sigma V_L}{r} \qquad [4]$$

for a cylindrical meniscus. The radii r_1 and r_2 are reckoned in the above formulas as positive or negative according as the corresponding center of curvature is on the vapor side of the surface, or is on the liquid side.

2. Typical Capillaries Which Fill and Empty Without Hysteresis

We consider the filling of conical and wedge-shaped cavities, composite conical capillaries, tubular capillaries with hemispherical ends, and pockets in the form of spherical caps, by a liquid which wets their surfaces.

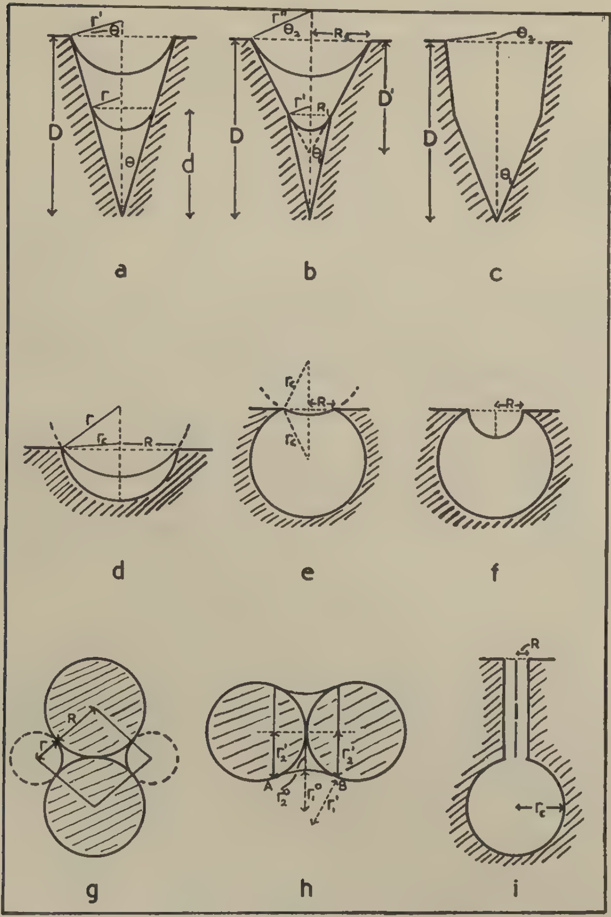

FIG. 1. Cross sections of capillaries, showing significance of symbols used in text.

a. Conical Capillaries. Consider an infinitely deep hollow cone of half angle θ. Let r be the radius of a sphere which fits inside this cone and R be the radius of the cone at the plane of contact with the sphere (Fig. 1*a*); d is the perpendicular distance from the vertex of the cone to this plane. For zero angle of wetting r will be the radius of curvature of the meniscus formed inside the cone, at a distance d from the vertex. Since capillary condensation will be preceded by the formation of an adsorbed layer on the walls of the capillary, the true dimensions of the capillary will be slightly different from the above dimensions. However, adsorption is not under discussion in any of the capillaries to be considered.

From the geometry of the cone, at the stage of filling described above, the volume V of capillary condensed liquid is

$$V = \frac{\pi r^3}{3} \frac{(\sin\theta - 1)^2}{\sin\theta}, \qquad [5]$$

where

$$r = -\frac{2\sigma V_L}{RT \ln \frac{p}{p_0}} \qquad \text{(Kelvin's Eq. [1]).}$$

Equation [5] is valid also for finite conical capillaries within the range where a meniscus can form with zero angle of contact with the capillary walls. If D is the depth of the cone, r', the maximum radius of curvature of the meniscus at which this will occur, is

$$r' = D \frac{\sin\theta}{\cos^2\theta}. \qquad [6]$$

At this stage, from Eq. [5], the volume condensed is

$$V' = \frac{\pi}{3} D^3 \frac{\sin^2\theta\,(\sin\theta - 1)^2}{\cos^6\theta}. \qquad [7]$$

For relative pressures p/p_0 greater than that corresponding to equilibrium with the meniscus of curvature r', the remaining volume of the cone will continue to fill until at $p/p_0 = 1$ the cone will be full and the liquid meniscus plane. During this phase the radius of curvature of the meniscus grows from r' to ∞. For $r > r'$ we obtain

$$V = \frac{\pi}{3} [D^3 \tan^2\theta - 2r^3 + \sqrt{r^2 - D^2 \tan^2\theta}(2r^2 + D^2 \tan^2\theta)]. \qquad [8]$$

When the cone is full ($r = \infty$, $p/p_0 = 1$)

$$V_{\text{sat.}} = \frac{\pi}{3} D^3 \tan^2\theta. \qquad [9]$$

Equation [1] still defines the relation between p/p_0 and r, and so the isotherm may be calculated.

b. Wedge-Shaped Capillaries. We consider a wedge-shaped capillary of depth D, and of length L sufficient for the neglect of end effects. Figure 1*a* may still represent the cross section of the partly filled wedge; r is now the radius of curvature of the cylindrical meniscus in the wedge. Then it was found for $r < r'$ (Fig. 1*a*) that

$$V = Lr^2 \left\{ \cot\theta - \frac{\pi}{2} + \theta \right\}, \qquad [10]$$

while for $r' \leqslant r \leqslant \infty$

$$V = L\left\{D^2 \tan\theta - \frac{\pi r^2}{2} + r^2 \sin^{-1}\frac{\sqrt{r^2 - D^2\tan^2\theta}}{r} + D\tan\theta\sqrt{r^2 - D^2\tan^2\theta}\right\}. \qquad [11]$$

In Eqs. [10] and [11] r is given by Cohan's equation (Eq. [4]). When the wedge is just filled

$$V_{\text{sat.}} = LD^2\tan\theta. \qquad [12]$$

c. Double-Cone Capillaries. Two forms of double cone are illustrated in Figs. 1*b* and 1*c*. The filling of the cone of Fig. 1*b* proceeds as follows. Formula [5] is valid up to the stage where the radius of curvature, r, of the hemispherical meniscus becomes r' in the cone of half-angle θ_1. Thereafter formula [8] is valid until the radius of curvature is such that a meniscus with zero angle of wetting first appears in the cone of half-angle θ_2. The value of r at this stage is $\mathrm{R}_1/\cos\theta_2$. From this stage on the volume, V, of capillary condensate, is given by

$$V = \frac{\pi r^3}{3}\frac{(\sin\theta_2 - 1)^2}{\sin\theta_2} + \frac{\pi \mathrm{R}_1^3}{3}(\cot\theta_1 - \cot\theta_2) \qquad [13]$$

until the last meniscus is formed which can have zero angle of wetting of the cone of half-angle θ_2; r then has the value $\mathrm{R}_2/\cos\theta_2$. The value of V is thereafter

$$V = \frac{\pi}{3}\{(D')^3\tan^2\theta_2 - 2r^3 + \sqrt{r^2 - (D')^2\tan^2\theta_2} \cdot (2r^2 + (D')^2\tan^2\theta_2) + \mathrm{R}_1^3(\cot\theta_1 - \cot\theta_2)\}, \qquad [14]$$

where $D' = D - \mathrm{R}_1(\cot\theta_1 - \cot\theta_2)$. In all these relations r and p/p_0 are connected by the Kelvin equation. When $p/p_0 = 1$ and the pore is full,

$$V_{\text{sat.}} = \frac{\pi}{3}(D')^3\tan^2\theta_2 + \frac{\pi}{3}\mathrm{R}_1^3(\cot\theta_1 - \cot\theta_2). \qquad [15]$$

The double cone of Fig. 1*c* fills in a more complex manner. Capillary condensate may appear not only at the apex of the cone of half-angle θ_1 but also around the circle of intersection of the two cones. The condensation around this circle will be more important the greater the angle θ_1. Moreover the layer of liquid there formed will have two radii of curvature r_1 and r_2 such that $(1/r_1 + 1/r_2)$ remains constant, but r_1 and r_2 individually vary at any point according to the vertical distance of the point above the vertex. Eventually both layers of capillary condensate will join, and the capillary over a still later stage will fill according to Eqs. like [13] and [14].

d. Capillaries Represented by a Cap of a Spherical Shell. No capillary condensation occurs until the relative pressure reaches a value corresponding to r_c in Fig. 1*d*, according to Kelvin's equation (Eq. [1]). For $r > r_c$ and so for larger values of p/p_0 the volume of capillary condensate is

$$V = \frac{\pi}{3}\{(2r_c^3 - 2r_c^2\sqrt{r_c^2 - \mathrm{R}^2} - \mathrm{R}^2\sqrt{r_c^2 - \mathrm{R}^2}) - (2r^3 - 2r^2\sqrt{r^2 - \mathrm{R}^2} - \mathrm{R}^2\sqrt{r^2 - \mathrm{R}^2})\}. \quad [16]$$

When the cap becomes hemispherical $\mathrm{R} = r_c$ and so

$$V = \frac{\pi}{3}\{2\mathrm{R}^3 - 2r^3 + \sqrt{r^2 - \mathrm{R}^2}(\mathrm{R}^2 + 2r^2)\}. \quad [17]$$

e. Cylindrical Capillary with Hemispherical End. For this capillary of radius R and depth D no filling occurs until $r = \mathrm{R} = -2\sigma V_L/(RT \ln p/p_0)$, at which point the volume condensed rises from zero to

$$V = \pi \mathrm{R}^2(D - \mathrm{R}). \quad [18]$$

At higher relative pressures the amount condensed is given by the sum of Eqs. [17] and [18], reaching at $p/p_0 = 1$ the value

$$V_{\mathrm{sat.}} = \pi \mathrm{R}^2(D - \mathrm{R}) + \frac{2\pi}{3}\mathrm{R}^3. \quad [19]$$

f. Capillary Space Formed by Cylinders in Contact. When two equal cylinders of radius R are in contact along their lengths, capillary condensation occurs along the line of contact to give cylindrical concave menisci of radius r (Fig. 1*g*). Then r is governed by the Cohan equation (eq. [4]), and if the cylinders are of length L sufficiently great to neglect end effects, the volume of capillary condensate is

$$V = L\left\{2\mathrm{R}\sqrt{(\mathrm{R} + r)^2 - \mathrm{R}^2} - r^2\left(\pi - 2\cos^{-1}\frac{\mathrm{R}}{\mathrm{R} + r}\right) - 2\mathrm{R}^2\cos^{-1}\frac{\mathrm{R}}{\mathrm{R} + r}\right\}. \quad [20]$$

When $p/p_0 = 1$,

$$V_{\mathrm{sat.}} = (4 - \pi)\mathrm{R}^2 L \quad [21]$$

For equal cylinders close packed longitudinally each pore is formed by three cylinders in mutual contact. Condensation first occurs at the three lines of contact and proceeds according to Eq. [20] until the radius of the meniscus, r, is given by $r = (2\sqrt{3} - 3)\mathrm{R}/3$, when the three menisci merge. At this critical stage the pore fills completely.

g. Capillary Space Formed by Spheres in Contact. When two equal spheres are in contact, capillary condensation occurs about the point of contact. This problem has been discussed recently (10), and the volume of capillary condensate was supposed to be determined by rolling a third sphere having a radius r equal to one radius of curvature of the meniscus (Fig. 1*h*) around the point of contact of the two equal spheres. The volume of capillary condensate was thereby defined for any radius of the rolling sphere, and isotherms were calculated.

This approach can in fact be only a crude one. Both radii r_1 and r_2 change as we move along the meniscus from A to B in Fig. 1*h*. It is only $(1/r_1 - 1/|r_2|)$ which is constant. Moreover, the points of contact of the rolling sphere of radius r with the other spheres do not define the true length of AB, since the rolling sphere argument is, as shown, not correct. The theory of the filling of the capillary space is rather complex, and is outlined in the Appendix.

3. Capillary Condensation Isotherms

Whereas various combinations of these types of capillary are possible, and more complex systems might also be investigated, the calculations of Section 2 may be regarded as typical. Capillary condensation isotherms have accordingly been calculated for the filling and emptying of some of the capillaries illustrated in Fig. 1, with water at 20°C.

In Fig. 2*a* and *b* the fraction of filling $(V/V_{\text{sat.}})$ is shown as a function of relative pressure for a series of conical capillaries. In Fig. 2*a*, the isotherms are shown for cones of constant half-angle, θ ($\theta = 10°$), and of different depths. In Fig. 2*b* the isotherms are also given for conical capillaries of constant depth (200 A.) but varying θ. In Figs. 2*c* and 2*d* similar isotherms are given for long wedge-shaped capillaries. All these isotherms have the form of Type V in the Brunauer classification (1), but the shape approaches that of Type III for very deep conical or wedge-shaped capillaries of small θ, or for shallow but wide-angle capillaries. In Fig. 3*a* is shown the isotherm for a double cone such as that illustrated in Fig. 1*b*. The isotherm is of Type V with a discontinuity. A similar form will be given by a double-wedge capillary.

Condensation isotherms between cylinders have been derived for two identical cylinders in contact along their length (Fig. 2*e*) and also for a large number of identical cylinders close packed longitudinally (Fig. 2*f*). A hemispherical pocket, or cylindrical capillaries with hemispherical ends give capillary condensation only above a critical relative pressure. This is shown in Fig. 3*c* for hemispherical pockets of 25 A. and 50 A. radius, while Fig. 3*b* shows the curves for cylindrical capillaries with hemispherical ends, of total length 250 A.

Only true capillary condensation has been evaluated in these calculations. If the total sorption is considered, a contribution in the form of a Type I isotherm would be added to each isotherm in Figs. 2 and 3. For small surface areas mono- or multilayer sorption is small in extent com-

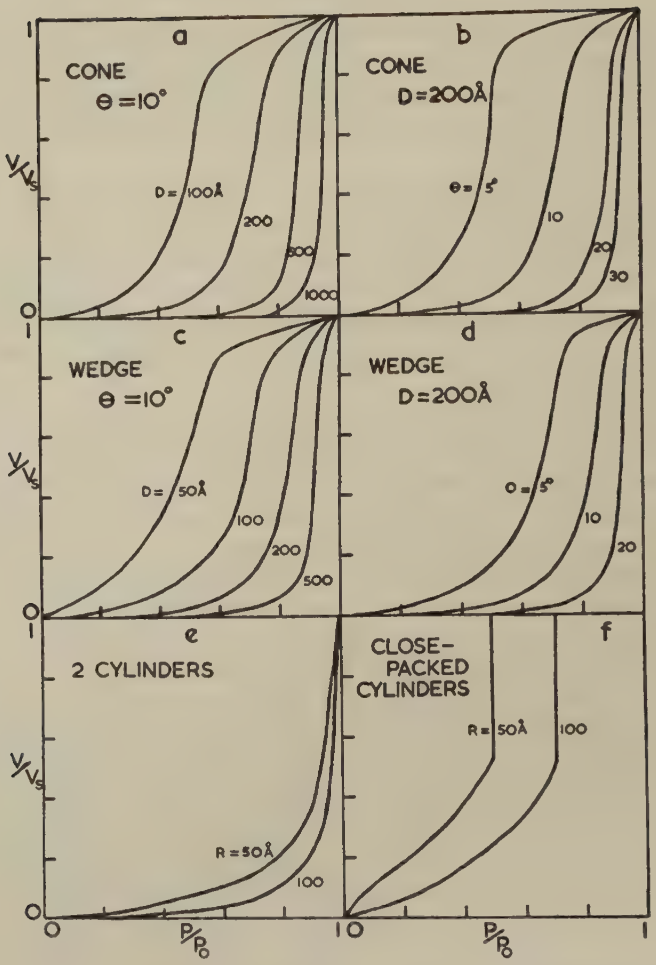

FIG. 2. Reversible condensation isotherms in capillaries.

pared with capillary condensation and isotherms will be little changed in contour. However, for large total surfaces adsorption will contribute substantially to the total uptake of sorbate and the condensation isotherms of Types V and III will become adsorption plus condensation isotherms of Types IV or II in the Brunauer classification.

4. Hysteresis

In none of the capillaries so far discussed will hysteresis occur in a condensation-evaporation cycle. As soon, however, as reentrant angles appear, hysteresis may be found (10–12). This view was challenged by Barkas (13), who claimed that the properties of the liquid condensed in a pore would be reversible. He considered, for example, that on desorption, after filling a

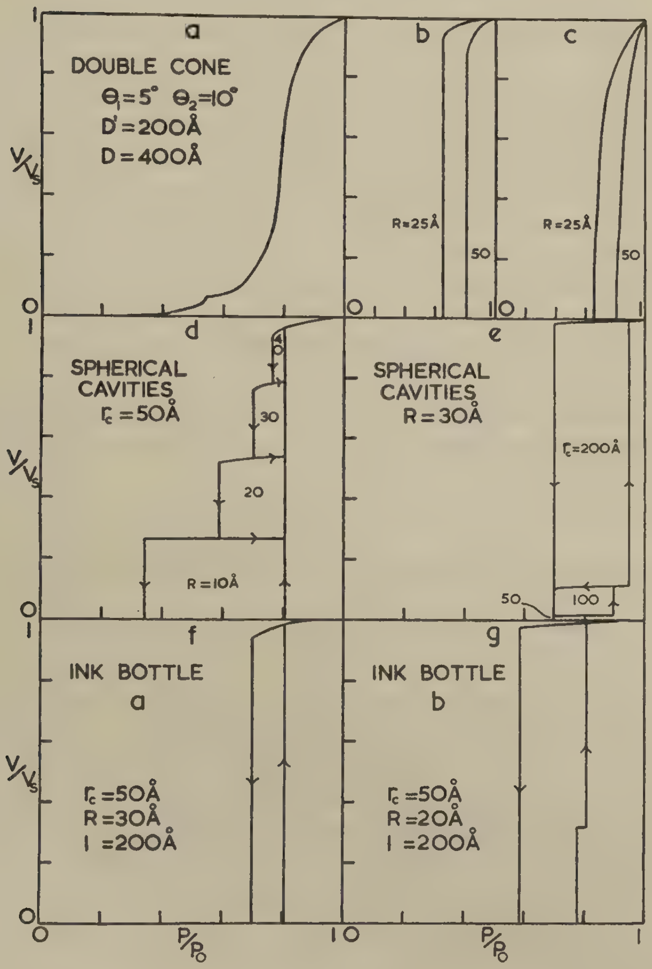

FIG. 3. (*a*) Condensation isotherm in a double cone (Fig. 1*b*). (*b*) Condensation isotherms in cylindrical capillaries with a hemispherical end. (*c*) Condensation isotherms in pockets of spherical symmetry. (*d*) and (*e*) Condensation isotherms in a small group of spherical cavities of differing geometry and each cavity with reentrant angles. (*f*) and (*g*) Condensation isotherms showing the two hysteresis loops associated with the two modes of filling ink-bottle capillaries, depending upon pore geometry.

McBain "ink bottle" capillary, a bubble would form in the body of the ink bottle, before the pressure had fallen sufficiently for the hemispherical meniscus to appear in the neck. The net result according to Barkas would be that the bottle would empty by the same path as it filled. However, if such a bubble formed it would at first have a smaller radius of curvature than that of the meniscus and so would be metastable and should be consumed again. This latter view was considered correct by McBain (12). Only if the condensate contained volatile dissolved gas could such an embryo bubble grow.

We may now consider the spheroidal cavity of Figs. 1*e* and 1*f*. As the relative pressure is increased no capillary condensate will form until a critical pressure is reached defined by the Kelvin equation $RT \ln p/p_0 = -2\sigma V_L/r_c$, where r_c is the radius of the sphere of which the capillary is the cap. At this pressure the capillary will fill to give a spherical meniscus of radius of curvature r_c (Fig. 1*e*). If the radius of the mouth of the capillary is R, then at this stage the volume of condensate is

$$V_a = \frac{\pi}{3}(4r_c^2 + 2\mathrm{R}^2)\sqrt{r_c^2 - \mathrm{R}^2}. \qquad [22]$$

From this point on the radius of curvature r increases as p/p_0 rises, so that the volume of condensate is

$$V_a = \frac{\pi}{3}\{2r_c^3 + (2r_c^2 + \mathrm{R}^2)\sqrt{r_c^2 - \mathrm{R}^2} - 2r^3 + (2r^2 + \mathrm{R}^2)\sqrt{r^2 - \mathrm{R}^2}\}. \qquad [23]$$

Eventually when $p/p_0 = 1$ and so $r = \infty$, this volume becomes

$$V_{\mathrm{sat.}} = \frac{\pi}{3}\{2r_c^3 - (2r_c^2 + \mathrm{R}^2)\sqrt{r_c^2 - \mathrm{R}^2}\}. \qquad [24]$$

The emptying process, however, follows a different path. As p/p_0 decreases, so does r the radius of curvature of the hemispherical meniscus, until it takes the value R, as shown in Fig. 1*f*. Any further removal of condensate as the pressure is lowered still more must *increase* r again. Thus, after this stage has been reached any lowering of p/p_0 results in complete evaporation of the condensate. In this critical state the volume of condensate is

$$V_d = \frac{\pi}{3}\{2r_c^3 + (2r_c^2 + \mathrm{R}^2)\sqrt{r_c^2 - \mathrm{R}^2} - 2\mathrm{R}^3\}. \qquad [25]$$

At the two critical stages, the one for forming condensate (Eq. [22]) and the other for removing condensate,

$$(V_a - V_d) = \frac{\pi}{3}\{(2r_c^2 - \mathrm{R}^2)\sqrt{r_c^2 - \mathrm{R}^2} - 2r_c^3 + 2\mathrm{R}^3\}. \qquad [26]$$

The relative pressures at which the capillary fills and empties, respectively, are then

$$\left(\frac{p}{p_0}\right)_a = \exp - \frac{2\sigma V_L}{r_c RT}; \qquad \left(\frac{p}{p_0}\right)_d = \exp - \frac{2\sigma V_L}{\mathrm{R}(RT)}.$$

It follows that the area, A, of the hysteresis loop is approximately

$$A \simeq \frac{(V_d + V_a)}{2}\left\{\exp - \frac{2\sigma V_L}{r_c RT} - \exp - \frac{2\sigma V_L}{\mathrm{R}(RT)}\right\}. \qquad [27]$$

The breadth of the hysteresis loops is thus related to pore geometry by the difference between r_c and R, and is zero when $r_c = \mathrm{R}$. The irreversible work W and entropy W/T associated with the hysteresis phenomenon can be calculated by plotting the amount sorbed in moles against $RT \ln p/p_0$ in calories, and finding the area of the loop. The work approaches

$$W \simeq \frac{n_a + n_d}{2}\left[-\frac{2\sigma V_L}{r_c} + \frac{2\sigma V_L}{\mathrm{R}}\right], \tag{28}$$

where n_a and n_d are the number of moles condensed at p_a and p_d, respectively.

Another simple form of capillary which exhibits hysteresis is a long troughlike capillary, open at both ends, of length L and with cross section as in Fig. 1*e*. Condensation first occurs at the pressure given by $RT \ln p/p_0 = -\sigma V_L/r_c$, when the volume condensed is given by

$$V_a = L\left\{\pi r_c^2 - 2r_c^2 \sin^{-1}\frac{\mathrm{R}}{r_c} + 2\mathrm{R}\sqrt{r_c^2 - \mathrm{R}^2}\right\}. \tag{29}$$

Above this relative pressure the volume of condensate is given by

$$V_a = L\left\{\pi r_c^2 - r_c^2 \sin^{-1}\frac{\mathrm{R}}{r_c} + \mathrm{R}\sqrt{r_c^2 - \mathrm{R}^2} - r^2 \sin^{-1}\frac{\mathrm{R}}{r} + \mathrm{R}\sqrt{r^2 - \mathrm{R}^2}\right\}, \tag{30}$$

where r is governed by the Cohan equation

$$V_{\text{sat.}} = L\left\{\pi r_c^2 - r_c^2 \sin^{-1}\frac{\mathrm{R}}{r_c} + \mathrm{R}\sqrt{r_c^2 - \mathrm{R}^2}\right\}. \tag{30a}$$

Desorption occurs according to Eq. [30] until $r = \mathrm{R}$ when the pore empties completely.

The "ink bottle" capillary discussed by McBain and Kraemer may be considered quantitatively as a third possible instance of hysteresis (Fig. 1*i*). Depending upon the relative dimensions of r_c and R there are two mechanisms of filling.

a. $2\mathrm{R} \geqslant r_c$. Condensation first occurs when the relative pressure corresponds to a meniscus r_c as given by the Kelvin equation. The capillary then fills until the volume condensed is

$$V_a = \frac{\pi}{3}\{(4r_c^2 + 2\mathrm{R}^2)\sqrt{r_c^2 - \mathrm{R}^2} + 3\mathrm{R}^2 l\} \tag{31}$$

where l denotes the length of the neck of the ink-bottle.

For higher relative pressures the meniscus fills according to the sum of [31] and [16].

b. $2\mathrm{R} < r_c$. Condensation begins in the neck of the ink bottle of radius R, the condensation pressure being governed by the Cohan equation ($RT \ln p/p_0 = -\sigma V_L/\mathrm{R}$). At this pressure the capillary will fill until

$$V = \frac{\pi}{3}\left\{3\mathrm{R}^2 l - 2\,[2r^3\sqrt{r^2 - \mathrm{R}^2}(\mathrm{R}^2 + 2r^2)]\right\}, \qquad [32]$$

where $RT \ln p/p_0 = -2\sigma V_L/r$ and so $r = 2\mathrm{R}$. Thereafter the filling is governed by the Kelvin equation, and until $r = r_c$ the volume condensed is related to the meniscus radius by Eq. [32]. At this point the whole bulb will fill, and the volume condensed will be given by Eq. [32] with $r = r_c$ together with an additional term $\frac{4}{3}\pi r_c^3$, which leads back to Eq. [31]. For still higher relative pressures filling proceeds according to the sum of Eqs. [31] and [16].

As p/p_0 falls the desorption process occurs by a decrease in the radius of curvature of the meniscus in the narrow neck of the ink bottle until a hemispherical meniscus of radius R appears, the pressure being that given by Kelvin's equation. At this pressure the system is no longer stable, and any further reduction in p/p_0 results in the complete emptying of the ink bottle. Thus a hysteresis appears which is different according as $2\mathrm{R} \geqslant r_c$ or $2\mathrm{R} < r_c$. In this latter case the filling of the ink bottle involves two discontinuous stages and its emptying only one such step. Calculated hysteresis loops for the two cases are shown in Figs. 3*f* and 3*g*.

The irreversible work and entropy associated with the hysteresis loop may readily be computed from Eq. [28]. Some values obtained for spheroidal cavities are shown in Table I, the numbers of spheroidal cavities being chosen so that the amount condensed when $p/p_0 = 1$ is a mole. Table II lists similar quantities for trough-shaped cavities. Values of W and of W/T have been obtained for hysteresis in montmorillonite (14) and in potassium benzene sulfonate (15), but these measurements referred to amounts of sorbent which cannot be directly compared in terms of capillary volume or structure with each other or with the cavities of Table I. At least part of the hysteresis was moreover associated with lattice changes

TABLE I

Irreversible Work and Entropy for Isotherms of Water at 20°C. in Spheroidal Cavities (Fig. 1e)

r_c (*A.*)	R(*A.*)	Work, W (cal. for no. of capillaries holding 1 mole H_2O at $p/p_0 = 1$)	Entropy $S = \frac{W}{T}$ (*e.u.*)
50	10	503	1.72
50	20	188	0.64
50	30	84	0.29
50	40	25.4	0.087
100	30	147	0.50
200	30	179	0.61

TABLE II

Irreversible Work and Entropy for Isotherms of Water at 20°C. in Troughs with Circular Cross Sections (Fig. 1e)

r_c (A.)	R(A.)	Work, W (cal. for length of capillary holding 1 mole H_2O at $p/p_0 = 1$)	Entropy $S = \frac{W}{T}$ (e.u.)
50	10	249	0.75
50	20	90	0.27
50	30	37	0.11
50	40	15.5	0.05
100	30	71.6	0.22
200	30	89	0.27

in the sorbent. Everett (16) has also recently considered the irreversible entropy arising from hysteresis in the benzene-charcoal system.

5. Scanning Behavior

Although there can be hysteresis in a single capillary, for no single capillary will scanning curves be found. There must, for the isotherm to exhibit scanning behavior, be a range of capillaries each giving a different hysteresis loop. The scanning behavior can be investigated for a series of spherical cavities such as that shown in Fig. 1*e* and *f*. Firstly, r_c was taken to be constant at 50 A., while R was given the values 10, 20, 30, 40 A. The isotherm is shown in Fig. 3*d*, it being assumed that there are equal numbers of cavities of each kind. All cavities fill at one relative pressure, but each group empties at a different pressure. Scanning is possible only during sorption following partial desorption, as indicated in the figure. The number of possible scanning curves is the same as the number of different capillary types.

A complementary behavior was found when R = 30 A. was taken to be constant for all capillaries, and r_c was assigned values of 50, 100, and 200 A. For equal numbers of cavities the isotherm contour is given in Fig. 3*e*. The filling of capillaries occurs in a series of steps, but the emptying takes place at one pressure only. Again the number of possible scanning curves is equal to the number of different kinds of capillary, but scanning can be observed only on desorption after partial filling of the capillary system. Similar isotherms are shown in Fig. 4*a* and 4*b* for equal lengths of trough-like cavities with circular cross sections.

If both R and r_c are varied, both sorption and desorption take place in steps, and if the number of capillary types becomes large, the stepwise hysteresis loop will be replaced by one with continuously sloping sorption and desorption branches. Moreover, scanning will be possible at any stage either of condensation or of desorption. This is the behavior normally observed (17, 18, 16).

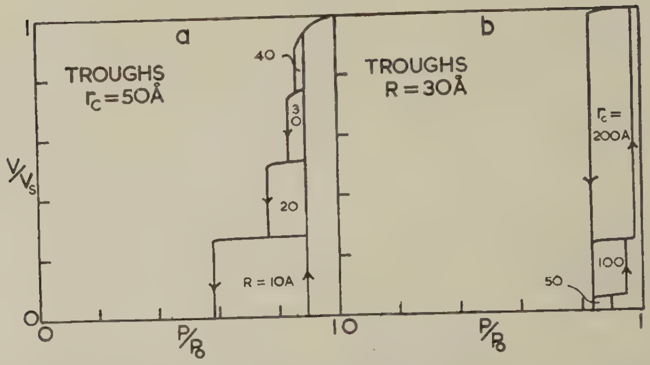

FIG. 4. Condensation isotherms in a small group of open-ended troughs of differing geometry, each trough with reentrant angles.

6. Discussion

Isotherms obtained for permanent gases in "Vycor" porous glass at 78° and 90°K. show hysteresis loops in which the desorption branch is very steep while the condensation branch is more sloping (19). This behavior tends to be that shown in Fig. 3*e*. The quantitative formulation of Section 5 then indicates that the hysteresis loop in porous glass is compatible with a distribution of pockets, or of drainlike channels, with reentrant angles, the cross sections of which are idealized in Fig. 1*e* or 1*i*. These capillaries must, however, be characterized by a diversity of bulb diameters together with openings which control desorption and which are rather uniform in dimensions. Thus desorption occurs over a narrow range in p/p_0, but not condensation.

Hysteresis has recently been considered in formal and general theories which require the existence of domains with different properties (20–24). In hysteresis associated with capillary condensation the domains evidently have physical reality if they comprise condensate in capillaries possessing reentrant angles. In condensation in micropore systems it is possible and even probable that in rigid micropore sorbents such domains do not interact perceptibly so that the situation resembles more nearly that discussed by Everett (20–22) than that treated by Enderby in his latest paper (24).

Only when capillaries are predominantly of one form will any reflection of their special geometry be likely to appear in the condensation isotherms. For example, it will be generally true that micropore systems involving only simple wedge- or cone-shaped capillaries will exhibit no hysteresis and will tend to be of Types III, IV, or V. This may be a more realistic interpretation than one based on multilayer formation restricted to a finite number of layers. Isotherms of Type V may also arise quite independently of either capillary condensation or restricted multilayer formation, and when the amount sorbed is less than a monolayer (25). Such an isotherm contour is found in the water-charcoal system for sorptions less than a monolayer, and can be attributed to lateral interaction between adsorbed molecules (26). Attention is thus directed to the need to measure more than isotherm contour in interpreting the processes involved.

In the calculations of isotherm contours given in the preceding sections we have used the normal bulk values of V_L and of σ. Direct measurements of these quantities have not been made down to such low capillary radii, although it has been suggested that liquid densities are approximately normal in capillaries of ~30 A. radius (27). A recent estimate of self potentials of molecules in very thin liquid-like slices has shown that these potentials assume values similar to those in bulk liquid or at the interface of that liquid when the slices are only a very few molecules thick (3 to 5 layers) (28). This in turn suggests that the surface tension may also be not very different in such multilayer slices from what it is for bulk liquid. Thus, whereas V_L and σ may in general not have exactly the same values for small aggregates of molecules as for large ones, these values should at least be comparable. Similarly whereas the idea of radii of curvature, r, of menisci may lose precision on a scale such that amplitudes of thermal vibrations become appreciable compared with r, we think that effects qualitatively similar to those calculated will arise. We have thus in some cases carried the calculations down to very small pore radii to show the general trend of the isotherms. The distortion of the menisci by gravity has not been considered. For small capillaries, except when $p/p_0 \rightarrow 1$, (and so $\Delta P \rightarrow 0$), such distortion is likely to be insignificant. Finally one may note that hysteresis can arise from causes other than the occurrence of rigid pores with reentrant angles. It may for example be associated with structural changes in the sorbent (29, 14, 15).

APPENDIX

Condensation in Space between Two Spheres in Contact

In the case of condensation between two spheres of radius a shown in Fig. 5 we have from Eq. [2]

$$\lambda = \frac{1}{r_1} - \frac{1}{|r_2|},$$

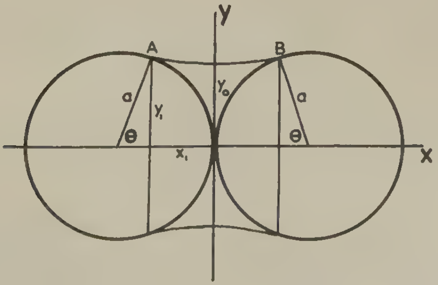

FIG. 5. The geometry of filling of the space between two spheres in contact.

where λ is a constant for any fixed value of p/p_0. By a standard procedure it follows that

$$\lambda = \frac{y''}{(1 + y'^2)^{3/2}} - \frac{1}{y}.$$

where $y' = dy/dx$ and $y'' = d^2y/dx^2$.
Accordingly

$$\frac{1}{2}\int \frac{dy'^2}{(1 + y'^2)^{3/2}} = \int \left(\lambda + \frac{1}{y}\right) dy,$$

i.e.,

$$-\frac{1}{[1 + (y')^2]^{1/2}} = \lambda y + \ln y + \text{const.} \qquad [33]$$

Since $y_1 = a \sin \theta$

$$\lambda y_1 + \ln y_1 + \text{const.} = -\frac{1}{\sqrt{1 + \cot^2}} = -\sin \theta. \qquad [34]$$

Thus from [33] and [34] the general equation of the curve AB is

$$\frac{1}{\sqrt{1 + y'^2}} = \lambda(y_1 - y) + \ln \frac{y_1}{y} + \sin \theta,$$

and therefore

$$y' = \left\{\frac{1}{[\sin \theta + \lambda(y_1 - y) + \ln (y_1/y)]^2} - 1\right\}^{1/2}. \qquad [35]$$

Integration of Eq. [35] from y_0 to y_1 then gives

$$\int_{y_0}^{y_1} \frac{dy}{\{1/[\sin \theta + \lambda(y_1 - y) + \ln (y_1/y)]^2 - 1\}^{1/2}} = x_1 = a - a \cos \theta. \qquad [36]$$

For fixed values of λ and θ this integral can be found graphically; λ is known for any value of p/p_0 and hence by trial and error the value of θ can be found which satisfies Eq. [36]. When θ and hence x_1 have been determined, the volume of condensate for fixed λ is given by

$$V = 2.2\pi \int_0^{x_1} y^2\, dx - 2.2\pi \int_0^{x_1} [a^2 - (a - x)^2]\, dx$$

$$= 4\pi \int_{y_0}^{y_1} \frac{y^2}{y'}\, dy - 4\pi \left(a x_1^2 - \frac{x_1^3}{3}\right).$$

ACKNOWLEDGMENTS

We are indebted to Professor H. Jones, F.R.S., of the Department of Mathematics of this College for the method outlined in the Appendix. Thanks are due to the D.S.I.R. for an award to N. McK. and to the Beit Trustees for an award to J.S.S.R.

REFERENCES

1. BRUNAUER, S., "Physical Adsorption of Gases and Vapours," p. 150. Oxford University Press, 1944.
2. HILL, T. L., *J. Phys. Chem.* **54,** 1186 (1950).
3. TOLLENAAR, D., *Appl. Sci. Research* **A4,** 453 (1954).
4. HIGUTI, I., AND UTSUGI, H., *J. Chem. Phys.* **20,** 1180 (1952).
5. CARMAN, P., *Proc. Roy. Soc. (London)* **A209,** 69 (1951); *J. Phys. Chem.* **57,** 56 (1953).
6. DAVIES, C. N., *Discussions Faraday Soc.* **3,** 123 (1948).
7. BATES, T. F., HILDEBRAND, F. A., AND SWINEFORD, A., *Am. Mineralogist* **35,** 463 (1950).
8. *cf.* ILER, R. K., "The Colloid Chemistry of Silica and Silicates," Figs. 45 and 46. Cornell University Press, Ithaca, New York, 1955.
9. BARRER, R. M., AND WHITE, E. A. D., *J. Chem. Soc.* **1951,** 1561, Plate 1.
10. COHAN, L. H., *J. Am. Chem. Soc.* **60,** 433 (1938).
11. KRAEMER, E. O., *in* H. S. Taylor's "A Treatise on Physical Chemistry," p. 1661. Van Nostrand, New York, 1931.
12. McBAIN, J. W., *J. Am. Chem. Soc.* **57,** 699 (1935).
13. BARKAS, W. W., *Discussions Faraday Soc.* **3,** 108 (1948).
14. BARRER, R. M., AND MACLEOD, D. M., *Trans. Faraday Soc.* **50,** 980 (1954).
15. BARRER, R. M., DRAKE, J., AND WHITTAM, T. V., *Proc. Roy. Soc. (London)* **A219,** 32 (1953).
16. EVERETT, D. H., AND WHITTON, W. I., *Proc. Roy. Soc. (London)* **A230,** 91 (1955).
17. *e.g.*, RAO, K. S., *J. Phys. Chem.* **45,** 500–539 (1941).
18. EMMETT, P. H., AND CINES, M., *J. Phys. & Colloid Chem.* **51,** 1248 (1947).
19. BARRER, R. M., AND BARRIE, J. A., *Proc. Roy. Soc. (London)* **A213,** 250 (1952).
20. EVERETT, D. H., AND WHITTON, W. I., *Trans. Faraday Soc.* **48,** 749 (1952).
21. EVERETT, D. H., AND SMITH, F. W., *Trans. Faraday Soc.* **50,** 187 (1954).
22. EVERETT, D. H., *Trans. Faraday Soc.* **50,** 1077 (1954).
23. ENDERBY, J. A., *Trans. Faraday Soc.* **51,** 835 (1955).
24. ENDERBY, J. A., *Trans. Faraday Soc.* **52,** 106 (1956).
25. DE BOER, J. H., "The Dynamical Character of Adsorption," Chapter 8. Oxford University Press, 1953.
26. DUBININ, M. M., ZAVERINA, E. D., AND SERPINSKY, V. V., *J. Chem. Soc.* **1955,** 1760.
27. CARMAN, P., *Proc. Roy. Soc. (London)* **A211,** 526 (1952).
28. BARRER, R. M., *Trans. Faraday Soc.* **50,** 1074 (1954).
29. MOONEY, R. W., KEENAN, A. G., AND WOOD, L. A., *J. Am. Chem. Soc.* **74,** 1367 (1952).

JOURNAL OF COLLOID SCIENCE **11,** 496–500 (1956)

THE KINETICS OF COLLECTIVE SEDIMENTATION

R. C. L. Bosworth

The Colonial Sugar Refining Co., Ltd., Research Department, Pyrmont, Australia

Received March 20, 1956

INTRODUCTION

The rate of fall of an isolated solid particle through a fluid and under the influence of gravitational and frictional forces has been described by a number of empirical laws, each a valid approximation within a certain range of conditions. In all instances the rate of fall varies with the particle size and the difference between the particle density and the density of the fluid. Sedimentation of an inhomogeneous batch of particles accordingly results in the segregation of particles of different sizes and densities. The occurrence of such segregation in dilute suspensions has indeed been used for the grading of particles and in particle size analysis (see, for example, ref. 1).

However, there are many instances, particularly in the technical arts, where suspensions of an inhomogeneous nature settle with no segregation and indeed with a sharp line of separation between the supernatant liquid and the precipitate (2). Such settling is referred to as collective sedimentation. Typical examples occur in the process of clarification by sedimentation in the sugar industry.

Figure 1 represents successive photographs of a test tube in which a clarified sugar cane juice has been allowed to settle. The photographs were taken, respectively, ½, 1, 2, 3, 5, and 20 minutes after the settling commenced. The precipitate, which appears black in the photographs, consists of particles of insoluble calcium salts of phosphoric, silicic, and aconitic acids and perhaps smaller amounts of other organic acids mixed with particles of wax, coagulated protein, and certain polysaccharide present in the juice. The particle sizes range from 10 $\mu\mu$ to 5 μ. In spite of this large range in sizes practically all the particles settle together and indeed the line of demarcation between supernatant liquid and precipitate becomes sharper as settling proceeds. It is obvious in this instance that we are dealing with a relatively concentrated suspension.

In such concentrated suspensions it is to be expected that the rate of fall of any particular particle should be modified by the fall of other neighboring particles. Bikerman (ref. 3, page 315) has listed mechanisms whereby

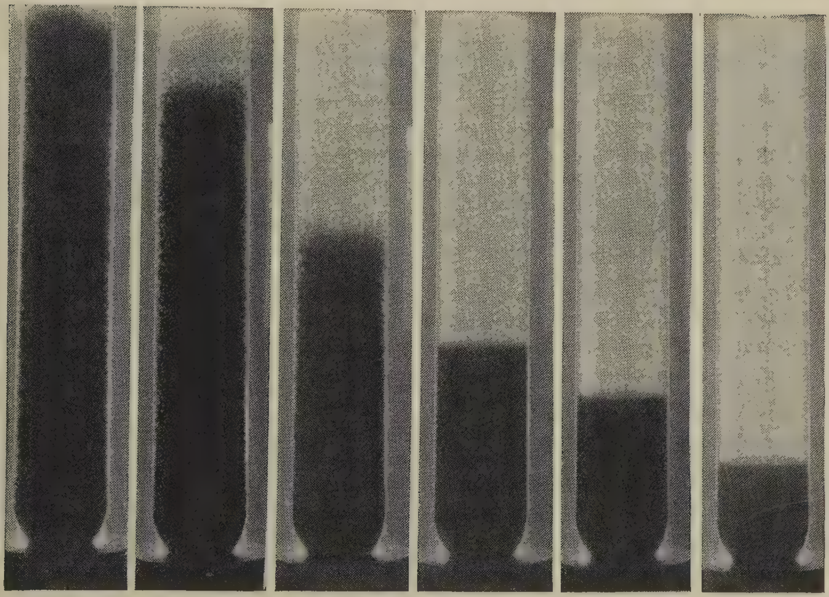

FIG. 1

such interaction can take place, and Kynch (4) has drawn some purely deductive conclusions on the possibility of the occurrence of critical phenomena during sedimentation of an incompressible solid.

The most comprehensive experimental study is that recorded by Steinour (5), who studied the rate of subsidence of slurries of spheres, angular particles, and loose flocculated aggregates of varying sizes. He gave a semi-empirical expression for the initial rate of subsidence of the slurries expressed as a sub-multiple of the free velocity of settling of an isolated average-sized particle falling under Stokes' law and obtained information on the amount of liquid immobilized by various-shaped angular and flocculated particles. However, the concept of the Stokesian velocities for the representative average-sized particle is not the type of property readily measurable for an ordinary slurry and the existence of many hundreds of sets of photographs of the type shown in Fig. 1 prepared the ground for a purely empirical study of the kinetics of sedimentations in terms of measurable properties of the slurry itself.

EXPERIMENTAL

Steinour's work, quoted above, shows that there are two important facts concerned with the rate of settling of slurry. These are:

1. The free rate of settling of the average-sized particles.

2. The total volume of the solid with due allowance for stagnant liquid immobilized between the particles.

The first factor in this set will clearly be related to the rate of settling at some standard state of dilution and thus standard state of interaction between particles.

The second factor is equally clearly related to the ultimate volume of the mud sediment after infinite time.

The empirical measurements of the volume of mud at five or six successive times could accurately be used to extrapolate to infinite time when it was found that the plot of the volume versus the reciprocal of the time tended to linearity in a very large number of instances.

Further the subsiding layers of mud are all in a comparable state of dilution when they reach a volume which is some fixed multiple of the final volume. The time taken to reach twice the final volume may perhaps be called the half-life time of the precipitate.

From these two measurements the kinetic properties of any particular batch of settling mud can then be expressed as a relation between dimensionless quantities:

x = the ratio of the volume at time t to the volume at infinite time,

and

y = the ratio of the actual time of partial settling t to the half-life time.

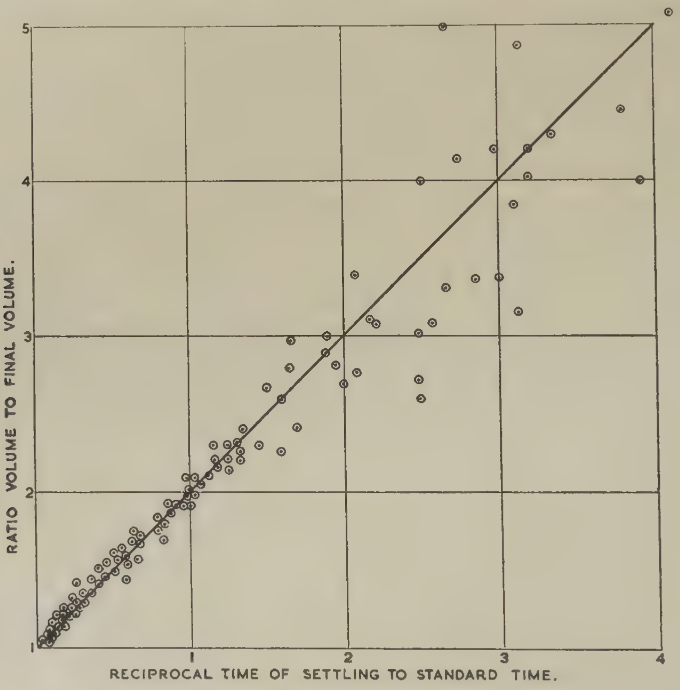

FIG. 2

RESULTS

The experimental relation between the dimensionless quantities x and y proves, as might have been anticipated, to be an hyperbolical one.

Figure 2 shows x, or the ratio of volume to final volume, plotted against the reciprocal of y, or the ratio of the actual time of settling to the half-life time. Although the figure shows a considerable scattering of points, the linear relation between the variables is apparent.

For the line of best fit we have:

$$x - 1 = \frac{0.95}{y} \qquad [1]$$

as an empirical expression for the kinetics of collective sedimentation.

DISCUSSION

The empirical law (Eq. [1]) connecting the relative volume (x) of the precipitate with its relative life period (y) may readily be differentiated to give an expression for the rate of settling at any particular stage.

For a liquid settling in a tube of constant sectional area an alternative expression for x reads:

$$x = \frac{h}{h_\infty},$$

where h is the height of the top of the precipitate at any time t and h_∞ is the final height. The variable y correspondingly becomes

$$y = \lambda t,$$

where λ is a measure of the rate of settling in some standard state and as such is related to the mean particle size and average particle shape. Equation [1] now becomes

$$\frac{h}{h_\infty} - 1 = \frac{0.95}{\lambda t},$$

or the $v = dh/dt$, the velocity of settling at time t becomes

$$v = \frac{1.05(h - h_\infty)^2}{\lambda h_\infty} \qquad [2]$$

The concentration C of the suspension is related to the ratio of h_∞ to h and if the final volume, because of water immobilized between particles is some multiple k of the true volume of the suspended particles, we have

$$C = \frac{h_\infty}{kh},$$

and Eq. [2] becomes:

$$v = \frac{1.05h_\infty}{\lambda}\left(\frac{k}{C} - 1\right)^2 \qquad [3]$$

and may be compared with the Powers' (6) equation developed for the sedimentation of cement pastes. Powers' equation reads

$$v = \frac{0.2}{\sigma^2}\frac{g\Delta\rho}{\eta}\frac{(1/C - k)^3}{(1/C) - 1} \qquad [4]$$

where

σ = the specific surface of the particles,
$\Delta\rho$ = the density difference between solid and fluid, and
η = the viscosity of the fluid.

Equation [3] differs from [4], however, in that all the terms concerned are directly measurable from the kinetic behavior of the slurry itself.

REFERENCES

1. ROSE, H. E., "The Measurement of Particle Size in Very Fine Powders." Constable, London, 1953.
2. WILSON, B. I. O., *Australian J. Appl. Sci.* **4,** 274–299 (1953).
3. BIKERMAN, J. J., "Surface Chemistry in Industrial Research." Academic Press, New York, 1945.
4. KYNCH, G. J., *Trans. Faraday Soc.* **48,** 166–176 (1952).
5. STEINOUR, H. A., *Ind. Eng. Chem.* **36,** 618–624, 840–847, 901–907 (1945).
6. POWERS, T. C., *Bull. Research Lab. Portland Cement Assoc. U. S. A.* **2** (1939).

JOURNAL OF COLLOID SCIENCE 11, 501–507 (1956)

INTERFACIAL ENERGIES

E. A. Moelwyn-Hughes

Department of Physical Chemistry, University of Cambridge, Cambridge, England

Received December 20, 1955

The energy of molecules in an interface, like that of molecules generally, consists of two parts: the kinetic energy depends on molecular motion, and the potential energy on the relation in which a molecule stands to the other molecules in the system. In this paper we consider only the potential energy. We shall review briefly, and in some respects extend, the theories hitherto advanced.

The Energy of Adsorption on a Plane Surface

Let a molecule be placed at a point P (Fig. 1) which is at a vertical distance d above the plane surface of a condensed phase containing n_α molecules per cubic centimeter. It is clear from Fig. 1 that its energy of interaction with all the molecules in the condensed phase is

$$\Phi = 2\pi n_\alpha \int_{z=d}^{z=\infty} dz \int_{a=z}^{a=\infty} \phi(a) a da, \qquad [1]$$

where $\phi(a)$ is the energy of interaction of the molecule placed at P with an isolated molecule of the kind appearing in the condensed phase. This we shall take to be given by Mie's equation (1)

$$\phi(a) = Aa^{-n} - Ba^{-m}, \qquad [2]$$

where n and m are integers ($n > m$), and A and B are constants. Then

$$\Phi = 2\pi n_\alpha \left[\frac{A}{(n-2)(n-3)} \cdot \frac{1}{d^{n-3}} - \frac{B}{(m-2)(m-3)} \cdot \frac{1}{d^{m-3}} \right]. \qquad [3]$$

If we ignore the energy due to repulsion, and take $m = 6$, we obtain

$$\Phi = -\frac{\pi n_\alpha B}{6d^3} \qquad [4]$$

This is the result obtained by F. London (2), and successfully applied by him to compute the energy of desorption of various gases from charcoal. His well-known dispersion theory allows of an independent evaluation of B. Among the striking experiments confirming London's theory may be

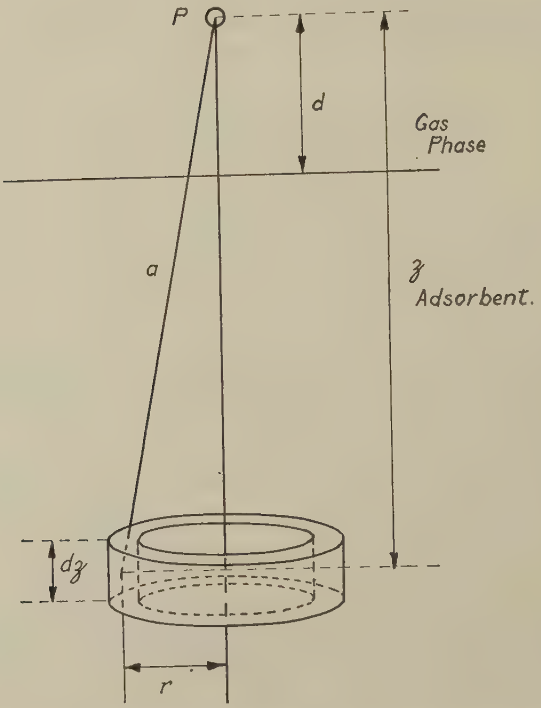

FIG. 1. To determine the interaction energy of a molecule of gas with a solid, when the molecule is at a vertical distance d above a plane surface.

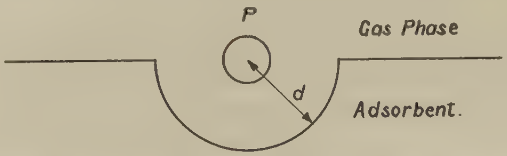

FIG. 2. A molecule adsorbed in the plane of the surface, above a hemispherical cavity.

mentioned those of R. M. Barrer (3) (hydrogen on graphite) and W. J. C. Orr (4) (argon on potassium chloride).

The Energy of Adsorption on a Hemispherical Cavity in a Plane Surface

When a molecule is centrally situated on a hemispherical cavity in an otherwise plane surface (Fig. 2), its energy of interaction with the condensed phase is clearly

$$\begin{aligned}\Phi &= 2\pi n_\alpha \int_d^\infty \phi(a)a^2 da \\ &= 2\pi n_\alpha \left[\frac{A}{(n-3)}\cdot\frac{1}{d^{n-3}} - \frac{B}{(m-3)}\cdot\frac{1}{d^{m-3}}\right].\end{aligned} \qquad [5]$$

If we again ignore repulsion and take m as 6, we find

$$\Phi = -\frac{2\pi n_\alpha B}{3d^3}, \tag{6}$$

which is four times as great as the former result (J. H. de Boer and J. F. H. Custers (5)). The force attracting a molecule to a curved surface is thus greater than that attracting it, at the same distance, to a plane surface. If, therefore, a surface thought to be planar is in fact marred by cracks and crevices, adsorption first occurs in them. As the fissures are gradually filled up, there is progressively more adsorption on the flat surface, and the heat of adsorption consequently gets smaller. J. K. Roberts (6), however, has shown that the experimental heat of adsorption from a plane surface increases as the surface becomes more and more covered. The two effects are in opposite directions, and taken jointly can account for the fact that the heat of adsorption in certain instances passes through a minimum (7).

A Comparison of the Two Energies of Adsorption

Equations [3] and [5] hold for arbitrary values of the distance d. The nearest distance to which a molecule can be drawn to the surface is given by the equation

$$d_0^{n-m} = \frac{(m-2)A}{(n-2)B} \tag{7}$$

in the planar system, and

$$d_0^{n-m} = \frac{A}{B} \tag{8}$$

in the hemispherical system. The corresponding minimum energies are

$$\Phi_0 = \frac{2\pi n_\alpha B}{(m-2)\, d_0^{m-3}} \left[\frac{1}{(n-3)} - \frac{1}{(m-3)}\right], \tag{9}$$

and

$$\Phi_0 = \frac{2\pi n_\alpha B}{d_0^{m-3}} \left[\frac{1}{(n-3)} - \frac{1}{(m-3)}\right]. \tag{10}$$

Hence

$$\frac{\Phi_0\ (curved)}{\Phi_0\ (planar)} = \left[\frac{(m-2)^{n-3}}{(n-2)^{m-3}}\right]^{\left(\frac{1}{n-m}\right)} \tag{11}$$

This ratio is smaller and more exact than that found using arbitrary values of d. Thus, for example, with $m = 6$ and $n = 9$, the ratio is $16/7 = 2.29$.

The Frequency of Vibration of an Adsorbed Molecule

By expanding $\Phi - \Phi_0$ in a power series of $(d - d_0)$, the gain in energy when the adsorbed molecule is displaced slightly from its equilibrium position is found to vary in proportion to $(d - d_0)^2$. Its motion in the dimension normal to the surface is consequently a simple harmonic vibration, with a frequency in the planar model given by

$$\nu_0 = \frac{1}{2\pi d_0} \sqrt{\frac{(m-3)(n-3)\lambda_0}{\mu}}, \qquad [12]$$

where $\lambda_0 = -\Phi_0$, and μ is the mass of the adsorbed molecule.

The Energy of Cohesion between Planar Surfaces

Instead of the molecule indicated by P in Fig. 1, let us consider a number of molecules placed in a horizontal slab of thickness δd and of extension O cm.^{2} at the same height d from the surface of the condensed phase α. The number of molecules in the slab is $On_\beta \delta d$, where n_β is the concentration of molecules in the upper phase. The total interaction energy between all the molecules in one phase with all the molecules in the other phase is

$$U = \int_d^\infty \Phi n_\beta O \delta d, \qquad [13]$$

where Φ is given by Eq. [3]. Hence

$$U = 2\pi n_\alpha n_\beta O \left[\frac{A}{(n-2)(n-3)(n-4)} \cdot \frac{1}{d^{n-4}} - \frac{B}{(m-2)(m-3)(m-4)} \cdot \frac{1}{d^{m-4}} \right]. \qquad [14]$$

The nearest distance to which the two phases approach is given by the equation

$$d_0^{n-m} = \frac{(m-2)(m-3)}{(n-2)(n-3)} \cdot \frac{A}{B}, \qquad [15]$$

and the minimum potential energy of the system is

$$U_0 = -\frac{(n-m)2\pi n_\alpha n_\beta BO}{(m-2)(m-3)(m-4)(n-4)d_0^{m-4}} = -bn_\alpha n_\beta O, \qquad [16]$$

where b is a positive constant. This is the energy of cohesion. The reference state of zero energy is that of the isolated phases at an infinite distance apart. An expression resembling Eq. [16] has been derived by T. S. Wheeler (8), who regarded it, however, as only one of three components in the total interaction energy.

We are now in a position to calculate the excess potential energy, U_σ, which a pure substance possesses when it exists in two phases, separated by a plane surface of area O, over the sum of the energies of the two isolated phases. It follows from Eq. [16] that

$$U_\sigma = (n_\alpha - n_\beta)^2 bO. \qquad [17]$$

An equation of this form has been derived by R. H. Fowler (9).

The excess energy due to the creation of an interfacial area of extent O between two phases of different substances is

$$U_\sigma = (b_{\alpha\alpha}n_\alpha^2 + b_{\beta\beta}n_\beta^2 - 2b_{\alpha\beta}n_\alpha n_\beta)O. \qquad [18]$$

When $m = 6$ and the forces of attraction are due to dispersion, the constants b can be calculated using London's theory (2).

The Surface Tension of a Pure Liquid

When a liquid is in thermal equilibrium with its vapor, the excess free energy per unit area of surface is numerically equal to the surface tension. In the absence of thermal motion, the free energy equals the total energy. Hence the extrapolated value of the surface tension at $T = 0$ is

$$\gamma_0 = \frac{U_\sigma}{O} = (n_\alpha - n_\beta)^2 b. \qquad [19]$$

When the concentration of molecules in the vapor phase can be neglected, we have

$$\gamma_0 = \frac{U_\sigma}{O} = n_\alpha^2 b.$$

On using Eq. [16], we obtain the result

$$\gamma_0 = \frac{(n - m)2\pi n_\alpha^2 B}{(m - 2)(m - 3)(m - 4)(n - 4)\ d_0^{m-4}}. \qquad [20]$$

Hildebrand, Wakeham, and Boyd (10) have shown that $n = 9$ and $m = 6$ for mercury. Hence

$$\gamma_0 = \left(\frac{\pi}{20}\right)\frac{n_\alpha^2 B}{d_0^2}. \qquad [21]$$

Moreover, for this liquid, $B = 4.90 \times 10^{-58}$ erg-cm.^{6} (11) and $d_0 = 1.944$ A. The computed value of γ_0 is thus 344 ergs/cm.^{2}.

By applying to molecules in the surface layer, and in the layers immediately beneath it, the radial distribution function established by Hildebrand for the liquid, G. Jura (12) calculates an excess surface potential energy of 500 ergs/cm.^{2}, in closer agreement with the experimental value of γ_0, which is 463.6 ergs/cm.^{2} (13).

Stefan's Ratio

J. Stefan (14) argued that the energy gained by a molecule on being transferred from the bulk of the liquid to its surface must be equal to the energy gained during a further transfer from the surface to the vapor. His argument has been corrected on theoretical (15) and experimental (16) grounds. The ratio of the excess energy for molecules in the surface to the latent heat of vaporization has been given an extremely simple interpretation in terms of the coordination numbers in the interface and in the bulk liquid (17). Another means of arriving at Stefan's ratio is provided by the general theory of intermolecular forces.

If the molecules in a fluid are uniformly distributed, and fluctuations in the concentration n_α are ignored, the total potential energy of N_α molecules of a liquid is

$$U = 2\pi N_\alpha n_\alpha \int \phi(a)a^2 da. \qquad [22]$$

On using Mie's equation [2], the minimum value of U is found to be

$$U_0 = -\frac{2\pi N_\alpha n_\alpha B}{a_0^{m-3}}\left[\frac{1}{(m-3)} - \frac{1}{(n-3)}\right], \qquad [23]$$

where

$$a_0^{n-m} = \frac{A}{B}. \qquad [24]$$

The excess energy ascribable to a surface of extension O cm.^{2} is found from Eqs. [16] and [17] to be

$$U_\sigma = \frac{2\pi n_\alpha^2(n-m)BO}{(m-2)(m-3)(m-4)(n-4)\, d_0^{m-4}}, \qquad [25]$$

where d_0 is given by Eq. [15]. The ratio of the heat of vaporization (at the absolute zero of temperature) to the excess energy due to the surface is thus

$$-\frac{U_0}{U_\sigma} = \frac{(N_\alpha/Od_0)}{n_\alpha} \cdot \frac{(m-2)(m-4)(n-4)}{(n-3)} \cdot \left(\frac{d_0}{a_0}\right)^{m-3}. \qquad [26]$$

The first term on the right-hand side is clearly unity. Hence, Stefan's ratio becomes

$$-\frac{U_0}{U_\sigma} = (m-4)(n-4)\left(\frac{m-2}{n-3}\right)^{\left(\frac{n-3}{n-m}\right)}\left(\frac{m-3}{n-2}\right)^{\left(\frac{m-3}{n-m}\right)}. \qquad [27]$$

With $m = 6$, we thus anticipate ratios in the neighborhood of 1.91 ($n = 9$), 2.60 ($n = 12$), and 3.12 ($n = 15$). These agree with the experimental ratios, as given by R. Haul (18) and H. Volkmann (19), which are 2.20 (He), 2.37 (Ne), 2.38 (A), 2.15 (Hg), 3.10 (CS_2), and 3.20 (CCl_4).

This article has been written as a tribute to Sir Eric Rideal. While writing it, I had also inevitably in mind the memory of his friend, the late Sir John Lennard-Jones. It has been one of the author's greatest privileges to enjoy over a number of years a close collaboration and friendship with both.

REFERENCES

1. MIE, G., *Ann. Physik* **11**, 657 (1903).
2. LONDON, F., *Z. physik. Chem.* **B11**, 222 (1930).
3. BARRER, R. M., *Proc. Roy. Soc. (London)* **A161**, 476 (1937).
4. ORR, W. J. C., *Trans. Faraday Soc.* **35**, 1247 (1939).
5. DE BOER, J. H., AND CUSTERS, J. F. H., *Z. physik. Chem.* **B25**, 225 (1934).
6. ROBERTS, J. K., "Some Problems in Adsorption." Cambridge, 1939.
7. POLANYI, M., AND WELKE, V., *Z. physik. Chem.* **A132**, 371 (1928).
8. WHEELER, T. S., *Trans. Natl. Inst. Sci. India* **1**, 333 (1938).
9. FOWLER, R. H., *Proc. Roy. Soc. (London)* **A159**, 229 (1937).
10. HILDEBRAND, J. H., WAKEHAM, H. R. R., AND BOYD, R. N., *J. Chem. Phys.* **7**, 1094 (1939).
11. MOELWYN-HUGHES, E. A., *J. Phys. & Colloid Chem.* **55**, 1246 (1951).
12. JURA, G., *J. Phys. & Colloid Chem.* **52**, 40 (1948).
13. BIRCUMSHAW, L. L., *Phil. Mag.* **12**, 596 (1931).
14. STEFAN, J., *Wied. Ann.* **29**, 655 (1886).
15. OSTWALD, W., *Z. physik. Chem.* **1**, 45 (1887).
16. HARKINS, W. D., AND ROBERTS, L. E., *J. Am. Chem. Soc.* **44**, 653 (1922).
17. WOLF, K. L., AND KLAPPROTH, K., *Z. physik. Chem.* **B46**, 276 (1940).
18. HAUL, R., *Z. physik. Chem.* **A53**, 331 (1943).
19. VOLKMANN, H., *FIAT Rev. Ger. Sci. Phys. Chem.* **30**, 205 (1947).

JOURNAL OF COLLOID SCIENCE **11**, 508–518 (1956)

LIGHT-SCATTERING MEASUREMENTS ON SOME BRANCHED POLYSTYRENES

M. H. Jones,[1] H. W. Melville, D. W. Ovenall, F. W. Peaker, and W. G. P. Robertson[2]

Chemistry Department, The University, Birmingham, England

Received April 5, 1956

Abstract

Light-scattering measurements are described on branched polystyrenes prepared by a bromination growth technique designed to produce polymers of known structure. The molecular weights and dimensions calculated from light scattering have been correlated with the structures predicted from the conditions of polymer synthesis.

Introduction

Attention has been drawn recently (1) to the paucity of precise experimental information yet available on the influence of branching on the physical properties of polymer molecules. This is largely due to the difficulty of producing, for investigation, suitable samples of branched polymers without introducing the added complication of any crosslinking (2, 3) and to the difficulty of determining with any precision the nature and extent of the branching effected.

Several methods have been described recently (1, 4–6) by which it is possible to synthesize branched vinyl polymers or graft copolymers fairly readily. The primary aim of one of these methods (1) was to make available some well-characterized samples of branched polystyrene so that the physical properties of the branched polymers, with particular reference to light scattering, could be compared with those of the linear species. Branched polystyrene was obtained by brominating polystyrene photochemically and subsequently irradiating the brominated product in the presence of fresh monomer. This paper reports the results of light-scattering measurements on some branched polystyrenes previously prepared (1) in this way.

Materials

The experimental procedure for the bromination of polystyrene and for the branch-growth polymerization has been previously described (1). The starting material for most of the branched polymers was a commercial polymer designated X (7). From this were derived the brominated polystyrenes A, C, and E, from which in turn were obtained branched polymers A1, C1, E3, and E4. A second sample of polystyrene used as a starting material was a laboratory preparation, Y. This was a first fraction (25%) from a polystyrene prepared photochemically from the pure monomer at 25°C. using 1-azo-bis-1-cyclohexanonitrile (0.1 g./l.) as initiator, the polymerization being carried to 5% conversion. The polystyrene Y was the parent polymer from which a brominated polystyrene F and its branched derivatives F1 and F2 were obtained. In Table I the two starting materials X and Y and their bromination products are listed with characterizing data. Table II lists the branched polymers.

---

[1] Present address: Ontario Research Foundation, Toronto.

[2] Present address: Weapons Research Establishment, Salisbury, South Australia.

The branched polystyrene C1 was prepared in the absence of transfer agent (carbon tetrachloride). Normally under these conditions insoluble

TABLE I

Polystyrene Starting Materials and Their Bromination Products

Polymer	% Bromine by analysis	[η] (dl./g.) [a]	$M_n \times 10^{-3}$ [b]
X	—	6.12	2000
A	10.8	1.04	190
C	0.05	4.41	1300
E	4.0	3.40	890
Y	—	2.58	650
F	4.8	0.827	150

[a] In benzene solution at 20°C.

[b] From viscosity measurements and data of Ewart and Tingey (18).

TABLE II

Branched Polymers

Polymer	% Branching[a]	P_n Branches[b]	Monomer units of backbone/branch	P_n backbone[e]	Average no. branches/molecule
C1	(25)[c]	8,000	(25,000)	12,500	(0.5)
A1	37	160	270	1,900	7
E3	39	310	480	8,500	19
E4	25	95	290	8,500	31
F1	34[d]	230	450	1,500	3.5
F2	37	230	390	1,500	4

[a] Calculated from fractionation data (1).

[b] Calculated degree of polymerization from kinetic data (19).

[c] Calculated from kinetic data (19).

[d] Radioactive branches. C^{14} assay indicated 34%, 38%, 35% branching for three fractions of the branched polymer. Bromine analysis indicated about 40% branching (1).

[e] Calculated degree of polymerization from M_n values of Table I.

cross-linked polymers are obtained (1), but in the case of C1 the extent of branching and crosslinking was too small to lead to insolubility (polymer C1 was not fractionated at all). The extent of branching was calculated from the observed polymerization during the branching reaction, on the assumption that half was due to branching and half to the formation of linear, bromine atom-initiated polymer. The apparent results may be quite misleading in view of the termination by combination of polystyrene radicals (8). The branching data given in Table II for the other branched polymers were calculated from fractionation results (1). Polymers F1 and F2 were prepared as nearly identically as practically possible except that styrene monomer labeled with C^{14} was used for the branches in F1. In the case of F1 the branching data calculated from fractionation results was checked by C^{14} assay and also by bromine analysis before and after branching. The results were in good agreement (1). The following polymers were examined by the light-scattering method:

Polystyrenes X and Y
Brominated polystyrenes E and F
Branched polystyrenes A1, C1, E3, E4, and F2.

Polymers X, E, A1, and C1 were examined unfractionated. A1 was considerably contaminated with low molecular weight polymer. The probable complexity of C1 is mentioned above. The branched polymers E3, E4, and F2 were fractionated to remove the linear low molecular weight impurity.

The values given in Table II for the chain lengths of the backbones of branched polymers assume no degradation during branch-growth polymerization. The number of branches per molecule will depend on the length of the backbone, being derived on the basis of the assumed backbone length from the figures for branch frequency.

EXPERIMENTAL

The instrument used for the light-scattering measurements was that previously described by Bosworth *et al.* (9). Pure dry methyl ethyl ketone was used as a solvent, since this gives a conveniently high value for the refractive index increment. The polymer solutions were filtered through a bed (thickness 1 cm.) of "Metasil," grade A, filtration medium (Metafiltration Co., Hounslow, Middlesex) supported on a No. 3 sintered glass filter. The concentrations of the solutions of brominated and branched polymers were measured by weighing samples of each (about 8 g.), evaporating off the solvent at room temperature on a vacuum line, and weighing the polymer residue. This technique was adopted because it was feared that heating these polymers might cause some degradation. Although constant weight was obtained in about 24 hours, it is likely that, owing to residual solvent, the concentrations measured in this way were about 5% too high. Polymer concentrations of 0.3 g. per 100 ml. and below were used.

The polymer solutions were contained in a cylindrical cell for measurement and scattering intensities obtained from 30° to 140° to the incident beam. A correction for back reflection of the incident beam was made (10). The apparatus was calibrated by using a magnesium carbonate block as a standard diffuse reflector (11).

The light-scattering measurements were interpreted in accordance with the equation

$$\frac{Kc}{R_\theta} = \frac{1}{M_w P(\theta)} + \frac{2B}{RT} C,$$

where R_θ is the reduced intensity of scattering at an angle θ of a solution of concentration C g. cm.$^{-3}$ and

$$K = \frac{2\pi^2 n_0^2 \left(\frac{\partial n}{\partial c}\right)^2}{N\lambda^4},$$

where n_0 is the refractive index of the solvent and $\partial n/\partial c$ the refractive index increment; N is Avogadro's number and λ the wavelength of the light in vacuum.

Weight-average molecular weights were calculated from the limiting relationship

$$\frac{1}{M_w} = \left(\frac{KC}{R_0}\right)_{c=0}$$

obtained by Zimm's method of plotting (12). The size of molecules in solution was obtained from the variation of the reciprocal of the reduced intensity with $\sin^2 (\theta/2)$ in the limit of zero concentration by using the equation (13)

$$D^2 = \frac{9\lambda^2}{8\pi^2 n_0^2} \frac{(\text{Limiting slope at } \theta = \theta^\circ)}{\text{Intercept}}.$$

For linear randomly coiled molecules D is the r.m.s. end-to-end distance. In the case of branched molecules D corresponds to $\sqrt{6}$ times the radius of gyration (13, 14).

From the characteristics of the mercury arc and filter used the effective wavelength of the light source was estimated as 4247 A. Errors quoted were estimated from the difficulties in extrapolation caused by scatter of the experimental points. All molecular weights, although consistant in themselves, are subject to any systematic error which may be present in the calibration of the apparatus (11).

Results and Discussion

The results of the light-scattering measurements are summarized in Table III. For convenience in the discussion of these results the polymers

TABLE III

Light-Scattering Results

Group	Sample	$M_w \times 10^{-6}$ from 0°	D from 0° (A.)	$\frac{2B}{RT}$ g.$^{-1}$cm.^{3}	$\frac{M_w}{D^2}$ ($A.^{-2}$)
	X	3.15 ± 0.1	2410	2.3×10^{-4}	0.54
1	A1	3.05 ± 0.1	2140	0.7×10^{-4}	0.67
	C1	3.8 ± 0.3	3000	0.35×10^{-4}	0.42
	E	1.00 ± 0.02	1375	0.48×10^{-4}	0.53
2	E3	1.41 ± 0.06	1300	1.15×10^{-4}	0.83
	E4	0.91 ± 0.02	941	3.3×10^{-4}	1.03
	Y	1.17 ± 0.02	1270	2.4×10^{-4}	0.72
3	F	0.16 ± 0.005	—	~ 0.0	—
	F2	0.31 ± 0.01	—	3.9×10^{-4}	—

have been divided into three groups. None of the polymers in the first group (Table III), polystyrene X and the two branched products A1 and C1, was fractionated prior to light-scattering measurements. Of the second group the brominated polymer, E, was unfractionated. The linear polystyrene Y and its branched derivatives of the third group were all fractionated polymers. The relationships between the polymers measured by light scattering are shown in Fig. 1.

1. Polymers X, A1, and C1

The graphs of the reciprocal of the reduced intensities for these polymers (Figs. 2, 3, and 4) are convex to the $\sin^2 (\theta/2)$ axis in all three cases. This behavior is to be expected for polydisperse materials. In such cases molecular weights calculated from reduced intensities at 90° and limiting dissymmetry values would give misleading results, since the angular variation of scattering intensity does not follow that for monodisperse random coils, the model usually chosen for the interpretation of the asymmetry of scattering by solutions of chainlike polymer molecules.

Subsequently Stead and Melville (15) have shown by the turbidimetric titration method that the polymer X had a wide molecular weight distribution with many peaks, and it seems likely that the scattering behavior is due to polydispersity. Hawkins and Smith (16) have also measured a sample of polystyrene X and obtained 2.94×10^6 for the weight-average molecular weight calculated from zero angle scattering at 5780 A, which is in fair agreement with the value in Table III.

Increases in the average molecular weights of these polymers due to branching may be masked by two effects. The degradation which occurs on bromination will result in a backbone of much lower molecular weight than the parent polymer (Table I), and the presence of low molecular weight polymer in the final product will decrease the weight-average molecular

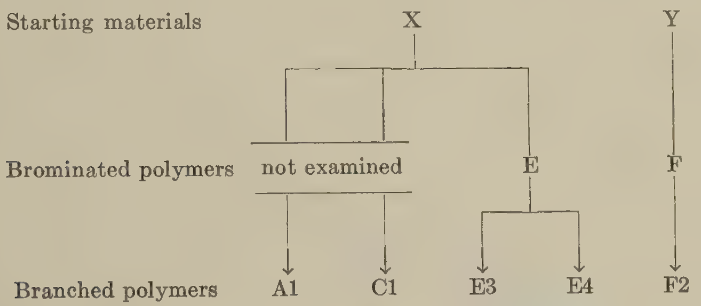

FIG. 1. Relationships between polymers examined by light scattering.

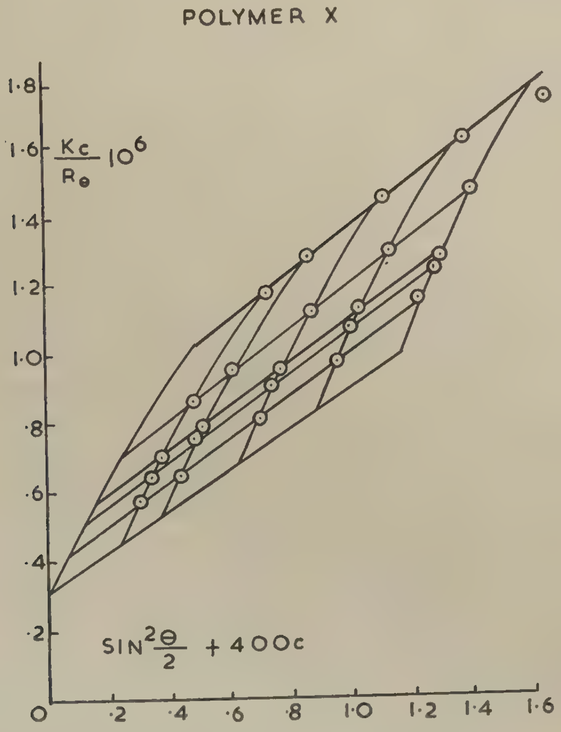

FIG. 2. Zimm plot for polymer X.

weight. In the case of the branched polystyrene C1 the latter results from bromine atom initiation and additionally in the case of A1 from the action of the transfer agent. The observed increase in molecular weight of some 20% in going from X to C1 (Table III) confirms that this polymer is branched. Polymer A1 had substantially the same molecular weight as X, which, bearing in mind the above effects, indicates that some branching has taken place. The variation in second virial coefficient (Table III) is

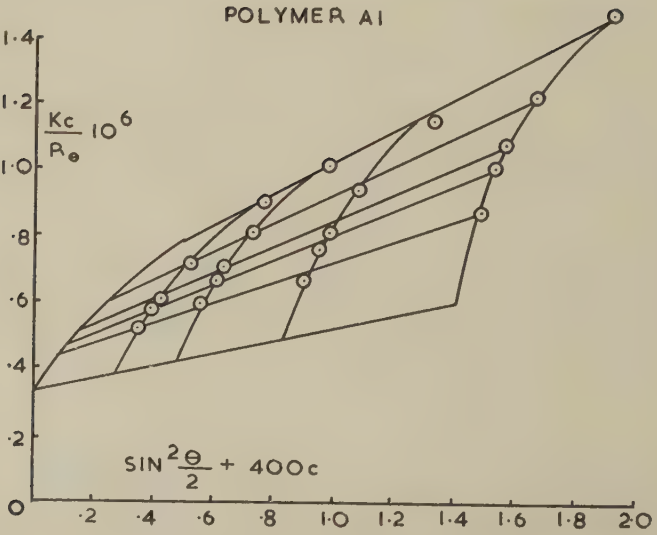

FIG. 3. Zimm plot for polymer A1.

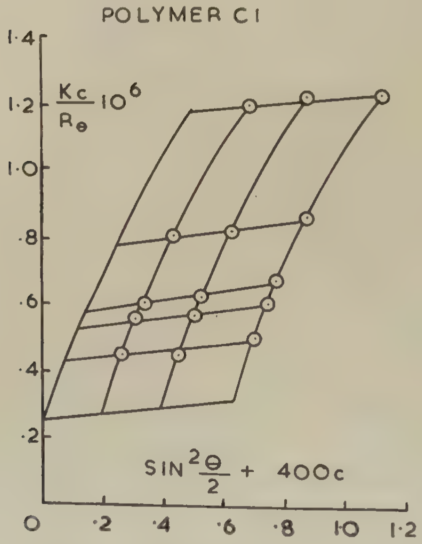

FIG. 4. Zimm plot for polymer C1.

paralleled by the behavior of the dissymmetry coefficients (Fig. 5). In the case of X the relatively high second virial coefficient and the large increase in dissymmetry which occurs on dilution indicate an extended molecular structure. Polymers A1 and C1 have lower second virial coefficients and show little change in dissymmetry on dilution. This suggests the presence of molecules of a more compact structure which are relatively independent

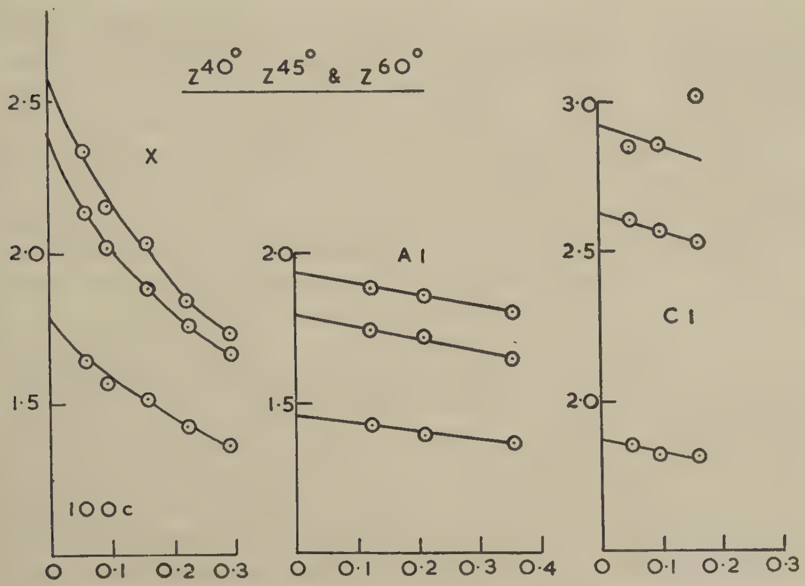

FIG. 5. Variation of dissymmetry coefficients with concentration for polymers X, A1, and C1.

at moderate concentrations. In the case of A1 this behavior could be partly due to residual bromine, but it is unlikely that a significant amount of bromine was present in polymer C1.

In view of the work of Bosworth *et al.* on polyvinyl acetate (9) it was hoped that it would be possible to follow changes in structure by variations in the ratio M_w/D^2. If nonrandom coil behavior and the excluded volume effect are neglected, this ratio should be independent of molecular weight for a given structure. Branched, and therefore more compact, molecules should give higher values than linear molecules. The interpretation here is complicated by the polydispersity of the polymers. The calculated r.m.s. end-to-end distance is that for a molecule with the Z average molecular weight. This may be considerably greater than the weight-average molecular weight. The ratio M_w/D^2 for the polymer X is considerably less than values which have been obtained for fractionated polystyrenes in methyl ethyl ketone (17). This is more probably due to polydispersity than to branching. The molecular weight distribution for the two unfractionated polymers A1 and C1 will be wider than for X. As it is difficult to estimate the limiting slopes of the Zimm plots owing to curvature, the observed variations in M_w/D^2 are probably not significant.

2. Polymers E, E3, and E4

In calculating the weight-average molecular weight of the brominated polymer E it has been assumed that the bromine content did not affect the value of the refractive index increment. The refractive indices of solutions of known concentration of E and the brominated polymer F (Section 3) were checked in a Rayleigh interferometer (11) and no significant difference from normal polystyrenes was found.

It is interesting to compare the data obtained for polymer E (Table III) with that for the parent polymer X. The similarity of the values for M_w/D^2 obtained for X and E indicates little change in structure. This is in apparent contradiction to the decrease in second virial coefficient. It would appear that although the brominated polymer E is less soluble than the original polymer X, it is not more tightly coiled in solution.

Unlike the polystyrene X and its bromination product E, the two derived branched polymers, E3 and E4, were fractionated. However, the fractionation was designed only to separate the high molecular weight branched material from the low molecular weight polymer present as a by-product of the branch-growth polymerization. Of the two polymers E3 and E4, only E3 showed an increase in molecular weight over polymer E (Table III). This is not altogether surprising for it must be assumed that, as in the case of the bromination reaction, there is opportunity during the branch-growth polymerization for some degradation of the backbone to occur. Not only was a greater proportion of branching introduced in E3 (39%) than in E4 (25%) but the shorter branch length obtained in E4 (Table II) required the use of more drastic conditions for the branching polymerization with consequently a greater chance of degradation.

The values for M_w/D^2 obtained for both E3 and E4 are significantly higher than the values obtained for the parent brominated polymer E or the starting material X and also higher than the value for the fractionated linear polystyrene Y (Table III). As it is unlikely that the fractionation of polymers E3 and E4 resulted in any appreciable narrowing of the molecular weight distribution of the branched polymer, it appears that the observed increase in M_w/D^2 may be attributed to the presence of branching.

3. Polymers Y, F, and F2

This polymer series exhibits similar behavior to those of the earlier sections. Bromination of the polystyrene Y has resulted in a considerable decrease in weight-average molecular weight. The branched polystyrene F2 has a molecular weight almost twice that for F.

Insufficient data were available to enable the second virial coefficient of F to be obtained with high accuracy. However it was certainly not far from zero. This decrease in second virial coefficient on bromination and its increase after the branch-growth polymerization, which was also observed in the series X, E, E3, and E4, may be attributed to the removal of bromine atoms from the polymer backbone during the latter process. No comparison between the second virial coefficients of Y and F2 is possible owing to the large difference in molecular weight.

Both F and F2 had symmetrical scattering envelopes. In the case of F this is not surprising since, owing to the low molecular weight, the r.m.s. end-to-end distance would be expected to be only of the order of a tenth of a light wavelength in solution. However, the weight-average molecular weight of F2, which is roughly twice that of F, suggests that for similar values of M_w/D^2 its r.m.s. end-to-end distance should be of the order of four-tenths of a wavelength. This would give rise to a measurable dissymmetry. Thus it appears that the branched polymer F2 is more compact in solution than the brominated polymer F.

CONCLUSIONS

From these measurements it is concluded that branched polymers can be produced by the bromination growth technique and that such branching can be detected by light scattering. However, in order to obtain unambiguous results the molecular weight distributions of the materials examined should be well defined. By its very nature branch-growth polymerization does not allow strict control. With a fractionated backbone and with neglect of the degradation during branch growth, there remains the spread of the degree of polymerization of the branches. It is felt, however, that although emphasizing the difficulties, these results do indicate the scope of light-scattering measurements in studies of this type.

ACKNOWLEDGMENTS

M. H. J. wishes to thank Bakelite Limited for a Research Fellowship, and D.W.O. wishes to thank The British Rayon Research Association for a Research Scholarship, during the tenure of which this work was carried out. W.G.P.R. thanks the Department of Supply, Commonwealth of Australia for the opportunity of participating in the work.

REFERENCES

1. JONES, M. H., MELVILLE, H. W., AND ROBERTSON, W. G. P., *Nature* **174,** 78 (1954).
2. MANSON, J. A., AND CRAGG, L. H., *Can. J. Chem.* **30,** 482 (1952); CRAGG, L. H., AND FERN, G. R. H., *J. Polymer Sci.* **10,** 185 (1953).
3. THURMOND, C. D., AND ZIMM, B. H., *J. Polymer Sci.* **8,** 477 (1952).
4. METZ, D. S., AND MESROBIAN, R. B., *J. Polymer Sci.* **16,** 345 (1955); HAHN, W., AND LECHTENBOHMER, H., *Makromol. Chem.* **16,** 50 (1955).
5. GUILLET, J. E., AND NORRISH, R. G. W., *Nature* **173,** 625 (1954).
6. SAEGUSA, T., NOZAKI, M., AND ODA, R., *J. Chem. Soc. Japan, Ind. Chem. Sect.* **57,** 243 (1954).
7. BEVINGTON, J. C., GUZMAN, G. M., AND MELVILLE, H. W., *Proc. Roy. Soc. (London)* **A221,** 453 (1954).
8. BEVINGTON, J. C., MELVILLE, H. W., AND TAYLOR, R. P., *J. Polymer Sci.* **12,** 449 (1954).
9. BOSWORTH, P., MASSON, C. R., MELVILLE, H. W., AND PEAKER, F. W., *J. Polymer Sci.* **9,** 565 (1952).
10. SHEFFER, H., AND HYDE, J. C., *Can. J. Chem.* **30,** 817 (1952).
11. MELVILLE, H. W., OVENALL, D. W., AND PEAKER, F. W., to be published.
12. ZIMM, B. H., *J. Chem. Phys.* **16,** 1093 (1948).

13. Benoit, H., Holtzer, A. M., and Doty, P., *J. Phys. Chem.* **58,** 635 (1954).
14. Benoit, H., and Doty, P., *J. Phys. Chem.* **57,** 958 (1953).
15. Stead, B. D., and Melville, H. W., *J. Polymer Sci.* **16,** 505 (1955).
16. Hawkins, S. W., and Smith, H. (ICI Alkali Division), private communication.
17. Data deduced from International Union of Pure and Applied Chemistry Reports on Molecular Weight Determinations of Polystryrene Fractions. *J. Polymer Sci.* **10,** 129 (1953); *ibid.* **17,** 1 (1955).
18. Ewart, R. W., and Tingey, H. C., unpublished data quoted in A. C. S. Monograph No. 115, p. 334 (1952).
19. Jones, M. H., unpublished results.

JOURNAL OF COLLOID SCIENCE **11**, 519-531 (1956)

NON-NEWTONIAN SURFACE VISCOSITY

M. Joly

Service de Chimie-Physique, Institut Pasteur, Paris

Received April 5, 1956

GENERAL BASIS OF SURFACE RHEOLOGY

The flow properties of monolayers show great similarity with those of bulk systems. For instance, one can observe with surface films Newtonian and non-Newtonian viscosity, thixotropy or rheopexy. But in consequence of the simplification due to the two-dimensional arrangement of the molecules, surface rheology gives us the possibility of developing a simple molecular model of the flow processes, and the rheological behavior of the monolayers can be quantitatively described (1–3).

The insoluble monolayers are spread on water surfaces, with their non-polar groups towards air and their polar groups towards water. The fixation of the molecules of the film on water is chiefly due to dipolar interactions and hydrogen bonds. It has been experimentally shown that there is no slipping (4, 5) between a flowing monolayer and its water substrate. All the neighboring water molecules close to the polar groups of a molecule of the film behave as if they were rigidly bound to this molecule. Since the dipolar interactions decrease rapidly with distance, the molecules of water not adjacent to the polar groups are not bound to the molecules of the film. Thus, when the film flows, the kinetic units are not the molecules of the insoluble monolayers but the aggregates made up by each of these molecules and the water molecules bound to it.

The coefficient of surface viscosity μ is defined as follows. Let us consider, in the plane xy, a monolayer, a small element $dx\ dy$ of which flows in the direction x at a velocity $u(y)$. This element undergoes (6, 7) from the adjacent monolayer elements a resisting force equal to $\mu(d^2u/dy^2)\ dx\ dy$. The dimensions of μ are MT^{-1} instead of $ML^{-1}T^{-1}$ as for the bulk viscosity. According to the type of film, the order of magnitude of μ varies between 10^{-6} and 10 c.g.s. The coefficient of surface viscosity can be calculated by several methods: from the rate of flow of a film through a narrow canal (6), from the damping of the oscillations, or from the torque due to the rotation of a light not wettable ring floating on the film (7, 8).

Eyring and collaborators developed a theory of viscosity considered as a particular case of activation process and applied it to monolayers (9, 10).

According to Eyring's point of view, each molecule of a liquid is in a potential trough, each of these corresponding to a possible equilibrium position for the molecules. So, for the flow of a molecule to occur, this molecule must acquire the energy of activation necessary to pass over the potential barrier which separates it from the neighboring equilibrium position. Applied to the monolayers, this theory leads to

$$\sinh \frac{\mu g \sigma}{2kT} = \frac{gh}{2kT} e^{\Delta F/kT} \tag{1}$$

with σ the molecular area, g the velocity gradient in the plane of the monolayer, T the absolute temperature, k the Boltzmann constant, h the Planck constant and ΔF the free energy of activation for the kinetic unit.

As shown in preceding papers (1, 11, 12), a film of mean molecular area σ is generally made up of a mixture of two molecular states i and $i - 1$ characterized by the molecular areas σ_i and σ_{i-1}. We can write

$$\sigma = (1 - \alpha)\sigma_i + \alpha\sigma_{i-1}, \tag{2}$$

α being the proportion of molecules in the state $i - 1$ compared with the total number of molecules for a square centimeter. Therefore the free energy of activation ΔF is a mean value and can be written

$$\Delta F = (1 - \alpha)\Delta F_i + \alpha\Delta F_{i-1}, \tag{3}$$

with ΔF_{i-1} and ΔF_i the free energies of activation in the pure states $i - 1$ and i. As a result, the curve $\Delta F(\sigma)$ is a kinked line, the angular points of which correspond to the successive transformation points of the film. Thus, the surface rheology gives us an experimental method for the determination of the characteristic areas corresponding to the transformation points of different orders in the monolayers.

NEWTONIAN SURFACE FLOW

The viscosity of a liquid is Newtonian when the viscosity coefficient does not depend upon the rate of shear. According to Eyring's theory the flow of a monolayer remains Newtonian as long as the inequality

$$\mu g \sigma \ll 2kT \tag{4}$$

is obeyed. In this case, Eq. [1] is reduced to

$$\mu = \frac{h}{\sigma} e^{\Delta F/kT}. \tag{5}$$

As a consequence of Eq. [3], ΔF is a function of the molecular area.

Practically all monolayers of fatty acids and triglycerides (2) are Newtonian. To show the orders of magnitude, Tables I*A*, I*B*, and I*C* give experimental values of the coefficient of surface viscosity at several molecular areas for gaseous, liquid, and mesomorphous films.

TABLE IA

Surface Viscosity of Newtonian Gaseous Monolayers

Substance	Substrate	Temp. (°C.)	$\sigma (A.^2)$	$\mu \times 10^5$ (*c.g.s. units*)
Tricaproin	H_2O	20	73	0.65
			110	3.35
			138	17.5
			300	27.5
			600	36
Tricaprylin	H_2O	20	79	5.6
			112	7.4
			142	13.8
			270	81
C_{20} Dicarboxylic acid	0.01 *M* HCl	20.5	80.5	6.2
			91.5	6.6
			107.5	15.4
Ethyl-11-oxystearate	H_2O	20	109	2.9
			123	3.6
			150	16
			186	50

TABLE IB

Surface Viscosity of Newtonian Liquid Monolayers

Substance	Substrate	Temp. (°C.)	$\sigma (A.^2)$	$\mu \times 10^5$ (*c.g.s. units*)
Oleic acid	0.01 *M* HCl	17	32.5	0.7
			34.9	3.8
			39.9	14.3
			47.7	16.8
Myristic acid	0.01 *M* HCl	22	29.6	1.7
			31.8	6.5
			34.5	9
			39	11.8
			43.9	15.2
Tricaprin	H_2O	19.5	68.6	7.3
			88.4	7.8
			109.6	8.2
			121.2	11
			130.5	12.8
Trilaurin	H_2O	22	89.8	7.5
			99.7	10.5
			111	14
Triolein	H_2O	20	100.5	3.1
			111	9.1
			121.5	13.8
			132	14.3
Triricinolein	H_2O	20	84	0.7
			104.5	0.7
			124	2.25
			143	6.15
			156	9.1
			168	11.1
			188	11.1

TABLE IC

Surface Viscosity of Newtonian Mesomorphous Monolayers

Substance	Substrate	Temp. (°C.)	σ(A.²)	$\mu \times 10^4$
Stearic acid	0.001 M HCl	18	20.1	11.6
			21	7.35
			21.65	4.35
			22.5	3.2
			23.05	2.65
Palmitic acid	0.01 M HCl	25.3	21.5	5
			22.4	3.1
			23.6	1.87
			25.4	1.44
			27.3	1.12
			28.1	1.32
			29	2.55
Myristic acid	0.01 M HCl	17	22.7	2.16
			23.4	1.8
			24.6	1.32
			26	1.2

Since the monolayer is rigidly bound to the substrate, the measured surface viscosity is that of the system including the insoluble film and the first layer of water molecules. Consequently ΔF can be written

$$\Delta F = \Delta F_c + \Delta F_{H_2O}, \qquad [6]$$

ΔF_c and ΔF_{H_2O} being the free energies of activation of the film and of the water layer. This equation explains the variation of μ with σ. Indeed, it has been shown (1, 12) that ΔF_c can be represented by a sum of terms in σ^{-3} and $\sigma^{-3/2}$, while ΔF_{H_2O} increases almost linearly with σ. Accordingly, for small values of σ, μ is a decreasing function of σ, while for high values of σ it is an increasing function. That is why the apparent viscosity of mesomorphous films increases by compression, whereas for liquid and gaseous films it decreases.

It is generally considered that the mean positions of the molecules in a fluid film, chiefly in the condensed states, correspond to a quasi-crystal structure and are locally arranged nearly as an hexagonal lattice. It has been postulated (11, 12) that the molecules of a monolayer can exist only in a finite number of stable equilibrium states $\cdots i - 1, i, \cdots$ corresponding to a series of discrete molecular areas $\cdots \sigma_{i-1}, \sigma_i, \cdots$ or intermolecular distances $\cdots r_{i-1}, r_i, \cdots$ and probably to different molecular forms. (The σ_i values are given by experiment, since these areas correspond to the transformation points of different orders on the isotherm curves.)

Since during the flow of a film in the state i the distance between certain molecules becomes lower than r_i, these molecules cannot remain in the state i. They jump suddenly into the state $i - k$ corresponding to the possible lattice distance immediately below the smallest distance attained. Thus one can assume that, during the flow of a film initially in the state i, the activation state of the molecules is $i - k$.

The relationship between the energy of activation ΔE and the free energy of activation ΔF is given by

$$\frac{\Delta F}{kT} = \frac{\Delta E}{hT} - \log \frac{f_+^{\;+}}{f}, \tag{7}$$

where $f_+^{\;+}$ and f are the partition functions of the flowing molecules, respectively, in the activated state and in the initial state. In a first approximation (13)

$$\frac{f_+^{\;+}}{f} \simeq \frac{\sigma_{i-k}}{\sigma_i}. \tag{8}$$

In the condensed state, σ_i and σ_{i-k} have almost the same values, and then, with a good accuracy,

$$\Delta F \simeq \Delta E. \tag{9}$$

Therefore, ΔF_i can be calculated in terms of molecular interactions. As the intermolecular forces are negligible beyond three or four molecular distances, we have only to consider very small regions around each molecule, and we can treat the film as a small domain of a hexagonal network.

The term ΔF_i includes two terms: the energy required to make a hole in the film into which an activated neighboring molecule may be moved, and the energy necessary to cause a molecule to pass from one equilibrium position to a free neighboring position.

If $W_j(r_i)$ is the value per kinetic unit (each molecule of the insoluble monolayer and the water molecules rigidly bound to it) of the interaction energy between one kinetic unit and all its neighbors assumed to be in the state j but at a distance r_i, the preceding first term of ΔF_i is equal to $W_i(r_i)$. The second term can be resolved into three parts: the energy necessary for the translation of the molecules, the energy corresponding to the local deformation of the network during this translation, and the energy of the change of the equilibrium stable form of the molecules during their displacements. The three corresponding values of the energy variations are, respectively, $0.7W_{i-k}(r_i)$, $-0.5W_{i-k}(r_i)$, and $6W_i(r_i) - W_{i-k}(r_i)$.

Therefore one finds

$$\Delta F_i \simeq 7W_i(r_i) - 5.8W_{i-k}(r_i). \tag{10}$$

The energy $W_j(r_i)$ can be derived from the potentials of interaction between the various functional groups of the molecules (1, 12). The agreement between the experimental and calculated values of ΔF_i is quite good. Table II gives several values of measured and calculated free energies of activation of viscous flow for Newtonian monolayers of fatty substances.

TABLE II

Free Energies of Activation of Flow

				$\Delta F \times 10^{13}$	
Substance	Substrate	Temp. (°C.)	$\sigma(A.^2)$	Measured	Calculated
Triricinolein	H_2O	20	82	6.4	6.41
			100	6.48	6.5
			155	7.74	7.69
			200	7.92	7.88
Triolein	H_2O	20	95	6.75	6.8
			115	7.73	7.72
			135	7.81	7.82
Tricaprylin	H_2O	20	120	7.5	7.55
			170	8.22	8.19
			210	8.78	8.7
Tricaproin	H_2O	20	110	7.19	7.16
			130	7.86	7.86
			210	8.23	8.22
			480	8.64	8.6
Myristic acid	0.01 *M* HCl	17	22	7.21	7.22
			23.5	7.17	7.19
			24.5	7.03	7.04
			26	7.02	7.02
			30	6.95	7.03
			33.5	7.23	7.25
			37	7.26	7.28
Palmitic acid	0.01 *M* HCl	17	22	7.29	7.31
			23.5	7.25	7.26
			24.5	7.19	7.19
			26	7.22	7.23
Stearic acid	0.01 *M* HCl	20	20.5	7.66	7.6
			22	7.4	7.36
			23.5	7.27	7.28

NON-NEWTONIAN SURFACE FLOW

As we have seen before, the flow of a monolayer remains Newtonian, according to Eyring's theory, as long as the inequality [4] is obeyed. Now, non-Newtonian behavior occurs, that is to say, one observes that the surface viscosity coefficient μ depends on the velocity gradient g, when experimental conditions satisfy the inequality [4]. Therefore it is necessary to admit that Eq. [5] is still valid but that the free energy of activation ΔF varies with increasing rate of shear. Table III gives several examples of such behavior.

I have given (3, 13) an interpretation of the non-Newtonian flow in monolayers. As shown before, the displacement of one molecule in the i state from its initial position to an adjacent free place in a molecule row parallel to the flow direction, produces the temporary removal of other molecules in the neighboring rows; if a second displacement occurs in the

TABLE III

Non-Newtonian Surface Viscosity

Substance	Substrate	Temp. (°C.)	$\sigma(A.^2)$	g	$\mu \times 10^3$
Lauryl alcohol	H_2O	20.5	37	0.6	2
				2.7	1
				6.5	0.4
Myristyl alcohol	H_2O	18.1	22	2.27	0.8
				5.9	0.4
				47	0.2
			20.5	0.57	2
				0.89	1.5
				1.25	1.2
				5.07	0.4
			20	0.54	5.6
				1.77	2
				2.9	1.1
Cetyl alcohol	H_2O	20	22	1	2.5
				3	1
				5	0.7
			20	0.5	7
				1.6	1.4
				2.6	0.8
Stearyl alcohol	H_2O	20.5	20.5	0.29	2.8
				0.56	1.2
			19.5	0.26	6.2
				0.55	2.5
Stearyl amide	H_2O	21	24.5	0.24	14
				0.4	6
				18	0.8
			21.5	0.24	44
				0.48	12

flowing row before the removed lateral molecules are again in their equilibrium initial positions, the activation energy for an elementary displacement is no longer ΔF_i but a smaller quantity, $\Delta F'_i$. This difference $\Delta F_i - \Delta F'_i$ chiefly corresponds to the fact that, in the second case, there is no new local deformation of the network and no new change of the equilibrium form of the neighboring molecules during the displacement of the second kinetic unit. As a first approximation

$$\Delta F_i - \Delta F'_i \simeq 4\,[W_i(r_i) - 1.1\,W_{i-k}(r_i)] \qquad [11]$$

when there is no hydrogen bond between the molecules of the insoluble monolayer.

If p_i is the probability that an i molecule removed from its initial position will not reoccupy its normal position before a second molecule goes beyond it, the free energy of activation for any elementary flow is given by

$$\Delta F(g) = \Delta F_i - p_i(\Delta F_i - \Delta F'_i) \qquad [12]$$

TABLE IV

Free Energy of Activation and Relaxation Time of Non-Newtonian Flow

Substance	$\sigma(A.^2)$	$\Delta F_i \times 10^{13}$	$\Delta F_i \times 10^{13}$	τ_i
Lauryl alcohol	37	8.44	7.79	0.44
Myristyl alcohol	23.5	8.18	7.42	0.497
	22	8.15	7.125	0.479
	20.5	8.17	7.175	0.647
	20	8.62	7.375	0.621
Cetyl alcohol	21.5	8.45	7.405	0.543
	20.5	8.73	7.07	0.656
	20	8.85	7.085	0.88
	19.5	9.06	7.65	1.837
Stearyl alcohol	20.5	8.8	7.12	3
	20	8.955	7.655	3.37
	19.5	9.16	7.71	3.8
Stearyl amide	24.5	9.33	7.475	2.34
	23.5	9.5	7.555	2.435
	21.5	10.03	8.025	3.66

with

$$p_i = e^{-1/g\tau_i} \tag{13}$$

and

$$\tau_i \simeq 0.94 r_i \sqrt{\frac{2\pi m}{kT}}\, e^{W_{i-k(0.94r_i)/kT}}, \tag{14}$$

where m is the mass of one kinetic unit of the film. Table IV shows a few experimental values of ΔF_i, $\Delta F'_i$, and τ_i derived from the curves $\mu(g)$ by means of Eqs. [5], [12], and [13].

In the preceding relationships τ_i behaves as a relaxation time. As a first approximation it can be considered as the mean time which is required by a disturbed kinetic unit to reoccupy its normal position.

Thus, the decrease of μ with increasing g is due to the high values of the relaxation times of the perturbation induced by the flow in the quasi-lattice structure. So the non-Newtonian character is related to the order decrease in an initially highly ordered system.

As a consequence of the lattice deformation a pressure appears, leading to the expansion of the monolayer. Therefore, the surface pressure at constant area increases with increasing rate of shear (3, 14). Consequently, one observes surface dilatancy with the non-Newtonian monolayers; that is to say, the surface area per kinetic unit (or the apparent molecular area) at constant surface pressure increases with the velocity gradient.

If σ_i is the molecular area at rest, the apparent molecular area $\sigma(g)$ at the rate of shear g is given by

$$\sigma(g) = (1 + 0.07\, p_i)\sigma_i\,. \tag{15}$$

When $W_i(r_i)$ and τ_i are large enough (for instance τ_i not negligible compared with the duration of a viscosity measurement), the monolayer shows thixotropy. In this case, the apparent value of the surface viscosity coefficient obviously depends upon the rate of shear, and also on the velocity of its variation. Consequently the curves $\mu(g)$ are no longer reversible with respect to the velocity gradient.

For simplification, we have assumed that at rest all the molecules of the film are in the state i. In the general case, the monolayer, for any point on its isotherm curve, is a mixture of the two molecular types $i - 1$ and i corresponding to the molecular areas σ_{i-1} and σ_i. The mean molecular area at rest is given by Eq. [2]. Relationship [12] becomes

$$\Delta F(g) = (1 - \alpha)\Delta F_i + \alpha\Delta F_{i-1} - p_i(1 - \alpha)(\Delta F_i - \Delta F'_i) - p_{i-1}\alpha(\Delta F_{i-1} - \Delta F'_{i-1}) \qquad [12']$$

where p_i is given by Eq. [13] and p_{i-1} by

$$p_{i-1} = e^{-1/g\tau_{i-1}}, \qquad [13']$$

with

$$\tau_{i-1} \simeq 0.94r_{i-1} \sqrt{\frac{2\pi m}{kT}}\, e^{[W_{i-1-l}(0.94r_{i-1})]/kT}. \qquad [14']$$

The definition of the state $i - 1 - l$ with regard to the state $i - 1$ is the same as the definition of $i - k$ with regard to i.

All the conclusions remain the same for the non-Newtonian behavior as a function of the velocity gradient.

SURFACE RHEOPEXY AND PHASE TRANSFORMATION INDUCED BY THE FLOW

As we have seen, in a flowing monolayer, the displacement of one i molecule causes the removal of its neighboring molecules from their equilibrium positions, and a temporary transition occurs from the state i to the state $i - k$. Because of the fluctuations due to the thermal agitation, it can happen that a disturbed molecule of the film, instead of coming back to the state i, aggregates with some of its neighbors by local condensation in the state $i - k$. The probability of the occurrence of such a process is

$$\pi_i = e^{-[W_{i-k}(r_{i-k}) - W_{i-k}(0.94r_i)]/[W_{i-k}(0.94r_i) - W_i(r_i)]}. \qquad [16]$$

Besides, the probability that the considered molecule will still be in the state $i - k$ at a time $1/g$ after its condensation is given by

$$\varphi_i = e^{-1/g\theta_i}, \qquad [17]$$

where θ_i can be considered as the mean life of one kinetic unit in the aggregates formed by the flow of the monolayer. As a first approximation

$$\theta_i \simeq r_{i-k} \sqrt{\frac{2\pi m}{kT}}\, e^{[W_{i-k}(r_{i-k})]/kT}. \qquad [18]$$

TABLE V

Decrease of the Apparent Molecular Area during the Flow

Substance	Substrate	Temp. (°C.)	$\sigma_i(A.^2)$	$\bar{g}(sec.^{-1})$	$t(min)$	$-\Delta\sigma/\sigma(\%)$
Cetyl alcohol	H_2O	20	19.5	1.27	12	1.6
					17	2.2
					35	2.4
Stearyl alcohol	H_2O	20	19.5	1.85	12	0.5
					35	1.1
					85	1.25
					145	1.4
Stearyl amide	H_2O	20	21.5	1.32	10	2.7
					20	3.6
					32	4.7
					56	5.3
					83	5.5
					105	5.8

As a consequence of such a process, if all the molecules are at rest in the state i, after a time t at the rate of shear g, the ratio of the molecules in the state $i - k$ becomes

$$z(t) = \pi_i\varphi_i \frac{[\varphi_i(1 - \pi_i)]^{gt} - 1}{\log \varphi_i(1 - \pi_i)}, \qquad [19]$$

with g constant.

Therefore the molecular composition of the monolayer changes during the flow. The film shows an evolution towards the condensed states. Thus a physical state change occurs on a molecular scale in the monolayer. According as the i and $i - k$ molecular forms are miscible or not, one observes in the film a first- or high-order phase change induced by the flow. This phase change results in a decrease of the apparent molecular area $\sigma(t)$ at constant surface pressure which is given by

$$\begin{aligned}\sigma(t) = {} & (1 + 0.07p_i)\sigma_i \\ & + \pi_i\varphi_i \frac{[\varphi_i(1 - \pi_i)]^{gt} - 1}{\log \varphi_i(1 - \pi_i)} [\sigma_{i-k} - (1 + 0.07p_i)\sigma_i],\end{aligned} \qquad [20]$$

where g remains constant. Table V gives experimental values of the relative decrease of the apparent molecular area under constant pressure.

Such a dynamic phase change is accompanied by surface rheopexy or surface shear hardening, that is to say, by a large increase of the surface viscosity during the flow. Indeed, as a consequence of the variation of the molecular composition of the film, ΔF_i is replaced by

$$\begin{aligned}\Delta F(t) = {} & \Delta F_i - p_i(\Delta F_i - \Delta F'_i) \\ & + \pi_i\varphi_i \frac{[\varphi_i(1 - \pi_i)]^{gt} - 1}{\log \varphi_i(1 - \pi_i)} [\Delta F_{i-k} - \Delta F_i + p_i(\Delta F_i - \Delta F'_i)],\end{aligned} \qquad [21]$$

the rate of shear g being constant. Table VI shows a few experimental values of the surface viscosity at constant velocity gradient for several

TABLE VI

Surface Shear Hardening

Substance	Substrate	Temp. (°C.)	$\sigma_i (A.^2)$	$\vec{g} (sec.^{-1})$	$t(min)$	$\mu \times 10^3$
Stearyl alcohol	H_2O	19	20.5	1.64	14	2.5
					29	3.4
					38	5.9
			20	1.8	4	3
					28	4.2
					44	5.1
					52	6.9
Stearyl amide	H_2O	20	21.5	1.39	8	10.2
					18	62.7
					25	67
					34	73.3
					40	88.2
					48	112
					57	125

TABLE VII

Non-Newtonian Surface Viscosity

Substance	σ_i $(A.^2)$	$\Delta F_i \times 10^{13}$	$\Delta F'_i \times 10^{13}$	τ_i	π_i $\times 10^3$	θ_i $\times 10^{-3}$	ΔF_{i-k} $\times 10^{13}$	$W_i(r_i)$ $\times 10^{12}$	$W_{i-k}(r_{i-k})$ $\times 10^{12}$
Cetyl alcohol	19.5	9.06	7.65	1.84	1.32	1.6	9.9	1.002	1.311
Stearyl alcohol	20.5	8.8	7.22	3	1.69	1.72	9.34	1.016	1.317
	20	8.955	7.655	3.37	1.76	1.72	9.34	1.023	1.317
	19.5	9.16	7.71	3.8	1.8	1.72	9.34	1.032	1.317
Stearyl amide	21.5	10.03	8.025	3.66	0.94	5.4	11.89	1.03	1.362

times of flow. From the experimental curves $\mu(t)_g$ can be derived, by means of the preceding equations, the values of ΔF_i, $\Delta F'_i$, τ_i, π_i, θ_i, ΔF_{i-k}, $W_i(r_i)$, and $W_{i-k}(r_{i-k})$. A few examples are given in Table VII.

In the general case where the monolayer is, at rest, a mixture of molecules in the states i and $i - 1$, the flow behavior of the film at constant rate of shear is the same in spite of the complication of the corresponding equations. Indeed, Eq. [21] must be replaced by

$$\Delta F(t) = (1 - \alpha)\Delta F''(t) + \alpha\, \Delta F'''(t) \qquad [21']$$

with

$$\Delta F''(t) = \Delta F_i - p_i(\Delta F_i - \Delta F'_i) + \pi_i \varphi_i \frac{[\varphi_i(1 - \pi_i)]^{gt} - 1}{\log \varphi_i(1 - \pi_i)} [\Delta F_{i-k} - \Delta F_i + p_i(\Delta F_i - \Delta F'_i)] \qquad [21'']$$

$$\Delta F'''(t) = \Delta F_{i-1} - p_{i-1}(\Delta F_{i-1} - \Delta F'_{i-1}) + \pi_{i-1}\varphi_{i-1} \frac{[\varphi_{i-1}(1 - \pi_{i-1})]^{gt} - 1}{\log \varphi_{i-1}(1 - \pi_{i-1})} [\Delta F_{i-1-l} - \Delta F_{i-1} + p_{i-1}(\Delta F_{i-1} - \Delta F'_{i-1})] \qquad [21''']$$

where

$$\pi_{i-1} = e^{-[W_{i-1-l}(r_{i-1-l})-W_{i-1-l}(0.94r_{i-1})]/[W_{i-1-l}(0.94r_{i-1})-W_{i-1}(r_{i-1})]} \qquad [16']$$

$$\varphi_{i-1} = e^{-1/g\theta_{i-1}} \qquad [17']$$

and

$$\theta_{i-1} \simeq r_{i-1-l} \sqrt{\frac{2\pi m}{kT}}\, e^{[W_{i-1-l}(r_{i-1-l})]/kT}. \qquad [18']$$

If the velocity gradient g varies with time, the behavior of a monolayer showing shear hardening is extremely complicated and the entirely quantitative calculation cannot be performed. In the flow mechanism for monolayers, the shearing forces tend simultaneously to disturb the actual structure and to promote the development of a new structure of higher order. One or other of these contradictory processes prevails according to the values of g, to the interaction energies between the kinetic units, and to the previous mechanical treatments of the monolayer, that is to say, its rheological history.

The simple case where a film initially in the pure molecular state i flows successively during a time t' at the velocity gradient g' and during a time t'' at the velocity gradient g'', has been treated elsewhere (3). This derivation leads to

$$\begin{aligned}\Delta F(t' + t'') = \Delta F_i - p_i(\Delta F_i - \Delta F'_i) + \pi_i[\Delta F_{i-k} - \Delta F_i \\ + p_i(\Delta F_i - \Delta F'_i)] \times \left\{\varphi'_i \frac{[\varphi'_i(1-\pi_i)]^{g't'} - 1}{\log \varphi'_i(1-\pi_i)}\right. \\ \left. + \varphi''_i[\varphi'_i(1-\pi_i)]^{g't'} \cdot \frac{[\varphi''_i(1-\pi_i)]^{g''t''} - 1}{\log \varphi''_i(1-\pi_i)}\right\}\end{aligned} \qquad [22]$$

with

$$\varphi'_i = e^{-1/g'\theta_i} \qquad [17'']$$

and

$$\varphi''_i = e^{-1/g''\theta_i}. \qquad [17''']$$

In such a relationship one sees the great number of parameters upon which depends the surface viscosity when the flow behavior of a monolayer is non-Newtonian.

We have previously shown (15) that the flow processes occurring in monolayers give us a good model of the rheological behavior of colloidal bulk systems. On the whole, the reciprocal relations between the structure and the state of motion can be extended from the two-dimensional fluids to the three-dimensional flowing systems. Besides surface rheology provides us a useful investigation method for the study of the molecular interactions.

SUMMARY

The results of surface rheology are explained and quantitatively described by the help of a simple molecular model of the flow behaviors in monolayers. The fundamental processes of this rheological pattern are:

1. The transport of substrate water molecules rigidly bound to the molecules of the flowing monolayers.

2. The deformation by the flow of the quasi-lattice structure of the film, the relaxation velocity of which determines the type of behavior, Newtonian or not, in relation to the respective values of the rate of shear and of the interaction energies between the kinetic units.

3. The microscopic or macroscopic phase changes induced in the monolayer by the flow and causing, for instance, the shear hardening phenomenon, the various time effects, and the decrease of the apparent molecular area.

The three types of processes are correlative and simultaneous. As a consequence of the reciprocal interaction between structure and rate of shear, the actual flow behavior of a monolayer depends upon its total rheological history.

REFERENCES

1. JOLY, M., *J. phys. radium* **7,** 83, 112 (1946).
2. JOLY, M., *J. chim. phys.* **44,** 206, 213 (1947).
3. JOLY, M., *Kolloid-Z.* **126,** 35 (1952).
4. MERIGOUX, R., *Compt. rend.* **202,** 2049 (1936); *ibid.* **203,** 848 (1936); *ibid.* **205,** 115 (1937).
5. SCHULMAN, J. H., AND TEORELL, T., *Trans. Faraday Soc.* **34,** 1337 (1938).
6. JOLY, M., *J. phys. radium* **8,** 471 (1947); *ibid.* **9,** 345 (1948).
7. JOLY, M., *Kolloid-Z.* **89,** 26 (1939).
8. CHAMINADE, R., DERVICHIAN, D. G., AND JOLY, M., *J. chim. phys.* **47,** 883 (1950).
9. EWELL, R. H., AND EYRING, H., *J. Chem. Phys.* **5,** 726 (1937).
10. MOORE, W. J., AND EYRING, H., *J. Chem. Phys.* **6,** 391 (1938).
11. JOLY, M., "Surface Chemistry," 37. London, 1949.
12. JOLY, M., *J. Colloid Sci.* **5,** 49 (1950).
13. JOLY, M., *J. phys. radium* **11,** 171 (1950).
14. JOLY, M., *Compt. rend. 2e Réunion chim. phys. (Paris 1952)*, p. 477.
15. JOLY, M., *Kolloid-Z.* **139,** 43 (1954).

JOURNAL OF COLLOID SCIENCE **11,** 532–542 (1956)

THE CATALYTIC HYDROGENATION OF ACETONE ON EVAPORATED METALLIC FILMS

C. T. H. Stoddart and C. Kemball

Department of Chemistry, The Queen's University of Belfast, Northern Ireland

Received March 26, 1956

ABSTRACT

The catalytic reaction between acetone vapor and hydrogen on evaporated metallic catalysts in a static system has been followed by means of a Nier-type mass spectrometer. The main reaction observed on platinum, nickel, tungsten, iron, palladium, and gold was the formation of isopropanol but small amounts of propane were also formed simultaneously on platinum and, to a lesser extent, on the other metals with the exception of palladium and gold.

Activation energies and frequency factors were measured for the production of isopropanol on all the metals and some pressure dependencies were obtained on nickel films. The order of activity of the metals was similar to the order for the hydrogenation of ethylene except for palladium, which was the least active of the five transition metals.

A series of values for the equilibrium constant for the dehydrogenation of isopropanol to acetone was obtained at substantially lower temperatures than have been used in previous measurements.

INTRODUCTION

Although a number of investigations have been made on the hydrogenation and deuteration of acetone on foils and on bulk metallic catalysts, no work has been reported using evaporated metallic catalysts. As there are various conflicting theories about the mechanism by which acetone is hydrogenated to isopropanol and propane, it was thought that valuable information might be obtained if a careful analysis were made of the isotopic content of the initial products formed from deuterium and acetone over evaporated metal films. However, preliminary investigation showed that it was not possible to interpret the complicated mass spectra of the deutero-isopropanols and deutero-propanes until information had been obtained about the relative amounts of isopropanol and propane formed by studying hydrogenation of acetone on films. The object of the present work was, therefore, to investigate the nature of the products resulting from the hydrogenation of acetone on these catalysts and also to determine the relative efficiency of different metals for the reduction of the carbonyl group.

EXPERIMENTAL

A. R. acetone was purified by refluxing over calcium oxide and potassium permanganate and then by distillation. The liquid was degassed in the vacuum apparatus and stored over liquid air to prevent attack on the stopcock grease. Isopropanol was refluxed over calcium oxide, distilled, and then handled in the same way as acetone. Hydrogen from a cylinder was purified by diffusion through a palladium thimble.

The apparatus consisted of a glass reaction vessel (200 ml.) in which films of metal could be formed by evaporation and which was attached to a normal high vacuum train. A fine glass capillary leak linked the reaction vessel to the gas inlet of the mass spectrometer and allowed the mixture in the reaction vessel to bleed continuously into the spectrometer. It was possible with this technique to obtain analyses of the reaction mixture throughout the course of each run. Detailed descriptions of the catalytic apparatus, the capillary leak, and the technique for the preparation of the evaporated films have been given previously (1, 2).

The normal gas mixture contained eight parts of hydrogen to one part of acetone. For experiments on tungsten, iron, palladium, and gold, the mixture was admitted to the reaction vessel at 0°C.; the partial pressure of acetone was 1.49 mm., and the number of acetone molecules in the reaction vessel was estimated as 1.04×10^{19}. For experiments on platinum and nickel, it was necessary to admit the mixture at lower temperatures, and the corresponding figures were 1.45 mm. and 1.10×10^{19} molecules. Temperatures below 0°C. were obtained by means of molten slurries and higher temperatures by the use of an electric furnace. A calibrated thermocouple was used to measure temperature.

The analyses in the mass spectrometer were made by using low-voltage electrons (17 v.) to ionize the molecules, thus avoiding extensive corrections for the formation of fragmentary ions. Isopropanol was estimated from the peak corresponding to ions formed by loss of a methyl group and an electron (mass 45) because the amount of the parent ions (mass 60) was small. Acetone was estimated from the peak corresponding to the parent ion (mass 58) after correction for a small contribution from a fragmentary ion formed from isopropanol. The estimation of propane was made from the peak corresponding to the parent ion (mass 44), but three corrections had to be included—to allow for the background of carbon dioxide in the spectrometer, for the presence of heavy isotopes in the ion $CH_3 \cdot CO^+$, which was a major component of the mass spectrum of acetone, and finally for small amounts of an ion formed by isopropanol. The analyses for propane were, therefore, subject to some uncertainty, and the error amounted to 1%–2% of the total amount of acetone present initially. Calibration experiments with acetone, isopropanol, and propane were carried out from time to time to check sensitivities and extents of fragmentation.

RESULTS

The main reaction observed on all the metals studied was the formation of isopropanol. It was found that the reverse reaction, the dehydrogenation of isopropanol to acetone, was also of importance at temperatures above 0°C. and that, on the more active metals, the equilibrium between acetone, isopropanol, and hydrogen was being established. Since no experimental values for the equilibrium constant for this reaction at temperatures below 105°C. have been published and since the apparatus was capable of measuring the small amounts of acetone remaining at temperatures above 23°C., a series of equilibrium constants were determined. Most of these values were obtained on nickel films because of their high activity, but gold films were suitable for measurements at higher temperatures because of the absence of side reactions on gold. The values of the equilibrium constant for the dehydrogenation of isopropanol (K_p, atmos.) are given in Table I. The errors in the values were approximately 15% except for the value at 23°C., which was less accurate owing to the small amount of acetone which had to be measured and to the correction for the ion from isopropanol, which was a substantial fraction of the observed peak for mass 58 under these conditions.

For all the metals at temperatures and times where the amount of the reverse reaction was small, the formation of isopropanol followed the equation

$$-\log_{10}(100 - x) = k_1 t/230.3 - \log_{10} 100, \qquad [1]$$

where x is the percentage of isopropanol formed at time t and k_1 is a constant. Typical plots are shown in Fig. 1, in which the decrease in rate due to the development of the reverse reaction can be seen for the experiment on tungsten. From such plots the initial rates of reaction k_1 expressed as percentage of acetone converted to isopropanol per minute were determined. These values were then expressed as a rate per 10 mg. of catalyst (k) and are shown in Fig. 2 plotted according to the Arrhenius equation. The activation energies so obtained are given in Table II, together with

TABLE I

Equilibrium Constants for the Dehydrogenation of Isopropanol

Temperature (°K.)	$\log_{10} K_p$
498.2	0.2232
408.2	$\bar{2}.7447$
383.0	$\bar{2}.4404$
349.0	$\bar{3}.5396$
321.2	$\bar{4}.8829$
296.2	$\bar{4}.3050$
355.0[a]	$\bar{3}.903$

[a] Derived from thermodynamic data.

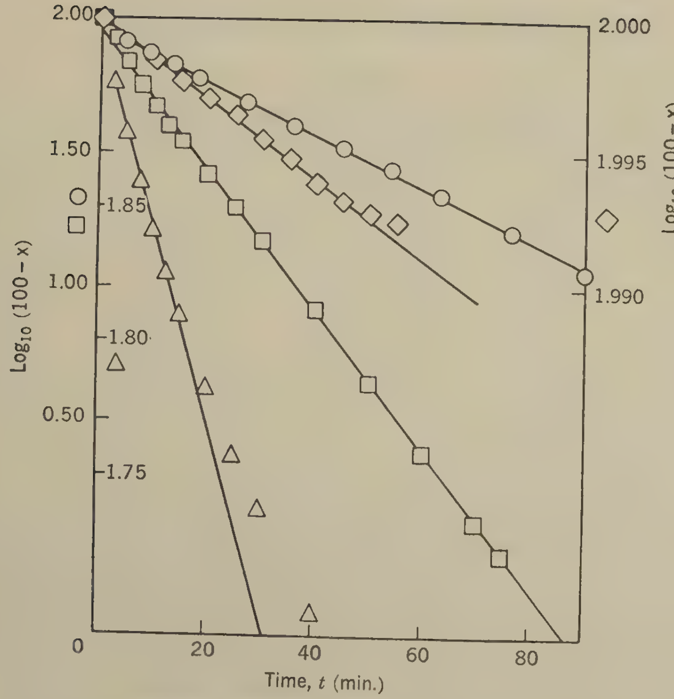

FIG. 1. Plots to determine the initial rates (k_1) of hydrogenation of acetone to isopropanol according to Eq. [1]. □, 8.7 mg. platinum at −21.7°C.; ○, 9.9 mg. nickel at 0°C.; ◇, 9.1 mg. palladium at 25.4°C.; △, 9.3 mg. tungsten at 88.3°C. L.H. outer scale, ○ and □; L.H. inner scale, △; R.H. scale, ◇.

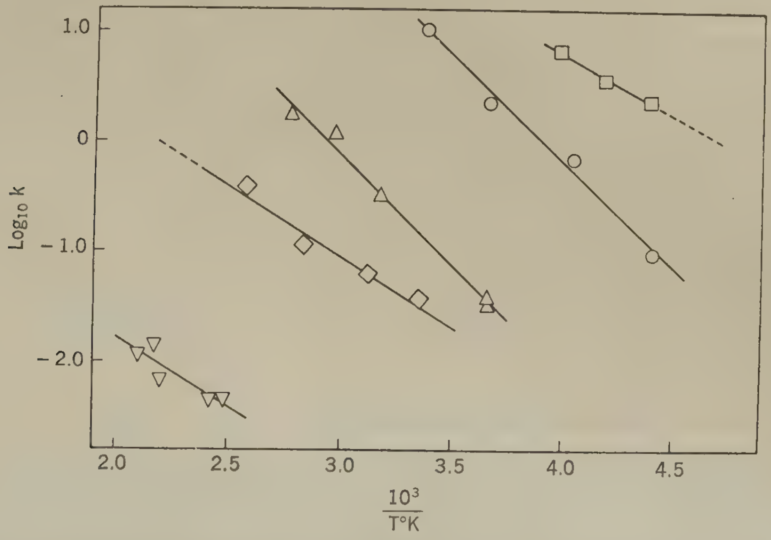

FIG. 2. The effect of temperature on the initial rate (k) of hydrogenation of acetone to isopropanol expressed as percentage of acetone removed per minute per 10 mg. of catalyst. Symbols as in Fig. 1. ▽, Gold (percentage/min. for 110 cm.^{2} apparent area of film).

TABLE II

Activation Energies and Frequency Factors

Catalyst	*E*(*kcal./mole*)	$\log_{10}$ A(*A in mol./sec. 10 mg.*)	Temp. range (°*C.*)	Temp. when rate is 1% /min. 10 mg. (°*C.*)
Platinum	5.0	20.5	−46 to −22	−61.6
Nickel	8.8	22.8	−45 to 24	−17.4
Iron	12.5	23.3	0 to 98	67.1
Tungsten	9.1	21.1	0 to 88	67.4
Palladium	5.8	18.0	25 to 116	185.4
Gold[a]	5.7	16.0	130 to 203	450

[a] A is given in molecules/sec. for 110 cm.^{2} apparent area of film. The approximate temperature at which the initial rate would be 0.1%/min. for 110 cm.^{2} apparent area is given.

the frequency factors expressed as molecules/sec.10 mg. and also the temperatures at which the initial rates were 1%/min.10 mg. The activation energies refer to constant concentration and not to constant pressure of the gases. As the activities of the gold films were not proportional to their weight presumably because of sintering, the initial rates k_1 were not converted to rates per 10 mg. of catalyst. The apparent areas of the gold films were approximately 110 cm.^{2}.

The reproducibility of the films was good except in the case of iron, from which it is difficult to produce clean films, and in the case of gold, where there was some variation in the apparent area of the films. In experiments on platinum below −34°C., condensation of the alcohol occurred in the later stages of the reaction, and it was necessary to find the initial rates using only measurements in the early part of the run before the saturation vapor pressure of the alcohol was exceeded. In a similar manner, on all metals studied at high temperature, the initial rates had to be obtained using only measurement from the first part of the run before the reverse reaction became appreciable.

A series of experiments was conducted on nickel films at 0°C. to ascertain the effect of alteration of pressures of the gases on the initial rate of the reaction. The results are shown in Table III; the first four experiments obeyed Eq. [1] or a modified form of this equation which was used when isopropanol was present in the initial mixture; the last two experiments yielded curved lines indicating that the rate of reaction was decreasing with time to a greater extent than would have been expected from Eq. [1]. A comparison of experiments 1, 2, and 6 shows that the rate of reaction was independent of the pressure of hydrogen at high pressures but became dependent at low pressures. Experiments 1, 3, and 4 showed that the reaction was inhibited by isopropanol and that the initial rate of reaction was reduced by slightly more than a factor of two by the presence of a pressure of isopropanol equal to the pressure of acetone present initially. Experi-

TABLE III

Rates of Conversion of Acetone to Isopropanol on Nickel Films at 0°C.

Expt.	Pressures (*mm.*)			Initial Rate (% *acetone/min. 10 mg.*)
	Acetone	Hydrogen	Isopropanol	
1	1.59	12.52	—	2.28
2	1.66	38.00	—	2.27
3	1.54	12.23	1.54	0.94
4	1.54	12.36	1.54	0.87
5	6.20	12.27	—	0.51
6	1.61	3.21	—	1.51

ments 1 and 5 indicated that the initial rate was independent of the pressure of acetone, since the percentage conversion was reduced by a factor of four for a mixture with four times the usual pressure.

The most extensive production of propane was observed on platinum films. The production of propane was initially quite rapid on this metal at temperatures between −45° and −22°C. but became slower and eventually ceased when about half the acetone had been used up. The production of the alcohol continued until all the acetone had disappeared, except that a decrease in rate was observed at the lowest temperature when the saturation pressure of the alcohol was exceeded. After the acetone had disappeared the products amounted to about 92% isopropanol and 8% propane. No further propane was observed on warming the reaction vessel to 0°C., but at higher temperatures acetone reappeared rapidly corresponding to the establishment of the equilibrium with isopropanol and hydrogen and then both acetone and isopropanol were converted slowly into propane. This production of propane on platinum at higher temperatures attained a rate of approximately 1%/min.10 mg. at 63°C. On nickel films up to 76°C. and on iron films up to 143°C., only trace amounts of about 2% of propane were observed. Tungsten showed slightly more activity for the formation of propane as some 4% was observed after 40 minutes on a 9.3-mg. film at 88.3°C., and on another film weighing 9.0 mg. about 10% of propane was found at 113°C. after 70 minutes. No propane was detected over palladium films at temperatures up to 115°C. nor over gold films up to 225°C.

DISCUSSION

Measurements of the equilibrium constant for the dehydrogenation of isopropanol to acetone and hydrogen have been reported by Rideal (3) for the temperature range 105–275°C. but his results were criticized by Parks and Kelley (4), who obtained values for the range 184–218°C. using a dynamic system with a copper catalyst. The values found by Parks and

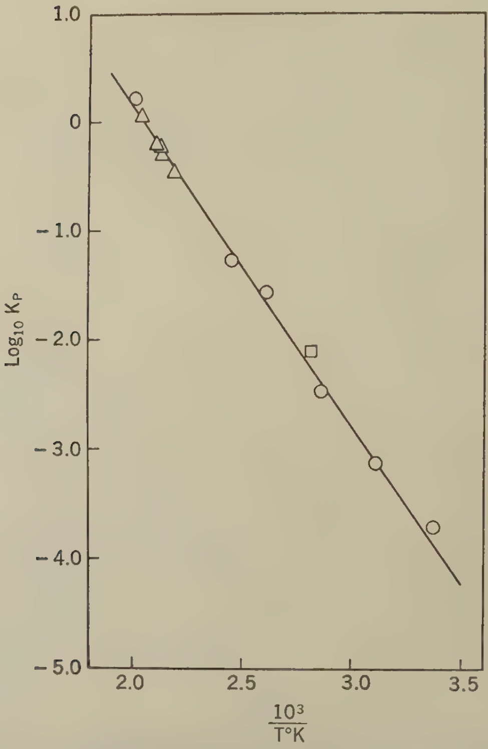

FIG. 3. The effect of temperature on the equilibrium constant, K_p (atmos.), for the dehydrogenation of isopropanol. ○, present work; △, Parks and Kelley; □, thermodynamic data.

Kelley and the results of the present work are shown in Fig. 3, and the two sets of values blend together well. A point is included on the figure for the theoretical equilibrium constant at 355°K. based on the heat of hydrogenation of −13,407 ± 100 cal./mole obtained by Dolliver *et al.* (5) and on values of 74.15, 78.29, and 32.25 cal./deg. mole for the standard entropies at this temperature of acetone, isopropanol, and hydrogen, respectively. The line drawn through the points corresponds to the equation

$$\log_{10} K_p = \frac{-13{,}340}{4.576T} + 5.969, \qquad [2]$$

and this gives a heat of reaction in excellent agreement with the value obtained by Dolliver *et al.*

The zero order dependence of the rate of isopropanol production on the pressures of both acetone and hydrogen, provided that the latter was in substantial excess, indicated that the surface was simultaneously saturated with acetone and hydrogen. Similar kinetics were found by van

Mechelen and Jungers (6) for the reaction in the liquid phase over Raney nickel at temperatures above 100°C. and by Herbo (7) for the reaction in the gas phase over a composite catalyst of nickel, zinc oxide, and chromium oxide at temperatures up to 175°C. Herbo invoked the idea of two types of sites to explain the observed kinetics, arguing that the surface could not be saturated simultaneously with both reactants if they occupied similar sites. An alternative explanation is possible in terms of the relative size of the acetone molecule and the hydrogen atom. The acetone, although strongly adsorbed, will not cover the surface completely because of the size of the molecule. The vacant sites between the acetone molecules will be covered by hydrogen atoms provided the ratio of the hydrogen pressure to the acetone pressure is sufficiently high but hydrogen will not displace the more strongly adsorbed acetone. On the other hand, if the ratio of the hydrogen pressure to the acetone pressure is reduced, the coverage of the vacant sites between the adsorbed acetone molecules becomes dependent on the pressure of hydrogen as indicated by the experimental results obtained.

The halving of the initial rate when a pressure of alcohol equal to the initial pressure of acetone was added, indicated that isopropanol competed with acetone for the surface and that the two substances were adsorbed with approximately equal strength. This inhibition by alcohol accounts for the apparent first-order dependence on acetone pressure of the rate of the reaction throughout the course of a run, implied by Eq. [1], despite the fact that the initial rate was independent of the acetone pressure. On the basis of equal competition for the surface by acetone and isopropanol and on the assumptions that both are strongly adsorbed and that the rate of the reaction is governed by the amount of adsorbed acetone, the following equation can be derived from equations of the Langmuir type,

$$\frac{dp_I}{dt} = \frac{k_2 p_A}{p_A + p_I}, \qquad [3]$$

where p_A and p_I refer to the pressures of acetone and isopropanol, respectively. If the pressures are replaced by the percentages of acetone and alcohol present, Eq. [3] becomes

$$\frac{dx}{dt} = \frac{k_1(100 - x)}{(100 - x) + x} = \frac{k_1(100 - x)}{100}, \qquad [4]$$

where x is the percentage of isopropanol at time t and k_1 is the initial rate of conversion in %/unit time. Integration of Eq. [4] leads to Eq. [1], which was obeyed by all the experiments where the ratio of hydrogen to acetone was high and provided the results were taken in the early part of the runs before the reverse reaction became appreciable. The curved lines obtained when the experiments 5 and 6 of Table III with a ratio of hydrogen to acetone of 2:1 were plotted according to Eq. [1] indicated that the simple kinetics implied by Eq. [3] were no longer adequate to explain the observations under these conditions.

The results in Table II show that the order of activity of the metals for the production of isopropanol as measured by the temperature required to attain a fixed rate of conversion, followed quite closely the order which has been reported by Beeck (8) for the hydrogenation of ethylene. Palladium was, however, exceptional in that it was the least active of the five transition metals for the hydrogenation of acetone, whereas it was the most active of the five for the hydrogenation of ethylene. The small but significant activity observed on gold films was interesting because it showed that activity for this reaction was not confined solely to transition metals. Table II also indicates that there was a tendency for the frequency factors to be larger on the metals with the higher activation energies. The value of 8.8 kcal./mole for the activation energy on evaporated nickel films may be compared with 9.5 kcal./mole obtained by van Mechelen and Jungers (6) in the liquid phase over Raney nickel at the higher temperature range of 100–150°C. and with 12 kcal./mole reported by Herbo (7) for his promoted nickel catalyst in the temperature range 140–170°C. At higher temperatures Herbo found that the apparent activation energy decreased and became negative above 200°C. He attempted to explain this behavior by suggesting that the adsorption of the reacting gases was decreasing with increase of temperature to a greater extent than the rate of hydrogenation was increasing. We believe that the explanation of his results is the establishment of the equilibrium between acetone, hydrogen, and isopropanol at the higher temperatures, and that at the highest temperatures he was measuring the heat of reaction and not an energy of activation. The equilibrium constant for the hydrogenation of acetone to isopropanol at 246°C. is 5.9×10^{-4} (mm.)$^{-1}$ and consequently in one of the experiments he quoted, starting with 245 mm. of acetone and 520 mm. of hydrogen, equilibrium would have been attained when 53 mm. of isopropanol had been formed. Furthermore, he established that the value of the quantity $v(p_A \cdot p_H)^{-1}$, where v was the reaction velocity in mg./hr. and p_A and p_H were the initial pressures of acetone and hydrogen in millimeters, was almost constant, varying only between 5.9×10^{-4} and 6.9×10^{-4}, at 246°C. We suggest that v was a measure not of the velocity but of the amount of isopropanol formed and that, since only small amounts of alcohol would have been formed, the final values of the pressures of acetone and hydrogen would not have differed substantially from the initial pressures and, consequently, that the quantity he reported was actually very similar to an equilibrium constant for the reaction. The approximate constancy of the quantity confirms, in our opinion, that equilibrium was established at 246°C.

The capacity of platinum to convert acetone to propane, which was observed, is in agreement with the work of Farkas and Farkas (9) on the deuteration of acetone over platinized-platinum foil, with that of Friedman and Turkevich (10), who used a catalyst containing 10% Pt on charcoal, and with that of Kauder and Taylor (11) on platinized platinum. However, there were substantial differences in the amounts of propane which were obtained on evaporated films in contrast to the other types of platinum catalyst. Farkas and Farkas used pressures of acetone between 40 and 100 mm. and comparable pressures of deuterium and found that the yield of propane was 68% at −42°C. and that this rose to almost 100% at 0°C. In contrast the evaporated films of platinum yielded only about 8% of propane in the same temperature range. Farkas and Farkas also showed that the formation of propane was slower from isopropanol than from the ketone, and they suggested that acetone underwent two independent reductions yielding either isopropanol or propane. They ruled out the possibility of the formation of propane by consecutive reactions with isopropanol as an intermediate product because of the relatively slow conversion to propane they observed with the alcohol as the initial reactant. Two factors are probably responsible for the different results obtained on evaporated films and on foil. Firstly, it will be noted that the production of propane on the evaporated films occurred only to a small extent at the beginning of the reaction and then ceased. This indicated that the direct formation of propane from acetone was due to the presence of a limited number of active sites on the evaporated film and that these sites became poisoned quite rapidly. There is evidence for this sort of behavior with evaporated films in the exchange of ethane with deuterium (12), since a very rapid production of small amounts of the deuteroethanes was observed in the first minute or two on some metals and then further exchange followed at the normal rate. The sites capable of inducing the catalytic fission of the carbon-oxygen bond of the ketone at low temperatures on the foil may have been either more numerous or less susceptible to poisoning than those on the evaporated film. Secondly, it is possible that both the desorption and the adsorption of isopropanol were substantially slower on the foil used by Farkas and Farkas than on the evaporated platinum film. This would have accounted for both the minor amounts of alcohol obtained from the ketone by them and also for the slow rate of conversion of the alcohol to propane on their catalyst.

A detailed discussion of the mechanisms of the reduction of acetone to isopropanol and to propane will be possible when the work, at present being undertaken, on the reaction of deuterium and acetone over evaporated films is completed.

The authors are grateful to the Council of the Royal Society for a grant towards the cost of materials. One of us (C.T.H.S.) wishes to thank the Ministry of Education, Northern Ireland, for a research grant.

References

1. Kemball, C., *Proc. Roy. Soc. (London)* **A207**, 539 (1951).
2. Kemball, C., *Proc. Roy. Soc. (London)* **A214**, 413 (1952).
3. Rideal, E. K., *Proc. Roy. Soc. (London)* **A99**, 153 (1921).
4. Parks, G. S., and Kelley, K. K., *J. Phys. Chem.* **32**, 734 (1928).
5. Dolliver, M. A., Gresham, T. L., Kistiakowsky, G. B., Smith, E. A., and Vaughan, W. E., *J. Am. Chem. Soc.* **60**, 440 (1938).
6. Van Mechelen, C., and Jungers, J. C., *Bull. soc. chim. Belges* **59**, 597 (1950).
7. Herbo, Cl., *J. chim. phys.* **47**, 454 (1950).
8. Beeck, O., *Discussions Faraday Soc. No.* **8**, 118 (1950).
9. Farkas, A., and Farkas, L., *J. Am. Chem. Soc.* **61**, 1336 (1939).
10. Friedman, L., and Turkevich, J., *J. Am. Chem. Soc.* **74**, 1669 (1952).
11. Kauder, L. N., and Taylor, T. I., *Science* **113**, 238 (1951).
12. Anderson, J. R., and Kemball, C., *Proc. Roy. Soc. (London)* **A223**, 361 (1954).

JOURNAL OF COLLOID SCIENCE **11**, 543–554 (1956)

THE INFLUENCE OF TEMPERATURE ON MONOLAYERS OF NONELECTROLYTIC LINEAR HIGH POLYMERS

J. Llopis and D. V. Rebollo

Instituto "A. de G. Rocasolano" de Quimica-Fisica, Madrid, Spain

Received April 6, 1956

ABSTRACT

The compression isotherms of monolayers of linear high polymers spread at the air/water interface have been obtained at different temperatures. The polymers studied were polyvinyl acetate (PVac), polyvinyl alcohol (PVA), and dimethylcellulose (DMC). The effect of temperature is insignificant on monolayers of DMC. With monolayers of PVAc we find that for a given value of the area per unit of polymer the surface pressure goes through a minimum with rising temperature. On the contrary, with monolayers of PVA the pressure goes through a maximum with rising temperature. From these variations of the surface pressure with temperature the spreading entropy and enthalpy have been obtained and conclusions have been reached concerning the coherence of these monolayers and their interactions with the substratum.

INTRODUCTION

The interest inherent in the study of the behavior of macromolecules at interfaces has been evident in the last few years from the growing number of publications appearing on this question (1–5).

Several papers deal with the surface pressure and potential as functions of the available area per molecule, as well as of the corresponding variations in the optical and mechanical properties (viscosity coefficient and moduli of elasticity) of the monolayers formed by macromolecules; interesting conclusions were reached in this way (6) concerning the arrangement of the macromolecules at the interfaces, their mutual interactions, and their interactions with the components of the phases which form the interface.

The interpretation of the surface pressure-area curves furnishes data about the cohesion of the monolayers. In the case of macromolecules, this cohesion is the result of the interactions of the skeletons and chains or lateral groups and of the internal effects among the segments of the same macromolecule (7), all of which are influenced by the nature and composition of the interface on which the monolayer is spread (8, 9).

The portion of these curves corresponding to the lowest pressures has the advantage of being easier to interpret in theory and also offers the possibility of drawing conclusions in some cases with regard to the flexibility and configuration taken by the macromolecules at the interfaces (10), apart from the possible determination of molecular weights, when extrapolation to an infinite area (11, 12) or zero pressure is practicable (13). Generally speaking, this extrapolation gives greater guarantees in favorable circumstances that the macromolecules will take on a compact and rigid configuration at the interface, whereas, on the contrary, those which favor the unfolding of the macromolecule on the interface and increase its internal flexibility, lead to a representation πA-π nonsuitable to this extrapolation (9). In this connection, in the last few years, surface balances have been developed that are suitable for measuring the lowest pressures (11, 14).

It must be stated that, although numerous papers have been published on the monolayers of high polymers, theoretical research work on their equation of state is very scanty. The Flory-Huggins method for macromolecule solutions in three dimensions has been used by Singer (15), whereas Saraga and Prigogine (16) have used Flory's more approximate treatment (5). The inter- and intramolecular electric effects on the equation of state of monolayers, formed by charged macromolecules, have been taken into account by Davies and Llopis (9).

Except in those cases in which intermolecular cohesion is very great, Singer's treatment is probably the best one for monolayers of polymers (5). However, this treatment is based on an idealized model and allows us only to give an account of the entropic variation with regard to ideality (17), since it introduces the approximations of not taking into account the interaction energies and assumes a random distribution of the macromolecule segments at the interface.

The lack of data concerning the dependence on the temperature of the surface pressure-area curves for monolayers of polymers results in ignorance of the effect of the first approximation. We have, therefore, thought it desirable to study, at different temperatures, the compression isotherms of monolayers of linear polymers, and attempt to correlate the results with the scant existing theory. In principle, and with a view to facilitating interpretation, more attention has been paid to the portion of the isotherms at low pressures, and nonelectrolytic polymers were chosen in order to avoid the electrical interactions in charged macromolecules. The polymers studied were polyvinyl acetate (PVAc), polyvinyl alcohol (PVA), and dimethylcellulose (DMC). The existence of lateral chains in PVAc and DMC may increase cohesion among the segments of the polymer.

EXPERIMENTAL TECHNIQUE

The surface pressures were determined by means of a Langmuir-Adam torsion balance, with a single wire and optical enlargement. The lowest pressure that can be measured, by using a 14.0 × 31.3 cm. trough, was 25 mdyne cm.$^{-1}$; and the highest, 20 dyne cm.$^{-1}$. The accuracy of each measurement was about ±10 mdyne $cm.^{-1}$. This balance was held in an air thermostat, the temperature of which was regulated by means of a bimetallic junction and an electromagnetic relay. The inner surface of this thermostat was metallic and directly connected to earth to permit the measurement of surface potential. The temperatures were measured with a thermometer introduced into the trough which was used to spread the monolayers, just behind the mobile barrier. This way of measuring the temperature may have been partly responsible for the dispersion of results, for the temperature which it would have been really interesting to know was that of the interface in question. However, this effect was lessened by the thermostatization of the atmosphere, as proved by the fact that the dispersion obtained was not excessive. Other causes of error were probably more important as regards this dispersion; for instance, the more or less complete spreading of the macromolecules which form the monolayer at the interface, the measure of the volume of the spread solution, and the measure of the area. The temperature could be measured with an accuracy of 0.1°C., and its variation in the course of an experiment was below 0.1°C.

The surface potentials were measured by an ionization method, by means of an electrometer fitted with an E.T.1. valve.

As substratum in all cases a solution of 0.001 *N* hydrochloric acid in doubly distilled water was used. The experiments described in this paper were carried out at the air/water interface, with a quartz trough with paraffined edges. The paraffin used for this purpose and also to cover the fixed and mobile barriers must be of high melting point (65°C.), making it possible to work easily in the temperature range at which we operated (15–50°C.)

Experimental Results

Dimethylcellulose

As is known, it is possible to study the behavior of some derivatives of cellulose when they are spread as monolayers at the air/water interface (18–21). A lengthy paper on this question was written by Adam, and a general discussion of the results is described in his well-known monograph (22). It can be inferred that the methyl derivatives of cellulose spread well as monolayers, but, as regards the influence of the temperature, Adam mentions only that, in the 15–50°C. range, this factor does not seriously affect the pressure-area curves. In this aspect, he refers only to the derivatives of cellulose that have been studied and does not concretely specify how far the results are certain.

On the other hand, we must bear in mind that when the cellulose chains spread out on the surface, the exose rings lie flat and the only flexibility of these macromolecules will be that allowed by the bending of the oxygen bonds between two successive rings. Consequently, it would seem desirable, with a view to a possible theoretical study, to know in detail the pressure-area and surface potential-area curves at different temperatures, since, in these polymers, the flexibility of the monomer groups themselves is null and the total flexibility of the macromolecule is the result of the union between them.

The derivative studied in this case was a noncrystallized dimethylcellulose. The sample used, after being purified, was washed with chloroform, which removed the more methylated fractions, that were soluble in this solvent; in the remainder, the CH_3O— groups were determined by analysis, and a value of 1.61 methoxyl groups per exose monomer was found. This methylcellulose dissolves in water, albeit slowly; and, for this reason, it is advisable to heat to 50°C. for a long time, in which way a perfectly transparent solution is obtained. To spread the monolayer, a solution in water containing about 0.25 mg./cm.^{3} of polymer was used, with the addition of 10% of its volume of isopropyl alcohol. The spreading of the monolayer is achieved by means of an Agla microsyringe and, generally speaking, it has been seen that the most reproducible results are attained when compression is applied 2 or 3 minutes after the spreading of the monolayer. If we wait until 30 minutes, no variations are observed in the low-pressure area; but slightly higher pressure values are found in the more compressed areas. This may be due, as in other cases (23), to the fact that, after a time, the macromolecules at the interface get a more unfolded configuration, although the chances of contamination of the surface also increase. Therefore, in view of the fact that in this case the effect is not appreciable, it was thought better to proceed as stated.

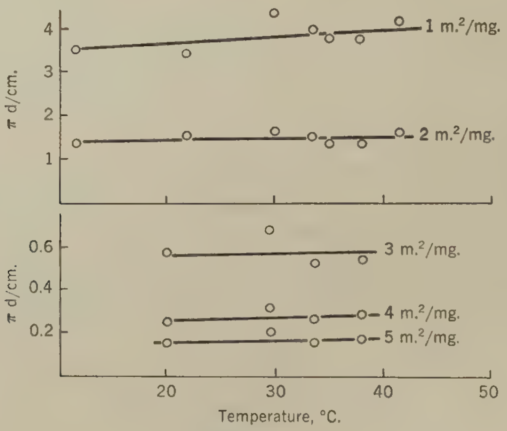

FIGURE 1

For each temperature value several π-A curves were obtained; and, from these, a median curve was drawn, on which the values represented in Fig. 1 were interpolated. In this figure, the surface pressures are shown in dyne cm.^{-1} as a function of the temperature in °C. and for five values of the available area expressed in $\text{m.}^2\ \text{mg.}^{-1}$. For the study of the lowest pressures we proceeded in the same way, with other experiments in which the quantity of substance spread in the formation of the monolayer was much less. The two series of experiments coincide fairly satisfactorily in the pressure values in which they overlap. The reproducibility achieved up to areas of 3 $\text{m.}^2\ \text{mg.}^{-1}$ is ± 0.02 dyne cm.^{-1} and for areas of 1.5 $\text{m.}^2\ \text{mg.}^{-1}$, ± 0.15 dyne cm.^{-1}; the dispersion of results increases rapidly when pressures exceeding 5 dyne cm.^{-1} are dealt with.

This figure shows that the effect of the temperature is insignificant on monolayers of these polymers, in accord with Adam's indications.

Surface potential-area curves were also obtained for two extreme temperatures (21.9°C. and 40°C.), and it was observed that the influence of the temperature is likewise very slight as regards the orientation adopted by the exose groups on the fluid surface. The effect observed, some 20 mv. for an area of 1 $\text{m.}^2\ \text{mg.}^{-1}$, indicates that the surface potential is somewhat lower in proportion as the temperature rises, and this effect is null for greater areas.

Polyvinyl Acetate

This polymer can be perfectly well spread in monolayers at the air/water interface (1). The π-A curves then obtained by compression do not depend on the time we wait after the formation of the monolayer. However, in tracing these curves it is advisable to let the compression occur slowly, for otherwise it takes some time to get the proper equilibrium pressure. In total, the π-A curves (the latter being expressed in $\text{m.}^2\ \text{mg.}^{-1}$) depend only slightly on the average molecular weight of the polymer in question, and only at the larger areas is a tendency observed to get higher pressures when the mol. wt. diminishes; at pressures exceeding 2 dyne cm.^{-1} the differences found fall within the usual dispersion of this kind of measurements. The compressibility of these monolayers is very great at low pressures and reaches a minimum with areas of 15.8 A.^2/monomer. The collapse pressure is 26.4 dyne cm.^{-1}, and it must be remarked that the monolayers of this polymer show no hysteresis in successive compression and expansion processes, even when the limiting values of pressure are reached (24, 25).

The determination of molecular weights by extrapolation to $\pi \rightarrow 0$, in the representation of πA against π, leads to very low values (26); this is due to the fact that, in this case, this representation is not linear but concave towards the axis of the pressure (27), even for very low pressure values. This deviation corresponds, according to Davies (8), to a high value of macromolecule flexibility, when the latter is expressed by the parameter z of Singer's equation. In this sense, we have calculated on the basis of our experiments carried out at 20°C., a value of $\omega = 1.10$, which does indeed belong to a very flexible molecule.

To study the influence of the temperature on monolayers of this polymer, we carried out the series of experiments the results of which are shown in Fig. 2. The polymer used was prepared by the block method and has a very high mol. wt. ($\simeq 450{,}000$). The monolayer is spread at the air/water interface, with a solution of 0.001 N hydrochloric acid as a substratum, and the spreading is achieved by means of a solution of the polymer in benzene, with a concentration of 1 mg. cm.$^{-3}$.

The average reproducibility attained in relation to the pressure for each series of experiments can be estimated at 3.5%. In this figure the pressures attained for different area values in m.^{2} mg.$^{-1}$ are represented as a function of temperature in °C. It is seen that, in this case, the effect of temperature is considerable, even for a large expansion of the monolayer. For a given value of the area per amount of polymer the surface pressure reaches a minimum with rising temperature.

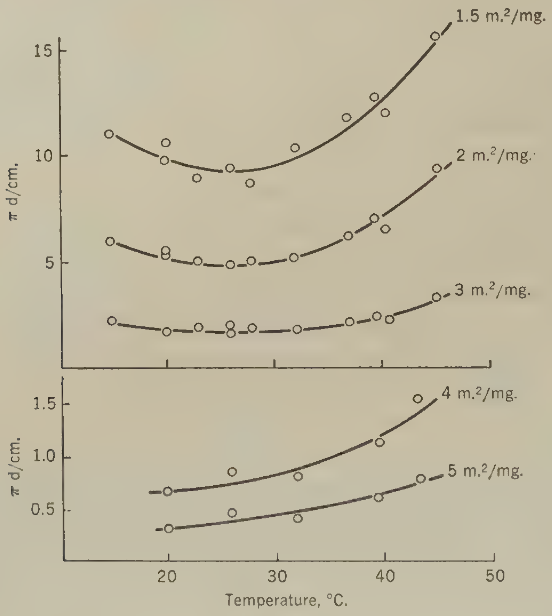

FIGURE 2

The influence of the variation in temperature on the surface potential is slight; only at 40°C. lower potentials are observed for areas of 4 m.^{2} mg.$^{-1}$.

Polyvinyl Alcohol

The monolayers of polyvinyl alcohol are fluid and very compressible. This polymer is soluble in water and it might be thought that its monolayers would be unstable and penetrate into the water, especially when com-

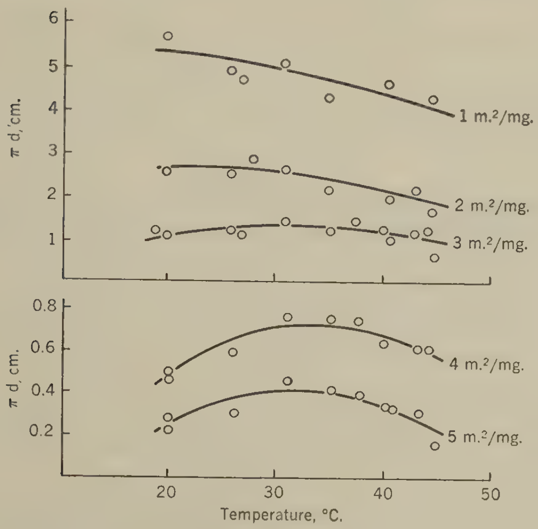

FIGURE 3

pressed. However, this does not occur, for no effect is seen owing to slow diffusion when the monolayer is expanded again (1). Monolayers of this polymer can be formed from a solution in a mixture of water and propyl or ethyl alcohol.

The polymer used in the experiments here described has an elevated molecular weight and is very pure, although it may contain some traces of acetyl. For the formation of the monolayer an aqueous solution is used, the polymer concentration of which is 1 mg. cm.$^{-3}$, with added isopropyl alcohol to 30% in volume. For these monolayers, no aging effects have been observed; but, as with polyvinyl acetate, the pressure drops somewhat after a rapid compression. In order to avoid this effect, in these cases we have proceeded by slow compression, regulating the latter by means of a motor.

As in the former cases, the results obtained are represented in Fig. 3, in which the pressures are set forth as a function of the temperature, for different values of the available area per milligram of substance.

It is of interest to point out that, in this case, the pressure passes through a maximum with rising temperature, and this maximum shifts towards lower temperatures as more compressed states of these monolayers are considered, until, for an area of 1 m.^{2} mg.$^{-1}$ the pressure is a maximum at 20°C., the lowest temperature used.

DISCUSSION

The dependence of the π-A curves on the temperature will allow us to draw certain conclusions about the energy of interaction existing in the macromolecules which form the monolayer in question.

Following Harkins (28) we define the thermodynamic magnitudes of spreading as:

$$g_s = \left(\frac{\partial G}{\partial \sigma_g}\right)_{E,T,A} \qquad h_s = \left(\frac{\partial H}{\partial \sigma_g}\right)_{E,T,A} \qquad s_s = \left(\frac{\partial S}{\partial \sigma_g}\right)_{E,T,A} \qquad [1]$$

in which the variation of the area of the film σ_g is obtained by means of a mobile barrier, and therefore, at the same time as this former area is increased the free surface of the substratum σ_a is decreased in the same proportion, the total surface, $E = \sigma_g + \sigma_a$, remaining constant.

If in the aforesaid variation the free surface of the substratum is not affected, the thermodynamic magnitudes of extension g_e, h_e, s_e, are obtained in the partial derivation.

Now $g_e = g_s + g_a$ and similar expressions for the entropy and enthalpy are evident, the corresponding magnitudes per unit of substratum surface being g_a, h_a, s_a.

From the variations in surface pressure with the temperature it is possible to calculate the spreading magnitudes by means of the expressions

$$g_s = -\pi \quad s_s = \left(\frac{\partial \pi}{\partial T}\right)_{A,E} \quad h_s = -\left[\frac{\partial(\pi/T)}{\partial(1/T)}\right] = T\left(\frac{\partial \pi}{\partial T}\right)_{A,E} - \pi \qquad [2]$$

In the case of DMC, it will be observed in Fig. 1 that π depends very little on the temperature, and the dispersion of experimental results prevents us from differentiating, even in the best of cases, if this dependence is not linear. Admitting that it is effectively so, for an area of 1 m.^{2} mg.$^{-1}$ we obtain a spreading entropy of $s_s = 0.01_4$ erg cm.$^{-2}$ dgr.$^{-1}$. At the same time we get a zero enthalpy h_s, which would seem to prove that with this polymer the molecular interactions are zero and, as regards the interactions with the molecules of the substratum, there is no variation by the differential expansion, at any rate up to the compressions studied; consequently, in the interpretation of the π-A curves, only the variations in entropy need be considered.

The same thing does not occur with the other polymers studied. With the results set forth in the relevant figures, by means of the expressions [2] we have found the spreading enthalpies and entropies for two temperature values, viz., 25°C. and 40°C. The results are summed up in Tables I

TABLE I

Spreading Entropy and Enthalpy Values for PVAc Monolayers at the Air/Water Interface

m.^{2} mg.$^{-1}$	h_s^{25}	s_s^{25}	h_s^{40}	s_s^{40}
1, 5	-18	-0.030_0	$+129$	0.45
2	$-9._4$	-0.01_5	$+87$	0.3_0
3	$-3._2$	$+0.00_5$	$+35$	0.1_2
4	$+3._9$	$+0.01_5$	$+17._7$	0.06_1
5	$+3._4$	$+0.01_2$	$+7._4$	0.02_6

(PVAc) and II (PVA) and represented, respectively, in Figs. 4 and 5, in relation to the areas available in m.^{2} mg.$^{-1}$.

The first thing observed when comparing these two figures and the tables of values mentioned above is that, for 25°C. we get in both cases similar

TABLE II

Spreading Entropy and Enthalpy Values for PVA Monolayers, at the Air/Water Interface (h_s in erg cm.$^{-2}$; s_s in erg cm.$^{-2}$ dgr.$^{-1}$)

m.^{2} mg.$^{-1}$	h_s^{25}	s_s^{25}	h_s^{40}	s_s^{40}
1	−16	-0.03_0	−23	-0.07_2
2	−2	0.00	−18	-0.05_6
3	$+5._8$	$+0.02_4$	−12	-0.03_6
4	$+5._3$	$+0.02_2$	$-5._4$	−0.015
5	+3.0	$+0.01_5$	$-5._3$	−0.016

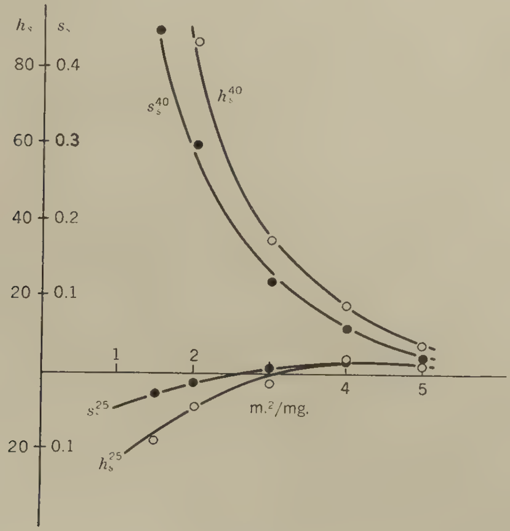

FIGURE 4

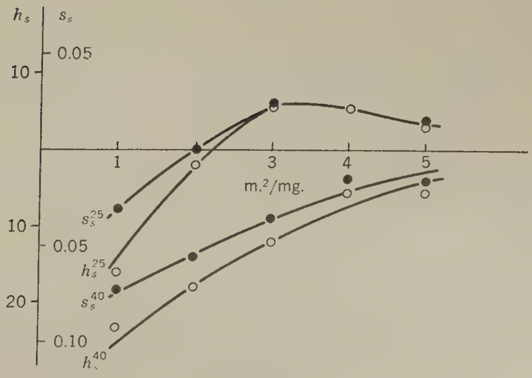

FIGURE 5

h_s and s_s values and an identical variation of these magnitudes with compression. However, at 40°C. the difference in behavior as regards these magnitudes is fundamental, since with PVA monolayers we get negative h_s and s_s values, which continue to decrease with compression, whereas with PVAc they are positive and increase with compression.

To interpret this different behavior we have to bear in mind that in monolayers formed by high polymers and up to pressures that are not excessively high, the variation with compression of the spreading entropy is due to the following causes: (*a*) the ideal variation depending on the assumption that the macromolecules are rigid; (*b*) the variation due to the flexibility of the long chains of the polymer; (*c*) the contribution arising from the possibility that some part of the macromolecule may penetrate into the substratum; and (*d*) the influence of the incomplete unfolding of the macromolecules at the interface. As regards the enthalpy, these causes will have an influence in so far as they affect the energy of interactions of a segment with the others of the same macromolecule, with those of another neighboring macromolecule, and with the molecules which constitute the interface.

As regards the first factor, the spreading entropy will be positive and increases with compression. The spreading enthalpy will be zero if there are no interactions among the macromolecules; if there exist attractions or repulsions, a factor of reality is introduced, which will cause the enthalpy to be positive or negative, as the case may be. In so far as these interactions depend on the average distance between neighboring molecules, the law of variation of this fraction of the spreading enthalpy with compression will result.

The deviation of the spreading entropy in relation to ideality, due to the flexibility of the macromolecules, is the only thing that has been studied by means of a statistical mechanical treatment, by the same process as was followed in the study of macromolecule solutions in three dimensions.

If we accept the definition of flexibility given by Davies (8) as $\omega = z - 2$, z being the coordination number of the monomers in the bidimensional postulate of the quasi-reticulum at the interface, it follows, according to Singer's equation, that the spreading entropy is positive and increases with compression more rapidly when more flexible macromolecules are considered.

But, in order to take into account the intramolecular cohesion in the equation of state, this factor may be introduced in the configurational term z (9), so that:

$$\omega = \omega_0 e^{-E/RT}, \qquad [8]$$

E being the energy barrier required to change the place of a monomer, previously leaving a hole to be filled. This hypothesis is not justified *a priori*, but it has given good results in the study of polyamino acid monolayers taking into account the intramolecular electric actions.

If it is assumed, in principle, that E does not depend on the available area per molecule, it follows from [3] that ω increases with T and owing to this increment in the flexibility of the macromolecule, the spreading entropy will be more positive. Naturally, the value of E will depend on the strength of the cohesion forces, and, therefore, it is to be expected that this thermal effect will be greater whenever the attraction among the segments is greater.

As regards the variation in the spreading enthalpy with the intramolecular actions, this will depend on the influence of the available area per macromolecule on the average distance between two segments.

We shall subsequently study the contribution arising from the possibility of a part of the macromolecule skeleton sinking into the substratum, thus diminishing the number of hydrophilic groups at the interface. It is evident that this penetration originates an increase of entropy and, at the same time, the introduction of $—CH_2—$ groups in the aqueous phase originates a disturbance in the H_2O structure with an increase of enthalpy, since the affinity of a $—CH_2—$ group for H_2O is negligible as compared with that of these molecules among themselves; nevertheless, this effect is partly compensated by the lessening of enthalpy, which involves a better solvation of the hydrophilic groups and, consequently, the result will depend on the balance existing in the macromolecule between the hydrophilic and hydrophobic groups.

When there is a differential expansion and, consequently, an access to the surface by the sunken part of the molecule in the monolayers here considered, a lessening both of the entropy and the enthalpy is to be expected.

The degree of unfolding of the macromolecules at the interface will depend on their state in the solution used to form the monolayer, and it is probable that, at the interface, at least a part of the macromolecule will still retain the configuration it had in the solution. Up to what point the molecule will be unfolded at the surface cannot be decided in principle; but if the intramolecular cohesion has an influence on this fact, the temperature may be expected to play an essential part in the unfolding and a major portion of the macromolecule is freed from tridimensional rolling and can participate more freely in the bidimensional thermal movement (29).

If in the light of these ideas we try to interpret the results found when studying the monolayers of polyvinyl alcohol and polyvinyl acetate, we infer that: *(1)* In both cases even for areas of 3 $m.^2\ mg.^{-1}$ cohesive forces are apparent at the air/water interface, which originate a spreading enthalpy that is not zero. *(2)* The influence of a partial penetration of the macromolecule into the substratum increases with the compression of the monolayer, and this effect, when the temperature rises, becomes very noticeable in the case of PVA, owing to the preponderance of the hydrophilic part of the macromolecule; on the contrary, with PVAc, when the temperature rises the other effects prevail. (*3*) In both cases, conclusions from a theoretical study of the π-A curves, should be substantiated by the results for pressures below 0.1 dyne cm.$^{-1}$.

REFERENCES

1. Crisp, D. J., *J. Colloid Sci.* **1,** 49, 161, (1946).
2. Cumper, C. W. N., and Alexander, A. E., *Revs. Pure and Appl. Chem. (Australia)* **1,** 121 (1951).
3. Cheesman, D. F., and Davies, J. T., *Advances in Protein Chem.* **9,** 439 (1954).
4. Isemura, T., Hirota, H., and Hamaguchi, K., *Mem. Inst. Sci. and Ind. Research, Osaka Univ.* **12,** 125 (1955).
5. Rideal, E. K., *J. Polymer Sci.* **17,** 531 (1955).
6. Cumper, C. W. N., and Alexander, A. E., *Trans. Faraday Soc.* **46,** 235 (1950).
7. Hirota, H., *J. Colloid Sci.* **9,** 504 (1954.)
8. Davies, J. T., *Biochim. et Biophys. Acta* **11,** 165 (1953).
9. Davies, J. T., and Llopis, J., *Proc. Roy. Soc. (London)* **227A,** 537 (1955).
10. Davies, J. T., *J. Colloid Sci. 9, Sup.* **1,** 9 (1954).
11. Guastalla, J., *Compt. rend.* **208,** 1078 (1939)
12. Guastalla, J., *J. chim. phys.* **48,** 621 (1951).
13. Bull, H. B., *J. Am. Chem. Soc.* **67,** 4 (1945).
14. Allan, A. J. G., and Alexander, A. E., *Trans. Faraday Soc.* **50,** 863 (1954).
15. Singer, S. J., *J. Chem. Phys.* **16,** 872 (1948).
16. Saraga, L., and Prigogine, I., *J. chim. phys.* **49,** 458 (1952).
17. Allan, A. J. G., and Alexander, A. E., *Trans. Faraday Soc.* **46,** 316 (1950).
18. Adam, N. K., *Trans. Faraday Soc.* **29,** 90 (1933).
19. Harding, J. B., and Adam, N. K., *Trans. Faraday Soc.* **29,** 837 (1933).
20. Parker, J., and Shereshafsky, J. L., *J. Phys. Chem.* **58,** 850 (1954).
21. Jaffe, J., *J. chim. phys.* **51,** 243 (1954).
22. Adam, N. K., "The Physics and Chemistry of Surfaces," p. 85. Oxford, 1941.
23. Cheesman, D. F., and Schuller, H., *J. Colloid Sci.* **9,** 112 (1954).
24. Müller, F. H., *Kolloid-Z.* **136,** 127 (1954).
25. Müller, F. H., *Z. Elektrochem.* **59,** 312 (1955).
26. Benson, G. C., and McIntosh, R. L., *J. Colloid Sci.* **3,** 323 (1948).
27. Isemura, T., Hotta, H., and Miwa, T., *Bull. Chem. Soc. (Japan)* **26,** 380 (1953).
28. Harkins, W. D., "The Physical Chemistry of Surface Films," p. 1721. Reinhold, New York, 1952.
29. Hamaguchi, K. A., *J. Biochem.* **42,** 705 (1955).

JOURNAL OF COLLOID SCIENCE **11**, 555–564 (1956)

METHODS OF STUDYING THE SURFACE STRUCTURE OF SOLIDS

F. P. Bowden

Research Laboratory for the Physics and Chemistry of Surfaces, Department of Physical Chemistry, Cambridge, England

Received May 21, 1956

INTRODUCTION

All who have worked with Sir Eric Rideal agree about his gay and infectious enthusiasm for scientific work and about his conviction not only that all problems are soluble but that it will be great fun solving them. I have been enormously grateful for this from the day of my arrival in Cambridge as a shy student from Tasmania when he set me to work on a table in the basement among the dustbins (the only space available). All difficulties disappeared, and we even solved, after some months of hard work, the problem of the removal of the dustbins. On the more scientific side we were interested in the real area of solid surfaces and one of our first pieces of work (1) together was the determination of the area of a metal surface by measurement of the electrical capacity of the interface when it was immersed in an electrolyte. These measurements showed that the "real" area (in this case the area accessible to hydrogen ions and to water molecules) of a smooth metal surface was appreciably greater than its apparent area and, if the surface was rough, it could be several times greater.

We are in this laboratory at the present time using a number of different physical methods for studying the contour and topography of solid surfaces. They all show that even when the surfaces are carefully prepared by polishing (or indeed by cleaving) they are not flat but contain irregularities and hills and valleys which are large compared with molecular dimensions. In this paper a brief account will be given of the methods of surface examination which we are finding most useful and, in particular, of some recent results of applying electron microscopy to a study of the nature of solid surfaces.

STYLUS METHODS

Instruments have been developed which amplify the movement of a tracer needle as it passes slowly over the surface and follows its contours.

The stylus is usually a conical diamond which may have a radius of curvature at its tip as small as 2×10^{-4} cm. The vertical movement of the stylus is amplified electrically and recorded on a moving paper. Considerable ingenuity and precision have been employed in the design and construction of these instruments, and they can operate successfully with a vertical magnification of 40,000. Certain inherent difficulties arise at high magnification, such as the difficulty of fixing accurately the reference datum level and, if the surface is soft, its damage by the stylus. A great advantage of this type of instrument is that it gives a record of the surface contour more quickly and conveniently than other methods, and it does not involve the destruction of the surfaces. Its ultimate sensitivity is limited by the finite size of the needle, which prevents it from penetrating the finest scratches or irregularities. It will, however, under favorable conditions, detect pits or scratches which are only 250 A. deep. An account of the underlying theory and of the value and the limitations of stylus methods has been given by Reason, Hopkins, and Garrod (2).

Taper Sectioning

A standard method of studying surface irregularities is to cut a cross section at right angles to the surface and examine it under the microscope. For small surface irregularities the highest powers must be used and the area of the field is therefore very restricted. Also, the minimum size of irregularity which can be observed is limited by the resolution of the microscope. Provided the surface irregularities are elongated in one direction—this is so, for example, with scratches caused by grinding or abrasion and with the surface damage caused by sliding—both these limitations can, to a considerable degree, be overcome by cutting the section obliquely to the surface. In this way a taper section is obtained with the vertical component of the surface contour greatly magnified relative to the horizontal one. The ratio of the magnification in the vertical and in the horizontal direction in the final section is the cosecant of the angle α. If the section is cut at an angle $\alpha = 5° 43'$ the ratio of the vertical to the horizontal magnification would be 10:1. It is necessary to protect the surface irregularities from damage by electroplating with a metal of similar hardness. This method of cutting is, of course, not new, but it appears to have first been described by Nelson (3).

It has been further developed by Dr. Moore and others working in this laboratory (4). With this method surface irregularities which are of the order of 10^{-5} cm. in height may be detected. It has the disadvantage that the surface is destroyed and it is a difficult and somewhat tedious technique. It does, however, have the great advantage that it reveals the structure of the solid *beneath* the surface.

Multiple Beam Interference

Simple two-beam interference methods for measuring surface contour have, of course, been in use for a long time. With the simple method the light and dark interference bands are comparatively broad. The variation of intensity from one maximum to the next is a sine squared function and the width of a "line" at half-maximum intensity is 50% of the spacing of the lines. This means that detail causing a shift of the maximum of less than ⅕ of an order would be almost invisible. Tolansky (5) has recently made notable advances by developing interference methods to a high degree of sensitivity. If the surfaces of the optical flat and the lens are coated with a layer of silver having a high reflecting coefficient (85–95%) and a significant transmission coefficient, the incident light will be reflected back and forth and the interference pattern will be the resultant of all these beams. The effect (which is analogous to increasing the number of lines on a diffraction grating) is to leave the maxima and minima of intensity as before, but to alter the distribution of intensity between one maximum and the next.

The intensity distribution is similar to that obtained in a Fabry-Perot interferometer: narrow bright lines in a dark field; the width at half-maximum intensity about 2% or 3% of the distance between orders. Fine detail of imperfections of surface finish corresponding to variations of thickness of the film $1/100$ of that between successive orders is easily visible. If $\lambda = 5000$ A., this corresponds to the detection of features 25 A. high.

By a modification of the method and the use of a spectrograph and white light the sensitivity can be increased still further, and steps and similar features in the surface as small as 6 A. can be detected and their magnitude measured to an accuracy of about 1 A. or 2 A. It is a most sensitive and exact method for measuring distances normal to the surface. Its resolution in a direction parallel to the surface is comparatively low.

Dr. Courtney-Pratt has used it to measure the chain length of hydrocarbons adsorbed as a monolayer on the surface (6). Dr. Bailey (7) has used it to measure molecular contact between cleaved mica surfaces. Recently she has made the remarkable observation (8) that if mica is cleaved in air and the surfaces placed together again so that molecular contact occurs the adhesion strength is almost the same as (about 17% less than) that of the virgin mica. If a monolayer of hydrocarbon is adsorbed on the surface the adhesion is enormously reduced.

Reflection Electron Microscopy

The electron microscope is, of course, a very powerful instrument for studying the detailed structure of surfaces. It normally works by transmission, and it is generally necessary to prepare transparent replicas of the surfaces. Apart from the fact that replica techniques are often a tricky business, it is never certain that they follow the original contour exactly, nor is the interpretation of the transmission micrograph obtained from the replica always unequivocal. These difficulties do not arise when the electron microscope is used as a reflection instrument. The general principle is to direct the electron beam at glancing incidence on to the surface under examination, and to focus the scattered electrons in the usual way. Active work on this is being done in the U.S.S.R., in France, and in England. A general review of this work has been given (9). The resultant electron micrograph reveals the surface contours somewhat in the same way as a pedestrian sees the surface irregularities of a road illuminated by oncoming car headlights. Long shadows are cast by surface irregularities, and they are foreshortened because of the small angle of viewing. Since we know the angle of the incident electron beam, it is easy to calculate the true height of the surface features. The great advantage of this technique is that replicas are not necessary: the surface itself is examined directly by the beam.

Some years ago Dr. Menter (10), working in this laboratory, showed that a very simple modification to a standard transmission microscope (the Metropolitan Vickers EM 3) would enable it to take reflection micrographs of great clarity, good resolution, and considerable depth of focus. The surface of a highly polished metal viewed by reflection electron microscopy is illustrated in Fig. 1. This photograph, taken by Mr. Seal, is of a gold surface which had been highly polished with alumina so that a Beilby layer is formed on it. To ordinary methods of examination it appears bright and smooth and the optical microscope would not reveal structure. The horizontal magnification of this picture is about 1000, and it will be seen that the surface is certainly not flat but is covered with a series of mountain ridges and furrows. It should be emphasized that this surface layer has been produced by a polishing process which involves high-temperature flow

FIG. 1. Reflection electron micrograph of a polished gold surface. The microroughness of the surface is apparent.

(11). It is not surprising when we can see such a surface that the area accessible to hydrogen ions is greater than unity.

Because of its great depth of focus this method is suitable for examining solids with a high degree of curvature such as fibers and Fig. 2 shows its

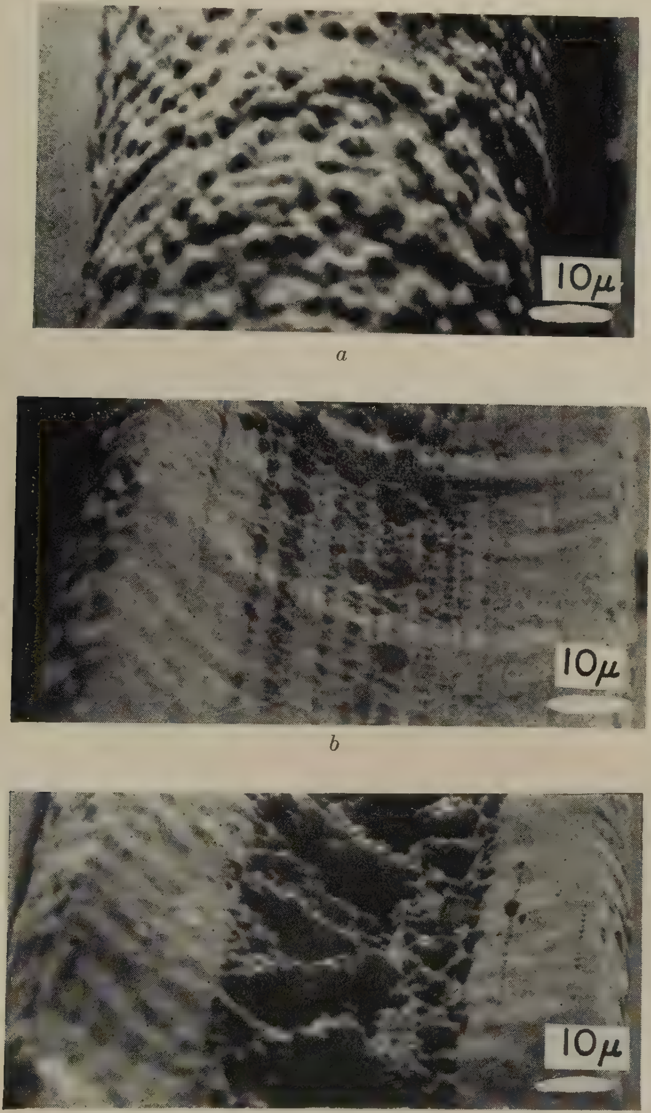

a

b

c

Fig. 2. Reflection electron microscopy of fibers. The deformation and damage occurring when a flat platinum slider is rubbed once along a drawn nylon fiber is shown: (*a*) undamaged fiber; (*b*) damage at a load of 200 g.; (*c*) damage at a load of 280 g.; heavy tearing occurs at the center of the track.

application to a study of the structure and wear of nylon fibers (12). This original fiber is illustrated in Fig. 2(*a*) and the cobblestone structure of the surface is apparent. Figure 2(*b*) shows the deformation and damage produced when a flat platinum slider at a moderate load is rubbed once over the surface. The more profound damage under a heavier load and the peculiar deformation of the fiber are illustrated in Fig. 2(*c*).

Decomposition of Crystals. The Use of a Scanning Microscope.

In electron microscopy precautions must be taken to ensure that the object under examination is not damaged by the electron beam. This is particularly important with biological specimens and with other solids which may decompose at a comparatively low temperature. The high-velocity electrons may themselves initiate chemical reaction or they may raise the bulk temperature of the object so that changes occur in it. We have been using the electron microscope to examine the mode of decomposition of explosive crystals and here the effect of the beam is of course particularly important. Recently Oatley and his colleagues (13) in the Engineering Laboratory at Cambridge have developed a scanning electron microscope which works in reflection or transmission. Here the electron beam which falls on the object is focused to a very small spot which may be less than 200 A. in diameter and is made to scan the object in a manner analogous to that of a television camera. In this way the average intensity is kept very low so that little damage is done. Mr. McAuslan in this laboratory is using this method to study in some detail the thermal decomposition of azide crystals. The crystal is placed in the microscope and rests on a metal plate which can be heated to any appropriate temperature. The successive stages of decomposition can be followed and photographed at convenient intervals.

Figure 3 illustrates the mode of thermal decomposition of a silver azide crystal. The crystal is a long, thin, needle about 1 μ in cross section and the left-hand end is in good thermal contact with the underlying plate so that it decomposes first. It will be seen that the decomposition of the crystal is not primarily a surface effect nor does it proceed in a uniform manner. Decomposition occurs within the crystal which breaks up into small blocklets a few tenths of a micron in size (14). These decompose into silver and nitrogen and the silver is left in the form of small nodules. This direct observation is yielding useful information about the modes of decomposition in the solid state.

Electron Microscopy and Electron Diffraction as a Joint Technique

Electron diffraction is of course widely used for studying the structure of solid surfaces. Since it gives us the atomic arrangement in the surface

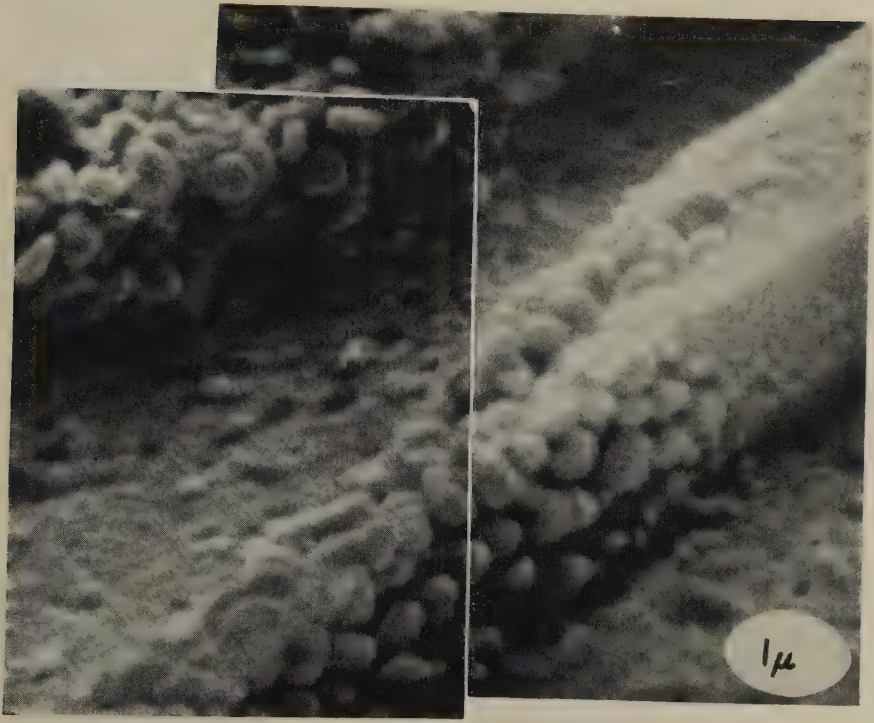

FIG. 3. Scanning electron micrograph of decomposing azide crystal. Reaction is occurring within the crystal which breaks up into small blocks $\sim 0.3\ \mu$.

layers it is a subtle and valuable tool. We are using it extensively for investigating the structure of mono- and polymolecular films on surfaces. More recently we have used it simultaneously with the electron microscope to follow the changes in a decomposing crystal. Mr. J. Sawkill (15) has investigated the decomposition of silver azide in this way. A thin crystal is placed on the stage of the electron microscope and examined in transmission. The action of the beam causes decomposition to occur and the growth of the tiny silver nuclei may be observed in the microscope. At various stages in the decomposition the instrument is switched over to electron diffraction so that the atomic arrangement in the crystal can be observed. The diffraction pattern changes slowly from that characteristic of silver azide to that characteristic of metallic silver. Two silver patterns are observed. One is highly oriented, the other randomly oriented. The highly oriented pattern appears to come from discrete nuclei of crystalline silver (about $\frac{1}{10}\ \mu$ in size) formed near the surface of the azide crystal. At first the atomic spacing in these nuclei is wider than that of an ordinary silver crystal (since they have to fit in to the silver azide lattice) but as reaction proceeds and the nitrogens are removed the atoms collapse to the normal silver spacing. The randomly oriented silver appears to separate at the boundaries of a substructure *within* the crystal. Again we have evidence for the occurrence of decomposition inside the crystal probably at the defects and imperfections which exist there.

The Direct Observation of Molecules in a Crystal Lattice

The resolution of electron microscopes is continually being improved and instruments (e.g., Siemens) are now available with a resolution that is a little better than 10 A. This is not fine enough to resolve the atomic spacing in most crystals since this spacing may be 3 A. or so. If, however, a crystal with lattice dimensions comparable with the resolution limit of the microscope were selected, it should be possible to "see" the atomic array in the crystal. Dr. Menter[1] has recently tried this experiment at the Tube Investments Research Laboratories, Hinxton Hall, Cambridge, where he is now working, and has examined crystals of copper and of platinum phthalocyanines (16). These are large flat molecules consisting primarily of carbon and nitrogen with the metal atom in the center. They form long flat ribbon-like crystals, the surface of the ribbon being (001) and the ribbon axis [010]. In platinum phthalocyanine, the angle $(001)\,\hat{}\,(20\bar{1})$ is 88° so that a crystal will lie on a horizontal supporting film with the $(20\bar{1})$ planes almost vertical. The spacing of these planes is 11.94 A. They should, therefore, lie in a suitable orientation for diffraction and the distance between them should be resolvable in the electron microscope. Figure 4 shows a photograph he has taken. This is taken in transmission on a crystal about 200 A. thick, and the magnification is about one and a half million times. It is seen that it consists of an extremely well-defined series of uniformly spaced parallel lines. The distance between these lines is 12 A., which corresponds to the spacing of the $20\bar{1}$ planes in platinum phthalocyanine (as determined by X-ray diffraction). This is an exciting picture, since it is the first direct observation of molecular array in a crystal. We are indeed peering into the heart of matter.

The failure of solids to reach their maximum theoretical strength was attributed by Taylor (17) in 1934 to the existence of defects in the crystal lattice in the form of dislocations. The indirect evidence for the existence of these dislocations is very strong (18) but since they are of molecular dimensions they have not hitherto been directly observed. Now that we can see the actual molecular array in a crystal can we see these defects? Close examination of Fig. 4 shows that over most of the area shown here the molecular arrangement is quite orderly. However, some defects are present. A very interesting one is shown inside the square. This appears to be a beautiful example of an edge dislocation. It will be seen that one row of molecules stops and the two adjacent rows then converge. It is likely that this dislocation traverses the full thickness of the crystal. In

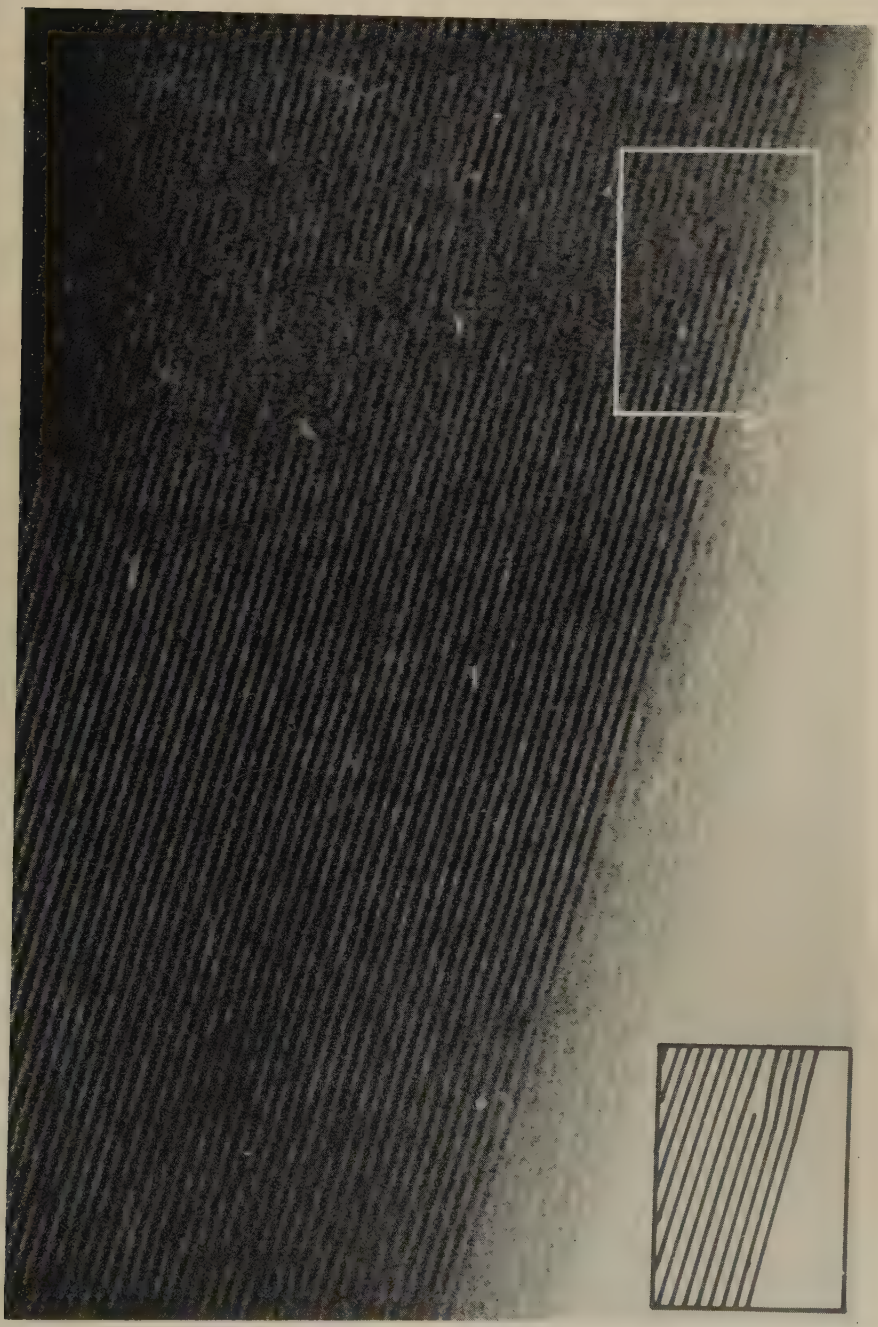

FIG. 4. Direct observation of molecular array in crystal of platinum phthalocyanine ca. × 1,500,000. The spacing between atomic planes is 12 A. Note the edge dislocation.

other crystals Menter has found screw dislocations and numerous and complicated arrays of dislocations. Since the strength properties of solids are governed by these dislocations it is clear that we have a powerful weapon for studying many problems in solid-state physics.

Preliminary examination of the edges of these crystals shows that in general there is no tendency for the spacing of the planes immediately adjacent to the surface to be different from that in the interior. Since we can examine the surface in such detail it should prove of great value in attacking a number of important problems in surface physics and chemistry.

References

1. Bowden, F. P., and Rideal, E. K., *Proc. Roy. Soc.* (*London*) **A120,** 80 (1928).
2. Reason, R. E., Hopkins, M. R., and Garrod, R. I., Report on Measurement of Surface Finish by Stylus Methods. Taylor-Hobson, Leicester, England.
3. Nelson, H. R., Proceedings of Conference on Friction and Surface Finish, Massachusetts Institute of Technology, p. 217, 1940.
4. Bowden, F. P., and Tabor, D., "The Friction and Lubrication of Solids." Oxford University Press, New York, 1950; rev. ed., 1954.
5. Tolansky, S., "Multiple Beam Interferometry of Surfaces and Films." Oxford University Press, New York, 1948.
6. Courtney-Pratt, J. S., *Nature* **165,** 346 (1950).
7. Bailey, A. I., and Courtney-Pratt, J. S., *Proc. Roy. Soc.* (*London*) **A227,** 500 (1955).
8. Bailey, A. I., Unpublished.
9. Cosslett, V. E., *Nature* **170,** 861 (1952).
10. Menter, J. W., *J. Inst. Metals* **81,** 163 (1952); *J. Photographic Sci.* (*London*) **1,** 12 (1953).
11. Bowden, F. P., and Ridler, K. E. W., *Proc. Roy. Soc.* (*London*) **A154,** 640 (1936).
12. Chapman, J. A., and Menter, J. W., *Proc. Roy. Soc.* (*London*) **A226,** 400 (1954).
13. Smith, K. C. A., and Oatley, C. W., *Brit. J. Appl. Phys.* **6,** 391 (1955).
14. Bowden, F. P., and Singh, K., *Proc. Roy. Soc.* (*London*) **A227,** 22 (1954).
15. Sawkill, J., *Proc. Roy. Soc.* (*London*) **A229,** 135 (1955); see also Bowden, F. P., "Selected Combustion Problems," p. 385. Advisory Group for Aeronautical Research and Development, 1953.
16. Menter, J. W., *Proc. Roy. Soc.* (*London*), **A236,** 119 (1956).
17. Taylor, G. I., *Proc. Roy. Soc.* (*London*) **A145,** 362 (1934).
18. See Cottrell, A. H., "Dislocations and Plastic Flow in Crystals." Clarendon Press, Oxford, 1953; Mott, N. F., *in* "Surveys in Mechanics" (Batchelor and Davies, eds.), p. 32. Cambridge University Press, 1956.

JOURNAL OF COLLOID SCIENCE **11**, 565–574 (1956)

EFFECTS OF X-RAYS ON DILUTE AQUEOUS SOLUTIONS OF AMINO ACIDS

Judith Nosworthy and C. B. Allsopp

Guy's Hospital Medical School, London, England

Received March 12, 1956

Abstract

The effects of X-rays on aqueous solutions of β-phenylalanine, tyrosine, and 3,4-dihydroxyphenylalanine in the presence of oxygen have been studied. Evidence has been obtained that, in addition to oxidative deamination, reactions occur in which dopa is formed from tyrosine, and an indole derivative is produced from dopa. It is thus possible that the irradiation of aqueous solutions of tyrosine can set in train the same sequence of oxidative changes as occurs during the metabolic oxidation of tyrosine to a melanin pigment.

Introduction

The chemical reactions which result when aqueous solutions are irradiated with X-rays or other ionizing radiations are predominantly oxidative in character, especially when oxygen itself is present, and massive irradiation of amino acids has been shown to cause oxidative deamination (1). Such radical changes, however, do not necessarily preclude the possibility that milder oxidation may also occur. The effects of X-rays on dilute aqueous solutions of three α-amino acids, β-phenylalanine, tyrosine, and 3,4-dihydroxyphenylalanine (dopa), and some related compounds have now been studied. These compounds were chosen not only because they have general biological interest but also because tyrosine and dopa are known to be intermediates in a metabolic system in which a melanin pigment is formed (2). It was thought also that the investigation might throw some light on the pigmentation which results in human skin after therapeutic doses of radiation. The results show, in fact, that reactions analogous to those of the metabolic system can be initiated by X-rays.

When an aqueous solution of tyrosine with the enzyme tyrosinase stands in air, it becomes red. The red color fades, the solution later becomes brown, and eventually a black precipitate of melanin forms. Raper (3) suggested the following sequence of reactions, which is now generally accepted, to account for these changes:

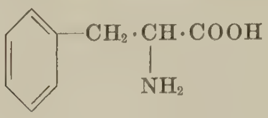

I β-Phenylalanine

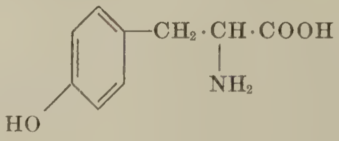

II Tyrosine

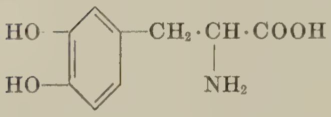

III Dopa

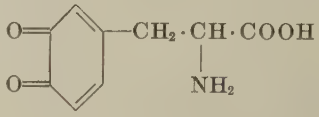

IV

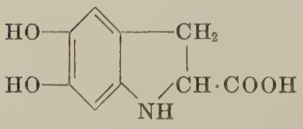

V

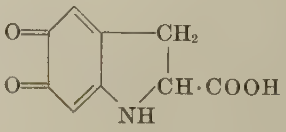

VI Dopachrome

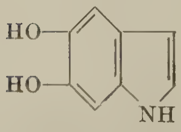

VII 5:6-Dihydoxyindole

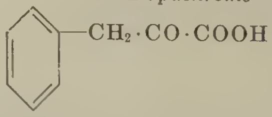

VIII Phenylpyruvic Acid

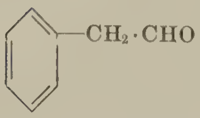

IX Phenylacetaldehyde

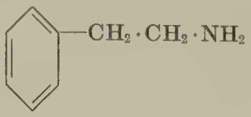

X β-Phenylethylamine

Tyrosine (monohydroxy-β-phenylalanine), II, oxidizes firstly to the dihydroxy compound dopa, III, and then to a quinone, IV. This molecule undergoes internal rearrangement and ring closure to form the intermediate dihydroxy compound, V, which oxidizes further to the quinone "dopachrome," VI. Another internal rearrangement yields 5,6-dihydroxyindole, VII, which forms a melanin on oxidation and polymerization. Raper isolated dopa from the original tyrosine solution and dimethoxyindole derivatives from the colorless solution which results when the red solution stands *in vacuo*. Dopachrome itself has not been isolated, but its *p*-bromophenylhydrazone and *p*-nitrophenylhydrazone have been obtained. Other experiments by Raper (3), by Mason (4), and by Bu'lock and Harley Mason (5) have confirmed the correctness of Raper's interpretation.

Arnow, who followed chemical changes by observing changes in absorption spectra, found dopa in aqueous solutions of tyrosine after exposure to ultraviolet radiation (6); and Nurnberger (7) obtained similar spectroscopic changes when tyrosine solutions were subjected to the action of either ultraviolet, 200-kv. X- or radon α-radiations. The tyrosine solutions became brown in color. Recently Rowbottom (8) irradiated tyrosine with X-rays and γ-rays and identified 3,4-dihydroxyphenylalanine as one of the products.

New Experiments

The observations made in the present experiments are set out below. It should be noted that at no stage was oxygen excluded from the apparatus in which solutions were irradiated, and hydrogen peroxide is known to accumulate in them.

β-Phenylalanine

A (colorless) dilute aqueous solution of this compound, I, slowly became yellow on irradiation with 240-kv. X-rays. In the absorption spectrum of the solution, the characteristic peak at 2580 A. increased in intensity with increasing dose of radiation, and a weak subsidiary maximum appeared at 3250 to 3350 A., followed by increasing absorption at shorter wavelengths (Fig. 1, Curves 7, 6, and 5). The yellow color deepened when the solution was warmed with alkali. When the solution was passed through an alumina column, the yellow substance remained at the top, but it could not be eluted.

Treatment of the irradiated phenylalanine solution with a freshly prepared 1% solution of 2,4-dinitrophenylhydrazine in 2 N HCl produced an orange-colored precipitate of a phenylhydrazone. This turned deep red with 10% sodium hydroxide. It could not be satisfactorily recrystallized. It could, however, be separated into two clearly defined components by paper chromatography: an ascending technique, with a mixture of phenol, n-butanol, and water as solvent, was employed. One component ran to the top of the chromatogram as do the 2,4-dinitrophenylhydrazones of benzaldehyde and of phenylacetaldehyde. The other spot had an R_f value corresponding to that of the 2,4-dinitrophenylhydrazine derivative of pyruvic acid when this compound was run simultaneously on the same chromatogram. Some irradiated samples gave no "phenylpyruvic spot." When the solvent was a mixture of cyclohexane, methanol, and ethyl acetate, a single spot resulted whose R_f corresponded to that of the phenylhydrazone of phenylacetaldehyde.

This evidence indicates that a mixture of dinitrophenylhydrazones is obtained from the irradiated solution. Phenylpyruvic acid readily undergoes decarboxylation (e.g., by standing in the presence of air). This may be the initial product of irradiation and phenylacetaldehyde the result of

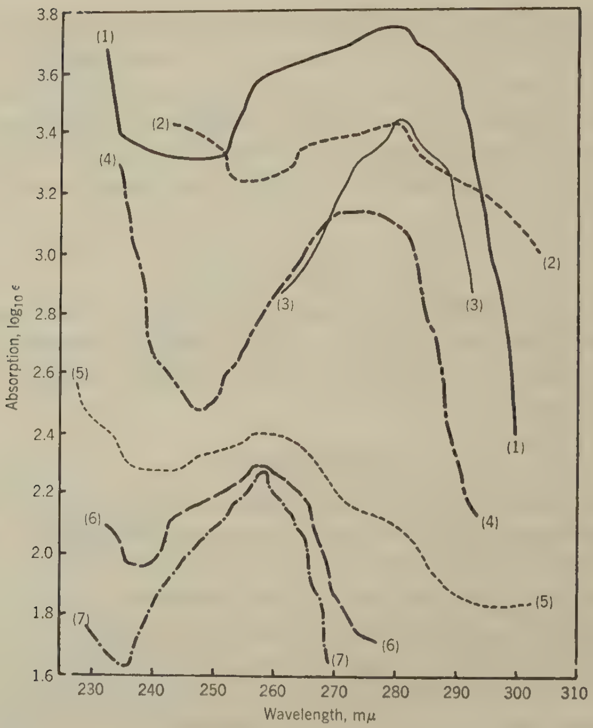

FIG. 1. Absorption curves for: 1. Tryptophan. 2. 3,4-Dihydroxyphenylalanine irradiated. 3. Unirradiated 3,4-dihydroxyphenylalanine. 4. Tyrosine. 5. β-Phenylalanine irradiated with 105,000 r. 6. β-Phenylalanine irradiated with 36,000 r, 7. Unirradiated β-phenylalanine. Curves for unirradiated tyrosine and tryptophan included for comparison.

subsequent reaction. Phenylacetaldehyde polymerizes readily. It forms a yellow solution on warming with 10% aqueous sodium hydroxide. On mixing the pure compound with β-phenylethylamine, X (a possible product from the decarboxylation of phenylalanine), a bright lemon yellow compound was formed with evolution of heat. No reaction was observed on simply mixing dilute solutions.

Other reactions of the irradiated phenylalanine solutions were: (*1*) with Nessler's reagent to give a yellow color: ammonia could be driven off from an alkaline solution; (*2*) with Millon's reagent to give a pink color. The latter reaction is not given by freshly prepared unirradiated phenylalanine solutions to which hydrogen peroxide has been added.

Synthetic mixtures of phenylalanine, tyrosine, and dopa could be separated in a few hours by circular paper chromatography when a phenol: water mixture was used as solvent, the amino acids being detected by spraying with ethanolic ninhydrin. Neither tyrosine nor dopa could be found in irradiated phenylalanine solutions in this way, however; but the method is incapable of detecting less than a 10% conversion of phenylalanine to tyrosine or of tyrosine to dopa.

Tyrosine

Irradiated tyrosine solutions reacted with Folin's reagent (phosphotungstic acid in aqueous phosphoric acid, which is believed to be specific for dihydroxyphenols) similarly to unirradiated dopa solutions, the blue color produced becoming greenish brown on addition of alkali. The reaction of this reagent with various dihydroxyphenyl compounds related to tyrosine has been compared by Dagliesh (9). Solutions of hydrogen peroxide or of tyrosine alone did not give the greenish brown color; but it was obtained from a tyrosine solution to which hydrogen peroxide had been added.

Under conditions similar to those used for phenylalanine, irradiated solutions of tyrosine and of dopa (and also of alanine) yielded 2,4-dinitrophenylhydrazones, the precipitate from irradiated tyrosine being reddish brown, and that from irradiated dopa, a dull brown in color.

Dopa

On irradiation, dopa solutions became pinkish-red and then brown, but the first stage was not always detectable. Unlike the absorption spectrum of irradiated phenylalanine, that of dopa in the earlier stages of irradiation did not show an increase of absorption at 2810 A. (Fig. 1, Curves 2 and 3). The pink solution, however, had a second broad absorption band whose maximum was at about 4800 A. (Fig. 2). This corresponds to the band attributed by Mason to dopachrome (4).

The irradiated dopa solutions gave a positive Ehrlich reaction for the indole nucleus, and the "indole" concentration was measured in this way (10). At a constant dosage rate of 1200 r/min. it built up to a maximum

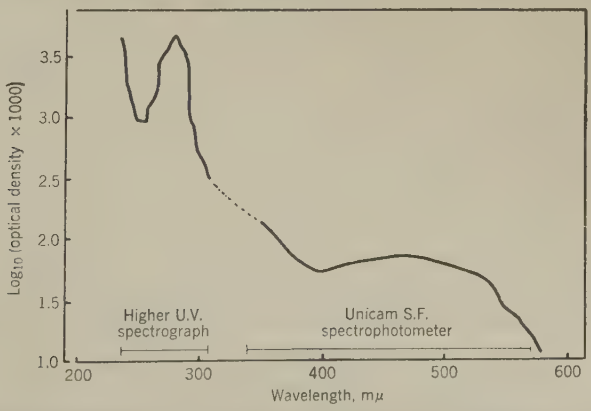

FIG. 2. Absorption spectrum of "dopa" solution after irradiation with 152,000 r.

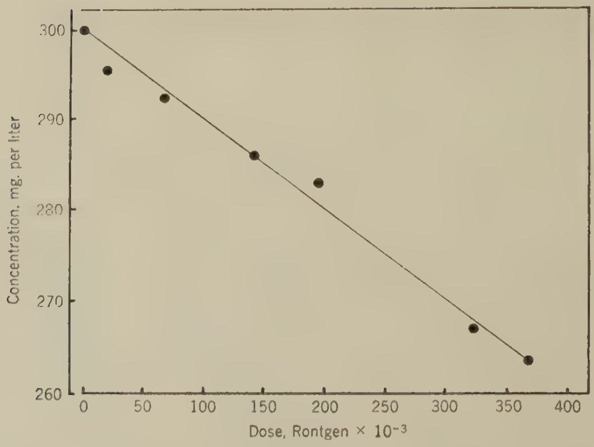

FIG. 3. Destruction of "dopa." Dose rate 1200 r/min.

value about which it seemed to oscillate as larger doses of radiation were given.

The destruction of dopa was followed by a colorimetric method based on its reaction with ninhydrin. The concentrations of the irradiated solutions fell linearly with dose (Fig. 3). At the concentration used (300 mg./l.), the concentration of "indole" formed was never more than 1% of that of dopa, and represented about one-tenth of the dopa destroyed.

Indole

In earlier experiments it was shown that at X-ray dosage rates of a few r/min. and for doses up to 50 r, indole itself is very sensitive to radiation, but that after this initial, sensitive, dosage range, the indole concentration as indicated by the Ehrlich reaction remained steady (11). Dosage rates between 130 and 1200 r/min. were now used, and the concentration was found to fall linearly with dose, without any significant dependence on dosage rate, down to concentrations of 1 to 2 mg./l., when the curves became exponential, the quantity of radiation needed to destroy a given quantity of indole at these very low concentrations being proportionately higher (Fig. 4). This is to be expected if the effect of X-rays is primarily on the solvent and not on the solute. At a dosage rate of 1200 r/min., the initial rate of disappearance of pure indole was comparable with that of dopa, so that the steady concentration of an indole derivative observed in the irradiated dopa solutions probably results from competition between dopa and the products of its decomposition for the oxidizing radicals released in the primarily radiolysis of the water solvent.

The identity of the indole derivative formed in the irradiated dopa solutions is not established, but it seems likely to be 5,6-dihydroxyindole

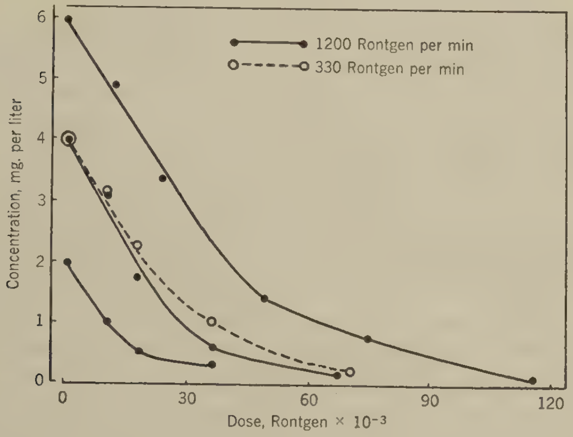

FIG. 4. Destruction of indole (low concentrations). Dose rate 1200 r/min.

(VII). With Ehrlich's reagent this compound gave a purple color whose absorption spectrum was practically identical with that obtained from indole with Ehrlich's reagent. The compound, however, is so subject to direct oxidation that it was considered that no reliable information would be derived by irradiating its aqueous solutions.

DISCUSSION

The results which have been described may be summarized as follows:

1. Irradiation of each of the three amino acids, β-phenylalanine, tyrosine, and dopa, produces compounds which can form 2,4-dinitrophenylhydrazones.

2. In the case of phenylalanine, this compound is phenylpyruvic acid, formed by deamination, the product readily undergoing decarboxylation:

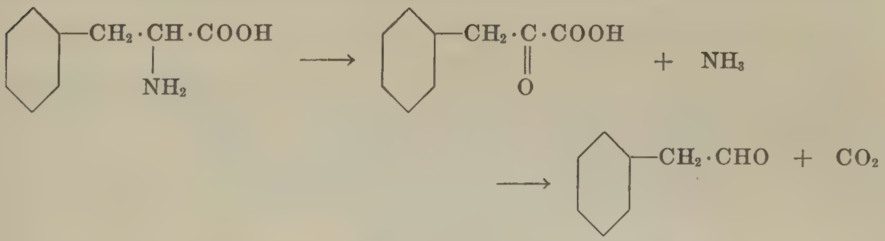

3. Irradiation of phenylalanine and of tyrosine gives rise to phenolic compounds, as indicated by Millon's reagent.

4. Tyrosine in addition gives a dihydroxyphenol as indicated by Folin's reagent.

5. The changes in absorption spectra observed during irradiation of tyrosine and phenylalanine are consistent with direct oxidation.

6. The changes in the absorption spectra during irradiation of dopa correspond to those recorded by Mason during its enzymatic oxidation.

7. During the irradiation of dopa, a compound reacting with Ehrlich's reagent and presumably containing the indole nucleus, is found.

These results are also in general accord with the changes which can be deduced from the changes in the absorption spectra of phenylalanine, tyrosine, and dopa during irradiation as described by Barron, Ambrose, and Johnson (12). These authors pointed out that it is not always possible to predict the effect of small X-ray doses by extrapolation from those of larger doses. They claimed that the *initial* effect of a *moderate* dose of X-rays, e.g., 46,000 r, on amino acids is oxidative deamination. Nevertheless, their measurements of the loss of phenolic OH in tyrosine during irradiation showed it to be comparable in amount to the deamination. Our experiments were made under conditions not very dissimilar to those of Barron, Ambrose, and Johnson and are in agreement with those of Rowbottom in respect to tyrosine. It is concluded that aromatic amino acids can be decomposed simultaneously in more than one way. It is therefore perhaps not correct to designate any particular reaction as "primary": If one, for example, oxidative deamination, appears to be the only one when small quantities of radiation are used, it may be only because of the difficulty of detecting the presence of small quantities of other products.

These and our earlier experiments indicate that, despite other reactions, there is a possibility that irradiation of tyrosine yields dopa, that the dopa may be converted to a derivative of indole which in turn oxidizes and polymerizes to a melanin, in fact that the irradiation can set in train the same sequence of changes as occur in the natural synthesis of melanin from tyrosine.

Experimental

RADIATION

Source and quality. Newton-Victor Raymax Machine working at 240 kv., 14.5 ma., with no added filtration. H.V.L. = 0.7 mm. of Cu.

Measurement. By Victoreen chamber connected to a d.-c. amplifier which was calibrated against a standard Victoreen meter. Results were checked against, and were in reasonable agreement with, those obtained by $FeSO_4$ dosimetry.

Irradiation vessel. For quantitative work, quartz stoppered tubes, capacity 2 ml., approximating in size to the Victoreen chamber. Alternatively solutions were irradiated in a Pyrex trough covered with a Perspex lid.

REAGENTS AND SOLUTIONS

Amino acids. DL forms except for L-tyrosine. Acids and indole prepared by Roche Products Ltd.

Solvent water. From an ion exchange column; or water twice distilled (once from alkaline permanganate) in Pyrex. It is known that extraneous organic or inorganic solutes may greatly affect radiation chemical yields, and also that the Zn^{++} ion catalyzes the isomeration of quinones in the dopa → dihydroxyindole reaction. No difference in behavior was observed between solutions made up with water from these two sources.

Solution concentrations.

(*1*) *Dopa.* For disappearance of dopa and formation of "indole", 300 mg. of dopa/l.

(*2*) *Indole.* For destruction measurements, initial concentrations of 16, 6, 4, and 2 mg./l.

Analytical reagents. All of A.R. grade from British Drug Houses Ltd. Millon's reagent: (*1*) 10 g. $HgSO_4$ ground into 90 ml. H_2SO_4 made up to 100 ml. with water. (*2*) Sodium nitrate 10%. Folin's reagent: (*1*) 10 g. sodium tungstate in 5 ml. 98% H_3PO_4 + 95 ml water. (*2*). Approx. 4 *N* NH_3 solution.

Sensitivities. With an initial concentration of amino acid of 1 mg./ml. and a dose rate of 1200 r/mm., Folin's reagent gave a just visible positive reaction after 30 minutes irradiation with "tyrosine" solution, and Millon's reagent a just visible color with "phenylalanine" solution. The colors were quite distinct after 45 minutes (54,000 r).

SYNTHESES

β-Phenylpyruvic acid. According to *Organic Syntheses.*

5,6-Dihydroxyindole. By the method of Beer, Clarke, Khorana, and Robertson (*13*) modified as follows: in the hydrolysis of 5,6-acetoxyindole, less dithionate was used, the reaction was made at room temperature, the mixture was extracted with ethyl acetate instead of with ether, the solvent was distilled off under N_2, and the residue was sublimed at 150°/0.01 mm.

ESTIMATIONS

Spectra. Recorded with a Hilger Spekker Spectrophotometer and Medium Quartz Spectrograph, and with a Unicam SP 60 Spectrophometer at longer wavelengths.

Absorptionmeter methods. Indole. with a Spekker Absorptionmeter and green filter, (9), or at $\lambda = 5660$ A. on the Unicam spectrophotometer.

Dopa. To 2-ml. dopa solution were added 2 ml. of *freshly prepared* 2% aqueous ninhydrin and 2 ml. of 10% aqueous pyridine. The mixture was heated for exactly 20 minutes in a boiling water bath and immediately diluted to 100 ml. with cold water. The depth of color was estimated at $\lambda = 5660$ A.

Chromatography

Filter paper: Whatman 3 MM.

The phenylhydrazones were applied in solution in ethyl acetate.

Solvent systems: (*1*) Phenol/butanol/water (the aqueous layer from a mixture of 3 parts *n*-butanol + 1 part water + 1 part of a 4:1 v.v. phenol-water mixture). (*2*) Two parts cyclohexane + 4 parts methanol + 0.1 part ethyl acetate.

ACKNOWLEDGMENTS

Our thanks are due to the British Empire Cancer Campaign which has given financial support throughout these researches; to Professor Sir Alexander Todd for allowing facilities in the Cambridge University Chemical Laboratory for the synthesis of 5,6-dihydroxyindole; and to Mr. J. Harley Mason for his invaluable advice about this; to our many colleagues in the Medical School who have given advice and loaned apparatus; and, of course, to Sir Eric Rideal for encouraging one of us to interest himself in these problems in the early days of radiation chemistry.

REFERENCES

1. Stein, G., and Weiss, J. *J. Chem. Soc.* **1948,** 3245.
2. Lerner, A. B., *Advances in Enzymol.* **14,** 73 (1953).
3. Raper, H. S., *Biochem. J.* **21,** 89 (1927); Duliere, W. L., and Raper, H. S., *Biochem. J.* **24,** 239 (1930); Raper, H. S., *Biochem. J.* **26,** 2000 (1932).
4. Mason, H. S. *J. Biol. Chem.* **172,** 83 (1948).
5. Bu'lock, J. D., and Harley Mason J., *J. Chem. Soc.* **1951,** 2248.
6. Arnow, L. E., *J. Phys. Chem.* **42,** 415 (1938).
7. Nurnberger, C. E., *Proc. Natl. Acad. Sci. U. S.* **23,** 187 (1937); *J. Chem. Phys.* **42,** 415 (1938).
8. Rowbottom, J., *J. Biol. Chem.* **212,** 299 (1955).
9. Dagliesh, C. E., *J. Chem. Soc.* **1952,** 3943.
10. Allsopp, C. B., *Biochem. J.* **35,** 965 (1941).
11. Allsopp, C. B., and Wilson, J., *Discussions Faraday Soc.* **12,** 299 (1952).
12. Barron, E. S. G., Ambrose, J., and Johnson, P., *Radiation Research* **2,** 145 (1955).
13. Beer, R. J. S., Clarke, K., Khorana, H. G., and Robertson, A., *J. Chem. Soc.* **1949**, 885.

JOURNAL OF COLLOID SCIENCE **11**, 575-584 (1956)

THE ADSORPTION OF SERUM ALBUMIN AND SODIUM DODECYL SULFATE AT EMULSION INTERFACES

E. G. Cockbain

The British Rubber Producers Research Association, Welwyn Garden City, Herts, England

Received March 27, 1956

ABSTRACT

The distribution of serum albumin and sodium dodecyl sulfate between the interface and aqueous phase of *n*-decane emulsions has been measured, and the total interfacial area of the emulsions determined. In the absence of dodecyl sulfate, the adsorbed albumin film is monomolecular in thickness, the area/residue agreeing closely with that found for compressed spread monolayers of serum albumin and other proteins. The area/residue is essentially independent of albumin concentration, pH, and ionic strength.

In the presence of sodium dodecyl sulfate, complex formation with the albumin occurs at the interface and in the aqueous phase. The composition of the interfacial complex and the thickness of the adsorbed film have been determined. Conditions under which the complex is displaced from the interface by excess dodecyl sulfate are described.

INTRODUCTION

The work of Gorter (1), Rideal (2, 3) and their collaborators established that many proteins could be spread quantitatively at the air-water surface to form stable, coherent, insoluble films whose average thickness corresponded closely to that of a monolayer of fully extended polypeptide chains. The properties and structure of such films have been the subject of many later investigations (4, 5), and similar studies have been made on protein monolayers spread at the benzene-water or petrol ether-water interface (6).

On the other hand, very little progress has been made in determining the thickness and orientation of protein films formed by adsorption from solution. In many cases, at least, adsorption involves irreversible changes in the structure of the protein which rule out all possibility of calculating the amount of adsorption from boundary tension data and the Gibbs equation, and no alternative experimental technique free from criticism has so far been proposed. Thus, the method described by du Noüy (7) is based on several unlikely assumptions, which have been fully discussed by Neurath and Bull (4). Langmuir's method (8) of measuring the thickness of spread films optically, after transference to prepared metal plates, cannot be applied quantitatively to adsorbed compounds at the air- or oil-water interface. By comparing the interfacial viscosities of both spread and adsorbed proteins at the same interface, Cumper and Alexander (9) have derived values for the thickness of adsorbed films of pepsin, insulin, and bovine β-globulin. The thicknesses varied from about 3 A. to more than 30 A., depending on such factors as the pH and ionic strength of the aqueous solutions. One of the assumptions of this method is that the spread monolayers and the adsorbed films have essentially the same structure.

To obtain a clearer understanding of the behavior and significance of adsorbed proteins in biological systems, quantitative information concerning the thickness and structure of proteins adsorbed at different interfaces is needed. In the present work, a quantitative study has been made of the adsorption of serum albumin at the *n*-decane–water interface, with and without the presence of sodium dodecyl sulfate in the aqueous phase.

EXPERIMENTAL

Emulsions of decane in buffered solutions of serum albumin were prepared by mechanical stirring, followed by passage three times through a stainless steel homogenizer. Aliquots of a given emulsion, normally containing 40% by volume of decane, were then diluted with equal volumes of buffer solution containing different amounts, including zero concentration, of sodium dodecyl sulfate (NaDS). The buffer solution also contained sufficient sodium alginate, as creaming agent, to give a final alginate content of 0.15%, calculated on the volume of aqueous phase. At this concentration the interfacial activity of sodium alginate at the decane-water interface is very small and, as will be shown later, does not affect the adsorption of albumin. All the diluted emulsions of a given series thus possessed the same initial interfacial area. After 2 to 5 hours sufficient clear serum had separated, as a lower layer, for it to be run off and analyzed for protein and NaDS.

The separation of serum, in the presence of creaming agent, is similar to the phenomenon of syneresis in gels, and does not involve coalescence of the emulsion particles unless the original emulsion is of low stability. Over the period of 2 to 5 hours mentioned above, analyses of the serum separating from a given diluted emulsion gave the same results, showing that coalescence of the emulsion particles was negligible. Analysis also proved that when the concentration of NaDS in the emulsions was high enough, all the albumin was displaced from the emulsion interface, leaving an adsorbed film of NaDS. The amount of NaDS adsorbed remained almost constant when its concentration in solution was further increased, showing that adsorption had reached a maximum. Since the area/molecule of NaDS alone at the decane-water interface, under the same conditions of maximum adsorption, pH, and ionic strength, was known from previous work (10), the interfacial area of the diluted emulsion could be calculated, thus permitting the amount of protein, or protein plus NaDS, adsorbed per unit area of interface to be obtained.

1. Determination of Albumin Concentration

Albumin concentrations were determined by light absorption measurements, using a Hilger Uvispek photoelectric spectrophotometer. Owing to the presence of sodium alginate and NaDS in many of the emulsion sera, optical density measurements at a single wavelength (278.5 mμ) did not give an accurate measure of protein concentration. However, as the absorption caused by both NaDS and sodium alginate was found to vary linearly with wavelength over the range 270 to 290 mμ, corrections for the background absorption of these two components were made by the method of Banes and Eby (11).[1] It can then be shown that if a solution containing albumin, sodium alginate, and NaDS has optical densities E_1, E_2, and E_3 at the wavelengths λ_1, λ_2, and λ_3,

$$\text{albumin concentration } [C] = \frac{\{E_2 - E_1(1 - n) - E_3 n\}}{l\{\epsilon_2 - \epsilon_1(1 - n) - \epsilon_3 n\}},$$

where l = cell length, $n = \dfrac{\lambda_3 - \lambda_2}{\lambda_3 - \lambda_1}$ and ϵ_1, ϵ_2, and ϵ_3 are the extinction coefficients for the pure protein at λ_1, λ_2, and λ_3, respectively. Using standard solutions of albumin containing various amounts of sodium alginate and NaDS, optical densities were measured at 270, 278.5, and 290 mμ, and $\{E_2 - E_1(1 - n) - E_3 n\}$ plotted against $[C]$. A straight line passing through the origin was obtained, as required by the above expression. The protein concentrations of the standard solutions were based on micro-Kjeldahl nitrogen determinations, using a value of 16.07% for the nitrogen content of pure serum albumin (12). The protein concentrations in the emulsion sera were also periodically checked by micro-Kjeldahl analysis.

2. Determination of Sodium Dodecyl Sulfate

The concentrations of NaDS in the emulsion sera were determined by titrating against a standard aqueous solution of cetyltrimethyl ammonium bromide (CTAB), using bromophenol blue as indicator. The method described by Barr, Oliver, and Stubbings (13) was used, except that the titration was carried out with a 2:1 mixture of chloroform and acetone instead of chloroform alone. Coloration of the chloroform-acetone phase by the dye occurs at the end point of the titration. This end point was affected by the presence of albumin in the sera, owing presumably to interaction between the albumin and the CTAB. In the analysis of each serum, therefore, it was necessary to carry out blank titrations on standard solutions containing known amounts of NaDS and the same concentrations of albumin, sodium alginate, and buffer salt as were present in the serum (variation in the alginate content between zero and 0.15% actually had very little effect on the end point). The concentration of NaDS in the serum was then obtained by interpolation.

---

[1] Our thanks are due to Mr. G. Higgins for proposing this method of analysis and for carrying out many of the absorption measurements.

Interfacial tensions were measured by the drop-volume method, using an apparatus similar to that described in a previous communication (14).

3. *Materials*

The albumin used was crystallized bovine serum albumin from the Armour Laboratories, and the sodium dodecyl sulfate was a sample of high purity kindly provided by Lankro Chemicals Ltd. Cetyltrimethyl ammonium bromide, sodium alginate, and *n*-decane were obtained from I.C.I. Ltd., Alginate Industries Ltd., and L. Light and Co. Ltd., respectively. The *n*-decane was freed from traces of polar impurities by passage through an alumina column, to give an interfacial tension against distilled water of 51 dynes/cm.

RESULTS

1. *Displacement of Adsorbed Albumin by NaDS*

In the experiments shown in Fig. 1., aliquots of a 40% decane emulsion in 0.1 *M* acetate buffer, pH 5.6, were diluted with equal volumes of the same buffer solution containing, in addition, 0.24% sodium alginate and NaDS in concentrations ranging from zero to 1%. The original emulsion,

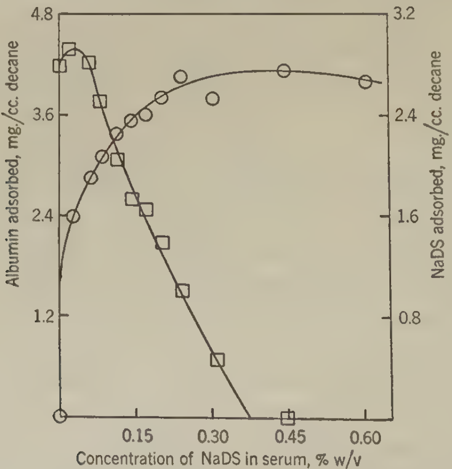

FIG. 1. Adsorption of serum albumin and sodium dodecyl sulfate at the emulsion interface *n*-decane/0.1 *M* acetate buffer, pH 5.6 (*n*-decane content of emulsion = 20% by volume; total albumin content = 0.18 g./100 ml. emulsion). □ serum albumin. ○ sodium dodecyl sulfate.

stabilized with serum albumin (0.6 g./100 ml. aqueous phase) was allowed to stand 30 minutes before diluting with the buffer solution, and another 2½ hours elapsed before the first samples of clear serum were removed for analysis. No significant change in the analytical figures was observed if longer periods were allowed for the creaming process, i.e., adsorption of both albumin and NaDS had reached steady values. In the emulsions containing no NaDS, creaming occurred slowly even in the absence of sodium alginate, and it was possible to confirm in these cases that the alginate did not affect the adsorption data.

Figure 1 shows the distribution of albumin and NaDS between the interface and aqueous phase. As $[\mathrm{NaDS}]_{\mathrm{aq.}}$ increased from zero to approximately 0.05%, adsorption of this component also increased rapidly without displacing albumin from the interface; indeed, the amount of adsorbed protein appeared to increase slightly. It is known (15) that the presence of a small concentration (e.g. 0.01%) of NaDS in 0.1% serum albumin solution gives an interfacial tension (I.T.), against benzene, which is considerably lower than that due to the protein or the dodecyl sulfate alone. The same effect was found to occur with *n*-decane as the oil phase, indicating that in the above emulsions penetration of the protein film by NaDS takes place, rather than adsorption of the detergent as a secondary layer underneath the protein.

Increases in $[\mathrm{NaDS}]_{\mathrm{aq.}}$ above 0.05% resulted in displacement of albumin from the interface and in increased adsorption of NaDS. It is clear from the method of analysis that the displaced protein was soluble in the aqueous phase, owing presumably to complex formation with the NaDS. Displacement of albumin was complete when $[\mathrm{NaDS}]_{\mathrm{aq.}}$ exceeded 0.37%, adsorption of NaDS reaching a maximum at about the same concentration. The critical micellar concentration (cmc) of sodium dodecyl sulfate in 0.1 *M* acetate buffer of pH 5.6, in the absence of albumin, is 0.04%. At this and higher concentrations, the I.T. of the solutions against *n*-decane at 20°C. was found to be 4.3 dynes/cm. Similar measurements on the emulsion sera showed that the tensions decreased from 9 dynes/cm. at $[\mathrm{NaDS}]_{\mathrm{aq.}} =$ 0.05% to 4.3 dynes/cm. at $[\mathrm{NaDS}]_{\mathrm{aq.}} = 0.34\%$., further increases in concentration producing negligible changes in tension. It is inferred, therefore, that the albumin in the aqueous phase retarded the formation of NaDS micelles until $[\mathrm{NaDS}]_{\mathrm{aq.}}$ reached 0.34%, thus accounting for the adsorption maximum in Fig. 1 at approximately the same concentration. The amount of albumin in the aqueous serum, after its complete displacement from the emulsion interface, was 0.225%.

2. Effect of Albumin Concentration on Adsorption

The adsorption data of Fig. 2 were obtained by diluting a 40% decane emulsion, stabilized by albumin (0.5 g./100 ml. aqueous phase), with equal volumes of albumin solutions of concentrations ranging from zero to 1.38%

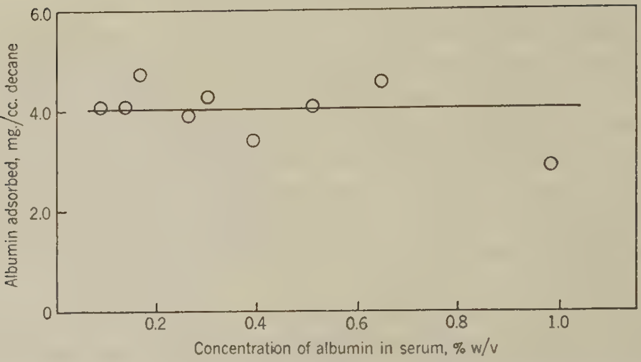

FIG. 2. Effect of serum albumin concentration on adsorption at the emulsion interface *n*-decane/0.1 *M* acetate buffer, pH 5.6 (*n*-decane content of emulsion = 20% by volume).

w/v. All aqueous solutions, including that used in the preparation of the original emulsion, were at pH 5.6 (0.1 *M* acetate buffer). Although the concentration of protein remaining in the aqueous phase varies by a factor of more than ten (Fig. 2), the amount adsorbed is essentially constant. It is also interesting to note that when the concentration of albumin in the diluting solution was less than in the aqueous phase of the original emulsion, no *desorption* of protein occurred from the interface of the emulsion particles.

3. *Effect of pH and Ionic Strength on Adsorption*

The results shown in full line in Fig. 3 were obtained by emulsifying *n*-decane in a 0.5% w/v solution of serum albumin in distilled water, and diluting portions of the emulsions with acetate or borax buffer solutions. The pH values of the diluted emulsions were 4.8, 5.6 (acetate buffers), and 9.2 (borax), and the ionic strengths of their aqueous phases 0.01, 0.10, and 0.30 at each pH. The diluted emulsion at pH 4.8 and ionic strength 0.01 did not cream sufficiently well for analysis of the serum to be carried out. In the other emulsions, the amount of protein adsorbed was approximately constant—a result which could conceivably be due to adsorption of protein being a maximum under the conditions of preparation of the original emulsion, subsequent desorption of protein on dilution being negligibly small, as indicated in the previous section.

This possibility was ruled out by preparing an emulsion of decane in 0.5% albumin solution adjusted to pH 10.0 with sodium hydroxide. Portions of the emulsion were diluted with equal volumes of acetate, borate, and phosphate buffers to give final pH values of 4.8, 5.6 (acetate), 7.2 (phosphate), and 9.2 (borate), each at ionic strengths of 0.01, 0.05, and 0.2. The adsorption results are shown in broken line, in Fig. 3, for those emulsions

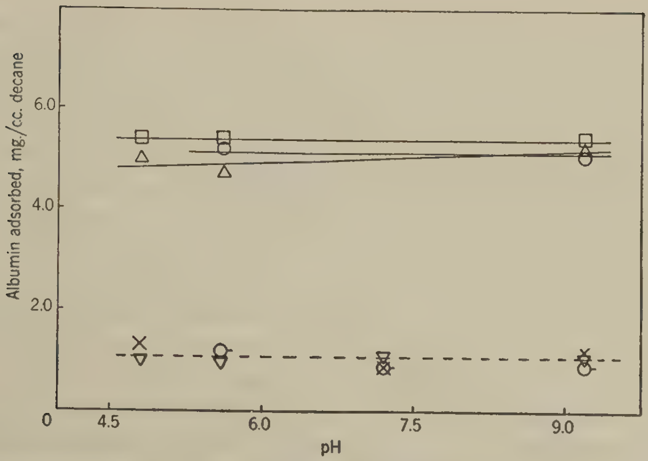

FIG. 3. Effect of ionic strength and pH on the adsorption of serum albumin at the n-decane emulsion interface (n-decane content of emulsion = 20% by volume; total albumin content = 0.15 g./100 ml. emulsion). ○ ionic strength 0.01; ○- ionic strength 0.01; × ionic strength 0.05; □ ionic strength 0.10; ▽ ionic strength 0.20; △ ionic strength 0.30.

which creamed sufficiently for analysis. In every case, the amount of protein adsorbed per cubic centimeter of decane was much less than in the previous series, since the initial emulsion was of larger particle size, as indicated by microscopic examination. This was probably due to the *rate* of adsorption of the albumin, at pH 10 and very low ionic strength, being relatively slow during preparation of the emulsion. However, the results in Fig. 3 confirm the negligible effect of both pH and ionic strength on the final adsorption, over the ranges covered.

DISCUSSION

Putnam and Neurath (16) showed by electrophoresis measurements that NaDS and serum albumin formed two well-defined soluble complexes at pH 6.8, of composition AD_n and AD_{2n}, where A and D represent albumin and dodecyl sulfate, respectively. Assuming a molecular weight of 70,000 for the albumin, n was found to be 55. The number of dodecyl sulfate molecules bound in the complex AD_{2n} thus corresponds closely to the total number of cationic groups (100 to 107) in the serum albumin molecule (12, 17). From interfacial tension measurements on mixed solutions of NaDS and serum albumin, it was shown by the author (15) that a similar well-defined complex was formed at the benzene-water interface in the presence of 0.1 M acetate buffer a' pH 5.6. The interfacial complex was assumed to be AD_{2n}, in which the ratio by weight of dodecyl sulfate to albumin (D/A) equals 0.44. Evidence was also obtained for the presence in solution of a higher complex of composition corresponding to AD_{4n}.

From the results of Fig. 1, the ratios D/A at the interface and in the aqueous phase of the emulsions can be calculated. At the concentration $[\text{NaDS}]_{\text{aq.}}$ at which displacement of albumin by NaDS commenced (*ca.* 0.05%), D/A was 0.44 at the interface and 0.42 in solution. Adsorption of NaDS without displacement of albumin can therefore be attributed to formation of the AD_{2n} complex. Complex formation appears to proceed preferentially at the interface, as indicated by the fact that D/A is greater at the interface than in solution, when $[\text{NaDS}]_{\text{aq.}}$ is less than 0.05%. This is understandable in view of the high surface activity of NaDS.

The presence of dodecyl sulfate in amounts larger than that required to form AD_{2n} results in the progressive displacement of complex from the interface by NaDS. This process is complete at approximately the same concentration of NaDS (0.34%) as that at which micelles of the latter are formed in the aqueous sera, as judged by interfacial tension measurements. Since the cmc of the dodecyl sulfate in absence of albumin was 0.04%, the difference should represent the amount of NaDS bound to the dissolved albumin (0.225%), the ratio D/A being 1.3. It is unlikely that this ratio has any special stoichiometric significance, the main point of interest being that serum albumin is able to bind such a large proportion of NaDS.

Thickness of Adsorbed Albumin Films

The interfacial area of the decane particles in the emulsions referred to in Fig. 1 has been calculated from the maximum amount of dodecyl sulfate adsorbed (2.74 mg./c.c. decane), after displacement of all the albumin from the interface, using a value of 41.5 A.^{2}/molecule for the molecular area of the adsorbed NaDS. This is the limiting molecular area recently determined by the author (10) for sodium dodecyl sulfate adsorbed at the decane-water interface from solutions of ionic strength 0.1. The area $S = 2.4 \times 10^4$ cm.^{2}/c.c. decane, so derived, applies to all the emulsions of Fig. 1, which were obtained from the same concentrated emulsion. Thus, in the absence of NaDS, the adsorption of 4.2 mg. albumin/c.c. decane is equivalent to a specific adsorption area for the albumin of 0.57×10^4 cm.^{2}/mg., corresponding to an average film thickness of 13.5 A. (assuming the density of the protein at the interface to be 1.30). These values, which are in very good agreement with those found (18, 19) for a highly compresed spread monolayer of serum albumin at the air-water or benzene-water interface, where the film area is approximately 0.5×10^4 cm.^{2}/mg. at a surface pressure of 20 dynes/cm., demonstrate the monomolecular character of the adsorbed albumin films.

Taking the average amino acid residue weight of serum albumin as 134 (20), the area/residue in the adsorbed film is 12.6 A.^{2}. If all the polypeptide chains were situated in the plane of the interface, the minimum area/residue as calculated from X-ray data and molecular models (6) would be 15.3 A.^{2}, corresponding to close-packed polypeptide chains in the β-keratin configuration, with the side chains oriented approximately perpendicularly to the interface. The smaller area of 12.6 A.^{2} found for adsorbed serum albumin is best explained by assuming that some of the polypeptide chains are in the aqueous phase. As the amount of adsorbed protein increases, a stage will be reached at which an unfolding molecule cannot be entirely accommodated in the interface for steric reasons. The average thickness of the film indicates, however, that at least a part of the molecule must unfold at the interface, i.e., adsorption of native albumin is negligible. The irreversibility of the adsorption process and the independence of adsorption on protein concentration point to the same conclusion.

The negligible effect of pH and ionic strength on the amount of albumin ultimately adsorbed, as distinct from the rate of adsorption (15), also supports the view that the area of interface available for close packing of the polypeptide chains determines the amount of albumin adsorbed. However, for constancy of adsorption it is necessary that the adsorbed film should be able to withstand increases in surface pressure caused, for example, by changes in pH or ionic strength. Albumin films at the decane-water interface can apparently do so, but there is evidence that other proteins at different interfaces are less stable. Thus, Cumper and Alexander (9) concluded from interfacial viscosity measurements that adsorbed pepsin films slowly collapsed with the formation of non-surface-active coagulated protein, permitting the occurrence of further adsorption from solution.

Figure 1 shows that the weight of albumin plus NaDS adsorbed at the emulsion interface, when $[\mathrm{NaDS}]_{\mathrm{aq.}} = 0.05\%$, is 6.15 mg./c.c. decane, the ratio of albumin to dodecyl sulfate corresponding to the complex AD_{2n}. Assuming a density of 1.25 for the complex at the interface, the average film thickness is 20.5 A., as compared with 13.5 A. for the albumin film alone. Since the polypeptide chains in the albumin film are already close-packed, and I.T. measurements indicate that NaDS molecules actually penetrate the film, the dodecyl sulfate must force some of the polypeptide chains above or, more probably, below, the plane of the interface. The large pressure exerted by the complex film (*ca.* 40 dynes/cm.) is evidence of its high stability. At concentrations of $[\mathrm{NaDS}]_{\mathrm{aq.}}$ greater than 0.05%, displacement of the AD_{2n} complex from the interface by dodecyl sulfate is accompanied by a gradual decrease in the total weight of albumin plus NaDS adsorbed.

This work forms part of the program of research undertaken by the Board of the British Rubber Producers' Research Association. Thanks are due to Mr. K. Day for assistance in the experimental work.

REFERENCES

1. ADAM, N. K. "Physics and Chemistry of Surfaces," p. 91. Oxford University Press, 1938.
2. HUGHES, A. H., AND RIDEAL, E. K., *Proc. Roy. Soc.* (*London*) **137,** 62 (1932).
3. HUGHES, A. H., SCHULMAN, J. H., AND RIDEAL, E. K., *Nature* **129,** 21 (1932).
4. NEURATH, H., AND BULL, H. B., *Chem. Revs.* **23,** 391 (1938).
5. BULL, H. B., *Advances in Protein Chem.* **3,** 95 (1947).
6. CHEESMAN, D. F., AND DAVIES, J. T., *Advances in Protein Chem.* **9,** 439 (1954).
7. DU NOÜY, P. L., "Surface Equilibria of Biological and Organic Colloids." Chemical Catalog Co., New York, 1926.
8. LANGMUIR, I., SCHAEFER, V. J., AND WRINCH, D. M., *Science* **85,** 76 (1937).
9. CUMPER, C. W. N., AND ALEXANDER, A. E., *Trans. Faraday Soc.* **46,** 235 (1950).
10. COCKBAIN, E. G., *Trans Faraday Soc.* **50,** 874 (1954).
11. BANES, F. W., AND EBY, L. T., *Ind. Eng. Chem., Anal. Ed.* **18,** 535 (1946).
12. BRAND, E., *Ann. N. Y. Acad. Sci.* **47,** 187 (1946).
13. BARR, T., OLIVER, J., AND STUBBINGS, W. V., *J. Soc. Chem. Ind.* (*London*) **67,** 45 (1948).
14. COCKBAIN, E. G., AND MCMULLEN, A. I., *Trans. Faraday Soc.* **47,** 322 (1951).
15. COCKBAIN, E. G., *Trans. Faraday Soc.* **49,** 104 (1953).
16. PUTNAM, F. W., AND NEURATH, H., *J. Biol. Chem.* **159,** 195 (1945).
17. TANFORD, C., *J. Am. Chem. Soc.* **72,** 441 (1950).
18. DERVICHIAN, D. G., *Kolloid-Z.* **126,** 15 (1952).
19. ALEXANDER, A. E., AND TEORELL, T., *Trans. Faraday Soc.* **35,** 734 (1939).
20. NEURATH, H., *J. Phys. Chem.* **44,** 300 (1940).

JOURNAL OF COLLOID SCIENCE **11**, 585–592 (1956)

SOLUBILITY IN SOAP SOLUTIONS. VI. THE EFFECT OF SOAP UPON UPPER AND LOWER CONSOLUTE TEMPERATURES IN THE NICOTINE-WATER AND TRIETHYLAMINE-WATER SYSTEMS

D. Langbridge, A. S. C. Lawrence, and R. Stenson

Sheffield University, Sheffield, England

Received April 5, 1956

INTRODUCTION

In previous parts of this work upon the solubility of organic substances in soap solutions (1–5), it was pointed out that, where the water and third component have limited mutual solubility, the addition of soap may be regarded as lowering the consolute temperature (C.T.) progressively. The whole solubility curve being lowered, the two-phase area becomes smaller corresponding with the increase of mutual solubility of the two liquids. One of us (3) has examined the effect of sodium stearate upon the upper and lower consolute temperatures of the well-known closed-ring phase diagram of the nicotine-water system and found that the soap lowered the upper value and raised the lower; observations were limited to 50:50 nicotine-water composition, and it was found that the upper and lower C.T. met at *ca.* 8% of sodium stearate so that only a homogeneous one-phase system exists when this or a greater amount of soap is present. We have now examined the whole system and the progressive closure of the ring with increasing amounts of both anionic and kationic soap. The effect of sodium dodecyl sulfate upon lower consolute temperatures in the triethylamine-water system has also been investigated.

EXPERIMENTAL

The critical solution temperatures were observed by heating the specimen in a sealed tube following Alexeev (6) and Hudson (7), who observed the nicotine-water closed ring. We, however, used larger tubes—4 mm. in internal diameter and about 10 cm. long—in order to accommodate a stirrer consisting of a small soft iron rod sealed into a Pyrex tube. The tube was heated in a suitable bath and the stirrer actuated by an external magnet. The triethylamine-water system was also observed in sealed tubes except for the points lying below 40°C. The thermometer used was calibrated in ⅕th of a degree and no difficulty was normally found in obtaining results accurately to ⅕th by taking the temperature up and down across the transition point. As the soap concentration was increased, the well-known opalescence appeared more noticeably just above the upper consolute temperature (U.C.T.). It was found that decomposition of the kationic soap set in above 200°C. and that the U.C.T. of specimens held above this temperature for more than a very short time rose steadily. For these higher values, therefore, heating and observation of the U.C.T. was carried out rapidly and repeats were not attempted.

MATERIALS

Commercial 95% nicotine was distilled twice under reduced pressure, and the fraction boiling between 141 and 143°C. at 29–30 mm. Hg pressure used. Its refractive index was 1.5243 at 24°C. Triethylamine was distilled from good quality commercial material with the addition of a small quantity of quicklime. The fraction boiling at 89–91°C. was used. The palmitic acid had molecular weight (by saponification value) of 255.7 (theory 256.3) and melting pt. 62.6 (lit. value 62.4°C.). The solutions of sodium palmitate were prepared by mixing calculated amounts of acid and sodium hydroxide solution made up in CO_2-free water in an atmosphere of nitrogen. The cetyl trimethylammonium bromide was recrystallized from a very pure sample kindly prepared for us by Imperial Chemical Industries, Blackley, from a sample of cetyl alcohol specially freed from homologous impurities.

The nicotine-water ring and triethylamine-water curve were determined without addition of soap as a further check on purity. Our results were identical with those of Hudson and Rothmund (9), respectively. The graph for the triethylamine-water system in Findlay's *Physical Chemistry* (p. 517 and p. 434 in the revised edition) shows a curious error; the flat lower consolute temperature (L.C.T.) minimum is drawn at 22°C., whereas it should be at 18.3°C.

RESULTS

Nicotine-Water System

Figure 1 shows the progressive reduction of the "ring" with increasing amounts of cetyl trimethylammonium bromide. The outermost curve (*a*) and the corresponding one in Fig. 2 are for nicotine and water without soap; the agreement with Hudson's results, confirmed by Tsakalotos (8), is satisfactory proof of the purity of the nicotine. The nicotine concentration is given in mole fractions because better separation of the curves results. With 20% of this soap, the nicotine and water are completely miscible over all concentrations and at temperatures from 15° to 250°C.

Figure 2 shows the results for sodium palmitate. It will be seen that the curve for 5% soap crosses the nicotine-water curve and that, at the nicotine-

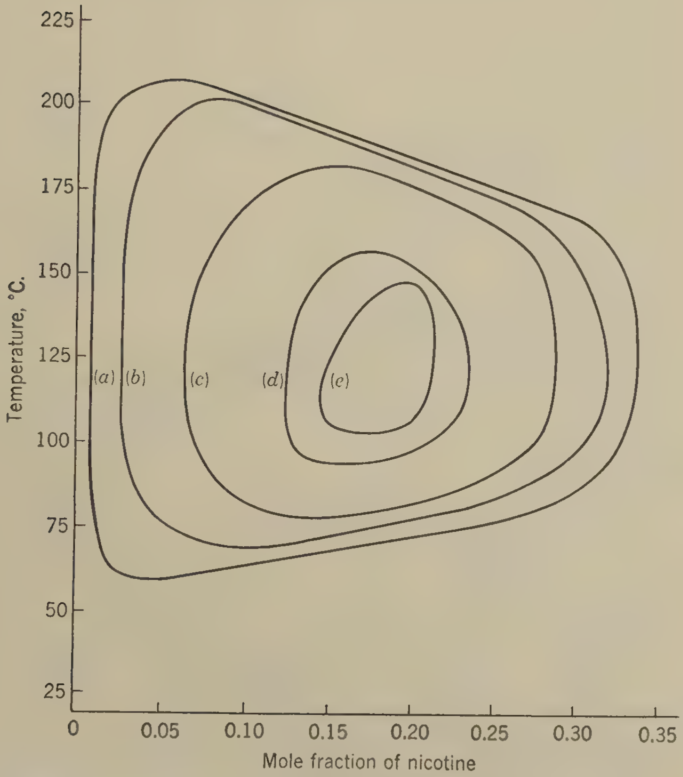

FIG. 1. Cetyltrimethyl ammonium bromide in nicotine-water system. (*a*) No soap; (*b*) 5%; (*c*) 10%; (*d*) 15%; (*e*) 18% soap.

rich side of the diagram, nicotine is less soluble in the presence of 5% soap than without any. With 10% of soap, the normal reduction of the "ring" proceeds. It was thought that fatty acid produced by hydrolysis might be responsible and the curve for 5% soap + 5% palmitic acid was then determined; this shows little difference from that of the soap alone, and 5% of palmitic acid was tried without any soap. The outer broken curve resulted; this suggests that the relatively greater hydrolysis in the 5% soap is in fact responsible for the effect.

Triethylamine-Water System

The occurrence of an L.C.T. in this system was recorded by V. Rothmund (9), who also examined a number of other cases including that of isobutyric acid. The U.C.T. has not been observed for triethylamine and water but would be expected to be very high.

Figure 3 shows the system over the whole range of triethylamine-water composition; we see, as before, the marked raising of the L.C.T. with in-

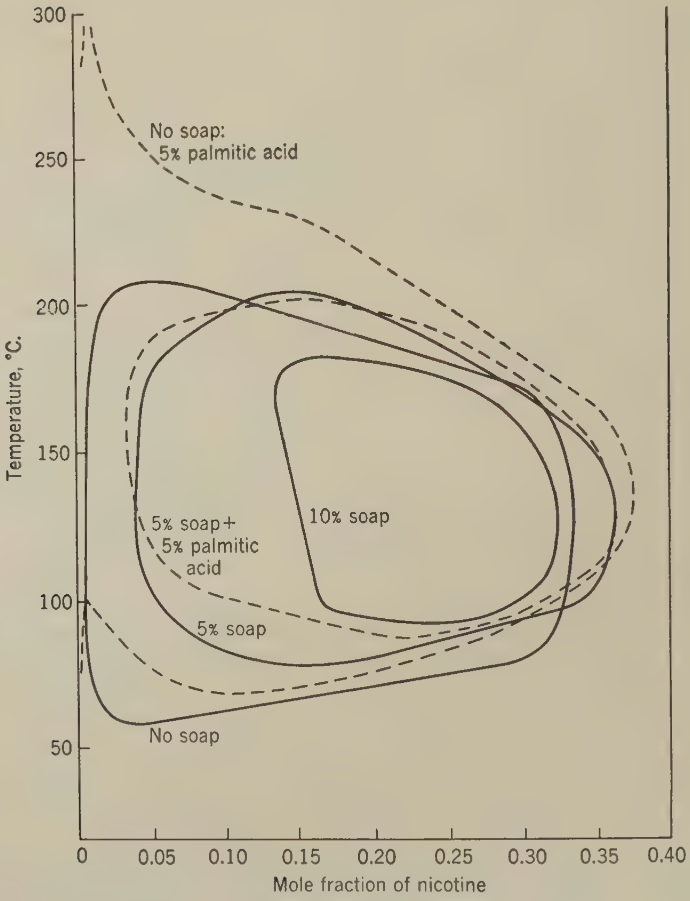

FIG. 2. Nicotine-water-sodium palmitate system.

crease of soap. Clearly even with 25% of soap we are a long way below the U.C.T. The 25% solution was taken up to 200°C. but did not clear; it was not heated above this because decomposition of the soap would have made the experiment meaningless.

Figure 4 shows the effects of sodium dodecyl sulfate upon the L.C.T.; the curve seems to consist of two straight lines with an abrupt change of slope at about 11% of soap. With the 20% and 25% soap systems a new and curious phenomenon was observed. The viscosity of these solutions, which was about that of water at room temperature, increased over 3° to 4° by a factor of at least 10^4; closer inspection revealed the slight turbidity which is characteristic of smectic liquid crystalline ternary systems. The heating when repeated under low magnification in a polarizing microscope showed that the smectic phase appeared suddenly in the isotropic solution,

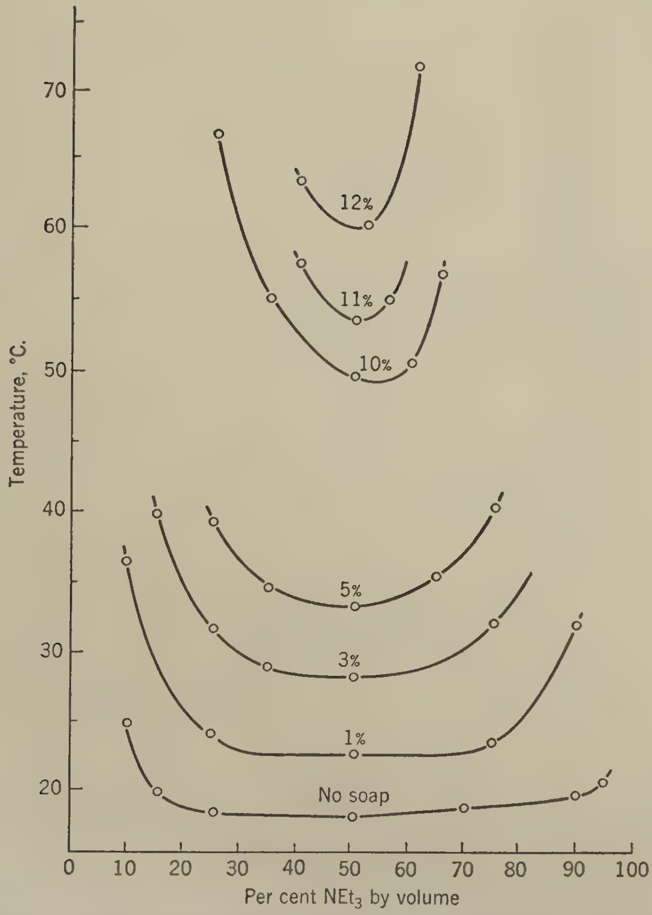

FIG. 3. Effect of soap upon lower consolute temperature of NEt_3-H_2O mixtures.

and in an interval of less than 2° the whole specimen had become a liquid crystalline mass. The second curve in Fig. 4 shows, as lower point, the temperature of appearance of the smectic phase and its re-solution to isotropic fluid solution occurring equally sharply at a higher temperature. The curve shows that a minimum of at least 19% of this soap is required for the liquid crystalline phase to separate; with 17.5% of soap in the 50:50 NEt_3-H_2O solvent mixture, no liquid crystalline phase appeared between room temperature and the L.C.T., which was 98°C. In view of the insolubility of the soap in anhydrous NEt_3, further experiments were carried out upon solutions in mixtures containing more than 50% NEt_3. Figure 5 shows the results as the temperatures at which the smectic phase appeared, that at which it disappeared, and, in the soap-NEt_3–rich solutions, the freezing

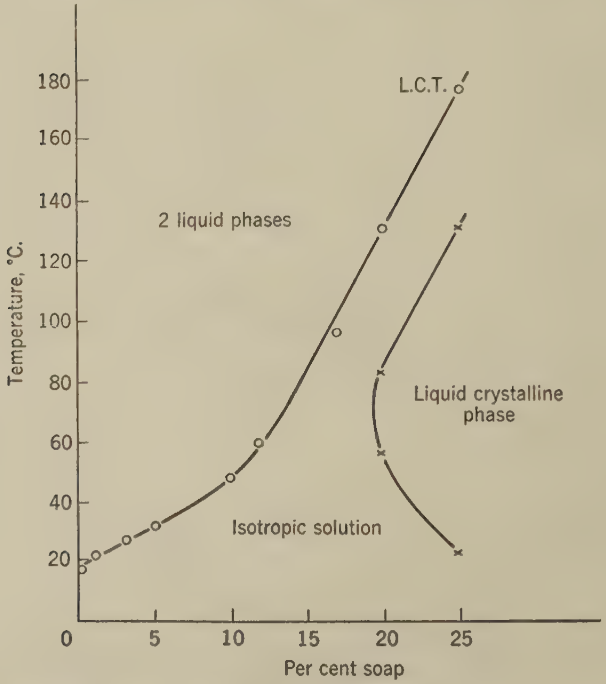

Fig. 4. Sodium dodecyl sulfate in 50:50 triethylamine-water mixture.

point at which the pure crystalline soap starts to separate (Krafft point).

The sudden appearance of the smectic phase on heating is shown by development of high birefringence and, in the medium concentrations of NEt_3, by a very large increase of viscosity. As the amount of water is reduced, this viscosity also falls and at the 90% NEt_3 level, the smectic phase is highly birefringent but quite fluid. This extreme fluidity of the smectic phase at the low-water, high-organic third component part of the phase diagram is general, although this viscosity increases moderately with increase of molecular weight of the third component.

In the 25% soap in 90% NEt_3 and in the 20 in 95, the mixture of solid soap and solution passes on heating directly to liquid crystal, the intermediate isotropic solution phase having been pinched out as shown in Fig. 5. For lower NEt_3 concentrations, some freezing points have been determined; they are not such sharp transitions as normal Krafft points in aqueous soap solutions and this fact, together with the quite remarkable fluidity of the isotropic solutions, suggests that the extent of colloidal aggregation is not nearly so great in these binary solvent mixtures as it is in water alone. It will be recalled that Ward considered that there is no colloid in solutions of soap in 40% ethyl alcohol in water (11). A single solution of a kationic soap, cetyl trimethylammonium bromide at 25% concentration in

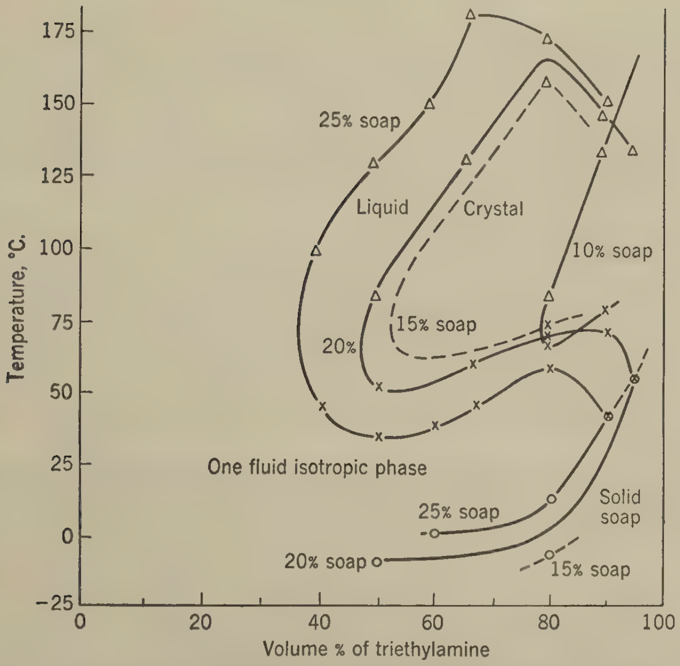

Fig. 5. Phase transitions in sodium dodecyl sulfate-triethylamine system. ○ Freezing point solid soap. × Lower temperature limit of liquid crystalline region. △ Upper limit of liquid crystals.

70% aqueous triethylamine was isotropic solution at room temperature and became liquid crystalline on warming.

Discussion

The results for the nicotine-water system show again the lack of any effects due to the charge on the soap (4). The CTAB curves are straightforward and show the progressive lowering of the U.C.T. and raising of the L.C.T. with increase of soap concentration. Ordinary electrolytes produce the opposite effect and the following figures illustrate the two contrary effects.

Solution	L.C.T.	ΔT	U.C.T.	ΔT
25% nicotine in water	62	—	207.5	—
25% nicotine + 1% KCl	57	−5	238	+30.5
50% nicotine in water	65	—	204	—
50% nicotine + 5% CTAB	71	+6	200	−4
50% nicotine + 5% CTAB + 0.5% KNO_3	62.5	−8.5	235	+35

If the mole fraction of nicotine is plotted against the concentration of soap for the intercepts on the rings at a chosen temperature, e.g., 140°, 150°, and

160°C., triangular graphs result with the apex in the neighborhood of 66% nicotine and 19%–20% of soap. The disappearance of the two-phase system will therefore require a minimum of soap of this order; 20% solutions of CTAB in 61%, 63%, and 66% nicotine were all single-phase systems from 15° to 250°C. For sodium palmitate the minimum concentration for complete miscibility is 13%.

Lower Consolute Temperatures have been discussed by a number of workers, especially in terms of hydrogen bonding and entropy considerations (10). However we find that triethylamine in water below the L.C.T. has an ionic conductivity falling with increase of concentration of amine and becoming very small above 40%. Nicotine-water mixtures also show small but peculiar conductivity effects. We feel that speculation about these solutions is unprofitable until more is known of their physical properties.

One of us (R. S.) is indebted to the University of Sheffield for the award of a Robert Styring Scholarship during the tenure of which this work was carried out.

References

1. Lawrence, A. S. C., *Trans. Faraday Soc.* **33**, 325 (1937).
2. Lawrence, A. S. C., *Trans. Faraday Soc.* **33**, 815 (1937).
3. Lawrence, A. S. C., "Wetting and Detergency," Leather Trades Chemists Society Symposium, p. 205, 1937.
4. Hyde, A. H., Lawrence, A. S. C., and Langbridge, D. M., *Discussions Faraday Soc.* on "Coagulation and Flocculation," **18**, p. 239 (1954).
5. Blakey, B. C., and Lawrence, A. S. C., *Discussions Faraday Soc.* on "Coagulation and Flocculation," **18**, p. 268 (1954).
6. Alexeev, W., *Wied. Ann.* **28**, 305 (1886); *Z. physik. Chem.* **58**, 129 (1907).
7. Hudson, C. S., *Z. physik. Chem.* **47**, 113 (1904).
8. Tsakalotos, D., *Bull. soc. chim. Belg.* **5**, 397 (1909).
9. Rothmund, V., *Z. physik. Chem.* **26**, 459 (1898).
10. Hirschfelder, J., Stevenson, D., and Eyring, H., *J. Chem. Phys.* **5**, 896 (1937); Rushbrooke, G. S., *Proc. Cambridge Phil. Soc.* **34**, 424 (1938); Copp, J. L., and Everett, D. H., *Discussions Faraday Soc.* **15**, 174 (1953).
11. Ward, A. F. H., *Proc. Roy. Soc. (London)* **A176**, 412 (1940).

JOURNAL OF COLLOID SCIENCE **11**, 593–607 (1956)

AN ESTIMATE OF THE CONTRIBUTION OF INDUCED DIPOLES TO THE ORIENTATIONAL POLARIZATION OF ADSORBATES

G. C. Benson[1], E. W. Channen[2], and R. McIntosh[3]

The Pure Chemistry Division, National Research Council, Ottawa, and the Chemistry Department, University of Toronto

Received March 5, 1956

Abstract

The orientational polarization of a polarizable dipolar molecule adsorbed above the {100} plane of a sodium chloride lattice has been evaluated. It has been shown that such polarization is small in spite of the large induced moment created by the electric field from the solid surface. It is also demonstrated that orientational effects of dipoles induced by surface fields are insignificant for nonpolar adsorbates. It therefore follows that apparent polarizabilities in excess of the polarizability of the molecule in the gaseous state, which are frequently reported for adsorbed molecules, are to be attributed to inexact formulas, in the estimation of the polarization of the adsorbate from the experimental data.

Introduction

In attempting to examine the state of physically adsorbed gas molecules on both porous and nonporous adsorbents, investigators have to contend with the problem of assigning a value of the internal field acting upon the adsorbate molecules, if the real part of the dielectric constant is to be interpreted in terms of molecular properties. Various authors (1–6) have employed different procedures for evaluating the internal field, and widely different results are obtained by the several methods. This aspect of the overall problem has been emphasized by Channen and McIntosh (1), who have themselves presented several procedures, none of which seemed generally satisfactory. In discussing the various procedures, Channen and McIntosh took as a useful criterion the comparison between the deduced polarizability of adsorbed nonpolar gases and the known value for the bulk material from refractive index data (or more correctly, dielectric data obtained at low frequencies). This criterion is useful only if the assumption is valid that induced dipoles, arising from the field of the solid, do not affect the observations. Thus if the polarizability of an adsorbate molecule is considered to be isotropic, the induced dipoles cancel out, since the direction of the induced dipole from the field of the surface may be considered as fixed on application of the field. The applied field merely polarizes the molecule in its direction to an extent dependent upon the polarizability. On the other hand, if the polarizability of the molecule is not isotropic, a preferred orientation for the adsorbed molecule will be established. On application of the field, the direction of the molecule may be changed in order to maintain the energy in its lowest state, so that the induced dipole may follow the field and thus contribute to the orientational polarization.

---

[1] Associate Research Officer, National Research Council.

[2] Graduate student and Holder of the Union Carbide Company Fellowship.

[3] Professor of Chemistry.

This latter conception has apparently led Kamiyoshi (3) to conclude that large apparent moments for adsorbed molecules of benzene and carbon tetrachloride exist owing to the influence of the field from the adsorbing solid. A similar view has been expressed by Miss Shimizu (6). Dipolar molecules would, on the same assumptions, reveal an enhanced value of the dipole moment, perhaps appreciably greater than that found for the substance in the gaseous state.

On the other hand, we consider that the deduction of large dipole moments for adsorbed molecules from experimental observations, arises from the use of incorrect formulas to separate the contribution of adsorbate from that of the rest of the experimental system. It seemed worth while, therefore, to try to establish the order of magnitude of the induced dipole and the contribution it would make to the orientational polarization. To do so a simplified model has been chosen to permit the solution of the problem. The solid adsorbent has been taken as an ideal crystal of sodium chloride. The adsorbate molecule has properties corresponding roughly to those of hydrogen chloride.

DETAILS OF THE MODEL AND SOLUTION OF THE PROBLEM

We consider the molecule of HCl to be represented by a model similar to that described by Debye (7). The distance between the two ions is r, and each ion has unit charge $\pm\epsilon$, which equals 4.8024×10^{-10} e.s.u. The positive ion is treated as a point charge, while the negative ion is assigned an effective polarizability, taken as 1.70×10^{-24} cm.^{3}, the value required to procure agreement with the known dipole moment of 1.05×10^{-18} e.s.u. For any separation r the potential energy of the molecule is $U^m(r) = -\frac{\epsilon^2}{r} + R(r) - \frac{1}{2}\alpha(\mathbf{E}_-^{\ +})^2$, where $\mathbf{E}_-^{\ +}$ is the electrostatic field at the negative ion due to the positive charge, and $R(r)$ represents the repulsive interaction between the ions. It is assumed that $R(r)$ depends only upon the two types of ion and their separation, and is not changed when other ions approach or when external fields are applied.

To a fair approximation $U^m(r) = U_0 + \frac{1}{2}k_m(r - r_0)^2$, for values of r near r_0, which is the equilibrium spacing of the gaseous molecule and is taken as 1.27×10^{-8} cm. U_0 is a constant, and $k_m = 5.0 \times 10^5$ dynes cm.$^{-1}$ is the vibrational force constant (8) from spectroscopic data.

The potential energy is next considered when the molecule is placed in the electrostatic field near the surface of the {100} face of a sodium chloride crystal in which the nearest neighbor distance is 2.81×10^{-8} cm. To make the calculation feasible the possible orientations of the molecule relative to the surface are restricted. If the molecule consisted of two point charges, and if the repulsive forces between the ions of the molecule and those of the crystal were nonspecific, the molecule would lie in a plane parallel to the surface and with its axis along the line joining two neighboring ions in the surface. The mid-point of the axis of the molecule would be vertically above the mid-point between the two surface ions, while the distance above the surface would depend upon the repulsive forces between the molecule and the surface. When the negative ion is polarizable as assumed, and the repulsive forces vary with the types of ion, the molecule will still tend to lie along the line between two surface neighbors, but the center of its axis will be displaced from the mid-point position and the axis will be tilted out of the plane parallel to the surface. In the present calculation details of the repulsive interaction with the surface are not considered and the above effects are not treated. The adsorbed molecule is assumed to have its mid-point fixed at a point a distance Z vertically above the mid-point between surface ions. Owing to its thermal energy the molecule may rotate and vibrate symmetrically about this point, but these motions are restricted to a plane parallel to the surface. Estimates of the orientational polarization of this model will be made for several values of Z. The model is considered sufficient to provide an estimate of this polarization term.

The energy of the molecule in the field of the crystal in configuration r, γ (see Figs. 1 and 2) is

$$U(r, \gamma) = \frac{-\epsilon^2}{r} + R(r) - \tfrac{1}{2}\alpha(\mathbf{E}_-^{+} + \mathbf{E}_-^{c})^2 + \epsilon(\phi_+^{c} - \phi_-^{c}),$$

where $\mathbf{E}_-^{c}$ is the electric field at the negative ion of the molecule due to the crystal and ϕ_+^{c} and ϕ_-^{c} are the electrostatic potentials at the positive and negative ions of the molecule, respectively.

$$U(r, \gamma) = U_0 + \tfrac{1}{2}k_m (r - r_0)^2 - \tfrac{1}{2}\alpha\, (2\mathbf{E}_-^{+} \cdot \mathbf{E}_-^{c} + (\mathbf{E}_-^{c})^2) + \epsilon(\phi_+^{c} - \phi_-^{c}).$$

If a uniform external electric field $\mathbf{E}$ is applied, the energy of the molecule may be written as

$$U(r, \gamma, \mathbf{E}) = U(r, \gamma) - \mathbf{E} \cdot (\epsilon\mathbf{r} + \alpha(\mathbf{E}_-^{+} + \mathbf{E}_-^{c})) - \frac{\alpha}{2}\mathbf{E}^2,$$

where $\mathbf{r}$ is directed from the negative to the positive ion along the axis of the molecule. The total dipole moment of the molecule is

$$\boldsymbol{\mu}_t = \epsilon\mathbf{r} + \alpha\, (\mathbf{E}_-^{+} + \mathbf{E}_-^{c} + \mathbf{E}),$$

and it is convenient to write this as

$$\boldsymbol{\mu}_t = \boldsymbol{\mu} + \alpha\mathbf{E}.$$

Thus

$$U(r, \gamma, \mathbf{E}) = U(r, \gamma) - \mathbf{E}\cdot\boldsymbol{\mu} - \frac{\alpha}{2}\mathbf{E}^2.$$

The location and permitted movements of the adsorbed molecule are described by means of the coordinate systems depicted in Figs. 1 and 2. The *ox* and *oy* axes fixed in the crystal coincide with two principal axes in the {100} surface of the crystal. A positive ion is at the origin *O*. The outward drawn normal is *oz*. The constant electric field **E** defines the *oX* direction for a second right-handed coordinate system *oXYZ* fixed in space. The polar angles of *oz* relative to this new set of axes are θ and ϕ. The pro-

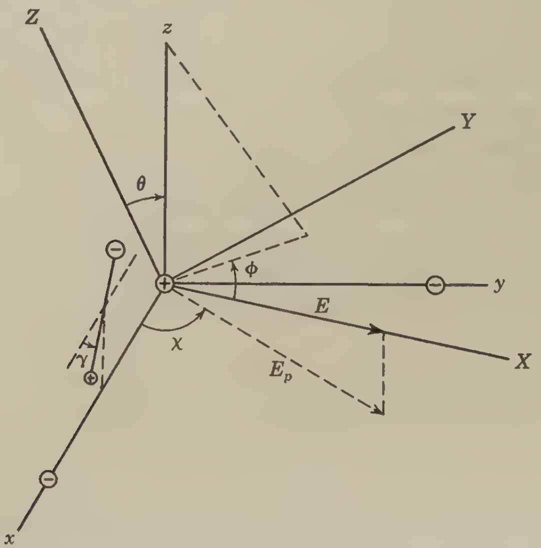

FIG. 1. Representation of crystal axes, space axes, and relative position of adsorbed molecule and applied field.

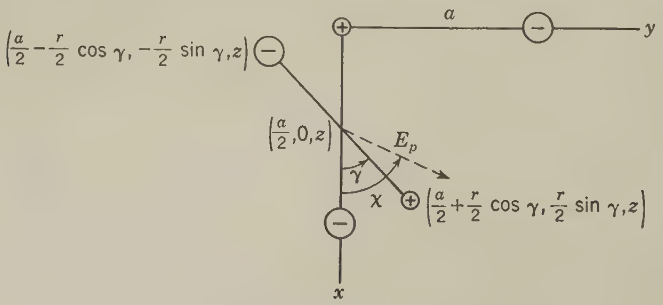
a
y
$\left(\frac{a}{2}-\frac{r}{2}\cos\gamma, -\frac{r}{2}\sin\gamma, z\right)$
$\left(\frac{a}{2}, 0, z\right)$
E_p
γ
χ
$\left(\frac{a}{2}+\frac{r}{2}\cos\gamma, \frac{r}{2}\sin\gamma, z\right)$
x

FIG. 2. Representation of molecule relative to surface ions.

jection of $\mathbf{E}$ on the oxy plane is $\mathbf{E}_P$ and makes an angle χ with the direction ox; $\mathbf{i}$, $\mathbf{j}$, $\mathbf{k}$ are unit vectors along ox, oy, oz.

The expressions for the potential and electric fields are:

$$\phi_-^+ = \frac{\epsilon}{r}; \qquad \mathbf{E}_-^+ = -\frac{\epsilon}{r^2}(\cos\gamma\mathbf{i} + \sin\gamma\mathbf{j});$$

$$\phi^c(x, y, z) = \frac{2\epsilon}{a}\sum_{\substack{-\infty \\ k_1\text{odd}}}^{+\infty}\ \sum_{\substack{-\infty \\ k_2\text{odd}}}^{+\infty} \frac{e^{-(\pi Z/a)\sqrt{k_1{}^2+k_2{}^2}}}{\sqrt{k_1^2 + k_2^2}(1 + e^{-\pi\sqrt{k_1{}^2+k_2{}^2}})} \cos\left(\pi k_1\frac{x}{a}\right)\cos\left(\pi k_2\frac{y}{a}\right).$$

The latter assumes a regular crystal lattice of point charges which is undistorted by the adsorbed molecule. For the purposes of this calculation ϕ^c is approximated by

$$\phi^c(x, y, z) = \frac{8\epsilon}{a\sqrt{2}}e^{-\pi Z\sqrt{2}/a}\cos\left(\frac{\pi x}{a}\right)\cos\left(\frac{\pi y}{a}\right) = A\cos\left(\frac{\pi x}{a}\right)\cos\left(\frac{\pi y}{a}\right).$$

The expression for ϕ^c was obtained by using the methods of van der Hoff and Benson (9), and the approximation is similar to that employed by Verwey (10) for the electrical field at the surface of a crystal.

$$\mathbf{E}^c = -\nabla\phi^c = \frac{\pi A}{a}\left(\sin\left(\frac{\pi x}{a}\right)\cos\left(\frac{\pi y}{a}\right)\mathbf{i} + \cos\left(\frac{\pi x}{a}\right)\sin\left(\frac{\pi y}{a}\right)\mathbf{j} + \sqrt{2}\cos\left(\frac{\pi x}{a}\right)\cos\left(\frac{\pi y}{a}\right)\mathbf{k}\right).$$

The coordinates of the positive and negative ions of the molecule are

$$\frac{a}{2} + \frac{r}{2}\cos\gamma, \qquad \frac{r}{2}\sin\gamma, Z$$

$$\frac{a}{2} - \frac{r}{2}\cos\gamma, \qquad \frac{-r}{2}\sin\gamma, Z,$$

respectively. Thus

$$\epsilon(\phi_+^c - \phi_-^c) = -2A\epsilon I,$$

where

$$I = \sin\left(\frac{\pi r}{2a}\cos\gamma\right)\cos\left(\frac{\pi r}{2a}\sin\gamma\right);$$

$$\mathbf{E}_-^c = \frac{\pi A}{a}\left[\cos\left(\frac{\pi r}{2a}\cos\gamma\right)\cos\left(\frac{\pi r}{2a}\sin\gamma\right)\mathbf{i} - \sin\left(\frac{\pi r}{2a}\cos\gamma\right) \times \sin\left(\frac{\pi r}{2a}\sin\gamma\right)\mathbf{j} + \sqrt{2}\sin\left(\frac{\pi r}{2a}\cos\gamma\right)\cos\left(\frac{\pi r}{2a}\sin\gamma\right)\mathbf{k}\right];$$

$$\mathbf{E}_-^c\cdot\mathbf{E}_-^+ = \frac{\epsilon A\pi}{ar^2}J;$$

where

$$J = \sin\gamma \sin\left(\frac{\pi r}{2a}\cos\gamma\right)\sin\left(\frac{\pi r}{2a}\sin\gamma\right) \\ - \cos\gamma\cos\left(\frac{\pi r}{2a}\cos\gamma\right)\cos\left(\frac{\pi r}{2a}\sin\gamma\right);$$

$$(\mathbf{E}_-{}^c)^2 = \frac{\pi^2 A^2}{a^2} K$$

where

$$K = \cos^2\left(\frac{\pi r}{2a}\sin\gamma\right) + \sin^2\left(\frac{r\pi}{2a}\cos\gamma\right).$$

Hence

$$U(r,\gamma) = U_0 + \tfrac{1}{2}k_m(r - r_0)^2 - \frac{\alpha\epsilon A\pi}{ar^2} J - \frac{\alpha}{2}\left(\frac{\pi}{a}\right)^2 A^2 K - 2A\,\epsilon\, I.$$

Next $\mathbf{E}\cdot\boldsymbol{\mu}$ is evaluated. Since $\mathbf{E} = \mathbf{E}_p + \mathbf{E}_n$, where $\mathbf{E}_p$ has already been defined as the projection of $\mathbf{E}$ on the *oxy* plane and $\mathbf{E}_n$ is in the *oz* direction,

$$E_n = E\sin\theta\cos\phi,$$

and

$$E_p = E(1 - \sin^2\theta\cos^2\phi)^{1/2},$$

so that

$$\mathbf{E} = E[(1 - \sin^2\theta\cos^2\phi)^{1/2}(\cos\chi\mathbf{i} + \sin\chi\mathbf{j}) + \sin\theta\cos\phi\mathbf{k}].$$

The moment $\boldsymbol{\mu}$ can also be expressed in terms of its components in the $\mathbf{i}$, $\mathbf{j}$, and $\mathbf{k}$ directions. Thus

$$\boldsymbol{\mu} = \epsilon\mathbf{r} + \alpha(\mathbf{E}_-{}^+ + \mathbf{E}_-{}^c) = \mu_x\mathbf{i} + \mu_y\mathbf{j} + \mu_z\mathbf{k}$$

where

$$\mu_x = \epsilon\left(r - \frac{\alpha}{r^2}\right)\cos\gamma + \frac{\alpha\pi A}{a}\cos\left(\frac{\pi r}{2a}\cos\gamma\right)\cos\left(\frac{\pi r}{2a}\sin\gamma\right).$$

$$\mu_y = \epsilon\left(r - \frac{\alpha}{r^2}\right)\sin\gamma - \frac{\alpha\pi A}{a}\sin\left(\frac{\pi r}{2a}\cos\gamma\right)\sin\left(\frac{\pi r}{2a}\sin\gamma\right)$$

$$\mu_z = \alpha\frac{A\pi\sqrt{2}}{a}\sin\left(\frac{\pi r}{2a}\cos\gamma\right)\cos\left(\frac{\pi r}{2a}\sin\gamma\right)$$

and μ_x, μ_y, μ_z are functions of r, γ. We define m as the component of $\boldsymbol{\mu}$ in the direction $\mathbf{E}$.

$$m = \frac{\mathbf{E}\cdot\boldsymbol{\mu}}{E} = (1 - \sin^2\theta\cos^2\phi)^{1/2}(\mu_x\cos\chi + \mu_y\sin\chi) + \mu_z\sin\theta\cos\phi.$$

The energy $U(r, \gamma, \mathbf{E})$ can then be written

$$U(r, \gamma, \mathbf{E}) = \Delta U + U_0 - Em - \frac{\alpha}{2}\mathbf{E}^2,$$

where

$$\Delta U = \tfrac{1}{2}k_m(r - r_0)^2 - \frac{\alpha\epsilon A\pi}{ar^2} J - \frac{\alpha A^2}{2}\frac{\pi^2}{a^2} K - 2A\epsilon I.$$

Now the total energy of the molecule in the field of the crystal plus the external field $\mathbf{E}$ is H, the sum of the kinetic and potential energies.

$$H = \tau + U(r, \gamma, \mathbf{E}) \qquad \text{where} \qquad \tau = \tfrac{1}{8}M\,(\dot{r}^2 + r^2\dot{\gamma}^2).$$

Here M is the mass of the molecule and the dot denotes differentiation with respect to time; τ is next written in terms of the conjugate momenta so that

$$\tau = \frac{2}{M}\left(p_r^2 + \frac{p_\gamma^2}{r^2}\right).$$

Let m_t be the value of the component of the total moment in the direction of $\mathbf{E}$. Then

$$m_t = \frac{\boldsymbol{\mu}_t \cdot \mathbf{E}}{E} = m + \alpha E.$$

The mean value of m_t for a molecule adsorbed on a surface with specified values of θ, ϕ, χ, is given by averaging over all permitted values of r, γ, p_r, p_γ after weighting with the Boltzmann factor $e^{-H/kT}$. Thus

$$\langle m_t \rangle_{\theta,\phi,\chi} = \frac{\displaystyle\int_{-\infty}^{\infty}\int_{-\infty}^{\infty}\int_0^{\infty}\int_{-\pi}^{\pi} (m + \alpha E)e^{-H/kT}\,d\gamma\,dr\,dp_r\,dp_\gamma}{\displaystyle\int_{-\infty}^{\infty}\int_{-\infty}^{\infty}\int_0^{\infty}\int_{-\pi}^{\pi} e^{-H/kT}\,d\gamma\,dr\,dp_r\,dp_\gamma}$$

where

$$H = U_0 - \frac{\alpha}{2}E^2 + \tau + \Delta U - Em.$$

Since U_0 and $(\alpha/2)E^2$ are independent of the variables of integration, the terms in these factors cancel in the numerator and denominator. Since m is not a function of the momenta, the integrations over these variables can be performed directly leading to the expression

$$\langle m_t \rangle_{\theta,\phi,\chi} = \alpha E + \frac{\displaystyle\int_0^{\infty}\int_{-\pi}^{\pi} mre^{-(\Delta u - Em/kT)}\,d\gamma\,dr}{\displaystyle\int_0^{\infty}\int_{-\pi}^{\pi} re^{-(\Delta u - Em/kT)}\,d\gamma\,dr}.$$

As E/kT is a small quantity, the ratio of the two integrals is expanded as a power series in E/kT, and only the first term in E/kT is retained. On this basis

$$\langle m_t \rangle_{\theta,\phi,\chi} = \alpha E + \frac{I_1}{I_0} - \frac{E}{kT}\left(\frac{I_1^2}{I_0^2} - \frac{I_2}{I_1 I_0}\right)$$

where I_0, I_1, and I_2 are defined by the integrals

$$I_0 = \int_0^\infty \int_{-\pi}^{\pi} re^{-\Delta u/kT}\, d\gamma\, dr.$$

$$I_1 = \int_0^\infty \int_{-\pi}^{\pi} mre^{-\Delta u/kT}\, d\gamma\, dr.$$

$$I_2 = \int_0^\infty \int_{-\pi}^{\pi} m^2re^{-\Delta u/kT}\, d\gamma\, dr.$$

To get the average value of m_t for all possible orientations of the crystal surface, the assumption is made that all orientations are equally probable. Then

$$\langle m_t \rangle = \frac{1}{8\pi^2} \int_0^{2\pi} \int_0^{2\pi} \int_0^{\pi} \langle m_t \rangle_{\theta,\phi,\chi} \sin\theta\, d\theta\, d\phi\, d\chi.$$

Since I_0 is independent of θ, ϕ, χ

$$\langle m_t \rangle = \alpha E + \frac{I_1}{I_0} + \left(\frac{E}{kT}\frac{I_2}{I_0} - \frac{I_3}{I_0^2}\right)$$

where

$$I_1 = \frac{1}{8\pi^2} \int_0^{2\pi} \int_0^{2\pi} \int_0^{\pi} I_1 \sin\theta\, d\theta\, d\phi\, d\chi.$$

$$I_2 = \frac{1}{8\pi^2} \int_0^{2\pi} \int_0^{2\pi} \int_0^{\pi} I_2 \sin\theta\, d\theta\, d\phi\, d\chi.$$

$$I_3 = \frac{1}{8\pi^2} \int_0^{2\pi} \int_0^{2\pi} \int_0^{\pi} I_1^2 \sin\theta\, d\theta\, d\phi\, d\chi.$$

On integration with respect to θ, ϕ, χ it is found that

$I_1 = 0,$

$$I_2 = \tfrac{1}{3} \int_0^\infty \int_{-\pi}^{\pi} (\mu_x^2 + \mu_y^2 + \mu_z^2) re^{-\Delta u/kT}\, d\gamma\, dr = \tfrac{1}{3} \int_0^\infty \int_{-\pi}^{\pi} \mu^2 re^{-\Delta u/kT}\, d\gamma\, dr$$

and

$$I_3 = \tfrac{1}{3}\left\{\left[\int_0^\infty \int_{-\pi}^{\pi} \mu_x re^{-\Delta u/kT}\, d\gamma\, dr\right]^2 + \left[\int_0^\infty \int_{-\pi}^{\pi} \mu_z re^{-\Delta u/kT}\, d\gamma\, dr\right]^2\right\}.$$

In obtaining the expression for I_3 the fact has been used that

$$\int_0^\infty \int_{-\pi}^{\pi} \mu_y r e^{-\Delta u/kT}\, d\gamma\, dr = 0$$

because Δu is an even function of γ and μ_y is an odd function of γ.

$$\langle m_t \rangle = \alpha E + \frac{E}{3kT} \left\{ \frac{\int_0^\infty \int_{-\pi}^{\pi} \mu^2 r e^{-\Delta u/kT}\, d\gamma\, dr}{\int_0^\infty \int_{-\pi}^{\pi} r e^{-\Delta u/kT}\, d\gamma\, dr} - \left[\frac{\int_0^\infty \int_{-\pi}^{\pi} \mu_x r e^{-\Delta u/kT}\, d\gamma\, dr}{\int_0^\infty \int_{-\pi}^{\pi} r e^{-\Delta u/kT}\, d\gamma\, dr} \right]^2 \right.$$
$$\left. - \left[\frac{\int_0^\infty \int_{-\pi}^{\pi} \mu_z r e^{-\Delta u/kT}\, d\gamma\, dr}{\int_0^\infty \int_{-\pi}^{\pi} r e^{-\Delta u/kT}\, d\gamma\, dr} \right]^2 \right\}.$$

To evaluate these integrals Δu, μ^2, μ_x, and μ_z are expanded in Taylor's series in r and γ about the equilibrium position with no external field applied. To obtain this equilibrium position the equilibrium values of r and γ are obtained from the simultaneous conditions that $\partial \Delta u/\partial r = 0$ and $\partial \Delta u/\partial \gamma = 0$. It should be noted that $\partial \Delta u/\partial \gamma = 0$ for $\gamma = 0$, which agrees with the original statement of the molecule lying parallel with the line between the ions of the crystal. Thus the equilibrium value of $\gamma_e = 0$, and r_e is obtained from the condition $\partial \Delta u/\partial r = 0$ at $\gamma = 0$. Recalling that

$$\Delta U = \tfrac{1}{2} k_m (r - r_0)^2 - 2A\epsilon I - \alpha \left(\frac{\epsilon A \pi}{a} J + \frac{A^2 \pi^2}{2a^2} K \right)$$

and evaluating

$$\left(\frac{\partial I}{\partial r} \right)_{\gamma=0}, \quad \left(\frac{\partial J}{\partial r} \right)_{\gamma=0}, \quad \left(\frac{\partial K}{\partial r} \right)_{\gamma=0}$$

results in the equation

$$O = k_m (r_e - r_0) - \frac{A\epsilon\pi}{a} \cos\left(\frac{\pi r_e}{2a} \right) - \alpha \left[\frac{2A\epsilon\pi}{a r_e^3} \cos\left(\frac{\pi r_e}{2a} \right) \right.$$
$$\left. + \frac{A\epsilon\pi^2}{2a^2 r_e^2} \sin\left(\frac{\pi r_e}{2a} \right) + \frac{A^2\pi^3}{2a^3} \sin\left(\frac{\pi r_e}{2a} \right) \cos\left(\frac{\pi r_e}{2a} \right) \right]$$

which can be solved numerically for r_e. Evaluation of higher derivatives of the energy indicates that this equilibrium is a stable one at distances $z = 2.0$ and 2.5×10^{-8} cm. but that it becomes unstable before

$$z = 3.0 \times 10^{-8} \text{ cm.}$$

If we define $(\pi r_e/2a) = w$.

The values of I, J, K and their first and second derivatives with respect to r and γ are worked out for the equilibrium position $r = r_e$ and $\gamma = 0$. The relations obtained are

$$I_e = \sin w, \qquad J_e = -\cos w, \qquad K_e = 1 + \sin^2 w$$

$$\left(\frac{\partial I}{\partial r}\right)_e = \frac{\pi}{2a}\cos w, \qquad \left(\frac{\partial J}{\partial r}\right)_e = \frac{\pi}{2a}\sin w, \qquad \left(\frac{\partial K}{\partial r}\right)_e = \frac{\pi}{a}\sin w \cos w$$

$$\left(\frac{\partial^2 I}{\partial r^2}\right)_e = \frac{-\pi^2}{4a^2}\sin w, \quad \left(\frac{\partial^2 J}{\partial r^2}\right)_e = \frac{\pi^2}{4a^2}\cos w, \quad \left(\frac{\partial^2 K}{\partial r^2}\right)_e = \frac{\pi^2}{2a^2}(\cos^2 w - \sin^2 w),$$

$$\left(\frac{\partial^2 I}{\partial \gamma^2}\right)_e = -w(\cos w + w \sin w), \qquad \left(\frac{\partial^2 J}{\partial \gamma^2}\right)_e = \cos w + w(\sin w + w \cos w),$$

$$\left(\frac{\partial^2 K}{\partial \gamma^2}\right)_e = -2w(w + \sin w \cos w)$$

and

$$(\Delta U)_e = \tfrac{1}{2}k_m(r_e - r_0)^2 - 2A\epsilon \sin w - \alpha\left[\frac{-\epsilon A\pi}{ar_e^2}\cos w + \frac{A^2\pi^2}{2a^2}(1 + \sin^2 w)\right]$$

which is independent of r and γ. The series for ΔU is

$$\Delta U = (\Delta U)_e + \tfrac{1}{2}k_r\,(r - r_e)^2 + \tfrac{1}{2}k_\gamma\gamma^2 + \text{etc.},$$

where

$$k_r = k_m + \frac{A\epsilon}{2}\left(\frac{\pi}{a}\right)^2 \sin w + \alpha\left[\frac{6A\epsilon\pi}{ar_e^4}\cos w + \frac{2A\epsilon}{r_e^3}\left(\frac{\pi}{a}\right)^2 \sin w - \frac{A\epsilon}{4r_e^2}\left(\frac{\pi}{a}\right)^3 \cos w - \frac{A^2}{4}\left(\frac{\pi}{a}\right)^4 \cos 2w\right],$$

and

$$k_\gamma = 2A\epsilon w(\cos w + w \sin w) - \alpha\left[\frac{\epsilon A}{4}\left(\frac{\pi}{a}\right)^3\left(\frac{\cos w}{w^2} + \frac{\sin w}{w} + \cos w\right) - A^2\left(\frac{\pi}{a}\right)^2 w(w + \sin w \cos w)\right].$$

Put $r - r_e = \varphi$ and thus

$$\Delta U = (\Delta U)_e + \tfrac{1}{2}k_r\varphi^2 + \tfrac{1}{2}k_\gamma\gamma^2 + \text{etc.}$$

In a similar fashion μ_x, μ_z, and μ^2 are developed as power series in r and γ, that is,

$$\mu_x = \xi_0 + \xi_1(r - r_e) + \tfrac{1}{2}\xi_2(r - r_e)^2 + \tfrac{1}{2}\xi_3\gamma^2;$$

$$\mu_z = \eta_0 + \eta_1(r - r_e) + \tfrac{1}{2}\eta_2(r - r_e)^2 + \tfrac{1}{2}\eta_3\gamma^2;$$

$$\mu^2 = \zeta_0 + \zeta_1(r - r_e) + \tfrac{1}{2}\zeta_2(r - r_e)^2 + \tfrac{1}{2}\zeta_3\gamma^2.$$

Since $(\partial\mu_x/\partial\gamma)_{\gamma=0}$ and $(\partial^2\mu_x/\partial\gamma\partial r)_{\gamma=0}$, etc., are zero,

$$\xi_0 = (\mu_x)_e \quad = \epsilon\left(r_e - \frac{\alpha}{r_e^{\,2}}\right) + \alpha\frac{A\pi}{a}\cos w;$$

$$\xi_1 = \left(\frac{\partial\mu_x}{\partial r}\right)_e = \epsilon\,(1 + 2\alpha/r_e^{\,3}) \;-\; \frac{\alpha A}{2}\left(\frac{\pi}{a}\right)^2\sin w;$$

$$\xi_2 = \left(\frac{\partial^2\mu_x}{\partial r^2}\right)_e = \frac{-6\epsilon\alpha}{r_e^{\,4}} - \frac{\alpha A}{4}\left(\frac{\pi}{a}\right)^3\cos w;$$

$$\xi_3 = \left(\frac{\partial^2\mu_x}{\partial\gamma^2}\right)_e = -\epsilon\left(r_e - \frac{\alpha}{r_e^{\,2}}\right) + \alpha A\,\frac{\pi}{a}\,(w\sin w - w^2\cos w);$$

$$\eta_0 = (\mu_z)_e \quad = \alpha\frac{A\pi}{a}\sin w;$$

$$\eta_1 = \left(\frac{\partial\mu_z}{\partial r}\right)_e = \frac{\alpha A}{2}\left(\frac{\pi}{a}\right)^2\sqrt{2}\cos w;$$

$$\eta_2 = \left(\frac{\partial^2\mu_z}{\partial r^2}\right)_e = \frac{-\alpha A}{4}\left(\frac{\pi}{a}\right)^3\sqrt{2}\sin w;$$

$$\eta_3 = \left(\frac{\partial^2\mu_z}{\partial\gamma^2}\right)_e = -\frac{\alpha A\pi}{a}\sqrt{2}w(\cos w + w\sin w);$$

$$\zeta_0 = (\mu^2)_e = \epsilon^2\left(r_e - \frac{\alpha}{r_e^{\,2}}\right)^2 + \frac{2\alpha A\pi\epsilon}{a}\left(r_e - \frac{\alpha}{r_e^{\,2}}\right)\cos w + \alpha^2A^2\left(\frac{\pi}{a}\right)^2$$
$$\times\,(1 + \sin^2 w);$$

$$\zeta_1 = \left(\frac{\partial\mu^2}{\partial r}\right)_e = \epsilon^2\left(r_e - \frac{\alpha}{r_e^{\,2}}\right)\left(1 + \frac{2\alpha}{r_e^{\,3}}\right) + \frac{2\alpha A\pi\epsilon}{a}$$
$$\left[\left(1 + \frac{2\alpha}{r_e^{\,3}}\right)\cos w - \left(r_e - \frac{\alpha}{r_e^{\,2}}\right)\frac{\pi}{2a}\sin w\right] + \alpha^2A^2\left(\frac{\pi}{a}\right)^3\sin w\cos w;$$

$$\zeta_2 = \left(\frac{\partial^2\mu^2}{\partial r^2}\right)_e = 2\epsilon^2\left[\left(1 + \frac{2\alpha}{r_e^{\,3}}\right)^2 - \frac{6\alpha}{r_e^{\,4}}\left(r_e - \frac{\alpha}{r_e^{\,2}}\right)\right]$$
$$-\frac{2\alpha A\pi\epsilon}{a}\left[\left(1 + \frac{2\alpha}{r_e^{\,3}}\right)\frac{\pi}{a}\sin w + \frac{6\alpha}{r_e^{\,4}}\cos w + \left(r_e - \frac{\alpha}{r_e^{\,2}}\right)\left(\frac{\pi}{a}\right)^2\frac{\cos w}{4}\right.$$
$$\left. + \frac{\alpha^2A^2}{2}\left(\frac{\pi}{a}\right)^4(\cos^2 w - \sin^2 w);\right.$$

$$\zeta_3 = \left(\frac{\partial^2\mu^2}{\partial\gamma^2}\right)_e = -\frac{2\alpha A\pi\epsilon}{a}\left(r_e - \frac{\alpha}{r_e^{\,2}}\right)(\cos w + w\sin w + w^2\cos w)$$
$$-2\alpha^2A^2\left(\frac{\pi}{a}\right)^2(w^2 + w\sin w\cos w).$$

Next the integrals given earlier in the expression for $\langle m_t \rangle$ are evaluated. On substituting $r - r_e = \varphi$, the first integral

$$\int_0^\infty \int_{-\pi}^{\pi} \mu^2 r e^{-\Delta u/kT} \, d\gamma \, dr \quad \text{becomes}$$

$$\int_{-r_e}^\infty \int_{-\pi}^{\pi} (\zeta_0 + \zeta_1 \varphi + \tfrac{1}{2}\zeta_2 \varphi^2 + \tfrac{1}{2}\zeta_3 \gamma^2) \cdot (r_e + \varphi) e^{-(\Delta u)_e/kT} e^{-k_r \varphi^2/2kT} e^{-k_\gamma \gamma^2/2kT} \, d\gamma \, d\varphi.$$

The limits of both integrals are changed to $-\infty$ and $+\infty$, which was shown to be justified by numerical evaluation. Furthermore, the integrals of odd functions betwen these limits are zero; hence we obtain the result

$$\int_0^\infty \int_{-\pi}^{\pi} \mu^2 r e^{-\Delta u/kT} \, d\gamma \, dr = \frac{2\pi kT e^{-(\Delta u)_e/kT} r_e}{(k_r k_\gamma)^{1/2}} \left[\zeta_0 + kT \left(\frac{\zeta_2}{2k_r} + \frac{\zeta_3}{2k_\gamma} + \frac{\zeta_1}{k_r r_e} \right) \right].$$

The two other integrals in the numerators of the expression for $\langle m_t \rangle$ are exactly the same form. There remains

$$\int_0^\infty \int_{-\pi}^{\pi} r e^{-(\Delta u)_e/kT} \, d\gamma \, dr = I_0$$

in the denominator. This is evaluated to be

$$\frac{r_e e^{-(\Delta u)_e/kT} \cdot 2\pi kT}{(k_r k_\gamma)^{1/2}}.$$

We thus obtain finally

$$\langle m_t \rangle = \alpha E + \frac{E}{3kT} \left[\zeta_0 + kT \left(\frac{\zeta_2}{2k_r} + \frac{\zeta_3}{2k_\gamma} + \frac{\zeta_1}{k_r r_e} \right) - \left(\xi_0 + kT \left(\frac{\xi_2}{2k_r} + \frac{\xi_3}{2k_\gamma} + \frac{\xi_1}{k_r r_e} \right) \right)^2 - \left(\eta_0 + kT \left(\frac{\eta_2}{2k_r} + \frac{\eta_3}{2k_\gamma} + \frac{\eta_1}{k_r r_e} \right) \right)^2 \right].$$

On using the explicit forms of ζ_0, ξ_0, η_0, it is then readily shown that $\zeta_0 - \xi_0^2 - \eta_0^2 = 0$ and $\zeta_1 - 2\xi_0\xi_1 - 2\eta_0\eta_1 = 0$. We thus obtain the approximate answer

$$\langle m_t \rangle = \alpha E + \frac{E}{3kT} \left[kT \left(\frac{\zeta_2 - 2\xi_0 \xi_2 - 2\eta_0 \eta_2}{2k_r} + \frac{\zeta_3 - 2\xi_0 \xi_3 - 2\eta_0 \eta_3}{2k_\gamma} \right) \right],$$

and this should be compared with the Debye term for orientational polarization $\frac{E}{3kT} \mu_g^2$, where μ_g is the dipole moment of the gaseous molecule.

Numerical results for the orientational part of $\langle m_t \rangle$ at a temperature of 200°K. and distances of 2.0 and 2.5×10^{-8} cm. from the surface are given in Table I. As noted earlier, the form employed for the energy of the molecule above the crystal surface leads to the result that at a distance of about 3.0×10^{-8} cm. from the surface the energy is not a minimum for the position $\gamma = 0$, since the constant k_γ has become negative. In view of the simplifications made in the model of the adsorbed molecule and its restricted movements, this result has not been investigated farther. The numerical values obtained at the two closer distances seem sufficient to establish the low value of the orientational polarization.

There is another point of interest arising from the numerical values of k_r and k_γ also given in Table I. The frequency of vibration along r and of rotational oscillation about the equilibrium position with no external field can be obtained from the approximate expressions

$$\frac{1}{\pi}\sqrt{\frac{k_r}{M}} \text{ and } \frac{1}{\pi r_e}\sqrt{\frac{k_\gamma}{M}},$$

respectively. Values of these frequencies are also given in the table. It is clear from the variation of rotational frequency with distance from the surface that a method of obtaining the equilibrium distance from the surface might be developed through observation of the rotational frequency, although in this case the rotational frequency of gaseous hydrogen chloride appears to be very close to that predicted for the oscillatory rotations of the adsorbed molecule (11).

Discussion

It has been shown that the contribution of a dipolar molecule adsorbed on an ionic surface to the orientational polarization will be much less than for the free gaseous molecule. This is true in spite of the large induced dipole created in the molecule by the field of the surface. It may be instructive also to mention a physically unrealistic model as a limiting case. If the surface field is considered to induce a dipole in the adsorbed molecule, and if this increased dipole is able to rotate freely on the surface under the influence of an applied field, the maximum effect from the induced dipole would be obtained. This case was worked out for a dipole consisting of point charges. The distance between the charges was assumed to have

TABLE I

Orientational Polarization and Frequencies of Oscillation for Hydrogen Chloride, Adsorbed on the {100} Face of Sodium Chloride at 200°K.

Distance from the surface (*cm.*)	Polarization of the adsorbed molecule $\times \frac{3kT}{E}$	Polarization of the free gaseous molecule $\times \frac{3kT}{E}$	Frequency vibration along r (*sec.*$^{-1}$)	Frequency of oscillation about $\gamma = 0$ (*sec.*$^{-1}$)	Value of k_r (*dynes cm.*$^{-1}$)	Value of k_γ (*ergs*)	Value of r_e (*cm.*)
2.0×10^{-8}	1.73×10^{-39}	1.10×10^{-36}	3.10×10^{13}	2.60×10^{12}	5.73×10^{5}	7.24×10^{-13}	$1.362_6 \times 10^{-8}$
2.5×10^{-8}	8.31×10^{-39}	1.10×10^{-36}	3.00×10^{13}	8.80×10^{11}	5.38×10^{5}	8.03×10^{-14}	$1.314_5 \times 10^{-8}$

the value required for the equilibrium separation of the charges in the field from the surface for all positions about the equilibrium position without applied external field. This condition was described approximately through the equation $\mu = \mu_g + \mu_i \cos\gamma$, where μ_g is the value of the dipole of the free gaseous molecule and μ_i is that of the induced dipole at $\gamma = 0$. The variation of the dipole with γ was found by numerical computation to be sufficiently well expressed by the equation up to angles of 30° for the surface potential field given by $\phi = A \cos\frac{\pi x}{a} \cos\frac{\pi y}{a}$. In conjunction with this expression for the dipole moment, the Boltzmann factor $e^{-\boldsymbol{\mu}\cdot\mathbf{E}/kT}$ was employed in the averaging process, which corresponds with the assumption that the dipole is a free rotator. The result for the orientational polarization was

$$\langle m \rangle = \frac{E}{3kT}\left(\mu_g^2 + \frac{\mu_i^2}{8}\right).$$

Thus, even if μ_i is as great as $\mu_g/2$, the contribution to the orientational polarization from the induced dipole is only about 3% of the total term.

Such a model is deficient in its neglect of the restoring force to the equilibrium position without applied field. To consider it emphasizes the negligible effect of induced dipoles. More important, however, is the realization that when the potential energy is correctly expressed, the motion must be oscillatory. For dipolar molecules in the first adsorbed layer on ionic solids this conclusion appears quite general. One would therefore not expect the orientational polarization to be as large as the Debye term.

It was pointed out in the introductory paragraph that nonpolar molecules with polarizabilities which are independent of direction will exhibit no tendency to align themselves in an applied field. If the polarizability does depend upon direction a preferred orientation on the surface will be established. On application of an electric field a dipole will be induced in the molecule, and since the polarizability is not isotropic, the resulting dipole in general will not be parallel to the applied field. Thus a torque tending to turn the molecule will result, but it will be of much smaller magnitude than for a dipolar molecule. Moreover, since the field from the surface remains fixed, if the molecule does turn its potential energy in the field from the surface will increase, and this will reduce the loss of potential energy to be expected from alignment in the applied field. Contributions to orientational polarization because of dipoles induced by the surface fields would thus appear to be unimportant. Where permanent moments have been computed for nonpolar adsorbates (1, 3), the cause must be the particular formulation used to derive the polarization from the experimental data.

CONCLUSION

The criterion suggested by Channen and McIntosh (1) for testing the formulas used to deduce polarization of adsorbed molecules in heterogeneous dielectric systems of adsorbate and adsorbent seems justified. This criterion is that nonpolar adsorbates, or polar adsorbates which are known not to contribute to orientational polarization, should reveal polarizabilities for the adsorbed state very similar to the distortion polarizability of the bulk material. This conclusion has been established by showing that dipoles induced by the surface fields do not raise the orientational polarization of an adsorbed dipolar molecule above that expected for the gaseous molecule. For nonpolar adsorbates no appreciable orientational polarization is to be expected owing to the existence of induced dipoles arising from the field at the surface of the crystal.

REFERENCES

1. CHANNEN, E. W., AND MCINTOSH, R., *Can. J. Chem.* **33**, 172 (1955).
2. HIGUTI, I., *Bull. Inst. Phys. Chem. Research (Tokyo)* **20**, 489 (1941).
3. KAMIYOSHI, K., *Science Repts. Research Insts. Tôhoku Univ.* **A3**, 513 (1951).
4. KURBATOV, L. N., *J. Phys. Chem. (U.S.S.R.)* **24**, 899 (1950).
5. KUROSAKI, S., *J. Phys. & Colloid Chem.* **58**, 320 (1954).
6. SHIMIZU, M., *Science Repts. Tôhoku Univ. First Ser.* **37**, 136 (1953).
7. DEBYE, P., "Polar Molecules," p. 59. Chemical Catalogue Co., New York, 1929.
8. HERZBERG, G., "Molecular Spectra and Molecular Structure. Spectra of Diatomic Molecules," pp. 82, 98. Van Nostrand, New York, 1950.
9. VAN DER HOFF, B. M. E., AND BENSON, G. C., *Can. J. Phys.* **31**, 1087 (1953).
10. VERWEY, E. J. W., *Rec. trav. chim.* **63**, 521 (1946).
11. HERZBERG, G., "Molecular Spectra and Molecular Structure. Spectra of Diatomic Molecules," p. 81. Van Nostrand, New York, 1950.

JOURNAL OF COLLOID SCIENCE **11,** 608–616 (1956)

THE TRANSFER OF SURFACE FILMS THROUGH SURFACE CHANNELS—GEOMETRICAL FACTORS

Victor K. La Mer and Martin Blank

The Department of Chemistry, Columbia University, New York, New York

Received June 8, 1956

I. Abstract

Mixtures of certain substances, spread as monolayers, can be separated into their components by a process of transferring the monolayer through channels from a higher to a lower surface pressure. When a mixture is separable, the order of separation of the components depends upon their surface pressures.

The mechanism of the transfer process has been investigated. The rate of transfer is directly proportional to the difference in surface pressures of the initial and final states of the film and inversely proportional to a "resistance" which is dependent upon the geometry of the channel. Expressions have been derived for the rate of transfer as affected by the angle of the groove of the channel and the height of the barrier over which the channel passes. These formulas have been verified using brass grooves wetted with water and cyclohexyl myristate spread as the monolayer on water.

II. Introduction

Abribat, Rosano, and Vaillet (A, R, and V) have reported recently in a note (1) that it was possible to separate a mixture of decyl alcohol, oleic acid, and methyl laurate by a method which they called "distillation isotherme superficielle." They deposited the mixture upon a subphase as a monolayer with the excess remaining as lenses. This surface was connected to a second water surface by a set of glass rods in contact with each other and bent as shown in Fig. 1. Flowing water removed continuously any film that was transferred by the rods to the receiving surface so that the surface pressure at this place was always effectively zero. It is essential that the glass rods be clean and well wetted by the water.

By measuring the surface pressure on surface 1 with a dipping plate surface manometer, they observed a surface pressure-time curve that resembled in appearance a titration curve of a tribasic acid or, perhaps better still, a polarographic curve of a ternary mixture. They pointed out that such a method should permit the identification and analysis of the components of a mixture.

In Fig. 2 we show one of our typical results for a mixture of Adol 22,[1]

---

[1] Archer Daniels Midland Company sample containing a mixture of fatty alcohols (88% erucyl, 8% oleyl, and 4% linoleyl).

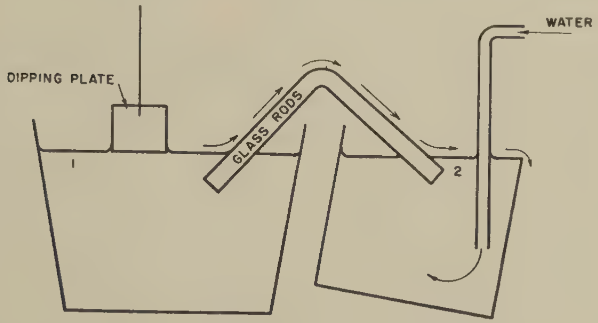

FIG. 1. Apparatus for film transfer.

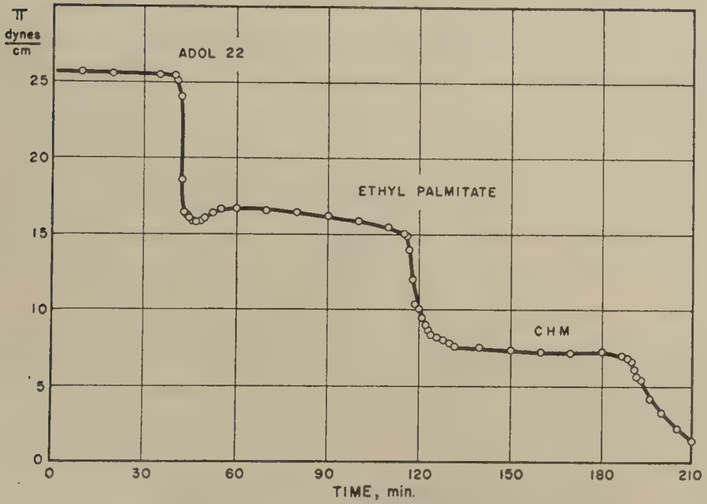

FIG. 2. Transfer curve for the ternary mixture of Adol 22, ethyl palmitate, and cyclohexyl myristate (CHM). Surface pressure (π) vs. time.

ethyl palmitate, and cyclohexyl myristate (CHM) using the technique just described, thus confirming the essential features of the preliminary result of A, R, and V. The components of the mixture transferred progressively in the order of decreasing surface pressures under suitable experimental conditions.

We do not find, however, a horizontal plateau in the transfer curve but rather one of small negative slope. We believe this is due to some mixing of components in the film.

We also confirm the comment of A, R, and V that it is not always possible to get separations of the type indicated in Fig. 2. Adol 22[1] can not be separated into the several fatty alcohols of which it is composed, presumably because the surface pressures of the components are not sufficiently different. However, there are also cases in which the pressures differ by 10 dynes $cm.^{-1}$ where separation does not occur.[2]

---

[2] See p. 688 for Note Added in Proof.

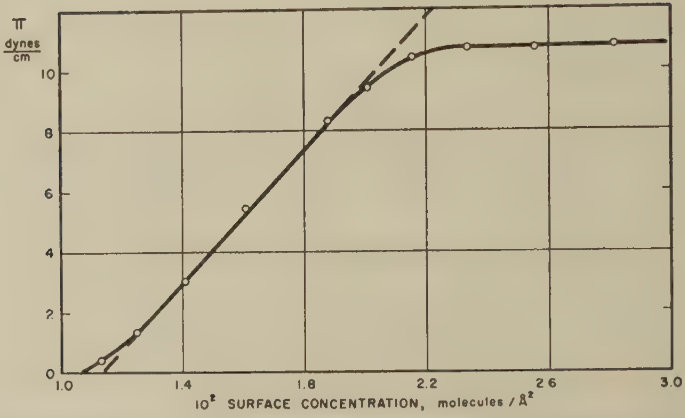

FIG. 3. Surface pressure vs. surface concentration for CHM at 27.0° C.

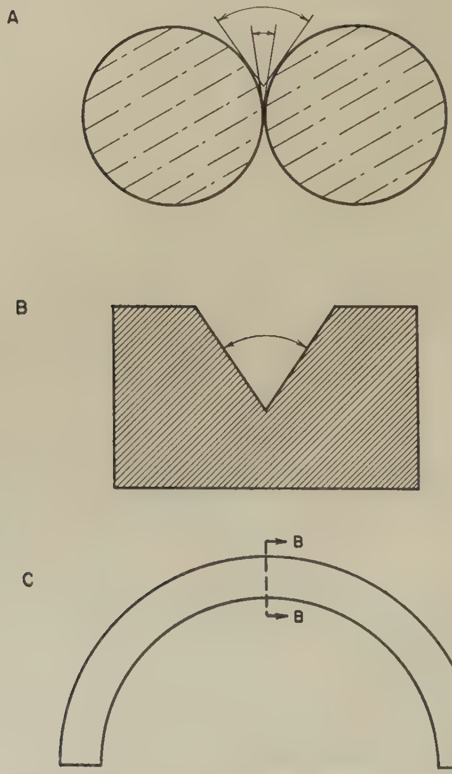

FIG. 4. Description of channel. *A:* cross section of glass rods, *B:* (cross section), *C:* (side view) brass groove.

Since this method obviously opens up a new field of endeavor with important possibilities, we have undertaken an investigation of the mechanism of the transfer process and of the types of curves obtained with different pure substances before proceeding further in the matter of the separation of mixtures.

This paper will be restricted to a study of the nature of the process whereby a film of cyclohexyl myristate (CHM) is transferred from one water surface to another on a machined groove in a brass ring.

Cyclohexyl myristate was chosen because it is a liquid at room temperature [(m.p. 25.8) index of refraction $n_D^{27.2} = 1.4536$] and has desirable surface properties (Fig. 3).

A brass ring was used in place of the glass rods for reasons evident from Figs. 4*A* and 4*B*. When a set of glass rods are in parallel orientation and in contact, they form a set of grooves. However, these grooves possess a variable angle depending upon the position at which the angle is measured. It is better to use a single groove having planar sides forming a well-defined angle (Fig. 4*B*), so that simple expressions for the rate of transfer can be derived and tested experimentally. The grooves in each ring used were machined at different angles to a precision of at least one degree. (See Figs. 4*B* and 4*C*.)

III. THE "GEOMETRIC RESISTANCE" *R*

We conceive of the transfer process as motivated by the difference in surface pressures between the two surfaces and retarded by a "Geometric Resistance" *R* determined by the shape of the path over which the film moves. In other words

$$\text{Rate} \propto \frac{\text{“Driving Force”}}{\text{“Geometric Resistance”}}. \qquad [1]$$

We assume that the "Geometric Resistance" is directly proportional to the length of the path and varies inversely as the width.

The calculation of *R* is somewhat involved. The water wets the brass ring along its groove, but the thickness of the water layer decreases with height owing to gravity. The fundamental equation of capillarity, which shows the effect of gravity, is

$$\gamma\left(\frac{1}{r} + \frac{1}{r'}\right) = gh(\rho - \rho'), \qquad [2]$$

where γ = surface tension, h = height, r, r' = radii of curvature of surface, $\rho - \rho'$ = difference in density (water, air), and $\rho - \rho' \cong \rho$.

Figure 5*A* illustrates the groove. From the equations relating the contact angle at an interface to the surface tensions it can be shown that the contact angle of the water in the groove (with a film on it) will remain prac-

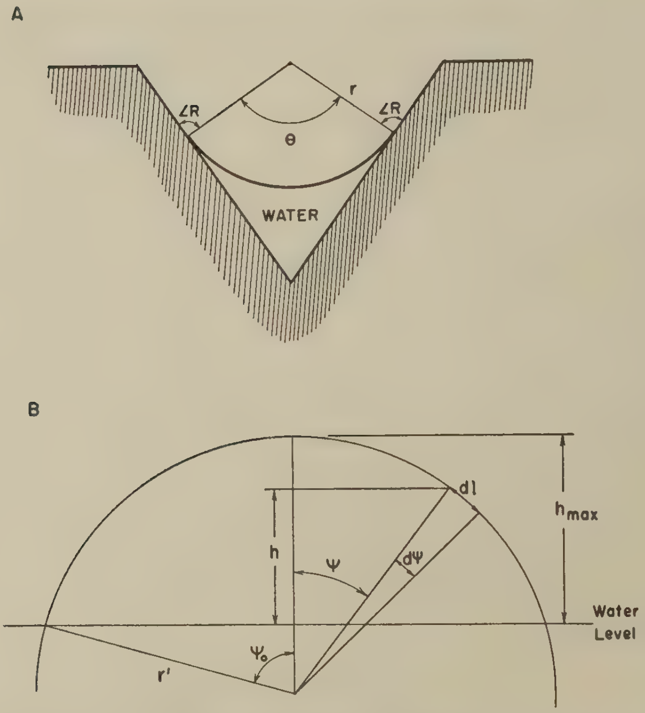

FIG. 5. Geometry of channel. Description in text.

tically constant and nearly zero degrees throughout the experiment. We take the contact angle as constant and equal to zero. The water wets the brass with the same contact angle at any height. The width of the path over which the film is transferred is $r\theta$ at all points.

To get the length of the path one integrates along that part of the groove above the water surface. From Fig. 5*B* we see that

$$\begin{aligned} dl &= r'\,d\psi; \\ h &= r'\cos\psi - r'\cos\psi_0\,. \end{aligned}$$

Utilizing Eq. [2] and substituting into

$$R = \frac{\text{length}}{\text{width}} = \int \frac{dl}{r\theta}$$

we get

$$R = \frac{2}{\theta}\int_0^{l/2}\left(\frac{\rho g h}{\gamma} - \frac{1}{r'}\right) dl.$$

It can be shown that $1/r'$ is negligible.

$$R = \frac{2\rho g}{\theta\gamma}\int_0^{\psi_0} (r'\cos\psi - r'\cos\psi_0) r'\,d\psi,$$

which upon integration yields

$$R = \frac{2\rho g r'^2}{\theta\gamma} (\sin\psi_0 - \psi_0 \cos\psi_0). \qquad [3]$$

Equation [3] gives the geometric resistance. R has the form

$$R = \frac{K}{\gamma}, \qquad [3a]$$

where $$K = \frac{2\rho g r'^2}{\theta} (\sin\psi_0 - \psi_0 \cos\psi_0).$$

IV. The Rate of Transfer of Film

From the surface pressure-surface concentration curve for CHM (Fig. 3) it can be seen that for the range 1–9 dynes cm.$^{-1}$ we can write to a good approximation that the surface concentration

$$c = -k'\gamma + k'', \qquad [4]$$

where k' is a positive number. From Eq. [1] we set

$$-\frac{dc}{dt} = k'\frac{d\gamma}{dt} = k\frac{(\gamma_0 - \gamma)}{K/\gamma},$$

where c = surface concentration, k = proportionality constant, γ_0 = surface tension of water, $\gamma_0 - \gamma = \pi$ = surface pressure, and $R = K/\gamma$ as in Eq. [3a]. Integration yields

$$\int_{\gamma_i}^{\gamma} \frac{d\gamma}{\gamma(\gamma_0 - \gamma)} = \int_0^t \frac{k\,dt}{k'K} \qquad [5]$$

$$\log\frac{\gamma_0 - \gamma}{\gamma} = -\frac{k\gamma_0}{k'K}t + \log\frac{\gamma_0 - \gamma_i}{\gamma_i} \qquad [6]$$

where γ_i = initial surface tension of film.

Upon substituting for K we get

$$\log\frac{\gamma_0 - \gamma}{\gamma} = -\frac{\gamma_0\theta k t}{2k'\rho g r'^2(\sin\psi_0 - \psi_0\cos\psi_0)} + \text{const.} \qquad [7]$$

Equation [7] was tested as follows.

a. Dependence upon Surface Tension. For constant θ and h (ψ_0 is a function of h only) Fig. 6 gives the data of a typical run. The agreement occurs in the range where Eq. [4] holds, i.e., the surface concentration is a linear function of the surface tension.

b. Dependence upon Groove Angle. Utilizing the approximation of Section III that the contact angle is zero degrees, it follows that θ in Eq. [7] is the supplement of the groove angle. Defining the slope K' of the line in Fig. 6 by the expression

$$\log\frac{\gamma_0 - \gamma}{\gamma} = K't + \text{constant},$$

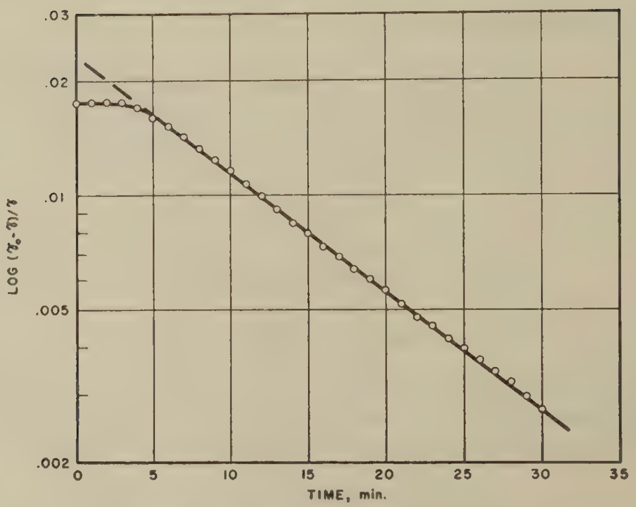

FIG. 6. Typical curve showing log $(\gamma_0 - \gamma)/\gamma$ vs. time. Slope $= -(\gamma_0\theta k)/2k'\rho g(\sin\psi_0 - \psi_0\cos\psi_0)$

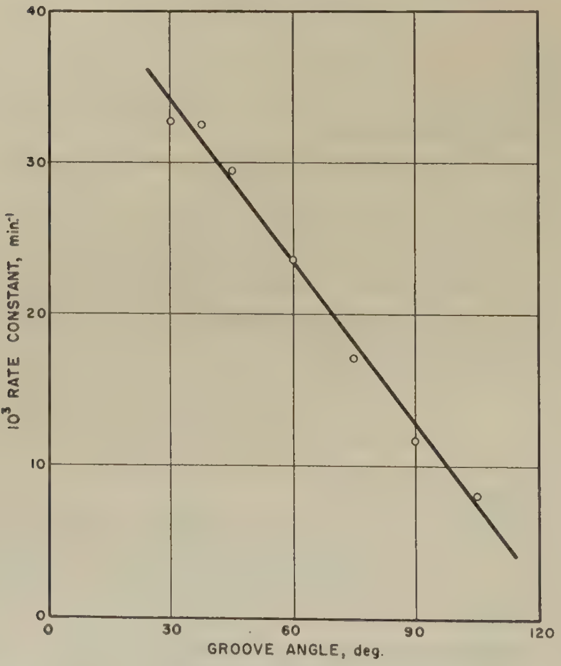

FIG. 7. Rate constant vs. groove angle.

we see that K' should vary directly as θ, and, therefore, directly as the groove angle. The results are shown in Fig. 7 and are in agreement with prediction.

c. *Dependence on Height.* The dependence of the transfer rate upon the

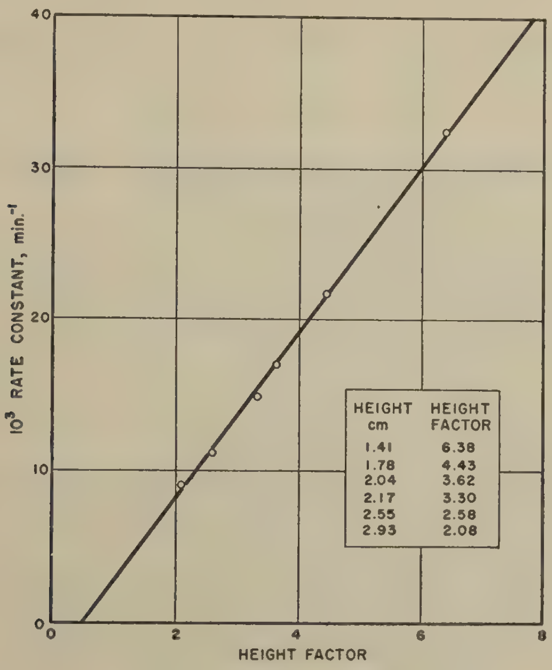

HEIGHT cm	HEIGHT FACTOR
1.41	6.38
1.78	4.43
2.04	3.62
2.17	3.30
2.55	2.58
2.93	2.08

FIG. 8. Rate constant vs. height factor.

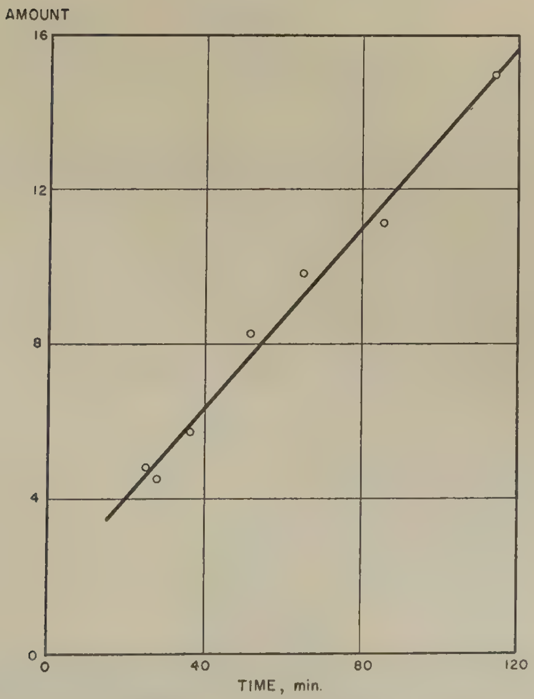

FIG. 9. Amount of CHM (in arbitrary units) vs. time for transfer.

maximum height of the barrier is given by a factor f defined as

$$f = \frac{1}{(\sin \psi_0 - \psi_0 \cos \psi_0)}$$

since $$\psi_0 = \cos^{-1}\left(\frac{r' - h_{\max}}{r'}\right).$$

The value of f was computed for several values of $h_{\max}$. The results given in Fig. 8 show that K' is linear with f in accord with prediction.

A further test was performed utilizing a constant surface pressure difference by having an excess of a pure surfactant during a run. The value of R was constant since all the quantities on which it depended, namely θ, γ, and $h_{\max}$ were constant. The rate of transport of film should, therefore, be constant, and the amount of time for the substance to be transported should be proportional to the amount present.

A lens was deposited using a calibrated micropipet, and the time measured until the surface pressure fell below its saturation value, indicating a change in the surface concentration (Fig. 3).

Figure 9 gives the data for varying amounts of CHM on the surface. The explanation for the non-zero intercept is that the end of a run occurs when a certain amount of substance remains as a saturated film on the water.

V. Discussion

The expression for the rate constant contains quantities which are determined by the geometry of the system and also quantities specific to the film and substrate.

Only the geometrical factors and the surface tension dependence have been tested in this paper. Both k', which is determined by the equilibrium properties of the film (Eq. [4]), and k, which should be related to flow properties, must be tested further. In measuring surface viscosity Harkins (2), Dervichian, Joly (3), and others have used systems in which films move through slits under small pressure differences. Our results, although not in complete agreement with previous work, have the advantage of describing the flow of film over a larger continuous range.

Acknowledgments

The problem of separating components was brought to our attention by Dr. Henri L. Rosano, while he was in this Laboratory.

We gratefully acknowledge the grant of a Fellowship to Martin Blank from Consumers' Union, which made this work possible, and also express our thanks to Dr. Thor A. Bak for his aid and interest during the course of this research.

References

1. Abribat, M., Rosano, H. L., and Vaillet, G., *Compt. rend.* **238**, 1219 (1954).
2. Harkins, W. D., and Myers, R. J., *J. Chem. Phys.* **5**, 601 (1937).
3. Dervichian, D. G., and Joly, M., *Compt. rend.* **204**, 1318 (1937).

JOURNAL OF COLLOID SCIENCE **11**, 617–622 (1956)

CALCULATION OF MEMBRANE PRESSURE FOR A SOL OF SPHERICAL PARTICLES

R. K Schofield[1]

With mathematical appendix by

D. H. Rees[1]

Received April 5, 1956

ABSTRACT

Electronic computation has been used to obtain the Poisson-Boltzmann distribution of counter ions between an outer spherical surface, radius R_0, where the potential gradient is zero, and an inner concentric surface, radius R, representing a uniformly charged spherical particle. Here c_0 is the concentration of the counter ions at the outer surface, and c_m is their mean concentration in the volume between the two surfaces. The results of the computations are given in a plot of c_0/c_m against $\ln \frac{R}{R_0}$. For given values of R and R_0, c_0 at first increases linearly with the number of counter ions per particle, but ultimately approaches a limit. Values of the membrane potential, p_0, are calculated from the equation $p_0 = NkT(c_0 + C)/1000$ for 1% and 0.1% sols of particles 10^{-6} cm. in radius.

INTRODUCTION

Using Donnan's theory to calculate the equilibrium pressure, p, across a membrane separating pure water from a dilute aqueous sol of charged spherical particles one obtains as a first approximation

$$p_m = \frac{NkT}{1000}(c_m + C). \qquad [1]$$

In this expression N is Avogadro's number, k Boltzmann's constant, T the absolute temperature, c_m the mean molar concentration of the counter ions, and C the molar concentration of the particles. Equation [1] gives an overestimate of the membrane pressure if the concentration, c, of the counter ions at the charged surfaces of the particles greatly exceeds their concentration, c_0, at points furthest away from the particles. It seems to the author that the equation

$$p_0 = \frac{NkT}{1000}(c_0 + C) \qquad [2]$$

should provide a better approximation to the membrane pressure than Eq. [1].

---

[1] Rothamsted Experimental Station, Department of Statistics, Harpenden, Herts., England.

METHOD

With this thought in mind the author enlisted the help of Dr. P. M. Grundy, who explored means for solving the Poisson-Boltzmann equation applied to the space between an outer spherical surface of radius R_0, at which the potential gradient is zero and the ionic concentration is c_0, and an inner concentric surface of radius R representing a uniformly charged spherical particle at which the ionic concentration is c. Taking the case where all the counter ions have the same valency ν, Dr. Grundy introduced a parameter t defined by the equation

$$t^2R^2c = t_0^2R_0^2c_0 = \frac{4}{\nu^2\beta} \qquad [3]$$

in which β stands for $\dfrac{8\pi\epsilon^2N}{1000\ DkT}$, ϵ being the electron charge and D the dielectric constant. For any chosen value of t_0, t can be related to $\ln\dfrac{R}{R_0}$ by numerical integration (see Appendix).

Integrations were carried out on the E.D.S.A.C. at Cambridge through the kind cooperation of Dr. J. C. P. Miller. These computations provided part of the data used in preparing Fig. 1. More recently Mr. D. H. Rees

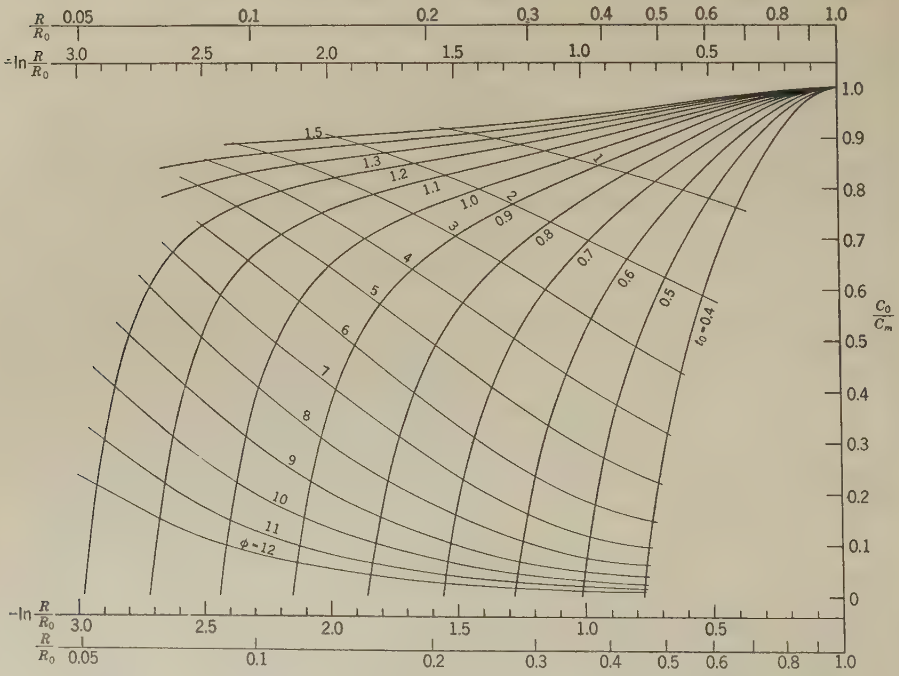

FIG. 1. c_0/c_n plotted against ln R/R_0 for constant values of t_0 and ϕ.

TABLE I

				For R = 10^{-6} cm.		
$\frac{R}{R_0}$	t_0	$\frac{c_0}{c_m}$	ϕ	c_0 (*millimoles per liter*)	p_0 (*cm. of water*)	$\frac{c_m}{C}$ counter ions per particle
			1% Sol			
0.217	0.69	∞	∞	0.374	9.4	∞
“	0.7	0.100	9.07	0.364	9.2	875
“	0.8	0.534	4.48	0.278	7.1	127
“	0.9	0.696	3.18	0.220	5.6	77
“	1.0	0.777	2.43	0.178	4.5	56
“	1.1	0.828	1.94	0.147	3.8	43
“	1.2	0.862	1.59	0.124	3.2	35
“	1.3	0.887	1.34	0.105	2.7	29
“	1.4	0.905	1.14	0.091	2.4	24
“	1.5	0.919	0.98	0.079	2.1	21
			0.1% Sol			
0.101	0.95	∞	∞	0.0428	1.1	∞
“	1.0	0.387	8.18	0.0386	1.0	242
“	1.1	0.656	5.78	0.0319	0.8	115
“	1.2	0.779	4.57	0.0268	0.7	84
“	1.3	0.832	3.77	0.0229	0.6	67
“	1.4	0.867	3.17	0.0198	0.5	55
“	1.5	0.890	2.72	0.0172	0.4	47

has used the computer at Rothamsted to trace the values of t to the limit $t = 0$ for $t_0 = 0.4, 0.5 \cdots 1.2$. At the same time values were obtained for the ratio c_0/c_m, where c_m is the mean molar concentration of counter ions in the volume between the concentric spheres of radii R_0 and R, respectively.

RESULTS

Figure 1 is a plot of c_0/c_m against $\ln \frac{R}{R_0}$. To illustrate its use let us consider its application to a sol in which uniform spherical particles are dispersed in 97 times their volume of water. Taking $(R_0/R)^3 = 98$ gives $R/R_0 = 0.217$, so we read off the values of c_0/c_m at which the curves for successive values of t_0 intersect the vertical for $R/R_0 = 0.217$. These values are set out in the third column of the upper part of Table I. The corresponding values of $\phi = \ln \frac{c}{c_0}$ are given in the fourth column. These can also be read roughly from Fig. 1. They are not used in the following calculations, but are included for general interest. A unit value of ϕ is approximately equal to 25 mv. difference in electrical potential between the outer sphere and the particle surface.

If we take $R = 10^{-6}$ cm., R_0 is 4.6×10^{-6} cm.; from Eq. [3]

$$c_0 = \frac{4}{t_0^2 R_0^2 \nu^2 \beta}.$$

Taking $\nu = 1$ and $\beta = 1.06 \times 10^{15}$ cm./millimoles, we obtain

$$c_0 = \frac{0.178}{t_0^2} \text{ millimoles/liter.}$$

The values of c_0 obtained in this way are entered in the fifth column of Table I, and the corresponding values of p_0 (Eq. [2]) in centimeters of water are given in the sixth column. The concentration of the particles themselves to the membrane pressure is only 1 mm., since in a solution containing 1 millimole/liter each molecule occupies 1.661×10^{-18} cm.^{3} and so

$$C = \frac{3 \times 1.661}{4\pi(4.6)^3} = 0.00407 \text{ millimoles/liter.}$$

The last column shows the number of univalent counter ions balancing the charge on each particle which is given by c_m/C.

A similar calculation was made for a more dilute sol of volume ration 970, i.e., $R/R_0 = 0.101$. The results are given in the lower part of Table I. The value of R was again taken to be 10^{-6} cm. so $R_0 = 9.9 \times 10^{-6}$ cm. Here C is just ten times smaller than before, but for the same charge per particle c_0 is not reduced to quite one-tenth. This reflects the fact that, for the same particle charge, c_0/c_m is greater for the more dilute sol.

DISCUSSION

It will be seen from both parts of Table I that as the charge on the particles increases the membrane pressure p_0, approaches a maximum value. Most of the surface charge densities implied in Table I are low; even 875 unit electron charges on the surface of a particle 10^{-6} cm. in radius corresponds to an area of 144 A.^{2} per unit charge.

The entries in the last three columns of Table I depend on the arbitrary choice of 10^{-6} cm. for R. To construct a table for $R = 2 \times 10^{-6}$ cm., the values of c_0 and p_0 in Table I must be divided by 4, while the values of c_m/C must be doubled. The surface densities of charge will be halved.

If R were increased to 10^{-5} cm., the maximum membrane pressure for a 1% sol would be only 1 mm. of water. If R were reduced to 10^{-7} cm., membrane pressures approaching 100 cm. of water would be given by a 0.1% sol, but the particles would carry only a few unit charges so that c_0 would not greatly exceed C. Thus the treatment developed in this paper is best suited to aqueous sols of spherical particles neither much larger nor much smaller than 10^{-6} cm. in radius. For larger particles the pressures could be increased by using more concentrated sols, but caution is needed in applying the treatment when R/R_0 exceeds 0.4.

In conclusion, brief consideration will be given to the effect of a small external electrolyte concentration on the equilibrium membrane pressure. We take the case represented by the fifth row of Table I, but suppose that externally there is 2×10^{-5} M concentration of uni-univalent electrolyte. The ion product, being 4×10^{-10} outside, must have the same value inside, the expected values being 0.179 and 0.002 millimole/liter. As before C is 0.004, so the total inside concentration is 0.185. Since the total outside concentration is 0.040, the concentration difference effective in producing the membrane pressure is 0.145, giving a pressure of 3.6 cm. of water instead of 4.5 cm.

Appendix

With only one kind of ion present the Poisson-Boltzmann equation takes the form

$$\nabla^2\psi = \frac{-4\pi\nu\epsilon N c_0}{1000D} e^{\frac{-\nu\epsilon\psi}{kT}}, \qquad [4]$$

where ψ is the electric potential, ν the valency of the counter ions, ϵ the electronic charge, N Avogadro's number, D the dielectric constant, k Boltzmann's constant, and T the absolute temperature. The molar concentration of the counter ions at the surface of an inner sphere of radius R whose potential is $-\psi$ is given by c. In particular, $c = c_0$ on the surface of the sphere of radius $R = R_0$ with zero potential.

By making the following substitutions and taking into account the spherical symmetry of the system, Eq. [4] can be reduced to

$$\frac{1}{r^2}\frac{d}{dr}\left(r^2\frac{d\phi}{dr}\right) = 2e^{\phi-\phi_0}, \qquad [5]$$

where

$$\phi = \frac{-\nu\epsilon\psi}{kT} = \ln\frac{c}{c_0}$$

$$\beta = \frac{8\pi\epsilon^2 N}{1000DkT} = \frac{4}{t^2R^2\nu^2c} \qquad \text{(by virtue of Eq. [3])}$$

$$r = \frac{R}{R_0}$$

$$t_0^{\,2} = e^{\phi_0}$$

The problem has been to find the first value of r (<1) for which ϕ becomes infinite given the initial values

$$\phi = \phi_0$$

$$\frac{d\phi}{dr} = 0$$

at $$r = 1.$$

The solutions calculated on the E.D.S.A.C. were derived from the numerical integration of an equation of the same form as Eq. [5]. Because of the rapid increase in the values of ϕ these results were useful only over a limited range of values of r. In particular, the limiting value of r as $\phi \rightarrow \infty$ could not be determined. In order to determine the whole range of values of r the substitution $u = \ln r$ was made. This reduced Eq. [5] to the pair of first-order differential equations

$$\frac{d\zeta}{du} = \frac{\zeta - \zeta t - t^2 - 1}{t}, \qquad \frac{dt}{du} = \zeta, \tag{6}$$

with the initial conditions

$$t = t_0, \qquad \frac{dt}{du} = -t_0 \quad \text{at} \quad u = 0.$$

The integration of these equations was carried out on the Elliott Bros. "401" digital computer, now located at Rothamsted Experimental Station, with the use of a modified form of the Runge Kutta process (1). An integration interval of 2^{-9} was used and at every 17th step values of u, t, $\frac{dt}{du}$, $\frac{c_0}{c_m}$, and $e^{-\frac{1}{2}\phi}$ were printed. When t first became $\leq 2^{-6}$ the program was reset automatically to print out every step of the integration.

The graphs in Fig. 1 for $t_0 = 0.4, 0.5 \cdots 1.2$ were drawn directly from the printed results. The graphs for $t_0 = 1.3, 1.4, 1.5$ were drawn from calculations based on E.C.S.A.C. results as far as they were valid. The curves for constant ϕ were determined by standard interpolation.

REFERENCE

1. Wilkes, M. V., Wheeler, D. S., and Gill, S., "Programs for an Electronic Digital Computer." Addison Wesley Press, Cambridge, Massachusetts, 1951.

JOURNAL OF COLLOID SCIENCE **11**, 623–636 (1956)

RECENT WORK ON SURFACE ACTIVITY, WETTING AND DEWETTING

Jean Guastalla

Laboratoire de Chimie Physique, Faculté des Sciences, Paris

Received April 5, 1956

SURFACE ACTIVITY

a. Theoretical

Let γ be the work necessary to increase isothermally and reversibly the free surface area of a pure liquid (i. e., the *surface tension*).

The liquid is placed in a trough. Let us imagine that one of its edges can be displaced; the work necessary to move horizontally this edge of length L over a distance dl in order to increase isothermally and reversibly the free surface area of the liquid an amount $dS = L\,dl$, is equal to $\gamma\,dS = \gamma L\,dl$. This work is done by a mechanical force f which moves the point at which it is applied over a distance dl; at equilibrium, $f\,dl = \gamma L\,dl$, or $\gamma = f/L$.

The pure liquid is then replaced by a very dilute solution of a surface-active substance; the work γ_{inst} which the experimenter would have to do *if no adsorption ocurred*, is in fact smaller since the experimenter recovers, while working to increase the area of the surface, the adsorption work on the newly created surface, this work being W_{ads} per cm.^{2} (provided he works isothermally and reversibly). Therefore, the work which the experimenter must supply (per cm.^{2}) is $\gamma_{\text{solut}} = \gamma_{\text{inst}} - W_{\text{ads}}$. The instantaneous tension γ_{inst} is practically identical with the surface tension γ_0 of the pure solvent if the solution is very dilute; the adsorption work W_{ads} is then represented by the lowering of the surface tension or *surface pressure* p:

$$\gamma_{\text{solut}} = \gamma_0 - p.$$ [1]

Experimentally, the trough with a movable edge cannot be used for measuring the surface tension γ because of friction and hydrostatic effects; but the wettable plate method (Wilhelmy, Lord Rayleigh) is an equivalent procedure which is very convenient and direct.

A rectangular plate is immersed in a liquid which wets it perfectly and is then partially withdrawn in such a way as to outreach the tangential position of the meniscus; if we then lift the plate a distance dh, the area of the liquid film wetting the plate will be increased by $dS = \varpi\, dh$ (ϖ = the perimeter of the plate), by doing work $\gamma\varpi\, dh$ against the surface tension γ. The work is supplied by a mechanical force f which displaces the point where it is applied vertically a distance dh; at equilibrium $\gamma\varpi\, dh = f\, dh$, $\gamma = f/\varpi$.

---

[1] This kind of approach will be particularly useful as applied to wetting, discussed later (1, 2).

To measure γ we use a direct-reading balance with an horizontal torsion wire; the movable equipment comprises a galvanometer mirror (R = 200 cm.) and a rod 2 cm. long, positioned nearly horizontally during measurements, at the end of which the wettable plate is suspended by a silk thread. Displacements of a spot are observed on a scale.

The buoyancy on the plate cannot be neglected. It is convenient to include its variations in the calibration of the apparatus (3, 4); the calibration is carried out by means of riders, while the wettable plate suspended from the balance is partially immersed in a liquid having a stable surface tension and the same density as the experimental solution. Then, after the spot is brought to the zero position, the surface of the solution is slowly brought into contact with the lower edge of the plate. As soon as contact is established the plate will be slightly immersed. The surface tension may then be directly calculated from the deviation of the spot along the scale.

The plates used are made of rough platinum or rough mica. The accuracy of the measurements may be better than 0.1 dyne/cm.

We have also frequently used the Dognon and Abribat tensiometer, where a wettable rough platinum plate is suspended from an electromagnetic balance (5).

b. Determination of the Traube Coefficient

The Traube rule states that in an homologous series of surface-active substances there is a constant ratio between the molar concentrations of two consecutive homologs giving rise to the same very small surface tension lowering in aqueous solutions. This law is true only in the limiting case, i. e., at extreme dilutions where adsorption films are supposed to be in the state of a two-dimensional ideal gas. According to Langmuir (6) the statistical adsorption equilibrium at great dilutions can be expressed as follows:

$$A_1 c_{\text{molec}} = A_2 \delta \exp(-W_0/kT),$$

where δ is the surface density or the number of adsorbed molecules per cm.^{2}, c_{molec} the molecular concentration, W_0 the immersion work of the hydrocarbon chain, k the Boltzmann's constant, T the absolute temperature; A_1 and A_2 are both constants which are available for a given series. If we compare two terms, respectively C_n and C_{n+1} in an homologous series, it follows that:

$$(\delta/c_{\text{molec}})_{n+1} = (\delta/c_{\text{molec}})_n \cdot \exp(\Delta W_0/kT),$$

ΔW_0 being the increase in immersion work of the hydrocarbon chain when the chain increases by one CH_2 group; n represents the number of carbons in the molecule.

The term $\exp(\Delta W_0/kT)$ is called the Traube coefficient (C_T).

On a perfect gaseous film,

$$\Delta\gamma = p = kT\delta; \qquad \frac{\delta}{c_{\text{molec}}} = \frac{1}{kT}\frac{p}{c_{\text{molec}}};$$

therefore the limit of the ratio δ/c_{molec} at extreme dilutions is obtained by dividing the slope of the tangent at the origin of the adsorption curve by kT (p is plotted against c_{molec}).

L. Guastalla has determined the Traube coefficient for the series of saturated acids and for the series of saturated alcohols (at around 22–23°C.) over a chain length range as wide as possible (n between 2 and 12, this range being limited by the insolubility of the higher homologs) (7, 8).

The fatty acids were dissolved in 0.01 *M* hydrochloric acid, since it was necessary to avoid dissociation. A dissociated molecule is much less surface-active than a nondissociated molecule. We know (according to G. Langlois (9)) that if a fatty acid is partially dissociated in solution, it seems that the adsorption layer is in equilibrium only with the undissociated molecules; for instance, if lauric acid is dissolved in 0.00002 *M* hydrochloric acid, whose pH is close to the pK_d of the fatty acid, the adsorption curve p–c is identical to the one obtained by increasing the abscissa of the lauric acid adsorption curve (0.01 *M* HCl) by a factor of 2.

The alcohols were dissolved in pure water, the results being substantially the same with alcohols dissolved in 0.01 *M* hydrochloric acid.

For each of the substances studied an adsorption curve p–c (c = molar concentration) was obtained and the tangent at the origin of the curve was drawn (see, for example, Figs. 1 and 2). The measurements are difficult with the higher members; for example, the pressure of the lauric acid adsorption film *in the gaseous state* does not go beyond 0.4 dyne/cm.

After $(\delta/c)_{\lim}$ has been calculated for each substance of the series, the logarithms of $(\delta/c)_{\lim}$ are plotted against n (n = number of carbon atoms in a molecule). If the Traube coefficient is constant it should be possible to draw a straight line through the points.

The results for a certain number of acids and alcohols are shown in Fig. 3. The following conclusions may be drawn from the figure. The Traube coefficient is constant over the whole range studied for both acids and alcohols. Its value is the same for the acids and for the alcohols. This value is approximately 2.65, which is rather smaller than the one generally accepted; the immersion work per CH_2 group (ΔW_0) is about 390×10^{-16} erg. The same conclusions would have been reached if the straight lines corresponding to the acids and alcohols were only *parallel*; but they are in

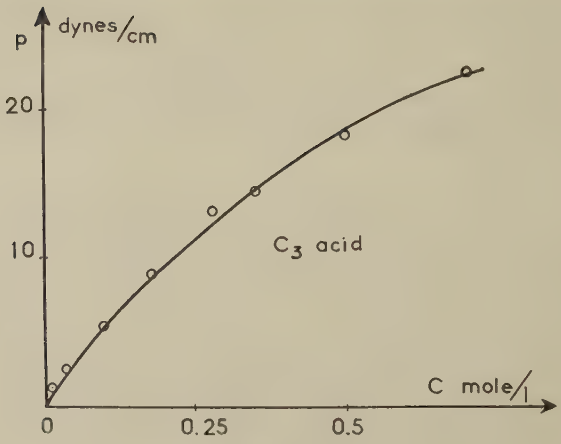

FIG. 1

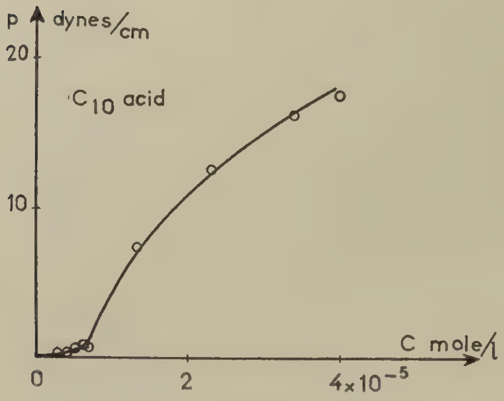

FIG. 2

fact *identical*, which can be interpreted by assuming that the average length of the chain above the water surface is the same for an acid as for an alcohol having the same number of carbon atoms.

Other experiments concerning the Traube rule have been performed with more concentrated solutions, giving real adsorption films (8). The relationship which expresses adsorption equilibrium takes the following form:

$$A_1 c_{\text{molec}} = A_2 \delta \exp\left[-\frac{(W_0 - W_e)}{kT}\right]$$

where, according to J. Guastalla (10), the expulsion energy is

$$W_e = \int_0^{p_s} \sigma \, dp_s$$

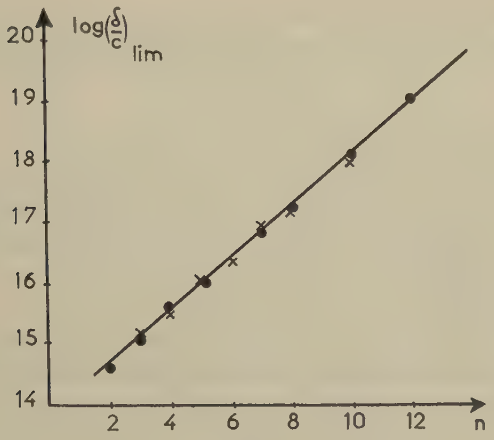

FIG. 3

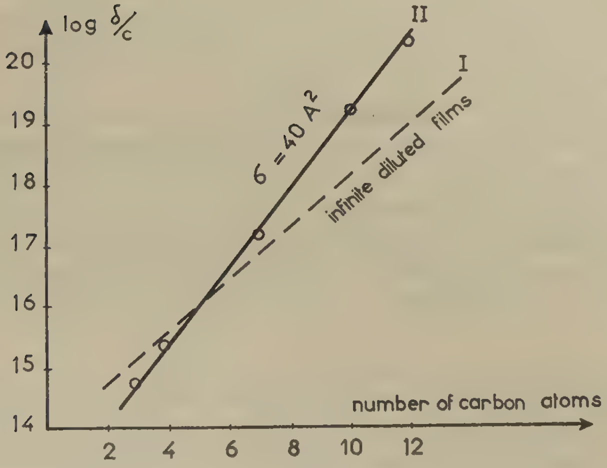

FIG. 4

($1/\delta = \sigma$, the molecular area; $p_s = p - kT\delta$). The term W_e is always positive for short-length acids and alcohols; it can be negative over a certain concentration range for long-chain members.

For different terms of a homologous series, a comparison is made for the ratios δ/c established for a given value δ (for example, $\delta = (1/40)\text{A.}^{-2}$) (we then use the isotherms p–σ calculated from the Gibbs equation).

It is possible to determine nearly correctly a Traube coefficient $C'_{T(\delta)}$ for a given value of δ; this coefficient is higher than the actual Traube coefficient determined at extreme dilutions. The logarithms of δ/c corresponding to $\delta = (1/40)\text{A.}^{-2}$ plotted against n are represented in Fig. 4. A straight line can be, well enough, drawn through the points; this line cuts the one plotted with the δ/c values extrapolated for extreme dilutions.

II. Wetting

a. Theoretical (11, 1, 2)

A very thin rectangular plate made of Plexiglas is suspended from a torsion balance with an horizontal wire. The plate is completely immersed in pure water (which wets it imperfectly). It is then withdrawn vertically and very slowly, while the vertical force to which the plate is subjected, is measured continuously.

First there is a meniscus formed which leans on the upper edge of the plate (as if it were wettable); but tangential contact is never obtained. At a certain moment the solid plate frees itself of the liquid and *seems* to be *dry*; henceforth the meniscus does not alter in shape and forms a constant angle with the solid. The graph of force vs. height of the plate (after correction for buoyancy) is represented in Fig. 5. The ascending branch of the curve represents the deformation of the meniscus, the plateau corresponding to the *constant* force measured from the moment at which the plate emerges dry from the meniscus of constant shape.

From this moment on, the experimenter does not work any more against surface tension or hydrostatic forces; the work supplied by him is used only *for the plate dewetting.*

Let τ be the work of dewetting per cm.^{2} (isothermal and reversible). The work of dewetting of the plate over a height dh is $\tau\, dS = \tau \varpi\, dh$ (ϖ being the perimeter of the plate); if the mechanical compensation work is $f'\, dh$ (force f'), it follows that

$$\tau \varpi\, dh = f'\, dh, \qquad \tau = f'/\varpi.$$

With Plexiglas and pure water, τ is positive. With a paraffin-coated plate and pure water, τ is negative; it is necessary to *supply* work to immerse vertically a paraffin-coated plate in pure water. A graph like the one of Fig. 6 is obtained when the vertical force is plotted against the *depth* of immersion of the lower edge of the plate.

Hysteresis. Wetting and dewetting an imperfectly wettable solid cannot

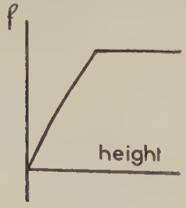

FIG. 5

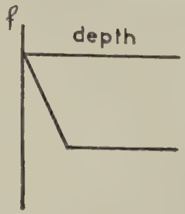

FIG. 6

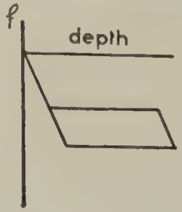

FIG. 7

be performed in a strictly reversible manner. If the paraffin-coated plate is partially immersed in pure water and then withdrawn, an *hysteresis cycle* is obtained on the graph representing the forces (Fig. 7). The area of the cycle represents the work lost. From the two "plateaux" of the forces (immersion and emersion) it is possible to calculate *the adhesion tension of immersion* τ_e (wetting work with opposite sign) and the *adhesion tension of emersion* τ_s (dewetting work).

The hysteresis of wetting is well known; it can arise from several causes (roughness of the solid surface, delays either in adsorption or desorption of solute or vapor . . .). In the case of paraffin and water, the hysteresis is due mainly to the roughness of the paraffin-coated surface. The hysteresis can be greatly decreased by polishing the surface by means of reheating in an oven (12).

Wetting by a Solution of an Adsorbable Substance at the Solid-Solution Interface. Let us assume for a moment that there is no hysteresis. The experimenter who would then immerse a paraffin-coated plate in a *dilute* solution of a substance able to adsorb itself at the paraffin-solution interface would work, *if no adsorption occurred*, to wet the paraffin surface with a liquid whose properties would be very close to those of pure water (work of wetting—τ_0). But adsorption takes place, and if the experimenter works reversibly, he recovers the adsorption work at the liquid-solid interface of the *solute* (W_{ads} per cm.^{2}) when he immerses the plate; he must therefore supply altogether, per cm.^{2}, $-\tau_{\text{solut}} = -\tau_0 - W_{\text{ads}}$ (he will *supply* work $+\tau_{\text{solut}}$ when *withdrawing* the plate if the adsorbed molecules go back into solution). The work W_{ads} is analogous to a *surface pressure*, and we shall represent this quantity by p_i (13). It then follows that

$$-\tau_{\text{solut}} = -\tau_0 - p_i \,;$$

$$p_i = \tau_{\text{solut}} - \tau_0 \,.$$

If τ_0 is negative (as, for instance, in the case of the system water-paraffin), it may happen that $p_i = W_{\text{ads}}$ is greater than $(-\tau_0)$; the work supplied by the experimenter when wetting the plate is therefore reduced to such an extent that the sign is changed; in this case the experimenter obtains positive work when wetting the plate.

Harkins and his co-workers (14) have calculated p_i, in a certain number of cases, from indirect measurements (determination of the contact angle); p_i can be determined much more easily by comparing the force vs. depth graphs established with pure water and with the solution, respectively (Fig. 8).

Hysteresis brings in a difficulty. If hysteresis is considerable in the case of pure water, it will be decreased by the presence of the wetting agent. But if the hysteresis is small with pure water (very smooth plates), it will be only slightly reduced by the wetting agent, and the values of $p_{i(e)}$ and $p_{i(s)}$ obtained by comparing the immersion and emersion plateaux are nearly identical.

Contact Angles. Formerly, the characteristics of wetting were frequently determined by measuring contact angles, these measurements being difficult to carry out. The angles of advance and withdrawal (θ_a and θ_r) are related to γ and to the two values of τ by the relationship $\tau = \gamma \cos \theta$, which is well known and easy to derive from energy considerations.

The direct measurement of τ by means of the plate is much more convenient than the measurement of θ; moreover, θ is generally of not much importance. The contact angle is to be considered only as an *effect*, being the result of γ competing with τ.[2] Regarding phenomena like the rise of a liquid in a capillary tube or its penetration in imperfectly wettable pores, the only interesting quantity would be τ; for instance, when rising to a height, h, in an imperfectly wettable capillary tube of radius, r, the liquid stops when the work against the hydrostatic forces, $\rho g h \pi r^2\, dh$, is equal to the work obtained from the wetting action, $2\pi r \tau\, dh$, wherefore $h = 2\tau/\rho g r$, where ρ is the specific mass of the liquid and g is the acceleration due to gravity.

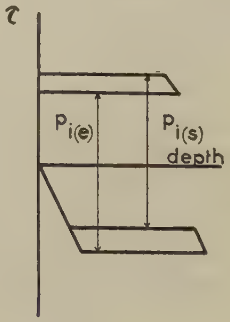

FIG. 8

b. *Apparatus and Technique (16, 2)*

The apparatus which we use for studying wetting (wetting tensiometer, Figs. 9 and 10) permits the simultaneous measurement of surface tension and adhesion tension (the *simultaneousness* of both measurements being necessary when equilibrium is not instantaneous). The apparatus comprises two torsion balances with horizontal wires which can be displaced a few centimeters, upwards or downwards, independent of each other, in two parallel planes very close to one another. The trough which contains the liquid is fixed. The wettable plate is suspended from one of the balances and the imperfectly wettable plate from the other one. The torsion balance

---

[2] The author would not be in agreement with Harkins on this point (15).

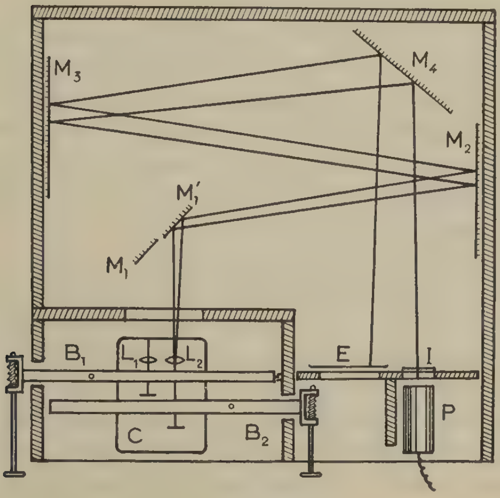

FIG. 9

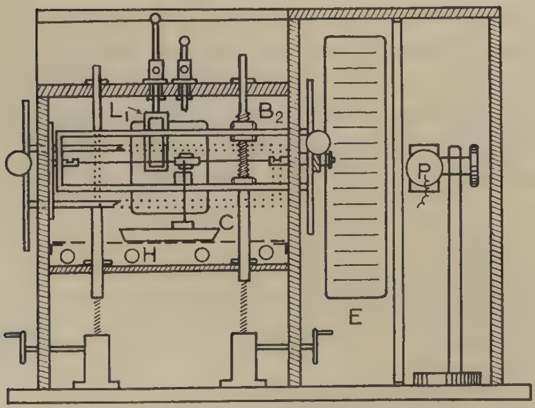

FIG. 10

FIGS. 9. and 10. *M*—vertical mirrors; *B*—torsion balances; *L*—lenses; *E*—scale; *I*—index; *P*—light source; *C*—trough; *H*—heating.

includes small *plane* mirrors. Light arrives at each of these mirrors in parallel beams after having passed through a convergent lens of long focal length (200 cm.), the light source and a big graduated scale being situated in the focal plane of the lens. The dimensions of the apparatus are reduced because of several reflections on vertical mirrors.

In this manner two spots are obtained on a single fixed scale; the position of each spot gives only the torsion angle of the corresponding balance and is not modified by the vertical displacements of the balance if the torsion angle remains constant.

Qualitative Experiment. Both the spots are brought to zero (center of the scale). The wettable plate is brought into contact with the surface of pure water; when contact is established, one of the spots rises. Then the second (paraffin-coated) plate is immersed in the water; the plate is pushed upwards and the second spot goes down ($\tau < 0$). When a small quantity of a surface-active compound is dissolved in the water, by introducing it on the tip of a rod, the first spot goes down but remains above zero (γ decreases); the second spot will then go up and will stabilize above zero (τ increases and becomes positive).

Wetting Curve; Corrections. Figure 11 represents actual wetting curves (*A*, paraffin-water; *B*, paraffin-solution of surfactant); the vertical forces acting on the plate are shown as a function of the displacement downwards of the balance, counted from the contact of the base of the plate with the surface of the liquid.

On these *rough* graphs, the plateaux of the adhesion tension are slightly inclined (buoyancy). In order to correct for this effect in the calculation of the adhesion tension, the two inclined straight lines are extrapolated to the ordinates.

If a rigorous treatment is desired, the change of the torsion angle during the experiment should be taken into account; the *depth* of the lower edge of the plate is a little different from the *displacement* of the balance-body, counted from the contact of the plate with the liquid. In order to correct for the differences (proportional to the displacements of the spot), a slightly inclined axis instead of the vertical ordinate is taken, the slope of which can be easily determined (broken line, Fig. 11).

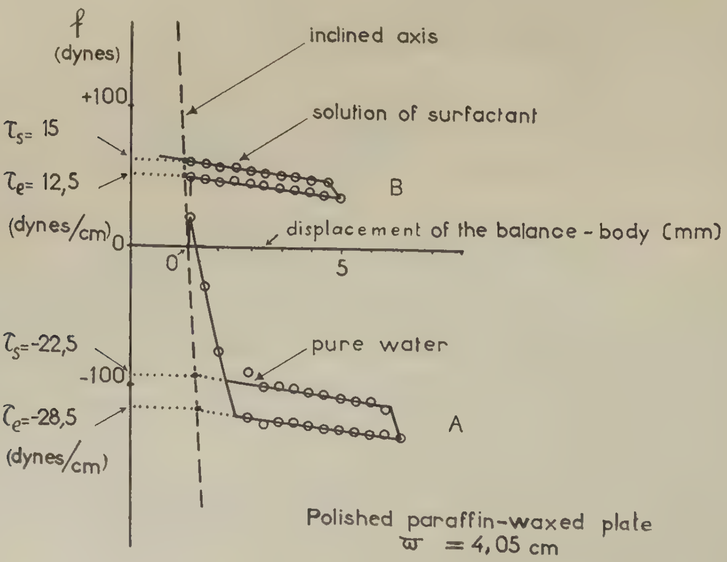

FIG. 11

c. Examples of Results Obtained

1. Curves p–c and p_i–c; Establishing of a Traube Rule. The wetting of paraffin by solutions of various acids and saturated alcohols has been studied by L. Guastalla at the same time as the surface tension of the same solutions.

For the first homologs, the curves p_i–c differ rather little from the curves p–c; the differences become more important when the length of the chain increases. Figure 12 shows the curves p_i–c and p–c for lauric acid (C_{12}). The ratio of the slopes of the tangents at the origin for both curves is about 20.

L. Guastalla has tried to define a kind of Traube coefficient from the slopes of the tangents to the curves p_i–c at the origin, for an homologous series. This coefficient is not constant. For the first members of each series, the coefficient is greater than the one for the free liquid surfaces (for instance, 3.8 for the first acids instead of 2.65). It will tend towards 2.65 for the long-chain members (17).

2. Curves γ-log c and τ-log c for an Industrial Product. It is convenient to plot γ, τ_e, and τ_s versus the logarithm of the concentration. The graph (example Fig. 13) indicates the C.M.C. The more the adhesion tension approaches the surface tension, the more efficient is the wetting agent. When the wetting is perfect, the adhesion tension curves rejoin the surface tension curve; this phenomenon is rather exceptional when the solid to be wetted is paraffin.

d. Dynamic Wetting

In industry, dynamical wetting has to be considered frequently. The results obtained by static measurements are applicable only if the phenomenon is practically reversible.

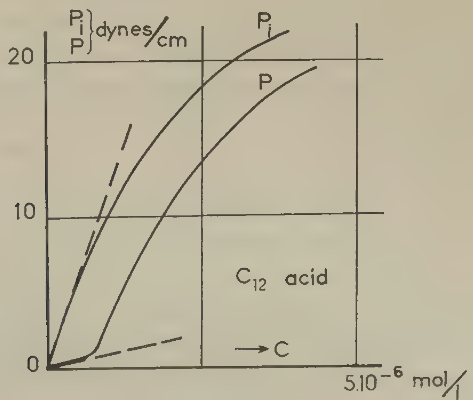

FIG. 12

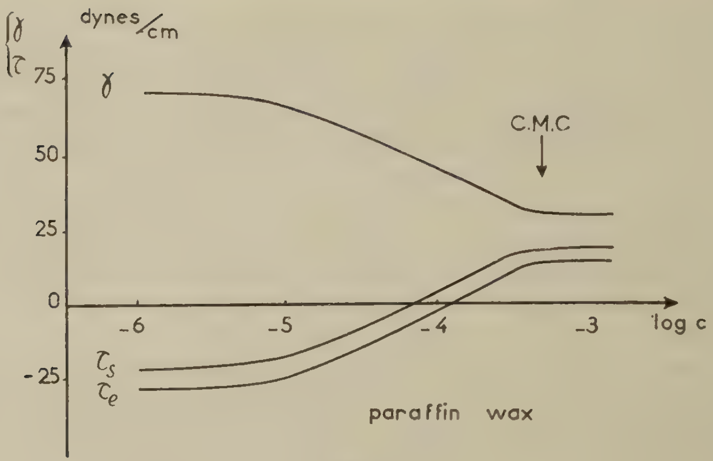

FIG. 13

Rosano (18, 19) has studied the rate of penetration of water and various solutions into small tubes which are paraffin-coated on the inside and into tubes of polyvinyl chloride, under different hydrostatic pressures. For pure liquids and for certain micellar wetting solutions, the progression (or retreat) follows correctly Washburn's law for displacements in wettable tubes, provided γ is replaced by τ_e (progression) or by τ_s (retreat). For non-micellar wetting solutions, the rate of progression is generally decreased, since the meniscus zone leaves molecules on the walls of the tube and since the supply of molecules from the solution is not instantaneous (dynamic loss). In case a network of very small micropores (tissue, porous material) has to be wetted, a definite loss may moreover take place (stop of progression) owing to the great adsorbing surface.

In order to study directly the penetration of a wetting solution in a porous material, a rectangular sample of the material may be suspended from a torsion balance, and the increase in weight of the sample may be followed as a function of time, after its lower edge is put in contact with the surface of the liquid. It is necessary to separate from the measured force the effect of the surface tension on the periphery of the sample (test devised by Rosano, Le Peintre and Baudier).

III. DEWETTING

A wetting agent for paraffin does not necessarily wet any other solid. For instance, the cationic surfactants, which are excellent wetting agents for paraffin, dewet glass or quartz within certain concentration limits. This phenomenon was studied by L. Ténèbre by means of the wetting tensiometer (20, 21). A mica plate having a rough surface was suspended from one of the balances in order to measure the surface tension and a glass plate (micro-

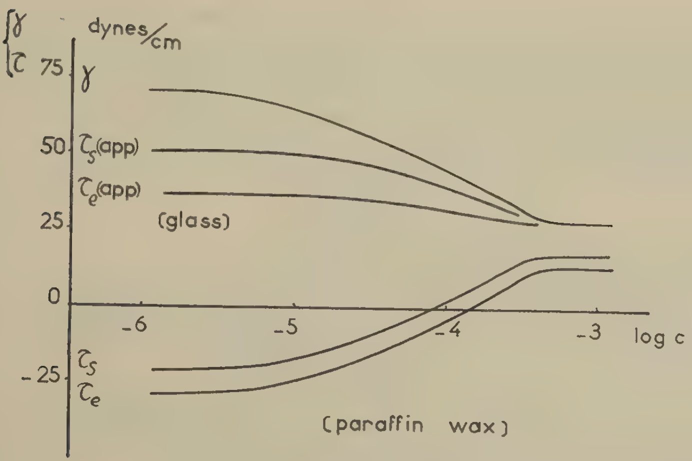

FIG. 14

scope cover glass) from the other balance. The wet glass plate is first immersed in the liquid (thermodynamically irreversible dewetting is then observed), and the *apparent adhesion tension* for glass-solution is measured from an emersion followed by another immersion.

As an example, Fig. 14 shows γ, τ_e , and τ_s paraffin-solution, $\tau_{e(\mathrm{app})}$ and $\tau_{s(\mathrm{app})}$ glass-solution, as a function of the logarithm of the concentrations for solution of lauryl-trimethyl-ammonium bromide.

The slope of the τ_{app} curves (glass-solution) has the same sign as the one of the curve of γ, i. e., opposite to the one of the slope for the curve τ paraffin-solution. The application of the Gibbs equation (as well as common sense) led to the idea that a film is fixed on the glass plate when it is withdrawn from the solution, the plate being apparently dry, and that this film is restored to the suface of the solution when the glass plate is again immersed. This withdrawal of a film is confirmed by the fact that in the case of nonmicellar solutions of cationic long-chain substances the surface tension increases temporarily while the glass plate is withdrawn and decreases temporarily while it is again immersed. (Ténèbre has succeeded in determining the rate at which material is deposited on the glass plate.) It is here a question of an *additional adsorption*, since the glass fixes already a certain number of surfactant molecules when it is immersed in the solution (this fact being confirmed by the rise in the surface tension of the solution after it has been stirred in the presence of glass wool). But, contrary to what may be expected, this additional adsorption *is not due* to the deposition of a second layer of molecules of surfactant, paraffin ends to paraffin ends, on a first layer already deposited in the bulk of the solution. This additional adsorption *would indeed look like an adsorption on the paraffin* (positive slope for the curve τ-log c). But the data rather lead to the assumption that the polar ends of the molecules of surfactant are fixed on the glass, during emersion, at the free places between the molecules already adsorbed, in the form of a rather loose network in the bulk of the solution.

This method may permit elucidation of the mechanism which lies at the basis of flotation phenomenon.

REFERENCES

1. GUASTALLA, J., *J. chim. phys.* **49,** 250 (1952).
2. GUASTALLA, J., *J. chim. phys.* **51,** 287 (1954).
3. DERVICHIAN, D. G., *J. phys. radium* **6,** 221 (1935).
4. HARKINS, W. D., AND ANDERSON, T. F., *J. Am. Chem. Soc.* **59,** 2189 (1937).
5. ABRIBAT, M., AND DOGNON, A., *J. phys. radium* **10,** 22 S (1939).
6. LANGMUIR, I., *J. Am. Chem. Soc.* **39,** 1848 (1917).
7. GUASTALLA, L., AND GUASTALLA, J., *Mém. services chim. état (Paris)* **38,** 99 (1953).
8. GUASTALLA, L., AND GUASTALLA, J., *Compt. rend.* **240,** 425 (1955).
9. LANGLOIS, G., *Mém. services chim. état (Paris)* **40,** 83 (1955).
10. GUASTALLA, J., *Compt. rend.* **228,** 820 (1949).
11. GUASTALLA, J., AND GUASTALLA, L., *Compt. rend.* **226,** 2054 (1948).
12. GUASTALLA, L., *Compt. rend.* **230,** 824 (1950).
13. GUASTALLA, J., GUASTALLA, L., LUZZATI, D., ROSANO, H. L., AND SARAGA, L., *Compt. rend.* **231,** 220 (1950).
14. FOWKES, F. M., AND HARKINS, W. D., *J. Am. Chem. Soc.* **62,** 3377 (1940).
15. HARKINS, W. D., AND LOESER, E. H., *J. Chem. Phys.* **18,** 556 (1950).
16. GUASTALLA, J., *J. chim. phys.* **51,** 583 (1954).
17. GUASTALLA, L., Thesis, unpublished.
18. ROSANO, H. L., *Mém. services chim. état (Paris)* **36,** 309, 437 (1951).
19. ROSANO, H. L., AND GUASTALLA, J., *Compt. rend.* **230,** 628 (1950)
20. TÉNÈBRE, L., *Mém. services chim. état (Paris)* **40,** 77 (1955).
21. TÉNÈBRE, L., *J. chim. phys.* **53,** 6 (1956).

JOURNAL OF COLLOID SCIENCE **11**, 637–646 (1956)

POLAR ION-SELECTIVE MEMBRANES AND CORROSION PROTECTION

Antonio Nasini and Giorgio Ostacoli

Dell 'Istituto Chimico, Dell 'Universita Di Torino, Torino, Italy

Received May 16, 1956

It has been pointed out previously (1–3) that layers of polar polymers could be considered as "membranes," and treated as such when laid on metal supports.

Some consequences of this hypothesis have already been drawn. Von Manegold (4) has subsequently treated the same problem as applied to different types of membrane models.

A polar film, considered as a membrane, can then be considered as consisting of a series of communicating pores and cavities on whose walls groups of polar molecules are to be found: swelling the film with water yields, by dissociation, fixed ions on the wall and mobile ions in the intermicellar water. Such conditions are like those existing in ion-selective membranes as described among others by Sollner (5).

If a metal test piece, coated with a film of the type described, is dipped in an electrolytic solution, it is anticipated that the selective property of the film will strongly influence the composition of the solution, originating from the liquid penetrating through the membrane, in contact with the metal; the concentration of this inner solution may be chiefly influenced either by corrosion phenomena or by ion diffusion from the outer solution, or by both.

The selective effect of the coating film can work in two ways: (*1*) by hydrolytic action, modifying the pH of the liquid in contact with the metal; (*2*) by allowing exchange among the ions having the same sign as the mobile ones of the membrane. The hydrolytic effect on the corrosion reaction varies according to the nature of the metal tested. The limits imposed on the ion exchange by the presence of the ion-selective films are general and can be easily described.

A cation-selective film should allow the passage from inside to outside the metal ions originated by the corrosion, whereas an anion-selective film should stop their diffusion.

The components used as varnishes offer only weakly selective properties, and where a selectivity exists, often the high polarity itself can originate the decrease of the selective properties owing to too large a swelling.

To realize the best possible experimental conditions to follow the penetration of electrolytic solutions through membranes covering metal test pieces, we used components which were suitable for this purpose, although they are not as efficient as real varnishes for protective purposes.

The films used were prepared from extremely dispersed suspensions of ion-exchange resins in ion-inert and film-forming components; the present technique differs from the one followed by Wyllie and Patnode (6) to obtain heterogeneous membranes from blends of ion-exchange resin, incorporated in polystyrene or polymethylmethacrylate, by molding under pressure.

To test the behavior of our membranes, we checked the degree of selectivity as measured on isolated films against varying concentrations of different electrolytes, with satisfactory results.

Silver and iron electrodes were used; for silver, corrosion phenomena are not important, and the potentiometric measurements of the coated electrodes against a solution of silver nitrate enabled us to follow the rate of exchange of metallic ions, through the film, versus time. For iron the measurements made against a solution initially not containing soluble iron salts, definitely show the effect of the ion-selectivity of the film upon corrosion phenomena.

Experimental

a. Silver Electrodes

The electrodes, shaped as small round-edged sticks, were coated by immersion in suspensions of ion-exchange resins in polystyrene solutions.

To prepare these suspensions, two types of ion-exchange resins were used: the Amberlite I.R. 100 A. G., cation-exchanger, and the Amberlite I.R.4 B, anion-exchanger. These resins, after grinding, were sieved through a 200-mesh sieve, and dispersed in a 20% solution of polystyrene in toluene. After a number of preliminary tests, the use of suspensions containing 25% of ion-exchange resins on the weight of polystyrene was preferred.

For measurements on separate films, membranes were obtained by laying the suspension on glass strips and then stripping off the film after the solvent evaporated. The degree of selectivity of the membranes was evaluated potentiometrically, following the method described by Meyer and Sievers (7), against solutions of potassium chloride, potassium nitrate, and silver nitrate in concentrations ranging from 0.17 to 0.01 M. The results of potentiometric measurements are reported in Table I for cationic membranes and in Table II for anionic membranes. Alongside the experimental values ($E_{\text{exp.}}$), the theoretical values are reported ($E_{\text{calc.}}$); these were cal-

TABLE I

Potentiometric Measurements for Cationic Membranes

	Conc. M C_1/C_2			
	0.17/0.085	0.085/.0042	0.042/0.021	0.021/0.105
KCl				
$E_{exp.}$	14	15	15	16
$E_{calc.}$	15.74	17.4	17.0	18.06
$t\pm$	0.89	0.86	0.87	0.88
KNO_3				
$E_{exp.}$	13.7	15	15.2	15.2
$E_{calc.}$	15.3	16.03	17.0	18.06
$t\pm$	0.89	0.94	0.84	0.84
$AgNO_3$				
$E_{exp.}$	13.7	15	15.2	15.2
$E_{calc.}$	16.03	17.0	17.0	17.79
$t\pm$	0.85	0.88	0.89	0.85

TABLE II

Potentiometric Measurements for Anionic Membranes

	Conc. M C_1/C_2			
	0.17/0.085	0.085/0.042	0.042/0.021	0.021/0.0105
KCl				
$E_{exp.}$	−10	−11.2	−11.2	−10
$E_{calc.}$	15.74	17.4	17.0	18.06
$t\pm$	0.64	0.64	0.66	0.50
KNO_3				
$E_{exp.}$	−12.5	−12.5	−12	−10
$E_{calc.}$	15.3	16.03	17	18.6
$t\pm$	0.81	0.77	0.70	0.55
$AgNO_3$				
$E_{exp.}$	−14.7	−15	−15	−15
$E_{calc.}$	16.03	17.0	17.0	17.79
$t\pm$	0.92	0.87	0.87	0.84

culated by means of the activity coefficients given by Harned and Owen (8) and by Landolt (9) with the following formula:

$$E = \frac{RT}{F} \log \frac{a_1}{a_2} \qquad [1]$$

valid in the case of an ideal perm-selective membrane. In Tables I and II is also reported the "apparent transport number," of the exchanging ion, evaluated for every measurement and referred to the average normality (10) by the formula:

$$t_{\mp} = \frac{E_{exp.}}{E_{calc.}}. \qquad [2]$$

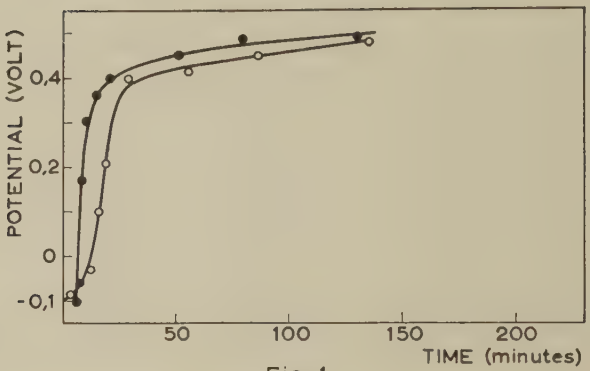

Fig. 1

FIG. 1. Silver electrodes coated with cation-selective films. Potential versus time diagram: ● film thickness 0.15 mm.; ○ film thickness 0.36 mm.

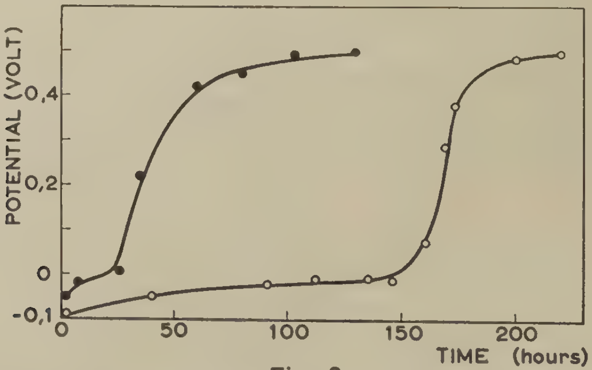

Fig. 2

FIG. 2. Silver electrodes coated with anion-selective films. Potential versus time diagram: ● film thickness 0.12 mm.; ○ film thickness 0.4 mm.

The coated electrodes were dipped into solutions of 0.17 *M* of silver nitrate. Their potentials were measured against a reference calomel electrode in a saturated solution of potassium chloride, connected to a solution of silver nitrate by ammonium nitrate bridges.

Immediate short circuiting between metal and solution was observed in every case. The results are shown in Figs. 1 and 2, respectively, for the electrodes coated with cation-exchange and with anion-exchange resins.

b. Iron Test-Electrodes

Potentiometric measurements were made in a solution of composition equivalent to that of sea water (11) using a reference calomel electrode in a saturated solution of KCl.

First experiments with polystyrene suspensions gave too short a time of observation (150–200 hours), given the strong water absorption on the film. In order to avoid this inconvenience, other measurements were made on test pieces coated with a layer of plasticized chlorinated rubber, activated with ion-exchange resins and coated with a second layer of plasticized chlorinated rubber, to limit the swelling. The suspensions contained 25% of ion-exchange resin on the dried residue.

In this case, measurements could be made even on an isolated film with 0.1 and 0.01 *M* solutions of KCl. Stable potentiometric values were obtained, in the present case, after about 72 hours. For cation-exchange membranes, a value of +50 mv. for ($E_{\text{exp.}}$) was obtained, and of −48 mv. for anion-exchange membranes. The theoretical value, calculated from formula [1], is ±55.6.

Together with the test pieces coated as described, some reference test pieces were used, which were protected only by nonionic films. In no case was an immediate short circuiting observed.

Measurements lasted a period of 22 months. The level of liquid in the containers was kept constant by periodic supplies of water. The results of potential versus time measurements are reported in Figs. 3, 4, and 5.

Some corrosion phenomena could be clearly observed after 16 months on test pieces C (cation-exchange film) and after 18 months on test pieces I (ion-inert film). The corrosion appeared with a yellow-greenish color of the solution, and with the formation of a rust deposit on the bottom of the containers.

The solution, however, did not appear colored and no formation of deposit was observed, after 22 months, in the containers holding test pieces A (anion-exchange film). It was possible to observe the formation of

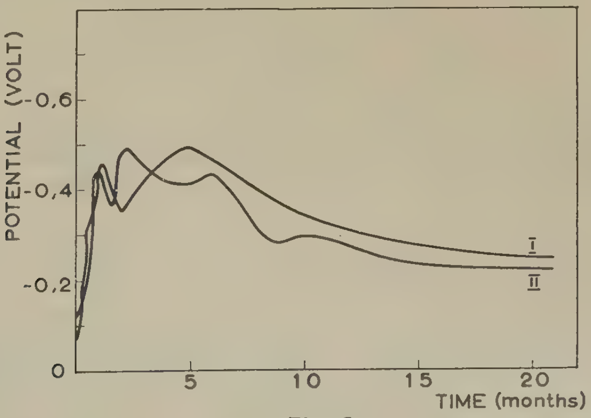

Fig. 3

FIG. 3. Iron test pieces, coated with anion-selective films (A). Potential versus time diagram: No. I film thickness 0.42 mm.; "time of contact" about 145 hours. No. II film thickness 0.45 mm.; "time of contact" about 170 hours.

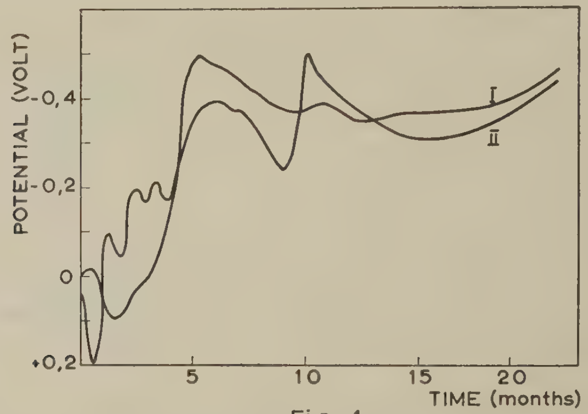

Fig. 4

FIG. 4. Iron test pieces, coated with cation-selective films (C). Potential versus time diagram: No. I film thickness 0.50 mm.; "time of contact" about 160 hours. No. II film thickness 0.47 mm.; "time of contact" about 135 hours.

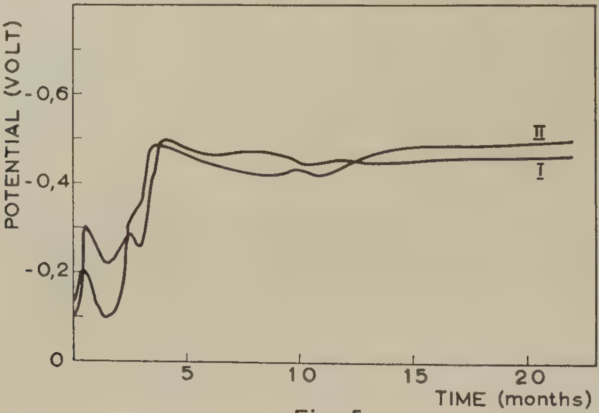

Fig. 5

FIG. 5. Iron test pieces, coated with ion-inert films (I), plasticized chlorinated rubber only. Potential versus time diagram: No. I film thickness 0.28 mm.; "time of contact" about 160 hours. No. II film thickness 0.22 mm.; "time of contact" about 190 hours.

blisters on the films, particularly in the test piece corresponding (diagram Fig. 5) to curve No. 2.

After removal of the film, on test pieces C, a pointlike corrosion was observed, owing to the presence of anodic and cathodic areas over all the dipped surfaces. On test pieces I, a similar corrosion was observed along with the formation of a dusty material and the presence of slight blisters on the varnish film. On the test pieces A the presence of some liquid under the varnish was observed, the surface appearing practically without corrosion.

TABLE III

Iron Test Pieces

Potential in volts	A		C		I	
	I	II	I	II	I	II
E_1 (initial)	−0.15	−0.07	+0.04	−0.01	−0.13	−0.1
E_2 (after 3 months)	−0.44	−0.43	−0.17	+0.1	−0.37	−0.25
E_3 (max.)	−0.50	−0.49	−0.49	−0.50	−0.48	−0.50
Time (in months)	5	2	5	10	3	4
E_4	−0.25	−0.22	−0.46	−0.43	−0.48	−0.46

In Table III are reported the potentials observed on the closing of contact (E_1) and after 3 months (E_2); in the same table the highest value obtained from each test piece (E_3) and the value observed at the end of the measurements are also given.

DISCUSSION

The measurements upon coated silver electrodes show that from the "times of contact" and from the values of the first constant potential able to be measured, the initial behavior of the electrodes is independent of the ionic nature of the film.

The silver ion concentration in the solution in contact with the metal can increase only by diffusion of ions existing in the outer solution, because of the slight solubility of the corrosion products. This should be possible only for electrodes coated with cationic membranes. Experimental results agree (Fig. 1) with this supposition. Figure 2 shows that the anion-exchange film maintains the initial conditions for a relatively long time (150 hours). It is obvious that the increase of values of the potential is due to the diffusion of the electrolyte through nonpolar pores. This fact becomes possible only when the film loses, by swelling, its selective properties.

According to what we have pointed out, it can be seen that the thickness of the film has very little influence on the behavior of the potential versus time diagram, obtained from electrodes coated by cation-exchange films (Fig. 1), whereas it appreciably modifies the curves obtained from electrodes coated with anion-exchange membranes.

From the measurements reported, we may reach the conclusion that the selective properties of coating films have a remarkable influence upon the ionic exchange through the solution in contact with the electrode and the electrolytic solution.

For iron the presence of rust deposits in the containers for test pieces C (cationic film) and the absence of corrosion products for the test pieces A (anionic film) confirm the suppositions formerly made on this subject. In the same way, the final surface conditions of the iron at the end of the test can be explained.

A visible anodic corrosion can be observed only on test pieces C; this fact can be related to the possibility that ferrous ions, forming at the anode, will migrate from the anodic zone by exchange with the moving ions existing in the neighborhood of the local piles. On the surfaces covered by anionic membranes, this possibility does not exist; the corrosion products are likely to remain in the zone where they have first formed.

The potentials E_1, E_2, and the time necessary to reach the maximum value E_3, point to a greater passivity for C than for A test pieces (Table III). At the end of the test, the values of E_4 indicate, on the other hand, a greater passivity for test pieces A, according to the visual examination of the surface conditions. The values of the "time of contact" reported in Figs. 3, 4, and 5 show that the test pieces are all in the same condition and indicate the uniformity of the film tested. It is therefore obvious that the different behavior of the curves shown on the potential versus time diagrams is due to the selective action of the films.

The differences observed can be referred to the hydrolytic effect of the ionic active layer. To make this effect noticeable it is necessary that, for a certain period of time, the concentration of ions having the same sign as the moving ones be greater in the external part of the film. This is not difficult to accept, even if the presence of the inert layer hinders the contact of the ion-selective film with the electrolytic solution in which the test piece is dipped.

From the general trend of the curves in Fig. 4 and 5, one can see that the initial behavior of test pieces C can be considered similar to that of test pieces I. It is therefore probable that the type of passivation observed is similar in both cases.

Crennel (12) has attributed the passivating effect of a varnish to the possibility that the accumulation of corrosion products on the metal surface makes the solution in contact with it alkaline. The passivating effect decreases with time because some corrosion products may, by a different mechanism, pass into the outer solution by exchanging with existing ions or salts. With test pieces C, ferrous ions exchange with mobile ions which are of opposite sign to the fixed ions, whereas with test pieces I, the exchange happens through nonpolar pores and in the presence of anions from the outer solution.

From the value of E_1 (Table III), for samples C and I, we observe that the former, when closing the contact, show a greater passivity, as indicated by a more positive potential. From the general trend of the potential values immediately after the contact time, the hydrolytic effect of the cationic-exchange membranes, contributing to passivation, is confirmed.

The hydrolytic effect, in the case of anion-exchange membranes, allows only a slow corrosion by the low pH (13) of the liquid penetrated through the membrane and in contact with the metal; in this case, then, we might suppose that the outer anions penetrate the membrane exchanging with the inner mobile anions, leading to the formation of soluble ferrous salts and to a subsequent saturation of the inner solution. In such a way the corrosion of the metal is stopped by mass effect. By osmotic effect a larger amount of water may swell the membrane and, by the case, penetrate through it, leading eventually also to a decrease of the adhesion of the coating film to the metal surface, then causing blisters by deformation of the membrane, in accordance with the experiments of Kittelberger and Elm (14).

It can be pointed out, too, that the corrosion phenomena observed upon test pieces I can be considered as intermediate between those from test pieces A and C. The anionic or cationic character of the film seems then to represent a limiting case in the protective action of a varnish film. As to the passivation of ferrous surfaces, the best results have been obtained with anion-exchange resins.

As previously mentioned, the film coatings used in the present work are not those required for a good varnish, but have been chosen for the purpose of proving the protective effect of a perm-selective membrane in the limited case of the experiments here described.

SUMMARY

Measurements have been made of potential versus time for silver and iron electrodes coated, respectively, with films of polystyrene and chlorinated rubber activated with ion-exchange resins of the cationic and anionic types, immersed in solutions of different electrolytes.

Upon silver electrodes coated with cation-selective films against solutions of $AgNO_3$, potentials near the equilibrium value are reached in a few minutes (15–20), whereas with anion-selective films the time required may reach 160 hours.

Upon coated iron electrodes against "sea water" solution a large initial passivation may be observed with cation-selective films, whereas with anion-selective films the passivation effect predominates towards the end of the experiments that have lasted 22 months.

Observation of the metal surfaces, made at the end of the experiments, has confirmed the deduction made from the potential measurements.

The results have been discussed in terms of the concept that the coating film behaves as a membrane.

REFERENCES

1. NASINI, A., POLI, G., AND RAVA, V., *1st Congr. tech. intern. ind. peintures et inds. assoc., Paris, 1947.*
2. NASINI, A., RAVA, V., AND OSTACOLI, G., *Chimica e industria (Milan)* **33**, 624 (1951).
3. NASINI, A., AND OSTACOLI, G., *Industria vernice (Milan)* **5**, 148 (1951).

4. Von Manegold, E., *Kolloid-Z.* **116,** 135 (1950).
5. Sollner, K., *J. Phys. Chem.* **49,** 47, 171 (1945).
6. Wyllie, M. R., and Patnode, H. W. *J. Phys. Chem.* **54,** 204 (1950).
7. Meyer, K. H., and Sievers, J. F., *Helv. Chim. Acta* **19,** 649, 665 (1936).
8. Harned, H. S., and Owen, B. B., "The Physical Chemistry of Electrolytic Solutions," p. 567. Reinhold, New York, 1950.
9. Landolt, "Physikalisch Chemische Tabellen," 5th ed.
10. Juda, W., and McRee, W. A., *J. Am. Chem. Soc.* **72,** 1044 (1950).
11. Uhlig, H. H., "Corrosion Handbook," p. 129. Wiley, New York, 1948.
12. Crennel, J. T., *J. Soc. Chem. Ind. (London)* **49,** 36 (1950).
13. Kabanov, B., Burstein, R., and Frumkin, A., *Discussions Faraday Soc.* **1,** 259 (1947).
14. Kittelberger, W., and Elm, A. C., *Ind. Eng. Chem.* **38,** 695 (1946).

JOURNAL OF COLLOID SCIENCE **11**, 647–652 (1956)

THE DECOMPOSITION OF HYDROGEN PEROXIDE BY MASSIVE COLLOIDAL METALLIC FERROCYANIDES

F. H. Constable

Director of the Institute of Physical Chemistry, Istanbul University, Istanbul, Turkey

Received March 12, 1956

An investigation by H. Erkut (1) in this laboratory has shown that, of the insoluble colloidal metallic ferrocyanides, only the highly colored ferrocyanides of copper and iron are catalysts for the decomposition of hydrogen peroxide in aqueous solution, and the copper compound is more active than the iron compound. There was considerable difficulty in obtaining stable colloidal solutions of these substances over wide ranges of pH, so that the present studies were made on the precipitates from equivalent quantities of salts in aqueous 0.2 *N* solutions mixed at 70°C. The precipitates were collected in a Büchner funnel, well washed with water at 70°C., dried in a vacuum desiccator over fused calcium choride, and passed though a 200 Tyler sieve.

Through the courtesy of Professor Fahir Yeniçay and Miss Müeyyet of the Physics Department, electron microscope photographs of the finest particles from aqueous emulsion of the two preparations were made at 24,000 magnification. The photographs show very clearly the colloidal nature of the particles. Preliminary experiments established that with a fixed mass of catalyst the velocity of the apparently unimolecular heterogeneous catalytic reaction was constant at all stirring velocities above the minimum required to keep the particles in suspension at constant pH; the velocity was proportional to the mass of catalyst at constant pH and was very sensitive to the pH of the solution.

I. CUPRIC FERROCYANIDE (HATCHETT'S BROWN)

Effect of pH on Reaction Velocity

The velocity was followed by withdrawal at convenient time intervals of 10-ml. samples of the reaction mixture kept in a thermostat. These samples were run into 10 ml. of 10% sulfuric acid in an Erlenmeyer flask, followed by titration with *V* ml. of 0.025 *N* potassium permanganate. The pH was maintained by phosphate buffers (5–10). With an effective concentration of cupric ferrocyanide of 0.1 mg./ml. it was found necessary to leave the catalyst in contact with the buffer for 30 minutes before commencing the experiment to obtain linear log *V* versus time graphs.

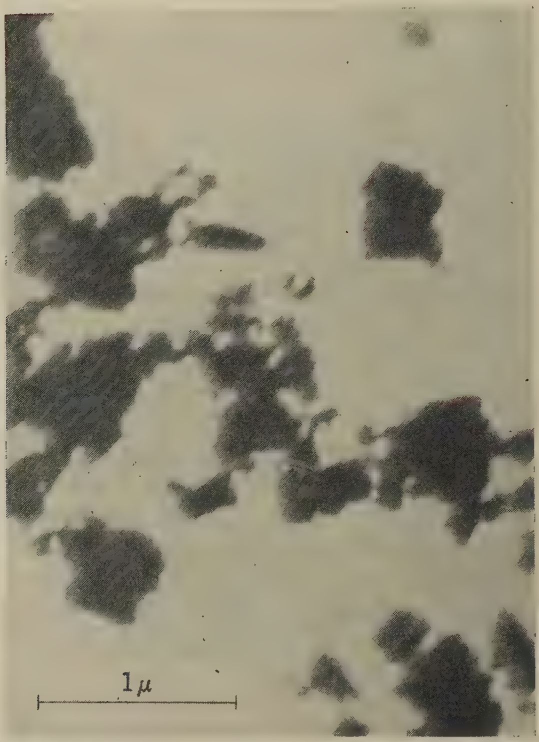

FIG. 1. Electron microscope photograph (× 24,000) of Hatchetts' brown (cupric ferrocyanide).

Figure 3 shows the great effect of pH on the linear (i.e., apparently unimolecular) log V versus time curves from pH 2 to 10 at 25.0°C. Similar linear results were obtained at 0°C. and 48°C. When the pH is kept above 10 with phosphate buffers, or above 9 with borate buffers, the apparently unimolecular velocity increases with the diminution of concentration of H_2O_2, but the overall velocity has continued to diminish as the pH increases above 9.7, and some color change was observed in the catalyst. Figure 4 is for borate buffers at 25°C. The onset of the effect is at a higher pH, the lower the temperature.

II. EFFECT OF pH AND TEMPERATURE

From all the results a curve was plotted for the logarithm of velocity constants (log k) versus pH. This is shown in Fig. 5. The lines are nearly parallel, but closer examination shows that the straight-line slope is proportional to the absolute temperature, T. Thus the reaction velocity may be represented by the equation,

$$\log_{10} k = a - \frac{b}{T} + \frac{c(\text{pH})}{T},$$

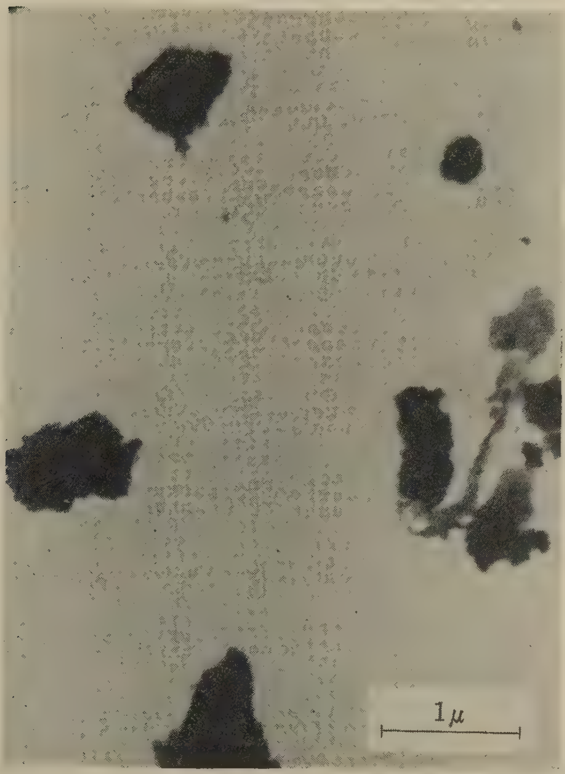

Fig. 2. Electron microscope photograph (× 24,000) of Prussian blue (ferric ferrocyanide).

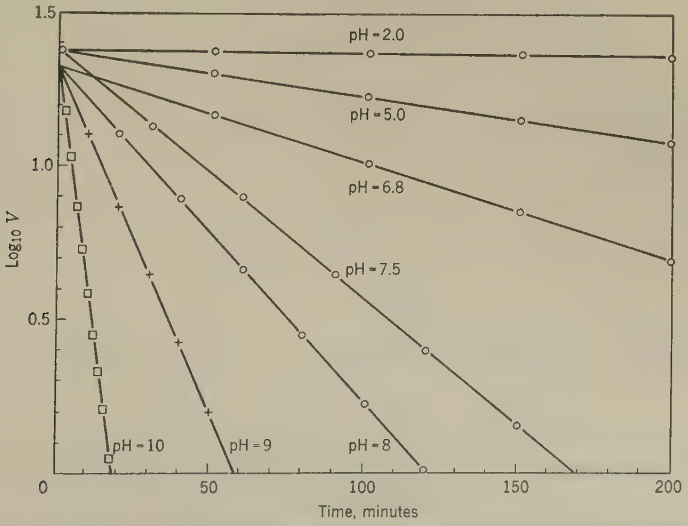

Fig. 3. The relation between the logarithm of the concentration of H_2O_2 and time for 50 mg. of $Cu_2Fe(CN)_6$ catalyst in 500 ml. solution from pH 2 to 10.

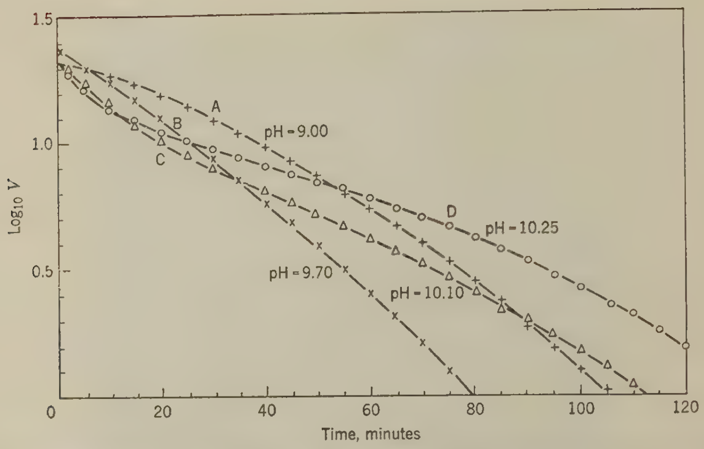

FIG. 4. Similar relation from pH 9 in borate buffer solution, showing retardation, and the commencement of the HO_2 ion reaction.

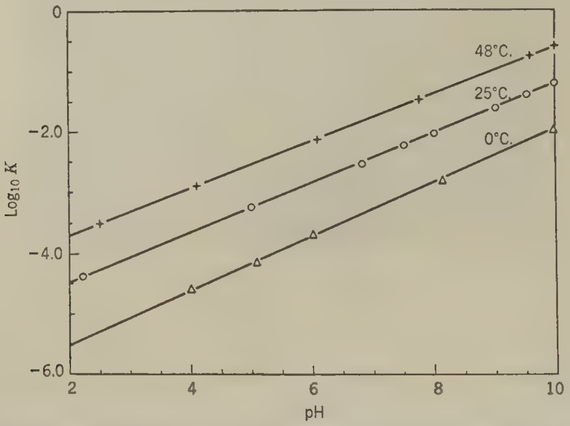

FIG. 5. The relation between $\log_{10}k$ and the pH of the solution at 0°C., 25°C., and 48°C.

where a, b, and c are constants. With the use of the value 7.311 for a obtained by a plot of $(\log_{10} k - c(\text{pH})/T)$ against $1/T$, it is possible to plot all the observations on one graph against pH in this form:

$$T(a - \log_{10} k) = b - c(\text{pH}).$$

In this way the equation for the reaction velocity was obtained:

$$\log_{10} k = 7.311 - \frac{3738}{T} + \frac{121.3\,\text{pH}}{T}$$

for a mass of 50 mg. of heterogeneously suspended cupric ferrocyanide in aqueous hydrogen peroxide. Since it has been shown that the reaction velocity is proportional to the mass, the general equation becomes

$$\log_{10} k = \log_{10} m + 5.612 - \frac{3738}{T} + \frac{121.3\,\text{pH}}{T},$$

in which the velocity constant k is obtained in units of $\frac{d}{dt}(\log_{10} C)$, time is in minutes, and m is in milligrams. C is H_2O_2 concentration.

III. Prussian Blue

Similar experiments were made with Prussian blue. For the region of pH between 1.3 and 8.2, the experiments with 200 mg. of Prussian blue which has passed a 200 Tyler sieve gave

$$\log_{10} k = 7.110 - \frac{3243}{T} + \frac{98.6\,\text{pH}}{T}.$$

Thus if m is the mass of the catalyst in milligrams the equation becomes

$$\log_{10} k = \log_{10} m + 4.809 - \frac{3243}{T} + \frac{98.6\,(\text{pH})}{T}.$$

IV. Turnbull's Blue

With 200 mg. of catalyst the experimental work gave the equation

$$\log_{10} k = 7.409 - \frac{3275}{T} + \frac{83.6\,\text{pH}}{T},$$

or if m is the mass of the catalyst in milligrams

$$\log_{10} k = \log_{10} m + 5.108 - \frac{3275}{T} + \frac{83.6\,\text{pH}}{T}.$$

V. Conclusion

Of the three highly colored active complex cyanides, showing marked resonance effects, cupric ferrocyanide is the most sensitive to the pH of the solution, while Turnbull's blue (ferrous ferricyanide) is the least sensitive. For each of these there is a definite range of pH in which the logarithm of the reaction velocity increases in a linear manner with pH. For each of the three there comes a pH at which the apparent monomolecular velocity increases with the dilution. This pH is sufficiently high to allow appreciable quantities of the ion of H_2O_2 in the solution, and it seems that the disturbing effect is due to this ion. At still higher pH values the catalysts are decomposed. It seems difficult to avoid the conclusion that the energy of activation for the decomposition falls with the pH of the solution in the range in which the linear relation exists between the logarithm of reaction velocity and pH.

I would like to thank Miss Kandare (2) of Ljubljana University, Captain Burhan Pekin (3), and Miss Ohanian (4) of Istanbul University, all of whom have taken part in some of the experimental work.

VI. SUMMARY

The catalytic activity of the highly colored supercomplex cyanides of copper and iron towards hydrogen peroxide in aqueous solution is summed up by the equations:

1. Hatchett's brown:

$$\log_{10} k = \log_{10} m + 5.612 - \frac{3738}{T} + \frac{121.3\,\mathrm{pH}}{T}.$$

2. Prussian blue:

$$\log_{10} k = \log_{10} m + 4.809 - \frac{3243}{T} + \frac{98.6\,\mathrm{pH}}{T}.$$

3. Turnbull's blue:

$$\log_{10} k = \log_{10} m + 5.108 - \frac{3275}{T} + \frac{83.6\,\mathrm{pH}}{T}.$$

Here k is the unimolecular velocity constant and the time, t, is expressed in minutes, m is the mass of catalyst in milligrams, T is the absolute temperature, and pH is $-\log_{10}$ of the hydrogen ion concentration. The catalysts are arranged in order of their activity, and it is observed that the more active catalyst is more sensitive to a change of pH, and that the apparent activation energy falls with increase of pH in all cases.

REFERENCES

1. ERKUT, H., *Rev. fac. sci. univ. Istanbul* **C**, 1–14 (1954).
2. KANDARE, S. AND CONSTABLE, F. H., *Rev. fac. sci. univ. Istanbul* **C**, 238–261, 62–65 (1954); *ibid.*, pp. 123–132 (1955).
3. CONSTABLE, F. H., AND PEKIN, B., *Rev. fac. sci. univ. Istanbul* **C**, pp. 121–129 (1956).
4. CONSTABLE, F. H., AND OHANIAN, V., *Rev. fac. sci. univ. Istanbul* **C**, pp. 123–128 (1955).

JOURNAL OF COLLOID SCIENCE **11**, 653–670 (1956)

THE KINETICS OF THE CATALYTIC OXIDATION OF NAPHTHALENE

A. F. D'Alessandro and A. Farkas*

Barrett Division, Allied Chemical & Dye Corporation, Glenolden, Pennsylvania

Received April 5, 1956

ABSTRACT

The vapor phase catalytic air oxidation of naphthalene was studied over various catalysts and in the presence of a large excess of oxygen. Over a catalyst of fairly regular shape made by fusing vanadium pentoxide into pellets, the progress of the reaction with time was investigated. Overall first-order rate constants obtained ranged from 0.56 sec.$^{-1}$ at 340°C. to 32.9 sec.$^{-1}$ at 475°C., with an activation energy of 29 kg.-cal.

Naphthoquinone, phthalic anhydride, and carbon dioxide were found to be formed from naphthalene in simultaneous reaction steps and in the approximate respective proportions of 0.4 to 0.4 to 0.2. Naphthoquinone underwent subsequent conversion to phthalic anhydride.

This branching of the primary step was found to occur with various vanadium pentoxide catalysts, and the extent of branching was compared.

For a fluidized vanadium pentoxide oxidation catalyst modified with a large content of potassium sulfate, a consecutive reaction mechanism was found to apply.

In the fixed bed laboratory operation, mass transfer effects became significant only above 450°C. Below this temperature, rates were controlled by chemical reaction.

I. INTRODUCTION

The production of phthalic anhydride by the catalytic vapor phase oxidation of naphthalene has been known since 1917. Nowadays, it is carried out in numerous commercial plants, each of which can produce tens of millions of pounds of highly refined phthalic anhydride per year.

Although the technical and patent literature of this reaction is rather extensive, very little fundamental work on its kinetics and mechanism has been published. It has been generally assumed (1) that the reaction follows a stepwise course leading successively to more highly oxidized products. In earlier presentation (2) of part of the present work, it was shown that the mechanism of the catalytic oxidation of naphthalene with certain catalysts involves branched reactions in which products oxidized to various degrees are formed simultaneously rather than in a stepwise sequence. Similar results were obtained by Calderbank (3) by measuring initial rates at very low conversions.

---

* Present address: Houdry Process Corporation, Marcus Hook, Pa.

In extending the work to different catalysts, the relative rates of the simultaneous reactions were found to vary with the nature of the catalyst, and, in at least one instance, a truly consecutive reaction sequence was also observed.

The purpose of this paper is to present the experimental data of these studies and to show how these data can be fitted into rate equations.

II. Experimental

1. *Apparatus and Mode of Operation*

The experiments were carried out in apparatus shown in Fig. 1 according to the following procedure:

Filtered air at 330 liters per hour at room conditions was metered by a controlled pressure-drop, needle-valve assembly; measured by a rotameter; and passed through a 25-mm. coarse fritted glass disc at the bottom of vaporizer *A*. The vaporizer, containing molten naphthalene, was immersed in a bath thermostatically controlled to within 0.1°C. Another air stream joined the emerging air-naphthalene mixture at the top of the vaporizer, and the combined stream passed through the preheater section and into

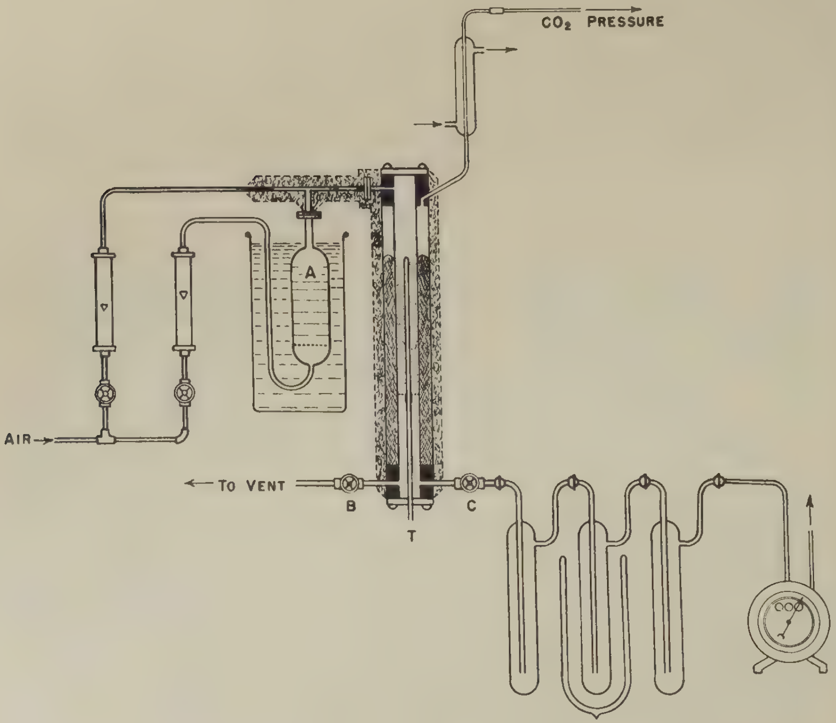

Fig. 1. Apparatus for the oxidation of naphthalene.

the reactor. Thus the concentration of naphthalene was fixed by adjusting the ratio of the two air streams and the temperature of the bath.

The reactor consisted of a 1-inch I.D. stainless steel tube fitted with an outer jacket containing liquid mercury, which was heated electrically. Reaction temperatures were controlled by adjusting the pressure of the carbon dioxide atmosphere maintained above the boiling mercury.

The catalyst was supported on a perforated disc welded to the ¼-inch O.D. thermowell assembly, which was attached to the reactor by a gasketed flange. The whole thermowell assembly was dropped for catalyst removal. Thermocouples were inserted in the thermowell to measure temperatures at points 2 cm. apart along the catalyst bed (slightly more than one point for every 10 ml. of catalyst charge). The average catalyst temperature was considered to be the arithmetical average of the temperatures measured at these points.

In operation, gaseous products issued from the reactor through Valve *B* to waste until equilibrium temperatures were established, at which point a timed product sample was passed through Valve *C* and collected in the trapping system. This system consisted of an air-cooled trap, a dry ice-cooled trap filled with wire mesh, and a glass wool-filled trap to filter out entrained solids.

The vaporizer was weighed before and after a full day's operation. Yields were calculated on the basis of the proportional amount of naphthalene evaporated during the sampling time.

The naphthalene concentration in the feed was kept low (about 0.28 mole %) to avoid generation of excessive heat and to minimize steep temperature gradients in the catalyst zone. In this manner, the average catalyst temperature was usually kept within 3° of the nominal temperature, and was never more than 6° removed. A slight hot spot which developed in the catalyst bed was always within 10° of the nominal temperature.

At the low naphthalene concentration used, oxygen was in large excess, the molar ratio of oxygen to naphthalene being about 75 to 1. The effect of oxygen partial pressure on the reaction rate thus was assumed to be constant, and was not considered in the treatment.

Relatively high flow rates of 50–60 cm. per second were used to lessen mass transfer effects. (See Section III, 4.)

For the experiments with the fluidized catalyst, the general procedure was the same, except that the reactor was replaced with a 2-inch I.D. Pyrex tube in which 150–700 ml. of the fluid catalyst was supported on a layer of sand. The tube was heated electrically without the provision of a heat transfer jacket. The reactants were introduced from the bottom at a flow rate sufficient to expand and "fluidize" the catalyst.

In these runs, the naphthalene concentration in the feed was 0.6 mole % and the air rate 210 liters per hour. Because of the mixing caused by the fluidization, the temperature through the catalyst bed was uniform.

To prevent "slugging" and by-passing of gas bubbles of reaction mixture, six 2-inch diameter discs of 50 mesh stainless steel screen were evenly spaced to form a baffling system in the catalyst bed.

2. Materials

The Barrett Division's "Polar" brand refined naphthalene (melting point 79.2°C. minimum) was used.

Since catalytic reactions are quite specific, care was taken to prepare a vanadium pentoxide catalyst of regular shape and reproducible properties. This was done by drawing melted c.p. vanadium pentoxide into 6 mm. I.D. Pyrex glass tubing, in which it was allowed to solidify. After carefully breaking the glass tube, the oxide cylinders were sawed into pellets having an average length of 6.7 mm. This catalyst is designated as catalyst A. Although the greater part of the work reported was done with this catalyst, in general the results do not differ greatly from those obtained with commercial-type catalysts (vanadium pentoxide precipitated on an inactive refractory support).

Catalyst B, prepared by the method of E. B. Punnett (4), in which 10% vanadium by weight was supported on "Alundum" granules, was a commercial-type catalyst.

Catalyst C was a $\frac{1}{8}$ x $\frac{3}{10}$-inch pelleted catalyst obtained from the Davison Chemical Company as Davison Grade 903. It contained 10% vanadium pentoxide and 23% potassium sulfate supported on silica gel.

Catalyst D was prepared by impregnating 4–8 mesh active alumina with 8% by weight of vanadium pentoxide according to the method of Punnett (4).

Catalyst E, a powdered catalyst (Code No. 202) supplied by the Davison Chemical Company, contained 10% vanadium pentoxide and 33% potassium sulfate on silica powder. This catalyst was screened to obtain the 150–210 μ size range, which was used in the fluidized catalyst experiments.

3. Analytical Methods

The reaction product in the sampling traps was washed out with acetone and diluted to a known volume. Total anhydride was determined by acid titration; maleic anhydride and naphthoquinone were measured by polarography (5).

Phthalic anhydride was calculated as the difference between maleic anhydride and total anhydride contents.

After carbon monoxide had been converted to carbon dioxide in a combustion furnace, $CO + CO_2$ were determined in the gases issuing from the product traps by absorption in caustic. Formation of CO_2 is reported as excess values over that formed in the reaction of naphthalene to phthalic anhydride or maleic anhydride, and is expressed as per cent naphthalene undergoing complete combustion.

Residual naphthalene was determined by difference and, in a few cases, by an ultraviolet absorption method.

III. Results and Discussion

Catalyst A

The oxidation of naphthalene was carried out over Catalyst A at five nominal temperatures, 340°, 375°, 410°, 450°, and 475°C. Conversions were measured at constant mass velocity. The residence time was varied by changing the catalyst volume in 10-ml. increments. In each series of runs, the average catalyst temperature usually was maintained within 3° of the nominal value. The maximum catalyst temperature in no case exceeded the average value by more than 7°. Experimental data are given in Table I.

Figure 2 shows the decay of the naphthalene concentration as a function of the residence time at different temperatures, and is a plot of the logarithm of the fraction of the residual naphthalene against the residence time. The residence time is defined herein as the ratio of the catalyst void volume to the volume feed rate corrected to the temperature of the reactor. The reasonably straight-line relationship indicates that the consumption of naphthalene can be expressed by a first-order equation. First-order velocity constants were calculated from the slopes of the lines according to the formula:[1]

$$\ln [\mathrm{Np}]/[\mathrm{Np}_0] = -kt. \qquad [1]$$

Here k differs from the specific rate constant by a factor for catalyst surface area per unit reactor volume, which is constant for a particular catalyst in a flow system, and by a factor for the oxygen partial pressure, which is also assumed to be constant. The rate constants are given in Table II.

In Fig. 3, the Arrhenius plot of the logarithm of the rate constant against the reciprocal temperature is shown. The slope of this plot corresponds to an activation energy of 29 kg.-cal.

Two typical sets of conversion curves showing the distribution of reaction products as a function of catalyst volume are reproduced in Figs. 4 and 5. Although the figures are for two different temperatures, the general shape of the curves is similar. The curves show the expected exponential decay of the naphthalene starting material with time. The curves for naphthoquinone show a maximum, and indicate that reactions leading to its formation and destruction are involved. A notable exception from the behavior of a consecutive reaction sequence, however, is the absence of a primary product (that is, the absence of a product that predominates at low con-

---

[1] All symbols are defined in Table VI.

TABLE I

Experimental results, Catalyst A

Run no.	Catalyst volume, (ml.)	Residence time (sec.)	Reaction products, mole % of naphthalene					
			Np	PA	MA	Nq	CO_2	CO
Experiment 1. Nominal Temperature 340°C.								
1	10	.023	97.8	0.90	0	0.84	0.30	0.12
2	20	.048	97.35	1.42	0	0.92	0.29	0.11
3	30	.073	96.0	2.11	0	0.78	0.59	0.39
4	40	.096	95.3	2.69	0	0.98	0.68	0.33
5	50	.117	94.7	2.99	0	1.32	0.68	0.33
6	57	.135	93.0	3.71	0	1.50	1.08	0.73
Experiment 2. Nominal Temperature 375°C.								
7	30	.069	91.2	4.24	0	3.09	1.06	0.43
8	40	.090	85.4	9.83	0	4.25	0.28	0.27
9	60	.144	86.7	7.30	.45	3.80	1.40	0.33
10	80	.182	64.0	25.9	1.30	3.87	3.83	1.20
11	100	.244	61.4	28.1	2.29	4.07	2.66	1.53
Experiment 3. Nominal Temperature 410°C.								
12	20	.044	75.4	15.2	0	6.74	1.95	0.68
13	30	.065	58.0	31.8	2.03	4.41	2.72	1.08
14	40	.086	51.0	35.9	3.37	5.51	3.28	0.94
15	60	.130	40.2	45.5	2.88	5.00	4.69	1.77
16	80	.171	31.3	52.7	3.56	4.12	6.62	1.93
17	100	.217	17.7	66.6	4.96	3.09	4.65	2.96
Experiment 4. Nominal Temperature 450°C.								
18	10	.021	57.3	31.8	1.98	4.79	1.95	2.02
19	20	.042	42.0	48.2	2.63	4.05	1.58	1.58
20	30	.061	26.2	61.2	4.10	4.00	2.40	2.10
21	40	.082	23.5	66.3	4.72	3.74	0.36	1.44
Experiment 5. Nominal Temperature 475°C.								
22	10	.020	45.4	42.0	2.36	6.48	1.65	2.16
23	20	.040	29.5	60.1	3.61	4.88	0.84	1.09
24	30	.050	17.3	70.5	4.52	4.22	1.25	2.15

versions but that decreases while the secondary products increase in concentration as the reaction progresses). The fact that phthalic anhydride concentration is larger than the naphthoquinone concentration even at the lowest conversions measured indicates that phthalic anhydride is not formed exclusively through naphthoquinone as an intermediate.

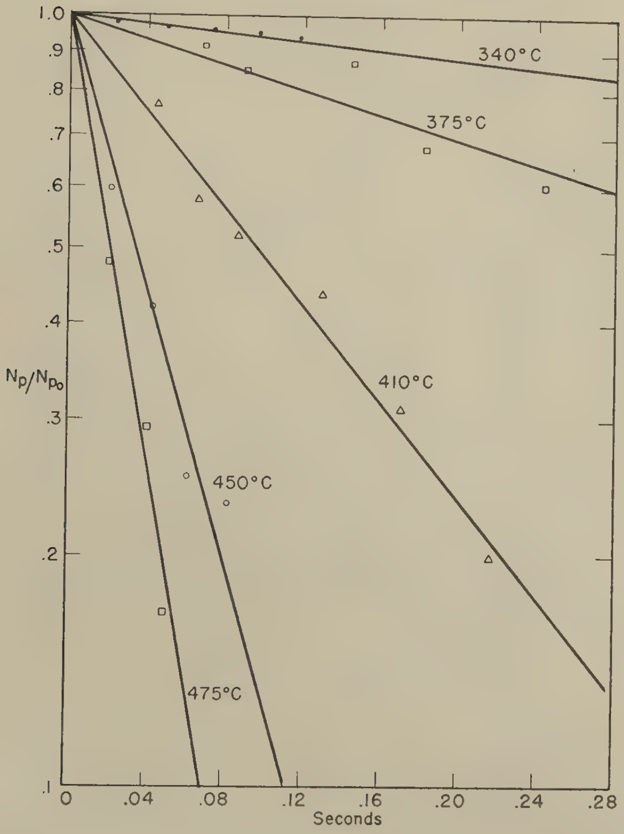

FIG. 2. Comparison of experimental points with first-order naphthalene consumption.

TABLE II

Overall Oxidation Rates over Catalyst A

Temperature (°C.)	*k* (*sec.*$^{-1}$)
340	0.56
375	1.70
410	7.36
450	20.4
475	32.9

The absence of a primary product is shown in another way in Fig. 6 in which the product yields based on the naphthalene attacked are plotted as a function of the conversion. Experimental points for all the temperatures used are included on the same plot. Extrapolation to zero conversion shows the distribution of products formed in the initial stages of the reaction. Again it is obvious that no single product predominates at low conversion. From the intercepts on the product yield ordinate, it appears that

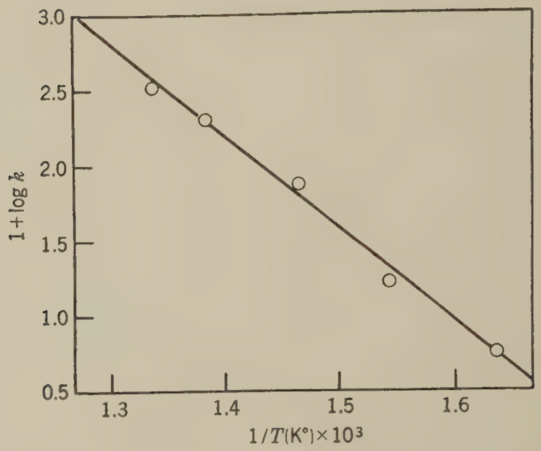

FIG. 3. Variation of rate constant with temperature for catalyst A.

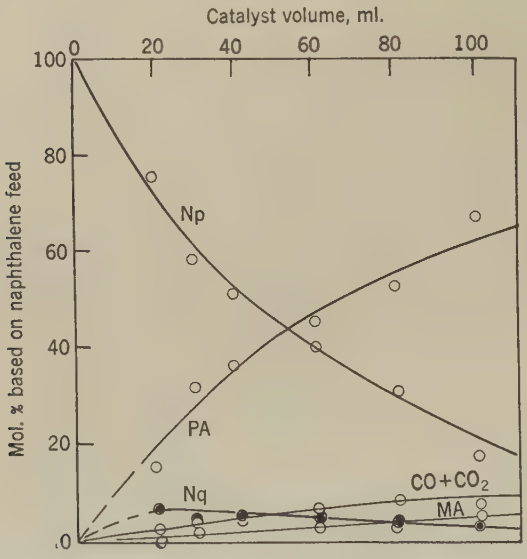

FIG. 4. Conversion curves for catalyst A at 410°C.

there is a branching of the primary reaction step into three simultaneous reactions that form phthalic anhydride, naphthoquinone, and carbon oxides in the approximate, respective proportions 0.4:0.4:0.2. Naphthoquinone undergoes further oxidation as indicated by the decrease in naphthoquinone concentration in the product with extent of attack.

The experimental points for the combined CO + CO_2 curve were not inserted to avoid possible confusion with those for naphthoquinone. In-

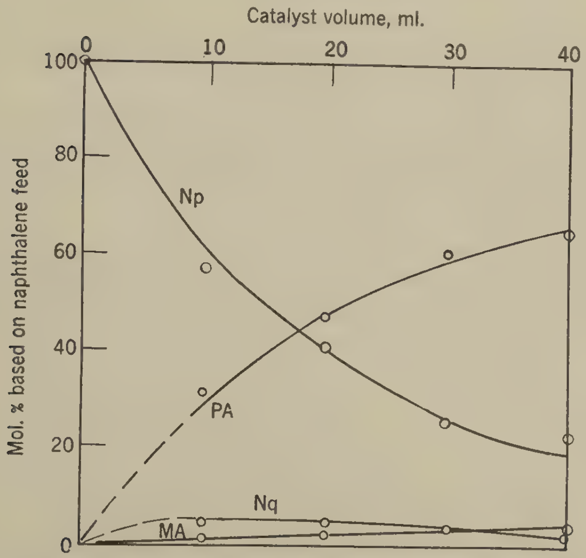

FIG. 5. Conversion curves for catalyst A at 450°C.

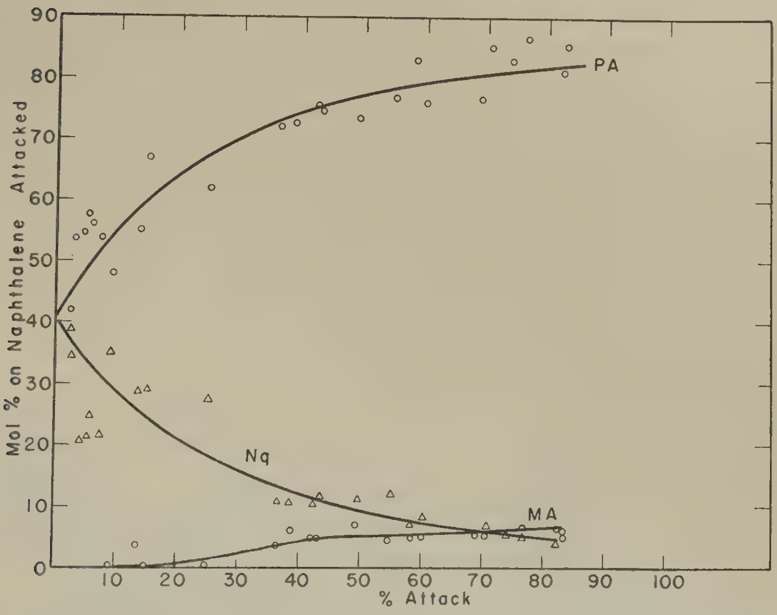

FIG. 6. Percentage in total product. Variation with per cent conversion.

cluding data for different temperatures in a plot of this kind is not correct unless the temperature coefficients of the individual steps are similar. Since the carbon oxides showed a tendency to decrease with increasing conversion, the temperature coefficient for $CO + CO_2$ formation apparently is lower than that for the other reaction steps.[2] Of the identified products, only maleic anhydride acts as a true secondary product by forming zero per cent of the products at zero conversion.

Any attempt to characterize a reaction scheme for this oxidation, therefore, must involve both consecutive and simultaneous reactions. Although a completely rigorous treatment for so complex a reaction is impossible, the following approximations are of interest.

If, for simplicity, those products more highly oxidized than the desired product, viz., maleic anhydride, CO, and CO_2, are grouped together and designated as CO_2, the reaction may be considered to follow a scheme such as this:

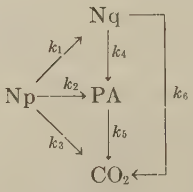

Naphthalene is consumed by three simultaneous reactions. A path is provided for the further oxidation of naphthoquinone and phthalic anhydride to each successively more oxidized stage. Such a scheme is necessarily true, but is trivial if the constants are allowed to have any value including zero. It is desirable to solve for values of the constants which will give agreement with the experimental data.

On the assumption of first-order reaction steps, the set of differential equations that govern the concentrations of each chemical species with time are:

$$\begin{aligned} d\,[\mathrm{Np}]/dt &= -(k_1 + k_2 + k_3)\,[\mathrm{Np}] \\ d\,[\mathrm{Nq}]/dt &= k_1\,[\mathrm{Np}] - (k_4 + k_6)\,[\mathrm{Nq}] \\ d\,[\mathrm{PA}]/dt &= k_2\,[\mathrm{Np}] + k_4\,[\mathrm{Nq}] - k_5\,[\mathrm{PA}] \\ d\,[\mathrm{CO_2}]/dt &= k_3\,[\mathrm{Np}] + k_6\,[\mathrm{Nq}] + k_5\,[\mathrm{PA}] \end{aligned} \qquad [2]$$

Even with the simplifying assumptions that have been made, analytic solutions for these differential equations, beyond the expressions for naphthalene and naphthoquinone, become unwieldy. If, however, values for the constants are assumed in advance and inserted, the equations become

[2] The decrease in the relative amount of CO + CO_2 in the reaction product as the conversion is increased by raising the temperature is surprising. This decrease is due either to a lower temperature coefficient for the reaction step or steps leading to complete combustion, or to a change in the catalyst with increasing temperature. This change may be a shift in the steady-state concentrations of the various oxides of vanadium in the catalyst under the reaction conditions, the proportions of which depend on temperature and composition of reacting gases.

TABLE III

Relative Values of the Rate Constants and Solutions of Rate Equations for Oxidation over Catalyst A

	Case 1	Case 2
k_1	0.45	0.45
k_2	0.45	0.45
k_3	0.10	0.10
k_4	7.50	2.00
k_5	0.04	0.02
k_6	2.50	0.25
Np	$Np_o e^{-t}$	$Np_o e^{-t}$
Nq	$0.05\ Np_o(e^{-t} - e^{-10t})$	$0.36\ Np_o(e^{-t} - e^{-2.25t})$
PA	$Np_o(-0.859e^{-t} + 0.0377^{-10t} + 0.822e^{-0.04t})$	$Np_o(-1.194e^{-t} + 0.323e^{-2.25t} + 0.871e^{-0.02t})$
$MA + CO + CO_2$	$Np_o - Np - Nq - PA$	$Np_o - Np - Nq - PA$

much more tractable and may be solved easily by the use of "operational methods" (6). The sum of the constants k_1, k_2, and k_3 is equal to the measured overall rate constant. Since the constants have already been shown to be in the approximate proportions of 0.4:0.4:0.2, it is necessary only to select relative values for the remaining rate constants, k_4, k_5, and k_6, to test the validity of the branching mechanism.

Two sets of values for the latter constants were assumed. These values together with the solutions for the integrated rate expressions for the products are given in Table III. The plots of these functions produce synthetic conversion curves (Figs. 7 and 8) which resemble the curves obtained from the experimental data.[3] The naphthoquinone curve falls below the phthalic anhydride curve and does not cut it at any point. However, the fit is not exact. The naphthoquinone maximum is too low in one case and too high in the other. Further adjustment of the three unknown constants could yield a better match.

Because the concentration of CO plus CO_2 in the product does not increase with conversion, the carbon oxides must be formed only by branched (simultaneous) steps. The concentration of maleic anhydride in the product does increase with conversion; therefore, it is improper to group these three products together. A better reaction scheme would be:

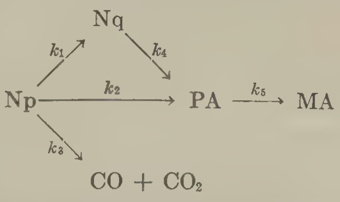

---

[3] For simplicity, relative rate constants for the reaction steps have been used in the integration rather than absolute values. The integrated rate expressions, therefore, involve relative rather than absolute values of the product concentrations. This procedure is valid for the purpose of comparing shapes of conversion curves.

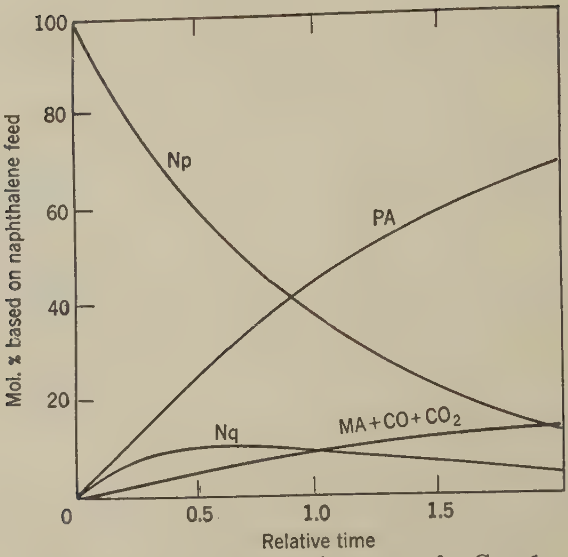

FIG. 7. Calculated conversion curves for Case 1.

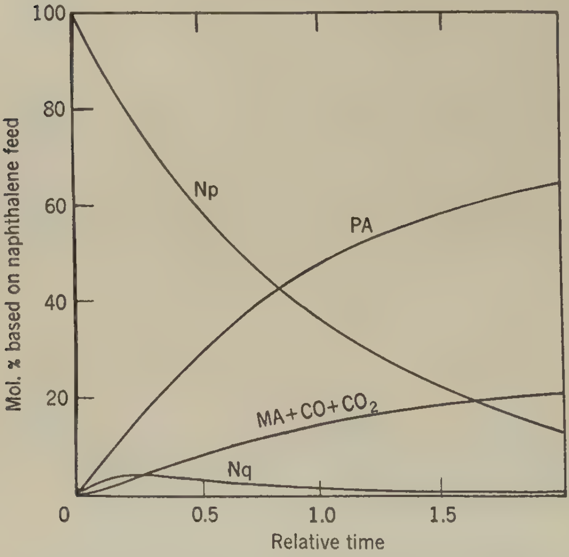

FIG. 8. Calculated conversion curves for Case 2.

The adjustment of only two constants, k_4 and k_5, should give much better agreement with the experimental curves.

2. Other Fixed Bed Catalysts

In the oxidation over catalyst A, the formation of CO + CO_2 through a simultaneous reaction from the starting naphthalene was the most serious limiting factor in realizing high conversions of the desired product, phthalic

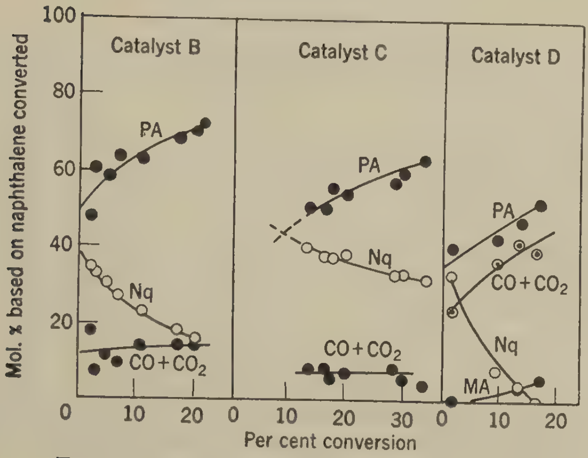

FIG. 9. Initial products for various catalysts.

anhydride. Therefore, the behavior of the reaction at low conversions was investigated for three other catalysts to determine the influence of the branching of the primary step. Again the results were plotted as yield based on naphthalene converted versus conversion, and were extrapolated to zero conversion. These plots are shown in Fig. 9.

For catalyst B, which was a granular Alundum-supported vanadium pentoxide catalyst, the curves look almost identical to those for the pelleted catalyst A. The same type of branching of the initial reaction step applies, and the formation of phthalic anhydride, naphthoquinone, and $CO + CO_2$ occurs at the approximate relative rates of 0.5:0.4:0.1.

With catalyst C, really low conversions were not achieved, but it appears that here, for the first time, the naphthoquinone and phthalic anhydride curves cross. The phthalic anhydride, therefore, is formed at least partially through naphthoquinone. The relative rate of naphthoquinone consumption is lower than that for the previously investigated catalysts. The $CO + CO_2$ curve again does not appear to increase with conversion, and, therefore, suggests that these materials form only through simultaneous steps. The $CO + CO_2$ curve is lower, however, with only about 7.5% of the naphthalene reacting along the branch to complete combustion.

In the case of catalyst D (vanadium pentoxide impregnated on γ-alumina), the maximum yield obtainable for phthalic anhydride is limited both by branching of the primary step to form CO and CO_2 and by subsequent combustion of the intermediate products. This conclusion follows from the observation that the $CO + CO_2$ curve cuts the ordinate at about 20% of total products and increases rapidly with extent of conversion. It is obvious that catalyst D would not form a good practical catalyst for phthalic anhydride production.

TABLE IV

Experimental Results, Catalyst E

Temperature 314°C.

Residence time, sec.	0.261	0.605	1.214
Conversions, mole %			
PA	43.5	72.2	89.2
Nq	16.0	5.0	2.1
MA	1.5	1.7	2.1
CO + CO_2	1.5	1.1	5.4
Total	62.5	80.0	98.8
Naphthalene unreacted, %	37.5	20.0	1.2

3. *Fluidized Catalyst*

The oxidation of naphthalene was carried out also with a fluidized catalyst, catalyst E. The residence time was varied by varying the catalyst volume from 150 to 700 ml. The naphthalene content of the feed mixture was 0.60–0.63 mole % in an air stream of 210 liters per hour. The results obtained at 314°C. are summarized in Table IV.

The data in this instance, though scant, can be represented by a sequence of first-order reactions:

$$\mathrm{Np} \xrightarrow{k_1} \mathrm{Nq} \xrightarrow{k_2} \mathrm{PA} \xrightarrow{k_3} \mathrm{CO_2}$$

where CO_2 now denotes the sum of maleic anhydride, carbon monoxide, and carbon dioxide.

The differential equations involved in consecutive reactions of this type can be integrated by the usual methods to give:

$$[\mathrm{Np}] = [\mathrm{Np_0}]e^{-k_1t} \tag{3}$$

$$[\mathrm{Nq}] = \frac{k_1}{k_2 - k_1}[\mathrm{Np_0}](e^{-k_1t} - e^{-k_2t}) \tag{4}$$

$$[\mathrm{PA}] = \frac{k_1 \cdot k_2}{k_1 - k_2}[\mathrm{Np_0}] \cdot \left[\frac{1}{k_1 - k_3}(e^{-k_1t} - e^{-k_3t}) - \frac{1}{k_2 - k_3}(e^{-k_2t} - e^{-k_3t})\right] \tag{5}$$

$$[\mathrm{CO_2}] = [\mathrm{Np_0}] - [\mathrm{Np}] - [\mathrm{Nq}] - [\mathrm{PA}] \tag{6}$$

The values of the constants k_1 and k_2 can be determined from Eq. [3] and from the maximum value for naphthoquinone ($\mathrm{Nq_{max}}$) that is given by:

$$[\mathrm{Nq}]_{\mathrm{max}} = \frac{k_1}{k_1 - k_2}[\mathrm{Np_0}]\left(\frac{k_2}{k_1}^{k_2/k_1-k_2} - \frac{k_2}{k_1}^{k_1/k_1-k_2}\right). \tag{7}$$

Since k_2 turns out to be much larger than k_1, the second reaction step can be omitted temporarily for the estimation of k_3. The value of k_3 can

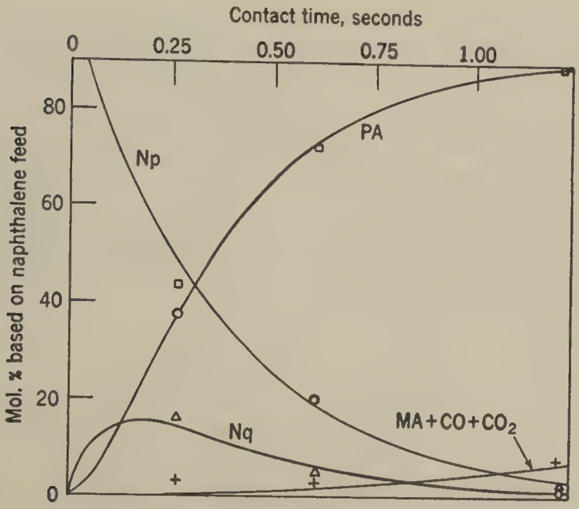

FIG. 10. Conversion curves for catalyst E.

then be calculated from an expression for $[PA]_{max}$ which is identical to Eq. [7].

On this basis, the following values of the velocity constants were chosen:

$$k_1 = 2.78 \text{ sec.}^{-1};$$

$$k_2 = 11.12 \text{ sec.}^{-1};$$

$$k_3 = 0.08 \text{ sec.}^{-1}.$$

With these constants, the values for phthalic anhydride, naphthoquinone, the sum of maleic anhydride, carbon monoxide, and carbon dioxide, and unattacked naphthalene were calculated as a function of time. The values thus obtained are represented in Fig. 10. The experimental points are plotted on the same figure. Comparison with the calculated conversion curves shows satisfactory agreement.

4. Role of Mass Transport

Since catalytic oxidations are very rapid reactions, it is not necessarily true that the mass transfer is sufficiently fast to supply reactants to the catalyst, with the result that the measured reaction rates may be more or less controlled by the transport phenomena.

The mass transport in catalytic reactions can occur by the following processes:

a. Knudsen diffusion in the fine pores of the catalyst.
b. Surface diffusion on the catalyst.
c. Eddy diffusion in the gas phase caused by turbulence.
d. Molecular diffusion in the gas phase.

In the present consideration, calculations will be made for catalyst A. Process *a* will be disregarded because of the rapidity of the reaction and the absence of fine pores in the pelleted catalyst A. Furthermore, for simplification, the surface diffusion on the catalyst (process (*b*)) is assumed to be sufficiently rapid compared to diffusion processes in the gas phase. Consequently, the primary purpose will be to estimate the diffusional processes (*c*) and (*d*) as compared to the rate of reaction.

For this discussion, use will be made of the concepts of height of transfer unit (H_t), height of catalytic unit (H_c), and height of reactor unit (H_r), defined by D. M. Hurt (7) as follows:

$$-dy/dZ = 1/H_t(y - y_1) \qquad [8]$$

$$-dy/dZ = 1/H_c(y_1 - y^*) \qquad [9]$$

$$-dy/dZ = 1/H_r(y - y^*) \qquad [10]$$

where Z is the height of the packed bed and y, y_1, and y^* are the mole fractions of reacting gas in the gas stream, at the gas-solid interface, and in equilibrium, respectively. In the case of naphthalene oxidation, y refers to naphthalene and $y^* = 0$.

For a first-order reaction, these various heights are connected by the relation:

$$H_r = H_c + H_t\,. \qquad [11]$$

Integrating Eq. [10] and comparing with Eq. [1] gives:

$$\ln \mathrm{Np}/\mathrm{Np}_0 = Z/H_r = -kt. \qquad [12]$$

Thus H_r is the height of catalyst bed required to reduce the naphthalene to $1/e$ of its original concentration; H_r can be determined from the attack ($\mathrm{Np}/\mathrm{Np}_0$) and the bed depth by using formula [12].

The value of H_t will now be calculated to determine the contribution it makes to H_r (8). Chilton and Coburn (9) have expressed H_t in terms of the mass transfer characteristics:

$$H_t a_v = 1/j_d(\mu/\rho D_v)^{2/3}, \qquad [13]$$

where a_v is the surface area of the catalyst in unit reactor volume. The mass transfer factor, j_d, is a function of the modified Reynolds number. Wilke and Hougen (10) have recommended:

$$j_d = 1.82(D_pG/\mu)^{0.51}, \qquad (D_pG/\mu < 350). \qquad [14]$$

Here D_p is the diameter of a sphere which has the same surface area as an average particle in the bed—in this case, a 6.0 by 6.7 mm. cylinder.

Using Eqs. [13] and [14], the height of the transfer unit was calculated

TABLE V

Calculation of Heights of Transfer and Reactor Units

	Temperature (°C.)					
	340	375	410	450	475	
D_v	0.219(9, 10)				0.307(11, 12)	cm.^{2} sec.$^{-1}$
μ	0.000307				0.000352	g. cm.$^{-1}$ sec.$^{-1}$
ρ	0.000576				0.000471	g. cm.$^{-3}$
Dp	0.763				0.763	cm.
G	0.357				0.357	g.cm.$^{-2}$ sec.$^{-1}$
a_v	5.30				5.30	cm.$^{-1}$
j_d	0.185				0.198	dimensionless
H_r	280.0	52.5	15.2	5.3	3.8	cm.
H_t	1.84				1.72	cm.

TABLE VI

Definition of Symbols

Np	Naphthalene
Np_o	Naphthalene concentration at start of reaction
PA	Phthalic anhydride
MA	Maleic anhydride
Nq	Naphthoquinone
k	Overall reaction rate constant, sec.$^{-1}$
k_n	Reaction rate constant for reaction n
t	Residence time, sec.
T	Temperature, °K.
H_r	Height of reactor unit, cm.
H_c	Height of catalytic unit, cm.
H_t	Height of transfer unit, cm.
Z	Height of catalyst bed, cm.
a_v	Surface area per unit vol. of catalyst, cm.$^{-1}$
μ	Viscosity, g. cm.$^{-1}$ sec.$^{-1}$
ρ	Density of reaction mixture, g. cm.$^{-3}$
D_v	Diffusivity, cm.^{2} sec.$^{-1}$
j_d	Mass transfer factor, dimensionless
D_p	Diameter of sphere with surface area of average catalyst particle, cm.
G	Mass velocity, g. cm.$^{-2}$ sec.$^{-1}$

for 340°C. and for 475°C. (the temperature range in which the naphthalene oxidation was studied over catalyst A). The values used for the physical properties and the results calculated for H_r and H_t are shown in Table V. From these results, the reactor height appears to be sufficiently larger than the transfer height, at least below 450°C. The measured rates, therefore, correspond to the chemical reaction rates below this temperature, but, above 450°C. mass transfer phenomena begin to make a significant contribution.

REFERENCES

1. MAREK, L. F., AND HAHN, D. A., "Catalytic Oxidation of Organic Compounds in the Vapor Phase." American Chemical Society Monograph Series No. 61, Chemical Catalog Company, New York, 1932.
2. FARKAS, A., "Kinetics of the catalytic oxidation of naphthalene," paper presented at Catalysis Session, Gordon Research Conferences, American Association for the Advancement of Science, 1950. D'ALESSANDRO, A. F., CLARK, C. R., and FARKAS, A., "Kinetics of the catalytic oxidation of naphthalene," paper presented at the Meeting in Miniature of the Philadelphia Section of the American Chemical Society, January 18, 1951.
3. CALDERBANK, P. H., *Ind. Chemist* **28,** 291 (1952).
4. PUNNETT, E. B. (to National Aniline and Chemical Co.), U. S. 1,978,506, October, 1934.
5. Barrett Standard Method, unpublished.
6. CARSLAW, H. S., AND JAEGER, J. C., "Operational Methods in Applied Mathematics." Oxford, 1947.
7. HURT, D. M., *Ind. Eng. Chem.* **35,** 522 (1943).
8. HOUGEN, O. A., AND WATSON, K. M., "Chemical Process Principles," Volume 3, Chapter 20, p. 973. Wiley, New York, 1947.
9. CHILTON, T. H., AND COBURN, A. P., *Ind. Eng. Chem.* **27,** 255 (1935).
10. WILKE, C. R., AND HOUGEN, O. A., *Trans. Am. Inst. Chem. Engrs.* **41,** 445 (1945).
11. MACK, E., JR., *J. Am. Chem. Soc.* **47,** 2468 (1925).
12. ARNOLD, J. H., *Ind. Eng. Chem.* **22,** 1091 (1930).

JOURNAL OF COLLOID SCIENCE **11**, 671–687 (1956)

DIELECTRIC RELAXATION TIMES OF SOME NONRIGID POLAR MOLECULES

A. Aihara[1] **and Mansel Davies**[2]

The Edward Davies Chemical Laboratories, University College of Wales, Aberystwyth

Received March 26, 1956

The molecular interpretation of the frequency dependence of molar polarization has been based largely upon Debye's treatment. This envisages a rigid spherical polar molecule having one relaxation time proportional to the macroscopic viscosity of the medium. Even for dilute solutions extensions of this treatment have been made to embrace nonspherical molecules, distributions of relaxation times, and the evaluation of the correct form of the viscosity factor (1). The particular concern of the present study is the influence of nonrigidity in the polar molecule. This factor has already received consideration both in theoretical terms (2) and in experimental accounts (3).

According to Budó the effective relaxation time of a molecule with a freely rotating polar group can be expressed as follows:

$$\tau_{\text{eff}} = \left(\frac{\mu_f}{\mu}\right)^2 \tau_f + \left(\frac{\mu_{f'}}{\mu}\right)^2 \tau_{f'} + \left(\frac{\mu_r}{\mu}\right)^2 \tau_r$$

Here μ_f and $\mu_{f'}$ are the fixed components of the moment in the direction of the axis of internal rotation and in the plane perpendicular to that axis, and μ_r is the component of the rotating moment also in the plane perpendicular to the axis. τ_f, $\tau_{f'}$, and τ_r are associated relaxation times and $\mu^2 = \mu_f^2 + \mu_{f'}^2 + \mu_r^2$. In general, $\mu \neq \mu_{\text{obs}}$. The value τ_{eff} is clearly a weighted mean relaxation time whose particular significance is that it can reasonably be expected to correspond to the relaxation time deduced on the assumption that the absorption measured at an appreciable interval from the individual frequencies is of a simple Debye type. This assumption is implicit in published experimental assessments of these cases. In simple instances where the direction of the fixed component of the moment coincides with the intramolecular rotational axis, the above equation becomes

$$\tau_{\text{eff}} = \left(\frac{\mu_f}{\mu}\right)^2 \tau_f + \left(\frac{\mu_r}{\mu}\right)^2 \tau_r,$$

---

[1] Permanent address: Shinshu University, Agata-machi, Matsumoto, Japan.

[2] Member of Colloid Science Laboratory, 1935–38.

whence, in the condition $\tau_r < \tau_f$, one finds that τ_{eff} will be less than the value expected for a rigid structure, which would be approximately τ_f. This provides the qualitative criterion for detecting nonrigidity in a polar molecule.

Particular interest attaches to such structures as the para-derivatives of benzene when the two substituents are identical. In these cases $\mu_f = \mu_{f'} = 0$ and Budó's equation becomes

$$\tau_{\text{eff}} = 2\left(\frac{\mu_r}{\mu}\right)^2 \tau_r.$$

For freely rotating groups $\mu_r = \mu/\sqrt{2}$, so that $\tau_{\text{eff}} = \tau_r$. However, τ_r does not itself give the relaxation time (τ_g) arising from the rotation of the polar group. The further relation

$$\frac{2}{\tau_r} = \frac{1}{\tau_{f'}} + \frac{1}{\tau_g}$$

is involved. Here, as previously, $\tau_{f'}$, is the relaxation time expected for the molecule if it merely had a rigid moment perpendicular to the axis of rotation; it can be estimated from the τ values for rigid molecules having nearly the same size and shape as those being considered. Proceeding along these lines both Hase and Fischer have evaluated τ_g in a number of cases; when its value agrees approximately with the relaxation time anticipated for a free rigid molecule of the same size as the rotating group, it is concluded that the latter suffers no hindrance within the molecule. Values of τ_g appreciably larger than those estimated from its size are taken to indicate hindered rotation. Budó has also examined such cases theoretically (2c).

EXPERIMENTAL

All the absorption measurements reported were made over the range 3×10^4–1×10^8 cycles per second (= 100 Mc. per second) with a Hartshorn-Ward apparatus; this measures the loss tangent ($\tan \delta = \epsilon''/\epsilon'$) in terms of the capacitance increment (ΔC) corresponding to the half-width of the voltage-resonance curve of the cell-containing circuit (4). Amongst the checks on its performance we can report the following observations. At each of eight frequencies between 0.2 and 50 Mc. per second the half-widths for air in the capacitance cell varied by no more than 2% when measured over intervals of weeks; for the small solution loss factor of $\tan \delta = 1 \times 10^{-3}$ at 70 Mc. per second, ΔC (solution) became 0.837 $\mu\mu$f compared with ΔC (air) = 0.667 $\mu\mu$f. Small loss factors up to 100 Mc. per second for a transformer oil agreed within a few per cent with measurements at the N.P.L.

For solutions, the loss factor (if any) of the solvent at the same frequency

TABLE I

Dielectric Properties of Solvent Xylene at 15°C.

f in Mc. per sec.	69.8	13.7	6.75	3.07	1.36	0.646
ϵ'	2.38	2.36	2.36	2.37	2.38	2.38
$10^3 \times \tan\delta$	0.08	0.06	0.03	0.04	0.01	0.05
	0.350	0.192	0.113			
	2.37	2.38	2.38			
	0.06	0.04	0.09			

must be subtracted in deducing that for the solute. Benzene and tetrachloroethylene were found (as expected) to have zero loss. For dioxane at 70 Mc per second the value of $\tan\delta$ was less than 0.05×10^{-3}. For the solvent xylene (mostly meta-) slightly varying values of $\tan\delta$ were found for different preparations; a typical sequence is quoted in Table I. Literature values of ϵ' for xylene are 2.57 (ortho), 2.37 (meta), and 2.27 (para), all at 20°C. In comparison, a 1.0 M phenol solution in xylene has $10^3 \times \tan\delta = 2.00$ at 70 Mc per second.

Our general procedure was checked by measuring a number of solutes of known relaxation times. In dilute solutions both the Debye and Onsager equations become (1a)

$$\tan\delta = \frac{(\epsilon' + 2)^2}{\epsilon'} \cdot \frac{4\pi s\mu^2}{27kT} \cdot \frac{\omega\tau}{1 + \omega^2\tau^2},$$

where ϵ' is the permittivity of the medium, s the number of polar molecules per cubic centimeter, ω the angular frequency ($\omega = 2\pi f$), and τ the relaxation time. When $\omega\tau \ll 1$, this relation reduces to

$$\tau = \frac{\tan\delta}{\omega \cdot c} \cdot \frac{6750\, kT}{\pi N\mu^2} \cdot \frac{\epsilon'}{(\epsilon' + 2)^2},$$

where N = Avogadro's number and c is the molar concentration. The constancy of $\tan\delta/\omega$ for a particular solution provides a simple test of the applicability of the Debye equations, and from its value τ may be calculated. Table II shows some results for a benzophenone solution.

Using a mean value $\tan\delta/\omega = 12.4 \times 10^{-12}$ and $\mu = 3.00\ D$ we find $\tau = 16.7 \times 10^{-12}$ sec. This is in excellent agreement with Jackson and Powles's value for the same solute in benzene, $\tau = 16.4 \times 10^{-12}$ sec. at 19°C., which is one of the most precise values in the literature (5). The

TABLE II

1.34 M Benzophenone in Xylene at 18°C.

f in Mc./sec.	69.8	28.5	13.7	6.75	3.07
ϵ'	3.82	2.82	2.82	2.82	2.82
$10^3 \times \tan\delta$	5.50	2.16	1.07	0.52	0.29
$10^{12} \times \tan\delta/\omega$	12.6	12.1	12.4	12.3	15.0

centipoise values of the viscosities at 21°C. are η (benzene)/η (xylene) = 0.638/0.650. Similar comparisons are contained in later tables.

As ϵ' is measured to within 2% and its value is usually of the order of 3, no significant error arises in the factor $\epsilon'/(\epsilon' + 2)^2$, so that apart from variations in tan $\delta/\omega c$, the only other appreciable uncertainty in the τ_{eff} values obtained in this way arises from uncertainty in μ. When values have to be transferred from another (similar) solvent, this uncertainty may amount to a few per cent, and $\tau \propto (1/\mu^2)$.

Unless otherwise mentioned all the dipole moment data not determined by ourselves have been taken from Wesson's tables (6). They are invariably given in Debye units. In a number of instances we have had to estimate μ for ourselves:

1. From measurements on a pure liquid, for which the appropriate Onsager equations (1a) are:

$$\mu^2 = \frac{9kT}{4\pi s} \cdot \frac{(\epsilon' - n_\infty^2)(2\epsilon' + n_\infty')}{\epsilon'(n_\infty^2 + 2)^2};$$

$$\tau = (\tan \delta/\omega) \cdot \epsilon'/(\epsilon' - n_\infty^2).$$

s is the number of molecules per cubic centimeter and for η_∞, the η_D value has been used.

2. From Higashi's form of the Debye equation for dilute solutions (7) which, for xylene at 20°C., reduces to $\mu = 0.96 \times 10^{-18} (\Delta\epsilon'/x)^{1/2}$. Here $\Delta\epsilon' = \epsilon'$ (solution) $- \epsilon'$ (solvent) and x is the mole fraction of solute whose moment is μ. Dipole moments estimated in these ways are given in Tables III and IV, where comparison is made in some instances with previous values; they are usually correct to 5% or 10%.

Measurements were normally made at room temperatures; these are recorded in the tables. Some few measurements were made in an auxiliary cell which could be kept at lower temperatures, but its useful range was limited to below 20 Mc. per second.

It must be noted that many of the dipole moments we have perforce used involve a more general uncertainty in the correction for the atomic polarization term. An abnormally large atomic polarization term such as might arise in nonrigid molecular structures would have the effect of making the dipole moment value—from the usual radiowave data—larger than that appropriate for the above equations. This itself would make our τ_{eff} values smaller than they should be. Thus we must envisage two by no means mutually exclusive conditions leading to $\tau_{\text{eff}} < \tau_{\text{rigid}}$; (*1*) the presence of $\tau_r < \tau_{\text{rigid}}$ in the absorption relations for the meter-wave region; (*2*) a contribution from a much higher frequency "atomic polarization" term whose immediate effect in our results is to make μ (experimental) $> \mu$ (rigid). The qualitative result and interpretation is the same in either case, i.e., the high frequency flexibility of the molecule—but only for case (*1*) does the Fischer-Budó treatment of the data apply. Further consideration of these factors is included in the discussion of relevant cases.

If we assume the applicability of the Pellat-Debye equations, our relaxation times should represent τ_{eff} to within 20%.

Materials

All chemicals, unless of Analar grade, were purified before use and their m.p.'s or b.p.'s checked against literature values. Some particular treatments should be mentioned. Solvent xylene (mostly meta) was shaken mechanically with concentrated H_2SO_4, washed with alkali and water, dried ($CaSO_4$) and the fraction distilling 138–140°C. used. An air stream was passed for 6–8 hours through dioxane treated with concentrated HCl to oxidize aldehyde impurities. After preliminary drying (Na_2CO_3, $CaSO_4$) it was kept over sodium before a final distillation.

Di-*n*-butyl terephthalate prepared from the acid and alcohol distilled at 211–212°C./18 mm. *p*-Phenylenediamine was first distilled at 18 mm. and recrystallized from $CHCl_3$; m.p. 130°C. (lit. 139.7°C.). Terephthaloyl chloride, recrystallized from Analar petroleum ether, had m.p. 83°C. (lit. 78°C.). Triphenylmethyl chloride prepared by passing dry HCl gas into a boiling benzene solution of the carbinol and subsequently recrystallizing from petroleum ether had m.p. 108–110°C. (lit. 109–112°C.).

Results

The tables summarize the observations made. The τ_{eff} values are deduced from the mean values of $\tan \delta/\omega \cdot c$ and a generous indication of the variation in this factor is appended to the figures quoted. The uncertainty is greatest in those cases where low solubility or small τ values lead to $\tan \delta$ values below 0.50×10^{-3}. Again, the equations used assume that the solutions are sufficiently dilute to eliminate solute-solute interactions. This has been confirmed for many cases by the proportionality of $(\tan \delta/\omega)$ to concentration; in other instances, notably the phenols and some amines, obvious concentration variation showed the influence of association. These instances have been detailed and will be further discussed. The abbreviations, xyl. = xylene; teth. = tetrachloroethylene; diox. = *p*-dioxane; benz. = benzene; liq. = pure liquid; O = Onsager's equations; H = Higashi's equations; are used. The unit for τ values is 10^{-12} sec.

Discussion

Two methods are available for assessing the rigidity of these molecules from their τ_{eff} values. Firstly, the τ_{eff} values may be compared with those of similar rigid molecules—preferably in the same solvent. Most such measurements have been made in benzene (1c); fortunately, as we have confirmed,

TABLE III

Solute	Solvent	Temp. (°C.)	μ solute (D)	$10^{12} \times \tau_{eff}$ (*sec.*)	Observations
1,4-Dimethoxybenzene	xyl.	15	1.70	6.3 ± 0.4	
	teth.	18	1.70	8.3 ± 0.8	
	diox.	17	1.70	9	
αα′-Dichloro-*p*-xylene	xyl.	18	2.17	5 ± ?	Very small tan δ for 0.4*M* solution
Dimethylterephthalate	xyl.	19	2.2	14 ± 3	0.11*M* solution; low solubility
Diethylterephthalate	xyl.	16	2.3	27.6	Uncertainty determined by μ
Diethylterephthalate	teth.	18	2.3	44 ± 1	
Diethyl-*o*-phthalate	xyl.	15	2.68	12.9 ± 1	
Diethyl-*o*-phthalate	teth.	18	2.68	16.1 ± 1	
Diethyl-*o*-phthalate	liq.	22	2.6	104 ± 3	ε′ (obs.) = 7.84; μ and τ from O
Diethyl-*o*-phthalate	liq.	−15	2.6	760 ± 40	
Di-*n*-butylterephthalate	xyl.	18	2.3	54 ± 3	μ = 2.2 from H
Di-*n*-butylterephthalate	teth.	19	2.3	69 ± 3	
Di-*n*-butylterephthalate	liq.	19	2.48	640 ± 15	ε′ (obs.) = 5.82 μ and τ from O
Terephthaloyl chloride	xyl.	18	0.90	12 ± ?	μ = 1.0 from H; μ = 0.92 for oxalyl chloride. Very small tan δ's for 1.25*M*
Triphenyl carbinol	benz.	20	2.11	11 ± 1	
	diox.	21	2.11	17 ± 1	
Triphenylmethyl chloride	xyl.	19	1.95	62 ± 2	
Dimethyloxalate	xyl.	21	2.0	3.8 ± 0.5	μ from H
Diethyloxalate	xyl.	22	2.49	4.4 ± 0.4	
	liq.	24	2.41	12.3 ± 0.5	ε′ (obs.) = 8.30; μ and τ from O
Ethylacetate	liq.	22	1.77	5.2 ± 0.5	ε′ (obs.) = 6.20; μ and τ from O
Methylcyclohexane	liq.	21	No loss from 0.1 to 70 Me./sec.		ε′ = 2.03
Cyclohexene	liq.	21	0.61	—	ε′ = 2.25; μ = 0.36 from O
Cyclohexanone	xyl.	16	2.75	5.3 ± 0.3	
o-Methylcyclohexanone	xyl.	22	(2.8)	5.6 ± 0.3	
o-Methylcyclohexanone	liq.	23	2.99	18 ± 2	ε′ = 14.05; μ and τ from O
1,4-Cyclohexanedione	xyl.	22	1.29	—	At 0.32*M* tan δ (solution) showed negligible increase from solvent. μ(apparent) = 1.2 from H
Cyclohexylamine	xyl.	22	1.32	1.2 ± ?	Very small tan δ for 1.87*M*
	liq.	22	1.40	5.2 ± 0.5	ε′(obs.) = 4.57; μ and τ from O
Nitromesitylene	xyl.	22	3.65	15.5 ± 0.4	
Benzil	xyl.	21	3.76	22.3 ± 1	
o-Methoxymethyl benzoate	xyl.	20	2.4	16	μ from H
o-Methoxymethyl benzoate	Nujol	20	2.4	250 ± 40	

TABLE IV

Solute	Solvent	Temp. (°C.)	Molar conc.	$10^{12} \times (\tan\delta/\omega c)$	Observations
Phenol	xyl.	20	1.75	6.1 ± 0.1	From extrapolated value 2.30 at $c = 0$ and μ (benz.) = 1.70, $\tau = 14.3 \pm 1.0$.
Phenol	xyl.	21	0.972	4.34 ± 0.08	
Phenol	xyl.	21	0.61	3.67 ± 0.15	
Phenol	teth.	21	1.70	7.2 ± 0.1	From extrapolated value 0.9_2 at $c = 0$ and μ (CCl_4) = 1.41, $\tau = 8.5 \pm 1$.
Phenol	teth.	22	0.793	3.8 ± 0.4	
3,5-Dimethylphenol	xyl.	20	1.45	11.1 ± 0.4	From extrapolated value 2.30 at $c = 0$ and μ (assumed) = 1.70, $\tau = 14.3 \pm 0.6$.
3,5-Dimethylphenol	xyl.	22	1.05	8.4 ± 0.2	
3,5-Dimethylphenol	xyl.	22	0.50	5.4 ± 0.2	
3,5-Dimethylphenol	xyl.	22	0.319	4.2 ± 0.3	
2,6-Dimethylphenol	xyl.	20	1.50	0.75 ± 0.10	Using $\mu = 1.36$ (mesitol), $\tau = 7 \pm 1$.
2,6-Dimethoxyphenol	xyl.	21	1.09	7.8 ± 0.2	$\mu = 2.5$ from H leads to $\tau = 21$.
2,6-Dinitrophenol	xyl.	22	0.87	17.7 ± 0.5	Using 18.0 and $\mu = 3.5$ from H, $\tau = 25$.
2,6-Dinitrophenol	xyl.	20	0.62	18.5 ± 0.5	
Picric acid	xyl.	23	0.32	6.9 ± 0.6	From $\mu = 1.75$ (Maryott (8)), $\tau = 41 \pm 4$.
Picric acid	diox.	22	1.16	28 ± 2	Using $\mu = 1.75$, $\tau = 160 \pm 15$.
Picryl chloride	xyl.	20	1.85	0.95 ± 0.10	Very small tan δ values. With $\mu = 0.9$ from H, mean $\tau = 19 \pm 2$.
Picryl chloride	xyl.	21	1.24	0.80 ± 0.10	
o-Nitrophenol	xyl.	20	2.30	4.1 ± 0.2	From extrapolated value 5.7 at $c = 0$ and $\mu = 3.11$, $\tau = 10.7 \pm 0.5$.
o-Nitrophenol	xyl.	20	1.15	4.8 ± 0.2	
	xyl.	20	0.23	5.6 ± 0.4	
o-Chlorophenol	xyl.	18	1.52	0.78 ± 0.08	Using $\mu = 1.31$, $\tau = 8.2 \pm 0.8$.
o-Chlorophenol	xyl.	−15	1.27	8.1 ± 0.4	Using $\mu = 1.31$, $\tau = 74 \pm 4$.
o-Chlorophenol	liq.	22	—	—	ϵ' (obs) = 6.46, from O. $\mu = 1.55$, $\tau = 60 \pm 4$.

TABLE IV—*Continued*

Solute	Solvent	Temp. (°C.)	Molar conc.	$10^{12} \times (\tan \delta/\omega c)$	Observations
2,4,6-Trichlorophenol	xyl.	20	1.43	1.79 ± 0.05	Using $\mu = 1.62$, $\tau = 12.0 \pm 0.5$.
2,4,6-Trichlorophenol	diox.	21	1.17	11.3 ± 0.5	Using $\mu = 1.62$, $\tau = 76 \pm 4$.
2,4,6-Tribromophenol	xyl.	23	1.01	2.3 ± 0.2	Using $\mu = 1.56$, $\tau = 17 \pm 2$.
2,4,6-Tribromophenol	diox.	21	0.80	14.0 ± 0.7	Using $\mu = 1.56$, $\tau = 100 \pm 5$.
2,6-Dimethyl aniline	xyl.	20	2.33	1.16 ± 0.08	From extrapolated value 1.43 at $c = 0$ and $\mu = 1.69$, $\tau = 10.1 \pm 1.0$.
2,6-Dimethyl aniline	xyl.	21	1.62	1.22 ± 0.04	
2,6-Dimethyl aniline	xyl.	21	1.25	1.29 ± 0.05	
2,6-Dimethyl aniline	liq.	21	—	—	ϵ' (obs) = 5.95; from O. $\mu = 1.60$, $\tau = 31 \pm 1$.
2,4,6-Tribromoaniline	xyl.	21	0.288	4.3 ± 0.3	Using $\mu = 1.80$, $\tau = 24 \pm 2$.
2,4,6-Tribromoaniline	diox.	21	1.00	15.6 ± 0.4	Using $\mu = 1.80$, $\tau = 85 \pm 2$.
2,4,6-Trinitroaniline	diox.	22	0.426	55.0 ± 0.5	Using $\mu = 3.25$, $\tau = 91 \pm 1$.
p-Phenylene-diamine	diox.	19	0.757	$0.58 \pm$?	Very small tan δ values. Using $\mu = 1.50$, $\tau \sim 4$.

the viscosity of our (meta-) xylene differs by less than 1% from that of benzene, and any solvation effects should be similar in these two media.

Secondly, we can make an *a priori* estimate of τ_{eff} assuming the molecule to be rigid. This starts from Perrin's equation

$$\tau = \frac{4\pi\eta}{kT} \cdot (a \cdot b \cdot c) \cdot f.$$

Here η represents the viscosity for solute rotation in the solvent (the "microscopic" solvent viscosity); a, b, and c are the semiaxes of the molecular rotational ellipsoid; and f is the "form factor" which is equal to the ratio of the relaxation time about one of the ellipsoid axes to that of a sphere of equal volume. This factor has been evaluated for various cases by Budó, Fischer, and Miyamoto (9). The geometrical terms (a, b, c, and f) are adequately established from direct measurements of Courtauld's models of the molecules concerned. The principal ambiguity arises for η. It is well known that the effective viscosity differs appreciably from the macroscopic value. What is needed is the effective viscosity of the solvent with respect to a particular solute molecule, and this is dependent upon such factors as the relative sizes of solute and solvent and their intermolecular force field (10). The most satisfactory evaluation of this factor yet available is the one due to Miss Hill (11). That, however, required detailed analysis of the solution viscosities. We have followed Fischer's empirical assessment—from experimental τ values he finds η (microscopic)/η (macroscopic) = 0.23 for a variety of solutes in benzene (3d). In transferring this factor to xylene appreciable error may be involved in individual cases. This means that, unless other evidence is available, only considerable differences between τ_{calc} and τ_{eff} are significant. As typical instances of rigid molecules we can quote the relaxation times calculated with the use of Fischer's factor for xylene solutions of picryl chloride, nitromesitylene, and triphenylmethyl chloride (all in 10^{-12} sec.), i.e., 18.2, 19.3, and 37.4. The observed values were 19, 15.5, and 62. Only for the triphenyl compound is the disagreement significant—it almost certainly arises from the influence of its relatively large molecular size upon the factor 0.23. It is well known that the micro-viscosity increases with the size of the solute molecule, approaching as a limit the macroscopic value (10). This form of deviation, it may be noted, would tend to mask any influence of nonrigidity in the comparison of relaxation times. We retain the use of τ_{eff} for the experimental values, τ_f for the rigid molecules, and τ_g for the relaxation time arising from the group rotation: in appropriate cases, as already explained, the latter is evaluated via τ_r. Related structures are discussed together; unless otherwise indicated the solvent is xylene and all the τ values are in units of 10^{-12} sec. Values of τ_f in solvents other than xylene are obtained by multiplying the values in the latter by the ratio of the macroscopic viscosities.

1,4-Dimethoxybenzene and αα′-Dichloro-p-xylene

These molecules have been measured in a number of solvents, and the results are seen in Table V.

TABLE V

Molecule	Solvent	τ_{eff}	Investigator
1,4-Dimethoxybenzene	$C_6H_4(CH_3)_2$	6.3	A.A. and M.D.
	C_2Cl_4	8.3	A.A. and M.D.
	$C_4H_8O_2$	9.0	A.A. and M.D.
	C_6H_6	6.9	Fischer (3f)
	CCl_4	9.4	Hase (3g)
αα′-Dichloro-*p*-xylene	$C_6H_4(CH_3)_2$	5	A.A. and M.D.
	C_6H_6	4.9	Fischer
	C_6H_6	6.7	D'Or and Henrion (3a)

The agreement between our own and previous values is satisfactory These are certainly instances of non-rigid structures as the minimum values of τ_f in xylene would be 10×10^{-12} sec. Fischer has estimated τ_g for the dimethoxybenzene as 4.1; completely free rotation of the methoxy group would make this nearer 3.0, perhaps suggesting some restraint in the C—O bond. Relative to xylene the τ_{eff} value in C_2Cl_4 increases almost in the ratio of their viscosities (1.31 and 1.40), but whilst the viscosity of dioxane is twice that of xylene, τ_{eff} is increased by only 40%. This, perhaps surprisingly, would correspond to completely free rotation of the methoxy groups in the dioxane solution. From his estimate of τ_g (=2.7) Fischer concluded there was unhindered rotation of the substituents in the dichloro-*p*-xylene.

Terephthalic and Phthalic Acid Derivatives

The relevant results are summarised in Table VI.

For the diethyl esters it appears there is no appreciable mobility within the molecules. Whilst for di-*n*-butyl terephthalate $\tau_{\text{eff}} > \tau_f$, this probably results from the underestimate of η (microscopic) for this bulky molecule. The dimethylterephthalate values perhaps indicate some mobility; Fischer found $\tau_{\text{eff}} = 14.5$ for the same ester in benzene. The contrast with other esters suggests that this may reside in the methyl rotation around the C—O bond in the ester grouping. This conforms to the absence of rotation about the C_{al}—C_{ar} bond indicated by the apparent rigidity of acetophenone, benzaldehyde, and terephthaldehyde—where C_{al}=O is also conjugated with the aromatic ring. Both for the dimethyl ester and for the more doubtful case of terephthaloyl chloride, the τ_g values indicate far from free rotation. These instances of $\tau_{\text{eff}} < \tau_f$ may, in fact, arise from an abnormally large contribution by the atomic polarization to the dipole moment used. Thus the most that can be claimed is that the data for the dimethylterephthalate suffice to indicate some form of flexibility in the molecular structure. The ratios $\tau_{\text{eff}}(C_2Cl_4)/\tau_{\text{eff}}(C_6H_4(CH_3)_2)$ for diethylphthalate, diethylterephthalate, and di-*n*-butylterephthalate are 1.22, 1.59, and 1.24—in approximate agreement with the solvent viscosity ratio, 1.40. In pure

TABLE VI

Molecule	τ_{eff}	τ_f	τ_r	τ_g
Dimethylterephthalate	14	18.2	18.2	11.9
Diethylterephthalate	27.7	24.0		
Diethylterephthalate in C_2Cl_4	44	(33.6)		
Di-*n*-butylterephthalate	54	36		
Di-*n*-butylterephthalate in C_2Cl_4	67	(50)		
Terephthaloylchloride	12	18.2	18.2	9.0
Diethylphthalate	16.4	18.2		
Diethylphthalate in C_2Cl_4	20	(25.4)		

diethylphthalate (see Table III) a temperature change of 37° changes τ_{eff} by a factor of 7.3, whilst the viscosity ratio is 9.9.

Triphenyl Carbinol

The calculated τ_f was 34.4 whilst τ_{eff} was only 10.7. This strongly suggests free rotation of the OH group in this molecule. For the certainly rigid triphenylmethyl chloride, τ_f was 37.4 and $\tau_{\text{eff}} = 62$. The reason for this difference has already been mentioned. If we assume that the angle COH is 115° and use accepted "bond moments," the justifiable use of $\tau_f = 62$ with $\tau_{\text{eff}} = 10.7$ for the carbinol leads to $\tau_r = 2.1$ and $\tau_g = 1.1$. The latter value probably conforms to unhindered rotation of the hydroxyl group. Dioxane again provides a lower τ_{eff} value than its viscosity relative to xylene would suggest; this may mean that its microscopic viscosity is being overestimated, but in any case the result emphasizes the existence of a loss process in triphenylcarbinol with a relaxation time much smaller than τ_f.

Both infrared (12) and dielectric absorption (13) studies of solid triphenylcarbinol have shown the comparative freedom of its hydroxyl group even in the crystalline state. It is essentially the result of steric protection.

Phenolic Structures

The τ values in Table VII are in xylene unless otherwise described.

The results given in Table IV show the influence of association in a number of the phenolic solutions. Figure 1 shows how tan $\delta/\omega \cdot c$, which should be independent of concentration, increases linearly with molarity (c) to an extent much greater than any viscosity change for the medium. *o*-Nitrophenol, whose association is unlikely to be significant here (14), shows a

TABLE VII

Molecule	τ_{eff}	τ_f	τ_r	τ_g
Phenol	14.3	9.7		
Phenol in teth.	8.5	13.6	7.1	4.8
Phenol in CCl_4 (3d)	9.3	12.6		
3,5 Dimethylphenol	14.3	13.0		
2,6 Dimethylphenol	6.8	13.0	5.5	3.5
2,6 Dimethoxyphenol	21.4	15.3		
o-Nitrophenol	10.7	12.1		
2,6-Dinitrophenol	24.5	15.3		
Picric acid	41	18.2		
Picric acid in diox.	160	36.4		
Picryl chloride	19	18.2		
o-Chlorophenol	8.2	9.9		
2,4,6-Trichlorophenol	12.0	15.9	11.0	8.4
2,4,6-Trichlorophenol in diox.	76	32		
2,4,6-Tribromophenol	17	19.8		
2,4,6-Tribromophenol in diox.	100	40		

much smaller decrease of τ_{eff} with increasing concentration. In the former cases the increase with concentration of the solute's mean particle size is probably responsible for the net effect observed. Measurements of the viscosities of xylene solutions at 21.0°C. support this contention. It is seen in Fig. 2 that for phenol and 3,5-dimethylphenol the solution viscosity increases more than proportionally to concentration and as the dielectric results suggest, the effect (of association) is the greater for 3,5-dimethylphenol. For 2,6-dimethylphenol, whose association will be much reduced by the steric "protection" of the hydroxyl, the viscosity increases at most linearly with concentration.

In cases where $\tan \delta/\omega \cdot c$ depends on concentration the τ_{eff} values in Table VII refer to zero concentration, and are open to the additional uncertainty of extrapolation from the observed values. Picryl chloride is relevant as an example of a rigid molecule, and it is seen that no departures from that condition can be claimed for 3,5-dimethylphenol, *o*-nitrophenol,

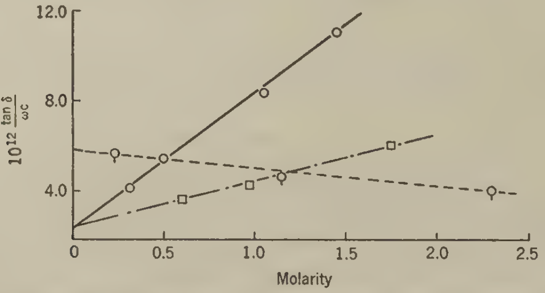

FIG. 1. Concentration dependence of relaxation times in xylene at 21 ± 1°C. ⊡ = phenol; ⊙ = 3,5 dimethylphenol; ⚲ = orthonitrophenol.

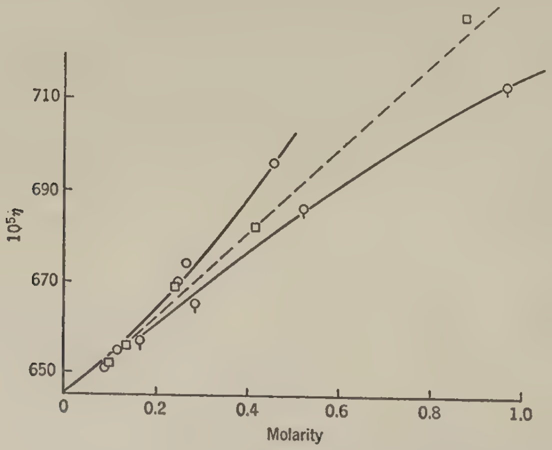

FIG. 2. Viscosity (η) in c.g.s. units of xylene solutions at 21.0°C. ⊡ = phenol; ⊙ = 3,5-dimethylphenol; ⚲ 2,6-dimethylphenol.

o-chlorophenol, or 2,4,6-tribromophenol. For phenol itself in tetrachloroethylene it seems that $\tau_{\text{eff}}(c = 0)$ is lower than τ_f by more than the experimental uncertainty; our result agrees well with Fischer's in carbon tetrachloride. However, the τ_g evaluated suggests a distinctly restricted rotation of the hydroxyl group.

In xylene the result $\tau_{\text{eff}} > \tau_f$ is found for phenol, for 2,6-dimethoxy and 2,6-dinitrophenol, and for picric acid. This condition is even more strikingly established in dioxane solutions. The anomaly is not due to any low-frequency conductance which these solutions might possess—such a factor leads to a tan δ decreasing with increasing frequency. In dioxane the result could correspond to the effective moment being increased by a factor of at least 2 relative to the benzene (or xylene) value; this might arise if a large proportion of ion pairs, $RO^-[HO_2C_4H_8]^+$, were formed in dioxane. This effect, if it occurred, would be found by low-frequency dipole moment measurements, but it is far in excess of what happens even with HCl dissolved in dioxane—the ratio of whose moments in dioxane and benzene is 2.12/1.25. In any case, this factor is inapplicable to xylene solutions, where only a negligible difference in moment from benzene can be expected.

Alternative interpretations of $\tau_{\text{eff}} > \tau_f$ in these cases are: Firstly, that solvation of the phenolic molecules occurs which markedly increases the effective size of the polar solute. This might be supported by the change in dipole moment of phenol itself: $\mu(\text{gas}) = 1.40$; $\mu(CCl_4)$ (15) $= 1.41$; $\mu(C_6H_6) = 1.70$; and also by the existence of the well-known aromatic hydrocarbon complexes of picric acid and 2,6-dinitrophenol. This possibility has been eliminated for picric acid by comparing the viscosities of its xylene solutions with those of picryl chloride which has a normal τ_{eff} value. At various molar concentrations (c) up to 0.35 M at 21.0°C. values of η (intrinsic) $= (\eta_{\text{solution}} - \eta_{\text{solvent}})/\eta_{\text{solvent}} \cdot c$ were, for picric acid, 0.604; 0.571; 0.559; 0.561; for picryl chloride, 0.592; 0.568; 0.570. This shows both solutes to be in a comparable state of solvation. Accordingly, we are driven to a second interpretation which is that an additional relaxation time to τ_f may arise from the switching of the OH group between two positions in the molecule (τ_t), each position equally stabilized by "hydrogen bridge" interactions with adjacent groups. Meakins (16) has, in fact, reported solid state results for 2,6-dinitrophenol and picric acid which show such a process, with $\tau_t > \tau_f$. This explanation is supported by the absence of the effect for dissolved *o*-nitro- and *o*-chlorophenol, where the hydrogen will essentially be tied to the side of the adjacent group, and, again, in 2,6-dimethyl- and 2,4,6-tribromophenols, where such interaction may be insignificant or, as 2,4,6-trichlorophenol suggests, perhaps $\tau_t \leqslant \tau_f$. Clearly, this bond rotation process is a type of proton-jumping mechanism and deserves further more detailed study.

The influence of dioxane in these cases is very striking; it has twice the viscosity of xylene, but for picric acid, trichlorophenol, and tribromophenol τ_{eff} is increased in the ratios 3.9, 6.3, and 5.9. It is very unlikely that this arises solely from its influence on the solute dipole moment, e.g., the μ value of trichlorophenol would have to be increased by a factor $\sqrt{6.3/2} = 1.77$, before the observations would conform to simple viscosity changes. Alternately, with μ constant, the solute molecular volume would have to be 3.15 times its value in xylene; solvation is unlikely to increase to this extent. Thus it seems that, apart from some influence on the μ values, dioxane may have a specific effect (increasing τ_t) on the proton-jumping process.

Aniline Derivatives

Fischer has claimed that the NH_2 group in aniline has at least a fairly large amplitude of torsional vibration about the C_{ar}—N bond. The τ_{eff} values for 2.6 dimethylaniline, 10.1, and 2,4,6-tribromoaniline, 24, in xylene approximate to those estimated for the rigid molecules, 13 and 20, respectively. However, the existence of the same anomaly as for the phenols is seen in the τ_{eff} values for the 2,4,6-tribromo and 2,4,6-trinitro anilines in dioxane, which are 85 and 91. For trinitroaniline we have used the dipole moment measured in dioxane, combined with $10^{12} \times \tan \delta/\omega$ values for a 0.426 *M* solution which were, at five frequencies from 6 to 70 Mc. per second, 23.1; 23.1; 23.5; 23.7; 23.4. The result $\tau_{\mathrm{eff}} \gg \tau_f$ seems particularly well established in this case. The magnitude and direction of this effect makes the results for phenylenediamine in dioxane all the more remarkable. The tan δ value for a 0.76 *M* solution (Table IV) was only 0.19×10^{-3} at 70 Mc. per second, corresponding to a maximum τ_{eff} of 4.4. This, however, conforms to Fischer's $\tau_{\mathrm{eff}} = 1.5$ in benzene; these values correspond to completely free rotation of the para-substituted amino groups. (See also "Alicyclic Compounds" below.)

Oxalic Acid Derivatives

From the values in Table VIII we can safely conclude that there is flexibility in these molecules, and from the small τ_g values it seems unlikely that rotation of the 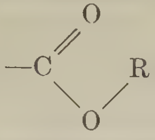 $-\mathrm{C}(=\mathrm{O})-\mathrm{O}-\mathrm{R}$ halves of the molecule is involved but rather that of the OR group about the C—O bond. Some evidence for the mobility of these groups was found in dimethylterephthalate (Table VI). Sutton (17) has observed that "the moments of aliphatic carboxylic esters, which

TABLE VIII

Molecule	τ_{eff}	τ_f	τ_r	τ_g
Dimethyloxalate	3.8	7.1	3.8	2.6
Diethyloxalate	4.4	10.6	4.4	2.8

vary from 1.6 to 1.9 D, agree roughly with the moment of 1.5 D calculated for the trans-configuration (A) with the alkyl groups turned away from each other. The alternative extreme configuration (B) would have a moment of about 3.5 D." The present data suggest limited rigidity in the oxalate esters—possibly owing to conjugation in the (O=C—C=O) system reducing the partial double-bond character of the C—O linkages. The value $\mu = 2.41$ D deduced from Onsager's equation and $\epsilon' = 8.30$ for pure diethyloxalate agrees with Smyth and Walls's value (18), 2.49 D; the ratio of τ_{eff} in the liquid (12.3) to that in xylene (4.4) is 2.8, whilst the ratio of viscosities is 3.0.

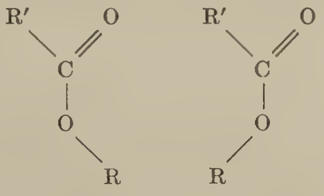

(A) (B)

Alicyclic Compounds

The value of $\tau_{\text{eff}} = 5.3 \pm 0.3$ for cyclohexanone in xylene may be compared with those of 6.5 and 10.5 in benzene due to Whiffen and Thompson (19) and to Cripwell and Sutherland (20). *o*-Methylcyclohexanone has a similar value in xylene—5.6 ± 0.3—the less certain value for the pure liquid (18 ± 2) showing an increase by 3.2, compared with the viscosity ratio of 2.6. Both these cyclohexanones have similar, compact, almost spherical molecules from whose volumes $\tau_f = 12$ is predicted for xylene. The appreciable difference between τ_{eff} and τ_f strongly tempts one to suggest a high-frequency absorption process arising from puckering of the cyclohexanone ring. The only other obvious source of the discrepancy is that the spherical form of these molecules reduces the micro-viscosity of the solvent much below its normal value in these cases. However, this explanation could not apply to the pure liquid value (*o*-methylcyclohexanone). We are inclined to the conclusion that the discrepancy shown by τ_{eff} in these cases arises from a large atomic polarization term, not properly assessed in the evaluation of the dipole moments. Results for 1,4-cyclohexanedione support this conclusion; we failed to detect any appreciable absorption at 0.32 *M* over our frequency range, which suggests a moment at most half that (1.29) recorded for it in the literature or calculated by us from Higashi's equation and ϵ' (solution). The atomic polarization term normally corresponds to a relaxation time smaller than that associated with group rotations—but this condition might well apply to distortions of the chair-form of the cyclohexane ring.

For liquid cyclohexylamine we have the abnormally low value $\tau_{\text{eff}} \cong 5$.

A 1.87 *M* solution of this amine in xylene showed such small tan δ values that only a maximum value, $\tau_{\text{eff}} = 3$, could be established. The same very small value has been found by Fischer for aniline in benzene. Certainly some intramolecular mobility is involved here. For the cyclohexylamine it might be:

1. high-frequency puckering of the cyclohexane ring with its polar substituent;

2. rotation of the NH_2 group about the C—N bond;

3. "inversion" of the H-atoms about the nitrogen.

The alternative (*1*) would not apply in the case of the similar results for aniline (and *p*-phenylenediamine), and the present data cannot distinguish between (*2*) and (*3*). At the same time (*2*) and (*3*) are irrelevant to the case of the cyclohexanones.

For the "miscellaneous" structures, nitromesitylene, *o*-methoxy-methyl benzoate, and benzil the measured τ_{eff} values agree within the experimental uncertainty with the estimated τ_f values.

General Conclusions

It is clear that nonrigidity in molecular structures may vary from almost completely free rotation of groups (e.g., OH in triphenylcarbinol) to restricted torsional vibrations. Only the more obvious cases can be definitely established by such exploratory studies as the present, but even these suffice for preliminary comparison of conditions in related molecules.

The influence of solvents upon relaxation times for both rigid and nonrigid molecules is well illustrated by some of our data for dioxane solutions. Now that the dependence of dipole moment upon solvent is sensibly well analyzed by Onsager's relations and the micro-viscosity can be evaluated from Miss Hill's treatment, the variation of relaxation time with solvent can disclose the extent of solute-solvent interaction. In the case of rigid molecules an assessment can be made of the size of the solvent sheath (if any) carried by the rotating polar solute.

Nonrigidity may arise in a number of forms—as in the case of the esters or cyclohexylamine—whose differentiation may be difficult but could be advanced by systematic comparison of variations due to molecular substitutions, etc. Most important of all, a more adequate frequency coverage (up to 10^{11} cycles per second) would allow of testing the appropriateness in these instances of the Pellat-Debye form of the loss equations, and it might resolve the various contributions to the low-frequency absorption into the individual components. In favorable cases it should be possible to distinguish between alternative modes of dipole relaxation from the integrated absorptions—as these will be proportional to the square of the dipole moment oscillations involved. Much, therefore, can be looked for in the development of this field of molecular structure studies.

ACKNOWLEDGMENTS

We wish to thank the British Council for an Overseas Fellowship (to A.A.) and the Royal Society for a grant for the purchase of apparatus. We are also grateful to the Dyestuffs Division of Messrs. I.C.I. Ltd., for providing a number of the compounds we have examined.

REFERENCES

1. See, for instance, (a) BÖTTCHER, C. J. F., "Theory of Dielectric Polarization." Elsevier, Amsterdam, 1953; (b) MÜLLER, F. H., AND SCHMELZER, Chr., *Ergeb. exakt. Naturw.* **25**, 359–475 (1951); (c) DAVIES, M., *Quart. Revs. (London)* **8**, 250 (1954).
2. (a) BUDÓ, A., *Physik. Z.* **39**, 706 (1938); (b) BUDÓ, A., *ibid.* **40**, 603 (1939); (c) BUDÓ, A., *J. Chem. Phys.* **17**, 686 (1949); (d) KIRKWOOD, J. G., AND FUOSS, R. M., *ibid.* **9**, 329 (1941).
3. (a) D'OR, L., AND HENRION, J., *Physik. Z.* **38**, 426 (1937); (b) FISCHER, E., AND FRANK, F. C., *ibid.* **40**, 345 (1939); (c) FISCHER, E., *ibid.* **40**, 645 (1949); (d) FISCHER, E., *Z. Naturforsch.* **a4**, 707 (1949); (e) FISCHER, E., *ibid.* **a8**, 168 (1953); (f) FISCHER, E., *ibid.* **a9**, 909 (1954); (g) HASE, H., *ibid.* **a8**, 695 (1950).
4. HARTSHORN, L., AND WARD, W. H., *J. Inst. Elec. Engrs.* p. 597 (1936).
5. JACKSON, W., AND POWLES, J. G., *Discussions Faraday Soc.* **A42**, 101 (1946).
6. WESSON, L. G., "Tables of Electric Dipole Moments." Massachusetts Institute of Technology Press, Cambridge, Mass., 1948.
7. HIGASHI, K., *Sci. Papers Inst. Phys. Chem. Research (Tokyo)* **22**, 805 (1943).
8. MARYOTT, A., *J. Research Natl. Bur. Standards* **41**, 1 (1948).
9. BUDÓ, A., FISCHER, E., AND MIYAMOTO, S., *Physik. Z.* **40**, 337 (1940).
10. SPERNOL, A., AND WIRTZ, K., *Z. Naturforsch.* **a8**, 122 (1953).
11. HILL, N. E., *Proc. Phys. Soc. (London)*, **B67**, 149 (1954).
12. DAVIES, M., *J. Chem. Phys.* **8**, 577 (1940).
13. MEAKINS, R. J., *Australian J. Chem.* **6**, 104 (1953).
14. TURNER, W. S., "Molecular Association." Longmans, London, 1917.
15. MECKE, R., REUTER, A., AND SCHUPP, R. L., *Z. Naturforsch.* **a4**, 182 (1949); and ref. 3(d).
16. MEAKINS, R. J., *Trans. Faraday Soc.* **51**, 371 (1955).
17. SUTTON, L. E., *in* E. A. Braude and F. C. Nachod, eds., "Determination of Organic Structures by Physical Methods," p. 405. Academic Press, New York, 1955.
18. SMYTH, C. P., AND WALLS, W. S., *J. Am. Chem. Soc.* **53**, 527 (1931).
19. WHIFFEN, D. H., AND THOMPSON, H. W., *Discussions Faraday Soc.* **A42**, 114 (1946).
20. CRIPWELL, F. J., AND SUTHERLAND, G. B. B. M., *Discussions Faraday Soc.* **A42**, 149 (1946).

NOTE ADDED IN PROOF

THE TRANSFER OF SURFACE FILMS THROUGH SURFACE CHANNELS—GEOMETRICAL FACTORS

Victor K. La Mer and Martin Blank

The data plotted in Fig. 2 are referred to in the text and legend as a ternary mixture. These data refer to an experiment in which a film and lens of Adol 22 was laid down and then separate lenses of ethyl plamitate and of CHM were deposited. The surface pressure was then measured as a function of time as monolayer was transferred. Figure 2 demonstrates the selective transfer of the substances from coexisting separate lenses, but does not demonstrate a separation of the components from a single lens. This problem will be treated in more detail in a later communication.

VINYL TYPE POLYMERIZATION AT SOLID SURFACES AND WITH COMPLEX CATALYSTS

F. Eirich and H. Mark

Institute of Polymer Research, Polytechnic Institute of Brooklyn
Brooklyn, New York

SUMMARY AND CONCLUSIONS

The so-called stereo-specific high polymer syntheses reported during the past few years, and their relation to heterogeneous catalysis, are briefly discussed. The likely courses of reactions during the formation of all-cis polybutadiene, of crystalline polypropylene oxide, and of the poly α-olefins during Ziegler type syntheses are analyzed in detail.

Reviewing the reaction mechanisms suggested, as well as those by the authors quoted, the inadequacy of the schemes to take care of many observations and details is fully recognized. In their present form these mechanisms will certainly require much revision in the light of the future, yet we believe it will be seen that a certain common pattern is apparent even now, the essential features of which permit the formulation of a distinct mechanism of catalysis.

Dividing this mechanism into two parts, i.e. acceleration and direction of reaction, the primary basis for the acceleration appears to be the coordination or complexing of the reactants to the same, or an adjacent, center. This increases the probability of suitable configurations prior to the transition state and thus lowers the entropy, and possibly also the energy, of the latter; the coordinating center participates also in the reaction by attracting electrons from the reactants and returning them to the product under a minimum of rearrangements of atoms. The activation process becomes thereby subdivided into several steps, each with much lower activation energy than that of the reaction as a whole. It is true that such processes have been postulated before in explanations of catalyses but this appears to be a new combination of "cage effect" and electron transfer through a temporary acceptor.

For the steering part of the mechanism, it seems to be essential that the reactive complex is situated on a surface so that one of the reactants is fixed with regard to its internal, rotational, degrees of freedom. The molecule to be added may then lose its energy to the surface, on its path from the transition to the final state, and may drop into a definite position of

lowest energy with respect to the other reactant and the surface. (This can be symbolized by the stacking of tripods which can be placed on each other in any rotational position when standing, but only in 3 distinct ways 120° apart when stacked lying sideways on a plane). This is quite different from the picture developed for some enzymatic or replica syntheses.

Among other features strongly suggested we mention the additional mechanism by which a polymerizable molecule becomes inserted into an existing bond, between the previously linked atoms. This is allied to ester, amide or silicon exchange reactions or even ion exchanges, and, as a double displacement reaction, requires a fairly polar bond. The catalysis of this insertion is tied to a site; consequently, one of the bond partners must be mobile tangentially along the surface, and the growth proceeds like that of a hair from a feeding root.

Finally, it seems required that the coordinating electron acceptor be tied to a electron donating substrate. Whether the donating quality is only needed to hold the coordination center, or is essential in the mechanism of catalysis, cannot be surmised yet, although the latter alternative is likely. There can be little doubt though that the elevated position of the coordinating center, lying on top of a crystal plane, will help in the complex formation.

In view of the rapid development of the field, the completion of this manuscript has been delayed and, for technical reasons, the article will appear in its entirety in the next issue of the *Journal of Colloid Science.*

JOURNAL OF COLLOID SCIENCE **11**, 661–696 (1956)

THE RATIO OF THE POSITIVE AND NEGATIVE LIGHT ION CONDUCTIVITIES WITHIN A NEUTRAL AEROSOL SPACE

Ross Gunn

Office of Physical Research, U. S. Weather Bureau, Washington, D. C.

Received September 11, 1956

Abstract

The diffusion of atmospheric ions onto an aerosol establishes a distribution of particle charges that depends on the ratio of the positive and negative light ion conductivities. When the aerosol space is electrically neutral, it is shown that this important ratio may be expressed in terms of the number of particles per unit volume, their size, the rate of ion pair formation, the light ion mobilities, and recombination coefficient. The derived relation is useful in defining the properties of an aerosol in terms of known and measurable atomic and electrical parameters.

It has been shown in a series of analytical and experimental articles that the net electrical charge carried by aerosol particles depends on the logarithm of the ratio of the electrical conductivities of the positive and negative light ions in the environmental air (2, 3, 4, 6). All ion-producing processes simultaneously generate a positive and negative ion so that except for the influence of combination processes and transport due to electric fields, there is a marked tendency for the establishment of equal ionic population densities. Therefore, since the mobility of the negative ion is some 40% larger than that of the positive ion there is a parallel tendency for the negative ion conductivity to exceed that due to the positive ions. The reality of this phenomenon has been made manifest by a recent series of measurements in a large closed vessel which was systematically cleared of condensation nuclei and pollution (5). It is found that the combination of ions with those of opposite sign and with the particles suspended in the environmental air, always influences the relative abundance of the positive and negative ions. The relative abundance depends not only on the number and size of the suspended particles and the recombination, but also upon the rate of ion production. It is our purpose here to determine analytically the relative ion population densities and electrical conductivities in an aerosol space when the ion production and combination are specified.

It has been shown in this laboratory that when the relatively large numbers of condensation nuclei and other pollution in the atmosphere are progressively removed; then the conductivity of the negative ions increases relative to the conductivity of the positive ions (5). This observed fact is a direct consequence of the notably greater mobility of the negative ions which normally diffuse onto the aerosol at a greater rate than do the corresponding positive ions. In this way a slight excess of positive ions is established outside the suspended particles which compensates for their lower mobility. Thus, when the particle density is large, the conductivities of the positive and negative ions approach equality. One may notice, too, that if the rate of ion pair production is greatly increased, then the equilibrium ionic densities will approach equality, and the conductivity ratio of the positive and negative ions will approximate the ratio of their respective ionic mobilities (4).

In the earth's atmosphere the air at high levels is relatively free of condensation nuclei and the diffusion of ions onto the particulate matter is not large. However, at lower and lower elevations, more and more pollution is encountered and both types of ions recombine with the suspended aerosol at a rate that depends significantly on their mobility. It is important to determine the interrelation between the size of the aerosol particles, their population density, and the ionic and electrical conductivity ratio in a given region. This ratio is useful because it determines the distribution of charges carried by any aerosol in equilibrium with its ionized environment. By employing the well-verified facts of ionic recombination and combination it has been possible to determine the nature of the established equilibrium and its dependence upon the rate of ion production and the mean number of aerosol particles per unit volume.

It is well established that the time rate of disappearance of positive and negative light ions due to recombination with each other is given by

$$\frac{dn_+}{dt} = \alpha n_+ n_- = \frac{dn_-}{dt}, \tag{1}$$

where n_+ and n_- are the positive and negative ionic densities, respectively and α is the recombination coefficient.

Similarly the time rate of disappearance of positive and negative ions that diffuse onto and combine with the aerosol particles of population density N_0 and radius a is given by (2)

$$\frac{dn_+}{dt} = \frac{4\pi Q u_+ n_+ N_0}{\exp\left[\frac{+Qe}{akT}\right] - 1} = \beta_+ n_+ N_0 \tag{2}$$

and

$$\frac{dn_-}{dt} = \frac{4\pi Q u_- n_- N_0}{1 - \exp\left[\frac{-Qe}{akT}\right]} = \beta_- n_- N_0, \tag{3}$$

where Q is free charge carried by the spherical aerosol particle, u_+ and u_- are the mobilities of the positive and negative light ions, k is the Boltzmann constant, T is the absolute temperature, N_0 is the number of aerosol particles of radius a in unit volume, and β_+ and β_- are the combination coefficients of the positive and negative ions on the spherical nuclei. One notices that Eqs. [2] and [3] may be extended to represent the average rate of ion combination if Q is assumed to represent the average charge carried by all the aerosol particles.

One imposes a further requirement by noticing that after a steady state is established any excess charge on the aerosol particles will be neutralized by ions of opposite sign in the aerosol space outside the particles. Thus if the aerosol space is neutral

$$N_0Q = -e(n_+ - n_-), \tag{4}$$

where Q is now the average net free charge carried by the particles and its value is given (2) by

$$Q = \frac{akT}{e} \ln \frac{n_+u_+}{n_-u_-} = \frac{akT}{e} \ln \frac{\lambda_+}{\lambda_-}, \tag{5}$$

where λ_+ and λ_- are the positive and negative light ion conductivities. Thus, mean steady-state values for Eqs. [2] and [3] become approximately

$$\frac{dn_+}{dt} = \frac{4\pi akTu_+}{e} \left(\frac{\ln \frac{\lambda_+}{\lambda_-}}{\frac{\lambda_+}{\lambda_-} - 1} \right) n_+N_0\,; \tag{6}$$

$$\frac{dn_-}{dt} = \frac{4\pi akTu_-}{e} \left(\frac{\ln \frac{\lambda_+}{\lambda_-}}{1 - \frac{\lambda_-}{\lambda_+}} \right) n_-N_0\,. \tag{7}$$

Now if the aerosol space is exposed to X-rays, radioactivity, or cosmic rays, and if such ionizing agencies produce q ion pairs per unit volume per unit time then one may write the equilibrium equations

$$q_- = (\alpha n_+ + \beta_-N_0)n_-\,; \tag{8}$$

$$q_+ = (\alpha n_- + \beta_+N_0)n_+\,. \tag{9}$$

Whence by elimination it is found that

$$n_- = \frac{\beta_+N_0}{2\alpha}\left[\left(1 + \frac{4q\alpha}{\beta_+\beta_-N_0^2}\right)^{1/2} - 1\right]; \tag{10}$$

$$n_+ = \frac{\beta_-N_0}{2\alpha}\left[\left(1 + \frac{4q\alpha}{\beta_+\beta_-N_0^2}\right)^{1/2} - 1\right], \tag{11}$$

where $q_+ = q_- = q$.

It may be noticed from Eqs. [10], [11], and [5] that

$$\frac{n_+}{n_-} = \frac{\beta_-}{\beta_+} = \frac{\lambda_+ u_-}{\lambda_- u_+}. \qquad [12]$$

By combining the above relations it is found that

$$\begin{aligned} \frac{N_0 akT}{e} \ln\left(\frac{\lambda_+}{\lambda_-}\right) &= e(n_- - n_+) \\ &= \frac{eN_0}{2\alpha}\left[\left(1 + \frac{4q\alpha}{\beta_+\beta_- N_0^2}\right)^{1/2} - 1\right](\beta_+ - \beta_-). \end{aligned} \qquad [13]$$

After some reduction one finds that in an aerosol space, free of appreciable electric fields,

$$\frac{N_0^2 a^2}{q} = \frac{e^4\left(1 - \dfrac{\lambda_+ u_-}{\lambda_- u_+}\right)^2}{k^2T^2\left(\ln\dfrac{\lambda_+}{\lambda_-}\right)^2 \dfrac{u_-\lambda_+}{u_+\lambda_-}\left[\alpha + \dfrac{4\pi e u_+\left(1 - \dfrac{\lambda_+ u_-}{\lambda_- u_+}\right)}{\dfrac{\lambda_+}{\lambda_-} - 1}\right]}. \qquad [14]$$

It may be noticed that this expression is a function only of known constants and the ratio of the light ion conductivities in the environment. By adopting $u_+ = 425$ cm./sec./statvolt/cm., $\alpha = 1.6 \times 10^{-6}$, $u_+/u_- = 0.77$, $e = 4.8 \times 10^{-10}$ e.s.u., and $kT = 4 \times 10^{-14}$ erg, the value of Eq. [14] is plotted in Fig. 1. This figure shows very clearly that as N_0 approaches zero, the conductivity ratio approaches the ratio of the ionic mobilities measured in clean air. On the other hand, as the particle density of the aerosol steadily increases or as the particles become larger, the light ion conductivity ratio becomes more nearly unity. Attention is drawn particularly to the fact that the rate of ion pair production q influences the conductivity ratio, just as our laboratory measurements have suggested (2, 3, 4, 6). Since the number of condensation nuclei in the atmosphere and their size changes with altitude, as does the ion production and the recombination coefficient; it is clear that the conductivity ratios existing in the free atmosphere will depend markedly upon the altitude. Moreover, the introduction of cloud droplets or rain into the region will obviously profoundly influence the equilibrium ratio.

It is illuminating to apply Eq. [14] to a practical case. For example, the number of cloud particles in a typical cloud approximates 400 droplets/cm.^{3} and their mean radius $a = 5 \times 10^{-4}$ cm. In the lower atmospheric levels $q = 10$ ion pair/cm.^{3} sec., while the recombination coefficient α will approximate 1.6×10^{-6}. Substituting in Eq. [14], one may verify that $N_0^2 a^2/q = 4 \times 10^{-3}$ and therefore λ_+/λ_- is nearly unity. Further calcula-

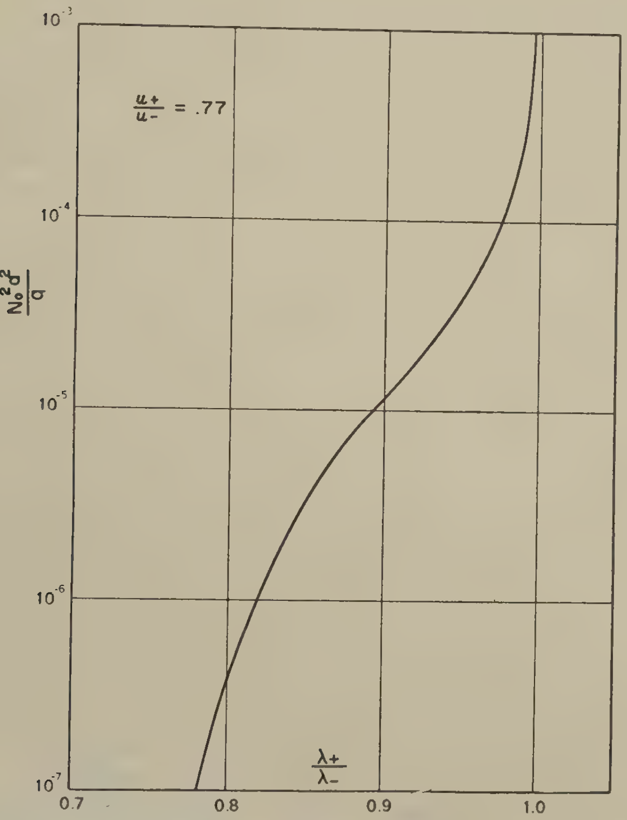

FIG. 1. The ratio of the positive and negative light ion conductivities as a function of the number of aerosol particles N_0 per unit volume, their radius a, and the rate of ion pair production q per unit volume per unit time. Calculated from Eq. [14].

tions will show that the conductivity will not depart greatly from unity unless the number of cloud droplets decreases to something like 40 droplets/cm.^{3}. In contrast to this result, one may notice that in the clear lower atmosphere there are frequently 10^3 to 10^4 condensation nuclei per cubic centimeter having a radius of the order of 10^{-5} cm. In this case $N_0^2a^2/q = 10^{-5}$ to 10^{-3} corresponding to $\lambda_+/\lambda_- = 0.89$ and 0.99, respectively. It is known that the population density of condensation nuclei decreases notably with increasing altitude. This implies that the conductivity ratio at several kilometers altitude will be much less than unity, just as the measurements of Wait and Gish appear to show (1).

A careful comparison of Eq. [14] with observed values has not been carried out, but it satisfactorily forecasts the approximate values of λ_+/λ_- observed both in the free atmosphere and in the giant closed cloud chamber used in a number of our earlier experiments.

In a series of earlier papers appearing in this Journal we have reported the observed distribution of the droplet charges accumulated by an aerosol exposed to a variety of physical conditions (2, 3, 4, 6). All these measurements were consistent with the view that the accumulated charges were established primarily by ionic diffusion and that the fractional number of particles F_x/F_t carrying a given number of elementary charges x is given by the basic aerosol electrification (3)

$$\frac{F_x}{F_t} = \frac{e}{(2\pi akT)^{1/2}} \exp\left[\frac{-\left(x - \frac{akT}{e^2}\ln\frac{\lambda_+}{\lambda_-}\right)^2}{2\left(\frac{akT}{e^2}\right)}\right], \qquad [15]$$

where F_x is the number of particles per unit volume, carrying x elementary charges, and F_t is the total number of particles per unit volume. An examination of this expression shows that the distribution is described by rather simple characteristics of the aerosol and by the ratio of the positive and negative light ion conductivities in the environmental air. Equation [14] provides a direct means of determining this conductivity ratio in terms of known constants and the size and population of the aerosol particles. Therefore, by its use one may describe, in the steady state, the entire behavior of an aerosol once its detailed characteristics and the ion production rate are known. Conversely if one measures the ratio of the electrical conductivities within an aerosol he may immediately infer the approximate number and size of the particles present. For example, it has been shown that if a sample of typical outside air is stored in a large sphere and the condensation nuclei and pollution therein systematically removed by any means, the electrical conductivity ratio increases until the ratio approximates the ratio of the respective ionic mobilities (5). Equation [14], therefore, will be of use in analyses that seek to determine and specify pollution of the free atmosphere.

REFERENCES

1. Gish, O. H., and Wait, G. R., "Thunderstorms and the earth's general electrification," *J. Geophys. Research* **55**, 473–484 (1950).
2. Gunn, Ross, "Diffusion charging of atmospheric droplets by ions, and the resulting combination coefficients," *J. Meteor.* **11**, 339–347 (1954).
3. Gunn, Ross, "The statistical electrification of aerosols by ionic diffusion," *J. Colloid Sci.* **10**, 107–119 (1955).
4. Gunn, Ross, and Woessner, R. H., "Measurements of the systematic electrification of aerosols," *J. Colloid Sci.* **11**, 254–259 (1956).
5. Phillips, B. B., Allee, P. A., Pales, J. C., and Woessner, R. H., "An experimental analysis of the effect of air pollution on the conductivity and ion balance of the atmosphere," *J. Geophys. Research* **60**, 289–296 (1955).
6. Woessner, R. H., and Gunn, Ross, "Measurements related to the fundamental processes of aerosol electrification," *J. Colloid Sci.* **11**, 69–76 (1956).

JOURNAL OF COLLOID SCIENCE 11, 697–703 (1956)

PRODUCTION AND CHARACTERISTICS OF SUBMICRON WATER AEROSOLS[1]

Guy G. Goyer and Frances D. Pidgeon

Central Research Laboratory, Canadian Industries, Ltd., McMasterville, Quebec, Canada, and Department of Occupational Therapy, Washington University, St. Louis, Missouri

Received December 12, 1955; revised April 23, 1956

ABSTRACT

A modification of the La Mer-Sinclair generator for the production of uniformly sized aerosol particles has been fitted with a special chimney to permit the aerosol to grow into solution droplets. The resulting droplets are of relatively uniform size and are in the submicron range. The modified generator provides a predictable source of small droplets for use in cloud physics experimentation.

INTRODUCTION

The production of water clouds for meteorological studies has been attempted in several ways by researchers in recent years. Uniformity of size and a high droplet concentration, as achieved by aerosol techniques (1), are the characteristics to be sought. To obtain these two conditions simultaneously is difficult with the present methods.

The spinning disk generator (2), the oscillating reed (3) in its many forms, the bursting bubble generator (4), and several other devices (5) produce streams of uniform droplets. However, their concentration is too low to be applicable to meteorological cloud physics studies other than droplet coalescence. Concentrated clouds of nonuniform droplets, on the other hand, are produced by the well-known techniques of the cloud chamber (6) and of the sprays (7). In these, the difficulty encountered in the measurement of the average droplet size and of the size distribution outweighs the advantages.

In certain experiments, where the presence of a solute in the droplet has no undesirable consequences, clouds of relatively uniform droplets can be produced through the condensation of water vapor on salt nuclei. The droplets thus produced are in the submicron size range. The measurement of size and concentration of the droplets is accomplished through the use of standard light-scattering techniques (8).

---

[1] The research reported in this paper has been sponsored by the Geophysics Research Directorate of the Air Force Cambridge Research Center, Air Research and Development Command, under Contracts AF 19(604)-618 and AF 19(604)-1388.

EXPERIMENTAL

The standard La Mer-Sinclair aerosol generator (8) as modified by Gendron (9) may be used to produce water aerosols on various nuclei. An investigation of an aerosol produced by the condensation of water vapor on sodium chloride nuclei obtained from a heated Nichrome coil generator is reported in this work. A study was made (*1*) on the diameters of nuclei produced by the source (10) and of those obtained from the evaporation of droplets, and (*2*) on the radii, electrical charge, and sodium chloride concentration of the droplets produced.

The La Mer-Sinclair generator fitted with a chimmey 135 cm. long could be used at room temperature, provided its chimney was heavily coated with tiny water droplets at the start of a run. The nuclei source consisted of a Nichrome coil, heavily coated with sodium chloride and operated at temperatures from 150°C. to 475°C. The coil temperature was measured with an iron-constantan thermocouple located in the center of the NaCl-coated Nichrome coil. The coils were wound from 20-cm. lengths of Nichrome wire No. 24 and No. 26 and were used from 4 to 8 hours. Flow rates of 900 cc./min. over the nuclei source and 20 cc./min. of filtered air were maintained in the generator. Because of the inhomogeneity of the nuclei and of their solubility in water, a strictly uniform cloud was not always obtained. However, even at the highest temperature, 500°C., a narrow enough size distribution (0.35 μ to 0.90 μ radius with 95% of the droplets ranging from 0.35 μ to 0.74 μ) was achieved for the use of an average particle size[2] to be valid.

In this case, standard light-scattering techniques could not be used to determine the size of the aerosol droplets. On the other hand, higher order Tyndall spectra could be observed on aerosols produced at the lower temperatures 140° to 300°C. (where over 80% of the droplets range between 0.3 and 0.5 μ in radius), and used to determine a valid average droplet size. As shown on Fig. 3, the size distribution of the aerosol widens with increasing coil temperature and consequently the brightness and sharpness of the Tyndall spectra decrease accordingly to the point of complete disappearance at coil temperatures above 300°C.

The radii of the aerosol droplets were determined by measuring their rate of fall in a Millikan oil drop apparatus. Aerosol droplets, in a comparable sample, were then evaporated by passing the cloud of droplets over a layer of phosphorus pentoxide in a 4 foot long glass tube, and the nuclei obtained therefrom allowed to settle upon electron microscope screens within the Millikan oil drop apparatus. The diameters of the nuclei so obtained were measured from electron microphotographs (10). Finally the diameters of the sodium chloride nuclei directly obtained from the salt coil were measured in a similar manner.

---

[2] Highly uniform droplets of NH_4Cl aqueous solutions were obtained with a generator developed in this laboratory and described elsewhere (11).

The aerosol droplet charge was determined by measuring the aerosol penetration through an electrostatic precipitator as a function of the electric field applied on the precipitator (11). Qualitative observations were also made in the Millikan oil drop apparatus.

RESULTS

The size distribution of the sodium chloride nuclei and of the solution droplets is plotted in Fig. 1 and Fig. 2. A comparison of the two figures shows that, for the most part, the nuclei run larger at the higher temperature of Fig. 2. Also, at the higher temperature the nuclei from evaporated droplets are larger than those produced directly, but this is not the case at the lower temperature. The difference suggests that more than one nucleus is involved in the formation of many of the droplets, uniting to form a single large nucleus upon evaporation.

The effect of the coil temperature on the size and size distribution of the salt solution droplets, over the range of temperature from 140°C. to 500°C., is shown in Fig. 3. The size increases and the size distribution widens with increasing coil temperature as shown by Gendron (12) for the salt nuclei. This result differs from that obtained with an oil aerosol where an increase in the nuclei source temperature gives rise to a larger number

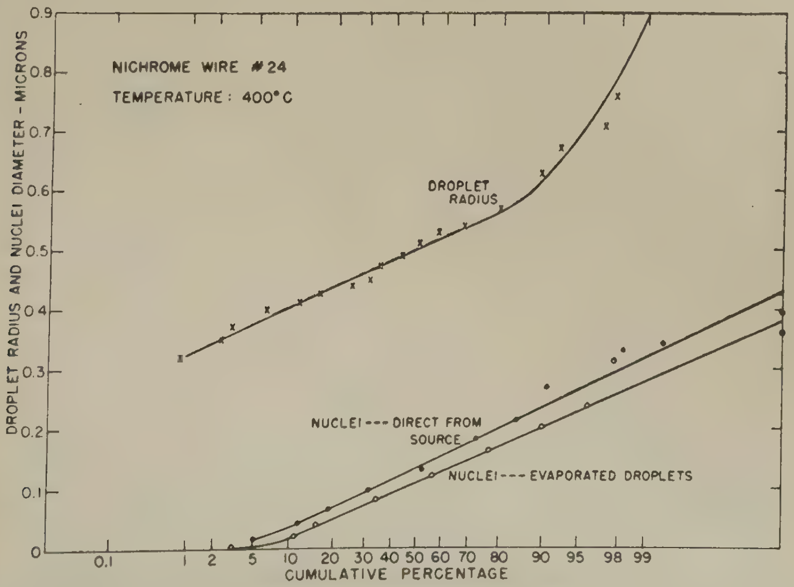

FIG. 1. Size distribution of sodium chloride nuclei and solution droplets obtained at an operating temperature of 400°C.

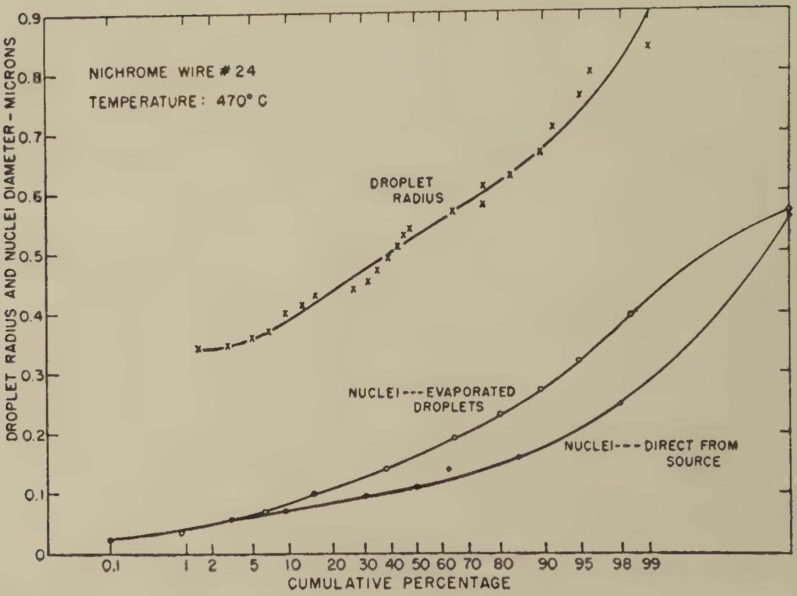

FIG. 2. Size distribution of sodium chloride nuclei and solution droplets obtained at an operating temperature of 470°C.

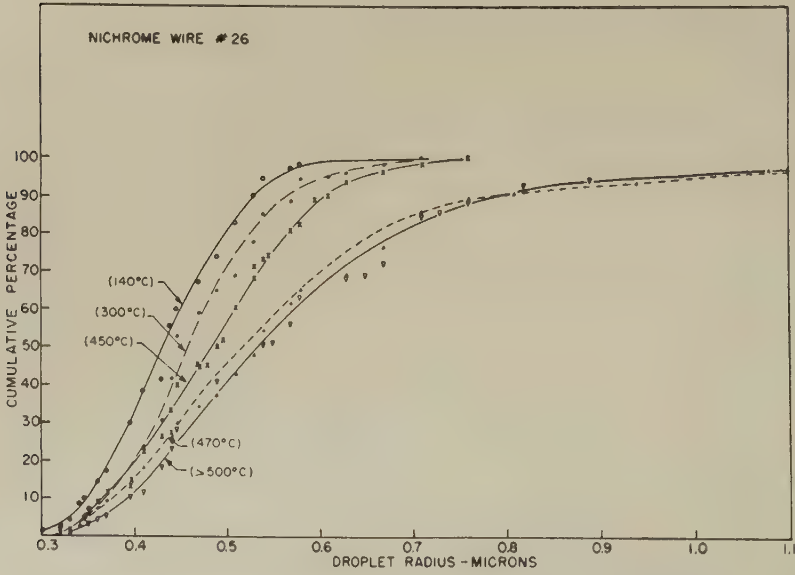

FIG. 3. Size distribution of solution droplets obtained from wire size No. 26 and various coil temperatures.

of smaller droplets (13). In the case of a water aerosol where the nucleus is soluble in the droplet, this result indicates that at the higher temperatures several nuclei unite to form a single droplet of a larger size.

Figure 4 shows the salt concentration in the droplets as a function of their size at two temperatures of the nuclei source. The bigger the droplet the greater is the salt concentration. This indicates that equilibrium conditions are not obtained in the time elapsed from the production of the droplets to the measurement of their sizes, because all droplets should eventually have the same salt concentration at a given water vapor supersaturation and temperature.

For a given droplet size, the salt concentration increases with the temperature of the coil as should be expected. It is interesting to note that the salt concentration is quite low over the whole range of droplet sizes, and suffices to stabilize the droplets over long periods of time. A sample of this cloud of salt solution droplets can be kept in a stoppered flask for as long as 6 to 8 hours without appreciable change.

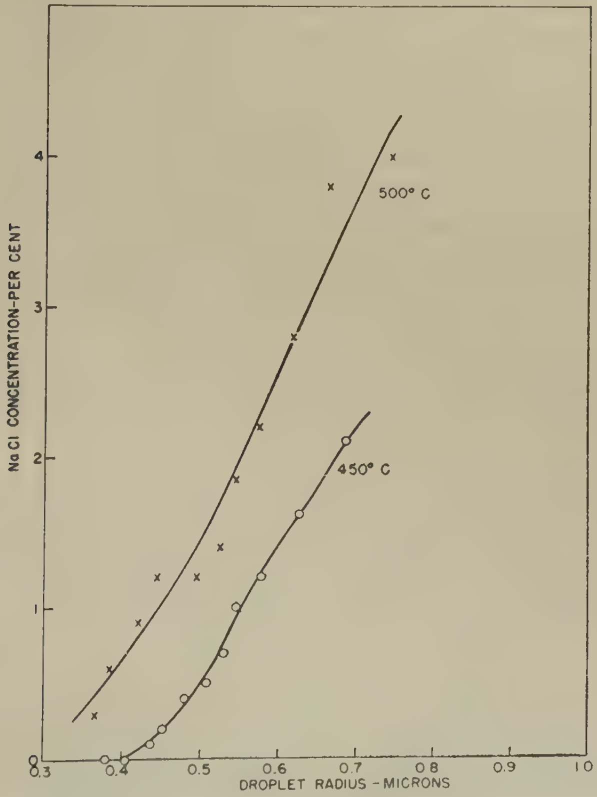

Fig. 4. Computed solution concentrations in droplets as a function of droplet size and coil temperature. Coil wire size No. 26.

The electrical charge carried by the droplets was measured by means of electrostatic precipitation and light scattering as described elsewhere (11). Most of the droplets were found to carry one or two electronic charges of either sign. A similar experiment was carried out on dioctyl phthalate aerosols produced in the standard La Mer-Sinclair generator and yielded similar results, in agreement with those of White and Hill (14), but contrary to the observations reported by Goyer (15) and Dalla Valle (16). Further qualitative observations showed the number of charged droplets to increase with increasing coil temperature as would be expected if thermal emission is the charging mechanism in this case. The conflicting observations, reported by several investigators, on the electric charge of aerosol droplets produced by condensation can thus be explained by the dependence of the charge on the temperature of the nuclei source.

Conclusions

The results reported in this work show the feasibility of producing reasonably stable and uniform clouds of submicron aqueous droplets for cloud physics studies. The most important control in their production is in the nuclei source. Several gauges of Nichrome wire were used and the results indicate a slight effect of the surface area of the wire. The dependence of droplet size on coil temperature is not as well defined for a No. 24 gauge as it is for a No. 26. In addition to coil area and coil temperature, several factors may explain this discepancy, such as the thickness and the age of the salt coating on the coil (10), the available moisture in the generator, and the flow rate of the air through the generator. A thorough study of these variables is necessary before a complete understanding of the formation and growth of salt solution droplets in this generator is obtained.

Nevertheless, this method fills a gap in water cloud production methods in the submicron range.

Acknowledgments

We are indebted to Prof. Horace R. Byers for his contribution in the analysis of the data, to Dr. Roscoe R. Braham, Jr. for numerous helpful suggestions on the improvement of the discussion, to Miss Barbara J. Tufts for her cooperation in supplying electron microphotographs of the sodium chloride nuclei, and to Mr. George S. Handler for measuring electrical charges on the droplets.

References

1. Sinclair, D., Handbook on Aerosols, Chapter 6. Atomic Energy Commission, Washington, D. C. (1950).
2. Walton, W. H., and Prewett, W. C., *Proc. Phys. Soc. (London)* **62B**, 341 (1949).
3. Dimmock, N. A., Nat. Gas. Turbine Establishment, Whetstone, Leics., England. Memorandum No. M-115 (1951).
4. Blanchard, D., *J. Colloid Sci.* **9**, 321 (1954).

5. Johnstone, H. F., "Bibliography on Aerosols," Atomic Energy Commission AT(30-3)-28, Chapter 2. February 28, 1951.
6. Wilson, J. G., "Cloud Chamber Technique," Chapter 1. Cambridge University Press, Cambridge, 1951.
7. DeJuhasz, K. J., and Meyer, W. E., "Bibliography on Sprays." The Texas Company, New York, 1949.
8. Sinclair, D., and La Mer, V. K., *Chem. Revs.* **44,** 245 (1949).
9. La Mer, V. K., and Gendron, P. R., *Chem. in Can.* **4,** 54 (1952).
10. Lodge, J. P., and Tufts, B. J., *J. Colloid Sci.* **10,** 256 (1955).
11. Goyer, G. G., and Handler, G. S., *J. Meteorol.* **12,** 569 (1955).
12. Gendron, P. R., Final Report to U.S. Air Force Materiel Command, Contract AF19(122)300, Department of Chemistry, University of Montreal. May 31, 1954, p. 19.
13. La Mer, V. K. *et al.*, Atomic Energy Commission Report. NYO-512, March (1951).
14. White, L., Jr., and Hill, D. G., *J. Colloid Sci.* **3,** 251 (1948).
15. Goyer, G., Gruen, R., and La Mer, V. K., *J. Phys. Chem.* **58,** 137 (1954).
16. Hinckle, B. L., Orr, C., Jr., and Dalla Valle, J. H., *J. Colloid Sci.* **9,** 70 (1954).

JOURNAL OF COLLOID SCIENCE **11**, 704–709 (1956)

FLOCCULATION, SUBSIDENCE, AND FILTRATION OF PHOSPHATE SLIMES[1]

I. General

Victor K. La Mer and Robert H. Smellie, Jr.

Department of Chemistry, Columbia University, New York, New York, and Department of Chemistry, Trinity College, Hartford, Connecticut

Received June 18, 1956

Abstract

This paper serves as an introduction to a series on the colloidal behavior of Florida phosphate slimes. The problems involved in improving the flocculation, subsidence, and filtration behavior of slimes are considered generally. A description of the slimes used in the investigations and the results of orienting experiments for determining the range of particle size and number and electrophoretic mobility are given. Electrolytes were found to be ineffective as aids in improving flocculation, subsidence, and filtration and the reasons for introducing special flocculating agents such as potato starch for such purposes are discussed.

I. Introduction

The results of an extended series of investigations on the dewatering of uraniferous phosphate slimes (originating in Florida) will be reported in this and subsequent papers. This program was initiated in June, 1951, by the U.S. Atomic Energy Commission with the ultimate objective of recovering uranium contained in the waste slimes of phosphate fertilizer production. The immediate objective was to undertake a study of the fundamental colloidal factors involved in flocculation, subsidence, and filtration in order to obtain information which would be of aid in the development of processes for the beneficiation of the uranium-bearing fractions; also methods for the possible economical recovery of phosphate values in these materials. From the practical point of view, the difficulties encountered in current processes involved primarily slow rates of settling of solids and slow rates of filtration due to the clogging of filters. Therefore, the basic problem in these investigations has been the study of factors related to and methods for accomplishing the economically successful dewatering of these slimes.

---

[1] Presented before the Colloid Division of the American Chemical Society, at the New York Meeting, September, 1954.

In the phosphate fertilizer industry, rock phosphate is ground under water and the fine pebble which settles rapidly is separated and sold as pebble phosphate fertilizer. After various flotation operations, slimes are left over which consist of fine particles which settle very slowly and effectively clog all types of filters. The construction of settling tanks and settling ponds for these waste slimes becomes a burdensome item of operation.

Various schemes, involving ultrasonic irradiation (1), electrokinetic methods (2), and even the cultivation of water lillies, have been proposed and tried on a relatively large scale in order to induce flocculation and subsidence or to facilitate the evaporation of water, but with only negligible improvement incommensurate with the cost.

The "scope of research" involved the following approaches. The results will be reported in detail in this series of papers.

1). The dewatering of slimes and the concentration of solids has been related to the subsidence rates as modified by dilution, the addition of electrolytes, and the addition of special flocculating agents such as starches, natural gums, and synthetic polyelectrolytes and uncharged polymers.

2). Investigation of improvement of the character of precipitates (or flocs) resulting from these treatments to locate the best combination of interdependent conditions to produce the most rapid filtration rate.

3). The analysis of subsidence as a function of time and final sediment volume and the general correlation of these with filtration behavior.

4). The correlation of improvement in rate of filtration and the optimum in amount of flocculating agent.

5). Correlation of these observations (1–4) of the behavior of phosphate slimes, with the degree of dispersion and the chemical nature of the particles of the natural suspensions and of synthetic dispersions of pure substances of known composition and particle size.

II. MATERIALS USED

The following types of materials have been used.

a). Native slimes resulting from standard plant operations.

b). Synthetic slimes prepared in the laboratory from naturally occurring conglomerates of phosphate rock ("leached zone" material).

c). Colloidal dispersions of finely divided pure substances such as calcium phosphate, aluminum phosphate, silica, and clays, prepared in the laboratory.

Only one representative member of the first two types will be described in this introductory paper. Others of type (*c*) have been used in more recent investigations of the effect of chemical composition of the solid and of particle size distributions and will be described in subsequent papers.

The first sample investigated, called Hopewell slime (I), was obtained from J. B. Cathcart of the U.S. Geological Survey at Plant City, Florida. It originated from an old slime pond of the Coronet Phosphate Co., Hopewell Mine. It is a thick, viscous dispersion, grey in color, with a solid content of 20% (oven-dried). Microscopic and light-scattering observations indicate that it consists of a small amount of coarse sand with some particles of 5 to 20 μ. The majority of particles, however, are less than 1 μ in equivalent radius.

Slime I never sedimented completely even after considerable dilution with water; i.e., there was always a significant amount of suspended matter in the supernatant liquid after the major portion of the heavier components had settled out. This behavior should be contrasted with the representatives of type (*b*), of which the slimes designated as III, VI, and VIII are replicas.

Slimes of type (*b*) were prepared in the laboratory from native leached zone phosphate rock by grinding the material under water in a pebble mill and then in a mortar. Since primary interest centered in the colloidal behavior of small particles of less than 200 mesh (74 μ), the larger particles were eliminated by screening. This procedure yields a slime with a sedimentation behavior different from that of slime I, since slime III and its replicas VI and VIII settle within 24 hours, leaving a clear supernatant liquid thus indicating that the majority of particles are greater than 1 μ in equivalent radius.

III. INTRODUCTORY THEORY

A. Effect of Electrolytes

It is useful to distinguish, at least qualitatively, between two classes of colloids: the lyophobic and the lyophilic. Typical examples of the first class are gold, sulfur, and silver iodide sols. Their stability depends primarily upon the repulsion between the electric charges on the particles which are modified by the surrounding electric double layers and further screened by the diffuse ionic atmospheres of the electrolytes in the solvent.

The validity of the diffusion theory of M. Smoluchowski for the kinetics of the rapid coagulation of lyophobic colloids has been amply demonstrated when the particles possess a low density of surface charge. This theory also holds for the kinetics of molecular reactions of low energy of activation, e.g., quenching of fluorescence. For ionic reactions, the rates calculated for uncharged molecules are subject to important electrostatic corrections (3, 4). In the case of most colloids where the particles exhibit high charge density and the double layer potential is correspondingly high, indiscriminate use of the linear approximation of the Debye-Hückel theory can lead to false and very misleading interpretations, as emphasized by Verwey and Overbeek (5). The recent work of these authors combines the repulsive effects arising from the electric double layers—calculated by solution of the unabridged Poisson-Boltzmann equation—and from the attractive forces of the London-Hamaker type. This model furnishes a satisfactory explanation of the stability relations for lyophobic colloids. As a consequence of the Smoluchowski law, the upper limit of particle number for stability is $n = 10^6/\text{cm.}^3$. Lyophobic colloids are sensitive to electrolyte additions and, broadly speaking, are not primarily dependent upon chemical interactions with the medium, although chemical interaction is by no means excluded (6).

On the other hand, gelatin or starch in water and high molecular weight polymers, are, in general, extreme types of lyophilic colloids. Here, the particle number may reach values as high as $n = 10^{15}$ to $10^{18}/\text{cm.}^3$. The "macromolecule" may be either a long threadlike molecule or a molecule of branched chains, rolled into a porous ball open to penetration by the solvent medium. The solvation of a lyophilic colloid involves direct absorption of solvent molecules throughout the entire macromolecule.

As contrasted to the instability of lyophobic colloids, the thermodynamic stability of lyophilic colloids depends primarily upon a combination with the solvent and the increase in entropy arising from the thermal expansion of the macromolecule on imbibition. Although these molecules often possess electric charges as a result of acid-base equilibria, they are comparatively insensitive to electrolyte additions but are peculiarly sensitive to chemical interactions with dissolved molecules as determined by molecular architectures.

The small native particles of interest in our research are, for the most part, flat platelike structures of substituted kaolin, gibbsite, and wavellite types (7), in addition to larger irregularly shaped particles of calcium phosphate, aluminum phosphate, and silica.

Thus, the smaller particles consist of more-or-less rigid layers of silicate, aluminum and calcium hydroxides. Stability is attributed to hydrogen bonding between the exposed OH groups and the solvent water molecules. It is believed that water molecules can penetrate at least partly into some of the lattice structures, but swelling in kaolinite is not as pronounced as in the montmorillonite or bentonite structure. The fine particles have major axes of less than 1 to 2 μ and are negatively charged with an electrophoretic velocity of 2 4 microns $\text{sec.}^{-1}\text{volt}^{-1}\text{cm.}^{-1}$. The charge is a function of the pH, and the presence on the surface of the particle of potential-determining ions such as Al^{+++} and PO_4^{---}.

From this brief description, it is obvious that a completely satisfactory study along the lines indicated would require a very detailed study of the particle size, number concentration, and electrokinetic behavior of each type of particle to understand the origin of the stability and the flocculation properties of each dispersion. Such a comprehensive study was considered to be both impractical and ill-advised at the time—until further orientation had been achieved. A combination of more direct empirical approaches combined with theoretical guidance has shown that factors of nonelectrostatic origin, i.e., of chemical origin, play a decisive role in the behavior of the dispersions.

Particle size was investigated in a preliminary way by direct microscopic observations when sufficiently above the limit of resolution, supplemented by light scattering when applicable. Electrophoretic mobility measurements were made by a micro method (8). The detailed data differ for each natural slime or each slime synthetically prepared in the laboratory from the natural rock.

The most significant orienting conclusion that can be drawn is that the smallest particles present in some of the original slimes had a number concentration of the order of $n = 10^{10}/\text{cm.}^3$ and radii corresponding to equivalent spheres of roughly 0.1 to 0.2 μ. From this value of n it is evident that the suspension of fine particles would be unstable if lyophobic. The stability of the suspension of fine particles is to be attributed primarily to the hydrophilic bonding between the OH group of the particle and the water in addition to any secondary repulsions arising from the interaction of the electric double layers surrounding each particle.

This view is substantiated by the effect of added electrolytes. The addition of considerable amounts of lime water, strong acids and bases, aluminum and ferric salts *produces in some cases moderate improvements in the rate of subsidence without producing any significant improvement in the filtration rate.* Sediment from electrolyte precipitation is more compact than that arising from special flocculating agents and is not sufficiently porous for the rapid passage of water through the filter cake. Electrolyte addition coagulates some of the finer particles into a compact floc, producing increased subsidence from the larger size of the floc without improving the porosity of the filter cake significantly. The search for an efficient electrolyte additive for the improvement of filtration was, therefore, abandoned.

B. Stability of Slimes—Special Flocculating Agents

Since the addition of electrolytes proved to be incapable of producing significant improvement in filtration rate, we have searched for specific flocculating agents.

Professor J. Th. G. Overbeek informed us (July, 1951) about the very successful use of starch as a flocculant for the finely divided particles in the effluent of coal mining operations carried out in Belgium and Holland and described in the Henry Patent (9). The applicability of starch as a flocculant for phosphate slimes was subsequently successfully demonstrated in our laboratories in September, 1951, when significant improvements in subsidence and filtration rates of Hopewell slime (I) were obtained by using Flocgel[2] as a flocculating agent. Van Iterson has given an explanation of the action of starch which we shall modify and extend in greater detail in paper II of this series (10).

---

[2] A modified potato starch sold by W. A. Scholten Chemische Fabrieken, Foxhol, the Netherlands.

Electrolytes will coagulate colloidally dispersed matter, whereas starch, in the absence of electrolytes, will preferentially coagulate the coarser particles. Van Iterson believes that the addition of electrolyte (like $Ca(OH_2)$) is necessary first to reduce the electric charge on the finer particles which are usually negative. Today, we would say that the electrostatic potential of the surrounding double layer is reduced, producing instability.

In paper No. II, evidence will be presented that the Van Iterson-Overbeek explanation is inadequate to account for all our present observations; it appears that specific cross-linking between the phosphate radicals which normally occur in the potato starch molecules with the calcium or other cations forming insoluble phosphates is responsible for the specific flocculating power of this starch and its derivations.

Regardless of the explanation, the observation of the Dutch School that very small amounts of starch sensitizes the coal effluent dispersion to flocculation and subsidence, whereas larger amounts of starch produce a deleterious stabilizing effect, has been observed for all our dispersions and for almost all the large list of specific flocculating agents that we have studied (including starches, starch derivatives, and various synthetic polyelectrolytes). There is also an optimum concentration of flocculant for the production of the most rapid and complete filtration. The location and interpretation of this optimum concentration, which appears to be dependent upon specific interactions between the dispersed particle and the particular flocculant, will be one primary objective of later papers in this series.

REFERENCES

1. THOMPSON, D., *Bull. Virginia Polytech. Inst. Eng. Expt. Sta. Ser.* **No. 75** (1950).
2. WALTHALL, J. H., Tennessee Valley Authority, Private communication.
3. DEBYE, P., *Trans. Electrochem Soc.* **82,** 7 (1942).
4. UMBERGER, J. Q., AND LAMER, V. K., *J. Am. Chem. Soc.* **67,** 1099 (1945).
5. VERWEY, E. J. W., AND OVERBEEK, J. TH. G., "Theory of the Stability of Lyophobic Colloids." Elsevier, New York, 1948.
6. DINEGAR, R. H., SMELLIE, R. H., JR., AND LAMER, V. K., *J. Am. Chem. Soc.* **73,** 2050 (1951); DINEGAR, R. H., AND SMELLIE, R. H., JR., *J. Colloid Sci.* **7,** 370 (1952).
7. ILER, R. K., "The Colloid Chemistry of Silica and the Silicates," Chapters 7, 8. Cornell Univ. Press, Ithaca, New York, 1955.
8. SMELLIE, R. H., JR., AND LAMER, V. K., *J. Phys. Chem.* **58,** 583 (1954).
9. HENRY, R. A., French Patent 658306 (1928).
10. VAN ITERSON, F. K., *Proc. Acad. Sci. Amsterdam* **41,** 81 (1938); also *Chem. Abstr.* **32,** 3580 (1938).

JOURNAL OF COLLOID SCIENCE **11**, 710–719 (1956)

FLOCCULATION, SUBSIDENCE, AND FILTRATION OF PHOSPHATE SLIMES[1]

II. Starches as Agents for Improving Flocculation, Subsidence, and Filtration of Phosphate Slimes[2]

Victor K. La Mer and Robert H. Smellie, Jr.

Columbia University, New York, New York, and Trinity College, Hartford, Connecticut

Received July 2, 1956

Abstract

The use of starches as flocculating agents for improving flocculation and filtration of Florida phosphate slimes is discussed in detail. The methods used in performing reproducible, quantitative filtration measurements are described. Potato starches were found to be the most effective and produced improvements in filtration rates up to 10- to 15-fold with some slimes. Corn starches were least effective.

The flocculating efficiency of potato starches has been related to their phosphate content. The presence of cations which form insoluble phosphates is also necessary to produce complete flocculation. A three-dimensional bridge structure formed between particles in the flocs is suggested as a picture of the flocculation. The OH groups of the starch adsorb on the surface of the solid particles followed by interlinking of the free ends of the adsorbed starch molecules (on different particles) through their phosphate radicals with Ca^{++} ion or other insoluble phosphate producing cation in solution.

Introduction

In paper I of this series we noted that a modified potato starch, Flocgel, was used successfully in improving the degree of flocculation and consequently the subsidence and filtration rates of phosphate slimes (1). Since much of the early experimental work, in which techniques for measuring subsidence and filtration rates were developed, was performed using starches of various types, this work will be described separately in this paper.

Basis for the Use of Flocgel and Other Starches

A description and an interpretation of the use of starch in connection with the flocculation of coal washery effluents has been given by Van

---

[1] Supported by funds from Contract AT-30-1189 between Columbia University and the A.E.C.

[2] Presented before the Colloid Division of the American Chemical Society, at the New York meeting, September, 1954.

Iterson (2). He explains the action of the starch (in this case also a prepared potato starch) more or less as follows: Electrolytes will precipitate colloidally dispersed matter; whereas the starch in the absence of electrolyte will preferentially flocculate the coarser particles. The addition of a small amount of electrolyte, usually $Ca(OH)_2$, is desirable to reduce the charge on the smaller particles of the suspended material, which is usually negative. This may be stated more correctly as the reduction of the repulsive forces between the electric double layers of different particles. The starch attaches itself to the surface of the particles (in coal washery effluents kaolin or some other clay), so that the OH groups of the starch point out with their pyranoid rings in a flat position. Clay particles with adsorbed starch now no longer attract water molecules as well as before, but now attract each other and are, therefore, flocculated.

According to Overbeek (3), in this interaction the two types of colloids show a strong attraction, irrespective of charge, and combine in all proportions. With relatively small amounts of lyophilic colloid, the lyophilic particles will be surrounded by the lyophobic particles and sensitization to flocculation results. When the concentration of the lyophobic colloid is relatively great, stabilization or protection against flocculation will result.

This protective action at higher starch concentration has been observed by us also in the use of starches as flocculating agents for phosphate slimes, although in some cases relatively very large amounts of starch must be present (>300 p.p.m.). On the other hand a much smaller amount (10–100 p.p.m.) will effect a rapid flocculation and produce a significant improvement in the filtration rate of a slime sample.

From our studies we have developed a more specific picture. After the demonstration of the effectiveness of Flocgel in improving the flocculation and filtration rates of Hopewell slime (see paper I of this series) was made, some studies of the nature of the necessary accompanying electrolyte were initiated. The results of the early orientation experiments suggested that the contribution of the added electrolyte in helping to produce flocculation with starches might be associated with the ability of the cation to form a relatively insoluble phosphate rather than being dependent only on the charge of the cation. That this is correct is demonstrated, for example, by the fact that salts of Na^+, K^+, etc., with Flocgel showed no visible flocculation, whereas Ag^+, which is also univalent, produced a marked improvement in the flocculating efficiency of a small amount (20 p.p.m.) of starch.

Table I shows that of all the cations studied essentially those which form relatively insoluble phosphates are effective in producing visible flocculation, regardless of the charge of the cation. In any case, it is evident that a Schulz-Hardy or lyotropic series effect is not the only factor involved.

The relationship between cations producing insoluble phosphates and the improved efficiency of Flocgel is interpreted by us on the basis of the phosphate content of the starch. It is postulated that the starch molecules

TABLE I

Effect upon Flocculation of Hopewell Slime (I) by Substituting Various Cations for Calcium Ion

In all cases the final concentration of the cation was 0.005 *N*. Samples of the slime also contain 20 p.p.m. of soluble starch (after Lintner)

Cation	Visible flocculation	Subsidence rate compared with that of sample containing Ca^{++} as cation
Ag^+	Immediate	Faster
Al^{+++}	Immediate	Slower
Ba^{++}	Immediate	Slower
Bi^{+++}	Immediate	Much slower
Cd^{++}	Immediate	Faster
Ce^{++++}	Immediate	Faster
Cr^{+++}	Immediate	Faster
Co^{++}	Immediate	Faster
Cu^{++}	Immediate	Faster
Fe^{+++}	Immediate	Slower
Pb^{++}	Immediate	Faster
Mg^{++}	Immediate	Faster
Hg_2^{++}	Immediate	Faster
Hg^{++}	Immediate	About the same
Ni^{++}	Immediate	Faster
Sr^{++}	Immediate	Faster
Zn^{++}	Immediate	Faster
Na^+	None	None
K^+	None	None
NH_4^+	None	None

adsorbed on different solid particles through the OH groups of the carbohydrate part (probably by hydrogen bonding) are cross-linked into a three-dimensional network through the phosphate part of the starch molecules by cations such as Ca^{++} which form insoluble phosphates. Experiments in 1951 showed that corn starch and other starches known to contain no phosphate were ineffective as flocculating agents for phosphate slimes even with relatively large amounts of electrolyte, whereas potato starches and Flocgel were very effective especially in the presence of added Ca^{++} or other cations producing insoluble phosphates.

TYPICAL RESULTS ON FLOCCULATION AND FILTRATION OF PHOSPHATE SLIMES WITH VARIOUS STARCHES

A. Introduction

The general method for the study of the flocculating efficiency of various starch and electrolyte combinations consisted of subsidence measurements on 100-ml. samples contained in 100-ml. graduated cylinders. The interpretation of the results of various subsidence measurements will be treated specifically in paper III of this series. This paper should also be consulted for a complete description of the experimental method.

In addition to subsidence rates, filtration rates were also determined as a measure of the degree of flocculation produced by starches. The laboratory data obtained in both types of measurements are convertible to larger scale processes where specifically dewatering, or concentration of solids, is desired by the use of thickeners (subsidence) or continuous filtration equipment.

B. Experimental Filtration Methods

In general, two methods of measuring filtration rate have been employed in our experiments. The first method, the gravity filtration method, was the one employed in the earlier experiments. It consisted in measuring the filtrate collected as a function of time from a slime sample which had been poured onto a #2 Whatman conical fluted filter paper in an ordinary conical funnel. The use of fluted paper avoided the effect of the liquid column in the stem of the filter, and limited the effects to the shape of the cone of the funnel, the initial volume of the liquid and the nature of the solid, degree of flocculation, and the amount of solid in the sample. A means of representing filtration data obtained by this method in a form equivalent to relative filtration rates will be discussed later in this paper.

Conforming more closely to industrial practice, the second method for measuring filtration rates was by use of vacuum filtrations. The vacuum filtrations were performed using a 7-cm. (and later a 5.5-cm.) Büchner funnel and #2 Whatman filter paper. A Cenco vacuum pump reduced the pressure inside the filter flask to 2 cm. Hence a constant pressure difference of 74 cm. Hg was maintained throughout the filtration. A 100-ml. graduated cylinder was placed inside the filter flask in order to measure the filtrate collected as a function of time.

C. Results of Some Quantitative Filtration Rate Measurements of Slimes Flocculated with Potato Starches

The first sample of phosphate slime studied quantitatively with respect to filtration after treatment with various amounts of Flocgel was Hopewell slime (I), described in paper I of this series. It is significant that the results obtained with this sample and Flocgel showed a pattern of behavior later shown by other phosphate slimes treated with a variety of flocculating agents such as starch derivatives, gums, and polyelectrolytes. An examination of the data for the Hopewell Slime (I) with Flocgel as flocculant revealed the following significant features.

1). Where the flocculation is not essentially complete (i.e., a relatively large number of fine particles remain in suspension) the filtration rate varies approximately inversely and in a few cases erratically with the subsidence rate. The occasional erratic behavior is probably due to clogging of the filters or the alternation of the pore size of the cake by the large

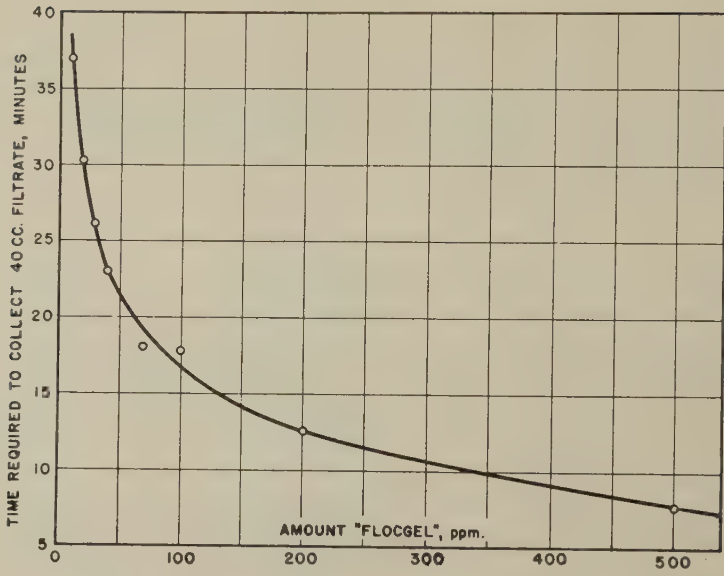

FIG. 1. Shows time required to collect 40 ml. of filtrate vs. amount of Flocgel in parts per million in terms of total slime. Slime: Hopewell (I) diluted to 5% solids. Each sample also contains 2 ml. of saturated $Ca(OH)_2$ per 100 ml. of slime.

number of primary particles still not flocculated. In cases where this was observed, the supernatant liquid above the subsidence level was quite turbid compared to those in which filtration rate and subsidence rate were directly related (see *4*, below).

2). For a given concentration of $Ca(OH)_2$, the rate of filtration increases with increasing Flocgel content (from 10 to 500 p.p.m.) (i.e., the time required to collect a given volume of filtrate decreases) (Fig. 1).

3). For a given Flocgel content, the rate of filtration increases with increasing $Ca(OH)_2$ concentration. In some cases a minimum in the rate of filtration is found (maximum in the time required to obtain a given volume of filtrate) (Fig. 2).

4). For well-flocculated samples, the rate of filtration follows the rate of subsidence. The *initial rate* of filtration vs. the square of the rate of subsidence is linear for Hopewell slime (I) with Flocgel contents of 40–200 p.p.m. (Fig. 3). The subsidence rate used for comparison is that obtained for the portion of the subsidence curve representing the greatest subsidence rate.

An explanation of this relationship follows from the Stokes' law of fall in a viscous medium and Poiseuille's law of flow through capillaries. The rate of free fall of the effective sphere, which is also the approximate subsidence rate, $-dh/dt$, depends primarily upon r^2 for flocs of constant density,

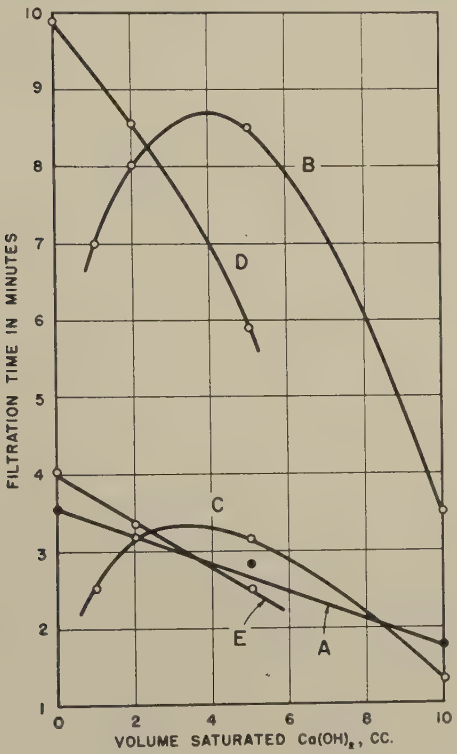

FIG. 2. Shows time required to collect various volumes of filtrate vs. volume of saturated $Ca(OH)_2$ added to 100 ml. of Hopewell slime (I).

	Solids (%)	Amt. Flocgel (p.p.m.)	Volume filtrate collected (ml.)
A	5	0	50
B	5	10	20
C	5	10	10
D	2.5	10	20
E	2.5	10	10

where r is the effective radius of a sphere equivalent to the floc; i.e.,

$$-\frac{dh}{dt} = Kr^2.$$

According to Poiseuille's law, the rate of flow of a liquid through a capillary is proportional to R^4, where R is the effective radius of the capillaries in the cake, or the pores in the filter, or in this case, the space between flocs.

In general, $R \propto r$, i.e., the radius of the capillary between flocs should be proportional to the radii of the flocs, when they are considered as closely packed spheres.

$$R^4 \propto (r^2)^2$$

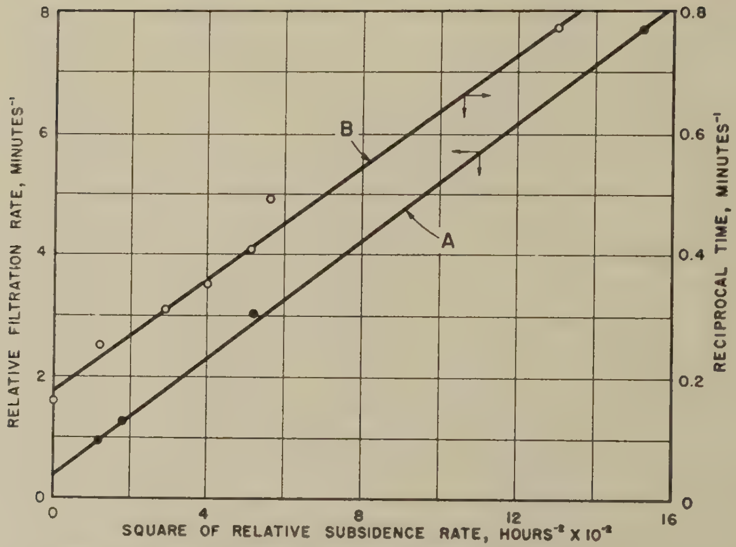

FIG. 3. Relative initial filtration rate (reciprocal of the time required to collect 10 ml. of filtrate) vs. the square of the relative subsidence rate in (graduations of cylinder)^2 hour^{-2}. Left axis: *A*—Hopewell slime 5% solids; 10 ml. sat. $Ca(OH)_2$ per 100 ml. slime. Flocgel contents 40–200 p.p.m. Right axis: *B*—Hopewell slime 2.5% solids; 2 ml. sat. $Ca(OH)_2$ per 100 ml. slime. Flocgel contents 20–200 p.p.m.

and

$$\frac{dv}{dt} \text{ (filtration rate) } \propto \left(-\frac{dh}{dt}\right)^2$$

or the rate of filtration is proportional to the square of the rate of subsidence, as observed (Fig. 3).

Another phosphate slime studied extensively in early investigations with starches was a slime prepared from so-called leached-zone material and designated as slime III (see paper I for description). The subsidence and filtration of this slime were studied using an ordinary potato starch marketed by A. Goodman Co., Long Island City, New York, as flocculant. The studies showed that the behavior of slimes I and III is qualitatively the same.

An interesting effect on filtration rates, especially noticeable in this case, was found when the time required to collect given volumes of filtrate is plotted against the added potato starch (Fig. 4). For starch contents of 0–25 p.p.m. the time required to obtain a given volume of filtrate *increases*, i.e., the rate of filtration *decreases*. For starch contents greater than 25 p.p.m. the filtration rate again increases steadily with increasing starch addition. Taking for comparison the time required to obtain 50 ml. of filtrate, it is shown that the filtration rate for 500 p.p.m. of starch present is

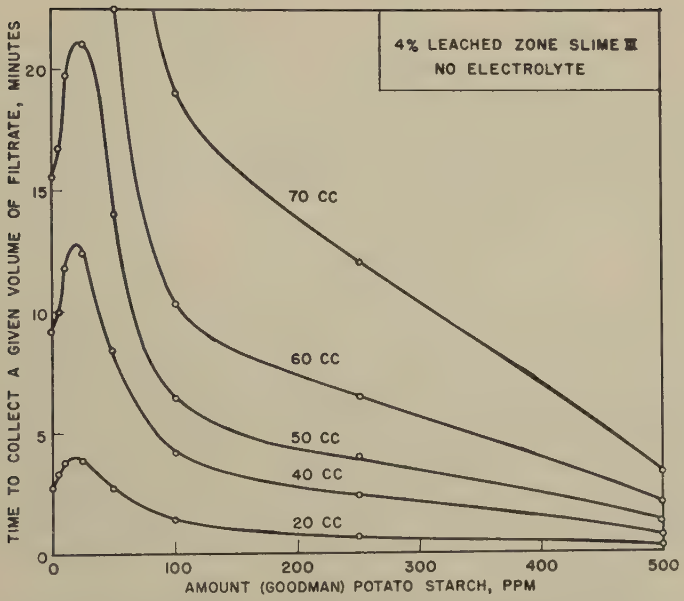

FIG. 4. Shows time required to collect different volumes of filtrate as a function of added Goodman potato starch. Leached zone slime III, 4% solids. No electrolyte added.

about 10 times as great as that for the untreated sample. This behavior was also observed for Hopewell slime (I) and evidently occurs only where little or no electrolyte is present.

In all these filtration experiments, fluted paper was used to avoid having a liquid column in the stem of the funnel. As the liquid passes through the filter the pressure (head) is reduced as the height of the liquid in the funnel falls. For a cone the volume is $\frac{1}{3}\pi r^2h$, where r = the radius of the base and h = the height of the cone, and also $\tan\theta = r/h$, where $\tan\theta$ is the tangent of ½ the angle of the cone at the apex, and is constant for a given funnel.

Therefore $r = kh$, where k is a constant and V (volume of the cone) $= \frac{1}{3}\pi k^2h^3$. The area of the side of a cone, $A = \pi r\sqrt{r^2 + h^2}$ or $A = \pi kh^2\sqrt{k^2 + 1}$.

For filtration through a conical fluted filter these expressions for volume and area represent approximately the volume of liquid in the cone and the area of escape, respectively.

The D'Arcy equation for rate of filtration may now be applied (4), i.e.,

$$\frac{dV}{dt} = \frac{KAP}{L},$$

where P = pressure difference across the cake;
A = filtration area;
L = thickness of the cake;

K = a characteristic factor determined by the particle size, porosity of the cake, and the nature of the solid material.

In the filtration experiments described here (for any given solid content), L is essentially constant as shown by experiment.

The pressure difference is proportional to h, the height of the liquid in the filter, and $A \propto h^2$. Therefore

$$\frac{dV}{dt} = \frac{KAP}{L} = K'h^3,$$

where K' is a constant involving K/L and other constants of proportionality between $A \propto h^2$ and $P \propto h$. The volume of the liquid in the funnel $= \frac{1}{3}\pi k^2h^3$ and dV/dt is proportional to the volume of the liquid in the funnel $= V_T$, where V_T = the original volume of water in the sample, V = the volume of filtrate already collected at time t. So that $dv/dt = K''(V_T - V)$, which integrates to $-\log(V_T - V) = K''/2.3\, t + c$, which

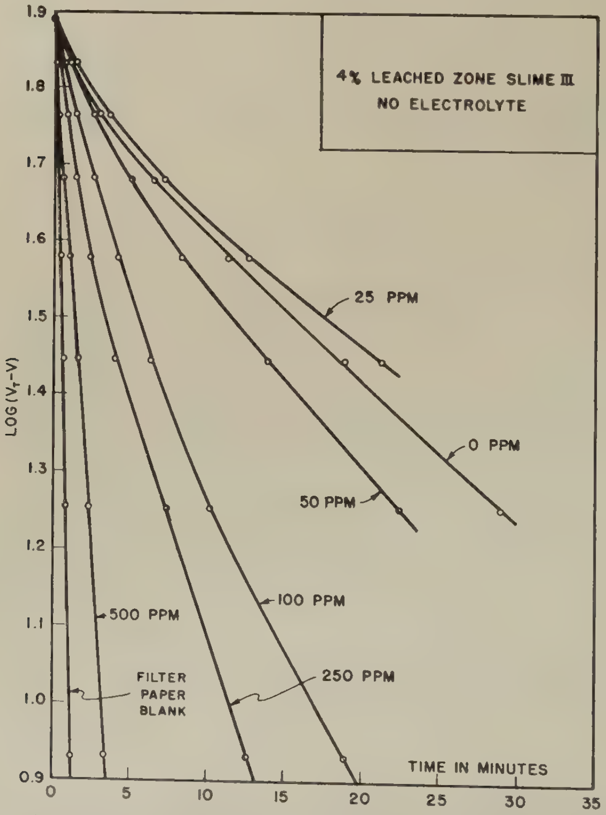

FIG. 5. The data of Fig. 4 plotted as $\log_{10}(V_T - V)$ vs. time in minutes, where V_T = total volume of water (ml.) in slime sample, and V = volume of filtrate collected in time t.

indicates that a plot of log $(V_T - V)$. vs. t should be linear, with the slope $K/2.3$ proportional to the actual filtration rate constant.

Figure 5 shows the data of Fig. 4 plotted in this way. A control with water and filter paper alone is included. For example, the actual volume of free water in the slime samples (V_T) was calculated to be 78 ml. for a 100-ml. sample of slime III (4% solids) used in these experiments. The data of Fig. 5 show some deviation from linearity in the early stages of filtration, which may be attributed to the deposition of solid on the paper during filtration. Thus the filtration rate gradually decreases at first and finally reaches a constant value after the deposition of the solid is completed.

A comparison of the linear portion for the slime III samples (4% solids) containing 0 and 500 p.p.m. of Goodman's potato starch shows that the rate of filtration of the latter is 13 times as great as the former. The sample containing 500 p.p.m. of starch filtered at a rate which was only 3 times as slow as the control with water alone. This method of representing the filtration data demonstrates that the use of potato starch in amounts up to 500 p.p.m. leads to improvements in filtration rate by a factor greater than 10.

Conclusion

The effectiveness of potato starches as compared to corn starches and other starches containing no phosphate was attributed to the cross-linking made possible by cations (such as Ca^{++}) producing insoluble phosphates with the production of a three-dimensional network and hence large flocs.

In all cases tested various purified corn starches, modified corn, or impure corn starches were found to be ineffective. The effectiveness of various potato starches is attributed to the phosphate content. Subsequently extensive tests of various commercially available starches and starch derivatives were made in our laboratories. All these products were tested qualitatively and in some cases quantitatively with respect to efficiency in improving flocculation, subsidence, and filtration.

Later a specifically detailed investigation of carboxylated, phosphorylated, and various aminated derivatives of corn starch and dextrans was carried out by Drs. Beckmann and Roger of the Columbia University Laboratories; it will be reported in a later paper of this series.

References

1. LaMer, V. K., and Smellie, R. H., Jr., *J. Colloid Sci.* **11**, 704 (1956).
2. Van Iterson, F. K., *Proc. Acad. Sci. Amsterdam* **41**, 81 (1938) (in English); also *Chem. Abstr.* **32**, 3580 (1938).
3. Overbeek, J. Th. G., *Chem. Weekblad* **35**, 117 (1938); also *Chem. Abstr.* **32**, 4044 (1938).
4. D'Arcy, H., Originally in "Les Fountaines Publique de la Ville de Dijon." Victor Dalmont, Paris, 1856. Treated by P. C. Carman, *J. Soc. Chem. Ind.* **15**, 150 (1937).

JOURNAL OF COLLOID SCIENCE **11**, 720–731 (1956)

FLOCCULATION, SUBSIDENCE, AND FILTRATION OF PHOSPHATE SLIMES[1]

III. Subsidence Behavior[2]

Robert H. Smellie, Jr., and Victor K. La Mer

Trinity College, Hartford, Connecticut, and Columbia University,
New York, New York

Received June 18, 1956

Abstract

Two types of subsidence curves have been observed depending upon whether flocculation is initially rapid or relatively slow, corresponding to the initial limiting slopes, on a time plot of the height of subsiding column, which are, respectively, very large or nearly zero. Rapid initial subsidence leads more often to a larger final subsidence volume than does a slower initial subsidence rate. An empirical equation which represents the subsidence data of well-flocculated slimes in linear form is shown to be identical with an equation derived theoretically using flow theory. The theoretical equation is identical with the empirical only if the volume density of solid is at any instant uniform throughout the subsiding column. This can be interpreted in terms of a three-dimensional network of particles being gradually and uniformly compressed during subsidence and shows that the process is not one of the independent settling of particles. The structure extends continuously throughout the sedimenting slime if sufficient solid, unflocculating agent is present.

A. Introduction

This is the third paper of a series reporting investigations on the flocculation, subsidence, and filtration of uraniferous phosphate slimes initiated by the Chemical Research and Raw Materials Divisions of the Atomic Energy Commission in 1951.

In this paper we treat the subsidence data quantitatively in terms of empirical and theoretical relations. A study of the subsidence of thick suspensions has been used by many investigators (1) in preference to the standard methods of sedimentation. In subsidence (in contradistinction to sedimentation), the rate of downward movement of the boundary between clear liquid and the solid is measured rather than the rate of accumulation of solid at the bottom. Sedimentation is more significant from the point of view of the present objectives of interest since it also measures the rate of decrease of the volume occupied by the solid, i.e., the packing rate. Steinour (2) has shown that the initial rate of subsidence of thick suspensions was proportional to a function of the initial volume fraction of liquid. Similar studies have been made by others, but only limited aspects of the problem were investigated. Recently, Kynch (3) developed an expression for subsidence which applies throughout the entire process. However, the method of testing data is cumbersome, since no complete analytical solutions could be obtained.

---

[1] Supported by funds from Contract AT(30-1) 1189 between Columbia University and the A.E.C.

[2] Presented before the Colloid Division of the American Chemical Society, at the New York meeting, September, 1954.

B. Experimental Method

Samples of slimes were prepared by dilution of stock slimes (see paper I of this series) with distilled water. In some series of experiments, the pH was adjusted to that of the stock slime to control this variable.

The slime sample and various amounts of the flocculating agent (final volume 100 ml.) were mixed in 100-ml. graduate cylinders. In those experiments in which starches were used as flocculating agents, $Ca(OH)_2$ was sometimes added. The slime and reagents were mixed by inverting the cylinder (10–40 times in 2 minutes) to obtain uniform mixing; the subsidence measurements were then made by recording the height of the solid-liquid boundary in terms of the graduations on the cylinder as a function of time. The subsidence rates of the untreated slimes, and slimes with $Ca(OH)_2$ only, were used as controls in each series of experiments. The graduated cylinders were selected so that the cross section, and hence the height of the graduations, were the same throughout.

C. Experimental Results

With phosphate slimes of different types of preparation and origin, two types of subsidence curves are observed depending upon whether the flocculation is initially rapid or relatively slow. On a time plot of the height of subsiding column these two types possess initial limiting slopes which are, respectively, very large or approach zero, as shown in Fig. 1. The shape of the subsidence curves can be interpreted on the basis of the following processes being operative.

1. In some cases a relatively slow flocculation takes place initially. In these cases, the rate of subsidence is initially slow and gradually increases, indicating that the particle size becomes progressively larger as a result of the flocculation process (region AI).

2. Eventually, a floc size is obtained after which the settling rate remains constant for some time (region BI). On the other hand, a constant subsidence rate is observed immediately where flocculation is rapid (II).

The interpretation given to the first parts of Curves I and II of Fig. 1

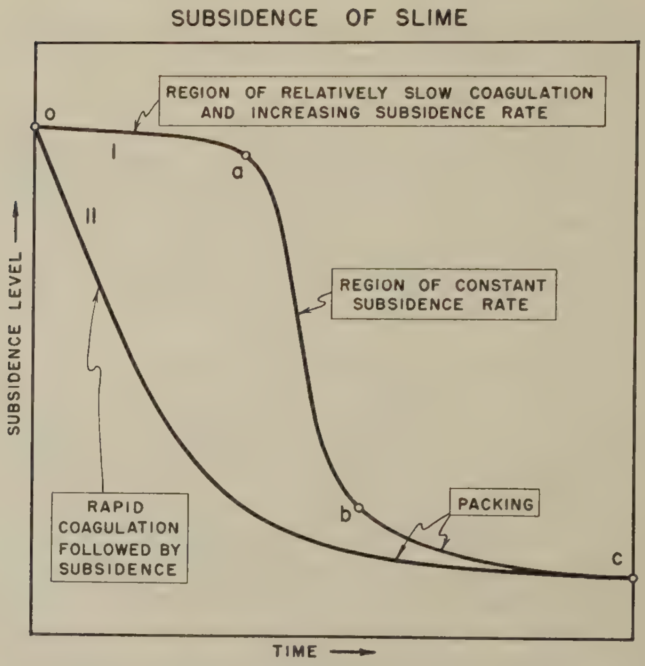

Fig. 1. Shows variation of subsidence vs. time for unflocculated and well-flocculated slimes.

is in accord with the interpretation of sedimentation (accumulation) curves of similar shape obtained by Odèn (4) by sedimentation analysis of concentrated sulfur and barium sulfate suspensions flocculated by the addition of various amounts of electrolytes.

a). The time required to reach point "*a*" on curves of type I will be greater, the slower the rate of flocculation.

b). The rate of subsidence from points "*a*" to "*b*" will be dependent on the final size and structure of flocs produced.

The factors determining the portions "*a*" and "*b*" above will be dependent on the size, number, and composition of the particles, the concentration and composition of the flocculation agent, and other chemical factors such as pH and electrolyte concentration.

In the region *c*, a final compression of the sediment occurs leading to a final volume which will be dependent upon the processes which occurred in both (*a*) and (*b*).

Some of the results obtained with a typical Florida phosphate slime (obtained from an old pond of the Hopewell Mine of the Coronet Phosphate Co.) and a certain flocculating agent (Flocgel[3]) are shown in Fig. 2. The

---

[3] Trade name for a modified potato starch sold by W. A. Scholten Chemische Fabrieken, Foxhol, Netherlands.

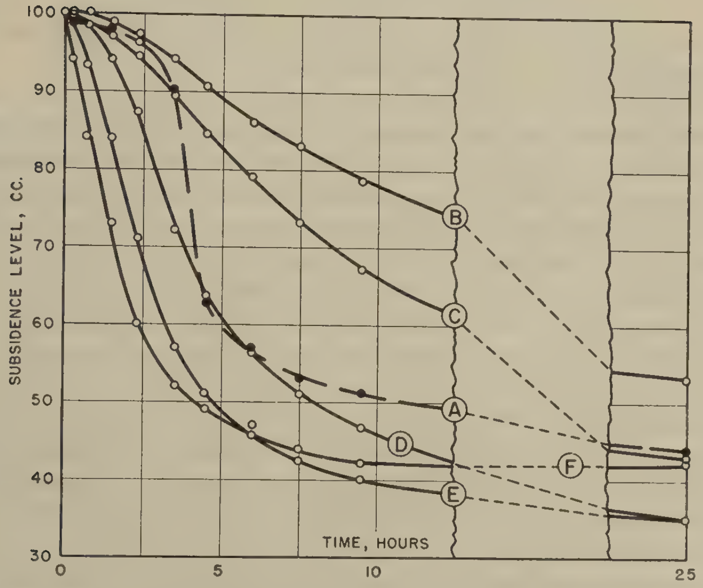

FIG. 2. Shows subsidence level (in terms of the graduations on the cylinder) vs. the time in hours after adding reagents. Hopewell slime (I) 5% solids. Each sample contains 10 ml. of added saturated $Ca(OH)_2$ per 100 ml. of slime and various amounts of added Flocgel to give the following final concentrations in p.p.m. *A*—0 p.p.m. *B*—10 p.p.m. *C*—20 p.p.m. *D*—40 p.p.m. *E*—70 p.p.m. *F*—200 p.p.m.

samples contained the same amount of $Ca(OH)_2$ and progressive amounts of Flocgel (0–200 p.p.m.). In general subsidence curves of the two types discussed above are obtained experimentally depending upon the amount of Flocgel added.

A blank of the untreated slime (not shown in the figure) exhibited fractional settling and the supernatant liquid remained very turbid. Since some of the particles in this slime were of the order of 0.2 μ equivalent radius, no settling of these particles occurred within the period of observation (25 hours). Consequently only various degrees of turbidity differences were observed between the top and the bottom of the column.

The blank containing no Flocgel but with added $Ca(OH)_2$ is typical of the behavior to be expected in the flocculation by electrolyte alone, leading to a more compact floc than that obtained with potato starch. More precisely, there results a packed granular precipitate which filters very poorly. In general, sufficient potato starch or synthetic polyelectrolyte produces a more loosely packed floc with an entirely different filtration behavior as compared to simple electrolyte flocculation.

The sample with electrolyte alone gave a subsidence rate that was initially slow (zero limiting slope) because of the slow flocculation process. The relatively rapid subsidence rate (after initial flocculation) may be attributed to the close packing of primary particles in the flocs having a relatively large density but still a relatively small size.

For a compact floc, the subsidence rate may be relatively rapid owing to the density's being relatively large for a small size. However, with a flocculating starch or polyelectrolyte present, the flocs formed are large and possess an open structure. Although the incorporation of water makes the average density of the floc smaller, the larger value of the radius contributes to a faster rate of subsidence, since settling rates depend (roughly) on the square of radius in accordance with Stokes' law.

For these reasons, a sample containing electrolyte alone could sediment more rapidly in a limited range than one containing extremely small amounts (in this case, 0–30 p.p.m.) of a flocculating starch. However, the sample containing $Ca(OH)_2$ alone is inferior to those which also contain 40–200 p.p.m. of Flocgel. With sufficient amounts of Flocgel (40–200 p.p.m.), the subsidence rate is initially fast and constant immediately after adding and mixing the reagents, showing that flocculation was completed.

Very small amounts of flocculating starches (0 to about 30 p.p.m.) produce slower sedimentation than those of a "blank" in at least one other slime, using Goodman's potato starch.[4] This behavior is reflected more clearly in the filtration rates to be discussed in paper IV.

For the samples containing relatively large amounts of flocculating starch, the final sediment volume is often larger than in those containing smaller amounts. Troelstra and Kruyt (5) and others explain the variations in final sediment volume as follows:

When the particles possess high electric charge, the suspensions are stable and settle slowly. However, it is usually observed that in this case the final settled volume of the solid is small because the particles eventually take positions of minimum potential with respect to each other. These positions lead to a relatively densely packed solid after sufficient time.

On the other hand, when the particles are flocculated by electrolytes and/or special agents (starches or polyelectrolytes) the particles are united rapidly and in a *haphazard* manner, forming a relatively loose or porous *structure*. Owing to the haphazard association of particles in rapid flocculation, the final settled volume of the sediment will be greater than in the case of the more stable suspensions. Although the data of this paper are primarily restricted to starch as the flocculating agent, later work (1953) with synthetic polyelectrolytes and gums corroborates the conclusions drawn from the starch studies.

D. REPRESENTATION OF DATA BY AN EMPIRICAL EQUATION

Much of the subsidence data obtained with these thick slimes can be well represented by the following simple equation

---

[4] A. Goodman & Company, Long Island City, New York.

$$\frac{t}{h_0 - h} = \alpha + \beta t, \qquad [1]$$

where h_0 = initial height of the subsidence level, h = height of the subsidence level after time, t, and α and β are constants independent of time.

This empirical equation applies only where (*1*) the flocculation was initially very rapid and complete, and (*2*) where the solid content is reasonably high. In cases where it does not apply, the deviations observed when the function is plotted are generally as follows (Fig. 3):

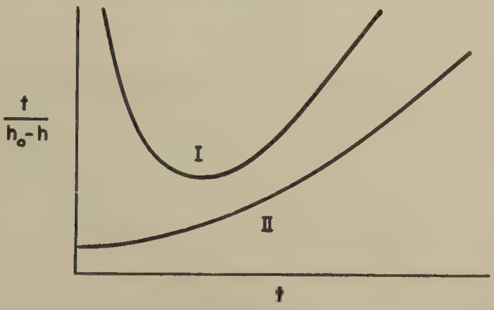

FIG. 3.

In cases where the $\frac{t}{h_0 - h}$ vs. t shows an appreciable early region of negative slope (I), the subsidence curve is of the type shown in Fig. 4,

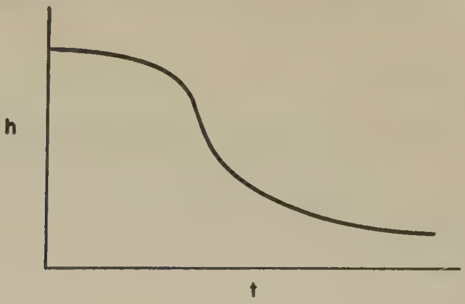

FIG. 4.

indicating that initially flocculation is slow. In cases where curves of type II are observed, the subsidence curves are usually of the type shown in Fig. 5.

The cases where Eq. [1] above is valid throughout exhibit subsidence curves similar to type II (see Fig. 6). The excellent conformity to Eq. [1] is exhibited by many different slimes of relatively high solid content when well flocculated. In cases where Eq. [1] is not valid throughout, one can obtain concordance with Eq. [1] by choosing a new and later reference time, i.e.,

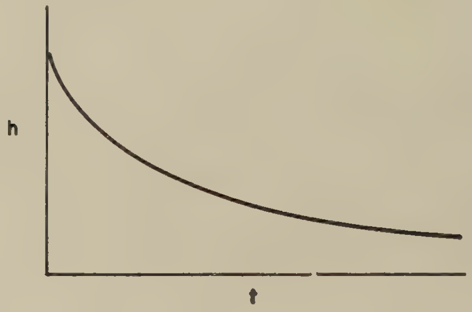

FIG. 5.

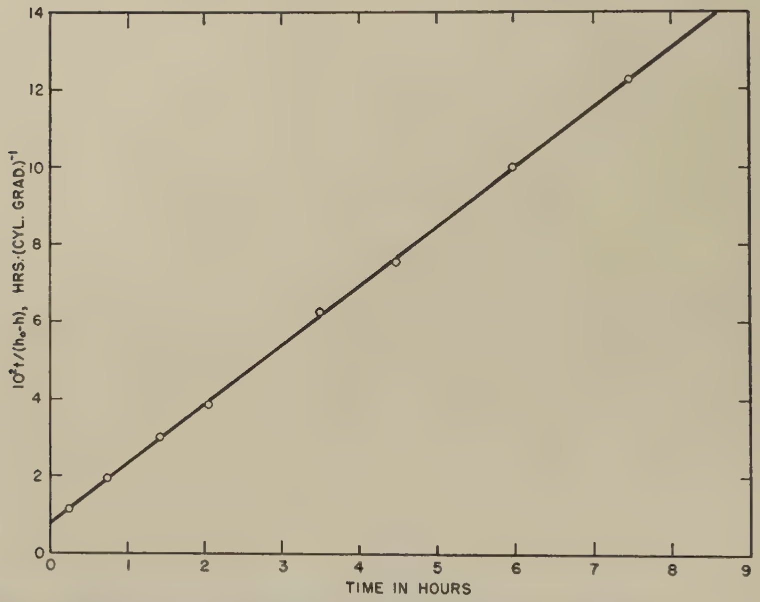

FIG. 6. Shows data on subsidence of Hopewell slime I (5% solids) treated with 500 p.p.m. of Flocgel and 10 ml. of saturated $Ca(OH)_2$ per 100 ml. of slime plotted according to Eq. [1] as $\frac{t}{h_0 - h}$ vs. t.

after subsidence has begun. The subsidence level is taken as h_0 for $t = 0$, as in Fig. 7.

Further consideration of Eq. [1] reveals that the slope $(\beta) = \frac{1}{h_0 - h_f}$, where h_f is the final height of the solid after subsidence is complete. The intercept $(\alpha) = \frac{1}{v_0}$, where v_0 is the initial velocity of subsidence. These relationships may be obtained as follows:

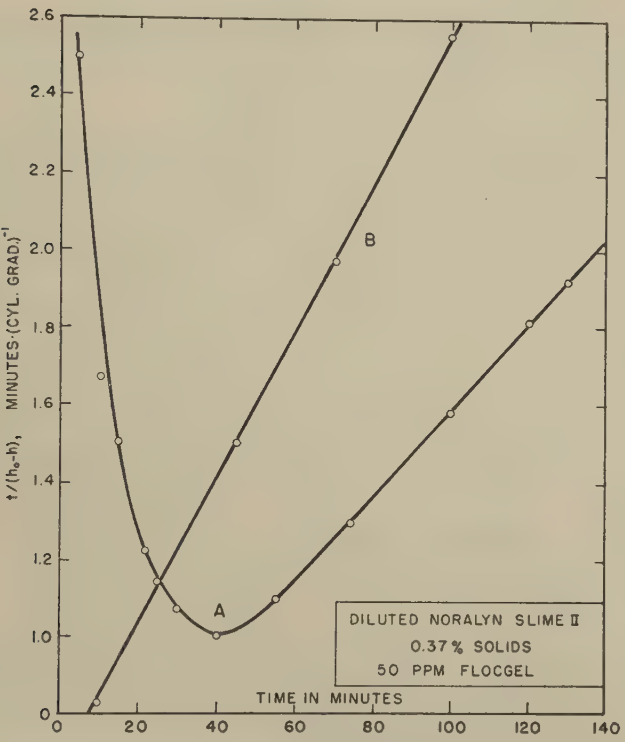

FIG. 7. Shows subsidence data for a diluted Noralyn slime (0.37% solids) II of the International Minerals & Chemical Co. (Mulberry, Florida) plotted according to Eq. [1].

A. Plot of $\frac{t}{h_0 - h}$ vs. t using original reference time $t = 0$. Original $h_0 = 100$.

B. Plot of $\frac{t}{h_0 - h}$ vs. t choosing as new reference time $t = 30$ min. as $t = 0$. New $h_0 = 72$. Sample contained 50 p.p.m. of added Flocgel.

To obtain β, divide Eq. [1] by t and let $t \rightarrow \infty$. Then $h \rightarrow h_f$ and $\frac{\alpha}{t} \rightarrow 0$ to give $\frac{1}{h_0 - h_f} = \beta$. From Eq. [1] it may be shown that $-\frac{dh}{dt} = v = \frac{\alpha}{(\alpha + \beta t)^2}$, where v is the velocity of subsidence. Let $t \rightarrow 0$, then $v \rightarrow v_0$ and $\alpha = \frac{1}{v_0}$.

The agreement between experimental and calculated values of β is satisfactory for cases where Eq. [1] applies and the subsidence is followed to completion.

Explanation: An explanation of the relation between the type of subsidence curve and the applicability of Eq. [1] follows:

Substituting for $\alpha + \beta t$ in terms of $\frac{t}{h_0 - h} = x$,

$$v = \frac{\alpha(h_0 - h)^2}{t} = \frac{\alpha}{x^2};$$

$$x = \sqrt{\frac{\alpha}{v}}.$$

$\therefore$ In the $\frac{t}{h_0 - h}$ vs. t plot, $\frac{t}{h_0 - h}$ decreases if v is increasing. This occurs in a slowly flocculating slime. If v is constant as in unhindered fall of particles of constant size, $\frac{t}{h_0 - h}$ is constant as expected, and if v is decreasing as in compression, then $\frac{t}{h_0 - h}$ vs. t increases. In the latter case, the result can be derived theoretically, as will now be shown.

E. DERIVATION OF THEORETICAL EQUATION

As the starting point for the derivation, an equation of continuity applicable to the subsidence process must be obtained. Such an equation has been derived elsewhere (6). The result is

$$\frac{\partial(\rho v)}{\partial h} = \frac{\partial \rho}{\partial t}, \tag{2}$$

or

$$\rho \frac{\partial v}{\partial h} + v \frac{\partial \rho}{\partial h} = \frac{\partial \rho}{\partial t}. \tag{3}$$

This is identical with an equation of continuity for a gas flow process (7) where in the present case, ρ = volume density of solid, i.e., the volume of solid per unit volume of free water. The volume of free water is the volume of water between the subsidence level and the bottom of the cylinder, since clear water above the subsidence level no longer contains any solid.

$v = -\frac{dh}{dt}$ = the rate of fall of the level between solid and clear liquid.

In order to derive a theoretical equation identical in form with Eq. [1], a significant requirement appeared, namely, it was necessary to assume that the volume density of solid (ρ) was at any instant the same throughout the whole subsiding column. This can be understood only if the flocculated solid forms a network of particles in close contact which is being gradually and uniformly compressed by the effect of gravity. Now

$$\rho = \frac{\text{total volume of solid}}{\text{volume of free water}}.$$

After complete compression has occurred, the final height of solid is h_f. The total amount of solid in the cylinder is constant. Therefore, the total volume of solid $V_s = A(h_f - c)$, where A = cross-sectional area of cylinder and c is a factor representing the water remaining in the network when h has reached h_f. The volume of free water is the total volume measured from the subsidence level, h, down to the bottom of the cylinder minus the volume of solid.

$$\therefore \text{ volume of free water } = A(h - h_f + c);$$

$$\therefore \rho = \frac{A(h_f - c)}{A(h - h_f + c)} = \frac{h_f - c}{h - h_f + c}; \qquad [4]$$

$$\therefore \frac{\partial \rho}{\partial t} = - \frac{(h_f - c)}{(h - h_f + c)^2} \cdot \frac{dh}{dt};$$

but

$$-\frac{dh}{dt} = v,$$

$$\frac{\partial \rho}{\partial t} = \frac{(h_f - c)v}{(h - h_f + c)^2}, \qquad [5]$$

and from [4]

$$\frac{\partial \rho}{\partial h} = - \frac{(h_f - c)}{(h - h_f + c)^2}. \qquad [6]$$

Substituting the values of [5] and [6] in [3]

$$\frac{(h_f - c)}{(h - h_f + c)} \frac{\partial v}{\partial h} + v\left(\frac{-(h_f - c)}{(h - h_f + c)^2}\right) = \frac{h_f - c}{(h - h_f + c)^2} v$$

or

$$\frac{dv}{dh} = \frac{2v}{h - h_f + c}$$

$$\frac{dv}{v} = \frac{2dh}{h - h_f + c} \quad \text{and} \quad \ln v = 2 \ln (h - h_f + c) + \text{const.}$$

Initially, when

$$h = h_0, \qquad v = v_0.$$

$$\therefore \text{ const.} = \ln v_0 - 2 \ln (h_0 - h_f + c)_0$$

$$\ln \frac{v}{v_0} = 2 \ln \frac{(h - h_f + c)}{(h_0 - h_f + c)},$$

or

$$\frac{v}{v_0} = \frac{(h - h_f + c)^2}{(h_0 - h_f + c)^2}.$$

(It is evident from the above and from Eq. [4] that $v = v_0 \cdot \frac{\rho_0}{\rho}$.

Since $v = -\frac{dh}{dt}$

$$-\frac{dh}{dt} = \frac{v_0(h - h_f + c)^2}{(h_0 - h_f + c)^2},$$

$$-\frac{dh}{(h - h_f + c)^2} = \frac{v_0\,dt}{(h_0 - h_f + c)^2},$$

and

$$\frac{1}{(h - h_f + c)} = \frac{v_0\,t}{(h_0 - h_f + c)^2} + \text{const.}$$

When $t = 0$, $h = h_0$

$$\therefore \text{ const.} = \frac{1}{h_0 - h_f + c}$$

and

$$\frac{h_0 - h}{(h - h_f + c)} = \frac{v_0\,t}{(h_0 - h_f + c)}.$$

The last equation may be rearranged to give

$$\frac{t}{h_0 - h} = \frac{1}{v_0} + \frac{t}{(h_0 - h_f + c)}.$$

This is exactly the form found empirically and as previously explained the slopes of the lines (β) equal $\frac{1}{h_0 - h_f}$. The effect produced by the constant c in the theoretical equation will be minor, since it will be small compared with $h_0 - h_f$. The intercept is $1/v_0$ as previously deduced.

It should be emphasized that the density, ρ, is defined such that one obtains $v \rightarrow 0$ at the end of the subsidence. This is equivalent to considering the actual subsidence distance allowable as $h_0 - h_f$, i.e., in practical terms $h = 0$ when $h = h_f$, since the column of solid can move no further.

CONCLUSION

In constructing a physical picture of the structure of the slime during subsidence, one significant requirement of the theory just described is that the particle density (ρ) be uniform at any instant throughout the subsiding column. Since particles would fall essentially at constant velocity if sufficient space were available, it is evident that for a slime obeying Eq. [1] the particles are in contact or in close proximity. In cases where the solid content is small (small h_f), some time must elapse before sufficient crowding occurs. Accordingly, Eq. [1] will not be valid up to this point. If flocculation is also occurring, then the variation in particle size will contribute, since ρ is changing horizontally as well as vertically. The value of ρ (as defined) will change during flocculation, since the volume occupied by the particles is so changed. The complete flocculation of a given slime of given solid content leads to a greater degree of conformity with Eq. [1] than in the case of the unflocculated material. This is understandable since in the flocculated slime h_f is usually greater than in the unflocculated case. Therefore, the effective volume of the particles is greater and contact of particles occurs higher in the suspension. Since at an earlier time flocculated slimes (initially) usually subside faster than unflocculated ones, the region of conformity to Eq. [1] is reached sooner for this reason also.

The values of h_f are useful in comparing effective floc size using some assumptions concerning geometry. Relationships between subsidence and filtration rate have been obtained. Further investigations are being made with promising results.

References

1. Ward, H., and Kammermeyer, K., *Ind. Eng. Chem.* **32,** 622 (1940). See this article for a good discussion of subsidence and references to earlier literature.
2. Steinour, H., *Ind. Eng. Chem.* **36,** 618, 840, 901 (1944).
3. Kynch, G. J., *Trans. Faraday Soc.* **48,** 166 (1952).
4. See article by S. Odèn *in* Alexander, ed., *Colloid Chemistry*, Vol. 1, p. 861, Chemical Catalog Co., New York, 1926.
5. Troelstra, S. A., and Kruyt, H. R., *Kolloid Beih.* **54,** 225 (1943); also *Chem. Abstr.* **37,** 6179^9 (1943).
6. Kynch, G. J., ref. 3 p. 167.
7. See F. L. Hitchcock and C. S. Robinson, "Differential Equations in Applied Chemistry," 2nd ed. p. 75. Wiley, New York, 1936.

JOURNAL OF COLLOID SCIENCE **11**, 732–747 (1956)

THE DEFORMATION AND STRENGTH OF NAPKIN RING METAL-ADHESIVE-METAL JOINTS

T. Gillespie[1] and Sir Eric Rideal

Department of Physical Chemistry, King's College, University of London, London W.C. 2

Received May 16, 1956

ABSTRACT

A study has been made of the deformation and strength in shear of joints between two identical thin-walled metal cylinders using paraffin wax and nitrocellulose as adhesives. The breaking strength was proportional to the apparent area of metal joint and was always less than the tensile strength of carefully prepared samples of the adhesive. There was a large variation in breaking strength which increased as the joints were made thinner. This variation is reflected in a correspondingly large variation in the viscoelastic properties of the joints. A detailed analysis of the deformation of typical joints has emphasized the necessity for further research on the mechanical behavior of carefully prepared samples of the adhesives.

It has been suggested by De Bruyne and Houwink (1) that the "napkin ring" test for adhesion has certain advantages and might be of considerable use in any attempt to further our knowledge of the factors which affect the strength of metal-adhesive-metal joints. In this test, two thin-walled cylinders are glued together with a layer of adhesive and the system is tested by applying a torque to one of the cylinders while the other is held stationary. It has been argued (1) that if the width of the adhesive layer δR is very much less than the radius of the cylinders, the stress in the joint will be uniform and some of the stress concentrations which occur in other types of joints may be avoided. On this basis the shear stress, denoted by F, would be given by

$$F = \frac{\text{Torque}}{2\pi \bar{R}^2 \delta R}, \qquad [1]$$

where $\bar{R}$ and δR are as illustrated in Fig. 1.

There is some doubt as to whether the stress on a napkin ring joint may be described in this simple manner, but the test has other merits which make an investigation of it worth while. In particular, it is relatively easy to measure the deformation of the joint at any stage prior to fracture. It is

---

[1] Present address: Suffield Experimental Station, Ralston, Alberta, Canada.

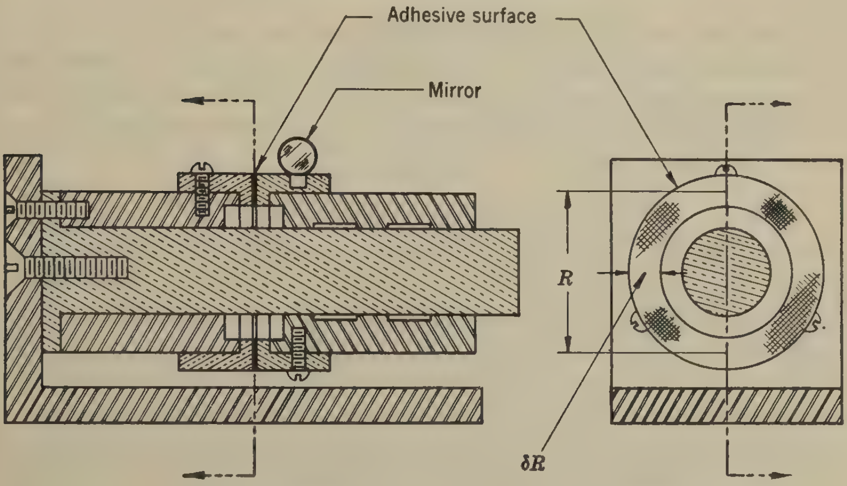

FIG. 1. A diagram of the napkin ring apparatus.

reasonable to suspect that the measurement of such deformation would lead to a much better understanding of the mechanism of adhesion than would be obtained in a simple breaking strength set of experiments. In consequence a napkin ring apparatus was constructed with provision for the measurement of joint deformation before fracture, and it was used to study the behavior of some typical metal-adhesive-metal joints.

THE NAPKIN RING APPARATUS

The apparatus illustrated in Fig. 1 consisted of two 5.1 cm. diameter steel cylinders which were supported on a 2.5 cm. bearing. The bearing ran right through the axes of the cylinders and was fixed at both ends. The bearing and cylinders were machined as accurately as possible with the available facilities. The actual clearance between the movable cylinder and the bearing was less than $\frac{1}{1000}$ inch and any possible play was reduced by lubrication which was primarily used to allow the movable cylinder to move easily and smoothly.

The joint to be tested was formed either between the steel cylinders or between the brass cylinders which were attached to the basic steel cylinder with four $\frac{3}{4}$-inch B.A. steel bolts (Fig. 1). Either of the brass cylinders could be machined as required by placing the corresponding steel one on a mandrel in a lathe. The final finish on the surfaces to be stuck together was achieved by wringing the cylinders together using the various grades of Carborundum powder and finishing with jewellers' rouge.

Application of the Torque

The load was applied to the handle of a large die holder which was firmly attached to the movable cylinder. To ensure a steady and reproducible rate of loading, the torque was applied by means of a calibrated spring attached to a flat metal tape connected to a 4-inch diameter drum which was driven by a slow-speed electric motor and a gear system. The rate of loading could be altered by either changing the spring or attaching the spring at various points on the handle of the die holder.

Measurement of Joint Deformation

The deformation of the joint was measured with either of two techniques. In the first, a small plane mirror was bolted to the movable cylinder and changes in the direction of a beam of light reflected from its surface were indicated on a scale 2.5 meters away. In the second method, a Fielden proximity meter was connected to a fixed and insulated metal plate 1 inch square. This electrode was placed alongside an earthed 1 inch diameter disc connected to the movable cylinder. The output of the proximity meter was connected to a micro galvanometer which formed part of a photographic paper drum recorder setup. After appropriate calibration (using the optical system) the traces obtained on the drum recorder could be interpreted. This arrangement was of particular use in experiments of long duration or in detecting rapid changes in deformation.

A preliminary test was made to check the rigidity of the system so that changes other than those occurring in the joint would not interfere in the deformation measurements. This was done by clamping the two rings together and applying various torques up to the maximum to be used in the main experiments. A small amount of slip occurred in the first trial each time the rigidity was tested. In repeats, the slip, if any, was not detectable and the system was elastic, behaving according to Hooke's law as indicated in Fig. 2. To avoid any possible spurious slip in subsequent experiments the apparatus was always prestrained if any part was removed for alteration.

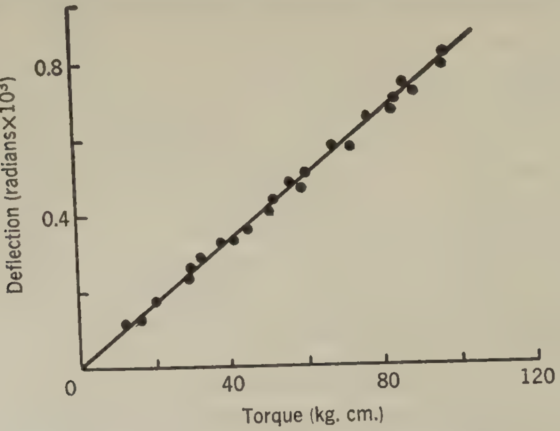

FIG. 2. Elastic strain of the napkin ring apparatus at various loads with the rings rigidly clamped together.

To check whether the connection between the rings was rigid enough in the above test, a solid brass ring was machined and connected to the steel cylinder in place of the two napkin rings. No appreciable difference was detected. Figure 2 was thus used with confidence in correcting the deformation observed in the main experiments.

Cleaning Procedure and Application of the Adhesives

The rings were first wiped with a clean cloth. They were then washed in a warm Tepol solution and rinsed profusely with distilled water. After this they were hung in a trichlorethylene vapor degreasing chamber and finally placed in a vacuum desiccator for 20 minutes.

Two adhesives were used, paraffin wax and nitrocellulose. To apply the paraffin wax, small pieces of it were placed on the metal surfaces which had been warmed in an oven. After the wax had run over the surface, the rings were wrung together. After allowing the joints to cool for 4 hours the excess wax was scraped off with a specially prepared metal tool, and the joint allowed to stand for a further 20 hours before testing.

Before applying the nitrocellulose the rings were rinsed in acetone. A solution of the nitrocellulose in acetone was then spread on each of the surfaces to be stuck with the aid of a clean glass rod. The rings were then wrung together. In some experiments the joints were allowed to set in air for a specified time and in others they were placed in a vacuum desiccator for various times. Before testing, the excess adhesive was removed as in the case of the paraffin wax joints. The thickness of the joint in each case was measured using a microscope with a 44 × objective and a 15 × eyepiece containing a calibrated scale.

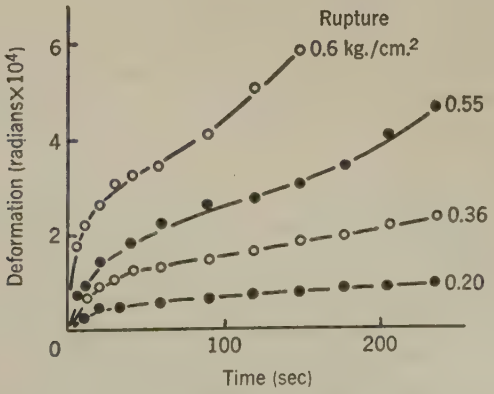

FIG. 3. The creep of a paraffin wax-brass joint. (Joint thickness 120 μ.)

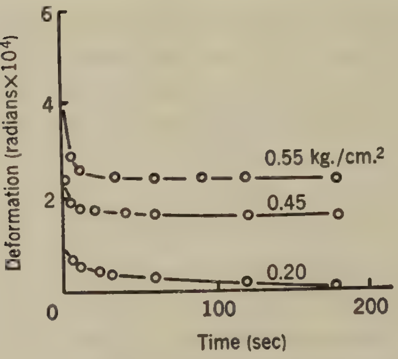

FIG. 4. The recovery of a paraffin wax-brass joint. (Joint thickness 120 μ.)

EXPERIMENTAL RESULTS

Paraffin Wax Joints

The creep of a typical paraffin wax-brass joint is illustrated in Fig. 3. All the results plotted are for the same joint. Figure 4 illustrates the recovery of a paraffin wax-brass joint after removal of the load. With steel rings the results were similar.

The load at which failure occurred was always less than 6.0 kg./cm.². The value obtained seemed to depend to some extent on the previous history of the joint. For example, a repeat experiment at the same load led to rupture in some cases.

Attempts to duplicate joints were not successful. Two joints formed in what appeared to be the same manner and of the same thickness behaved quite differently under load, and there was considerable difference in the breaking strength. However, it was a general rule that the easier a joint deformed the easier it was to break it.

Nitrocellulose-Brass Joints

The deformation of a nitrocellulose-brass joint is illustrated in Fig. 5, both during stress and after removal of the load. It was generally found that the more easily a joint could be deformed the stronger it was, as illustrated in Fig. 6. This behavior was the reverse to that found with paraffin wax-brass joints.

The nitrocellulose joints were easier to form than the wax joints and the deformation, being larger, was easier to measure. For these reasons they were examined in more detail than the wax joints.

Figure 7 illustrates the breaking strength observed in creep experiments for nitrocellulose-brass joints of various thicknesses after being left in the air for 24 hours. These results were not affected to any marked degree either by placing the joints in a vacuum desiccator for various times or by

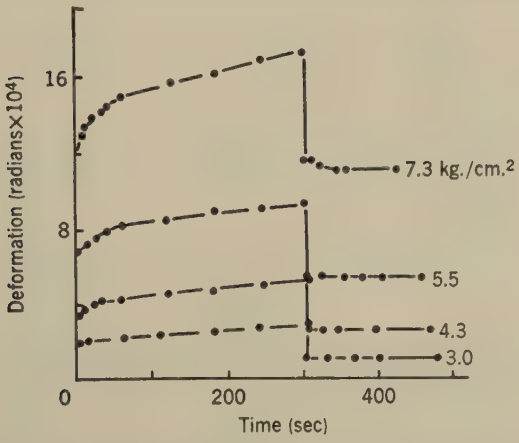

FIG. 5. The deformation of a nitrocellulose-brass joint.

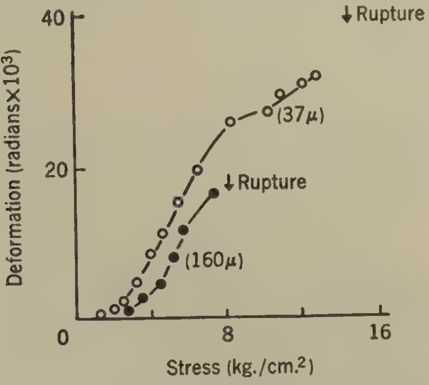

FIG. 6. The variation of the total deformation with stress for two typical nitrocellulose-brass joints.

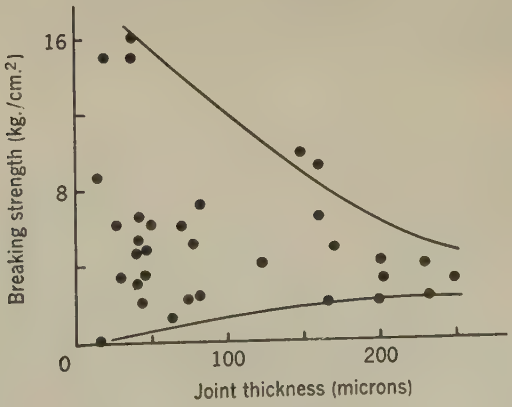

FIG. 7. The variation of the breaking strength of nitrocellulose-brass joints with changes in joint thickness.

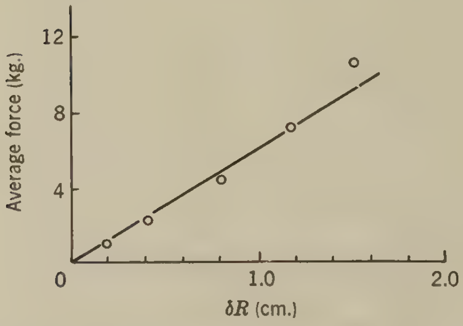

FIG. 8. Illustration of the proportionality between the average force required to break a nitrocellulose-brass joint and the area of metal covered by adhesive.

allowing them to set in air for as long as two weeks. There seems to be quite a large variation in the breaking strength of joints (as measured in shear creep experiments), and this variation increases as the joint thickness is decreased.

Figure 8 illustrates the effect of changing the width of the adhesive layer, i.e., δR. The average force required to break a joint was proportional to the apparent area of the metal surfaces stuck together by the adhesive.

ANALYSIS OF THE RESULTS

Since it is not possible in most practical cases to be sure whether a joint fails in the adhesive rather than at the metal-adhesive interface, it is convenient to analyze the results of the experiments such as those described above on the basis that all the deformation occurs in the adhesive. Any differences between the actual results obtained and what may be expected from the behavior of large samples of the adhesive may then be examined to see whether they may be attributed (*a*) to interface effects or (*b*) to the fact that in adhesion experiments only very small samples of the adhesive are involved.

Paraffin Wax-Metal Joints

It is reasonable to expect that a layer of paraffin wax under stress would act in either of two ways. It might act as a suspension of elastic bodies (the crystals) suspended in a very viscous liquid (the amorphous region) or, on the other hand, it might act as a polycrystalline material. In the first case the theory of Frohlich and Sack (2) would be applicable. If the second behavior were more likely we would expect that Andrade's empirical equation for the creep of polycrystalline materials would apply. Those joints which were strong enough to be adequately tested in the present experiments all acted as polycrystalline materials.

It has been found (4) that at low stresses the creep of polycrystalline metals is given by the simple empirical expression

$$D_\beta = \beta t^{1/3}, \qquad [2]$$

where D_β denotes the creep at time t and β is a constant for a given load. Figure 9 illustrates the creep of a typical paraffin wax-brass joint plotted

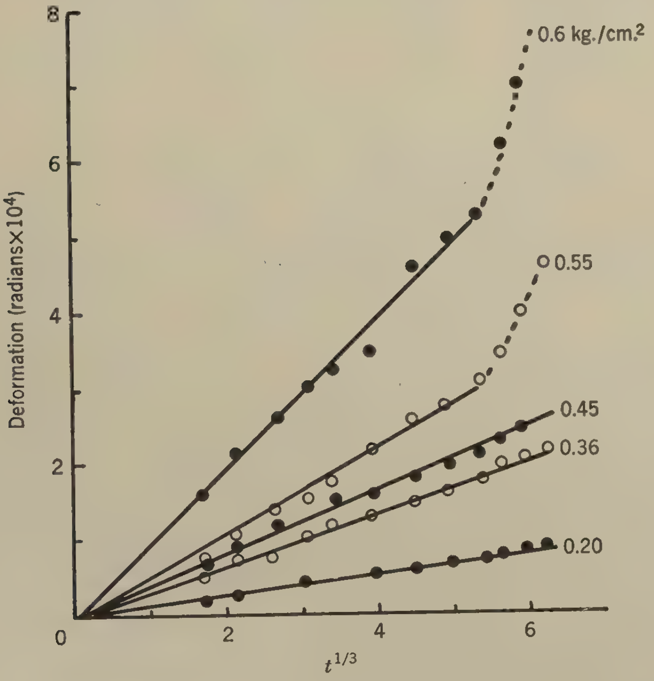

FIG. 9. The deformation t plots$^{1/3}$ of a typical paraffin wax-brass joint.

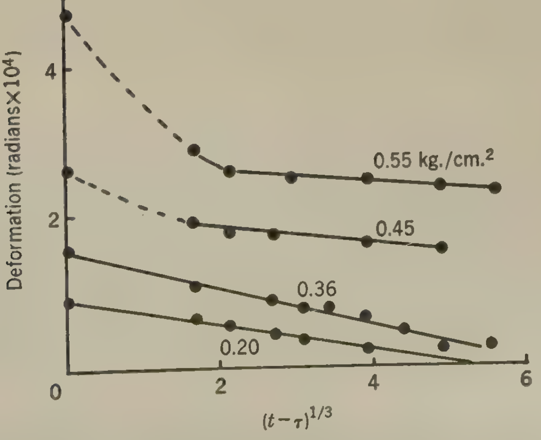

FIG. 10. The recovery of a typical paraffin wax-brass joint which has been stressed for 5 minutes at the loads indicated.

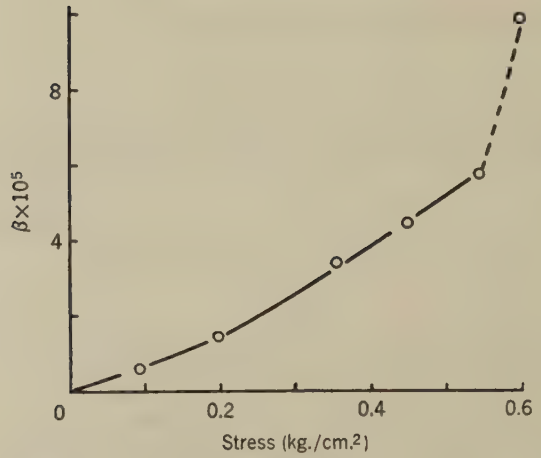

FIG. 11. The variation of the forward creep rate with stress for a paraffin wax-brass joint.

as suggested by Eq. [2]. This would indicate that paraffin wax-metal joints which were strong enough to test exhibit "β flow" up to or near to the failure point where more rapid deformation occurs.

If the rapid flow has occurred during an experiment there appears to be an initial rapid recovery followed by a β recovery which is less than the forward creep rate. In addition the recovery is not complete (Fig. 10).

The slope of the straight-line portion of the plots in Fig. 9 is equal to β in each case; β is descriptive of the rate of β flow and depends on the stress as illustrated in Fig. 11.

One obvious method of altering conditions so as to be able to determine the relative effects of the interface and the bulk adhesive would be to change the thickness of the joint. Unfortunately in practice it was not possible to do this and to be certain that the same crystalline structure and system of residual stresses prevailed in the adhesive.

Nitrocellulose-Metal Joints

An attempt was made to analyze the nitrocellulose joint deformation results using the well-known spring and dashpot models (5, 6) which are intended to represent the molecular behavior involving separation of atomic centers against attractive forces, orientation of chain segments, and the slippage of molecular chains past each other. Except at very low stress values it was necessary to introduce so many complicating factors that it was considered worth while to look for a different method of analyzing the results.

Figure 12 illustrates the result of plotting the total deformation (D_T) of a nitrocellulose-brass joint against $t^{1/3}$. Although highly curved for small

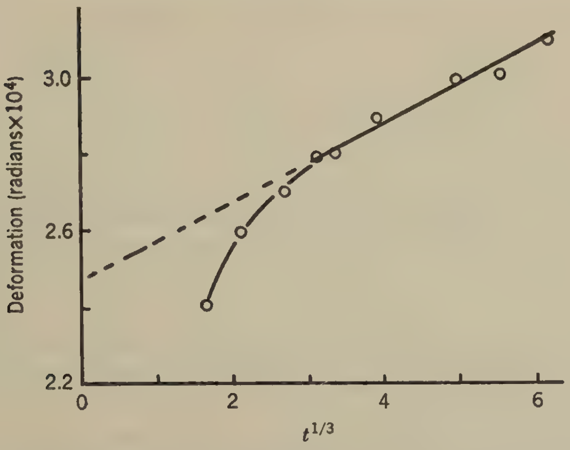

FIG. 12. Deformation of a nitrocellulose-brass joint plotted against $t^{1/3}$.

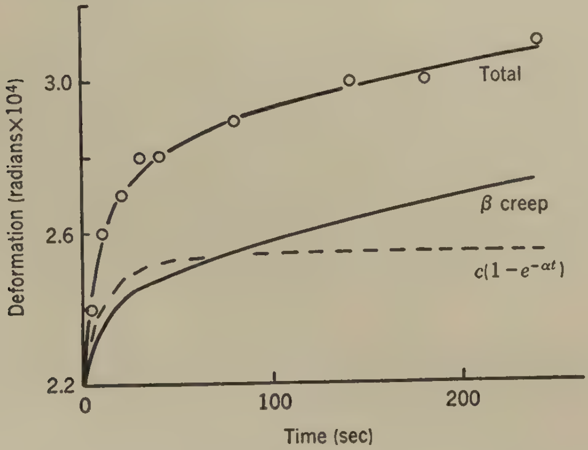

FIG. 13. Illustration of the splitting up of the total deformation of a nitrocellulose-brass joint into its various parts.

values of t, such plots became linear as t increased. This suggests that β creep occurs in nitrocellulose-brass joints. The slope of the dotted line as shown in Fig. 12 was taken as β in each case. This enabled the β creep to be calculated in each experiment as illustrated in Fig. 13.

Subtracting the β creep (D_β) at any time from the corresponding total deformation (D_T) resulted in curves such as illustrated by the dotted curve in Fig. 13. In all cases the equations representing these curves were found to be of the form

$$\Phi = D_T - D_\beta = D_I + C(1 - e^{-\alpha t}), \qquad [3]$$

where D_I, C, and α were constants for a given deformation experiment. Hence

$$D_T = D_I + \beta t^{1/3} + C(1 - e^{-\alpha t}) \qquad [4]$$

where D_I may be taken as the instantaneous deformation of application of stress.

After time τ the load was released in each experiment and the total deformation decreased from $D_{T\tau}$ and was adequately described by

$$D_T = D_{T\tau} - D_R - \beta_1(t - \tau)^{1/3}, \qquad D_T \leqslant D_P \quad [5]$$

where D_P is the permanent creep, D_R is the instantaneous recovery, and β_1 is a constant descriptive of the rate of flow in recovery and is not necessarily equal to β in Eq. [4].

All of the quantities in Eqs. [4] and [5] were determined for each joint under various loads. A typical result is summarized in Table I.

A successful attempt to establish the significance of each of these quantities and to see whether there were any effects which could not be attributed to the adhesive itself must be regarded as a subject for further research, possibly involving a variety of experimental techniques. It is, however, worth while to examine data such as given in Table I. This is done briefly below and the points that warrant future research emphasized.

a). *Instantaneous Recovery.* The instantaneous recovery of a joint (D_R) varied uniformly with stress. The elastic strain is defined by

$$\text{Elastic strain} = \frac{\bar{R} D_R}{h}, \qquad [6]$$

where h is the thickness of the joint and D_R is the instantaneous recoverable deformation measured in radians. A typical example of plotting the recoverable elastic strain against stress is illustrated in Fig. 14.

The decrease in the elastic modulus for instantaneous recovery as the

TABLE I

Data Derived from a Typical Cellulose Nitrate-Brass Napkin Ring Joint Experiment
($h = 160\ \mu$, $R = 0.8$ cm., $\bar{R} = 2.4$ cm., $\tau = 300$ sec.)

Stress kg./cm.²	$D_{T\tau}$ $\times 10^4$	D_I $\times 10^4$	D_R $\times 10^4$	D_P $\times 10^4$	β $\times 10^6$	$D_{\beta\tau}$ $\times 10^4$	C $\times 10^4$	α	β_1 $\times 10^6$
1.28	0.21	0.15	0.11	0.10	0	0	0.06	0.04	0
1.91	0.58	0.46	0.26	0.32	0	0	0.12	0.019	0
2.32	0.70	0.52	0.32	0.38	2.58	0.17	0.01	—	0
2.96	4.01	3.55	0.41	3.54	2.58	0.17	0.29	0.073	0
3.54	2.97	2.77	0.51	2.42	2.10	0.14	0.06	0.029	1.08
3.94	1.81	1.57	0.57	1.24	1.94	0.13	0.11	0.043	0
4.75	4.69	4.49	0.73	3.84	1.45	0.10	0.10	0.011	1.60
5.13	2.84	2.60	0.88	1.88	1.93	0.13	0.61	0.011	1.08
5.91	2.47	2.31	0.99	1.42	1.77	0.12	0.04	0.073	1.70

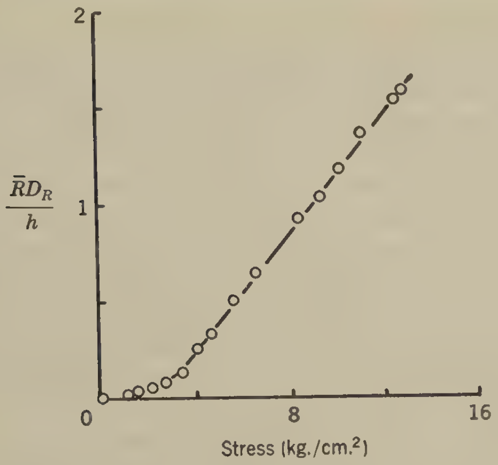

FIG. 14. The stress-strain relation for a typical nitrocellulose-brass joint.

stress was increased was apparent in all the joints which could be adequately examined. For convenience in discussing joints the slopes of the straight-line portion of curves such as the one given in Fig. 14 may be taken as being $1/G_R(\infty)$, where $G_R(\infty)$ is the final value of the modulus of elasticity for instantaneous recovery. This modulus varied from 4 to 100 kg./cm.^{2} for the joints which could be adequately tested.

Despite repeated attempts to control some of the various factors involved in the formation of joints which might affect $G_R(\infty)$ it was not possible to form deliberately two joints having the same value of this modulus.

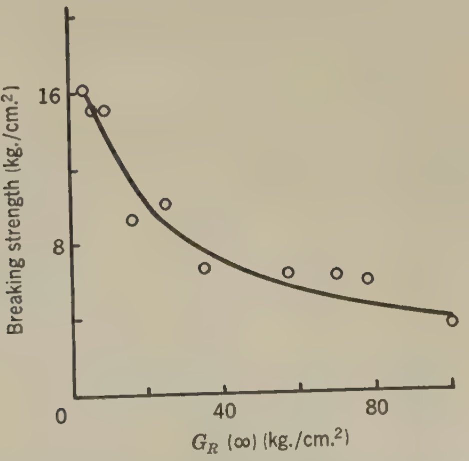

FIG. 15. Variation of the breaking strength of nitrocellulose-brass joints and the modulus $G_R(\infty)$.

It was noticed that the smaller the modulus of elasticity, $G_R(\infty)$, the greater was the joint strength. This is illustrated in Fig. 15.

The small values of this modulus would seem to mean that there is some sort of stress concentration or that the elasticity arises from weak elastic elements in the joint. The fact that joints which show the largest elastic deformation are the strongest would seem to rule out the first possibility unless some unrecognized factor is playing a part.

As far as the instantaneous recovery of a joint is concerned three large problems remain to be solved. These are (*a*) the reason for the change in the modulus of elasticity with increase in stress, (*b*) the reason for the apparent relationship between $G_R(\infty)$ and the strength of a joint, and (*c*) the reason for the great difficulty encountered in preparing joints of similar elastic properties.

b). *The Instantaneous Nonrecoverable Deformation.* The difference between D_I, the instantaneous deformation of a joint on application of a load and D_R, the instantaneous recovery, may arise either from a rapid extension of easily extended elements in the system followed by a partial permanent set or from a possible brittle fracture of links. In a subsidiary set of experiments a joint was stressed for time τ, allowed to recover, and the process repeated several times using the same load. A typical result is summarized in Table II.

These results can be qualitatively interpreted on the basis that on the first application of the load, all the links in a joint which cannot stand the stress are broken instantaneously. On the second application of the stress fewer links are broken. If this is the correct interpretation, the erratic nature of the quantity $D_I - D_R$ in the main experiments with nitrocellulose-metal joints is understandable, since in adhesion tests very small samples of the adhesive are being sheared and also the stresses chosen in a given experiment were not evenly spaced.

TABLE II

Data Derived from a Cellulose Nitrate-Brass Napkin Ring Joint Experiment in Which a Stress of 2.7 kg./cm.² was Applied Repeatedly

($h = 40\ \mu$, $\bar{R} = 1.5$ cm., $R = 2.4$ cm., $\tau = 300$ sec.)

Expt.	$D_{T\tau}$ $\times 10^4$	D_I $\times 10^4$	D_R $\times 10^4$	D_P $\times 10^4$	β $\times 10^6$	$D_{\beta\tau}$ $\times 10^4$	C $\times 10^4$	β_1 $\times 10^6$
1	9.04	8.94	0.48	8.50	0.9	0.06	0.04	1.1
2	0.60	0.54	0.48	0.10	0.8	0.05	0.01	0.36
3	0.50	0.44	0.44	0.03	1.0	0.07	0.01	0.6
4	0.51	0.42	0.44	0.05	1.32	0.09	0.04	0
5	0.46	0.42	0.40	0.02	0	0	0.04	0.6
6	0.82	0.78	0.54	0.23	0	0	0.04	0.8
7	1.85	1.81	0.78	0.93	0	0	0.04	0
8	0.44	0.42	0.42	0	0	0	0.02	0
9	0.44	0.44	0.42	0	0	0	0	0
10	0.52	0.50	0.50	0	0	0	0.02	0

This interpretation suggests a more convenient method of assessing $D_I - D_R$ in any experiment. If it is a brittle rupture of links, then one would expect that the total "give" up to and including the application of the nth stress in a given experiment, denoted by χ, would be

$$\chi = \sum_1^n (D_I - D_R). \qquad [7]$$

As would be expected this quantity varies much more uniformly with stress than the separate values of $D_I - D_R$. Figure 16 illustrates its variation with stress for two typical joints having the same adhesive layer thickness. The stronger joint would seem to be more resistant to instantaneous permanent "give."

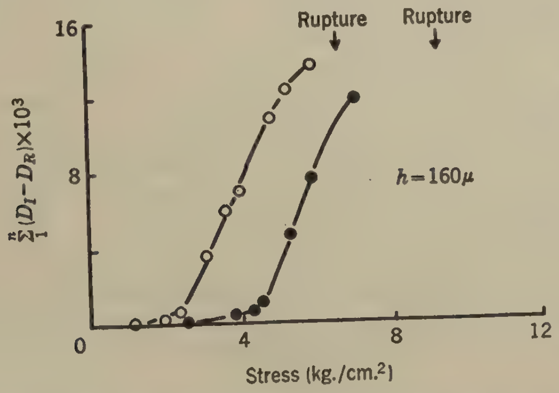

FIG. 16. Variation of the total instantaneous permanent "give" for two nitrocellulose brass joints of the same adhesive layer thickness.

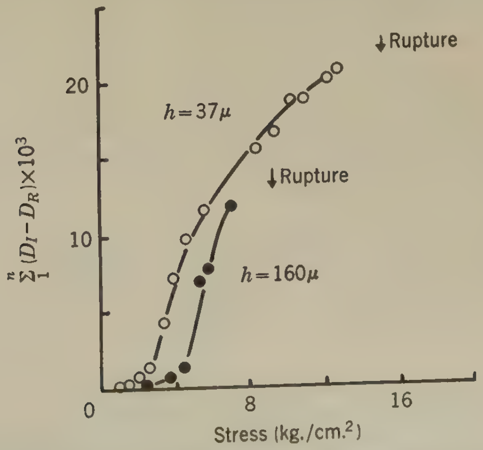

FIG. 17. Variation of the total instantaneous permanent "give" for two nitrocellulose-brass joints with different adhesive layer thicknesses.

Figure 17 illustrates the variation of χ with stress for two joints of different thickness. For some reason the strong thin joint was more permanently deformed by instantaneous "give."

It was not possible to trace the origin of this instantaneous "give" with certainty. It would be very interesting to know whether it is related to the well-known appearance of cracks in a substance like nitrocellulose giving it a milky appearance prior to rupture.

c). *Time-Dependent Deformation.* The creep of nitrocellulose-metal joints is apparently made up of two parts (*a*) a β flow which is either wholly or partially recoverable and (*b*) a flow which is described by $C(1 - e^{-\alpha t})$.

The significance of this second type of deformation is an open question. It may be due to an extension of flexible elements in the nitrocellulose (or at interfaces) against a viscous resistance followed by a permanent set, or it may be time-dependent breakage.

d). *Breaking Strength.* The large variation in the breaking strength of nitrocellulose-metal joints is not surprising in view of the corresponding variation in the viscoelastic properties of the joints.

It is interesting to note that although it is possible to get the strongest joints by making the layer of adhesive thin, there is no guarantee that a thin joint will always be stronger than a thick one.

The value of the breaking strength was always very much less than the tensile strength of well-orientated nitrocellulose film. There are a variety of possible reasons for this, among which the relatively crude way in which films are prepared in adhesion experiments is probably of considerable importance.

Finally, the data illustrated in Fig. 8 would seem to indicate that edge effects such as occur in lap joints are either not present in the napkin ring test or are masked by some other factor.

Conclusion

The present examination of the napkin ring type of joint has revealed that it should be a most useful technique in future adhesion research, especially if the viscoelastic behavior as well as the breaking strength of joints is assessed.

The outstanding problem in adhesion experiments is the difficulty encountered in trying to form joints having the same viscoelastic properties. This difficulty is reflected in the large variation in the practical strength of joints.

The failure of a joint appears to be intimately related to the rupture of the adhesive and to sort out the factors which are peculiar to adhesion at the interface it will be necessary to know more about the adhesives themselves at high stress.

ACKNOWLEDGMENTS

This work was made possible by the financial support of the Ministry of Supply and the Canadian Defence Research Board. Their assistance is appreciated.

REFERENCES

1. DE BRUYNE, N. A., AND HOUWINK, R., "Adhesion and Adhesives." Elsevier, London, 1951.
2. FROHLICH, H., AND SACK, R., *Proc. Roy. Soc. (London)*, **A185,** 415 (1946).
3. ANDRADE, E. N. DA C., *Proc. Roy. Soc. (London)*, **A84,** 1 (1910).
4. ANDRADE, E. N. DA C., AND JOLLIFFE, K. H., *Proc. Roy. Soc. (London)*, **A213,** 3 (1952).
5. FRITH, R. M., AND TUCKETT, R. F., "Linear Polymers." Longmann's, Green, London, 1950.
6. ELEY, D. D., AND PEPPER, D. C., *Trans. Faraday Soc.* **43,** 583 (1947).

JOURNAL OF COLLOID SCIENCE **11**, 748–766 (1956)

VINYL TYPE POLYMERIZATION AT SOLID SURFACES AND WITH COMPLEX CATALYSTS

F. Eirich and H. Mark

Institute of Polymer Research, Polytechnic Institute of Brooklyn, Brooklyn, N. Y.

Received September 7, 1956

I. Introduction

The term "catalysis" used in connection with vinyl-type addition polymerization designates in reality an initiation of an exothermic chain reaction. Whether the starting of the chains is effected by free radicals, positive carbonium ions, or negative carbanions, the so-called catalysts are essentially providing active centers for the initiation of chain growth. In the course of the last 25 years a considerable knowledge and know-how has been accumulated concerning our capacity to produce such active centers at desired concentrations over predetermined periods of time, and it is fair to say that we have a considerable fundamental understanding and practical control of the starting of vinyl-type polymer chains. We also can influence to a certain degree the termination of chain growth by the introduction of telomers or modifiers both of which accelerate the cessation reaction and bring the whole process of polymerization to an end. Vice versa, we can delay the recombination of radicals by increasing the viscosity of the medium and thereby reducing the probability of the termination steps.

Until recently, however, we have not been able to affect in any way the propagation reaction, that is, the manner in which each new individual unit is added to the growing chain by the methods now known. Once a chain is started it keeps on growing according to the laws of random collisions between the active chain ends and the monomer molecules. Apart from transfer steps which actually do not interrupt the kinetic but only the physical chains, or such either trivial or ineffective influences at our disposal as enhancing or delaying the exchange of the heat of reaction, changing the solvent, or changing the dielectric constant, there were no means to accelerate or delay the elementary step of addition, nor were we in the position to control the geometrical arrangement of the individual monomers and their substituents as they enter the growing chain.

It now seems that developments of the last 10 years begin to yield clues and perspectives as to how to gain a certain control over the details of the propagation step in vinyl-type polymerization. In most cases the essential step is to induce chain growth at a liquid-solid interface in such a manner that specific sites may exert a strong activating and directing influence on the actual process of addition of the individual monomer units to the growing chain. It is the purpose of this article to give a brief review of certain phases of this rapidly growing field.

II. Specific Instances of Interface Polymerization

As early as 1935 E. K. Rideal and his collaborators (1) started to investigate the mechanism of vinyl-type polymerization, including polymerization at interfaces, and found that vinylacetate can be polymerized at an aqueous surface at a considerable rate, and that butadiene polymerizes rapidly when brought into contact with a solution of H_2O_2 in water.

In 1948 C. E. Schildknecht (2) reported that he had succeeded in obtaining two different types of polyvinyl isobutyl ether, one essentially resulting from polymerization at low temperatures, and another which is formed whenever the reaction is carried out at more elevated temperatures but is moderated by using Friedel-Crafts' etherates. The "low-temperature" polymer, produced by a so-called proliferous reaction in the course of which a gel-liquid interface does appear in the system, is a crystalline, hard, and resinous material which melts around 70°C., whereas the "high-temperature" material is a soft, amorphous, rubbery mass which resembles polyisobutylene, rubber, or GR-S. Both materials can be dissolved, although the rubbery modification is more easily soluble; their osmotic molecular weights are of the same order of magnitude and there is no indication that one is more branched than the other. It was therefore assumed (3) that the difference in behavior is caused by a different arrangement of the substituents along the length of the macromolecular backbone chains whereby the hard resinous modification possesses the more regular arrangement and, therefore, a higher tendency to crystallize. Schildknecht points out that this modification is regularly obtained when the system is heterogeneous, whereas the soft rubbery material results if polymerization takes place in a homogeneous environment.

At about the same time A. A. Morton (4) reported the discovery of a new type of polybutadiene prepared with the aid of special catalytic systems, the so-called Alfin catalysts. It was well known that butadiene can be polymerized by free radical, as well as by ionic, initiation to give rubbery polymers which contain the individual monomer units in 1,4- and 1,2-addition, and which have a great tendency to cross-link at later stages of the reaction because of the presence of the relatively reactive pending vinyl double bonds, resulting from the 1,2-additions. The double bonds which are located in the backbone chains resulting from the 1,4-additions are partly in the *trans-* and partly in the *cis*-configuration, with the result that these "normal" butadiene polymers have a rather irregular chain structure and are not capable of crystallizing even if the samples are oriented by stretching for several hundred per cent. Morton, however, was able to prepare polybutadienes of very high molecular weights (up to several millions) at high rates and conversion without running into the difficulty of gelation. Infrared analysis demonstrated that the macromolocules contained only a few 1,2-additions, and that the double bonds in the chains were essentially in the *trans* configuration (5).

The specific catalysts for this type of reaction were prepared by reacting sodium isopropylate in a hydrocarbon solvent with allylcholoride, which leads to the formation of NaCl, sodium allylate, and an alcoholate-olefin complex. From the variations of this system the essential characteristics seem to be that a finely divided salt is suspended in a hydrocarbon vehicle and that an organometallic compound is complexed with the olefin and the complex adsorbed on the dispersed solid salt.

In an important modification of the older sodium butadiene polymerization, Stavely and co-workers (6) of the Firestone Company showed that an all-*cis* isoprene can be obtained by an apparent gel phase polymerization of the liquid monomer initiated by finely divided lithium metal. The same polymer has further been prepared by workers of the Goodrich Company with the aid of a metal halide-metal alkyl catalyst (7). Recently it was announced in a preliminary fashion by workers of the Eastman Kodak Company (8) that crystallizable polystyrene can be obtained in liquid phase by employing an Alfin catalyst.

In 1953 K. Ziegler (9) discovered that ethylene can be polymerized at normal pressures and at room temperature in hydrocarbon solvents with the aid of aluminum alkyls, forming α-olefins containing 10–20 carbon atoms. In a systematic effort to control the molecular weight distribution of the resulting product Ziegler made the additional discovery that polyethylene of very high molecular weight and unusual properties can be obtained at normal pressure and temperatures with a high rate of conversion if the aluminum alkyls are used in the presence of metal halides which can be reduced to states of lower valency. The principal combination which Ziegler disclosed in his first patents (10) was $TiCl_4$ and $AlEt_3$ in heptane or another aliphatic hydrocarbon vehicle.

However, it appears that this composition is just one of many possible embodiments of a general principle, namely, the effectiveness of a surface complex, produced in the reaction of a metal alkyl and a metal halide, in which the halide metal atom is not in its highest state of valency. More than a dozen metallic elements have been claimed to be effective complexing agents when used as the halide, and several (Be, Mg, Zn, Tl, and In) when forming the alkyl. Moreover, it seems that easily reducible organometallic compounds such as acetyl acetonates also can be used instead of the halide, and that Grignard compounds, sesquihalides, complex hydrides, and mixed alkyl hydrides may take the place of tri-alkyl aluminum. This is also shown by a large body of work which paralleled Ziegler's as quoted, e.g., under Ref. (7, 12, 28).

As far as the present information goes (11) it requires a dispersed solid phase of particles larger than colloidal size to provide the specific characteristics of the Ziegler reaction. These characteristics are not only the rapid formation of polymer of high molecular weight (up to several millions) at normal pressures and ordinary temperatures, but comprise also regularity of monomer addition as well as the absence of short-chain branching, so that the Ziegler polyethylene, e.g., is essentially a polymethylene and, as a consequence, has a higher tendency to crystallize, a higher density (0.95–0.96), a distinctly higher melting point (above 130°C.), and a greater resistance to the action of solvents and swelling agents than high-pressure polyethylene.

G. Natta (12) extended Ziegler's discovery shortly afterwards. By first using typical Ziegler catalysts, and later applying the principle of solid dispersed complexes between inorganic and organic metal compounds to a series of other combinations, he studied the polymerization of α-olefins and the nature of the resulting products. He found that, in fact, propylene, α-butylene, and styrene can be converted into high molecular weight materials with the aid of this technique; he also established that the resulting polymers differed essentially from the corresponding "normal" materials prepared in a homogeneous environment with the aid of free radicals or ionic catalysts. Whereas the known species of polypropylene, polybutylene, and polystyrene are linear (or slightly branched), amorphous polymers with relatively low softening ranges and with no indication of crystallinity even in the highly oriented state, Natta discovered that the polymers obtained with metal alkyl-metal halide complexes were linear macromolecules with a strong tendency to crystallize, having typical melting points at temperatures much higher than the softening ranges of the amorphous species. This is quite analogous to the two polyvinyl isobutylethers of Schildknecht, and suggests a similar explanation for both phenomena.

By a very careful X-ray study of well-oriented samples of crystalline polypropylene, polystyrene, and other α-olefins (13), Natta succeeded in establishing recently that in all these cases the substituents are arranged with a peculiar regularity which has never been found previously in vinyl polymers. Inside of the crystalline domains of polystyrene the chains are arranged in a helicoidal form such that the substituents have all the same steric configuration in respect to the backbone chain and that each monomer unit is turned 120°C. from the axes of its neighbors; thus forming an identity period of three units. Molecular models show this so-called *gauche* conformation to be the one of least interference between substituents and hydrogen atoms. If one would straighten out the backbone of a molecule as a planar zigzag paraffin chain, all phenyl groups would be on the same side of the plane over a certain length of the chain, followed by a change-over to the other side of the plane and a stretch of substituents in this configuration, and so on. One arrives in this manner at a system of blocks of substituents in the *d*-configuration separated from each other by blocks of substituents in the *l*-configuration, or to what essentially is a "block" *meso*-form of polystyrene. Natta has proposed the adjective "isotactic" for vinyl polymers with this specific arrangement of their substituents (12, 14) and has emphasized that the presence of a solid surface seems to be essential for inducing such a regularity of individual propagation steps.

In a later paper (13) Natta demonstrated the existence of an all 1,2-polybutadiene in which the pending vinyl groups are regularly arranged in respect to the planar backbone chain in such a manner that there is a continuous alternation from *d* to *l*, back to *d*, and so on. Natta proposes for this type of regularity in the configuration of the substituents the name "syndyotactic." This type of polybutadiene is entirely different from all previously obtained polymers of butadiene and represents a rigid crystalline resin with a melting point of about 140°C. The structure of its crystalline domains has been elucidated by Natta in a very thorough investigation with the aid of X-ray and electron diffraction (13) which established not only the regular *d-l* alternation of the pending vinyl groups but also the exact arrangements of the backbone chains in the lattice.

Using a rather different system, namely, chromium oxide supported on silica, workers of the Phillips Petroleum Company (15) indicated in a trade journal that, after the earlier successful synthesis of polyethylene on the same catalyst, they were able to produce also all-*cis*-, all-*trans*-, and all 1,2 polybutadiene. It should be noted that this catalyst appears to be of the spinel structure and thus to belong to a family of catalysts which has been used frequently in the past for catalytic reactions of unsaturated hydrocarbons. Similar systems are reported by the Standard Oil Co. of Indiana (15).

Still more recently C. C. Price (16) and co-workers have uncovered a case of stereospecific synthesis which, although not vinyl polymerization, throws much light on the molecular configurations in the transition state. It was shown that *l*-propylene oxide, prepared by enzymatic reduction of hydroxyacetone, when polymerized in organic solvents in the presence of potassium hydroxide powder yields a solid polymer of melting point 56°C. with a strong optical activity. The same polymerization process starting from inactive isopropylene oxide yielded only a low molecular weight oil which freezes at −65°C. When ferric chloride was used as catalyst (a process developed by the Dow Company (17) yielding about 30% high molecular weight crystalline, optically inactive, material melting at 70°C. from racemic monomer) and applied to the *l*-isomer, only about 25% of crystalline, optically active, material was obtained. It follows that polymerization on potassium hydroxide surfaces does not lead to racemization, nor does it induce optical activity, whereas ferric chloride gives rise to a synthesis by a process which must involve some stereospecific direction, but without forming regular sequences.

III. Some Concepts of Stereospecific Catalysis

In trying to postulate mechanisms for these stereospecific reactions it is, first of all, not certain or even likely that they all follow similar mechanisms. It is not unlikely, however, that these reactions proceed by some common, basic steps, in the same way as, e.g., free radical polymerization, cationic polymerization by Friedel-Crafts' catalysts, popcorn polymerizations, etc., are characterized by common steps.

Assuming then that it is permissible to speak of common features, the following seem to hold for all stereospecific syntheses (18):

a. Fairly fast overall rates at low temperatures and pressures.

b. A distinct preponderance of linear polymerization over side reactions.

c. The regularity of the resulting chains, in particular with respect to *d-* and *l*-configuration.

We propose to attribute these characteristics to the following reaction features:

α. Adsorption or complex formation, the energy of which permits the adoption of well-defined configurations of the reactants prior to, or in, the transition state (18).

β. An effective cataysis, by polarization, adsorption and electron transfer, lowering the activation energies of the initiation as well as of the propagation step.

γ. A structure and a life time of the transition state which either leads to a specific freezing of rotation or permits a suitable rearrangement between saddle points with relatively small energy differences.

The mechanisms quoted under α–γ should not be expected to correspond directly to the features quoted under *a*–*c*, but may combine with one another in producing the observed behavior. Certain conditions under α in particular may eliminate, for example, the need for others under γ. In view of the large number of factors and of their combinations that will have to be taken into account, we shall only briefly summarize those generally known features of complex formation and of heterogeneous catalysis which appear to be pertinent to our case.

According to the concepts of surface catalysis, the surface may be the site of permanent, or adsorbed, particles which enhance the formation of the transition state (activated complex) or enter into it and are released again after the reaction. Alternatively, the surface may possess the ability to adsorb the reactant molecules, to displace electrons or electron pairs and thus loosen bonds, or even to dissociate adsorbed molecules into groups which react with others arriving from the surrounding phase. Such chemical adsorption is quantitatively different from physical adsorption, in which the electron configuration of the adsorbed particles is only insignificantly altered.

Further, for effective catalytic functions, the reacting groups have to be formed and removed at appropriate rates and the binding energy to the surface must be such that the heat and the activation energy of adsorption will not compete with those of the rearrangement. Finally, the often observed changes in the heats of adsorption with percentage surface covered must not lead to poor utilization of the surface area, and the proper balance between mobile adsorption, which enhances a high rate of combination, and immobile adsorption, which is conducive to fixing specific configurations, must be preserved.

As for the often assumed ability of the catalytic surface to act as electron sink, draining bonding electrons from the adsorbed molecules into unfilled orbitals of the catalyst (say into the *d*-shells of the transition elements) (18, 32) we shall have to consider in addition, the ability of the catalytic surface to supply electrons and thus act as a "Lewis base."

The factors responsible for heterogeneous catalysis referred to so far pertained to the lowering of the activation energies of initiation and propagation and thus to a speeding up of the reaction. In order to account for stereospecificity we must assume further that certain configurations of the transition state of the propagation step are favored by the catalytic surface. It will be remembered that W. Kuhn (19) has shown it to be necessary for optically active syntheses that the reactants join in a three-point contact at the moment of coupling. Only in this way may a specific optical configuration of the one component enforce a specific configuration in the other component. A two-point contact is sufficient if there is a group exerting strong steric hindrance (amounting in effect to a third contact). We can see that in many cases the presence of a surface may provide steric hindrance to rotation and permit a directive influence of one configuration on to the other.

In general, two joining groups are able to rotate around the axis of their approach (19). One has to expect for a stereospecific synthesis that the relation between average rotational energy and the magnitude of the rotational barriers be such that the energetically most favorable position can be reached and temporarily maintained. In uncatalyzed reactions which require full supply of the activation energy, i.e., which proceed at elevated temperatures, the rotational degrees of freedom will contain sufficient energy so as to prevent a dropping into the lowest potential energy well. In the presence of a catalytic surface, the reaction may proceed at a sufficiently low temperature, or the surface may act as a sufficiently strong rotation barrier, to permit the two- or three-point contact necessary for stereosynthesis. Surfaces will assist further in conducting away the heat of reaction, and thus will again favor the assumption of specific positions.

In the particular case of vinyl monomers with bulky side groups joining the growing end of a homo-polymer chain, it is to be expected that the side groups will be directed into the *gauche* position, provided the path and the energetics of the reaction will permit this. *Gauche* positions require substituents on the same side of the chain, though 120° displaced, so that a succession of *gauche* conformations amounts to a helicoidal succession of the same steric species. The adsorption of such chains will require very high specificity and thus be highly selective as regards the catalyst.

Finally, we shall have to employ the concept of steric complexes and of their formation and, in view of their widely varying nature from very loose molecular types held by van der Waals' forces to rather stable ionic, or partly covalent, complexes or chelates we shall discuss the nature of the complex from case to case.

IV. Suggested Mechanisms of Stereospecific Syntheses

a. In starting to analyze the limited number of known facts in the light of the above general principles, the chemically simplest case appears to be that of the polymerization of dienes by lithium metal. This system contains only dispersed metal, inert solvent, and the monomer and is presumably related to the sodium polymerization of butadiene (20). The primary interaction of lithium is, very probably, related to that of other cations with olefinic double bonds, as, for example, studied by Chatt, Dewar and others (18, 21) on platinous, silver, and other ion complexes, including the metals at the end of the transition series in the periodic groups Ib, IIb, and VIII. Dewar visualizes $\sigma - \pi$ complex bonds in which the π electrons of the olefin overlap with the empty *s* orbital, or the *dsp* hybrid orbitals, of the metal while the *d*-electrons of the latter overlap with the antibonding π-orbitals of the olefin. The reactivity of these compounds depends on the presence of other electronegative groups. Generally, the complexes are moderately stable, and no catalytic activity has, as yet, been observed.

Alkali metals which can participate in σ-type bonds only, form loose complexes with olefins, in line with the more recent concepts of proton or Br^+ addition to olefins, which postulate fast complex formation with the π-electrons followed by slow proton addition and carbonium ion formation (22):

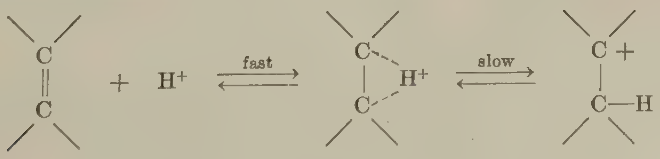

The adsorption of dienes on metallic surfaces should follow this pattern, whereby electron separation of atomic lithium will lead to metallation and to the formation of small amounts of lithium alkyl which in turn may act as the catalytically effective compound. A possible course of reaction is indicated below:

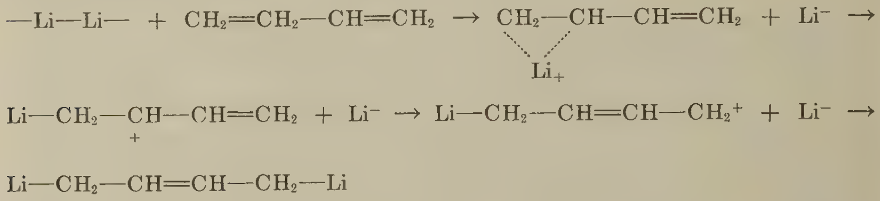

$$-\mathrm{Li}-\mathrm{Li}- + CH_2{=}CH_2-CH{=}CH_2 \rightarrow \underset{\mathrm{Li}_+}{CH_2-CH}-CH{=}CH_2 + \mathrm{Li}^- \rightarrow$$

$$\mathrm{Li}-CH_2-\underset{+}{CH}-CH{=}CH_2 + \mathrm{Li}^- \rightarrow \mathrm{Li}-CH_2-CH{=}CH-CH_2^+ + \mathrm{Li}^- \rightarrow$$

$$\mathrm{Li}-CH_2-CH{=}CH-CH_2-\mathrm{Li}$$

There is, however, a difficulty pertaining to this scheme, in that Grignard reagents, which are known to complex readily with olefins, lead in their reactions mostly to *cis*-compounds, whereas Li-alkyls, as lesser complexing agents, lead to a higher ratio of 1–2 addition (23)[1]. Since Coral rubber is an all-*cis*, 1–4 polymer, one should not expect ordinary, free Li-alkyls to be the catalytic agent. It is not implausible, though, that the conditions for *cis*-complexing are improved by the adsorption of both, the Li-alkyl and the olefin (I); alternatively, in view of the adsorption of the olefin, Li-alkyl may not even be required as intermediary, but complexing might take place directly at surface steps, or corners, of the metal lattice, II:

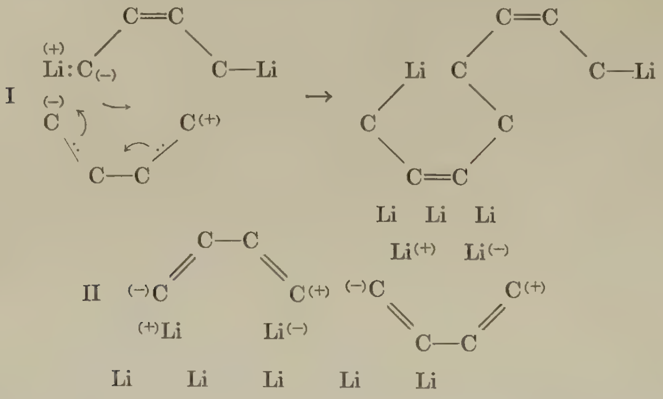

It should be remarked that if adsorption is less locally specific, but strong and unspecific, dense surface packing will favor all-*trans* configurations of the adsorbed molecules. In such an almost crystalline surface layer, Li^+–Li^- initiation should lead to an all-*trans*, 1–4 polymer, and Li-alkyl initiation would produce an all 1–2 polymer.

---

[1] In his lecture before the Chemical Society, London, December 15, 1955, L. E. Orgel, Cambridge, postulated ferrocene type complexes of cyclo butadiene, which in this case might be formulated as: $2Li + C_4H_6 \rightleftarrows (LiH)_2 \cdot C_4H_4$.

b. In the scheme above, the stereospecificity of the diolefin polymerization was restricted to the distinction between addition in *cis*- or *trans*- configuration by the energy difference between various forms of surface complexing or adsorption. In addition polymerization of racemic propylene oxide we are confronted with a stereospecific direction of approaching, optically active, monomers (24).

In suggesting a mechanism, we refer first to the generally accepted view that the ring opening of propylene oxide by bases occurs rather specifically by S_N2 attach on the less substituted carbon, whereas ring opening by acids occurs in varying, but not very different, proportions on both carbon atoms. In agreement with this, the data of Huston *et al.* (23) show that propylene oxide in ethyl alcohol catalyzed with sodium ethoxide produces 85 % of 2-hydroxy propyl ethyl ether (I), while in the acid polymerization 25 % of the same ether and 31 % of 2-ethoxy n-propanol (II) were found. It will be seen that the basic attack on #1 carbon

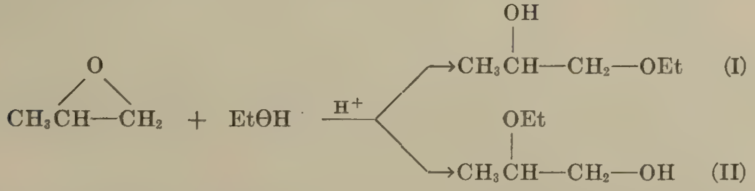

preserves the optical configuration of the central, #2 carbon, whereas in more than half the instances of acid attack, i.e., those on the optically active carbon, the latter passes through a carbonium ion stage with consequent inversion. Moreover, lately, acid catalyzed epoxy ring opening without any inversion has been discussed (23).

Price found in his very interesting studies of propylene oxide polymerization that solid KOH as catalyst produces crystalline, 1-active polymer in high yield but of low molecular weight. This is readily understandable on the basis of the above scheme, as the optically active carbon will remain preserved, and as in the displacement by the alkoxy oxygen on the #1 carbon the monomer units have only one path of approach. When ferric

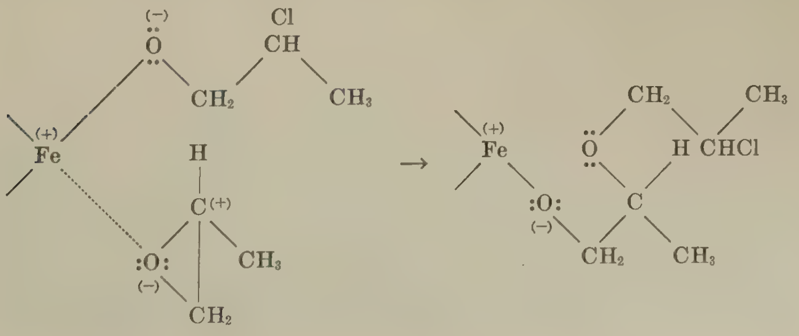

chloride was employed as catalyst for 1-monomer, about the same ratio as reported above of optically active and of inactive polymer was produced. Ferric chloride and racemic monomer produced partly crystalline inactive, and partly amorphous polymer.

According to Price, the catalyst contains basic sites consisting of ferric alkoxide which formed when the catalytic solution was prepared by propylene oxide addition to the ferric chloride in ether whereby a subsequent turbidity and formation of precipitate were observed.

These sites activate polymerization by a coordinating process of a character in between anionic and cationic attack, as also shown above. The directive effect is here postulated as emanating from the optically active carbon in the ferric alkoxide, which switches the configuration of the oncoming monomer while the central carbon ion becomes planar in the transition state. Additional catalyst sites of different nature are invoked, but not specified, as being responsible for random, or racemizing, addition.

It may be taken for granted, however, that the ferric chloride is never quite free of water or of hydrochloric acid. In this case the catalyst formation may proceed as indicated by Overberger (25); this would help to explain the absence of chloroform-soluble products in the catalyst, or of any chlorohydrin which should be found according to Price's scheme.

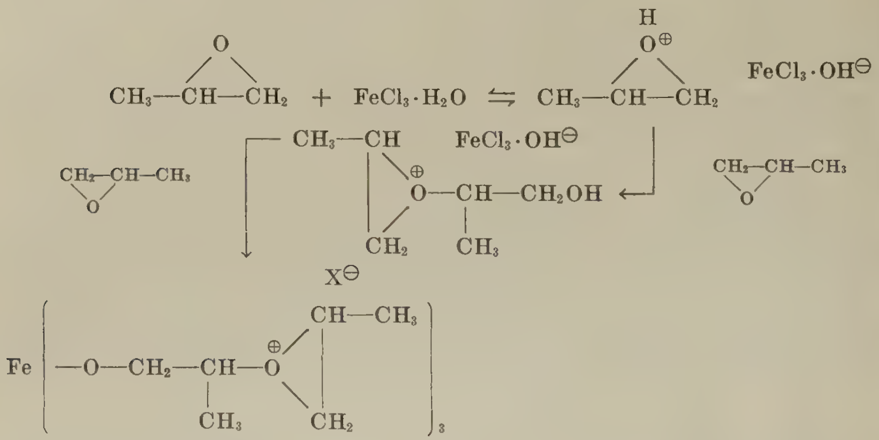

The attack of the basic oxygen on the more substituted carbon, further, is not supported by ordinary experience; furthermore, it is difficult to see how the asymmetric carbon atom of the bound alkoxy group can influence the configuration of the attacked carbon atom, from which it is separated by two intervening atoms. In an alternative explanation of the partial stereospecificity exhibited by ferric chloride acting on racemic monomer, one might postulate fixation of a ferric chloride hydrate, or of a hydrochloride, on a surface, followed by the coordination of two propylene oxide molecules to Fe^{3+} ion, satisfying the coordination number six. This complex, too, should be insoluble in ether because of the displacement of solvating ether molecules. The driving forces of the polymerization reaction will then be the addition of the unprotonated to the protonated of the two coordinated propylene oxide molecules—a process which simultaneously vacates a coordination site for a new molecule to be complexed. This typical S_N2 attack is

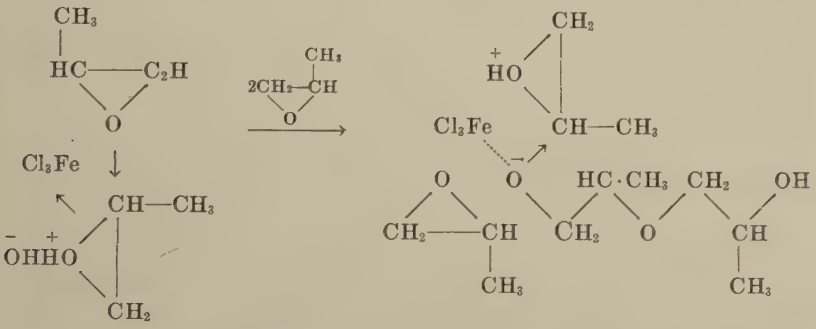

preceded by proton transfer from the water to the oxygen of the attacked monomer, and therefore is again subject to the two alternative routes discussed above. The attack on carbon ☀2 will lead to a planar carbon in the transition state and is, therefore, capable of rearranging the monomer to that of configuration which, on joining of the bond, will give the lowest configuration energy. Attack on carbon ☀1 will preserve the configuration of the new monomer and thus fail to influence it.

Accordingly, there would be only one type of site, and the differences in addition are attributed to the known ambiguity of the proton-initiated attack. The stereospecific direction occurs during the racemizing path and the directive influence does not stem, or stems only partly, from the distant active carbon, but is due to adsorption, coordination, and inversion of the new monomer, cooperating so as to bring it into a position and configuration equivalent to that taken up by the incumbent alkoxy groups. Since these are alternating approaches and positions in the complex, a syndyotactic structure is more likely than isotactic blocks.

c. Turning to catalysts of the Ziegler type, we have an inert solvent, a metal chloride, an aluminum alkyl, or a Friedel-Crafts' catalyst, and the olefinic monomer. In order to appreciate the parts played by these constituents, the following facts have to be borne in mind.

The aluminum halides and alkyls, and also many other metal halides and alkyls, occur as dimers since their coordination numbers are, as a rule, larger than the number of their valencies. In aluminum alkyls in particular, where the valency is 3 and the coordination number 4, the dimerization tendency of the lower alkyls is very strong, even in the vapor phase. Only in electron-donating solvents does one find the monomers, and such solvents cannot be used for polymerization. The dimerization is strongest for the tri-methyl aluminum and falls off to the tri-pentyl aluminum, since there the volume of the three substituents has become so large as to exclude occupancy of the fourth coördination site.

The structure of most of these dimers, and especially of AlX_3 and AlR_3, is the so-called bridge structure: 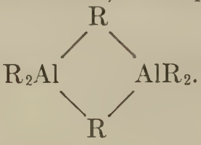. The halides can be assigned partially polar bonds 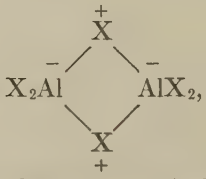, but the alkyls require electron-deficient bonds or central 3-center orbitals (26). Mixed alkyl halides should, therefore be more stable than the pure alkyls and, in general, all compounds tend to become monomeric by expanding, as Lewis acids, their electron shells. It is the strong tendency of these aluminum alkyls to form more stable compounds which represent the driving force of their reducing power.

We might, therefore, expect the reaction between the aluminum alkyl and the titanium tetrachloride to proceed by a number of routes written below summarily:

$$Al_2R_6 + TiCl_4 \rightarrow Al_2Cl_2R_4 + TiCl_2R_2$$

$$TiCl_2R_2 + TiCl_4 \rightarrow 2TiCl_3R$$

$$2TiCl_3R \rightarrow 2TiCl_3 + R_2$$

According to this scheme, the dimers of aluminum chloroalkyls would be produced by exchange reactions under simultaneous formation of titanium chloroalkyls. The latter compounds are rather unstable and decompose to insoluble titanium chlorides (which form dark suspensions) and dimerized alkyls.

The structures of titanium chloride, ferric chloride, and, in fact, of most of the chlorides of the transition elements and even of tin and lead, have many features in common. All these chlorides form close-packed layer lattices either of the cubic, or of the hexagonal, type. $TiCl_3$ and $TiCl_2$ are typical in possessing the CdI_2 structure in which the titanium ions lie in hexagonally packed planes and are surrounded by six chlorine ions, three above and three below the plane. Every layer of Ti-ions thus is sandwiched between two outer layers of chlorine ions which face each other from sandwich to sandwich. The difference between $TiCl_2$ and $TiCl_3$ consists merely in the fact that in the lattice of the latter every one out of three titanium ions is missing, and the same is true for the ferrous and ferric chlorides and many others. In view of the symmetry of the crystal structure one has to assume that the unshared valence electrons of the reduced titanium are symmetrically distributed, forming an *s* shell around the Ti^{2+} with a certain amount of bonding between these ions. The Ti^{3+} may form bonds between two ions which uncouple approximately at room temperature, as seen by a strong increase of the magnetic susceptibility of $TiCl_3$ at 300°K (27). Thus, titanium ions do not readily occur in any crystal surface except at faults. Further, the exterior chlorine ion layers will be distinguished by the covalent bonding that they can exert with respect to similar chlorine compounds; they will further have a strong electron-donating, basic, character in that, apart from the completed electron octet of Cl^-, the reduced titanium ions beneath can also act as ready electron suppliers.

It is, then, safe to assume that in an inert solvent the surface of a dispersed, solid, titanium chloride will be able to act as a multi-base on which dimeric aluminum chloroalkyls will dissociate and become adsorbed as monomers. After some progress of the reaction between $TiCl_4$ and AlR_3, the catalyst will thus consist of titanium chloride crystals of small dimensions with adsorbed layers of aluminum chloroalkyl, titanium chloroalkyl, and of some other odd ions or radicals. Obviously the composition of this catalyst can be widely varied by changing the molar ratio of $TiCl_4$ and AlR_3, but while the effectiveness of the catalyst increases and eventually levels off with decreasing this ratio, its mode of functioning is almost independent of composition (28). Finally, the same catalyst can be produced by dispersing $TiCl_3$ and $AlClR_2$ directly. Poorer catalysts result from combining other valence states of titanium and higher aluminum chloroalkyls. Halogens other than chlorine are also effective, though less so, and the same is true for other titanium salts, and even titanates and the salts of a number of transition metals (11, 28). The main property required of the catalyst seems to be that it consists of a dispersed reduced metal compound with basic surface properties and adsorbed acid sites. The relative base-acid strength of this pair, also expressable as a redox potential, seems to be very important for the specific olefin to be polymerized.

Adding olefins to the catalyst solution, it is hardly conceivable that molecules of olefinic electron structure become extensively adsorbed on such electron-rich surfaces as those of titanium chloride. Trivalent titanium chloroalkyls should be adsorbed as dimers. Ti^{4+}-compounds, which act as Lewis acids, should be very weakly adsorbed because of their solubility. Consequently, it seems more likely that the best catalytic surface sites are provided by adsorbed aluminum chloroalkyls.

The complexing of the latter with the monomer may proceed either by a competing action for the Lewis acid between surface and olefin or by the olefin's becoming complexes by the polarized aluminum-carbon bond. In both cases the olefin molecule will become itself polarized as shown diagrammatically below and may eventually be able to interpose itself between the aluminum and one of its alkyls by the mechanism of polarized bond polymerization as suggested by Price (29). The fact that the rate of polymerization depends linearly on the olefin concentration is also a sign that the propagation step is not based on a densely adsorbed layer of olefin but rather proceeds from individual centers. Natta (30) is inclined to consider the polymerization as initiated by carbanions of adsorbed metallo organic compounds but as the adsorption process certainly occurs first, it is probably more appropriate to speak of a polar, coordinate polymerization as envisaged in the polar bond mechanism. The termination step occurs probably by hydrogen or hydride ion transfer from the alkyl to the olefin or metal ion and electron switch from the aluminum alkyl bond and formation of a new bond between the monomer and the aluminum. One should, therefore, expect the polymer molecules to be terminated on one end by a double bond, and at the other by the original alkyl or aryl group on the aluminum. Evidence for this, including chain transfer, has been produced by Natta (31).

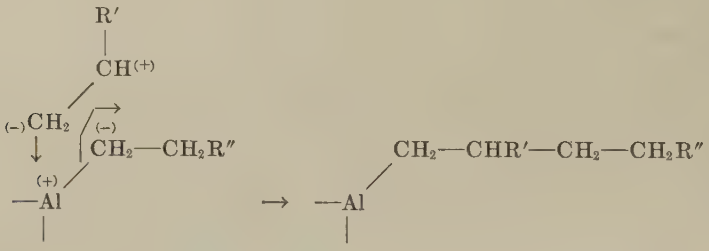

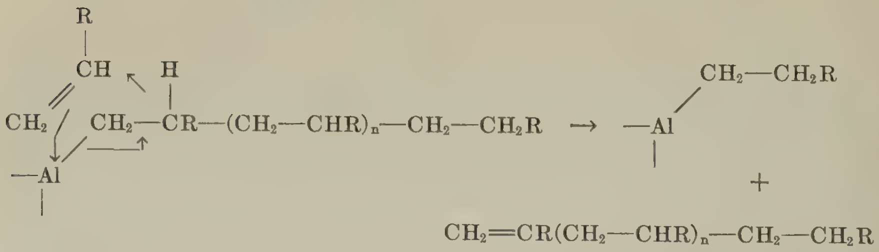

In the picture developed so far an attempt has been made to explain the catalytic enhancement of the reaction at low pressures and temperatures by postulating transition state complexes of presumed low energy. To explain stereospecific direction we may again assume that the adsorbed aluminum or titanium alkyl will occur primarily in a specific position of lowest energy of adsorption, say, for instance, with the chlorine atoms closest to the surface, and the alkyl group being restricted in its rotation. The new monomer in the initial stages of becoming coordinated will have rotational freedom. When reaction occurs it will be steered into the azimuthal position of the lowest energy with respect to rotation around the forming bond. In the case of asymmetrical monomers this will be the *gauche* position with respect to the fixed alkyl. The stereospecific direction thus arises from the adsorbed state of the growing chain end and should be enhanced by the vicinity of the surface which will assist in reducing the rotational freedom of the adding monomer. Apparently, different surface sites will encourage different positions of adsorption of the alkyl group and different routes of access for the new monomer, thus affording a qualitative picture of the formation of the regular forms of the polymer chains and, in case of adsorption which allows rotation on the alkyl groups, of irregular chains.

The above mechanism has been described in detail not yet justified, in order to indicate in which direction explanations might be sought on the basis of present-day direct or indirect evidence. The situation is presumably much more complex, as seen by the rapidly increasing number of reports of stereospecific polymerizations by means of rather diverse catalysts. The titanium chloride-aluminum alkyl system was singled out because the chemistry of its components is rather well investigated, and because it seems to produce a particularly efficient catalyst. As has been mentioned, though, even in this system rather different reaction routes may eventually be established. It is for instance not impossible that the titanium chloride may react with traces of water or acid and thus produce a Lewis acid-co-catalyst system of the type known to be effective in cationic polymerization. Schildknecht's vinyl ether polymerization appears to be a case of ionic polymerization in a condensed film on a liquid-liquid (BF_2-ether: solvent) interface. There are other possibilities that cannot be excluded, e.g., that in the presence of a strong reducing agent such as a hydride, besides a reducible metal salt, metal alkyl compounds may be formed with monomer, thus obviating the necessity of their addition. Finally, it may be possible that adsorption layers of very complex structure may permit dense adsorption of olefins and thus polymerization mechanisms similar to that described under (*a*) for the lithium polymerization of di-olefins. Alfin catalysts seem to belong to this category.

d. Mentioning briefly the Phillips catalyst, of heat-activated chromium oxide on a silica support, we believe the catalytic process to be of a rather different nature. It is true that the oxygen atoms will again provide basic surface sites. In this case, however, the chromium ions present possess an unfilled *d*-shell which is generally accredited as effecting catalytic processes by loosening bond electrons and drawing them into the adsorbing surface (32). The nature of the chromium oxide is not known to us, but presumably is of either the spinel type, O^{2-} ions arranged in cubic close packing and forming tetrahedral holes or the ReO_3 structure, which is cubic close-packed with the metal ion forming the corners and with the anions in the centers of the edges. Consequently, the chromium atoms will be much more accessible at the surface than the reduced ions in the layer structures. Electrons may then be donated to the catalyst in order to be returned whenever this can occur under promoting a polymerization step and with the consequent lowering of the energy of the system as a whole.

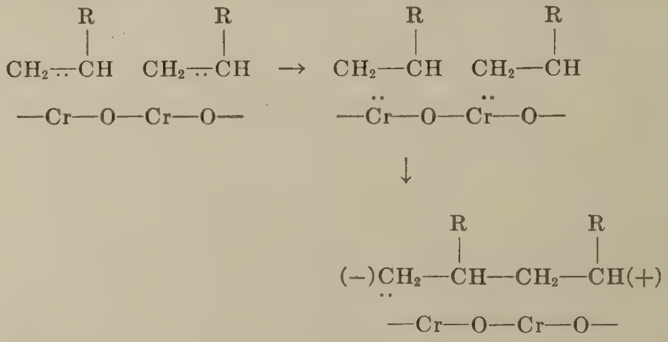

$$\begin{array}{c} \mathrm{R}\qquad\qquad\quad \mathrm{R} \\ |\qquad\qquad\quad | \\ \mathrm{CH_2{\cdots}CH}\quad \mathrm{CH_2{\cdots}CH} \\ \mathrm{—Cr—O—Cr—O—} \end{array} \rightarrow \begin{array}{c} \mathrm{R}\qquad\qquad\quad \mathrm{R} \\ |\qquad\qquad\quad | \\ \mathrm{CH_2—CH}\quad \mathrm{CH_2—CH} \\ \mathrm{—\ddot{C}r—O—\ddot{C}r—O—} \end{array}$$

$$\downarrow$$

$$\begin{array}{c} \mathrm{R}\qquad\qquad\qquad \mathrm{R} \\ |\qquad\qquad\qquad | \\ \mathrm{(-)\underset{\cdot\cdot}{C}H_2—CH—CH_2—CH(+)} \\ \mathrm{—Cr—O—Cr—O—} \end{array}$$

The surface thus acts like a Lewis acid, i.e., like the adsorbed complexes on the Ziegler catalyst surface, and should have primary affinity for olefins. Again adsorption and minimizing of rotational energy will exert stereospecific direction. On the other hand, the supported oxide catalysts of the Standard Oil Co. of Indiana have to be reduced and require reducing agents as activators for best efficiency (33), and therefore seem to play the part of the reduced metal halide surfaces.

V. Conclusions

The so-called stereo-specific high polymer syntheses reported during the past few years, and their relation to heterogeneous catalysis, are briefly discussed. The likely courses of reactions during the formation of all-cis polybutadiene, of crystalline polypropylene oxide, and of the poly α-olefins during Ziegler type syntheses are analyzed in detail.

Reviewing the reaction mechanisms suggested, as well as those by the authors quoted, the inadequacy of the schemes to take care of many observations and details is fully recognized. In their present form these mechanisms will certainly require much revision in the light of the future, yet we believe it will be seen that a certain common pattern is apparent even now, the essential features of which permit the formulation of a distinct mechanism of catalysis.

Dividing this mechanism into two parts, i.e. acceleration and direction of reaction, the primary basis for the acceleration appears to be the coordination or complexing of the reactants to the same, or an adjacent, center. This increases the probability of suitable configurations prior to the transition state and thus lowers the entropy, and possibly also the energy, of the latter; the coordinating center participates also in the reaction by attracting electrons from the reactants and returning them to the product under a minimum of rearrangements of atoms. The activation process becomes thereby subdivided into several steps, each with much lower activation energy than that of the reaction as a whole. It is true that such processes have been postulated before in explanations of catalyses but this appears to be a new combination of "cage effect" and electron transfer through a temporary acceptor.

For the steering part of the mechanism, it seems to be essential that the reactive complex is situated on a surface so that one of the reactants is fixed with regard to its internal, rotational, degrees of freedom. The molecule to be added may then lose its energy to the surface, on its path from the transition to the final state, and may drop into a definite position of lowest energy with respect to the other reactant and the surface. (This can be symbolized by the stacking of tripods which can be placed on each other in any rotational position when standing, but only in 3 distinct ways 120° apart when stacked lying sideways on a plane). This is quite different from the picture developed for some enzymatic or replica syntheses.

Among other features strongly suggested we mention the additional mechanism by which a polymerizable molecule becomes inserted into an existing bond, between the previously linked atoms. This is allied to ester, amide or silicon exchange reactions or even ion exchanges, and, as a double displacement reaction, requires a fairly polar bond. The catalysis of this insertion is tied to a site; consequently, one of the bond partners must be mobile tangentially along the surface, and the growth proceeds like that of a hair from a feeding root.

Finally, it seems required that the coordinating electron acceptor be tied to a electron donating substrate. Whether the donating quality is only needed to hold the coordination center, or is essential in the mechanism of catalysis, cannot be surmised yet, although the latter alternative is likely. There can be little doubt though that the elevated position of the coordinating center, lying on top of a crystal plane, will help in the complex formation.

REFERENCES

1. Compare, e.g., GEE, G., AND RIDEAL, E. K., *Trans. Faraday Soc.* **31**, 996 (1935); GEE, G., DAVIES, C. B., AND MELVILLE, H. W., *Trans. Faraday Soc.* **35**, 1298 (1939).
2. SCHILDKNECHT, C. E., GROSS, S. T., DAVIDSON, H. R., LAMBERT, J. M., AND ZOSS, A. O., *Ind. Eng. Chem.* **40**, 2104 (1948); SCHILDKNECHT, C. E., GROSS, S. T., AND ZOSS, A. O., *Ind. Eng. Chem.* **41**, 1998, 2891 (1949).
3. MARK, H., *Trans. N. Y. Acad. Sci.* **11**, 51 (1948).
4. MORTON, A. A., *Ind. Eng. Chem.* **42**, 1488 (1950).

5. Stewart, R. A., *et al.*, *Ind. Eng. Chem.* **45,** 173 (1953).
6. Stavely, F. W., and co-workers, *Ind. Eng. Chem.* **48,** 778–783 (1956).
7. Horne, S. W., Kiehl, J. P., *et al.*, *Ind. Eng. Chem.* **48,** 784–791 (1956).
8. Williams, F. C., *et al.*, *J. Am. Chem. Soc.* **78,** 1260 (1956).
9. Ziegler, K., *Brennstoff-Chem.* **33,** 193 (1953); *Angew. Chem.* **64,** 323 (1952).
10. Ziegler, K., Belgian Patents 533,362; 534,792; 534,888.
11. Ziegler, K., Belgian Patent 543,259.
12. Natta, G., *J. Polymer Sci.* **16,** 143 (1955).
13. Natta, G., *Chimica e industria, Milan* **37,** 888 (1955); Natta, G., and Corradini, P., *J. Polymer Sci.* **95,** 251 (1956).
14. Natta, G., *et al.*, *J. Am. Chem. Soc.* **77,** 1708 (1955).
15. Philipps Petroleum Co., Belgian Patent 530,617; 535,082; Australian Patent Appl. 6193/56; Standard Oil of Indiana, U.S. Patent 2,692,257.
16. Price, C. C., Osgan, M., Hughes, R. E., and Shambelan, C., *J. Am. Chem. Soc.* **78,** 690 (1956).
17. Pruitt, M. E. and Baggett, J. M., U. S. Patent 2,706,181. April 12 (1955).
18. See articles by: Skinner, H. A.; Chatt, J.; Rijnders, G. W. A., and Schuit, G. E. A. *in* "Cationic Polymerization and Related Complexes" (P. H. Plesch, ed.). Academic Press, New York, 1953; Walling, C., *J. Am. Chem. Soc.* **72,** 1164 (1950); cf. also, Eirich, F. and Mark, H., *Kunststoffe,* in press.
19. Freudenberg, K., "Stereo-Chemie," Vol. 1, p. 317. F. Deuticke, Vienna, 1933; Glasstone, S., Laidler, K. J., and Eyring, H., "The Theory of Rate Processes." McGraw-Hill, New York, 1941.
20. Talalay, A., and Magat, M., "Synthetic Rubber from Alcohol." Interscience, New York, 1945.
21. Chatt, J., *Proc. Univ. Coll. North Staffordshire, Engl. 1952* p. 10–56 (Publ. 1953).
22. Bilery, J., Taft, R. W., and Hammet, L. P., *J. Am. Chem. Soc.* **75,** 1253 (1953); Taft, R. W., *et al.*, *ibid.*, **77,** 1584 (1955); but compare also, Evans, A. G., *et al.*, *J. Chem. Soc.*, 2757, (1956).
23. Lutz, R. E., and Revely, W. G., *J. Am. Chem. Soc.* **63,** 3184 (1941); Gilman, H., and Kirby, R. H., *J. Am. Chem. Soc.* **63,** 2046 (1941); Huston, R. C., *et al.*, *J. Org. Chem.* **6,** 123 (1941); *ibid.* **12,** 90 (1947); *ibid.* **13,** 331 (1948); cf. also, Brewster, J., *J. Amer. Chem. Soc.* **78,** 4061 (1956); Wassermann, A., and Aubrey, N. E., *ibid.* **78,** 1726 (1956).
24. Price, C. C., *J. Am. Chem. Soc.* **78,** 690 (1956).
25. Overberger, Private communication.
26. For a detailed discussion, see Moeller, T., "Inorganic Chemistry," Wiley, New York, 1952; also, Cartmell, E., and Fowles, G. W. A., "Valency and Molecular Structure," Academic Press, New York, 1956.
27. Klemm, W., and Krose, E., *Z. anorg. Chem.* **253,** 209 (1947).
28. Friedlander, H. N., and Oita, K., American Chemical Society Fall Meeting, Lecture (1956).
29. Price, C. C., *Ann. N. Y. Acad. Sci.* **44,** 368 (1943); Pepper, D. C., *Quart. Rev. (London)* **8,** 88 (1954).
30. Natta, G., *Makromol. Chem.* **16,** 213–237 (1955).
31. Natta, G., Private communication.
32. Gomer, R., and Smith, C. S., "Structure and Properties of Solid Surfaces," U. of Chicago Press, Chicago, Illinois, 1953.
33. Field, E., and Feller, M., American Chemical Society Fall Meeting, Lecture (1956).

JOURNAL OF COLLOID SCIENCE **11**, 767–768 (1956)

BOOK REVIEW

Principles and Problems in Energetics. By J. N. Brønsted. Translated from Danish by R. P. Bell. Interscience Publishers, Inc., New York, 1955. 119 pp. Price $3.50.

Lewis and Randall, in the preface to their classical book *Thermodynamics*, compare some domains of science, e.g., thermodynamics, with ancient cathedrals, inspiring solemity and awe. That awe might be the reason why for a long time critical scrutiny of its foundation and its presentation in textbooks was scarce. The textbooks mostly used when I was a young student did not present the matter in a very clear way and consequently thermodynamics was generally considered to be rather hard stuff. The notations of Lewis and Randall were a great boon which made the presentation of thermodynamics incomparably clearer than before.

However, the first clear presentation of its foundations I found in an article by Landé in the *Handbuch der Physik*, where he gave an account of Caratheodory's work. But how far from experimental work was this mathematical treatise. Later, when I became a professor, I could not use this presentation for my students, who had a very limited mathematical training. But I happened to read Sadi Carnot's little pamphlet from 1824 and Ostwald's remark to it, that Carnot's term "calorique" should be translated by "entropy" and not "heat," whereas "chaleur" should be rendered as "heat." I felt at once that chemical thermodynamics would be much easier to understand if one started with entropy as the fundamental thermal concept and not heat, and so I taught my students.

Glad was I when I found that Professor Brønsted at that time had written some papers on the foundations of thermodynamics along similar lines, but departing much more radically from the conventional presentation. Regrettably most of these papers were published in Danish in a journal with limited circulation. It is therefore to be welcomed that Dr. R. P. Bell, who is a master of that language since he many years ago worked in Brønsted's laboratory, has translated his last monograph on the matter, written only one year before the author's death in 1947.

I think a good deal of the difficulties in chemical thermodynamics arise from the fact that thermodynamics started as steam engine theory, and too much of that approach was taken over by the chemists, who at that time were not able to grasp J. Willard Gibbs' rather abstract presentation, although it became accessible also to European chemists at large through Ostwald's German translation.

Brønsted starts with an overhaul of the work concept and states his *work principle*, corresponding to the classical First Law;

$$\Sigma\delta A = \Sigma(P_1 - P_2)\delta K = 0,$$

where the several terms are called *work*, even in the case of P = temperature and K = entropy. Only reversible processes are discussed at the first moment. Of course some people might be annoyed by the extension of the work concept; it is the same thing as when Brønsted many years earlier redefined acids and bases as proton donors and proton acceptors.

He then proceeds to the temperature concept. From reversible processes only differences of absolute temperature can be defined, but no absolute zero. When a thermal reservoir changes its temperature our attention should be directed to its simultaneous change in entropy content rather than the heat involved. Whereas the entropy is defined as a function that is constant in a system in which only reversible processes are going on, this function turns out to increase in the case of irreversible processes. Brønsted's approach to the problem is compared with that of Planck, Caratheodory, and Born.

The transport of heat by conduction is regarded as a transport of entropy coupled, not with another sort of work, as in a reversible process, but with a production of entropy. The corresponding amount of heat TdS makes the total heat arriving at the colder reservoir equal the heat leaving the warmer one.

It is the comparison of an amount of entropy produced in an irreversible process and the corresponding amount of heat that makes it possible to define an absolute zero of temperature as Caratheodory first stressed. I should like to remark that the irreversibility does not matter, but the production does. There exists in energetics another quantity that in contrast to entropy can both be produced and annihilated, viz., a liquid surface. Accordingly it is possible to define an absolute zero for surface tension. But the zero pressure in a cold vacuum is conventional and not absolute in the same sense as zero temperature and surface tension; it is possible to obtain negative pressures in liquids. Chemical substances can also be produced, but only simultaneous with the annihilation of others, and hence chemical potentials have no absolute zero.

The book concludes with a discussion of thermoelectric and electrochemical phenomena. It was written before much of the modern thermodynamics of irreversible phenomena had been developed, so there is no connection with the work of Onsager, de Groot and Prigogine.

This book and the papers by Brønsted and by LaMer referred to in the foreword and the Introduction should be of great interest to all teachers of thermodynamics. Authors of physicochemical textbooks are legion. Their presentation of these matters would certainly be improved if they studied Brønsted's points of view.

Arne Ölander, University of Stockholm, Sweden

AUTHOR INDEX

A

Aihara, A., 671
Alexander, A. E., 419
Alfrey, T., Jr., 135
Allsopp, C. B., 565

B

Barrer, R. M., 479
Baum, H., 428
Benson, G. C., 593
Bhattacharya, Abani K., 124
Bhattacharya, Amal K., 124, 171
Bigelow, W. C., 60
Bikerman, J. J., 299
Blank, Martin, 608
Bloksma, A. H., 286
Bobalek, Edward G., 21
Bose, A. N., 240
Bosworth, R. C. L., 496
Bowden, F. P., 555
Bradford, E. B., 135
Bradley, R. S., 237
Brockway, L. O., 60

C

Catsiff, E., 48
Channen, E. W., 593
Cockbain, E. G., 575
Constable, F. H., 647
Crisp, D. J., 356

D

D'Alessandro, A. F., 653
Davies, J. T., 377
Davies, Mansel, 671

E

Eirich, F., 689, 748
Eley, D. D., 445
Epel, Joseph N., 195
Evans, U. R., 314

F

Farkas, A., 653
Farlow, N. H., 177, 184
Few, A. V., 34
Fok, Shiu-Ming, 21
Fraser, M. J., 451
French, F. A., 183
Fuchs, N., 107

G

George, Philip, 327
Gilbert, G. A., 428
Gillespie, T., 732
Goyer, Guy G., 697
Greene-Kelly, R., 77
Guastalla, Jean, 623
Gunn, Ross, 69, 108, 254, 691

H

Hawke, J. G., 419
Hedge, D., 445
Heller, Wilfried, 195
Hughes, W. J., 340
Hurd, Charles B., 15
Hutchinson, Eric, 352

I

Inagaki, Hiroshi, 226
Irvine, D. H., 327

J

Johnson, P., 340
Joly, M., 519
Jones, M. H., 508

K

Kemball, C., 532

L

Lahiri, A., 240
La Mer, Victor K., 295, 608, 704, 710, 720
Langbridge, D., 585
Lawrence, A. S. C., 585
Linton, M., 391
Lissowski, P., 107
Llopis, J., 543
Lucchesi, Peter J., 113

M

Maclay, William N., 272
McIntosh, R., 593
McKenzie, N., 479
Mark, H., 689, 748
Maron, Samuel H., 21, 80
Mehrotra, K. N., 250
Melville, H. W., 508
Merrill, Edward W., 1
Mitchell, J. S., 317
Moelwyn-Hughes, E. A., 501
Mosher, Carol S., 352
Mukherjee, P. N., 240

N

Nasini, Antonio, 637
Nosworthy, Judith, 565

O

O'Connor, D. J., 158
O'Driscoll, K. F., 244
Offenbach, J. A., 39, 48
Onogi, Shigeharu, 214
Ostacoli, Girogio, 637
Ottewill, R. H., 34, 340
Ovenall, D. W., 508

P

Packter, A., 96, 150
Peaker, F. W., 508
Pidgeon, Frances D., 697
Pierce, Percy E., 80
Pilpel, N., 51
Pinfold, T. A., 471

R

Rawlins, F. I. G., 324
Rebollo, D. V., 543
Reay, J. S. S., 479
Rees, D. H., 617
Rideal, Sir Eric, 732
Robertson, A. J. B., 308
Robertson, W. G. P., 508

S

Sanders, J. V., 158
Sanders, J. W., 260
Saunders, F. L., 260
Scheludko, A., 167
Schofield, R. K., 617
Schulman, J. H., 451
Sebba, F., 471
Smellie, Robert H., Jr., 704, 710, 720
Sobotka, Harry, 435
Stenson, R., 585
Stoddart, C. T. H., 532
Sutherland, K. L., 391

T

Tabibian, Richard M., 195
Taylor, Hugh, 296
Ter Minassian-Saraga, L., 398
Thomas, Jess W., 107
Tobolsky, A. V., 39, 48, 244

U

Ui, Kyuzaburo, 214

V

Vanderhoff, J. W., 135

W

Winterberger, Alan R., 15
Woessner, R. H., 69, 254

SUBJECT INDEX

A

Acetone, hydrogenation, Stoddart and Kemball, 532

Adhesion, metal-adhesive-metal joints, Gillespie and Sir Rideal, 732

Adsorption, molecules adsorbed at benzene-water interface, Pilpel, 51;—adsorbed films of fatty acids, Bigelow and Brockway, 60;—on alumina, Crisp, 356;—polarization of adsorbates, Benson *et al.*, 593

Aerosol, electrification, Woessner and Gunn, 69;—and ionic diffusion, Fuchs and Lissowski, 107;—reply, Gunn, 108;—collector, Farlow and French, 177;—water aerosol measurement, Farlow, 184;—electrification, Gunn and Woessner, 254;—and light ion conductives, Gunn, 691;—submicron water aerosols, Goyer and Pidgeon, 697

Alkyl sulfates, molal volumes, Hutchinson and Mosher, 352

Amino acids, and x-rays, Nosworthy and Allsopp, 565

Antifoams, surface studies, Hawke and Alexander, 419

Appreciation, Sir Eric Rideal, Taylor, 296

B

Butanol, solubilization of butanol and methylbutanol, Bose and Mehrotra, 250

C

Capillary condensation, Barrer *et al.*, 479

Carbon blacks, surface area, Maron *et al.*, 21

Chemical physics, at the National Gallery, Rawlins, 324

Coagulation, of lyophobic sols, Bhattacharya and Bhattacharya, 124

Coalescence, of liquid drops, Linton and Sutherland, 391

Colloidal particles, molecular weight determination, Scheludko, 167

Colloidal spheres, light scattering, Tabibian *et al.*, 195

Colors, by thin films on metal, Evans, 314

Corrosion, membranes and corrosion protection, Nasini and Ostacoli, 637

D

Dedication, to Sir Eric Rideal, La Mer, 295

Deoxyribonucleic acid, and macromolecular lesion, Mitchell, 317

Detergents, cationic, determination, Few and Ottewill, 34, 294

Diffusion battery, Thomas, 107

Drainage, and surface roughness, Bikerman, 299

E

Electrolyte, concentration and time of coagulation, Bhattacharya, 171

Emulsifiers, solubility of nonionic, Maclay, 272

Emulsion, polymerization, mechanism, Bradford *et al.*, 135;—adsorption at emulsion interfaces, Cockbain, 575

F

Ferrimyoglobin, and hydrogen peroxide, George and Irvine, 327

Flow, pseudoplastic, Merrill, 1; generalized flow theory, Maron and Pierce, 80

Formic acid, electrochemistry of anhydrous, overcurrent suppression, Sebba and Pinfold, 471

H

Humic acid, rheology, Mukherjee and Lahiri, 240

Hydrogen peroxide, and ferrocyanides, Constable, 647

Hydrophobic monolayers, on platinum, mica and silica, O'CONNOR AND SANDERS, 158

I

Ion exchange, statistical theory, BLOKSMA, 286

L

Latexes, electrolyte stability, SAUNDERS AND SANDERS, 260
Layers, penetrability of molecular, SOBOTKA, 435
Liescgang, phenomenon, PACKTER, 96, 150
Light scattering, calibration, HUGHES *et al.*, 340

M

Membrane pressure, calculation, SCHOFIELD AND REES, 617
Methylmethacrylate, polymerization, O'DRISCOLL AND TOBOLSKY, 244
Methylsiliconic acid, gels, HURD AND WINTERBERGER, 15
Monolayers, surface equation, DAVIES, 377;—adsorption and desorption, TER MINASSIAN-SARAGA, 398
Montmorillonites, swelling, GREENE-KELLY, 77

N

Naphthalene, catalytic oxidation, D'ALESSANDRO AND FARKAS, 653

P

Phosphate slimes, flocculation, LA MER AND SMELLIE, 704, 710, 720
Polyelectrolytes, spinnability and viscosity, INAGAKI, 226
Polymers, properties of crystalline polymers, CATSIFF *et al.*, 48; frequency and temperature dispersions of high polymers, ONOGI AND UI, 214; temperature and high polymers, LLOPIS AND REBOLLO, 543
Polystyrenes, light scattering, JONES *et al.*, 508
Polyurethan elastomers, stress relaxation, OFFENBACH AND TOBOLSKY, 39
Protein, protein-lipid interactions, ELEY AND HEDGE, 445

R

Relaxation times, of nonrigid polar molecules, AIHARA AND DAVIES, 671
RIDEAL, SIR ERIC, dedication, LA MER 295; appreciation, TAYLOR, 296
Rubber, and carbon black, BRADLEY, 237

S

Sedimentation, kinetics of collective, BOSWORTH, 496
Soap, solubility in soap solutions, LANGBRIDGE *et al.*, 585
Starch, fractionation, BAUM AND GILBERT, 428
Sulfates, oscillometric precipitation behavior of sparingly soluble sulfates (Ba, Pb, Sr), LUCCHESI, 113
Surface, reactions on metal surfaces, ROBERTSON, 308; interfacial energies, MOELWYN-HUGHES, 501; non-Newtonian viscosity, JOLY, 519;—of solids, BOWDEN, 555; transfer of surface films through channels, LA MER AND BLANK, 608, 688;—activity, wetting and dewetting, GUASTALLA, 623

T

Trypsin, interfacial, FRASER AND SCHULMAN, 451

V

Vinyl, vinyl type polymerization at solid surfaces, EIRICH AND MARK, 689, 748

INDEX OF BOOK REVIEWS

Brønsted, J. N., Principles and Problems in Energetics (Ölander, Å.), 767

Chargaff, E., and Davidson, J. N. (eds.), The Nucleic Acids: Chemistry and Biology (Steinhardt, J.), 111

Crawford, A. E., Ultrasonic Engineering with Particular Reference to High Power Applications (Sollner, K.), 291

Denbigh, K. G., The Principles of Chemical Equilibrium (King, C. V.), 292

Ferris, S. W., Handbook of Hydrocarbons (La Mer, V. K.), 288

Guggenheim, E. A., and Prue, J. E. Physicochemical Calculations (Smellie, R. H.), 288

Insley, H., and Fréchette, Van Derck, Microscopy of Ceramics and Cements (Mason, C. W.), 110

Linstead, R. P., *et al.*, A Course in Modern Techniques of Organic Chemistry (Stork, G.), 193

McDonald, H. J., Ionography. Electrophoresis in Stabilized Media (Becker, R. R.), 291

Morgan, P. (ed.), Glass-reinforced Plastics (Davies, R. E.), 110

Robinson, R. A., and Stokes, R. H., Electrolyte Solutions. The Measurement and Interpretation of Conductance, Chemical Potential and Diffusion (Scatchard, G.), 289

Trotman-Dickenson, A. F., Gas Kinetics: An Introduction to the Kinetics of Homogeneous Gas Reactions (Steacie, E. W. R.), 193

Williams, T. I., The Elements of Chromatography (Thomas, A. W.), 194

JOURNAL OF
COLLOID SCIENCE

Editor-in-Chief
Victor K. La Mer, Columbia University, New York

Advisory Board

C. O. Beckmann
K. F. Bonhoeffer
J. A. Christiansen
P. J. W. Debye
John T. Edsall
I. Fankuchen
John D. Ferry
Wilfried Heller
John G. Kirkwood
E. C. Lingafelter
L. G. Longsworth
S. G. Mason
J. Th. G. Overbeek
R. Ruyssen
William Seifriz
Leo Shedlovsky
Theodore Shedlovsky
Robert Simha
R. H. Smellie
Jacinto Steinhardt
The Svedberg
Hugh S. Taylor
Arne Tiselius
Robert D. Vold
Bernard Vonnegut
Ralph W. G. Wyckoff
Bruno H. Zimm

VOLUME 11
1956

ACADEMIC PRESS INC.—PUBLISHERS
NEW YORK, N. Y.

Copyright© 1956, by Academic Press Inc.
Made in United States of America

Contents of Volume 11

Number 1, February, 1956

Edward W. Merrill. Pseudoplastic Flow: Viscometry, Correlations of Shear Stress vs. Shear Rate, and Prediction of Laminar Flow in Tubes........ 1
Charles B. Hurd and Alan R. Winterberger. Gels of Methyl Siliconic Acid. I. Method of Formation and Energy of Activation. 15
Samuel H. Maron, Edward G. Bobalek and Shiu-Ming Fox. Determination of Surface Areas of Carbon Blacks by Soap Adsorption........ 21
A. V. Few and R. H. Ottewill. Determination of Cationic Detergents 34
J. A. Offenbach and A. V. Tobolsky. Chemical Relaxation of Stress in Polyurethane Elastomers........ 39
E. Catsiff, J. Offenbach and A. V. Tobolsky. Viscoelastic Properties of Crystalline Polymers: Polyethylene........ 48
N. Pilpel. The Sizes of Molecules Adsorbed at the Benzene-Water Interface........ 51
W. C. Bigelow and L. O. Brockway. Variation of Contact Angle and Structure with Molecular Length and Surface Density in Adsorbed Films of Fatty Acids........ 60
R. H. Woessner and Ross Gunn. Measurements Related to the Fundamental Processes of Aerosol Electrification........ 69
R. Greene-Kelly. The Swelling of Organophilic Montmorillonites in Liquids........ 77
Samuel H. Maron and Percy E. Pierce. Application of Ree-Eyring Generalized Flow Theory to Suspensions of Spherical Particles.... 80
A. Packter. The Liesegang Phenomenon. II. Addition of Protecting Agents........ 96

LETTERS TO THE EDITOR

Jess W. Thomas. Diffusion Battery........ 107
N. Fuchs and P. Lissowski. The Charging of Aerosols by Ionic Diffusion........ 107
Ross Gunn. Reply to Letter to the Editor by N. Fuchs and P. Lissowski........ 108

BOOK REVIEWS

Richard E. Davies. Glass-Reinforced Plastics........ 110
C. W. Mason. Microscopy of Ceramics and Cements........ 110

Jacinto Steinhardt. The Nucleic Acids: Chemistry and Biology. Volumes I and II 111

Number 2, April, 1956

Peter J. Lucchesi. Oscillometric Investigation of Precipitation and Dissolution Rates of Sparingly Soluble Sulfates 113
Amal K. Bhattacharya and Abani K. Bhattacharya. Verification of a New Equation in the Study of the Slow Coagulation of Lyophobic Sols by Different Techniques 124
E. B. Bradford, J. W. Vanderhoff and T. Alfrey, Jr., The Use of Monodisperse Latexes in an Electron Microscope Investigation of the Mechanism of Emulsion Polymerization 135
A. Packter. The Liesegang Phenomenon. III. The Structure of the Gel Medium 150
D. J. O'Connor and J. V. Sanders. Hydrophobic Monolayers on Platinum, Mica, and Silica 158
A. Scheludko. A Possibility for the Determination of Molecular Weights of Colloidal Particles by Ultracentrifugation in an Electric Field 167
Amal K. Bhattacharya. A Tyndallometric Study Connecting Electrolyte Concentration and Time of Coagulation 171
N. H. Farlow and F. A. French. Calibration of Liquid Aerosol Collectors by Droplets Containing Uniform Size Particles 177
N. H. Farlow. A Physicochemical System for Water Aerosol Measurement 184

BOOK REVIEWS

E. W. R. Steacie. Gas Kinetics 193
Gilbert Stork. A Course in Modern Techniques of Organic Chemistry 193
Arthur W. Thomas. The Elements of Chromatography 194

Number 3, June, 1956

Richard M. Tabibian, Wilfried Heller, and Joseph N. Epel. Experimental Investigations on the Light Scattering of Colloidal Spheres. I. The Specific Turbidity 195
Shigeharu Onogi and Kyuzaburo Ui. Frequency and Temperature Dispersions of High Polymers 214
Hiroshi Inagaki. On Concentrated Solutions of Polyelectrolytes. I. Spinnability and Non-Newtonian Viscosity 226
R. S. Bradley. The Reinforcement of Rubber by Carbon Black. A Study of the Cohesion Between the Particles of Filler 237
P. N. Mukherjee and A. Lahiri. Studies on the Rheological Properties of Humic Acid from Coal 240
K. F. O'Driscoll and A. V. Tobolsky. Kinetics of Polymerization of Methylmethacrylate Initiated by the System Benzoyl Peroxide-Dimethylaniline 244

A. N. Bose and K. N. Mehrotra. Effect of Oleic Acid and Sodium Hydroxide on the Solubilization of Butanol-1 and 3-Methyl Butanol-1 in Aqueous Solution of Sodium Oleate.............. 250
Ross Gunn and R. H. Woessner. Measurements of the Systematic Electrification of Aerosols....................................... 254
F. L. Saunders and J. W. Sanders. The Effect of Methylcellulose on the Electrolyte Stability of Dilute Synthetic Latexes.......... 260
William N. Maclay. Factors Affecting the Solubility of Nonionic Emulsifiers....................................... 272

LETTER TO THE EDITOR

A. H. Bloksma. On a Hidden Assumption in the Statistical Theory of Ion Exchange of Davis and Rible.......................... 286

BOOK REVIEWS

Victor K. La Mer. Handbook of Hydrocarbons.................. 288
R. H. Smellie, Jr. Physicochemical Calculations.................. 288
George Scatchard. Electrolyte Solutions. The Measurement and Interpretation of Conductance, Chemical Potential and Diffusion 289
Karl Sollner. Ultrasonic Engineering with Particular Reference to High Power Applications................................. 291
Robert R. Becker. Ionography. Electrophoresis in Stabilized Media. 291
Cecil V. King. The Principles of Chemical Equilibrium........... 292
Announcement....................................... 294

Numbers 4 and 5, August, October, 1956

Victor K. La Mer. Dedication................................ 295
Hugh Taylor. Sir Eric Rideal—An Appreciation................ 296
J. J. Bikerman. Drainage of Liquid from Surfaces of Different Rugosites.. 299
A. J. B. Robertson. The Absolute Rate of Certain First-Order Reactions on Metal Surfaces............................... 308
U. R. Evans. Colors Exhibited by Thin Films on Metal........... 314
J. S. Mitchell. The "Macromolecular Lesion" Involving Deoxyribonucleic Acid in Radiobiology and Radiotherapy........... 317
F. I. G. Rawlins. Chemical Physics at the National Gallery, London. 324
Philip George and D. H. Irvine. A Kinetic Study of the Reaction Between Ferrimyoglobin and Hydrogen Peroxide.............. 327
W. J. Hughes, P. Johnson, and R. H. Ottewill. Experimental Studies on the Light-Scattering Method and its Calibration.... 340
Eric Hutchinson and Carol S. Mosher. Partial Molal Volumes in Alkyl Sulfate Solutions................................. 352
D. J. Crisp. The Adsorption of Alcohols and Phenols from Nonpolar Solvents on to Alumina................................. 356
J. T. Davies. A Surface Equation of State for Charged Monolayers.. 377
M. Linton and K. L. Sutherland. The Coalescence of Liquid Drops. 391

L. TER MINASSIAN-SARAGA. Recent Work on Spread Monolayers, Adsorption and Desorption 398
J. G. HAWKE AND A. E. ALEXANDER. Some Surface Studies of Antifoams 419
H. BAUM AND G. A. GILBERT. The Fractionation of Potato Starch by Centrifugation in Alkali 428
HARRY SOBOTKA. Penetrability of Molecular Layers 435
D. D. ELEY AND D. HEDGE. Protein Interactions with Lecithin and Cephalin Monolayers 445
M. J. FRASER AND J. H. SCHULMAN. Activity of Trypsin-Lipid Complexes at Oil/Water Interfaces 451
F. SEBBA AND T. A. PINFOLD. Electrochemical Studies in Anhydrous Formic Acid. III. The Suppression of Polarographic Overcurrents (Maxima) 471
R. M. BARRER, N. MCKENZIE, AND J. S. S. REAY. Capillary Condensation in Single Pores 479
R. C. L. BOSWORTH. The Kinetics of Collective Sedimentation 496
E. A. MOELWYN-HUGHES. Interfacial Energies 501
M. H. JONES, H. W. MELVILLE, D. W. OVENALL, F. W. PEAKER, AND W. G. P. ROBERTSON. Light-Scattering Measurements on Some Branched Polystyrenes 508
M. JOLY. Non-Newtonian Surface Viscosity 519
C. T. H. STODDART AND C. KEMBALL. The Catalytic Hydrogenation of Acetone on Evaporated Metallic Films 532
J. LLOPIS AND D. V. REBOLLO. The Influence of Temperature on Monolayers of Nonelectrolytic Linear High Polymers 543
F. P. BOWDEN. Methods of Studying the Surface Structure of Solids 555
JUDITH NOSWORTHY AND C. B. ALLSOPP. Effects of X-Rays on Dilute Aqueous Solutions of Amino Acids 565
E. G. COCKBAIN. The Adsorption of Serum Albumin and Sodium Dodecyl Sulfate at Emulsion Interfaces 575
D. LANGBRIDGE, A. S. C. LAWRENCE, AND R. STENSON. Solubility in Soap Solutions. VI. The Effect of Soap upon Upper and Lower Consolute Temperatures in the Nicotine-Water and Triethylamine-Water Systems 585
G. C. BENSON, E. W. CHANNEN, AND R. MCINTOSH. An Estimate of Induced Dipoles to the Orientational Polarization of Adsorbates . 593
VICTOR K. LA MER AND MARTIN BLANK. The Transfer of Surface Films Through Surface Channels—Geometrical Factors 608
R. K. SCHOFIELD AND D. H. REES. Calculation of Membrane Pressure for a Sol of Spherical Particles 617
JEAN GUASTALLA. Recent Work on Surface Activity, Wetting and Dewetting 623
ANTONIO NASINI AND GIORGIO OSTACOLI. Polar Ion-Selective Membranes and Corrosion Protection 637

F. H. Constable. The Decomposition of Hydrogen Peroxide by Massive Colloidal Metallic Ferrocyanides.................... 647
A. F. D'Alessandro and A. Farkas. The Kinetics of the Catalytic Oxidation of Naphthalene.............................. 653
A. Aihara and Mansel Davies. Dielectric Relaxation Times of Some Non-Rigid Polar Molecules.............................. 671
F. Eirich and H. Mark. Vinyl Type Polymerization at Solid Surfaces and with Complex Catalysts (Summary and Conclusions)...... 689

Number 6, December 1956

Ross Gunn. The Ratio of the Positive and Negative Light Ion Conductivities within a Neutral Aerosol Space.................... 691
Guy G. Goyer and Frances D. Pidgeon. Production and Characteristics of Submicron Water Aerosols.......................... 697
Victor K. La Mer and Robert H. Smellie, Jr. Flocculation, Subsidence, and Filtration of Phosphate Slimes. I. General........ 704
Victor K. La Mer and Robert H. Smellie, Jr. Flocculation, Subsidence, and Filtration of Phosphate Slimes. II. Starches as Agents for Improving Flocculation, Subsidence, and Filtration of Phosphate Slimes.. 710
Robert H. Smellie, Jr., and Victor K. La Mer. Flocculation, Subsidence, and Filtration of Phosphate Slimes. III. Subsidence Behavior.. 720
T. Gillespie and Sir Eric Rideal. The Deformation and Strength of Napkin Ring Metal-Adhesive-Metal Joints................. 732
F. Eirich and H. Mark. Vinyl Type Polymerization at Solid Surfaces and with Complex Catalysts............................. 748

BOOK REVIEW

Arne Olander. Principles and Problems in Energetics........... 767

Author Index... 769
Subject Index.. 771
Index of Book Reviews...................................... 773